AD NUMBER
AD802293
LIMITATION CHANGES
TO: **Approved for public release; distribution is unlimited.**
FROM: **Distribution authorized to U.S. Gov't. agencies and their contractors; Administrative/Operational Use; 30 JUN 1966. Other requests shall be referred to Army Missile Command, Redstone Arsenal, AL.**
AUTHORITY
MICOM ltr 26 Feb 1968

VOLUME I

AERODYNAMIC FORCE ANALYSIS

By Branimir D. Djordjevic

JUNE 1966

DISTRIBUTION LIMITED SEE NOTICES PAGE

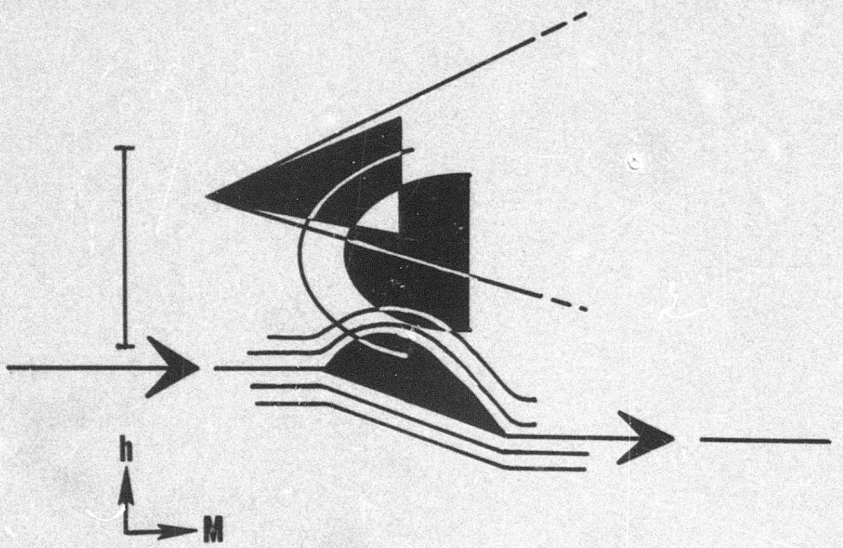

CONTRACT NO. DA-01-009-506-ORD-851 (Z)

AEROSPACE DEPARTMENT
AUBURN UNIVERSITY

For

U.S. ARMY MISSILE COMMAND
REDSTONE ARSENAL, ALABAMA

DISPOSITION INSTRUCTIONS

Destroy this report when it is no longer needed. Do not return it to the originator.

DISCLAIMER

The findings in this report are not to be construed as an official Department of the Army position, unless so designated by other authorized documents.

DISTRIBUTION LIMITATION

This document is subject to special export controls and each transmittal to foreign governments or foreign nationals may be made only with prior approval of this Command, Attn: AMSMI-RF.

30 June 1966

AERODYNAMIC FORCE ANALYSIS

by

BRANIMIR D. DJORDJEVIC

Prepared for

FUTURE MISSILE SYSTEMS DIVISION
RESEARCH AND DEVELOPMENT DIRECTORATE
U. S. ARMY MISSILE COMMAND
REDSTONE ARSENAL, ALABAMA

By

DEPARTMENT OF AEROSPACE ENGINEERING
AUBURN UNIVERSITY

CONTRACT DA-01-009-506-ORD-851(Z)

DA Project 1S222901A206
AMCMSC 5221.11.148

ABSTRACT

Aerodynamic Force Analysis methods and technology from an extensive bibliography, originally prepared as an internal reference for the U. S. Army Missile Command, is presented in conjunction with definitive guidance for use and applicability. An altitude range from 0 to 400,000 feet and a Mach number range from low subsonic through orbital-re-entry level hypersonic is encompassed, with appropriate continuum, slip and free molecule flow treatments. The extensive coverage should prove useful as a reference for engineering analysis and for introductory educational purposes. The user is also directed to the extensive bibliography of source material for rigid proofs and intensive subject treatment.

FOREWORD

The methods and technology presented herein are the result of considerable condensation and regrouping of an original reference prepared by the Aerospace Department of Auburn University. The original was prepared as an internal reference for the U. S. Army Missile Command under Contract DA-01-009-506-ORD-851 (Z) with Auburn Research Foundation, Inc. The extensive coverage and usefulness indicated educational and reference value of significance to warrant wide distribution. This revision of the original work retains the quality of an extensive engineering reference, but directs the user to source material for rigid proofs and intensive subject treatment. Revision has been accomplished under a supplement to the original contract, with distribution rights reserved by the U. S. Army Missile Command.

The principal author and technical supervisor for the original effort, Professor Branimir D. Djordjevic, supervised the format revision and condensation. Extensive participation in support of the effort, by the Aerospace Engineering Staff and many of its graduate and undergraduate students is acknowledged.

PART I

INTRODUCTION

BLANK PAGE

TABLE OF CONTENTS

Part I Introduction

LIST OF FIGURES

Part I Introduction

LIST OF TABLES

Part I Introduction

BLANK PAGE

1.1 PLAN AND SUMMARY OF PART I.

The material presented in Part I is a rudimental introduction to some of the basic aerodynamic and flight dynamic elements and definitions. It is thought that this part will prove to be a useful framework for a discriminating application to the differing aerodynamic design requirements and criteria of the explicit aerodynamic force data presented in Part II. It may prove, however, either superficial or inadequate when a broader and deeper knowledge in the subject already exists.

Part I is subdivided into eight sections. Each section is conceived of as an independent unit, but related to the rest in that they constitute sets of basic premises that are used later in the proposed methods of flight performance computations. Equations and page numberings are independent in each section, as is the explanation of symbols which is effected immediately and relative to the analytical expressions in the text. All accompanying figures and tables follow the respective context as closely as possible. They serve illustrative purposes and consequently are not meant as source data for direct numerical computations, with a few exceptions. Definitions, equations and underlying analytical methodology are not fully derived. Rather, it is felt better to indicate in each case the related source references where a thorough mathematical and phenomenological elaboration can be found. The list of references is supplied in the final Section 1.9.

Section 1.2 comprises the main limitations pertaining to the material presented both in this part, Part I, and in subsequent parts. The general restrictions and assumptions are specified for both the theoretical analysis and the physical nature of the flow as related to the evaluation of the aerodynamic forces required for practical aerodynamic design and flight dynamics analysis. Further limitations and approximations, however, which may appear respective to specific body geometry, flight regime and air flow type, are stated as the particular case is treated.

In Section 1.3 the general aerodynamic force concept and its components are analytically defined and are formulated respective to an arbitrary reference coordinate system. These expressions, quite general in form, are intended to serve as a basis for more specialized interpretations respective to a few of the most common reference frames used in atmospheric flight dynamics.

A few of the most important specialized coordinate systems are defined and presented in Section 1.4. They are grouped according to their usage into reference frames related to the trajectory, to the vehicle itself, and to the Earth respectively. In order to establish their mutual interrelationship and to clarify the corresponding transformation matrices, the intermediate or transformation-sequential coordinate systems are specified and illustrated graphically. Related analytical expressions for the evolutory angular velocities and the transformation tables for the aerodynamic force components are given without an elaborate derivation. The supplied self-explanatory illustrative figures and the quoted references are meant to fill this need. Special attention is given to the classical aerodynamic system, which is presented both in its left-hand and its right-hand version, since basically the theoretical and experimental aerodynamic force data are referred to them.

In Section 1.5 the transformation expressions for the aerodynamic force components between different reference frames are elaborated in detail.

Section 1.6 contains the definitions of two principal aerodynamic angles, i.e. the angle-of-attack and the sideslip angle conventions. Formulation of the lift, the drag and the sideforce concepts is then presented in terms of the two angles. Due to its fundamental importance the material is elaborated at length, including the special restrictive case of the vertical plane and a related example. In this context, the aerodynamic force coefficients and their dependence on the local normal pressure and the local skin friction coefficients are defined in a general analytical form.

In order to enable a later methodical presentation of explicit aerodynamic force data, a practical subdivision of the characteristic flight dynamics and fluid mechanics realms is outlined at the beginning of Section 1.7. Since only the relative distinctions between

themare intended, no particular rigourosity or extensive argumentation is used. Instead, ample graphical illustration of the various flight and fluid flow regimes as encountered for a few representative missile configurations is supplied. In accordance with the characteristic airflow regimes (continuum, slip, transitional and free molecular) and the flight speed regimes (incompressible subsonic, compressible subsonic, transonic, supersonic and hypersonic), a unified explicit aerodynamic force coefficient functional dependence on the aerodynamic angle-of-attack, the control surface delection angle, the Mach Number, the Reynolds Number, and the flight altitude is conditionally formulated. Special considerations are given to the zero-lift and the lifting conditions, as well as to a general interpretation of the aerodynamic drag polar and the aerodynamic efficiency in the different flight speed regimes. The accompanying graphs are for illustrative purposes only. On the basis of the above definitions, a general aerodynamic drag force breakdown scheme for compound vehicle configurations is then formulated in terms of the constituent vehicle parts and the physical flow conditions. The respective zero-lift and induced drag decomposition schemes are tabulated and defined in detail since they are intended to serve later as a fundamental scheme for presentation of the related aerodynamic force data in all flight and flow speed regimes.

Finally, in Section 1.8 a summary of the principal physical and theoretical aspects of the fluid flow patterns at subsonic, transonic, supersonic, and hypersonic speeds are globally interpreted, in as much as the restrictive aerodynamic force analysis is concerned. The subject treatment is still quite general and intended solely for the purpose of defining more closely various critical Mach Number concepts which serve as boundaries between the different speed regimes.

In conclusion, it is stressed again that the material presented in the Part I is meant as a basic orienting introduction to the use of the aerodynamic force data for practical purposes. As such, it lacks rigourousness and depth, both theoretically and phenomenologically, and may prove to be superfluous for an advanced reader.

1.2 PRINCIPAL LIMITATIONS OF THE PRESENTED MATERIAL

The aerodynamic force and moment analyses constitute only one aspect of the complex problem of vehicle design. Since the ultimate goal is to design a practical vehicle capable of performing specified tasks, the aerodynamic considerations must of necessity, be viewed in light of their relationships to other design factors, such as overall vehicle size, shape, and weight; flying performance; trajectory dynamics; stability and control; structural integrity; payload capacity; power plant selection; operational safety; production and maintenance costs; liability; etc. A successful integration of such a variety of design problems into a final vehicle configuration cannot be accomplished in a straight-forward analytical manner, but rather presents a complex problem of an artful compromise between the noncomplimentary requirements and solutions from the different engineering aspects. Indeed, before reaching its final form, a given vehicle design undergoes many phases of aerodynamic, structural, and system modifications which are the results of successive refining compromises. Evidently, during such a design evolution, the required accuracy of aerodynamic force and moment evaluations will tend to vary as a respective design phase or a particular design aspect might require. As a criterion of practical expediency, the required accuracy of the aerodynamic predictions should be, if possible, conformable in each particular case to the accuracy with which the overall design problem is treated. This implies use of aerodynamic force and moment evaluation methods which differ both by degree of complexity and by form of analysis, to meet the particular requirements of a given design phase.

In presenting the aerodynamic drag force methods of estimates and the related aerodynamic data of various degrees of accuracy, no attempt is made to elaborate explicitly their respective applicability relative to the different aerodynamic vehicle design optimization criteria, since this problem belongs in the complex realm of the overall art and philosophy of design and definitely lies beyond the limited scope of this treatise. A proper selection of a particular aerodynamic force evaluation procedure from the compiled material is thus left to the discretion and the judgment of the individual. In general, both the acquisition of theoretical and experimental data and their selective engineering applications involve, by necessity, a considerable number of idealizations and approximations. While a reasonable effort is made to enumerate the specifically restrictive analytical and physical assumptions and approximations as they pertain to each particular set of aerodynamic data, the following limitations can be considered to be common to all the proposed aerodynamic force estimates:

(i) The atmospheric flight conditions are restricted to flight speeds in the Mach number range of $0 < M < 20$ and flight altitudes in the range of $0 < H < 400{,}000$ ft.

(ii) The compiled aerodynamic data pertain to conventional aircraft and missile configurations, such as the ground-to-air, ground-to-ground, air-to-air and air-to-ground ballistic, semiballistic, and winged missile categories; the high-speed, high-altitude gliders; and the classical ground take-off and landing aircraft designs. The more specialized aerodynamic features and aspects of the sea-born aircrafts, VTOL, STOL, and the less-common re-entry, spacecraft and paraglider shapes are not treated.

(iii) All the constituent parts of a given missile configuration are assumed to be absolutely rigid, i.e. no aeroelastic or thermoelastic effects are considered.

(iv) A steady-state Standard Atmosphere (void of turbulence, winds, gusts and meteorological phenomena) is assumed, rotating as a unit with the Earth. Variations of the gravitational field patterns and of all the significant physical and chemical air properties with altitude follow the respectively prescribed standard analytical laws. In this treatise the compiled numerical data associated with the variable altitude flight conditions are taken directly from the original sources of information, which in most cases have been based on the ARDC 1956 or the ARDC 1959 Standard Atmospheres. It should be noted that the lately officially accepted U. S. Standard Atmosphere '62[1] shows marked differences in overall physical and chemical air-properties for altitudes above 100,000 ft. when compared with the ARDC 56 and 59 standards. Since

further modifications in the Standard Atmosphere structure are expected to take place at an increased rate as new and improved data become available, it was considered that a unique reduction of the differently based aerodynamic data to a specific common Standard Atmosphere form would be premature. In each case, the necessary corrections and/or conversions are thus left to be performed in accordance with the user's preference or need.

(v) Although the proposed aerodynamic force analyses are meant to be applicable to Standard Atmosphere flight dynamics problems in general, the pertinent aerodynamic data have been obtained exclusively from the theories and experiments of steady equilibrium flow. The proposed aerodynamic force estimates shall be, therefore, dynamically restricted to steady, rectilinear flight conditions. Consequently, when extended to accelerated and/or intrinsically unsteady flight regimes, the presented data are conditionally valid only, i.e., the data may be utilized provided the unsteady, time-dependent, Standard Atmosphere flight phenomena are treated tentatively as "quasi steady" by introduction of the following two conditional approximations:

First, so-called "apparent mass" effects common to fluid-solid body systems are neglected. The "apparent mass" phenomenon, wherein fractional masses of fluid are (by induction) dragged along with a solid body moving relative to and with an acceleration through a fluid medium, is transient in nature, disappearing when the body acquires a steady uniform linear motion. The net effect of this phenomenon is an increase in overall fluid resistance to body motion, thereby causing a restriction to the applicability of the well-known principle of "reciprocity of relative motion" from the classical dynamics of (solid) bodies.(2) This conditionality is explained in the following paragraph:

In accordance with the principles of classical mechanics a valid formulation of any dynamical occurrence is expressible in terms of relative motions of the involved mass particles, provided the relative motions are referred to a supposedly inertial (Newtonian) coordinate system. Choice of such an inertial reference frame is generally quite arbitrary, and an application of the associated reciprocity principle of relative motions is fully valid in any Newtonian reference frame, regardless of the type of motions or accelerations involved. However, in choosing such an inertial reference frame for fluid-solid body bounded systems, the principle of reciprocity of relative motions acquires the restrictive form: to regard the consequences of relative fluid-body motions as invariantly reciprocal, whether the body be considered at rest in a relatively flowing fluid or the fluid be taken at rest while the immersed body is moving relative to it, is strictly valid only if either the fluid is flowing perfectly uniformly and steadily with respect to the body, or the fluid at rest is completely void of any turbulence or unsteadiness of any nature while the body moves steadily through it.

Accelerated or unsteady transient flow phases which are associated with the "apparent mass" effects, are beyond the classical theoretical concepts according to which steady flow patterns are presumed to be established in an impulsive manner from an initially irrotational condition of the rest fluid.(2) Fundamentals of some special theoretical methods of analysis of both the irrotational non-uniform (accelerated) flows and the nonuniform flows with discontinuity surfaces (gusts, for instance) can be found in Ref. (2), (3), (10) and (14). Unfortunately, straightforward, simple, and reliable engineering-type computational techniques of the nonuniform flow phenomena associated with accelerated atmospheric flight conditions are as yet unavailable.

Second, all the time-dependent physical and chemical nonequilibrium characteristics associated with different unsteady and/or transient flow patterns are neglected. They may be broadly classified as the specific time-lags in acquiring respective equilibrium pressure, density, temperature, air composition, dissociation, and ionization states or flow profiles. Under the unsteady and/or accelerated flight conditions such steady equilibrium states of various gas parameters may never be realized for major portions of actual vehicle flight trajectories. In such cases, the proposed "quasi steady" aerodynamic force predictions should be treated with restraint. The unsteady and/or accelerated flow time-lag effects are most prominent in determining the nonequilibrium distributions of air parameters

and the air composition behind strong shocks and in boundary layers. Within the present context of the aerodynamic force analysis, these aerothermal transient effects are treated in some of the proposed methods in a very approximate form only (i.e., within the overall level of accuracy of the aerodynamic force predictions at large). Any more detailed analysis of unsteady, nonequilibrium flows, as eventually will be needed for optimization of technological, structural, or other aerothermodynamic and flight dynamic aspects, is considered beyond the scope of the gross aerodynamic force predictions for the limited flight dynamics analysis purposes.

(vi) In addition to the steady or the "quasi steady" equilibrium flow limitations, it is assumed that no pronounced flow separation occurs. The permissible angle-of-attack values are, thus, restricted to domains well below stall.

(vii) Most of the theoretically derived data incorporate the approximations inherent to the classical Prandtl's postulate, which allows for separate analytical treatments of completely uncoupled perfect inviscid and viscous boundary layer fluid-flow models, the respective partial results being then superimposed to form total aerodynamic force effects. The mutual interaction phenomena between the two types of flows are then eventually added as semiempirical or experimental correction factors, when possible.

Although originally defined and verified by experimental evidence for subsonic flow patterns, this concept has also been successfully extended to theoretical analyses of supersonic and hypersonic continuum flow with proper inclusion of the across-the-shock conditions.

The separation of the very complex totality of aerothermodynamic flow patterns around arbitrary body shapes into the supposedly predominantly inviscid perfect fluid flow and the predominantly viscous continuum fluid flow regions, becomes an invaluable theoretical proposition because of the severe lack of mathematical capacity for finding valid, closed-type solutions for the equations governing fluid flow problems in general. The situation may be briefly outlined as follows:

The acquisition of any particular bounded set of theoretical aerodynamic data demands a valid simultaneous solution of a necessary and sufficient number of the governing partial differential equations. These equations shall be fully descriptive of the assumed analytical model, representing the investigated aerothermodynamic phenomena within the prescribed boundaries of a specified fluid-body dynamic system. The related descriptive set of governing differential equations is only a limiting mathematical formulation of the classical physical principles of the conservation of mass, momentum and energy, to which an adequate number of auxiliary internal functional relationships between the involved physical properties of the bounded aerothermodynamical system is added to make the total number of independent equations equal to the number of the constituent independent variables. Nominally, there is a strong interaction between the influential physical parameters entering into the expression for conservation of momentum and energy. Therefore, the fundamental proposition of a simultaneous validity of the three conservational principles is tacitly accepted even when, in some specific or approximately treated cases, non-simultaneous solutions of conditionally uncoupled momentum and energy equations are performed.

For very simple body geometries and significantly idealized (for instance, thermally and calorically perfect gas, subsonic regimes) viscous flow patterns, and within the first-order theoretical gas model propositions, the resulting momentum expressions take the classical Navier-Stokes[2,10,14] partial differential equations form. A direct attempt for their general solution leads to formidable mathematical difficulties. Instead, by application of the Prandtl's postulate, the considerably simplified inviscid fluid flow momentum (and energy) expressions allow, in some special cases, a reasonable analytical handling, leading to acceptable aerodynamic data for the perfect fluid inviscid flow field regions. The subsequent confinement of viscous flow effects within a thin boundary layer allows for an eventual approximative reduction of the Navier-Stokes equations to an analytically simplified boundary layer form, which, in some restrictive cases, may also be tentatively solved with some acceptable degree of accuracy.

Thus, although the Prandtl's concept proves an invaluable analytical tool, it gives no direct information regarding any possible real flow interference effects between the inviscid flow pressure distributions and the viscous boundary layer frictional phenomena. Actually the mutual interplay between pressure fields and the associated pressure, density, temperature and velocity discontinuity surfaces or shock-waves of the inviscid flow patterns and the boundary layer frictional phenomena may be rather pronounced. In such cases, adequate semi-empirical or experimental interference corrections should be applied (if available) either to final theoretical results or as corresponding modifications of the presumed flow patterns. For instance, for slender, streamlined body shapes, which are of primary interest in engineering applications, this type of interference may result in effects such as:

(1) A pressure field change, produced by an apparent body shape deformation caused by thickening of the surrounding boundary layer.

(2) A partial flow separation phenomena, particularly at the rear portions of a body, promoted through combined interplay between the angle-of-attack variations, the inherent susceptibility of the boundary layer flow mechanism to external pressure fields and the shockwave-boundary layer interference (for transonic speeds especially).

(3) Complex interaction patterns between the slipping boundary layer and the shock waves in the dead air region (or wake) at the body base, affecting the base pressure and temperature distributions, etc.

Furthermore, since the individual simple body shapes will finally be assembled into a compound vehicle configuration, additional interference effects between the assembled simple body shapes in situ are introduced, altering both the pressure and the frictional stress distributions around the total configuration and in the wake.

Thus, interference corrections should be made in principle for both the Prandtl's analysis of simple body geometries (nose cones, cylindrical bodies, wings, fins, etc.) and the assembled configuration, if and in as much as the related corrective data are available from the related experimental, the compatible semi-empirical, or the simplified theoretical sources.

(viii) From a physical standpoint there are ever present approximations and errors caused by both analytical and experimental limitations with which the overall aerodynamic problems can be best understood, formulated, solved and measured. Both the idealized mathematical models and the necessarily simplified experimental techniques are thus inherently limited in adequately reproducing or representing the extremely complex reality of the actual aerothermodynamic phenomena in toto. The degree of sophistication to which an analytical model can be developed reflects, at best, the level of accuracy with which a fluid flow occurrence may be formulated or measured. In establishing both physically representative and analytically manageable real gas flow models the complexities and difficulties become especially pronounced under high speed, high temperature flow conditions. The problem is further aggrevated by an insufficient factual knowledge of the internal interdependency and dynamics of the different physical and chemical gas properties on molecular and atomic levels for such highly elevated and dynamically reacting energetic states.

(ix) Theoretically, there are additional simplifications and approximations because of the inability to find physically meaningful mathematical solutions for the tentatively defined analytical models. In the case of fluid flows even the simplest first-order highly idealized theoretical models result in a set of partial differential equations[3][4][5] which are only conditionally solvable in a closed type form for some simple body geometries and for special boundary conditions.

Once a representative form of governing equations is specified as a conditional formulation of the investigated flow pattern around a given body geometry in terms of an accepted essential number of influential physical parameters and their internal functional relationships (auxiliary equations), the analytical degree of relative accuracy with which a valid solution is obtainable within the specified boundary conditions can be traced to and expressed in terms of the mathematical approximations introduced. Here a reservation must be made regarding the claimed mathematical

"exactness" of some solutions, as frequently encountered in a wide spectrum of fluid flow theories. When either electronic computers or various numerical analysis techniques are used, the exactness is evidently expressed either by the number of significant figures or by the discarded residue values, plus the approximations which might be introduced in the overall analytical treatment. However, the relative validity of such "exact" solutions still remains questionable within and does not exceed the relative physical correctness of the fundamental premises upon which the theory and the formulation of the problem are based. It is still dependent on the relevant accuracy with which the influential physical parameters, variables and constants may be understood, measured or evaluated, and their mutual interrelations properly formulated. Therefore, it is considered justifiable to judge the overall validity and acceptability of a theory not primarily in terms of its mathematical exactness or its theoretical degree of sophistication per se, but rather by a direct comparison with correspondingly coordinated and conscientiously cleared experimental data. In accepting such a correlating criteria it is essential to bear in mind that the supporting experimental evidence is necessarily conditional and restrictive itself, the comparative agreement between a controlled (necessarily simplified) experiment and a full scale (far more complex) physical occurrence remaining still questionable. For instance, the high speed and the viscous fluid flow problems, which are of primary importance today, present such a formidable array of physical and chemical complexities and parametric uncertainities, that even the habitual expectancy that a more detailed higher-order theory or a more exact analytical treatment would yield a result closer to reality may not necessarily hold. Moreover, some rather simple analytical models and assumptions, which can hardly be claimed as well-representative of a real fluid flow internal mechanism, may prove comparable by their relative accuracy of results to many a more sophisticated and mathematically more elaborate treatment.[6,9] As another interesting illustration of the question of exactness, it may be mentioned that the long-claimed, and the well-accepted Blasius[8] "exact" mathematical solution of incompressible laminar boundary layer along a smooth, insulated flat plate at zero-angle of attack has been achieved by expansion into a series which in a much later investigation[7] proved to become divergent after some thirtieth term. Nevertheless, the Blasius solution is still one of the best available for the restricted type of incompressible laminar boundary layers to which it pertains.

(x) Finally, there are usually analytical or numerical approximations in computing the overall resultant aerodynamic forces for a given set of body-fluid flow conditions. Both the actual physical relationships between a solid body and a fluid medium in relative motion and the corresponding analytical set of descriptive differential equations reflect the space-time distributed nature of the local pressure and shear stress loads, be it within the continuum or the discrete particle structural concepts of fluid mediums. In order to define and solve the flight dynamics of a solid body using the classical Newtonian force postulates, an integration of the relevant variable local (normal and tangential) stress distributions is required. This leads to the conditional formulation of a resultant external aerodynamic force and its point-of-action location. For most practical purposes this summation or integration procedure is conveniently performed in a suitably simplified way, especially so in the case of usual compound body geometries. The corresponding error can be readily determined in terms of the approximations introduced in the adopted integration technique.

1.3 THE RESULTANT AERODYNAMIC FORCE AND ITS COMPONENTS

Within the overall limitations specified in Section 1.2, the resultant force with which the ambient equilibrium atmosphere opposes the steady uniform motion of a vehicle may be conveniently traced to two basic physical sources: the resistance caused by normal pressure and the resistance caused by viscous shear distributions on a given body contour. This conceptual division is well coincident with both Prandtl's postulate and the classical mechanistic force definitions. Thus, the local resultant aerodynamic force exerted by the flowing gas on each surface element of a body in relative motion can be analytically determined as a vectorial sum of the local normal (pressure) and the local tangential (frictional) force components. A subsequent integration of the local components over the entire exposed body surface gives the sum of the total pressure and the total frictional resistance force components respectively as

$$\vec{R} = \int_{S_{wet}} (\Delta p \vec{n} + \tau \vec{t})\, dS \qquad (1.3\text{-}1)$$

where: $\vec{n}$ is a unit vector normal to the surface element, dS, positively directed inward; $\vec{t}$ is a unit vector tangent to the surface element, dS, parallel to and positively directed in the same sense as the local free stream velocity vector, $\vec{V}_l$, of the inviscid fluid flow outside the boundary layer; $\Delta p = (p - p_A)$ represents the difference between the local (at the body surface) and the ambient (free stream at infinity) static (normal) pressures; and τ is the local shear stress value.

Two principal conceptual features intrinsic to the above definition are:

(1) Choice of a reference datum for measuring the local static pressures is in principle a quite arbitrary convention. Neither the physical flow pattern nor the form of the governing differential equations are influenced by it. But, for ascertainment of a minimum number of the flow similitude requirements as well as for general atmospheric flight dynamics purposes, it is convenient to measure the local static pressures, p, relative to the ambient atmospheric pressure datum, p_A, i.e. to select the static pressure "at infinity," $p_A = p_\infty$, as the basic zero-datum value in the fluid flow analysis in general.

(2) For powered atmospheric flight conditions the resultant aerodynamic force concept should be specified exclusive of some conventionally adopted thrust force definition.(11) Thus, in the case of rocket-propelled vehicles, it has become customary in most technical flight dynamics analyses to restrict the local normal and the local tangential force integrations to the actual solid body exposed (wetted) areas. In the case of jet-propelled vehicles it is customary to extend the above integration procedure to the sum of the vehicle wetted areas, the stream tube area ahead of the engine duct, and the engine afterbody area protruding in the jet stream. In both cases the base pressure effects, as due to the overall body geometry and the associated wake, are included in the "wetted area" term.

The general expression for the total aerodynamic resistance force, Eq. (1.3-1), is usually vectorially resolved into three directional components respective to a suitably defined reference coordinate system. The selection of a particular reference frame depends largely on the type and the analytical aspects of the aerodynamic or flight dynamics problem itself, the final aim of the respective flight dynamics analysis, and the form of the available theoretical or experimental data.
Given a conventional Cartesian orthogonal space reference frame, $Oxyz$, the respective resultant aerodynamic force components are specifically:

$$\begin{aligned}
\vec{R} &= \vec{X} + \vec{Y} + \vec{Z} = X\vec{i} + Y\vec{j} + Z\vec{k} \\
X &= \int_{S_{wet}} (\Delta p \vec{n}\cdot\vec{i} + \tau \vec{t}\cdot\vec{i})\, dS \\
Y &= \int_{S_{wet}} (\Delta p \vec{n}\cdot\vec{j} + \tau \vec{t}\cdot\vec{j})\, dS \\
Z &= \int_{S_{wet}} (\Delta p \vec{n}\cdot\vec{k} + \tau \vec{t}\cdot\vec{k})\, dS
\end{aligned} \qquad (1.3\text{-}2)$$

Specific reference frame cases of the above aerodynamic force resolutions are treated in Sections 1.4 and 1.6 in detail.

For the purpose of establishing valid comparative aerodynamic force and similitude criteria when different fluid-body systems are investigated, as well as for a generalization of theo-

retical results, the conventional concepts of non-dimensional aerodynamic force coefficients are introduced:

$$C_x = \frac{X}{q_A S_{ref}}, \quad C_y = \frac{Y}{q_A S_{ref}}, \quad C_z = \frac{Z}{q_A S_{ref}} \qquad (1.3\text{-}3)$$

Similarily and for the same reasons, instead of the dimensional pressure and shear stresses, the non-dimensional local pressure coefficient and local skin-friction coefficent definitions are introduced in the forms

$$C_p = \frac{\Delta p}{q_A} = \frac{p - p_A}{q_A}, \quad C_f = \frac{\tau_w}{q_A} \qquad (1.3\text{-}4)$$

respectively.

Consequently, the three resultant aerodynamic force component expressions (1.3-2) acquire the respectively dimensionless forms:

$$C_x = \frac{1}{S_{ref}} \int_{S_{wet}} (C_p \vec{n}\cdot\vec{i} + C_f \vec{t}\cdot\vec{i}) dS$$

$$C_y = \frac{1}{S_{ref}} \int_{S_{wet}} (C_p \vec{n}\cdot\vec{j} + C_f \vec{t}\cdot\vec{j}) dS \qquad (1.3\text{-}5)$$

$$C_z = \frac{1}{S_{ref}} \int_{S_{wet}} (C_p \vec{n}\cdot\vec{k} + C_f \vec{t}\cdot\vec{k}) dS$$

where:

$q_A = \frac{\rho_A V_A^2}{2}$ is the ambient atmospheric reference dynamic pressure, or the free stream dynamic pressure "at infinity," $q_A = q_\infty$.

V_A and ρ_A are respectively the ambient atmospheric-flight relative speed of the vehicle CG and the ambient atmospheric density. Again, by fixing the reference frame to the aircraft CG, these become by magnitude the "free stream at infinity" values, i.e. $V_A = V_\infty$, $\rho_A = \rho_\infty$.

The process of non-dimensionalization involves two significent conventions. First, the choice of a reference area, S_{ref}, is completely arbitrary, not necessarily representing the actual exposed (wetted) surfaces of any specific vehicle part or of the vehicle as a whole, i.e. in general, $S_{ref} \neq S_{wet}$. There is but one important restriction regarding the reference area: it must be a common non-dimensionalizing factor for all the different configurational parts of a given vehicle geometry. Customarily, the common reference area is chosen to be either the wing platform (projected to the Oxy plane) area, or the maximum body (fuselage) cross-sectional area. The specific choices, apart from serving the non-dimensionalizing convention, reflect physically important features of the winged (lifting surface) missile and the ballistic (drag characterized) missile configurations respectively.

Second, for the sake of preserving the uniformity of definitions, the reference dynamic pressure "at infinity," $q_A = q_\infty$, has been extended from the initially incompressible or negligibly compressible, low subsonic fluid flow regions to supersonic and hypersonic flow conditions as well. Inasmuch as analytically convenient formal definitions of the resultant force and the local pressure and skin-friction coefficients are concerned, the selection of any one specific and common reference non-dimensionalizing dynamic pressure value is a proposition of uniformity and convenience. But, if the physically important role of actual local dynamic pressures upon the local numerical values of C_p and C_f are investigated, the compressibility effects and the related behind-the-shock velocity, density, and temperature changes should be properly included. Clearly if the local pressure and the local skin friction coefficients are treated as the respective actual dimensionless local forces per unit area (subscript $_l$),

$$C_{p_l} = \frac{\Delta p}{q_l}, \quad C_{f_l} = \frac{\tau_w}{q_l}, \quad q_l = \frac{\rho_l V_l^2}{2} \qquad (1.3\text{-}6)$$

then their correlations with the respective reference values (subscript $_A$) are:

$$X = C_x q_A S_{ref} = \int_{S_{wet}} (C_{p_l} q_l \vec{n}\cdot\vec{i} + C_{f_l} q_l \vec{t}\cdot\vec{i}) dS$$

$$= \int_{S_{wet}} (C_p q_A \vec{n}\cdot\vec{i} + C_f q_A \vec{t}\cdot\vec{i}) dS \qquad (1.3\text{-}7)$$

$$\therefore \quad C_x = \frac{1}{q_A S_{ref}} \int_{S_{wet}} (C_{p_l} q_l \vec{n}\cdot\vec{i} + C_{f_l} q_l \vec{t}\cdot\vec{i}) dS$$

$$= \frac{1}{S_{ref}} \int_{S_{wet}} (C_p \vec{n}\cdot\vec{i} + C_f \vec{t}\cdot\vec{i}) dS \qquad (1.3\text{-}8)$$

etc.,

and $$C_p = \frac{q_l}{q_A} C_{p_l}, \quad C_f = \frac{q_l}{q_A} C_{f_l} \qquad (1.3\text{-}9)$$

Furthermore, in the particular case of the local skin friction coefficient, C_{f_l}, the actual local dynamic pressure, q_l, is referred to the local inviscid

flow conditions outside the boundary layer, so that in terms of the conditions at the surface proper:

$$C_{f_1} = \frac{\tau_w}{q_1} \quad , \quad C_{f_w} = \frac{\tau_w}{q_w} \quad , \quad q_w = \frac{\rho_w V_1^2}{2} \qquad (1.3\text{-}10)$$

$$\therefore \; C_{f_1} = \frac{q_w}{q_1} C_{f_w} \qquad (1.3\text{-}11)$$

where the wall local density value, ρ_w, is a function of the overall aerothermal flow conditions at the surface, as shall be discussed later.

Before a further elaboration of the aerodynamic force concept in terms of the involved physical variables, a formalistic vectorial resolution of the aerodynamic resistance force onto a few most common flight dynamics coordinate systems is defined in Sections 1.4 and 1.6.

1.4 COORDINATE SYSTEM CONVENTIONS

In many engineering problems it appears most convenient to resolve the resultant aerodynamic resistance, $\vec{R}$, into three components, i.e., the resultant lift, $\vec{L}$, the resultant drag, $\vec{D}$, and the resultant side force, $\vec{Q}$, in the modified right-hand aerodynamic coordinate system, $Ox_a y_Q z_a$. Their physical interpretations are given later, while their conditional vectorial definitions and transformations respective to various other flight dynamics reference coordinate systems are considered below and in Section 1.6.

The flight dynamics analysis may, in general, require several different reference coordinate systems, each coordinate system being advantageous for some specific investigation or a particular computational procedure. Subsequently, a respective number of transformations of all vectorial quantities from one reference frame to another may be needed. Assuming an arbitrary space flight trajectory and a rotating spherical earth, a few Cartesian right-hand orthogonal reference frames and the involved aerodynamic force component transformations most commonly used in the overall flight dynamics analysis are:

Reference frames related to trajectory

(i) Modified aerodynamic coordinate system, $Ox_a y_Q z_a$, used as a basic reference frame for the resultant aerodynamic lift, $\vec{L}$, the drag, $\vec{D}$, and the side force, $\vec{Q}$, definitions.

(ii) Wind axes coordinate system, $Ox_w y_w z_w$, convenient for both the three degrees of freedom (point mass) and the six degrees of freedom (rigid body) trajectory dynamics analyses.

(iii) Principal trihedral coordinate system, $Otbn$, representing a natural reference frame for the centripetal, $\vec{F}_c$, and the tangential, $\vec{F}_t$, force investigations.

(iv) Local horizon coordinate system, $Ox_h y_h z_h$, defining the local space attitude orientation of a vehicle on its trajectory.

Reference frames related to vehicle (Eulerian axes)

(v) Body axes coordinate system, $Ox_b y_b z_b$, convenient for the normal, $\vec{N}$, the axial, $\vec{C}$, and the lateral, $\vec{Y}$, force definitions, as well as for the moments-and-products of inertia computations.

(vi) Stability axes coordinate system, $Ox_s y_s z_s$, used for static and dynamic stability investigations.

Reference frames related to earth (Newtonian systems)

(vii) Curvilinear ground reference system, $EXYZ$, determining the instantaneous geographical position of the vehicle.

(viii) Rotating Earth axes system, $Ex_e y_e z_e$, used as the launching or impact point reference frame.

(ix) Star fixed reference frame, $O\xi\eta\zeta$, the fundamental inertial coordinate system necessary for a valid formulation of the governing dynamic equations of motion within the classical Newtonian concepts in the case of a rotating Earth.

Intermediate reference frames

When performing the rotational transformations, the final relative position between two rotated coordinate systems can be conveniently defined by specifying an orderly sequence of successive partial rotations through three characteristic (Eulerian) angles. In order to perform an analytical transformation of the aerodynamic force components (and of any other resolved vector quantities entering the governing sets of equations of motion) from one coordinate system to another by this method of sequential Eulerian angular conventions, it is necessary to introduce respectively defined intermediate coordinate systems, designated by subscripts 1, 2, 3, etc. This method is commonly preferred to the alternative method of direct projections from each of the three axes of the initial coordinate system onto the three axes of the final (rotated) reference frame, since such a procedure requires manipulation of nine directional cosines (or six directional cosines and three auxiliary cosine relationships) which are necessary for a statical definition

of the six axes orientations of the two rotated coordinate systems[11, 12, 13].

The relative disposition of essential flight dynamics coordinate reference frames is illustrated in Fig. 1.1.

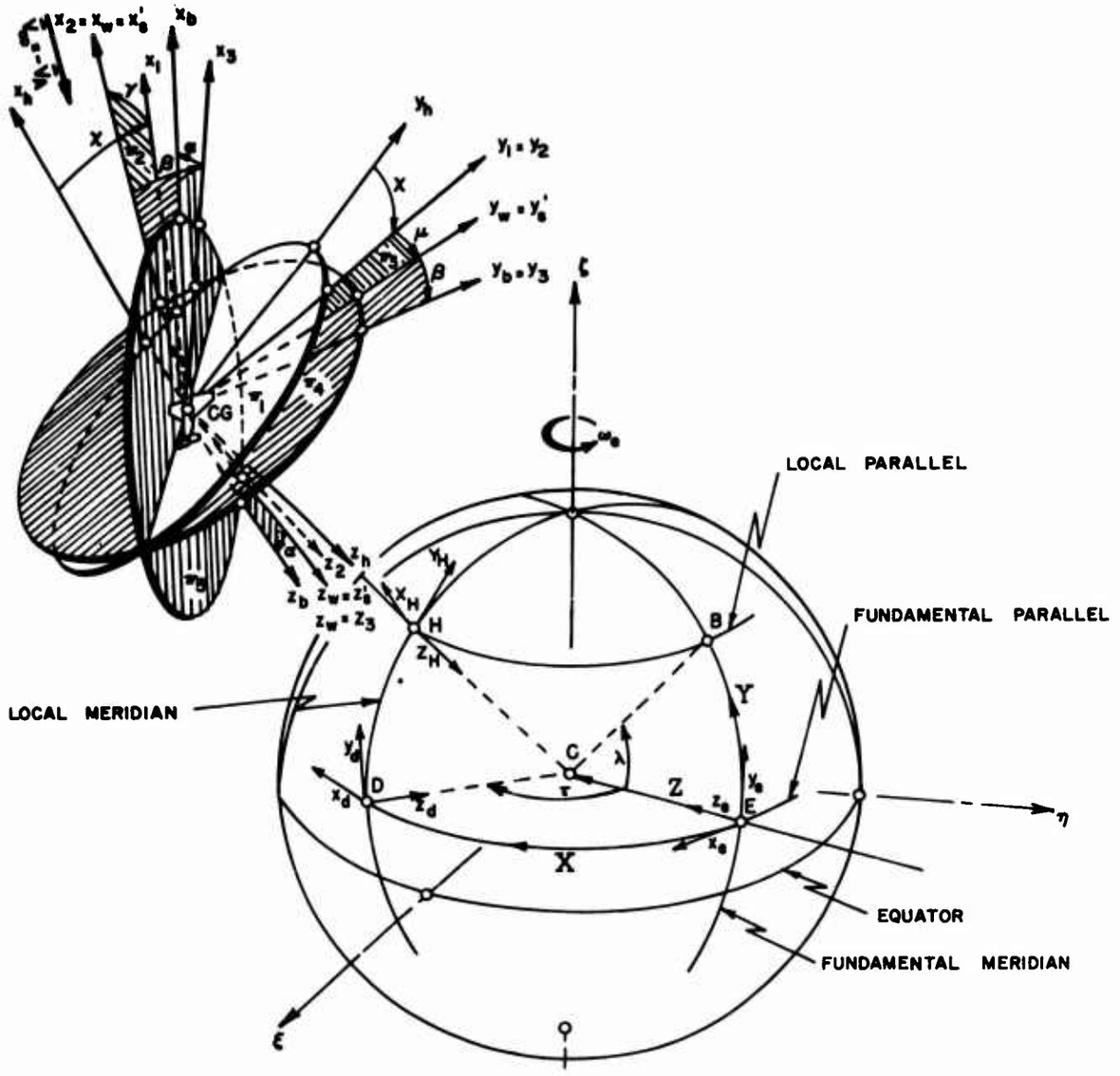

FIG. 1.1 Relative disposition of basic flight dynamics reference frames with respect to a rotating, spherical Earth.

Definitions of the individual coordinate systems are given in Sections 1.4.1 to 1.4.6. The few comparative reference planes pertaining to the spatial dispositions in Fig. 1.1, and comprising the adopted sequence of Eulerian angle definitions are:

The π_1 plane is the velocity yaw angle (χ) plane. It is parallel to the Earth's local horizon (tangential) plane, Hx_Hy_H, and contains both the trajectory local horizon plane, Ox_hy_h, and the first intermediate coordinate system plane, Ox_1y_1. A partial counterclockwise rotation of the Ox_h into Ox_1 axis (i.e. Oy_h into Oy_1) around the $Oz_h = Oz_1$ axis defines the velocity yaw angle, χ.

The π_2 plane is the velocity pitch angle (γ) plane. It contains both the first intermediate coordinate system Ox_1z_1 (coplanar to Ox_1z_h) plane and the second intermediate coordinate system Ox_2z_2 (coplanar to Ox_wz_2) planes. A partial counterclockwise rotation of the Ox_1 into $Ox_w \equiv Ox_2$ axis (i.e. $Oz_1 \equiv Oz_h$ into Oz_2) around the $Oy_1 \equiv Oy_2$ defines the velocity pitch angle, γ .

The π_3 plane is the velocity roll angle (μ) plane. It contains both the wind axes Oy_wz_w and the initial stability axes $Oy_s'z_s'$ planes, as well as the second intermediate coordinate system Oy_2z_2 plane. A partial counterclockwise rotation of the $Oy_1 = Oy_2$ into $Oy_s' = Oy_w$ axis (i.e. Oz_2 into $Oz_w = Oz_s'$) around the $Ox_w \equiv Ox_2 = Ox_s'$ axis defines the velocity roll angle, μ .

The π_4 plane is the side-slip angle (β) plane. It contains the wind axes Ox_wy_w and the initial stability axes $Ox_s'y_s'$ planes, as well as the third intermediate coordinate system Ox_3y_3 (coplanar to Ox_3y_b) plane. A partial counterclockwise rotation of the $Ox_w = Ox_s'$ into Ox_3 axis (i.e. $Oy_w = Oy_s'$ into $Oy_3 = Oy_b$) around the $Oz_w = Oz_3 = Oz_s'$ axis defines the side-slip angle, β .

The π_5 plane is the geometric angle-of-attack (α) plane, usually taken coplanar with the reference (vertical) plane of symmetry for classical vehicle geometries. It contains the body axes Ox_bz_b plane and the third intermediate coordinate system Ox_3z_3 (coplanar to Ox_3z_w and Ox_3z_s') plane. A partial counterclockwise rotation of the Ox_3 into Ox_b axis (i.e. of $Oz_3 \equiv Oz_w = Oz_s'$ into Oz_b) around the $Oy_3 = Oy_b$ axis defines the geometric angle-of-attack, .

1.4.1 CLASSICAL AERODYNAMIC COORDINATE SYSTEMS $Ox_a y_a z_a$ AND $Ox_a y_Q z_a$

The aerodynamic left-hand orthogonal reference frame, $Ox_a y_a z_a$, and its alternative right-hand version, $Ox_a y_Q z_a$, are historical legacies. The fundamental two- and three-dimensional low speed airfoil and wing theories and the respective basic aerodynamic force and moment concepts have been postulated with respect to them. Although numerous later refinements and extensions of the respective aerodynamic theories to higher speeds and to various three-dimensional body effects have introduced a number of other more convenient reference frames better suited for specific theoretical

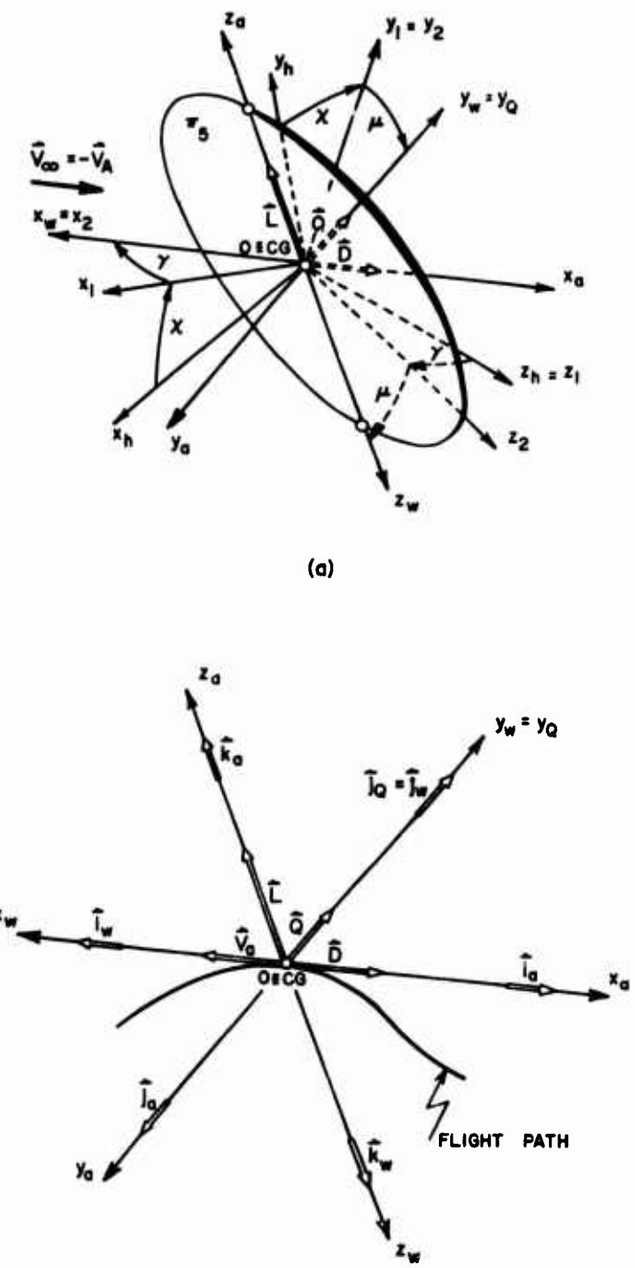

FIG. 1.2 Spatial definitions of the classical left and right-hand orthogonal aerodynamic coordinate systems, $Ox_a y_a z_a$, and $Ox_a y_Q z_a$, relative to the wind axes, $Ox_w y_w z_w$, and the trajectory local horizon axes, $Ox_h y_h z_h$, right-hand orthogonal coordinate systems.

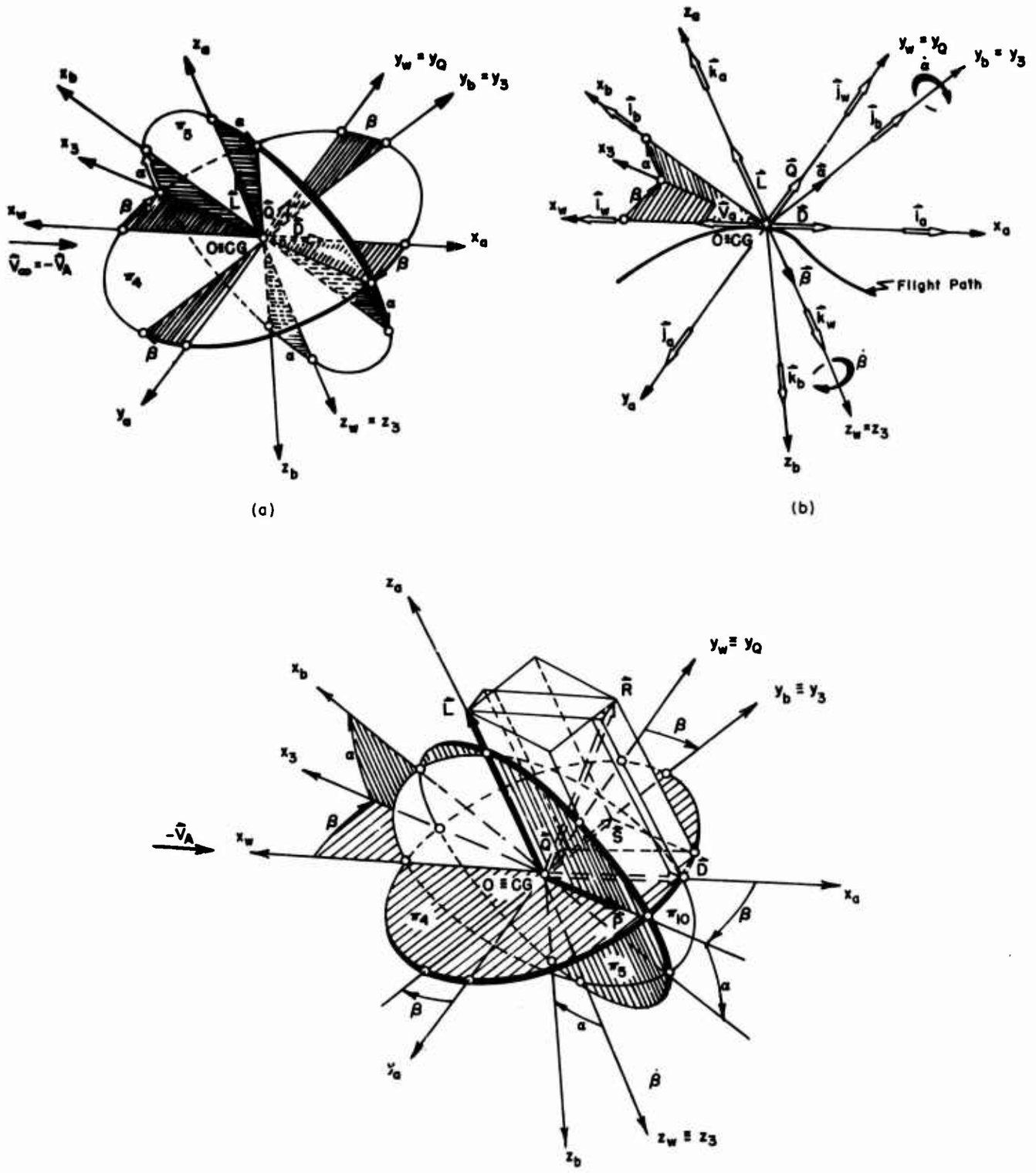

FIG. I.3 Spatial definitions of the classical left and right hand orthogonal aerodynamic coordinate systems, $Ox_a y_a z_a$ and $Ox_a y_Q z_a$, relative to the wind axes, $Ox_w y_w z_w$, and the body axes, $Ox_b y_b z_b$, right hand orthogonal coordinate systems.

developments, the practice of expressing the final analytical and/or experimental total aerodynamic force components relative to these classical aerodynamic frames has, in general, been retained.

Comparative spatial relations between the aerodynamic reference frames, $Ox_a y_a z_a$ and $Ox_a y_Q z_a$, and the flight dynamics basic reference systems (the wind axes, $Ox_w y_w z_w$, the local trajectory horizon axes, $Ox_h y_h z_h$, and the body axes, $Ox_b y_b z_b$) is illustrated in Figs. 1.2 and 1.3. From their respective spatial dispositions it is evident that the left-hand aerodynamic and the right-hand wind axes coordinate systems are related by a direct inversion.

GLOSSARY for Figs. 1.2 and 1.3

The π_4 plane contains the side-slip angle, β, defined by a partial counterclockwise rotation of the Ox_w into Ox_3 axis, (i.e. $Oy_w \equiv Oy_Q$ into $Oy_b \equiv Oy_3$) around the $Oz_w \equiv Oz_3$ axis. The π_4 plane is coincident with the $Ox_w y_w$, the $Ox_a y_a$, the $Ox_a y_Q$, and the $Ox_3 y_3 = Ox_3 y_b$ planes. It is generally not coincident with the local principal trihedral tangent plane, O_{tb}, on a space trajectory.

The π_5 plane is the reference (vertical) plane of symmetry of the vehicle geometry. It contains the geometric angle-of-attack, α, defined by a partial counterclockwise rotation of the Ox_3 into the Ox_b axis (i.e. $Oz_3 \equiv Oz_w$ into Oz_b) around the $Oy_3 \equiv Oy_b$ axis. The plane is coplanar with the $Ox_b z_b$ and the $Ox_3 z_3 \equiv Ox_3 z_w$ planes. It is generally not coincident with the principal trihedral local osculating plane, O_{tn}, on a space trajectory.

Aerodynamic forces

The total lift force for the overall vehicle configuration, $\vec{L} = L\vec{k}_a$, is contained in the reference plane of symmetry, π_5. The total drag force, $\vec{D} = D\vec{i}_a$ is in the π_4 plane. The total side-force, $\vec{Q} = Q\vec{j}_Q$ and the total cross-wind force $\vec{Y} = Y\vec{j}_a$ are perpendicular to the reference plane of symmetry, π_5, following the right-hand and the left-hand coordinate system conventions respectively.

The left-hand aerodynamic coordinate system

The aerodynamic coordinate system is conditionally treated as instantaneously inertial for the presumed steady or quasi-stead flow (or atmospheric flight) conditions. Its origin, O, is arbitrarily fixed at the vehicle's center of gravity, CG, when the rigid body flight dynamics problems are investigated. At any local point (i.e. at any instant of time) on a given trajectory, orientations of the aerodynamic axes are conventionally defined as follows:

The Ox_a axis is taken collinear and positive in the sense of the relative free stream "at infinity" velocity vector, $\vec{V}_\infty = -\vec{V}_A$. The Ox_a axis is thus always locally tangential to the flight path and oriented in the $(-\vec{i})$ sense. The relative free stream velocity vector, $\vec{V}_\infty$, is defined "at infinity," i.e. well ahead of vehicle, where the steady uniform flow conditions are assumed. Reciprocally, this implies that the instantaneous ambient flight velocity, $\vec{V}_A$, at any point (or at any instant) on a given trajectory should be referred to a steady equilibrium Standard Atmosphere, free of turbulence, winds, and gusts. The atmosphere is assumed to rotate with the earth, its angular velocity, $\vec{\omega}_e$, being constant. Furthermore, in accordance with basic assumptions in Section 1.2, the effects of instantaneous flight accelerations upon the overall flow pattern are neglected.

The Oz_a axis is, by convention, always contained in the reference π_5 plane of symmetry of a vehicle, regardless of the relative position of the vehicle respective to the flight trajectory. It is taken perpendicular to the Ox_a axis (which is not generally in the plane of symmetry) and sensed positively "upward" for a noninverted vehicle flight attitude. For classical aircraft configurations the reference plane of symmetry is usually the initially "vertical" plane of symmetry for a no bank (wings level) flight condition. For axially symmetric vehicle configurations the reference plane of symmetry should be conveniently specified in terms of some initial flight conditions, so that both the velocity yaw angle, χ, and the side-slip angle, β, may be uniquely specified.

The Oy_a axis (or the cross-wind axis) is perpendicular to the $Ox_a z_a$ plane, sensed so as to form a left-hand orthogonal coordinate system.

When the definitions of the aerodynamic (or absolute) angle-of-attack, α_a, and the side-slip angle, β, are adopted as specified later in Section 1.6 the total lift, $\vec{L}$, the total drag, $\vec{D}$, and the total cross-wind force, $\vec{Y}_a$, are

collinear with the aerodynamic axes Oz_a, Ox_a, and Oy_a respectively. For positive values of the aerodynamic angle, α_a, the lift force, $\vec{L}$, is thus made conditionally positive. The drag force, $\vec{D}$, is always positive. Due to the adopted dynamic convention for the definition of angles, the cross-wind force, $\vec{Y}_a$, becomes negative for the adopted positive values of the side-slip angle, β.

It is noted that the left-hand aerodynamic reference frame, $Ox_a y_a z_a$, is directly related to the dynamic wind axes coordinate system, $Ox_w y_w z_w$, through the simple unit vector relationships:

$$\begin{aligned} \vec{i}_a &= -\vec{i}_w \\ \vec{j}_a &= -\vec{j}_w \\ \vec{k}_a &= -\vec{k}_w \end{aligned} \qquad (1.4\text{-}1)$$

Consequently, the Eulerian vectorial matrices for the resultant aerodynamic lift, drag, and cross-wind force component transformations from the aerodynamic coordinate system into other flight dynamic reference frames are formally the same as later specified for the wind axes coordinate system, Section 1.4.2, provided the unit vector sign convention, Eq. (1.4-1), is correctively taken into account.

The right-hand modified aerodynamic reference frame

In order to bring into a better accord the sign convention between the positive incidence angles and the positive forces, the original aerodynamic left-hand coordinate system, $Ox_a y_a z_a$, in the flight dynamics and mathematical theories[14] is replaced by the right-hand modified aerodynamic reference frame, $Ox_a y_Q z_a$. That is, the cross-wind force, $\vec{Y}_a$, is replaced by the side-force (or aerodynamic lateral force) $Q = -\vec{Y}_a$ by changing the cross-wind axis, Oy_a, into the lateral axis, Oy_Q. The changed unit vector $\vec{i}, \vec{j}, \vec{k}$ relationships respective to the wind axis then become:

$$\begin{aligned} \vec{i}_a &= -\vec{i}_w \\ \vec{j}_Q &= +\vec{j}_w \\ \vec{k}_a &= -\vec{k}_w \end{aligned} \qquad (1.4\text{-}2)$$

Aerodynamic force components

In both aerodynamic reference frames the aerodynamic force components comprise the integrated static pressures and the frictional effects caused by the relative airflow only; see Eq. (1.3-1), Section 1.3, i.e. the gravity, the thrust and all the other (if present) external force components are excluded from this purely aerodynamic definition.

Rotational sequence convention

Using the Eulerian angles convention, the adopted order of successive counterclockwise partial rotations indicated in Figs. 1.2 and 1.3 are as follows:

Starting with the trajectory local horizon axes, $Ox_h y_h z_h$, the first intermediate coordinate system, $Ox_1 y_1 z_1$, is defined by the first partial counterclockwise rotation for the velocity yaw angle, χ, around the $Oz_h \equiv Oz_1$ axis. The second partial counterclockwise rotation for the velocity pitch angle, γ, around the intermediate $Oy_1 \equiv Oy_2$ axis results in the second intermediate coordinate system, $Ox_2 y_2 z_2$.

The final partial counterclockwise rotation for the velocity roll angle, μ, around the final $Ox_w = Ox_2$ axis, forms the local right-hand orthogonal wind axes coordinate system.

The classical left-hand orthogonal aerodynamic coordinate system, $Ox_a y_a z_a$, is then obtained by reversing the positive senses of the wind axes, while the modified right-hand aerodynamic coordinate system, $Ox_a y_Q z_a$, is formed by retaining the lateral axis $Oy_Q \equiv Oy_w$.

A further partial counterclockwise rotation of the local wind axes coordinate system, $Ox_w y_w z_w$, around the $Oz_w = Oz_3$ axis, through the side-slip angle, β, results in the third intermediate coordinate system, $Ox_3 y_3 z_3$. Finally, a second partial counterclockwise rotation around the $Oy_b = Oy_3$ axis, through the geometric angle-of-attack, α, yields the right-hand, orthogonal, body axis coordinate system, $Ox_b y_b z_b$.

1.4.2 LOCAL WIND AXES COORDINATE SYSTEM $Ox_w y_w z_w$

The right-hand, orthogonal, local wind axes reference frame, $Ox_w y_w z_w$, is one convenient choice for the rigid body trajectory and the flight performance analyses. Since it is collinear with and oriented inversely to the left-hand classical aerodynamic coordinate system, $Ox_a y_a z_a$, the respective local orientations of its axes relative to the flight

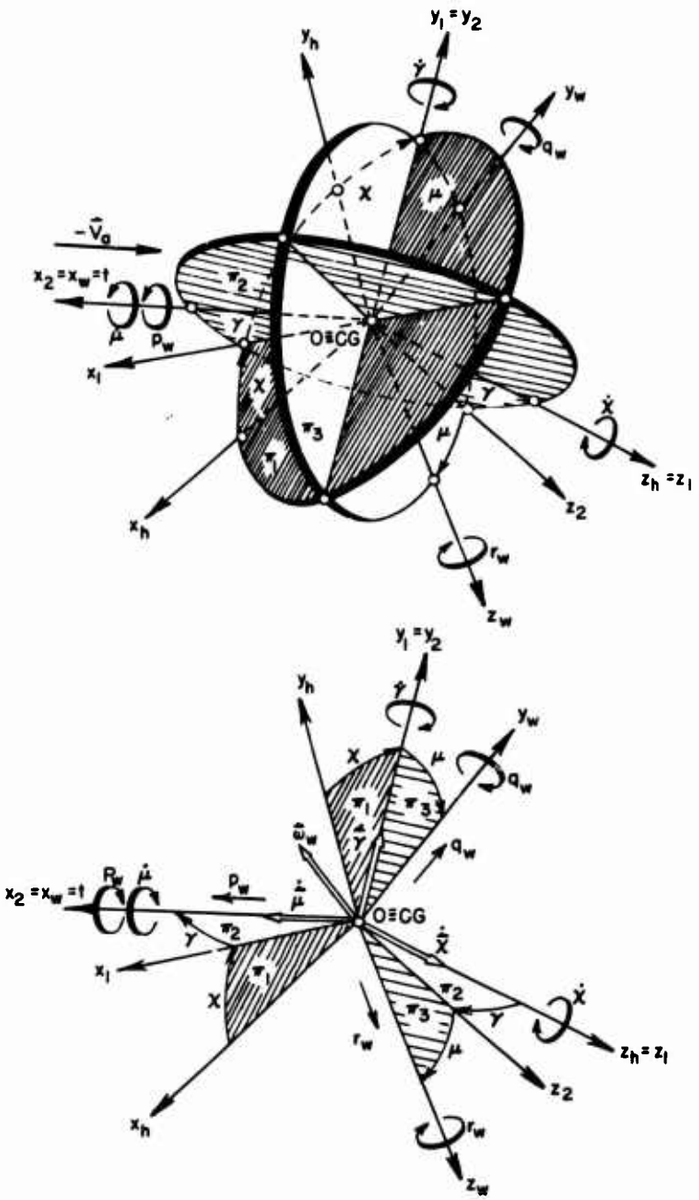

FIG. 1.4 Adopted Eulerian sequence of partial counterclockwise rotations from the trajectory local horizon reference frame, $Ox_h y_h z_h$, to the wind axes local coordinate system $Ox_w y_w z_w$.

trajectory and the geometrical reference (vertical) plane of vehicle symmetry follow the specifications already discussed for the $Ox_a y_a z_a$ or $Ox_a y_a z_a$ reference frames. That is, the positive sign convention is given by the simple unit vector transformation shown in Eqs. (1.4-1) and (1.4-2). For the adopted sequence of the partial angular rotations, the spatial angular elements of the Eulerian transformation from the trajectory local horizon axes, $Ox_h y_h z_h$, to the wind axes, $Ox_w y_w z_w$, are explicitly given in Fig. 1.4.

GLOSSARY for Fig. 1.4

The π_1, π_2 and π_3 planes contain the velocity yaw, χ, the velocity pitch, γ, and the velocity roll, μ, angles.

The Ox_w axis is collinear to the local tangent on a space trajectory, $Ox_w \equiv Ot$.

The adopted sequence of partial angular rotations of the $Ox_h y_h z_h$, into the $Ox_w y_w z_w$ axes, positive counterclockwise, is as follows:

(1) First, a rotation about the $Oz_h \equiv Oz_1$ axis for the velocity yaw angle, χ.

(2) Second, a rotation about the $Oy_1 \equiv Oy_2$ axis for the velocity pitch angle, γ.

(3) Third, a rotation about the $Ox_2 \equiv Ox_w$ axis for the velocity roll angle, μ.

The corresponding pattern of Eulerian transformations of the components of any vector (i.e. force, moment, velocity, acceleration) from the wind axes into the horizon axes reference frame is given by the following unit vector transformation matrix, or by its alternative tabular form, which is convenient for direct transformations both ways:

$$\begin{bmatrix} \bar{i}_h \\ \bar{j}_h \\ \bar{k}_h \end{bmatrix} = \begin{bmatrix} \cos\gamma\cos\chi & (\sin\mu\sin\gamma\cos\chi - \cos\mu\sin\chi) & (\cos\mu\sin\gamma\cos\chi + \sin\mu\sin\chi) \\ \cos\gamma\sin\chi & (\sin\mu\sin\gamma\sin\chi + \cos\mu\cos\chi) & (\cos\mu\sin\gamma\sin\chi - \sin\mu\cos\chi) \\ -\sin\gamma & \sin\mu\cos\gamma & \cos\mu\cos\gamma \end{bmatrix} \begin{bmatrix} \bar{i}_w \\ \bar{j}_w \\ \bar{k}_w \end{bmatrix} \qquad (1.4\text{-}3)$$

	$\vec{i}_w = -\vec{i}_a$	$\vec{j}_w = -\vec{j}_a = \vec{j}_Q$	$\vec{k}_w = -\vec{k}_a$
$\vec{i}_h$	$\cos\gamma\cos\chi$	$(\sin\mu\sin\gamma\cos\chi - \cos\mu\sin\chi)$	$(\cos\mu\sin\gamma\cos\chi + \sin\mu\sin\chi)$
$\vec{j}_h$	$\cos\gamma\sin\chi$	$(\sin\mu\sin\gamma\sin\chi + \cos\mu\cos\chi)$	$(\cos\mu\sin\gamma\sin\chi - \sin\mu\cos\chi)$
$\vec{k}_h$	$-\sin\gamma$	$\sin\mu\cos\gamma$	$\cos\mu\cos\gamma$

(1.4-4)

i.e. explicitly

$$\vec{i}_h = \vec{i}_w\cos\gamma\cos\chi + \vec{j}_w(\sin\mu\sin\gamma\cos\chi - \cos\mu\sin\chi) + \vec{k}_w(\cos\mu\sin\gamma\cos\chi + \sin\mu\sin\chi) \quad (1.4\text{-}5)$$

or

$$\vec{i}_h = -\vec{i}_a\cos\gamma\cos\chi + \vec{j}_Q(\sin\mu\sin\gamma\cos\chi - \cos\mu\sin\chi) - \vec{k}_a(\cos\mu\sin\gamma\cos\chi + \sin\mu\sin\chi) \quad (1.4\text{-}6)$$

etc., and vice versa

$$\vec{i}_w = -\vec{i}_a = \vec{i}_h\cos\gamma\cos\chi + \vec{j}_h\cos\gamma\sin\chi - \vec{k}_h\sin\gamma \quad (1.4\text{-}7)$$

etc.

The evolutory angular velocity, $\vec{\omega}_w$, of the wind axes, $Ox_wy_wz_w$, relative to the trajectory local horizon axes, $Ox_hy_hz_h$ is:

$$\vec{\omega}_w = \dot{\vec{\mu}} + \dot{\vec{\gamma}} + \dot{\vec{\chi}} \equiv \dot{\mu}\vec{i}_2 + \dot{\gamma}\vec{j}_1 + \dot{\chi}\vec{k}_h \equiv \dot{\mu}\vec{i}_w + \dot{\gamma}\vec{j}_2 \quad (1.4\text{-}8)$$

The resolution of the evolutory angular velocity, $\vec{\omega}_w$, onto the wind axes, $Ox_wy_wz_w$, is specified by the transformation matrix:

$$\begin{bmatrix} p_w \\ q_w \\ r_w \end{bmatrix} = \begin{bmatrix} 1 & 0 & -\sin\gamma \\ 0 & \cos\mu & \sin\mu\cos\gamma \\ 0 & -\sin\mu & \cos\mu\cos\gamma \end{bmatrix} \begin{bmatrix} \dot{\mu} \\ \dot{\gamma} \\ \dot{\chi} \end{bmatrix} \quad (1.4\text{-}9)$$

$$\therefore \quad \vec{\omega}_w = \vec{p}_w + \vec{q}_w + \vec{r}_w \equiv p_w\vec{i}_w + q_w\vec{j}_w + r_w\vec{k}_w \quad (1.4\text{-}10)$$

	$\dot{\mu}$	$\dot{\gamma}$	$\dot{\chi}$
p_w or $(-p_a)$	1	0	$-\sin\gamma$
$q_w = q_Q$ or $(-q_a)$	0	$\cos\mu$	$\sin\mu\cos\gamma$
r_w or $(-r_a)$	0	$-\sin\mu$	$\cos\mu\cos\gamma$

(1.4-11)

Alternatively, the mutual relationships between the evolutory angular velocity components, $\dot{\vec{\mu}}$, $\dot{\vec{\gamma}}$, $\dot{\vec{\chi}}$ and its wind axes components, $\vec{p}_w$, $\vec{q}_w$, $\vec{r}_w$ are readily obtainable from the corresponding transformation table, Eq. 1.4-11, valid both ways:

The trajectory local horizon axes components, $\vec{p}_{wh}$, $\vec{q}_{wh}$, $\vec{r}_{wh}$, of the wind axes angular evolutory velocity, $\vec{\omega}_w$, in terms of its wind axes initial componental values, $\vec{p}_w$, $\vec{q}_w$, $\vec{r}_w$, and vice versa, are directly obtainable by use of the respective unit transformation matrix, Eq. (1.4-13) or the corresponding unit vectors transformation table, Eq. (1.4-14):

$$\vec{\omega}_w = p_w\vec{i}_w + q_w\vec{j}_w + r_w\vec{k}_w = p_{wh}\vec{i}_h + q_{wh}\vec{j}_h + r_{wh}\vec{k}_h \quad (1.4\text{-}12)$$

$$\begin{bmatrix} p_{wh} \\ q_{wh} \\ r_{wh} \end{bmatrix} = \begin{bmatrix} \cos\gamma\cos\chi & (\sin\mu\sin\gamma\cos\chi - \cos\mu\sin\chi) & (\cos\mu\sin\gamma\cos\chi + \sin\mu\sin\chi) \\ \cos\gamma\sin\chi & (\sin\mu\sin\gamma\sin\chi + \cos\mu\cos\chi) & (\cos\mu\sin\gamma\sin\chi - \sin\mu\cos\chi) \\ -\sin\gamma & \sin\mu\cos\gamma & \cos\mu\cos\gamma \end{bmatrix} \begin{bmatrix} p_w \\ q_w \\ r_w \end{bmatrix} \quad (1.4\text{-}13)$$

	p_w or $(-p_a)$	$q_w = q_Q$ or $(-q_a)$	r_w or $(-r_a)$
p_{wh}	$\cos\gamma\cos\chi$	$(\sin\mu\sin\gamma\cos\chi - \cos\mu\sin\chi)$	$(\cos\mu\sin\gamma\cos\chi + \sin\mu\sin\chi)$
q_{wh}	$\cos\gamma\sin\chi$	$(\sin\mu\sin\gamma\sin\chi + \cos\mu\cos\chi)$	$(\cos\mu\sin\gamma\sin\chi - \sin\mu\cos\chi)$
r_{wh}	$-\sin\gamma$	$\sin\mu\cos\gamma$	$\cos\mu\cos\gamma$

(1.4-14)

The body axes components, $\vec{p}_{wb}$, $\vec{q}_{wb}$, $\vec{r}_{wb}$, of the wind axes evolutory angular velocity vector, $\vec{\omega}_w$, are defined either by the respective unit vector transformation table (1.4-14) in terms of $\vec{p}_w$, $\vec{q}_w$, $\vec{r}_w$:

	p_w or $(-p_a)$	q_w or $(-q_a)$	r_w or $(-r_a)$
p_{wb}	$\cos\alpha\cos\beta$	$\cos\alpha\sin\beta$	$-\sin\alpha$
q_{wb}	$-\sin\beta$	$\cos\beta$	0
r_{wb}	$\sin\alpha\cos\beta$	$\sin\alpha\sin\beta$	$\cos\alpha$

(1.4-15)

or, alternatively in terms of $\dot{\mu}$, $\dot{\gamma}$, $\dot{\chi}$ by the transformation matrix

$$\begin{bmatrix} p_{wb} \\ q_{wb} \\ r_{wb} \end{bmatrix} = \begin{bmatrix} \cos\alpha\cos\beta & \cos\alpha\sin\beta & -\sin\alpha \\ -\sin\beta & \cos\beta & 0 \\ \sin\alpha\cos\beta & \sin\alpha\sin\beta & \cos\alpha \end{bmatrix} \begin{bmatrix} 1 & 0 & -\sin\gamma \\ 0 & \cos\mu & \sin\mu\cos\gamma \\ 0 & -\sin\mu & \cos\mu\cos\gamma \end{bmatrix} \begin{bmatrix} \dot{\mu} \\ \dot{\gamma} \\ \dot{\chi} \end{bmatrix} \qquad (1.4\text{-}17)$$

i.e. in the alternative tabular form, convenient for transformations both ways:

	$\dot{\mu}$	$\dot{\gamma}$	$\dot{\chi}$
p_{wb}	$(\cos\alpha\cos\beta)$	$(\cos\mu)(\cos\alpha\sin\beta)$ $+(-\sin\mu)(-\sin\alpha)$	$(-\sin\gamma)(\cos\alpha\cos\beta)$ $+(\sin\mu\cos\gamma)(\cos\alpha\sin\beta)$ $+(\cos\mu\cos\gamma)(-\sin\alpha)$
q_{wb}	$(-\sin\beta)$	$(\cos\mu)(\cos\beta)$	$(-\sin\gamma)(-\sin\beta)$ $+(\sin\mu\cos\gamma)(\cos\beta)$
r_{wb}	$(\sin\alpha\cos\beta)$	$(\cos\mu)(\sin\alpha\sin\beta)$ $+(-\sin\mu)(\cos\alpha)$	$(-\sin\gamma)(\sin\alpha\cos\beta)$ $+(\sin\mu\cos\gamma)(\sin\alpha\sin\beta)$ $+(\cos\mu\cos\gamma)(\cos\alpha)$

(1.4-18)

1.4.3 BODY AXES COORDINATE SYSTEM $Ox_by_bz_b$

A body axes reference frame is presumed to be rigidly fixed respective to the vehicle geometry. It is sometimes referred to as an Eulerian coordinate system, the name implying that it participates in all the translational, rotational and oscillatory motions of the specified rigid body, the relative motions being defined from another, presumably inertial, Newtonian reference frame. Depending on the inherent physical characteristics of the investigated dynamic occurences, the correspondingly suitable specific choices of the Eulerian body axes, $Ox_by_bz_b$, may facilitate both the numerical computations and the related definitions of the involved mass inertial parameters. In the flight dynamics analysis it is usually convenient to fix the body axes origin, O, coincident with the vehicle center of gravity, CG, which allows for a corresponding simplification of the general form of the governing equations of motion.(11) In accordance with the adopted aerodynamic force definitions, a representative right-hand, orthogonal, body axes reference frame, $Ox_by_bz_b$, is illustrated in Fig. 1.5. A subsequent choice of the relative positions for two of the individual axes, Ox_b and Oy_b or Oz_b, respective to the vehicle geometry and mass distribution, shall implicate the following fundamental aspects of rigid body flight dynamics:

(i) Any arbitrary body fixed reference frame renders the moments and the products of inertias invariant of the rotational time-histories of a flying vehicle for a fixed CG position and a constant mass distribution. Since the body-fixed coordinate system rotates along with the vehicle, the time-derivatives of any vector referred to it shall acquire the correspondingly expanded Eulerian (i.e. non Gallilean) forms.(11,13,16,17)

(ii) When body fixed axes are chosen to be the principal inertial axes of the given vehicle mass distribution, the products of mass inertia vanish and two out of the three moments of inertia become maxima and minima respectively. For vehicle configurations having one reference plane of symmetry, in which the Ox_b and the Oz_b body axes are conventionally contained, the respective product of inertia terms become zero:

$$\int_m x_b\, y_b\, dm = \int_m y_b\, z_b\, dm = 0 \qquad (1.4\text{-}19)$$

If in addition, the Ox_b and the Oz_b axes are the principal axes, the remaining product of inertia term also becomes zero.

$$\int_m x_b z_b \, dm \equiv 0 \qquad (1.4\text{-}20)$$

Then, the Oy_b axis (which is, by virtue of orthogonality, perpendicular to the $Ox_b z_b$ plane) becomes a principal axis also, and the moments of inertia about the Ox_b, Oy_b and Oz_b axes respectively

$$\begin{aligned} \int_m (y_b^2 + z_b^2) dm &= I_{xx} \\ \int_m (x_b^2 + z_b^2) dm &= I_{yy} \\ \int_m (x_b^2 + y_b^2) dm &= I_{zz} \end{aligned} \qquad (1.4\text{-}21)$$

become maxima and minima, since the origin of the rigid body axes system is assumed to be central (O≡CG).

(iii) For sting-balance wind tunnel aerodynamic force and moment measurements, as well as for some analytical aerodynamic force and moment considerations in the case of axisymmetric body geometries, the body fixed reference frame is conveniently defined when the Ox_b axis is made collinear with the body center line.

(iv) From an overall aerodynamic force analysis point of view, a chosen body fixed reference frame of a given vehicle configuration serves for conditional definitions of the representative geometric angle-of-attack, α, and the side-slip angle, β.

(v) A special case arises when the Ox_b axis is so fixed in relation to the vehicle configuration (if possible) that the reference geometric angle-of-attack becomes equal to the representative aerodynamic (or absolute) angle-of-attack of the overall vehicle geometry

$$\alpha_a = \alpha \ , \ \alpha_o = 0 \qquad (1.4\text{-}22)$$

The Ox_b axis is then termed the first aerodynamic axis of the body configuration. This case is more specifically elaborated in Section 1.6.

GLOSSARY for Fig. 1.5

The π_4 and π_5 planes contain the side-slip angle, β, and the geometric angle-of-attack, α, respectively (see Figs. 1.2 and 1.3 for further specifications).

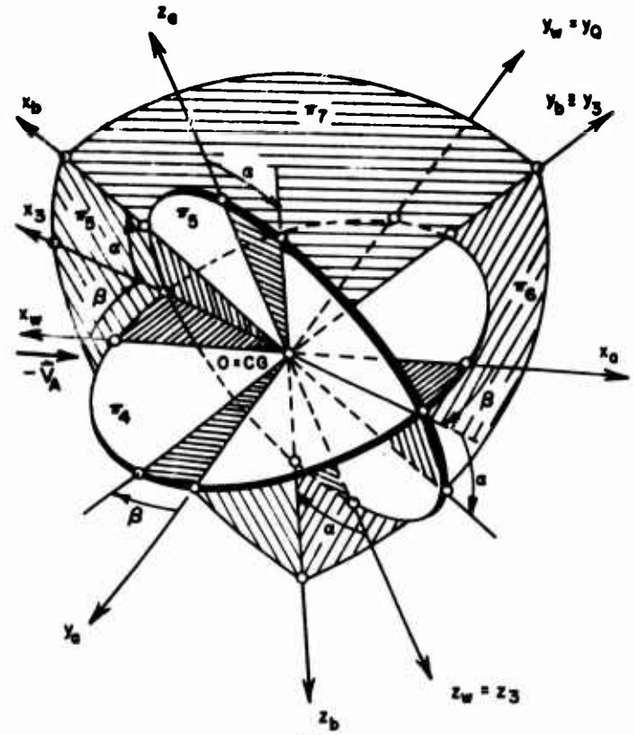

(a)

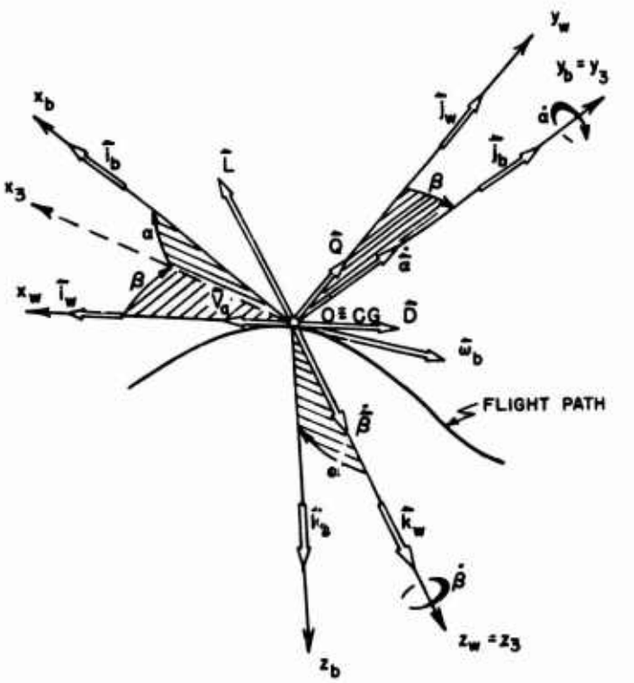

(b)

FIG. 1.5 Spatial definition of the right-hand, orthogonal, body axes coordinate system, $Ox_b y_b z_b$.

The π_6 plane is the lateral body axes plane, Oy_bz_b or Oy_3z_b .

The π_7 plane is the axial body axes plane, Ox_by_b or Ox_by_3 .

The convention for sequence of rotations from the wind axis, $Ox_wy_wz_w$, to the body axes, $Ox_by_bz_b$, coordinate systems is as follows:

(1) First, a partial rotation around the $Oz_w \equiv Oz_3$ axis in a counter-clockwise sense for a positive side-slip angle, β , defines the third intermediate coordinate system, $Ox_3y_3z_3$.

(2) Second, a partial rotation around the $Oy_3 \equiv Oy_b$ axis in a counter-clockwise sense for a positive geometric angle-of-attack, α , results in the adopted body axes coordinate system, $Ox_by_bz_b$.

The unit vector transformation matrices and the respective tabular forms, which are convenient for transformation both ways of the respective sets of components of any vectorial quantity, are:

(i) Body axes - Wind axes unit vector transformation, and vice versa:

	$\hat{i}_b$	$\hat{j}_b$	$\hat{k}_b$
$-\hat{i}_a$ or $\hat{i}_w$	$\cos\alpha\cos\beta$	$-\sin\beta$	$\sin\alpha\cos\beta$
$-\hat{j}_a$ or $\hat{j}_w = \hat{j}_Q$	$\cos\alpha\sin\beta$	$\cos\beta$	$\sin\alpha\sin\beta$
$-\hat{k}_a$ or $\hat{k}_w$	$-\sin\alpha$	0	$\cos\alpha$

(1.4-23)

(ii) Body axes - Local horizon axes unit vector transformation matrix:

$$\begin{bmatrix} \hat{i}_b \\ \hat{j}_b \\ \hat{k}_b \end{bmatrix} = \begin{bmatrix} \cos\alpha\cos\beta & \cos\alpha\sin\beta & -\sin\alpha \\ -\sin\beta & \cos\beta & 0 \\ \sin\alpha\cos\beta & \sin\alpha\sin\beta & \cos\alpha \end{bmatrix} \begin{bmatrix} \cos\gamma\cos\chi & \cos\gamma\sin\chi & -\sin\gamma \\ (\sin\mu\sin\gamma\cos\chi - \cos\mu\sin\chi) & (\sin\mu\sin\gamma\sin\chi + \cos\mu\cos\chi) & \sin\mu\cos\gamma \\ (\cos\mu\sin\gamma\cos\chi + \sin\mu\sin\chi) & (\cos\mu\sin\gamma\sin\chi - \sin\mu\cos\chi) & \cos\mu\cos\gamma \end{bmatrix} \begin{bmatrix} \hat{i}_h \\ \hat{j}_h \\ \hat{k}_h \end{bmatrix}$$

(1.4-24)

i.e. in the convenient tabular form, valid both ways:

	$\hat{i}_h$	$\hat{j}_h$	$\hat{k}_h$
$\hat{i}_b$	$(\cos\gamma\cos\chi)(\cos\alpha\cos\beta)$ $+(\sin\mu\sin\gamma\cos\chi - \cos\mu\sin\chi)(\cos\alpha\sin\beta)$ $+(\cos\mu\sin\gamma\cos\chi + \sin\mu\sin\chi)(-\sin\alpha)$	$(\cos\gamma\sin\chi)(\cos\alpha\cos\beta)$ $+(\sin\mu\sin\gamma\sin\chi + \cos\mu\cos\chi)(\cos\alpha\sin\beta)$ $+(\cos\mu\sin\gamma\sin\chi - \sin\mu\cos\chi)(-\sin\alpha)$	$(-\sin\gamma)(\cos\alpha\cos\beta)$ $+(\sin\mu\cos\gamma)(\cos\alpha\sin\beta)$ $+(\cos\mu\cos\gamma)(-\sin\alpha)$
$\hat{j}_b$	$(\cos\gamma\cos\chi)(-\sin\beta)$ $+(\sin\mu\sin\gamma\cos\chi - \cos\mu\sin\chi)(\cos\beta)$	$(\cos\gamma\sin\chi)(-\sin\beta)$ $+(\sin\mu\sin\gamma\sin\chi + \cos\mu\cos\chi)(\cos\beta)$	$(-\sin\gamma)(-\sin\beta)$ $+(\sin\mu\cos\gamma)(\cos\beta)$
$\hat{k}_b$	$(\cos\gamma\cos\chi)(\sin\alpha\cos\beta)$ $+(\sin\mu\sin\gamma\cos\chi - \cos\mu\sin\chi)(\sin\alpha\sin\beta)$ $+(\cos\mu\sin\gamma\cos\chi + \sin\mu\sin\chi)(\cos\alpha)$	$(\cos\gamma\sin\chi)(\sin\alpha\cos\beta)$ $+(\sin\mu\sin\gamma\sin\chi + \cos\mu\cos\chi)(\sin\alpha\sin\beta)$ $+(\cos\mu\sin\gamma\sin\chi - \sin\mu\cos\chi)(\cos\alpha)$	$(-\sin\gamma)(\sin\alpha\cos\beta)$ $+(\sin\mu\cos\gamma)(\sin\alpha\sin\beta)$ $+(\cos\mu\cos\gamma)(\cos\alpha)$

(1.4-25)

The evolutory angular velocity of the body axes coordinate system is

$$\vec{\omega}_b = \dot{\vec{\alpha}} + \dot{\vec{\beta}} = \dot{\alpha}\vec{i}_b + \dot{\beta}\vec{k}_w \equiv \dot{\alpha}\vec{j}_3 + \dot{\beta}\vec{k}_3 \qquad (1.4\text{-}26)$$

The body axes evolutory angular velocity components, $\bar{p}_b$, $\bar{q}_b$, $\bar{r}_b$, in terms of the defining angular velocities $\dot{\vec{\alpha}}$ and $\dot{\vec{\beta}}$ are given by the transformation matrix:

$$\begin{bmatrix} p_b \\ q_b \\ r_b \end{bmatrix} = \begin{bmatrix} 0 & 0 & -\sin\alpha \\ 0 & 1 & 0 \\ 0 & 0 & \cos\alpha \end{bmatrix} \begin{bmatrix} 0 \\ \dot{\alpha} \\ \dot{\beta} \end{bmatrix} \qquad (1.4\text{-}27)$$

or in a convenient tabular form, valid both ways:

	0	$\dot{\alpha}$	$\dot{\beta}$
p_b	0	0	$-\sin\alpha$
q_b	0	1	0
r_b	0	0	$\cos\alpha$

(1.4-28)

since by definition

$$\vec{\omega}_b = \dot{\alpha}\vec{j}_b + \dot{\beta}\vec{k}_w = r_b\vec{i}_b + q_b\vec{j}_b + r_b\vec{k}_b \qquad (1.4\text{-}29)$$

Similarly, a resolution respect ve to the wind axes components, $\vec{p}_{wb}$, $\vec{q}_{wb}$, $\vec{r}_{wb}$ in terms of the $\dot{\vec{\alpha}}$ and $\dot{\vec{\beta}}$ components of the body axes evolutory angular velocity, $\vec{\omega}_b$, is given by the transformation table:

	0	$\dot{\alpha}$	$\dot{\beta}$
$-p_{ba}$ or p_{bw}	0	0	$-\sin\beta$
$-q_{ba}$ or q_{bw}	0	$\cos\beta$	0
$-r_{ba}$ or r_{bw}	0	0	1

(1.4-30)

In accordance with the unit vectors transformation matrices, the following transformation tables for the body axes evolutory angular velocity components respective to other coordinate systems are obtained:

(i) Body axes components - Wind axes components transformation, and vice versa, from the corresponding unit vectors transformation table , Eq. (1.4-23):

$$\vec{\omega}_b = p_b\vec{i}_b + q_b\vec{j}_b + r_b\vec{k}_b = p_{bw}\vec{i}_w + q_{bw}\vec{j}_w + r_{bw}\vec{k}_w \qquad (1.4\text{-}31)$$

	p_b	q_b	r_b
$-p_{ba}$ or p_{bw}	$\cos\alpha\cos\beta$	$-\sin\beta$	$\sin\alpha\cos\beta$
$-q_{ba}$ or p_{bw}	$\cos\alpha\sin\beta$	$\cos\beta$	$\sin\alpha\sin\beta$
$-r_{ba}$ or r_{bw}	$-\sin\alpha$	0	$\cos\alpha$

(1.4-32)

(ii) Body axes components - Trajectory local horizon axes components transformation, and vice versa:

$$\vec{\omega}_b = p_b\vec{i}_b + q_b\vec{j}_b + r_b\vec{k}_b = p_{bh}\vec{i}_h + q_{bh}\vec{j}_h + r_{bh}\vec{k}_h \qquad (1.4\text{-}33)$$

i.e. from the corresponding unit vectors transformation matrix, Eq. (1-4-24):

	p_{bh}	q_{bh}	r_{bh}
p_b	$(\cos\gamma\cos\chi)(\cos\alpha\cos\beta)$ $+(\sin\mu\sin\gamma\cos\chi - \cos\mu\sin\chi)(\cos\alpha\sin\beta)$ $+(\cos\mu\sin\gamma\cos\chi + \sin\mu\sin\chi)(-\sin\alpha)$	$(\cos\gamma\sin\chi)(\cos\alpha\cos\beta)$ $+(\sin\mu\sin\gamma\sin\chi + \cos\mu\cos\chi)(\cos\alpha\sin\beta)$ $+(\cos\mu\sin\gamma\sin\chi - \sin\mu\cos\chi)(-\sin\alpha)$	$(-\sin\gamma)(\cos\alpha\cos\beta)$ $+(\sin\mu\cos\gamma)(\cos\alpha\sin\beta)$ $+(\cos\mu\cos\gamma)(-\sin\alpha)$
q_b	$(\cos\gamma\cos\chi)(-\sin\beta)$ $+(\sin\mu\sin\gamma\cos\chi - \cos\mu\sin\chi)(\cos\beta)$	$(\cos\gamma\sin\chi)(-\sin\beta)$ $+(\sin\mu\sin\gamma\sin\chi + \cos\mu\cos\chi)(\cos\beta)$	$(-\sin\gamma)(-\sin\beta)$ $+(\sin\mu\cos\gamma)(\cos\beta)$
r_b	$(\cos\gamma\cos\chi)(\sin\alpha\cos\beta)$ $+(\sin\mu\sin\gamma\cos\chi - \cos\mu\sin\chi)(\sin\alpha\sin\beta)$ $+(\cos\mu\sin\gamma\cos\chi + \sin\mu\sin\chi)(\cos\alpha)$	$(\cos\gamma\sin\chi)(\sin\alpha\cos\beta)$ $+(\sin\mu\sin\gamma\sin\chi + \cos\mu\cos\chi)(\sin\alpha\sin\beta)$ $+(\cos\mu\sin\gamma\sin\chi - \sin\mu\cos\chi)(\cos\alpha)$	$(-\sin\gamma)(\sin\alpha\cos\beta)$ $+(\sin\mu\cos\gamma)(\sin\alpha\sin\beta)$ $+(\cos\mu\cos\gamma)(\cos\alpha)$

(1.4-34)

Resultant evolutory angular velocity, $\vec{\Omega}_B$, for an overall rotation from the trajectory local horizon axes, $Ox_hy_hz_h$, to the body axes, $Ox_by_bz_b$, in terms of the adopted sequence of partial rotation through the Eulerian angles, χ, γ, μ, β, α, becomes:

$$\vec{\Omega}_B = \vec{\omega}_w + \vec{\omega}_b = (\dot{\mu}\vec{i}_2 + \dot{\gamma}\vec{j}_2 + \dot{\chi}\vec{k}_1) + (\dot{\alpha}\vec{j}_3 + \dot{\beta}\vec{k}_3)$$
$$= (\dot{\mu}\vec{i}_w + \dot{\gamma}\vec{j}_1 + \dot{\chi}\vec{k}_h) + (\dot{\alpha}\vec{j}_b + \dot{\beta}\vec{k}_w) \qquad (1.4\text{-}35)$$

Then, a resolution of the resultant evolutory angular velocity, $\vec{\Omega}_B$, onto the body axes is given in a convenient tabular form by use of the respective transformation matrices, Eqs. (1.4-17) and (1.4-27):

$$\vec{\Omega}_B = p_B\vec{i}_b + q_B\vec{j}_b + r_B\vec{k}_b = (p_{wb} + p_b)\vec{i}_b$$
$$+ (q_{wb} + q_b)\vec{j}_b + (r_{wb} + r_b)\vec{k}_b \qquad (1.4\text{-}36)$$

or explicitly in terms of $\dot{\chi}$, $\dot{\gamma}$, $\dot{\mu}$, $\dot{\beta}$, $\dot{\alpha}$:

	$\dot{\mu}$	$\dot{\gamma}$	$\dot{\chi}$	$\dot{\alpha}$	$\dot{\beta}$
$p_B = p_{wb} + p_b$	$(\cos\alpha\cos\beta)$	$(\cos\mu)(\cos\alpha\sin\beta)$ $+(-\sin\mu)(-\sin\alpha)$	$(-\sin\gamma)(\cos\alpha\cos\beta)$ $+(\sin\mu\cos\gamma)(\cos\alpha\sin\beta)$ $+(\cos\mu\cos\gamma)(-\sin\alpha)$	0	$-\sin\alpha$
$q_B = q_{wb} + q_b$	$(-\sin\beta)$	$(\cos\mu)(\cos\beta)$	$(-\sin\gamma)(-\sin\beta)$ $+(\sin\mu\cos\gamma)(\cos\beta)$	1	0
$r_B = r_{wb} + r_b$	$(\sin\alpha\cos\beta)$	$(\cos\mu)(\sin\alpha\sin\beta)$ $+(-\sin\mu)(\cos\alpha)$	$(-\sin\gamma)(\sin\alpha\cos\beta)$ $+(\sin\mu\cos\gamma)(\sin\alpha\sin\beta)$ $+(\cos\mu\cos\gamma)(\cos\alpha)$	0	$\cos\alpha$

(1.4-37)

Similarly, a resolution of the resultant angular velocity, $\vec{\Omega}_B$, onto the wind axes is given in a convenient tabular form by use of the respective transformation matrices, Eqs. (1.4-11) and (1.4-29):

$$\vec{\omega}_B = p_{Bw}\vec{i}_w + q_{Bw}\vec{j}_w + r_{Bw}\vec{k}_w$$
$$= (p_w + p_{bw})\vec{i}_w + (q_w + q_{bw})\vec{j}_w$$
$$+ (r_w + r_{bw})\vec{k}_w \qquad (1.4\text{-}38)$$

or explicitly in terms of $\dot{\chi}$, $\dot{\gamma}$, $\dot{\mu}$, $\dot{\beta}$, $\dot{\alpha}$:

	$\dot{\mu}$	$\dot{\gamma}$	$\dot{\chi}$	$\dot{\alpha}$	$\dot{\beta}$
$p_{Bw} = p_w + p_{bw}$	1	0	$(-\sin\gamma)$	0	$(-\sin\beta)$
$q_{Bw} = q_w + q_{bw}$	0	$\cos\mu$	$\sin\mu\cos\gamma$	$\cos\beta$	0
$r_{Bw} = r_w + r_{bw}$	0	$(-\sin\mu)$	$\cos\mu\cos\gamma$	0	1

(1.4-39)

1.4.4 STABILITY AXES COORDINATE SYSTEMS $Ox_s'y_s'z_s'$ AND $Ox_sy_sz_s$

The stability axes coordinate system represents a specific variant of a right-hand, orthogonal, body-fixed reference frame with its origin at the vehicle CG. Commonly used in the dynamic stability analysis, it is specified at the initial dynamic equilibrium flight condition to which the subsequent dynamic disturbances and control inputs are then related. By definition, the reference initial stability axes orientations are as follows (see Fig. 1.7)

Ox_s' axis is locally and instantaneously tangential to the flight path at the point of the initial symmetric flight equilibrium (undisturbed) condition, i.e. it is collinear and cosensed with the instantaneous flight velocity vector, $\vec{V}_A$, of the vehicle CG at the initial time instant, t_0.

Oz_s' axis is in the reference plane of symmetry ("vertical" plane for wings-level flight condition), sensed positively downward in a non-inverted flight attitude.

Oy_s' axis is perpendicular to the $Ox_s'y_s'$ reference plane of symmetry, sen-

sed positively to form a right-hand, orthogonal coordinate system.

Thus, the stability axes reference frame, $Ox_s y_s z_s$, is initially coincident with the local wind axes system, $Ox_w y_w z_w$, at the reference initial equilibrium flight instant of time, provided the side-slip angle, β , is zero. However, since the stability axes are not fixed to the trajectory, but to the vehicle, in any subsequent dynamically disturbed flight condition they participate in the six rigid-body degrees of freedom of the disturbed vehicle motion. In doing so they behave as a special set of Eulerian body axes, having the Ox_s axis conditionally fixed with respect to the vehicle configuration prior to the dynamic disturbance onset such that $Ox'_s \equiv Ox_w$, for $\beta=0$. As a consequence, the stability axes reference frame, $Ox'_s y'_s z'_s$, is conditionally ($\beta=0$) coincident with the wind axes, $Ox_w y_w z_w$, at an initial flight equilibrium instant of time, t_o, only. At any other arbitrary instant of time, $t > t_o$, during a dynamical flight disturbance, the spatial correlations between the instantaneous stability axes, $Ox_s y_s z_s$, and the local horizon axes, $Ox_h y_h z_h$, are as specified in Fig. 1.6

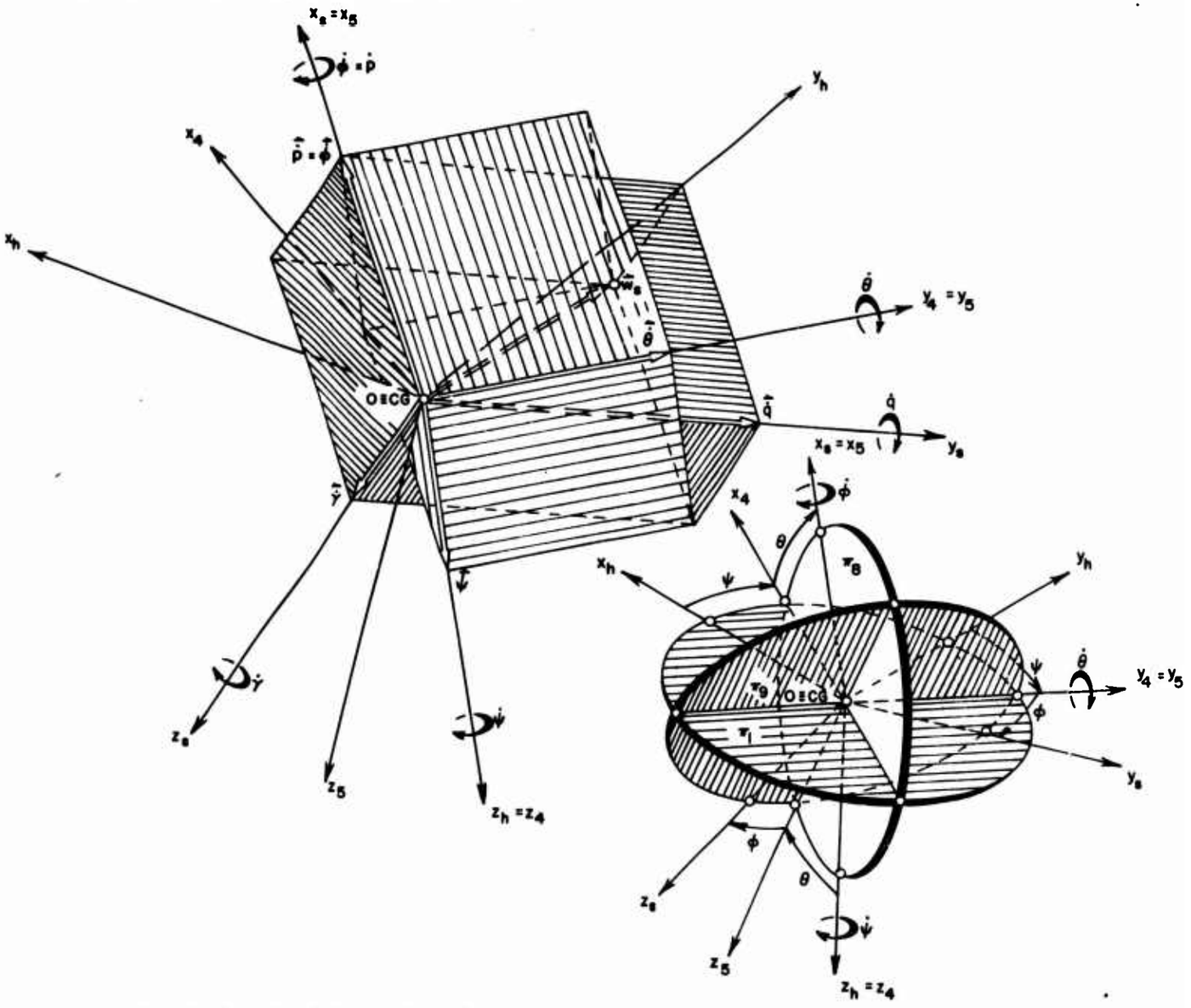

FIG. 1.6 Spatial relative position of the right hand orthogonal stability axes coordinate system, $Ox_s y_s z_s$, respective to the instantaneous local horizon axes, $Ox_h y_h z_h$, at any arbitrary instant of time during a dynamical flight disturbance.

GLOSSARY for Fig. 1.6

$Ox_hy_hz_h$ is the local horizon reference frame at any instant of time, fixed to the corresponding point on a given flight trajectory.

$Ox_sy_sz_s$ is the stability axes reference frame at the same instant of time, fixed to the vehicle.

$Ox_4y_4z_4$ and $Ox_5y_5z_5$ are the intermediate reference frames, resulting from the respective partial angular rotations ψ, θ and ϕ.

π_1 plane is coplanar with the Ox_hy_h and Ox_4y_4 planes. It is perpendicular to the $Oz_h \equiv Oz_4$ axis, containing the instantaneous azimuth angle ψ.

π_2 plane is coplanar with the Ox_4z_4 and Ox_5z_5 planes. It is perpendicular to the $Oy_4 \equiv Oy_5$ axis, containing the instantaneous elevation angle. θ.

π_3 plane is coplanar with Oy_5z_5 and Oy_sz_s planes. It is perpendicular to the $Ox_5 \equiv Ox_s$ axis, containing the instantaneous bank angle, ϕ.

The adopted sequence of the successive angular rotations from the local horizon axes, $Ox_hy_hz_h$, to the instantaneous stability axes, $Ox_sy_sz_s$, is as follows:

(1) The first partial rotation through the instantaneous azimuth angle, ψ, about the $Oz_4 \equiv Oz_h$ axis results in the intermediate reference frame $Ox_5y_5z_5$.

(2) The second partial rotation through the instantaneous elevation angle, θ, about the $Oy_4 \equiv Oy_5$ axis results in the intermediate reference frame $Ox_5y_5z_5$.

(3) The third partial rotation through the instantaneous bank angle, ϕ, about the $Ox_5 \equiv Ox_s$ axis results in the final stability axis coordinate system, $Ox_sy_sz_s$.

The evolutory angular velocity, $\vec{\omega}_s$, for the specified sequence of angular rotations is:

$$\vec{\omega}_s = \dot{\psi}\vec{k}_h + \dot{\theta}\vec{j}_4 + \dot{\phi}\vec{i}_5 \equiv \dot{\psi}\vec{k}_4 + \dot{\theta}\vec{j}_5 + \dot{\phi}\vec{i}_s \qquad (1.4\text{-}40)$$

The stability axes components, $\vec{p}_s$, $\vec{q}_s$, $\vec{r}_s$, of the evolutory angular velocity,

$$\vec{\omega}_s = p_s\vec{i}_s + q_s\vec{j}_s + r_s\vec{k}_s \qquad (1.4\text{-}41)$$

are related formally to the Eulerian angles derivatives, $\dot{\psi}$, $\dot{\theta}$, $\dot{\phi}$, by the same type of transfer matrix as specified for the rotation of local horizon to wind axes system: The same is true for the respective unit vectors transformation matrix.

$$\begin{bmatrix} \vec{i}_s \\ \vec{j}_s \\ \vec{k}_s \end{bmatrix} = \begin{bmatrix} \cos\psi\cos\theta & \cos\theta\sin\psi & (-\sin\theta) \\ (\sin\phi\sin\theta\cos\psi - \cos\phi\sin\psi) & (\sin\phi\sin\theta\sin\psi + \cos\phi\cos\psi) & \sin\phi\cos\theta \\ (\cos\phi\sin\theta\cos\psi + \sin\phi\sin\psi) & (\cos\phi\sin\theta\sin\psi - \sin\phi\cos\psi) & \cos\phi\cos\theta \end{bmatrix} \begin{bmatrix} \vec{i}_h \\ \vec{j}_h \\ \vec{k}_h \end{bmatrix} \qquad (1.4\text{-}42)$$

$$\begin{bmatrix} p_s \\ q_s \\ r_s \end{bmatrix} = \begin{bmatrix} 1 & 0 & (-\sin\theta) \\ 0 & \cos\phi & (\sin\phi\cos\theta) \\ 0 & (-\sin\phi) & (\cos\phi\cos\theta) \end{bmatrix} \begin{bmatrix} \dot{\phi} \\ \dot{\theta} \\ \dot{\psi} \end{bmatrix} \qquad (1.4\text{-}43)$$

Alternatively, in a convenient tabular form, valid both ways:

	$\vec{i}_h$	$\vec{j}_h$	$\vec{k}_h$
$\vec{i}_s$	$\cos\psi\cos\theta$	$(\sin\phi\sin\theta\cos\psi - \cos\phi\sin\psi)$	$(\cos\phi\sin\theta\cos\psi + \sin\phi\sin\psi)$
$\vec{j}_s$	$\cos\theta\sin\psi$	$(\sin\phi\sin\theta\sin\psi + \cos\phi\cos\psi)$	$(\cos\phi\sin\theta\sin\psi - \sin\phi\cos\psi)$
$\vec{k}_s$	$(-\sin\theta)$	$\sin\phi\cos\theta$	$\cos\phi\cos\theta$

(1.4-44)

	$\dot{\phi}$	$\dot{\theta}$	$\dot{\psi}$
p_s	1	0	0
q_s	0	$\cos\phi$	$(-\sin\phi)$
r_s	$(-\sin\theta)$	$\sin\phi\cos\theta$	$\cos\phi\cos\theta$

(1.4-45)

The above spatial and functional relationships and the related illustration, Fig. 1.6, are valid at any arbitrary instant of time, t, on a disturbed trajectory.

Since the body-fixed stability axes are formally coincident with the wind axes only at the inital equilibrium flight instant of time, t_0, the evolutory angular velocity components (p_s,

q_s, r_s), as well as instantaneous Eulerian angles and rotational velocities ($\theta, \phi, \psi, \dot{\theta}, \dot{\phi}, \dot{\psi}$), are time dependent functions, even for $\vec{\omega}_s$=const, for any other time interval, $t > t_0$, on the disturbed trajectory.

A generalized illustration of the spatial relationships between the local horizon axes, $Ox_h y_h z_h$, and the stability axes, $Ox'_s y'_s z'_s$ prior to and $Ox_s y_s z_s$ during a dynamic disturbance, is presented in Fig. 1.7.

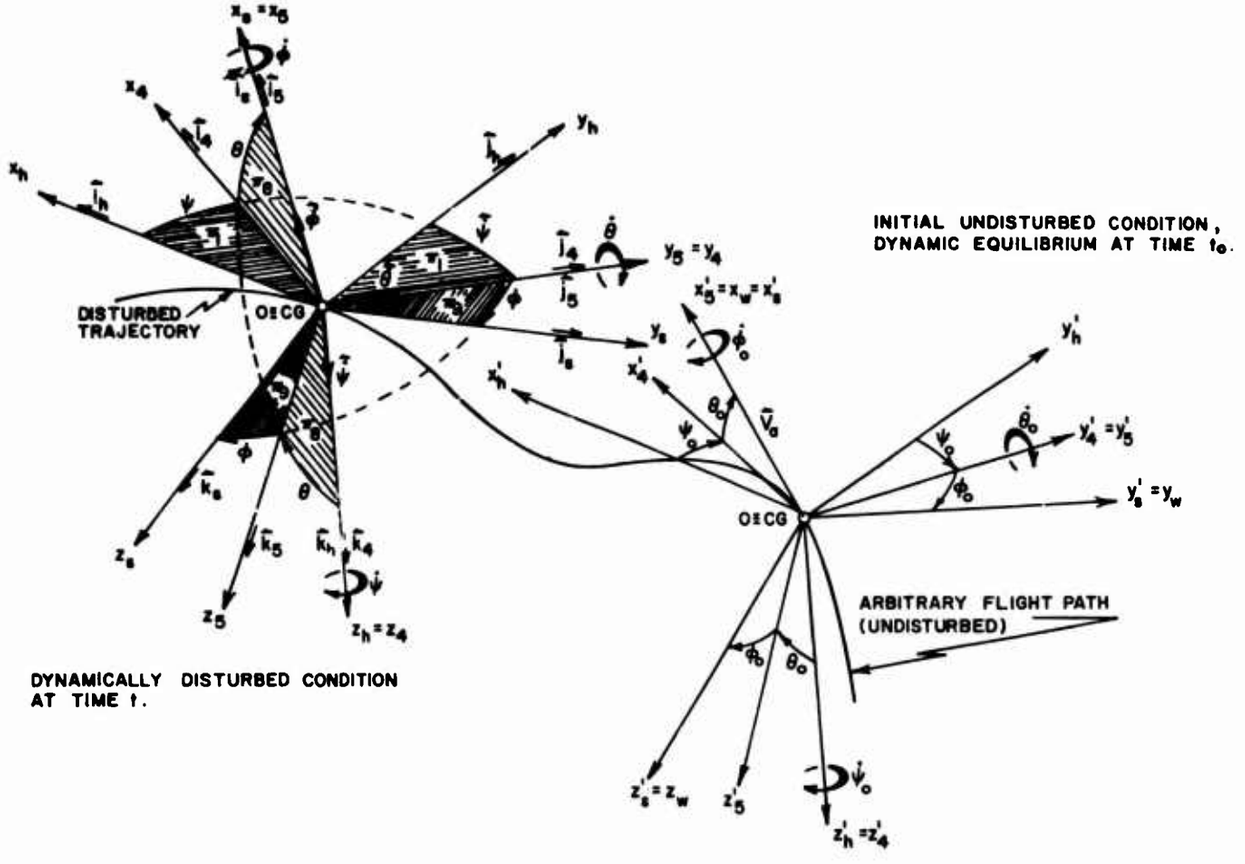

FIG. 1.7 Spatial relative position of the right hand orthogonal stability axes coordinate systems, $Ox'_s y'_s z'_s$, and $Ox_s y_s z_s$ relative to the instantaneous local horizon axes coordinate systems, $Ox'_h y'_h z'_h$ and $Ox_h y_h z_h$, at the dynamic equilibrium time instant, t_o, and at any arbitrary time instant during a dynamic disturbance, t, respectively.

GLOSSARY for Fig. 1.7

$Ox'_h y'_h z'_h$ is the initial local horizon reference frame, fixed at the dynamic equilibrium flight condition at some initial instant of time, t_0 . It serves as the conditional, reference inertial (Newtonian) coordinate system in the small perturbations dynamic stability analysis.

$Ox'_s y'_s z'_s$ is the initial stability axes coordinate system for the dynamic equilibrium flight condition at the initial instant of time, t_0 . The body fixed axes, $Ox'_s y'_s z'_s$, and the trajectory local wind axes, $Ox_w y_w z_w$, are coincident. The $Ox'_s z'_s$ and $Ox_w z_w$ planes are conditionally coplanar with the vehicle's reference plane of symmetry for a no sideslip initial equilibrium flight condition, β=0. The $Ox'_s y'_s z'_s$ stability axes are obtained from the second intermediate coordinate system, $Ox'_5 y'_5 z'_5$, by the third partial rotation through the inital angle-of-bank ϕ_0 about the $Ox'_5 \equiv Ox'_s$ axis.

$Ox_h y_h z_h$ is the local horizon reference frame at any subsequent instant of time, $t > t_0$, on the disturbed flight trajectory.

$Ox_s y_s z_s$ is the body-fixed stability axes coordinate system at the corresponding time instant, $t > t_0$, on the disturbed flight trajectory. The $Ox_s z_s$ plane is coplanar with the vehicle's vertical plane of symmetry. The $Ox_s y_s z_s$ stability axes are obtained from the second intermediate coordinate system, $Ox_5 y_5 z_5$, by the third partial rotation

through the instantaneous angle of bank ϕ about the $Ox_5 \equiv Ox_s$ axis.

$Ox'_4y'_4z'_4$ and $Ox_4y_4z_4$ are the first intermediate coordinate systems, at the time instants $t=t_0$ and $t>t_0$ respectively. They are obtained from the local horizon reference frames $Ox'_hy'_hz'_h$ and $Ox_hy_hz_h$ by the first partial rotations, about $Oz'_h \equiv Oz'_4$ and $Oz_h \equiv Oz_4$ axes through the corresponding initial and instantaneous azimuth angles ψ_0 and ψ respectively.

$Ox'_5y'_5z'_5$ and $Ox_5y_5z_5$ are the second intermediate coordinate systems, at the time instants t_0 and $t>t_0$ respectively, obtained from the first intermediate coordinate systems $Ox'_4y'_4z'_4$ and $Ox_4y_4z_4$ by the second partial rotations about $Oy'_4 \equiv Oy'_5$ and $Oy_4 \equiv Oy_5$ axes through the corresponding initial and instantaneous elevation angles θ_0 and θ respectively.

In small perturbation dynamic stability investigations[15] it is customary to resolve all instantaneous vector quantities (velocities, accelerations, forces, moments) onto the disturbed Eulerian stability axes, $Ox_sy_sz_s$, and to treat any such resultant disturbed vectorial component (subscript s) as the vectorial sum of its respective initial equilibrium (subscript o or s') and its disturbance incremental (Δ) values:

$$\begin{aligned} \vec{X}_s &= \vec{X}_o + \Delta\vec{X} \\ \vec{Y}_s &= \vec{Y}_o + \Delta\vec{Y} \\ \vec{Z}_s &= \vec{Z}_o + \Delta\vec{Z} \end{aligned} \qquad (1.4\text{-}46)$$

i.e. the incremental force disturbances are referred to and measured from the initial equilibrium condition at time t_0. Within the adopted premises for the coordinate systems and the defining angular rotational sequences in Fig. 1.7, a direct correlation between the respective componental addends of any vectorial quantity may prove rather involved in general. For instance, the magnitudes and directions of the instantaneous aerodynamic force components will depend on the aerodynamic angle-of-attack, α, the side-slip angle, β, and the adopted angular evolutory sequences (ψ, θ, ϕ) of the rotating coordinate systems. An illustration of the few significant relationships between the (Newtonian) local horizon axes, $Ox'_hy'_hz'_h$ and $Ox_hy_hz_h$, the (trajectory) wind axes, $Ox_wy_wz_w$, the initial stability axes, $Ox'_sy'_sz'_s$, the instantaneous disturbed (Eulerian) stability axes, $Ox_sy_sz_s$, and the reference body fixed axes, $Ox_by_bz_b$, shall indicate their conditional use in the dynamic stability computations:

(1) At the initial (subscript o) equilibrium flight condition at t_0, the wind axes, $Ox_wy_wz_w$, and the initial stability axes, $Ox'_sy'_sz'_s$, are coparallel for $\beta=0$, rendering the initial azimuth, elevation, and bank angles, ψ_0, θ_0, ϕ_0 equal and coincident to the initial velocity yaw, velocity pitch, and velocity roll angles, χ_0, γ_0, μ_0, respectively:

$$\begin{aligned} \vec{\psi}_o &\equiv \vec{\chi}_o \;,\; \vec{i}_w = \vec{i}_s \\ \vec{\theta}_o &\equiv \vec{\gamma}_o \;,\; \vec{j}_w = \vec{j}_s \\ \vec{\phi}_o &\equiv \vec{\mu}_o \;,\; \vec{k}_w = \vec{k}_s \end{aligned} \qquad (1.4\text{-}47)$$

Consequently, the transformation matrices for the evolutory angular velocity, $\vec{\omega}_s = \vec{\omega}_w$, for the unit vectors and aerodynamic force components, from the initial local horizon axes, $Ox'_hy'_hz'_h$, to the initial stability axes, $Ox'_sy'_sz'_s$, are formally the same as indicated for the transformation from the initial local horizon axes, $Ox_hy_hz_h$, to the wind axes, $Ox_wy_wz_w$; see Eqs. (1.4-3) to (1.4-7), Section 1.4.2.

At the same initial instant of time, t_0, the reference body axes coordinate system, $Ox_by_bz_b$, is spatially related to the initial stability axes, $Ox'_sy'_sz'_s \parallel Ox_wy_wz_w$, through the initial geometric angle-of-attack, α_0, (provided the side-slip angle, β, is zero) in terms of which the total aerodynamic resistance force, $\vec{R}(\alpha)$, is defined (see Fig. 1.7).

The reference body axes, $Ox_by_bz_b$, in general are not coparallel to the body fixed principal axes, $Ox_py_pz_p$, with respect to which the moments and products of inertia are analytically computed in simple form in terms of the vehicle mass and geometric symmetry conditions. A subsequent resolution of the moments and products of inertia from the principal axes, $Ox_py_pz_p$, onto the initial stability axes, $Ox'_sy'_sz'_s$, requires a special transformation, involving a set of three additional evolutory angles. Once properly transformed into $Ox'_sy'_sz'_s$, the moments and products of inertia remain constant during the subsequent time dependent disturbed motion of the vehicle, if the CG is kept fixed. The necessary transformation matrix takes a simple form (15) if the restraint of no initial side-slip angle, $\beta=0$, is introduced, rendering the $Ox'_s = Ox_w$, the Ox_p and Ox_b axes coplanar.

(2) For a "flat earth" trajectory and dynamic stability analysis, the local horizon axes $Ox'_hy'_hz'_h$ and $Ox_hy_hz_h$ are coparallel.

For a "spherical earth" trajectory and dynamic stability analysis (viz., high speed, high altitude, prolonged duration, slightly damped perturbations) the additional evolutory angular transformations representing the relative rotations between the $Ox'_h y'_h z'_h$ and $Ox_h y_h z_h$ local horizon axes are required (see Fig. 1.1, Section 1.4).

(3) When the "flat earth" approximation is acceptable, the instantaneous ψ, θ, ϕ, and the initial ψ_0, θ_0, ϕ_0, azimuth, elevation and bank angles are referred to the same reference (Newtonian) local horizon coordinate system, since $Ox_h y_h z_h$ and $Ox'_h y'_h z'_h$ local trajectory axes are then coparallel, both mutually and relative to the fixed (Newtonian) flat earth coordinate system $Ex_H y_H z_H$, which is the basic reference frame for the trajectory analysis (see Fig. 1.1 and Section 1.3). The instantaneous ($t>t_0$) evolutory angular velocity, $\vec{\omega}_s$, of the stability axes, $Ox_s y_s z_s$, respective to the local horizon axes $Ox_h y_h z_h$, is then defined, both in terms of its evolutory angular components and in terms of its stability axes components, formally in the same way and by the same type of transformation matrices as already specified for the initial angular velocity vector $\vec{\omega}_s$ at time t_0.

If the instantaneous ($t>t_0$) Eulerian angles, ψ_s, θ_s, ϕ_s, are tentatively expressed as sums of their respective initial values and relative angular increments between the $Ox_s y_s z_s$ and $Ox'_s y'_s z'_s$ axes, as is customarily done in the small perturbations dynamic stability analysis, then their vectorial equivalents of the Eqs.(1.4-46) are:

$$\begin{aligned} \vec{\psi}_s &= \vec{\psi}_0 + \Delta\vec{\psi} = \vec{\chi} + \Delta\vec{\psi} \\ \vec{\theta}_s &= \vec{\theta}_0 + \Delta\vec{\theta} = \vec{\gamma} + \Delta\vec{\theta} \\ \vec{\phi}_s &= \vec{\phi}_0 + \Delta\vec{\phi} = \vec{\mu} + \Delta\vec{\phi} \end{aligned} \qquad (1.4\text{-}48)$$

and in terms of scalars

$$\begin{aligned} \psi_s &= \psi_0 + \Delta\psi = \chi + \Delta\psi \\ \theta_s &= \theta_0 + \Delta\theta = \gamma + \Delta\theta \\ \phi_s &= \phi_0 + \Delta\phi = \mu + \Delta\phi \end{aligned} \qquad (1.4\text{-}49)$$

The above relationships represent a first order approximation, acceptable within the validity of the first order small perturbation theory at large.(15) The incremental angles $\Delta\psi, \Delta\theta, \Delta\phi$ are sometimes referred to as the disturbance, yaw, pitch and roll angles.

Similarly, at any perturbed time $t>t_0$, the position of instantaneous body axes, $Ox_b y_b z_b$, relative to the initial equilibrium wind axes, $Ox'_w y'_w z'_w$, at time t_0 is, in a first order of approximation, given by:

$$\begin{aligned} \beta &= \Delta\beta \quad \text{for } \beta_0 = 0, \\ \alpha &= \alpha_0 + \Delta\alpha. \end{aligned} \qquad (1.4\text{-}50)$$

(4) In the small perturbations dynamic stability analysis the dynamic equations of motion and all the constituent external forces and moments (as well as all velocities and accelerations) at any arbitrary instant of time $t>t_0$ during a small disturbance, are necessarily related to the initial equilibrium local horizon axes, $Ox'_h y'_h z'_h$, at the initial time instant t_0. These axes in the case of a flat earth, are coparallel with the earth fixed Newtonian coordinate system, $Ex_H y_H z_H$, as well as with any other instantaneous local horizon axes, $Ox_h y_h z_h$, at time instant $t>t_0$. A subsequent resolution of all the constituent vectors onto the instantaneous Eulerian stability axes is performed by introducing the above stated first order approximations for the relative angular rotations. The corresponding transformation matrices are of the type specified in paragraph (3) of this section. The explicit forms of the resulting system of differential equations of motion are given in the literature.(15)

1.4.5 PRINCIPAL TRIHEDRAL COORDINATE SYSTEM Otnb

The principal trihedral coordinate system, Otnb, serves well for the point mass, three degrees of freedom, trajectory analysis. It should not be confused with the local tangent, normal and lateral axes coordinate system at a given local point of the body contour, as used in the aerodynamic force components definitions in Sections 1.3 and 1.6.

The principal trihedral coordinate system is conventionally defined as a right-hand oriented set of orthogonal axes, Ot, On and Ob, such that (a) the intrinsic geometrical characteristics of a space curve (trajectory) are easily expressed in terms of the analytic geometric motions and (b) the Otnb axes represent a natural reference frame for vectoral presentation of linear velocities, linear accelerations, and centripetal accelerations. At any instant of time, t, the principal trihed-

ral origin is fixed at the respective generic point O≡CG along the space trajectory which a point mass (i.e. vehicle CG) describes in its three degrees of

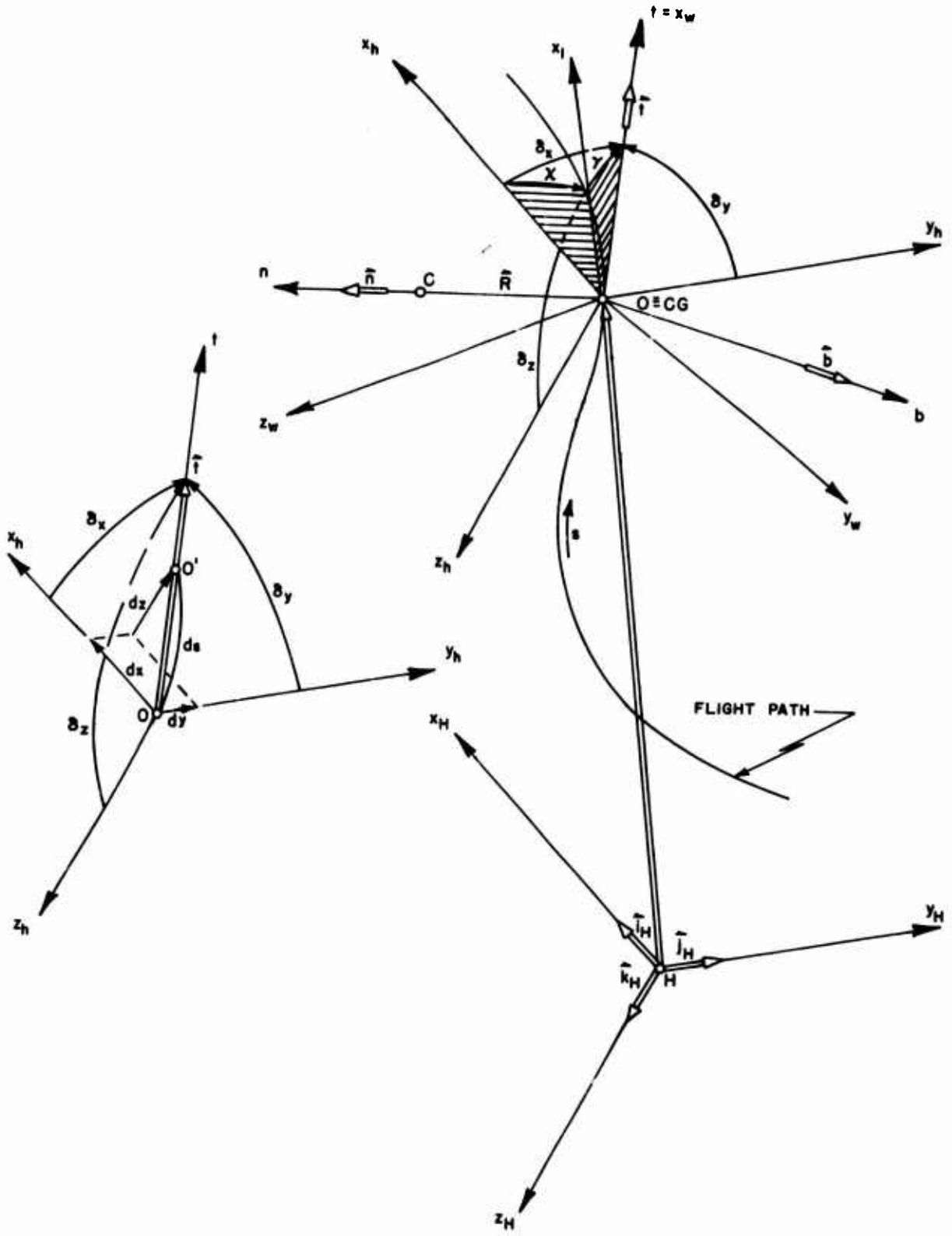

FIG. 1.8(a)

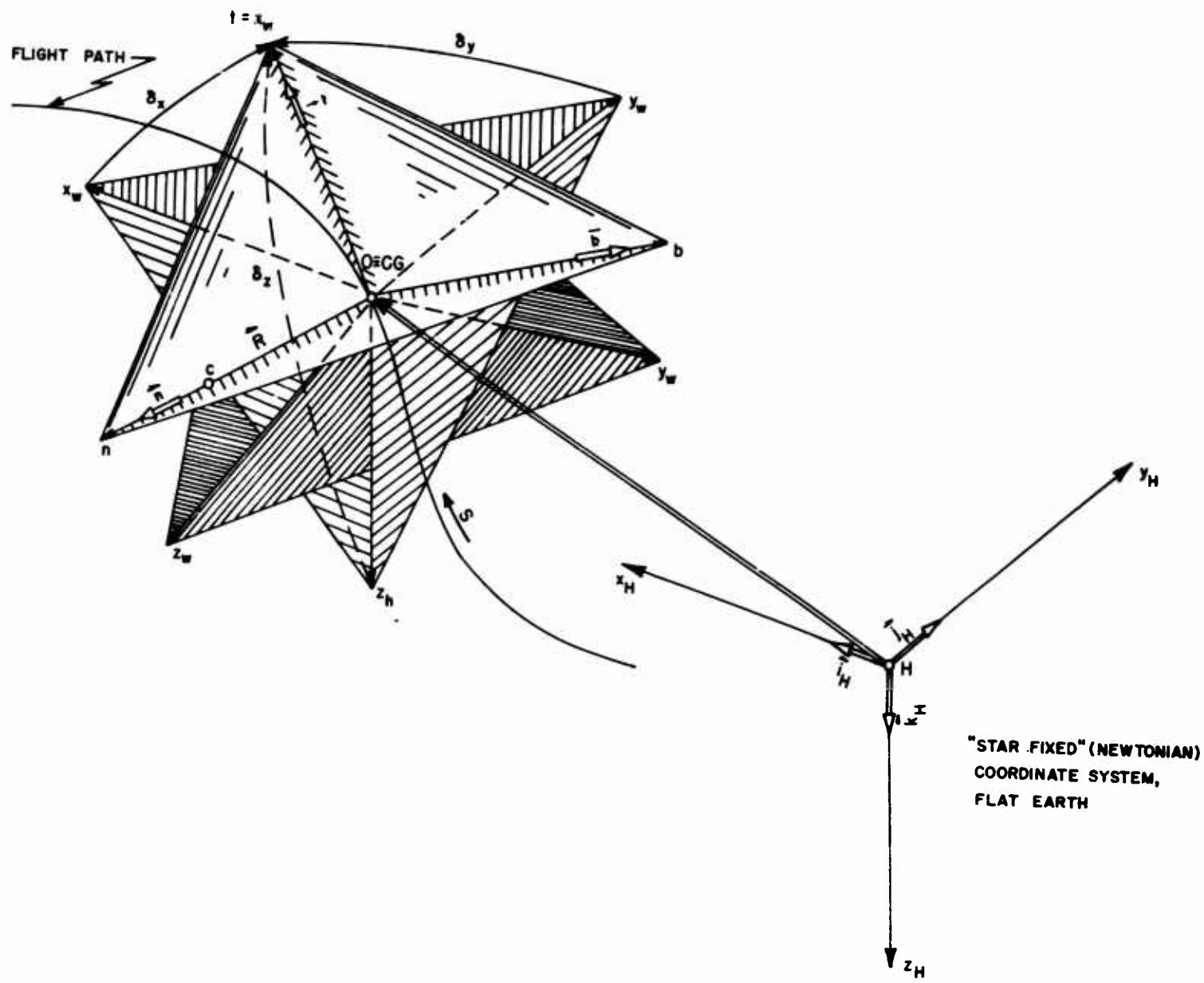

FIG. 1.8 (b)

FIG. 1.8 Right hand orthogonal principle trihedral coordinate system, Otbn.

freedom motion:

The Ot axis is locally tangential to the trajectory, taken collinear and cosensed with the instantaneous linear velocity vector, $\vec{V}_A$, of the vehicle CG.

The Ow axis is perpendicular to the Ot axis and collinear with the local radius of curvature, sensed positive towards the local center of curvature.

The Ob axis is perpendicular to the local osculating plane (the Otb plane), sensed positive to form a right-hand orthogonal coordinate system.

The respective local unit tangent, $\vec{t}$, unit normal, $\vec{n}$, and unit binormal, $\vec{b}$, vectors on the principal trihedral axes are thus defined, at any instantaneous position of the generic point O≡CG, in terms of the respective geometrical trajectory elements as follows:

In general the parametric equations of a known space curve in terms of the curvilinear abscissa, s(t),

$$\begin{aligned} x &= x(s) \\ y &= y(s) \\ z &= z(s) \end{aligned} \qquad (1.4\text{-}51)$$

are referred to a basic Newtonian ("star-fixed") coordinate system, in which the flight trajectory is specified. For a flat non-rotating earth, it is the earth horizon $Hx_Hy_Hz_H$ axes system, which is coparallel to the local horizon axes, $Ox_hy_hz_h$. The position vector of the generic point is then

$$\vec{HO}(t) = x_H\vec{i}_H + y_H\vec{j}_H + z_H\vec{k}_H$$

$$\therefore d\vec{HO} = \vec{OO'} = dx_h\vec{i}_h + dy_h\vec{j}_h + dz_h\vec{k}_h = d\vec{s} \qquad (1.4\text{-}52)$$

and the Ot axis forms the geometric angles $\delta_x(t)$, $\delta_y(t)$, $\delta_z(t)$ with the respective local horizon axes $Ox_hy_hz_h$.

$$\begin{aligned} \cos\delta_x &= \frac{dx_h}{ds} \\ \cos\delta_y &= \frac{dy_h}{ds} \\ \cos\delta_z &= \frac{dz_h}{ds} \end{aligned} \qquad (1.4\text{-}53)$$

$$\cos^2\delta_x + \cos^2\delta_y + \cos^2\delta_z = 1 \qquad (1.4\text{-}54)$$

$$\begin{aligned} x_H = x(s)\ ,\ dx_h &= dx_H\ ,\ \vec{i}_h \| \vec{i}_H \\ y_H = y(s)\ ,\ dy_h &= dy_H\ ,\ \vec{j}_h \| \vec{j}_H \\ z_H = z(s)\ ,\ dz_h &= dz_H\ ,\ \vec{k}_h \| \vec{k}_H \end{aligned} \qquad (1.4\text{-}55)$$

The vectorial equation of the space curve is

$$\vec{HO} = \vec{HO}(s)\ ,\ s = s(t) \qquad (1.4\text{-}56)$$

while the unit vectors of the principal trihedral are:(11)

$$\vec{t} = \vec{i}_h\cos\gamma_x + \vec{j}_h\cos\delta_y + \vec{k}_h\cos\delta_z = \frac{d\vec{HO}}{ds}$$

$$\vec{n} = \frac{\vec{dt}/ds}{|\vec{dt}/ds|} = R\frac{\vec{dt}}{ds} \qquad (1.4\text{-}57)$$

$$\vec{b} = \vec{t} \times \vec{n}$$

where the radius of local curvature is

$$R = \frac{1}{\left|\frac{d\vec{t}}{ds}\right|} = \frac{1}{\left|\frac{d^2\vec{r}}{ds^2}\right|}$$

$$ds = (dx_H^2 + dy_H^2 + dz_H^2)^{1/2} \qquad (1.4\text{-}58)$$

and $t\frac{d\vec{t}}{ds} = 0$ defines the local osculating plane, containing the unit vectors $\vec{t}$ and $\vec{n}$, as well as $\vec{R}$ and $\frac{d\vec{t}}{ds}$.

It is noted that the local tangent axis, Ot, is always collinear and cosensed with the local Ox_w wind axis.

Resolutions of the aerodynamic forces $\vec{L}$, $\vec{D}$ and $\vec{Q}$, at a given generic point O≡CG, onto the principal trihedral axes require that the instantaneous geometric angles $\delta_x(t)$, $\delta_y(t)$, $\delta_z(t)$ are known from the above given trajectory data, or that the relative spatial positions of the principal trihedral axes Otnb respective to the local horizon axes, $Ox_hy_hz_h$, are known. Two special cases in the flat earth flight dynamics performance analysis permit simplified transformation procedures:

(i) In case of a trajectory completely confined in the vertical plane, the Oz_w and On axes, in addition to the Ox_w and Ot, become collinear. This leads to an overall collinearity of the Otnb and the $Ox_wy_wz_w$ coordinate systems, provided the following geometrical, kinematic and dynamic conditions are satisifed:

(a) Vehicle possesses a vertical plane of symmetry.
(b) The thrust, $\vec{T}$, and the velocity vector, $\vec{V}_A$, are in the same plane of symmetry.
(c) $\mu = \beta = 0$
(d) $\vec{Q} = 0$

The unit vectors and the evolutory angular velocity transformation matrices are then specified for the wind axes, $Ox_wy_wz_w$, coordinate system, Section 1.4.2.

(ii) In the case of trajectories confined to the horizon plane, Ox_hy_h, of the local horizon axes, $Ox_hy_hz_h$, (which are coparallel with the $Hx_Hy_Hz_H$ and the $Ex_ey_ez_e$ on a "flat earth") the local wind axes, $Ox_wy_wz_w$, and the principal trihedral axes, Otnb, are not collinear. The thrust, $\vec{T}$, and the velocity, $\vec{V}_A$, vectors are contained in the vertical plane of symmetry, Ox_wz_w, i.e. the side-slip angle, β, is zero, rendering the aerodynamic side-slip force zero, $\vec{Q}=0$, for configurations geometrically symmetric with respect to the vertical plane. In addition, there is no velocity pitch, $\gamma=0$, since the trajectory is in the horizontal plane. Then, a direct cosine projection of all the vectorial components from the local trajectory wind axes onto the local principal trihedral axes yields a dynamically simplified set of the governing equations of motion,(15) with the centrifugal force appearing naturally as a single force in the direction of the On axis.

1.4.6 BASIC NEWTONIAN FIXED REFERENCE FRAMES $Hx_Hy_Hz_H$ and $Ex_ey_ez_e$

Valid formulations of flight dynamics occurrences within the classical Newtonian concepts and dynamics postulates necessitate that the governing equations of motion be defined and related to reference frames which can be conditionally regarded as inertial. In view of the nonexistance of such inertial reference frames in terms of the absolute, all motions being but relative in a classical sense, a conditional choice of such a basic inertial reference frame depends largely on the type of investigation and the time-spatial scope of the flight dynamics problem. Thus, in different analyses a number of conditionally acceptable inertial reference frames may be formulated. In Fig. 1.1, a few tentative dynamics of flight choices of such basic reference coordinate systems are indicated. Inasmuch as they are the dynamically defined basic reference for a later componental resolution of the vectorial governing equations of motion upon other, more convenient, non-Newtonian trajectory-bound or body-rotating coordinate systems, i.e. for the respective aerodynamic force components transformation in particular, their formulations and their relative spatial relationships are briefly outlined below.

The instantaneous right-hand, orthogonal, local horizon reference frame, $Ox_hy_hz_h$, has its origin at the vehicle CG and its axes sensed with and coparallel to the instantaneous ground horizon coordinate system, $Hx_Hy_Hz_H$. The Oz_h axis is the local vertical, positive downward. The Ox_h and Oy_h axes are in the π_l plane which is parallel to the earth local horizon plane, Hx_Hy_H, so that the Ox_h axis is coparallel to the tangent t_o, the instantaneous parallel passing through H; while the Oy_h axis is coparallel to the instantaneous meridian passing through H.

The earth axis right-hand orthogonal coordinate system, $Ex_ey_ez_e$, is assumed rigidly attached to the observer's fundamental reference point E on the earth surface; the Ez_e axis is oriented towards the centroid of the spherical earth, while the Ex_e and Ey_e axes are tangential locally to the fundamental parallel and the fundamental meridian, respectively, i.e. they form the fundamental local horizon plane, Ex_ey_e. The Ey_e axis is sensed positively toward the pole, causing the Ex_e axis to be positive in a clockwise sense for the Northern Hemisphere. Note that the fundamental parallel and the fundamental meridian are in general arbitrary reference circles, i.e. they are neither the equator nor the zero meridian.

The $Ex_ey_ez_e$ coordinate system can be interpreted as the initial surface reference (launch sight) for a spherical earth. For a flat earth the $Hx_Hy_Hz_H$ and the $Ex_ey_ez_e$ axes are coparallel.

The intermediate instantaneous local horizon reference frames, $Dx_dy_dz_d$ and $Hx_Hy_Hz_H$ are defined consistently with the $Ex_ey_ez_e$ system, i.e. they are obtained from it by successive partial rotations through the relative longitude angle, τ, and the relative latitude angle, λ, plus the corresponding translation. Note that the relative longitude angle, τ, is the only angle conditionally taken positive in a clockwise sense (Northern Hemisphere).

The curvilinear orthogonal coordinate system, EXYZ, is defined consistently with the fundamental reference frame, $Ex_ey_ez_e$. The curvilinear coordinates X and Y determine (in degrees) the instantaneous position of the vehicle CG with respect to E. Since

$$\begin{aligned} X &= r_0\tau, \\ Y &= r_0\lambda, \\ |\vec{r}_0| &= CE = CD = CH, \end{aligned} \qquad (1.4\text{-}59)$$

the resultant unit vector transformation matrix between the $Hx_Hy_Hz_H$ (or $Ox_hy_hz_h$) and the $Ex_ey_ez_e$ reference frame is:(15)

$$\begin{bmatrix}\vec{i}_h\\ \vec{j}_h\\ \vec{k}_h\end{bmatrix}=\begin{bmatrix}\cos\left(\frac{X}{r_0}\right) & 0 & \sin\left(\frac{X}{r_0}\right)\\ -\sin\left(\frac{X}{r_0}\right)\sin\left(\frac{Y}{r_0}\right) & \cos\left(\frac{Y}{r_0}\right) & \cos\left(\frac{X}{r_0}\right)\sin\left(\frac{Y}{r_0}\right)\\ -\sin\left(\frac{X}{r_0}\right)\cos\left(\frac{Y}{r_0}\right) & -\sin\left(\frac{Y}{r_0}\right) & \cos\left(\frac{X}{r_0}\right)\cos\left(\frac{Y}{r_0}\right)\end{bmatrix}\begin{bmatrix}\vec{i}_e\\ \vec{j}_e\\ \vec{k}_e\end{bmatrix} \qquad (1.4\text{-}60)$$

or, in a suitable tabular form, valid both ways:

	$\vec{i}_e$	$\vec{j}_e$	$\vec{k}_e$
$\vec{i}_h$	$\cos\left(\frac{X}{r_0}\right)$	0	$\sin\left(\frac{X}{r_0}\right)$
$\vec{j}_h$	$-\sin\left(\frac{X}{r_0}\right)\sin\left(\frac{Y}{r_0}\right)$	$\cos\left(\frac{Y}{r_0}\right)$	$\cos\left(\frac{X}{r_0}\right)\sin\left(\frac{Y}{r_0}\right)$
$\vec{k}_h$	$-\sin\left(\frac{X}{r_0}\right)\cos\left(\frac{Y}{r_0}\right)$	$-\sin\left(\frac{Y}{r_0}\right)$	$\cos\left(\frac{X}{r_0}\right)\cos\left(\frac{Y}{r_0}\right)$

(1.4-61)

Since in case of a "flat earth," the $Ex_ey_ez_e$ and the $Hx_Hy_Hz_H$ coordinate systems are coparallel, i.e. the unit vector transformation matrix, Eq. (1.4-60) becomes a unit matrix, rendering:

$$\begin{aligned}\vec{i}_H &\parallel \vec{i}_e\\ \vec{j}_H &\parallel \vec{j}_e\\ \vec{k}_H &\parallel \vec{k}_e\end{aligned} \qquad (1.4\text{-}62)$$

In case of a spherical earth, the evolutory angular velocity, $\vec{\Omega}_H$, specifying the adopted sequence of partial rotations of the $Ex_ey_ez_e$ into the $Hx_Hy_Hz_H$ (or $Ox_hy_hz_h$) reference frame through the evolutory angular components $(-\dot{\tau})=\frac{\dot{X}}{r_0}$ and $\dot{\lambda}=\frac{\dot{Y}}{r_0}$, is

$$\vec{\Omega}_H=\dot{\lambda}\vec{i}_H-\dot{\tau}\vec{j}_d=\dot{\lambda}\vec{i}_H-\dot{\tau}(\vec{j}_H\cos\lambda-\vec{k}_H\sin\lambda)$$
$$\vec{\Omega}_H=\left(\frac{\dot{Y}}{r_0}\right)\vec{i}_H-\left(\frac{\dot{X}}{r_0}\right)\cos\left(\frac{Y}{r_0}\right)\vec{j}_H+\left(\frac{\dot{X}}{r_0}\right)\sin\left(\frac{Y}{r_0}\right)\vec{k}_H \qquad (1.4\text{-}63)$$

$$\vec{\Omega}_H\parallel\vec{\Omega}_h,\quad |\vec{\Omega}_H|=|\vec{\Omega}_h| \quad \text{since} \quad \begin{aligned}\vec{i}_H &\parallel \vec{i}_h\\ \vec{j}_H &\parallel \vec{j}_h\\ \vec{k}_H &\parallel \vec{k}_h\end{aligned} \qquad (1.4\text{-}64)$$

For a flat earth case, a pure translation takes place, $\vec{\Omega}_H\equiv\vec{\Omega}_h=0$.

The resultant evolutory angular velocity for an overall rotation of the $Ex_ey_ez_e$ into the $Ox_wy_wz_w$ trajectory reference frame becomes, for a spherical earth:

$$\vec{\Omega}_w=\vec{\Omega}_H+\vec{\omega}_w=(\dot{\lambda}-\dot{\tau})+(\dot{\mu}+\dot{\gamma}+\dot{\chi}),$$
$$\therefore\ \vec{\Omega}_w=(\dot{\lambda}\vec{i}_H-\dot{\tau}\vec{j}_d)+(\dot{\mu}\vec{i}_w+\dot{\gamma}\vec{j}_2+\dot{\chi}\vec{k}_h), \qquad (1.4\text{-}65)$$

where, according to Section 1.4.2:

$$\vec{\omega}_w=\dot{\mu}\vec{i}_2+\dot{\gamma}\vec{j}_1+\dot{\chi}\vec{k}\equiv\dot{\mu}\vec{i}_w+\dot{\gamma}\vec{j}_2+\dot{\chi}\vec{k}_h \qquad (1.4\text{-}66)$$

and

$$\begin{bmatrix}\vec{i}_2=\vec{i}_w\\ \vec{j}_1=\vec{j}_2\\ \vec{k}_1=\vec{k}_h\end{bmatrix}=\begin{bmatrix}1 & 0 & 0\\ 0 & \cos\mu & (-\sin\mu)\\ (-\sin\gamma) & \sin\mu\cos\gamma & \cos\mu\cos\gamma\end{bmatrix}\begin{bmatrix}\vec{i}_w\\ \vec{j}_w\\ \vec{k}_w\end{bmatrix} \qquad (1.4\text{-}67)$$

Again, since in terms of the angular velocity wind axes components, $\vec{P}_w$, $\vec{Q}_w$, $\vec{R}_w$, the resultant evolutory angular velocity $\vec{\Omega}_w$ is alternatively given by:

$$\vec{\Omega}_w=P_w\vec{i}_w+Q_w\vec{j}_w+R_w\vec{k}_w=(\dot{\lambda}\vec{i}_H-\dot{\tau}\vec{j}_d)+(\dot{\mu}\vec{i}_w+\dot{\gamma}\vec{j}_2+\dot{\chi}\vec{k}_h) \qquad (1.4\text{-}68)$$

$$\therefore P_w\vec{i}_w+Q_w\vec{j}_w+R_w\vec{k}_w=(\dot{\mu}\vec{i}_w+\dot{\gamma}\vec{j}_2+\dot{\chi}\vec{k}_h)+\left(\frac{\dot{Y}}{r_0}\right)\vec{i}_H-\left(\frac{\dot{X}}{r_0}\right)\cos\left(\frac{Y}{r_0}\right)\vec{j}_H+\left(\frac{\dot{X}}{r_0}\right)\sin\left(\frac{Y}{r_0}\right)\vec{k}_H \qquad (1.4\text{-}69)$$

The respective transformation matrix is then obtained by combining the corresponding unit vector matrix transformations, Eqs. (1.4-67) and (1.4-3):

$$\begin{bmatrix}P_w\\ Q_w\\ R_w\end{bmatrix}=\begin{bmatrix}1 & 0 & -\sin\gamma\\ 0 & \cos\mu & \sin\mu\cos\gamma\\ 0 & -\sin\mu & \cos\mu\cos\gamma\end{bmatrix}\begin{bmatrix}\dot{\mu}\\ \dot{\gamma}\\ \dot{\chi}\end{bmatrix}+\begin{bmatrix}(\cos\gamma\cos\chi) & (\cos\gamma\sin\chi) & (-\sin\gamma)\\ (\sin\mu\sin\gamma\cos\chi-\cos\mu\sin\chi) & (\sin\mu\sin\gamma\sin\chi+\cos\mu\cos\chi) & (\sin\mu\cos\gamma)\\ (\cos\mu\sin\gamma\cos\chi+\sin\mu\sin\chi) & (\cos\mu\sin\gamma\sin\chi-\sin\mu\cos\chi) & (\cos\mu\cos\gamma)\end{bmatrix}\begin{bmatrix}\left(\frac{\dot{Y}}{r_0}\right)\\ -\frac{\dot{X}}{r_0}\cos\left(\frac{Y}{r_0}\right)\\ \frac{\dot{X}}{r_0}\sin\left(\frac{Y}{r_0}\right)\end{bmatrix} \qquad (1.4\text{-}70)$$

For the flat earth case: $r_0\to\infty$, the angular evolutory velocity $\vec{\Omega}_H\equiv 0$ and $\vec{\Omega}_w\equiv\vec{\omega}_w$, (see Section 1.4.2).

In conclusion, it is pointed out that the evolutory angular velocity matrices reflect the respective coordinate systems relative rotations only; the wind axes components $\vec{p}_{ew}$, $\vec{q}_{ew}$, $\vec{r}_{ew}$ of the earth angular velocity of rotation, $\vec{\omega}_e$, in terms of $\vec{p}_e$, $\vec{q}_e$, $\vec{r}_e$ components are then determined (when necessary as in case of the Coriolis force) by use of the respective unit vector transformation matrices between the $Ex_ey_ez_e$ and $Ox_wy_wz_w$ coordinate systems, i.e. the earth rotational angular velocity $\vec{\omega}_e$ is treated as any substantial vector quantity whose resolution is sought in consistence with the respective vector transformation rules:

$$\vec{\omega}_e = p_e\vec{i}_e + q_e\vec{j}_e + r_e\vec{k}_e = p_{ew}\vec{i}_w + q_{ew}\vec{j}_w + r_{ew}\vec{k}_w \tag{1.4-71}$$

$$\begin{bmatrix} p_{ew} \\ q_{ew} \\ r_{ew} \end{bmatrix} = \begin{bmatrix} \text{unit vector transformation matrix, Eq. I.4-70, expressing relative rotations of } Ox_w y_w z_w \text{ and } Hx_H y_H z_H \text{ (or } Ox_h y_h z_h \parallel Hx_H y_H z_H \text{) axes.} \end{bmatrix} \begin{bmatrix} p_{eH} \\ q_{eH} \\ r_{eH} \end{bmatrix}$$

$$= \begin{bmatrix} \text{unit vector transformation matrix, Eq. I.4-70, expressing relative rotations of } Ox_w y_w z_w \text{ and } Hx_H y_H z_H \parallel Ox_h y_h z_h \text{ axes.} \end{bmatrix} \begin{bmatrix} \text{unit vector transformation matrix, Eq. I.4-60, expressing relative rotations of } Hx_H y_H z_H \parallel Ox_h y_h z_h \text{ and } Ex_e y_e z_e \text{ axes.} \end{bmatrix} \begin{bmatrix} p_e \\ q_e \\ r_e \end{bmatrix} \tag{1.4-72}$$

1.5 TRANSFORMATIONS OF THE AERODYNAMIC FORCE COMPONENTS

A formal resolution of the resultant aerodynamic force

$$\vec{R} = \vec{R}(\alpha) + \vec{R}(\beta) \qquad (1.5\text{-}1)$$

onto the adopted modified right-hand, orthogonal, aerodynamic coordinate system, $O x_a y_Q z_a$, (Sections 1.3 and 1.6, Fig.1.12) in accordance with the definitions of the geometric angle-of-attack, α, and the side-slip angle β, yields basic expressions for the lift, $\vec{L}$, the drag, $\vec{D}$, and the side-force, $\vec{Q}$, vectors. These, along with the corresponding coefficients, are

$$\vec{L} = L\vec{k}_a = (C_L q_A S_{ref})\vec{k}_a \qquad (1.5\text{-}2)$$

$$C_L = \frac{1}{S_{ref}}\int_{S_{wet}} Cp(\alpha)\vec{n}\cdot\vec{k}_a\, dS \qquad (1.5\text{-}3)$$

$$\vec{D} = \vec{D}(\alpha) + \vec{D}(\beta) = D\vec{i}_a = (C_D q_A S_{ref})\vec{i}_a \qquad (1.5\text{-}4)$$

$$C_D = C_D(\alpha) + C_D(\beta)$$

$$= \frac{1}{S_{ref}}\int_{S_{wet}}\left[Cp(\alpha)\vec{n}\cdot\vec{i}_a + C_f(\alpha)\vec{i}_a\vec{i}_a\right]dS \qquad (1.5\text{-}5)$$

$$+ \frac{1}{S_{ref}}\int_{S_{wet}}\left[Cp(\beta)\vec{n}\cdot\vec{i}_\beta + C_f(\beta)\vec{i}_\beta\vec{i}_a\right]dS$$

$$\vec{Q} = Q\vec{j}_Q = (C_Q q_A S_{ref})\vec{j}_Q \qquad (1.5\text{-}6)$$

$$C_Q = \frac{1}{S_{ref}}\int_{S_{wet}} Cp(\beta)\vec{n}\cdot\vec{j}_Q\, dS \qquad (1.5\text{-}7)$$

Subsequent transformations of the $\vec{L}$, $\vec{D}$, and $\vec{Q}$ aerodynamic force components from the modified right-hand aerodynamic coordinate system, $O x_a y_Q z_a$, onto other flight dynamics reference frames can be affected either by the method of direct projections (involving nine cosine relationships, six of which are independent) or by use of the adopted set of three sequential Eulerian angular rotations. Through use of the respective unit vector transformation matrices from Section 1.4, the latter method yields the following transformation sets for the lift, the drag, and the side-force aerodynamic force components:

(i) Local wind axes aerodynamic force components, $\bar{X}_w$, $\bar{Y}_w$, $\bar{Z}_w$, are,

$$\vec{R} = D\vec{i}_a + Q\vec{j}_Q + L\vec{k}_a = \vec{X}_w + \vec{Y}_w + \vec{Z}_w \qquad (1.5\text{-}8)$$

$$\vec{X}_w = -D\vec{i}_w = D\vec{i}_a$$
$$\vec{Y}_w = Q\vec{j}_w = Q\vec{j}_Q \qquad (1.5\text{-}9)$$
$$\vec{Z}_w = -L\vec{k}_w = L\vec{k}_a$$

$$\therefore \vec{R} = \vec{X}_w + \vec{Y}_w + \vec{Z}_w \equiv -D\vec{i}_w + Q\vec{j}_w - L\vec{k}_w \qquad (1.5\text{-}10)$$

(ii) Local horizon axes aerodynamic force components, $\bar{X}_h$, $\bar{Y}_h$, $\bar{Z}_h$, are, from the unit vector transformation matrix Eq. (1.4-3), Section 1.4.2,

$$\vec{R} = \vec{X}_h + \vec{Y}_h + \vec{Z}_h = X_h\vec{i}_h + Y_h\vec{j}_h + Z_h\vec{k}_h \qquad (1.5\text{-}11)$$

$$X_h\vec{i}_h\cdot\vec{i}_h = (-\cos\gamma\cos\chi)\vec{i}_a\cdot D\vec{i}_a$$
$$+(-\cos\mu\sin\chi + \sin\mu\sin\gamma\cos\chi)\vec{j}_Q\cdot Q\vec{j}_Q \qquad (1.5\text{-}12)$$
$$+(-\cos\mu\sin\gamma\cos\chi - \sin\mu\sin\chi)\vec{k}_a\cdot L\vec{k}_a$$

etc.,

$$\therefore X_h = -D(\cos\gamma\cos\chi)$$
$$-Q(\cos\mu\sin\chi - \sin\mu\sin\gamma\cos\chi)$$
$$-L(\cos\mu\sin\gamma\cos\chi + \sin\mu\sin\chi)$$
$$Y_h = -D(\cos\gamma\sin\chi) \qquad (1.5\text{-}13)$$
$$+Q(\cos\mu\cos\chi + \sin\mu\sin\gamma\sin\chi)$$
$$-L(\cos\mu\sin\gamma\sin\chi - \sin\mu\cos\chi)$$
$$Z_h = D\sin\gamma + Q\sin\mu\cos\gamma - L\cos\mu\cos\gamma$$

(iii) Initial stability axes aerodynamic force components, $\bar{X}_s$, $\bar{Y}_s$, $\bar{Z}_s$ for $\beta=0$ are from Section 1.4.1,

$$R = \vec{X}_s' + \vec{Y}_s' + \vec{Z}_s' = X_s'\vec{i}_s' + Y_s'\vec{j}_s' + Z_s'\vec{k}_s' \equiv -D\vec{i}_s' + Q\vec{j}_s' - L\vec{k}_s' \qquad (1.5\text{-}14)$$

where X_s' , Y_s' , Z_s' are given by Eq. (1.5-9), since

$$\vec{X}_s' = \vec{X}_w$$
$$\vec{Y}_s' = \vec{Y}_w \qquad (1.5\text{-}15)$$
$$\vec{Z}_s' = \vec{Z}_w$$

(iv) Spherical earth fixed axes aerodynamic force components, $\bar{X}_e$, $\bar{Y}_e$, $\bar{Z}_e$, are, from the unit vector transformation matrix Eq. (1.4-60), Section 1.4.6,

$$\vec{R} = \vec{X}_e + \vec{Y}_e + \vec{Z}_e = X_e\vec{i}_e + Y_e\vec{j}_e + Z_e\vec{k}_e \qquad (1.5\text{-}16)$$

$$X_e = X_h\vec{i}_h\cos\left(\frac{X}{r_o}\right)\vec{i}_h$$
$$+Y_h\vec{j}_h\left[-\sin\left(\frac{X}{r_o}\right)\sin\left(\frac{Y}{r_o}\right)\right]\vec{j}_h \qquad (1.5\text{-}17)$$
$$+Z_h\vec{k}_h\left[-\sin\left(\frac{X}{r_o}\right)\cos\left(\frac{Y}{r_o}\right)\right]\vec{k}_h$$

etc.,

$$\therefore X_e = X_h\cos\left(\frac{X}{r_o}\right) + Y_h\left[-\sin\left(\frac{X}{r_o}\right)\sin\left(\frac{Y}{r_o}\right)\right]$$
$$+Z_h\left[-\sin\left(\frac{X}{r_o}\right)\cos\left(\frac{Y}{r_o}\right)\right] \qquad (1.5\text{-}18)$$

$$Y_e = Y_h\cos\left(\frac{Y}{r_o}\right) + Z_h\left[-\sin\left(\frac{Y}{r_o}\right)\right]$$

$$Z_e = X_h\sin\left(\frac{X}{r_o}\right) + Y_h\left[\cos\left(\frac{X}{r_o}\right)\sin\left(\frac{Y}{r_o}\right)\right] \qquad (1.5\text{-}19)$$
$$+Z_h\left[\cos\left(\frac{X}{r_o}\right)\cos\left(\frac{Y}{r_o}\right)\right]$$

where X_h , Y_h , Z_h are given by Eq. (1.5-13).

(v) Body axes aerodynamic force components, X_b , Y_b , Z_b , are, from the unit vector transformation matrix, Eq. (1.4-23), Section 1.4.3,

$$\vec{R} = \vec{X}_b + \vec{Y}_b + \vec{Z}_b = X_b\vec{i}_b + Y_b\vec{j}_b + Z_b\vec{k}_b$$
$$= D\vec{i}_a + Q\vec{j}_Q + L\vec{k}_a \qquad (1.5\text{-}20)$$

$$X_b = -D\cos\alpha\cos\beta + Q\cos\alpha\sin\beta + L\sin\alpha$$
$$Y_b = D\sin\beta + Q\cos\beta \qquad (1.5\text{-}21)$$
$$Z_b = -D\sin\alpha\cos\beta + Q\sin\alpha\sin\beta - L\cos\alpha$$

For a general illustrative purpose, the method of graphical stepwise resolution of the aerodynamic force components on body axes by following the adopted sequence of angular rotations is presented in Figs. 1.9, 1.10 and 1.11. Similar stepwise geometrical presentations can be worked out for other transformation cases.

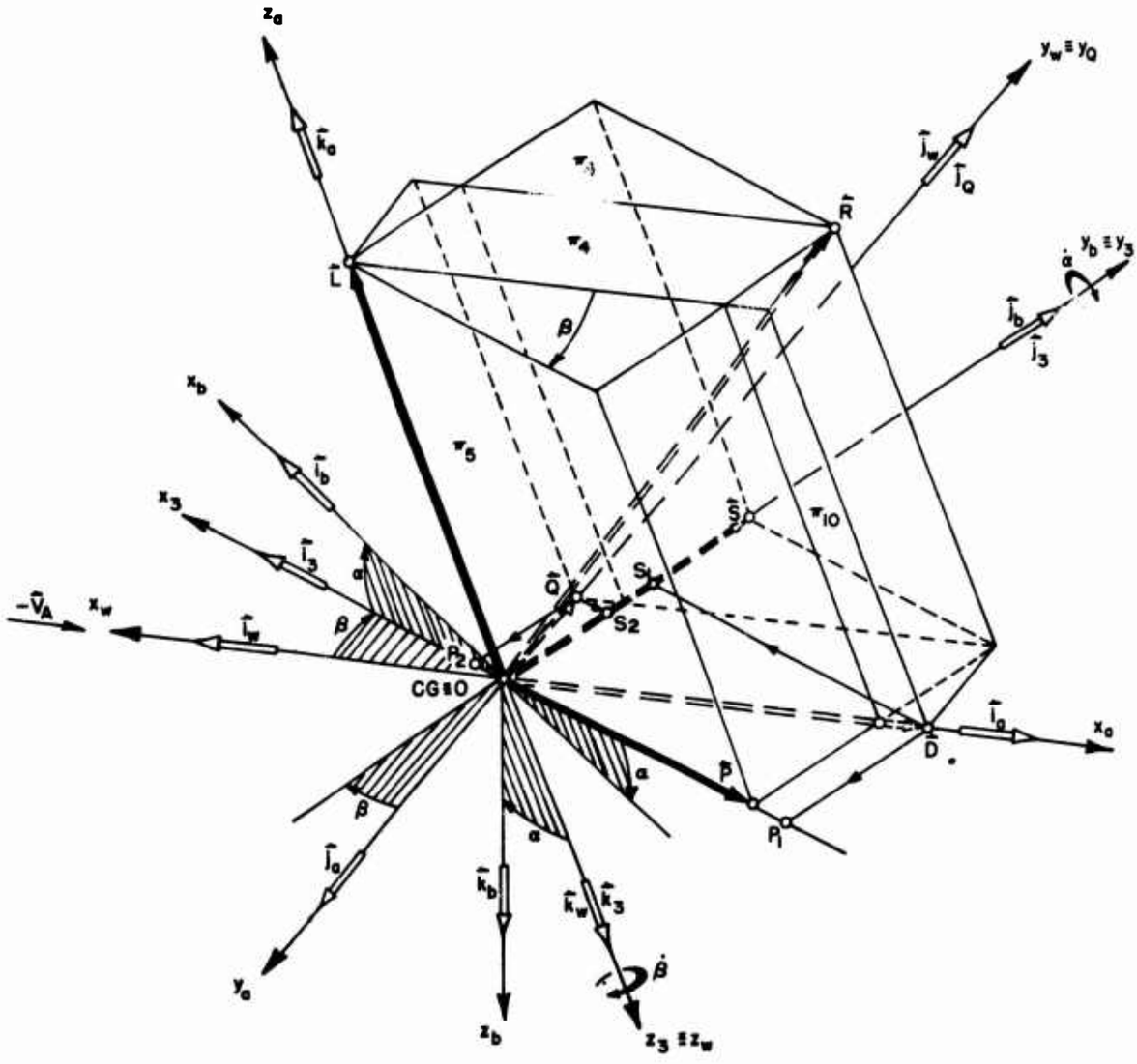

FIG. 1.9 (a)

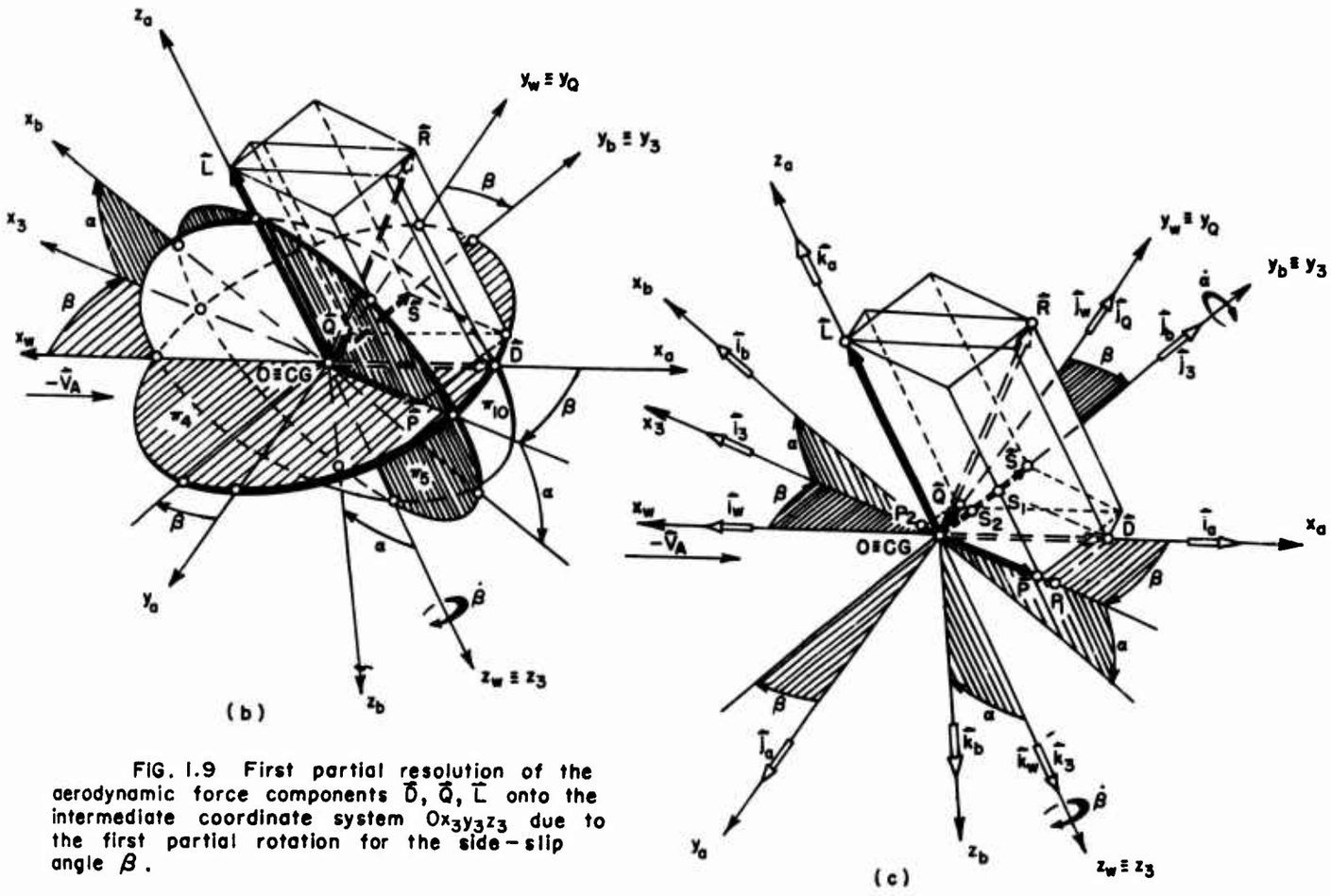

FIG. 1.9 First partial resolution of the aerodynamic force components $\vec{D}$, $\vec{Q}$, $\vec{L}$ onto the intermediate coordinate system $Ox_3y_3z_3$ due to the first partial rotation for the side-slip angle β.

GLOSSARY for Fig. 1.9

$Ox_3y_3z_3$ is the intermediate coordinate system obtained by the first partial rotation of the wind axes, $Ox_wy_wz_w$, through the side-slip angle, β, about the $Oz_3 \equiv Oz_w$ axis. The $Ox_3y_3z_3$ intermediate axes are collinear and cosensed with the respective $Ox_3y_bz_w$ axes.

The π_4, π_5 and π_{10} planes are as specified earlier (Section 1.4.3) i.e.:

The π_4 plane is coplanar with the Ox_wy_w (i.e. the Ox_ay_Q or the Ox_ay_a) plane. It contains the side-slip angle, β, as well as the Ox_a, Ox_w, Ox_3 and the Oy_a, $Oy_w \equiv Oy_Q$, Oy_3 and Oy_b axes. The π_4 plane is generally not the local geometrical tangent plane on a space trajectory.

The π_5 plane is coplanar with the Ox_bz_b (i.e. the Ox_3z_3) plane, which is the reference vertical plane of vehicle geometric symmetry. It contains the geometric angle-of-attack, α, as well as the Ox_3, Ox_b, and the Oz_3, Oz_w, Oz_a and Oz_b axes. The π_5 plane is generally not the geometrical local osculating plane on a space trajectory.

The π_{10} plane is coplanar with the Ox_az_a (i.e. the Ox_wz_w) plane, containing the $\vec{L}$ and $\vec{D}$ force vectors. The Oy_wz_w (i.e. the Ox_ay_a and Ox_ay_Q) plane is coplanar with the π_3 plane (see Fig. 1.12) containing the side force vector, $\vec{Q}$.

The resultant aerodynamic force components:

(i) In the $Ox_ay_Qz_a$ modified aerodynamic reference frame

$$\vec{R} = \vec{D} + \vec{Q} + \vec{L} = D\vec{i}_a + Q\vec{j}_Q + L\vec{k}_a \qquad (1.5\text{-}22)$$

(ii) In the first intermediate reference frame, $Ox_3y_3z_3$, resulting from a partial rotation through the side-slip angle, β,

$$\vec{R} = \vec{P} + \vec{S} + \vec{L} = P\vec{i}_3 + S\vec{j}_3 + L\vec{k}_3 \qquad (1.5\text{-}23)$$

$$\vec{P} = \vec{OP}_1 + \vec{OP}_2 = -(D\cos\beta - Q\sin\beta)\vec{i}_3 = -P\vec{i}_3 \qquad (1.5\text{-}24)$$

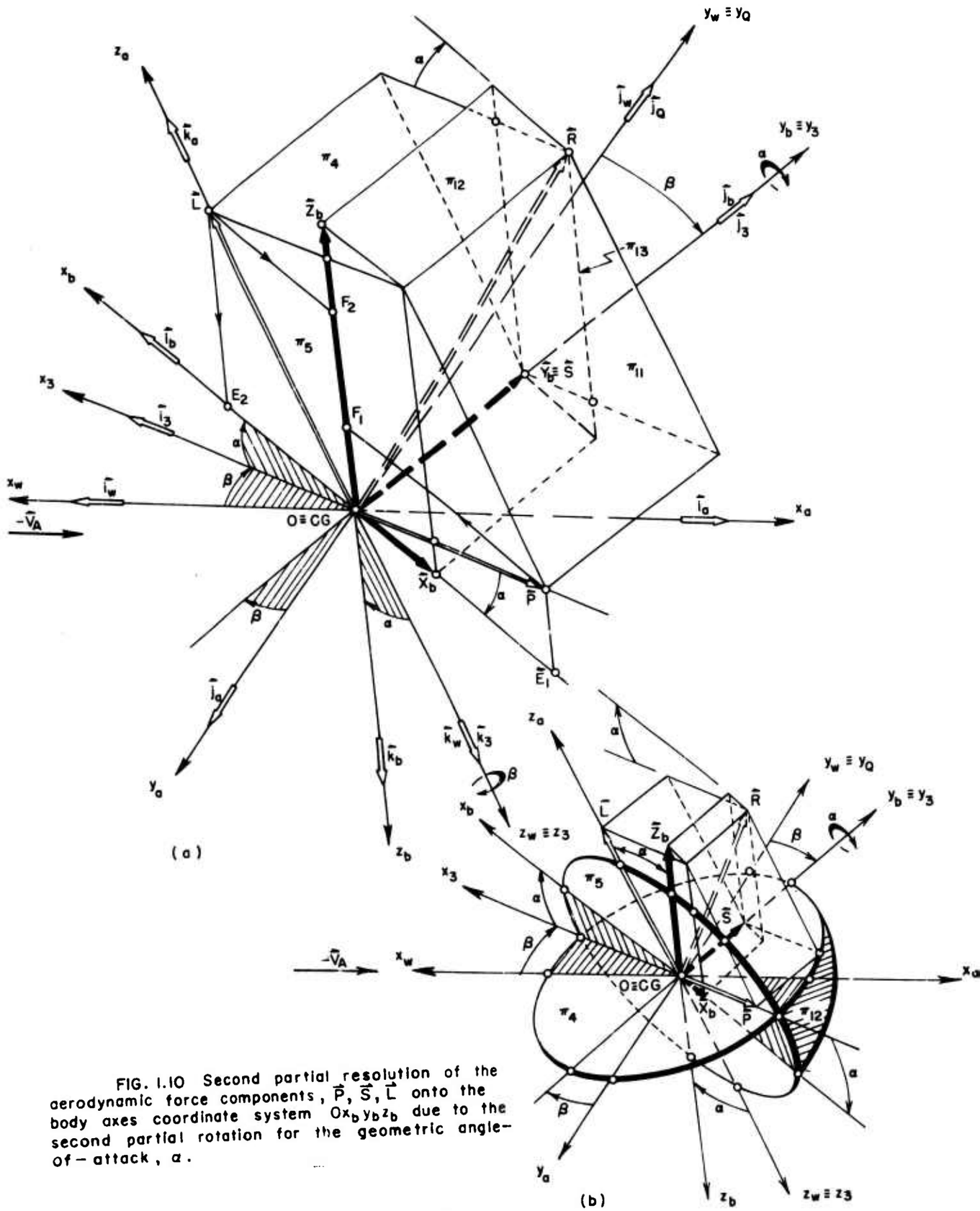

FIG. 1.10 Second partial resolution of the aerodynamic force components, $\vec{P}, \vec{S}, \vec{L}$ onto the body axes coordinate system $Ox_by_bz_b$ due to the second partial rotation for the geometric angle-of-attack, α.

$$\vec{S} = \vec{OS}_1 + \vec{OS}_2$$
$$= (D \sin\beta + Q\cos\beta)\vec{j}_3 = S\vec{j}_3 \qquad (1.5\text{-}25)$$
$$\therefore \vec{R} = -(D\cos\beta - Q\sin\beta)\vec{i}_3$$
$$+ (D\sin\beta + Q\cos\beta)\vec{j}_3 - L\vec{k}_3 \qquad (1.5\text{-}26)$$

GLOSSARY for Fig. 1.10

$Ox_by_bz_b$ is the body axes coordinate system, obtained by the second partial rotation of the intermediate coordinate system, $Ox_3y_3z_3$, through the geometric angle-of-attack, α, about the $Oy_b \equiv Oy_3$ axis.

The π_{12} plane is parallel to the Ox_by_b plane, i.e. to the π_7 plane in Fig. 1.5.

The π_{13} plane is parallel to the Ox_bz_b reference plane of symmetry, i.e. to the π_5 plane in Fig. 1.5.

The π_{11} plane is parallel to the Oy_bz_a (i.e. to the Oy_bz_w) plane.

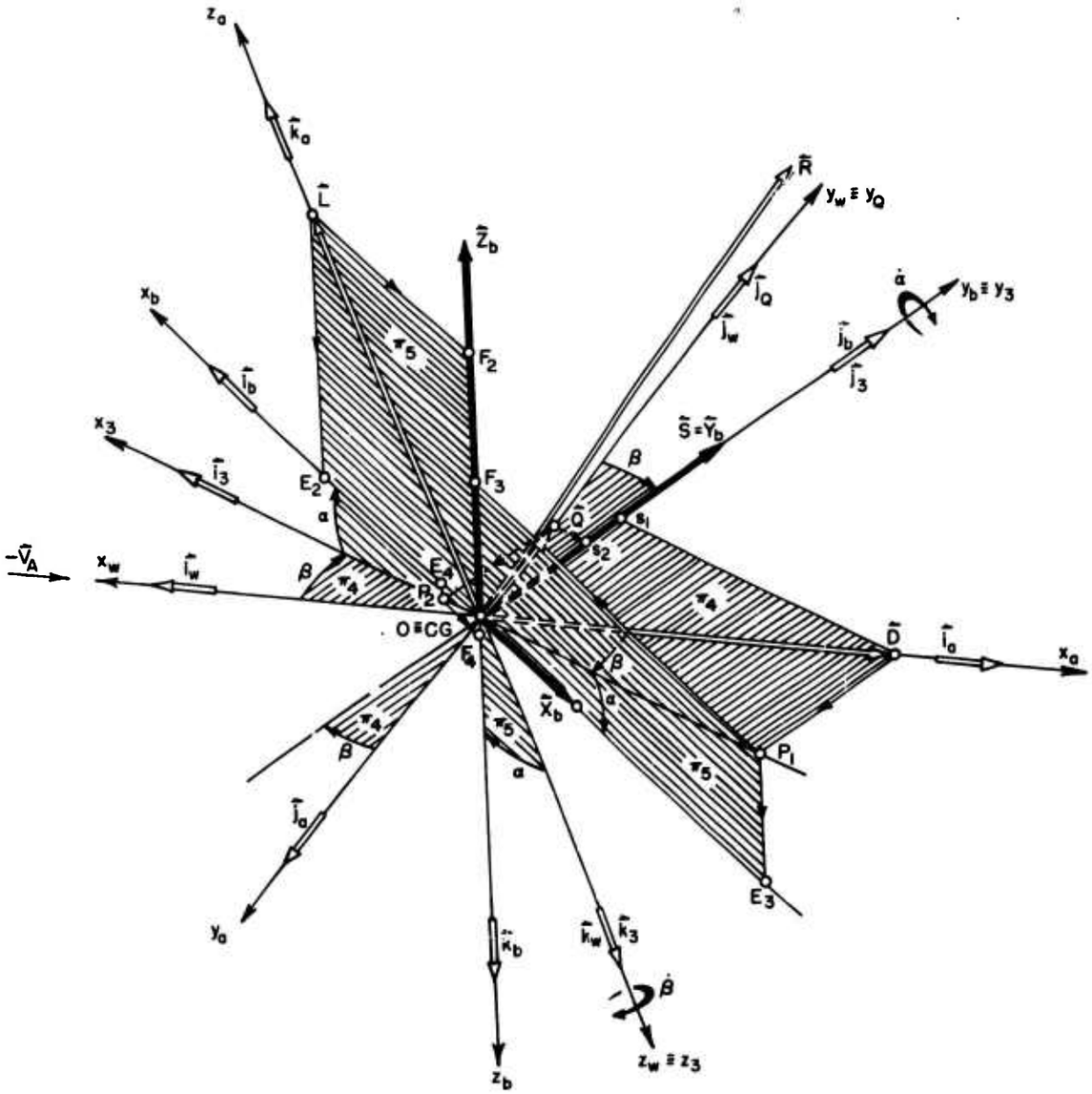

FIG. 1.11 Resultant resolution of the lift, $\vec{L}$, the drag, $\vec{D}$, and the side-force, $\vec{Q}$, vectors onto the body axes, $Ox_by_bz_b$, defining the normal, $\vec{Z}_b$, the axial, $\vec{X}_b$, and the lateral, $\vec{Y}_b$, forces.

The resultant aerodynamic force components:

(i) In the first intermediate reference frame, $Ox_3y_3z_3$, resulting from partial rotation through the side-slip angle, β,

$$\vec{R} = \vec{P} + \vec{S} + \vec{L} = P\vec{i}_3 + S\vec{j}_3 + L\vec{k}_3 \qquad (1.5\text{-}27)$$

$$\therefore R = (-D\cos\beta + Q\sin\beta)\vec{i}_3 + (D\sin\beta + Q\cos\beta)\vec{j}_3 - L\vec{k}_3 \qquad (1.5\text{-}28)$$

(ii) In the body axes reference frame resulting from partial rotation through the geometric angle-of-attack, α,

$$\vec{R} = \vec{X}_b + \vec{Y}_b + \vec{Z}_b = X_b\vec{i}_b + Y_b\vec{j}_b + Z_b\vec{k}_b \qquad (1.5\text{-}29)$$

$$\vec{X}_b = \overrightarrow{OE}_1 + \overrightarrow{OE}_2 = (-P\cos\alpha + L\sin\alpha)\vec{i}_b = \left[(-D\cos\beta + Q\sin\beta)\cos\alpha + L\sin\alpha\right]\vec{i}_b \qquad (1.5\text{-}30)$$

$$\vec{Y}_b = \vec{S} = (D\sin\beta + Q\cos\beta)\vec{j}_b \qquad (1.5\text{-}31)$$

$$\vec{Z}_b = \overrightarrow{OF}_1 + \overrightarrow{OF}_2 = (-P\sin\alpha - L\cos\alpha)\vec{k}_b = \left[(-D\cos\beta + Q\sin\beta)\sin\alpha - L\cos\alpha\right]\vec{k}_b \qquad (1.5\text{-}32)$$

$$\therefore \vec{R} = (-D\cos\beta\cos\alpha + Q\sin\beta\cos\alpha + L\sin\alpha)\vec{i}_b + (D\sin\beta + Q\cos\beta)\vec{j}_b + (-D\cos\beta\sin\alpha + Q\sin\beta\sin\alpha + L\cos\alpha)\vec{k}_b \qquad (1.5\text{-}33)$$

GLOSSARY for Fig. 1.11

Resolution of the aerodynamic force components on the $Ox_by_bz_b$ axes by direct geometrical projections, in terms of the side-slip angle, β, and the geometric angle-of-attack, α, are

$$\vec{R} = \vec{D} + \vec{Q} + \vec{L} = \vec{X}_b + \vec{Y}_b + \vec{Z}_b \qquad (1.5\text{-}34)$$

$$\vec{R} = D\vec{i}_a + Q\vec{j}_Q + L\vec{k}_a = -D\vec{i}_w + Q\vec{j}_w - L\vec{k}_w \qquad (1.5\text{-}35)$$

$$\vec{R} = X_b\vec{i}_b + Y_b\vec{j}_b + Z_b\vec{k}_b \qquad (1.5\text{-}36)$$

$$\vec{X}_b = \overrightarrow{OE}_3 + \overrightarrow{OE}_4 + \overrightarrow{OE}_2$$
$$\vec{X}_b = (D\cos\beta\cos\alpha)(-\vec{i}_b) + (Q\sin\beta\cos\alpha)\vec{i}_b + (L\sin\alpha)\vec{i}_b$$
$$\vec{X}_b = X_b\vec{i}_b = (-D\cos\beta\cos\alpha + Q\sin\beta\cos\alpha + L\sin\alpha)\vec{i}_b \qquad (1.5\text{-}37)$$

$$\vec{Y}_b = \overrightarrow{OS}_1 + \overrightarrow{OS}_2$$
$$\vec{Y}_b = (D\sin\beta)\vec{j}_b + (Q\cos\beta)\vec{j}_b \qquad (1.5\text{-}38)$$
$$\vec{Y}_b = Y_b\vec{j}_b = (D\sin\beta + Q\cos\beta)\vec{j}_b$$

$$\vec{Z}_b = \overrightarrow{OF}_3 + \overrightarrow{OF}_4 + \overrightarrow{OF}_2$$
$$\vec{Z}_b = (D\cos\beta\sin\alpha)(-\vec{k}_b) + (Q\sin\beta\sin\alpha)\vec{k}_b + L\cos\alpha(-\vec{k}_b)$$
$$\vec{Z}_b = Z_b\vec{k}_b = (-D\cos\beta\sin\alpha + Q\sin\beta\sin\alpha - L\cos\alpha)\vec{k}_b \qquad (1.5\text{-}39)$$

i.e. by algebraic values:

$$X_b = (-D\cos\alpha\cos\beta + Q\sin\beta\cos\alpha + L\sin\alpha)$$
$$Y_b = (D\sin\beta + Q\cos\beta) \qquad (1.5\text{-}40)$$
$$Z_b = (-D\cos\beta\sin\alpha + Q\sin\beta\sin\alpha - L\cos\alpha)$$

Alternatively by using the respective unit vectors transformation matrix, Eq. (1.4-23), Section 1.4:

$$\begin{bmatrix} X_b\vec{i}_b\cdot\vec{i}_b \\ Y_b\vec{j}_b\cdot\vec{j}_b \\ Z_b\vec{k}_b\cdot\vec{k}_b \end{bmatrix} = \begin{bmatrix} (-\cos\alpha\cos\beta) & (\cos\alpha\sin\beta) & (\sin\alpha) \\ (\sin\alpha) & (\cos\beta) & 0 \\ (-\sin\alpha\cos\beta) & (\sin\alpha\sin\beta) & (-\cos\alpha) \end{bmatrix} \begin{bmatrix} D\vec{i}_a\cdot\vec{i}_a \\ Q\vec{j}_Q\cdot\vec{j}_Q \\ L\vec{k}_a\cdot\vec{k}_a \end{bmatrix} \qquad (1.5\text{-}41)$$

$$X_b = \left[-D\cos\alpha\cos\beta + Q\cos\alpha\sin\beta + L\sin\alpha\right]$$
$$Y_b = \left[D\sin\alpha + Q\cos\beta\right] \qquad (1.5\text{-}42)$$
$$Z_b = \left[-D\sin\alpha\cos\beta + Q\sin\alpha\sin\beta - L\cos\alpha\right]$$

$$\therefore \vec{X}_b = X_b\vec{i}_b = \left[-D\cos\alpha\cos\beta + Q\cos\alpha\sin\beta + L\sin\alpha\right]\vec{i}_b$$
$$\vec{Y}_b = Y_b\vec{j}_b = \left[D\sin\alpha + Q\cos\beta\right]\vec{j}_b \qquad (1.5\text{-}43)$$
$$\vec{Z}_b = Z_b\vec{k}_b = \left[-D\sin\alpha\cos\beta + Q\sin\alpha\sin\beta - L\cos\alpha\right]\vec{k}_b$$

For the special case of no side-slip, $\beta=0$, and no side-force, $Q=0$, (i.e. a steady, rectilinear flight condition with no velocity roll angle, $\mu=0$, no bank angle, $\phi=0$, and no side-slip angle $\beta=0$; the Ox_bz_b plane being the geometric plane of symmetry for the overall vehicle configuration), the transformation equation (1.5-42) reduces to the simple form

$$X_b = -D\cos\alpha + L\sin\alpha$$
$$Y_b = 0 \qquad (1.5\text{-}44)$$
$$Z_b = -D\sin\alpha - L\cos\alpha$$

Alternatively, by introducing the aerodynamic normal force, $\vec{N}$, and the aerodynamic axial force, $\vec{C}$, concepts, viz.

$$\vec{C} = -X_b\vec{i}_b = -\vec{X}_b$$
$$\vec{N} = -Z_b\vec{k}_b = -\vec{Z}_b \qquad (1.5\text{-}45)$$

the Eq. (1.5-45) takes the familiar scalar form

$$C = D\cos\alpha - L\sin\alpha$$
$$N = D\sin\alpha + L\cos\alpha \qquad (1.5\text{-}46)$$

1.6 GEOMETRIC ANGLE-OF-ATTACK, α, AND SIDE-SLIP ANGLE, β, DEFINITIONS

The geometric angle-of-attack, α, and the side-slip angle, β, of a composite vehicle configuration are conventionally defined by the two respective sequences of partial rotations which would bring the local wind axes system, $Ox_w y_w z_w$, into the arbitrarily chosen body axes system, $Ox_b y_b z_b$ (see Fig. 1.12). The reference body axis, Ox_b, may be any convenient body-fixed reference line. It might be taken as a body-fixed line parallel to the mean aerodynamic chord, $\bar{c}_a$, or the mean geometric chord, $\bar{c}$. For bodies of revolution (non-lifting missiles), the reference axes might be taken as the center-line of the body. In general, the reference axis can be any line with respect to which the geometric angle-of-attack of a compound vehicle configuration can be purposefully specified.

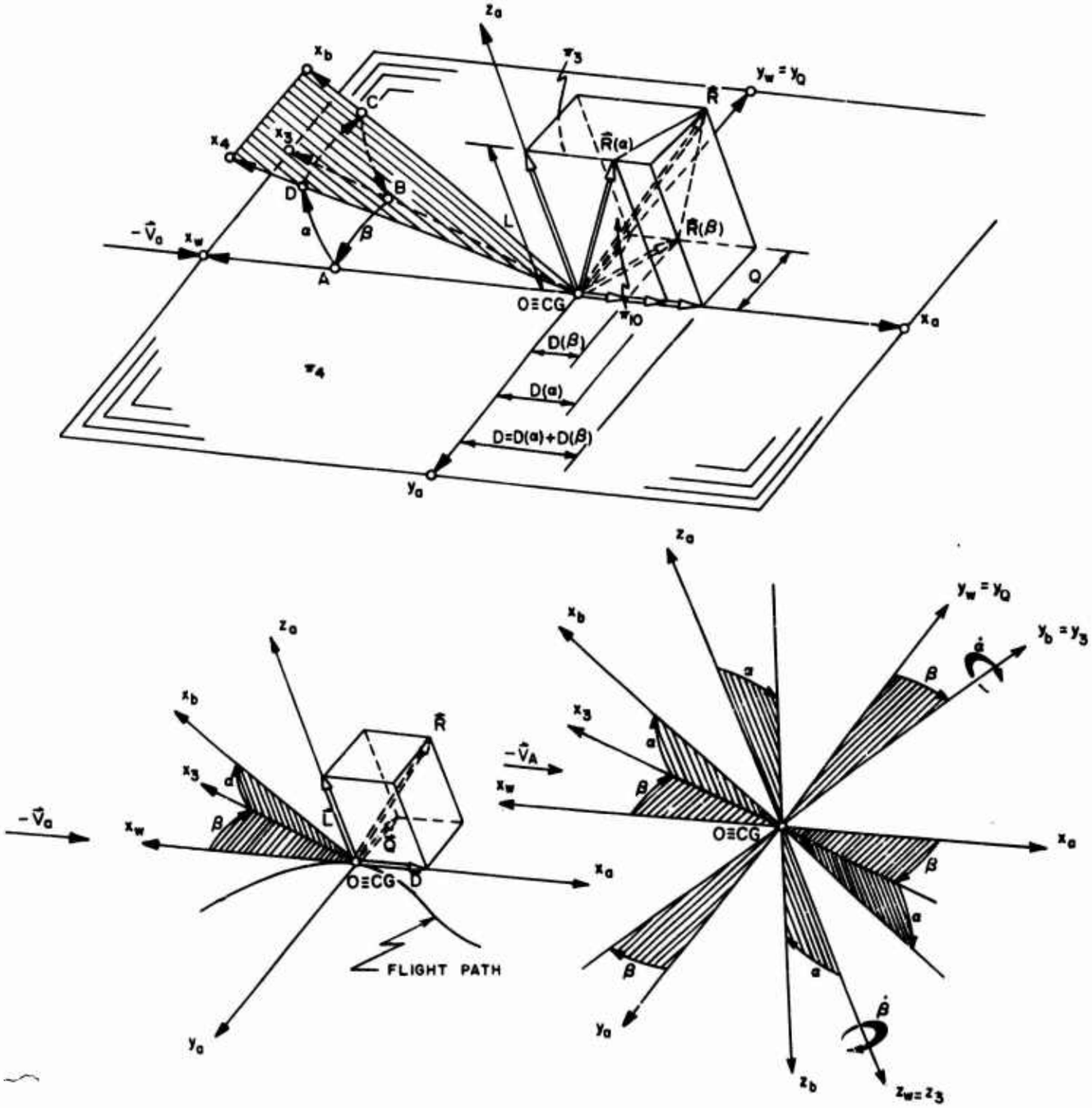

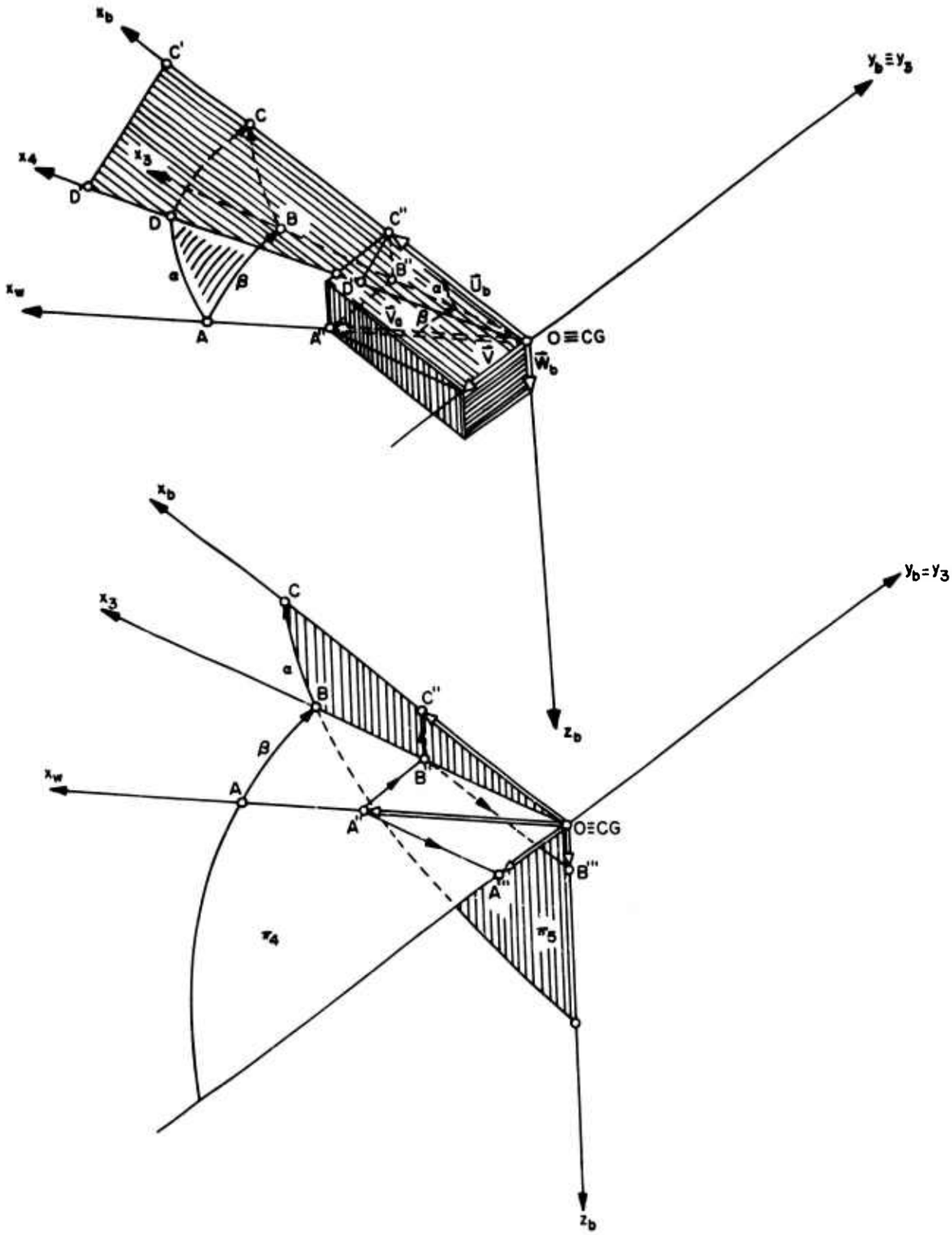

FIG. I.12 The adopted conventions for the aerodynamic force components and the aerodynamic angles definitions.

GLOSSARY for Fig. 1.12

The π_4 and π_5 planes contain the side-slip angle, β, and the geometric angle-of-attack, α, respectively. The π_4 and the $Ox_a y_a$, $Ox_w y_w$, $Ox_3 y_3$ and $Ox_b y_b$ planes are coplanar; they are generally not coplanar with the local tangent plane, Oz_b, on a space trajectory. The π_4 plane contains $\vec{D}(\beta)$, $\vec{D}(\alpha)$, $\vec{D}$, $\vec{Q}$, and $\vec{R}(\beta)$ force vectors. The π_5 plane is the reference (vertical) plane of symmetry, i.e. it is coplanar with the $Ox_b y_b$ and $Ox_3 y_b$ planes.

The π_3 plane is coplanar with the $Oy_a z_a$ and $Oy_w z_w$ planes, containing the $\vec{L}$ and $\vec{Q}$ aerodynamic force components.

The π_{10} plane is coplanar with the $Ox_a z_a$, $Ox_w z_w$ and $Ox_4 z_a$ planes, containing the $\vec{L}$, $\vec{D}$, $\vec{D}(\alpha)$, $\vec{D}(\beta)$ and $\vec{R}(\alpha)$ aerodynamic force components.

$Ox_a y_a z_a$, $Ox_a y_a z_a$, $Ox_w y_w z_w$ and $Ox_b y_b z_b$ are the classical left-hand aerodynamic, the modified right-hand aerodynamic, and the right-hand body axes reference frames respectively. The Ox_3 axis becomes conditionally the Ox_b body axis for $\alpha=0$. The Ox_4 axis becomes conditionally the Ox_b body axis for $\beta=0$.

Arc conventions. Arc $\widehat{DC}$ is in the $Ox_4 x_b$ skew plane. However, $\widehat{DC} \nparallel \widehat{AB}$ although $\widehat{DC}=\widehat{AB}=\beta$. In the same manner, $\widehat{AD} \nparallel \widehat{BC}$ although $\widehat{AD}=\widehat{BC}=\alpha$.

Velocity vectors conventions. $\vec{V}_A$ is the instantaneous, ambient flight, linear velocity vector of the vehicle CG, relative to the Standard Atmosphere at rest. $\vec{U}_b$, $\vec{V}_b$, and $\vec{W}_b$ are the instantaneous, ambient flight velocity vector components in the Eulerian, body-fixed reference frame $Ox_b y_b z_b$. The magnitudes and relative geometry of the velocity vectors are as follows:

$$\vec{V}_A = \vec{U}_b + \vec{V}_b + \vec{W}_b$$

$$\sphericalangle B''OC'' = \alpha = \tan^{-1}\frac{W_b}{U_b} = \sin^{-1}\frac{W_b}{V_A\cos\beta}$$

$$\sphericalangle A''OB'' = \beta = \sin^{-1}\frac{V_b}{V_A} = \tan^{-1}\frac{V_b}{V_A\cos\beta}$$

$$\overline{DC} \parallel \overline{D'C'} \parallel \overline{D''C''}$$

$$V_A = |\overrightarrow{OA''}|$$

$$U_b = |\overrightarrow{OC''}| = |\overrightarrow{B''B'''}|$$

$$V_b = |\overrightarrow{OA'''}| = |\overrightarrow{A''B''}| = V_A \sin\beta$$

$$W_b = |\overrightarrow{OB'''}| = |\overrightarrow{B''C''}|$$

$$W_b \csc\alpha = U_b \cos\alpha = |\overrightarrow{OB'''}| = |\overrightarrow{A''A'''}|$$

$$V_b \tan\beta = V_A \cos\beta = |\overrightarrow{OB'''}| = |\overrightarrow{A''A'''}| \qquad (1.6\text{-}1)$$

1.6.1 BASIC CONVENTIONS FOR THE GEOMETRIC ANGLE-OF-ATTACK, α, AND THE SIDE-SLIP ANGLE, β

The geometric angle-of-attack, α, is in the vehicle reference ("vertical") plane of symmetry, $Ox_b z_b$, contained between the Ox_3 and Ox_b axes. When the dynamic pressure "at infinity," is taken as a common reference for the aerodynamic force component definitions, $\vec{L}$, $\vec{D}$ and $\vec{Q}$, and when it is assumed that the individual flow patterns due to the geometric angle-of-attack, α, and the angle-of-side-slip, β, can be treated as partial and uncoupled; then the lift, $\vec{L}$, and the drag, $\vec{D}(\alpha)$, components are conditionally determined as if β were zero:

$$\vec{L} = L\vec{k}_a = [C_L q_A S_{ref}]\vec{k}_a = f_1(\alpha_a, M, Re, Pr, St, Kn) \qquad (1.6\text{-}2)$$

$$\vec{D}(\alpha) = D(\alpha)\vec{i}_a = [C_{D(\alpha)} q_A S_{ref}]\vec{i}_a = f_2(\alpha_a, M, Re, Pr, St, Kn) \qquad (1.6\text{-}3)$$

i.e. as if the geometric angle-of-attack, α, were in the $Ox_w z_w$ plane

$$\alpha \propto |\widehat{AD}| = |\widehat{BC}| \;;\; \widehat{AD} \nparallel \widehat{BC} \qquad (1.6\text{-}4)$$

In the same manner, assuming $\alpha=0$, the side-slip angle defines the $\vec{Q}$ and the $\vec{D}(\beta)$ components,

$$\vec{Q} = Q\vec{j}_Q = -Q\vec{j}_a = [C_Q q_A S_{ref}]\vec{j}_Q = f_3(\beta, M, Re, Pr, St, Kn) \qquad (1.6\text{-}5)$$

$$\vec{D}(\beta) = D(\beta)\vec{i}_a = [C_{D(\beta)} q_A S_{ref}]\vec{i}_a = f_4(\beta, M, Re, Pr, St, Kn) \qquad (1.6\text{-}6)$$

with the side-slip angle, β, contained in the $Ox_w y_w$ plane, i.e.:

$$\beta \propto |\widehat{AB}| = |\widehat{DC}| \;;\; \widehat{AB} \parallel \widehat{DC} \qquad (1.6\text{-}7)$$

Thus, the combined effects of the geometric angle-of-attack and the side-slip angle upon the aerodynamic force components are

$$\vec{R} = \vec{R}(\alpha) + \vec{R}(\beta) = \vec{L} + \vec{D} + \vec{Q} = \vec{L} + [\vec{D}(\alpha) + \vec{D}(\beta)] + \vec{Q} \quad (1.6\text{-}8)$$

for $\alpha \neq 0$ and $\beta \neq 0$, where

$$\vec{R}(\alpha) = \vec{L} + \vec{D}(\alpha); \quad \beta = 0, \ \alpha \neq 0$$

$$\vec{R}(\beta) = \vec{Q} + \vec{D}(\beta); \quad \beta \neq 0, \ \alpha = 0 \quad (1.6\text{-}9)$$

$$\vec{D} = \vec{D}(\alpha) + \vec{D}(\beta); \quad \beta \neq 0, \ \alpha \neq 0$$

For flight dynamics analysis purposes the α and the β angles are sometimes expressed in terms of the ambient flight velocity vector components, $\vec{U}_b$, $\vec{V}_b$, $\vec{W}_b$, on the body-fixed Eulerian, $Ox_b y_b z_b$, reference frame as

$$\alpha = \tan^{-1} \frac{W_b}{U_b} = \sin^{-1} \frac{W_b}{V_A \cos\beta} \quad (1.6\text{-}10)$$

$$\beta = \sin^{-1} \frac{V_b}{V_A} = \tan^{-1} \frac{V_b}{V_A \cos\beta} \quad (1.6\text{-}11)$$

$$\vec{V}_A = \vec{U}_b + \vec{V}_b + \vec{W}_b \quad (1.6\text{-}12)$$

As already stated in Section 1.4, a dynamically positive side-slip angle, β , creates a negative side-slip force, $\vec{Q}$, due to the adopted convention of a left-hand basic aerodynamic reference frame, $Ox_a y_a z_a$. In aerodynamic wind-tunnel practice, the equivalent negative aerodynamic "angle-of-yaw," σ , is sometimes substituted for the positive side-slip angle, β ,

$$\beta = -\sigma \quad (1.6\text{-}13)$$

thus coincidently allowing for a positive aerodynamic side-force, $\vec{Q}$, corresponding to a positive aerodynamic "angle-of-yaw," σ. This conditional "angle-of-yaw" convention is different from the actual "yaw" definition in flight dynamics trajectory analysis.(3,7)

Discounting the wind tunnel practices, the accepted counterclockwise positive senses of the partial angular rotations, β and α , by which the wind-axes, $Ox_w y_w z_w$, are brought to the body-axes, $Ox_b y_b z_b$, lead to the following conditions:

(i) In the right-hand, wind-axes reference frame, $Ox_w y_w z_w$, the lift, $\vec{L}$, and the drag, $\vec{D}$, aerodynamic force components are negative for positive values of the angle-of-attack, α , and the side-slip angle, β , while the side-force, $\vec{Q}$, is positive for positive values of the side-slip angle, β ,

$$\vec{L} = -L\vec{k}_w \text{ and } \vec{D} = -D\vec{i}_w \text{ for } (+\alpha), (+\beta) \quad (1.6\text{-}14)$$

$$\vec{Q} = +Q\vec{j}_w \text{ for } (+\beta) \quad (1.6\text{-}15)$$

(ii) In the modified right-hand aerodynamic reference frame, $Ox_a y_a z_a$, the lift, $\vec{L}$, and the drag, $\vec{D}$, aerodynamic force components are positive for positive values of the angle-of-attack, α , and the side-slip angle, β , while the side-force, $\vec{Q}$, is positive for a positive value of the side-slip angle, β ,

$$\vec{L} = L\vec{k}_a \text{ and } \vec{D} = D\vec{i}_a \text{ for } (+\alpha), (+\beta) \quad (1.6\text{-}16)$$

$$\vec{Q} = -Q\vec{j}_a = Q\vec{j}_Q \text{ for } (+\beta) \quad (1.6\text{-}17)$$

Following the adopted conventions for the breakdown of aerodynamic force components in terms of α and β, as illustrated in Fig. 1.12, the partial evaluations of L and D(α) in terms of α and of Q and D(β) in terms of β are performed separately, i.e. by treating the cases $\alpha \neq 0$, $\beta = 0$ and $\alpha = 0$, $\beta \neq 0$ independently. The resultant aerodynamic force components $\vec{L}$, $\vec{Q}$, and $\vec{D}$ for the more general case, when both α and β are not zero, is then conditionally obtained by the linear vectorial superposition of $\vec{L}$, $\vec{D}(\alpha)$, $\vec{D}(\beta)$ and $\vec{Q}$ as indicated by Eqs. (1.6-2) to (1.6-6). The interference effects between the partial flow patterns due to α and those due to β, in terms of the configuration elements, are thus not included. The linear superposition assumption is formally valid in terms of the vectorial resolution in Fig. 1.12, and may eventually be acceptable within idealized fluid flow theoretical premises. However, the real flow patterns, including the interferences between various configuration parts as assembled in a compound vehicle configuration, will not necessarily be represented by the supposed linear superposition of the α and the β effects. But, due to the extreme complexities of the real fluid flows, even when treated in their simplest forms, the tentative linear superposition of the partially evaluated aerodynamic components is retained by necessity in engineering practice. An illustration of the method, as applied to compound vehicle configurations, is given next.

1.6.2 AN ILLUSTRATION OF THE REPRESENTATIVE ANGLE-OF-ATTACK AND THE DEFINITION FOR COMPOUND VEHICLE GEOMETRIES

For actual flight dynamics conditions, on a general space trajectory, the instantaneous values of the aerodynamic lift, $\vec{L}$, the aerodynamic drag, $\vec{D}$, and the aerodynamic side-force, $\vec{Q}$, at a given instant of time, t, are in

general intricate functions of all the involved geometrical, dynamical and aerodynamical governing parameters, as they pertain to the investigated flight occurrence and the compound vehicle geometry. Even in cases where a quasi-steady equilibrium flight condition is assumed, at an instant of time on an arbitrary flight trajectory under Standard Atmospheric conditions, the aerodynamic forces are intricate functions of many fluid flow and flight dynamics parameters. Thus, for instance, the total lift force $\vec{L}$, comprises (under the above restrictive conditions) the sum of the individual lift vectors of all the assembled parts of a given compound vehicle configuration, including many forms of aerodynamic interference effects of the resultant flow pattern:

$$\vec{L} = \sum^{n} \vec{L}_i = \sum^{n} L_i \vec{K}_a \qquad (1.6\text{-}18)$$

$$\sum_{i=1}^{n} L_i = f(\alpha_i, \beta_i, M_i, Ke_i, St_i, \qquad (1.6\text{-}19)$$

$$Pr_i, \delta_E, \delta_A, \delta_R, \ldots)$$

Similar implicit functional dependencies may be written for the total drag, $\tilde{D}$, and the total side-force, $\tilde{Q}$.

Assuming that the governing physical properties of the gaseous medium and the fluid flow pattern are known for a steady flight speed, flight altitude and a standard atmospheric density at a given instant of time; the resultant aerodynamic lift, $\tilde{L}$, the aerodynamic drag, $\tilde{D}$, and the aerodynamic side-force, $\tilde{Q}$, can be expressed as functions of the conditionally defined, representative aerodynamic angle-of-attack, α_a, and the representative aerodynamic side-slip angle, β_a, of the overall vehicle configuration by using the classical uniform steady flow aerodynamic conventions

$$L = C_L q_A S_{ref}, \quad C_L = f_1(\alpha_a, \beta_a)$$

$$Q = C_Q q_A S_{ref}, \quad C_Q = f_2(\alpha_a, \beta_a) \qquad (1.6\text{-}20)$$

$$D = C_D q_A S_{ref}, \quad C_D = f_3(\alpha_a, \beta_a)$$

The representative values of α_a and β_a can then be obtained by a simultaneous solution of the respective six governing equations of motion, under the instantaneous dynamic steady state equilibrium flight conditions, in terms of: the required aerodynamic control deflections, δ_E, δ_A, δ_R; the velocity yaw, χ; the velocity pitch, γ: the velocity roll, μ; and the thrust vector parameters. For direct aerodynamic force estimates the six degrees of freedom procedure is complex. Instead, the aerodynamic force dependence on the representative angle-of-attack, α_a, and the representative side-slip angle, β_a, is evaluated separately, i.e. by assuming conditionally uncoupled cases of $\alpha_a \neq 0$, $\beta = 0$ and of $\alpha_a = 0$, $\beta_a \neq 0$.

The simplified case of $\alpha_a \neq 0, \beta_a = 0$ is presented below. In this case: the flight trajectory is necessarily confined to the vertical plane $Ox_h z_h$ respective to a flat EARTH; the vehicle possesses a geometrical plane of symmetry $Ox_b z_b$, coincident with the $Ox_h z_h$ and the $Ox_w z_w$ planes; the velocity roll angle is zero, $\mu = 0$; and $\delta_A = \delta_R = 0$; i.e. $\tilde{Q} = 0$ and $\tilde{D}(\beta) = 0$.

For the equilibrium steady flight condition in the vertical plane, including all other restraints specified above, the instantaneous resultant lift, $\tilde{L}$, and drag, $\tilde{D}(\alpha)$, aerodynamic force components become functions of a conditionally defined representative aerodynamic angle-of-attack of the overall vehicle configuration

$$\alpha_a = \alpha - \alpha_0 \qquad (1.6\text{-}21)$$

where α_0 is called the representative zero-lift angle-of-attack. Only when the reference body axis, Ox_b, is specifically chosen such that $\alpha_0 = 0$, does the geometric angle-of-attack, α, become numerically equal to the aerodynamic angle-of-attack, α_a. A convenient fixing of the reference body axis, Ox_b, is dependant upon the body geometry as illustrated in Figs. 1.13 and 1.14.

For simple and isolated body geometries taken individually, the specific zero-lift condition for each is acquired when the respective aerodynamic angle-of-attack, $(\alpha_a)_i$, which is defined with respect to the first aerodynamic axis (or the zero-lift line) is equal to zero,

$$(\alpha_a)_i = (\alpha)_i - (\alpha_0)_i = 0$$

where $(\alpha_0)_i$, (usually numerically negative) is sometimes called the zero-lift angle, contained between the chosen geometric reference line, Ox_b, (i.e. between the reference wing or airfoil chord, $\bar{c}$ or $\bar{c}_a$, or the body ℓ, etc.) and the first aerodynamic axes (see Fig. 1.13). Historicaly, both the zero-lift angle, $(\alpha_0)_i$, and the geometric angle-of-attack, $(\alpha)_i$, are a consequence of analytical expressions adopted for the airfoil geometry definitions, which are either functionally or numerically

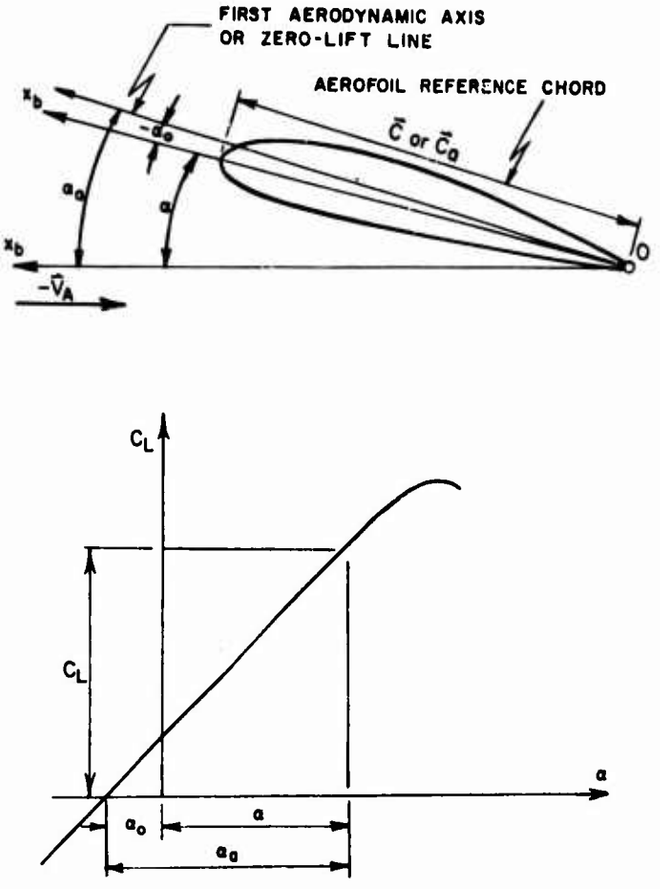

FIG. 1.13 The conventional angle-of-attack definitions for two-dimensional aerofoils, $\beta=0$.

referred to a geometrically convenient, but aerodynamically arbitrary, configurational reference chord, $\vec{c}$.(2,10) Axisymmetric bodies of revolution and symmetric two-dimensional (with respect to Ox_b or $\vec{c}$) airfoils have the singular aerodynamic properties

$$(\alpha_0)_i = 0 \qquad (\alpha_a)_i = (\alpha)_i \qquad (1.6\text{-}22)$$

For all other simple and isolated body geometries which do not possess a geometric axis of symmetry, such as general three-dimensional aerodynamic shapes, two-dimensional cambered airfoils, three-dimensional airfoil shapes composed of cambered two-dimensional airfoils (i.e. for body geometries having aerodynamic and/or geometric spanwise twist, etc.), the general condition is that $\alpha_0 \neq 0$. Evidently this holds for three-dimensional airfoils having a geometric twist, even in case of a spanwise distribution of symmetric sectional airfoils.

For compound vehicle configurations, a common Ox_b reference line is defined which may or may not be coincident with the aerodynamic or geometric angle-of-attack reference line of any one of the individual components. A representative geometric angle-of-attack, α, for the total vehicle configuration is thus referred to such an arbitrarily chosen, common Ox_b axis. The conditional definitions of the representative geometric angle-of-attack, α, and the zero-lift angle, α_0, of such compound configurations depend in each case on both the choice of the common geometric reference, Ox_b, and the related aerodynamic characteristics of various individual parts. The problem of finding the representative values of α and α_0 is thus necessarily treated specifically for every given overall design concept of a vehicle. As an example, in Fig. 1.15 a tentative formulation of the geometric angles-of-attack $(\alpha)_i$, and the zero-lift angles-of-attack $(\alpha_0)_i$, for the individual constituent parts of a vehicle geometry is illustrated. Analytical expressions for the overall representative angle-of-attack and the representative zero-lift angle of the specified compound vehicle configuration are of the type illustrated by Eqs. (1.6-56) and (1.6-57), respectively.

GLOSSARY for Fig. 1.14

Angular convention in aerodynamic analysis. All aerodynamic and geometric angles sensed clockwise from the $(-V_A)$ direction toward the respective reference lines are positive. The zero-lift angles-of-attack are measured from the first aerodynamic axis to the reference lines, positive clockwise (i.e. they are negative in the illustrative example). The wing and the horizontal tail built-in angles, i_W and i_T, are positive when measured clockwise from the common reference line, ℓ, to $\vec{c}_W$ and $\vec{c}_T$ respectively (i.e. i_W is positive and i_T is negative in the illustration). The elevator deflection angle, δ_E, is positive clockwise (i.e. downward) from the horizontal tail mean chord, $\vec{c}_T$, in accordance with the general rule, valid for all control surfaces: a positive angular control deflection results in a negative moment increment about the vehicle CG.

Reference lines. Ox_b is an arbitrary, body-fixed common reference line. For convenience it is usually chosen through the vehicle CG. In the illustration it is assumed that Ox_b is collinear with the body ℓ. $\vec{c}_W$ and $\vec{c}_T$ are the mean geometric (or mean aerodynamic)

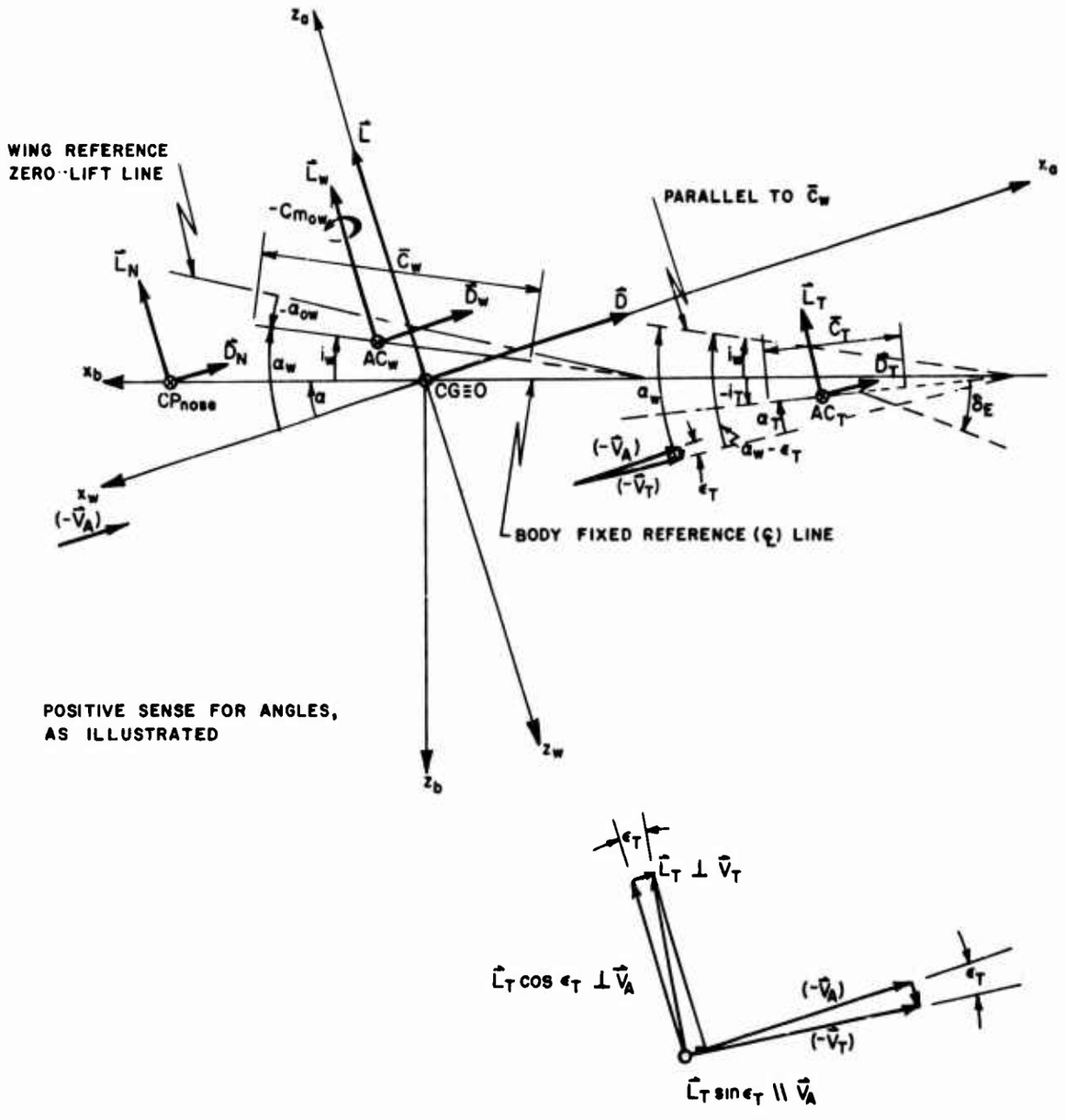

FIG. 1.14 A schematic illustration of the representative geometric angle-of-attack definitions for a compound vehicle configuration, consisting of a body with a nose-cone (or ogive), a wing, and a horizontal and vertical tail, arranged in a classical manner. No propulsion or base pressure effects included. The equivalent to a zero side slip condition assumed, $\beta = 0$.

chords of the wing and the horizontal tail, respectively.

The first aerodynamic axis (or the zero-lift line) of the wing (or of the horizontal tail) exists when cambered airfoils are used. It is assumed that the horizontal tail is composed of symmetric airfoils with no geometric twist spanwise.

Angular values. $\epsilon_T = [\epsilon_o + (\partial\epsilon_T/\partial\alpha_w)\alpha_w]$ is the linear functional form of the downwash angle (negative) due to the wing, evaluated at the horizontal tail. No other interference effects (fuselage, power unit, etc.) on the downwash are considered.

α_W is the wing geometric angle-of-attack, assuming no upwash due to fore-

body presence, blanking of the wing central portion due to the body and no power plant effects (jets or propellers). A tentative combined wing plus central body plus power plant value of a_{wb} and $a_{o_{wb}}$ can be defined and a correspondingly corrected form of the $C_{L_{wb}} = a_{wb}(a_{wb} - a_{o_{wb}})$ functional law correctly introduced.

Local force and moment reduction points. CP_{NOSE} is the center-of-pressure for a conical (or ogive) nose section, representing the action point for the $\vec{L}_N \perp \vec{V}_A$ and $\vec{D}_N \perp \vec{V}_A$ forces. When the influence of the front part of the body (fuselage) is introduced, the CP_N, $\vec{L}_N$ and $\vec{D}_N$ numerically change to their combined forebody (nose plus front-part of body proper) values. AC_w and AC_T are the wing and the horizontal tail aerodynamic centers respectively, as defined in the aerodynamic theory. $CG \equiv O$ is the common force and moment reduction point for the overall vehicle configuration.

Aerodynamic forces. L, D, L_N, D_N, L_W, D_W, L_T, D_T are the total, the nose cone, the wing and the horizontal tail individual lift and drag force components, normal and parallel to the local relative flow velocity vectors respectively, i.e. in accordance with the introduced assumptions that: L, L_N and L_W are normal to $(-\vec{V}_A)$; D, D_N and D_W are coparallel to $(-\vec{V}_A)$; L_T is normal to $\vec{V}_T$; and D_T is parallel to $\vec{V}_T$.

No pitching moments are indicated except for $C_{m_{o_w}}$ which implies a cambered wing.

The expression for lift force is

$$L = L_N + L_w + L_T \cos\epsilon_T - D_T \sin\epsilon_T$$

$$\epsilon_T = \epsilon_0 + \frac{\partial \epsilon_T}{\partial a_w} a_w \qquad (1.6\text{-}23)$$

then for small values of a_w and ϵ_T:

$$\cos\epsilon_T \approx 1, \quad \sin\epsilon_T \approx \epsilon_T, \quad D_T \ll L_T, \quad D_T \epsilon_T \approx 0$$

$$\vec{L} \approx \vec{L}_N + \vec{L}_W + \vec{L}_T \qquad (1.6\text{-}24)$$

$$\vec{L} = L\vec{k}_a \approx (L_N + L_W + L_T)\vec{k}_a \qquad (1.6\text{-}25)$$

$$\therefore L = L_N + L_W + L_T \qquad (1.6\text{-}26)$$

$$C_L \frac{\rho_A V_A^2}{2} S_{ref} = C_{L_N} \frac{\rho_A V_A^2}{2} S_N + C_{L_W} \frac{\rho_w V_w^2}{2} S_W + C_{L_T} \frac{\rho_T V_T^2}{2} S_T \qquad (1.6\text{-}27)$$

$$\therefore C_L = C_{L_N} \frac{S_N}{S_{ref}} + C_{L_W} \frac{S_W}{S_{ref}} + C_{L_T} \frac{S_T}{S_{ref}} \eta_T \qquad (1.6\text{-}28)$$

where:

ϵ_T is the angle of downwash at the horizontal tail.

S_N, S_W, S_T are individual reference areas of the nose cone, the wing and the horizontal tail, respectively.

S_{ref} is any common representative reference area of the total vehicle configuration.

q_A, q_W, q_T are the common free stream at infinity, and the corrected wing and horizontal tail dynamic pressures, respectively.

The specific q_W and q_T values comprise the upwash, the downwash and the power unit interference effects on the wing and the horizontal tail dynamic pressures values "in situ" (i.e. in the assembly). For subsonic speeds[18] $V_W/V_A \sim O(1)$ and $V_T/V_A \sim O(0.9\text{-}1.1)$. In this illustrative case it will be assumed that $q_A \approx q_W$, while the factor $q_T/q_A = \eta_T$ is retained. Further, it is customary that:

S_W is taken as the wing planform area, i.e. the projected area in the $Ox_b y_b$ plane of either the total or the exposed wing area, depending on the choice of the method of aerodynamic analysis.

S_{ref} is taken as the cone base area,

S_N is taken as the horizontal tail platform area, i.e. its projected area (total or exposed) in the $Ox_b y_b$ plane.

S_T is usually taken either equal to S_W (aircraft) or equal to the maximum cross-sectional area of the vehicle body (missiles). More generally, it can be any convenient common reference area for the compound missile configuration.

Within the concepts of the perfect inviscid fluid flow theory, the individual lift coefficients of the constituent parts can be conditionally expressed in terms of the respective individual aerodynamic angles-of-attack, $(a_a)_i$, and the individual lift curve slopes, $(a_i) \equiv (C_{L_a})_i \equiv (\partial C_L/\partial a)_i$.

Thus for the given illustrative example, assuming that the nose cone is substantially the lift producing representative part of the missile forebody:

$$a_{aN} = a_N - a_{ON} \qquad (1.6\text{-}29)$$

$$C_{L_N} = a_N a_{aN} = a_N a_N = a_N a, \quad a_{ON} \equiv O; \quad \epsilon_N \equiv O \qquad (1.6\text{-}30)$$

$$\alpha_{o_W} = \alpha_W - \alpha_{OW} \tag{1.6-32}$$

$$C_{L_W} = a_W(\alpha_W - \alpha_{OW}) = a_W(\alpha + i_W + \alpha_{OW});\ \epsilon_W = 0 \tag{1.6-33}$$

$$\alpha_{o_T} = \alpha_T - \alpha_{OT};\ \alpha_{OT} = 0,\ \epsilon_T = \epsilon_0 + \frac{\partial \epsilon_T}{\partial \alpha_W}\alpha_W \tag{1.6-34}$$

$$C_{L_T} = a_T\alpha_{o_T} + a_E\delta_E = a_T\alpha_T + \frac{\partial C_{L_T}}{\partial \alpha_T}\frac{\partial \alpha_T}{\partial \delta_E}\delta_E \tag{1.6-35}$$

$$C_{L_T} = a_T(\alpha_T + \frac{\partial \alpha_T}{\partial \delta_E}\delta_E);\ a_T = \frac{\partial C_{L_T}}{\partial \alpha_T} \tag{1.6-36}$$

$$\alpha_T = (\alpha_W - \epsilon_T + i_T - i_W) \tag{1.6-37}$$

$$C_{L_T} = a_T(\alpha_W - \epsilon_T + i_T - i_W) + a_T\frac{\partial \alpha_T}{\partial \delta_E}\delta_E \tag{1.6-38}$$

$$C_{L_T} = a_T(\alpha_W - \epsilon_0 - \frac{\partial \epsilon_T}{\partial \alpha_W}\alpha_W + i_T - i_W) + a_T\frac{\partial \alpha_T}{\partial \delta_E}\delta_E \tag{1.6-39}$$

$$C_{L_T} = a_T\alpha_W(1 - \frac{\partial \epsilon_T}{\partial \alpha_W}) - a_T(\epsilon_0 - i_T + i_W) + a_T\frac{\partial \alpha_T}{\partial \delta_E}\delta_E \tag{1.6-40}$$

$$C_{L_T} = a_T(\alpha + i_W)(1 - \frac{\partial \epsilon_T}{\partial \alpha_W}) - a_T(\epsilon_0 - i_T + i_W) + a_T\frac{\partial \alpha_T}{\partial \delta_E}\delta_E \tag{1.6-41}$$

$$C_{L_T} = a_T\alpha(1 - \frac{\partial \epsilon_T}{\partial \alpha_W}) - a_T(\epsilon_0 - i_T + i_W\frac{\partial \epsilon_T}{\partial \alpha_W}) + a_T\frac{\partial \alpha_T}{\partial \delta_E}\delta_E \tag{1.6-42}$$

$$a_N = \frac{\partial C_{L_N}}{\partial \alpha_N} = \frac{\partial C_{L_N}}{\partial \alpha};\ \alpha_N = \alpha,\ \alpha_{ON} \equiv 0,\ \epsilon_N \equiv 0 \tag{1.6-43}$$

$$a_W = \frac{\partial C_{L_W}}{\partial \alpha_W} = \frac{\partial C_{L_W}}{\partial \alpha};\ \alpha_{OW} = \text{const.},\ i_W = \text{const.},\ \epsilon_W \equiv 0 \tag{1.6-44}$$

$$a_T = \frac{\partial C_{L_T}}{\partial \alpha_T};\ \alpha_{OT} \equiv 0,\ i_T = \text{const.},\ i_W = \text{const.},\ \epsilon_T = \epsilon_0 + \frac{\partial \epsilon_T}{\partial \alpha_W}\alpha_W, \tag{1.6-45}$$

and $a_E = \frac{\partial C_{L_T}}{\partial \delta_E} = \frac{\partial C_{L_T}}{\partial \alpha_T}\frac{\partial \alpha_T}{\partial \delta_E}$ is the elevator lift effectiveness referred to S_T and q_T, where $\partial \alpha_T/\partial \delta_E$ is the elevator angle effectiveness, i.e. the rate of change of α_T due to δ_E. Also

$$\alpha_{o_N} = \alpha_N - \alpha_{o_N} = \alpha_N = \alpha;\ \alpha_{o_N} \equiv 0,\ \epsilon_N \equiv 0 \tag{1.6-46}$$

$$\alpha_{o_W} = \alpha_W - \alpha_{o_W} = \alpha + i_W - \alpha_{o_W};\ \epsilon_W \equiv 0 \tag{1.6-47}$$

$$\alpha_{o_T} = \alpha_T - \alpha_{o_T} = \alpha_T = (\alpha_W - i_W + i_T - \epsilon_T);\ \alpha_{o_T} \equiv 0 \tag{1.6-48}$$

$$\therefore \alpha_{o_T} = \alpha_T = (\alpha_W - \epsilon_0 - \frac{\partial \epsilon_T}{\partial \alpha_W}\alpha_W - i_W + i_T);\ \epsilon_0 \approx \text{constant} \tag{1.6-49}$$

where ϵ_0 is the downwash angle at the horizontal tail due to zero geometric angle-of-attack of the wing, $\alpha_W = 0$. Also i_W and i_T are the geometric "built-in" incidence angles of the wing and the horizontal tail respectively, relative to the adopted common reference line, Ox_b, conditionally positive measured clockwise from the Ox_b axis. For the sake of generalization in the above expressions, both i_W and i_T appear as algebraic terms, i.e. they are algebraically added to the respective α_W and α_T geometric angle-of-attack values. As a result, in this specific case, the i_W angle of geometric incidence is positive and the i_T angle of geometric incidence is negative, i.e. their respective positive and negative numerical values should be substituted in the algebraic equations above.

Note that the nose section lift coefficient is explicitly:

$$C_{L_N} = \frac{L_N}{\frac{1}{2}\rho_A V_A^2 S_N} \tag{1.6-50}$$

where, according to Fig. 1.15

$$\vec{L}_N = \vec{L}_{N_1} + \vec{L}_{N_2}$$
$$\vec{L}_N = L_N\vec{k}_a = (L_{N_1} + L_{N_2})\vec{k}_a \tag{1.6-51}$$
$$L_N = Z_b\cos\alpha_N - X_b\sin\alpha_N$$

Note also that, in general, a_w, a_W and a_{ow} are the average values for the three-dimensional effects, the fuselage-wing interference effects, the upwash, the partial "shading" of the central portion of the wing planform by the fuselage, the aerodynamic and geometric spanwise wing airfoil twisting, the power plant (pull propeller) effects, etc. The same implicitly holds for the respective horizontal tail average values of a_T, α_T and α_{oT}, in addition to the explicit corrections due to ϵ_T, q_T, etc. as sketched in Fig. 1.14.

Explicitly, the total lift coefficient for the compound vehicle configuration is then obtained conditionally by the aerodynamic definition analogy

$$C_L = a(\alpha - \alpha_o) \tag{1.6-52}$$

or in terms of the componental parts:

$$C_L = a_N \alpha \frac{S_N}{S_{ref}} + a_W(\alpha + i_W - \alpha_{OW})\frac{S_W}{S_{ref}} + \left[a_T \alpha\left(1-\frac{\partial \epsilon_T}{\partial \alpha_W}\right) - a_T(\epsilon_O - i_T + i_W \frac{\partial \epsilon_T}{\partial \epsilon_W}) + a_T \frac{\partial \alpha_T}{\partial \delta_E}\delta_E\right]\frac{S_T}{S_{ref}}\eta_T \quad (1.6\text{-}53)$$

$$C_L = a_W \frac{S_W}{S_{ref}}\left[\left(\frac{a_N}{a_W}\frac{S_N}{S_W}+1\right)+\frac{a_T}{a_W}\frac{S_T}{S_W}\eta_T\left(1-\frac{\partial \epsilon_T}{\partial \alpha_W}\right)\right] \cdot \left[\alpha - \frac{(\alpha_{OW}-i_W)+\frac{a_T}{a_W}\frac{S_T}{S_W}\eta_T\left[(\epsilon_O - i_T + i_W\frac{\partial \epsilon_T}{\partial \alpha_W}) - \frac{\partial \alpha_T}{\partial \delta_E}\delta_E\right]}{\left(\frac{a_N}{a_W}\frac{S_N}{S_W}+1\right)+\frac{a_T}{a_W}\frac{S_T}{S_W}\eta_T\left(1-\frac{\partial \epsilon_T}{\partial \alpha_W}\right)}\right] \quad (1.6\text{-}54)$$

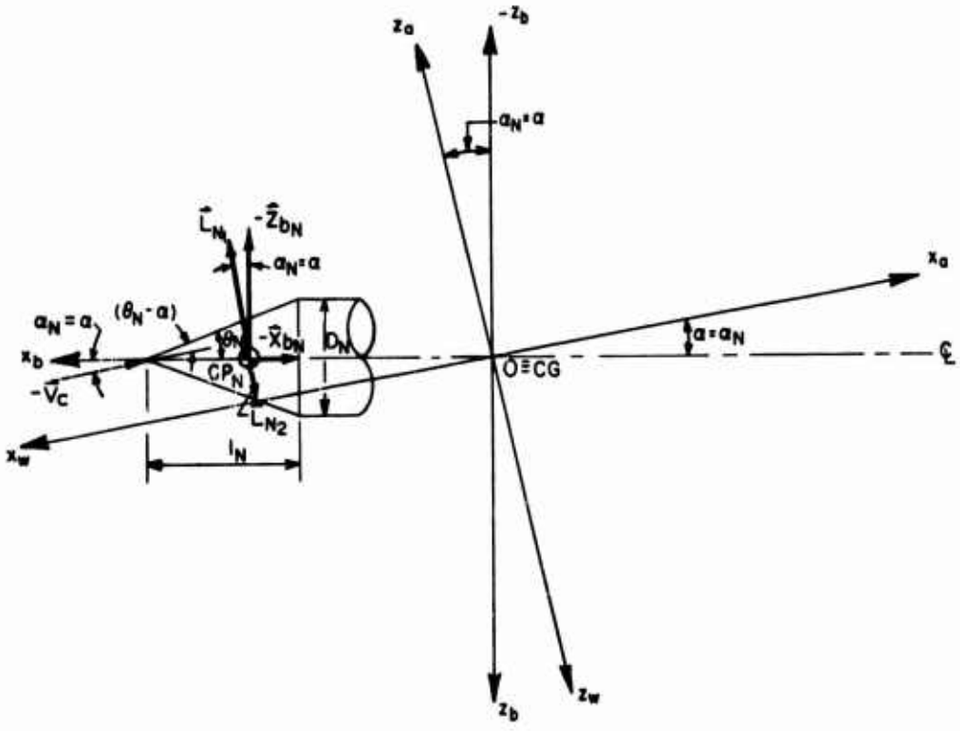

FIG. 1.15 Adopted convention for the nose cone lift coefficient, L_N, in terms of normal and axial force components, $(-\bar{Z}_{bN})$, $(-\bar{X}_{bN})$, respectively.

By a direct comparison of the aerodynamic expression for the defined total lift coefficient, Eq. (1.6-52), and the derived total lift coefficient expression, Eq. (1.6-53), it is evident that the total lift curve slope, a, the representative geometric angle-of-attack, α, and the representative zero-lift angle, α_o, for the compound configuration are

$$a = a_W \frac{S_W}{S_{ref}}\left[\left(\frac{a_N}{a_W}\frac{S_N}{S_W}+1\right)+\frac{a_T}{a_W}\frac{S_T}{S_W}\eta_T\left(1-\frac{\partial \epsilon_T}{\partial \alpha_W}\right)\right] \quad (1.6\text{-}55)$$

$$\alpha = \alpha_W - i_W = \alpha_N = \alpha_T + \epsilon_T - i_T \quad (1.6\text{-}56)$$

$$\alpha_o = \frac{(\alpha_{OW}-i_W)+\frac{a_T}{a_W}\frac{S_T}{S_W}\eta_T\left[(\epsilon_O - i_T + i_W\frac{\partial \epsilon_T}{\partial \alpha_W}) - (\frac{\partial \alpha_T}{\partial \delta_E}\delta_E)\right]}{\left(\frac{a_N}{a_W}\frac{S_N}{S_W}+1\right)+\frac{a_T}{a_W}\frac{S_T}{S_W}\eta_T\left(1-\frac{\partial \epsilon_T}{\partial \alpha_W}\right)} \quad (1.6\text{-}57)$$

Where, provided $\partial \epsilon_T / \partial \alpha_w$ is constant, the total lift curve slope, a, is constant.

For the vertical plane, steady-state equilibrium flight regime, at a fixed instant of time, the representative zero-lift angle-of-attack becomes a function of the equilibrium elevator deflection angle, δ_E, provided $\partial \alpha_T / \partial \delta_E$ is a constant. The corresponding numerical values of δ_E and α are obtained from a simultaneous solution of the respective force and moment equations. (11,17)

The above expressions for the representative lift curve slope, a, the representative geometric angle-of-attack, α, and the representative zero-lift angle, α_o, of the compound vehicle configuration are conditional, i.e. for the special case illustrated in Fig. 1.14, and with the assumptions stated therein.

In each other case, similar representative aerodynamic expressions for σ, α and α_o can then be defined accordingly.

1.6.3 REPRESENTATIVE SIDE-SLIP ANGLE DEFINITIONS FOR COMPOUND VEHICLE GEOMETRIES ASSUMING $\alpha = 0$

For each specific compound configuration an explicit expression for the representative side-slip angle, β, is determined. Then the total side-slip force, $\tilde{Q}$, is aerodynamically defined through a procedure similar to that outlined for the lift force, $\tilde{L}$, the main difference between the two being the fact that the aircraft and the missile configurations generally are not geometrically symmetric with respect to the $Ox_b y_b$ plane. In the case of cruciform configurations, the double symmetry respective to both the $Ox_b z_b$ and the $Ox_b y_b$ planes is specifically satisfied, and the $\tilde{Q}$ force evaluation follows identically the analytical pattern of the $\tilde{L}$ force. The side-slip angle, β, then acquires its specific aerodynamic and zero-side-force definitions:

$$\beta_a = \beta - \beta_0 \quad , \quad \text{or} \quad \beta = \beta_a + \beta_0 \qquad (1.6\text{-}58)$$

where the interpretations for β_o and β_a are equivalent to the already-specified definitions for α_o and α_a. For body geometries possessing only one ($Ox_b z_b$) plane of symmetry, the side-slip angle, β, has in the first approximation only a conditional geometrical meaning, i.e.

$$\beta = \beta_c \quad , \quad \beta_0 = 0 \qquad (1.6\text{-}59)$$

provided the reference Ox_b axis has the quality of the body center line, and the vertical fin airfoil is symmetrical, which is commonly the case.

1.6.4 GENERAL DEFINITIONS OF AERODYNAMIC FORCE COMPONENTS IN TERMS OF THE REPRESENTATIVE ANGLE-OF-ATTACK α, AND THE REPRESENTATIVE SIDE-SLIP ANGLE, β

Once the representative angle-of-attack, α, and the representative side-slip angle, β, are defined for a given vehicle configuration under specified steady equilibrium flight conditions (i.e. for a given set of $\tilde{V}_A$ and ρ_A values), the total aerodynamic lift coefficient, C_L, and the total side-force coefficent, C_Q, are obtainable from the fundamental perfect-fluid potential theory definitions

$$C_L = \frac{\partial C_L}{\partial \alpha}(\alpha - \alpha_0) \qquad (1.6\text{-}60)$$

$$C_Q = \frac{\partial C_Q}{\partial \beta}(\beta - \beta_0) \qquad (1.6\text{-}61)$$

The inherent underlying assumption of the potential flow theory excludes any frictional or viscous effects; consequently, these effects are not included in the expressions (1.6-60) and (1.6-61). This approximation is conditionally correct for all practical purposes, provided the configurations are aerodynamically slender and the representative angles α and β are small.

Except in the case of simple Newtonian impact theory analysis, there are no correspondingly simple expressions for the drag force components, $D(\alpha)$ and $D(\beta)$, since the drag phenomena include (directly or indirectly) strong frictional effects. Thus, evaluation of the drag force components is generally a far more tedious and involved procedure. Procedures for the evaluation of drag force components will be elaborated later in sufficient detail for engineering purposes. Here, following the classical vectorial aerodynamic force definitions from Section 1.3 and the adopted vectorial interpretation as illustrated in Fig. 1.12, analytical examples of general expressions for the aerodynamic lift, $\hat{L}$, the aerodynamic drag, $\hat{D}$, and the aerodynamic side-force, $\hat{Q}$, are developed.

The total aerodynamic resistance force, $\tilde{R}$, which opposes the vehicle motion through an ambient atmosphere, has been conveniently defined in terms of the classical concept of the normal and the tangential stress distributions taken around the vehicle contour

$$\vec{R} = \int_{S_{wet}} \left[(p - p_\infty)\vec{n} + \tau \vec{t} \right] dS \qquad (1.6\text{-}62)$$

where the numerical values of p, p_∞, and τ are evaluated locally (note that $\Delta p = p - p_\infty$). The local normal, $\vec{n}$, and the local tangent, $\vec{t}$, unit vectors at the small wetted surface element, dS, are taken respectively as normal to and collinear with the local zero-streamline. The local unit vectors $\vec{t}$ and $\vec{n}$ obviously should not be confused with the principal trihedral reference frame $Otnb$ in Section 1.4.

A subsequent resolution of the resultant aerodynamic resistance force, $\tilde{R}$, into the lift, $\hat{L}$, drag, $\hat{D}$, and side-force, $\hat{Q}$, components on the Oz_a, Ox_a

and Oy_Q axes respectively, leads to the corresponding expressions

$$\vec{L} = L\vec{k}_a = \vec{k}_a \int_{S_{wet}} (\Delta p \vec{n}\cdot\vec{k}_a + \tau \vec{t}\cdot\vec{k}_a)\, dS \qquad (1.6\text{-}63)$$

$$\vec{D} = D\vec{i}_a = \vec{i}_a \int_{S_{wet}} (\Delta p \vec{n}\cdot\vec{i}_a + \tau \vec{t}\cdot\vec{i}_a)\, dS \qquad (1.6\text{-}64)$$

$$\vec{Q} = Q\vec{j}_Q = \vec{j}_Q \int_{S} (\Delta p \vec{n}\cdot\vec{j}_Q + \tau \vec{t}\cdot\vec{j}_Q)\, dS \qquad (1.6\text{-}65)$$

The above expressions are representative for general three-dimensional flow patterns. The unit vector dot products involve the cosines of the locally subtended angles between the $\vec{t}$, $\vec{n}$, $\vec{i}$, $\vec{j}$, and $\vec{k}$ vectors respectively. Since the local $\vec{t}$ and $\vec{n}$ unit vectors follow the zero-streamline of a three-dimensional flow pattern the explicit forms of the general vectorial expressions (1.6-63) to (1.6-65) are individually defined for any given body geometry and flow regime. If the combined aerodynamic effects of the angle-of-attack, α, and the side-slip angle, β, are treated as a linear sum of their partial aerodynamic contributions, then, from the adopted vectorial force conventions in the Fig. 1.12, it follows conditionally that

$$\vec{R} = \vec{R}(\alpha) + \vec{R}(\beta) \;;\; \alpha \neq 0,\ \beta \neq 0$$

$$\vec{R}(\alpha) = \vec{L} + \vec{D}(\alpha) \;;\; \beta = 0,\ \alpha \neq 0$$

$$\vec{R}(\beta) = \vec{Q} + \vec{D}(\beta) \;;\; \alpha = 0,\ \beta \neq 0$$

$$\therefore \vec{R} = \vec{L} + \vec{D}(\alpha) + \vec{D}(\beta) + \vec{Q} = \vec{L} + \vec{D} + \vec{Q} \qquad (1.6\text{-}66)$$

with $(-\vec{V}_A)$ being the representative relative flight velocity. Following the fundamental aerodynamic force definitions in Section 1.3, the non-dimensional aerodynamic expressions for $\vec{R}$, $\vec{L}$, $\vec{D}$ and $\vec{Q}$ can then be formulated as shown in the following paragraphs.

Resultant aerodynamic resistance force

$$\vec{R} = R\vec{r} = \int_{S_{wet}} d\vec{R} = \int_{S_{wet}} (C_{p_l} q_l \vec{n} + C_{f_l} q_l \vec{t})\, dS = q_A \int_{S_{wet}} (C_p \vec{n} + C_f \vec{t})\, dS$$

$$= \left[q_A \int_{S_{wet}} (C_p \vec{n}\cdot\vec{r} + C_f \vec{t}\cdot\vec{r})\, dS \right] \vec{r} \qquad (1.6\text{-}67)$$

$$R = C_R q_A S_{ref} = q_A \int_{S_{wet}} (C_p \vec{n}\cdot\vec{r} + C_f \vec{t}\cdot\vec{r})\, dS \qquad (1.6\text{-}68)$$

$$C_R = \frac{1}{S_{ref}} \int_{S_{wet}} (C_p \vec{n}\cdot\vec{r} + C_f \vec{t}\cdot\vec{r})\, dS \qquad (1.6\text{-}69)$$

$$C_p = \frac{p - p_A}{q_A} = \frac{\Delta p}{q_A} \;,\quad C_{p_l} = \frac{p - p_A}{q_l} = \frac{\Delta p}{q_l} \;,\quad C_f = \frac{\tau_w}{q_A}$$

$$C_{f_l} = \frac{\tau_w}{q_l} \;,\quad q_A = \frac{\rho_A V_A^2}{2} \;,\quad q_l = \frac{\rho_l V_l^2}{2}$$

where C_p and C_f are the local pressure and local skin friction coefficients of the resultant flow pattern due to both the angle-of-attack, α, and the side-slip angle, β. Also, $\vec{n}$ and $\vec{t}$ are the local normal and the local tangent unit vectors at any surface point of the body contour; $\vec{t}$ being totally tangent to the resultant streamline (positive in the sense of the local stream velocity, $\vec{V}_l$) and $\vec{n}$ being locally normal to the surface element dS (positive inward).

Furthermore, by a formal vector resolution:

$$\vec{R} = \vec{R}(\alpha) + \vec{R}(\beta) = R(\alpha)\vec{r}_\alpha + R(\beta)\vec{r}_\beta$$

$$= |\vec{R}\cdot\vec{r}_\alpha|\vec{r}_\alpha + |\vec{R}\cdot\vec{r}_\beta|\vec{r}_\beta \qquad (1.6\text{-}70)$$

$$\vec{R}(\alpha) = R(\alpha)\vec{r}_\alpha = \left[q_A \int_{S_{wet}} (C_p \vec{n}\cdot\vec{r}_\alpha + C_f \vec{t}\cdot\vec{r}_\alpha)\, dS \right] \vec{r}_\alpha \qquad (1.6\text{-}71)$$

$$R(\alpha) = C_R(\alpha) q_A S_{ref} = q_A \int_{S_{wet}} (C_p \vec{n}\cdot\vec{r}_\alpha + C_f \vec{t}\cdot\vec{r}_\alpha)\, dS \qquad (1.6\text{-}72)$$

$$\therefore C_R(\alpha) = \frac{1}{S_{ref}} \int_{S_{wet}} (C_p \vec{n}\cdot\vec{r}_\alpha + C_f \vec{t}\cdot\vec{r}_\alpha)\, dS \qquad (1.6\text{-}73)$$

$$\vec{R}(\beta) = R(\beta)\vec{r}_\beta = \left[q_A \int_{S} (C_p \vec{n}\cdot\vec{r}_\beta + C_f \vec{t}\cdot\vec{r}_\beta)\, dS \right] \vec{r}_\beta \qquad (1.6\text{-}74)$$

$$R(\beta) = C_R(\beta) q_A S_{ref} = q_A \int_{S_{wet}} (C_p \vec{n}\cdot\vec{r}_\beta + C_f \vec{t}\cdot\vec{r}_\beta)\, dS \qquad (1.6\text{-}75)$$

$$\therefore C_R(\beta) = \frac{1}{S_{ref}} \int_{S_{wet}} (C_p \vec{n}\cdot\vec{r}_\beta + C_f \vec{t}\cdot\vec{r}_\beta)\, dS \qquad (1.6\text{-}76)$$

The above formal vectorial resolutions imply the following restrictive aerodynamic and geometric conditions:

The resultant three-dimensional fluid flow field around the vehicle is presumed to correspond to a total angle of incidence, $\vec{\alpha}+\vec{\beta}$, measured between the reference body axis, Ox_b, and the total air stream velocity vector. In the more general flight dynamics cases the instantaneous total air stream velocity is a vectorial sum of the air stream velocity tangent to the flight path, $\vec{V}_\infty = -\vec{V}_A$, the atmospheric wind or turbulence velocity, $\vec{V}_w$, and the resultant translatory disturbance velocity, $\vec{V}_D$, presuming a no-spin flight condition. For the more limited aspects of the present aerodynamic force analysis, under steady equilibrium flow conditions, it is assumed that $\vec{V}_w = \vec{V}_D = 0$.

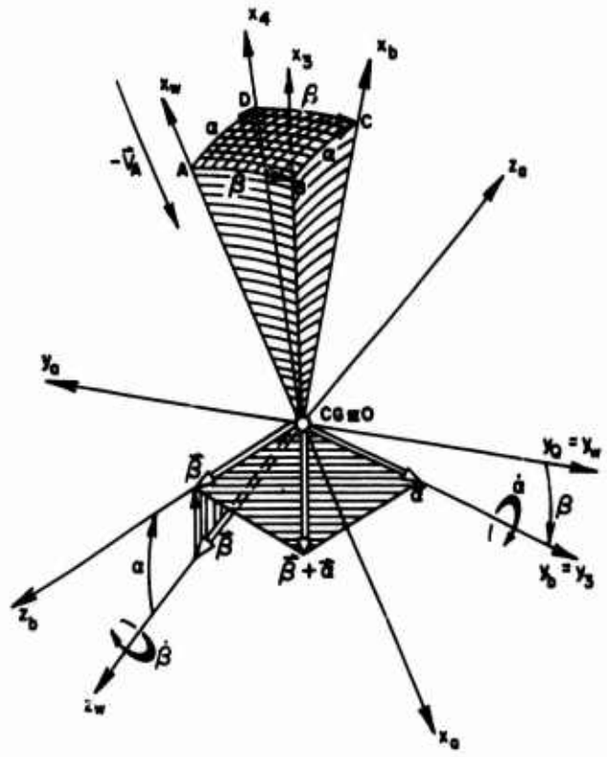

Fig. 1.16 Total angle of incidence, $\vec{\alpha}+\vec{\beta}$, measured between the Ox_w and the Ox_b axes, in a plane normal to the $(\vec{\alpha}+\vec{\beta})$ vector. Note: $\vec{\alpha}+\vec{\beta} \neq \vec{\beta}+\vec{\alpha}$.

The resultant aerodynamic resistance force, $\vec{R}$, and the corresponding local pressure and local skin friction coefficients (C_p, C_f) are due to the total incidence angle, $\alpha+\beta$. A direct analytical investigation of the complex flow pattern around compound vehicle configurations is unattainable. Thus the local C_p and C_f values in the formal vectorial expressions (1.6-67) to (1.6-76) can be adequately extablished by experiment only. In order to allow for a theoretical evaluation procedure, the complex flow pattern is conditionally resolved into vectorially additive componental flows, assuming the conditions of $\beta=0$, $\alpha\neq0$, and $\beta\neq0$, $\alpha=0$ respectively. Then, according to Figs. 1.12 and 1.15,

$$R(\alpha) = C_R(\alpha) q_A S_{ref} = q_A \int_{S_{wet}} \left[C_p(\alpha)\hat{n}\cdot\hat{r}_\alpha + C_f(\alpha)\hat{t}_\alpha\cdot\hat{r}_\alpha \right] dS \qquad (1.6\text{-}77)$$

$$C_R(\alpha) = \frac{1}{S_{ref}} \int_{S_{wet}} \left[C_p(\alpha)\hat{n}\cdot\hat{r}_\alpha + C_f(\alpha)\hat{t}_\alpha\cdot\hat{r}_\alpha \right] dS \qquad (1.6\text{-}78)$$

$$R(\beta) = C_R(\beta) q_A S_{ref} = q_A \int_{S_{wet}} \left[C_p(\beta)\hat{n}\cdot\hat{r}_\beta + C_f(\beta)\hat{t}_\beta\cdot\hat{r}_\beta \right] dS \qquad (1.6\text{-}79)$$

$$C_R(\beta) = \frac{1}{S_{ref}} \int_{S_{wet}} \left[C_p(\beta)\hat{n}\cdot\hat{r}_\beta + C_f(\beta)\hat{t}_\beta\cdot\hat{r}_\beta \right] dS \qquad (1.6\text{-}80)$$

where $C_p(\alpha)$, $C_f(\alpha)$, and $C_p(\beta)$, $C_f(\beta)$ are the normal pressure and the tangential shear stress coefficients evaluated locally under the partial flow conditions of $\alpha\neq0$, $\beta=0$ and $\alpha=0$, $\beta\neq0$ respectively. It is important to realize that each of the two partial flow patterns is still three-dimensional. The local unit vector, $\hat{n}$, is normal to the local surface element, dS, of the body contour (positive inward) while the local unit vectors $\hat{r}_\alpha$ and $\hat{r}_\beta$ are tangential to the local surface element, dS, and directed along the respective componental zero-streamlines for the $\alpha\neq0$, $\beta=0$ and $\alpha=0$, $\beta\neq0$ inviscid flow patterns.

When comparing the corresponding conditional pairs of equations (1.6-72) and (1.6-77) for $\vec{R}(\alpha)$, and (1.6-75) and (1.6-79) for $\vec{R}(\beta)$, it should be noted that they are equal only if locally, for any surface element, dS,

$$C_p\hat{n} = \left[C_p(\alpha) + C_p(\beta) \right]\hat{n} \qquad (1.6\text{-}81)$$

$$C_f\hat{t} = C_f(\alpha)\hat{t}_\alpha + C_f(\beta)\hat{t}_\beta \qquad (1.6\text{-}82)$$

and for the total compound configuration

$$\int_{S_{wet}} C_p\hat{n}\cdot\hat{r}_\alpha\, dS = \int_{S_{wet}} C_p(\alpha)\hat{n}\cdot\hat{r}_\alpha\, dS \qquad (1.6\text{-}83)$$

$$\int_{S_{wet}} C_p\hat{n}\cdot\hat{r}_\beta\, dS = \int_{S_{wet}} C_p(\beta)\hat{n}\cdot\hat{r}_\beta\, dS \qquad (1.6\text{-}84)$$

$$\int_{S_{wet}} C_f\hat{t}\cdot\hat{r}_\alpha\, dS = \int_{S_{wet}} C_f(\alpha)\hat{t}_\alpha\hat{r}_\alpha\, dS \qquad (1.6\text{-}85)$$

$$\int_{S_{wet}} C_f\hat{t}\cdot\hat{r}_\beta\, dS = \int_{S_{wet}} C_f(\beta)\hat{t}_\beta\hat{r}_\beta\, dS \qquad (1.6\text{-}86)$$

where the conditions (1.6-83) to (1.6-86) are possible due to the double integration procedures performed in different respective planes.

In order to satisfy the conditions of Eqs. (1.6-81) and (1.6-82), the componental values of $C_p(\alpha)$, $C_f(\alpha)$ and $C_p(\beta)$, $C_f(\beta)$, although evaluated under the partial restraints of $\alpha\neq0$, $\beta=0$ and $\alpha=0$, $\beta\neq0$ respectively, should incorpor-

ate the partial corrections for resultant induced effects and the resultant interference effects between different parts of a compound vehicle configuration. The task is usually beyond the theoretical possibilities. Instead, in a first approximation the uncoupled analyses of the partial flow cases for $\alpha \neq 0, \beta = 0$ and $\alpha = 0, \beta \neq 0$ are conducted, the respective partially evaluated interference effects introduced separately, if available and the $\tilde{R}(\alpha)$ and the $\tilde{R}(\beta)$ components added vectorially.

Lift force

Using the formal vectorial resolution in Fig. 1.12 and Eqs. (1.6-67) and (1.6-71), the lift force and related coefficient can be formulated as follows:

$$\tilde{L} = L\tilde{k}_a = (\tilde{R}\cdot\tilde{k}_a)\tilde{k}_a = \left[q_A \int_{S_{wet}} (C_p \tilde{n}\cdot\tilde{k}_a + C_f \tilde{t}\cdot\tilde{k}_a)\,dS\right]\cdot\tilde{k}_a \tag{1.6-87}$$

$$\tilde{L} = L\tilde{k}_a = \left[\tilde{R}(\alpha)\cdot\tilde{k}_a\right]\tilde{k}_a = \left\{q_A \int_{S_{wet}} \left[C_p(\alpha)\tilde{n}\cdot\tilde{k}_a + C_f(\alpha)\tilde{t}_\alpha\cdot\tilde{k}_a\right]dS\right\}\tilde{k}_a \tag{1.6-88}$$

$$L = C_L(\alpha) q_A S_{ref}$$

$$\therefore C_L = \frac{1}{S_{ref}} \int_{S_{wet}} \left[C_p(\alpha)\tilde{n}\cdot\tilde{k}_a + C_f(\alpha)\tilde{t}\cdot\tilde{k}_a\right]dS \tag{1.6-89}$$

Side force

Again employing the vectorial resolution in Fig. 1.12 and using Eqs. (1.6-71) and (1.6-74)

$$\tilde{Q} = Q\tilde{j}_Q = \left[\tilde{R}(\beta)\tilde{j}_Q\right]\tilde{j}_Q = \left\{q_A \int_S \left[C_p(\beta)\tilde{n}\cdot\tilde{j}_Q + C_f(\beta)\tilde{t}_\beta\cdot\tilde{j}_Q\right]dS\right\}\tilde{j}_Q \tag{1.6-90}$$

$$Q = C_Q\, q_A\, S_{ref}$$

$$\therefore C_Q = \frac{1}{S_{ref}} \int_{S_{wet}} \left[C_p(\beta)\tilde{n}\cdot\tilde{j}_Q + C_f(\beta)\tilde{t}_\beta\cdot\tilde{j}_Q\right]dS \tag{1.6-91}$$

Drag force

The drag force and related coefficient are formulated in a manner completely analogous to that in which the lift expressions are formulated as:

$$\tilde{D} = \tilde{D}(\alpha) + \tilde{D}(\beta) \tag{1.6-92}$$

$$\tilde{D}(\alpha) = D(\alpha)\tilde{i}_a = \left[\tilde{R}(\alpha)\tilde{i}_a\right]\tilde{i}_a = \left\{q_A \int_{S_{wet}} \left[C_p(\alpha)\tilde{n}\cdot\tilde{i}_a + C_f(\alpha)\tilde{t}_\alpha\cdot\tilde{i}_a\right]dS\right\}\cdot\tilde{i}_a \tag{1.6-93}$$

$$D(\alpha) = C_D(\alpha) q_A S_{ref} \tag{1.6-94}$$

$$\therefore C_D(\alpha) = \frac{1}{S_{ref}} \int_{S_{wet}} \left[C_p(\alpha)\tilde{n}\cdot\tilde{i}_a + C_f(\alpha)\tilde{t}_\alpha\cdot\tilde{i}_a\right]dS \tag{1.6-95}$$

$$\tilde{D}(\beta) = D(\beta)\tilde{i}_a = \left[\tilde{R}(\beta)\tilde{i}_a\right]\tilde{i}_a = \left\{q_A \int_{S_{wet}} \left[C_p(\beta)\tilde{n}\cdot\tilde{i}_a + C_f(\beta)\tilde{t}_\beta\cdot\tilde{i}_a\right]dS\right\}\cdot\tilde{i}_a \tag{1.6-96}$$

$$D(\beta) = C_D(\beta) q_A S_{ref}$$

$$\therefore C_D(\beta) = \frac{1}{S_{ref}} \int_{S_{wet}} \left[C_p(\beta)\tilde{n}\cdot\tilde{i}_a + C_f(\beta)\tilde{t}_\beta\cdot\tilde{i}_a\right]dS \tag{1.6-97}$$

$$C_D = C_D(\alpha) + C_D(\beta) = \frac{1}{S_{ref}} \int_{S_{wet}} \left\{\left[C_p(\alpha) + C_p(\beta)\right]\tilde{n}\cdot\tilde{i}_a + \left[C_f(\alpha)\tilde{t}_\alpha + C_f(\beta)\tilde{t}_\beta\right]\tilde{i}_a\right\}dS \tag{1.6-98}$$

1.6.5 PHYSICAL CONSIDERATIONS AND SPECIAL CASES

For a given body geometry and for a specified instantaneously steady or quasi-steady flight occurrence, the aerodynamic force coefficients are explicit functions of the representative angle-of-attack, α, and the representative side-slip angle, β. Thus, keeping constant all the dynamical and physical variables governing a specific flight occurrence, the aerodynamic force coefficients C_L, C_Q, $C_D(\alpha)$, $C_D(\beta)$ are obtained by a double integration of the local normal and the local tangential stress coefficients $C_p(\alpha)$, $C_p(\beta)$, $C_f(\alpha)$, $C_f(\beta)$ around the body contour as indicated in Eqs. (1.6-89), (1.6-91), (1.6-95) and (1.6 97). In performing the formal mathematical operations, the following physically important conditions and restrictions should be recognized:

(i) When the geometric representative angles α and β are used, the integrated $C_p(\alpha)$ and $C_p(\beta)$ values are generally not zero for $\alpha = 0$ and $\beta = 0$ respectively. However, according to the inviscid, perfect fluid theory, the integrated dot products

$$\int_{S_{wet}} C_p(\alpha)\tilde{n}\cdot\tilde{k}_a\,dS \tag{1.6-99}$$

and

$$\int_{S_{wet}} C_p(\beta)\tilde{n}\cdot\tilde{j}_Q\,dS \tag{1.6-100}$$

become zero for zero values of the respective aerodynamic angles, $\alpha_a = 0$ and $\beta_a = 0$. At the same time

$$\int_{S_{wet}} C_p(\alpha)\vec{n}\cdot\vec{i}_a \, dS$$

and (1.6-101)

$$\int_{S_{wet}} C_p(\beta)\vec{n}\cdot\vec{i}_a \, dS$$

still have, in general, finite values which depend upon the real three-dimensional flow pattern, body geometry and relative attitude with respect to the fluid flow, including: effects of the forebody and the base slopes, the outside flow streamline distortions due to boundary layer thickness changing the effective body shape, the boundary layer-shock wave inteferences and the entropic losses through strong detached bow shocks.

(ii) The integrated frictional contributions

$$\int_{S_{wet}} C_f(\alpha)\vec{i}_\alpha\cdot\vec{k}_a \, dS \ , \quad \int_{S_{wet}} C_f(\beta)\vec{i}_\beta\cdot\vec{k}_a \, dS$$

$$\int_{S_{wet}} C_f(\alpha)\vec{i}_\alpha\cdot\vec{j}_Q \, dS \ , \quad \int_{S_{wet}} C_f(\beta)\vec{i}_\beta\cdot\vec{j}_Q \, dS$$

$$\int_{S_{wet}} C_f(\alpha)\vec{i}_\alpha\cdot\vec{i}_a \, dS \ , \quad \int_{S_{wet}} C_f(\beta)\vec{i}_\beta\cdot\vec{i}_a \, dS \qquad (1.6\text{-}102)$$

are always present.

(iii) Following the customary aerodynamic representation for the total drag and drag coefficients in the case of three-dimensional flows

$$C_D(\alpha) = C_{D_o}(\alpha) + C_{D_i}(\alpha)$$
$$C_D(\beta) = C_{D_o}(\beta) + C_{D_i}(\beta) \qquad (1.6\text{-}103)$$

where $C_{D_o}(\alpha)$ and $C_{D_o}(\beta)$ are the zero-lift, and the zero side-force drag coefficients, while $C_{D_i}(\alpha)$ and $C_{D_i}(\beta)$ are the drag coefficient increments due to non-zero values of the lift and the side-force, it follows from the above that

$$C_{D_o}(\alpha) = \frac{1}{S_{ref}}\int_{S_{wet}}\left[C_p(\alpha)\vec{n}\cdot\vec{i}_a + C_f(\alpha)\vec{i}_\alpha\cdot\vec{i}_a\right]dS \quad \text{when } \alpha_a = \alpha - \alpha_o = 0 \qquad (1.6\text{-}104)$$

$$C_{D_o}(\beta) = \frac{1}{S_{ref}}\int_{S_{wet}}\left[C_p(\beta)\vec{n}\cdot\vec{i}_a + C_f(\beta)\vec{i}_\beta\cdot\vec{i}_a\right]dS \quad \text{when } \beta_a = \beta - \beta_o = 0 \qquad (1.6\text{-}105)$$

The above expressions are very general and involved for actual computations. Useful engineering simplifications are, therefore, introduced, taking into account the order of magnitude of the respective integrals and the overall limitations in accuracy with which the pressure and the frictional effects can be evaluated theoretically and/or measured experimentally. Thus, for aerodynamically slender body shapes it is usually acceptable for practical purposes to neglect frictional force contributions to the lift, L , and the side-force, Q . The approximation reflects the experimentally well substantiated Prandtl's postulate, of the inviscid perfect fluid theory, that the lift and the side-force are functions of the pressure distribution components in the respective directions normal to the uniform free stream flow at infinity, while the skin-friction contributions are, substantially, creating only a drag increment. Furthermore, in view of the considerable uncertainty with which the frictional contribution to the drag force, D , can be either theoretically predicted or experimentally measured, it proves acceptable to consider the local $C_f(\alpha)$ and the $C_f(\beta)$ coefficients practically independent of the respective α and β values, provided these angles are relatively small, i.e. the local $C_f(\alpha)\vec{i}_\alpha\cdot\vec{i}_a$ and the local $C_f(\beta)\vec{i}_\beta\cdot\vec{i}_a$ components are usually estimated under $\alpha_a = \alpha - \alpha_o$ and $\beta_a = \beta - \beta_o = 0$ conditions and the estimates subsequently considered constants for small $\alpha_a \neq 0$ and $\beta_a \neq 0$ values. With these conditional approximations, restrictively valid for aerodynamically slender configurations at small angles respective to $\vec{V}_\infty$, presuming steady flow conditions without separation, the general expressions (1.6-89), (1.6-91), (1.6-95), (1.6-97) attain the respectively simpler forms:

$$C_L = \frac{1}{S_{ref}}\int_{S_{wet}}\left[C_p(\alpha)\right]_{\alpha_a}\vec{n}\cdot\vec{k}_a \, dS \qquad (1.6\text{-}106)$$

$$C_Q = \frac{1}{S_{ref}}\int_{S_{wet}}\left[C_p(\beta)\right]_{\beta_a}\vec{n}\cdot\vec{j}_Q \, dS \qquad (1.6\text{-}107)$$

$$C_D(\alpha) = \frac{1}{S_{ref}}\int_{S_{wet}}\left[C_p(\alpha)\vec{n}\cdot\vec{i}_a + C_f(\alpha)\vec{i}_\alpha\cdot\vec{i}_a\right]dS \qquad (1.6\text{-}108)$$

$$\therefore C_D(\alpha) = C_{D_o}(\alpha) + C_{D_i}(\alpha)$$
$$= \frac{1}{S_{ref}}\int_{S_{wet}}\left(\left[C_p(\alpha)\right]_{\alpha_a=0}\vec{n}\cdot\vec{i}_a + \left[C_f(\alpha)\right]_{\alpha_a=0}\vec{i}_\alpha\cdot\vec{i}_a\right)dS$$
$$+ \frac{1}{S_{ref}}\int_{S_{wet}}\left[\Delta C_p(\alpha)\right]_{\alpha_a}\vec{n}\cdot\vec{i}_a \, dS$$
$$= \frac{1}{S_{ref}}\int_{S_{wet}}\left\{\left(\left[C_p(\alpha)\right]_{\alpha_a=0} + \left[\Delta C_p(\alpha)\right]_{\alpha_a}\right)\vec{n}\cdot\vec{i}_a + \left[C_f(\alpha)\right]_{\alpha_a=0}\vec{i}_\alpha\cdot\vec{i}_a\right\}dS \qquad (1.6\text{-}109)$$

$$C_D(\beta) = \frac{1}{S_{ref}} \int_{S_{wet}} \left[C_p(\beta) \vec{n} \cdot \vec{i}_a + C_f(\beta) \vec{i}_\beta \cdot \vec{i}_a \right] dS \tag{1.6-110}$$

$$\therefore C_D(\beta) = C_{D_o}(\beta) + C_{D_i}(\beta)$$

$$= \frac{1}{S_{ref}} \int_{S_{wet}} \left\{ \left[C_p(\beta) \right]_{\beta_a=0} \vec{n} \cdot \vec{i}_a + \left[C_f(\beta) \right]_{\beta_a=0} \vec{i}_\beta \cdot \vec{i}_a \right\} dS$$

$$+ \frac{1}{S_{ref}} \int_{S_{wet}} \left[\Delta C_p(\beta) \right]_{\beta_a} \vec{n} \cdot \vec{i}_a \, dS$$

$$= \frac{1}{S_{ref}} \int_{S_{wet}} \left\{ \left(\left[C_p(\beta) \right]_{\beta_a=0} + \left[\Delta C_p(\beta) \right]_{\beta_a} \right) \vec{n} \cdot \vec{i}_a \right.$$

$$\left. + \left[C_f(\beta) \right]_{\beta_a=0} \vec{i}_\beta \cdot \vec{i}_a \right\} dS \tag{1.6-111}$$

$$C_D = C_D(\alpha) + C_D(\beta) = C_{D_o} + C_{D_i} \tag{1.6-112}$$

$$= \frac{1}{S_{ref}} \int_{S_{wet}} \left\{ \left(\left[C_p(\alpha) \right]_{\alpha_a=0} + \left[C_p(\beta) \right]_{\beta_a=0} \right) \vec{n} \cdot \vec{i}_a \right.$$

$$\left. + \left(\left[C_f(\alpha) \right]_{\alpha_a=0} \vec{i}_a \cdot \vec{i}_a + \left[C_f(\beta) \right]_{\beta_a=0} \vec{i}_\beta \cdot \vec{i}_a \right) \right\} dS$$

$$+ \frac{1}{S_{ref}} \int_{S_{wet}} \left(\left[\Delta C_p(\alpha) \right]_{\alpha_a} + \left[\Delta C_p(\beta) \right]_{\beta_a} \right) \vec{n} \cdot \vec{i}_a \, dS \tag{1.6-113}$$

where the $C_p(\alpha)$ and $C_p(\beta)$ are necessarily defined for the respective partial three-dimensional flow patterns corresponding to the $\alpha_a \neq 0, \beta_a = 0$ and $\alpha_a = 0, \beta_a \neq 0$ uncoupled conditions.

Consider the special case of a flight trajectory confined to the vertical plane $Ox_h z_h$, respective to the flat earth local horizon axes, as illustrated in detail in Subsection 1.6.2, i.e. assuming at a given instant of time an equilibrium quasi-steady flight condition for a vehicle possessing a geometrical plane of symmetry $Ox_b z_b$ coincident with the $Ox_h z_h$ and the $Ox_w z_w$ planes so that

$$\beta = \beta \equiv 0$$
$$\delta_A = \delta_R \equiv 0$$
$$\mu \equiv 0, \quad \phi \equiv 0 \tag{1.6-114}$$

the aerodynamic side-slip force, $\tilde{Q}$, and the aerodynamic drag component, $\tilde{D}(\beta)$, become zero. Then, the corresponding expressions of the lift, $\tilde{L}$, and the drag, $\tilde{D}(\alpha)$, force components take the classical simple coefficient forms

$$C_L = \frac{1}{S_{ref}} \int_{S_{wet}} C_p \vec{n} \cdot \vec{k}_a \, dS = a(\alpha - \alpha_o) = a\alpha_a \tag{1.6-115}$$

$$C_D = \frac{1}{S_{ref}} \int_{S_{wet}} (C_p \vec{n} \cdot \vec{i}_a + C_f \vec{t} \cdot \vec{i}_a) \, dS \tag{1.6-116}$$

$$\therefore C_D = C_{D_o} + C_{D_i} = \frac{1}{S_{ref}} \int_{S_{wet}} \left\{ \left[(C_p)_{\alpha_a=0} \vec{n} \cdot \vec{i}_a \right.\right.$$

$$\left.\left. + (C_f)_{\alpha_a=0} \vec{t} \cdot \vec{i}_a \right] + \left[(\Delta C_p)_{\alpha_a} \vec{n} \cdot \vec{i}_a \right] \right\} dS \tag{1.6-117}$$

where:

(1) The local pressure coefficient on any surface element, dS,

$$C_p = \frac{p - p_\infty}{q_A}$$

$$\therefore C_p = \left[C_p \right]_{\alpha_a=0} + \left[\Delta C_p \right]_{\alpha_a} = \left[\frac{p - p_\infty}{q_A} \right]_{\alpha_a=0} + \Delta \left[\frac{p - p_\infty}{q_A} \right]_{\alpha_a} \tag{1.6-118}$$

is evaluated for three-dimensional flow conditions.

(2) The local skin friction coefficient on any surface element, dS, is

$$C_f = (C_f)_{\alpha_a=0} \; ; \quad \vec{t} \equiv \vec{i}_a \tag{1.6-119}$$

(3) The representative geometric angle-of-attack, the representative zero-lift angle-of-attack, α_o, and the respective total lift curve slope, a, of a compound vehicle configuration are given by Eqs. (1.6-56), (1.6-57) and (1.6-55) respectively, as determined from the overall vehicle geometry and the instantaneous equilibrium flight conditions.(11)

The local C_p and C_f values are evaluated for three-dimensional flow conditions, and double integrated for each i-th part (in situ) of a compound vehicle configuration. The individual results of the integrations are then summed:

$$C_L = \frac{1}{S_{ref}} \int_{S_{wet}} (\Delta C_p)_{\alpha_a} \vec{n} \cdot \vec{k}_a \, dS = \frac{1}{S_{ref}} \sum_{i=1}^{n} \int_{(S_{wet})_i} (\Delta C_{p_i})_{\alpha_a} \vec{n}_i \cdot \vec{k}_a \, dS_i \tag{1.6-120}$$

$$C_D = \frac{1}{S_{ref}} \int_{S_{wet}} \left\{ \left[(C_p)_{\alpha_a=0} \vec{n} \cdot \vec{i}_a + (C_f)_{\alpha_a=0} \vec{t} \cdot \vec{i}_a \right] + \left[(\Delta C_p)_{\alpha_a} \vec{n} \cdot \vec{i}_a \right] \right\} dS \tag{1.6-121}$$

$$C_D = \frac{1}{S_{ref}} \sum_{i=1}^{n} \int_{(S_{wet})_i} \left\{ \left[(C_{p_i})_{\alpha_a=0} \vec{n}_i \cdot \vec{i}_a + (C_{f_i})_{\alpha_a=0} \vec{t}_i \cdot \vec{i}_a \right] + \left[(\Delta C_{p_i})_{\alpha_a} \vec{n}_i \cdot \vec{i}_a \right] \right\} dS \tag{1.6-122}$$

where, for each i-th part in situ, at any surface element, dS_i,

$$C_{p_i} = \left[C_{p_i} \right]_{\alpha_a=0} + \left[\Delta C_{p_i} \right]_{\alpha_a} = \left[\frac{p_i - p_\infty}{q_A} \right]_{\alpha_a=0} + \Delta \left[\frac{p_i - p_\infty}{q_A} \right]_{\alpha_a} \tag{1.6-123}$$

$$C_{f_i} = \left[C_{f_i} \right]_{\alpha_a=0} \approx \left[C_{f_i} \right]_{\alpha_{a_i}=0} \tag{1.6-124}$$

$$\left[C_{p_i} \right]_{\alpha_a=0} = f_1(\alpha_i, \alpha_{o_i}, \theta_i)$$

$$\left[\Delta C_{p_i} \right]_{\alpha_a} = f_2(\alpha_i, \alpha_{i_o}, \theta_i) \tag{1.6-125}$$

with θ_i being the local incidence angle of the surface element dS_i with respect to the common reference line Ox_b of the compound vehicle configuration, while the individual geometric angle-of-attack, α_i , and the individual zero-lift angle-of-attack, α_{0_i} , of the i-th part are expressed in terms of the representative aerodynamic angle $\alpha_0 = \alpha - \alpha_0$ definition for the overall vehicle configuration (see Eqs. (1.6-46), (1.6-47), (1.6-48), (1.6-56) and (1.6-57) of the illustrative example of Subsection 1.6.2).

1.7 FLIGHT DYNAMICS AND FLUID MECHANICS REALMS

Atmospheric flight dynamics involve, in general, flight regimes varying from low subsonic to high hypersonic speeds and flight altitudes ranging from sea-level to the extremely rarefied outer limits of the atmosphere. Consequently, at any given instant of time on a specified flight trajectory, the aerodynamic force coefficients may become functions of a rather complex and intercoupled array of varying aerothermodynamic, chemical and electromagnetic properties of the air-body interacting system, even when quasi-equilibrium flight conditions and a Standard Atmosphere are assumed. The functional dependence of the aerodynamic force coefficients

$$C_L = C_L(\alpha_a, \delta_E, p, \rho, V, \mu, k, \gamma, T, \text{etc})$$

$$C_D = C_D(\alpha_a, \delta_E, p, \rho, V, \mu, k, \gamma, T, \text{etc}) \quad (1.7\text{-}1)$$

takes a corresponding specific form for a given vehicle at any instant of time during a flight performance.

In order to establish a more generalized functional relationship between the aerodynamic forces and the significant physical parameters governing the fluid-body interacting mechanism, the non-dimensional similarity parameters (natural variables) are introduced in place of the dimensional substantial physical variables. A reduced number of the nondimensional variables is obtained in place of the larger number of individual physical parameters. The nondimensional relationships are then valid for families of dynamically and geometrically similar fluid-body bounded systems.

In order to perform the task, a proper understanding of the role of substantial physical variables and of their conditional grouping into respective nondimensional ratios under widely differing fluid flow and speed regimes is necessitated. A unified analytical approach to the problem in its most general form, comprising simultaneous and extremely complex aerothermal interplays of all the influential physical variables, is both theoretically and practically unwieldy. Instead, a partial grouping of possible real flow aspects according to their relative significance is restrictively performed for conditionally simplified fluid-body systems. Several analytical methods[19] are available which lead to suitable non-dimensionalization of the governing flow equations and to a meaningful formulation of the resulting non-dimensional similarity parameters. When the non-dimensionalization procedures are applied, corresponding sets of significant non-dimensional natural variables are obtained in terms of which the respective similarity generalizations are easily performed. Results and solutions of such relatively simplified investigations are then partially and restrictively applicable to specific flight speed and flow regimes.

In the application of aerodynamic force analysis very convenient and useful groupings of different fluid flow patterns are obtained on the basis of two significant physical criteria: the degree of ambient atmospheric rarefaction and the degree of fluid compression when in motion relative to a given body geometry. The corresponding non-dimensional natural variables, serving as the generalized similarity criteria for various fluid-body systems, are the free stream Knudsen Number, Kn_A, and the free stream Mach Number, M_A, respectively.

The rarefaction criteria, Kn_A, is used for distinguishing between four intrinsically different fluid flow types from an internal kinetics point of view: the continuum, the slip, the transitional and the free molecular flow regimes. The second criterion, M_A, serves as a measure of the relative significance of the compressibility and the associated thermal effects, leading to a useful formulation of five characteristic flight speed regimes: The incompressible subsonic, the compressible subsonic, the transonic, the supersonic and the hypersonic speed domains. As stated already, in both cases the criteria are used in conjunction with correspondingly simplified fluid-body analytical models, including the viscous flow effects which are represented by the respective free stream Reynolds Number value, Re_A. The generally transient and nonequilibrium effects of thermal, radiative, and chemical nature are then treated separately when necessary as corrective factors of the aerodynamic force estimates.

1.7.1 KNUDSEN NUMBER CRITERIA AND FLUID FLOW REGIMES

A systematized investigation of the rarefaction effects on the grounds of the kinetic theory of isothermal equilibrium steady gas flows and a tentative formulation of the four major flow regimes (continuum, slip, transitional, free molecular) is defined in the classical works on the subject by Knudsen[26] Maxwell[27], Kennard[28], Loeb[29], Tsien[30,31], Chapman and Cowling[32], Shaaf[33], Shaaf and Chambre[34], Roberts[35], Donaldson[36], Siegel[37] and others. The governing natural variable is the Knudsen Number,

$$Kn_L = \frac{\bar{\lambda}}{L} \qquad (1.7\text{-}2)$$

where $\bar{\lambda}$ is the mean free molecular path in a gaseous medium, and L is the body characteristic length. The Knudsen Number criterion leads to two characteristic fow patterns of an isothermal steady gas flow in equilibrium at near ordinary temperatures:

$(Kn_L \ll 1)$ defines the classical continuum flow regime. Ambient (atmospheric) gas conditions are near standard, and the relative influence of the Knudsen Number as a natural variable may be neglected.

$(Kn_L \sim 1)$ defines the domain where the rarefied gas flow effects become important. When the mean free molecular path, $\bar{\lambda}$, is comparable to the characteristic body length, L, the statistically averaged effects of the fluid discrete molecular structure cannot be acceptably approximated by the continuum medium concepts. The term "characteristic length", L, may apply to any representative external body dimension (diameter of an internal flow duct, boundary layer thickness, shock wave thickness, etc.) depending upon the type of problem and the aim of the investigation conducted. It is pointed out that the qualification of "rarefied gas effects" is not exclusively related to low gas densities only, but rather to any gas flow condition characterized by very sharp pressure, velocity or temperature gradients in a distance of a few mean free molecular paths, regardless of the absolute gas density values.

The "rarefied gas" flow domain $(Kn_L \sim 1)$, is further subdivided into three flow regimes, based on rarefactional levels involved:

1. Slip flow regime--characterized by slightly rarefied gas conditions,
2. Transitional flow regime--characterized by moderately rarefied gas condition,
3. Free molecular flow regime--characterized by a highly rarefied gas condition.

Boundaries between the characteristic regimes are conditionally defined by assuming nearly isothermal conditions and a fixed specific heats ratio, γ, in a steady, viscous, compressible, non-conducting gas flow around insulated bodies. The significant natural variables under such restrictive conditions are the Mach Number, the Reynolds Number, and the Knudsen Number. When referred to the "free stream at infinity" or the ambient Standard Atmosphere conditions, they become the main representative similarity parameters for a given instant of time on a given flight trajectory:

$$M_A = \left(\frac{V}{a}\right)_A, \quad Re_A = \left(\frac{VL\rho}{\mu}\right)_A, \quad Kn_A = \left(\frac{\bar{\lambda}}{L}\right)_A \qquad (1.7\text{-}3)$$

Using as the characteristic measure either the overall body length, L, or the boundary layer thickness, δ, the three similarity parameters can be conditionally interrelated on the grounds of the equilibrium kinetic theory of gases:

$$Kn_L = \frac{\bar{\lambda}}{L} = \frac{\mu}{\rho}\left(\frac{\pi}{2RT}\right)^{1/2}\left(\frac{\gamma}{\gamma}\right)^{1/2}\frac{V}{LV} = \left(\frac{\pi\gamma}{2}\right)^{1/2}\frac{M}{Re_L}$$

or, alternatively:

$$Kn_L = \frac{\bar{\lambda}}{L} \sim \frac{\nu}{aL} = \frac{\mu}{\rho VL}\frac{V}{a} = \frac{M}{Re_L} \qquad (1.7\text{-}4)$$

$$Kn_\delta = \frac{\bar{\lambda}}{\delta} = \frac{\bar{\lambda}}{L}\frac{L}{\delta} = \frac{L}{\delta}Kn_L \sim \frac{L}{\delta}\frac{M}{Re_L} \sim \frac{M}{Re_L^{1/2}} \qquad (1.7\text{-}5)$$

where $M = \frac{V}{a}$, $Re_L = \frac{VL}{\nu}$

$$\bar{\lambda} = \nu\left(\frac{\pi}{2RT}\right)^{1/2} = \frac{\mu}{\rho}\left(\frac{\pi}{2RT}\right)^{1/2} \qquad (1.7\text{-}6)$$

according to Chapman's law. Therefore,

$$\bar{\lambda} = 2\frac{\nu}{\bar{C}} = \frac{2\nu}{\left(\frac{8}{\pi}\frac{\rho}{\rho}\right)^{1/2}} = 2\nu\frac{\sqrt{\gamma}}{1.59a} = 1.26\sqrt{\gamma}\,\frac{\nu}{a}$$

where a is the speed of sound,

$$a = \left(\gamma\frac{p}{\rho}\right)^{1/2} = \left(\gamma RT\right)^{1/2} \qquad (1.7\text{-}7)$$

$\bar{c}$ is the mean speed of the molecular random motion,

$$\bar{c} = \left(\frac{8}{\pi}\frac{p}{\rho}\right)^{1/2} \qquad (1.7\text{-}8)$$

V is the reference ordered flow speed,
T is the absolute temperature of gas stream,
R is the gas constant,
$\nu = \mu/\rho$ is the kinematic coefficient of viscosity,
$\gamma = c_p/c_v$ is the specific heat ratio,
δ is the boundary layer thickness.

When a laminar boundary layer on a flat, insulated plate is assumed, it becomes approximately

$$\frac{\delta}{L} = \frac{\text{const}}{(Re_L)^{1/2}} \sim \frac{1}{(Re_L)^{1/2}} \qquad (1.7\text{-}9)$$

The laminar boundary assumption is justifiable as a representative criteria, since under atmospheric flight conditions significant rarefaction effects for actual vehicle geometries are encountered only at considerable altitudes, where the boundary layer (if existing) is predominantly of a modified laminar type.

Depending on the numerical values of the three interrelated natural variables, M , Re and Kn , the respective boundaries between the four essentially different flow regimes are tentatively specified as follows: (see Figs. 1.17 to 1.20)

(1) Continuum flow regime prevails for relatively high Reynolds Number and relatively low Mach Number values, their ratio resulting in a negligibly small Knudsen Number:

$$Kn_\delta = \frac{\bar{\lambda}}{\delta} \sim \frac{M}{Re_L^{1/2}} < 10^{-2}$$

$$Kn_L = \frac{\bar{\lambda}}{L} \sim \frac{M}{Re_L} \ll 1$$

$$Re_L \gg 1\,, \quad 0 < M < 15 \qquad (1.7\text{-}10)$$

In the continuum flow regime the classical aerodynamic theories for incompressible subsonic, compressible subsonic, transonic, supersonic and hypersonic flow speeds are used. In absence of adequate data they can be, in a first approximation, tentatively extrapolated to the slip and even to the transitional flow regimes.

The continuum flow regime is encountered during most of the time history of atmospheric flights; notable exceptions are the satellite orbit, the skip-and-dive and the initial phase of re-entry trajectories.

(2) Slip flow regime boundaries have been approximately set at (34)

$$10^{-2} < \frac{M}{Re_L^{1/2}} \sim Kn_\delta = \frac{\bar{\lambda}}{\delta} < 10^{-1}$$

$$Re_L > 1\,, \quad M > 1 \qquad (1.7\text{-}11)$$

The Knudsen Number is still relatively small, but not negligible, indicating an onset of gas rarefaction. The effects are primarily confined to changed conditions inside the thickening viscous laminar boundary layer along the exposed body surfaces, and to the relative weakening of the shock wave profiles. The outer, inviscid stream patterns remain practically unchanged, (see Fig. 1.19). This is due to the fact that the mean free molecular path, $\bar{\lambda}$, becomes comparable to the characteristic viscous flow thickness, δ , (although $\bar{\lambda}$ is still, by order of magnitude, smaller than L), and the emerging discerningly discrete molecular structure brings about changes in the formulation of the internal (body surface) boundary conditions. As a result, the relatively rarefied molecular gas layer immediately adjacent to the immersed solid surface can no longer be assumed to be "at rest." The no-slip continuum flow assumption is no more valid, since the next-to-the-surface gas layer acquires a finite tangential velocity. This fact explains the corresponding term, "slip flow." Moreover, the velocity discontinuity at the body surface is accompanied by a corresponding "temperature jump" condition.

Generally, the slip flow regime criteria implies that either the Reynolds Number should be rather small or that the Mach Number should be very large. Their permissible variations within the slip flow regime must satisfy the indicated inequality limits of Eqs. (1.7-11). From the criteria it is evident that the slip flow rarefied gas effects occur in connection with either strong viscous or pronounced compressibility phenomena. Under actual high altitude, high speed atmospheric flight conditions, the "slip flow" rarefied gas regime is created predominantly due to strong compressibility effects, provided the Mach Number is still not excessively great while the corresponding Reynolds Number is great enough, so

that the two combined still ensure existence of a laminar boundary layer concept. This restriction is important, since at hypersonic speeds, coupled with extreme rarefactions (very low Re_L), the very concept of a boundary layer in the classical sense used for formulation of the above criteria loses its meaning. It should be noted that the laminar boundary layer assumption used in forming the proportionality in Eq. (1.7-11) is not restrictive for atmospheric flight conditions, since with the specified Reynolds and Mach Number values the flow laminarity on actual body geometries is assured (when the condition, $Re_L < 10^6$ is taken to approximate the upper limit of a laminar boundary layer existence at large.), see illustrative Fig. 1.20.

(3) Transitional flow regime, also called "mixed flow regime", is defined for flows in which the Knudsen Number variation is between

$$Kn_\delta = \frac{\bar{\lambda}}{\delta} \sim \frac{M}{Re_L^{1/2}} > 10^{-1} \quad \text{lower boundary}$$

$$Kn_L = \frac{\bar{\lambda}}{L} \sim \frac{M}{Re_L} < 3 \quad \text{upper boundary} \qquad (1.7\text{-}12)$$

It is characterized by a mean free molecular path of the same order of magnitude as the characteristic body length itself. As a consequence, the molecule-surface collisions and the molecule-molecule free stream collisions in the immediate vicinity of the immersed body are of the same importance, which renders the analysis of the transitional flow phenomena extremely complex. Existing theoretical solutions are so highly limited and the related empirical evidence so scarce that no reliable aerodynamic analysis is as yet available. Consequently, the aerodynamic force data related to either slip flow or to free molecular flow regimes are usually extrapolated to cover the transitional flow regime as well.

(4) Free molecular flow regime

A further increase in rarefaction makes the mean free molecular path, $\bar{\lambda}$, greater than a characteristic body dimension, L. The discrete molecular gas structure then becomes the governing factor, affecting the flow pattern formation around an immersed body in several ways, the two most important being:

(i) the classical concepts of a boundary layer and a shock wave are completely invalidated,

(ii) the individual molecules of such a highly rarefied gas impinge freely and without interference on the solid boundary, and after being re-emitted from the body surface travel several mean free molecular paths before becoming involved in an intermolecular collision at distances relatively far away from the immersed body. Obviously, the flow boundary conditions at the body surface are thus radically different from those of the classical continuum and the slip flow regime. The very mechanism of the molecular collisions with the body surface is changed to a far greater extent than in the previous cases of "slip" and "transitional" flows.

The lower boundary of the free molecular flow region cannot be determined on the basis of Kn_δ due to the absence of a boundary layer notion in its classical form. Instead, it is necessary that the Knudsen Number be interpreted in terms of $\bar{\lambda}$ and L. Then the onset of a free molecular flow regime can be tentatively defined by the condition

$$Kn_L = \frac{\bar{\lambda}}{L} \sim \frac{M}{Re_L} > 3 \ , \ Re_L \sim O(1) \qquad (1.7\text{-}13)$$

Obviously, this implies primarily hypersonic flight Mach Numbers and high flight altitudes, although any other lower Mach Number - Reynolds Number combination satisfying the above inequality is not ruled out, provided Re_L is kept below one in order to ensure a proper relatively high rarefaction existance.

In Fig. (1.19), the boundaries of the continuum, slip, transitional and free molecular flow regimes as functions of altitude and flight velocity, are illustrated with the vehicle characteristic length, L, taken as a parameter. The boundaries have been computed using data from Figs. (1.17) and (1.18) assuming a steady isothermal flow condition over an insulated flat plate at zero-angle-of-attack.

Under extremely rarefied atmospheric flight conditions the aerodynamic forces may bec me negligibly small compared with gravitational and inertial forces. Nevertheless, their computation in the free molecular flow regime becomes of relative importance in cases where they are applied over long periods of time, producing significant cumulative effects on the orbital and the skip and glide trajectory decay rates.

The high altitude, high speed flight regimes are characterized by extreme skin temperatures which eventually promote dissociation, ionization, chemical and electromagnetic reactions. Nevertheless, for practical aerodynamic force analysis purposes it is deemed convenient to analyze the rarefied gas effects by assuming nearly isothermal flow conditions at first, and then to add correctively the high temperature effects and the dissociation, ionization, chemical, ablative and other aspects in as much as they may significantly affect the aerodynamic force estimates. Figs. 1.21 to 1.28 a few illustrative samples of missile trajectories with indicated boundaries of different flow regimes are given as overplotted from Fig. 1.19.

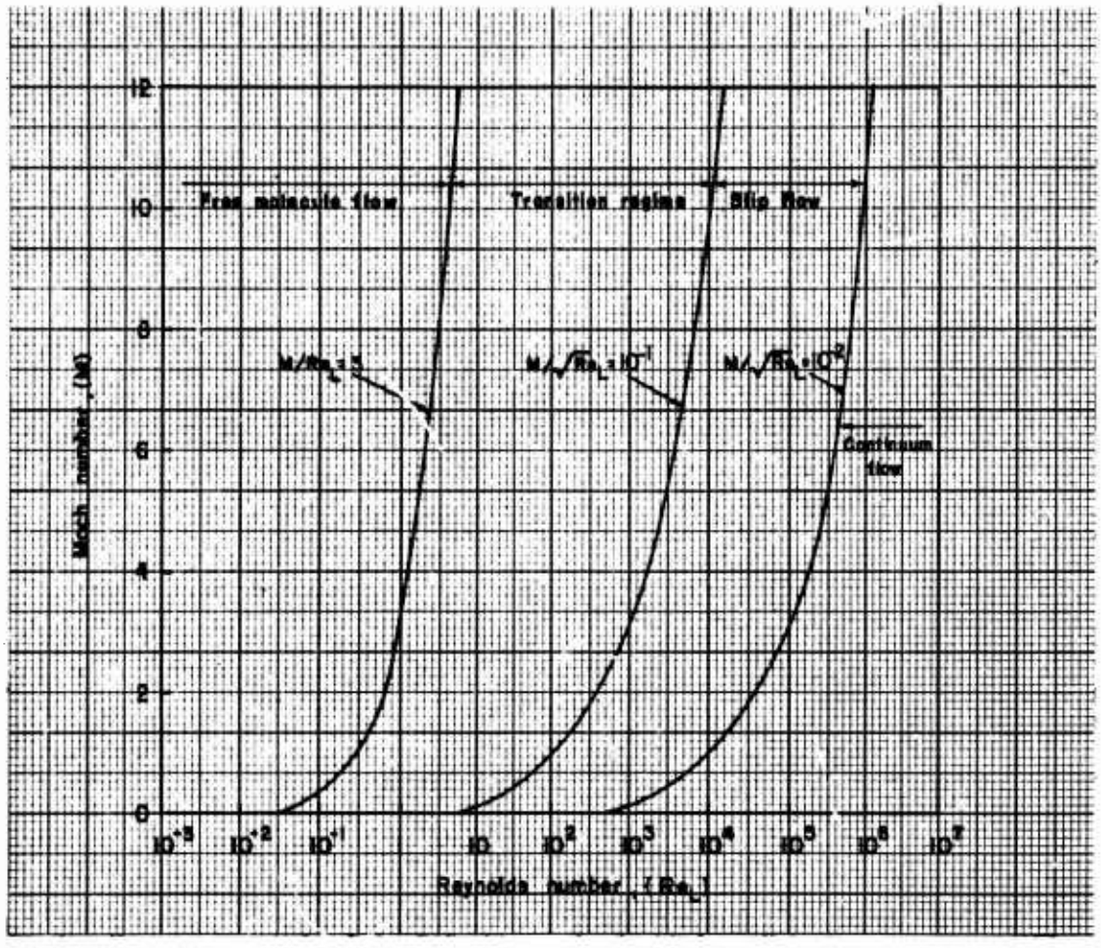

FIG. 1.17 The regimes of gas dynamics. (Ref. 34)

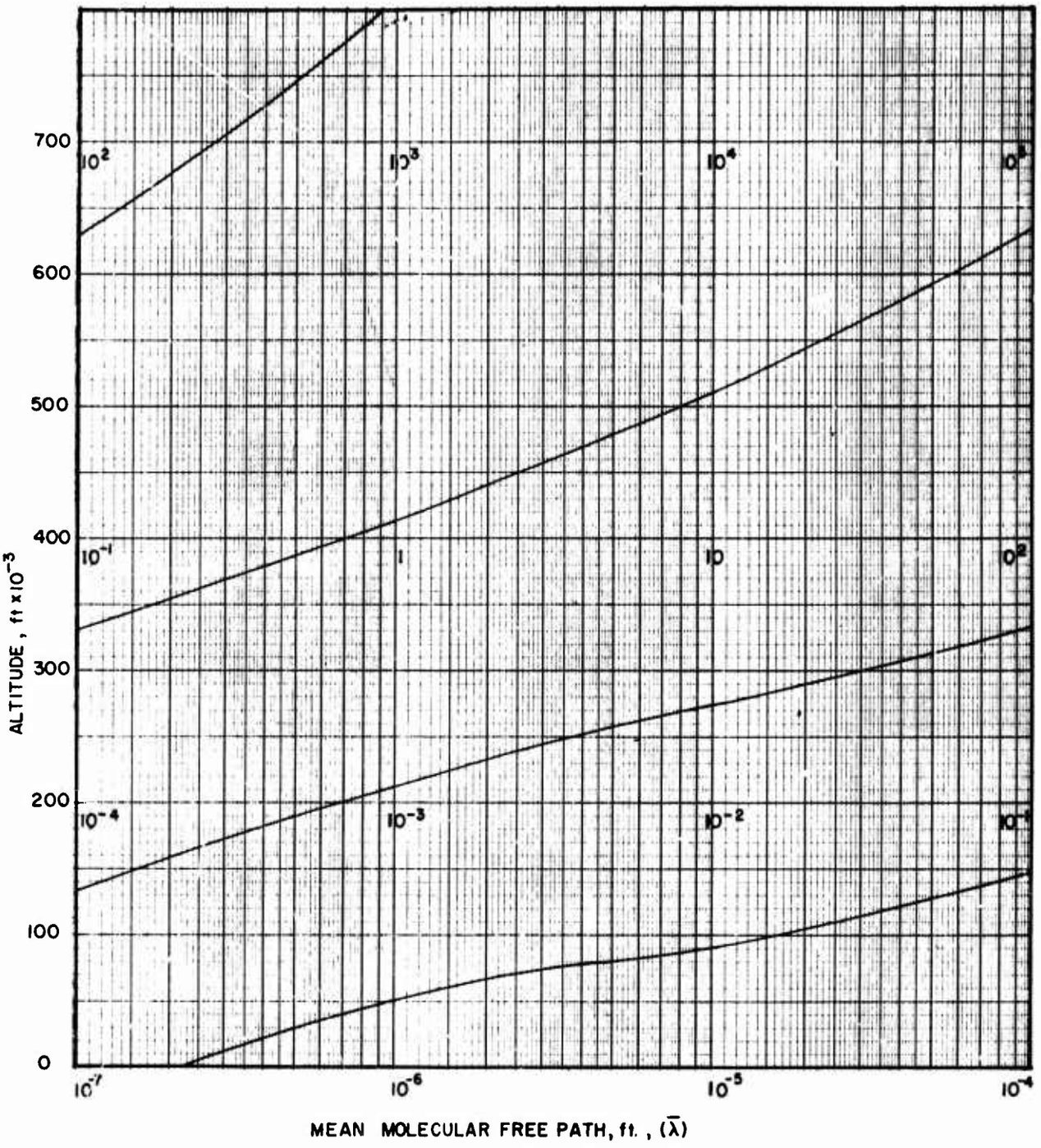

FIG. 1.18 Variation of the mean free molecular path with altitude in the NACA Standard Atmosphere. (347, Ref. 34)

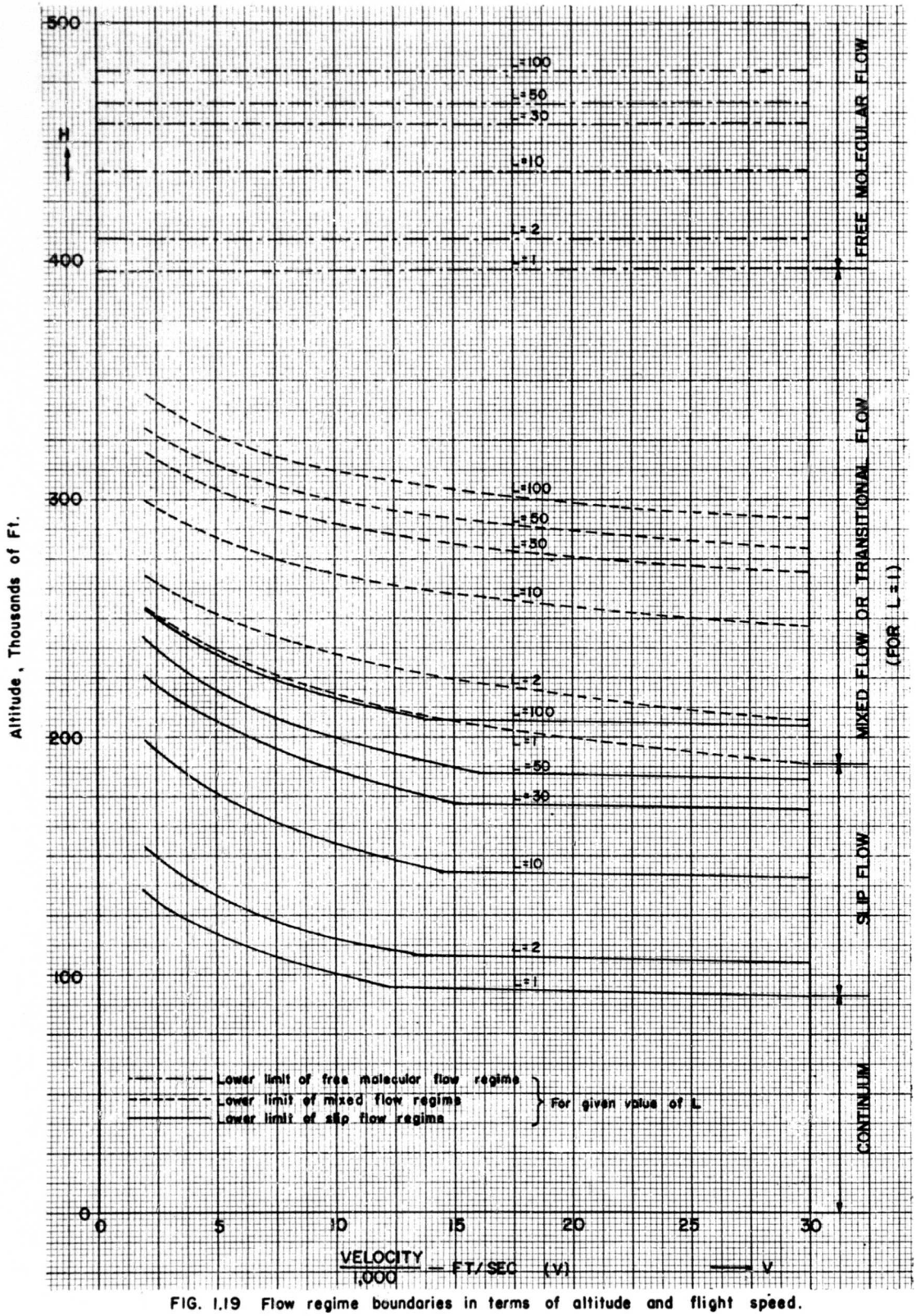

FIG. 1.19 Flow regime boundaries in terms of altitude and flight speed.

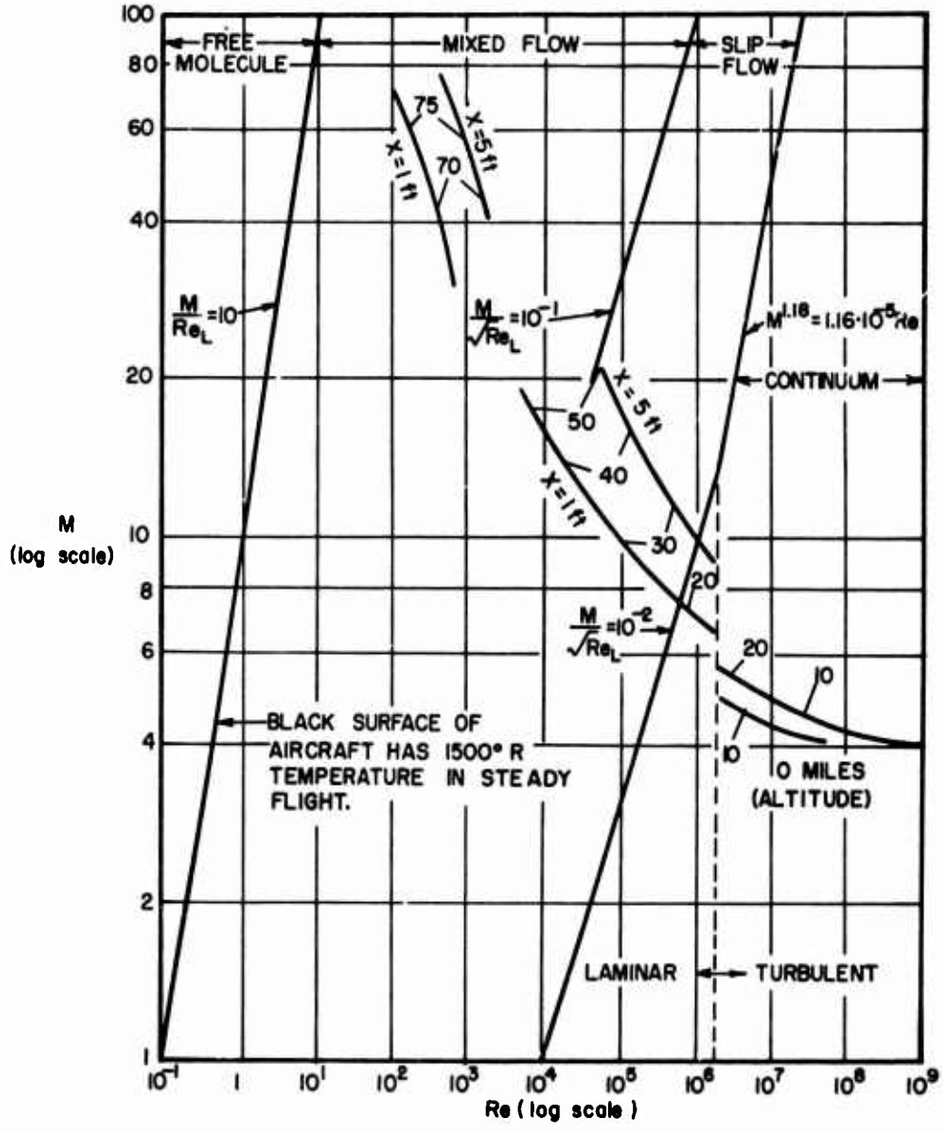

FIG. 1.20 Flow regimes in terms of ambient Mach Number (M) and Reynolds Number (Re_L) values. X is the distance from wing leading edge. (Ref. 37)

GLOSSARY - FIGURES 1.21 - 1.28

Notation

C_D -total drag force coefficient, dimensionless.
S -reference area, $ft.^2$
M -vehicle gross mass, slugs.
H -flight altitude, 10^3 ft.
Tew -maximum permissible equilibrium skin temperature for a presumed high grade steel material, ^oK; plotted for sustained flight conditions as a function of speed and altitude.
V -flight speed, 10^3 ft./sec.
I.R.B.M. -Intermediate Range Ballistic Missile.
I.C.B.M. -Intercontinental Ballistic Missile.
W -vehicle gross weight, lbf.
CF -centrifugal force, lbf.
L -aerodynamic lift force, lbf.

Description

Illustrative flight envelopes for a few missile categories are tentatively presented. Fig. 1.21, 1.24 and 1.26 are for ballistic vehicles for which no aerodynamic lift is required. Fig. 1.22 is for satellites and glide missiles. Fig. 1.23 and 1.27 are for skip and glide vehicles. Fig. 1.25 and 1.28 are for sustained flight and anti-missile missiles. Other related general flight data are tabulated in Table 1.7-1.

The space between the limit of aerodynamic lift and the allowable equilibrium surface temperature represents the "corridor" in which continuous prolonged flight is possible. The "allowable" skin temperature is defined in terms of inherent structural material properties without artificial heat-relieving devices (ablation, heat sink, etc.)

The illustrative ballistic missile curves in Fig. 1.21 are representative for presumably high drag-mass ratios ($C_D S/M \approx 4$) with a corresponding low re-entry angle, and for low drag-mass ratios ($C_D S/M \approx .05$) with a corresponding higher re-entry angle, respective to both categories illustrated in Fig. 1.21

The segments of the actual flight envelopes lying below the curves of the presumed maximum permissible equilibrium skin-temperature, Tew , curves indicate the necessity for an eventual introduction of artificial cooling techniques, taking into account the actual time-intervals during which the vehicle is exposed to the excessive heating rates. In this respect the relative advantage of high drag-mass ratio configurations at lower altitudes (H < 100,000 ft.) and at flight speeds less than 10,000 ft./sec. is evident. In general, a re-entering missile is likely to penetrate the imposed permissible equilibrium skin-temperature limit.

Vehicles involved in long range and orbital re-entry flight regimes, such as in Fig. 1.23, generally require aerodynamic lift for sustained flight conditions.

No lift is necessary for the spiralling-in part of a glide-vehicle trajectory during the re-entry phase and for the ballistic part of the skip-vehicle trajectory.

The air-breathing power plant missiles and the high-maneuverability anti-aircraft (or anti-missile) missiles in Fig. 1.25 require a sustaining lift force, the air-breathing missile to a greater extent due to its more prolonged sustained flight regime durations.

The actual skin-temperature conditions appear to be temporarily more severe for the anti-aircraft missiles, due to relatively higher flight speeds.

Both missile categories in Fig. 1.25 are operational at relatively lower altitudes (H < 150,000).

L – AERODYNAMIC LIFT FORCE, lbf
D – TOTAL AERODYNAMIC DRAG FORCE, lbf
$\frac{L}{D}$ – AERODYNAMIC CLEANLINESS OR AERODYNAMIC FINENESS FACTOR

	MANNED	NORMAL (LIFTING) 'g'	LONGITUDINAL (DECELERATING) 'g'	MAX C_N	C_{D_o}	MAX C_{D_i}	L/D	HEATING	ORDER OF WEIGHT lb	DESIGN ALTITUDE* 1000 FT
BALLISTIC RE-ENTRY										
LOW DRAG	NO	ZERO	VERY LARGE	ZERO	SMALL	ZERO	ZERO	VERY SEVERE	10^3-10^4	40 – 100
HIGH DRAG	NO	ZERO	VERY LARGE	ZERO	LARGE	ZERO	ZERO	SEVERE	10^3-10^4	70 – 150
SKIP VEHICLES										
LONG RANGE	NO	LARGE	MODERATE	VERY LARGE	MODERATE	LARGE	LARGE	INTERMITTENTLY SEVERE	10^3-10^5	100 – 250
ORBITAL RE-ENTRY	YES	LARGE	MODERATE	VERY LARGE	MODERATE	VERY LARGE	SMALL	INTERMITTENTLY SEVERE	10^4-10^5	150 – 300
GLIDE VEHICLES										
LONG RANGE	NO	SMALL	SMALL	LARGE	MODERATE	MODERATE	LARGE	MODERATE	10^3-10^5	180 – 240
ORBITAL RE-ENTRY	YES	SMALL	MODERATE	VERY LARGE	MODERATE	VERY LARGE	SMALL	MODERATE	10^4-10^5	200 – 300
SUSTAINED FLIGHT	YES	SMALL	VERY SMALL	MODERATE	SMALL	MODERATE	LARGE	MODERATE	10^5-10^6	80 – 150
ANTI-AIRCRAFT AND ANTI-MISSILE MISSILES	NO	VERY LARGE	LARGE	LARGE	SMALL	MODERATE	MODERATE	POSSIBLY SEVERE FOR SHORT TIME	10^3-10^4	40 – 100

* ALTITUDE AT WHICH DESIGN PROBLEMS ARE MOST SEVERE.

TABLE 1.7-1 – ILLUSTRATIVE REPRESENTATIVE BASIC DATA FOR THE MISSILE CATEGORIES REPRESENTED IN FIGURES 1.21, 1.23, 1.25 (REF. 38)

g - GRAVITATIONAL CONSTANT, ft/sec^2
C_N - NORMAL FORCE COEFFICIENT, DIMENSIONLESS, $C_N \sim C_L$
C_{D_o} - ZERO ANGLE OF ATTACK DRAG COEFFICIENT, DIMENSIONLESS
C_{D_i} - "INDUCED" (DUE TO LIFT) DRAG COEFFICIENT, DIMENSIONLESS
C_L - AERODYNAMIC LIFT FORCE COEFFICIENT, DIMENSIONLESS

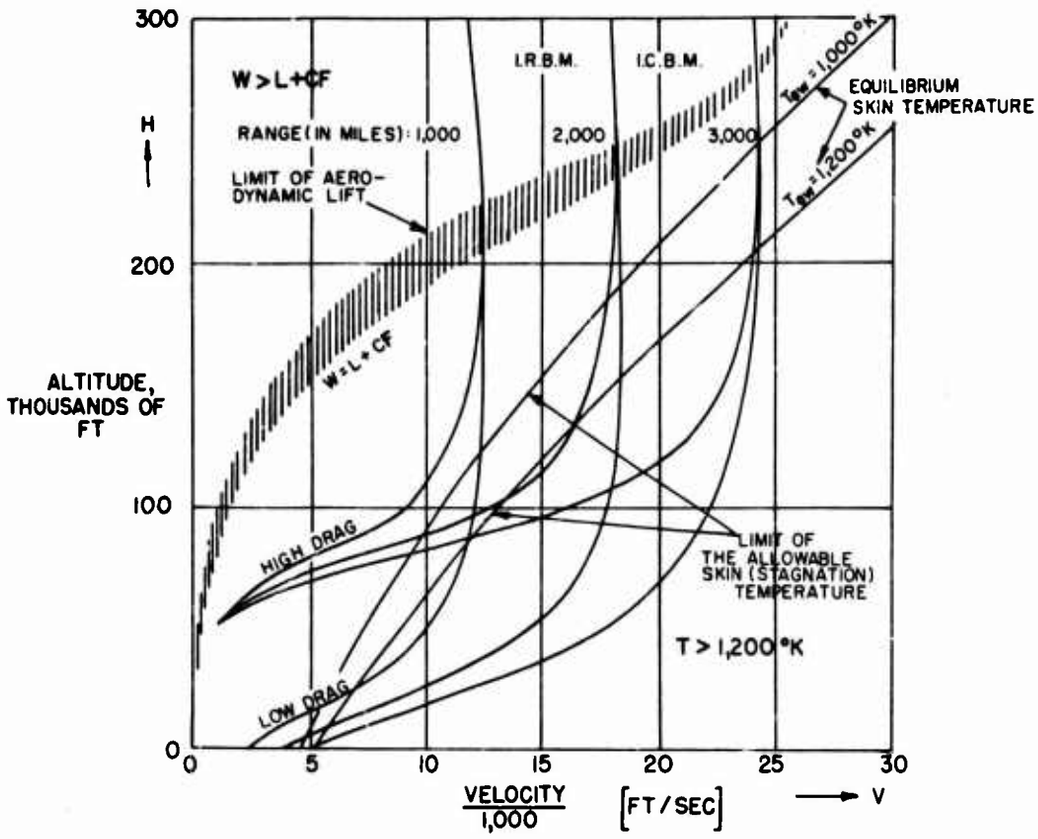

FIG. 1.21 Flight regimes for ballistic vehicles. No aerodynamic lift is required. (Ref. 38)
Space between the limit of aerodynamic lift and the allowable equilibrium surface temperature represents the "corridor" in which continuous prolonged flight is possible.
'Allowable' skin temperature defined in terms of inherent structural material properties without artificial heat-relieving devices (ablation, heat sink, etc.)

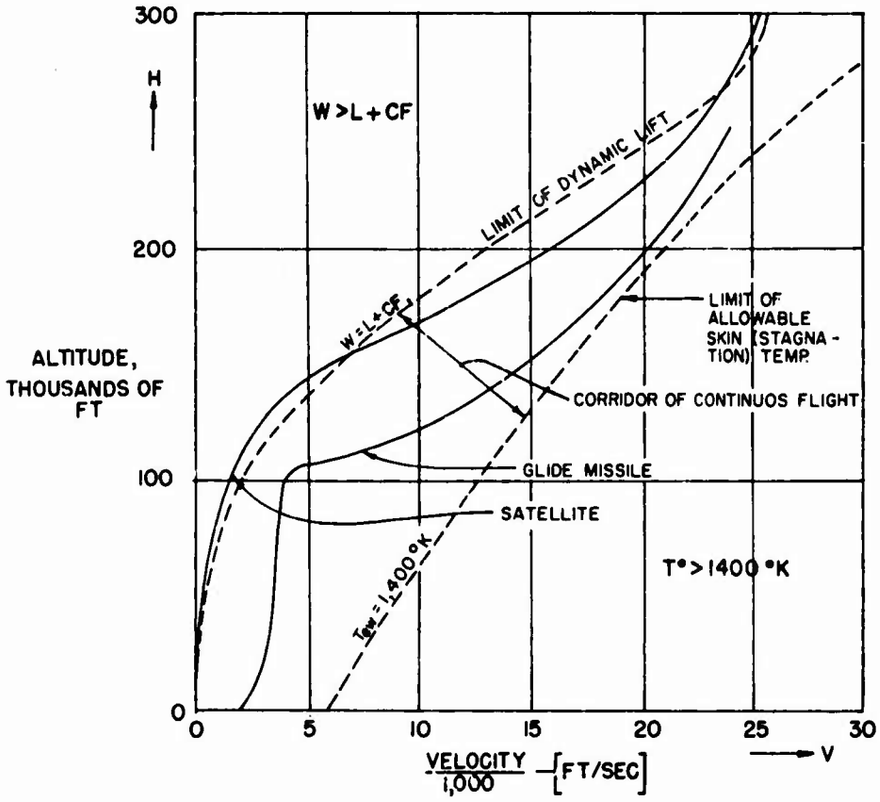

FIG. 1.22 Flight regimes for glide missile. (Ref. 38)
Space between the limit of aerodynamic lift and allowable equilibrium surface temperature represents the "corridor" in which continuous prolonged flight possible.
"Allowable" skin temperature defined in terms of inherent structural material properties, without artificial heat-relieving devices (ablation, heat sink, etc.)

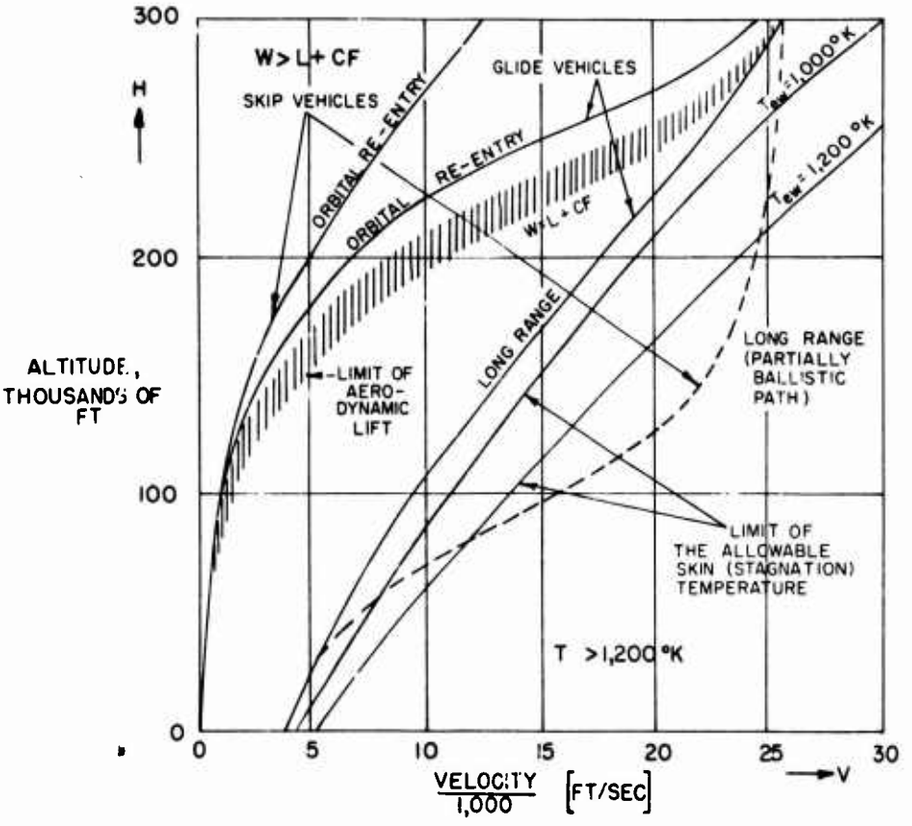

FIG. I.23 Flight regimes for skip and glide vehicles. (Ref.38) Space between the limit of aerodynamic lift and the allowable equilibrium surface temperature represents the "corridor" in which the continuous prolonged flight is possible. "Allowable" skin temperature defined in terms of inherent structural material properties without heat-relieving devices (ablation, heat sink, etc.)

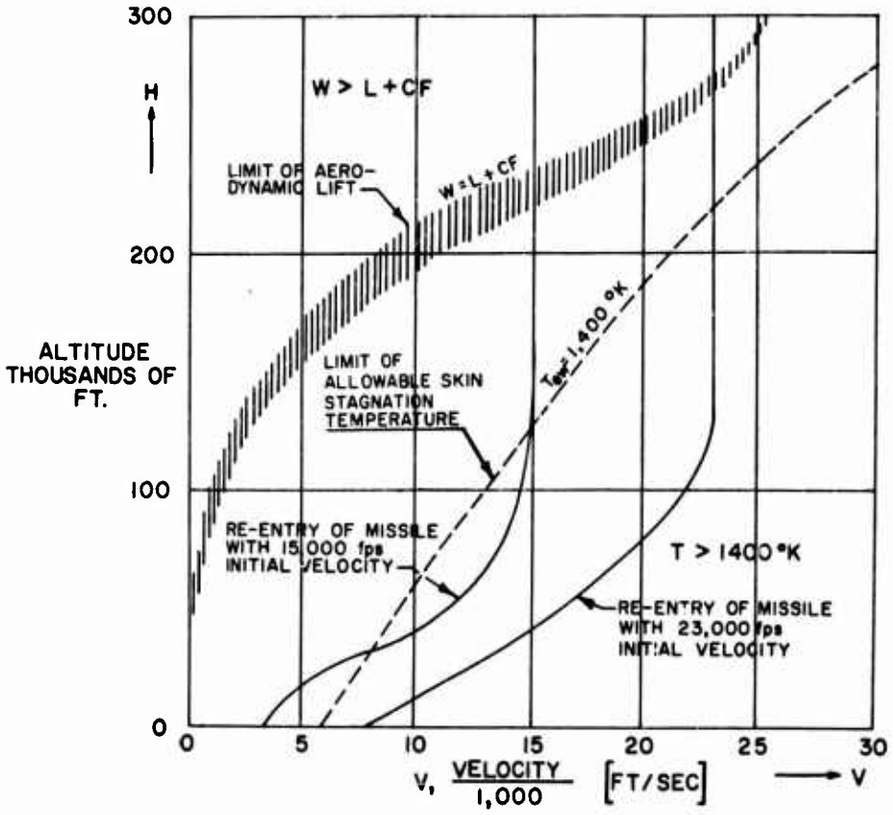

FIG 1.24 Flight regimes for ballistic vehicles.(Ref. 38)
Space between the limit of aerodynamic lift and allowable equilibrium surface temperature represents the "corridor" in which continuous prolonged flight is possible.
"Allowable" skin temperature defined in terms of inherent structural material properties without artificial heat-relieving devices (ablation, heat sink, etc.)

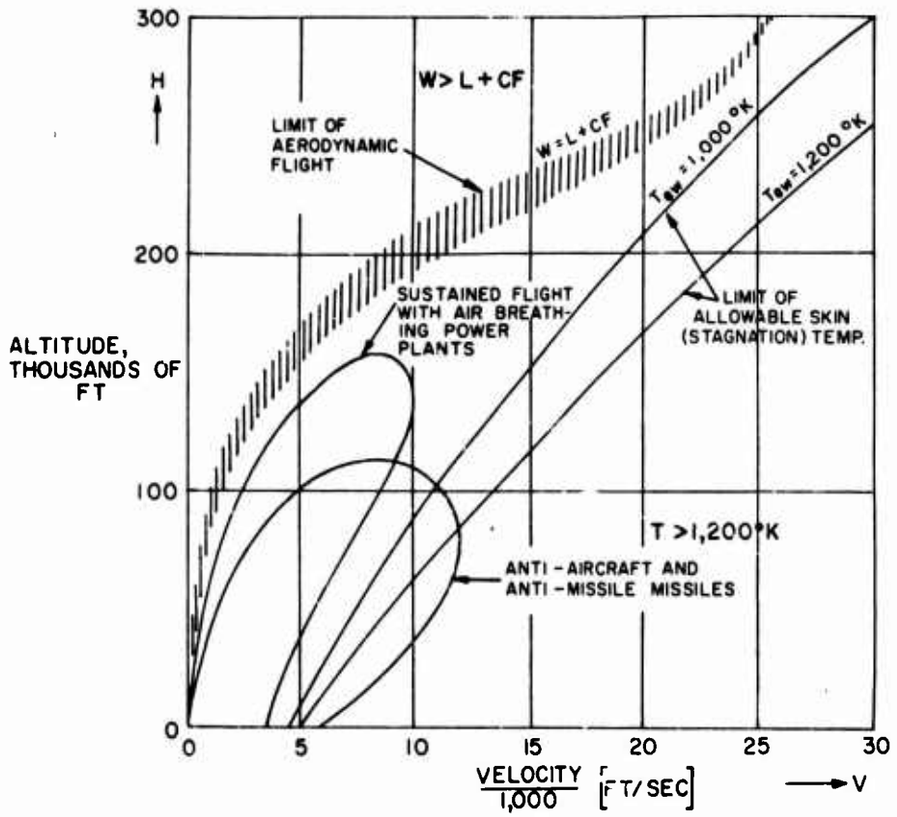

FIG. 1.25 Flight regimes for sustained flight and anti-missile missiles. (Ref. 38)
Space between the limit of aerodynamic lift and the allowable equilibrium surface temperature represents the "corridor" in which the continuous prolonged flight is possible.
"Allowable" skin temperature defined in terms of inherent structural material properties without artificial heat-relieving devices (ablation, heat sink, etc.)

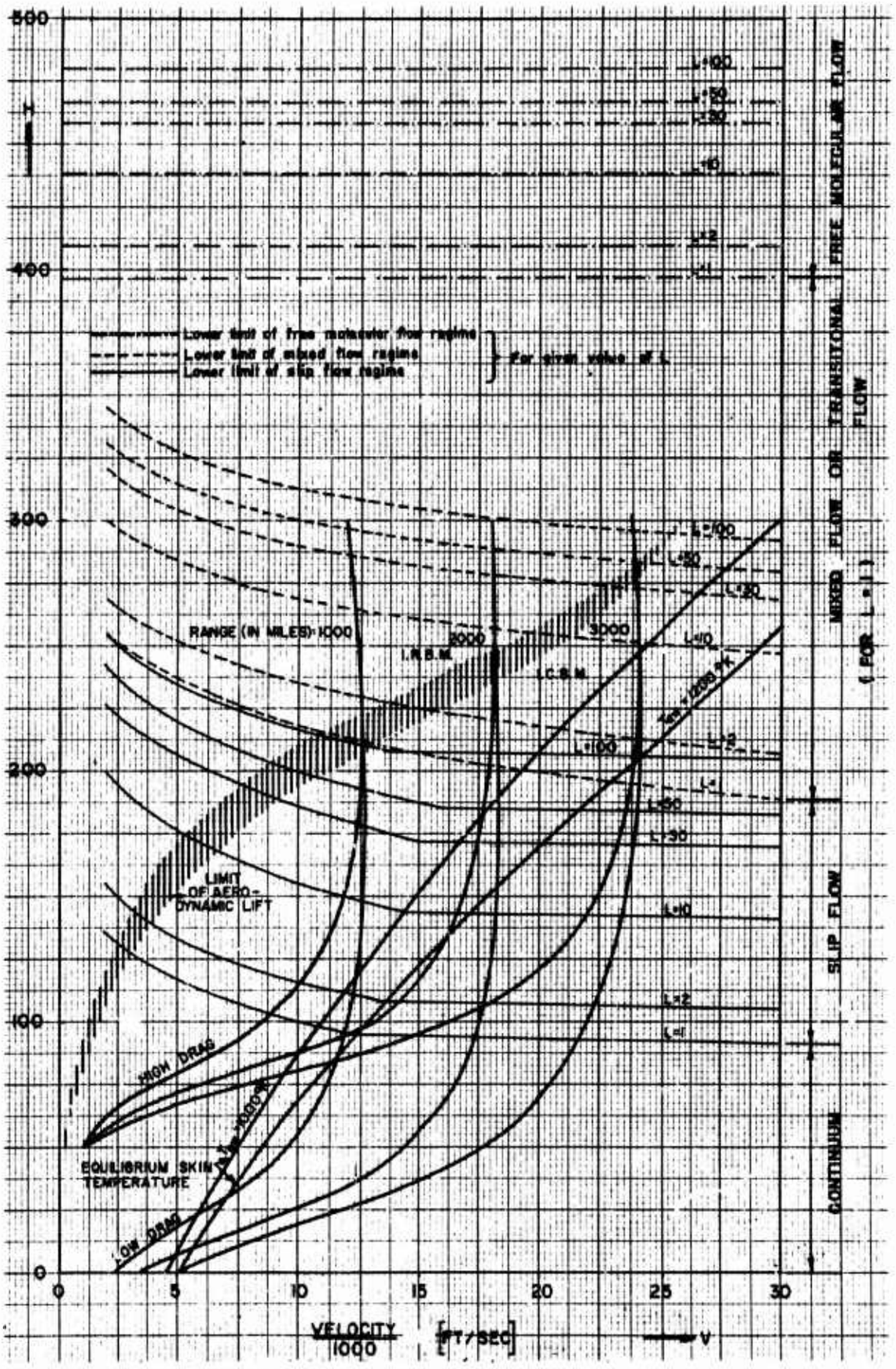

FIG. 1.26 Flow regime boundaries for ballistic vehicles.

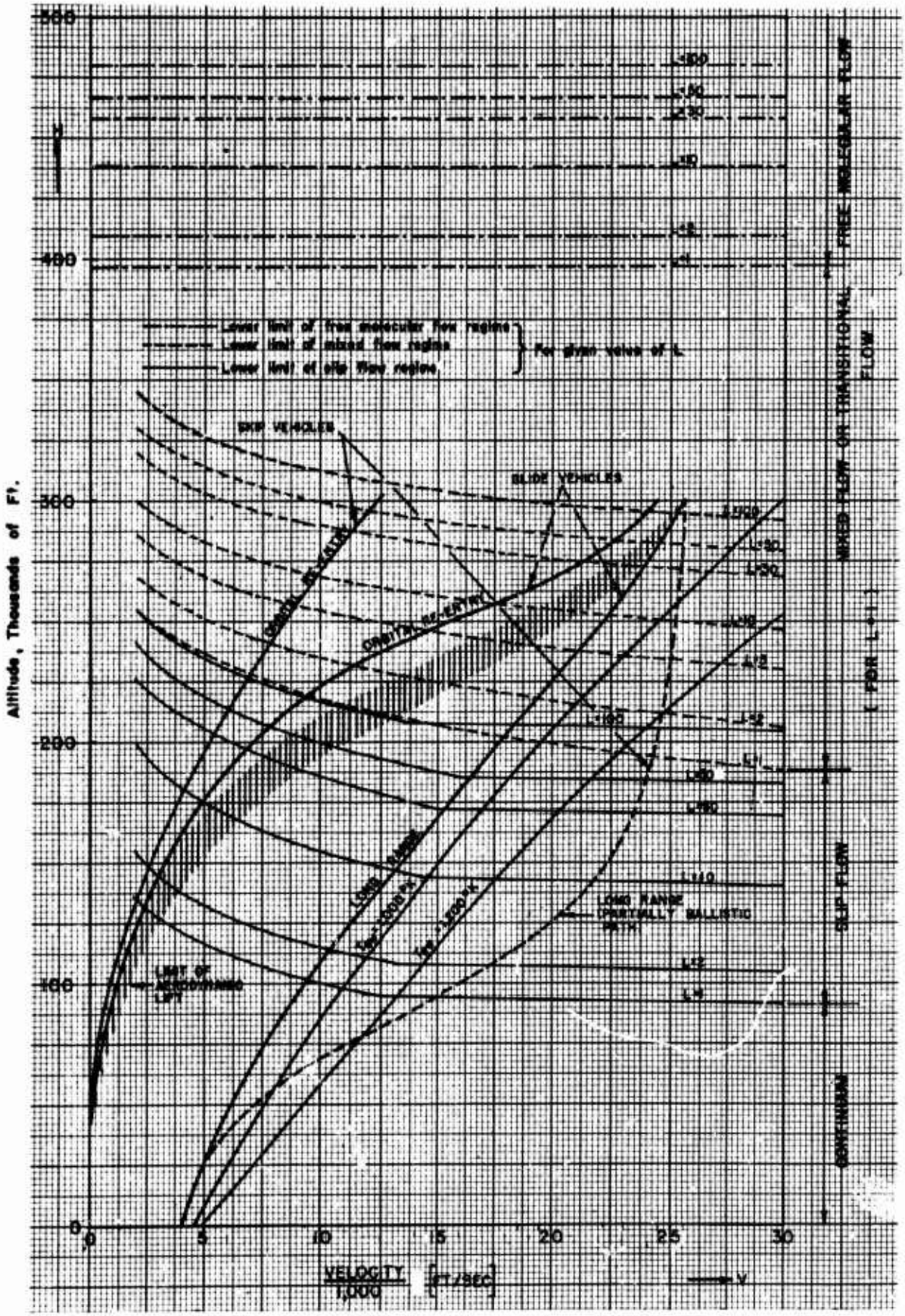

FIG. I.27 Flow regime boundaries for skip and glide vehicles.

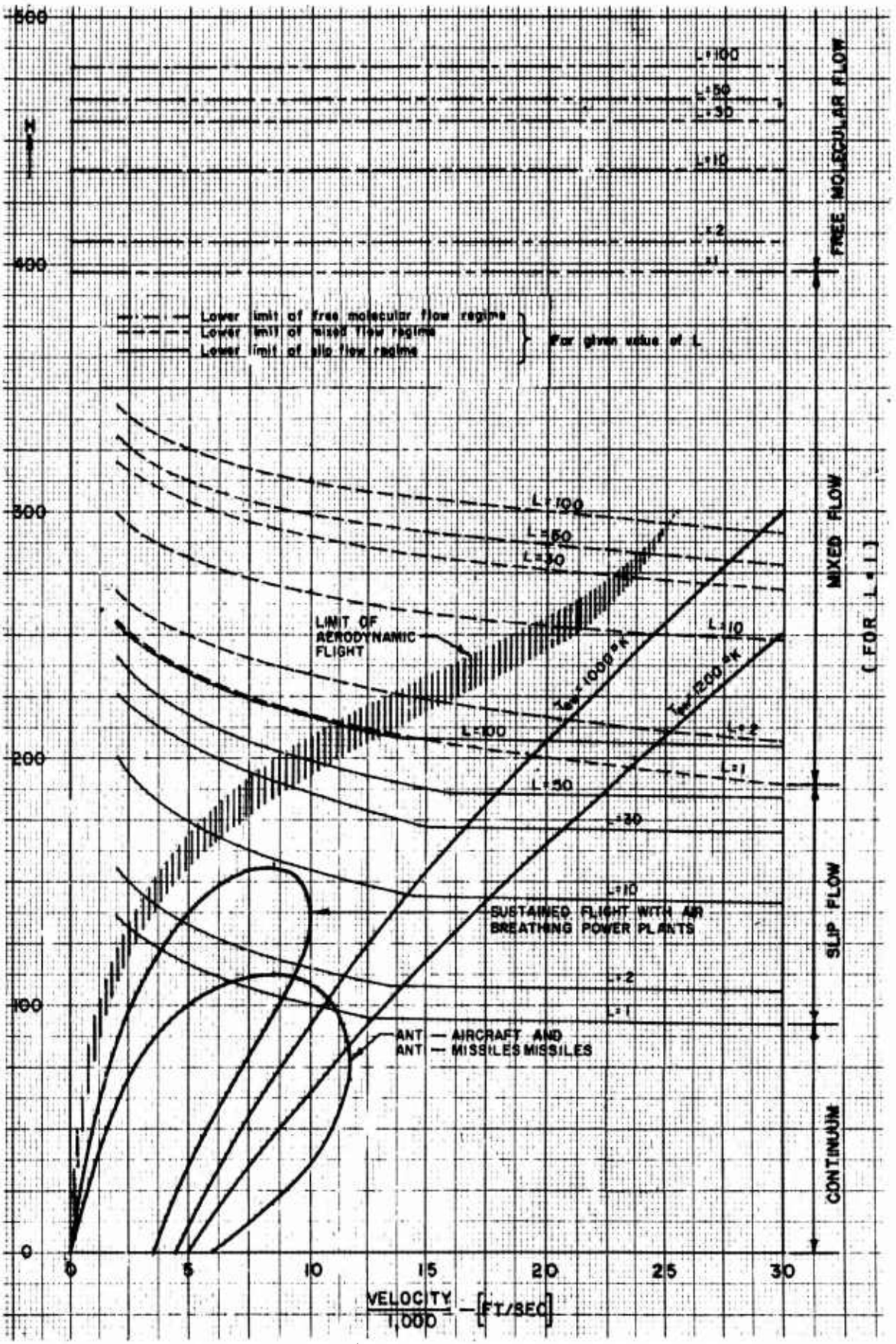

FIG. 1.28 Flow regime boundaries for sustained flight and anti-missile missiles.

1.7.2 FLIGHT SPEED REGIMES FOR CONTINUUM FLOW

The second practically useful subdivision of possible flow patterns in terms of the relative intensity of compressibility effects entails two basic premises:

(1) It is strictly meaningful for the continuum flow regime only, i.e., for flow patterns characterized by

$$Kn_L = \frac{M}{Re_L} << 1 \ , \ Re_L >> 1 \ , \ 0 < M < O(15) \qquad (1.7\text{-}14)$$

In the rarefied gas flow domains, the inter-relationship between physical flow parameters and the associated fluid-body interaction mechanism are being essentially changed, rendering the classical flow compressibility formulations through the Mach Number concept the more inapt the higher degree of rarefaction is realized. Thus, although the Mach Number definition is nominally retained, the shock wave pattern and the boundary layer structure become increasingly diffuse from slip to transitional flow regimes, finally disappearing completely at the free molecular flow conditions. This, coupled with the changes in solid boundary conditions and the very nature of momentum, mass and energy transport mechanisms makes the flight speed regimes distinction based on the Mach Number compressibility criteria progressively invalid with the onset of rarefied flow conditions.

However, despite the above argumentation, the aerodynamic force analysis of the continuum flow regime is tentatively extended, with slight modifications, to the slip flow and sometimes even to the transitional flow regimes, primarily due to lack of respective theoretical and/or experimental data. Therefore, the restriction (1.7-14) necessarily becomes conditional.

(2) The theoretically extremely useful Prandtl's postulate is maintained: the overall flow field is conceived to consist of a relatively thin, pronouncedly viscous flow region over exposed surfaces (boundary layer) and of an outer inviscid streamlined flow pattern, the two being treated separately by respective theoretical methods of analysis.

Then, depending upon the degree of compressibility and its impact upon the internal aerothermodynamic flow mechanism, both the viscous and the inviscid continuum flow states can be conveniently subdivided into five major speed regimes using the Mach Number as a primary reference. Furthermore, the subdivision can be performed according to either flight dynamics or aerodynamic considerations. Thus:

(i) When the value of the ambient flight Mach Number

$$M_A = \left(\frac{V}{a}\right)_A \qquad (1.7\text{-}15)$$

is used as a criterion, five characteristic "flight speed regimes" are defined:

(1) incompressible subsonic flight regime, $0<M_A<.4$
(2) compressible subsonic flight regime, $.4<M_A<.8$
(3) transonic flight regime, $.8<M_A<1.2$
(4) supersonic flight regime, $1.2<M_A<5$
(5) hypersonic flight regime, $5<M_A<O(15)$

When extending thus formulated boundaries to more general (and in flight more common) cases of curvilinear (maneuver) and unsteady (accelerated) atmospheric flight regimes, two main alternatives are possible:

Either the established steady, rectilinear flight speed criteria are applied assuming that they are conditionally valid instantaneously at the corresponding points on the trajectory for a vehicle in an accelerated, curvilinear flight condition. The trajectory is locally approximated by its tangent (or its chord). The curvilinear flow, apparent mass and other unsteady, time dependent, aerodynamic and inertial effects due to acceleration are neglected. This treatment is conditionally called "quasi-steady."

Or, the assumed steady, rectilinear criteria are corrected and re-evaluated at each point on the general curvilinear flight trajectory, by accounting for the specific curved flow geometry, the acceleration effects, the time-lag effects upon the aerodynamic pressure distribution and heat transfer rates under the generally non-equilibrium aerothermal conditions, etc.. Such a corrective analysis is clearly of an unsteady transient type and therefore usually lengthy, involved, and pronouncedly lacking in reliable theoretical and/or experimental evidence needed for general practical

purposes.

It is evident that, in general, the cited flight speed boundaries in terms of the flight Mach Number values, M_A, body geometry and its attitude are necessarily of an indicative order-of-magnitude nature. In cases of compound vehicle geometries, the actual numerical values of the boundaries between different flight (and flow) speed regimes should be evaluated for every individual componental body shape in situ, i.e. including interference effects when possible. Then, the most critical M_A values for lower and upper boundaries are taken when establishing the extent of each flight speed regime.

(ii) A similar subdivision can be effected on theoretical grounds. The somewhat changed boundaries, reflecting both the differing analytical form of the governing equations of motion and the degree of approximation with which the underlying physical flow aspects are mathematically handled within specified fluid-body systems. The corresponding flow states are then tentatively called "flow speed regimes", and the valid criterion for subdivision becomes the local Mach Number value at any critical point on a given body configuration:

(1) steady incompressible flow speed regime, $0<M<.4$
(2) steady compressible subsonic flow speed regime, $.4<M<M_{CR}=1$
(3) (unsteady) transonic flow regime, $M=M_{CR}=1$
(4) supersonic flow regime, $(M_{CR}=1)<M<5$
(5) steady hypersonic flow regime, $M>5$

Near the critical value of local Mach Number, $M_{CR}=1$, the theoretical subdivision is rather fictitious from an experimental point of view. The transonic flow regime, characterized by the onset of an unstable shock wave pattern, is intrinsically of an unsteady, transient nature for a span of Mach Number values greater than one. A steady supersonic flow speed regime actually sets in only after both the bow and the trailing shock wave patterns are firmly established. The extension of the transonic flow realm beyond the $M_{CR}=1$ value depends on the body geometry and its attitude with respect to the assumed uniform stream conditions at infinity.

1.7.3 CONVENTIONAL FUNCTIONAL REPRESENTATIONS OF AERODYNAMIC FORCE COEFFICIENTS

In terms of properly defined natural variables for a given vehicle geometry, flight speed and flow regime, the lift and the drag force given in Eq. (1.7-1) take the convenient dimensionless functional form

$$C_L = \frac{L}{(\rho_A V_A^2/2)S_{ref}} = \frac{L}{(1/2)p_A \gamma_A M_A^2} =$$

$$= C_L(\alpha_a, \delta_E, \gamma, M, Re, Kn, Pr, St....)$$

$$C_D = \frac{D}{(\rho_A V_A^2/2)S_{ref}} = \frac{D}{(1/2)p_A \gamma_A M_A^2} =$$

$$= C_D(\alpha_a, \delta_E, \gamma, M, Re, Kn, Pr, St....) \qquad (1.7\text{-}16)$$

where the number of involved similarity parameters depends on the nature of the actual physical occurrence. The nondimensionalizing factor

$$(\rho_A V_A^2/2)S_{ref} = \frac{\rho_A V_A^2}{2}\frac{\gamma_A R T_A}{a_A^2} S_{ref} = \frac{p_A \gamma_A M_A^2}{2} \qquad (1.7\text{-}17)$$

renders the numerical value of C_L and C_D implicitly dependent on the dynamic pressure variation with flight altitude and the choice of the common reference area of a compound vehicle configuration.

As pointed out in Sections 1.7.1 and 1.7.2, for flight dynamics and general aerodynamics computational and comparative purposes, it is customary to express the lift and the drag coefficients conditionally as explicit functions of the aerodynamic angle-of-attack, α_a, the elevator deflection angle, δ_E, the Knudsen Number, the Mach Number, and the Reynolds Number only.

All other influential natural variables, reflecting rarefaction and thermal effects, are then contained implicitly in the different forms of the related functional laws of the involved local skin friction coefficients, C_f, and the local pressure coefficients, C_p, as applicable to a given flight speed and flow type regime.

$$C_L = C_L(\alpha_a, \delta_E, M, Re, Kn)$$

$$C_D = C_D(\alpha_a, \delta_E, M, Re, Kn) \qquad (1.7\text{-}18)$$

Furthermore, it is formally assumed that, as long as there is no pronounced flow separation, the variation of the normal pressure distribution is independent of the Reynolds Number, and that the tangential shear stress distribution on the wetted surfaces is practically independent of the presumed small variations in angle-of-attack. Then, within the overall restrictions and the approximations stated in Section 1.6, the fundamental lift and drag coefficients, Eqs. (1.6 - 120) to (1.6 - 125), for a given vehicle configuration, flight speed and flow regime are treated conventionally in the explicit parametric forms:

$$C_{p_i} = \left[C_{p_i}\right]_{\alpha_a=0} + \left[\Delta C_{p_i}\right]_{\alpha_a}$$

$$\left[C_{p_i}\right]_{\alpha_a=0} = C_p(\theta_i, \alpha_{0_i}, \alpha_i, M, Kn, \gamma, Pr, St .....)_{\alpha_a=0}$$

$$\left[\Delta C_{p_i}\right]_{\alpha_a} = C_p(\theta_i, \alpha_{0_i}, \alpha_i, M, Kn, \gamma, Pr, St .....)_{\alpha_a}$$

$$C_{f_i} = \left[C_{f_i}\right]_{\alpha_a=0} = C_f(\theta_i, M, Kn, Re, \gamma, Pr, St .....)_{\alpha_a=0} \qquad (1.7\text{-}19)$$

and

$$C_L = \frac{1}{S_{ref}} \sum_{i=1}^{n} \int_{(S_{wet})_i} (\Delta C_{p_i})_{\alpha_a} \vec{n}_i \cdot \vec{k}_a \, dS_i = C_L(\alpha_a, \delta_E, M, Kn) \qquad (1.7\text{-}20)$$

$$\sum_{i=1}^{n} \int_{(S_{wet})_i} (C_{p_i})_{\alpha_a=0} \vec{n}_i \cdot \vec{k}_a \, dS_i = 0$$

$$\sum_{i=1}^{n} \int_{(S_{wet})_i} (\Delta C_{f_i})_{\alpha_a=0} \vec{t}_i \cdot \vec{k}_a \, dS_i = 0 \qquad (1.7\text{-}21)$$

$$C_D = C_{D_0} + C_{D_i} = \frac{1}{S_{ref}} \sum_{i=1}^{n} \int_{(S_{wet})_i} \left[(C_{p_i})_{\substack{\alpha_a=0 \\ \alpha_a=0}} \vec{n}_i \cdot \vec{i}_a + (C_{f_i})_{\alpha_a=0} \vec{t}_i \cdot \vec{i}_a\right] dS_i$$

$$+ \frac{1}{S_{ref}} \sum_{i=1}^{n} \int_{S_{wet}} (\Delta C_{p_i})_{\alpha_a} \vec{n}_i \cdot \vec{i}_a \, dS_i \qquad (1.7\text{-}22)$$

and

$$C_D = C_D(\alpha_a, \delta_E, M, Re, Kn)$$
$$C_{D_0} = C_D(\delta_E, M, Re, Kn)$$
$$C_{D_i} = C_D(\alpha_a, \delta_E, M, Kn) \qquad (1.7\text{-}23)$$

where (except for C_{D_i} subscript "i" denotes the "i"-th individual part of a compound configuration, θ_i is the local incidence angle of the surface element dS_i respective to a common reference line Ox_b of the compound vehicle configuration, while the individual zero-lift angle-of-attack, α_{0_i}, and the individual geometric angle-of-attack, α_i, of the "i"-th configurational part are expressed in terms

of the representative aerodynamic angle-of-attack, $\alpha_a = \alpha - \alpha_o$, for the overall vehicle configuration. (See Eqs. (1.6 - 46) to (1.6 - 57), Section 1.6.2).

For a given set of Reynolds and Mach Numbers, the basic parametric relationships in Eqs. (1.7 - 20) and (1.7 - 22) are graphically illustrated in Fig. 1.29. The illustration is restrictively representative for subsonic and supersonic speed regimes within the continuum flow concepts. The lift force coefficient is presumed independent of Reynolds Number for relatively small angles-of-attack and follows approximately a straight line law in terms of the representative angle-of-attack nearly to the stall point, S, where the pronounced flow separation and the Reynolds Number effects become all important, usually reducing abruptly the lift coefficient values.

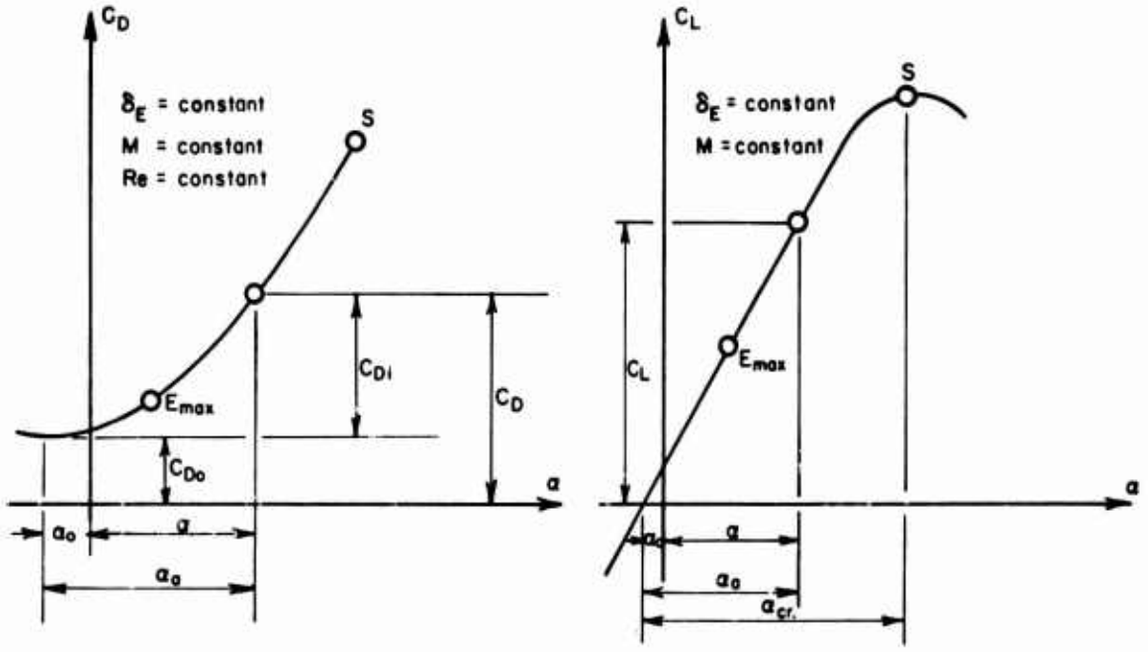

FIG. 1.29 Illustrative plots of drag force coefficient, C_D, and lift force coefficient, C_L, versus representative angle of attack, α, at subsonic or supersonic speeds in the continuum flow regime for vehicles possessing a vertical plane of geometric symmetry. (S = stall point, E_{max} = maximum aerodynamic efficiency point)

The total drag coefficient dependence on the representative angle-of-attack, α, is generally of a pseudoparobolic type, the zero-lift drag coefficient value corresponding to the $\alpha_a = 0$ condition being automatically the minimum drag coefficient value if the vehicle geometry has a vertical plane of symmetry. At hypersonic speeds the $C_L = C_L(\alpha_a)$ law becomes non-linear even for small angles-of-attack.

GENERALIZED DRAG POLAR CONCEPT

The total drag force coefficient, C_D, is subdivided into two parts, Eq. (1.7-22): the zero lift (or the zero aerodynamic angle-of-attack) drag coefficient, C_{D_o}, and the "lift induced" drag coefficient, C_{D_i}. This subdivision leads to the generalized drag polar concept, which has advantages for some flight dynamics and fluid mechanics purposes and it is obtained by introducing the formalistic relationships:

$$C_{Di} = \frac{1}{S_{ref}} \sum_{i=1}^{n} \int_{(S_{wet})_i} (\Delta C_{p_i})_{\alpha_a=0} \vec{n}_i \cdot \vec{i}_a \, dS_i =$$

$$= \frac{\kappa}{(S_{ref})^x} \left[\sum_{i=1}^{n} \int_{(S_{wet})_i} (\Delta C_{p_i})_{\alpha_a} \vec{n}_i \cdot \vec{k}_a \, dS_i \right]^x \qquad (1.7\text{-}24)$$

$C_{D_i} = \kappa C_L^{x}$

$C_L = C_L(\alpha_e, \delta_E, M, Re)$

$\kappa = \kappa(M, Re, \text{body geometry})$

$x = x(M, Re)$

$$C_D = C_{D_o} + C_{D_i} = C_{D_o} + \kappa C_L^{x} = C_D(\delta_E, C_L, M, Re) \qquad (1.7\text{-}25)$$

The parameters $\kappa(M,Re)$ and $x(M,Re)$ are called the induced drag factor and the drag polar exponent respectively. For a given body geometry they are generally functions of both Mach and Reynolds Numbers. In that way both parameters account for the flow separation phenomena and the boundary layer displacement effects upon the inviscid outer flow normal pressure distribution, i.e. upon the lift coefficient and the induced drag inter-relationship given in Eq. (1.7-24). As already stated, for small angles-of-attack and for given explicit values of lift coefficients, it is sometimes permissible to assume (in a first approximation) that the respective induced drag coefficients, C_{D_i}, are independent of Reynolds Number over the entire domain of flight speeds, i.e. $C_L = C_L(\alpha_e, \delta_E, M)$, $\kappa = \kappa(M)$, $x = x(M)$. The approximation is conditionally justifiable provided the rear flow separation is negligible, as in the case of some not-too-thin aerodynamically smooth configurations, (sharp trailing edges, pointed or properly boattailed bodies) when the boundary layer displacement thicknesses are small in comparison to actual relative thicknesses of the solid body crossections. Moreover, for low (incompressible) subsonic and higher hypersonic speeds, $M > 15$, both the induced drag coefficient and the zero-lift drag coefficient dependence on Mach Number is negligible (Newtonian Impact Theory).

In addition to the Mach Number and the Reynolds Number dependence, the induced drag factor, κ, is a strong function of the overall vehicle configuration, the geometry of lifting surfaces (wings primarily) being the most influential factor. The drag polar exponent, x, is primarily influenced by the speed regime (for a given value of C_L).

For symmetric, relatively thin winged and aerodynamically smooth vehicle configurations at relatively small angles-of-attack, the following κ and x values may be considered representative in a first approximation:

Incompressible subsonic speed regime, $0 < M < .4$:

$C_{D_o} = C_D(\delta_E, Re)$

$C_{D_i} = C_D(C_L)$

$x = 2 \qquad \kappa = \text{const}$

$$\therefore C_D = C_{D_o} + \kappa C_L^2 = C_D(\delta_E, C_L, Re) \qquad (1.7\text{-}27)$$

i.e. the drag polar takes a parabolic form, where κ is merely a constant characteristic for a given vehicle configuration.

Compressible subsonic flight speed regime, $.4 < M_A < M_{CR} \sim .8$

$C_{D_o} = C_D(\delta_E, Re, M)$

$C_{D_i} = C_D(C_L, M)$

$x = 2 \qquad \kappa = \kappa(M)$

$$\therefore C_D = C_{D_o} + \kappa C_L^2 = C_D(\delta_E, C_L, M, Re) \qquad (1.7\text{-}28)$$

Transonic flight speed regime, $\sim .8 < M_A < \sim 1.2$

$C_{D_o} = C_D(\delta_E, Re, M)$

$C_{D_i} = C_D(C_L, M, Re)$

$x = 2 \qquad \kappa = \kappa(M, Re)$

$$\therefore C_D = C_{D_o} + \kappa C_L^2 = C_D(\delta_E, C_L, M, Re) \qquad (1.7\text{-}29)$$

Note that the parabolic approximation for the inherently unsteady transonic flow conditions represents an engineering convenience only, the relative validity of the approximation remaining questionable.

Supersonic flight speed regime, $\sim 1.2 < M_A < 5$

$C_{D_o} = C_D(\delta_E, Re, M)$

$C_{D_i} = C_D(C_L, M)$

$x = 2 \qquad \kappa = \kappa(M)$

$$\therefore C_D = C_{D_o} + \kappa C_L^2 = C_D(\delta_E, C_L, M, Re) \qquad (1.7\text{-}30)$$

High hypersonic flight speed regime, $M_A \gg 1$

$C_{D_o} = C_D(\delta_E, Re)$

$C_{D_i} = C_D(C_L)$

$x = 3/2 \qquad \kappa = \text{const}$

$$\therefore C_D = C_{D_o} + \kappa C_L^{3/2} = C_D(\delta_E, C_L, Re) \qquad (1.7\text{-}31)$$

i.e. the drag polar follows a 3/2 exponent law (Newtonian Impact theory approximation).

AERODYNAMIC EFFICIENCY

The aerodynamic efficiency, E , or the lift-to-drag ratio is another useful criterion in flight dynamics computations. On the basis of the drag polar definition:

$$E = \frac{C_L}{C_D} = \frac{C_L}{C_{D_o} + C_{D_i}} = \frac{C_L}{C_{D_o} + \kappa C_L^x} \qquad (1.7\text{-}32)$$

For a definite vehicle configuration and a given elevator deflection angle, δ_E , and given Mach and Reynolds Numbers, its maximum value, E_{max} , is graphically determined by the tangent from the origin to the polar curve $C_D = C_D(\delta_E, C_L, M, R_e)$, as shown in Fig. 1.30 Algebraically, the necessary condition of maxima

$$\left(\frac{dE}{dC_L}\right)_{\delta_E, M, Re, const} = 0$$

$$\kappa = \kappa(M, Re) = const$$

$$x = x(M, Re) = const \qquad (1.7\text{-}33)$$

leads to the lift coefficient value

$$(C_L)_{E_{max}} = \left[\frac{C_{D_o}}{\kappa(x-1)}\right]^{1/x} \qquad (1.7\text{-}34)$$

and consequently to

$$E_{max} = \frac{1}{x}\left(\frac{x-1}{C_{D_o}}\right)^{\frac{x-1}{x}} \left(\frac{1}{\kappa}\right)^{1/x} \qquad (1.7\text{-}35)$$

from which the corresponding ratio of induced-to-zero lift drag ratio is obtained as

$$\frac{C_{D_i}}{C_{D_o}} = \frac{1}{x-1} \qquad (1.7\text{-}36)$$

Referring to the representative x values, Eqs. (1.7-27) to (1.7-30), it follows that for the subsonic, transonic and supersonic speed regimes ($x = 2$) the maximum aerodynamic efficiency is obtained when

$$C_{D_i} = C_{D_o} = \kappa C_L^2$$

$$(C_L)_{E_{max}} = \left[a(\alpha - \alpha_o)\right]_{E_{max}} = \left[\frac{C_{D_o}}{\kappa}\right]^{1/2}$$

$$(\alpha)_{E_{max}} = \left[\frac{1}{a}\left(\frac{C_{D_o}}{\kappa}\right)^{1/2} + \alpha_o\right]$$

$$a = \frac{\partial C_L}{\partial \alpha} \qquad (1.7\text{-}37)$$

while at high hypersonic speeds with $X = 3/2$

$$C_{D_i} = 2C_{D_o} = 2\kappa C_L^{3/2}$$

$$(C_L)_{E_{max}} = \left[a(\alpha - \alpha_o)\right]_{E_{max}} = \left(\frac{C_{D_o}}{2\kappa}\right)^{2/3}$$

$$(\alpha)_{E_{max}} = \left[\frac{1}{a}\left(\frac{C_{D_o}}{2\kappa}\right)^{2/3} + \alpha_o\right] \qquad (1.7\text{-}38)$$

The term "induced drag" coefficient originated in the classical incompressible subsonic theory of perfect, inviscid gas flows around three dimensional aerofoil shapes, i.e. it was originally associated with the vortex system shedding from the trailing edge and the tips of lifting surfaces. Here, the term is conditionally retained and extended to all speed regimes, but its meaning is respectively changed: the "induced drag" coefficient comprises any kind of drag coefficient increment due to lifting conditions ($\alpha_o \neq 0$), not only the "vortex drag" contribution.

DRAG COEFFICIENT DEPENDENCE ON MACH NUMBER

In aerodynamic practice it is also customary to express the explicit dependence of the drag coefficient on Mach Number, treating the other primary variables, $(\alpha_o, \delta_E, R_e, H)$ as conditional parametric constants. Then, retaining the drag polar concept, the resulting parametric families of curves $C_D = C_{D_o} + C_{D_i} = C_D(M)$ serve as a very convenient basic reference for aerodynamic drag force data in flight dynamics, performance and stability and control computations. For a given vehicle configuration, possessing at least one (vertical) plane of geometric symmetry and within the general approximations and limitations specified in Sections 1.6 and 1.7, the explicit parametric dependence $C_D = C_D(M)$ is thus conditionally established as follows:

(1) For a given set of δ_E and M_A values and a fixed flight altitude, H , the zero-lift drag force coefficient value ($\alpha_o = 0$) is computed first in terms of the reference Reynolds Numbers of

the individual (i) parts of a given compound vehicle configuration:

$$(Re_{L_i})_A = \frac{\rho_A V_A L_i}{\mu_A}$$

$$M_A, \delta_E, H = \text{const}$$

$$C_{D_0} = C_{D_0}(Re_{L_i})_A \qquad (1.7\text{-}39)$$

In order to facilitate numerical evaluations of the corresponding reference $M_A = M_H$ and $(Re_{L_i})_A = (Re_{L_i})_H$ values at a given flight altitude, H, i.e. for a given ambient flight speed, V_A, and the characteristic body length L_i of the "i"-th part, the related data $(Re/L)_H = f(M_A, H)$ in Figs. 1.31 and 1.32 and in Table 1.7-2 are presented for convenience. There, the Standard ARDC 1958 Atmosphere is assumed, and the computations are performed using the relationships:

$$\left(\frac{Re}{L}\right)_H = \left(\frac{Re}{L_i}\right)_A = \frac{V_A \rho_A}{\mu_A}$$

$$\rho_A = \rho(H)$$

$$\mu_A = \mu(H)$$

$$V_A = a_A M_A$$

$$a_A = a(H) \qquad (1.7\text{-}40)$$

$$\therefore \left(\frac{Re}{L}\right)_H = M_A \frac{a_A \rho_A}{\mu_A} = M_A \cdot K(H)$$

$$K(H) = \frac{a_A \rho_A}{\mu_A} = \frac{a_A}{\nu_A} \qquad (1.7\text{-}41)$$

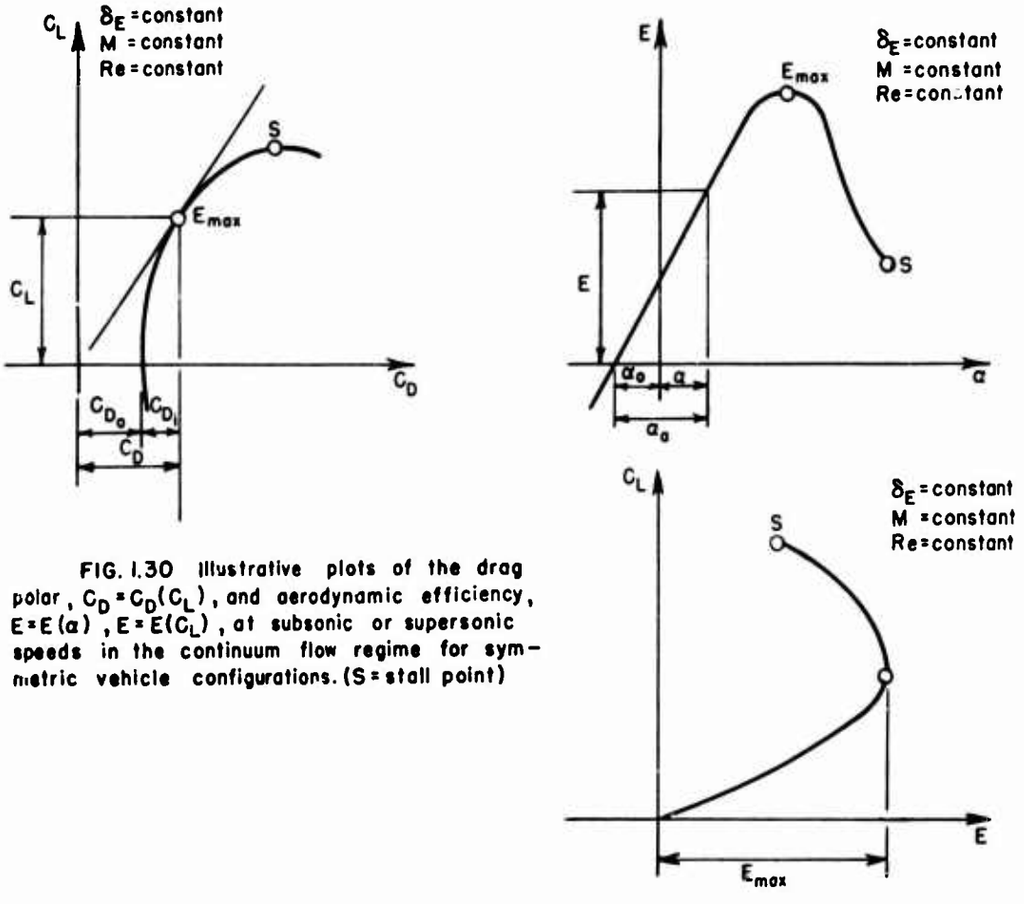

FIG. 1.30 Illustrative plots of the drag polar, $C_D = C_D(C_L)$, and aerodynamic efficiency, $E = E(\alpha)$, $E = E(C_L)$, at subsonic or supersonic speeds in the continuum flow regime for symmetric vehicle configurations. (S = stall point)

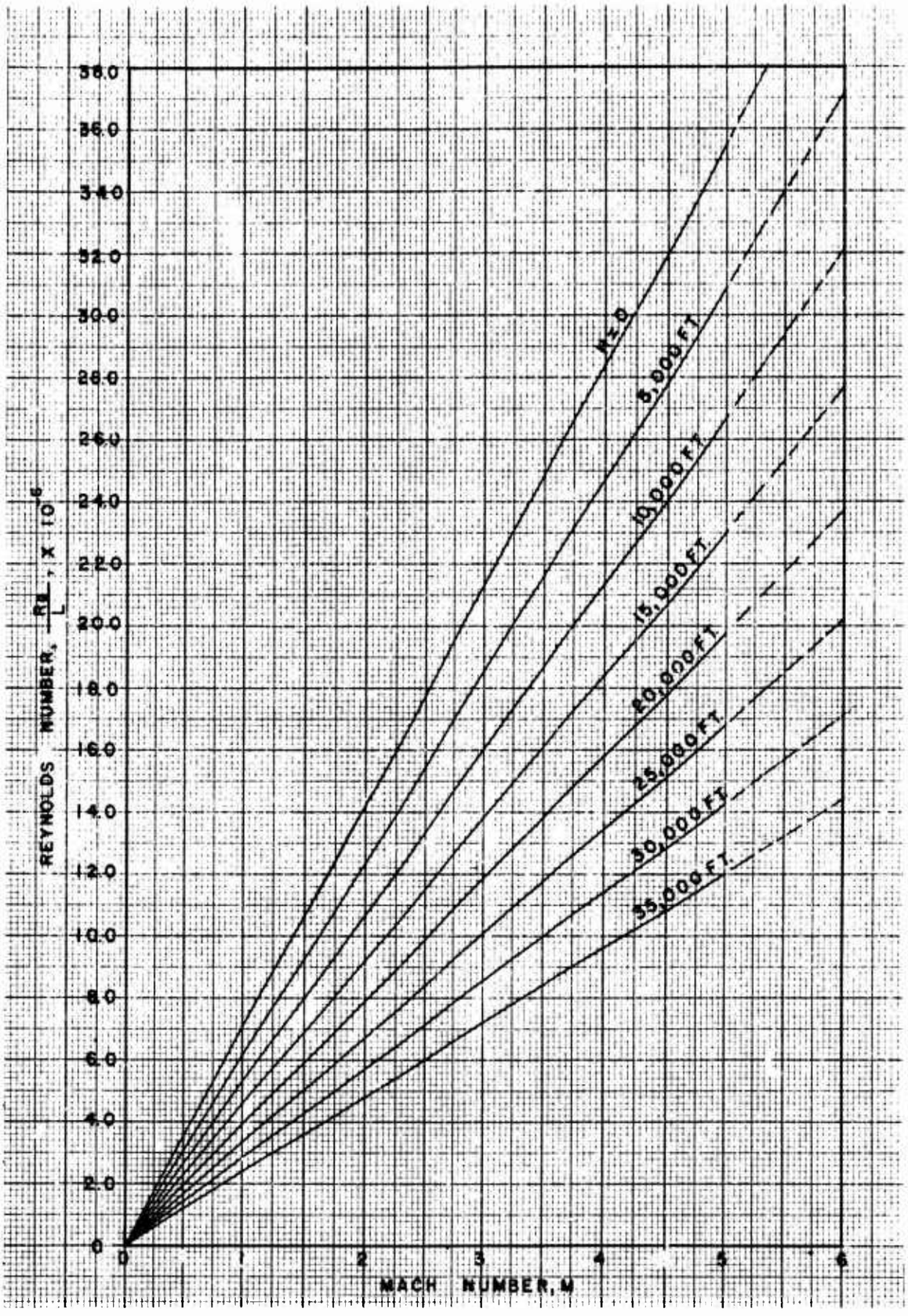

FIG. 1.31 Plot of REYNOLDS NUMBER vs. MACH NUMBER for altitudes from 0 to 35,000 feet.

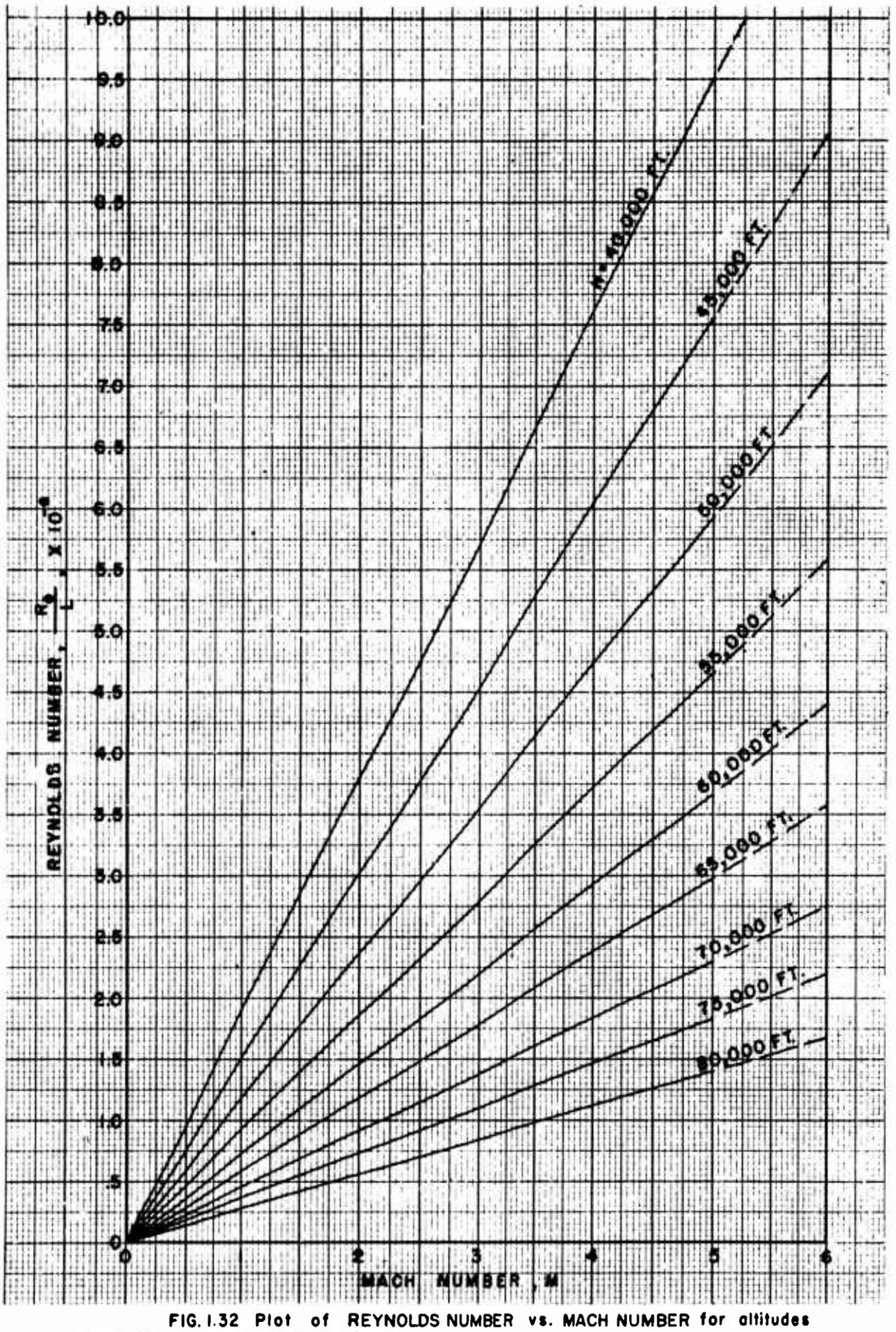

FIG. I.32 Plot of REYNOLDS NUMBER vs. MACH NUMBER for altitudes from 40,000 to 80,000 feet.

TABLE 1.7-2

ALTITUDE IN FEET	MACH NUMBER, M									
	0.5	1.0	1.5	2.0	2.5	3.0	3.5	4.0	4.5	5.0
0	355	710	1065	1420	1775	2130	2485	2840	3195	3550
5,000	309	618	927	1236	1545	1854	2163	2472	2781	3090
10,000	268	535	802	1070	1338	1605	1872	2140	2408	2675
15,000	230	461	692	922	1152	1383	1614	1844	2074	2305
20,000	197.6	395.2	593	790	988	1186	1383	1581	1778	1976
25,000	168.5	337	505.5	674	842.5	1011	1180	1348	1516	1685
30,000	142.5	285	427.5	570	712.5	855	997.5	1140	1282	1425
35,000	120	240	360	480	600	720	840	960	1080	1200
40,000	95.5	191	286.5	382	477.5	573	668.5	764	859.5	955
45,000	75.5	151	226.5	302	377.5	453	528.5	604	679.5	755
50,000	59.5	119	178.5	238	297.5	357	416.5	476	535.5	595
55,000	46.7	93.4	140.1	186.8	233.5	280.2	326.9	373.6	420.3	467
60,000	36.75	73.50	110.25	147	183.75	220.5	257.25	294	330.75	367.5
65,000	29.8	59.6	89.4	119.2	149	178.8	208.6	238.4	268.2	298
70,000	22.8	45.6	68.4	91.2	114	136.8	159.6	182.4	205.4	228
75,000	18.5	37	55.5	74	92.5	111	129.5	148	166.5	185
80,000	14.15	28.3	42.45	56.6	70.75	84.9	99.05	113.2	127.35	141.5
	REYNOLDS NUMBER, $\frac{R_e}{L} \times 10^{-4}$									

SEE FIGS 1.31 AND 1.32

In order to estimate the average zero-lift drag coefficient for each individual "i"-th part, the related local values of Mach and Reynolds Numbers corresponding to the indicated reference ambient values in Eq. (1.7-40) must be found, and the integration indicated by Eq. (1.7-22) performed. The bilateral relationship between the local and the ambient Reynolds Number values is obtained by use of the corresponding theoretical relationships pertaining to the particular body geometry, flight speed and flow type regime. The proper local Reynolds and Mach Number values determine the laminar and/or the turbulent boundary layer extents across the individual body part, the intensity of aerothermal effects, the boundary layer-inviscid outer flow interaction pattern, the degree of flow separation at the body base or at the wing trailing edge, etc.

(2) Holding δ_E, M , and H constant, the variation in the representative aerodynamic angle-of-attack is introduced. The induced drag coefficient C_{Di} functional dependence is computed

$$C_{Di} = C_{D_i}[\alpha_a]$$

$$\alpha_a \neq 0 \ , \ \delta_E, M_A, H = \text{const.} \qquad (1.7\text{-}42)$$

In cases where the Reynolds Number

effects upon the induced drag coefficient (i.e. the normal pressure distribution) are not considered negligible, the same general approach as outlined above for C_{D_o} may be used to establish the respective functional dependence

$$C_{D_i} = C_{D_i}\left[(Re_{L_l})_A, \alpha_a\right]$$

$$(Re_{L_l})_A = \frac{\rho_A V_A L_l}{\mu_A}$$

$$\alpha_a \neq 0$$

$$\delta_E, M_A, H = \text{const}$$

(1.7-43)

where α_a serves as the primary variable parameter in presenting the results.

(3) The total drag coefficient conditionally becomes then explicitly dependent on the aerodynamic angle-of-attack, α_a, only:

$$C_D = C_{D_o} + C_{D_i} = C_D(\alpha_a)$$
$$M_A, H, \delta_E = \text{const}$$

(1.7-44)

or, alternatively, an explicit function of the corresponding lift coefficient, C_L,

$$C_D = C_{D_o} + C_{D_i} = C_{D_o} + \kappa C_L^x = C_D(C_L)$$

$$C_L = a\alpha_a$$

$$x, \kappa = \text{const}$$

$$M_A, H, \delta_E = \text{const}$$

(1.7-45)

The respective graphs are given in Figs. 1.29 and 1.30.

(4) The above procedure is then repeated for a series of Mach Number values, still keeping δ_E=const. and H = const. conditions. As a result, a family of parametric curves

$$\left[C_D\right]_{\alpha_a} = C_{D_o} + \left[C_{D_i}\right]_{\alpha_a} = \left[C_D(M_A)\right]_{\alpha_a}$$
$$H, \delta_E = \text{const}$$

(1.7-46)

with α_a as the variable parameter is obtained.

The respective illustrative plot is given in Fig. 1.33. Evidently the α_a variation influences the induced drag term only.

(5) A repetition of all the steps (1) to (4), with the additional removal of the restriction δ_E = const., yields the double-parametric families of curves

$$\left[C_D\right]_{\alpha_a, \delta_E} = \left[C_{D_o} + (C_{D_i})_{\alpha_a}\right]_{\delta_E} = \left[C_D(M_A)\right]_{\alpha_a, \delta_E}$$
$$H = \text{const}$$

(1.7-47)

with δ_E influencing both the zero-lift and the induced drag coefficient values.

It should be noted that the α_a and δ_E variations are unrelated in general. But, when specific flight dynamics applications are performed, the required instantaneous equilibrium α_a and the trim δ_E values are functionally interrelated for any given flight altitude and a specified flight trajectory through the respective sets of simultaneous dynamical equations of the vehicle motion. For instance, for a no-spin vehicle possessing a vertical plane of symmetry in a steady rectilinear horizontal flight condition, wings level, and zero slideslip (β=0), the respective system of dynamical equilibrium equations of motion in the wind-axes coordinate $Ox_wy_wz_w$ reference frame is (17):

$$\sum X_w = 0 \;:\; T\cos\epsilon - D = 0$$
$$\sum Z_w = 0 \;:\; W + T\sin\epsilon - L = 0$$
$$\sum M_{yy} = 0 \;:\; M(T) + M(\alpha_a)_{\delta_E=0} + M(\delta_E) = 0$$

(1.7-48)

where $M(T)$ is the thrust force pitching moment,
$M(\alpha_a)_{\delta_E=0}$ is the aerodynamic force pitching moment for zero elevator deflection
$M(\delta_E)$ is the elevator balancing moment
ϵ is the thrust force angle, positive or negative, contained between the thrust line and the Ox_w axis.

The corresponding nondimensional form of the system of Eqs. (1.7-48) yields

$$C_D = C_{D_o} + C_{D_i} = \frac{T\cos\epsilon}{(\rho_A V_A^2/2)S_{ref}} = \frac{T\cos\epsilon}{(1/2)p_A\gamma_A M_A^2 S_{ref}}$$

$$C_L = \left[C_L\right]_{\delta_E=0} + C_{L_\delta}\delta_E = \left[a(\alpha-\alpha_o)\right]_{\delta_E=0} +$$

$$+ C_{L_\delta}\delta_E = \frac{W+T\sin\epsilon}{(\rho_A V_A^2/2)S_{ref}} = \frac{W+T\sin\epsilon}{(1/2)p_A\gamma_A M_A^2 S_{ref}}$$

$$C_m = \left[C_{m_o}\right]_{\delta_E=0} + \left[C_{m_\alpha}(\alpha-\alpha_o)\right]_{\delta_E=0} +$$

$$+ C_{m_\delta}\delta_E = \frac{M(T)}{(\rho_A V_A^2/2)S_{ref}} = \frac{M(T)}{(1/2)p_A\gamma_A M_A^2 S_{ref}}$$

$H = \text{const}$, $CG = \text{const}$, $M_A = \text{const}$

(1.7-49)

where (see Section 1.6.2)

$$C_D = C_{D_o} + \kappa C_L^* = C_D(C_L) = C_D(\alpha_a, \delta_E)$$

(1.7-50)

$$\alpha = a_w\frac{S_W}{S_{ref}}\left[\left(\frac{a_N}{a_w}\frac{S_N}{S_W}+1\right) + \frac{a_T}{a_w}\frac{S_T}{S_W}\eta_T\left(1-\frac{\partial\epsilon_T}{\partial\alpha_w}\right)\right] = \text{const.}$$

Eq(1.6-55)

$$\alpha_a = \alpha - \alpha_o \qquad (1.7\text{-}51)$$

$$\alpha = \alpha_w - i_w$$

Eq.(1.6-56)

$$\alpha_o = \frac{(\alpha_{ow}-i_w) + \frac{a_T}{a_w}\frac{S_T}{S_W}\eta_T\left(\epsilon_o - i_T + i_w\frac{\partial\epsilon_T}{\partial\alpha_w}\right)}{\left(\frac{a_N}{a_w}\frac{S_N}{S_W}+1\right) + \frac{a_T}{a_w}\frac{S_T}{S_W}\eta_T\left(1-\frac{\partial\epsilon_T}{\partial\alpha_w}\right)} = \text{const.}$$

(1.7-52)

$$C_{L_\delta} = \left(\frac{\partial C_{L_T}}{\partial\alpha_T}\frac{\partial\alpha_T}{\partial\delta_E}\right)\frac{S_T}{S_{REF}}\eta_T = a_T\frac{S_T}{S_W}\frac{S_W}{S_{REF}}\eta_T\frac{\partial\alpha_T}{\partial\delta_E} = \text{const}$$

(1.7-53)

$$C_{m_\alpha} = \left(\frac{\partial C_m}{\partial\alpha}\right)_{\delta_E=0} = a(h-h_n) = \text{const}$$

(1.7-54)

$(h-h_n)$ = const. is the static longitudinal stability margin, stick-fixed(17),

$(C_{mo})_{\delta_E=0}$ = const. is the zero-lift pitching moment coefficient for the $\delta_E=0$ condition(17)

$$C_{m_\delta} = \left(\frac{\partial C_m}{\partial\delta_E}\right) = -a_T V_H\frac{\partial\alpha_T}{\partial\delta_E}\frac{S_W}{S_{ref}} = \text{const} \qquad (1.7\text{-}55)$$

$V_H = \frac{S_T L_T}{S_W L_{ref}}$ = const. is the volumetric tail coefficient(17)

L_{ref} is the reference length, usually mean geometric wing chord, $\bar{C}$, or the maximum body diameter, D_{max}

W is the vehicle gross weight, assumed constant

$S_{ref} = S_w$ or $S_{ref} = \frac{\pi D_{max}^2}{4}$

Thus, for a fixed value of Mach Number, M_A (or ambient flight speed, V_a, at a given flight altitude, H, once the basic aerodynamic and configurational data are known, a simultaneous solution of the system of Eqs (1.7-49) yields the required thrust force, the equilibrium aerodynamic angle-of-attac, α_a, and the elevator trim angle, δ_E. As a result, at any fixed altitude, H = const., a single family of the drag coefficient curves results:

$$\left[C_D\right]_{\alpha_a,\delta_E} = \left[C_{D_o} + (C_{D_i})_{\alpha_a}\right]_{\delta_E} = \left[C_D(M_A)\right]$$

$$\alpha_a = f_1(M_A) = \alpha_{EQ}$$

$$\delta_E = f_2(M_A) = \delta_{E_{trim}}$$

(1.7-56)

Evidently any change in the flight dynamics conditions (Eqs. (1.7-48) or flight altitude will result in different sets of α_a and δ_E values. Therefore, for general aerodynamic analysis purposes, the generally unrelated arbitrary double parametric sets of curves,

$$\left[C_D\right]_{\substack{\alpha_a \\ \delta_E=\text{const}}} = \left[C_{D_o} + (C_{D_i})_{\alpha_a}\right]_{\delta_E=\text{const}} = \left[C_D(M_A)\right]_{\substack{\alpha_a \\ \delta_E=\text{const}}}$$

(1.7-57)

and

$$\left[C_D\right]_{\substack{\delta_E \\ \alpha_a=\text{const}}} = \left[C_{D_o} + (C_{D_i})_{\alpha_a=\text{const}}\right]_{\delta_E} = \left[C_D(M_A)\right]_{\substack{\delta_E \\ \alpha_a=\text{const}}}$$

(1.7-58)

for H = const., are required.

(6) Finally, the altitude variation effects are introduced and steps (1) to (5) are repeated. It is important to

realize that altitude variations affect not only the specific coupled values of the equilibrium angle-of-attack, $\alpha_{o_{EQ}}$, and the elevator trim angle, $\delta_{E_{TRIM}}$, for some explicitly prescribed dynamical flight condition and a chosen flight Mach Number, but that altitude variations may considerably affect the zero-lift drag coefficient (and in a lesser degree the induced drag coefficient) value per se, even if a specific flow type regime (for instance continuum) is maintained. The theoretical "constancy" of C_{D_o} for a given Mach Number (or eventually Mach Number range, as in low subsonic speed domain) and its independence of the "free stream" dynamic pressure $\frac{1}{2}\rho_A V_A^2 = \frac{1}{2}\rho_A \gamma_A M_A^2$, influence, is strictly conditional: (1) it presupposes a constant boundary layer pattern (laminar and/or turbulent), unaffected by the Reynolds Number variations (due to density and viscosity changes with altitude) and, (2) it presupposes a negligible change of the estimated skin-friction drag coefficient in terms of the said Reynolds Number variations with altitude. The latter assumption is usually argued on the basis that, under actual atmospheric flight conditions, the relatively high Reynolds Numbers involved (and other unsteady atmospheric effects) cause the boundary layers to be predominantly of a turbulent type, and thus the skin friction coefficient values to be nearly invariant with altitude for all practical purposes. (See illustrative Fig. 1.35). The argument is definitely conditional and should be applied with caution. As indicated in Fig. 1.35, with altitude increase and the respective density drop a considerable effect of the Reynolds Number variations upon both the boundary layer type and the skin-friction coefficient value may be encountered for a given flight Mach Number or a given ambient flight speed. In general, for any constant flight Mach Number, the altitude increase progressively decreases the corresponding Reynolds Number values (see Figs. 1.31 and 1.37) and consequently promotes a possible spread and gradual prevailance of the laminar boundary layer, which considerably affects the overall skin-friction coefficient values.

As an illustration, in Fig. 1.34 an estimate of the zero lift coefficient dependence on altitude is presented for a hypothetical supersonic aircraft with H as a parameter, assuming $\delta_E = 0$. Obviously, even if the C_{D_i} dependence on Reynolds Number is neglected, the total drag coefficient, C_D, is affected by C_{D_o} variations with altitude, requiring in general a triple parametric set of independent aerodynamic drag coefficient data given by

$$\left[C_D\right]_{\substack{\alpha_o \\ \delta_E, H=\text{const}}} = \left[C_{D_o} + (C_{D_i})_{\alpha_o}\right]_{\substack{\delta_E, H=\text{const}}} = \left[C_D(M_A)\right]_{\substack{\alpha_o \\ \delta_E, H=\text{const}}} \tag{1.7-59}$$

$$\left[C_D\right]_{\substack{\delta_E \\ \alpha_o, H=\text{const}}} = \left[C_{D_o} + (C_{D_i})_{\alpha_o=\text{const}}\right]_{\substack{\delta_E \\ H=\text{const}}} = \left[C_D(M_A)\right]_{\substack{\delta_E \\ \alpha_o, H=\text{const}}} \tag{1.7-60}$$

$$\left[C_D\right]_{\substack{H \\ \alpha_o, \delta_E=\text{const}}} = \left[(C_{D_o})_H + C_{D_i}\right]_{\substack{H \\ \alpha_o, \delta_E=\text{const}}} = \left[C_D(M_A)\right]_{\substack{H \\ \alpha_o, \delta_E=\text{const}}} \tag{1.7-61}$$

where α_o, δ_E and H are successively treated as primary parameters. The number of independent graphs in each parametric case is equal to the number of the (δ_E, H), (α_o, H) and (δ_E, α_o) arbitrary sets of constant values respectively.

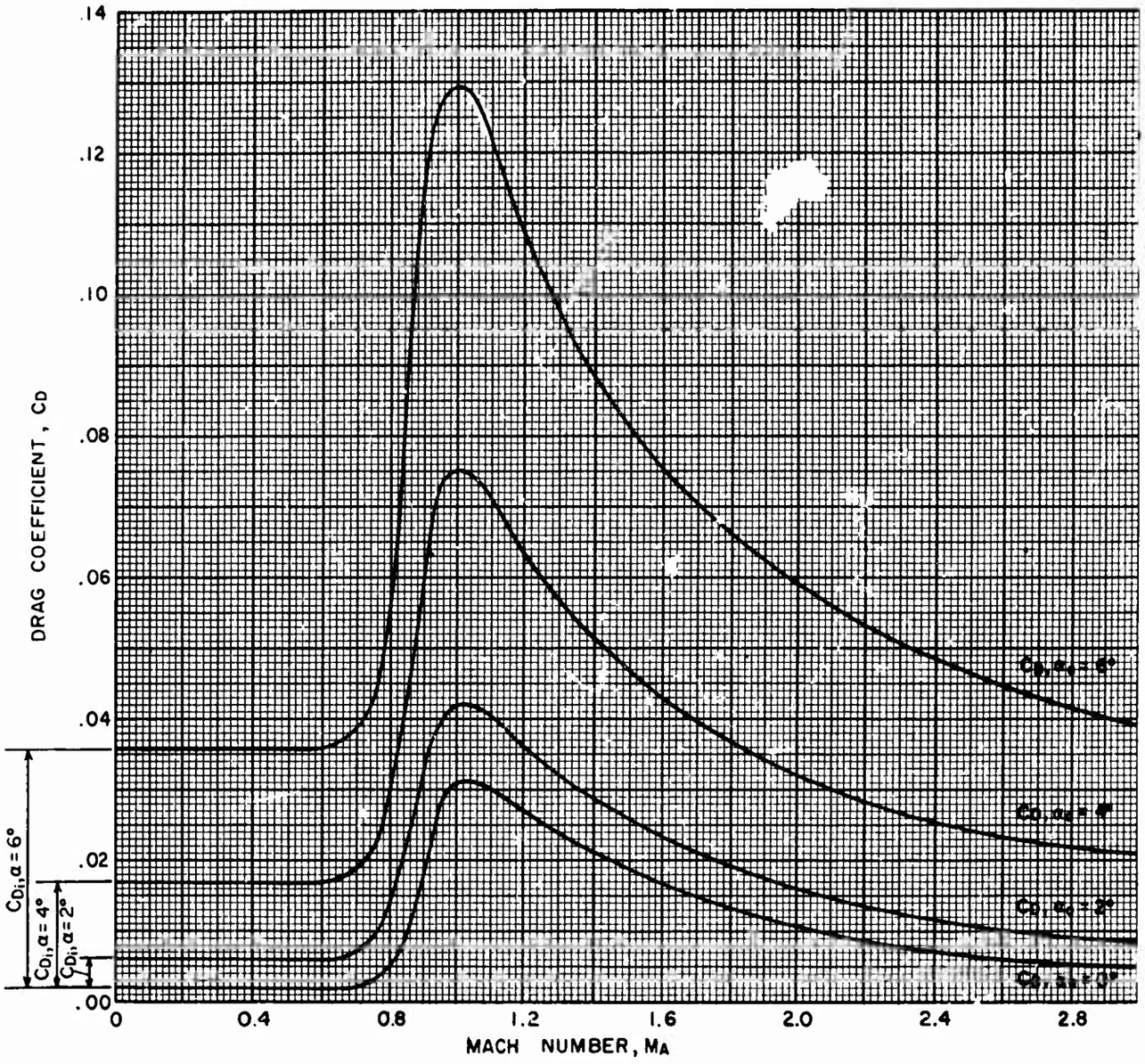

FIG. 1.33 Total drag coefficient versus mach number for a hypothetical vehicle steady rectilinear flow regime, sea level conditions (reference area S_{WEXP} = 6.75 sq. ft.)

Fig. 1.33 continued

						$\alpha_o = 2°$		$\alpha_o = 4°$		$\alpha_o = 6°$	
M	κ	C_{D_o}	C_{L_α}	$C_{L_\alpha}^2$	κ_1	C_{D_i}	C_D	C_{D_i}	C_D	C_{D_i}	C_D
.2	.145	.0219	.080	.0064	.00093	.0037	.0256	.0149	.0368	.0335	.0554
.5	.145	.0219	.080	.0064	.00093	.0037	.0256	.0149	.0368	.0335	.0554
.9	.223	.0380	.085	.0072	.00160	.0064	.0444	.0256	.0636	.0576	.0956
1.0	.242	.0507	.106	.0113	.00274	.0110	.0617	.0440	.0947	.0985	.1492
1.2	.262	.0470	.093	.0086	.00225	.0090	.0560	.0360	.0830	.0810	.1280
1.5	.332	.0380	.072	.0052	.00173	.0069	.0449	.0277	.0657	.0624	.1004
2.0	.442	.0300	.056	.0031	.00137	.0055	.0355	.0220	.0520	.0493	.0793
2.5	.546	.0268	.045	.0020	.00109	.0044	.0312	.0174	.0442	.0393	.0651
3.0	.650	.0243	.038	.00145	.00095	.0038	.0281	.0152	.0395	.0342	.0585

$$C_D = \frac{D}{\frac{1}{2} \rho_A \gamma_A M_A^2 S_{REF}} = \left[C_{D_o} + (C_{D_i})_{\alpha_o}\right]_{\delta_E = 0} = \left[C_D(M_A)\right]_{\substack{\alpha_o \\ \delta_E = 0}}$$

H = 0 ft. $\quad C_{D_i} = \kappa C_L^2 = \kappa C_{L_\alpha}^2 \alpha^2 = \kappa_1 \alpha^2$

$C_L = C_L(M, \alpha_o)$

$\kappa = \kappa(M_A)$

$S_{REF} = S_{WEXP} = 6.75$ sq. ft.

$\alpha_o = \alpha - \alpha_o$

$\alpha_o = 0 \ , \ \delta_E = 0$

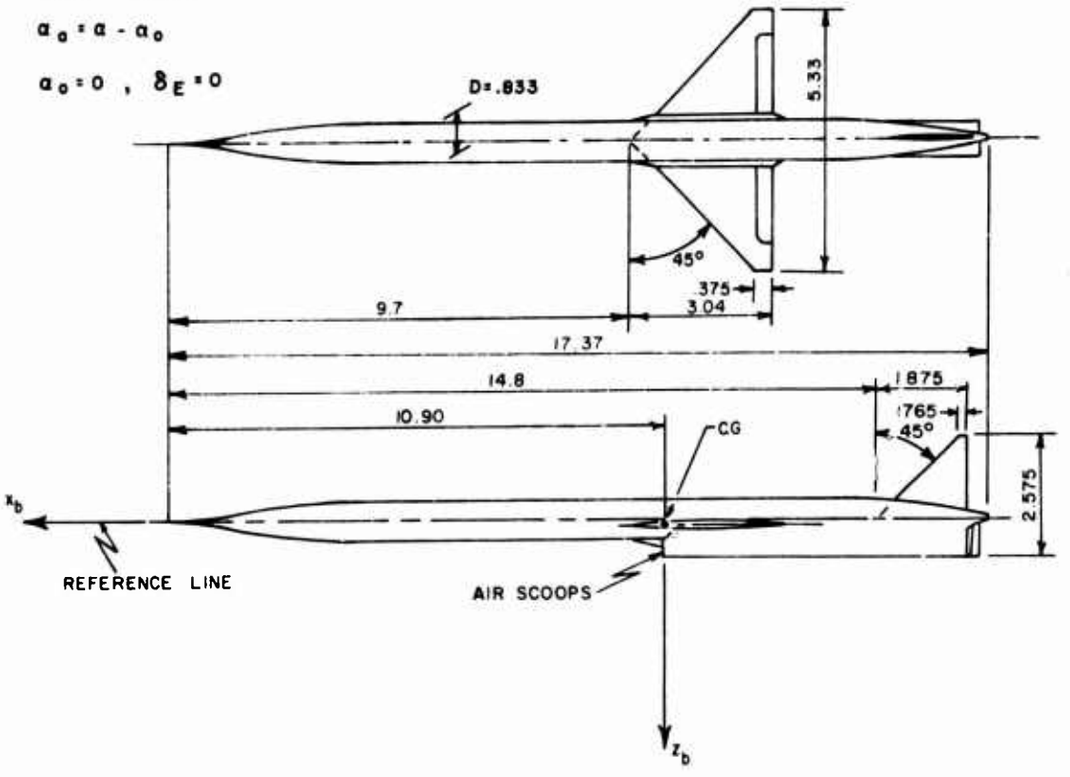

BASIC DATA - FIG. 1.33

Wing

Circular arc airfoil, 4% thick

Exposed wing planform area, S_{WEXP} = 6.75 sq. ft.

Exposed wing span, b_{WEXP} = 4.5 ft.

Exposed wing root chord, $(C_{WEXP})_r$ = 2.625 ft.

Exposed wing tip chord, $(C_{WEXP})_t$ = .375 ft.

Taper ratio, $(C_{WEXP})_t / (C_{WEXP})_r$ = .1425

Exposed wing mean geometric chord, C_{WEXP} = 1 5 ft.

Exposed wing aspect ratio, $AR_{WEXP} = \frac{b^2_{WEXP}}{S_{WEXP}}$ = 3.0

Leading edge sweepback angle, Λ = 45°

Built-in incidence angle, i_w = 0°

Dihedral angle Γ_w = 0°

Fuselage

Length, L_F = 17.37 ft.

Diameter, $D = D_{max}$ = .833 ft.

Fineness ratio, L/D = 20.84

Vertical Fin

Circular arc airfoil, 5% thick

Total area, S_{vt} = 1.74 sq. ft.

Mean geometric chord, $\bar{C}_{vt}$ = 1.025 ft.

Height from fuselage, ℓ = 1.70 ft.

Aspect ratio, AR_{vt} = 1.66

Taper ratio, $(C_{vt})_t / C_{vt}$ = 0.094

Leading edge sweepback angle, Λ_{VTLE} = 45°

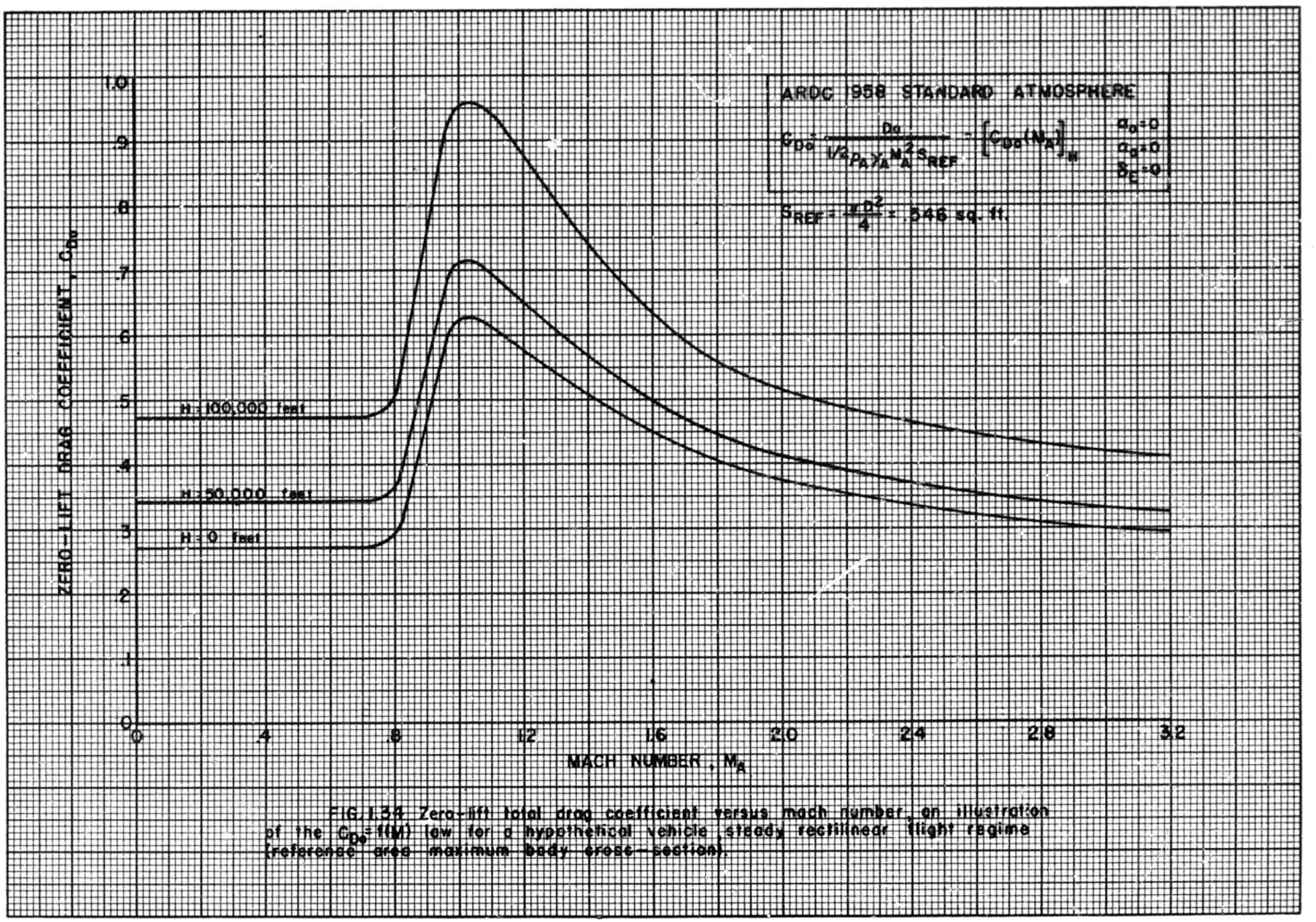

FIG. I.3A Zero-lift total drag coefficient versus mach number, an illustration of the $C_{D_0} = f(M)$ law for a hypothetical vehicle, steady rectilinear flight regime (reference area maximum body cross-section).

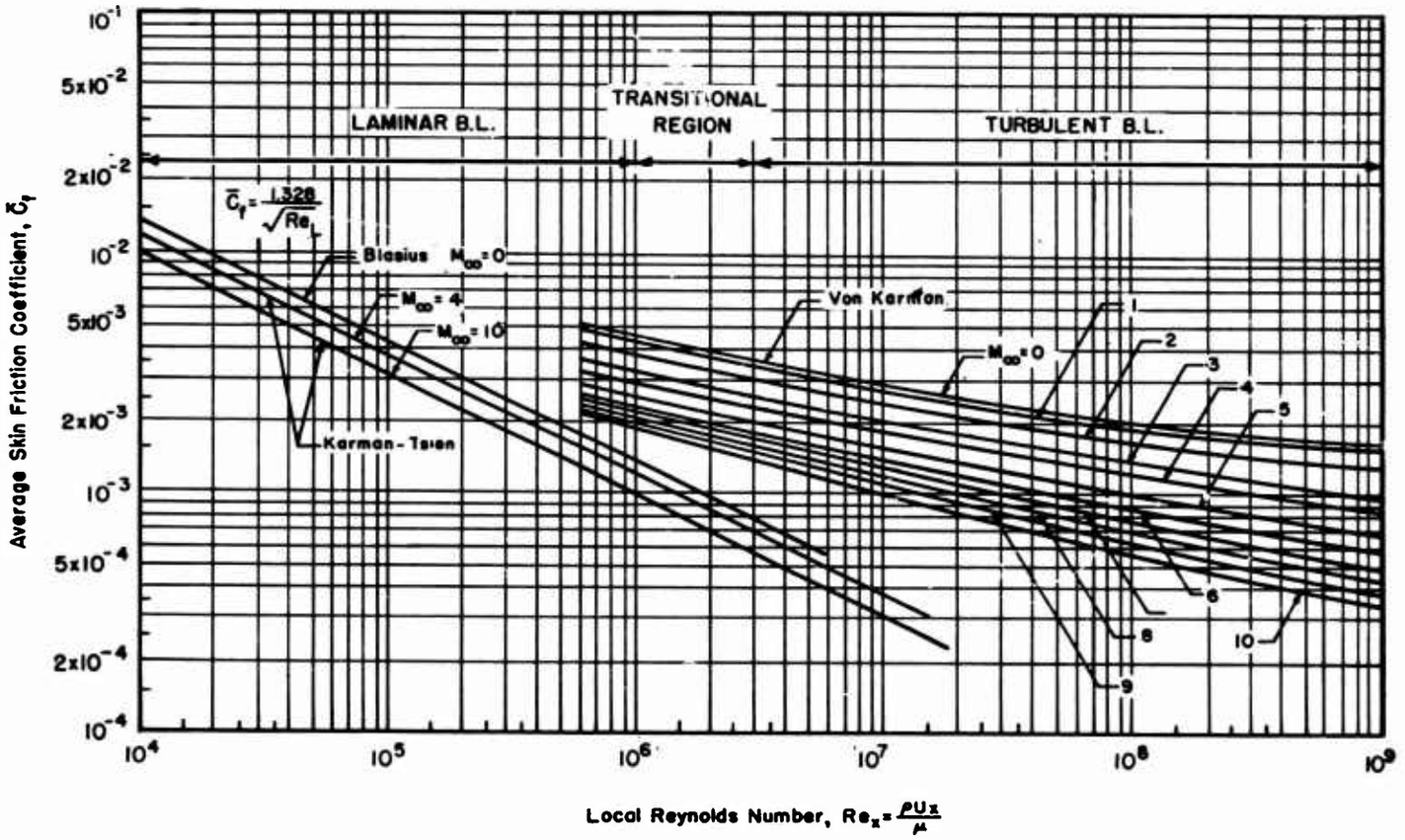

X = distance along the flat plate

L = total length of the flat plate

$$\bar{C}f = \frac{\int_{S_{WET}} q\, Cf\, d\, S}{q_A\, S_{WET}} = \frac{\int_{S_{WET}} \tau\, dS}{q_A\, S_{WET}} = \frac{\bar{\tau}}{q_A}$$

$$Cf = \frac{\tau}{q},$$

$$\bar{\tau} = \frac{\int_{S_{WET}} \tau\, d\, S}{S_{WET}}$$

FIG. 1.35 Average skin friction coefficient versus Reynolds Number on an insulated, smooth flat plate (one side), zero angle-of-attack. (Ref 39)

1.7.4 AERODYNAMIC FORCE TERMINOLOGY AND GENERALIZED DECOMPOSITION SCHEME

The fundamental definition of aerodynamic force coefficients allows for several decomposition schemes applicable to the total drag coefficient[22-25] for compound vehicle configurations. Any of the different schemes may be best suited for a particular set of conditions, such as body geometry, flight speed and flow regime, type of related analytical and/or experimental aerodynamic evidence, degree of required accuracy of drag force estimates, aim of the overall aerodynamic force analysis, etc. For the present restrictive aerodynamics and flight dynamics applications as specified in Sections 1.6 and 1.7, the following aerodynamic force breakdown scheme, which can later be easily applied to various numerical evaluation procedures, is adopted:

(1) The Prandtl's postulate from classical fluid mechanics permitting a separation of the inviscid (normal pressure) and the viscous (frictional) flow phenomena is formally retained for all gas flow regimes. This allows for an independent application of the corresponding theoretical analyses of the perfect fluid flows and the boundary layers respectively. In terms of the classical lift and the drag force definitions, it leads to the approximate expressions

$$L = (\rho_A V_A^2/2) S_{ref} C_L = q_A \sum_{i=1}^{n} \int_{(S_{wet})_i} (\Delta C_{p_i})_{\alpha_a} \vec{n}_i \cdot \vec{k}_a \, dS_i \tag{1.7-62}$$

$$D = (\rho_A V_A^2/2) S_{ref} C_D = q_A \sum_{i=1}^{n} \int_{(S_{wet})_i} \left[(C_{p_i})_{\alpha_a=0} \vec{n}_i \cdot \vec{i}_a + (C_{f_i})_{\alpha_a=0} \vec{i}_i \cdot \vec{i}_a \right] dS_i + q_A \sum_{i=1}^{n} (\Delta C_{p_i})_{\alpha_a} \vec{n}_i \cdot \vec{i}_a \, dS_i = D_o + D_i \tag{1.7-63}$$

which are valid for slender symmetrical body shapes and restricted flight conditions in the reference vertical plane, Section 1.6.

The lift and the drag forces are presumed to act at a particular point called the Center of Pressure of a given body configuration. Its location is commonly represented as an explicit function of the body geometry, body attitude relative to the free stream direction (angle-of-attack), and the Mach and Reynolds Numbers.

A subsequent reduction of the lift and the drag forces to the configurational center of gravity, C. G., results in a pitching moment about the axis. The total pitching moment of simple, aerodynamically slender body configurations and airfoil shapes is composed of two terms: one is due to the aerodynamic force reduction, and the other is due to an aerodynamic force couple which is, within some limits, invariant of changes in angle-of-attack. The invariant part of the overall pitching moment around the configurational C. G. is called the zero-lift pitching moment, (see Eq. (1.7-49)).

(2) The drag polar concept is retained for all speed regimes conveniently allowing for separate zero lift drag force and induced drag force analyses:

$$D = q_A S_{ref} (C_{Do} + C_{Di}) = q_A \sum_{i=1}^{n} \int_{(S_{wet})_i} \left[(C_{p_i})_{\alpha_a=0} \vec{n}_i \cdot \vec{i}_a + (C_{f_i})_{\alpha_a=0} \vec{i}_i \cdot \vec{i}_a \right] dS_i + \kappa q_A \left[\sum_{i=1}^{n} \int_{(S_{wet})_i} (\Delta C_{p_i})_{\alpha_a} \vec{n} \cdot \vec{k}_a \, dS_i \right]^X \cdot \left(\frac{1}{S_{ref}} \right)^{X-1} \tag{1.7-64}$$

(3) In accordance with Section 1.7.3, the explicit primary dependence of the force coefficients upon the Knudsen, Mach and Reynolds Numbers, the aerodynamic angle-of-attack, and the elevator deflection angle for a given body geometry is formally maintained for all gas flow and flight speed regimes. Effects of other influential physical parameters are then implicitly contained in the correspondingly corrected values of the pressure, C_{p_i}, and skin friction coefficients, C_{f_i}, for each individual body part, as the actual physical case may require.

(4) Application of the generalized Eqs. (1.7-62), (1.7-63) and (1.7-64) to compound vehicle configurations is then performed by the following procedure:

(i) The individual lift and drag force coefficient values for each "i-th" simple component of the body geometry are estimated separately using the corresponding theoretical and/or experimental aerodynmaic data, whichever are more readily available.

(ii) Such isolated partial values

are conditionally summed, as indicated by Eqs. (1.7-62), (1.7-63), and (1.7-64), after first being reduced to the common representative flight Mach and Reynolds Numbers. The procedure is exemplified in Section 1.6.

(iii) The assembly of individual constituent parts into the resulting compound vehicle configuration introduces interference effects which may prove important for specific flow and flight regimes. Subsequently the interference effects due to both the changed fluid flow interaction patterns between various body geometries "in situ", the bilateral interaction between viscous boundary layers, shock waves, base area flow separation on one side, and the outer inviscid flow streamlined conditions on the other, are introduced as corrective terms in Eqs. (1.7-62), (1.7-63) and (1.7-64). It is stressed that the availability of theoretical and/or experimental data for evaluation of the generally complex interference effects in various fluid flow and flight speed regimes is usually very limited and the corrective procedure very involved.

(5) For purposes of drag force analyses, a compound vehicle configuration may then, in general, be treated as an assembly of the following individual simple geometries or main individual parts:

(i) Body - The body section is generally of an arbitrary shape. For classical missile configurations, however, it can be subdivided into: the "forebody", comprising the section from the nose tip to the wing junction (or the fin junction on wingless missiles); the "midbody" consisting of the central part subtended by the wing root chord (for winged missiles); and the "afterbody", comprising the rest of the body behind the wing (with or without exclusion of the section subtended by the horizontal and vertical fins.)

For bodies of revolution, the forebody usually consists of a nose section and a subsequent cylindrical part. Simpler nose section forms are conically, ogivally, hemispherically or ellipsoidally shaped. The tip of the nose can be sharp, spiked or partially blunted. The midbody section is sometimes specially formed to fit transonic or supersonic area rules. The afterbody section is, in many cases, aerodynamically boattailed to alleviate the unavoidable flow separation phenomena and the strong shock wave-boundary layer-wake flow interactions at the blunt base region.

The enumerated simplifying body subdivisions are necessarily limited, but convenient for theoretical aerodynamic force estimates. More general or irregular body shapes require experimental or semi-empirical aerodynamic data.

(ii) Wings - The wings are of distinct planform shapes, aspect ratios and airfoil cross-sections. The relative position of the wings with respect to the body center line is characterized by the wing incidence angle, i_w, and its vertical location (low, middle, or high).

When the midbody section is treated as a separate unit, the exposed wing planform becomes the representative reference area for the wing aerodynamic force estimates.

(iii) Fins - The fins or horizontal and vertical tail surfaces follow specifications similar to wings.

(iv) Air inlet (scoops) area(s), - The air inlet area effects are considered in the external aerodynamic force concept if airbreathing power units are installed.

(v) Elevators (or elevons) - The elevators are treated as pitch controls.

All other possible constituent parts which may be found in manned vehicles, such as canopies, cabins, landing gears, turrets, slots, flaps, antennas, etc., are not explicitly considered in the present missile restricted drag force analysis. Their contribution should be evaluated as shown in the literature(23,40).

Applying propositions (1) to (5) listed above, the adopted drag force breakdown is schematically presented in Tables (1.7-3) to (1.7-5). The evaluation procedure is then outlined by the following main steps:

The total drag force of a given compound vehicle configuration is decomposed into its main constituent parts. (See the illustrative Figs. (1.36) and (1.37)):

$$D = D_B + D_W + D_F + D_{AI} + D_{EL} \qquad (1.7\text{-}65)$$

where the subscript B denotes body, W refers to wings, F to fins, AI to air inlets or scoops, and EL to elevators or elevons.

For non-dimensionalization of the drag force expressions, the following common representative quantities are chosen:

Reference area: $S_{ref} = \frac{\pi D^2}{4}_{max}$ or $S_{ref} = S_{WEXP}$

Reference length: D_{max}, L_{max}, or $\bar{C}_{WEXP}$

Reference dynamic pressure: $q_A = \frac{\rho_A V_A^2}{2} = \frac{1}{2} p_A \gamma_A M_A^2$

$$\therefore \quad C_D = \frac{D}{q_A S_{REF}} = C_{D_B} + C_{D_W} + C_{D_F} + C_{D_{Al}} + C_{D_{EL}} \tag{1.7-66}$$

With a Standard Atmosphere adopted, the four characteristic fluid flow regimes, i.e. continuum, slip, transitional and free molecular are determined to a first approximation with the body length L as a common criterion, using the related data from Figs. (1.31) and (1.32). In more detailed numerical computations, the individual reference lengths for each constituent part can be used in order to establish the correspondingly more accurate individual boundaries of the characteristic fluid flow regimes.

Similarly, the subdivision into five characteristic flight regimes, which is strictly valid in the continuum flow domain, is introduced in terms of the representative ambient flight Mach Number, M_A : incompressible subsonic, high subsonic, transonic, supersonic and hypersonic speed domains respectively, (see Eqs. (1.7-15)). The subdivision is tentatively extended to the slip and eventually to the transitional flow regimes when necessary due to lack of data.

From a general configurational layout in the vehicle vertical plane of symmetry (see illustrative Fig. (1.14)) the local values of individual aerodynamic, α_{a_i} , and zero-lift, α_{o_i} , angles of attack for each vehicle part are defined in terms of the representative angles-of-attack, α_a , and α_o , of the overall configuration (see exemplary Eqs. (1.6-46) to (1.6-49)). In the process, the elevator deflection angle, δ_E, is treated separately. Then, for each of the possible and dynamically unrelated combinations of α_a and δ_E the corresponding sets of drag polar expressions are obtained as

$$\left[C_D(M_A)\right]_{\alpha_a, \delta_E} = \left[C_{Do} + (C_{Di})_{\alpha_a}\right]_{\delta_E}$$

$$H = \text{const} \tag{1.7-67}$$

where M_A is considered the primary variable, while α_a and δ_E serve as independent variable parameters, and the flight altitude is kept constant. A subsequent variation in H will then result in two more similar parametric expressions as given by Eqs. (1.7-58) to (1.7-60) in Section 1.7-3.

Explicitly,

$$\left[C_D(M_A)\right]_{\alpha_a, \delta_E} =$$

$$= \left[C_{Do_B} + C_{Do_W} + C_{Do_F} + C_{Do_{Al}} + C_{Do_{EL}}\right]_{\alpha_a = 0, \delta_E} +$$

$$+ \left[C_{Di_B} + C_{Di_W} + C_{Di_F} + C_{Di_{Al}} + C_{Di_{EL}}\right]_{\alpha_a, \delta_E}$$

where:

$$\left[C_{Do_B}\right]_{\alpha_a = 0, \delta_E} = \tag{1.7-68}$$

$$= \frac{1}{S_{ref}} \left[\int_{(S_{wet})_B} \left(C_{f_B} \vec{i}_B \cdot \vec{i}_a + C_{p_B} \vec{n}_B \cdot \vec{i}_a\right) dS_B\right]_{\alpha_a = 0, \delta_E} \tag{1.7-69}$$

etc.

$$\left[C_{Di_B}\right]_{\alpha_a, \delta_E} = \frac{1}{S_{ref}} \left[\int_{(S_{wet})_B} \Delta C_{p_B} \vec{n}_B \vec{i}_a dS\right]_{\alpha_a, \delta_E}$$

etc. (1.7-70)

Alternatively,

$$\left[C_D(M_A)\right]_{\alpha_a, \delta_E} =$$

$$\left[C_{Do_B} + C_{Do_W} + C_{Do_F} + C_{Do_{Al}} + C_{Do_{EL}}\right]_{\alpha_a = 0, \delta_E}$$

$$+ \left[\kappa (C_L)^x\right]_{\alpha_a, \delta_E}$$

(1.7-71)

where, in general, as specified in Sections 1.6 and 1.7:

$$\kappa = \kappa(M_A, Re_A)$$

$$x = x(M_A, Re_A)$$

$$(C_L)_{\alpha_a, \delta_E} = (C_L)_{\substack{\alpha_a \\ \delta_E = 0}} + (\Delta C_L)_{\substack{\alpha_a = 0 \\ \delta_E}} \tag{1.7-72}$$

$$(C_L)_{\substack{\alpha_a \\ \delta_E = 0}} = \frac{1}{S_{REF}} \left[\sum_{i=1}^{n} \int_{(S_{wet})_i} (\Delta C_{p_i}) \vec{n}_i \cdot \vec{k}_a dS_i\right]_{\substack{\alpha_a \\ \delta_E = 0}} =$$

$$\left[a(\alpha - \alpha_0)\right]_{\delta_E = 0} \tag{1.7-73}$$

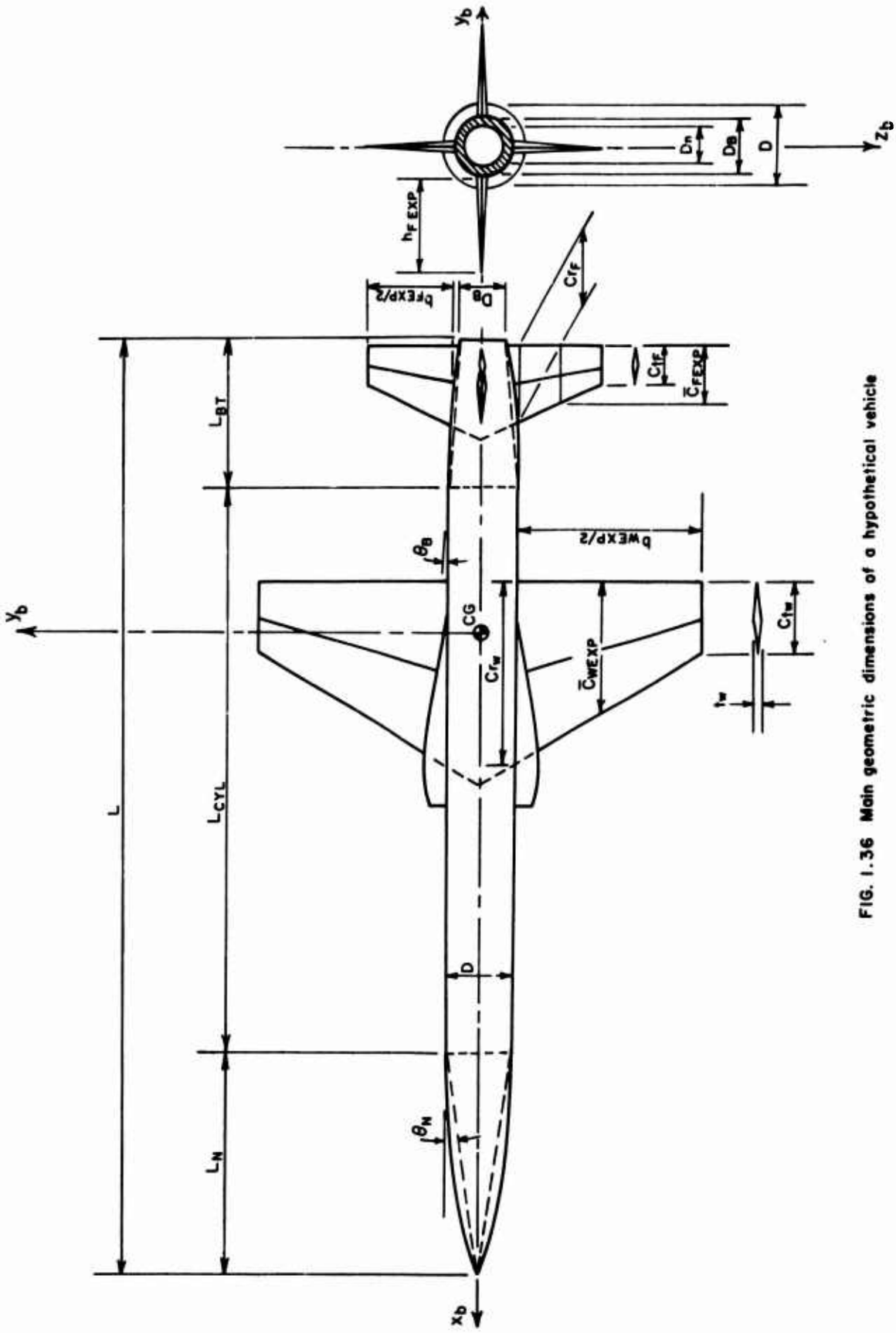

FIG. I.36 Main geometric dimensions of a hypothetical vehicle

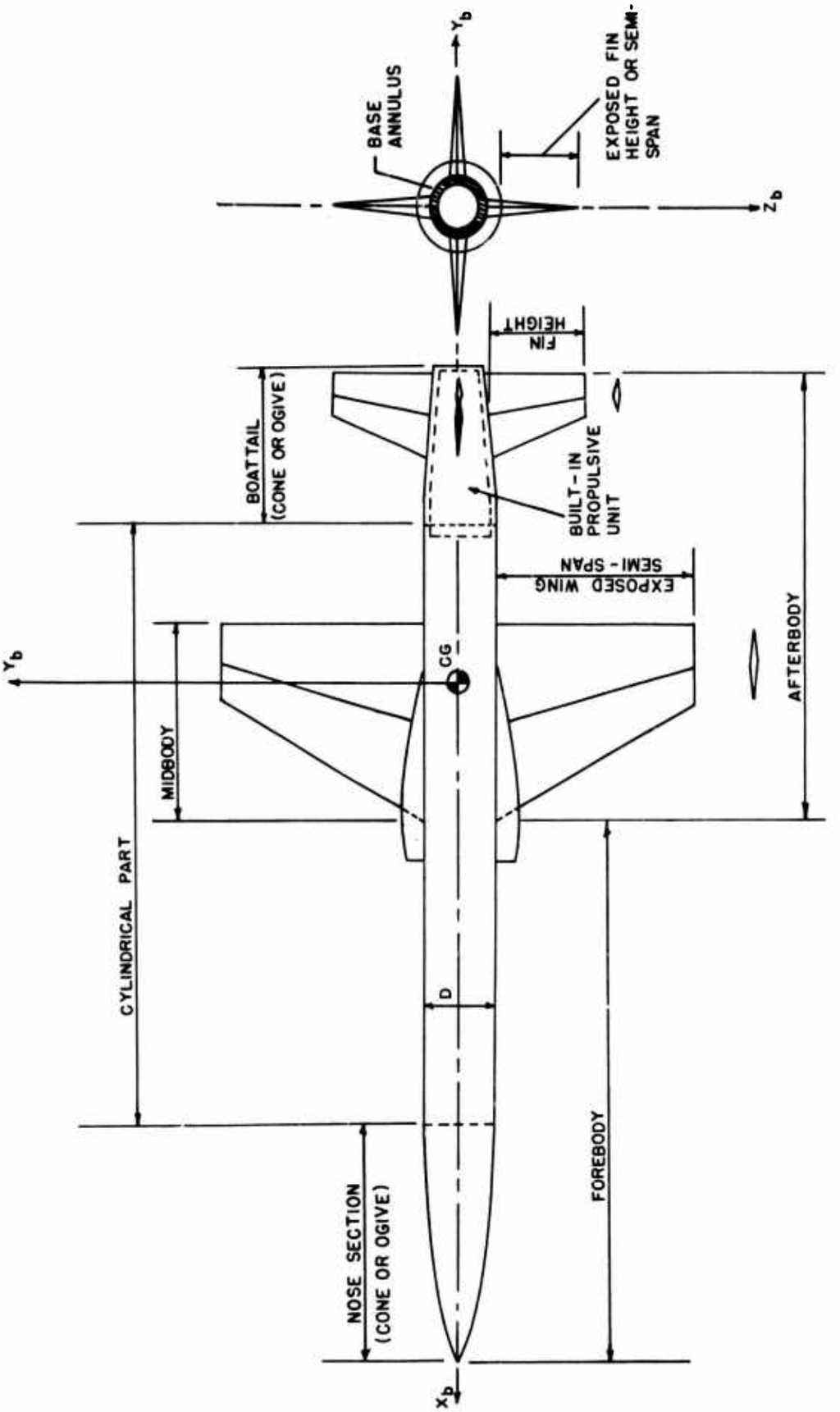

FIG. I.37 Illustration of a general missile configuration.

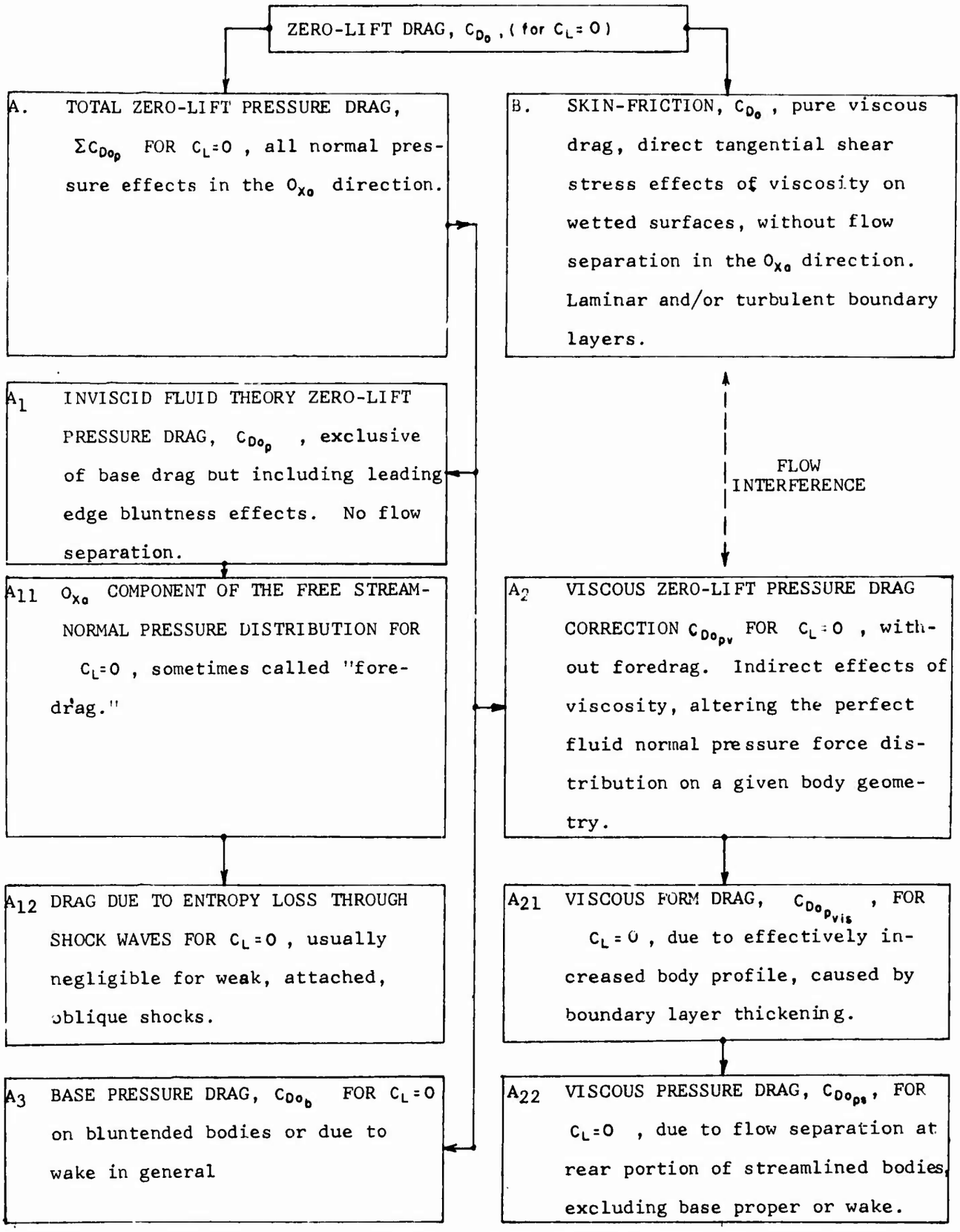

TABLE 1.7-3 ZERO-LIFT DRAG FORCE BREAK-DOWN-PHYSICAL INTERPRETATION, CONTINUUM FLOW REGIME

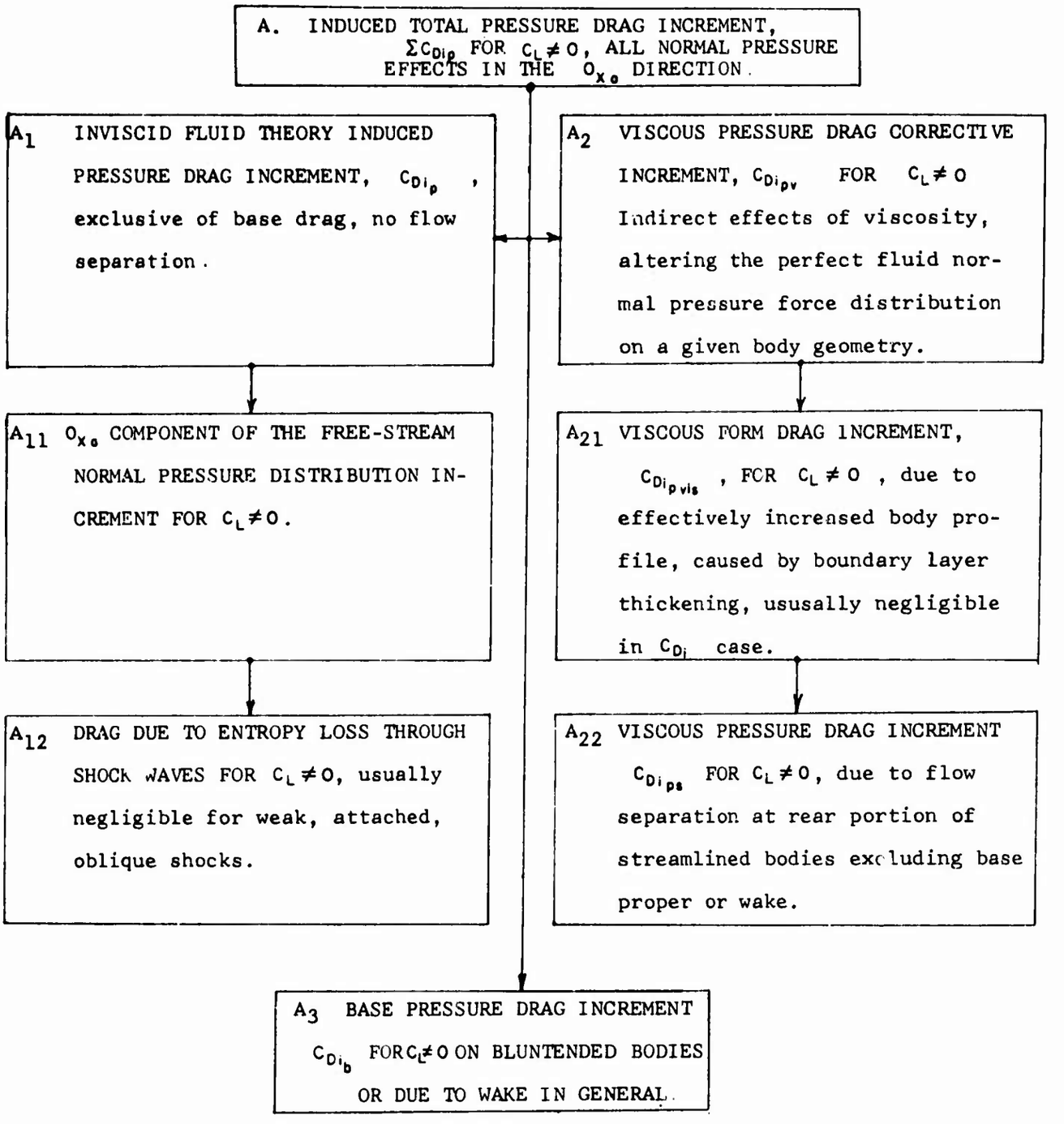

TABLE 1.7-4 INDUCED DRAG FORCE BREAK-DOWN-PHYSICAL INTERPRETATION CONTINUUM FLOW REGIME

MAIN GEOMETRY CONTRIBUTIONS			TOTAL SKIN FRICTION DRAG COEFFICIENT, C_{Do_f}		TOTAL INVISCID PRESSURE DRAG COEFFICIENT, C_{Do_p}		TOTAL VISCOUS PRESSURE DRAG INCREMENT, $C_{Do_{pv}}$		TOTAL BASE PRESSURE DRAG COEFFICIENT, C_{Do_f}
MISSLE BODY	FORE	NOSE	$C_{Do_{f_N}}$	$C_{Do_{f_B}}$	$\pm\Delta C_{Do_{p_{B(W)}}}$	$C_{Do_{p_B}}$	$C_{Do_{pv_B}}$	$C_{Do_{pv_{FORE}}}$	———
		MIDDLE	$C_{Do_{f_{CYL}}}$		$\pm\Delta C_{Do_{p_{B(AI)}}}$			———	———
	AFT (BOATTAIL)		$C_{Do_{f_{BT}}}$		$\sum C_{Do_{pBT}} = C_{Do_{pBT}} \pm \Delta C_{Do_{pBT(F)}} \pm \Delta C_{Do_{pBT(W)}} \pm \Delta C_{Do_{pBT(FORE)}} \pm \Delta C_{Do_{pBT(J)}}$			$C_{Do_{pv_{BT}}}$	$C_{Do_{b_{BA}}} = C_{Do_{b_{BA(B)}}} \pm \Delta C_{Do_{b(BT)}} \pm \Delta C_{Do_{b(JET)}} \pm \Delta C_{Do_{b(F)}} \pm \Delta C_{Do_{b(FORE)}}$
WINGS			$C_{Do_{f_W}}$		$C_{Do_{pW}} = C_{Do_{pWEXP}} \pm \Delta C_{Do_{pWLE}} \pm \Delta C_{Do_{pMB(W)}} \pm \Delta C_{Do_{pW(FORE)}} \pm \Delta C_{Do_{pW(AI)}}$			$C_{Do_{pv_W}}$	$C_{Do_{b_{WTE}}}$
FINS			$C_{Do_{f_F}}$		$C_{Do_{pF}} = C_{Do_{pFEXP}} \pm \Delta C_{Do_{pFLE}} \pm \Delta C_{Do_{pF(W)}} \pm \Delta C_{Do_{p_{F(B)}}} \pm \Delta C_{Do_{p_{F(S)}}} \pm \Delta C_{Do_{pF(BT)}}$			$C_{Do_{pv_F}}$	$C_{Do_{b_{FTE}}}$
AIR INLETS			———		$C_{Do_{p_{AI}}}$			———	———
ELEVATOR			———		$C_{Do_{p_{EL}}}$			———	———

Table 1.7-5 Detailed zero lift drag force coefficient breakdown scheme for classical missile configurations

$$(\Delta C_L)_{\substack{\alpha_a=0 \\ \delta_E}} = C_{L_\delta}\delta_E = \frac{1}{S_{ref}}\left[\sum_{i=1}^{n}\int_{(S_{wet})_i}(\Delta C_{p_i})\, n_i \cdot k_a\, dS_i\right]_{\substack{\alpha_a=0 \\ \delta_E}} \qquad (1.7\text{-}74)$$

with the approximation that

$$C_{L_\delta} = a_T \frac{\partial \alpha_T}{\partial \delta_E}\frac{S_T}{S_W}\frac{S_W}{S_{ref}}$$

As stated earlier, the above expressions (1.7-67) to (1.7-74) include as corrective terms the important interference effects between individual parts in situ and between the associated inviscid and viscous flow patterns. In order to introduce them explicitly, both the zero-lift and the induced drag force components for each individual part of a compound vehicle configuration are further decomposed into four main physical constituents:

C_{Dop} or C_{Dip} , represents the pressure (or wave) drag as obtained from the respective inviscid flow theories for aerodynamically shaped geometries, exclusive of the base drag effects (specified below). Inasmuch as nose tip or leading edge bluntness effects are involved they are included as additional separate corrective factors.

C_{Dopv} or C_{Dipv} , which is called viscous form drag and represents normal pressure changes of the external inviscid flow field due to the viscous boundary layer displacement thickness. It reflects the apparent distortion of body geometry, which is most prominent at its rear portions, accompanied by a partial flow separation (and a subsequent formation of a wake), even when the end point or the trailing edge is manufactured to be sharp. The wake effects are excluded.

C_{Dob} or C_{Dib} , represents the base drag due to pressures acting in the dead air region at the rear of bodies, where pressures result both because of actual body base bluntness and the inevitable effective base thickening caused by the boundary layer and the rear shock-expansion wave presence, and the boattail, fins, and jet interference effects.

C_{Dof} , comprises the skin friction drag due to viscous shear stresses within the associated laminar or turbulent boundary layers. It includes surface roughness and thermal effects.

Each of these four zero-lift drag components is evaluated ro the main configurational parts of a design vehicle, the individual parts being taken as isolated geometric forms. The results are then corrected for interference effects which arise when the missile parts are grouped together. Such a breakdown permits a quick correction and only a partial re-evaluation of the initial drag data as the geometry and location of various missile parts are being changed during various design development phases.

The self-explanatory graphical scheme of the drag force breakdown from the physical point of view is presented in Tables (1.7-3) and (1.7-4) for the zero-lift drag force and the induced drag force coefficients respectively. Evidently, when exceptionally convenient the total drag coefficient can be tentatively treated as a whole along the same lines without an explicit subdivision into C_{Do} and C_{Di} components, i.e. without introducing the drag polar concept.

Analytically, omitting for convenience subscripts α_a and δ_E and introducing the convention that small letter subscripts refer to physical conditions, that capital letter subscripts refer to geometry, and that subscripts in brackets refer to interference effects:

$$C_D = (C_{Dof} + C_{Dop} + C_{Dopv} + C_{Dob}) + (C_{Dip} + C_{Dipv} + C_{Dib}) \qquad (1.7\text{-}75)$$

where:

$$C_{Dof} = C_{Dof_B} + C_{Dof_W} + C_{Dof_F} + C_{Dof_{PARTS}}$$

$$C_{Dop} = C_{Dop_B} + C_{Dop_W} + C_{Dop_F} + C_{Dop_{AI}} + C_{Dop_{EL}} + C_{Dop_{PARTS}}$$

$$C_{Dopv} = C_{Dopv_B} + C_{Dopv_W} + C_{Dopv_F} + C_{Dopv_{PARTS}}$$

$$C_{Dob} = C_{Dob_{BA}} + C_{Dob_{WTE}} + C_{Dob_{PARTS}} \qquad (1.7\text{-}76)$$

and

$$C_{Dip} = C_{Dip_B} + C_{Dip_W} + C_{Dip_F} + C_{Dip_{AI}} + C_{Dip_{EL}} + C_{Dip_{PARTS}}$$

$$C_{Dipv} = C_{Dipv_B} + C_{Dipv_W} + C_{Dipv_F} + C_{Dipv_{EL}} + C_{Dipv_{PARTS}}$$

$$C_{Dib} = C_{Dib_{BA}} + C_{Dib_{PARTS}} \qquad (1.7\text{-}77)$$

In Eqs. (1.7-76):

(i) <u>In the skin-friction drag</u>

coefficient expression, C_{Dof} :

(1) C_{Dof_B} is the laminar and/or turbulent boundary skin friction drag coefficient of the body in the presence of wings and fins, without flow separation:

$$C_{Dof_B} = C_{Dof_{\substack{\text{Total wetted}\\ \text{body area,}\\ \text{exclusive of}\\ \text{base.}}}} - \Delta C_{Dof_{\substack{\text{Area segments}\\ \text{occupied by wing}\\ \text{and fin junctions}}}} \qquad (1.7\text{-}78)$$

In view of the inherent inaccuracy of C_{Dof} estimates, the last term in the expression (1.7-78) is neglected. Referring to the illustrative Figs. (1.36 and 1.37), more explicitly:

$$C_{Dof_B} = C_{Dof_{\text{Nose Section}}} + C_{Dof_{\text{CYL Body + Boat Tail}}}$$

$$\therefore C_{Dof_B} = C_{Dof_N} + C_{Dof_{CYL+BT}} \qquad (1.7\text{-}79)$$

where estimeates of $C_{Dof_{CYL+BT}}$ values entail consideration of the prior history and state of the boundary layer development on the nose section.

$$C_{Dof_N} = \frac{1}{S_{ref}} \int_{(S_{wet})_N} (C_{f_N})_{\alpha_a=0}\, \vec{t}_N \cdot \vec{i}_a\, dS_N = \bar{C}_{f_N} \frac{(S_{wet})_N}{S_{ref}} \qquad (1.7\text{-}80)$$

$$C_{Dof_{CYL+BT}} = \frac{1}{S_{ref}} \int_{(S_{wet})_{CYL+BT}} (C_{f_{CYL+BT}})_{\alpha_a=0}\, \vec{t}_{CYL+BT} \cdot \vec{i}_a\, dS_{CYL+BT} = \bar{C}_{f_{CYL+BT}} \frac{(S_{wet})_{CYL+BT}}{S_{ref}} \qquad (1.7\text{-}81)$$

where

$$\bar{C}_f = (\bar{C}_f)_{\alpha_a=0} = \frac{1}{S_{wet}} \int_{S_{wet}} (C_f)_{\alpha_a=0}\, \vec{t} \cdot \vec{i}_a\, dS \qquad (1.7\text{-}82)$$

is in general the average skin friction coefficient, while locally at any point (x,y,z) defined by a dS surface element,

$$C_f = (C_f)_{\alpha_a=0} = \left(\frac{\tau_w}{q_A}\right)_{\alpha_a=0} \qquad (1.7\text{-}83)$$

$$\tau_w = \tau(Re, M, Kn, \gamma, St, Pr\ldots) \sim \frac{\kappa}{(Re_x)^{\kappa_2}}$$

$$Re_x = \frac{V_A x}{\nu_A}\,, \quad \kappa_1 = \kappa(Re, M, Kn, \gamma, St, Pr\ldots)$$
$$\kappa_2 = \kappa(Re, M, Kn, \gamma, St, Pr\ldots) \qquad (1.7\text{-}84)$$

(2) C_{Dof_W} is the laminar and/or turbulent boundary layer skin friction drag coefficient of the wetted exposed wing surfaces

$$C_{Dof_W} = C_{Dof_{WEXP}} = \frac{1}{S_{ref}} \int_{(S_{wet})_{WEXP}} (C_{f_{WEXP}})_{\alpha_a=0}\, \vec{t}_{WEXP} \cdot \vec{i}_a\, dS_{WEXP} = \bar{C}_{f_{WEXP}} \frac{(S_{wet})_{WEXP}}{S_{ref}} \qquad (1.7\text{-}85)$$

(3) C_{Dof_F} is the laminar and/or turbulent boundary layer skin friction drag coefficient of the wetted exposed fin surfaces

$$C_{Dof_F} = C_{Dof_{FEXP}} = \frac{1}{S_{ref}} \int_{(S_{wet})_{FEXP}} (C_{f_{FEXP}})_{\alpha_a=0}\, \vec{t}_{FEXP} \cdot \vec{i}_a\, dS_{FEXP} = \bar{C}_{f_{FEXP}} \frac{(S_{wet})_{FEXP}}{S_{ref}} \qquad (1.7\text{-}86)$$

(4) $C_{Dof_{PARTS}}$ is the laminar and/or turbulent boundary layer skin friction drag coefficient on the wetted surfaces of secondary vehicle parts such as canopies, nacelles, exterior engine cowlings, turrets, etc.

(ii) In the zero-lift inviscid pressure drag coefficient expression, C_{Dop} :

(1) C_{Dop_B} is the overall body inviscid flow zero-lift pressure drag coefficient, excluding the blunt base pressure effects for $\alpha_a=0$ condition. The midbody section, contained by the wing root chord, as well as the aftbody section contained by fins junction are included in the overall body geometry, and the interference pressure corrections due to presence of wings, fins, air inlets and other external geometries are then additionally introduced. Explicitly:

$$C_{Dop_B} = C_{Dop_{\substack{\text{Slender}\\ \text{Forebody}}}} + \Delta C_{Dop_{\substack{\text{Nose tip}\\ \text{bluntness}}}} + C_{Dop_{\text{Midbody}}} + C_{Dop_{\text{Aftbody}}} \pm \Delta C_{Dop_{\substack{\text{Wing}\\ \text{Interference}}}} \pm \Delta C_{Dop_{\substack{\text{Air Inlets}\\ \text{Interference}}}} \pm C_{Dop_{\substack{\text{PARTS}\\ \text{Interference}}}} + \Sigma C_{Dop_{\text{Boat Tail}}} \qquad (1.7\text{-}87)$$

overall zero-lift drag contribution is commonly estimated globally.

(iv) In the zero-lift base drag coefficient expression, C_{Dob} :

(1) $C_{Dob_{BA}}$ is the zero-lift base pressure drag coefficient, with or without boattailing and jet effects, in presence of fins, taken over the effective base or wake area:

$$C_{Dob_{BA}} = C_{Dob_{\text{Body base without boattailing effects}}} \pm \Delta C_{Dob_{\text{Body base due to boattailing}}} \pm \Delta C_{Dob_{\text{Body base due to jet effects}}} \pm \Delta C_{Dob_{\text{Body base due to fins interference}}} \pm \Delta C_{Dob_{\text{Body base due to forebody and wings interference}}} \quad (1.7\text{-}105)$$

$$\therefore C_{Dob_{BA}} = C_{Dob_{BA(B)}} \pm C_{Dob_{BA(BT)}} \pm \Delta C_{Dob_{BA(J)}} \pm \Delta C_{Dob_{BA(Fore)}} \pm \Delta C_{Dob_{BA(F)}} \quad (1.7\text{-}106)$$

(2) $C_{Dob_{WTE}}$ and $C_{Dob_{FTE}}$ are the wings and fins trailing edge zero lift base pressure drag coefficients, due to the trailing edge bluntness and wake flow effects for condition.

(3) $C_{Dob_{PARTS}}$ is the base pressure drag coefficient for blunt base secondary vehicle parts such as canopies, nacelles, turrets, landing gears, etc.

Physical and geometrical interpretations of individual terms in the lift induced drag coefficient expressions (1.7-77) are conducted in a similar way. Alternatively, the overall induced drag term can be, in a first approximation, treated by way of the total lift coefficient expression (1.7-64) or (1.7-71).

A summary scheme for the above innumerated zero-lift drag force coefficient breakdown is presented in Table (1.7-5).

When using the scheme, several important aspects should be realized: The breakdown is of a quite generalized indicative nature. Depending upon the overall required accuracy of the drag force analysis and the available theoretical and/or experimental data sources, various recombinations, approximations and neglections can be introduced. Also, for different flight speeds and flow type regimes, the conditional existence and the relative importance of different drag force coefficient terms additionally requires respective modifications and rearrangements of the involved expressions. These points will be elaborated in detail later, when the explicit methods of drag force evaluations are presented. In any case, the final drag force coefficient estimates in terms of the adopted primary parameters (Mach Number, Reynolds Number, Knudsen Number, α_0, δ_E and flight altitude) should be critically compared with the related wind-tunnel or free flight evidence, whenever possible. In doing so, the fundamental underlying limitations of the indicated drag force analysis should be remembered at all times:

(1) Only steady, or quasi-steady flight regimes without appreciable accelerations are considered, under no-spin, no sideslip and wings-level conditions.

(2) All missile parts are treated as absolutely rigid, the configuration having a vertical plane of symmetry.

(3) The Standard Atmosphere is regarded as void of turbulence or gusts; or otherwise, the fluid flow is supposedly steady and uniform at infinity.

(4) Entropic energy losses through oblique, presumably weak, shocks are neglected for the aerodynamically relatively high fineness ratio configurations.

(5) There is no pronounced actual flow separation, except eventually at aft body portions (small angles of attack.)

1.8 DRAG FORCE COEFFICIENT DEPENDENCE ON MACH NUMBER - GENERAL TRENDS

From the point of view of atmospheric flight dynamics, the continuum flow regime is of predominant importance and is defined by the inequality:

$$\frac{\bar{\lambda}}{\delta} = Kn_{\delta} \sim \frac{M_A}{\left[Re_L\right]_A^{1/2}} < 10^{-2} \qquad (1.8\text{-}1)$$

where

$$\left[Re_L\right]_A >> 1 \qquad 0 < M_A < O(15)$$

Within the continuum flow regime there are five characteristic flight speeds which in terms of the zero-lift drag coefficient, C_{D_o}, and the ambient flight Mach Number M_A, are illustrated in Fig. (1.38). The functional dependence of the drag coefficient, C_{D_o}, with Mach Number M_A:

$$C_{D_o} = \left[C_{D_c}(M_A)\right]_{\substack{\alpha_a=0 \\ \delta_E, H = \text{const.}}} \qquad (1.8\text{-}2)$$

serves the purpose of distinguishing between the different speed regimes in terms of the characteristic or critical Mach Numbers. Aerodynamic angle-of-attack effects will, in general, cause a shift of the indicated boundaries.

Six critical free stream (ambient flight) Mach Number values characterize the changing trend of the zero-lift drag force coefficient in the five basic speed regimes:

$(M_A)_I \sim 0(.4)$ representing the upper limit of applicability for idealized incompressible subsonic flow theory.

$(M_A)_C \sim 0(.8)$ called the Critical Mach Number, indicating the onset of sonic flow at some point on the vehicle.

$(M_A)_D \sim 0(.8)$ called the Drag Divergence Mach Number, characterizing a noticeable and rather abrupt rise in the drag force coefficient value.

$(M_A)_P \sim 0(1.0)$ corresponding to the peak or maximum value of the drag force coefficient.

$(M_A)_S \sim 0(1.2)$ indicating establishment of a completely supersonic flow pattern over the whole of the craft configuration (not valid for blunt bodies).

$(M_A)_H \sim 0(5)$ characterizing the onset of hypersonic flow conditions.

The indicated Mach Number values are of an order of magnitude nature only. They depend strongly on the actual compound vehicle geometry, the angle of attack, the control surface deflections, and the flight altitude. They are subsequently used as criteria for setting boundaries between different flight speed regimes and the associated theoretical fluid flow analyses.

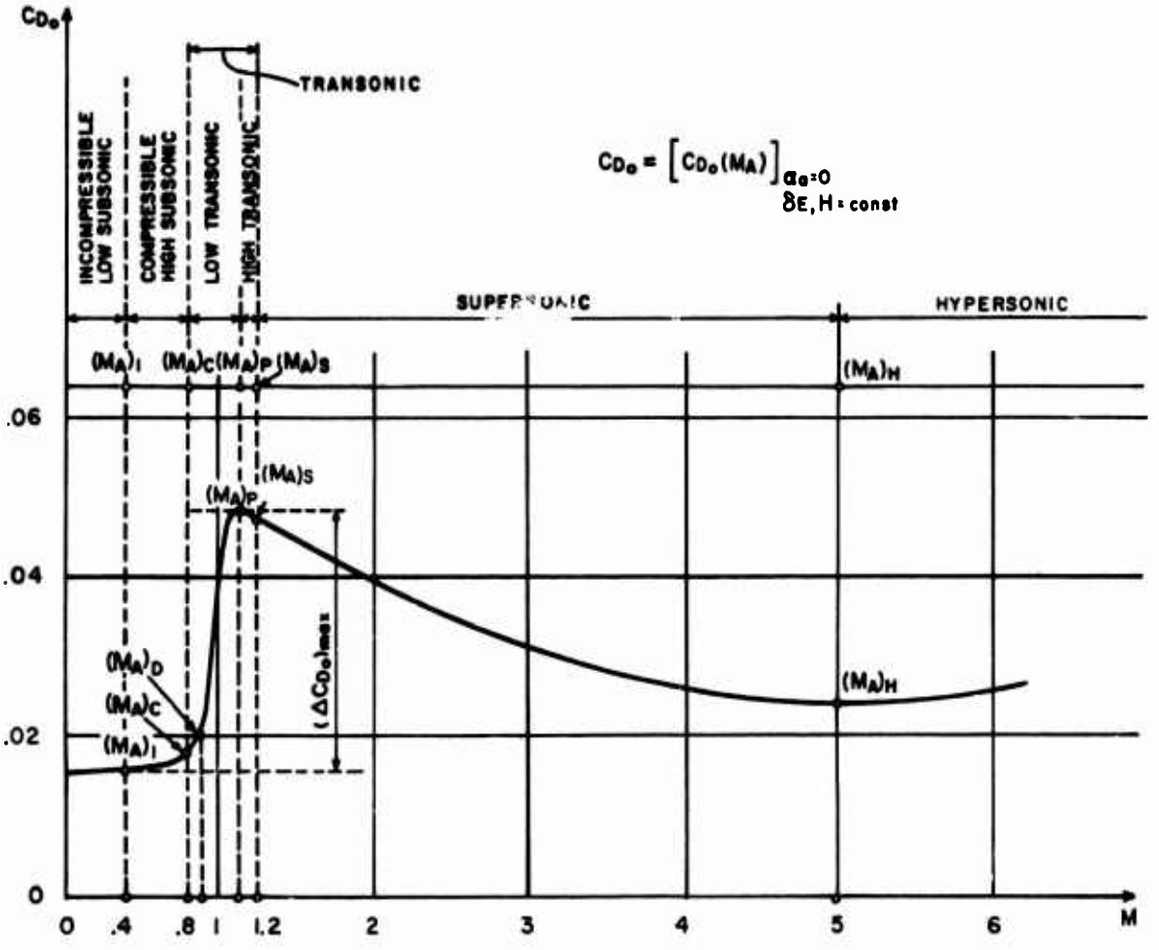

FIG. 1.38 Critical free stream Mach Numbers and boundaries between continuum flow speed regimes, zero lift drag coefficient, $C_{D_o}(M)$

1.8.1 INCOMPRESSIBLE SUBSONIC FLIGHT SPEED REGIME, $M_A < .4$

At incompressible subsonic flight speeds, the aerodynamic force and moment coefficients are invariants with Mach Number. The steady relative airflow is considered to be adiabatic, thermally and calorically perfect and incompressible. Actual small temperature variations and the associated thermal transport processes are neglected both in the viscous boundary layer and in the outer inviscid and theoretically irrotational flow field.

(i) Error due to incompressibility assumption

The assumption of incompressible flow up to $M_A < .4$ introduces an error of less than 4% in the theoretical estimates of pressure coefficients[40], see Fig. (1.39).

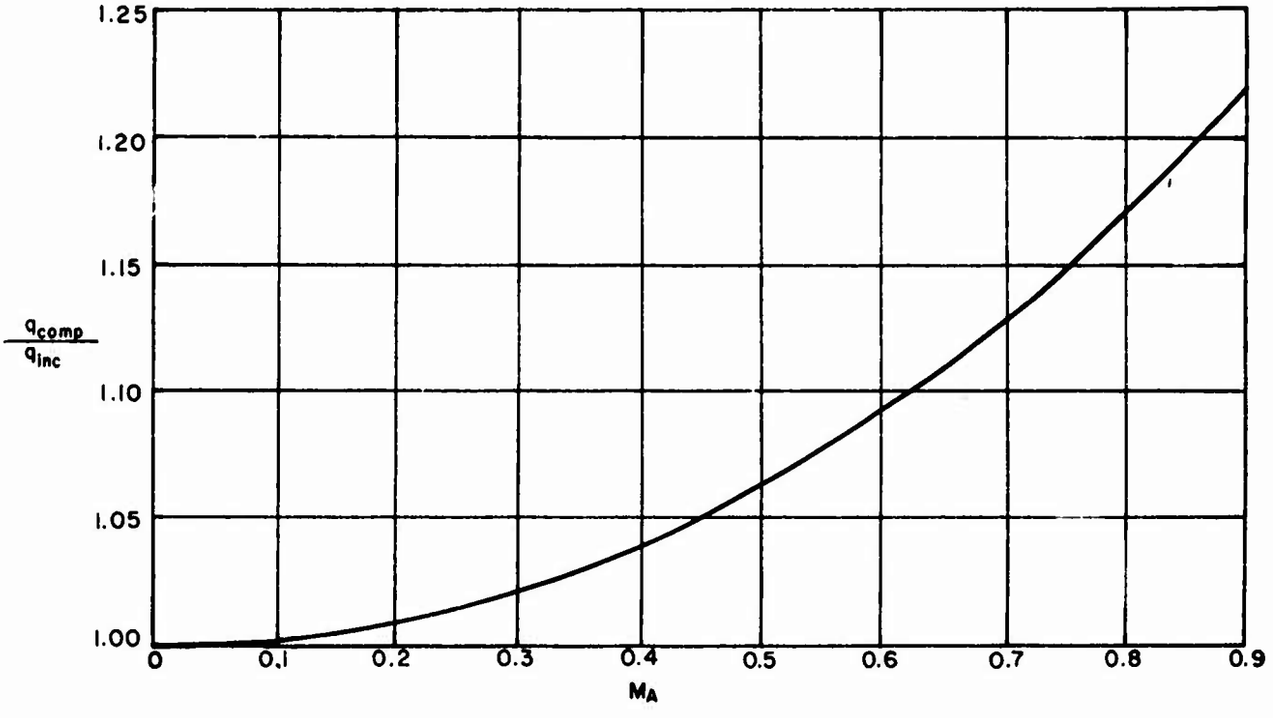

FIG. 1.39 Illustration of the compressible dynamic pressure to incompressible dynamic pressure ratio as a function of Mach Number in a standard atmosphere. Ref. 40.

For steady isentropic perfect fluid flows, the pressure ratio along a streamline in terms of the stagnation point and the free stream at infinity conditions is given by[40]

$$\frac{P_S}{P_A} = \left[1 + \frac{\gamma-1}{2} M_A^2\right]^{\frac{\gamma}{\gamma-1}}$$

$$M_A = \frac{V_A}{a_A} \qquad (1.8\text{-}3)$$

and, expanding in power series (for $M_A < 1$), the stagnation point pressure for compressible subsonic flows becomes:

$$P_S = P_A + \frac{1}{2}\rho_A V_A^2 + \frac{1}{2}\rho_A V_A^2\left[\frac{1}{4}M_A^2 + \frac{2-\gamma}{24}M_A^4 + \cdots\right] \qquad (1.8\text{-}4)$$

or, for incompressible fluid flows, $M_A \sim 0$:

$$P_S = P_A + \frac{1}{2}\rho_A V_A^2 \qquad (1.8\text{-}5)$$

Then, using the pressure coefficient definition, and denoting the ambient free stream, the local compressible, the local incompressible, and the stagnation point conditions by subscripts (A), (comp), (inc) and (s) respectively:

$$C_p = \frac{P-P_A}{q_A} = \frac{1}{2\gamma_A M_A^2}\left(\frac{P}{P_A}-1\right) \quad (1.8\text{-}6)$$

$$\therefore C_{p_s} = \frac{P_s-P_A}{q_A} \quad (1.8\text{-}7)$$

$$(P_s-P_A)_{inc} = \frac{1}{2}\rho_A V_A^2 = q_A = q_{inc} \quad (1.8\text{-}8)$$

$$(P_s-P_A)_{comp} = q_A + q_A\left[\frac{1}{4}M_A^2 + \frac{2-\gamma}{24}M_A^4 + \cdots\right] = q \quad (1.8\text{-}9)$$

one gets:

$$\left[C_{p_s}\right]_{inc} = \frac{(P_s-P_A)_{inc}}{q_A} = 1 \quad (1.8\text{-}10)$$

$$\left[C_{p_s}\right]_{comp} = \frac{(P_s-P_A)_{comp}}{q_A} = \frac{q_{comp}}{q_{inc}} \quad (1.8\text{-}11)$$

and

$$\frac{\left[C_{p_s}\right]_{comp}}{\left[C_{p_s}\right]_{inc}} = \frac{q_{comp}}{q_{inc}} = 1 + \frac{1}{4}M_A^2 + \frac{2-\gamma}{24}M_A^4 + \cdots \quad (1.8\text{-}12)$$

The ratio is plotted in Fig. (1.39) in a Standard International Atmosphere (40). Since the average aerodynamic pressure force (and moment) coefficients C_L and C_{D_p} are directly proportional to the respectively integrated values of the local pressure coefficients, C_p, it is evident that the incompressibility approximation shall result in a respectively negligible error for the $M_A < .4$ condition.

(ii) Drag force terminology at subsonic speeds.

Foundations of the aerodynamics theory and the wind tunnel experiments were developed at subsonic speeds. Consequently most of the basic aerodynamic terminology was formulated at relatively low speeds, where air compressibility and thermodynamic considerations played but a negligible role. This necessitates a corresponding partial reinterpretation of various componental terms in the proposed general drag force breakdown scheme in Section 1.7.4.

(1) Zero-lift drag coefficient, C_{D_o}.

For aerodynamically streamlined configurations at low subsonic speeds the frictional drag component, $C_{D_{pf}}$, is of primary importance and numerically greater than the pressure drag component $C_{D_{op}}$ under $\alpha_a = 0$ conditions (see Fig. (1.40)). As a matter of fact, the inviscid incompressible perfect fluid flow theory past aerodynamically shaped bodies predicts for $\alpha_a = 0$ a zero inviscid flow pressure drag term (D'Alambert paradox). Actual existence of the pressure drag component then is due to boundary layer presence, altering the ideal inviscid flow pattern and causing subsequent partial flow separation at the body base, even in case of ideally sharp trailing edges (wings) and slender pointed bodies. The resulting pressure drag component is classically called form drag at subsonic speeds, the term being used both for $\alpha_a = 0$ and $\alpha_a \neq 0$ conditions. In the adopted general drag force breakdown scheme, the subsonic "form drag" thus represents the viscous pressure drag $C_{D_{opv}}$ or $C_{D_{ipv}}$, while $C_{D_{op}}$ is automatically zero (see Table 1.7-3). The viscous drag term should not be confused with the base pressure term, $C_{D_{ob}}$ or $C_{D_{ib}}$, which is due to actual bluntness of the body base, if any. Note also that $C_{D_{ip}} \neq 0$ for three dimensional body geometries.

Since most actual subsonic drag force data for finite aspect ratio wings are available either from wind tunnel tests or are correctively computed from a rather extensive collection of two-dimensional airfoil data(41) both for $\alpha_a = 0$ and $\alpha_a \neq 0$ conditions, the form drag and the skin friction drag are sometimes found lumped together. In the case of two-dimensional airfoils they are then classically referred to as profile drag. Under lifting conditions, $\alpha_a \neq 0$, the profile drag does not include the induced drag term, C_{D_i} which is computed separately as a three dimensional flow characteristic in terms of the lifting surface geometry, Mach Number and aerodynamic angle-of-attack.

Both the skin friction drag $C_{D_{of}}$ and the form drag $C_{D_{o_{form}}}$ coeffi-

cients are evidently strong functions of all the influential viscous flow parameters: Reynolds Number, boundary layer type (laminar and/or turbulent), surface roughness, airfoil shape, etc., the skin friction being by far the predominent factor. The relative importance of the form drag (or the viscous pressure drag) contribution depends evidently on the body thickness ratio, t , as illustrated in Fig. 1.40:

$$t = \left(\frac{t_{max}}{C}\right) \text{ or } t_B = \left(\frac{D_{max}}{L}\right) \qquad (1.8\text{-}13)$$

for typical two dimensional subsonic airfoils and bodies of revolution respectively, where:

t_{max}	is the maximum airfoil thickness
C	is the airfoil chord
D_{max}	is the maximum body diameter
L	is the overall body length

Correct skin friction drag coefficient estimates, C_{Do_f} , are thus of primary importance in the subsonic flow regime. The pressure field and interference effects have no appreciable influence on skin friction, and in the absence of excessive flow-separations (below lift-stall conditions), relatively reliable estimates of the frictional effects for adiabatic incompressible viscous flow conditions over streamlined body shapes are obtainable from both theoretical and semiempirical data, provided the surface roughness effects and the relative extent of the laminar and the turbulent boundary layer portions are properly determined in terms of the surface finish conditions and the transitional critical Reynolds Number, respectively.

In view of the qualitative considerations stated above, the interpretation of the zero-lift drag force coefficient at low subsonic speeds results in a simplified decomposition scheme compared to its more general form, (see Section (1.7.4)):

$$C_{Do} = \left(C_{Do_f} + C_{Do_{form}}\right) + C_{Do_{p_{EL}}} + C_{Do_{p_{AI}}} + C_{Do_b} + \Delta C_{Do_{INT}} \qquad (1.8\text{-}14)$$

and

$$C_{Do_{form}} = \left(C_{Do_{p_v}}\right)_B + \left(C_{Do_{p_v}}\right)_{Wexp} + \left(C_{Do_{p_v}}\right)_{Fexp} \qquad (1.8\text{-}15)$$

where the rest of the terms in Eq. (1.8-14) are as specified in Section 1.7.4. The flow and the geometry interference effects of an assembly of various simple body geometries is introduced as $\Delta C_{Do_{INT}}$ when related or similar experimental data are available.

In application to missiles, the incompressible low speed zero-lift drag coefficient data are of relatively limited importance during the launch and the beginning of the boost phases. For landing craft categories they play a considerably more important role in many performance phases. Combined with the induced drag coefficient component, the total zero-lift drag coefficient values affect take-off and landing characteristics of most aircraft, as well as the ceiling, the stall and some of climb, descent and level flight performance cases.

For all vehicle categories estimates of the zero-lift drag forces are a valuable basic reference for comparisons of the respective high speed computations.

(2) Induced drag coefficient - C_{D_i} - basic concept.

The induced drag at subsonic speeds is primarily associated with the vortices shedded from the trailing edge and the tips of a lifting surface for the $\alpha_a \neq 0$ condition. The phenomenon is strictly of a three dimensional nature, producing an additional (induced) pressure drag component which is sometimes called the vortex drag or the drag due to lift. Any changes in the skin friction drag C_{Do_f} and the form drag $C_{Do_{form}}$ force under lifting conditions, $\alpha_a \neq 0$, may be considered negligible, provided no significant spread of the flow separation takes place, i.e. provided the aerodynamic angle-of-attack values are kept below the stall condition, $\alpha_a < \alpha_{cr}$.

Fuselage contributions to the induced drag term are negligible at low subsonic speeds. Theoretically, pointed slender symmetric bodies of revolution at an angle of attack in an inviscid incompressible steady stream acquire a pressure distribution which results in a pure couple (pitching moment) i.e. no resultant lifting force is created.(40)

The lifting surface trailing edge vortex sheet constitutes an integral part of the vortex line concept by which the actual wing (or fin) structure is theoretically represented.

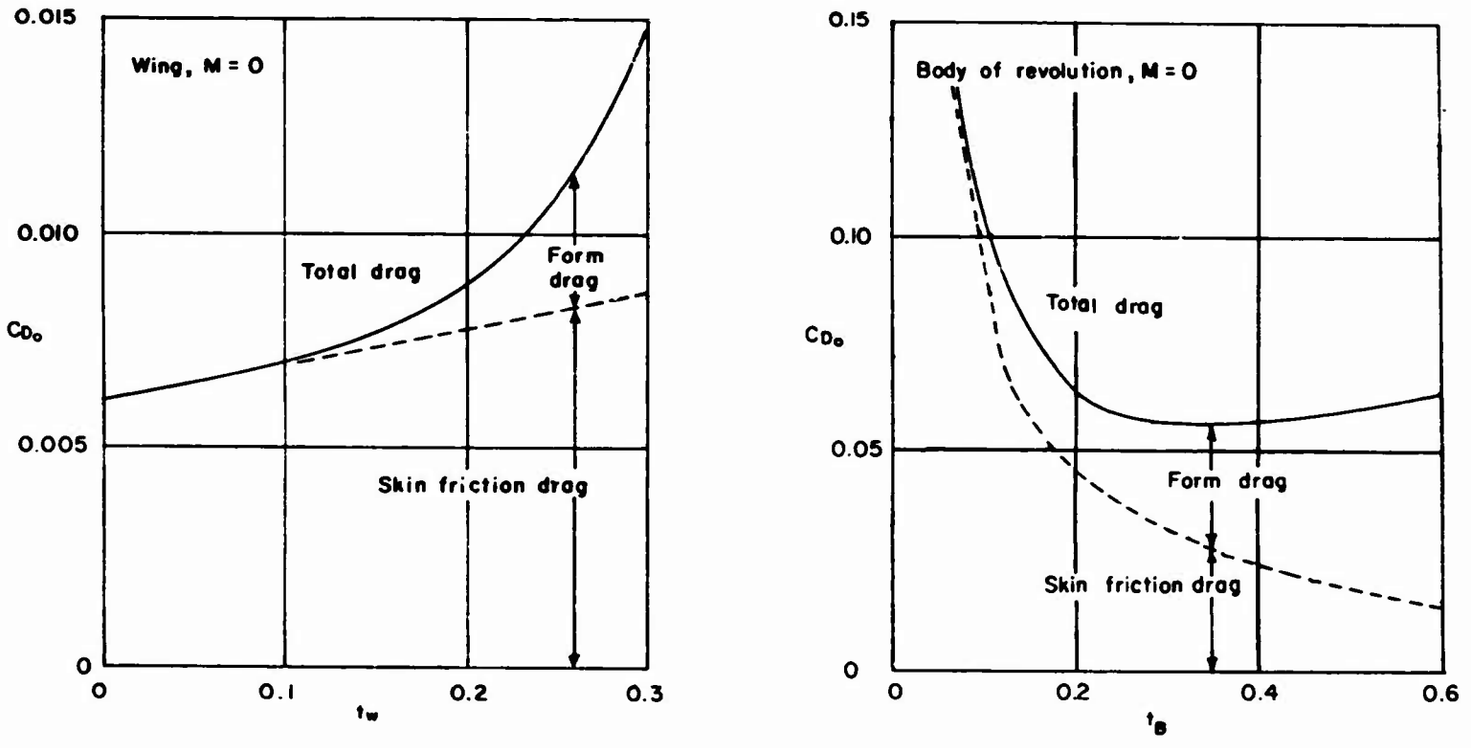

FIG. 1.40 Incompressible zero-lift drag coefficient of a typical subsonic two-dimensional airfoil and a typical body of revolution versus the thickness ratio. Ref. 11.

The lifting line vortex strength distribution possesses the same spanwise circulation variation as the actual wing[3], i.e. it is in accordance with the actual wing geometry and its aerodynamic characteristics, such as planform shape, aspect ratio, taper ratio, airfoil spanwise distribution, geometrical and aerodynamic twist, etc. The shedded vortex sheet pattern deflects the air stream downward, creating a "downwash" velocity component and a corresponding "induced angle" of stream deflection. The warping and downward deflection of the trailing vortex sheet, including tip vortices, varies longitudinally, reflecting the actual geometrical and aerodynamical wing characteristics. In order to enable a unified analytical expression of the lift induced effects for different wing configurations, it is customary to define first the induced angle, α_i , and the induced drag coefficient, C_{D_i} , for an idealized elliptical circulation distribution along the span of a hypothetical wing whose aerodynamical and geometrical properties are given by the condition that the local (subscript " $_l$ ") product $(a_0 a_e c)_l$ has also an elliptical spanwise variation, where:

$(\alpha_e)_l = (\alpha_0)_l + \alpha_i$ is the local effective angle-of-attack, varying spanwise, $(\alpha_e)_l = \alpha_e(y)$.

$(\alpha_0)_l$ is the local aerodynamic angle-of-attack varying spanwise, $(\alpha_0)_l = \alpha_0(y)$.

α_i is the local induced angle-of-attack, implicitly negative, and constant along the span.

$(a_0)_l$ is the local two-dimensional lift curve slope of an aerofoil, varying spanwise, $(a_0)_l = a_0(y)$.

$(C)_l$ is the local geometrical chord, varying spanwise, $(C)_l = C(y)$.

Such a hypothetical wing has a minimum of induced effects; their spanwise integrated values give the representative or average wing characteristics (subscript w)[3]:

$$(\alpha_i)_w = -\frac{C_{L_w}}{\pi AR_w} = \text{const along the span} \qquad (1.8\text{-}16)$$

$$(C_{D_i})_w = -(C_{L_w}\alpha_{i_w}) = \frac{C_{L_w}^2}{\pi AR_w} \qquad (1.8\text{-}17)$$

$$C_{L_w} = a_w \alpha_{a_w} = a_w(\alpha_w - \alpha_{0_w}) \qquad (1.8\text{-}18)$$

$$a_w = \frac{a_{0_w}}{1 + \frac{a_{0_w}}{\pi AR_w}} \qquad (1.8\text{-}19)$$

$$\alpha_{a_w} = (\alpha_{e_w} - \alpha_{i_w}) = (\alpha_w - \alpha_{0_w}) \qquad (1.8\text{-}20)$$

where

a_{0_w} is the average two-dimensional lift curve slope of the aerofoil at the mean aerodynamic chord when an aerodynamic spanwise twist exists, $(a_0)_l = a_0(y)$

α_{e_w} is the average effective angle-of-attack of the aerofoil at the mean aerodynamic chord in the case of a spanwise aerodynamic and geometric twist, $(\alpha_e)_l = \alpha_e(y) = \alpha_0(y) + \alpha_g(y) + \alpha_i$.

α_{a_w} is the average aerodynamic angle-of attack of the aerofoil at the mean aerodynamic chord in the case of a spanwise aerodynamic twist, $(\alpha_c)_l = \alpha_a(y) = \alpha(y) - \alpha_0(y)$.

α_{i_N} is the downwash or the induced angle, constant along the span for an elliptical spanwise circulation distribution and an elliptical spanwise variation of the local products $(a_0 a_e C)$.

α_w is the wing representative geometrical angle-of-attack, (see Section 1.6 for definition).

α_{0_w} is the wing zero-lift representative angle of attack, (see Section 1.6 for definition).

General Remarks:

In the expression (1.8-20) the representative angles α_{e_w}, α_{i_w}, α_w and α_{0_w} are defined on different premises, and therefore are not directly related, i.e.:

$$\alpha_{e_w} \neq \alpha_w$$
$$\alpha_{i_w} \neq \alpha_{0_w} \qquad (1.8\text{-}21)$$

The necessary condition that the local products $(a_0 a_e C)_l$ have an elliptical spanwise variation, for the

idealized elliptical circulation distribution along the span of a hypothetical wing, is a generalized requirement, allowing for spanwise variation of the airfoil characteristics, $a_0(y)$, $a_e(y)$, $C(y)$. As a consequence, the wing planform is not necessarily elliptical in shape. Only in the special case of $a_0 = \text{const.}$ and $a_e = \text{const.}$, along the span, does the necessary elliptical $C(y)$ spanwise variation result in an elliptical wing planform.

The theoretical lifting line or vortex line of elliptically varying circulation is assumed to pass through the local quarter-chord points along the wing span.

The mean aerodynamic chord, $\bar{C}_a$, introduced as an equivalent aerodynamic substitute for the actual wing, is assumed to be projected onto the wing center line of symmetry. All representative angles, a_{a_w} , a_{e_w} , a_{i_w} , a_w , a_{0_w} , are then defined respective to this mean aerodynamic chord.

The induced angle-of-attack, a_{i_w} , is constant along the span for the presumed elliptical conditions. Its value, given by Eq. (1.8-16), is at the quarter-chord (lifting line) position.

For the three dimensional flow conditions around finite aspect ratio wings the resultant pressure force vector is tilted backward due to the induced angle-of-attack, resulting in the induced drag term (1.8-17), (see Fig. (1.41)). According to the adopted lift and drag force definitions:

$$\vec{L}_w = \vec{L}_{R_w} - \vec{D}_{i_w}$$

$$L_w = C_{L_w} \frac{\rho_\infty V_\infty^2}{2} S_w$$

$$D_{i_w} = C_{D_{i_w}} \frac{\rho_\infty V_\infty^2}{2} S_w = \frac{C_{L_w}^2}{\pi AR_w} \frac{\rho_\infty V_\infty^2}{2} S_w$$

(1.8-22)

where

$\vec{L_w}$ is normal to the undeflected direction of free stream flow at infinity, (i.e. normal to $\vec{V_\infty}$).

$\vec{L_{RW}}$ is normal to the deflected flow direction (i.e. normal to $V_\infty + \vec{w}$).

$\vec{D_{i_w}}$ is in the undeflected direction of freestream flow at infinity (i.e. coparallel to $\vec{V_\infty}$).

(3) Induced drag coefficient - C_{D_i} - arbitrary wing planforms and compound vehicle configurations.

The induced drag coefficient for wings of arbitrary planform is obtained by introducing a corrective coefficient, σ , into the basic expression (1.8-17), for idealized elliptical conditions(3):

$$C_{D_{i_w}} = \kappa C_{L_w}^2 = \frac{dC_{D_w}}{dC_{L_w}^2} C_{L_w}^2 = \frac{1+\sigma}{\pi AR_w} C_{L_w}^2$$

(1.8-23)

where the numerical value of the corrective coefficient ($\sigma << 1$) depends on the wing geometrical and aerodynamic characteristics in general, as exemplified later in Part 2.

Expression (1.8-23) is sometimes written in the alternative form

$$C_{D_{i_w}} = \frac{C_L^2}{\pi e AR_w}$$

(1.8-24)

where

$e = \frac{1}{1+\sigma}$ is called Oswald's efficiency factor,

$e AR_w$ represents the effective aspect ratio of a hypothetical equivalent wing having an elliptical lift distribution which, when integrated, results in the same total lift coefficient as of the actual wing.

When Eq. (1.8-24) is extended to compound vehicle configurations the meaning of Oswald's efficiency factor is modified to account for nonellipticy of actual planforms and of actual spanwise pressure distributions on all lifting surfaces (wings and fins), as well as for the actual increase in the skin-friction and the viscous pressure drag coefficients under lifting conditions ($a_a \neq 0$) for all vehicle parts. Correct determination of the numerical value of the factor e for wings and/or compound vehicle configurations can be attained only from either free flight tests or from properly reduced wind-tunnel data. Then expressed as:

$$C_D = C_{D_o} + \frac{C_L^2}{\pi e AR_w}$$

(1.8-25)

$$\therefore\ e = \frac{1}{\kappa \pi AR_w} = \frac{dC_D}{dC_L{}^2}\ \frac{1}{\pi AR_w} \qquad (1.8\text{-}26)$$

where

C_L is the total lift coefficient for the whole vehicle.

Approximate preliminary design estimates of e are given later in Part 2.

$$\alpha_i = \tan^{-1}\frac{w}{V_\infty} \sim \frac{w}{V_\infty} \quad \text{(Implicitly Negative)}$$

$$\Gamma = \Gamma(y_a = 0)\sqrt{1-\left(\frac{y}{b/2}\right)^2}$$

$$a_0 \alpha_e C = 2\frac{\Gamma(y_a=0)}{(V_\infty^2 + w^2)^{1/2}}\sqrt{1-\left(\frac{y}{b/2}\right)^2}$$

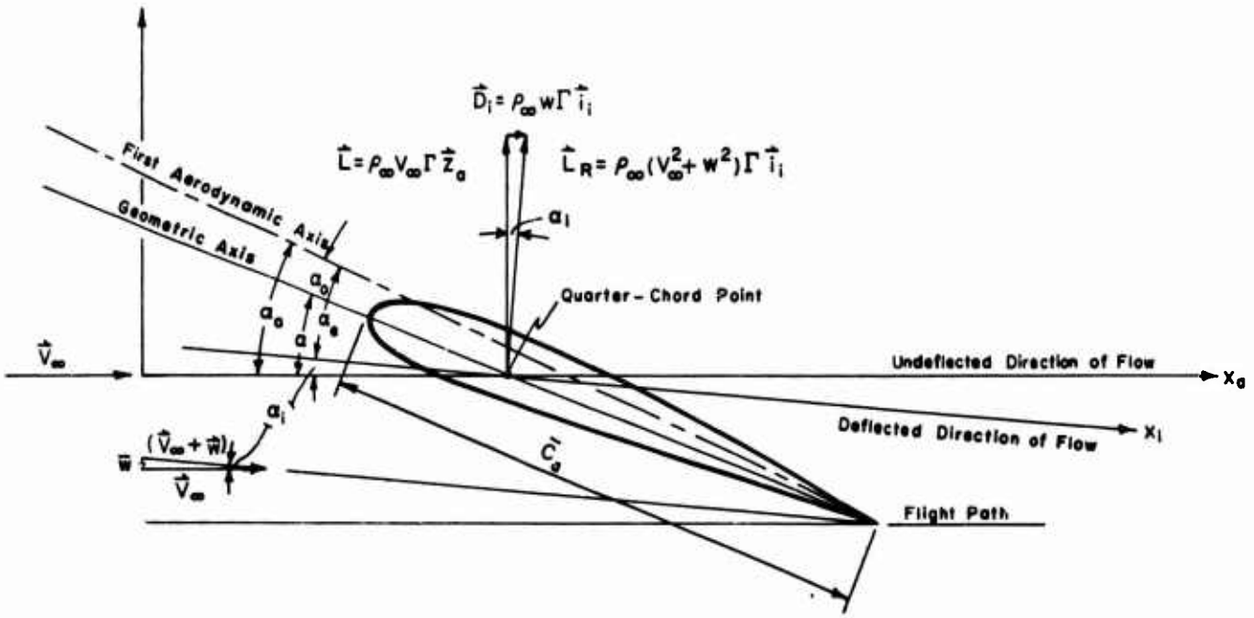

FIG. 1.41 Illustrative sketch of the induced drag origin in the vertical plane, OX_aZ_a, of symmetry, subsonic three dimensional incompressible flow conditions (finite aspect ratio wings).

1.8.2 SUBSONIC COMPRESSIBLE FLOW SPEED REGIME, $.4 < M_A < (M_A)_C = O(.8)$

From Fig. (1.39) the compressibility of air begins to affect the local pressure coefficient values noticeably when the free stream Mach Number is in excess of ~.4. When the compressibility effects are taken into account, drag and lift coefficients change respective to their incompressible flow values. To a first approximation, the Glauert's compressibility factor[42] for subsonic flow conditions

$$\frac{1}{\sqrt{1 - M_A^2}} \qquad (1.8\text{-}27)$$

can be used as a correction for the compressible C_L and C_{D_i} values, while the zero-lift drag coefficient, C_{D_o}, is correspondingly changed through the increased values of Reynolds Number and the flow compressibility effects inside the boundary layers, i.e. primarily due to the altered skin friction coefficient functional dependence $C_f(M,Re)$, which continues to be of a predominant importance under the non-lifting ($\alpha_o \neq 0$) conditions for C_{D_o} estimates. Thus, retaining the basic definitions from the incompressible flow domain, the slightly changed values of aerodynamic force coefficients due to air flow compressibility at subsonic speeds are indicated implicitly by

$$C_D(M,Re) = C_{D_o}(M,Re) + \kappa(M,Re)\,C_L^2(M) \qquad (1.8\text{-}28)$$

$$C_{L_{comp}} = C_L(M) = \frac{C_{L_{inc.}}}{\sqrt{1 - M_A^2}} \qquad (1.8\text{-}29)$$

$$\kappa(M,Re) = \frac{1}{\pi e_{comp} AR_w} \qquad (1.8\text{-}30)$$

where the Oswald's factor, e_{comp}, is only a weak function of compressibility up to the critical Mach Number value $(M_A)_C$, which represents the upper limit of the subsonic flow domain. A typical qualitative trend of the dependence,

$$e_{comp} = e(M,Re) \qquad (1.8\text{-}31)$$

is illustrated in Fig. (1.46) for a wide range of Mach Number values[42]. The plotted functional dependence $e(M,Re)$, indicates the same trend as obtained for the related induced drag factor, $\kappa(M,Re)$, as independently computed in the illustrative example of Section 1.7.3, (see Fig. 1.33). Actual numerical estimates of the Oswald's factor in terms of the overall geometrical and aerodynamical characteristics for different compound vehicle configurations are deferred until Part II.

The subsonic compressible flow is theoretically treated as a calorically and thermally perfect fluid flow, with the Mach and the Reynolds Numbers being the predominant natural variables. Thermal effects are still of a secondary importance, appearing mainly in the slightly modified viscous compressible boundary layer analyses. The upper limit of the subsonic compressible flow regime is reached when the highest local Mach Number at any point on a compound vehicle geometry becomes equal to one, indicating the onset of transonic flow conditions. The corresponding free stream or ambient flight Mach Number value is called the critical Mach Number, $(M_A)_C$.

1.8.3 TRANSONIC FLIGHT SPEED REGIME
$(M_A)_C \sim O(.8) < M_A < (M_A)_S \sim O(1.2)$

The transonic flow conditions are characterized by a considerable increase in the pressure drag term, both for the lifting and the zero-lift conditions. The pressure drag rise is associated with the local shock waves and is therefore alternatively called the wave drag component. A subsequent spread of the local supersonic flow regions over the vehicle surfaces occurs as flight Mach Number increases. Between the subsonic and supersonic flow regions, a system of intrinsically unstable shock wave patterns is established. Their subsequent spread results in markedly unsteady mixed flow conditions.

When the first local sonic condition is reached, a Mach wave of infinitesimal strength is established. Only after the corresponding free stream critical Mach Number $(M_A)_C$ is exceeded by a finite margin does the accompanying increase in shock wave strength become appriciable enough to cause a noticeable pressure drag rise. The corresponding free stream Mach Number is called the drag divergence Mach Number, $(M_A)_D$, indicating an abrupt and markedly steep increase in the drag coefficient, see Fig. (1.38). A manifold drag coefficient rise is finally achieved at a peak value; the corresponding free stream Mach Number is consequently denoted as $(M_A)_P$. The mixed subsonic - supersonic flow conditions still continue to exist over some parts of the vehicle configuration until finally a completely supersonic flow is reached over all surfaces and a steady shock-expansion wave pattern is established. The respective free stream Mach Number is denoted as $(M_A)_S$

A reliable estimate of the unsteady transonic flow boundaries, $(M_A)_C$ and $(M_A)_S$, is theoretically a quite difficult task, as are the evaluations of the zero-lift and the induced drag coefficient increments under the unstable transonic flow conditions, in particular their peak values. Therefore, for comparative and corrective purposes, either reliable wind tunnel and free flight test data or ample experience with geometrically and aerodynamically similar vehicle configurations is needed. The pronounced transonic unsteady flow characteristics are further aggravated by a very strong viscous-inviscid flow interaction and by significant interference effects between various individual parts of a compound vehicle geometry. Since the mutually interfering shock wave and the boundary layer structures are highly sensitive to both local Mach Number and Reynolds Number values, extensive corrections for the "scale effects" and the "wall and sting interference effects" are required when wind tunnel data are used. It is therefore always recommendable to resort, whenever possible, to the actual free flight measurements, or to apply a reasonable judgement from experimental evidence for similar configurations. As an example, comparative data of the C_{D_0} , C_{D_i} and $C_{L_\alpha = 0}$ variations with Mach Number at transonic flight speeds for three high speed aircraft configurations are illustrated in Ref. 43.

As stated, the main characteristic of the transonic speed domain is a substantial rise in the pressure (or wave) drag component. The skin-friction drag looses its dominant role in the overall drag force estimates, even under nonlifting ($\alpha_a = 0$) conditions. This trend is further intensified as the Mach Number increases toward the supersonic and the hypersonic flow domains.

For classical winged configurations, the local sonic speed, $M = 1$, is ordinarily first reached at some chord-wise position on the wing surface. This is due to the existence of comparatively greater local velocity perturbations on airfoils as compared to those on other body shapes[44] for the same reference flight Mach Number, M_A, values. Consequently, in order to postpone the onset of the drag divergence, it is desirable to design wings aerodynamically for the maximum possible $(M_A)_C$ value. For an isolated wing at a given angle-of-attack, the local critical Mach Number is in general affected by the airfoil sectional properties and their spanwise distribution (geometrical and aerodynamic twist), the wing planform, the wing taper ratio, the wing aspect ratio and the leading edge sweep back angle, Λ_{WLE} . The sweep-back angle effect is especially very pronounced. In particular, for a two-dimensional wing, the critical Mach Number, $(M_A)_C$, theoretically increases proportionally to the factor $1/\cos \Lambda_{WLE}$ since the chordwise velocity disturbances are essentially affected by the

free stream velocity component normal to the leading edge only, provided the spanwise stream effects on the boundary layer thickening and the subsequent viscous pressure drag disturbances are neglected.(44) Unfortunately, the three dimensional wing-tip effects, the generally strong boundary layer-inviscid flow interaction effects and the central body (or fuselage) interference effects considerably offset the favorable theoretical influence of sweep-back. The relative influences of the sweep-back angle, Λ_{WLE}, the representative airfoil thickness ratio, $t_w = \left(\frac{t_{max}}{c}\right)_w$ and the aspect ratio, AR_w, of a typical isolated wing on the critical Mach Number value, $(M_A)_c$, are illustrated(17) in Fig. (1.42). Influence of the same wing characteristic on the peak zero-lift drag coefficient increment are similarly illustrated in Fig. (1.43). The existence of a real peak drag coefficient value is in accord with linearized theoretical considerations for two-dimensional airfoils(3), whereby the compressibility corrective factors before and after the sonic speed is reached locally are

$$\frac{1}{\sqrt{1 - M_\infty^2}} \quad \text{and} \quad \frac{1}{\sqrt{M_\infty^2 - 1}} \qquad (1.8\text{-}32)$$

respectively, indicating the existence of a real flow maximum value of $C_D(M)$ near the condition of $M_\infty \approx 1$. Two important aspects of a general significance for design purposes may be drawn from the considerations of the $(C_{D_o})_p$ value:

(1) It is desirable to keep the peak drag force coefficient as low as possible if a vehicle is intended for operations at low supersonic flight speeds. This is achieved by first selecting such geometrical and aerodynamical shapes for each part of a vehicle configuration which minimize the strengths of associated shock waves, and then by investigating the intricate interaction pattern of the shock wave system for the vehicle assembly as a whole. The latter is of a crucial importance, since the complex interference effects at transonic speeds are especially pronounced. A preliminary design approach to the problem of a prospective minimization of the peak drag is most easily achieved by use of the semi-empirical Whitcomb's area rule(4), based on an experimental conclusion that the pressure and the velocity disturbances at great distances from a given wing-body assembly are primarily influenced by the assembly's longitudinal cross-sectional area distribution, while the particularity of the wing-body relative arrangement is practically unimportant. A consequential deduction is that for each wing-body combination there exists an equivalent body of revolution having the same cross-sectional area distribution and a correspondingly equivalent disturbed flow pattern, i.e. the same overall wave drag characteristics. A subsequent smoothing off of such an equivalent body cross-sectional area distribution in the longitudinal direction results in a respective improvement of its wave drag characteristics. Then, if the actual wing-body combination is to fit the new, improved equivalency requirement of the improved idealized body of revolution, the actual fuselage shape has to become indented to accomodate the addition of the wing cross-sections at their joint. Although devised for pure wing-body assemblies, the method can be extended to incorporate other parts of a vehicle configuration, in as much as it proves practical from structural, payload capacity and other general considerations. It is to be remembered that the area rule criteria is of a semi-empirical nature, and that many other real flow aspects may additionally affect the total drag coefficient value, such as boattailing, base area pressure, etc. Effectiveness of the area rule for wing-body combinations is at its best for wing planforms satisfying the condition:

$$AR_w (t_w)^{\frac{1}{3}} < 1 \qquad (1.8\text{-}33)$$

where

$$AR_w = \frac{b_w^2}{S_w} \qquad t_w = \left(\frac{t_{max}}{c}\right)_w \qquad (1.8\text{-}34)$$

(2) The change in the corrective compressibility factor, expression (1.8-32), in passing from the $M_\infty < 1$ to $M_\infty > 1$ condition is in accord with the respective subsonic and supersonic linearized theories, assuming in both cases a thermally and calorically perfect, inviscid, isentropic and irrotational fluid flow.(3) The resulting differences in the linearized differential equations governing the sub-

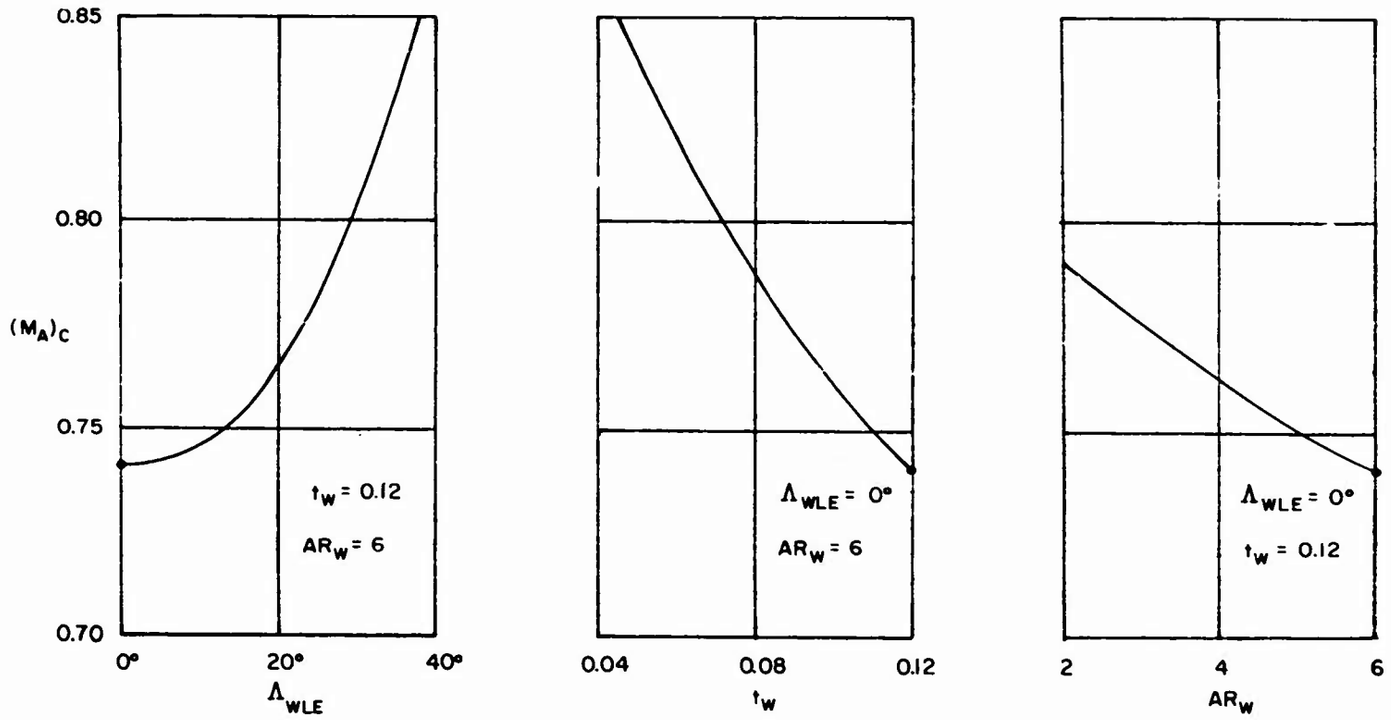

FIG. 1.42 Influence of the angle of sweep, the thickness ratio, and the aspect ratio on the critical Mach Number of a typical wing. Ref. 17.

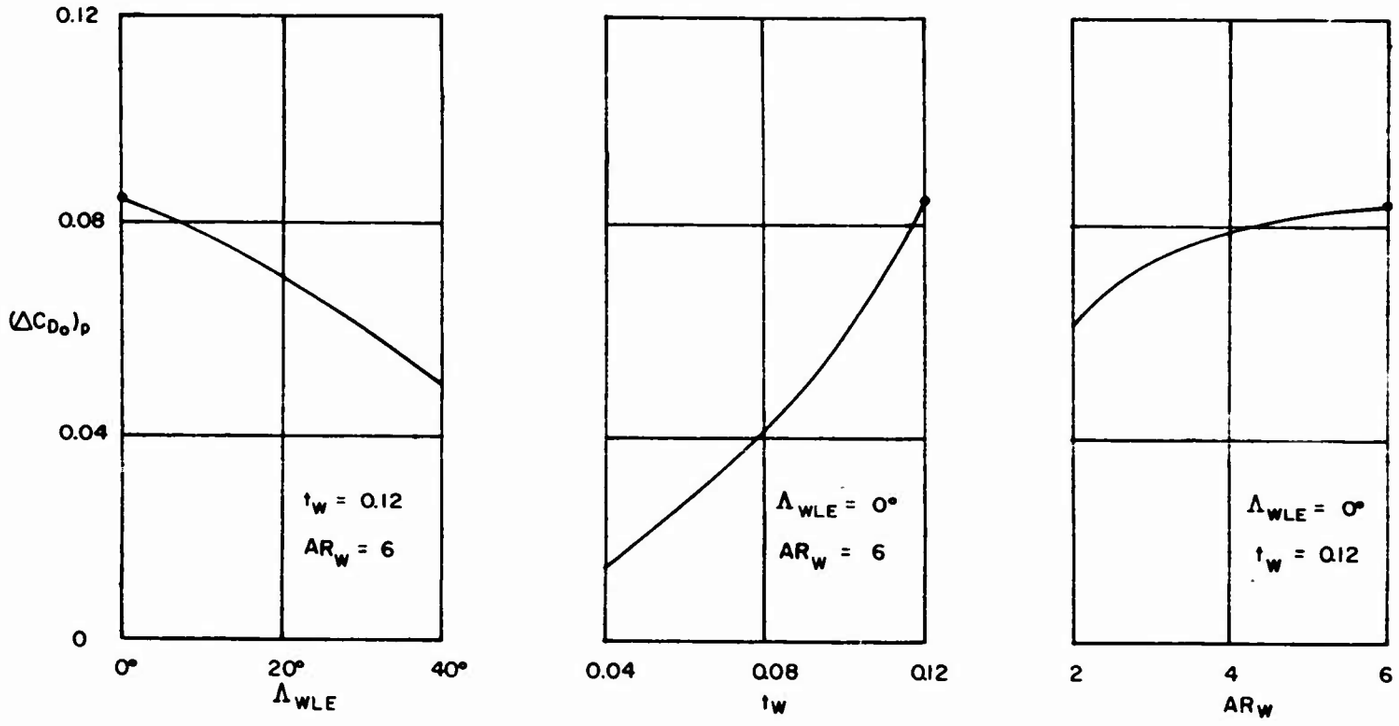

FIG. 1.43 Influence of the angle of sweep, the thickness ratio, and the aspect ratio on the peak drag coefficient of a typical wing. Ref. 17.

sonic and supersonic steady fluid flows entail a corresponding change of form of the compressibility factor, Eq. (1.8-32). Their applicability is restrictive to slender, aerodynamically smooth shapes and to small angle-of-attack values, as specified by the so called small pertubation theory requirements. Neither the steady subsonic nor the steady supersonic theory analyses are strictly applicable to the inherently unsteady transonic flow domain. Therefore, when due to lack of reliable data the corrective compressibility factors, (1.8-32), are applied to the transonic speed regime, due reservations regarding their validity should be exercised.

For the same practical ends, the transonic speed regime is sometimes split into two domains: the low transonic speed regime, $(M_A)_C < M_A < (M_A)_p$ and the high transonic speed regime, $(M_A)_p < M_A < (M_A)_S$ (see Fig. (1.38)). In the first, most of the attention is concentrated on the drag divergence problem; in the second on the peak drag value and the ultimate acquisition of completely steady supersonic flow conditions. A helpful physical interpretation of the formation and the subsequent unsteady shift of the local wave patterns throughout the transonic speed domain can be found in Ref. 4 and 43, accompanied by explanations of the relative importance and the impact exerted by the various transonic flow phases respective to practical design considerations.

The viscous flow phenomenology in the transonic speed regime is even more difficult and involved for an adequate physical formulation and a theoretical analysis. But, in view of a decreasing importance of the skin-friction drag respective to the pressure and the viscous pressure drag contributions, it is customary in applications to treat the transonic boundary layers on the basis of the steady compressible flow premises. The approach is one of expediency and necessity, and is treated as such with all due reservations.

1.8.4 SUPERSONIC FLIGHT SPEED REGIME $(MA)_S \sim O(1.2) < MA < (MA)_H \sim O(5)$

The steady supersonic flow conditions over the entire vehicle configuration are set on when the latest critical local Mach Number (M=1) at any point on the vehicle configuration is realized. The corresponding free stream Mach Number is denoted as $(M_A)_S$. The criteria applies to aerodynamically smooth and slender body shapes in an inviscid outer stream, excluding the partial flow separation phenomena, the viscous subsonic sublayers within the boundary layers proper and the near stagnation point regions behind detached shock waves due to local body bluntness effects. Steady supersonic flow conditions are thus assumed to be characterized by body attached shock-expansion systems as obtained from idealized flow conditions and as eventually closely approximated by the real oblique shock patterns for relatively small angles-of-attack.

Under the fully developed steady supersonic flow conditions, the zero-lift pressure (or wave) drag term steadily gains in importance over the skin-friction drag term as the flight Mach Number is increased. For an isolated two-dimensional aerofoil the zero-lift inviscid pressure-to-viscous skin friction drag coefficient ratio increases proportionally to the square of the aerofoil thickness ratio, (see illustrative Fig. (1.44)). This is due to the fact that the pressure drag increases as the square of airfoil thickness ratio, t , while the skin-friction drag is practically independent of it for thin airfoils. The viscous pressure drag and the base pressure drag (due to inevitable trailing-edge bluntness) as well as the leading-edge bluntness contributions are not represented in the example.

For isolated slender, pointed bodies of revolution, the inviscid pressure drag to viscous flow skin friction drag coefficient rate is illustrated for zero-lift conditions in Fig. (1.45) in terms of a varible fineness ratio

$$F = \frac{l}{t} = \frac{l}{D_{max}} \qquad (1.8\text{-}35)$$

keeping the maximum cross-sectional area $\frac{\pi D_{max}^2}{4}$ constant. Under these conditions, and excluding all other real flow contributions as in the case of wings, the inviscid flow pressure (or wave) drag coefficient contribution is inversely proportional to the square of the fineness ratio, F , while the skin friction drag increases in a direct (nonlinear) proportion to F . As a result, for a given cross-sectional area of a pointed body of revolution there is an optimum fineness ratio for which the total C_{D_0} value acquires a minimum, which in the illustrative example is for a F value between 14 and 15 . If the maximum cross-sectional area is varied while the volume of a body of revolution is being kept constant (as sometimes required by payload considerations), the above trends in the zero-lift inviscid flow pressure drag and the skin friction drag coefficient variations with fineness ratio acquire the functional forms of $(\frac{1}{F})^{8/3}$ and $F^{1/3}$ respectively, while the optimum of the total zero-lift drag coefficient is reached for F~25 . A survey of optimization techniques for slender body shapes respective to different restraint criteria at supersonic speeds may be found in Ref. 6 and elsewhere. It is stressed that the theoretical optimization considerations are necessarily performed under idealized inviscid flow conditions. The actual total zero-lift drag coefficient values shall incorporate the viscous pressure drag and the base drag terms, as well as other contributions, (see general Eq. (1.7-76), Section 1.7.4.)

At steady supersonic flow conditions the induced drag term, C_{D_i} , shall be influenced not only by wing (and fin) lift characteristics, but to a considerable extent by the lift generated by the pointed body itself, which may constitute a considerable fraction of the total lift coefficient of a compound vehicle configuration. Thus, the induced drag at supersonic speeds is primarily due to:

(1) the pressure (or wave) drag component of the lifting surfaces, which is not zero, even under idealized, two-dimensional inviscid flow conditions as compared to the subsonic case,

(2) the vortex drag proper, associated with the system of shedded vortices from the wing trailing edge and the wing tips. At subsonic speeds,

it is the sole source contributing to the wind induced drag term,

(3) the pressure drag component in the free stream direction due to the resultant supersonic pressure distribution over the pointed slender bodies of revolution at small angles-of-attack.

According to linearized supersonic flow theories, both the inviscid pressure drag and the vortex drag components are still proportional to the total C_L^2, and a parabolic law for the drag polar, Eq. (1.8-25), can be assumed still valid in a first approximation, provided the body contribution to the total lift coefficient is properly accounted for. This treatment is obviously idealized, and the corrections due to the viscous pressure drag, the base drag and the interference effects under lifting conditions, ($\alpha_0 \neq 0$), shall be added by a correspondingly altered value of the Oswald's factor, e, or the induced drag corrective factor κ. Since the procedure is rather involved and uncertain, it seems more advisable to compute the induced drag directly term by term, as indicated in the explicit breakdown scheme in Table (1.7-5), (Section (1.7.4)). When the e or κ value is thus obtained, a formal drag polar expression of C_{D_i} in terms of the total lift coefficient is easily defined for various sets of Mach Number, angle-of-attack, control deflection angle and flight altitude values, (see Eq. (1.7-45)). Illustrative examples of the general trends of the $e(M)$ and $\kappa(M)$ functional dependence are given in Figs. (1.46) and (1.47).

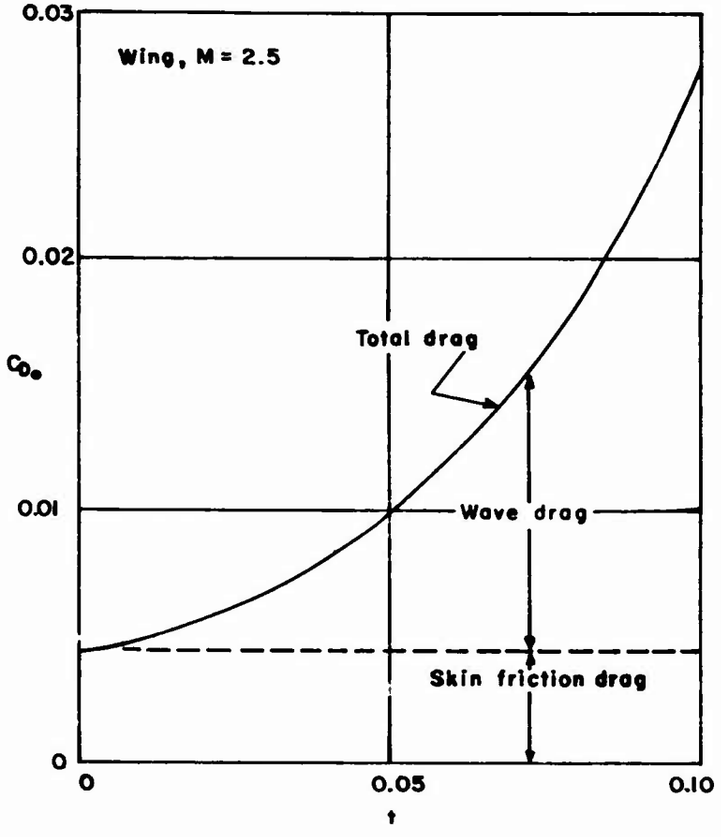

FIG. 1.44 Zero-lift drag coefficient of a typical two-dimensional wing versus the thickness ratio. Ref. 17.

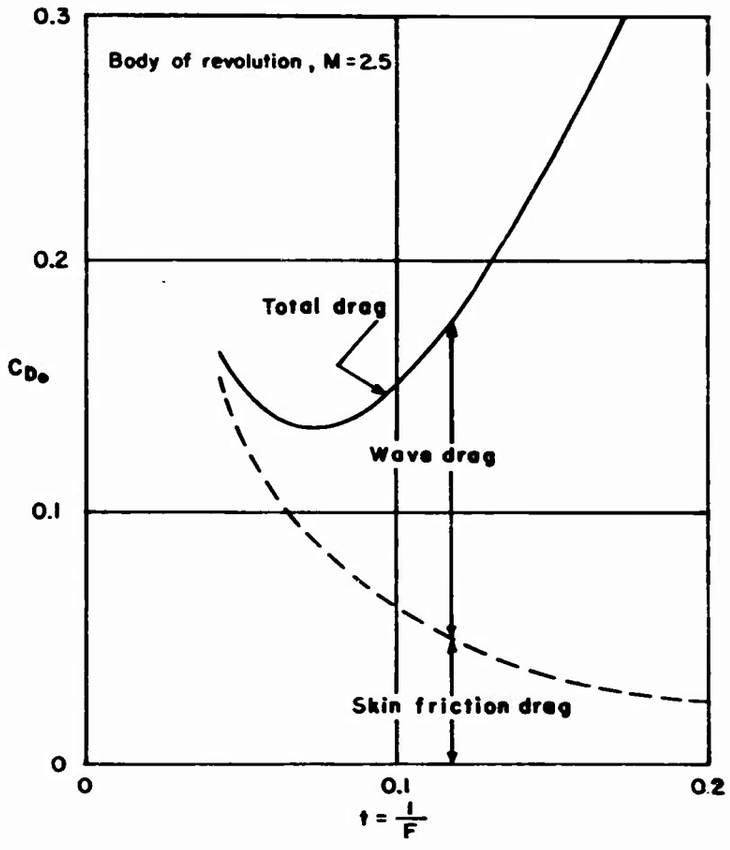

FIG. 1.45 Zero-lift drag coefficient of a typical body of revolution versus the thickness ratio, for a given cross-sectional area. Ref. 17.

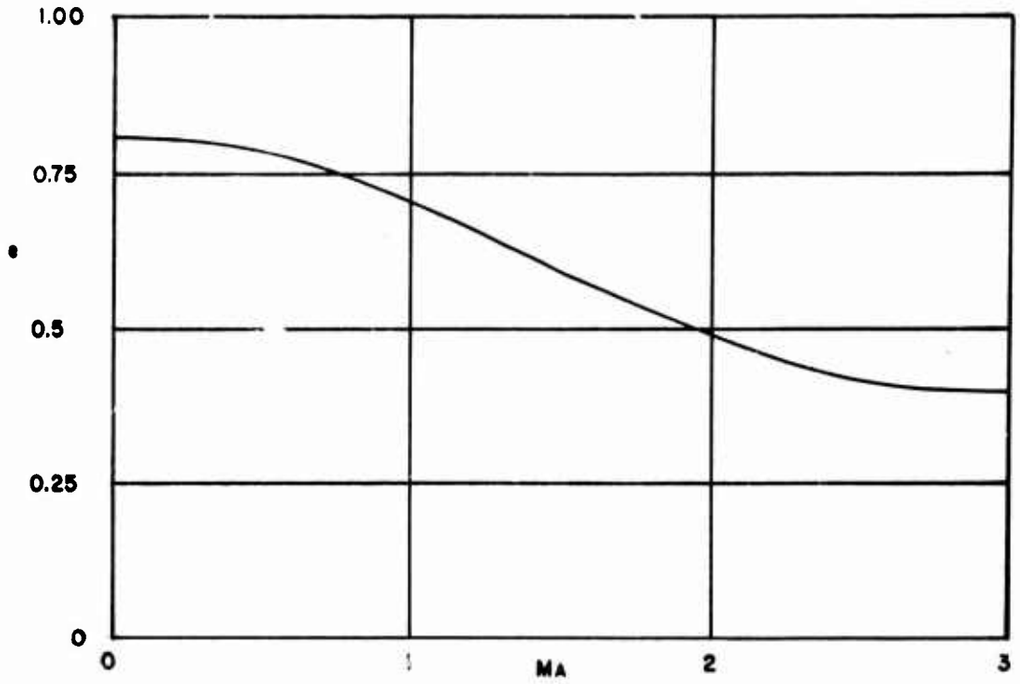

FIG. I.46 Illustrative graph of Oswald's factor dependence on Mach Number for a lifting vehicles. Ref. 42.

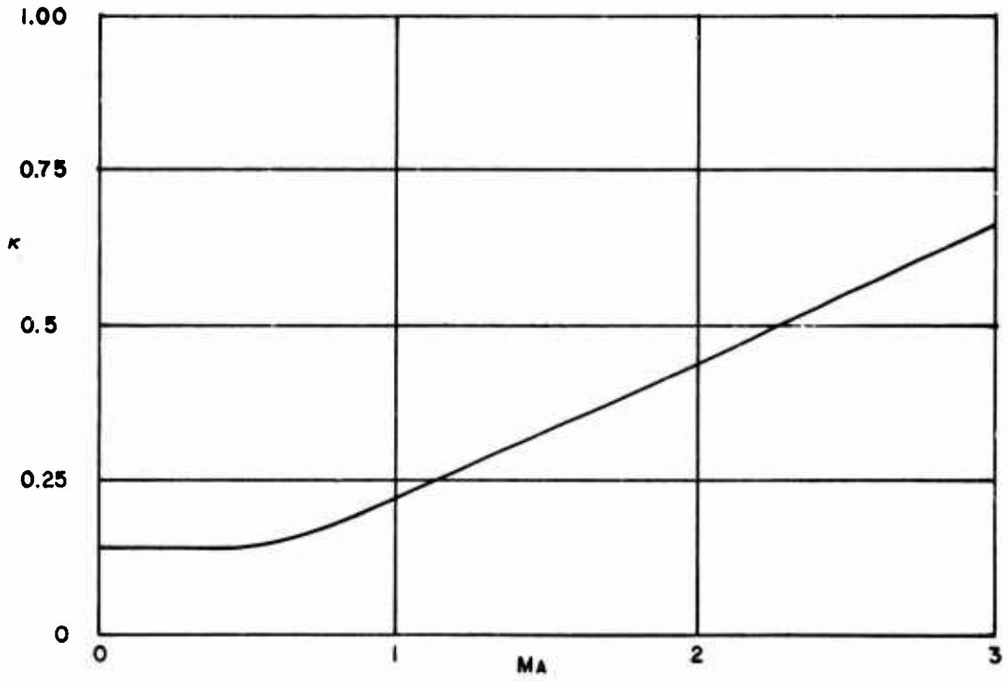

FIG. I.47 The induced drag factor, κ, variation with Mach Number for the illustrative example in Fig. I.33.

1.8.5 HYPERSONIC FLIGHT SPEED REGIME

$M_A > (M_A)_H \sim O(5)$

With a progressive increase of flight Mach Number the bow shock wave at the leading edge of wings or at the front tip point of slender bodies becomes more oblique, with a tendency to close upon the wing or the body contour. As a result, there is an ever increasing interaction between the growing viscous hypersonic boundary layer and the diminishing corridor of inviscid flow behind the shock. Furthermore, with the increase of flight Mach Number, the progressively higher temperature regions behind the shock and in the hypersonic viscous boundary layer itself successively excite the inert (vibration, dissociation, ionization) molecular degrees of freedom of various air components. Thus it may be necessary to analyze the real gas effects of a mixture of different components under general non-equilibrium conditions. This task is extremely complex, especially so when introducing chemical reactions on the body surface and different heat sink, ablative or coolant-injecting protective measures.

For practical and limited purposes of the aerodynamic force analysis, extensive simplifications and quasi-equilibrium thermal and compositional conditions of the real gas are usually assumed, i.e. the severe and complex heat transfer phenomena both in the inviscid and in the viscous flow regions are treated very approximately and only in as much as they may have bearings on the skin friction and the normal pressure coefficients. The situation is obviously of a quite different order of magnitude when the thermal and the structural problems are posed.

On the basis of permissible theoretical and physical approximations, the aerodynamic force analysis in the hypersonic flow domain is performed along the following lines:

The lower limit of the hypersonic flight speed regime is loosely set to be of the order of $M_A \sim 5$ for slender configurations on the grounds that up to that Mach Number the air can be still approximately treated as a thermally and calorically ideal gas. The temperatures realized behind shocks and within the boundary layers do not affect appreciably the thermodynamic and the structural properties of air, so that slightly modified classical supersonic flow theories and their shock-expansion relationships yield acceptable aerodynamic force predictions for most configurations.

Since the relative importance of high temperatures on the changes of internal gas properties and the overall hypersonic air flow characteristics are strongly affected not only by the free stream Mach Number criteria, but also by the body shape, the angle of attack and the ambient atmospheric conditions, several helpful subdivisions are made. Accordingly, a rather sharp distinction is made between the slender, sharp edged or pointed configurations and the blunted body shapes. The former are presumed to have attached, relative weaker bow wave patterns, while the latter are characterized by pronouncedly strong, detached bow shocks. The main difference between the two is in the intensity of entropy losses and the associated changes in pressures, temperatures, densities and flow speeds across the shocks, resulting in essentially different sets of airflow characteristics and the respective methods of approximated analyses.

Thus, the inviscid flow theories for sharp or pointed slender configurations at relatively small angles-of-attack are theoretically treated, in a first approximation by an order-of-magnitude modification of the supersonic flow equations and the shock-expansion relationships assuming that the air is still a perfect gas, taking into account that the small velocity perturbations near the body and the speed of sound are of the same order of magnitude. The latter fact represents the main difference between the supersonic and the hypersonic inviscid flow analyses under the idealized perfect gas conditions and renders the modified hypersonic flow equations nonlinear.[45] Neglecting across the shock entropy losses, their solutions, as obtained by several approximate two-dimensional and three-dimensional theories[6], are found to be in a reasonably good agreement with corresponding experimental data up to free stream Mach Numbers of the order of 15. The upper limit reflects an empirical indication of a subsequent onset of the real gas effects of such an intensity that the assumed idealized gas

approximations do not yield numerically acceptable results in predicting the normal pressure coefficients.

The blunt body configurations require quite a different type of analysis.[6] The relatively strong, detached bow shock waves involve appreciable entropy losses and subsequently pronounced jumps in gas parameters. Regions of subsonic, transonic and supersonic flow conditions are encountered after the detached shock waves near the forward stagnation point. The interference effects between inviscid and the viscous flow patterns, coupled with the real gas effects, are appreciably enhanced as the free stream (ambient flight) Mach Number increases. The analytical treatments of such mixed, real gas flow conditions are involved, even in the case of ample simplifications customary in the prediction of aerodynamic forces. In this context, it is of importance to realize that the body bluntening is introduced as a necessary compromise between the contradictory aerodynamic and the heat transfer design requirements, i.e. for the purpose of deliberately creating a detached shock wave pattern of a sufficient strength, so that appreciable entropic losses are realized across the strong, detached shock wave, and an energy dissipative buffer zone established between the shock and the body itself. Structurally, allowance must be made for a realization of the necessary mass accumulation at the blunted nose-section which serves as a heat sink and prevents its eventual melting.

As the free stream Mach Number approaches infinity, it can be argued that the bow shock approaches the body contour itself[6]. In such a limiting case, the simple Newtonian impact theory and its eventual modifications incorporating centrifugal force effects become applicable for normal pressure coefficient predictions. These methods of analysis are relatively simple and they are not restricted either by body shape or by angle-of-attack, i.e. they are applicable both to slender and blunt geometries. They do not allow for any flow interference effects among different components of a compound vehicle configurations, heat transfer, and skin friction phenomena. Relative validity of the Newtonian impact theory and of its derivatives is restricted to extreme Mach Numbers. Practically, it is conditionally used for overall aerodynamic force predictions above the Mach Number of 15 for arbitrary and compound body configurations.

Treatment of the boundary layer flows at hypersonic speeds up to the Mach Number of 20 is performed along the same methodological lines as at supersonic speeds, with due care given to the intensified momentum and energy transport mechanisms at elevated temperatures, assuming steady, equilibrium conditions. The approximate extrapolated analyses are restrictive to the skin friction coefficient estimates, and may not be adequate for heat transfer and structural design purposes.

Extreme atmospheric flight altitudes affect considerably the validity of the continuum flow concept. When the free molecular flow conditions are realized, the normal pressure and the skin friction coefficients are easiest computed on the premises of the equilibrium kinetic theory of gases, as mentioned earlier. Since, in reality, the extreme hypersonic flight speeds are encountered predominantly during the atmospheric-reentry of ballistic missiles, hypersonic gliders and space capsules, both the free molecule flow and the hypersonic continuum flow conditions may appear in various phases of the reentering vehicle trajectory. As already stated, the associated very severe problem of heat transfer rates necessitates use of blunt noses and blunt leading edges of finite radii, which in general alleviate the peak heating rates through the accompanying realization of a forebody high pressure drag component. The overall aerodynamic drag force break down scheme remains as given in Section 1.7.4, with the overall pressure or wave drag component being predominant. As an illustration, the zero-lift coefficient dependence on Mach Number for a typical long range missile, a typical high drag reentry capsule and a hypersonic glider are given in Fig. (1.48). In the case of the glider, the pronounced sweep back of a delta wing configuration is considered effective in improving the necessary aerodynamic efficiency which is otherwise offset by the unavoidable leading edge bluntness.

The induced drag for winged hypervelocity configurations at small angles of attack and relatively high Mach Numbers tends toward the limiting value[6]

$$C_{D_I} = \kappa C_L^{\,n} = \frac{C_L^{3/2}}{\sqrt{2}}$$

$$\kappa = \frac{1}{\sqrt{2}}$$

$$n = 3/2$$

(1.8-36)

if the simple Newtonian impact theory is used in a first approximation. A more accurate induced drag expression is obtained by taking into account all the individual drag force components of the actual vehicle configurations as specified in Section 1.7.4 for lifting conditions.

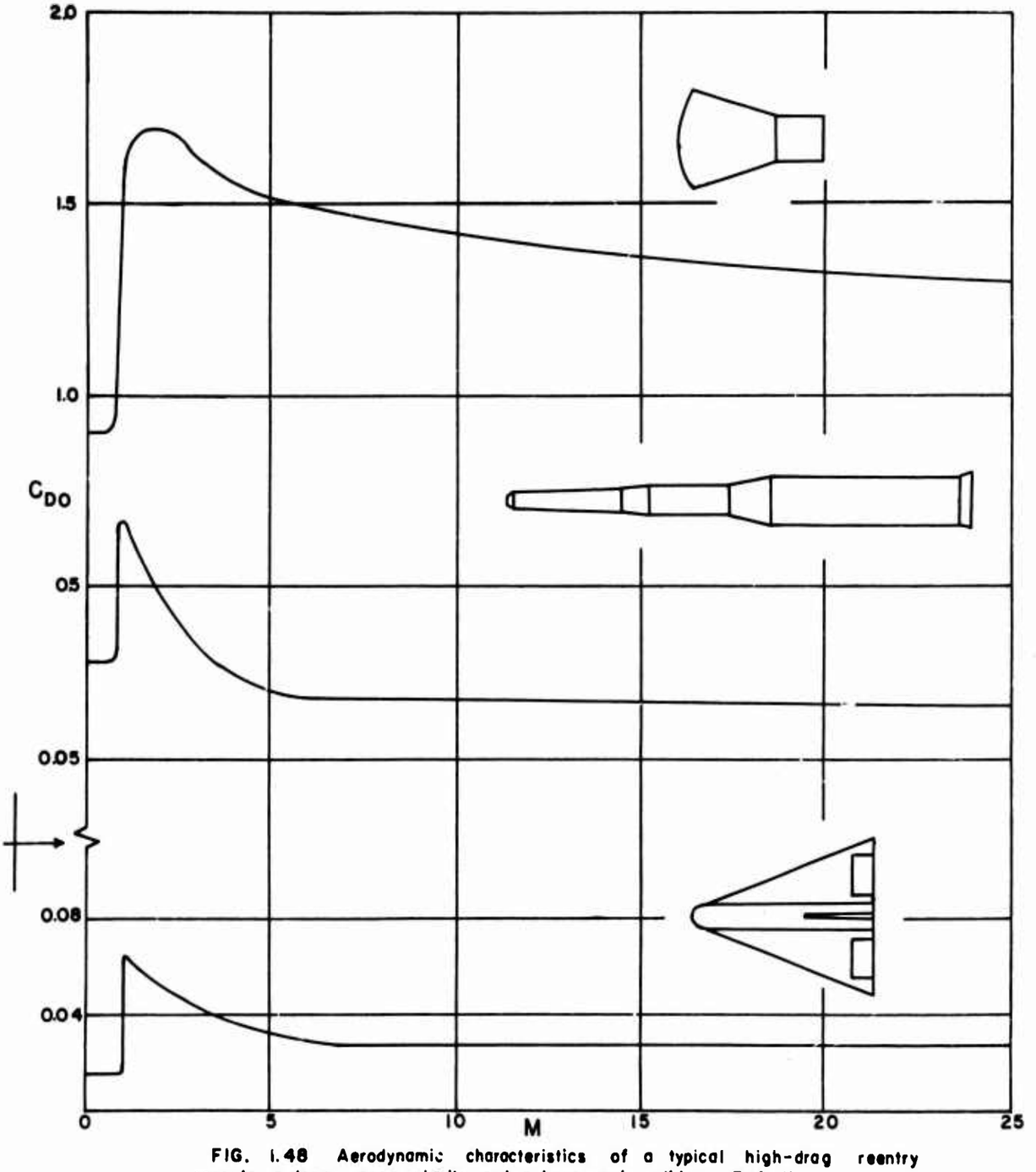

FIG. 1.48 Aerodynamic characteristics of a typical high-drag reentry capsule, a long-range missile, and a hypersonic glider. Ref. 11.

1.9 REFERENCES

1. NASA, USAF, USWB. "U. S. Standard Atmosphere, 1962."

2. Prandtl, L. Essentials of Fluid Dynamics. London: Blackie and Sons, Ltd., 1960.

3. Kuethe, A. M., Schetzer, T. L. Foundations of Aerodynamics, Second Edition. New York: John Wiley and Sons, Inc., 1963.

4. Liepman, H. W. and Roshko, A. Elements of Gasdynamics. New York: John Wiley and Sons, Inc., 1957.

5. Emmons, H. W. High Speed Aerodynamics and Jet Propulsion, Vol. III, Fundamentals of Gasdynamics. Princeton, New Jersey: 1958.

6. Truitt, R. W. Hypersonic Aerodynamics. New York: The Ronald Press Company, 1959.

7. Rubesin, M. W. and Johnson, H. A. "A Critical Review of Skin Friction and Heat Transfer Solutions of the Laminar Boundary Layer of a Flat Plate," ASME Trans., Vol. 71, No. 5, July, 1949.

8. Goldstein, S. Modern Developments in Fluid Dynamics. New York: Oxford University Press, 1938.

9. Tendeland, T. "Effects of Mach Number and Wall Temperature Ratio on Turbulent Heat Transfer at Mach Numbers From 3 to 5", NASA TR-16, 1959.

10. Sears, W. R. High Speed Aerodynamics and Jet Propulsion, Vol. VI, General Theory of High Speed Aerodynamics. Princeton, New Jersey: 1954.

11. Miele, A. Flight Mechanics, Vol. I. Reading, Massachusetts: Addison-Wesley Publishing Company, Inc., 1962.

12. Nielsen, Y. N. Missile Aerodynamics. New York: McGraw-Hill Book Company, Inc., 1960.

13. Loh, W. H. T. Dynamics and Thermodynamics of Planetary Entry. Englewood Cliffs, New Jersey: Prentice-Hall, Inc., 1963.

14. Schlichting, H. Boundary Layer Theory. New York: McGraw-Hill Book Company, Inc., 1955.

15. "Glossary of Aeronautical Terms", British Standards Institution, Part I, Part II, and Part III, British Standards House, London, England, 1950-51.

16. Duncan, W. T. The Principles of the Control and Stability of Aircraft. Cambridge, England: Cambridge University Press, 1959.

17. Etkin, B. Dynamics of Flight. New York: John Wiley and Sons, Inc., 1959.

18. Perkins, C. D. and Hage, R. E. Airplane Performance, Stability and Control. New York: John Wiley and Sons, Inc., 1953.

19. Ipsen, D. C. Units, Dimensions and Dimensionless Numbers. New York: McGraw-Hill Book Company, Inc., 1960.

20. Nelson, W. C. and Loft, E. E. Space Mechanics. Englewood Cliffs, New Jersey: Prentice-Hall, Inc., 1962.

21. Babister, A. W. Aircraft Stability and Control, International Series of Monographs on Aeronautics and Astronautics, Vol. I.

22. Donovan, A. F. and Lawrence, H. R. High Speed Aerodynamics and Jet Propulsion, Vol. VII, Aerodynamic Components of Aircraft at High Speeds. Princeton, New Jersey: 1957.

23. Hoerner, S. F. Fluid Dynamics Drag: Author's publication.

24. Hoerner, S. F. "Report of the Definitions Panel of Definitions to be Used in the Description and Analysis on Drag," British A.R.C.C.P. No. 369, London, 1958.

25. Truitt, R. W. Fundamentals of Aerodynamic Heating. New York: The Ronald Press Company, 1960.

26. Knudsen, M. The Kinetic Theory of Gases. London: Methuen and Company, Ltd., 1934.

27. Maxwell, T. C. Collected Works. Cambridge, England: Cambridge University Press, 1890.

28. Kennard, E. H. Kinetic Theory of Gases. New York: McGraw-Hill Book Company, 1938.

29. Loeb, L. B. Kinetic Theory of Gases. New York: McGraw-Hill Book Company, 1934.

30. Tsien, H. S "Superaerodynamics, Mechanics of Rarefied Gases", Journal Aerospace Science, Vol. 13, 1946.

31. Tsien, H. S. Journal Aerospace Science, Vol. 15, 1948.

32. Chapman, S. and Cowling, T. G. Mathematical Theory of Non-Uniform Gases. Cambridge, England: Cambridge University Press, 1951.

33. Shaaf, S. A. "Theoretical Considerations in Rarefied Gas Dynamics," University of Michigan, Engineering Research Institute, Heat Transfer Symposium, 1953.

34. Emmons, H. W. (Ed.) High Speed Aerodynamics and Jet Propulsion Series, Vol. III, Fundamentals of Gas Dynamics, Section H by Chambre and Shaaf. Princeton, New Jersey: Princeton University Press, 1958.

35. Kuo, Y. H. Journal of Mathematics and Physics, Vol. 5, 1954.

36. Drake, R. M. and Kanc, E. D. "A Summary of the Present Status of Heat Transfer in Rarefied Gases" University of California, Institute of Engineering Research, Report HE-150-73, 1950.

37. Eckert, E. R. G. "Mass, Momentum and Heat Transfer - A Survey of the Field" Recent Advances in Engineering Sciences, Proceedings of Conference on Science and Technology, September 9-12, 1957, Purdue University, Lafayette, Indiana.

38. Milne-Thompson, L. M. Theoretical Hydrodynamics. New York: The MacMillan Company, 1957.

39. Stoney, E. W. "Collection of Zero-Lift Drag Data on Bodies of Revolution from Free Flight Investigations" NACA TN 4201.

40. "Royal Aeronautical Society Data Sheets - Aerodynamics" Vol. I, II, III, England, 1960.

41. Abbott, H. I. and Doenhoff, E. A. Theory of Wing Sections. New York: Dover Publications, Inc., 1959.

42. Dommasch, D. O., Sherby, S. S. and Connolly, T. F., Airplane Aerodynamics. New York: Pitman Publishing Corp., 1961.

43. "Dynamics of the Airframe - Addendum." Publication AE-6-4-II, Norair, Hawthorne, California.

44. Hilton, W. F. High Speed Aerodynamics. New York: Longmans, Green and Company, 1951.

PART II

AERODYNAMIC DRAG FORCE ANALYSIS

TABLE OF CONTENTS

Part II Aerodynamic Drag Force Analysis

PART II - AERODYNAMIC DRAG FORCE ANALYSIS

2.1 Plan and Summary of Part II.

The primary aim of the Part II is to provide the essential methods and data for the aerodynamic drag force estimates in aerodynamic design and flight dynamics applications within the general limitations specified in the Sections 1.2 and 1.7. In presenting the different evaluation procedures, the emphasis is laid on the zero-lift aerodynamic drag force predictions. Following the specific aerodynamic force definitions and the decomposition scheme in PART I, the same methods can be easily adjusted for the induced drag computations, using the corresponding pressure distribution data under the lifting conditions. The elaborated methods of the drag force estimates are conceived in a self explanatory, stepwise computational form, clearly indicated in the respective computational tables, allowing for easy extensions and modifications when different aerodynamic data and different vehicle configurations are eventually considered.

The compiled aerodynamic data are mostly limited to simple missile configurations. They are presented in form of graphs, intended for an easy, direct computational use. Additional design references containing other or similar data, are indicated in most cases.

The whole treatment of the drag force analysis is based on the drag force decomposition scheme from Section 1.7.4, and on the general assumptions and limitations specified in the Section 1.2. The selection of individual drag force data is in all cases supported by the respective theoretical and engineering considerations. Since the related supporting theoretical and/or experimental evidence is in some instances quite lengthy and involved, the following general guidelines can be used in obtaining more quickly the particularly desired resulting information :

There are seven Sections in the Part II. Excluding the introductory Section 2.1, each of the six remaining deals with a basic component of the aerodynamic drag force decomposition scheme. Each of the six Sections 2.2 to 2.7 is subdivided into several sub-sections, denoted by three digits, such as 2.2.1, 2.2.2, etc. The subsections are further decomposed into paragraphs, designated by small Roman numerals (i), (ii), (iii), (iv), etc., which, in their turn, are eventually further subdivided into enumerating units, such as (1), (2), (3), etc.

The pages, tables and equations in each of the six Sections are numbered individually, bearing in the first two digits the particular Section designation. For instance, in the Section 2.3: page 2.3-15, Fig (2.3-5), Table (2.3-7), Eq (2.3-235), etc.

At the beginning of each of the six Sections, the particular Table of Contents, the list of figures, the list of tables and the list of symbols are provided. The corresponding list of references is supplied at the end of each Section, the reference numbering bearing the same convention as for the figures or tables, i.e. for instance, Ref (2.3-35) refers to the Section 2.3. In the main text of each Section, the meanings of all new symbols are clearly specified when they appear at first; the summary list of symbols at the beginning of each Section thus serving as an additional aid. It should be noted that due to the considerable extent and variety of the presented material, there appears sometime a lack of uniformity in the notation from one Section to another, i.e. the same letter-symbols or subscripts may undergo a change in meaning in different Sections.

In order to distinguish between the supporting theoretical and/or experimental evidence and the actual computational methods and data, most of the "working" Figures and Tables are compiled at the end of the particular Section, while the illustrative Figures and Tables, related directly to the analytical and theoretical developments, are found in the text itself. For a general reference, the distinction between the theoretical and/or experimental background material, and the compiled aerodynamic design data proper, can be obtained by following this plan through the Sections:

In Section 2.2 the theoretical and the physical fundamentals of fluid dynamics are briefly stated in a summary form, serving as a general reference

background for later specific theoretical and experimental data, see the subsections 2.2.1 through 2.2.5. The material has not a direct bearing on the later proposed methods of engineering applications, but is rather meant as a guiding framework of the aerodynamic force analysis in general. As such, the material can be dispensed of when so desired. In the subsections 2.2.6 and 2.2.7, the Standard Atmosphere data and the main air properties under atmospheric flight conditions are briefly stated, as they may be needed for the aerodynamic force predictions at a specified atmospheric flight regime.

Section 2.3 comprises the skin-friction drag force analysis for the continuum flow regimes and the quasi-steady flight conditions. The subsections 2.3.1 and 2.3.2 are devoted to the laminar boundary layer fundamentals, while the subsection 2.3.3 refers to the turbulent boundary layers in the same way. The subsections 2.3.4 and 2.3.5 deal with the three-dimensional and the pressure gradient effects, and with the surface roughness effects respectively. All four subsections are of the supporting theoretical and/or experimental evidence type. The actually important data for direct computational purposes are contained in the subsections 2.3.6 through 2.3.13. The methods of analysis and the stepwise tabular instructions for the skin-friction drag coefficient estimates under varying atmospheric flight conditions and with a varying degree of desired accuracy are there elaborated.

An extension of the skin-friction drag coefficient analysis to the accelerated flight regimes on a prescribed atmospheric flight trajectory is presented in the next Section 2.4, including the rarefied gas effects. The subsections 2.4.1 and 2.4.2 deal with the general aerothermal flow aspects in the free molecule flow regime, while the subsections 2.4.3 and 2.4.4 are related to the total drag force (skin-friction and pressure drag) estimates for simple body geometries in the free molecule flow regime. Similar theoretical fundamentals and their respective comparison with the continuum flow aspects are given in the subsections 2.4.5 and 2.4.6 for the slip flow regime. Finally, the actual drag force computational methods for the transient accelerated flight conditions on a prescribed atmospheric trajectory are worked out in the concluding subsection 2.4.7 for the continuum, the slip, the transitional and the free molecule flow regimes.

The combined inviscid and the viscous pressure drag analysis for the zero-lift conditions are contained in the Section 2.5. There, for general theoretical and the supporting experimental evidence are briefly summarized in the subsections 2.5.1 and 2.5.2, while in the subsections 2.5.3 through 2.5.5 the actual computational data and the computational procedures are worked out in the generally adopted self explanatory tabular form.

The Section 2.6 is designated for the base drag analysis. A brief survey of the related reference works and a summary comparative analysis of the most important influential parameters are given in the subsections 2.6.1, 2.6.2 and 2.6.3. The proposed methods for the base drag coefficient estimates and the related graphical data are presented in the concluding subsections 2.6.4 and 2.6.5.

Finally, in the closing Section 2.7 the summary tabular form for the total zero-lift drag force coefficient estimates for a compound vehicle configuration is given in terms of the main data and the partial computations as performed in the preceding Sections 2.3 through 2.6.

As already stated, the specifically illustrated computational methods for the zero-lift conditions can be easily further adjusted or modified in order to incorporate different and eventually more extensive sets of aerodynamic data than those presented here, including the induced drag estimates.

TABLE OF CONTENTS

Section 2.2 Governing Equations of Fluid Dynamics, Physical Variables and Laws

LIST OF FIGURES

Section 2.2 Governing Equations of Fluid Dynamics, Physical Variables and Laws

LIST OF TABLES

Section 2.2 Governing Equations of Fluid Dynamics, Physical Variables and Laws

LIST OF SYMBOLS

Section 2.2 Governing Equations of Fluid Dynamics
Physical Variables and Laws

I. PHYSICAL AND GEOMETRIC

G_F - Grashof Number

G_Z - Gratz Number

β - Coefficient of thermal expansion

R - Individual gas constant

s - Entropy per unit mass

e - Internal energy

δ_q - Heat added to gaseous system per unit mass

δ_w - External work done by surroundings on the fluid

dV - Infiniesimal change of specific volume

h - Enthalpy per unit mass

e_t - Kinetic energy of translation of molecules or atoms

e_r - Rotational energy of diatomic and polyatomic molecules

e_v - Vibrational energy of diatomic and polyatomic molecules e_v

e_d - Energy of dissociation (and recombination) of diatomic and polyatomic molecules into atoms or groups of atoms

e_e - Energy of electronic excitation (ionization) of molecules and atoms

e_{rad} - Electromagnetic or radiation energy of molecules and atoms

K - Boltzmann's universal constant

x, y, z, t - Coordinates of dimensionless point (space-time point)

$\vec{V}$ - Relative velocity of fluid motion

T^* - Absolute temperature

ρ - Mass density

γ - Specific heats ratio

$[M]$ - Mass

$[L]$ - Length

$[T]$ - Time

$[°K]$ - Absolute degrees Kelvin

n_i - Nondimensional molal function of the "i-th" gaseous component

i - Number of gaseous species

w_i - Reaction rate of the "i-th" gaseous component

u_i, v_i, w_i - Local average velocity components in O_x, O_y, O_z, direction respectively

U_i, V_i, W_i - Diffusive velocity components of the "i-th" species in O_x, O_y, O_z, directions respectively.

v, u, w - Average macroscopic stream velocity components in O_x, O_y, O_z directions respectively

F_x, F_y, F_z - Generalized external force field components (per unit mass) of the conservative body "forces"

p - Resultant local static pressure of the air mixture

J_x, J_y, J_z - Electric current components in an electrically charged field

B_x, B_y, B_z - The magnetic field intensity components

μ - Local field value of first coefficient of viscosity

λ - Local field value of second coefficient of viscosity

τ_{ik} - Resultant stress tensor of the second order

Q - Total internal heat generation (per unit volume) received locally by an identified fluid particle

ϕ - Viscous mechanical dissipation function

q_x, q_y, q_z - Local components of the heat flux vector, , for a fluid particle

k - Local (bulk matter) field value of the coefficient of thermal conductivity

q_{rx}, q_{ry}, q_{rz} - Local radiation heat flux vector components

E - Total specific (per unit mass) internal energy of a fluid particle

σ - Electric conductivity coefficient of a conducting fluid

H - Specific enthalpy or total heat content of fluid particle

C_p - Field value of the specific heat at constant pressure

C_v - Field value of the specific heat at constant volume

S - Specific entropy (per unit mass) of a fluid particle

a - Speed of sound

α - Angle of attack

β - Side-slip angle

N - Number of molecules

C_p - Local pressure coefficient

C_f - Local skin friction coefficient

M - Mach Number

Re - Reynolds Number

L/D - Body fineness ratio

e_i - Average internal energy of a single "i-th" degree of freedom per molecule under equilibrium conditions

Rm - Gas constant per molecule

Ro - Mean radius of a spherical earth at 45^o north latitude

H - Altitude

δ - Product of the coefficient of air compressibility at constant temperature and the static (absolute) pressure. Also b.l. thickness.

ϵ - Product of coefficient of thermal expansion at constant pressure and absolute temperature

D - Characteristic length of the body (diameter)

L - Characteristic length of system

P_c - The Peclet Number

ν - Kinematic coefficient of viscosity

G - Mass velocity, $G=\rho V$, or momentum of density

δ_β - B.C. thickness

F_r - Froude Number

We - Weber Number

σ - Surface tension

dS - Infinitesimal area

D_{ij} - Diffusion coefficient for solute and solution at given temperature

Pr - Prandtl Number

Nu - Nusselt Number

St - Stanton Number

h - A dimensional heat transfer coefficient

Q - Heat energy

S - Area to direction of heat flow

t - Time

m - $\frac{dm}{dt}$ mass flow rate

L-$\bar{\lambda}$ - Mean free path

σ - Effective molecular diameter

κ - Sutherland's constant

ξ - Velocity dilatation constant

T_m° - Molecular scale temperature

H - Geopotential altitude

Z - Geometric altitude

n - Number density of air

w - Specific weight

$\bar{v}$ - Mean air-particle speed

ν - Average collision frequency

C_s - Speed of sound

η - Kinematic viscosity

β - Shock wave angle

II. SUBSCRIPTS

l - Local free stream (outside relatively thin BC)

w - Local wall

A - Ambient atmospheric conditions (at infinity)

e - Edge of b.l.

t - Translational degree of freedom

r - Rotational degree of freedom

v - Vibrational degree of freedom

d - Dissociated degree of freedom

e - Ionized degree of freedom

w - Wall

BLANK PAGE

2.2 GOVERNING EQUATIONS OF FLUID DYNAMICS, PHYSICAL VARIABLES AND LAWS

The aerodynamic force data presented in the succeeding sections are conditionally valid within respectively specified and mathematically and physically restrained and/or approximated models of the actual fluid-body interacting and bounded systems. The data are given without explicit derivations and/or elaborations of the involved theoretical procedures and methods of solutions, i.e., the data are given in their final nondimensional aerodynamic force coefficient forms, ready for engineering aerodynamic design applications. But, in each case the underlying basic assumptions, limitations and approximations are briefly specified, including quotations of the related reference works from which the data are taken, so that a comprehensive judgment of their restrictive validity and applicability to a considered set of real physical flight dynamics and fluid flow conditions may be critically effected, when necessary.

In order to enable a general discriminating placement of any such specific theoretical or semiempirical solution within the overall context of the fluid flow phenomenology, the few most fundamental and necessary concepts and definitions pertaining to the bounded fluid-body systems in relative motion are summarized in this section. In doing so, no pretension for completeness of the given definitions is envoked.

2.2.1 CARTESIAN SCALAR FORM OF THE GOVERNING EQUATIONS FOR CONTINUUM FLUID FLOWS

(i) Description of the Fluid Dynamics Model

Fluid is assumed to be homogeneous, continuous, viscous, compressible and heat conducting. It is in a generally unsteady motion relative to an immersed rigid body at rest to which a reference Cartesian orthogonal coordinate system is fixed. The fluid-body system is presumed insulated and bounded by the exposed body surface (inner boundary) and the fluid conditions at a great distance from it (outer boundary "at infinity"). When unsteady flow cases are considered, the limitations in validity of the principle of reciprocity of relative motions for fluid-body systems should be observed, see Part I.

Investigations of such physically bounded (closed) systems are performed by application of the fundamental principles of mass, momentum and energy conservation. The three postulates are mutually completely independent and should be applied simultaneously within the Newtonian mass-space-time concept. Their respective analytic forms are named the equation of continuity, the momentum equation(s) and the energy equation.

The usual differential forms of the continuity, momentum and energy equations can be derived:

(1) Indirectly, considering an internally discrete molecular structure of the fluid matter. The three conservation principles are applied to the discrete molecular fluid structure using, for instance, the equilibrium statistical mechanics analysis (i.e. the classical kinetic theory method). The results thus obtained are then suitably transformed into the conventional "bulk matter" or "continuum" differential equations forms by some proper mean averaging procedure[8,10].

(2) Directly, treating the flowing fluid as macroscopically homogeneous and continuous.

By this method[1 to 7] the mass, momentum and energy conservation principles are applied to some conveniently small fluid "control volume" of an arbitrary shape, which is then subsequently reduced to "a mathematical point" in a space fixed continuous and homogeneous "fluid field", characterized by presumably known time-spatial distributions of the involved physical properties. The term "fluid particle" denotes an arbitrarily shaped representative "control volume" of relatively infinitesimal dimensions, i.e. in the limes the "fluid particle" reduces to the concept of a mathematical (dimensionless) point (x,y,z,t), although still possessing respectively properly defined physical properties

of mass density, pressure, velocity, temperature, etc. The field concept comprises a functional continuous representation of any physical variable or quantity in terms of the absolute space and the absolute time independent coordinates. Evidently, the spatial reference coordinate system is inertial and fixed, the fluid being in relative motion respective to it.

A scalar field relates to a space-time distribution function of a scalar physical variable, such as the absolute temperature, T°, the mass density, ρ, etc. It is characterized at each space-time point (x,y,z,t), by a single functional number.

A vector field is the space-time functional distribution of a vectorial physical quantity, such as the relative velocity of fluid motion, $\vec{V}$, having at each space-time point (x,y,z,t), a particular functional magnitude, direction and sense. In the adopted Cartesian orthogonal reference frame a vector field is conditionally resolved into three componental scalar fields by a correct vectorial resolution into the three axes directions of the involved vectorial quantity.

In order to acquire the differential form of the mass, momentum and energy conservation principles within the fluid field concept, the differentiation is necessarily performed "by following a fluid particle motion through the fluid field", since a correct application of the conservational principles and the involved space-time changes of physical quantities require that the identity of a fluid particle (or of an infinitesimal control volume) be preserved as it moves through the prescribed fluid field. As a consequence, a special scalar differentiation operation, D/Dt, is performed on any scalar field variable, $A(x,y,z,t)$, such that:

$$\frac{D}{Dt} = \frac{\partial}{\partial t} + u\frac{\partial}{\partial x} + v\frac{\partial}{\partial y} + w\frac{\partial}{\partial z}$$

$$A = A(x,y,z,t)$$

$$\therefore \frac{DA}{Dt} = \frac{\partial A}{\partial t} + u\frac{\partial A}{\partial x} + v\frac{\partial A}{\partial y} + w\frac{\partial A}{\partial z} \qquad (2.2\text{-}1)$$

In case of a vector field variable, $\vec{A}(x,y,z,t)$, the above operation is performed on its scalar components in the given three axes directions:

$$\vec{A} = \hat{i}A_x + \hat{j}A_y + \hat{k}A_z$$

$$\frac{DA_x}{Dt} = \frac{\partial A_x}{\partial t} + u\frac{\partial A_x}{\partial x} + v\frac{\partial A_x}{\partial y} + w\frac{\partial A_x}{\partial z}$$

$$\frac{DA_y}{Dt} = \frac{\partial A_y}{\partial t} + u\frac{\partial A_y}{\partial x} + v\frac{\partial A_y}{\partial y} + w\frac{\partial A_y}{\partial z}$$

$$\frac{DA_z}{Dt} = \frac{\partial A_z}{\partial t} + u\frac{\partial A_z}{\partial x} + v\frac{\partial A_z}{\partial y} + w\frac{\partial A_z}{\partial z} \qquad (2.2\text{-}2)$$

Performance of the scalar operation, $\frac{D}{Dt}$, results in the so-called "substantial derivative" of the respective particle physical quantity in the fluid field. Then the partial time rate of change, $\partial/\partial t$, is the local derivative for unsteady fluid flows, while the partial spatial rates of changes, $\partial/\partial x$, $\partial/\partial y$, $\partial/\partial z$, are called convective derivatives due to the particle motion through the field both for steady and unsteady fluid flows.

The relative accuracy of the scalar operator D/Dt is of the order of the first (linear) term in the Taylor's expansion series taken around any fixed local point (x,y,z) in a fluid field. Its counterpart in the vector notation is

$$\frac{D}{Dt} \equiv \frac{\partial}{\partial t} + (\nabla\cdot\nabla) \qquad (2.2\text{-}3)$$

A condensed formalistic survey of various analytical forms of the basic equations in fluid dynamics can be found in Ref. 11. Their rigourous derivations should be sought elsewhere (1,2,3,4,5,6,10,12). With a slight modification, the Cartesian scalar forms of the governing equations (or equations of change) are presented here for a quick reference convenience. The modification comprises treatment of the continuity equation both explicitly in terms of the possible constituent different species of air (i.e. treating air as a physically and chemically active gaseous mixture), and in its more usual global form, treating air conditionally as a single uniform diatomic gas having an average specific heats ratio value of $\gamma = 1.4$ at near-standard conditions. It is noted that most aerodynamic force problems can be adequately formulated by writing either explicitly the compound species

form of the continuity equation, or by using implicitly its global form with the different species effects stated separately and properly accounted for by mean averaging procedures. The momentum and the energy equations require the global forms only.

NOTE: All equations of change are given "per unit volume". A subsequent division by the mass density, ρ , shall bring them into "per unit mass" form. All physical quantities are expressed in the $[(MLT)^\circ K]$ system of dimensions, where M stands for mass, L for length, T for time, and °K for absolute degrees Kelvin. Dimensions of all physical quantities are given in brackets [ ] indicating their definition. When not used as a symbol for time dimension [T] , T° stands in equations for absolute temperature, while time is denoted by t .

(ii) Continuity Equation

The continuity equation represents an analytical expression of the principle of conservation of mass for bounded fluid-body systems in relative motion.

(1) The explicit form of the continuity equation in terms of the constituent gaseous species, assuming that their reaction rates are known throughout the fluid field:

$$\frac{\partial n_i}{\partial t} + \frac{\partial (n_i u_i)}{\partial x} + \frac{\partial (n_i v_i)}{\partial y} + \frac{\partial (n_i w_i)}{\partial z} = \dot{\omega}_i \qquad (2.2\text{-}4)$$

where

$n_i = n_i(x,y,z,t)$ - is the nondimensional molal fraction of the "i-th" gaseous component

i - is the number of gaseous species, such as $N_2, O_2, H_2, N, O, NO, H, A, O^-, e$, etc.

$\dot{\omega}_i = \dot{\omega}_i(x,y,z,t)$ - is the reaction rate of the "i-th" gaseous component, i.e., the rate at which formation or depletion of the "i-th" reactant is taking place locally at a given instant of time in a reacting gaseous medium, $[T^{-1}]$.

$u_i = u_i(x,y,z,t)$, $v_i = v_i(x,y,z,t)$, $w_i = w_i(x,y,z,t)$ are the local average velocity components of the "i-th" species in the Ox, Oy, Oz, directions respectively, $[LT^{-1}]$.

Note that:

$$\begin{aligned} u_i &= U_i + u \\ v_i &= V_i + v \\ w_i &= W_i + w \end{aligned} \qquad i = 1,2,3\ldots k \qquad (2.2\text{-}5)$$

where

$U_i = U_i(x,y,z,t)$, $V_i = V_i(x,y,z,t)$, $W_i = W_i(x,y,z,t)$ are the diffusion velocity components of the "i-th" species in the Ox, Oy , and Oz directions respectively, $[LT^{-1}]$.

$u = u(x,y,z,t)$, $v = v(x,y,z,t)$, $w = w(x,y,z,t)$ are the average macroscopic stream velocity components in the Ox , Oy , and Oz directions respectively, $[LT^{-1}]$.

(2) The global differential form of the continuity equation. Alternate forms:

$$\frac{\partial \rho}{\partial t} + \frac{\partial (\rho u)}{\partial x} + \frac{\partial (\rho v)}{\partial y} + \frac{\partial (\rho w)}{\partial z} = 0 \qquad (2.2\text{-}6)$$

$$\frac{\partial \rho}{\partial t} + \rho\left(\frac{\partial u}{\partial x} + \frac{\partial v}{\partial y} + \frac{\partial w}{\partial z}\right) + u\frac{\partial \rho}{\partial x} + v\frac{\partial \rho}{\partial y} + w\frac{\partial \rho}{\partial z} = 0 \qquad (2.2\text{-}7)$$

$$\frac{D\rho}{Dt} + \rho\left(\frac{\partial u}{\partial x} + \frac{\partial v}{\partial y} + \frac{\partial w}{\partial z}\right) = 0 \qquad (2.2\text{-}8)$$

where

$\rho = \rho(x,y,z,t)$ - is the global mass density, $[ML^{-3}]$.

M_i - is the molecular mass (weight) of "i-th" component, $[ML^{-3}]$.

Note that the global forms (2.2-6) to (2.2-8) are obtained from the system of k equations of species (2.2-5) by multiplying the latter by M_i , and then summing them up, while:

$$\sum_1^k n_i M_i U_i = 0$$

$$\sum_1^k n_i M_i V_i = 0$$

$$\sum_1^k n_i M_i W_i = 0$$

$$\sum_1^k M_i \dot{\omega}_i = 0$$

$$\rho = \sum_1^k n_i M_i \qquad (2.2\text{-}9)$$

(iii) Momentum Equations in the Classic Navier-Stokes Form

The Navier-Stokes differential equations of motion represent one conventional analytical form of the principle of conservation of momentum as applied to the fluid field concept. The three scalar components are:

$$\rho\left(\frac{\partial u}{\partial t}+u\frac{\partial u}{\partial x}+v\frac{\partial u}{\partial y}+w\frac{\partial u}{\partial z}\right)=\rho F_x+(JyBz-JzBy)-$$
$$-\frac{\partial p}{\partial x}-\mu\left(\frac{\partial^2 v}{\partial y\partial x}-\frac{\partial^2 u}{\partial y^2}-\frac{\partial^2 u}{\partial z^2}+\frac{\partial^2 w}{\partial z\partial x}\right)+$$
$$+\frac{4}{3}\mu\frac{\partial}{\partial x}\left(\frac{\partial u}{\partial x}+\frac{\partial y}{\partial y}+\frac{\partial w}{\partial z}\right)+$$
$$+2\left(\frac{\partial\mu}{\partial x}\frac{\partial u}{\partial x}+\frac{\partial\mu}{\partial y}\frac{\partial u}{\partial x}+\frac{\partial\mu}{\partial z}\frac{\partial u}{\partial z}\right)+\frac{\partial\mu}{\partial y}\left(\frac{\partial v}{\partial x}-\frac{\partial u}{\partial y}\right)-$$
$$-\frac{\partial\mu}{\partial z}\left(\frac{\partial u}{\partial z}-\frac{\partial w}{\partial x}\right)-\frac{2}{3}\frac{\partial\mu}{\partial x}\left(\frac{\partial u}{\partial x}+\frac{\partial v}{\partial y}+\frac{\partial w}{\partial z}\right),$$

(2.2-10)

$$\rho\left(\frac{\partial v}{\partial t}+u\frac{\partial v}{\partial x}+v\frac{\partial v}{\partial y}+w\frac{\partial v}{\partial z}\right)=\rho F_y+(JxBz-JzBx)-$$
$$-\frac{\partial p}{\partial y}-\mu\left(\frac{\partial^2 w}{\partial z\partial y}-\frac{\partial^2 v}{\partial z^2}-\frac{\partial^2 v}{\partial x^2}+\frac{\partial^2 u}{\partial x\partial y}\right)+$$
$$+\frac{4}{3}\mu\frac{\partial}{\partial y}\left(\frac{\partial u}{\partial x}-\frac{\partial v}{\partial y}-\frac{\partial w}{\partial z}\right)+$$
$$+2\left(\frac{\partial\mu}{\partial x}\frac{\partial v}{\partial x}+\frac{\partial\mu}{\partial y}\frac{\partial v}{\partial y}+\frac{\partial\mu}{\partial z}\frac{\partial v}{\partial z}\right)+\frac{\partial\mu}{\partial z}\left(\frac{\partial w}{\partial z}-\frac{\partial v}{\partial z}\right)-$$
$$-\frac{\partial\mu}{\partial x}\left(\frac{\partial v}{\partial x}-\frac{\partial u}{\partial y}\right)-\frac{2}{3}\frac{\partial\mu}{\partial y}\left(\frac{\partial u}{\partial x}+\frac{\partial v}{\partial y}+\frac{\partial w}{\partial z}\right),$$

(2.2-11)

$$\rho\left(\frac{\partial w}{\partial t}+u\frac{\partial w}{\partial x}+w\frac{\partial w}{\partial y}+w\frac{\partial w}{\partial z}\right)=\rho F_z+(JxBy-JyBx)-$$
$$-\frac{\partial p}{\partial z}-\mu\left(\frac{\partial^2 u}{\partial x\partial z}-\frac{\partial^2 w}{\partial x^2}-\frac{\partial^2 w}{\partial y^2}+\frac{\partial^2 v}{\partial y\partial z}\right)+$$
$$+\frac{4}{3}\mu\frac{\partial}{\partial z}\left(\frac{\partial u}{\partial x}+\frac{\partial v}{\partial y}+\frac{\partial w}{\partial z}\right)+$$
$$+2\left(\frac{\partial\mu}{\partial x}\frac{\partial w}{\partial x}+\frac{\partial\mu}{\partial y}\frac{\partial w}{\partial y}+\frac{\partial\mu}{\partial z}\frac{\partial w}{\partial z}\right)+\frac{\partial\mu}{\partial x}\left(\frac{\partial u}{\partial z}-\frac{\partial w}{\partial x}\right)-$$
$$-\frac{\partial\mu}{\partial y}\left(\frac{\partial w}{\partial y}-\frac{\partial v}{\partial z}\right)-\frac{2}{3}\frac{\partial\mu}{\partial z}\left(\frac{\partial u}{\partial x}+\frac{\partial v}{\partial y}+\frac{\partial w}{\partial z}\right)$$

(2.2-12)

In terms of the "substantial derivative" notation, the left hand sides of the equations (2.2-10) to (2.2-11) can be alternatively written as:

$$\rho\frac{Du}{Dt},\quad \rho\frac{Dv}{Dt},\quad \rho\frac{Dw}{Dt}$$

Notation:

$\rho=\rho(x,y,z,t)$ - is the field fluid mass density, $[ML^{-3}]$.

$u=u(x,y,z,t)$, $v=v(x,y,z,t)$, $w=w(x,y,z,t)$ - are the field relative velocity components of the ordered or "bulk matter" fluid motion in the Ox, Oy, and Oz axes directions respectively, $[LT^{-1}]$.

Fx, Fy, and Fz - are generalized external force field components (per unit mass) of the conservative body "forces", i.e. forces proportional to mass and possessing a potential, such as gravity force, $[(MLT^{-2})(M^{-1})]$. In vector notation:

$$\vec{F}=\vec{i}Fx+\vec{j}Fy+\vec{k}Fz=-\nabla\phi$$

$$\nabla=\vec{i}\frac{\partial}{\partial x}+\vec{j}\frac{\partial}{\partial y}+\vec{k}\frac{\partial}{\partial z} \qquad (2.2\text{-}13)$$

$p=p(x,y,z,t)$ - is the resultant (Dalton's Law) local static (or normal) pressure of the air mixture (per unit area), $[(MLT^{-2})(L^{-2})]$.

Jx, Jy, and Jz - are the electric current components in an electrically charged field,

$$\vec{J}(x,y,z,t)=\vec{i}Jx(x,y,z,t)+\vec{j}Jy(x,y,z,t)+$$
$$+\vec{k}Jz(x,y,z,t) \qquad (2.2\text{-}14)$$

Bx, By, and Bz - are the magnetic field intensity components,

$$\vec{B}(x,y,z,t)=\vec{i}Bx(x,y,z,t)+\vec{j}By(x,y,z,t)+$$
$$+\vec{k}Bz(x,y,z,t) \qquad (2.2\text{-}15)$$

Note that the scalar componental expressions (JyBz - JzBy) etc. have necessarily dimension $[(MLT^{-2})(L^{-3})]$, and that they are obtained from the associated vectorial force field concept:

$$\vec{J}x\vec{B}=\begin{vmatrix}\vec{i}&\vec{j}&\vec{k}\\Jx&Jy&Jz\\Bx&By&Bz\end{vmatrix}=\vec{i}(JyBz-JzBy)+$$
$$+\vec{j}(JxBz-JzBx)+\vec{k}(JxBy-JyBx)$$

(2.2-16)

$\mu=\mu(x,y,z,t)$ - is the local field value of the coefficient of viscosity, called "the first coefficient" of viscosity, $[ML^{-1}T^{-1}]$

$\lambda = \lambda(x,y,z,t)$ - is the local field value of "the second coefficient" of viscosity. It can be thought of as a delation($\partial u/\partial x + \partial v/\partial y + \partial w/\partial z$) proportionality factor related to the effects of compressibility on the shear in a fluid. With an average static pressure defined as[7,14]

$$p = p_{av} = -\left(\frac{\tau_{11}+\tau_{22}+\tau_{33}}{3}\right)$$

the relationship between λ and μ ,

$$\lambda = -\frac{2}{3}\mu \quad , \tag{2.2-17}$$

can be established using the equilibrium kinetic theory analysis, where

$[\tau_{ik}]$ - is the resultant stress tensor of the second order,

$$[\tau_{ik}] = \begin{bmatrix} \tau_{11} & \tau_{12} & \tau_{13} \\ \tau_{21} & \tau_{22} & \tau_{23} \\ \tau_{31} & \tau_{32} & \tau_{33} \end{bmatrix} \tag{2.2-18}$$

It possesses the quality of symmetry, i.e.:

$$\tau_{ik} = \tau_{ki}$$

and thus,

$$[\tau_{ik}] = \begin{bmatrix} \tau_{11} & \tau_{12} & \tau_{13} \\ \tau_{12} & \tau_{22} & \tau_{23} \\ \tau_{13} & \tau_{23} & \tau_{33} \end{bmatrix} \tag{2.2-19}$$

where τ_{11} , τ_{22} and τ_{33} are the "direct" or "normal" stresses ($i = k$) , and the $\tau_{12} = \tau_{21}$, $\tau_{13} = \tau_{31}$, $\tau_{23} = \tau_{32}$ are the "shear" or "tangential" stresses.

Convention for stress signs: tensile stresses are considered positive, compressive stresses negative.

(iv) Energy Equation

Energy equation represents the total energy balance or energy conservation in an infinitesimally small "control volume" at any point in the fluid field. Several commonly used general forms of the energy equation appear, depending on the way in which the fluid thermodynamic characteristics are treated. Thus:

(1) Energy Equation in Terms of the Specific Internal Energy,E

$$\frac{\partial Q}{\partial t} + \frac{\partial}{\partial x}\left(k\frac{\partial T}{\partial x}\right) + \frac{\partial}{\partial y}\left(k\frac{\partial T}{\partial y}\right) + \frac{\partial}{\partial z}\left(k\frac{\partial T}{\partial z}\right) -$$

$$-\left(\frac{\partial q_{rx}}{\partial x} + \frac{\partial q_{ry}}{\partial y} + \frac{\partial q_{rz}}{\partial z}\right) + \frac{J^2}{\sigma} + \phi =$$

$$= \rho\left[\frac{DE}{Dt} + p\frac{D}{Dt}\frac{1}{\rho}\right] = \rho\frac{DE}{Dt} + p\left(\frac{\partial u}{\partial x} + \frac{\partial v}{\partial y} + \frac{\partial w}{\partial z}\right) \tag{2.2-20}$$

where

$Q = Q(x,y,z,t)$ - is the total internal heat generation (per unit volume) received locally by an identified fluid particle, such as that due to Joule heating effects, chemical reactions, etc., not including the viscous dissipation work, which is represented by the mechanical dissipative function ϕ , and not including the Ohmic heating in a conducting fluid, $\left[(ML\,T^{-2})(L)(L^{-3})\right] = \left[(ML^2T^{-2})(L^{-3})\right]$.

q_x , q_y , q_z - are the local components of the heat flux vector, $\vec{q}$, for a fluid particle, such that

$$\vec{q}(x,y,z,t) = \vec{i}q_x(x,y,z,t) + \vec{j}q_y(x,y,z,t) + \vec{k}q_z(x\,y\,z\,t) \tag{2.2-21}$$

where, by definition,

$$q_x = k\frac{\partial T^\circ}{\partial x} \qquad \left[(ML\,T^{-2})(L^{-2})(T^{-1})\right]$$

$$q_y = k\frac{\partial T^\circ}{\partial y} \qquad \text{- " -}$$

$$q_z = k\frac{\partial T^\circ}{\partial z} \qquad \text{- " -} \tag{2.2-22}$$

and

$$\frac{\partial q_x}{\partial x} + \frac{\partial q_y}{\partial y} + \frac{\partial q_z}{\partial z} = \nabla\cdot\vec{q} = \left[\frac{\partial}{\partial x}\left(k\frac{\partial T^\circ}{\partial x}\right) + \right.$$

$$\left. + \frac{\partial}{\partial y}\left(k\frac{\partial T^\circ}{\partial y}\right) + \frac{\partial}{\partial z}\left(k\frac{\partial T^\circ}{\partial z}\right)\right] \tag{2.2-23}$$

$$\left[(ML^2\,T^{-2})(L^{-3})(T^{-1})\right]$$

$T^\circ = T^\circ(x,y,z,t)$ - is the local absolute temperature, $[^\circ R]$.

$k = k(x,y,z,t)$ - is the local (bulk matter) field value of the coefficient of thermal conductivity for a given fluid, $\left[(ML^2T^{-2})(L^{-1})(T^{-1})(^\circ R^{-1})\right]$.

q_{rx}, q_{ry}, q_{rz} - are the local radiation

heat flux vector components, $\left[(ML^2T^{-2})(L^{-2})(T^{-1})\right]$

$$\vec{q}_r(x,y,z,t) = \vec{i}\,q_{rx}(x,y,z,t) + \vec{j}\,q_{ry}(x,y,z,t) + \vec{k}\,q_{rz}(x,y,z,t) \tag{2.2-24}$$

$$\left(\frac{\partial q_{rx}}{\partial x} + \frac{\partial q_{ry}}{\partial y} + \frac{\partial q_{rz}}{\partial z}\right) = \nabla \cdot \vec{q}_r \tag{2.2-25}$$

$E = E(x,y,z,t)$ - is the total specific (per unit mass) internal energy of a fluid particle as it moves through the fluid field $\left[(ML^2T^{-2})(M^{-1})\right]$

$\frac{J^2}{\sigma}$ - is the local ohmic heating density (per unit volume) time rate of a fluid particle, $\left[(ML^2T^{-2})(L^{-3})(T^{-1})\right]$.

$\sigma = \sigma(x,y,z,t)$ - is the electric conductivity coefficient of a conducting fluid.

$\phi = \phi(x,y,z,t)$ - is the viscous dissipation function, always positive and unaffected in form by field variations of the first, μ, and second, λ, coefficients of viscosity. Dimensionally, it is expressed in Eq. (2.2-20) in the form of a heat density time rate (per unit volume per unit time), $\left[(ML^2T^{-2})(L^{-3})(T^{-1})\right]$.

Most common alternate forms of the dissipation function, with $\lambda = (-2/3)\mu$, are:

$$\phi = \frac{2}{3}\mu\left[\left(\frac{\partial u}{\partial x} - \frac{\partial v}{\partial y}\right)^2 + \left(\frac{\partial v}{\partial y} - \frac{\partial w}{\partial z}\right)^2 + \left(\frac{\partial w}{\partial z} - \frac{\partial u}{\partial x}\right)^2\right] + \mu\left[\left(\frac{\partial u}{\partial z} + \frac{\partial w}{\partial x}\right)^2 + \left(\frac{\partial v}{\partial x} + \frac{\partial u}{\partial y}\right)^2 + \left(\frac{\partial w}{\partial y} + \frac{\partial v}{\partial z}\right)^2\right] \geq 0 \tag{2.2-26}$$

$$\phi = \mu\left[\left(\frac{\partial u_1}{\partial x_3} + \frac{\partial u_3}{\partial x_1}\right)^2 + \left(\frac{\partial u_2}{\partial x_1} + \frac{\partial u_1}{\partial x_2}\right)^2 + \left(\frac{\partial u_3}{\partial x_2} + \frac{\partial u_2}{\partial x_3}\right)^2\right] - \lambda\left[\left(\frac{\partial u_1}{\partial x_1} - \frac{\partial u_2}{\partial x_2}\right)^2 + \left(\frac{\partial u_2}{\partial x_2} - \frac{\partial u_3}{\partial x_3}\right)^2 + \left(\frac{\partial u_3}{\partial x_3} - \frac{\partial u_1}{\partial x_1}\right)^2\right] \geq 0 \tag{2.2-27}$$

$$\phi = 2\mu\left\{\left(\frac{\partial u}{\partial x}\right)^2 + \left(\frac{\partial v}{\partial y}\right)^2 + \left(\frac{\partial w}{\partial z}\right)^2 + \frac{1}{2}\left[\left(\frac{\partial u}{\partial y} + \frac{\partial v}{\partial x}\right)^2 + \left(\frac{\partial u}{\partial z} + \frac{\partial w}{\partial x}\right)^2 + \left(\frac{\partial w}{\partial y} + \frac{\partial v}{\partial z}\right)^2\right]\right\} + \lambda\left[\frac{\partial u}{\partial x} + \frac{\partial v}{\partial y} + \frac{\partial w}{\partial z}\right]^2 \geq 0 \tag{2.2-28}$$

(2) Energy Equation in Terms of the Specific Enthalpy, H.

$$\rho\frac{DH}{Dt} = \frac{Dp}{Dt} + \frac{\partial Q}{\partial t} + \frac{\partial}{\partial x}\left(k\frac{\partial T}{\partial x}\right) + \frac{\partial}{\partial y}\left(k\frac{\partial T}{\partial y}\right) + \frac{\partial}{\partial z}\left(k\frac{\partial T}{\partial z}\right) - \left(\frac{\partial q_{rx}}{\partial x} + \frac{\partial q_{ry}}{\partial y} + \frac{\partial q_{rz}}{\partial z}\right) + \frac{J^2}{\sigma} + \phi \tag{2.2-29}$$

where

$H = H(x,y,z,t)$ - is the specific enthalpy (per unit mass) or the total heat content of a fluid particle as it moves through the fluid field. By definition,

$$H = E + \frac{p}{\rho} = C_p T \left[(ML^2T^{-2})(M^{-1})\right] \tag{2.2-30}$$

where C_p - is the field value of the specific heat (per unit mass) at constant pressure, and

$$C_p = \gamma C_v \qquad \left[(ML^2T^{-2})(M^{-1})(^\circ K)\right] \tag{2.2-31}$$

(3) Energy Equation in Terms of the Specific Entropy, S.

$$\rho T\frac{DS}{Dt} = \frac{\partial Q}{\partial t} + \frac{\partial}{\partial x}\left(k\frac{\partial T}{\partial x}\right) + \frac{\partial}{\partial y}\left(k\frac{\partial T}{\partial y}\right) + \frac{\partial}{\partial z}\left(k\frac{\partial T}{\partial z}\right) - \left(\frac{\partial q_{rx}}{\partial x} + \frac{\partial q_{ry}}{\partial y} + \frac{\partial q_{rz}}{\partial z}\right) + \frac{J^2}{\sigma} + \phi \tag{2.2-32}$$

where

$S = S(x,y,z,t)$ - is the specific entropy (per unit mass) of a fluid particle as it moves through the fluid field. By definition:

$$S = \int_0^T \frac{\delta Q}{T} \qquad \left[(ML^2T^{-2})(M^{-1})(^\circ K^{-1})\right] \tag{2.2-33}$$

Since the dissipation function, ϕ, represents the rate of dissipative work done by viscous stresses, and since it is always positive, it increases the internal heat content in a viscous fluid. Consequently, the dissipation function, ϕ, is related to the entropy, H, increase in the fluid:

$$\rho\frac{DE}{Dt} = -p\nabla\cdot\vec{V} + \frac{\partial Q}{\partial t} + \nabla\cdot\vec{q} - \nabla\cdot\vec{q}_r + \frac{J^2}{\sigma} + \phi$$

$$\rho T\frac{DS}{Dt} = \rho\frac{DE}{Dt} + p\nabla\cdot\vec{V} = \rho\frac{DQ}{Dt} \tag{2.2-34}$$

$$\therefore \rho T\frac{DS}{Dt} = \frac{\partial Q}{\partial t} + \nabla\cdot\vec{q} - \nabla\cdot\vec{q}_r + \frac{J^2}{\sigma} + \phi \tag{2.2-35}$$

where in the shorthand vectorial notation:

$$\nabla \cdot \vec{V} = \frac{\partial u}{\partial x} + \frac{\partial v}{\partial y} + \frac{\partial w}{\partial z} \qquad (2.2\text{-}36)$$

while $\nabla \cdot \vec{q}$ and $\nabla \cdot \vec{q}_r$ are given by Eqs. (2.2-23) and (2.2-25) respectively.

(v) Discussion of the General Forms of the Governing Fluid Flow Equations (Equations of Change)

The resulting simultaneous system of five governing differential equations of motion (one continuity equation, three componental momentum equations and one energy equation) are above expressed per unit volume. The equations are valid locally at a given instant of time in the respectively fixed fluid field, all the constituent physical variables in the equations being necessarily functionally treated as given space-time field properties.

When a physical quantity in the equations is defined per unit mass, the term "specific" is used. Likewise, when a physical quantity is defined per unit volume, the term "density" is used. Dimensions for each physical quantity are indicated in brackets, [ ] , as specified earlier.

The necessary and sufficient number of primary dependent substantial physical variables is five, all other physical variables requiring the corresponding sets of auxiliary functional expressions, which shall define them additionally in the adopted space-time fluid field terms locally at any point. Alternatively, by introduction of some assumptions and/or approximations, the rest of physical variables and parameters over the five primary ones can be conditionally treated either as constants throughout the investigated fluid field, or eventually directly related by known and explicitly defined physical laws and internal flow conditions to some of the basic five independent physical variables. Thus, customarily and in accordance with the essential meanings of the mass, momentum and energy conservational principles when applied to the fluid field concept, the primary dependent substantial physical variables in the five governing equations of motion are the (Cartesian) velocity components, u , v , w , the mass density, ρ , and the absolute temperature, $T°$:

$$\begin{aligned} u &= u(x,y,z,t) \\ v &= v(x,y,z,t) \\ w &= w(x,y,z,t) \\ \rho &= \rho(x,y,z,t) \\ T° &= T°(x,y,z,t) \end{aligned} \qquad (2.2\text{-}37)$$

The rest of physical variables, such as the static pressure, p , the coefficient of viscosity, μ , the coefficient of heat conductivity, k , and the specific heats, C_p and C_v , are usually expressed by auxiliary, explicitly known physical relationships:

$$\begin{aligned} p &= p(\rho, R, T°) \\ \mu &= \mu(T°) \\ k &= k(T°) \\ C_v &= C_v(T°) \\ C_p &= \gamma C_v \text{ , etc.} \end{aligned} \qquad (2.2\text{-}38)$$

which are valid throughout the given fluid field in terms of $\rho(x,y,z,t)$, $T°(x,y,z,t)$ and the gas constant R . Other physical parameters and/or more complex fluid field space-time characteristics may require correspondingly different and more involved functional relationships respectively.

In as much as the present aerodynamic force analysis is concerned, the thermal effects shall be in most cases of a secondary importance. Consequently, the functional dependence of the μ, k, C_v, γ, etc. variables on the absolute temperature, $T°$, shall take correspondingly simplified and idealized forms which are elaborated later. Contrary to it, the static pressure, p , impact on the aerodynamic force results is of a primary significance for a given fluid-body system, although it is not represented in an explicit $p(x,y,z,t)$ fluid field functional form, but rather as an implicit function of mass density, ρ , by use of the auxiliary thermodynamic equation of state, $F(p, \rho, R, T°) = 0$. The convention is one of convenience in theoretical works, since the functional relationship $p = p(\rho, R, T°)$ can be in most cases of practical interest mathematically further simplified either by specifying specially idealized isentropic flow conditions, $p = \text{const.}\ \rho^{\gamma}$, or by using the concept of speed of sound, $a = \left(\gamma \frac{p}{\rho}\right)^{1/2}$.

Except in a few very idealized and simplified flow cases, the system of the five governing equations requires a simultaneous solution within a prescribed set of boundary conditions at

the body surface and "at infinity." Within the continuum flow concepts, the boundary conditions at the body surface are diametrically opposed for two fundamentally idealized flow cases (Prandtl's postulate):

(1) For a calorically and thermally perfect and inviscid fluid flow, a "perfect slip" condition is assumed on the body contour, which is there treated as a zero-reference streamline, i.e. the local tangential velocity component is completely preserved, while the local normal velocity component is zero.

(2) For a viscous fluid flow confined within the thin boundary layer concept, the "no slip" condition is assumed at the wetted body surfaces, i.e. the local tangential velocity component is also zero.

The boundary condition "at infinity" for steady continuum fluid flow fields is usually taken to be represented by a steady, uniform velocity distribution.

The integration procedure of the five differential equations of change should be validly performed throughout the bounded fluid-body system in terms of the independent field variables (x,y,z,t) and u,v,w,ρ and T° as primary dependent variables. The results of the solutions are then finally represented in form of the aerodynamic pressure and skin friction force distribution around the given body contour.

Unfortunately, the system of the simultaneous governing differential equations of motion in its general form cannot be mathematically solved by rigourous analytical methods. (Machine computations are considered as variants of the approximate numerical analysis methods; the relative degree of accuracy remaining an option). Therefore, the general forms of the governing equations, the auxiliary relationships and the boundary conditions are by necessity usually simplified and modified in such a way that a reasonably approximated analytical procedure may be applied and the required solutions obtained within a specified degree of accuracy. The approximated theoretical modifying procedures are numerous, each eventually and conditionally acceptable for the respectively simplified and idealized fluid flow physical models. As already outlined in Part I, a classification of the multitude of the existing approximate theoretical and/or experimental procedures can be conveniently grouped according to a few most important physical characteristics of the fluid-body bounded systems, such as:

- Body shape and thickness distribution: aerodynamically smooth (pointed) or blunted, slender or thick configurations.

- Body attitude relative to the fluid flow direction "at infinity": the aerodynamic angle-of-attack, α, and the side-slip angle, β, criterion.

- Fluid flow time pattern: unsteady, time dependent fluid flow field conditions, (x,y,z,t), or steady fluid flow field conditions (x,y,z).

- Fluid flow space pattern: streamlined (laminated) or turbulent fluid flow characteristics. The distinction is applicable to both inviscid and viscous flow regions. The simple inviscid fluid flow analyses of engineering importance are mostly restricted to streamlined flows. The viscous (boundary layer) flow patterns of both laminar and turbulent types are inevitably investigated, the latter requiring a more complex analysis, which usually involves some time-and-space mean averaging procedures. Another flow pattern criterion is the flow separation phenomena. Except for the blunted base regions, the simplified theoretical analyses are customarily conducted under "no separation" assumption by imposing restraints respective to the body thickness distribution, its overall shape and its attitude relative to a given set of fluid flow parameters at large.

- Flow field dimensionality: one-dimensional, two-dimensional and three dimensional spatial variations of the involved physical parameters and the rigid body configurations.

- Intrinsic structural, physical and chemical properties of air as a flight medium, i.e. variations of its composition, its thermal, chemical and electromagnetic state and variations of its compressibility, viscosity and heat conductivity characteristics with flight altitude and flight speed. The criteria lead (1) to the conditional subdivision into continuum, slip, transitional and free molecular airflow regimes, which are basically affected by flight altitude, and (2) to the low, incompressible subsonic, compressible subsonic, transonic, supersonic and hypersonic speed regime subdivision in terms of the compressibility and thermal

effects intensity, see Part I.

The relatively low viscosity of air flows around immersed bodies leads to another extremely convenient subdivision of the overall fluid flow field (1) into a predominantly inviscid and streamlined fluid flow pattern, spread across most of the field, and (2) into a relatively thin, predominantly viscous boundary layer, confined next to the exposed body surfaces (Prandtl's postulate). The respectively differing analytical methods represent a major criteria in modifying and simplifying the general governing equations of motion.

The temperature distribution and the associated heat transport mechanism through a given fluid flow field are usually treated as secondary effects in the aerodynamic force analyses, i.e. they are introduced only in as much as they may appreciably affect the final aerodynamic force data. The situation is one of necessity, since any extensive involvement of thermal effects complicates considerably the already mathematically complex task of acquiring practically expedient aerodynamic solutions. Thus, although the high-temperature effects become increasingly prominent at hypersonic speeds, most of the slender body small perturbation inviscid flow theories[9,10] do not treat the thermal effects explicitly to any great extent, and yet the aerodynamic force results thus obtained are fairly acceptable (within the imposed restrictions) for aerodynamic design purposes. Contrary to it, the blunt body problem at high speeds and the boundary layer frictional effects in general, are strongly affected by the aerothermodynamic mechanism at large, and the temperature and heat transport effects upon the overall fluid flow conditions must be correctively taken into account to a greater extent.

Explicitly simplified physical and analytical fluid flow models in terms of the introduced assumptions and approximations are individually specified when the respective aerodynamic force data are given in later sections. Some simplifications of the equations of change due to a few most common approximating assumptions are presented below in a general form.

(vi) Simplified Forms of the Governing Equations of Motion

(1) For steady fluid flow fields, all derivatives respective to time are identically zero, $\partial/\partial t \equiv 0$, i.e. all physical variables are functions of spatial field coordinates (x,y,z) only. The substantial derivative then degenerates to:

$$\frac{D}{Dt} = u\frac{\partial}{\partial x} + v\frac{\partial}{\partial y} + w\frac{\partial}{\partial z} \qquad (2.2\text{-}39)$$

(2) For electrically non-conducting gaseous mixtures the electro-magnetic force and energy terms are identically zero.

(3) The "body force" term which is mainly due to gravity field is neglected whenever the fluid particle paths do not involve appreciable differences in gravity potential values.

(4) For steady, non-conducting, low subsonic speed flows $M_\infty < .4$ at near-standard conditions, the compressibility effects are negligible. Spatial temperature variations are relatively insignificant, so that the coefficient of viscosity, μ, and the coefficient of thermal conductivity, k, are nearly constant throughout the fluid field. Thermal radiation effects, which are normally associated with high temperatures, are also negligible. With these assumptions, including (2) and (3), the governing equations of motion acquire their simplified incompressible subsonic flow forms:

Continuity Equation:

$$\rho = \text{const.}$$

$$\frac{\partial u}{\partial x} - \frac{\partial v}{\partial y} - \frac{\partial w}{\partial z} = 0 \qquad (2.2\text{-}40)$$

Navier-Stokes Equations:

$$\rho\frac{Du}{Dt} = -\frac{\partial p}{\partial x} + \mu\left(\frac{\partial^2 u}{\partial x^2} + \frac{\partial^2 u}{\partial y^2} + \frac{\partial^2 u}{\partial z^2}\right)$$

$$\rho\frac{Dv}{Dt} = -\frac{\partial p}{\partial y} + \mu\left(\frac{\partial^2 v}{\partial x^2} + \frac{\partial^2 v}{\partial y^2} + \frac{\partial^2 v}{\partial z^2}\right)$$

$$\rho\frac{Dw}{Dt} = -\frac{\partial p}{\partial z} + \mu\left(\frac{\partial^2 w}{\partial x^2} + \frac{\partial^2 w}{\partial y^2} + \frac{\partial^2 w}{\partial z^2}\right) \qquad (2.2\text{-}41)$$

Energy Equation:

$$\frac{\partial Q}{\partial t} + k\left(\frac{\partial^2 T^\circ}{\partial x^2} + \frac{\partial^2 T^\circ}{\partial y^2} + \frac{\partial^2 T^\circ}{\partial z^2}\right) + \phi = \rho\frac{DE}{Dt} \qquad (2.2\text{-}42)$$

where in the explicit expressions (2.2-26) -(2.2-28) for the dissipation function, ϕ, all terms comprising the second coefficient (compressibility effects) of viscosity, λ, should be dropped.

(5) For thermally perfect gases, obeying the ideal form of the equation of state

$$p = \rho R T^{\circ} \qquad (2.2\text{-}43)$$

the substantial derivative terms of internal specific energy, DE/Dt, and of specific enthalpy, DH/Dt, in the equations (2.2-20) and (2.2-29), can be substituted by $Cv\ DT^{\circ}/dt$ and $Cp\ DT^{\circ}/dt$ respectively, i.e.:

$$\frac{DE}{Dt} = Cv\frac{DT^{\circ}}{Dt}$$

$$\frac{DH}{Dt} = Cp\frac{DT^{\circ}}{Dt}$$

$$Cp = \gamma Cv \qquad (2.2\text{-}44)$$

The removal of the specific heats, Cp, and Cv, from the derivative operation is permissible regardless of whether they are functions of temperature or not, i.e. regardless of whether or not the gas is calorically perfect.

When the isentropic (adiabatic reversible) conditions are introduced through a proper definition of the stagnation temperature concept[14] (as in case of idealized inviscid perfect gas flows):

$$\frac{DS}{Dt} \equiv 0 \qquad \phi \equiv 0 \qquad (2.2\text{-}45)$$

(6) The majority of steady aerodynamic force analyses are conducted by separate and unrelated investigations of the idealized perfect gas inviscid and viscous flow patterns respectively (Prandtl's postulate). The correspondingly simplified forms of the Eulerian and the Boundary Layer (laminar and turbulent) governing equations of motion are given later in sections dealing explicitly with the pressure and the skin-friction force analyses. Their common underlying general form of the equations of motion is given here, sometimes referred to as the compact Navier-Stokes equations. They are considered to be representative equations of change in a steady, electrically non-conducting and chemically non-reacting compressible fluid flow field, gravity forces neglected. The fluid is treated as thermally perfect, ($p=\rho RT^{\circ}$), its pressure temperature and density variations remaining near-standard conditions, i.e., below their critical values for which the inert degrees of molecular freedom (vibration, dissociation, ionization) are aroused. The assumptions relating stresses and strains due to fluid viscosity and compressibility are presumed valid within the second order approximations of the Maxwell's molecular velocity distribution function[7,13]. The heat transport mechanism within the fluid field is assumed to be predominantly by conduction. The adiabatic irreversible conditions are imposed, and the internal energy (per unit mass) is presumed to be defined by

$$E = \int_0^T Cv\,dT^{\circ} \qquad (2.2\text{-}46)$$

Furthermore, the fluid density, ρ, definition retains a valid physical meaning at all points of the fluid field, i.e., the local static pressure, p, is nowhere so small and the local absolute temperature, T°, is nowhere so high as to render the analytical density definition:

$$\rho = \frac{dM}{dV} = mN$$

physically meaningless, i.e., the necessary condition that the number of molecules, N, contained in an infinitesimally small particle volume, dV, must be always very great from the statistical averaging procedure point of view[7] is satisfied throughout the fluid field. The latter restraint excludes rarefied gas flow domains (transitional and free molecular flow regimes): the presumed second-order approximations of the Maxwell's velocity distribution function for continuum flow conditions are then inadequate, i.e., higher order terms for the viscous and the heat conducting transport processes are required, which is achieved by introducing a third order correction for the stress tensor and the heat flux vector definitions (called Burnett Equations)[7].

With the cited restrictions, the common compact Navier-Stokes forms of the governing equations for continuum fluid flows are:

(1) Equations of Change

Continuity equation:

$$\frac{\partial \rho}{\partial t} + u\frac{\partial \rho}{\partial x} + v\frac{\partial \rho}{\partial y} + w\frac{\partial \rho}{\partial z} + \rho\left(\frac{\partial u}{\partial x} + \frac{\partial u}{\partial y} + \frac{\partial u}{\partial z}\right) = 0 \qquad (2.2\text{-}47)$$

Momentum equations:

$$\rho\left(u\frac{\partial u}{\partial x}+v\frac{\partial u}{\partial y}+w\frac{\partial u}{\partial z}\right)=\rho F_x-\frac{\partial p}{\partial x}-\mu\left(\frac{\partial^2 v}{\partial y\partial x}-\frac{\partial^2 u}{\partial y^2}-\right.$$
$$\left.-\frac{\partial^2 u}{\partial z^2}+\frac{\partial^2 w}{\partial z\partial x}\right)+\frac{4}{3}\mu\frac{\partial}{\partial x}\left(\frac{\partial u}{\partial x}+\frac{\partial v}{\partial y}+\frac{\partial w}{\partial z}\right)+$$
$$+2\left(\frac{\partial\mu}{\partial x}\frac{\partial u}{\partial x}+\frac{\partial\mu}{\partial y}\frac{\partial u}{\partial x}+\frac{\partial\mu}{\partial z}\frac{\partial u}{\partial z}\right)+\frac{\partial\mu}{\partial y}\left(\frac{\partial v}{\partial x}-\frac{\partial u}{\partial y}\right)-$$
$$-\frac{\partial\mu}{\partial z}\left(\frac{\partial u}{\partial z}-\frac{\partial w}{\partial x}\right)-\frac{2}{3}\frac{\partial\mu}{\partial x}\left(\frac{\partial u}{\partial x}+\frac{\partial v}{\partial y}+\frac{\partial w}{\partial z}\right), \qquad (2.2\text{-}48)$$

$$\rho\left(u\frac{\partial v}{\partial x}+v\frac{\partial v}{\partial y}+w\frac{\partial v}{\partial z}\right)=\rho F_y-\frac{\partial p}{\partial v}-\mu\left(\frac{\partial^2 w}{\partial z\partial y}-\frac{\partial^2 v}{\partial z^2}-\right.$$
$$\left.-\frac{\partial^2 v}{\partial x^2}+\frac{\partial^2 u}{\partial x\partial y}\right)+\frac{4}{3}\mu\frac{\partial}{\partial y}\left(\frac{\partial u}{\partial x}+\frac{\partial v}{\partial y}+\frac{\partial w}{\partial z}\right)+$$
$$+2\left(\frac{\partial\mu}{\partial x}\frac{\partial v}{\partial x}+\frac{\partial\mu}{\partial y}\frac{\partial v}{\partial y}+\frac{\partial\mu}{\partial z}\frac{\partial v}{\partial z}\right)+\frac{\partial\mu}{\partial z}\left(\frac{\partial w}{\partial z}-\frac{\partial v}{\partial z}\right)-$$
$$-\frac{\partial\mu}{\partial x}\left(\frac{\partial v}{\partial x}-\frac{\partial u}{\partial y}\right)-\frac{2}{3}\frac{\partial\mu}{\partial y}\left(\frac{\partial u}{\partial x}+\frac{\partial v}{\partial y}+\frac{\partial w}{\partial z}\right) \qquad (2.2\text{-}49)$$

$$\rho\left(u\frac{\partial w}{\partial x}+w\frac{\partial w}{\partial y}+w\frac{\partial w}{\partial z}\right)=\rho F_z-\frac{\partial p}{\partial z}-\mu\left(\frac{\partial^2 u}{\partial x\partial z}-\frac{\partial^2 w}{\partial x^2}-\right.$$
$$\left.-\frac{\partial^2 w}{\partial y^2}+\frac{\partial^2 v}{\partial y\partial z}\right)+\frac{4}{3}\mu\frac{\partial}{\partial z}\left(\frac{\partial u}{\partial x}+\frac{\partial v}{\partial y}+\frac{\partial w}{\partial z}\right)+$$
$$+2\left(\frac{\partial\mu}{\partial x}\frac{\partial w}{\partial x}+\frac{\partial\mu}{\partial y}\frac{\partial w}{\partial y}+\frac{\partial\mu}{\partial z}\frac{\partial w}{\partial z}\right)+\frac{\partial\mu}{\partial x}\left(\frac{\partial u}{\partial z}-\frac{\partial w}{\partial x}\right)-$$
$$-\frac{\partial\mu}{\partial y}\left(\frac{\partial w}{\partial y}-\frac{\partial v}{\partial z}\right)-\frac{2}{3}\frac{\partial\mu}{\partial z}\left(\frac{\partial u}{\partial x}+\frac{\partial v}{\partial y}+\frac{\partial w}{\partial z}\right) \qquad (2.2\text{-}50)$$

Energy equation:

$$\rho\left(u\frac{\partial E}{\partial x}+v\frac{\partial E}{\partial y}+w\frac{\partial E}{\partial z}\right)=-p\left(\frac{\partial u}{\partial x}+\frac{\partial v}{\partial y}+\frac{\partial w}{\partial z}\right)+$$
$$+\left[\frac{\partial}{\partial x}\left(k\frac{\partial T^\circ}{\partial x}\right)+\frac{\partial}{\partial y}\left(k\frac{\partial T^\circ}{\partial y}\right)+\frac{\partial}{\partial z}\left(k\frac{\partial T^\circ}{\partial z}\right)\right]+$$
$$+\frac{2}{3}\mu\left[\left(\frac{\partial u}{\partial x}-\frac{\partial v}{\partial y}\right)^2+\left(\frac{\partial v}{\partial y}-\frac{\partial w}{\partial z}\right)^2+\left(\frac{\partial w}{\partial z}-\frac{\partial u}{\partial x}\right)^2\right]$$
$$+\mu\left[\left(\frac{\partial u}{\partial z}+\frac{\partial w}{\partial x}\right)^2+\left(\frac{\partial v}{\partial x}+\frac{\partial u}{\partial y}\right)^2+\left(\frac{\partial w}{\partial y}+\frac{\partial v}{\partial z}\right)^2\right] \qquad (2.2\text{-}51)$$

(2) Auxiliary Equation

Perfect gas equation of state:

$$p=\rho R T^\circ \qquad (2.2\text{-}52)$$

or, more generally for variable entropy cases:

$$F(p,\rho,R,T^\circ)=0$$

$$\mu=\mu(x,y,z) \quad \text{or} \quad \mu=\mu(T^\circ)$$
$$k=k(x,y,z) \quad \text{or} \quad k=k(T^\circ)$$
$$C_v=C_v(x,y,z)=C_p-RT^\circ=C_{p/\gamma} \quad \text{or} \quad C_v=C_v(T^\circ)$$
$$\lambda=-\frac{2}{3}\mu \qquad C_p=C_p(T^\circ) \qquad (2.2\text{-}53)$$

(3) Primary Variables

$$u=u(x,y,z)$$
$$v=v(x,y,z)$$
$$w=w(x,y,z)$$
$$\rho=\rho(x,y,z)$$
$$T^\circ=T^\circ(x,y,z) \qquad (2.2\text{-}54)$$

As already stated, a solution to the system of equations of change, together with the auxiliary relationships and within prescribed boundary conditions, is unobtainable in a mathematically rigorous closed form, i.e., their further simplification is required, customarily achieved through application of the Prandtl's postulate and by introduction of other physical and analytical assumptions and approximations.

In most cases of aerodynamic force and moment investigations, such respectively simplified governing equations of motion are analytically transformed to yield a solution in terms of the local pressure coefficient, C_p, and the local skin-friction coefficient, C_f, at any given point (x,y,z) in the steady fluid field, see Part I. A subsequent averaging summation of the local values across the exposed body surfaces gives then the total pressure and the total skin friction aerodynamic force components. As a further step, the solutions are usually sought in a non-dimensionalized similarity form, valid for families of body shapes, body attitudes and fluid flow conditions, provided that they satisfy identity of the respectively necessary and sufficient number of fixed similarity parameters or so called natural variables. The achieved "generalization" of such nondimensional similarity solutions is evidently of tremendous practical advantage. The basic underlying principles are summarized in the next Section, 2.2.2.

2.2.2 FUNDAMENTAL PHYSICAL UNITS AND VARIABLES

(i) Physical Variables

A physical variable is any physical concept to which a definite numerical value (or number) can be assigned, i.e., it represents a measurable physical quantity which is observed and specified as a pertinent quantitative component of a physical occurrence. All physical variables can be grouped into two categories, depending on the type of comparative external standards (units) used for their numerical formulation:

(1) Substantial physical variables are expressed in terms of a chosen set of the corresponding standard units (or unit measures), which must necessarily be of the same kind as the respective physical variable itself. The specific choice of such a system of unit measures is a matter of convention. Consequently, the substantial physical variables are represented by a dimensional number. Examples of substantial physical variables are mass, length, time, velocity, area, etc. Substantial physical variables are therefore dimensional by definition.

(2) Natural physical variables do not require for their definition any specific external measuring standards. They derive their meaning from a proper understanding of the intrinsic nature of a physical phenomena and from a subsequent establishment of a corresponding internal relationship between meaningful groups of compatible substantial variables which are governing the investigated nature of the physical occurrence. In order to define a natural physical variable the underlying substantial physical variable should be recognized first, and then, by the correct application of physical laws and principles that are pertinent to the investigated physical phenomena, the meaningful ratios of the dimensionally compatible substantial variables (or of their combinations) should be formed. Such a dimensionless ratio is a pure number defining the particular natural physical variable. Examples of natural physical variables are Mach Number, M ; Reynolds Number, Re ; body fineness ratio, (L/D) ; specific heat ratio, γ ; etc.

Both the basic substantial and the respectively derived natural physical variables can then be used for a valid description and an analytical formulation of the involved physical concepts and laws as they are applicable to a given physical occurrence. But the roles of the substantial and the natural physical variables in such analytic descriptions of the investigated physical phenomena are different. The substantial variables describe the fundamental measurable aspects of a physical state within the investigated physical system; they constitute and reflect a dimensional physical understanding of the internal structure and the dynamic mechanism of a physical occurrence.

The natural variables are formed only when such valid internal relationships between the substantial derivatives are already understood and functionally formulated. Since the natural variables represent non-dimensional ratios of compatible substantial physical variables, the following advantageous consequences appear:

(1) The analytical laws describing a physical occurrence are expressed in terms of a relatively reduced number of variables when the natural non-dimensional parameters are introduced.

(2) A convenient generalization of the non-dimensionalized analytical descriptions pertaining to physical systems which quantitatively possess the same natural variables and are governed by the same physical laws becomes possible. Such physical systems are said to be "similar", and the pertinent natural variables become the necessary and sufficient similarity conditions.

(3) The effective reduction in the number of non-dimensional influential variables and their similarity role make it easier and simpler to conduct comparative studies of varying conditions both within one particular physical system and for a family of aerodynamically similar systems in general.

(ii) Physical Meaning of Substantial Units

A unit is a conventionally selected magnitude of a substantial physical variable, in terms of which all other possible magnitudes of that physical variable can be specified numerically. The measuring concept requires that an unrestricted duplication or subdivision quality of the chosen unit can

be effected, so that any other physical magnitude of the same kind may be expressed numerically with a theoretically unlimited accuracy. This condition is automatically satisfied by such physical variables which in themselves can be quantitatively changed to any desirable extent by adding or subtracting their smaller amounts. Physical variables of this type are called "extensive variables", and their corresponding unit measures "extensive units." Examples are mass, length, time, etc. For instance: a length of five feet is readily conceived as a fivefold reduplication of a length of one foot.

But, there are possible conceptual definitions of some substantial physical variables which cannot be meaningfully interpreted in this additive manner. For example, if the "unit density" is defined by a specified volume of water at some reference ambient condition, then simple addition of such five units does not yield a fivefold density of a bulk of water five times greater by volume, although the unit can be used as a relative comparative measure of similarly defined densities of other substances. Such substantial physical variables, which do not possess naturally the simple additive qualities in forming greater or lesser amounts, are called "intensive variables." The lack of a meaningful additive property prevents their use in valid analytical expressions of physical laws. Consequently, any physical variable and its unit must be, by necessity, either directly or indirectly defined in terms of a compatible extensive physical variable of the same kind, or eventually in terms of other extensive variables, so that which possesses the necessary property of an unlimited reduplication is satisfied. For instance, such a physical intensive variable as "density" should be defined in terms of the actually involved mass (extensive variable) of the respective matter per unit volume, and the corresponding unit of density specified as a unit mass of the same matter per unit volume. Then, five density units represent by simple additive process fivefold mass per unit volume, or a fivefold density of the measured substance under differing ambient conditions.

The valid physical measuring concepts as defined above, imply two basic ideas: the unrestricted simple reduplication possibility, and the continuum homogeniety quality of a physical event. Consequently, whenever these classical measuring concepts are conditionally extended to such physical variables which describe conceptually discrete systems or indivisible entities (as is frequently done), it should be kept in mind that such an extended measuring notion is a mathematically convenient artifice, strictly limited in meaning by use of adequate statistical averaging procedures, i.e., only after the continuum or bulk-matter properties are ascertained.

(iii) Physical Meaning of Natural Units

In accordance with the fundamental concept of a natural variable, the corresponding natural unit is defined independently of any arbitrary external measuring standard, i.e., it reflects the intrinsic internal quality of a physical system or occurrence. A natural unit is, by virtue of the underlying ratio concept, quantitatively equal to the mathematical concept of unity. For example, a unit Mach Number is simply equal to the pure number of one.

Valid descriptive interpretations of a natural unit may be effected in different ways without changing its real meaning and definition. Thus, since Mach Number is defined as a ratio of some actual speed and the respective ambient speed of sound, the unit Mach Number may be interpreted as that speed of a body which is equal to the speed of sound, with the speed of sound taken as a measuring standard.

(iv) Basic Substantial Units

By a valid application of the fundamental physical laws and concepts, all substantial physical units can be suitably expressed in terms of a fewer number of conveniently chosen basic units. Both the number and the kind of basic units are conventional, depending on the choice of physical notions which are regarded as fundamental. Once a system of basic units is accepted, all the other physical units can be derived in terms of the few fundamental ones by applying individually valid physical laws and mathematical concepts, provided the condition of extensive quality of such a derived unit is maintained in the process.

(v) Mathematical Interpretation of Physical Variables and Units

The concept of units is introduced as a logical necessity, allowing for

a numerical representation of any physical magnitude as a simple reduplication (or subdivision) of the chosen unit measure. The additive quality of measuring processes in terms of numbers allows for a mathematical treatment of physical variables and events: the recognized physical laws and relationships governing an investigated physical occurrence are symbolically represented as conditionally meaningful mathematical equalities. The transition from physical reality to mathematical abstractions by means of units and measuring processes can in general proceed along several alternative routes, since formulation of meaningful links between the physical ideas and the mathematical symbolism depends on the chosen conventions for mathematical interpretations of physical units. Once such a conventionally accepted translation of physical recordings into the idealized language of mathematical symbols is performed, the powerful speculative potentialities of the mathematical analytic processes can be used, leading to many conclusions, deductions and generalizations that otherwise would hardly be conceived by pure physical methods and their random observational comparisons.

From the point of view of uniformity of the resulting dimensional mathematical equations (regardless of the chosen system of units), an acceptable (although by no means the only logical alternative) mathematical interpretation of a physical unit can be formulated as follows:

Any physically defined unit is regarded as an integral part of the adopted mathematical description of the respective physical variable. In other words, an equivalent mathematical quantitative definition of a substantial physical variable is represented as the product of a number times the respective unit measure. The quantitative value of a substantial physical variable is thus a dimensional number. When so mathematically interpreted, the magnitude of the measured physical variable is invariant with change in the choice of the corresponding physical system of units. For example, the equality

$$L = K_1\,\text{ft} = K_2\,\text{meters} \qquad (2.2\text{-}55)$$

holds only under the above stated "invariant" mathematical representation of the measured physical variable, i.e., when its absolute magnitude is defined as a conditional number times the chosen physical unit. In both "foot" and "meter" systems of units, the measured length, L, remains mathematically the same variable by its absolute physical magnitude. A change from feet to meters changes both the "measuring" number and the basic unit, but the product of the respective measuring number and the respective "unit" remains invariant in the transformation. In both cases the respective physical units are equivalent to the mathematical concept of a "unit entity," although the two physical units are unequal by magnitude, namely foot and meter respectively. So interpreted, the concept of the mathematical "unit entity" becomes strictly conditional.

(vi) Dimensions

Any set of basic units (for instance: cm, gr, sec) in a chosen system of basic extensive variables (for instance: length, mass, time) must satisfy the conditions of consistency, i.e., it should allow for definition of any other derived unit using the same valid standard expression by which the related derived physical variable is formulated. Example:

The standard physical definition of the uniform speed concept, V, (derived variable) is defined in terms of that distance, L, (basic variable) which is covered in the time interval, T, (basic variable) during which the uniform motion is observed. The resulting expression is a physical equation

$$V = \frac{L}{T} \qquad (2.2\text{-}56)$$

Therefore, the choice of any valid set of units for measuring the magnitude of the uniform speed, V, must be made consistent with above standard definition of the uniform speed. If the (cm sec) kinematic system of basic units is chosen, the derived unit of speed should be "cm per sec", so that the physical conceptual definition (2.2-56) is valid for the set of chosen units also, i.e.,

$$\text{cm per sec} = \frac{\text{cm}}{\text{sec}}\,. \qquad (2.2\text{-}57)$$

A change from one set of basic consistent units, (cm sec), to another set of basic consistent units, (ft sec) should then change only the measured magnitude of the observed uniform speed, while both sets of the derived (speed) and the basic (length, time) units are

consistent with the standard definition of the derived physical variable (speed) itself:

$$\text{ft-sec system:} \quad \text{ft per sec} = \frac{\text{ft}}{\text{sec}}$$

$$\text{cm-sec system:} \quad \text{cm per sec} = \frac{\text{cm}}{\text{sec}}$$

$$V = K_1 \frac{\text{cm}}{\text{sec}} = K_2 \frac{\text{ft}}{\text{sec}} \cdot \qquad (2.2\text{-}58)$$

Conclusion: A valid physical equation should be invariant with respect to any set of chosen consistent physical units (basic and derived).

Consequence: A quite general (i.e., unspecified by unit magnitudes) consistent system of basic and derived measures may be introduced: it is called the dimensional system or the dimension of a given physical variable (basic or derived) in particular. For example, any valid physical concept that can be measured in terms of some arbitrary unit of length is said to have the dimension of length, $[L]$.

Dimensions are never associated with any specific set of numbers and are expressed in terms of generalized letters, conventionally put into square brackets for distinction. A chosen set of basic units corresponds to a respective system of basic dimensions. Dimensions of derived physical variables are formed by a consistent combination of the involved basic dimensions, i.e.,by following the respective standard definition of the derived physical variable in question. For example, the dimension of velocity, V , is defined as length, L , divided by time, T :

$$[V] = \frac{[L]}{[T]} \qquad (2.2\text{-}59)$$

Basic dimensions and units are related to the concepts which define the basic physical variables and specify the basic governing laws for the investigated type of physical occurrence. Within the Newtonian absolute space and absolute time continuum environmental concepts, the defining equation of dynamics of motion is the Newton's second law. Consequently, the time, length and force (or mass), are usually chosen to represent the fundamental physical variables and dimensions. In accord with this choice, a multitude of specific systems of units may be defined; the foot-pound force-second, the centimeter-gram mass-second and the meter-newton-second systems are presently mostly in use. The length, the time and the mass represent three extensive physical variables.

For treatment of thermodynamic phenomena, the concept of temperature is introduced as the fourth fundamental variable. The temperature is actually an intensive physical variable, which can be indirectly defined through the extensive concepts of entropy and heat. Under suitable restrictions, the absolute temperature may be expressed as equal to the heat transfer per unit of entropy increase

$$T^\circ = \frac{\delta Q}{\delta S} \qquad (2.2\text{-}60)$$

where symbol δ denotes an infinitesimal increment. But, since the entropy definition is historically derived from temperature, and not vice versa, instead of employing the above correct definition the unit temperature has been quite arbitrarily formulated as a linear scaled difference between two physical conditions of a chosen substance, which makes it then explicitly an intensive physical variable.

The ambiguous situation with respect to the temperature definition can be summarized as follows:

(1) The second law of thermodynamics relates the fundamental concepts of entropy, heat and temperature, Eq. (2.2- 60). It can be used to define correctly the concept of absolute temperature, T°, in terms of heat, Q , and entropy, S , which are valid extensive physical variables.

(2) Alternatively, in the equilibrium kinetic theory of gases the absolute temperature is regarded as a measure of the total molecular energetic level, expressed in terms of the existing molecular degrees of freedom of motion, i.e.,in terms of the internal energy associated with each degree of freedom per molecule:

$$T^\circ = \frac{\Sigma e_i}{(1/2)R_m} \qquad (2.2\text{-}61)$$

where e_i is the average internal energy of a single "i-th" degree of freedom per molecule under equilibrium conditions, and R_m is the gas constant per molecule.

The first law of thermodynamics relates heat to work, and may serve as the principal analytic expression for relating other derived thermodynamic units, once the temperature is chosen as the fourth basic variable (i.e., in addition to mass, length and time) of the thermodynamic systems.

(3) In practice, a quite arbitrary (and hardly physically justifiable) historic definition of temperature and its unit has been customarily adopted in terms of two differently (Celsius, Fahrenheit, Reomur) scaled and differently specified reference physical conditions of water. Thus defined, the concept of temperature is then artificially expressed in terms of elongation properties of arbitrary materials (thermometers), which are calibrated relative to two distinct thermal conditions (solidification and evaporization points) of water. The arbitrary temperature definition is unrelated either to the internal energy contents from kinetic theory of gases, or to the classical thermodynamic postulates and laws.

Similar to the case of temperature, the accepted units of heat for measuring the heat as a particular form of energy suffer from historic anachronisms. Furthermore, there are several heat units in existence nowadays, even within one system of fundamental units. Moreover, if a fundamental system of units is changed, the definition of unit of heat is also changed as a consequence.

When the first thermodynamic law for closed cyclic processes is analytically expressed in its simplest restrictive form for insentropic inviscid conditions

$$\oint dQ = \oint dW \qquad (2.2\text{-}62)$$

the unit of heat, Q, becomes properly identical to the extensive unit of work, W, (i.e., energy) in any specified basic system of units. For instance, (ft - lbf) in the (ft - slug - sec) system; (ergs) in the metric (cgs) system of basic units, etc.

If the old calorimetric (water) definition of heat content is chosen instead, (i.e., when the heat content is defined without resorting to the direct relation of heat to work), the corresponding heat units are BTU and Calorie in the British and metric systems of fundamental units respectively. As a consequence, in expressing analytically the first law of thermodynamics, the Joule's constant

$$J = 778 \frac{\text{ft-lbf}}{\text{Btu}}$$

$$J = 4.186 \frac{\text{Joules}}{\text{Calorie}} \qquad (2.2\text{-}63)$$

must be introduced in Eq. (2.2-62), which then takes the form

$$J \oint dQ = \oint dW \qquad (2.2\text{-}64)$$

There are no unique standards in defining the heat transfer units, neither within a chosen fundamental system of units, nor in any particular country. In each individual case, a careful examination of the adopted conventions must be performed.

(vii) Main Systems of Units

The most commonly used systems of units in physics and engineering are divided into two primary groups according to the adopted fundamental systems of dimensions or measures:

(1) The [MLT] absolute physical systems of measures, based on the primary dynamic quantities, is mass, [M], length, [L], and time, [T]. The corresponding basic units in the [MLT] system are usually metric. In accordance with the Eleventh General Conference on Weights and Measures(15) of October, 1960, the primary metric standards are defined, and the corresponding English and American units are unilaterally related to their metric counterparts as follows:

Unit of length is 1 meter = 1650763.73 wave lengths of Krypton 86 orange-red radiation in vacuum. Then, 1 yard = .9144 meters, 1 ft = 1/3 yard.

Unit of mass is 1 kgm, identical to the prototype mass of the primary standard in Paris, called "the international prototype kilogram-mass." Then, 1 lbm = .45359237 kgm.

Unit of time is 1 ephemeris second. It is an arbitrarily defined time interval, made invariant by definition and not by its physical nature: 1 ephemeris second = 1/(31556925.9747) part of the tropical year for 1900, January $0^d\ 12^h$ ephemeris time, when the tropical year was $365^d\ 05^h\ 48^m\ 45.6661^s$.

Table (2.2-1)

	MLT Absolute System FUNDAMENTAL: Kgm - m - sec			FLT Gravitational System PRIMARY: lbf - ft - sec		
Basic Dimensions	ENGLISH or USA	METRIC		ENGLISH or USA	METRIC	
	lbm ft sec (Derived)	kgm m sec (Fundament.)	grm cm sec (Physics)	lbf ft sec (Primary)	kgf m sec (Derived)	grf cm sec (Derived)
Mass, M	POUND-MASS lbm (Basic)	KILOGRAM-MASS kgm (Fundament.)	GRAM-MASS grm (Physics)	SLUG* slug (Derived)	NO UNIT**	NO UNIT**
Force, F	POUNDAL --- (Derived)	NEWTON n (Derived)	DYNE d (Derived)	POUND-FORCE lbf (Basic)	KILOGRAM-FORCE kgf (Derived)	GRAM-FORCE grf (Derived)
Length, L	FOOT ft (Basic)	METER m (Fundament.)	CENTIMETER cm (Physics)	FOOT ft (Basic)	METER m (Fundament.)	CENTIMETER cm (Physics)
Time, T	EPHEMERIS SECOND sec (Fundamental)					

* The gravitational unit mass in the basic (lbf - ft - sec) system at sea-level standard conditions is

$$1\ \text{slug} = \frac{1\ \text{lbf}}{1\ (\text{ft/sec}^2)} = 32.174049\ \text{lbm}$$

Its value decreases with altitude, H , since,

$$g_H = \frac{g_S}{(Ro+H)^2} \qquad (2.2\text{-}65)$$

where Ro is the mean radius of a spherical earth at 45° north latitude.

** There are no named mass units in the derived (kgf - m - sec) and (grf - cm - sec) metric systems. At sea-level conditions, a weight of 1 kgf has a mass of 1 kgm, which is the fundamental unit of mass in the absolute (kgm - m - sec) system of units. It is invariant with altitude, since the inertial and the gravitational mass are then equivalent. A conditional unit mass, similarly defined as slug, in the (kgf - m - sec) and the (grf - m - sec) derived systems would be the sea-level numerical equivalents of slug:

9.80665 kgm
and 980.665 grm

which are undergoing the same variation with altitude as in the case of slug.

The thermodynamic concept of absolute temperature, T°, used whenever internal energetic levels in a flowing fluid are important, is the fourth basic unit.

As already stated, the absolute temperature is measured on a thermodynamic scale from the absolute zero condition. As an intensive variable the absolute temperature is then conditionally expressed either in the centigrade degrees absolute, which are named "degrees Kelvin," or in the Fahrenheit degrees absolute, which are named "degrees Rankine ":

$$°K = °C + 273.16°.$$

$$°R = °F + 459.69°$$

$$°R = \left(\frac{9}{5}\right) °K$$

$$\frac{°C}{5} = \frac{°F - 32°}{9} = \frac{°K - 273.16}{5} = \frac{°R - 491.69°}{9}$$

In the fundamental [MLT] system of measures, the unit of force is 1 newton. It is a derived quantity:

1 n = .10197612 kgf

1 kgf = 1 kgm x 9.80665 m/sec^2,

where the conventional standard gravity

$$g_s = 9.80665 \text{ m/sec}^2 = 32.174049 \frac{\text{ft}}{\text{sec}^2}$$

closely corresponds to its actually measured value at 45° north latitude, sea-level conditions

(2) The [FLT] gravitational systems of measures, based on the primary dynamic quantities of force, [F], length, [L], and time, [T]. The corresponding basic units in the [FLT] system are usually English. They are derived by internationally adopted standards as follows:

Unit of force is one pound-force:
1 lbf = .45359237 kgf
1 kgf = 1 kgm x 9.80665 m/sec^2

Unit of length is one yard:
1 yd = .9144 meters

Unit of time is one ephemeris second.

In the gravitational [FLT] system of measures the unit of mass is one slug. It is a derived quantity:
1 slug = 32.174049 ft/sec^2 x 1 lbm
1 lbm = .45359237 kgm.

Conversion constants between the [MLT] and the [FLT] basic units and their respective multiples are:

Length

m = 10^2 cm = 10^3 mm = 10^6 μ = 10^9 mμ = $10^{12}\mu\mu$

= 10^{10} Å (Angstroms)

= 39.37008 in

= 3.280840 ft

= 1.093613 yd

1 yd = 3 ft = 36 in = .9144 m
1 ft = .3048 m

1 in = 2.54 cm

Mass

1 kgm = 2.20462262 lbm

1 lbm = .45359237 kgm

1 slug = 32.174049 lbm

Force

1 kgf = 9.80665 newtons
= 2.20462262 lbf
= 70.931635 poundals

1 n = .10197612 kfg
= .22480894 lbf
= 7.2330139 poundals

1 lbf = .45359237 kgf
= 32.174049 poundals
= 4.4482217 newtons

1 poundal = .0310809497 lbf
= .014098082 kgf
= .13825495 newtons

The two fundamental dynamic systems of units, together with some others still in use, are comparatively presented for convenience in Table (2.2-1).

(viii) Description of Methods for Defining Natural Variables

The fundamental physical laws and definitions can be expressed as valid physical dimensional equations, provided the dimensional consistency of each term in the equations is satisfied. Since the dimensions of all algebraic terms in a valid physical equation must necessarily be the same, it is also always possible, as a consequence, to convert a physical equation into a mathematically non-dimensional form by a proper introduction of the natural nondimensional variables instead of the corresponding primary substantial physical variables. For instance, the familiar dimensional form of Newton's second law,

$$F = ma \qquad (2.2\text{-}66)$$

can be alternatively written as an equivalent nondimensional expression

$$\frac{F}{ma} = 1 \qquad (2.2\text{-}67)$$

stating that the natural variable F/ma is equal to unity.

There are, in general, two ways to ascertain a proper physically meaningful form and a minimum number of natural variables that fully describe a given physical occurrence:

(1) Dimensional Analysis Methods

By a direct use of dimensional analysis methods, it is possible to discern the constituent natural variables within a physical system without investigating the actual governing differential equations. The most obvious advantage of the dimensional analysis methods lies in the fact that an exact mathematical derivation of the physical functional relationships between the involved physical variables is rendered unnecessary for a proper formulation of the key natural variables which determine both the general behavior of the physical system and the similarity requirements. In the application of the dimensional analysis methods, however, it is imperative that all pertinent physical substantial variables and dimensions be recognized initially. For this to be possible, one must possess some understanding of, and an insight into, the internal mechanism of the physical process, i.e., one must realize the possible lawful interrelationships between all substantial variables determining the physical pattern of the investigated occurrence. Use of the dimensional analysis method may lead to formulation of the consistent natural variables, and thus set the stage for a subsequent definition of the similarity requirements, but it neither discloses the explicit analytic form of functional relationships between the natural variables, nor yields numerical solutions of problems.

In applications, the following two basic dimensional analysis approaches are characteristic (each of them is, in its turn, prone to many minor variants):

(a) The Step-by-Step Elimination Method[16]

This method involves an organized stepwise elimination of fundamental dimensions from a correctly recognized implicit functional relationship between the substantial physical variables that define the investigated physical system. The process leads to a direct definition of the governing natural variables. Choice of the fundamental dimensions for elimination purposes should correspond to the physical nature of the investigated system.

(b) The Buckingham π Theorem

The Buckingham π Theorem states that the number of natural variables (i.e., the number of independent nondimensional groups of substantial physical variables) which can be meaningfully formed within a physical system is equal to the difference between the number of assumed (or recognized) characteristic substantial variables and the number of independent basic dimensions involved. In simple words, this theorem tells how many nondimensional numbers to expect, provided a correct number of the physical substantial variables has first been determined. Once such knowledge is secured, the technique of applying the Buckingham π Theorem method in determining the natural variables (similarity parameters) is routine. For reference, any textbook on the subject will do.

(c) General Limitations of the Dimensional Analysis Methods

Both the step-by-step method and the Buckingham π Theorem require a preliminary intuitive insight into, or factual knowledge of, all the important substantial physical variables which constitute the investigated physical occurrence. If a physical occurrence is not well understood, and if the wrong type or an insufficient number of substantial physical variables is presumed, an erroneous or insufficient number of dimensionless natural parameters is obtained. The dimensional analysis technique does not yield an automatic clarification in the matter of a proper choice of the minimum but sufficient number of substantial physical variables.

Furthermore, the Buckingham π Theorem is founded on the supposition that a correct minimum number of independent basic dimensions $[L, M, T, T^*]$ pertinent to the investigated physical occurrence, is known "a priori." The theorem does not give itself any assurance that the presumed number of independent basic dimensions is in actuality, the minimum number. In many

cases it is easy to secure that knowledge in advance, but in some more complex physical events the existing evidence has shown that, due to an initial error in assuming more independent dimensions than really necessary, the number of natural variables derived by the Buckingham π Theorem turned out to be less than actually in existence, although formally correctly found by the theorem's technique. In such cases, the adopted minimum number of independent basic dimensions did not prove to be the actual minimum, and the theorem itself yielded no provisions for correcting the situation. In such cases the step-by-step method will secure means of discovering the actual minimum number of the really independent basic dimensions (independent variables).

(2) Direct Non-dimensionalization of the Governing Equations

On many occasions, the necessary intuitive insight, or the corresponding experimental evidence, may prove insufficient to guarantee a fully comprehensive treatment of a physical occurrence "a priori," and a subsequent coherent application of the dimensional analysis methods. Under such inadequate circumstances, the natural variables can be fully defined only by methods involving a direct study of the explicit physical equations and the boundary conditions governing the physical system under consideration. The equations are usually in the form of a system of simultaneous differential equations, which must be first derived by application of the corresponding physical laws as applicable to the particular physical closed system. For the limited purpose of defining the natural variables, a knowledge of how to solve the usually involved differential equations is not required.

There are several common techniques of handling the governing differential equations for the purpose of ascertaining the necessary and sufficient number of natural variables (i.e., similarity parameters), such as the scale factoring technique, nondimensionalization by use of characteristic parameters, etc. The method is considerably used in the existing technical literature, which should serve as a general reference in the matter. A special illustrative and purposeful example of nondimensionalization of the Navier-Stokes equations (compact form) is presented in Section 2.2.3.

(ix) Similitude Concepts

(1) Conditions for Similitude

A physically defined similitude concept is analogous to its more familiar geometric interpretation: similarity conditions are satisfied if the same shapes or proportions are maintained in two individual physical occurrences. Since the natural variables, by virtue of their very definitions, describe shapes or proportions, a similarity between two physical events is satisfied if the involved natural variables are fixed and of the same kind respectively. This requirement is both necessary and sufficient.

From an analytical point of view, two specific fluid flow occurrences around immersed bodies are similar only if they are represented by identical forms of the dimensional governing equations, auxiliary relationships, and boundary conditions, i.e., only if all the determining physical substantial variables of the fluid-body system and the boundary conditions for the two physical flow occurrences are so interrelated that the resulting identical differential equations yield the same types of particular solutions for the involved dependent variables (for instance velocity field components) in terms of the respective independent variables (space point coordinates for steady flow conditions or space point coordinates and time for unsteady conditions).

A broader, and at the same time simpler, similarity criteria is reached by introduction of the natural nondimensional variables instead of the substantial physical variables. Using either the direct analytical methods of non-dimensionalization of the governing flow equations and boundary conditions, or the dimensional analysis methods, it can be shown that the respective fixed identity of the representative natural variables for the two fluid-body systems represents the necessary and sufficient requirement for their physical similarity, i.e., the natural variables are the necessary and sufficient similarity parameters. The criteria of the respective identity of the representative natural variables can be then extended to conditions when the natural variables are not fixed (i.e., not related to a particular solution of the problem), but are allowed to vary while remaining correlatively

identical, and thus depict validly the similar physical behaviors of the comparative fluid-body physical systems in all their successively compatible changes. It means that if the equality of the respective representative natural variables is continuously preserved, the two systems are undergoing similar states. Furthermore, within a single fluid-body system, two different physical states, as defined by two different sets of substantial dimensional physical variables, are similar by pattern and type if the representative natural dimensionless variables are kept fixed. Evidently the same conditionality holds for two fluid-body systems, provided the respective pairs of natural variables are kept equal and fixed, and provided the geometric similarity or affinity conditions are preserved.

(2) Distinction Between Identity and Similarity

The dimensional substantial physical variables of a fluid-body system are also called characteristic parameters of the system. By equalizing and fixing all the respective dimensional characteristic parameters, two fluid-body systems are made absolutely identical.

The conditions for absolute identity of two fluid-body systems are not to be confused with the necessary and sufficient conditions for their similarity. The similarity requirements are not so restrictive as the requirements for identity, although in both cases the same characteristic parameters are involved. Two flows can be made similar by application of a constant scale factor to every dimensional characteristic parameter, i.e., the substantial physical variables are not necessarily kept individually identical. The nuance is analogous to the more familiar notion of the difference between two geometrically identical and similar figures, here applied on physical flow systems. Two similar physical systems will be represented by the same type of differential equations and boundary conditions, and shall have the same type of particular solutions, only numerically shifted by the introduced scale factors: for two similar physical systems the internal structural relationships, underlying natural laws and deductions, shall be conditionally identical by type, and only different by absolute magnitude; they are not absolutely identical.

It should be noted that similarity between two physical systems does not necessarily imply existence of the same overall geometry. Although usually presupposed, the geometric similitude is not an inclusive requirement for physical similarity at large. For instance, some two-dimensional steady flows about elliptic cylinders with longitudinal axes perpendicular to the uniform free stream direction, can be conditionally matched with corresponding two-dimensional flows about circular cylinders by applying additionally different scale factors to the independent spatial variables (coordinates x, y), and to the corresponding velocity components (u, v). Such types of similar flows are sometimes called "distorted similar flows," the name pointing out that the scaling process has been extended not only to the characteristic physical flow parameters, but to the flow field independent variables also including body contours.

Thus an apparently unrelated variety of fluid flows can conveniently be grouped into a few representative types. Such a conditional categorization allows for relatively simplified and generalized analytical and physical investigations of a considerably reduced number of affine fluid flows. The grouping can be conveniently performed according to the relative importance of those basic physical variables which appear essential in expressing the respective internal mechanisms of various flow patterns such as, for instance, flow speed regimes (low subsonic, compressible subsonic, transonic, supersonic, hypersonic, see Part I).

The important role that natural variables play in establishing similarity concepts can be summarized as follows:

(1) The natural variables indicate similarity conditions for a number of individual physical systems, i.e., they lead to generalized conclusions and enable investigations of otherwise experimentally unattainable full scale events by use of properly scaled model systems.

(2) They enable formulation and prediction of functional laws for similar physical systems by use of a reduced number of nondimensional variables, fully substituting a greater number of characteristic substantial physical variables.

(3) They permit a convenient classification of various physical phenomena according to significance and im-

portance of the pertinent natural numbers. For this limited purpose, only the natural numbers which are predominant for the internal mechanism of the investigated physical occurrence are considered, i.e., excluding from such an analysis various efficiency factors, natural constants, etc., which might be otherwise also treated (by virtue of their nondimensionality) as natural numbers at large.

Explicit forms of the similarity laws for subsonic, transonic supersonic and hypersonic continuum flow speed regimes are stated in the respective sections later, while a limited interpretation for subsonic and supersonic speed regimes is illustrated in Section 2.2.3 in a broad, non-specific way.

2.2.3 NON-DIMENSIONALIZATION OF THE COMPACT FORM OF THE NAVIER-STOKES EQUATIONS AND ANALYTICAL DEFINITIONS OF THE CONTINUUM FLOW NATURAL VARIABLES

In engineering applications, the non-dimensional aerodynamic force coefficients are customarily expressed as explicit functions of influential natural variables or similarity parameters. A meaningful formulation of each non-dimensional parameter, or natural variable, reflects some essential aerothermodynamic characteristic of the investigated fluid flow type, such as comparative significance of effects of viscosity, compressibility, thermal conductivity, etc. Each non-dimensional natural parameter can be treated as a partial quantitative indicator of the relative importance of a particular set of aerothermodynamic fluid flow substantial variables. The necessary number of the representative nondimensional natural variables depends upon the overall complexity of the investigated fluid flow type and upon the underlying assumptions and approximations used in formulation of the correspondingly representative fluid flow analytical model. The proposition is readily illustrated by a direct nondimensionalization of the governing equations and the boundary conditions for a simple two-dimensional, steady, subsonic compressible and viscous continuum fluid flow model around an infinite insulated cylinder having its longitudinal axis perpendicular to the direction of uniform steady free stream at infinity. It is assumed that air is a dry, chemically and electrically neutral mixture of a predominantly diatomic nature. The examplary simplified case serves well the purpose of illustrating the analytical definitions of the most important natural variables which are representative for the adopted continuum flow models described by the compact form of the Navier-Stokes equations of change (2.2-47) to (2.2-51). The energy equation (2.2-51) is for adiabatic flow field conditions; it is rewritten in its enthalpy form, the body forces are neglected, and the coefficients of air viscosity, μ, and heat conductivity, k, are assumed nearly constant throughout the field, which simplifies considerably the momentum equations (2.2-48) to (2.2-50) and the dissipation function, ϕ. Due to the imposed approximations, the validity of the illustrative analysis is restricted to subsonic and eventually to low supersonic speed regimes.

Main restrictive assumptions are:

(1) the air composition is near-standard and may be treated as a homogeneous continuum, viscous and compressible medium, chemically and electromagnetically neutral,

(2) the flow is steady, stable, and adiabatically irreversible,

(3) the steady flow conditions are not dependent on the way (history) in which they have been established,

(4) the viscous no-slip condition is satisfied at the body boundary,

(5) the flow conditions at infinity are unaffected by the body presence and are steady and uniform,

(6) the body surface is aerodynamically smooth (no roughness effects) and insulated,

(7) the initial (at infinity) flow conditions are not far from standard, i.e., no high temperature or rarefied effects are present initially.

The dimensional form of the governing equations (per unit volume) for the illustrative case is:

Continuity:

$$\frac{\partial}{\partial x}(\rho u) + \frac{\partial}{\partial y}(\rho v) = 0 \quad , \qquad (2.2\text{-}68)$$

Momentum:

$$\rho u \frac{\partial u}{\partial x} + \rho v \frac{\partial u}{\partial y} = -\frac{\partial (p - p_\infty)}{\partial x} + \mu\left(\frac{\partial^2 u}{\partial x^2} + \frac{\partial^2 u}{\partial y^2}\right) + \frac{1}{3}\mu \frac{\partial}{\partial x}\left(\frac{\partial u}{\partial x} + \frac{\partial v}{\partial y}\right) \quad , \qquad (2.2\text{-}69)$$

$$\rho u \frac{\partial v}{\partial x} + \rho v \frac{\partial v}{\partial y} = -\frac{\partial (p - p_\infty)}{\partial y} + \mu\left(\frac{\partial^2 v}{\partial x^2} + \frac{\partial^2 v}{\partial y^2}\right) + \frac{1}{3}\mu \frac{\partial}{\partial y}\left(\frac{\partial u}{\partial x} + \frac{\partial v}{\partial y}\right) \quad .$$

Energy: (2.2-70)

$$\rho u \frac{\partial H}{\partial x} + \rho v \frac{\partial H}{\partial y} = u \frac{\partial p}{\partial x} + v \frac{\partial p}{\partial y} - k\left(\frac{\partial^2 T}{\partial x^2} + \frac{\partial^2 T}{\partial y^2}\right) + \phi \qquad (2.2\text{-}71)$$

where:

$$\phi = \mu\left[\left(\frac{\partial u}{\partial y}\right)^2+\left(\frac{\partial v}{\partial x}\right)^2\right] + \frac{4}{3}\mu\left[\frac{\partial u}{\partial x}+\frac{\partial v}{\partial y}\right]^2 \qquad (2.2\text{-}72)$$

Note that both μ and k are assumed nearly constant, and that the sign convention is here defined for heat flux gain per unit control volume (since the temperature gradient is negative):

$$\left(\frac{\partial q_x}{\partial x}+\frac{\partial q_y}{\partial y}\right) = -k\left[\frac{\partial}{\partial x}\left(\frac{\partial T}{\partial x}\right)+\frac{\partial}{\partial y}\left(\frac{\partial T}{\partial y}\right)\right] \qquad (2.2\text{-}73)$$

(i) Boundary Conditions

At ∞ : $u = V_\infty$ $\rho = \rho_\infty$ $p = p_\infty$

$v = 0$, $T^\circ = T^\circ_\infty$ $i = i_\infty$

At the cylinder surface

$x^2 + y^2 = D^2/4$: $u = 0, v = 0$, $\frac{\partial T^\circ}{\partial n} = 0$

i.e., the local normal derivative of (T°) is zero for the assumed insulated cylinder surface.

Dimensions of all physical variables in the governing equations (2.2-68) to (2.2-71) are given in Section 2.2.2.

(ii) Primary Variables

In the equations of change, (2.2-68) to (2.2-71), (x) and (y) are the independent variables of the flow field, i.e., the spatial coordinates of any local point, (x) in direction of the local steady uniform free stream, and (y) perpendicular to it, following the usual right hand convention of a space fixed orthogonal Cartesian coordinate system. The four substantial field variables

$$u = u(x, y),$$

$$v = v(x, y),$$

$$p = p(x, y),$$

$$T^\circ = T(x, y),$$

are then taken as primary dependent variables in terms of which the solutions or the system of the four simultaneous differential equations should be defined, the particular integrals satisfying the cited boundary conditions, provided the remaining six physical variables $(\phi, \rho, H, k, \gamma, \mu)$ are specified through a sufficient number of physically meaningful parametric relationships in terms of the primary variables, or eventually treated as constant.

(iii) Auxiliary Relationships

The dissipation function, ϕ, depends on viscosity, compressibility and velocity gradients within the flow field, i.e., depends in general on the present types of the energy dissipating forms of the internal flow mechanism, such as the ordered momentum dissipation on a molecular level (energy absorption through the viscous distortion and rotation of a fluid particle), the work consumed in producing volumetric changes of a fluid particle due to its elasticity (or compressibility), etc. With the presumed constant values for the first, μ, and the second $[\lambda = -(2/3)\mu]$ coefficients of viscosity, the dissipative function takes the simplified form (2.2-72).

In a more general case, a proper functional representation of the five physical parameters, $(\rho, H, k, \gamma, \mu)$ in terms of the adopted primary physical variables, (u, v, p, T°), involves a respectively valid application of the gas-dynamic and thermodynamic concepts to the specific fluid flow case under investigation. In this respect, the following main notions may be considered:

For a given gas composition, the pressure, p, density, ρ, and absolute temperature, T°, are the characteristic independent thermodynamic variables. If and when the gas is in a state of stable thermodynamic equilibrium, an implicit functional relationship between the variables is established, which can be analytically represented in a generalized form

$$F(p, \rho, R, T^\circ) = 0 \qquad (2.2\text{-}74)$$

where R (gas "constant") is a specific structural characteristic of the gas, and the function F remains to be defined in terms of the overall state of gas.

Assuming a chemically and electromagnetically neutral gas at near-standard conditions, a special idealized form of the equation of state and the so called calorie equation are used in a first approximation.

$$C_p = C_v + R, \qquad (2.2\text{-}75)$$

$$p = \rho R T^\circ \qquad (2.2\text{-}76)$$

and the gas is then labeled as thermally perfect, where C_p and C_v represent specific heats at constant pressure and constant volume respectively.

For non-flowing (no bulk matter ordered motion) thermodynamic processes (which are conceived as an infinite sequence of infinitely small and continuous changes of the presumed equilibrium states, realized infinitely slowly) of adiabatic type (i.e., closed, insulated systems), the caloric equation (2.2-75) can be, for perfect gases, combined with the equation of state (2.2-75) in a general expression:

$$\gamma = \frac{C_p}{C_v} = 1 + R = \frac{\rho}{p}\left(\frac{\partial p}{\partial \rho}\right)_s \qquad (2.2\text{-}77)$$

$$\therefore \frac{dp}{p} = \gamma \frac{d\rho}{\rho}, \quad \gamma = \gamma(T) \qquad (2.2\text{-}78)$$

where subscript s stands for the constant entropy restraint. If, furthermore, the specific heats ratio, γ, is assumed constant, the gas is called calorically perfect, and the expression (2.2-79) reduces to the constant entropy adiabatic law:

$$\frac{p}{\rho^\gamma} = \text{const} \qquad (2.2\text{-}79)$$

A valid application of the above classical thermodynamic notions to flowing gases required further restraints:

The approximated idealized relationship (2.2-75) and (2.2-76) can be conditionally applied to processes in flowing gases, assuming that at any instant of time, each of the infinite number of gas flow states throughout a fluid field is in a thermodynamic equilibrium and that difference between any two flow states are infinitesimally small and continuous analytically.

The constant entropy (isentropic) forms for thermally perfect gases (2.2-77) and (2.2-78), as well as the isentropic form (2.2-79) for thermally and calorically perfect gases, require that the flowing gas be inviscid, ($\mu \equiv 0$), thermally non-conducting, ($k \equiv 0$), in addition to all other thermodynamic restraints.

In conclusion, compressible flows of thermally perfect gases, having no viscosity, ($\mu \equiv 0$), and no heat-conductivity, ($k \equiv 0$), can satisfy the isentropic conditions, and a direct pressure-density relationship may be expressed by Eqs (2.2-77) and (2.2-78). If, in addition to it, the flowing gas is considered to be also calorically perfect, (γ = const), the pressure-density relationship, $p = p(\rho)$, assumes the simple isentropic form (2.2-79).

Since for compressible viscous flows the entropy is not constant, a simple isentropic assumption of, $p = p(\rho)$, is not applicable. Instead, the variable density, ρ, should be expressed as a function of both the local static pressure, p, and the local absolute temperature, T°, according to the general form of the equation of state for thermally perfect gases, Eq (2.2-74), with the pressure, p, and the temperature, T°, taken as independent thermodynamic variables (i.e., as primary dependent variables in the governing equations (2.2-68) to (2.2-71)). The pressure-density relationship is then conveniently expressed in a more general form:

$$\frac{d\rho}{\rho} = \delta \frac{dp}{p} - \epsilon \frac{dT^\circ}{T^\circ}, \qquad (2.2\text{-}80)$$

where the coefficients δ and ϵ are defined as[16]:

$$\frac{d\rho}{\rho} = \delta \frac{dp}{p} - \epsilon \frac{dT^\circ}{T^\circ} \qquad (2.2\text{-}81)$$

$$\delta = \frac{p}{\rho}\left(\frac{\partial \rho}{\partial p}\right)_{T^\circ} = p\delta_1 \qquad (2.2\text{-}82)$$

$$\epsilon = -\frac{T^\circ}{\rho}\left(\frac{\partial \rho}{\partial T^\circ}\right)_p = -T^\circ \epsilon_1 \qquad (2.2\text{-}83)$$

$$dH = C_p dT^\circ + (1-\epsilon)\frac{dp}{\rho} \qquad (2.2\text{-}84)$$

$$\frac{1}{\gamma} = \delta - \frac{\epsilon^2}{C_p}\frac{p}{\rho T^\circ} \qquad (2.2\text{-}85)$$

with δ, ϵ and γ having comparable meanings:

δ - represents product of the coefficient of air compressibility at constant temperature, $\delta_1 = (1/\rho)(\partial\rho/\partial p)_{T^\circ}$, and the static (absolute) pressure, p.

ϵ - represents product of the coefficient of thermal expansion at constant pressure, $\epsilon_1 = (-1/\rho)(\partial\rho/\partial T)_p$, and the absolute temperature, T°.

The above relationships allow for either p or ρ to be treated as one of the primary dependent variables.

It should be noted that Eqs (2.2-80)

and (2.2-85) indicate that the specific heats ratio, γ, and the specific heat coefficient at constant pressure, C_p, are not constants in general, and do not necessarily follow the same functional law in terms of p, ρ, T° and internal viscous, δ, and elastic, ϵ, (or compressible) characteristics of air for the assumed variable entropy flow cases.

Note that by virtue of the auxiliary expression (2.2-80) to (2.2-81), the three physically important variable parameters ρ, H, and γ are considered functions of the primary dependent variables p and T°, and the three new thermodynamic coefficients, δ, ϵ, and C_p, which are in this analysis assumed to be and are often evaluated at some "reference state." The reference level may be, in general, different from any particular local free stream condition, i.e., it can be referred to some representative average gas condition, which yields a workable justification for an assumed constancy of δ, ϵ and C_p. The same trend of argumentation may be applicable to the coefficients k and μ, if conditionally treated as constants.

(iv) Nondimensionalization Procedure

For the present purpose, assuming that the governing physical relationships (2.2-68) to (2.2-72) and the auxilliary parametric expressions (2.2-81) to (2.2-85) are sufficient to specify all the variable physical quantities as direct and indirect functions of the space independent variables x and y, the required nondimensionalization can be performed as follows:

(1) Reference units are chosen to be p_∞, V_∞, D and $C_{p\infty}$, where D stands for diameter of the cylinder, and the subscript ∞ refers to the undisturbed free stream conditions.

(2) Reference levels for the substantial variables ρ, T°, and H are chosen as ρ_∞, T°_∞, and H_∞ respectively. Nondimensionalization of the governing differential equations, the auxiliary relationships, and the respective boundary conditions is then obtained on the basis of (1) and (2) by specification of the respective nondimensional variables

$$x' = \frac{x}{D},\quad y' = \frac{y}{D},\quad p' = \frac{p-p_\infty}{\rho_\infty V_\infty^2},\quad u' = \frac{u}{V_\infty},$$

$$\rho' = \frac{\rho}{\rho_\infty},\quad v' = \frac{v}{V_\infty},\quad T^{\circ\prime} = \frac{T^\circ - T^\circ_\infty}{V_\infty^2/C_{p\infty}},\quad H' = \frac{H-H_\infty}{V_\infty^2},$$

(2.2-86)

with k, μ, δ, and ϵ taken at some conditionally fixed representative values.

The nondimensional governing equations are:

$$\frac{\partial}{\partial x'}(\rho' u') + \frac{\partial}{\partial y'}(\rho' v') = 0 \quad , \tag{2.2-87}$$

$$\rho' u' \frac{\partial u'}{\partial x'} + \rho' v' \frac{\partial u'}{\partial y'} = -\frac{\partial p'}{\partial x'} + \frac{\mu}{\rho_\infty V_\infty D}\left[\frac{\partial^2 u'}{\partial x'^2} + \frac{\partial^2 u'}{\partial y'^2} + \frac{1}{3}\frac{\partial}{\partial x'}\left(\frac{\partial u'}{\partial x'} + \frac{\partial v'}{\partial y'}\right)\right] \tag{2.2-88}$$

$$\rho' u' \frac{\partial v'}{\partial x'} + \rho' v' \frac{\partial v'}{\partial y'} = -\frac{\partial p'}{\partial y'} + \frac{\mu}{\rho_\infty V_\infty D}\left[\frac{\partial^2 v'}{\partial x'^2} + \frac{\partial^2 v'}{\partial y'^2} + \frac{1}{3}\frac{\partial}{\partial y'}\left(\frac{\partial u'}{\partial x'} + \frac{\partial v'}{\partial y'}\right)\right] \tag{2.2-89}$$

$$\rho' u' \frac{\partial H'}{\partial x'} + \rho' v' \frac{\partial H'}{\partial y'} - \left(u' \frac{\partial p'}{\partial x'} + v' \frac{\partial p'}{\partial y'}\right) = -\frac{k}{\rho_\infty C_{p\infty} V D}\left(\frac{\partial^2 T^{\circ\prime}}{\partial x'^2} + \frac{\partial^2 T^{\circ\prime}}{\partial y'^2}\right) + \frac{\mu}{\rho_\infty V_\infty D}\left[\left(\frac{\partial u'}{\partial y'}\right)^2 + \text{similar terms}\right] \tag{2.2-90}$$

The nondimensional boundary conditions are:

At ∞ : $u'=1$, $\rho'=1$, $p'=0$, $v'=0$, $T^{\circ\prime}=0$, $H'=0$,

At the circular cylinder surface,

$$x'^2 + y'^2 = \frac{1}{4}\ ;\ u'=0,\ v'=0,\ \left(\frac{\partial T^{\circ\prime}}{\partial n}\right)=0,$$

where $\left(\frac{\partial T'}{\partial n}\right)$ is the local normal derivative of $(T^{\circ\prime})$ for the assumed insulated skin.

The nondimensional auxiliary parametric equations:

$$\frac{\mu}{\rho_\infty V_\infty D}\left[\left(\frac{\partial u'}{\partial y'}\right)^2 + \text{similar terms}\right] \quad , \tag{2.2-91}$$

$$\frac{d\rho'}{f} = \delta \frac{dp'}{p' + p_\infty/\rho_\infty V_\infty^2} + \epsilon \frac{dT^{\circ\prime}}{T^{\circ\prime} + C_{p_\infty} T^\circ_\infty / V_\infty^2} \quad , \tag{2.2-92}$$

$$dH' = \frac{C_p}{C_{p_\infty}} dT^{\circ\prime} + (1-\epsilon)\frac{dp'}{\rho'} \quad , \tag{2.2-93}$$

$$\frac{1}{\gamma} = \delta - \epsilon^2 \frac{C_{p_\infty}}{C_p} \frac{p'}{\rho' T^{\circ\prime}} \tag{2.2-94}$$

Note that in the dimensional form of the governing equations of motion the reference datum for measuring the local pressure, p, is unspecified. The choice of such a pressure datum has no influence on the flow pattern and the differential form of equations of change. But if left so undetermined, it would raise the number of requirements for similarity through the boundary condition specifications. Commonly, the local static pressure, p, is measured with respect to the reference constant pressure at infinity, p_∞, which then represents a relative zero datum level. Such a practice is in accord with the accepted definition of the pressure coefficient

$$C_p = \frac{p - p_\infty}{1/2 \rho_\infty V_\infty^2} \qquad (2.2\text{-}95)$$

and does not affect the form of the general equations, (2.2-68) to (2.2-71), since the derivatives of a fixed datum, p_∞, with respect to (x) and (y) are automatically zero:

$$-\frac{\partial (p - p_\infty)}{\partial x} = -\frac{\partial p}{\partial x}\,, \qquad -\frac{\partial (p - p_\infty)}{\partial y} = -\frac{\partial p}{\partial y}\,. \qquad (2.2\text{-}96)$$

As a consequence, the characteristic substantial variable becomes $(p - p_\infty)$, rather than an unspecified value p. Furthermore, the choice of the steady p_∞ reference value for static pressures coincides with the similarly steady $(\rho_\infty V_\infty^2/2)$ reference value for dynamic pressures, which satisfies the requirement that the datum static pressure and the datum dynamic pressure references must be the same and identically scaled to conform with the definition for a dimensionless pressure coefficient as a single similarity parameter; otherwise, two separate similarity parameters for static and dynamic pressures would be introduced respectively.

A similar consideration holds for the reference absolute temperature datum.

With the assumed independent and constant representative values of k, δ, ϵ, γ and μ, corresponding to some characteristic reference state of the gaseous internal molecular and thermal transport mechanism, the system of nondimensionalized equations (2.2-87) to (2.2-94) yields the following similarity parameters (i.e., natural variables):

$$\frac{\mu}{\rho_\infty V_\infty D}\,,\ \frac{k}{\rho_\infty C_{p_\infty} V_\infty D}\,,\ \frac{p_\infty}{\rho_\infty V_\infty^2}\,,\ \frac{C_{p_\infty} T_\infty}{V_\infty^2}\,,\ \frac{C_p}{C_{p_\infty}}\,,\ \delta\,,\ \gamma \text{ and } \epsilon \qquad (2.2\text{-}97)$$

Some of these eight natural variables may be mutually interrelated through the following additional considerations:

The first natural variable expresses the familiar Reynolds Number criteria,

$$Re = \frac{\rho_\infty V_\infty D}{\mu} = Re_D \qquad (2.2\text{-}98)$$

the subscript D referring the Reynolds Number to the characteristic length (i.e., diameter) of the body.

The second natural variable is called the Peclet Number, representing one of the conditions of similarity for heat transfer phenomena. Since in a compressible flow, the dynamic and the thermal similitudes are interconnected through the internal molecular interaction mechanism, the Peclet Number can be tentatively expressed in terms of the Reynolds Number and another heat transport natural variable, called the Prandtl Number (within the continuum flow concept) as follows:

$$P_e = \frac{\rho_\infty C_{p_\infty} V_\infty D}{k} = \frac{\rho_\infty V_\infty D}{\mu} \frac{C_{p_\infty} \mu}{k} = Re \cdot P_r\,, \qquad (2.2\text{-}99)$$

where

$$P_r = \frac{C_{p_\infty} \mu}{k}\,, \qquad (2.2\text{-}100)$$

is the Prandtl Number.

The third natural variable,

$$\frac{p_\infty}{\rho_\infty V_\infty^2}\,, \qquad (2.2\text{-}101)$$

can be conveniently expressed in terms of the Mach Number, M_∞, and the specific heats ratio, γ_∞, by introducing the conventional definition of the speed of sound (i.e., speed of progagation of small disturbances) under

steady isentropic conditions at infinity:

$$a_\infty = \sqrt{\gamma_\infty \frac{p_\infty}{\rho_\infty}} \quad , \qquad (2.2\text{-}102)$$

$$\therefore \quad \frac{\rho_\infty V_\infty^2}{p_\infty} = \gamma_\infty \left(\frac{V_\infty}{a_\infty}\right)^2 = \gamma_\infty M_\infty^2 \qquad (2.2\text{-}103)$$

The fourth natural variable

$$\frac{C_{p_\infty} T_\infty^\circ}{V^2} \quad , \qquad (2.2\text{-}104)$$

can be tentatively related (and thus eliminated as independent) to the sixth natural variable, δ , the seventh natural variable, ϵ , the Mach Number, M_∞ , and the specific heats ratio, γ_∞ , by evaluating the equation (2.2-94) at infinity conditions, and by combining the result with the equation (2.2-103):

$$\frac{1}{\gamma_\infty} = \delta_\infty - \frac{\epsilon_\infty^2 \rho_\infty}{C_{p_\infty} \rho_\infty T_\infty^\circ} \left(\frac{V_\infty^2}{V_\infty^2}\right) \qquad (2.2\text{-}105)$$

$$\therefore \frac{V_\infty^2}{C_{p_\infty} T_\infty^\circ} = \frac{V_\infty \delta_\infty - 1}{\epsilon_\infty^2} M_\infty^2 \qquad (2.2\text{-}106)$$

The fifth natural variable

$$\frac{C_p}{C_{p_\infty}} \quad , \qquad (2.2\text{-}107)$$

can also be eliminated through γ , δ , and ϵ from the equation (2.2-94):

$$\frac{C_{p_\infty}}{C_p} = \frac{\rho' T'}{\epsilon^2 p'} \left(\delta - \frac{1}{\gamma}\right) \qquad (2.2\text{-}108)$$

(v) Flow Similarity Requirements for Geometrically Similar Bodies at Subsonic Speeds.

On grounds of the above analysis, the following similarity conclusions may be drawn:

(1) For adiabatic, compressible, viscous, steady, continuum flows around insulated bodies, with the assumption of a presumed reference constancy of the coefficients γ , μ , k , δ , ϵ , (suitably defined), the similarity requirements are, in general, expressed by identity of the eight natural variables:

$$\frac{\mu}{\rho_\infty V D} \ , \ \frac{k}{\rho_\infty C_{p_\infty} V D} \ , \ \frac{p_\infty}{\rho_\infty V^2} \ , \ \frac{C_{p_\infty} T_\infty^\circ}{V_\infty^2} \ , \ \frac{C_p}{C_{p_\infty}} \ , \ \delta \text{ and } \epsilon \qquad (2.2\text{-}109)$$

or, alternatively, by identity of the reduced set of six natural variables:

$$Re \ , P_r \text{ (or } P_c), M, \gamma, \delta \text{ and } \epsilon \ , \qquad (2.2\text{-}110)$$

provided the relationships (2.2-99) to (2.2-108) are used.

When two geometrically similar (scaled) systems are compared, the natural flow variables γ , δ and ϵ , (which may be considered for each flow case as conditional, but individually evaluated constants) must be nevertheless, in both cases the same functions (f_1 , f_2, f_3, f_4) of the respective p' , ρ', and T' nondimensional variables:

$$\frac{1}{\gamma} = \delta - \epsilon^2 \frac{C_{p_\infty}}{C_p} \frac{p'}{\rho' T'} = f_1(p', T', \rho') \qquad (2.2\text{-}111)$$

$$\delta = \frac{p'}{\rho'} \frac{\partial \rho'}{\partial p'} = f_2(p', T', \rho') \qquad (2.2\text{-}112)$$

$$\epsilon = -\frac{T'}{\rho'} \frac{\partial \rho'}{\partial T'} = f_3(p', T', \rho') \qquad (2.2\text{-}113)$$

$$\rho' = f_4(p', T') \qquad (2.2\text{-}114)$$

$$p' = \frac{p_\infty}{\rho_\infty V_\infty^2} \left(\frac{p}{p_\infty} - 1\right) \qquad (2.2\text{-}115)$$

$$T' = \frac{C_{p_\infty} T_\infty^\circ}{V_\infty^2} \left(\frac{T^\circ}{T_\infty^\circ} - 1\right) \qquad (2.2\text{-}116)$$

The identity of the rest of similarity parameters (M , Re , P_r) is readily secured by their respective nondimensional definitions (2.2-98) to (2.2-103), provided μ and k are treated as absolute and identical constants for the two similar flow cases. But, if the viscosity, μ , and the heat conductivity, k , are considered to be relative constants only, i.e., fixed differently at some "representative values" for the two comparative flows, further restraint on μ and k are needed in order to achieve similitude. Thus,

if μ and k were functions of the absolute temperature, T^*, only (which is a good working assumption in many cases), i.e., if:

$$\frac{d\mu}{\mu} = f_1(T^{*\prime})\frac{dT^*}{T^*} \qquad (2.2\text{-}117)$$

$$\frac{dk}{k} = f_2(T^{*\prime})\frac{dT^*}{T^*} \qquad (2.2\text{-}118)$$

the necessary similarity requirement would be that f_5 and f_6 are the same functions of $T^{*\prime}$.

(2) If for the same general flow conditions as cited under (1), the gas is treated as thermally perfect, the parameters δ and ϵ are both equal to unity, and only three natural variables are left

$$Re \ , M \text{ and } \gamma, \qquad (2.2\text{-}119)$$

since for thermally (but not necessarily calorically) perfect gases

$$P_r = \frac{C_{p_\infty}\mu}{k} = f(\rho,\rho) = \psi(\gamma) \ , \qquad (2.2\text{-}120)$$

$$p=\rho R T^*$$

according to the thermally perfect gas equation of state. Here, the required fixed identity of the similarity parameter, γ, means that it must be the same function of the nondimensional variables, p', $T^{*\prime}$ and ρ' for two similar flow occurrences, as stated by expressions (2.2-111) to (2.2-116).

When the gas is assumed to be both thermally and calorically perfect, $\gamma = \text{const.}$

(3) Furthermore, if the gas is treated as thermally perfect and inviscid, conforming to the isentropic flow conditions ($\mu = k = 0$, $S = \text{const}$), the Reynolds Number, Re, and the Prandtl Number, Pr, criteria are automatically eliminated, and the similarity requirements are reduced to only two natural variables,

$$M \text{ and } \gamma \qquad (2.2\text{-}121)$$

the specific heats ratio, γ, becoming a constant when a calorically perfect gas assumption is additionally introduced.

(4) A viscous incompressible flow with a constant viscosity, $\mu = \text{const.}$, and including the rest of basic and thermodynamic simplifying assumptions, is characterized by a single natural variable, the Reynolds Number, Re.

As a general note, it is pointed out that the relatively simplified similarity considerations stated in the above example are restrictive to compressible subsonic speeds, a zero angle-of-attack condition for a family of geometrically similar bodies (cylinders, differently scaled). In more general cases, the local similitude requirements may include the angle-of-attack, α_a, and a more general body thickness distribution law in the flow direction as additional similarity conditions, as well as a necessity for an affine spatial coordinate system transformation (supersonic and hypersonic speeds), i.e., a broadening the concept of geometrical similitude. Also whenever a shock-wave pattern is present, the necessary compatibility of across-the-shock relationships between the corresponding physical variables (p, ρ, T^*, V, S) must be matched and added to the boundary conditions for two similar systems.

2.2.4 PHYSICAL INTERPRETATIONS OF NATURAL VARIABLES

In accord with the formal definitions of natural variables the main phenomenological features of the most characteristic natural variables for continuum flow regimes are summarized next. For an easy interpretation, the natural variables pertaining to classical fluid mechanics are treated separately from those related to the heat transport process. It is noted that the subdivision is artificial, since the mass, momentum and energy (heat) processes are necessarily interconnected and simultaneous in a flow occurrence. The transport processes are formally characterized by the auxiliary relationships (2.2-80) to (2.2-85), strongly influencing the actual interdependence of the governing equations (2.2-68) and (2.2-72) and the form of field solutions of their primary dependent variables (ρ, T, u, v).

(i) Natural Variable of Classical Fluid Mechanics

(1) Reynolds Number, Re

Under the restrictions and assumptions specified in the previous sections, Reynolds Number appeared as the only similarity criteria for streamlined, incompressible, viscous fluid flows, provided the reference datum for static pressure is chosen to be its free stream value, p_∞ .

The familiar alternative forms of the Reynolds Number expressions are:

$$\frac{\rho VL}{\mu} = \frac{VL}{\nu} = \frac{GL}{\nu} \qquad (2.2\text{-}122)$$

where

ρ = fluid density, $[ML^{-3}]$

V = characteristic flow velocity, $[LT^{-1}]$

L = characteristic length of the system, $[L]$

μ = first coefficient of viscosity, $[ML^{-1}T^{-1}]$

ν = kinematic coefficient of viscosity, $[L^2T^{-1}]$

G = mass velocity, $G = \rho V$, or momentum of density, $[ML^2T^{-1}]$

Choice of the characteristic length, L , is a matter of convention and convenience. It is not necessarily associated with the solid body itself, since in a fluid-body system in a steady relative motion, the ensuing viscous effects characterize the frictional interaction phenomena within the system, and thus the datum characteristic length can be as well related to the associated fluid flow pattern itself, if convenient. For instance, the characteristic length may be related to the boundary layer thickness, δ , as it is done in handling of the Knudsen Number criteria for fixing boundaries between slip and transitional flow regimes, see Part I.

Physically, Reynolds Number can be interpreted as an independent nondimensional parameter (natural variable) which expresses the ratio of the inertia to the frictional forces in viscous fluid flows. This can be analytically demonstrated by a direct dimensional comparison of the related terms in the governing momentum equations for visions flows[16], and nominally illustrated by:

$$Re_L = \frac{\rho VL}{\mu} = \frac{\rho VL}{\mu} \cdot \frac{V}{V} \cdot \frac{L}{L} = \frac{\frac{\rho V^2}{L}}{\frac{\mu V}{L^2}} \qquad (2.2\text{-}123)$$

where

$(\rho V^2)/L$ - is proportional to the time rate of change of momentum, i.e., to the associated inertial force per unit volume.

$(\mu V)/L^2$ - is proportional to the viscous or frictional force per unit volume.

The above definition of Reynolds Number in terms of the first coefficient of viscosity, μ , is strictly valid for incompressible fluids flowing in an orderly laminated or layered pattern. When allowance for compressibility effects in viscous fluids is made, a second coefficient of viscosity, λ , appears due to both density change and the rate of density change in the flow direction[14]. Introducing a conditional assumption that the normal (static) pressure is a function of density only

$$p = p(\rho)$$
$$\rho = \rho(x,y,z,t) \qquad (2.2\text{-}124)$$

and assuming that the total rate of density change in the flow direction

$$\frac{D\rho}{Dt} = \frac{\partial \rho}{\partial t} + u\frac{\partial \rho}{\partial x} + v\frac{\partial \rho}{\partial y} + w\frac{\partial \rho}{\partial z} \qquad (2.2\text{-}125)$$

has but negligible influence on the static pressure acting upon a fluid particle as it moves through the flow field

$$\rho = \rho(x,y,z,t)$$
$$u = u(x,y,z,t)$$
$$v = v(x,y,z,t) \qquad (2.2\text{-}126)$$
$$w = w(x,y,z,t)$$

the second coefficient of viscosity, λ, becomes restrictively related to the first coefficient of viscosity, μ,

$$\lambda = -\frac{2}{3}\mu \qquad (2.2\text{-}127)$$

The error involved in using the simple relationship (2.2-127) becomes appreciable only if the total (substantial) density derivative (2.2-126) becomes large, as inside a shock wave itself. For the rest of compressible fluid flow field the theoretical approximation (2.2-127) is in good agreement with corresponding experimental evidence for dry air.

Thus, on the basis of the conditionally acceptable expression (2.2-127), the classical incompressible flow Reynolds Number definition (2.2-122) is tentatively extended to serve as a partial viscosity criteria for compressible laminated continuum fluid flows in general. Furthermore, it is further conditionally extended to the slip flow regime also, where a modified laminar boundary layer under the slip conditions at the solid surface is defined[9]. In the free molecular flow regime, due to the prevailing aspects of a discrete molecular structure, the classical physical interpretation of the Reynolds Number looses its meaning, i.e., the concept can be conditionally retained as a formalistic mathematical convenience only, in a similar manner as the rest of the continuum (bulk) matter definitions, such as the speed of sound, the Mach Number, etc.

Within the cited restrictive conditions, an increase in the Reynolds Number value can be interpreted as an indication that the inertial forces are becoming relatively more important, and vice versa, a decrease in Reynolds Number value signifies an increasing dominance of viscous forces. This conclusion should be nevertheless, interpreted cautiously: the Reynolds Number criteria may be applied only if the viscous flow pattern does not change; unfortunately, a change in Reynolds Number usually invokes a change in flow pattern also, as it is affected by variations of the flow speed regime, V, the flow density, ρ, and the temperature, T°.

Another conditionally valid use of the Reynolds Number criteria can be formulated as follows: if at some particular Reynolds Number value the inertia forces become predominant within a specified flow system, their predominance shall be maintained for all higher Reynolds Numbers also, and vice versa, if the viscous forces become of an overwhelming importance at some Reynolds Number value, they shall retain the primary influence at all lower Reynolds Numbers also. Between the two limiting cases there is obviously a Reynolds Number range in which both the inertia and the viscous forces may be of the same order of magnitude and importance.

By application of the Prandtl's postulate to the continuum incompressible or compressible flow regimes, all the viscous effects in a gaseous flow over exposed solid surfaces are confined to the relatively thin boundary layer next to the solid surface itself. The recognized two distinct types of boundary layers that can occur, i.e., the laminar and the turbulent, are conditionally discriminated by the so called critical value of the Reynolds Number, Re_{cr}, which, for all practical purposes, may be supposed to be of the order of 10^6. Note that the classical Reynolds Number definition (2.2-122), although strictly valid for laminated viscous flows, is extended to the turbulent boundary

layers with an implication that all the constituent physical variables (ρ, μ, V) should be defined as mean averages in space and time. In more detailed turbulent boundary layers analyses, the overall viscous effects are considered due to both the molecular and the eddying diffusive mechanisms(18), so that the above Reynolds Number definition does not represent a complete criterion in comparing the relative importance of the viscous and the inertial forces respectively.

The four substantial physical variables (ρ, μ, V, L), which enter into the Reynolds Number definition, can be referred to different spatial conditions in a given flow field. In terms of such reference choices, the following explicitly inferred Reynolds Number specifications are commonly encountered:

(1) The local Reynolds Number, referred to a specified point on the body contour, which is located S ft from the tip point in the direction of the zero-streamline:

$$\left[Re_s\right]_{n=0} = \left[Re_s\right]_w = \frac{S\rho_w V_1}{\mu_w} \qquad (2.2\text{-}128)$$

$$\left[Re_s\right]_{n=\delta_s} = \frac{S V_1 \rho_1}{\mu_1} = \left[Re_s\right]_w \frac{\mu_1}{\mu_w}\frac{\rho_w}{\rho_1} \qquad (2.2\text{-}129)$$

$$\left[Re_s\right]_A = \left[\frac{S V_A \rho_A}{\mu_A}\right] = \left[Re_s\right]_{n=\delta_s} \frac{V_1}{V_A}\frac{\rho_1}{\rho_A}\frac{\mu_A}{\mu_1} = \left[Re_s\right]_w \frac{V_1}{V_A}\frac{\rho_w}{\rho_A}\frac{\mu_A}{\mu_w} \qquad (2.2\text{-}130)$$

where subscripts 1 , w , A refer to the local free stream (outside the relatively thin boundary layer), local wall and ambient atmospheric conditions (at infinity) respectively, with $\vec{n}$ taken normal to the local S direction of the zero stream line (body contour). The theoretical local condition, (subscript 1) is fulfilled for all practical purposes at the outer edge of the boundary layer with $n = \delta_s$, where δ_s is the local boundary layer thickness.

(2) The average Reynolds Number for any given "i-th" part of a body assembly, Re_{L_i} , is referred to the overall length, L_i , of the investigated contour in the direction of the zero stream line. It is usually expressed in terms of the ambient atmospheric conditions and serves in a first approximation, as a practical criterion when evaluating the relative extents of the laminar and of the turbulent boundary layer flows over the contour of the "i-th" body part.

$$Re_{L_i} = \frac{\rho_A L_i V_A}{\mu_A} \qquad (2.2\text{-}131)$$

With the restrictive approximations, the Reynolds Number can be used as a <u>partial</u> similarity criterion, implying that for two similar viscous flow systems the ratios of inertia to viscous forces should be the same for any pair of comparative local points, i.e., at the matching points having their coordinates (x, y, z) matched in the scale ratio

$$\frac{x_1}{L_1} = \frac{x_2}{L_2} \qquad \frac{y_1}{L_1} = \frac{y_2}{L_2} \qquad \frac{z_1}{L_1} = \frac{z_2}{L_2}$$

the corresponding numerical values of the local Reynolds Numbers

$$Re_1 = \frac{\rho_1 V_1 L_1}{\mu_1} \qquad Re_2 = \frac{\rho_2 V_2 L_2}{\mu_2} \qquad (2.2\text{-}132)$$

must be such that $Re_1 = Re_2$ locally, where subscripts 1 and 2 refer to the two comparative viscous fluid-body systems.

(2) <u>Froude Number, Fr</u>

The Froude Number concept is restricted to gravitation effects within fluid-body systems:

$$Fr = \frac{V}{(Lg)^{1/2}} \qquad (2.2\text{-}133)$$

Square of the Froude Number can be interpreted as a ratio of the inertia to gravity forces, acting on a fluid element of unit volume(16):

$$Fr^2 = \frac{V^2}{Lg} = \frac{V^2}{Lg}\frac{\rho}{\rho} = \frac{\frac{\rho V^2}{L}}{\rho g} \qquad (2.2\text{-}134)$$

where

$\rho V^2/L$ - is proportional to inertia force

per unit volume,

ρg - is proportional to gravity force per unit volume.

Froude Number appears as an important natural number in incompressible flows with free surfaces (gravity waves).

In compressible flows the Fronde Number can additionally appear whenever a free convection (which is maintained by gravity) is present.

For fluid-body systems, the Froude Number can be in some cases conveniently used to express the gravitational effects acting upon the body itself, and thus become usefully associated with the equivalent equilibriums lift coefficient, for instance in dynamic stability investigations(19).

(3) Weber Number, We

The Weber Number is another natural variable that becomes significant when the fluid free surface tension effects (surface-tension waves) are investigated; it represents a ratio of the inertial to the surface-tension forces, expressed in terms of the respective pressure differences as follows:(16)

The inertial pressure difference in the x-direction of a free-surface two-dimensional fluid in motion, acting on the corresponding unit areas a distance Δx apart, is:

$$\Delta p_{inertial} \sim \left(\rho u \frac{\partial u}{\partial x} + \rho v \frac{\partial u}{\partial y}\right)\Delta x \sim \rho V^2 \qquad (2.2\text{-}135)$$

The surface-tension pressure difference across a curved surface is equal to the ratio of the surface tension, σ, and the radius of the surface curvature, R :

$$\Delta p_{\substack{surface \\ tension}} = \frac{\sigma}{R} \sim \frac{\sigma}{L} \qquad (2.2\text{-}136)$$

The Weber Number is then defined as:

$$We = \frac{\rho V^2}{\sigma/L} = \frac{\rho V^2 L}{\sigma} \sim \frac{\Delta p_{inertial}}{\Delta p_{\substack{surface \\ tension}}} \qquad (2.2\text{-}137)$$

(4) Mach Number, M

The Mach Number represents a determining natural variable and a partial similarity parameter for investigations of compressibility effects at large. It becomes the only similarity parameter for inviscid, isentropic, compressible, perfect gas flows at near ordinary temperatures, i.e., provided the gas is assumed to be ideal ($\mu = k \equiv 0$), and both thermally and calorically perfect, while the body surface is insulated. Under the restrictive conditions, the allowance for compressibility is physically represented by variable density, which is then a function of pressure only. The pressure-density functional relationship is under the circumstances validly expressed by the adiabatic exponential law at constant entropy:

$$p = p(\rho), \quad \gamma = \frac{\rho}{p}\left(\frac{\partial p}{\partial \rho}\right)_s, \quad \therefore \quad \frac{dp}{p} = \gamma \frac{d\rho}{\rho} \qquad (2.2\text{-}138)$$

which, for near standard conditions and with $\gamma = const$, reduces the equation of state for thermally perfect gases

$$p = \rho R T^{\circ} \qquad (2.2\text{-}139)$$

to the simple isentropic form

$$p = \rho^{\gamma} \cdot const. \qquad (2.2\text{-}140)$$

This, combined with the illustrated nondimensionalization of governing equations and with a reference choice of ρ_∞ and p_∞ as datum values, renders the compressibility similarity requirement to

$$\frac{p_\infty}{\rho_\infty V_\infty^2}, \quad \gamma_\infty = const. \qquad (2.2\text{-}141)$$

which, by introduction of the speed of sound as representing the characteristic speed of propagation of small disturbances,

$$a_\infty = \left(\gamma_\infty \frac{p_\infty}{\rho_\infty}\right)^{1/2} \qquad (2.2\text{-}142)$$

reduces the compressibility criteria to the familiar practical definition of the Mach Number

$$\frac{\rho_\infty V_\infty^2}{p_\infty} = \gamma_\infty \left(\frac{V_\infty}{a_\infty}\right)^2 = \gamma_\infty M_\infty^2 \quad \therefore \; M_\infty = \frac{V_\infty}{a_\infty} \; . \qquad (2.2\text{-}143)$$

In general, a partial similarity of two comparative compressible flows around geometrically similar or affine bodies requires that the respective local Mach Number values at any two corresponding (dimensionless) points (x', y', z') in the two flow fields be the same. The requirement is both necessary and sufficient for thermally and calorically perfect gases, and necessary only for thermally perfect gases, since then $\gamma = \gamma(T^\circ)$ becomes the second compressibility parameter of importance.

It is noted that in a highly rarefied free molecular flow regime, the classical definition of speed of sound, conceived as the characteristic speed of propagation of small disturbances through an elastic medium, looses its true physical meaning and consequently the Mach Number definition as well. Nevertheless, the concepts are retained formally, with the speed of sound being conveniently related mathematically to the mean or to the most probable molecular speed by statistical probability methods of the classical equilibrium kinetic theory of gases.(7)

(5) Specific Heats Ratio, γ

It is the second compressibility parameter, which, together with Mach Number, forms the necessary and sufficient similarity criteria for calorically imperfect gases near standard conditions, all other restrictions remaining as stated in the paragraph (4).

The specific heats ratio, γ , depends, in general, on the thermal and structural characteristics of a gas, (its internal molecular and atomic composition), i.e., on the number and type of excited internal degrees of freedom (active and inert), on the relative equilibrium of dissociated, ionized and chemically reacting components, on the partial pressures and densities, etc. Such a broad functional dependence of γ is analytically too complex and well beyond the existing theoretical possibilities(7), requiring a considerable semi-empirical supporting evidence and data. Excluding both the very high and the very low thermal states (i.e., assuming a prevailance of active translatory and rotational degrees of molecular freedom only at near standard pressures and densities), the specific heat ratio, γ , can be conveniently defined in terms of the ordinary physical bulk matter properties as

$$\gamma = \gamma(p, \rho, T^\circ, R) \qquad (2.2\text{-}144)$$

for a given gas composition. When, as implied, the substantial physical variables, p , ρ , T° , are kept near standard conditions, the specific heats ratio, γ , for many real gases proves to be only a weak function of pressure and density variations, i.e., in a first approximation:

$$\gamma = \gamma(T^\circ). \qquad (2.2\text{-}145)$$

If, in addition, the temperature variations are further so restricted that the expression (2.2-145) degenerates to a weak functional dependence, the specific heat ratio is taken to be constant for all practical purposes, and gas is considered calorically perfect:

$$\gamma = \text{const.} \qquad (2.2\text{-}146)$$

(ii) Heat Transfer Natural Variables for Flowing Gases

Although the heat (energy) transfer phenomena in flowing gases are only for convenience considered separately, actually, they are closely interrelated to the mass and momentum transport processes. Formulation of the transport processes is expressed by the governing equations of change and the auxiliary relationships (2.2-68) to (2.2-85), which, in general, would take into account the actual composition and contributions of various species in a reacting mixture of gases within specified boundaries of a closed system.

(1) Atmospheric Gaseous Model

A closed gas dynamics system comprises a specified working medium (gas), flowing relative to a stationary immersed body, and separated from external environments by a defined outer enclosure (any closed mathematical or real surface), and by the body contour

itself (inner boundary).

In the extremes, the boundaries may be treated either as ideal mass and heat insulators, or as permitting heat and mass transmission into or out of the closed system. Flowing processes within ideally insulated closed systems are called adiabatic in general. If the necessary conditions for the constancy of entropy (see previous section) are satisfied, the respective flowing process becomes isentropic.

Relative to the structural state of gaseous medium, three distinct types of fluid-body closed systems are of a primary concern for practical aerodynamic purposes:

(a) Medium is treated as a homogeneous, individual gas,

(b) Medium is treated as a homogeneous mixture of gases,

(c) Medium is treated as a heterogeneous compostion of gaseous phases of various species.

For flight dynamics force evaluation purposes, the following simplified atmospheric aerothermal models are commonly considered:

At subsonic, transonic and moderate supersonic steady flight speed regimes in a Standard Atmosphere up to 100,000 feet, the ambient air is treated as a dry, predominantly diatomic, thermally and calorically perfect gas, possessing only active degrees of molecular freedom (three translations and two rotations of a dumbell molecular model) in equilibrium, so that the classical thermodynamic relationships as formulated for a continuous, macroscopically homogeneous, non-reacting, near-perfect gaseous medium, are tentatively applicable. The thermal equilibrium concept implies that a closed system reaches a state of equilibrium spontaneously, if sufficient time is allowed during which no mass or energy is transmitted to (or from) the system. Applied to flowing processes, the concept implies a continuous succession of an infinite number of steady states, achieved by infinitesimal and continuous changes in pressures, densities and temperatures, so that at each point in a fluid flow field a thermal equilibrium is realized at any instant of time. This implication is practically approached under steady prolonged flight conditions.

For higher flight altitude ($H > 100,000$) and/or hypersonic flight speeds, $M > 5$, especially for blunt body and stagnation point regions, the above simplified and idealized assumptions may prove in many cases inadequate. The so called real gas effects should be then correctively introduced, in as much as they may have substantial bearings upon the restrictive aerodynamic force data.

An increase in temperature levels activates successively the inert degrees of molecular freedom (vibration, dissociation and ionization), each of which has its own characteristic relaxation time required to reach its respective equilibrium state.

Different atmospheric gas components have different critical temperature levels for a measurable activation of their successive inert degrees of freedom: for a given pressure, density and temperature, air becomes a mixture of distinct gaseous phases in various states of molecular, atomic and ion excitation levels. The involved relaxation time intervals are again individual functions of (p, ρ, T°) for each gaseous component.

At highly rarefied (free molecular) flow conditions, the continuum flow supposition is necessarily substituted by the statistical probability concepts of the (equilibrium) kinetic theory of gases.(7)

(2) Descriptive Analytical Methods

As mathematically explicitly formulated in Section 2.2.2, a meaningful representation of various fluid flow-immersed body closed systems can be undertaken by three distinct analytic methods, depending upon the way in which a model of the physical system is best conceived: microscopic, molecular or macroscopic.

The fluid-body system analysis on a microscopic scale leads to the familiar set of five scalar differential equations of change, representing the mass, momentum and energy conservation principles. Consideration of a discrete molecular system results in the respective analytic expressions of the equilibrium kinetic theory of gases. Macroscopic model studies yield a finite, overall mass, momentum and energy balance in a system, without reference to the way in which the finite changes are realized. All the

three approaches are commonly in use, the relative preference depending on the intrinsic nature of a particular airflow model, the required degree of accuracy and the type of final data.

When either microscopic or molecular models are used, the resulting analytic expressions for the three conservation principles may be eventually brought to the same differential equations form, although the initial conceptional and analytical approaches are intrinsically different. In both cases the internal mechanism of the mass, momentum and energy transport processes inside a closed physical system can be most conveniently expressed by use of the so called transport coefficients, which are briefly termed in the following text.

In case of rarefied gas flows, the discrete molecular concept allows eventually a best physical interpretation of the actual internal mass, momentum and energy transport mechanisms, although the mathematical treatment and a subsequent acquisition of particular solutions is eventually cumbersome. This difficulty can be bridged by relating the ascertained discrete molecular properties and the observed molecular interaction patterns to overall physical characteristics of an appropriately small bulk amount of matter. The task falls into the realm of averaging procedures of the statistical mechanics, which can be broadly split into two main branches:

(a) Equilibrium state statistical thermodynamics or classical equilibrium kinetic theory of gases which bonds together the governing equations of state for various presumed fluid models (perfect, ideal, real, etc.) and the related equilibrium thermodynamic concepts.

(b) Nonequilibrium statistical mechanics, or the kinetic theory proper, describing the internal transport processes in terms of the inherent discrete molecular concepts in the presence of active forcing (nonequilibrium) components.

(3) Transport Coefficients

One advantage of the simplified equilibrium kinetic theory discrete molecular approach is that the internal structure of the mass, momentum, and energy transport mechanisms can be more easily grasped, and the related mass, momentum and energy transport coefficients more readily analyzed under varying gas flow conditions. Both the analytical and the numerical treatments of thermal, molecular and mass currents within a closed fluid-body system are very conveniently expressed on a microscopic scale by use of the respective "transport coefficient," which must be properly defined for the investigated physical flow model.

As a simplified illustrative example, when a steady, viscous and heat conducting fluid flow with a coolant injection is conceived to be one-dimensional and of a laminated flow pattern, the formulation of mass, momentum and energy transport coefficients, D_{ij}, μ and k may be attained by use of the corresponding fundamental laws (radiation effects excluded):[17]

(a) Fick's first law for a diffusive mixing of two gaseous components (binary mixtures) in absence of convective currents, i.e., for a mass transfer due entirely to processes effected on the atomic or molecular scale. The diffusion proceeds from points of more concentration to points of less concentration at a time rate proportional to the potential concentration gradient:

$$\dot{M}_{ix} = - D_{ij} \frac{d\rho_i}{d_x} \qquad (2.2\text{-}147)$$

where

$\dot{M}_{ix} = \frac{dM_i}{dSdt}$ - is the mass flux of the "i-th" species (solute) in the x-direction, $[ML^{-2}T^{-1}]$.

dS - is the infinitesimal area, normal to the x-direction, $[L^2]$.

$\frac{d\rho_i}{dx}$ - is the mass concentration gradient of the "i-th" species in the x-direction, $[(ML^{-3})(L^{-1})]$.

D_{ij} - is the diffusion coefficient for sclute and solution at a given temperature, $\left[\frac{L^2}{T^2}\right]$.

(b) Newton's law of viscosity,

$$\dot{T}_{yx} = -\mu \frac{du}{dy} \qquad (2.2\text{-}148)$$

expressing that the molecular momentum flux in the y-direction (or the shearing stress in the x-direction), $\dot{T}_{yx}$, is proportional, μ, to the gradient in the same y-direction, du/dy, of the velocity component, u, of the

ordered motion in the x-direction, where

μ - is the first coefficient of viscosity. The law is, strictly speaking, valid for incompressible, laminar fluid flows. The compressibility effects do affect the viscosity characteristics of a gas, but they are usually treated indirectly only by the introduction of the second coefficient of viscosity, λ, into the energy dissipation function, ϕ.

(c) Fourier's law of heat conduction,

$$q_x = - k \frac{dT^\circ}{dx} \qquad (2.2\text{-}149)$$

expressing that the flux of (heat) energy in the x-direction, q_x, is proportional, k, to the absolute temperature gradient in the same direction, dT°/dx.

where

$q = \frac{dQ}{dt\,dS}$ -is the heat flux, $[(ML^2T^{-2})(T^{-1})(L^{-2})]$.

k -is the coefficient of heat conductivity, $[(ML^2T^{-2})(L^{-1}T^{-1})(^\circ K)^{-1}]$.

T° -is the absolute temperature, °K.

The negative sign in Eq (2.2-149) is conventionally affixed, denoting a positive value for Q.

The above proportionality constants, D_{ij}, μ, and k, bear the name of transport coefficients, since they intrinsically describe the internal mechanism by which the mass, momentum, and energy currents are transported in the given direction and under the specified one-dimensional flow conditions.

As pointed out, the three transport coefficients (and others, depending upon the flow type and complexity, such as three-dimensional, laminar, turbulent, dissociating, ablating, radiative, etc.) are internally related to the constituent actual molecular properties and intermolecular forces in each particular case. As a consequence, their formulation in terms of the existing molecular structures shall vary; so will the relatively simple forms of the above laws.

The form of the above laws suggests a strong similarity of the mass, momentum and energy transport modes. This point is further illustrated in a comparative table of Ref. 15, (Eckert) for more general flow cases.

(4) Peclet Number - A Fundamental Heat Transfer Natural Variable

In laminar continuum fluid flows at near standard pressures and densities (i.e., excluding pronouncedly dense and rarefied states), and at temperatures below the critical levels for excitation of the inert degrees of freedom (see next Section, 2.2.5), the thermal similitude condition is basically represented through the concept of Peclet Number:

$$Pc = \frac{\rho C_p V D}{k} \qquad (2.2\text{-}153)$$

which has been illustratively (but not restrictively) identified earlier (see Section 2.2.3) and defined on the assumption that the heat transfer from the surface to the flow (or vice-versa) is absent (insulated surfaces, adiabatic flow). It is recognized that the "insulated surface" premise does not eliminate the internal gas conductive and convective heat transfer phenomena, especially for viscous flows, since the heat generation and transport is then realized through an internal frictional dissipation of the kinetic energy of the ordered or directed molecular flow. An introduction of non-insulated (or non-adiabatic) surface conditions shall additionally affect the heat transport mechanism and the temperature profile across the boundary layer, the non-insulated body acting as a heat sink (or source); the inner boundary conditions, the temperature profiles across the fluid flow field and the energy exchange mechanism are altered, while the Peclet Number concept formally stays valid, provided the laminar (or streamlined) flow pattern is preserved. The latter condition is restrictive, since a tentative extension of the Peclet Number concept to turbulent flows requires a prior time-spatial mean averaging lamination of all fluctuating and eddying flow characteristics.

In general, the Peclet Number role is of importance whenever overall thermal conditions within a viscous or a nonviscous but heat conducting (laminar continuum) compressible fluid flow-body closed systems are investigated, the eventually conductive pro-

perties of the exposed body surfaces primarily affecting the heat transfer rates and the local heat flux gradients. As already pointed out, the additional effect of a non-insulated surface may be treated as a specified heat sink or source within the closed system, and extends theoretically the domain of the heat transfer phenomena even to inviscid incompressible flows eventually (i.e., by allowing for real gas polytropic flow conditions). For practical purposes, the following discriminating guidelines are suggested:

In an incompressible and inviscid fluid flow, the Peclet Number can appear as a meaningful natural variable only if there is a significant heat source or sink, i.e., a non-insulated surface, artifically cooled or heated. The situation is but of limited practical importance, eventually realized at the landing phase of a controlled space capsule, and in some especially simulated experiments with heated surfaces transiently exposed to a low subsonic flow speed ($M_\infty < .4$).

In a compressible, heat-conducting flow, inviscid or viscous, with insulated or non-insulated surfaces, the Peclet Number role becomes respectively more pronounced. Its relative significance depends upon the specific flow type and upon the extent of allowed approximations in treating a real gas as near-perfect. Generally, the dynamic and the thermal flow conditions and the similitude requirements are interconnected even for a presumed thermally and calorically perfect gas, and the Peclet Number (or its alternative substitutes, Re and Pr) can be neglected only if the fluid conductivity, k , is permittedly disregarded. Evidently, with an increase in flow speeds and temperature variations, the Peclet Number significance becomes respectively more prominent.

As a broad generalization, it can be said that whenever there is any type of heat transport (regardless of its origins) in a fluid flow, the Peclet Number plays a role regarding the thermal flow aspects comparable to the Reynolds Number role for viscous flow aspects. The likeness can be deduced from their respective expressions:

$$Re_L = \frac{\rho V L}{\mu} = \frac{(\rho V)(V)}{(\mu/L)(V)} = \frac{(\rho V)(V)}{(\mu L^2/L^3)(V)} \qquad (2.2\text{-}154)$$

$$P_C = \frac{\rho C_p V L}{k} = \frac{(\rho C_p \Delta T^\circ V)}{(k\Delta T^\circ)/L} \qquad (2.2\text{-}155)$$

where, by dimensions:

ρ -is the mass density, $[ML^{-3}]$.

C_p -is the specific heat at constant pressure, $[(ML^2T^{-2})(M^{-1})(^\circ K)^{-1}]$.

ΔT° -is the absolute temperature increment, $[^\circ K]$.

V -is the ordered speed of flow, $[LT^{-1}]$.

k -is the coefficient of heat conductivity, $[(ML^2T^{-2})(T^{-1})(L^{-1})(^\circ K)^{-1}]$.

μ -is the first coefficient of viscosity, $[MLT^{-1}]$.

(ρV) -is the density momentum of ordered motion, $[(ML^{-3})\times(LT^{-1})] = [(MLT^{-1})(L^{-3})]$.

$(\mu L^2/L^3)$ -is the dissipated density momentum of ordered motion, $[(ML^{-1}T^{-1})\times(L^2)\times(L^{-3})] = [(MLT^{-1})\times(L^{-3})]$.

$(\rho C_p \Delta T^\circ V)$ -is the heat flux in the direction of ordered motion, $[(ML^{-3})\times(ML^2T^{-2})(M^{-1})(^\circ K)^{-1}\times(^\circ K)\times(LT^{-1})] = [(ML^2T^{-2})\times(L^{-2})\times(T^{-1})]$.

i.e., the time rate $[T^{-1}]$ per unit area $[L^{-2}]$ of the heat energy $[ML^2T^{-2}]$.

$(k\Delta T^\circ/L)$ -is the heat flux dissipa by random molecular motio in the direction normal to the ordered flow $[(ML^2T^{-2})(T^{-1})(L^{-1})(^\circ K)^{-1}\times(^\circ K)\times(L^{-1})] = [(ML^2T^{-2})\times(L^{-2})\times(T^{-1})]$.

i.e., the time rate $[T^{-1}]$ per unit area $[L^{-2}]$ of the heat energy $[ML^2T^{-2}]$ or, alternatively, it is the rate $[LT^{-1}]$ at which a fraction of the ordered flow thermal energy $[ML^2T^{-2}]$ per unit volume $[L^{-3}]$ is dissipated by random molecular motion.

$(\rho V)(V)$ -is the pressure drop or inertial force $[MLT^{-2}]$ per unit area $[L^{-2}]$ acting in the direction of the ordered motion, $[(MLT^{-1})(L^{-3})(L)(T^{-1})] = [(MLT^{-2})\times(L^{-2})]$.

$(\mu L^2/L^3)(V)$ -is the viscous tangential stress, or the dissipative force $[MLT^{-2}]$ per unit area $[L^{-2}]$ in the direction of

ordered flow motion,
$[(MLT^{-1})(L^{-3})(L)(T^{-1})] = [(MLT^{-2})(L^{-2})]$

or alternatively, it is the fraction of the dissipated energy [ML^2T^{-2}] per unit volume [L^{-3}] of the ordered flow due to random molecular motion.

In words:

The Reynolds Number represents the ratio of the rate at which the density momentum (ρV) of ordered motion is transported by the bulk matter fluid flow (numerator), to the rate at which the density momentum of ordered motion is dissipated ($\mu L^2 / L^3$) by the random molecular motion in a viscous fluid (denominator).

The Peclet Number represents the ratio of the ordered heat flux ($\rho C_p \Delta T^\circ V$) or the time rate per unit area at which the thermal energy is transported by the ordered fluid flow (numerator), to the random heat flux ($k\Delta T^\circ / L$) or the time rate at which the thermal energy is dissipated by the random molecular motion (denominator), i.e., the Peclet Number may be related to the thermal energy transport effects in thermally conducting flows in the same pattern as the Reynolds Number is related to the momentum transport effects in viscous fluid flows.

When restrictively applied to laminar and conditionally extended turbulent boundary layer flows, the Peclet and the Reynolds numbers may be interpreted as (1) representing the inverse of lateral diffusive rates of the ordered thermal ($k\Delta T^\circ / L$) and momentum $(\mu/L)(V)$ flow energies respectively for a given ordered laminar flow, and (2) as expressing the ratios of turbulent mean average transports of thermal ($\rho C_p \Delta T^\circ V$) and momentum (ρV) (V) energies to their mean average molecular dissipative transport rates, ($k \Delta T^\circ / L$) and $(\mu / L)(V)$, respectively for turbulent flows.

As already pointed out in Section 2.2.3 due to the intrinsic interdependence between dynamic and thermal flow characteristics, the Peclet Number can be alternatively treated as a product of the corresponding Reynolds and Prandtl Numbers, provided the fluid flow is of a viscous type:

$$P_c = \frac{\rho C_p V L}{k} = \frac{\rho V L}{\mu} \quad \frac{C_p \mu}{k} = Re_L \cdot P_r \qquad (2.2\text{-}156)$$

i.e., the relative significance of the Peclet Number may be analyzed tentatively in terms of the comparative importances of the associated Reynolds and Prandtl Numbers in each particular flow case. For instance, in the simplest case of a heat-conducting viscous gas flow over insulated surfaces, if the gas is treated as thermally ideal ($p = \rho RT^\circ$) and calorically perfect ($k = const$, $\mu = const$, $C_p = const$), the Prandtl Number is not a function of temperature,

$$P_r = \frac{C_p \mu}{k} = const \qquad (2.2\text{-}157)$$

and the Peclet Number

$$P_c = Re_L P_r = f(Re_L) \qquad (2.2\text{-}158)$$

becomes a direct function of the Reynolds Number, i.e., of the viscous flow type (laminar or turbulent). For laminar boundary layers this leads to a correspondingly straightforward heat transfer - skin friction coefficient relationship, which is referred to as the simple Reynolds Analogy concept in the respectively simplified boundary layer theories. For instance, for a laminar compressible boundary layer (of a thermally and calorically perfect gas and with $k = const$ and $\mu = const$) over a flat plate at a zero angle-of-attack (Pohlhausen)[14] the Reynolds Analogy takes the alternate simple analytical forms:

$$\left(P_r^{-2/3}\right)\frac{C_f}{2} = St = \frac{h}{\rho C_p V_\infty} = \frac{Nu}{P_r Re_L} = \frac{.664}{(P_r^{2/3})(Re_L^{1/2})} \qquad (2.2\text{-}159)$$

where

C_f -is the skin friction coefficient,

Nu -is the Nusselt Number,

St -is the Stanton Number,

h -is a dimensional heat transfer coefficient.

The coefficients (C_f, Nu, S_t, h) are defined in the ensuing text.

Similarly, when an allowance for variations of μ, k, and C_p with the absolute temperature is made, indicating a more general type of the internal random molecular transport mechanisms, the respectively more elaborate functional relationships between the heat transfer and the skin friction coefficients can be established, which are then called modified Reynolds Analogy concepts (when the skin-friction coefficient data are of a primary interest).

Since either simple, Eq (2.2-154), or modified Reynolds Analogy expressions are functionally presented in terms of alternate combinations of S_t, Pr, Nu on one side (heat effects), and C_f, Re on the other (viscous effects), it is customary in engineering applications to use as the representative non-dimensional heat transfer coefficients either the Stanton and the Prandtl Number, or the Nusselt and the Prandtl Number combination instead of the more generalized Peclet Number concept, ($Pc_L = Pr\,Re_L$).

To summarize: restrictively for viscous, heat conducting fluid flows, the four thermal natural variables (Pr, Pc, S_t, Nu) are mutually interconnected and functionally related to the Reynolds Number and the skin-friction coefficient definitions by Reynolds Analogy concepts. The Prandtl Number, Pr, may be conceived as a partial, exclusively thermal substitution for the broader Peclet Number concept, Pc, which reflects a more generalized interrelationship between heat conductivity and viscosity currents. The Stanton Number, S_t, and the Nusselt Number, Nu, definitions are directly based on the dimensional heat transfer coefficient concept, h, and are only indirectly related to the Peclet Number, Pc, through an adequately introduced Reynolds Analogy criteria. Since the Nusselt Number and the Stanton Number, although mutually simply interrelated, are nevertheless mutually exclusive in practical applications, a preference for their individual choice depending on the essential dynamic aspects of different fluid flow types, see paragraph (6).

Prior to a further investigation of the Stanton and the Nusselt Number roles, a word of caution is necessary respective to the definitions of their common link - the dimensional coefficient of heat conduction, h.

(5) Definition of the Dimensional Coefficient of Heat Conduction, h

The dimensional heat conduction coefficient, h, is a fundamental substantial variable which defines the conductive heat transport characteristic of a continuum, streamlined fluid flow. The transport mechanism by conduction includes both the insulated (adiabatic) and the non-insulated body surface conditions, i.e., the coefficient of heat conductivity, h, may be referred to both the variable temperature distributions (or temperature profiles) within an (adiabatic or non-adiabatic) fluid flow proper, and to the local temperature differences between a non-insulated surface (heat sink or source) and the fluid flow layers adjacent to it. The thermal boundary conditions at the surface, and the resulting temperature differences between it and the fluid, can be, in general, functions of many variables, such as surface skin heat capacity, the viscous and/or compressible fluid flow characteristics, the fluid flow pattern (streamlined or turbulent), etc. Therefore, depending upon the overall characteristics of a fluid-body system and the adopted premises of a chosen method of analysis, there are several specific heat transfer coefficient definitions in common use. Consequently, when interpreting and comparing the respectively diversified heat transfer data, it becomes necessary to establish first a required common comparative criterion.

In general, the dimensional forms of the heat transfer coefficient, h, are conceived as the ratio of a defined heat flux and of some characteristic absolute temperature difference:

$$h = \frac{q}{\Delta T^\circ} = \frac{q}{T^\circ - T^\circ} \qquad \left[\frac{(ML^2T^{-2})}{(L^2T)(^\circ K)}\right] \tag{2.2-160}$$

$$q = \frac{dQ}{dS\,dt} \qquad \left[\frac{(ML^2T^{-2})}{L^2T}\right] \tag{2.2-161}$$

$$\Delta T^\circ = (T - T_r)^\circ \quad [^\circ K] \tag{2.2-162}$$

where

Q -is the heat energy, $[(ML^2T^{-2})]$.

S -is the area, normal to the

direction of heat flow, [L^2],

t -is the time, [T],

T° -is the local absolute temperature, [°K].

T_r° -is some reference absolute temperature, [°K].

The specification of the temperature differences, ΔT°, involves both the explicit choice of a reference temperature, T_r°, and the magnitude of the temperature interval $(T^\circ - T_r^\circ)$. The actual temperature difference, ΔT°, between any local point, T°, and a chosen reference, T_r°, depends on the overall dynamical and thermal characteristics of given fluid flow field, since the thermal and the dynamical physical properties are mutually interdependent. The heat flux intensity (numerator) and the magnitude of the temperature difference, ΔT°, (denominator) in the defining expression (2.2-160) are therefore both directly interrelated on a thermal basis, and additionally and separately influenced by the intrinsic dynamical and thermal correlations in a flowing fluid in toto. As a consequence, when the formulation (2.2-160) is introduced, the dimensional conductive heat transfer coefficient, h, lacks the necessary qualities of a clear and distinct comparative measure of exclusively thermal transport properties either in a given fluid flow or between different aerothermal systems. In order to circumverate the ambiguous situation, in practice it is usually assumed that the energetic flux properties in fluid flows are not appreciably affected by finite temperature differences, provided the temperature intervals are not very large. The question of how large a temperature difference is permissible, stays open. The uncertainty can be rendered less cumbersome by restating that the heat transfer coefficient, h, is theoretically defined for vanishingly small temperature intervals, a practically acceptable meaning of the term "small" remaining a matter of choice.

(6) Stanton and Nusselt Numbers as Practical Heat Transfer Natural Variables in the Aerodynamic Force (Skin-friction) Analyses

The Stanton Number

$$St = \frac{h}{\rho C_p V} = \frac{h\Delta T^\circ}{(\rho C_p \Delta T^\circ)V} \qquad (2.2\text{-}163)$$

can be interpreted as the nondimensional ratio of the time rate at which the heat energy is transferred to the fluid per unit area, $h\Delta T^\circ$, and the time rate at which the convective thermal energy (per unit area) is carried along by the order flow motion, $(\rho C_p \Delta T^\circ V)$, (i.e., the heat flux in the direction of ordered motion, see preceding paragraphs 4 and 5).

The Nusselt Number

$$Nu = \frac{hL}{k} = \frac{h\Delta T^\circ}{(k\Delta T^\circ)/L} \qquad (2.2\text{-}164)$$

can be likewise interpreted as the nondimensional ratio of the time rate at which the heat is transferred to the fluid per unit area $h\Delta T^\circ$, and the time rate at which the conductive thermal energy $(k\Delta T^\circ/L)$, is dissipated (per unit area) by random molecular motion (i.e., the heat flux dissipation, see preceding paragraphs 4 and 5).

In both cases (ΔT°) represents a suitably chosen reference temperature difference.

From the above definitions it may be argued that the Stanton Number and the Nusselt Number are the natural variables representing, in a limiting case, the pure convective (i.e., effected by an ordered, bulk matter motion) and the pure conductive (i.e., effected by molecular random motion) heat transport currents respectively. In reality, the two types of heat transport mechanism do not exist exclusively: the convective transfer from a surface to a flowing gas shall always involve the conduction concept also (due to the everpresent mechanism of molecular random motion). Thus, choice of either of them as a representative heat transfer natural variable depends on the predominant physical aspects of the investigated fluid flow type: if an ordered flow pattern is prevailing, (for instance laminar boundary layers), the Stanton Number is an acceptable good representative of the overall (predominantly convective) heat transfer phenomena, while if the random molecular motion is in predominance, the Nusselt Number (i.e., heat conduction) appears as a better choice in describing the heat transfer mechanism, particularly for conditions where the ordered flow motion is slow ($V \approx 0$). Despite the phenomenological difference, it is customary in practice to refer

to the heat transport mechanism and to the heat transfer coefficient by using the term "conduction" only, which is but a terminology convenience.

(7) Prandtl Number, Pr

The Prandtl Number is obtained as a direct ratio of Peclet and Reynolds Numbers:

$$Pr = \frac{Cp\mu}{k} = \frac{(\rho Cp\, VL)/k}{(\rho VL)/\mu} = \frac{Pc}{Re_L} \cdot \qquad (2.2\text{-}165)$$

Consequently, any viscous thermal flow can be alternatively investigated by means of the Reynolds and the Prandtl Numbers or by a combination of the Peclet and the Prandtl Numbers.

Advantages of an alternative use of the Prandtl Number instead of the Peclet Number, are:

(a) It involves directly only three physical variables, (Cp, μ, k), instead of five (as required for the Peclet Number),

(b) For perfect gases the three physical variables are direct functions of the specific heats ratio, γ. Thus, since the specific heat ratio is in itself a fundamental similarity parameter, the Prandtl Number under the conditions is not appearing as any additional similarity requirement, provided k and γ are treated as constants.

(c) The Prandtl Number reflects a relationship between the intrinsic viscous and thermal transport properties of a fluid as a medium, rather than under some specific ordered flow conditions.

Limitations in the applicability of the Prandtl Number as a convenient substitute for the Peclet Number can be illustrated as follows:

(a) Prandtl Number is in its best use for describing diffusive tendencies in a viscous laminar type of fluid motion, i.e., in describing phenomena completely dependent on Reynolds Number and γ as governing similarity parameters. According to its definition (2.2-165), the Prandtl Number represents then a ratio of the ordered momentum diffusive tendencies (inverse of the Reynolds Number), to the diffusive tendencies of the thermal energy (inverse of the Peclet Number), both due to random molecular motion (see paragraphs 3 and 4). Consequently, with the thermal diffusivity due to molecular motion defined as

$$a = \frac{k}{\rho Cp} \qquad (2.2\text{-}166)$$

and the momentum molecular diffusivity expressed through the concept of the kinematic viscosity

$$\nu = \frac{\mu}{\rho} \qquad (2.2\text{-}167)$$

the Prandtl Number may be written alternatively as the ratio

$$Pr = \frac{\nu}{a} = \frac{(\rho Cp VL)\, k}{(\rho VL)\,\mu} \cdot \qquad (2.2\text{-}168)$$

(b) Prandtl Number is not a meaningful substitute for the more basic Peclet Number criteria whenever an inviscid type of flow is considered, or, for slightly viscous flows, whenever the Reynolds Number is not considered as an important similarity criteria. For instance, inviscid laminar flows or viscous turbulent flows of a general type cannot be defined adequately in terms of the Reynolds Number similarity criteria (the first due to absence of Re, and the second due to its eddying nature), i.e., the two flow types do not justify a meaningful use of the Prandtl Number concept. For such cases, the Nusselt Number, Nu, or the Stanton Number, St, should be used instead, since both of them can be represented in terms of the Peclet Number only.

(8) Gratz Number, Gz

When investigating thermal effects for unaccelerated laminar flows in pipes, the Peclet Number multiplied by a factor $(\pi/4\ D/L)$ serves as a fundamental heat transfer natural variable, bearing the name of Gratz Number.

$$Gz = \frac{\dot{m}\, Cp}{k\, L} = \frac{\pi D^2}{4}\,\frac{\rho V Cp}{kL} = \left(\frac{\pi D}{4L}\right)\left(\frac{\rho Cp VD}{k}\right) = \left(\frac{\pi D}{4L}\right) Pc_D \qquad (2.2\text{-}169)$$

where

$\dot{m} = \frac{dm}{dt}$ is the mass flow rate, $[MT^{-1}]$, alternatively expressed through the concept of mass density as

$$\dot{m} = \rho V \frac{\pi D}{4}, \qquad \left[(ML^{-3})(LT^{-1})(L^2)\right] = \left[MT^{-1}\right] \qquad (2.2\text{-}170)$$

L - is the pipe length, [L]

D - is the pipe diameter, [L]

Thus the Gratz Number is simply a variant of Peclet Number, used in thermal similitude investigations for unaccelerated, viscous, laminar ducted flows.

(9) Grashof Number, G_F

Grashof Number is a natural variable associated with free convection, which is present when gravity and variations in density are characteristic for heat transfer in a slowly moving gas,

$$G_F = \frac{\rho^2 g \beta D^2 (\Delta T^\circ)}{\mu^2} \qquad (2.2\text{-}171)$$

where (β) is the coefficient of thermal expansion of a gas.(17)

The Grashof Number can be interpreted as Reynolds Number squared times ($\beta \Delta T^\circ$) divided by Froude Number squared, or, alternatively, as representing the ratio of inertia force times buoyant force divided by viscous force squared.(16)

2.2.5 A BRIEF SUMMARY OF BASIC THERMODYNAMIC CONCEPTS IN FLOWING GASES

As a brief reference supplement to the preceding text in Sections (2.2.2) to (2.2.4), the few most important thermodynamic definitions and concepts relevant to and commonly used in gas flow analyses are summarized below. The presentation is limited to a discriminatory phenomenological and conceptual essentials, i.e., only to the extent, and in as much as, it may be needed for restrictively practical aerodynamic force analyses purposes.

(i) Equations of State for Ideal and Perfect Gases

A closed thermodynamic system of a gas in equilibrium is characterized by three bulk matter variables of state: the pressure, p, the density, ρ, (or specific volume v), and the absolute temperature, T°.

For near-standard (sea-level or so called slightly rarefied) conditions, most of real gases are well approximated by a generalized ideal gas model, for which the functional relationship between the variables of state takes the conveniently simple explicit form of the classical equation of state

$$p = \rho R T^\circ \qquad (2.2\text{-}172)$$

where

p - is absolute static pressure, $[(MLT^{-2})(L^{-2})]$,

ρ - is density, $[ML^{-3}]$,

T° - is absolute temperature, $[^\circ K]$,

R - is individual gas constant. $[(ML^2T^{-2})(M^{-1})(^\circ K)^{-1}]$

The thermal equation of state of an ideal gas represents combinations of the Boyle Mariotte's and Gay-Lussac's or Charles' (approximate) empirical laws for near standard conditions, the Avogadro's law and the complementary results from the equilibrium Kinetic theory of gases.(7)

Boyle-Mariotte's empirical law: At a constant temperature, the volumes of a given quantity of a gas vary inversely as the pressure exerted on it:

$$pV = \text{const.} = C_1 \qquad (2.2\text{-}173)$$

$$\therefore p\frac{V}{M} = \frac{p}{\rho}\ \text{const} = C_2 \qquad T^\circ = \text{const.} \qquad (2.2\text{-}174)$$

Charles' empirical law: At a constant volume, the pressures of a given quantity of a gas vary proportionally to its absolute temperature:

$$\frac{p}{T} = \text{const} = C_3 \qquad (2.2\text{-}175)$$

$$V = \text{const} \quad \text{or} \quad \frac{M}{V} = \rho = \text{const}$$

Avogadro's law: Equal volumes of all gases at the same temperature and pressure contain the same number of molecules, which for a mole of a gas at standard pressure and temperature is 6.023×10^{23} (Avogadro's Number). A mole is the quantity of a substance which has a "number of unit weights" equal to its "molecular weight number." In the CGS system of units, one mole is the matter content whose weight in grams is numerically equal to its molecular weight.

Gay Lussac's empirical law: In an expansion, the change in volume of a given quantity of gas is proportional to its absolute temperature:

$$\Delta V = V - V_\circ = \alpha V_\circ \Delta T^\circ \qquad (2.2\text{-}176)$$

where

$V_\circ$ - is the reference initial volume of a gas at a reference initial absolute temperature, $T^\circ_\circ$,

V - is the volume of a gas at any absolute temperature, T°,

$\Delta T^\circ = T^\circ - T^\circ_\circ$ - is the absolute temperature difference,

α - is the constant of proportionality; for air, $\alpha = .0036613$; for most gases $\alpha \sim \frac{1}{273}$.

Under the restrictive near-standard conditions, another idealization of empirical evidence (Joule) leads to the

relationship

$$e = e(T^\circ) \qquad (2.2\text{-}177)$$

where e is the internal energy (per unit mass) content of a gas under static equilibrium conditions.

By convention, the idealized gases satisfying simultaneously both Eq (2.2-172) and Eq (2.2-177) are called thermally perfect.

On the basis of empirical evidence, at near-standard (sea-level) pressure, densities and temperatures the internal energy content (per unit mass) of some real gases in the Eq (2.2-177) can be further approximated by:

$$e = \text{const} \cdot T^\circ = C_v T^\circ \qquad (2.2\text{-}178)$$

Such idealized gases are then called calorically perfect, the constant in the above equation being suitably defined as specific heat (per unit mass) at constant volume, C_v .

The idealized perfect gas equation of state, Eq (2.2-172) and the Gay Lussac's empirical law (2.2-176), when extended indiscriminantly to the domains of ever decreasing temperatures lead to the concept of the absolute zero temperature.

$$T^\circ = -273.16^\circ C = -459.69^\circ F \qquad (2.2\text{-}179)$$

which represents a conditional lower limit of possible thermal states. Temperature measurements referred to the absolute zero standard are called the "absolute temperature" scales (in degrees of Kelvin or Rankin) respectively,

$$T^\circ K = T^\circ C + 273.16$$
$$T^\circ R = T^\circ F + 459.69 \qquad (2.2\text{-}180)$$

The absolute zero temperature concept is artificially introduced by an idealized extrapolation of the perfect gas laws beyond any empirical evidence, i.e., assuming that the gaseous phase persists through the low temperature region in accord with Eq (2.2-172), while all gases actually liquify at various critical pressures, p_c , and temperature, T_c° , combinations. Nevertheless, the ideally postulated absolute zero temperature proves to be (on other grounds) a theoretical thermal limit for all aggregate states of matter when the actual internal molecular properties are fully taken into account.

The thermal equation of state, Eq (2.2-172) and the internal energy, e , as a state variable, Eq (2.2-177) or Eq (2.2-182) are but one necessary condition for the existence of a static thermal equilibrium state in general. Another variable of state

$$s = s(\rho, T^\circ) \qquad (2.2\text{-}181)$$

called entropy (per unit mass) is required, serving as a criteria for stability of a static equilibrium state. The two taken together represent the necessary and sufficient conditions for a statically stable thermal equilibrium state. The equation (2.2-181) is sometimes called the "caloric" equation of state.

(ii) First Law of Thermodynamics

Whenever there is an exchange of heat and/or work across the boundaries of a static closed gaseous system, the concept of internal energy, e , is introduced as a representative variable of change of state by formulation of the first law of thermodynamics (per unit mass):

$$e = e(v, T^\circ)$$

$$\delta e = \delta q + \delta w$$

$$v = \frac{1}{\rho} \qquad (2.2\text{-}182)$$

for small continuous and infinitely slow changes of state.

where

e - is the internal energy per unit mass at near-standard conditions,

δq - is the heat added (positive) to the gaseous system per unit mass,

δw - is the external work done by surroundings (positive) on the fluid.

In absence of dissipative (frictional) work, Eq (2.2-182) can be alternatively expressed in the form:

$$\delta e = \delta q - p\,dv \qquad (2.2\text{-}183)$$

where

dv - is the infinitesimal change of

specific volume, positive for expansion processes.

(iii) Irreversibility of Thermodynamic Processes

The first law of thermodynamics specifies only a formal possibility of changes of equilibrium states in a thermodynamic system, without restricting the sense of the process itself, i.e.:

$$\delta e \leftrightarrows \delta q + \delta w \qquad (2.2\text{-}184)$$

According to the "zeroth law of thermodynamics", two systems that are in thermal contact, i.e., separated by a heat transmitting boundary are in an equilibrium only if their respective temperatures are the same.

Furthermore, empirical evidence introduces the additional restriction that for real gases all natural or "spontaneous" thermodynamic processes are irreversible, or single sensed:

$$\delta e \rightarrow \delta q + \delta w \qquad (2.2\text{-}185)$$

i.e., the heat and the work addition for a presumed infinitesimal and continuous change of an initial equilibrium state into another equilibrium state is necessarily realized through simple-sensed from a higher to a lower level) currents or fluxes by which heat, work, mass, etc. are transmitted. For real gases these "current" processes are irreversible, the irreversibility being an accepted empirical fact, supported by theoretical considerations of the so called "highest probability" criteria. The unavoidable existance of currents as means of transportation for heat and other physical quantities between two subsequent equilibrium states, serves as a criteria for definition of equilibrium itself: a closed system is in a state of equilibrium, if it is free of currents. Such an idealized closed system, void of currents, becomes theoretically reversible. An idealized reversible thermodynamic process can be then tentatively defined as if the work and the heat were added in such a manner that no currents were produced between any two successive equilibrium states. The idealization serves as one of the necessary (but not yet sufficient) requirements in specifying adiabatic reversible conditions for flowing gases, i.e., the condition $\mu \equiv k \equiv 0$. In reality, since $\mu \neq 0$ and $k \neq 0$ for flowing gases, all processes are irreversible due to an unavoidable dissipation of the ordered momentum and the heat energy through the random molecular mechanism in presence of μ and k, as already described in Section 2.2.4.

(iv) Second Law of Thermodynamics

The empirical concept of irreversibility of real processes and the entropy concept as a measure of relative stability of an equilibrium state, lead to one of many forms in which the second law of thermodynamics can be expressed: for an isolated, closed system, (i.e., one that does not exchange either heat or work with surroundings), the entropy is increased in any internal spontaneous process, and the system reaches a stable static equilibrium when entropy becomes maximum.

The analytical expression for entropy (per unit mass) as a variable of state is

$$s = s(v, T^\circ) \qquad (2.2\text{-}186)$$

while the basic concept of entropy is given by definition

$$ds = \frac{\delta q}{T^\circ} . \qquad (2.2\text{-}187)$$

In Section (2.2.3), it is pointed out that the Eq (2.2-187) can be used also to define correctly a naturally intensive variable, T°, in terms of two extensive physical quantities, S and Q, instead of resorting to "thermometer" temperature concepts.

Both the internal energy, e, and the entropy, s, are thus equilibrium state variables. The formal mathematical introduction of the entropy definition, (2.2-187), is conceptually related to the idealization of reversible processes with external heat addition as follows:

An idealized reversible (expansion) change of state for any gas in an adiabatically (insulated) enclosed system is represented (per unit mass) by:

$$\delta e = -p\, dv$$

$$\delta q \equiv 0$$

$$\therefore p = -\frac{\partial e}{\partial v} \qquad (2.2\text{-}188)$$

Since, in general, $e = e(v, T^\circ)$, a new variable of state, $s = s(v, T^\circ)$ (related to the absolute temperature, T° , by Eq (2.2-187)), can be formally introduced in such a way that the reversibility quality is (by idealization) extended to processes involving non-adiabatic conditions also. Then, the general form of the thermal equation of state

$$e = e(v, T^\circ) \qquad (2.2-189)$$

takes the corresponding mathematical form

$$\delta e = \frac{\partial e}{\partial v}\,\delta v + \frac{\partial e}{\partial s}\,\delta s = -p\,\delta v + T^\circ \delta s = -p\,\delta v + \delta q\,,$$

$$\delta q \neq 0\,, \qquad \delta s = \frac{\delta q}{T^\circ}\,, \qquad (2.2-190)$$

$$\therefore\ e = e(s, v) \quad \text{and} \quad s_2 - s_1 = \int_1^2 \frac{\delta q}{T} \qquad (2.2-191)$$

for reversible nonadiabatic idealized processes between two equilibrium states 1 and 2.

Now the second law of thermodynamics formally asserts that

$$s_2 - s_1 > \int_1^2 \frac{\delta q}{T} > 0 \qquad (2.2-192)$$

for all thermodynamic systems involving heat addition (nonadiabatic systems), and for all real adiabatic processes with unavoidable dissipative currents, i.e., the law states that there is always a simple-sensed entropy increase, tending towards a stable equilibrium, even if the closed system is considered ideally isolated.

The conception of a reversible adiabatic process represents then a limiting idealized approximation only, expressed inclusively by

$$s_2 - s_1 = \int_1^2 \frac{\delta q}{T^\circ} \geq 0\,. \qquad (2.2-193)$$

(v) Specific Heats and Reversible Processes

The specific heats are defined within the concept of the first law of thermodynamics (per unit mass)

$$\delta e = \delta q - p\,dv \qquad (2.2-194)$$

as the amount of heat required for one degree of temperature rise (per unit mass) under the constant volume and the constant pressure processes respectively:

$$Cv = \left(\frac{\delta q}{\delta T^\circ}\right)_v \quad \text{and} \quad Cp = \left(\frac{\delta q}{\delta T^\circ}\right)_p\,. \qquad (2.2-195)$$

If idealized gases, satisfying the simple form of the equation of state,

$$p = \rho R T^\circ \quad \text{or} \quad pv = R T^\circ\,, \qquad (2.2-196)$$

are considered to undergo any idealized reversible (not necessarily adiabatic) thermodynamic process, the first law of thermodynamics takes conditionally a total differential form:

$$de = dq - p\,dv = \left(\frac{\partial e}{\partial v}\right)_{T^\circ} dv + \left(\frac{\partial e}{\partial T^\circ}\right)_v dT^\circ$$

$$e = e(v, T^\circ) \qquad (2.2-197)$$

expressing that the final states for reversible processes are independent of the path of integration. Then,

$$Cv = \left(\frac{dq}{dT^\circ}\right)_v = \left(\frac{de}{dT^\circ}\right)_v = Cv(T^\circ, v)\,, \qquad (2.2-198)$$

$$Cp = \left(\frac{dq}{dT^\circ}\right)_p = \left(\frac{\partial e}{\partial T^\circ}\right)_v + \left[\left(\frac{\partial e}{\partial v}\right)_{T^\circ} + p\right]\left(\frac{\partial v}{\partial T^\circ}\right)_p =$$

$$= Cp(T^\circ, v)\,. \qquad (2.2-199)$$

For thermally perfect gases

$$e = e(T^\circ) = \int Cv\,dT^\circ + \text{const}\,, \qquad (2.2-200)$$

$$Cv = \left(\frac{dq}{dT^\circ}\right)_v = \left(\frac{de}{dT^\circ}\right)_v = Cv(T^\circ)\,, \qquad (2.2-201)$$

$$Cp = Cv + p\left(\frac{dv}{dT^\circ}\right)_p = Cv + R = Cp(T^\circ)\,. \qquad (2.2-202)$$

For thermally and calorically perfect gases, Cp , and Cv are independent of temperature

$$Cv = \left(\frac{de}{dT^\circ}\right)_v = \text{const}'\,, \qquad (2.2-203)$$

$$Cp = Cv + R = \text{const}''\,, \qquad (2.2-204)$$

$$\therefore\ e = Cv\,T^\circ + \text{const}\,. \qquad (2.2-205)$$

(vi) Enthalpy or Heat Function

The first law of thermodynamics specifies the internal energy concept under static conditions, i.e., assuming that the involved thermodynamic processes and the respective changes of state are an infinitely slow sequence of equilibrium states (reversible or irreversible), void of any ordered (bulk matter) flow characteristics.

When the first law is applied to flowing fluids, the enthalpy concept is conveniently introduced to express the heat energetic aspects. Although the measure of enthalpy or heat function is readily illustrated in a limiting case of the classical adiabatic throttling (resistance) process of Joule-Thompson, its definition can be extended to any flowing process in general. The effect of the ordered (bulk matter) motion on the first law of thermodynamics is formally expressed through an additional term vdp, i.e.,

$$\delta h = \delta e + pdv + vdp = \delta q + vdp \quad (2.2\text{-}206)$$

i.e., the enthalpy (per unit mass), δh, becoming the overall energy (or heat function) characteristic of the flowing process (instead of δe), with p and T° as primary variables of state.

If the flowing process were considered reversible, the expression (2.2-206) takes the total differential form,

$$dh = \frac{\partial h}{\partial p}dp + \frac{\partial h}{\partial T^\circ}dT^\circ = de + pdv = dq + vdp \quad (2.2\text{-}207)$$

$$\therefore\ h = e + pv = h(p, T^\circ) \quad (2.2\text{-}208)$$

$$Cv = \left(\frac{dq}{\partial T^\circ}\right)_v = \left(\frac{\partial h}{\partial T^\circ}\right)_v + \left[\left(\frac{\partial h}{\partial p}\right)_v - v\right]\left(\frac{\partial p}{\partial T^\circ}\right)_v = Cv(T^\circ, v) \quad (2.2\text{-}209)$$

$$Cp = \left(\frac{dq}{dT^\circ}\right)_p = \left(\frac{\partial h}{\partial T^\circ}\right)_p \quad (2.2\text{-}210)$$

If the flowing gas is assumed to be thermally perfect,

$$e = e(T^\circ),\ Cv = Cv(T^\circ),\ Cp = Cp(T^\circ),$$

$$Cp = \frac{dh}{dT^\circ} = Cp(T^\circ),$$

$$Cv = \frac{dh}{dT^\circ} - v\left(\frac{\partial p}{\partial T^\circ}\right)_v = Cp - R, \quad (2.2\text{-}211)$$

$$h = e(T^\circ) + pv = e(T^\circ) + RT^\circ = h(T^\circ) = \int CpdT^\circ + \text{const.} \quad (2.2\text{-}212)$$

If the flowing gas is in addition treated as calorically perfect,

$$Cp = \text{const} \qquad Cv = \text{const}$$
$$h = CpT^\circ + \text{const}. \quad (2.2\text{-}213)$$

(vii) Adiabatic Reversible Processes

Processes in which no heat is transferred from or to a closed system (insulated systems) and the work is presumed completely reversible (no currents), are called adiabatic reversible in general. The gas as a medium is necessarily treated as ideal, i.e., satisfying the simple equation of state, although it may not be necessarily either thermally or calorically perfect. In case of flowing gases, possessing an ordered bulk matter velocity which necessitates a respective pressure drop (and work, vdp) in the flow direction, the adiabatic reversible process implies as a necessary condition a complete absence of dissipative effects, i.e., the gas is necessarily treated as ideally inviscid $\mu = 0$ and non-conducting $k = 0$. Since under the adiabatic reversible premises no entropy changes occur,

$$dS = 0, \quad (2.2\text{-}214)$$

the process is called isentropic. Respectively useful specific thermodynamic relationships for ideal gases are (no restrictions regarding thermal and calorical qualities):

$$e = e(T^\circ, v),\ h = h(T^\circ, p),\ pv = RT^\circ,\ v = \frac{1}{\rho}, \quad (2.2\text{-}215)$$

$$de = \left(\frac{\partial e}{\partial v}\right)_T dv + \left(\frac{\partial e}{\partial T^\circ}\right)dT^\circ = -pdv, \quad (2.2\text{-}216)$$

$$dh = \left(\frac{\partial h}{\partial p}\right)_T dp + \left(\frac{\partial h}{\partial T^\circ}\right)dT^\circ = de + pdv + vdp = vdp, \quad (2.2\text{-}217)$$

$$\therefore\ \frac{dT}{dv} = -\frac{1}{Cv}\left[\left(\frac{\partial e}{\partial v}\right)_T + p\right] \quad (2.2\text{-}218)$$

$$\frac{dT}{dp} = -\frac{1}{Cp}\left[\left(\frac{\partial h}{\partial p}\right)_T - v\right], \quad (2.2\text{-}219)$$

$$\frac{dp}{dv} = -\frac{p}{v}\frac{dh}{de} \cdot \qquad (2.2\text{-}220)$$

For a thermally perfect gas:

$$e = e(T^\circ), \quad h = h(T^\circ), \quad C_p = C_p(T^\circ), \quad C_v = C_v(T^\circ)$$

$$R = C_p C_v, \quad \gamma = \frac{C_p}{C_v} = \gamma(T^\circ) , \qquad (2.2\text{-}221)$$

$$\frac{v}{T^\circ}\frac{dT^\circ}{dv} = -\frac{R}{C_v} = 1-\gamma , \qquad (2.2\text{-}222)$$

$$\frac{p}{T^\circ}\frac{dT^\circ}{dp} = \frac{R}{C_p} = \gamma - 1 , \qquad (2.2\text{-}223)$$

$$\frac{d}{p}\frac{dp}{dv} = -\frac{C_p}{C_v} = -\gamma . \qquad (2.2\text{-}224)$$

For a thermally and calorically perfect gas:

$$C_p = \text{const}, \quad C_v = \text{const}, \quad \gamma = \text{const}, \qquad (2.2\text{-}225)$$

$$v = \text{const} \times T^{-1/(\gamma-1)} , \qquad (2.2\text{-}226)$$

$$p = \text{const} \times T^{\gamma/(\gamma-1)} , \qquad (2.2\text{-}227)$$

$$p = \text{const} \times v^{-\gamma} = \text{const}\ \rho^{\gamma} . \qquad (2.2\text{-}228)$$

(viii) Special Adiabatic Irreversible Processes

In presence of viscosity, μ, and internal heat conductivity, k, the adiabatic processes in flowing gases become irreversible. The following specific statements are then conditionally valid:

(a) The internal energy content (per unit mass), e, in a spontaneous expansion process under adiabatic conditions remains unchanged for the initial and the final equilibrium states, i.e., after the thermal (heat conduction) and the molecular (viscous) internal currents have subsided:

$$e_2 = e_1 . \qquad (2.2\text{-}229)$$

If the gas is additionally presumed to be thermally perfect, the initial and the final equilibrium temperatures are the same

$$T_2^\circ = T_1^\circ . \qquad (2.2\text{-}230)$$

(b) In a limiting case, the enthalpy (per unit mass), h, at any two points of an ideal gas flowing through a discrete resistance is the same, $h_1 = h_2$, provided the system is adiabatic (insulated) and the fluid flow is slow enough so that the kinetic energy of the ordered motion (per unit mass), $\frac{1}{2}V^2$, is negligible compared with enthalpy (per unit mass). (Joule-Thompson's classical experiment)

For thermally perfect gases, the equilibrium temperatures are the same

$$T_2^\circ = T_1^\circ . \qquad (2.2\text{-}230)$$

(c) The introduction of isentropic conditions results in the thermodynamic expressions and the energy equations cited in the preceding paragraph.

(ix) Real Gas Effects

In a broad sense, any deviations from the idealized gas concept

$$pv = RT^\circ \qquad (2.2\text{-}231)$$

reflects real gas effects. The real gas effects become increasingly important as the pressure, temperature, density increments or decrements and the associated structural, kinetic, chemical and electromagnetic internal properties of a flowing gas start deviating appreciably from their near-standard reference values.

For atmospheric flight conditions, the real gas effects become of importance whenever the ambient air flow undergoes large changes in state variables. The situation is readily encountered at hypersonic flow speeds in general, and for blunt body configurations in particular, primarily due to appearance of strong bow shocks which may cause considerable jumps in pressures, temperatures and densities. As a consequence, in the regions behind strong shocks the thermodynamic, chemical and electromagnetic properties of air depart considerably from the usual near-standard conditions, and the usual near-perfect idealizations of gas states cease to be a valid approximation.

For practical purposes, it is convenient to distinguish between real

gas effects in the continuum and in the rarefied (slip, transitional and free molecular) flow regimes. In the subsequent text the continuum flow case is treated mainly. Furthermore, the real gas effects may be usefully traced to three main physical sources: (1) due to high temperatures, (2) due to high pressures or densities, (3) due to radiation. The high temperature effects are of a predominant interest for aerodynamic force analysis.

(x) Limitation of the Gaseous Phase

Equation of state of an ideal gas concept implied a preservation of its gaseous phase up to the absolute zero. The extrapolation is unreal, since according to the third law of thermodynamics, it is impossible in reality by any finite number of processes to reduce any system to the absolute zero temperature, even if the processes were idealized.

Actually, every real gas becomes liquified for some specific combinations of temperature, pressure and density. Provided the chemical molecular properties of a gas are kept intact (no dissociation and ionization), the highest temperature at which the liquification is possible is termed the critical absolute temperature of the particular gas, T_c°, and the corresponding pressure and density are called critical pressure, p_c, and critical density, ρ_c, respectively.

(xi) Real Gas Equation of State - Analytical Considerations

A real gas equation of state that may be extended beyond the restrictions of near-standard conditions, includes the modifications in pressure-temperature-density functional relationships as any of the three variables change, i.e., beyond the approximations of Boyle-Mariotte, Gay-Lussac and Charles classical near-standard laws, which constitute special cases of the idealized equation of state.

For highly variable thermal and dynamic conditions, possibly as encountered during different atmospheric flight and re-entry phases, the variety of accompanying real gas effects can be analytically represented by an implicit "compressibility function Z," in the thermal equation of state(12)

$$\frac{pv}{RT^\circ} = Z(p, T^\circ) \qquad (2.2\text{-}232)$$

where the different explicit forms of the Z-function depend upon the pressure and the temperature induced changes in dynamical, structural, chemical and electromagnetic states of gas on molecular and atomic levels.

(xii) High Density Effects

At near standard (sea-level) reference pressures and temperatures, air is treated as a slightly rarefied gas whose equilibrium thermodynamic condition is well approximated by the simple idealized equation of state with $Z = 1$, see Eq (2.2-231).

At near-standard and/or not-too-low temperatures (cryogenics excluded) but at higher pressures, the increased gas densities cause considerable changes in intensities of intermolecular acting forces. Provided the gaseous phase is preserved, i.e., above the highest critical temperature, T_c, and the corresponding critical pressure, p_c, of liquification, the changes in equilibrium states of a gas due to enhanced compressions are expressed by the Van der Waal's equation of state in a first approximation:

$$\frac{pv}{RT^\circ} = Z(p, T^\circ) = 1 + b(T^\circ)\frac{p}{RT^\circ}, \qquad (2.2\text{-}233)$$

where

$b(T^\circ)\frac{b}{RT^\circ}$ - is called the "second virial coefficient", which is a dimensionless quantity. It is a characteristic function for a particular gas, i.e., its value is different for different real gases,

$b(T^\circ)$ - is a volumetric term, expressing the second virial change of volume per unit mass.

Introducing the individual gas characteristic critical temperature, T_c°, pressure, p_c, and specific volume, v_c, Eq (2.2-233) takes a more explicit dimensionless form

$$\frac{pv}{RT^\circ} = 1 + \frac{p_c v_c}{RT_c^\circ}\,\frac{p}{p_c}\,\frac{T_c^\circ}{T^\circ}\,\frac{b(T^\circ)}{v_c}. \qquad (2.2\text{-}235)$$

Furthermore, with $(p\,v)/(R\,T^\circ) = k \sim .295$ and with $b(T^\circ)/v_c = \phi(T_c^\circ/T^\circ)$ treated as a universal function for most of atmospheric air gaseous components, the Eq (2.2-235) takes a generalized approximate form:

$$\frac{p\,v}{R\,T^\circ} = 1 + \frac{p}{p_c}\,\phi\left(\frac{T_c^\circ}{T^\circ}\right) \qquad (2.2\text{-}236)\cdot$$

Critical data and characteristic temperatures for most important atmospheric air gaseous components, and the respective numerical values of the generalized ϕ-function (in the CGS system of units) are[12]:

	p_c (atm)	T_c° (°K)	R $\left(\frac{atm\ cm^3}{gr\ °k}\right)$	$\frac{p_c v_c}{R\,T_c^\circ}$	T_v° (°K)	T_D° (°K)	T_i° (°K)	
O_2	49.7	154.3	2.54	.292	2230	59,000	158,000	O
N_2	33.5	126.0	2.93	.292	3340	113,300	168,800	N
NO	65.0	179.1	2.73	.255	2690	75,500	--	
H_2	12.8	33.2	40.7	.306	6100	52,400	157,800	H
He	2.26	5.2	20.5	.306	--	--	285,400	He
Ar	48.0	151.1	2.05	.291	--	--	182,900	Ar
CO_2	73.0	304.2	1.86	.280	954	~40,000	130,800	C

T_c°/T°	.1	.2	.4	.6	.8
ϕ	.009	.015	-.005	-.067	-.18

where T_v°, T_D° and T_i° refer to the characteristic temperatures of vibration, dissociation, and ionization respectively, as specified in the next paragraph.

For moderately dense gases[12] at near standard reference temperatures, another convenient form of the Van der Waal's equation of state can be used as a criteria of errors in treating the real gases as ideally perfect. In it, the critical (highest) temperature of liquification, T_c°, and the corresponding critical pressure, p_c, appear as two additional individual gas constants, the third being the classical individual gas constant, R:

$$p = \rho\,RT^\circ\left[\frac{1}{1-\beta\rho} - \frac{a\rho}{RT^\circ}\right], \qquad (2.2\text{-}237)$$

$$\frac{a}{\beta} = \frac{27}{8}\,RT^\circ, \qquad \frac{a}{\beta^2} = 27\,p_c \cdot \qquad (2.2\text{-}238)$$

The corresponding Van der Waal's internal energy expression is (per unit mass)

$$e(v, T^\circ) = e_o(T^\circ) - \frac{a}{v} \qquad (2.2\text{-}239)$$

where $e_o(T^\circ)$ is the ideal gas internal energy content.

For gases at lower pressures, the ideal gas law takes the form of the Berthelot Equation[17] (per unit mass):

$$\frac{p\,v}{RT^\circ} = \left\{1 + \frac{9}{128}\,\frac{p\,T_c^\circ}{p_c T^\circ}\left[1 - 6\left(\frac{T_c^\circ}{T^\circ}\right)^2\right]\right\}. \qquad (2.2\text{-}240)$$

Note: Eq (2.2-240) does not apply to really rarefied gas domains.

(xiii) <u>High Temperature Effects</u>

At higher temperatures and relatively

moderate pressures the inert degrees of molecular freedom (vibration, dissociation and ionization) become aroused in the indicated sequence, the corresponding critical temperatures being individual characteristics of each gas. Monoatomic gases are subject to ionization exclusively.

For gaseous mixtures (air), the chemically activated components may bring reactions in the dissociated (diatomic) and ionized monoatomic states, such as formation of NO.

The equation of state of a dissociating diatomic gas in equilibrium (the rate of dissociation equal to the rate of recombination) is (per unit mass)(28)

$$\frac{pv}{R_2 T^\circ} = Z(p, T^\circ) = 1 + \alpha \qquad (2.2\text{-}241)$$

$$\alpha = \frac{m_1}{m_1 + m_2} = \alpha(p, T^\circ) \qquad (2.2\text{-}242)$$

where

R_2 - is the molecular gas constant of an individual diatomic gas undergoing dissociation (O_2, N_2, H_2, NO, etc.),

α - defines the equilibrium degree of dissociation, $\alpha = M_1 / M_1 + M_2$,

M_1 and M_2 - are the fractional masses of atoms and molecules of a diatomic gas in dissociative equilibrium, $M_1 + M_2 = 1$.

The equilibrium degree of dissociation, $\alpha(p, T^\circ)$, has in general, different numerical values for different (p, T°) combinations, the variational law being individual for each specific diatomic real gas. In a first approximation, a generalized functional relationship for all diatomic gases

$$\alpha\left(\frac{T^\circ}{T_D^\circ}, p\right) \qquad (2.2\text{-}243)$$

can be accepted, since the individual diatomic gas differences in the expression (2.2-242) are relatively small when the ratio of the actual temperature, T°, and the so-called "characteristic temperature" for dissociation, T_D°, is introduced:

$$\frac{T^\circ}{T_D^\circ} < 1, \qquad T_D^\circ = \frac{I_D}{R_2}, \qquad (2.2\text{-}244)$$

where

$I_D = (h_1 - h_2)$ - is the characteristic heat of dissociation, i.e., the latent heat required to dissociate a unit mass of diatomic molecules into atoms (for instance ($O_2 \rightarrow 2O$) at constant T° and p),

h_1 and h_2 - are enthalpies per unit mass of the completely dissociated atoms (subscript 1), and of the initial diatomic molecules (subscript 2),

R_2 - is the individual gas constant of the initial diatomic molecular gas.

The approximate generalized families of curves $\alpha = \alpha(T^\circ/T_D^\circ, p)$ and $(h/I_D) = f(T^\circ/T_D^\circ, p)$ for all diatomic gases are presented in Fig (2.2-1) and (2.2-2), while the actual individual values of T_D° for different diatomic gases are tabulated on p. 2.2-51.

Note: the "characteristic" temperature of dissociation, T_D°, should not be confused with the notion of the actual critical temperature of dissociation, which is denoted by T° in the numerator of the expression (2.2-243). The equation of state for an ionized gas can be represented in the same functional form as (2.2-241) and (2.2-242) by conducting an approximate unified treatment along the same lines as in the case of dissociation(28) For instance, when the temperature, T°, becomes sufficiently high, the oxygen dissociated atoms become a mixture of O^+ + , e and O species (in supposed equilibrium):

$$O^+ + e \rightleftarrows O \qquad (2.2\text{-}245)$$

to which the above approximate analysis is correspondingly fitted, with the "characteristic" temperature of ionization, T_I° tabulated on p.(2.2-51). Obviously, the respective families of unified curves will be similar but numerically different from those in Figs. (2.2-1) and (2.2-2)

Note that the characteristic heat of dissociation, I_D, represents the amount of energy required to break the interatomic binding forces within a

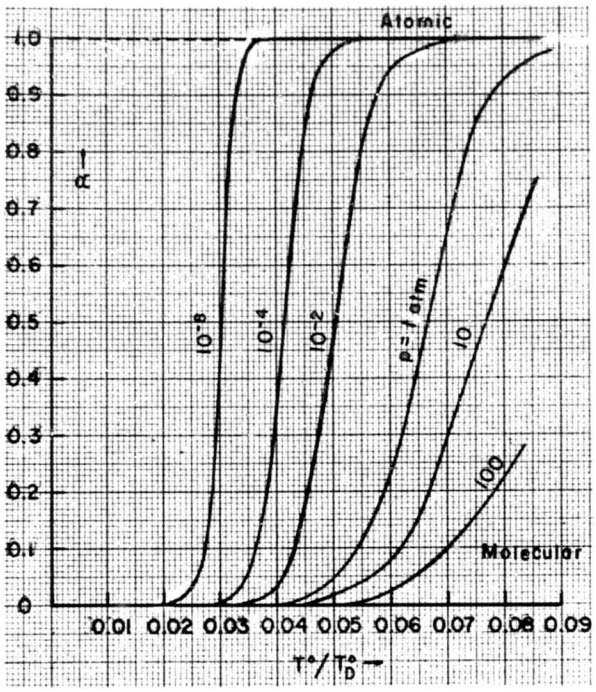

FIG. 2.2-1 Degree of dissociation versus reduced temperature for a dissociating diatomic gas. Ref. 28.

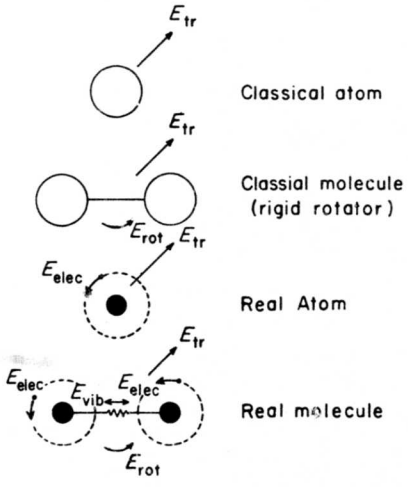

Fig. 2.2-3. Real diatomic gas models. Ref. 29.

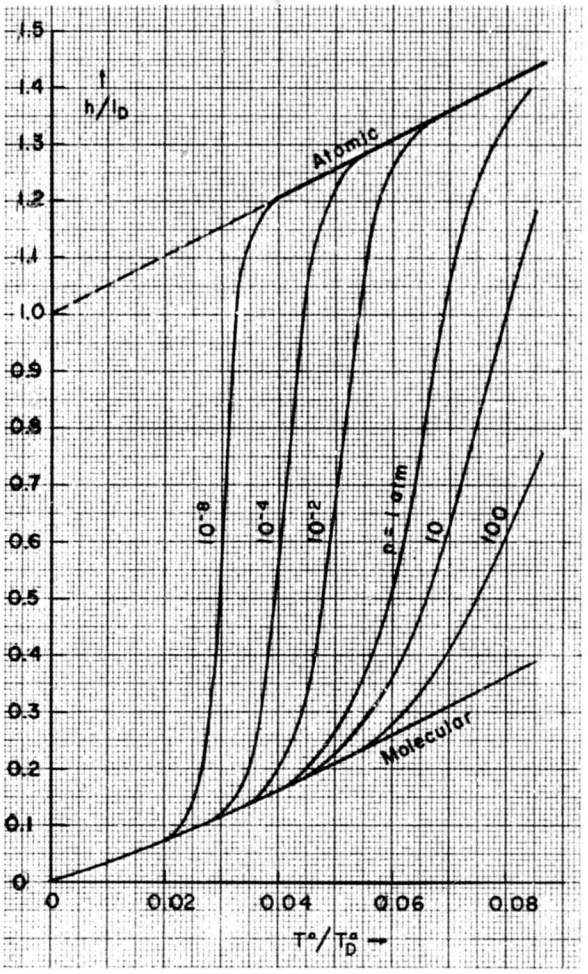

FIG. 2.2-2 Reduced enthalpy versus reduced temperature for a dissociating diatomic gas. Ref. 28.

molecule. Similarly, it can be argued that the Van der Waal's z-function represents some binding intermolecular energy, I_m, reflecting the intermolecular cohesive force effects for dense gases. Since

$$I_D \gg I_m \quad , \qquad (2.2\text{-}246)$$

and since the temperature and density ranges for dissociation and liquification are wide apart, there is no need to introduce in the dissociation Eq (2.2-241) any additional corrective terms of the dense gas (Van der Waal's) form, even if densities when dissociation takes place are considerably above near-standard.

(xiv) Internal Energy Content and Degrees of Molecular Freedom

The total internal energy content (per unit mass) of a real gas is conveniently broken into six main physically significant components(31):

- Kinetic energy of translation of molecules or atoms, e_t .
- Rotational energy of diatomic and polyatomic molecules, e_r .
- Vibrational energy of diatomic and polyatomic molecules, e_v .
- Energy of dissociation (and recombination) of diatomic and polyatomic molecules into atoms or groups of atoms, e_d .
- Energy of electronic excitation (ionization) of molecules and atoms, e_e .
- Electromagnetic or radiation energy of molecules and atoms, e_{rad}.

The above subdivision (except for radiation term) is based on the concept of totality of possible internal degrees of freedom for polyatomic gases in general, as recognized in the classical kinetic, the statistical mechanics and the quantum mechanics theories. The triple theoretical combination is necessary in order to account for all the internal degrees of freedom, the first two theories being inadequate for the complex purpose. Furthermore, in all cases the empirical corrections are unavoidably introduced, reflecting the actual energetic deviations of individual gases from the theoretically predicted values.

Theoretically, the total or mean internal energy of a molecule is a partial linear sum of the six independent energetic components. Expressed per unit mass:

$$e = e_t + e_r + e_v + e_d + e_e + e_{rad} \, . \qquad (2.2\text{-}247)$$

The expression (2.2-247) is conditionally based on three fundamental assumptions:

(a) An average equilibrium level in each of the degrees of freedom is presumed for a given amount of gas,

(b) Each degree of freedom is independent of all the others, i.e., there is no interaction between them,

(c) Each degree of freedom (except radiation) contributes $(kT^\circ/2)$ to the mean energy of a molecule, where k is the Boltzmann's constant. The assumption is known as the "energy equipartition" theorem(7).

In the partial listing of energies, the adopted sequence of degrees of freedom corresponds to the succession in which they are normally aroused with increasing temperature levels. Although all of them may in a variable degree of intensity exist similtaneously at any given temperature, T°, the significant average excitation levels for each group of degrees of freedom are reached (in average, and for a great number of molecules) only at specific critical temperatures (and pressures), the critical T_c° values varying for different individual gases.

Before a rational numerical assessment of the internal energies is attained, the few pertinent premises from the equilibrium kinetic theory of gases and from empirical evidence are briefly stated next.

(xv) Simplified Molecular Models and Degrees of Freedom

Four distinct categories of gaseous molecules are conceived:

(a) A monoatomic molecule, (He, A, etc.)
(b) A diatomic molecule of a "dumbell" model (H_2, O_2, N_2, NO, etc.)
(c) A polyatomic molecule, having all the atoms arrayed in a straight line, i.e., in the form of an extrapolated "dumbell" (CO_2 etc.)
(d) A polyatomic molecule with an arbitrary spatial arrangement of atoms.

The models are a theoretical supposition, each of them being representative for all the monoatomic, diatomic

and polyatomic gases respectively, i.e., eventual individual gas deviations from the idealized representative model should be, when necessary, correctively introduced on the basis of respective empirical evidence. The idealized models and the respective possible degrees of freedom in translation, rotation and vibration are illustrated in Fig (2.2-3).

Degrees of Freedom	Translation n_t	Rotation n_r	Vibration n_v
Monoatomic	3	--	--
Diatomic	3	2	$(3N_a - 5) = 1$
Polyatomic in line	3	2	$(3N_a - 5)$
Polyatomic in general	3	3	$(3N_a - 6)$

Note: N_a is the number of atoms in a polyatomic molecule

The possible degrees of freedom are classed into "active" (translation and rotation) and "inert" (vibration, dissociation and ionization). The distinction is based on the usual state of gas at near-standard ($p, \rho, T°$) reference states, as represented by the "active" degrees exclusively, while the "inert" degrees are aroused (in an abrupt manner) only at the respective higher (critical) temperatures and pressures. For instance, at near-standard conditions a diatomic gas is approximated by a rigid "dumbell" or "rigid rotor" model. The rigid model possesses then only the "active" degrees of freedom: three in translation and two in rotation, the third rotational degree of freedom about the rigid axis taken as negligible energetically. At a specified higher critical temperature, $T°_{cv}$, the vibrational degree of freedom is aroused, i.e., the link is treated as a simple harmonic oscillator.

(xvi) The Representative Monoatomic Molecular Model and Basic Definitions in the Classical Kinetic Theory in Gases

In the kinetic theory of gases[7] the term MOLECULE is conditionally used to represent either the physical concept of some regular neutral arrangement of atoms and electrons of a specified element, or composition of elements, or a single free atom and electron, or an ion.

Each molecule of a liquid can be treated as the center of a dual force field; repulsive for two molecules at close range, attractive (cohesive) at larger distances. A neutral equilibrium molecular distance defines a boundary between the two opposite fields.

In the gaseous state of matter the force fields are relatively weak and occur only for either extremely dense gases or during molecular collisions. Thus, during most of their individual time histories, the gas molecules are free, moving independently of each other with very wide variations in velocities of their individual random motion. The mean dimensions of molecules are small relative to the mean average distances between them, so that the Boltzmann's assumption of a molecular chaos can be introduced as a suitable representative model for the discrete internal molecular structure of a gas. As a consequence, there is no relation between the initial and instantaneous motions of various molecules, and there is no correlation between individual molecular position in any arbitrarily small volume of gas.

The kinetic theory in its simplest form works with idealized notions regarding the shape of individual molecules and the manner in which collisions between molecules occur. With the Boltzmann's concept of a molecular chaos, and some other simplifying assumptions, a relatively uncomplicated mathematical model is built:

(a) It is assumed that gas is at near-standard conditions, ($p, \rho, T°$), when it can be regarded as "slightly rarefied" possessing only weak force fields.

(b) Molecules of a gas are conceived as smooth, spherical masses of uniform diameters and possessing an unlimited rigidity and elasticity. Consequently, during collisions there is no interchange between internal (subatomic) energies, nor is there any loss of energy (deformations) during the idealized completely elastic encounters.

(c) The supposition of an idealized spherical shape is strictly justified for monoatomic molecules only. Actual polyatomic molecules would be better represented by a correspondingly multi-shaped combination of partially interpenetrated spheres, the number of "buldges" depending upon the number and the spatial arrangement of constituent atoms. Nevertheless, the simple spherical concept, corresponding strictly to monoatomic molecular structures, yields analytic results which, in a first approximation, can be taken as valid for diatomic and some polyatomic gases also, the additional corrections for the shape difference being eventually introduced from empirical evidence. The simple spherical shape implies existance of only translational degrees of freedom, i.e., it does not account for rotational and vibrational modes, which may become especially significant for polyatomic molecules. Furthermore, the introduction of a representative monoatomic spherical molecular model is equivalent to the assumption that physical properties of a gas depend primarily on the random translatory molecular motion, and not on their actual internal structure.

(d) Molecules of a gas may be alternatively conceived as possessing spherical symmetric repulsive force fields, acting at short distances between colliding pairs of molecules, the diameter of the force sphere being greater than for the assumed mass sphere. This concept used in investigation of molecular collisions for dense gases and in nonisentropic interactions between molecules and solid surfaces.

(e) The molecular collisions are presumed to be binary, i.e, involving only two molecules. This supposition seems well justifiable, since other more complex multiple forms of possible collisions are found to be statistically rare. Furthermore, the collisions are regarded as frictionless encounters.

(f) All the assumptions permit a direct and simple application of the classical principles of the conservation of momentum, energy and mass, without resorting to the more complex quantum mechanics analytic methods.

The final "bulk matter" expressions of the conservation principles in fluid dynamics theories are mathematically represented by the respective differential equations, which refer to microscopic (infinitesimal) arbitrary volumes (or mass contents) and thus necessarily require a continuum medium concept. The internal discrete molecular behavior is, on the other hand, investigated on the basis of representative binary collisions of molecules using the statistical methods and time-space mean averaging procedures. In order to express the kinetic theory molecular gas properties and findings in terms of the differential equations of the continuum concepts, it is necessary to define all mean-averaged physical quantities in such a way that a valid correlation between the real discrete molecular structure of matter and the continuum matter (microscopic) idealized suppositions is adequately ascertained. The objective is reached in the general form of the Boltzmann's integro-differential equation and in the more restrictive Maxwell's velocity distribution functions for isentropic and slightly non-isentropic equilibrium flow conditions[7], which can be then transformed into the usual differential form of the continuity, momentum and energy equations of the classical fluid mechanics.

(xvii) Main Results From the Monoatomic Kinetic Theory of Gases for Isentropic Conditions

Note: Some of the following expressions are alternatively given in terms of the universal Boltzmann's constant, k, and the individual gas constant, R. The respective definitions and inter-relationships are

$$k = \frac{R_o}{L} = \frac{\rho}{n} R = mR = R_M \quad , \quad (2.2\text{-}248)$$

where

k - is the Boltzmann's universal constant, defined per mole of a gas, $k = 1.380 \times 10^{-16}$ [erg deg^{-1}] $= 1.380 \times 10^{-1}$ [joule deg^{-1}]

R_o - is the universal gas constant, defined per mole of a gas, i.e., the same for all gases, $R_o = Lk = 8.31432$ [joule (°K)$^{-1}$mol

L - is the Avogadro's number per mole of a gas, the same for all gases, see definition p. (2.2-44)
$L = 6.02257 \times 10^{26}\,(kg\text{-}mol)^{-1}$, $= 6.02257 \times 10^{23}\,(gr\text{-}mol)^{-1}$

ρ - is the individual gas density, $\rho = mn = kn/R$.

n - is the individual gas number of molecules per unit volume, $[cm^{-3}]$.

R - is the individual gas constant per unit mass, $R = k/\rho$.

m - is the mass of a molecule, $[gr]$.

R_m - is the individual gas constant of a molecule, numerically equal to k, $R_m = k$.

For <u>isentropic</u> flows, characterized by a correspondingly special form of the Maxwellian velocity distribution function[7], the following physical parameters are conditionally defined:

- the mean (average) random molecular speed of translation:

$$\bar{c} = 2\left(\frac{2}{3}\frac{\overline{c^2}}{\pi}\right)^{\frac{1}{2}} = 2\left(\frac{2RT^\circ}{\pi}\right)^{\frac{1}{2}} . \qquad (2.2\text{-}249)$$

- the most probable random molecular speed of translation (i.e., the value possessed by the greatest number of molecules):

$$c_m = \left(\frac{2\overline{c^2}}{3}\right)^{\frac{1}{2}} = \left(2RT^\circ\right)^{\frac{1}{2}} . \qquad (2.2\text{-}250)$$

- The root-mean-square molecular speed of translation:

$$\left(\overline{c^2}\right)^{\frac{1}{2}} = 1.225 c_m = 1.086\,\bar{c} . \qquad (2.2\text{-}251)$$

- The mean (average) free path (between two collisions):

$$\bar{\lambda} = \frac{1}{2^{1/2}\pi n \sigma^2} . \qquad (2.2\text{-}252)$$

Under standard conditions, for air:

$$\bar{\lambda} = 6 \times 10^{-6}\ cm., \quad \sigma = 3.7 \times 10^{-8}\ cm. \qquad (2.2\text{-}253)$$

- Speed of sound (speed of propagation of small disturbances through a gas in thermal equilibrium) is a function of $\overline{c^2}$ or T° only, and independent of the source conditions of the small disturbance:

$$a = \left[\frac{2}{3}\left(\frac{1}{3}\overline{c^2}\right)\right]^{\frac{1}{2}} = \left(\gamma RT\right)^{\frac{1}{2}} = \left(\frac{\gamma p}{\rho}\right)^{\frac{1}{2}} . \qquad (2.2\text{-}254)$$

- Mach Number:

$$M = \frac{\bar{q}}{a} , \qquad \bar{q} = \left(\bar{u}^2 + \bar{v}^2 + \bar{w}^2\right)^{\frac{1}{2}} , \qquad (2.2\text{-}255)$$

where $\bar{q} = V$ is the mean (average) velocity of ordered motion for a great number of molecules.

- Specific heats ratio, γ:

The classical thermodynamics defines

$$\gamma = \frac{C_p}{C_v} , \qquad (2.2\text{-}256)$$

where C_p and C_v are specific heats per unit mass at constant pressure and at constant volume respectively. A connection between the above continuum thermodynamic definitions and the kinetic theory concepts is obtained as follows:

The constant-volume temperature rise, dT°, per unit mass of a flowing gas appears as an increment of the average internal (heat) energy per unit mass, $d\bar{E}/m$, only, without affecting the ordered gas motion:

$$C_v = \frac{1}{m}\left(\frac{d\bar{E}}{dT^\circ}\right)_{vol.} , \qquad (2.2\text{-}257)$$

where

m - is the mass of a molecule in grams,

$\bar{E}$ - is the mean-average internal energy of a molecule.

The constant-pressure temperature rise, dT°, per unit mass of a flowing gas appears both as an increment in the average internal (heat) energy, $d\bar{E}/m$ per unit mass, and as a mechanical work, $p = d(\frac{1}{\rho})$, per unit mass:

$$C_p\,dT^\circ = p\,d\left(\frac{1}{\rho}\right) + \frac{d\bar{E}}{m} , \qquad (2.2\text{-}258)$$

i.e., with

$$p = \rho R T^\circ, \qquad \therefore\ p\,d\left(\frac{1}{\rho}\right) = R\,dT^\circ, \tag{2.2-259}$$

it follows that

$$C_p = R + \frac{1}{m}\left(\frac{d\bar{E}}{dT^\circ}\right)_v = R + C_v \tag{2.2-260}$$

For monoatomic gases possessing translatory degrees of freedom only,

$$n\bar{E} = \frac{1}{2} m\bar{c^2} n = \frac{1}{2}\rho\bar{c^2}, \qquad \therefore\ \frac{\bar{E}}{m} = \frac{1}{2}\bar{c^2}, \tag{2.2-261}$$

where (n) is the number of molecules per unit volume, and thus:

$$\frac{E}{m} = \frac{3}{2} R T^\circ, \tag{2.2-262}$$

$$\therefore C_v = \frac{3}{2} R T^\circ = \frac{3}{2}\frac{nk}{\rho} T^\circ \tag{2.2-263}$$

and

$$C_p = \frac{5}{2} R T^\circ = \frac{5}{2}\frac{nk}{\rho} T^\circ . \tag{2.2-264}$$

In the above expressions, R , is the gas constant per unit mass, related to the gas constant for one molecule $R_M = k$, by:

$$R_M = mR = k . \tag{2.2-265}$$

In general, denoting the total number of all the degrees of freedom possessed by a molecule with N , Eqs (2.2-260), (2.2-261) and (2.2-262) become:

$$\frac{\bar{E}}{m} = \frac{1}{2} N R T^\circ , \tag{2.2-266}$$

$$C_v = \frac{1}{2} N R , \tag{2.2-267}$$

$$C_p = R\left(1 + \frac{N}{2}\right) , \tag{2.2-268}$$

$$\gamma = \left(1 + \frac{2}{N}\right) . \tag{2.2-269}$$

where the underlying assumption is that an average internal energy per molecule

$$\bar{E} = \frac{1}{2} R_m T^\circ = \frac{1}{2} mRT^\circ = \frac{\bar{mc}^2}{2} \tag{2.2-270}$$

can be associated with each of the N degrees of freedom, provided the gas is in an equilibrium state (Equipartition of energy postulate).

Pressure in a monoatomic gas:

$$p = \frac{1}{3}\rho\bar{c}^2 = \frac{1}{3} mn\bar{c}^2 = \rho R T^\circ \qquad \therefore\ p = nkT^\circ . \tag{2.2-271}$$

Density:

$$\rho = mn = \frac{kn}{R} . \tag{2.2-272}$$

Temperature:

$$T^\circ = \frac{\bar{c}^2}{3R} = \frac{m\bar{c}^2}{3k} . \tag{2.2-273}$$

General relationships between the gas parameters for two points (1 and 2) in an isentropic flow:

$$\frac{a_1}{a_2} = \left(\frac{T_1^\circ}{T_2^\circ}\right)^{\frac{1}{2}} = \left(\frac{\rho}{\rho_2}\right)^{\frac{\gamma-1}{2}} = \left(\frac{p_1}{p_2}\right)^{\frac{\gamma-1}{2\gamma}} ,$$

$$\frac{\bar{\lambda}_1}{\bar{\lambda}_2} = \frac{\rho_2}{\rho_1} = \left(\frac{a_2}{a_1}\right)^{\frac{2}{\gamma-1}} . \tag{2.2-274}$$

(xviii) General Remarks Respective to the Presented Isentropic Flow Data:

(a) The concept of pressure as formulated in Eq (2.2-271) applies to all points within the gas, assuming mathematical surfaces and free molecule collisions. The expression (2.2-271) is recognized as ideal gas equation of state for non-flowing processes.

In case of flowing gases over real surfaces (bodies), the interaction between the impinging molecules and the real body surface may not, in general, follow the laws of the free intermolecular collisions, eventually requiring subsequent modifications in the pressure definition, see paragraph (x).

Furthermore, the adopted monoatomic molecular model represented by smooth, hard and absolutely elastic spheres, leads to the conclusion that the static pressure in a gas arises solely from the momentum transfer of random molecular motion in free collisions, which is an acceptable approximation for ordinary homogeneous gases at slightly rarefied conditions. A more general molecular model, including the effects of molecular finite size and shape, the effects of intermolecular forces etc., shall cause corresponding modifications of the above expressions.

(b) The introduced simplified monoatomic molecular model yields results which are in a good agreement with the microscopic concepts and observations of the ordinary continuum theory and experiments for the restrictive isentropic conditions. This is due to the fact that in a flowing gas only the component of the ordered motion, $\bar{q} = V$, is directly discernible and easily specified by the mass flow rate measurements, while the random molecular motion remains undetected. Nevertheless, due care should be exercised in applying the above simplified concepts to any particular real gas flow case. The energy of the random molecular motion is termed as "heat" in the equilibrium kinetic theory of gases, i.e., as a "hidden" energy form, which may be partially converted into a corresponding increase of the "visible" ordered motion of gas, or vice versa. As defined above, the heat energy is due to translatory random molecular motion only (monoatomic gas concept), the molecular collisions of the perfectly elastic molecular spheres resulting in a simple momentum exchange mechanism. For more complicated molecular models, having additional vibrational and rotational degrees of freedom, further terms shall appear in the correspondingly more general expression for the heat energy.

(c) The concept of temperature is arbitrarily introduced as a basic variable and a basic measure of the heat effects. The empirical definitions of temperature are given elsewhere (see p. 2.2-18). In the simplified equilibrium kinetic theory of gases, the temperature definition is based on the assumption that the molecules possess only the translatory degrees of freedom:

$$T^{\circ} = \frac{\bar{c}^2}{3R} = \frac{m\bar{c}^2}{3k} \quad , \qquad (2.2\text{-}275)$$

where the individual gas constant, R , is referred to unit mass, and k is the Boltzmann's universal constant.

A subsequent introduction of the rotational degrees of freedom for polyatomic gases shall not affect the kinetic theory definition of temperature, since the translatory and the rotational degrees coexist independent of each other. But, the total internal energy content of a polyatomic and diatomic molecule shall be correspondingly greater than for monoatomic at the same kinetic temperature level, a fact which is also expressed by the respectively changed values of specific heats. When, due to any external heat sources or bulk matter flow characteristics (shock waves), the absolute temperatures are sufficiently raised, and the inert degrees of freedom (vibration, dissociation, ionization) are excited, part of the translational kinetic energy of particle motion shall be used up in the process of activation of the inert degrees, resulting in a corresponding drop of kinetic temperature, see Fig (2.2-4). These temperature changes cannot be expressed on the grounds of the monoatomic equilibrium kinetic theory of gases, i.e., the simple ideal gas equation of state needs to be modified so that the effects of changed internal energetic levels, associated with the excitation of other degrees of molecular freedom, can be assessed.

(d) The adopted idealized molecular model as represented by completely hard and infinitely elastic spheres in a chaotic motion, possessing translational velocity components only (monoatomic

gases), leads to the conclusion that the individual binary molecular collisions are a reversible process. Nevertheless, according to the second law of thermodynamics, the time-trend of the successive states of a whole system of a great number of molecules is not a priori reversible: the state of a gas as a whole is determined by all molecular encounters at any instant of time, and thus either may remain stationary, or else must definitely have a trend towards an increase in entropy as the time passes. Consequently, there is need to define a specific function which would reflect

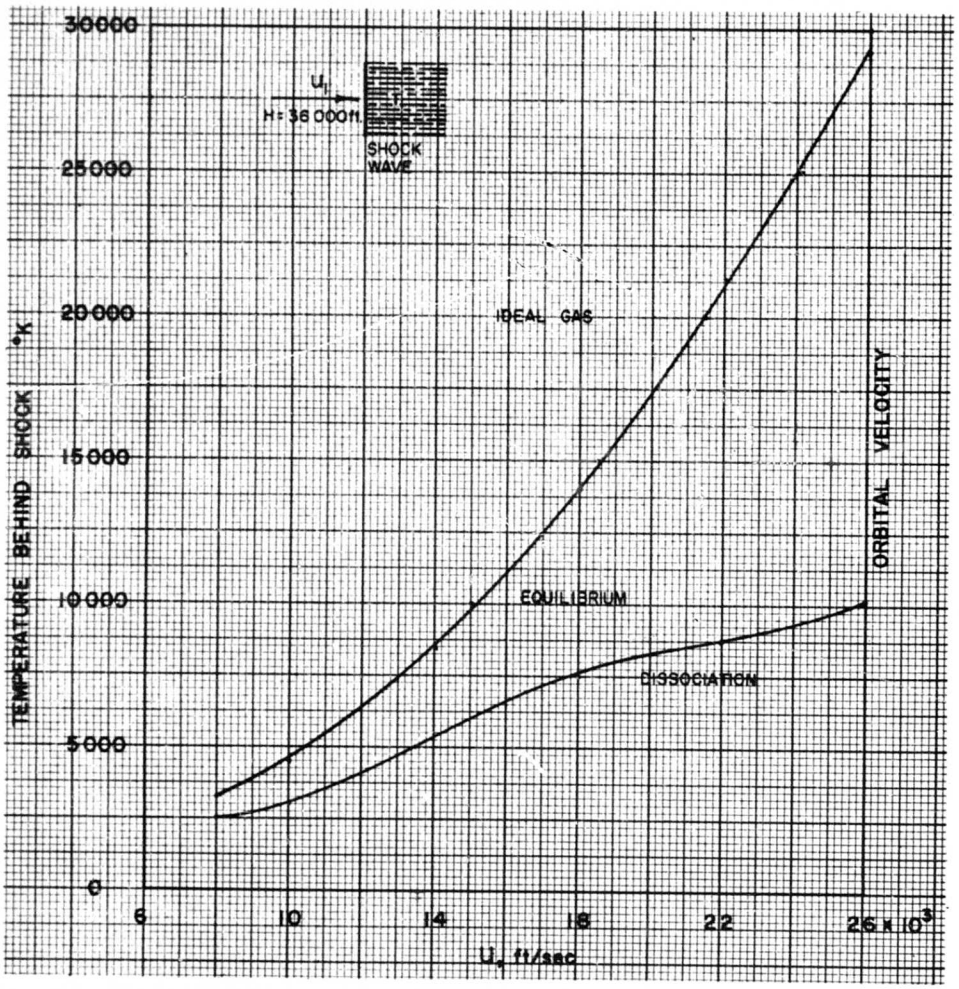

FIG (2.2-4) COMPARISON OF REAL AND IDEAL TEMPERATURES BEHIND A NORMAL SHOCK WAVE.

this irreversible tendency of successive states. This function, which is called the Boltzmann's H-function for a molecular system, must be in an explicit way related to the classical thermodynamic concept of entropy, S . Due to restrictions in the thermodynamic definition of S , the sought relationship between H and S can be reached only under condition of a stationary equilibrium state, yielding for monoatomic gases per unit mass(7):

$$S = -mRH + \text{const.}, \qquad (2.2\text{-}276)$$

where

$$S = R \log_e \left(\frac{T_o^{3/2}}{\rho}\right) + \text{const.} \qquad (2.2\text{-}277)$$

is derived for stationary equilibrium state, and

$$H_m = \frac{1}{m} \log_e \left[n\left(\frac{3}{2\pi \bar{c}^2}\right)^{3/2} \right] + \text{const.} \qquad (2.2\text{-}278)$$

is the "H" function per unit mass, derived and valid for both stationary and flowing gas equilibrium states.

(e) The equilibrium state of a gas (stationary or flowing) in the kinetic theory of gases is defined as the special case when the Boltzmann's integro-differential equation(7) reduces to zero. Such a special equilibrium motion (or state of rest) of a gas is said to have a "Maxwellian velocity distribution"(7). This Maxwellian condition of the kinetic theory corresponds to the isentropic change of state of the classical thermodynamics.

(f) Although the entropy relationship (2.2-276) is strictly valid for stationary (nonflowing) equilibrium states only, it is conditionally extended to cover the isentropic (flowing) equilibrium states also. The argumentative supposition is that for an exclusively isentropic flow, the Maxwellian law of molecular velocity distribution, (i.e., the adiabatic reversible equilibrium), holds throughout, if the initial molecular motion (at "infinity") in the gas occurs while the gas is at rest in an initially stationary equilibrium state.

(xix) Internal Energy Content in Flowing Gases

The classical equilibrium kinetic theory of slightly rarefied gases (i.e., at near standard conditions) is based on a simple monoatomic molecular model. For more complex molecular structures, as well as for gas conditions appreciably different from near-standard, the additional degrees of freedom of the molecular motion appear, changing subsequently the numerical values of all the physical variables and the form of the associated physical concepts and laws.

The conceptional modifications associated with the increased number of molecular degrees of freedom can be best formulated by investigating their effects on the overall internal energetic content of a gas, since this energetic level is a direct function of the state of intrinsic molecular motion. In general, the total internal energy per unit mass for a stationary gas can be expressed as

$$e = \beta \frac{p}{\rho}, \qquad (2.2\text{-}279)$$

where β is a dimensionless coefficient. Its value depends on the existing number of degrees of freedom of molecular motion.

Assuming that the ideal gas equation of state

$$p = \rho R T^\circ, \qquad (2.2\text{-}280)$$

remains valid (i.e., excluding both markedly dense and rarefied gaseous states), the expression (2.2-279) becomes

$$e = \beta \frac{p}{\rho} = \beta R T^\circ. \qquad (2.2\text{-}281)$$

For flowing gases, restricted to steady equilibrium isentropic conditions, the overall energy equation can be written in the convenient finite form (dissipation $\phi \equiv 0; k \equiv \mu \equiv 0$),

$$e + \frac{1}{2}\bar{q}^2 = \bar{e} + \frac{p}{\rho} = \beta \frac{p}{\rho} = \beta R T^\circ \qquad (2.2\text{-}282)$$

$$\therefore\ e = (\beta - 1)\frac{p}{\rho} = (\beta - 1) R T^\circ, \qquad (2.2\text{-}283)$$

where

$\bar{q}^2 = (\bar{u}^2 + \bar{v}^2 + \bar{w}^2)$ - is the speed of

ordered motion of a flowing gas.

$(1/2)^{-2}q$ - is the kinetic energy per unit mass. For isentropic flows, it is equal to the work done by pressure per unit mass, p/ρ. The coefficient β is nondimensional and refers to the total energy of flowing gases per unit mass:

$$\beta = \frac{e + \frac{p}{\rho}}{\frac{p}{\rho}} = e + 1, \qquad (2.2\text{-}284)$$

and since according to Eq. (2.2-247):

$$e = e_t + e_r + e_v + e_d + e_e, \qquad (2.2\text{-}284A)$$

it follows that

$$\beta = \beta_t + \beta_r + \beta_v + \beta_d + \beta_e + 1. \qquad (2.2\text{-}285)$$

where subscripts t, r, v, d, e refer to the translational, rotational, vibrational, dissociated and ionized degrees of freedom, respectively.

(xx) Internal Energy Due to Active Degrees of Molecular Freedom

The three translational ($n_t = 3$) degrees of freedom exist with all molecules; they are the only degrees of freedom for monoatomic molecular structures at near-standard conditions in particular. Since according to kinetic theory for monoatomic gases,

$$n_t = 3, \quad e_t = \frac{\bar{E}_t}{m} = \frac{n_t}{2}\frac{p}{\rho} = \frac{3}{2}RT^\circ, \qquad (2.2\text{-}286)$$

it follows that (per unit mass) for all gases:

$$\beta_t = \frac{e_t}{RT^\circ} = \frac{n_t}{2} = \frac{3}{2}, \qquad (2.2\text{-}287)$$

$$Cv_t = \frac{n_t}{2}\frac{p}{\rho T^\circ} = \frac{3}{2}R.$$

The internal energy (per unit mass), $\bar{e}_r$, due to rotational degrees for all gases is as predicted by the corrected average values from kinetic theory of gases:

For monoatomic gases:

$$n_r = 0, \quad e_r = 0, \quad \beta_r = 0, \quad Cv_r = 0. \qquad (2.2\text{-}288)$$

For diatomic gases (except H_2) and polyatomic gases with atoms arranged along a straight line (such as CO_2):

$$n_r = 2, \quad e = \frac{n_r}{2}\frac{p}{\rho} = RT^\circ,$$

$$\beta_r = \frac{e_r}{RT^\circ} = 1,$$

$$Cv_r = \frac{n_r}{2}\frac{p}{\rho T^\circ} = R. \qquad (2.2\text{-}289)$$

For all other polyatomic gases:

$$n_r = 3, \quad e_r = \frac{n_r}{2}\frac{p}{\rho} = \frac{3}{2}RT^\circ,$$

$$Cv = \frac{n_r}{2}\frac{p}{\rho T^\circ} = \frac{3}{2}R. \qquad (2.2\text{-}290)$$

Combining the translational and the rotational degrees of freedom, the following summary expressions for idealized gases near standard conditions, i.e., possessing only the active degrees of freedom (subscript a), are obtained:

For monoatomic gases:

$$n_a = n_t = 3,$$

$$e_a = e_t = \frac{n_t}{2}RT^\circ = \frac{3}{2}RT^\circ,$$

$$\beta_a = \beta_t = \frac{e_t}{RT^\circ} = \frac{3}{2},$$

$$Cv = Cv_t = \frac{n_t}{2}R = \frac{3}{2}R,$$

$$Cp = Cv + R = \frac{(n_t+2)}{2}R = \frac{5}{2}R,$$

$$\gamma = \frac{Cp}{Cv} = \frac{(n_t+2)}{n_t} = \frac{5}{3}. \qquad (2.2\text{-}291)$$

For diatomic gases (except H_2) and polyatomic gases with atoms arranged in a straight line:

$$n_a = n_t + n_r = 5,$$

$$e_a = e_t + e_r = \frac{(n_t + n_r)}{2} RT^\circ = \frac{5}{2} RT^\circ,$$

$$\beta_a = \beta_t + \beta_r = \frac{Ca}{RT^\circ} = \frac{5}{2},$$

$$Cv = Cv_t + Cv_r = \frac{(n_t + n_r)}{2} R = \frac{5}{2} R,$$

$$Cp = Cv + R = \frac{(n_t + n_r) + 2}{2} R = \frac{7}{2} R,$$

$$\gamma = \frac{Cp}{Cv} = \frac{(n_t + n_r) + 2}{(n_t + n_r)} = \frac{7}{5}.$$

(2.2-292)

For all other polyatomic gases:

$$n_a = n_t + n_r = 6,$$

$$e_a = e_t + e_r = \frac{(n_t + n_r)}{2} RT^\circ = 3RT^\circ,$$

$$\beta_a = \beta_t + \beta_r = \frac{e_a}{RT^\circ} = 3,$$

$$Cv = Cv_t + Cv_r = \frac{(n_t + n_r)}{2} R = 3R,$$

$$Cp = Cv + R = \frac{(n_t + n_r) + 2}{2} R = 4R,$$

$$\gamma = \frac{Cp}{Cv} = \frac{(n_t + n_r) + 2}{(n_t + n_r)} = 1 + \frac{2}{(n_t + n_r)} = 1 + \frac{2}{n_a} = \frac{4}{3}.$$

(2.2-293)

(xxi) Internal Energy Due to Vibrational Degrees of Freedom

As the temperatures are raised and the inert degrees of freedom for each gaseous component are successively aroused, the idealized approximation of the classical kinetic theory of gases become increasingly inaccurate. The corresponding predictions of the

$$e = e(p, T^\circ),$$

$$Cp = Cp(p, T^\circ),$$

$$Cv = Cv(p, T^\circ).$$

(2.2-294)

functional variations are beyond the scopes of the classical thermodynamic theory, and the functional variations must be obtained by a combined experimental and quantum statistical mechanics methods.

When the inert degrees of freedom are excited, the gases cannot be treated (even approximately) as thermally and calorically perfect. In general, the deviations from the idealized gas concepts are implicitly expressed by the respectively more general forms of the thermal and the caloric equations of state (per unit mass),[29]

$$pv = Z(p, T^\circ) RT^\circ, \quad v = \frac{1}{\rho}, \qquad (2.2\text{-}295)$$

$$\frac{\partial h}{\partial p} = v - T^\circ \left(\frac{\partial v}{\partial T^\circ}\right)_p = -\frac{RT^{\circ 2}}{p} \left[\frac{\partial Z(p, T^\circ)}{\partial T^\circ}\right]_p,$$

(2.2-296)

$$Cp - Cv = \left(v - \frac{\partial h}{\partial p}\right)\left(\frac{\partial p}{\partial T^\circ}\right)_v = R \frac{\left[Z(p, T^\circ) + T^\circ \left(\frac{\partial Z(p, T^\circ)}{\partial T^\circ}\right)_p\right]^2}{Z(p, T^\circ) - p\left(\frac{\partial Z(p, T^\circ)}{\partial p}\right)_{T^\circ}}.$$

(2.2-297)

The vibrational degrees of freedom are appreciably aroused once the critical temperature, T°_{cv}, for a given gas is reached. The contribution of vibrational degrees of freedom to the internal energy level can be estimated by normal modes of vibrational, each mode interpreted as a harmonic oscillator. Thus, denoting the number of atoms in a molecule by Na, the respective numbers of normal modes (or vibrational degrees of freedom) are:

Gas Molecule	Number of Atoms	Number of Normal Modes
Monoatomic	Na = 1	$n_v = 0$
Diatomic	Na = 2	$n_v = (3Na - 5) = 1$
Polyatomic, atoms in a straight line	Na	$n_v = (3Na - 5)$
All other polyatomics	Na	$n_v = (3Na - 6)$

The internal energy rise per unit mass due to any one normal mode is then expressed by(7):

$$\frac{e_v}{n_v} = \Delta e_v = f(z)RT^\circ = \frac{z}{e^z-1}RT^\circ = \frac{z}{e^z-1}\frac{p}{\rho} ,$$

$$\text{or } \frac{e_v}{n_v} = f(z)RT^\circ = \frac{\beta_v}{N_v}RT^\circ = \beta_v' RT^\circ ,$$

(2.2-298)

$$z = \frac{h\nu}{kT^\circ} = \frac{h\nu}{mRT^\circ} = \frac{h\nu}{R_m T^\circ} ,$$

(2.2-299)

$$\text{or } z = \frac{1.438}{\lambda T^\circ} ,$$

where

$f(z) = z/e^z-1 = \beta_v' = \beta_v/n_v$ - is the vibrational internal energy coefficient per mode,

h - is the Planck's constant, $h = 6.625 \times 10^{-27}$ [erg sec],

k - is the Boltzmann's constant, $k = 1.380\ 10^{-16}$ [erg deg^{-1}]

ν - is the frequency of vibration of a normal mode, (waves per cm = cm^{-1}),

Na - is the number of atoms,

T° - is the absolute temperature, [deg.],

λ - is the wave length, [cm^{-1}],

$\lambda = 2345$ cm^{-1} for N_2

$\lambda = 1570$ cm^{-} for O_2

R - is the individual gas constant, [erg gr^{-1} deg^{-1}],

R_m - is the individual gas constant of a molecule, [erg deg^{-1}],

m - is the mass of a molecule, [gr],

$m = k/R = R_m/R$.

The frequency of molecular vibrations in any normal model, $\nu = 1/\lambda$, is obtainable from the respective band spectrum for each gas:

Gas molecule	Number of normal modes	Frequency in waves per cm
N_2	$n_v = (3Na - 5) = 1$	$\nu_{N_2} = 2345$
O_2	$n_v = (3Na - 5) = 1$	$\nu_{O_2} = 1570$
CO_2	$n_v = (3Na - 5) = 4$	$\nu_{CO_2} = 667$
		$\nu_{CO_2} = 667$
		$\nu_{CO_2} = 1336$
		$\nu_{CO_2} = 2350$

The vibrational internal energies (per unit mass) are:

For monoatomic gases ($N_v = 0$):

$$e_v = 0, \quad \beta_v = 0. \qquad (2.2\text{-}300)$$

For diatomic gases, except H_v ($N_v = 1$),

$$e_v = n_v RT^\circ \frac{z}{e^z-1} = \frac{z}{e^z-1}RT^\circ = \beta_v' RT^\circ = \beta_v RT^\circ ,$$

$$\beta_v = \frac{e_v}{RT^\circ} = \frac{z}{e^z-1} = n_v\beta_v' = \beta_v . \qquad (2.2\text{-}301)$$

For polyatomic gases with atoms arranged in a straight line ($N_v = 3Na-5$):

$$e_v = n_v RT^\circ \frac{z}{e^z-1} = (3Na-5)RT^\circ \frac{z}{e^z-1} = (3Na-5)\beta_v' RT^\circ ,$$

$$\beta_v = \frac{e_v}{RT^\circ} = n_v\beta_v' = (3Na-5)\beta_v' . \qquad (2.2\text{-}302)$$

For all other polyatomic gases:

$$e_v = n_v RT^\circ \frac{z}{e^z-1} = (3Na-6)RT^\circ \frac{z}{e^z-1} = (3Na-6)\beta_v' RT^\circ ,$$

$$\beta_v = \frac{e_v}{RT^\circ} = n_v\beta_v' = (3Na-6)\beta_v' . \qquad (2.2\text{-}303)$$

The coefficient $\beta = f(z) = z/(e^z - 1)$ (per mole) for diatomic gases can be obtained from Fig(2.2-5)as a function of temperature, provided pressures are not too high (dense gases) or not too low (rarefied gases).

The vibrational energy of many diatomic gases (such as N_2, O_2) is negligibly small at ordinary temperatures, but for some other gases, as CO_2 for instance, the vibrational energy may be appreciable, even for near-standard conditions.

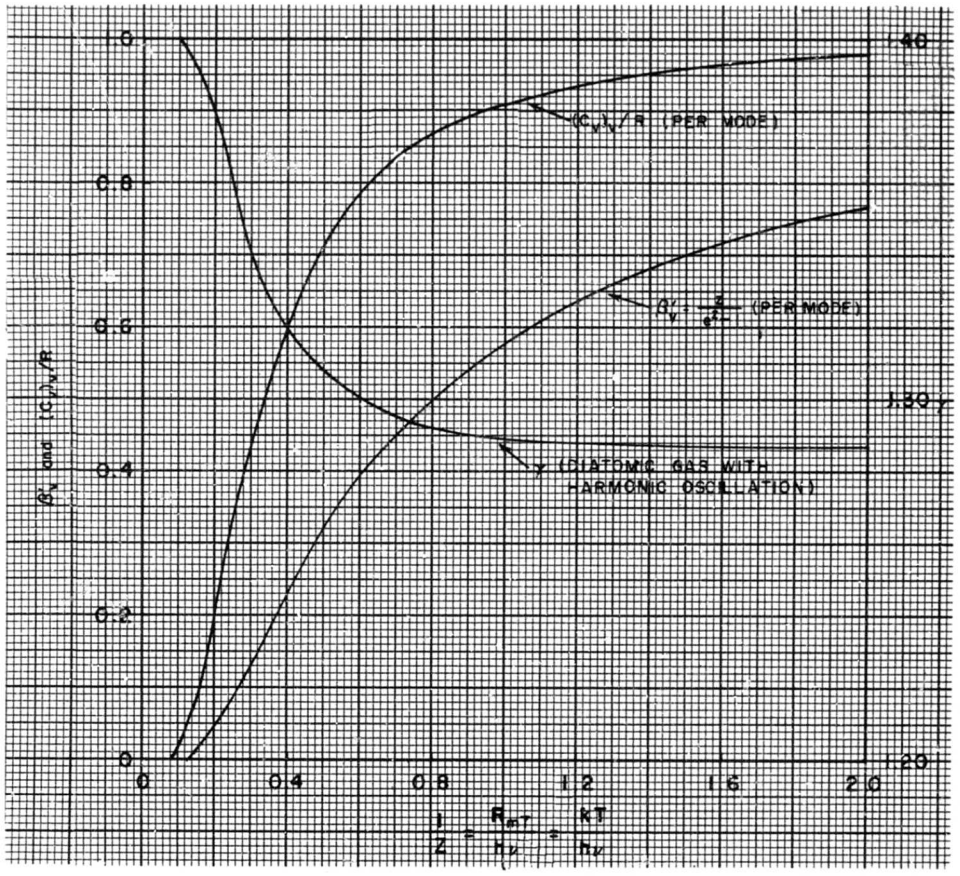

FIG(2.2-5) PROPERTIES OF THE HARMONIC OSCILLATOR FOR DIATOMIC GASES. REF. 31.

The above expressions are restricted to some not-too-high domain of temperatures, the limits being an individual intrinsic property of each gas. At very elevated temperatures, there appears a pronounced interaction between the rotational and the vibrational molecular motions. The vibrational modes can no more be regarded as pure harmonics, and one of them tends toward the value of RT°. For instance, the assumption of pure harmonic oscillations results in an error of 7% for N_2 at 5000° K.

The effect of vibrational modes on <u>specific heats</u> is treated in a similar way. Assuming that the supposed harmonic nature of the vibrational modes is valid, the contribution of each normal mode to the specific heat at constant volume is

$$\frac{Cv}{n} = \Delta Cv = \frac{d}{dT^\circ}\left[f(z)RT^\circ\right] = \frac{d}{dT^\circ}(\beta' RT^\circ),$$

$$f(z) = \beta_v' = \frac{\beta_v}{n_v} = \frac{e_v}{n_v RT^\circ} = \frac{z}{e^z - 1}.$$

(2.2-304)

Explicitly, the total contribution for all the vibrational modes is then:

For monoatomic gases ($N_v = 0$):

$$Cv_v = n_v \Delta Cv = 0. \qquad (2.2\text{-}305)$$

For diatomic gases ($N_v = 1$):

$$Cv_v = n_v \Delta Cv = \Delta Cv = \frac{d}{dT^\circ}(\beta_v' RT^\circ).$$

(2.2-306)

For polyatomic gases with Na atoms in a straight line ($N_v = 3Na - 5$):

$$Cv_v = n_v \Delta Cv = (3Na - 5)\frac{d}{dT^\circ}(\beta_v' RT^\circ).$$

(2.2-307)

For all other polyatomic gases ($N = 3Na - 6$):

$$Cv_v = n_v \Delta Cv = (3Na - 6)\frac{d}{dT^\circ}(\beta_v' RT^\circ).$$

(2.2-308)

Note: in the above expressions it is tacitely assumed that the internal energy and the specific heats are functions of temperature only, which can be taken as an acceptable approximation, provided pressures are kept near-standard. Then assuming that the simple form of the thermal equation of state still holds,

$$p = \rho RT^\circ, \qquad (2.2\text{-}309)$$

the density and the pressure dependence on the temperature is also obtained from the differential energy equation for isentropic flows as

$$\frac{d\rho}{\rho} = \frac{Cv}{RT}dT^\circ$$

$$\therefore \log_e \rho = \frac{1}{R}\int \frac{Cv}{T^\circ}dT^\circ \qquad (2.2\text{-}310)$$

$$\frac{dp}{p} = \frac{Cp}{RT^\circ}dT^\circ$$

$$\therefore \log_e p = \frac{1}{R}\int \frac{Cp}{T^\circ}dT^\circ. \qquad (2.2\text{-}311)$$

(xxii) Summary Expressions for Translational, Rotational and Vibrational Degrees of Freedom

$$n = n_t = 3,$$

$$e = e_t = \frac{n_t}{2}RT^\circ = \frac{3}{2}RT^\circ,$$

$$\beta = \beta_t = \frac{e_t}{RT^\circ} = \frac{3}{2},$$

$$Cv = Cv_t = \frac{n_t}{2}R = \frac{3}{2}R,$$

$$Cp = Cv + R = \frac{(n_t+2)}{2}R = \frac{5}{2}R,$$

$$\gamma = \frac{Cp}{Cv} = \frac{(n_t+2)}{n_t}R = \frac{5}{3}R,$$

$$p = \rho RT^\circ.$$

(2.2-312)

Diatomic gases (except H_2):

$$n = n_t + n_r + n_v = 3+2+1 = 6,$$

$$e = e_t + e_r + e_v = \left[\frac{(n_t+n_r)}{2} + \beta_v\right]RT^\circ = \left[\frac{5}{2} + \beta_v\right]RT^\circ,$$

$$\beta = \beta_t + \beta_r + \beta_v\left[\frac{n_t}{2} + \frac{n_r}{2} + n_v\beta_v'\right] = \left[\frac{5}{2} + \frac{z}{e^z - 1}\right],$$

$$Cv = Cv_t + Cv_r + Cv_v = \left[\frac{(n_t+n_r)}{2}R + \frac{d}{dT^\circ}(\beta_v' RT^\circ)\right] =$$

$$= \left[\frac{5}{2}R + \frac{d}{dT^\circ}\left(\frac{zRT^\circ}{e^z - 1}\right)\right],$$

$$Cp = Cv + R = \left[1 + \frac{n_t+n_r}{2}R + \frac{d}{dT^\circ}(\beta_v' RT^\circ)\right] =$$

$$= \left[\frac{7}{2}R + \frac{d}{dT^\circ}\left(\frac{zRT^\circ}{e^z - 1}\right)\right],$$

$$\gamma = \frac{Cp}{Cv} = \left[\frac{\frac{7}{2}R + \frac{d}{dT^\circ}\left(\frac{zRT^\circ}{e^z - 1}\right)}{\frac{5}{2}R + \frac{d}{dT^\circ}\left(\frac{zRT^\circ}{e^z - 1}\right)}\right],$$

$$p = \rho RT^\circ.$$

(2.2-313)

Polyatomic gases with Na atoms in a straight line:

$$n = n_t + n_r + n_v = 3 + 2 + (3Na-5),$$

$$e = e_t + e_r + e_v = \left[\frac{n_t+n_r}{2} + (3Na-5)\beta_v \right] RT^\circ =$$

$$= \left[\frac{5}{2} + (3Na-5)\beta_v \right] RT^\circ,$$

$$\beta = \beta_t + \beta_r + \beta_v = \left[\frac{n_t}{2} + \frac{n_r}{2} + (3Na-5)\beta'_v \right] =$$

$$= \left[\frac{5}{2} + (3Na-5)\frac{z}{e^z-1} \right],$$

$$Cv = Cv_t + Cv_r + Cv_v = \left[\frac{(n_t+n_r)}{2} R + (3Na-5)\frac{d}{dT^\circ}(\beta'_v RT^\circ) \right] =$$

$$= \left[\frac{5}{2}R + (3Na-5)\frac{d}{dT^\circ}\left(\frac{zRT^\circ}{e^z-1}\right) \right],$$

$$Cp = Cv + R = \left[\left(1 + \frac{n_t+n_r}{2}\right) R + (3Na-5)\frac{d}{dT^\circ}(\beta'_v RT^\circ) \right] =$$

$$= \left[\frac{7}{2}R + (3Na-5)\frac{d}{dT^\circ}\left(\frac{zRT^\circ}{e^z-1}\right) \right],$$

$$\gamma = \frac{Cp}{Cv} = \left[\frac{\frac{7}{2}R + (3Na-5)\frac{d}{dT^\circ}\left(\frac{zRT^\circ}{e^z-1}\right)}{\frac{5}{2}R + (3Na-5)\frac{d}{dT^\circ}\left(\frac{zRT^\circ}{e^z-1}\right)} \right],$$

$$p = \rho RT^\circ.$$

(2.2-314)

For all other polyatomic gases:

$$n = n_t + n_r + n_v = 3 + 3 + (3Na-6),$$

$$e = e_t + e_r + e_v = \left[\frac{n_t+n_r}{2} + (3Na-6)\beta_v \right] RT^\circ =$$

$$= \left[3 + (3Na-6)\beta_v \right] RT^\circ,$$

$$\beta = \beta_t + \beta_r + \beta_v = \left[\frac{n_t}{2} + \frac{n_r}{2} + (3Na-6)\beta'_v \right] =$$

$$= \left[3 + (3Na-6)\frac{z}{e^z-1} \right],$$

$$Cv = Cv_t + Cv_r + Cv_v = \left[\frac{(n_t+n_r)}{2} R + (3Na-6)\frac{d}{dT^\circ}(\beta'_v RT^\circ) \right] =$$

$$= \left[3R + (3Na-6)\frac{d}{dT^\circ}\left(\frac{zRT^\circ}{e^z-1}\right) \right],$$

$$Cp = Cv + R = \left[\left(1 + \frac{n_t+n_r}{2}\right) R + (3Na-6)\frac{d}{dT^\circ}(\beta_v RT^\circ) \right] =$$

$$= \left[4R + (Na-6)\frac{d}{dT^\circ}\left(\frac{zRT^\circ}{e^z-1}\right) \right],$$

$$\gamma = \frac{Cp}{Cv} = \left[\frac{4R + (3Na-6)\frac{d}{dT^\circ}\frac{zRT^\circ}{e^z-1}}{3R + (3Na-6)\frac{d}{dT^\circ}\frac{zRT^\circ}{e^z-1}} \right],$$

$$p = \rho RT^\circ.$$

(2.2-315)

(xxiii) Dissociation and Ionization Effects and the Internal Energy Content

The high temperatures, associated in free flights with either very high speeds or very strong shocks, can cause dissociation and ionization of gas molecules and atoms.

The resulting electronic excitation of the ionized gas particles does not contribute significantly to the internal energy content of gas, and in a first approximation can be neglected, i.e.: $e_e \sim 0$.

The molecular vibrations and the dissociation effects can appreciably contribute to the internal energy at the elevated temperatures.

For a dissociating gas the following expressions may be used(7):

Equation of state:

$$p = \rho RT^\circ(1 + \alpha_d), \qquad (2.2\text{-}316)$$

$\alpha = f(p, \rho, T^\circ)$ is the fraction of molecules dissociated, or the degree of dissociation. It is a strong function of T°, and a weak function of p and ρ:

$$\alpha_d = \left(\frac{k_d}{k_d + 4p}\right)^{1/2}, \qquad (2.2\text{-}317)$$

where, according to Ref. 31:

$$k_d = \frac{p_A^2}{p_M} \quad , \qquad (2.2\text{-}318)$$

with p_M and p_A being the partial pressures of atoms and molecules respectively. The numerical values of k_d can be found tabulated in Ref. 31.

Coefficient of internal energy content, β_d , for dissociating gases is:

$$\beta_d = \left(\frac{1-\alpha_d}{1+\alpha_d}\right)\beta_M + \left(\frac{\alpha_d}{1+\alpha_d}\right)\left(\frac{e_d}{RT^\circ} + 2\beta_A\right) \quad , \qquad (2.2\text{-}319)$$

where the subscripts (d), (M) , and (A) refer to the dissociating mixture, the molecules and the atoms respectively, and:

e_d - is the energy of dissociation per unit mass,

β_M - is the total coefficient of internal energy for molecules, obtained by adding the partial contributions due to translational, rotational, vibrational (and electronic excitation) degrees of freedom, see paragraph 17.

$$\beta_M = \beta_t + \beta_r + \beta_v + \beta_e \quad ,$$

$$\beta_e \approx 0 \quad , \qquad (2.2\text{-}320)$$

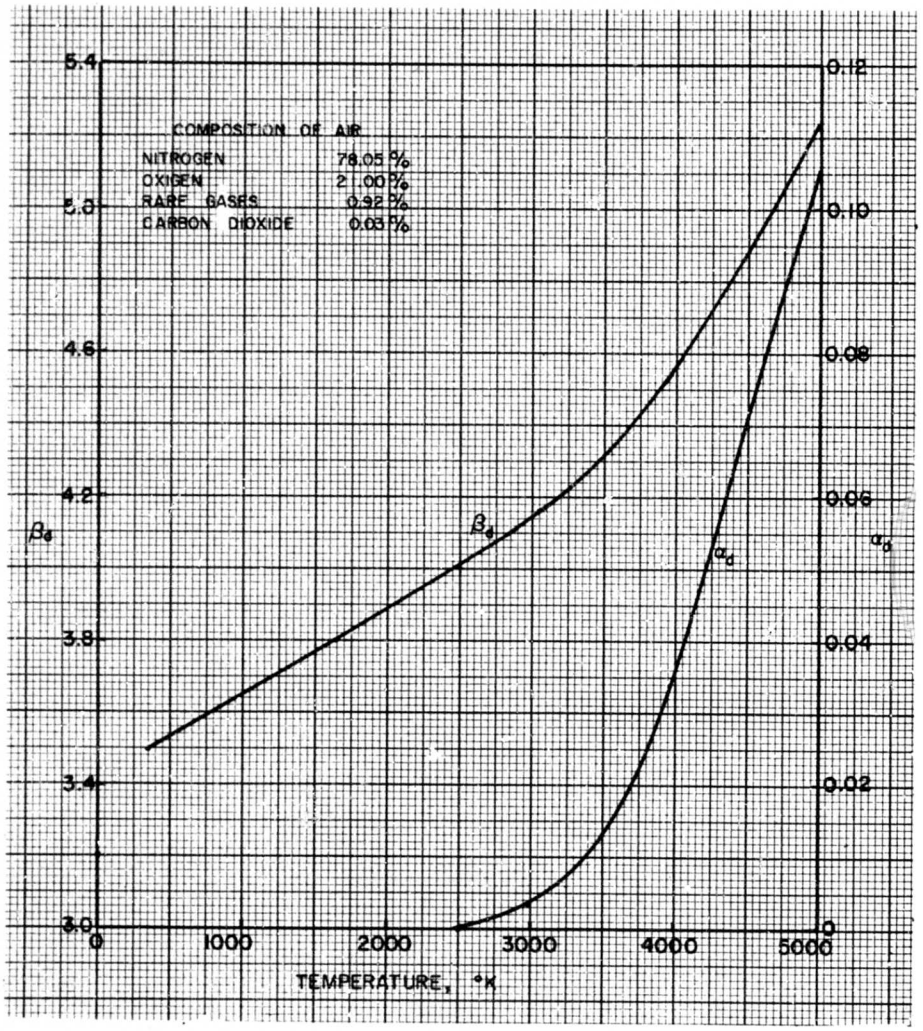

FIG (2.2-6) DISSOCIATION OF AIR AS A FUNCTION OF TEMPERATURE (REF 31)

β_A - is the coefficient of internal energy for (dissociated) atoms, comprising only translational degrees of freedom,

$$\beta_A = \frac{5}{2} \cdot \qquad (2.2\text{-}321)$$

Values of (β_d) and (α_d) for dissociating air are plotted versus temperature T° in Fig. (2.2-6), taken from Ref. 31.

(xxiv) Relaxation Times

The preceding thermodynamic definitions are based on one fundamental premise: the successive equilibrium states are supposed to be achieved by relatively slow changes, i.e., theoretically in infinite time intervals. Practically, they hold approximately for any not-too-rapidly developing thermodynamic process.

When rapid changes of state are encountered, the finite time interval required for any degree of freedom to reach the new respective energetic level is called the "relaxation time". This means that the internal molecular energy levels are in general lagging behind the rate of change of the state of a flowing gas. As the time intervals in which large temperature variations occur become smaller and less than the "relaxation time", indicating a speeded up process, there is an increase in time lag between the instantaneous energy contents for each degree of freedom and the corresponding anticipated equilibrium values (that could be achieved if sufficient time for each of the successive gaseous states was allowed). Thus, in general, the achievement of an actual new redistribution of the internal energy content among various degrees of freedom is delayed in time, i.e., only after the associated "relaxation times" have passed, the new equilibrium state is realized. This internal lag of adjustment is an irreversible process, accompanied by a corresponding increase in entropy.

The "relaxation time" reflects actually the number of collisions required for a complete transfer of the individually changed molecular energy levels between molecules (or molecular classes). As the efficiency of the energy transfer processes through collisions varies with different types of molecular motions, so will vary the associated "relaxation times". The translational degrees of freedom have the shortest (negligible) "relaxation time" intervals: substantial changes in the translational molecular motions are effected even through one single set of collisions. A complete new equilibrium state may be thus achieved in a very short time interval, Δt, which is appreciably less than the time interval dt, corresponding to the basic definition of the gas density, ρ, within a control space volume, $d\tau$.

The partial internal energy transfer which is associated with the rotational degrees of molecular freedom in a flowing gas (undergoing successive changes of state), requires a slightly greater number (10 to 100) of the intermolecular collisions to become effective, depending upon the actual molecular shape of the specific gas. The corresponding "relaxation time" intervals are thus slightly greater than for the translational degrees of freedom, but eventually still practically negligible.

The intermolecular energy transfer processes related to the vibrational degrees of freedom are, on the contrary, comparatively very slow, and the "relaxation times" involved are appreciable, being a function of both the temperature and the molecular structure. Example: for CO_2 about 33,000 collisions at 325° C. and at a pressure of 1 atmosphere are required to accomplish the vibrational energy transfer with a difference less than $(1/e)$ of its equilibrium value[31].

Practical conclusions are:

The translational and rotational degrees of freedom are considered "active", causing an almost discontinuous (negligible relaxation times) exchange of the internal energies between molecules, the new equilibrium state being effected in a few molecular collisions (or mean free paths). Consequently, the equilibrium isentropic expressions,

$$\bar{e}_a + \frac{p}{\rho} = \beta_a R T^\circ, \qquad \bar{e}_a = C_{v_a} R T^\circ,$$
$$T^\circ_{equ} = T^\circ \qquad (2.2\text{-}322)$$

are approximately valid instantaneously at any point in a steady flow field, where the subscript (a) denotes the "active" (translational and rotational) degrees of freedom and the subscript (equ) relates to the equilibrium temperature.

The vibrational degrees of freedom are considered "inert", involving appreciable relaxation time intervals before the equilibrium temperatures and the equilibrium gaseous states are achieved, the internal intermolecular energy exchange requiring a considerable number of collisions for the purpose. When the initially lagging equilibrium state ($T^\circ \rightarrow T^\circ_{equ}$) in steady flows is reached, the total internal energy expressions, with the additional vibrational degrees completely aroused, is

$$e = e_a + e_v = C_{va}\ RT^\circ + C_{v_v}\ T^\circ R\ , \qquad (2.2\text{-}323)$$

where the subscripts (a) and (v) refer to the sums of active and vibrational degrees of freedom respectively. The gradient of the temperature lag is obtained from

$$\frac{dT}{dt} = X(T^\circ_{equ} - T^\circ)\ , \qquad (2.2\text{-}324)$$

where $X(\rho, T^\circ)$ is the retardation factor.

(xxv) Free Molecular Interaction with Solid Surfaces and Slightly Nonisentropic Flows

The presence of a solid body immersed in a flowing gas is identified by specifying the boundary conditions on the washed surfaces, determining the corresponding particular solutions of the general equations of gas motion. In the kinetic theory of gases, it is recognized that the internal mechanism of the mass, momentum and energy transfer is affected and changed in the flow field around the immersed body. Specifically, the earlier adopted simple molecular model of completely free molecules and the subsequently derived conclusions, do not necessarily hold when interaction between the gas molecules and a solid boundary (surface) are investigated. Depending upon assumptions introduced in handling various real flow-immersed body conditions, different modifications of the interacting molecular mechanism are obtained.

(xxvi) Specular Reflections -- A Perfect Slip Flow Concept

By assuming a molecular interaction with a smooth, insulated solid surface (wall) corresponding to the isentropic flow conditions, ($\phi = \mu = \nu = 0$), a so called "specular" type of molecular reflection is defined, whereby the spherical molecules are reflected in a perfectly elastic manner from a smooth surface, the molecular model being otherwise of the same restricted idealized pattern as specified in the previous paragraphs. For such specular encounters there are no changes in the molecular velocity components locally tangential to the surface before and after collision with the solid boundary, while the respective normal molecular velocity components before and after collision are reversed in direction but unchanged in magnitude. The case of a perfect slip flow is obtained, see Fig (2.2-7), whereby the velocity of the ordered flow $\bar{q} = (\bar{u}^2 + \bar{w}^2)^{1/2}$ tangential to the elemental plane dS is preserved. The normal pressure (molecule-surface collisions) on the surface is then the same as the static pressure (molecule-molecule collisions) in the gas (locally), and there are no shear stresses. These boundary conditions on the kinetic theory scale match the isentropic boundary conditions from the perfect, inviscid and non-conducting adiabatic continuum flow theory, in which the zero-streamline of the ordered mass motion is identified with the body contour itself. The Maxwellian velocity distribution function for isentropic flow conditions remains valid at the body surface also, and consequently all the relationships among physical flow variables from previous paragraphs remain in force.

(xxvii) Slightly Nonisentropic Flows for Monoatomic Gases

In reality, the pure specular reflection of molecules in a Maxwellian (isentropic) flow across solid boundaries is not realized. The state of gas adjacent to the solid surface is actually affected both by the viscous and the heat conductive processes, which are functionally related to the thermal conditions of the immersed solid boundary, and thus the real flows are intrinsically nonisentropic. This fact is recognized in the classical continuum flow theory by introduction of the concept of a thin boundary layer adjacent to the surface. Its presence can be interpreted within the simple concepts of the equilibrium kinetic theory of gases by introducing the following modifications(7) on a molecular scale:

- A more accurate molecular model, allowing for heat transfer and momentum dissipation effects is needed.

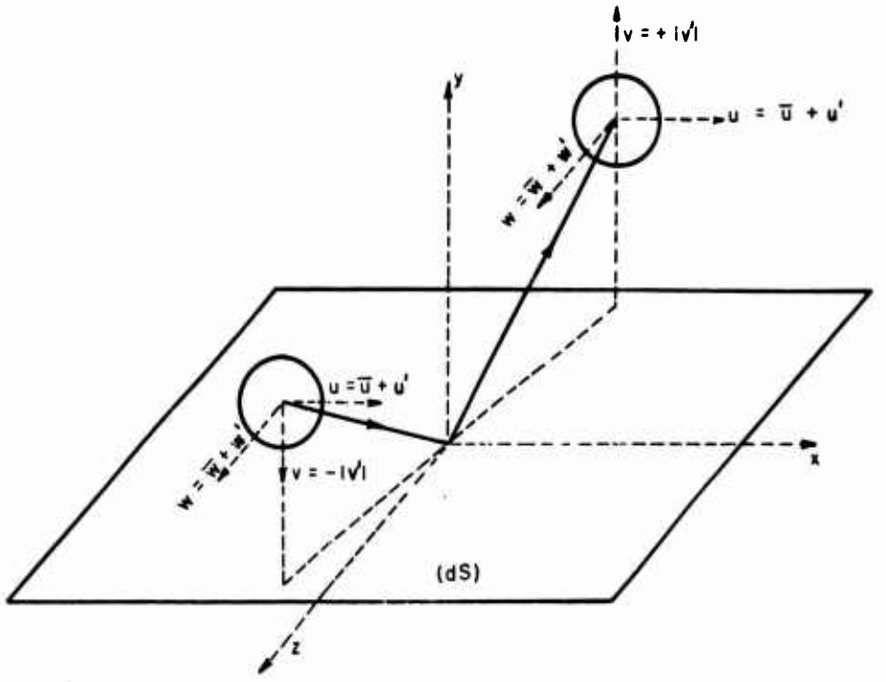

u', w', v' - are components of the velocity of random molecular motion

ū and w̄ - are components of the velocity of ordered flow (v̄ assumed zero)

FIG (2.2-7) SPECULAR REFLECTION — A BOUNDARY CONDITION FOR ISENTROPIC FLOW (REF 7.)

ALTERNATE FIG. (2.4-4)

This is achieved by analyzing the molecular collisions while the molecules are treated as "point centers of force" instead of regarding them as perfectly elastic spheres. The force field concept is based on the experimental evidence that gas molecules exert a weak force of attraction on each other when placed at large distances, and a strong force of repulsion when at short distances apart.

- The molecular motion is regarded as slightly nonisentropic only, i.e., the velocity distribution function deviates but slightly from the isentropic Maxwellian law. Consequently, although the expressions for the mass, momentum and energy conservation shall acquire a more general form, it remains similar to the respective isentropic case.

- The boundary conditions at the solid surface are changed in order to satisfy the new physical nature of a diffused reflection process, so that the results of the modified expressions of mass, momentum and energy transfer are brought in a closer agreement with the velocity distribution laws and the thermal conditions at the immersed solid surfaces.

The changed equations for the presumed slightly nonisentropic flows have been developed by several analytical approaches, with the following two being representative:

(a) The direct mathematical method of solving the general Boltzmann's equation for a modified velocity distribution function, developed by Enskog[32].

(b) The method of Chapman[33, 34, 35] which is mathematically simpler and physically more descriptive, based on the initial premises defined by Maxwell[36].

- The relatively changed results of the slightly modified molecular interaction model are:

The pressure definition is somewhat changed by inclusion of small additional terms, representing the effects of the molecular force fields.

The absolute temperature definition remains the same as in isentropic case, remaining related to the translational degrees of freedom only (monoatomic model).

The velocity distribution function deviates from the Maxwellian law in the neighborhood of the wall (i.e., in the boundary layer): the impinging molecules have initially motions consistent with the state of a free gas and possess the internal energy of a free gas, but the reflected molecules shall have their motion and their thermal conditions changed to accommodate partially for the nonisentropic conditions at the wall. The reflection is no more specular, and an intermingling of the impinging (Maxwellian) stream and the nonisentropically reflected molecular stream produces a departure from the initial Maxwellian (isentropic) velocity distribution law after the relections occur.

The mean free path expression is the same for both isentropic and slightly nonisentropic flows

$$\bar{\lambda} = \frac{1}{\sqrt{2}\,\pi\, n\, \sigma^2} \quad , \qquad (2.2\text{-}325)$$

provided gas densities are not too high and a new effective molecular diameter

$$\sigma = \sigma(T^\circ) = \frac{5 m \bar{c}}{32 (2\mu)^{1/2}} \qquad (2.2\text{-}326)$$

is introduced, so that the mean free molecular path becomes explicitly:

$$\bar{\lambda} = \frac{1}{(2)^{1/2} n \pi \sigma^2} = \frac{32}{\sqrt{\pi}} \frac{\mu}{\rho \bar{c}} = \qquad (2.2\text{-}327)$$

$$= \frac{16}{5} \frac{\mu}{\rho (2\pi R T)^{1/2}} \quad .$$

Since the expression for $\overline{c^2}$ is invariant in the form from the velocity distribution function for both isentropic and nonisentropic flows[7], and since the static pressure definition,

$$p = \frac{1}{3} \rho \overline{c^2} \quad , \qquad (2.2\text{-}328)$$

and the temperature concept,

$$R T^\circ = \frac{1}{3} \overline{c^2} \quad , \qquad (2.2\text{-}329)$$

are the same in form for both isentropic and slightly nonisentropic flows, it follows that the speed of sound in a monoatomic gas flowing nonisentropically is the same as defined for isentropic flows:

$$a = \left[\frac{5}{3} \left(\frac{1}{3} \overline{c^2} \right) \right]^{1/2} = (\gamma R T^\circ)^{1/2} \cdot \qquad (2.2\text{-}330)$$

The definition of the specific heats C_p and C_v hold as specified for isentropic flows.

The first coefficient of viscosity, μ, under the slightly nonisentropic conditions is defined as follows:

Physically viscosity represents the transfer of molecular momentum between any two adjacent laminated layers of the ordered mass flow due to the mechanism of molecular random motion, i.e., due to both the free molecular translation (monoatomic gases) and the intermolecular collisions. The transfer process results in a tendency for equalization of the ordered velocities of the two adjacent flow layers.

In the kinetic theory concepts, the gaseous flows are considered viscous if the molecular velocity distribution function departs from the Maxwellian law, and vice versa, in an isentropic flow, conforming with the Maxwellian molecular velocity distribution law, the tendency is absent, and the adjacent molecular layers slip freely above each other.

The coefficient of viscosity, μ, depends only on the mean kinetic energy of the random molecular motion $\overline{c^2}$:

$$\mu = \frac{5m}{16\sqrt{\pi}\,\sigma^2}\left(\frac{\overline{c^2}}{3}\right)^{\frac{1}{2}}, \qquad (2.2\text{-}331)$$

or expressed by the temperature concept,

$$\frac{\mu}{\mu_1} = \left(\frac{T^\circ}{T_1^\circ}\right)^{\omega}, \qquad (2.2\text{-}332)$$

where (1) refers to any reference local point, and ω depends on mathematical model chosen to represent the gas molecule:

$\omega = 1/2$ for monoatomic spherical molecules,

$\omega > 1/2$ for real monoatomic gases,

$\omega = 1/2 + 2(\upsilon_1 - 1)$ for monoatomic molecules, represented as point centers of force, with υ_1 being an exponent in the law of the repulsive molecular force field(30).

Assuming near-normal gas conditions, the experimental results of the viscosity-temperature law for different

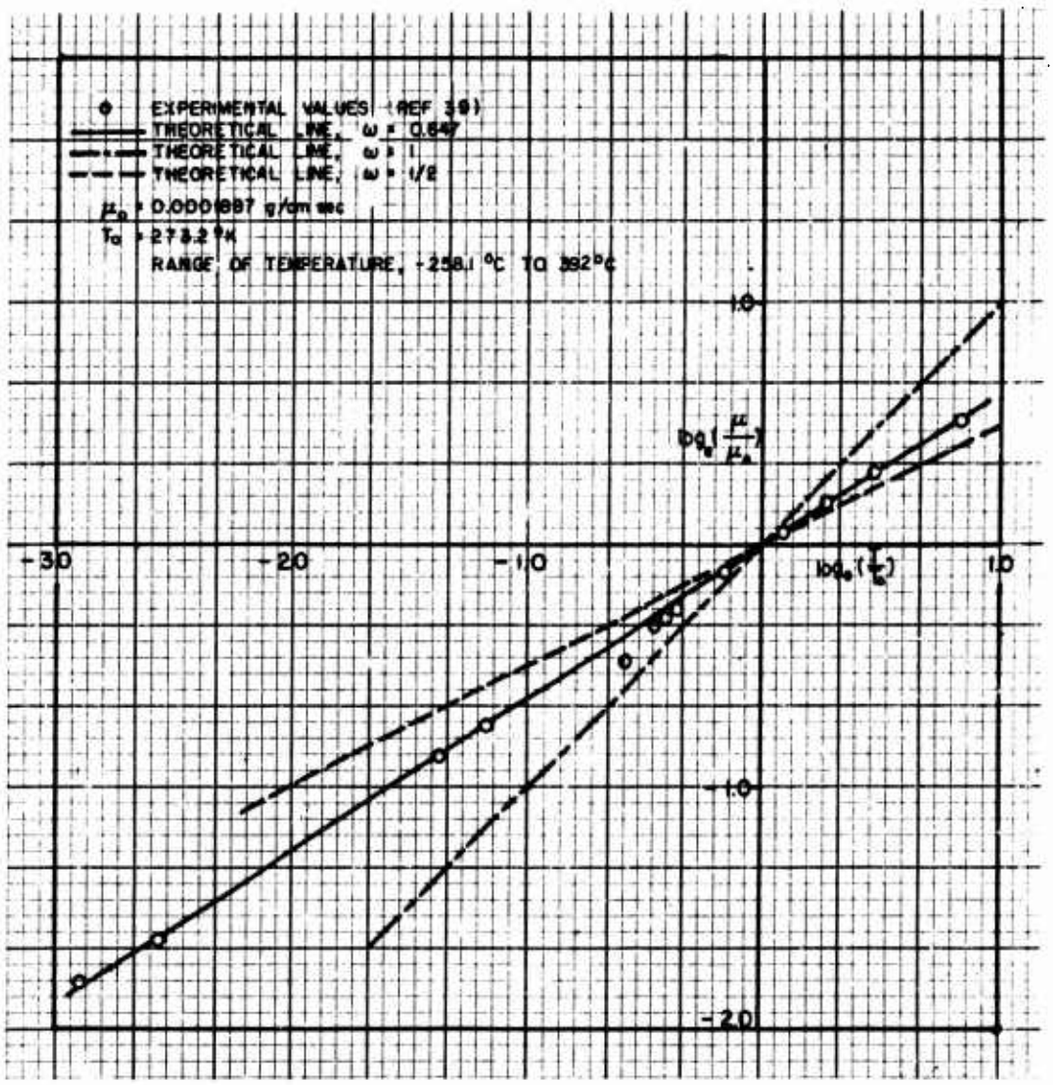

FIG (2.2-8) VARIATION OF VISCOSITY OF HELIUM WITH TEMPERATURE (REF 37)

real monoatomic gases show appreciable differences in the values of the exponent ω . Thus, for helium the experimentally determined variation of viscosity with temperature is replotted in Fig (2.2-8) from Ref. 37, (Dryden), indicating that the theoretical point-center repulsive force molecular model ($\nu = 14.6$ $\omega = .647$) is a very good approximation of the real viscosity effects in helium. The same conclusion holds for hydrogen, too. But for many other real gases (both monoatomic and diatomic), a different molecular model proves to be more satisfactory, leading to the Sutherland's law(38),

$$\frac{\mu}{\mu_1} = \left(\frac{T^\circ}{T_1^\circ}\right)^{\frac{3}{2}} \left(\frac{T_1^\circ + \kappa}{T^\circ + \kappa}\right) \quad , \quad (2.2\text{-}333)$$

where (μ_1) and (T_1°) are the given reference values, and molecules are conceived as smooth, elastic spheres surrounded by a weak, attractive field of force, which, when attached to a spherical molecule, reduces the mean free path, λ , and increases the collision frequency, (ν_1) . The same result may be obtained by supplementing the attractive force field by a corresponding variation of the spherical molecule diameter with temperature changes, $\sigma' = \sigma(T^\circ)$, the apparent diameter (σ') becoming smaller as the temperature increases according to the relationship

$$\sigma' = \sigma \left(1 + \frac{\kappa}{T^\circ}\right)^{\frac{1}{2}} \quad , \quad (2.2\text{-}334)$$

where

σ' - is the apparent molecular diameter,

σ - is the theoretical (geometric) molecular diameter,

κ - is the Sutherland's constant.

The Sutherland's law (2.2-233) is recommended(40) for air within the following limits

$$\kappa = 114 \quad , \quad 0 \le T^\circ \le 300^\circ C \quad , \quad T_1^\circ = 273.2^\circ K \quad .$$

$$\mu = 1.709 \times 10^{-4} \text{ gr cm}^{-1}\text{sec}^{-1} \quad . \quad (2.2\text{-}335)$$

A further refinement of the molecular model has been introduced by Lennard-Jones(41) by assuming that the point-center force field is either attractive or repulsive, depending on whether the molecular distance is large or small, leading to a temperature-viscosity law,

$$\frac{\mu}{\mu_1} = \left(\frac{T^\circ}{T_1^\circ}\right)^{\frac{3}{2}} \left(\frac{T_1^{\circ\,(\omega-3)/(\omega-1)} + \kappa}{T^{\circ\,(\omega-3)/(\omega-1)} + \kappa}\right)$$

(2.2-336)

It should be emphasized that whatever exponential temperature-viscosity law is assumed, considerable complications are encountered in finding the closed type solutions for the fundamental viscous flow equations in the boundary layer theories. Therefore, in practice a simpler and yet sufficiently accurate law of the form,

$$\frac{\mu}{\mu_1} = \kappa_1 \left(\frac{T^\circ}{T_1^\circ}\right) \quad , \quad (2.2\text{-}337)$$

is usually accepted, where the constant κ_1 is chosen to fit some reference gas conditions, T_1° , and μ_1 , which are well representative in the overall range of the T° and μ variations for the particular problem at hand. For standard atmosphere continuum flow flight conditions, the non-exponential viscosity-temperature law (2.2-237) involves an error of less than 6% in laminar boundary layer calculations.(42)

Simultaneously with the dissipative momentum transfer of the ordered mass flow, the non-Maxwellian random molecular motion results in a conductive heat transfer between adjacent laminated layers. In an isentropic (Maxwellian) flow, the mean molecular velocity, c^2 , is a function of the density number, n_1 , of molecules in the control space volume $d\tau$ only. In the absence of heat conduction and viscosity (isentropic idealization) no adjustment between the internal energy of a gas and the thermal conditions at the solid boundary is possible. And contrary to it, an accommodation between the gas temperature, $T^\circ \sim c^2$, and the solid surface temperature, T_w° , can be achieved in a non-isentropic flow by allowing for a respective deviation of the random molecular motion from the Maxwellian velocity distribution law.

The coefficient of heat conduction, κ , is a thermal counterpart to the coefficient of viscosity, μ , and it is similarly defined in terms of temperature as:

$$\frac{k}{k_1} = \left(\frac{T^\circ}{T_1^\circ}\right)^{\omega} , \qquad (2.2\text{-}338)$$

i.e., it is a function of the mean molecular speed, $\bar{c}^2$, only. A connection between the two coefficients for monoatomic gases is given by the relationship,

$$k = 2.5\, C_v\, \mu , \qquad (2.2\text{-}339)$$

which is in a good agreement with experimental results for monoatomic gases. For diatomic and polyatomic gases, another semi-empirical expression, developed by Eucken(43),

$$k = .25(9\gamma - 5)\mu C_v , \qquad (2.2\text{-}340)$$

represents a satisfactory approximation, with the γ value taken to correspond to the molecular structure (monoatomic, diatomic, polyatomic), and the respective number of degrees of freedom, see paragraph (22).

(xxviii) Viscosity and Heat Conductivity in Dense Monoatomic Gases (Laminar Flows)

The preceding definitions of the coefficients of viscosity, μ , and of the heat conductivity, k , (as well as of the static pressure and of the equation of state) for monoatomic, slightly rarefied gases at nearly standard sea-level conditions, are based on the assumption that the molecular diameter, σ , is negligibly small compared with the mean free molecular path, $\bar{\lambda}$. For highly compressed regions in a gas flow, the molecular diameter, σ , becomes comparable to the molecular mean free path, λ , and the momentum transfer, the heat conduction and the static pressures are affected additionally by the respectively altered molecular force fields and the subsequently changed molecular collision rates, ν . Consequently, for the dense monoatomic gases, new expressions for μ' , k' , and p' are required(17), where the prime superscript ($'$) denotes the changed "dense" values:

$$\mu' = \mu\left[1 + R_{m1}(T^\circ)\rho + R_{m2}(T^\circ)\rho^2\right] , \qquad (2.2\text{-}341)$$

or

$$\mu' = \mu(1 + .0875\theta + .217\theta^2), \qquad (2.2\text{-}342)$$

$$k' = k(1 + .287\theta + .216\theta^2) , \qquad (2.2\text{-}343)$$

$$p' = \rho R T^\circ\left[1 + (1/2)\theta + (5/32)\theta^2\right] - (3/4)\theta^2\mu\xi \qquad (2.2\text{-}344)$$

or

$$p' = \rho R T^\circ\left[1 + R_{m3}(T^\circ)\rho + R_{m4}(T^\circ)\rho^2\right] - \mu_b\xi , \qquad (2.2\text{-}345)$$

where

$R_{m3} = \frac{1}{2} R_m$, $R_{m1} = .0875 R_m$,

$R_{m4} = \frac{5}{32} R_m^2$, $R_{m2} = .217 R_m^2$,

$\mu_b = \frac{3}{4}\theta^2$ - coefficient of "bulk viscosity", appearing in flowing gases due to the finite molecular sizes.

$\theta = \frac{4}{3}\pi n \sigma^3 = R_m(T^\circ)\rho$ - is a mathematical term, expressing the ratio of the decrease in volume of the force-contact spheres for two colliding molecules, (molecules conceived as centers of point forces), to the total control volume, $d\tau$; or, the ratio of the excluded volume to the total control volume $d\tau$, see Fig (2.2-9).

$\sigma'(T^\circ)$ - an effective diameter of molecule, see Fig. (2.2-9).

$\xi = (\bar{u}_x + \bar{v}_y + \bar{w}_z)$ a velocity dilatation factor, i.e.,

$$\xi = \left(\frac{\partial \bar{u}}{\partial x} + \frac{\partial \bar{v}}{\partial y} + \frac{\partial \bar{w}}{\partial z}\right) ,$$

$R_m(T^\circ) = \frac{4\pi\sigma^3}{3m} = \frac{\rho}{\rho}$ = the gas constant per molecule.

σ = the geometrical diameter of a molecule, see Fig. (2.2-9).

Note that the equation of state (2.2-339) is valid for flowing dense gases. When gas is at rest, the equation takes a form similar to the Van der Waal's expression by neglecting

the velocity dilatation term in the expression (2.2-245),

$$p' = \rho R T^{\circ}\left[1 + R_{m3}(T^{\circ})\rho + R_{m4}(T^{\circ})\rho^2\right], \qquad (2.2\text{-}346)$$

or with further approximation (a special form of the Van der Waal's equation):

$$p' = \rho R T^{\circ}\left[1 + R_{m3}(T^{\circ})\rho\right]. \qquad (2.2\text{-}347)$$

In Fig. (2.2-10) the ratio of (μ'/μ) in terms of pressure (p') is replotted from Ref. 44 for carbon dioxide and from Ref. 45 for nitrogen.

The "bulk viscosity", (μ_b), is unimportant in monoatomic gases, but has a strong effect in diatomic and polyatomic gas flows[46,47,48].

(xxix) Viscosity and Heat Conductivity in Turbulent Flows

The interpretations of viscosity and heat conductivity in previous paragraphs have been based on the assumption of a laminar non-isentropic flow concept, i.e., when the radial velocity distribution of the ordered mass motion is essentially parabolic.

With an increase in Reynolds Number to a critical value, Re_{cr} , the mass motion becomes turbulent, and the velocity distribution in the viscous flow departs radically from the laminar parabolic law. The simple binary molecular encounters of individual molecules are no more an acceptable molecular model, since the energy, momentum and mass transfer mechanisms in a turbulent flow are performed by large molecular cluster

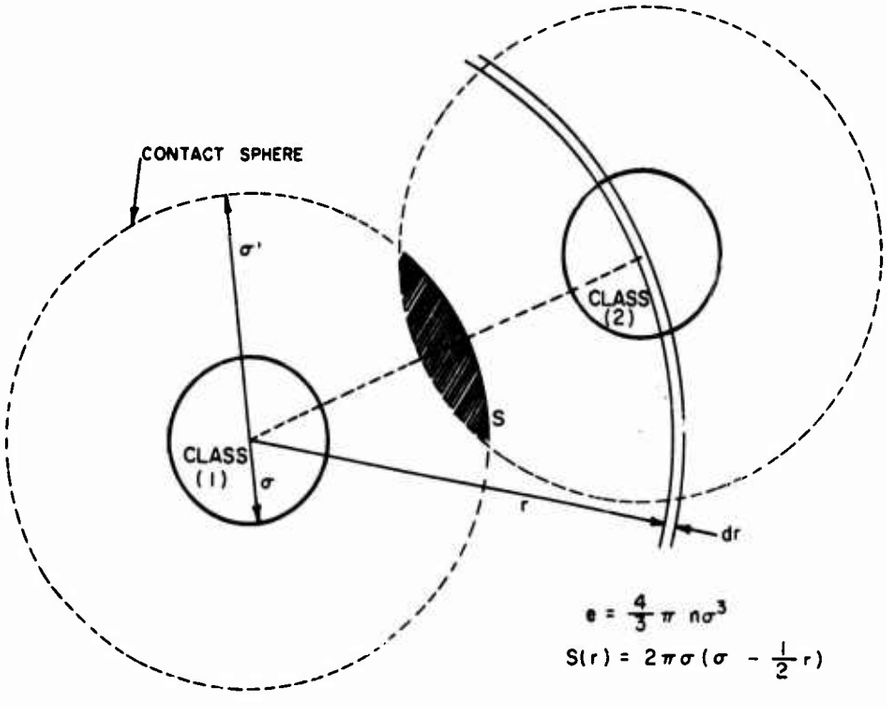

FIG (2.2-9) SHIELDING OF ONE MOLECULE BY ANOTHER (REF 7)

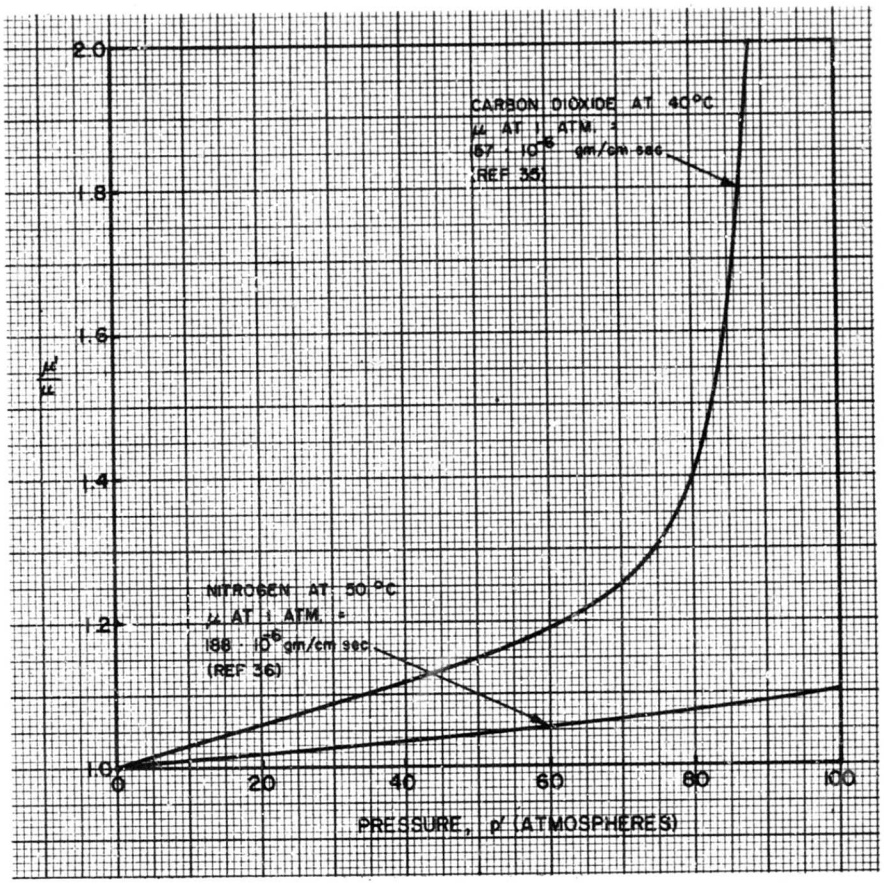

FIG (2.2-10) EXPERIMENTAL DETERMINATION OF THE VARIATION OF VISCOSITY WITH PRESSURE FOR DENSE GASES (REF 44 AND 45)

encounters, resulting in multiple molecular collisions. Consequently, the expressions for various physical variables from paragraphs(25) and(26) (and in particular the expressions for μ and k) are not valid for such multiple molecular encounters. A correspondingly modified kinetic theory approach, accounting for the multiple molecular encounters, has been developed by Born and Green[49]. Practical applications of the modified concepts are elaborated later in the section on turbulent boundary layers.

2.2.6 VARIATIONS OF AIR FLOW PARAMETERS AT ATMOSPHERIC FLIGHT CONDITIONS

The general context of the essential notions of physical parameters and laws, which are important in aerodynamic force analyses at large, are summarized in Section 2.2.5.

In this section, a brief discussion of the effects of physical parameters and of their functional variation during different flight regimes in a Standard Atmosphere is presented. The related factual data, as may be needed for the practical aerodynamic force analysis purposes, are not given in an all inclusive form, but the key reference sources are quoted instead.

(1) The Standard Atmosphere data

At the present moment, the adopted U. S. Standard[27] Atmosphere (1962) is recommended as the latest reference for the atmospheric flight environment data. It is subdivided into four altitude regions:

(a) From (-5) to (+20) km of geopotential altitude, designated as standard.

(b) From (+20) to (+32) km of geopotential altitude, designated as proposed standard.

(c) From (+32) to (+90) km of geopotential altitude, designated as tentative.

(d) From (+90) to (+700) km of geometric altitude, designated as speculative.

The variations of the atmospheric air parameters are presented in terms of both the geometric and the geopotential altitudes. All tabulated data are both in the metric (mks °K) system of units, i.e., meter (m), kilogram mass (k), second (s), degrees absolute Kelvin (°K), and in the English (ft-lb-sec-°R) systems of units. The definitions and the reference sea-level values of physical variables should be noted prior to use of the respective tabulated values. Since they may serve as a general common base for use and for conversion of any other theoretical and/or experimental data, they are briefly restated here. All notations are as specified in Ref. 27.

Air properties

Air is assumed to be in a steady, static equilibrium, devoid of moisture, water, vapor and dust, and obeying the perfect gas law and the hydrostatic equation:

$$\rho = \frac{Mp}{R_o T^\bullet} \quad , \qquad (2.2\text{-}349)$$

$$dP = -\rho g dZ \; . \qquad (2.2\text{-}350)$$

Definitions of primary constants:

P_o - Sea-level pressure is, by definition, 1.013250×10^5 newtons m^{-2}. This corresponds to the pressure exerted by a column of mercury 0.760 m high, having a density of 1.35951×10^4 kg m^{-3} and subject to an acceleration due to gravity of 9.80665 m sec^{-2}.

ρ_o, t_o - Sea-level density and temperature, respectively, are those values published in the ICAO Standard Atmosphere, Ref. 50.

g_o - The value for g_o, sea-level acceleration due to gravity, was adopted by the ICAO for the ICAO Standard Atmosphere and is adopted here as the value at exactly 45° geographic latitude, Ref. 50.

S, β - Sutherland's constant S and β, also a constant, are used in Sutherland's viscosity equation. These constants are determined from empirical data on the viscosity of air (ref. 51) in accordance with Sutherland's equation, and in general engineering practice the values shown in Table 1.2-1 are used.

$T_i^\bullet$ - Temperature of the ice point is 273.15° K. This value results from the decision in October 1954, by the Tenth General Conference on Weights and Measures, meeting in Paris, France, to redefine the temperature scale by selecting the triple point of water as the fundamental, fixed point and assigning it the temperature 273.16° K (0.01° C).

γ - The ratio of the specific heat of air at constant pressure to the

The normal composition of the clean, dry air near sea-level (Table 2.2-2 Ref. 27)

Constituent gas and formula	Content, percent by volume	Content variable relative to its normal	Molecular weight*
Nitrogen (N_2)	78.084	--	28.0134
Oxygen (O_2)	20.9476	--	31.9988
Argon (Ar)	0.934	--	39.948
Carbon dioxide (CO_2)	0.0314	**	44.00995
Neon (Ne)	0.001818	--	20.183
Helium (He)	0.000524	--	4.0026
Krypton (Kr)	0.000114	--	83.80
Xenon (Xe)	0.0000087	--	131.30
Hydrogen (H_2)	0.00005	?	2.01594
Methane (CH_4)	0.0002	**	16.04303
Nitrous oxide (N_2O)	0.00005	--	44.0128
Ozone (O_3)	Summer: 0 to 0.000007	**	47.9982
	Winter: 0 to 0.000002	**	47.9982
Sulfur dioxide (SO_2)	0 to 0.0001	**	64.0628
Nitrogen dioxide (NO_2)	0 to 0.000002	**	46.0055
Ammonia (NH_3)	0 to trace	**	17.03061
Carbon Monoxide (CO)	0 to trace	**	28.01055
Iodine (I_2)	0 to 0.000001	**	253.8088

*On basis of carbon-12 isotope scale for which $C^{12} = 12$.
**The content of these gases may undergo significant variations from time to time or from place to place relative to the normal indicated for those gases.

Primary constants of the adopted earth's atmosphere, with subscript (o) referring to sea-level conditions, are (Table 2.2-3 Ref 27):

Variable Quantity	Symbol	Metric Units (mks)	English Units (ft-lb-sec)
Sea-level pressure	P_o	1.013250×10^5 newtons m^{-2}	2116.22 lbf ft^{-2}
Sea-level density	ρ_o	1.2250 kg m^{-3}	0.076474 lb ft^{-3}
Sea-level temperature	t_o	150° C	59.0° F
Sea-level gravity constant	g_o	9.80665 m sec^{-2}	32.1741 ft sec^{-2}
Sutherland's constant	S	110.4° K	198.72° R
Temperature of the ice point	T_i°	273.15° K	491.67° R
Viscosity law constant	β	1.458×10^{-6} kg sec^{-1} m^{-1} $(^\circ K)^{-\frac{1}{2}}$	7.302×10^{-7} lb $ft^{-1}sec^{-1}(^\circ R)^{-\frac{1}{2}}$
Specific heats ratio	γ	1.40 (dimensionless)	1.40 (dimensionless)
Mean collision diameter	σ	3.65×10^{-10} m	1.1975×10^{-9} ft
Avogadro's number	N	6.02257×10^{26} $(kg\text{-}mol)^{-1}$	2.73179×10^{26} $(lb\text{-}mol)^{-1}$
Universal gas constant	R^*	8.31432 joules $(^\circ K)^{-1}$ mol^{-1}	1545.31 ft lb $(lb\text{-}mol)^{-1}(^\circ R)^{-1}$

Sea-level values of primary variables (super-script *) and derived quantities of the standard air (Table 2.2-4 Ref. 27)

Variable Quantity	Symbol	Metric	English
Speed of sound	$C_{s,o}$	340.294 m sec^{-1}	1116.45 ft sec^{-1}
Gravity constant	$^*g_o$	9.80665 m sec^{-2}	32.1741 ft sec^{-2}
Pressure scale height	H_{Ro}	8434.5 m	27,672 ft
Thermal conductivity	k_o	6.0530×10^{-6} kg-cal $m^{-1}sec^{-1}$ $(^oK)^{-1}$	4.0674×10^{-6} BTU $ft^{-1}sec^{-1}(^oR)^{-1}$
Mean free path	L_o	6.6328×10^{-8} m	2.1761×10^{-7} ft
Mean molecular weight	M_o	28.9644 (dimensionless)	28.9644 (dimensionless)
Number density	n_o	2.5471×10^{25} m^{-3}	7.2127×10^{23} ft^{-3}
Static pressure	$^*P_o$	1.013250×10^5 newtons m^{-2}	2116.22 lbf ft^{-2}
Absolute temperature	$^*T_o^\circ$	288.15° K	518.67° R
Mean particle speed	$\overline{V_o}$	458.94 m sec^{-1}	1505.7 ft sec^{-1}
Kinematic viscosity	η_o	1.4607×10^{-5} m^2 sec^{-1}	1.5723×10^{-4} ft^2 sec^{-1}
Coefficient of viscosity	μ_o	1.7894×10^{-5} kg m^{-1} sec^{-1}	1.2024×10^{-5} lb ft^{-1} sec^{-1}
Mole volume	ν_o	6.9193×10^9 sec^{-1}	6.9193×10^9 sec^{-1}
Density	$^*\rho_o$	1.2250 kg m^{-3}	0.076474 lb ft^{-3}
Mean Collision diameter	$^*\sigma_o$	3.65×10^{-10} m	11.975×10^{-10} ft
Specific weight	ω_o	12.013 kg m^{-2} sec^{-2}	2.4605 lb ft^{-2} sec^{-2}

specific heat of air at constant volume is adopted as 1.40 (dimensionless).

σ - The mean collision diameter for air is assumed to be a constant for all altitudes (Ref. 52).

N - Avogadro's Number based on the scale $C^{12} = 12.0000$. (The International Union of Pure and Applied Chemistry, meeting in Montreal in 1961, adopted a new table of atomic weights based on the assignment of atomic weight 12.0000 to the C^{12} isotope.)

$^{*}R$ - The value of R adopted here is that given in reference 53 when the latter is corrected for the aforementioned change in the atomic-weight scale.

Definitions of physical variables:

Acceleration of gravity, $\vec{g}$

g - is the absolute value of acceleration due to gravity force per unit mass,

$$g = \left|\vec{g}\right| = \left|\nabla\phi\right| \qquad (2.2\text{-}351)$$

$$\vec{g} = -\nabla\phi \qquad (2.2\text{-}352)$$

where $\nabla\phi$ is the ascendant gradient of the geopotential per unit mass:

$$\phi = \phi_G + \phi_C \qquad (2\text{-}2\text{-}353)$$

The gravity force field is conceived as a conservative field defined respective to a rotating earth fixed reference frame. Therefore, the potential energy per unit mass of the field (or shortly the geopotential), ϕ, becomes an algebraic sum of (1) the potential energy, ϕ_G, (per unit mass) of the gravitational attraction in accordance with the Newton's universal law of gravitation, and (2) the potential energy, ϕ_C, (per unit mass) associated with the centrifugal force effects due to the rotating reference frame choice (Earth and a steady atmosphere rotating as one unit).

The resultant geopotential, ϕ, has constant values at the "equipotential level" surfaces of the resultant gravity field. The lines of gravity force are everywhere normal to the equipotential surfaces. At each point on any line of gravity force the gravity force vector, $\vec{g}$, is in the direction of the local tangent, positively sensed in accordance with the expression (2.2-352).

The earth's surface is taken as the reference zero equipotential ($\phi = 0$) surface, in form of an ellipsoid of revolution, whose ellipticity is defined by

$$f = 1 - \frac{b}{a} = \frac{1}{298.32} \,, \qquad (2.2\text{-}354)$$

where b is the semininor axis (or polar radium), and a is the equatorial radius of the earth, numerically given in Ref. 54.

The sea-level standard conditions are specified at a precise geographic latitude $\phi = 45°$ (geocentric latitude $\psi = 44.808°$), yielding the reference sea-level values in Table 2.2-4 of Ref. 27, (subscript o). The Standard Atmosphere is postulated along any of the gravity force curves passing through the points $\phi = 0$ and $g = g_o$ and at $\phi = 45°$, i.e., independent of the longitude angle θ, see Fig. (2.2-11).

The geometric altitude, Z, of a point is defined as the distance measured along the reference curved "line of force":

$$d\phi = g\,dZ$$
$$\therefore \phi = \int_0^Z g\,dZ \,. \qquad (2.2\text{-}355)$$

The analytical expressions for ϕ, ϕ_C, ϕ_G and the integral values of Z are specified in Ref. 27. The acceleration due to gravity, g, as a function of the geometric altitude, Z, is given in Fig. (2.2-12). Note that the difference between the geometric altitude as measured along the representative curved "line of force", and the corresponding distances along the several straight line distances shown in Fig. (2.2-11), are negligible in the altitude range in which the Standard Atmosphere is defined.

The geopotential altitude, H, is defined in Ref. 27 as:

$$\frac{1}{g_o}(\phi - \phi_o) = \frac{1}{g_z}\Delta\phi = \int_0^Z \frac{g}{g_z}\,dZ \,,$$

$$\phi_o \equiv 0$$

$$\therefore \frac{1}{g_o}\phi = \int_o^z \frac{g}{g_z}\,dZ = H \qquad (2.2\text{-}356)$$

where the integration is performed along the same curved "line of force" as in case of geometric altitude. Physically, the quantity H is equivalent to the concept of ϕ, which is the work done in elevating unit mass from sea-level to a geometric altitude Z, while dimensionally the quantity H in Eq (2.2-356) is reduced to the dimension of length. Note that the definition of H in the Ref. 27 does not correspond to its meteorological definition. The adopted definition (2.2-356) of H is expressed in the actual "standard meters", m, and is numerically equal to the corresponding geopotential altitude measured by a "geopotential standard meter", m', where,

$$1m' = 9.80665\ m^2\ sec^{-2}, \qquad (2.2\text{-}357)$$

i.e., m' is not an actual length, but rather a physical quantity compatible with the physical meaning of the geopotential altitude as work $[ML^2T^{-2}]$ done per unit mass $[M]$. Evidently, it is necessary to distinguish between an actual measuring operation by a real meter-rod (geometric altitude definition) and a physical process, related to the altitude concept, which can be dimensionally expressed in units of length (but not directly obtained by an active successive transposition of a fixed real meter rod). This is due to the fact that the real spatial distance between successive geopotential surfaces one geopotential unit apart, $(\phi_{n+1}-\phi_n = 1)$, increases with altitude, i.e., the successive geometric distances, ΔZ, between the successively equal geopotential differences $(\phi_{n+1}-\phi_n = \Delta\phi)$, are not the same when measured by a real meter rod. The spatial variability of the equal $\Delta\phi$ intervals is the inherent property of the resultant gravity field, see Eqs. (2.2-353) and (2.2-356) combined.

Molecular weight, M

The mean molecular weight of air, M, is assumed constant up to $Z = 90$ km. Above that geometric altitude M varies because of an increasing dissociation and a diffusive separation of various single components in the atomospheric air mixture, see Fig (2.2-13). With the reference scale,

$$M = M_o = 28.9644\ \left[\frac{kg}{kg\ mol}\right]. \qquad (2.2\text{-}357A)$$

Atmospheric pressure, p, see Fig (2.2-14)

The functional variation $p = p(z)$ is computed from the perfect gas law (2.2-349) and the hydrostatic equation (2.2-350).

Atmospheric density, ρ, see Fig. (2.2-15)

The functional variation $\rho = \rho(z)$ is computed from the perfect gas law expressed in terms of the molecular-scale temperature, T_M°:

$$\rho = \frac{M_o}{R^*}\,\frac{P}{T_M^\circ}\ \left[kg\ m^{-3}\right]. \qquad (2.2\text{-}358)$$

Absolute (kinetic) temperature, T°, see Fig. (2.2-16)

Based on the adopted, T_l°, reference value (see Table) any other absolute temperature, T°, is given by

$$T^\circ K = T_l^\circ K + t^\circ c \qquad (2.2\text{-}359)$$

where the magnitudes of the degrees Celsius and Kelvin are equal.

Molecular-scale temperature, T_M°

The molecular-scale temperature is defined by

$$T_M^\circ = \frac{M_o}{M}\,T^\circ \qquad (2.2\text{-}360)$$

up to $Z = 90$km, $M_o = M$, and $T^\circ = T_M^\circ$. Above $Z = 90$ km, $M = M(Z)$, see Fig (2.2-13), and thus $T^\circ \neq T_M^\circ$, see Fig (2.2-17).

Note that the kinetic absolute temperature, T°, is defined in terms of the translational molecular degrees of freedom only, while the molecular scale temperature, T_M°, comprises the

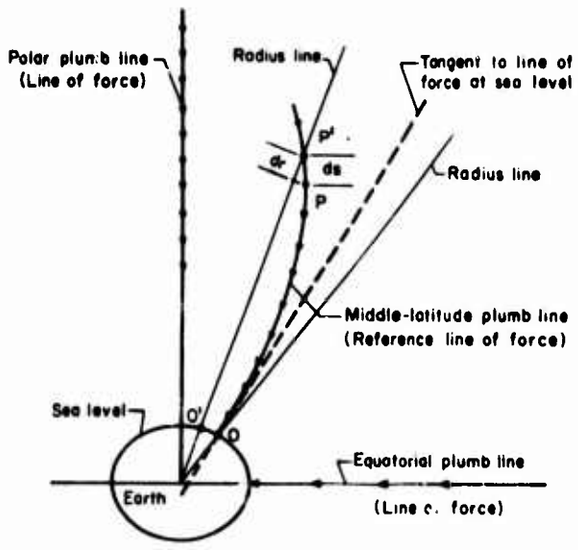

Fig. (2.2-11) Relationships between various heights. Scale exaggerated. (Ref. 27).

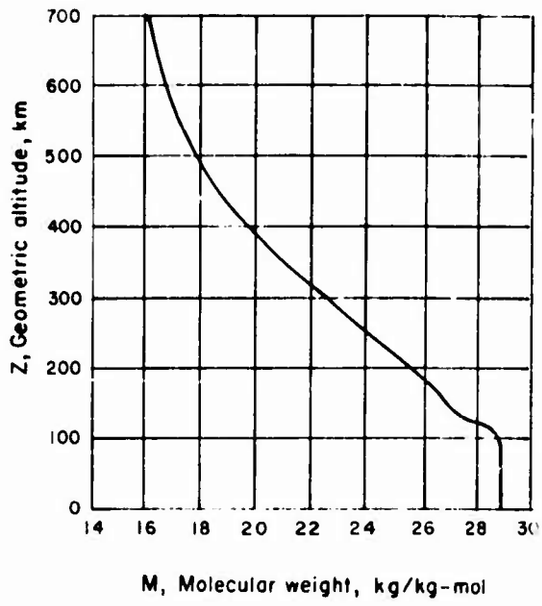

Fig. (2.2-13) Molecular weight M as a function of geometric altitude Z. (Ref. 55)

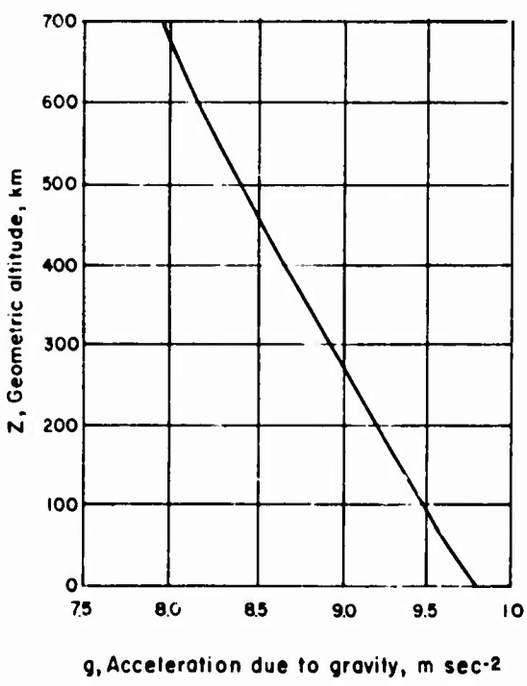

Fig. (2.2-12) Acceleration due to gravity g as a function of geometric altitude Z. (Ref. 27)

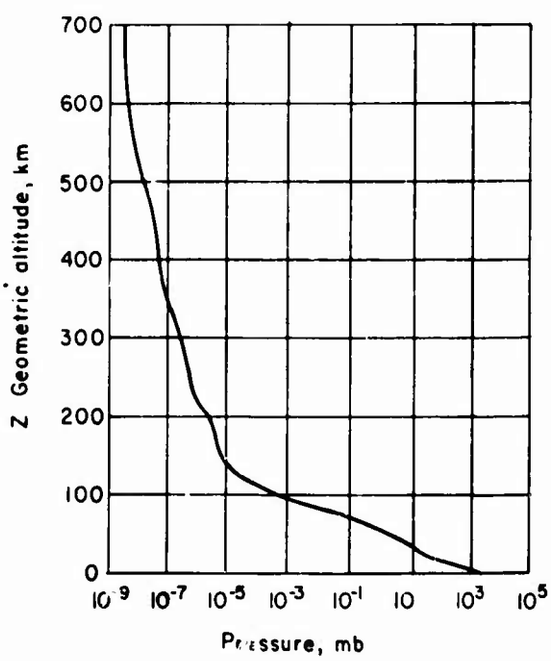

Fig. (2.2-14) Pressure P as a function of geometric altitude Z. (Ref. 27).

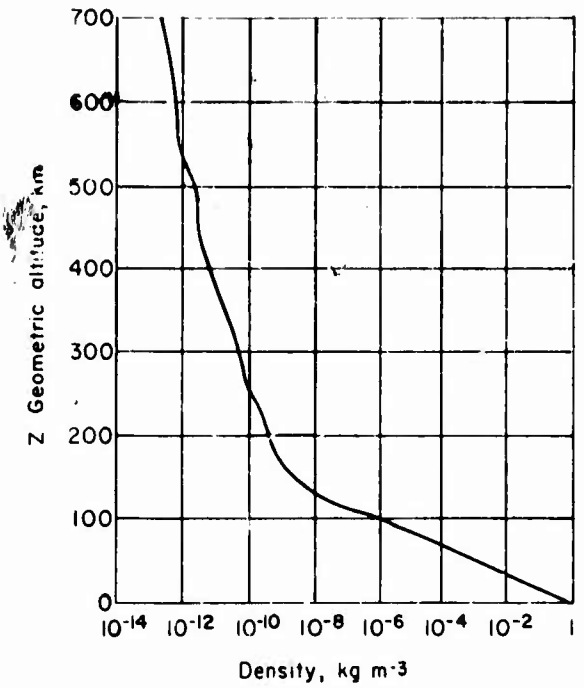

Fig.(2.2-15) Density ρ as a function of geometric altitude Z. (Ref. 27).

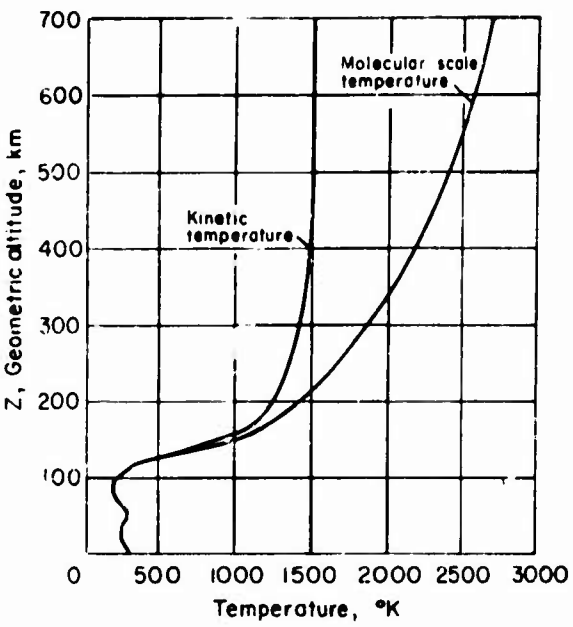

Fig (2.2-17) Molecular-scale temperature T_M° and kinetic temperature T° as functions of geometric altitude Z. (Ref. 27).

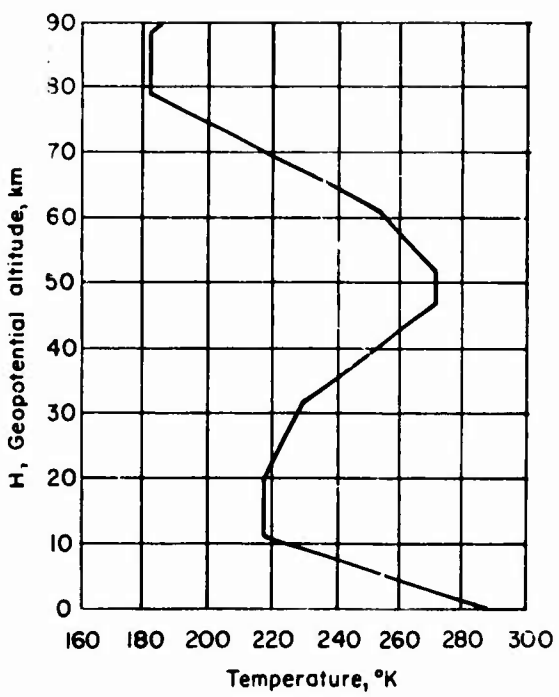

Fig. (2.2-16) Temperature T° as a function of geopotential altitude H. ($T_M^\circ = T^\circ$ below Z = 90km or H = 88.743 km.) (Ref. 27).

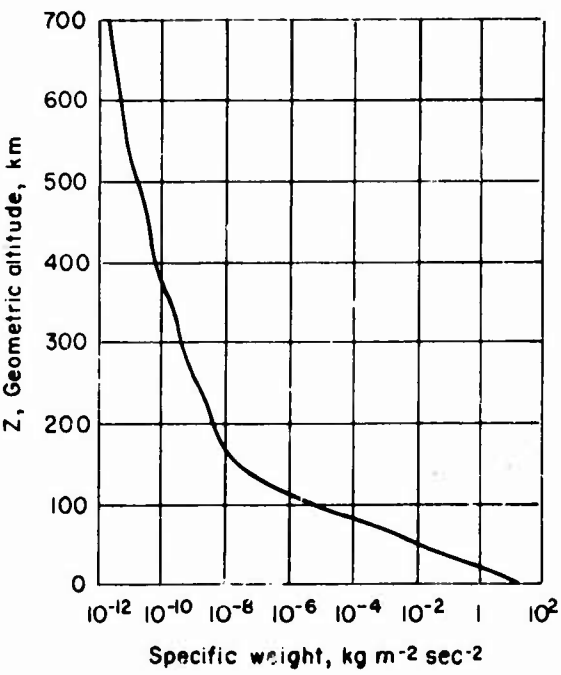

Fig.(2.2-18) Specific weight ω as a function of geometric altitude Z. (Ref. 27).

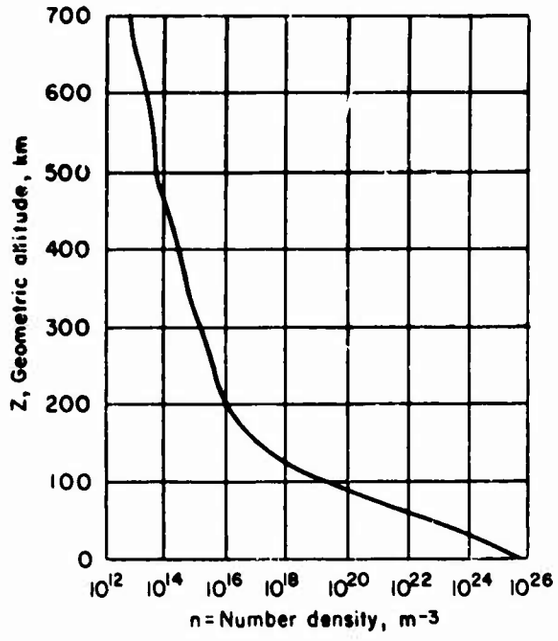

Fig. (2.2-19) Number density n as a function of geometric altitude Z. (Ref. 27).

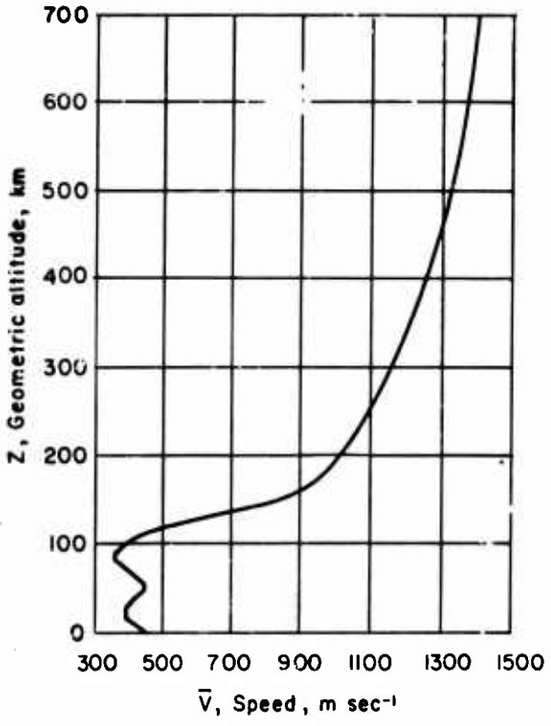

Fig. (2.2-20) Mean particle speed $\bar{V}$ as a function of geometric altitude Z. (Ref. 27).

molecular weight changes due to the diffusive separation of the dissociated air molecules, resulting in a variable species stratification by altitude.

Specific weight, w , see Fig (2.2-18)

ω - is defined as weight per unit volume:

$$w = \frac{dw}{dV} = g\frac{dm}{dV} = g\rho \left[kg\ m^{-2} sec^{-2} \right]. \qquad (2.2\text{-}361)$$

Number density of air, n , see Fig (2.2-19)

n - is defined as the number of atmospheric particles of various single species per unit volume. The particles are considered to be neutral:

$$n = \frac{M_o}{R^*}\frac{NP}{MT_M^o} \left[m^{-3} \right]. \qquad (2.2\text{-}362)$$

Mean air-particle speed, $\bar{V}$, see Fig (2.2-20)

$\bar{V}$ - is defined in Ref. 27 as the arithmetic average of the speed of all particles in a given volume element assuming a sufficiently great number of neutral particles and no pressure and temperature gradients within the volume element:

$$\bar{V} = \left(\frac{8}{\pi}\frac{R^*}{M_o}T_M^o \right)^{1/2} \left[m\ sec^{-1} \right]. \qquad (2.2\text{-}363)$$

Mean free path, L , see Fig (2.2-21

L - is the mean value of the distances traveled by individual neutral particles between successive collisions in a given volume:

$$L = \frac{1}{\sqrt{2}\,\pi N \sigma^2}\frac{R^*}{M_o}\frac{MT_M^o}{P} \left[m \right], \qquad (2.2\text{-}364)$$

where σ is the effective collision diameter of the representative mean air particle.

Average collision frequency, ν , see Fig (2.2-22)

ν - is the ratio of the average spee of the air particles, $\bar{V}$, and the mean free path, L , of the air particles treated as neutral in a given volume:

$$\nu = \frac{\bar{V}}{L} = 4\sigma^2 N \left(\pi \frac{M_o}{R^*} \right)^{1/2} \frac{P}{M(T_M^o)^{1/2}} \left[sec^{-1} \right]. \qquad (2.2\text{-}365)$$

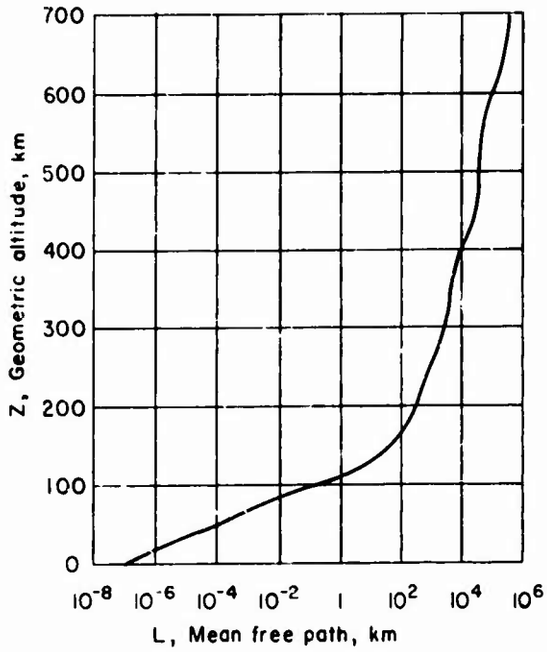

Fig. (2.2-21) Mean free path L as a function of geometric altitude Z. (Ref. 27).

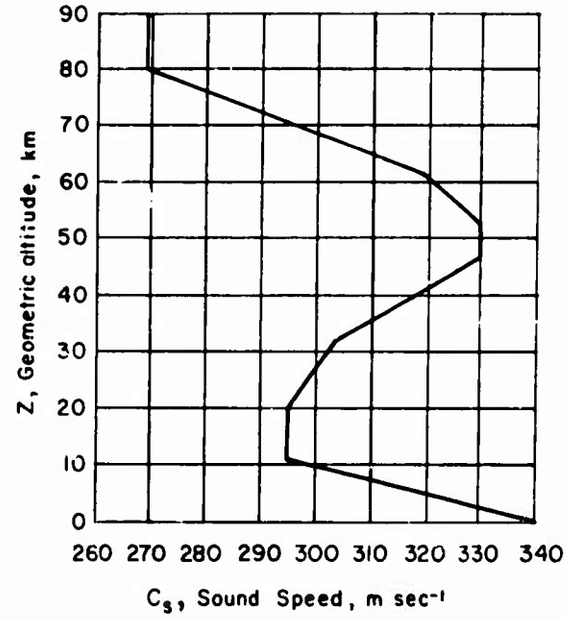

Fig. (2.2-23) Sound speed C_s as a function of geometric altitude Z. (Ref. 27).

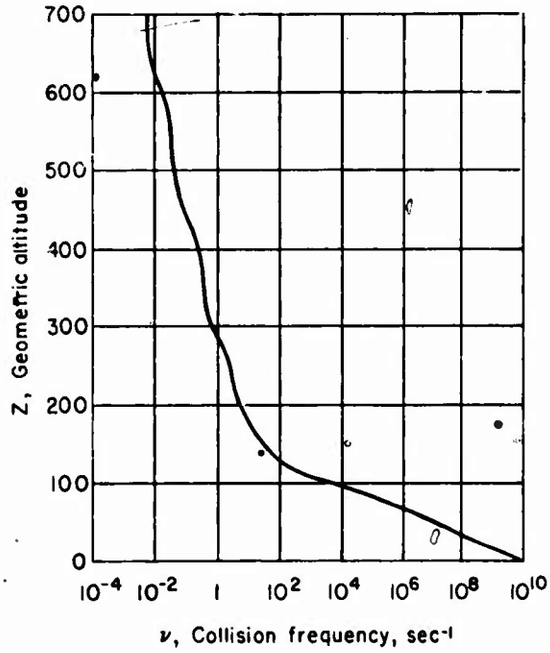

Fig. (2.2-22) Collision frequency ν as a function of geoaltitude Z. (Ref. 27).

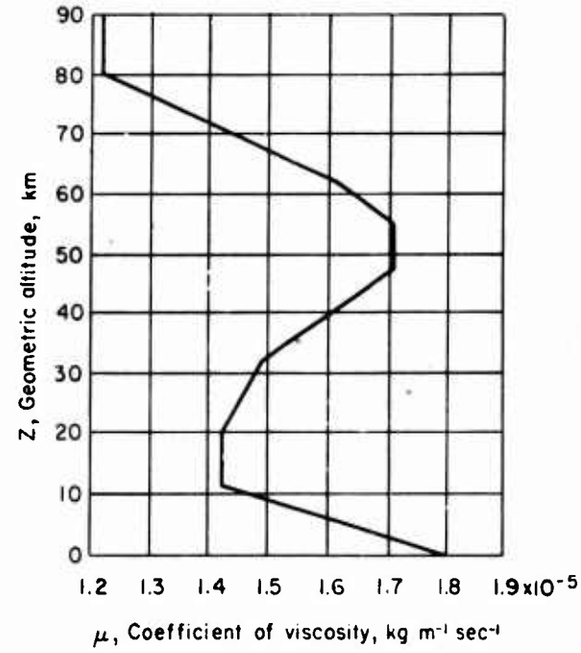

Fig. (2.2-24) Coefficient of viscosity μ as a function of geometric altitude Z. (Ref. 27).

(1) Speed of sound, C_s , see Fig (2.2-23)

$$C_s = \left(\gamma \frac{R^*}{M_o} T_M^\circ\right)^{1/2} \quad \left[m \ sec^{-1}\right]$$

$$\gamma = \frac{C_p}{C_v} = 1.40$$

(2.2-366)

Note: the speed of sound concept looses its meaning at higher altitudes (Z = 90 km) due to the excessive air rarefaction (free molecular conditions at low pressures and densities and high mean free path intervals).

Coefficient of viscosity, μ , see Fig (2.2-24)

The basic definition of μ is taken from the kinetic theory of gases, and then numerically modified by introduction of two temperature-dependent experimental constants, β and S (Sutherland's constant):

$$\mu = \frac{\beta T^{3/2}}{T + S} \quad \left[kg \ m^{-1} \ sec^{-1}\right] ,$$

$$\beta = 1.458 \times 10^{-6} \quad \left[kg \ sec^{-1} \ m^{-1} \ (^\circ K)^{-1/2}\right] ,$$

$$S = 110.4^\circ K . \qquad (2.2-367)$$

Eq (2.2-367) fails at very high and very low temperatures, as well as at altitudes in excess of 90 km.

Kinematic viscosity, η , see Fig (2.2-25)

η - is defined as:

$$\eta = \frac{\mu}{\rho} \quad \left[m^2 \ sec^{-1}\right] \qquad (2.2-368)$$

with all limitations pertaining to μ.

Coefficient of thermal conductivity, k , see Fig (2.2-26)

k for air mixture up to 90 km is defined by the empirical expression from Ref. 51:

$$k = \frac{6.325 \times 10^{-7} \ T^{3/2}}{T^\circ + 245.4 \times 10^{-(2/T^\circ)}} \left[k \ cal \ m^{-1} \ sec^{-1} (^\circ K)^{-1}\right] .$$

(2.2-369)

Mole volume, v , see Fig (2.2-27)

$$v = \frac{M}{\rho} = \frac{R^*}{M_o} \frac{M T_M^\circ}{P} \quad \left[m^3\right] .$$

(2.2-370)

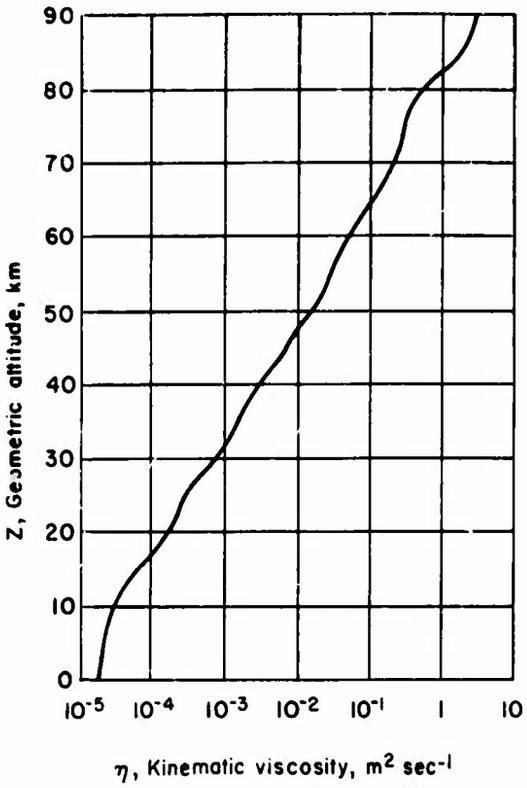

Fig.(2.2-25) Kinematic viscosity η as a function of geometric altitude Z. (Ref. 27).

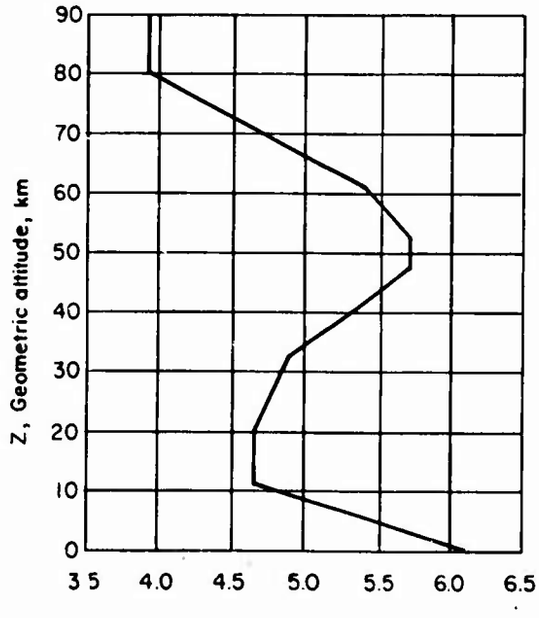

Fig.(2.2-26) Coefficient of thermal conductivity k as a function of geometric altitude Z. (Ref. 51)

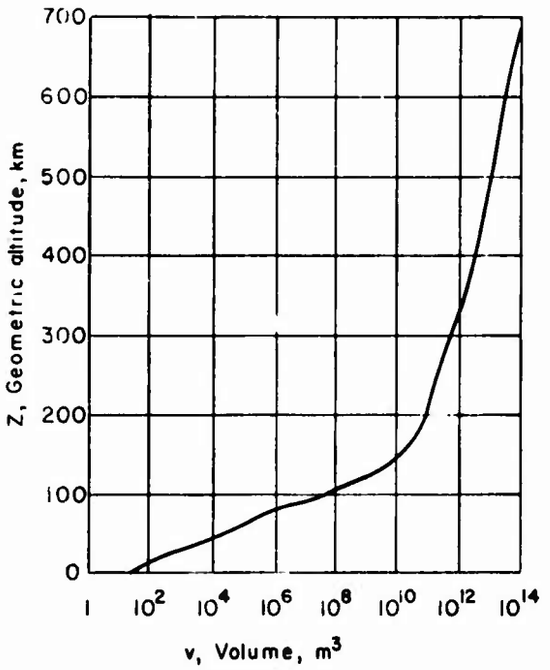

Fig.(2.2-27) Mole volume v as a function of geometric altitude Z. (Ref. 27).

Table I.4(a). METRIC TO ENGLISH CONVERSIONS OF UNITS OF LENGTH, MASS, AND GEOPOTENTIAL

A. Defined relations (the constants are adopted as being exact):

1 foot	= 0.3048 meter
1 i.n. mi	= 1,852 meters
1 pound	= 0.45359237 kilogram
1 standard geopotential foot	= 0.3048 standard geopotential meter

B. Derived relations:

1 meter	= 3.2808399...feet
1 meter	= 5.3995680...x 10^{-4} i.n.mi
1 kilogram	= 2.2046226...pounds
1 i.n. mi	= 6,076.1155...feet
1 foot	= 1.6457883...x 10^{-4} i.n.mi
1 standard geopotential meter	= 3.2808399...standard geopotential feet

Table I.4(b) METRIC TO ENGLISH AND ABSOLUTE TO NONABSOLUTE CONVERSIONS OF TEMPERATURE UNITS

A. Defined

$t(^oC) = T(^oK) - T_i(^oK)$, where $T_i(^oK) = 273.15(^oK)$

$T(^oR) = 1.8T(^oK)$

$t(^oF) - t_i(^oF) = T(^oR)$, where $t_i(^oF) = 32(^oF)$

B. Derived relations:

$t_i(^oC) = 0(^oC)$

$T_i(^oR) = 491.670(^oR)$

$t(^oC) = [T(^oR) - T_i(^oR)]/1.8 = [t(^oF) - t_i(^oF)]/1.8$

$T(^oR) = 1.8[t(^oC) + 273.15(^oC)] = t(^oF) - t_i(^oF) + 491.670(^oR)$

$t(^oF) - 32(^oF) = 1.8t(^oC) = 1.8[T(^oK) - 273.15(^oK)]$

Table I.4(c) ABSOLUTE SYSTEMS OF UNITS TO ABSOLUTE-FORCE, GRAVITATIONAL SYSTEM OF UNITS, METRIC-ENGLISH

A. Defined:

1 force unit = 1 mass unit x g_o

B. Derived relations:

1 kgf = 9.80665 kg m sec^{-2}

1 kg = $\frac{1}{9.80665}$ kgf sec^2 m^{-1} = 0.10197162 kgf sec^2 m^{-1}

1 lbf = 0.45359237 kgf

1 lbf = 32.174049 lb ft sec^{-2}

1 lb = 0.031080950 lbf sec^2 ft^{-1} = 0.031080950 slug

1 slug = 32.174049 lb

Table 2.2-5(d) THERMAL TO MECHANICAL UNITS, METRIC-ENGLISH

A. Defined relations:*

$$1 \text{ kg-cal} = \frac{1}{860} \text{ kw-hr (exact)}$$

$$1 \text{ kg-cal} = \frac{1.8}{0.45359237} \text{ BTU} = 3.9683207 \text{ BTU}$$

1 joule = 1 watt-sec

B. Derived relations:

$$1 \text{ kw-hr} = 3.6 \times 10^6 \text{ watt sec} = 3.6 \times 10^6 \text{ joules}$$

$$1 \text{ kg-cal} = \frac{3.6 \times 10^6}{860} \text{ joules} = 4{,}186.0465 \text{ joules}$$
$$= 4{,}186.0465 \text{ kg m}^2 \text{ sec}^{-2}$$

$$1 \text{ kg-cal} = \frac{3.6 \times 10^6}{860 \times 9.80665} \text{ m kgf} = 426.85795 \text{ m kgf}$$

$$1 \text{ kg-cal} = \frac{3.6 \times 10^6}{860 \times 9.80665 \times 0.45359237 \times 0.3048} \text{ ft lbf}$$
$$= 3087.4696 \text{ ft lbf}$$

$$1 \text{ BTU} = \frac{0.45359237}{1.8} \text{ kg-cal} = 0.25199576 \text{ kg-cal}$$

$$1 \text{ BTU} = \frac{3.6 \times 10^6}{860 \times 0.3048 \times 9.80665 \times 1.8} \text{ ft lbf}$$
$$= 778.02922 \text{ ft lbf}$$

$$1 \text{ BTU} = \frac{3.6 \times 10^6}{860 \times (0.3048)^2 \times 1.8} \text{ lb ft}^2 \text{ sec}^{-2}$$
$$= 25032.349 \text{ lb ft}^2 \text{ sec}^{-2}$$

*The calorie used here is the International Steam Table calorie and the joule is the mean international joule.

(2) Ambient Atmospheric Data for Various Flight Speeds and Flight Altitudes

The Standard Atmosphere data need to be reinterpreted in terms of different flight speeds and airflow regimes specified in Section 1.7. The few respective data are compiled below in form of generalized graphs, indicating the relative importance and order-of-magnitude of the primary atmospheric airflow parameters, which can serve as a first criterion for a later choice of the corresponding explicit theoretical or experimental methods in evaluating the aerodynamic force components for a given vehicle configuration and its operational atmospheric flight specifications.

(i) Initial Conditions

The static equilibrium change in atmospheric air composition with altitude is illustrated in Fig (2.2-28). For subsonic, transonic, and supersonic flight speed regimes, which are largely confined to lower atmospheric strata, the initial ("at infinity") air composition remains near-standard, as specified in the preceding paragraph (1) of this section. The same holds for hypersonic flight speeds, if realized at lower altitudes. However, the hypersonic flight regimes are normally achieved at considerably higher altitudes, where the corresponding change in the initial (static) state of the atmospheric air composition becomes the proper condition "at infinity" for the relative airflow analysis around a given body configuration. The respective variations in all important physical parameters under the static conditions are obtainable from the Standard Atmosphere tables and figures.

(ii) Flow Regimes

For a given flight trajectory, the four characteristic flow regimes (continuum, slip, transitional, and free molecular) can be estimated in terms of flight Mach Number and flight altitude from the respective data presented in Sections 1.4 and 1.5.

For a more general illustrative purpose, the few flight plans of some typical vehicle categories and the respectively realized flow regimes and wall (stagnation) temperatures in terms of flight altitudes and flight speeds are illustratively given in Figs. (2.2-29) and (2.2-30)

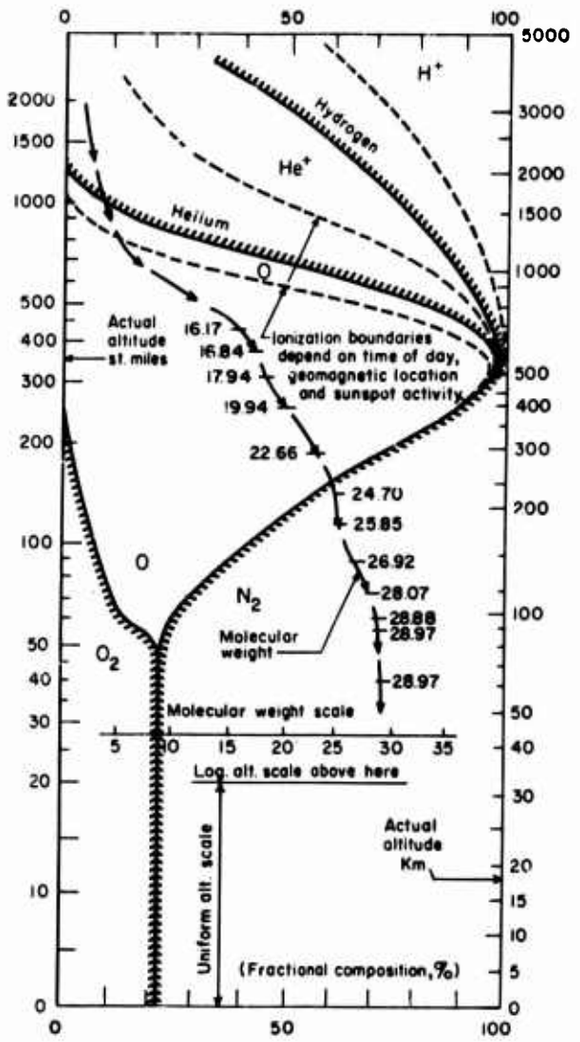

Fig. (2.2-28). Estimated (1962) fractional composition of the atmosphere, and molecular weight, as a function of altitude. Data above 500 km somewhat uncertain. (Ref. 57).

(iii) Temperature Effects at Different Flight Regimes

For a given set of initial atmospheric conditions and a specified flow regime, it is necessary to take into account variations in air properties as affected by the respective changes of the airstream flow pattern around a given body geometry. The analysis is usually done by considering the inviscid and the viscous (boundary layer) flow regions separately. The specific aerothermal considerations respective to the latter are relatively much more complex and involved, and therefore are treated separately in the section on skin-friction

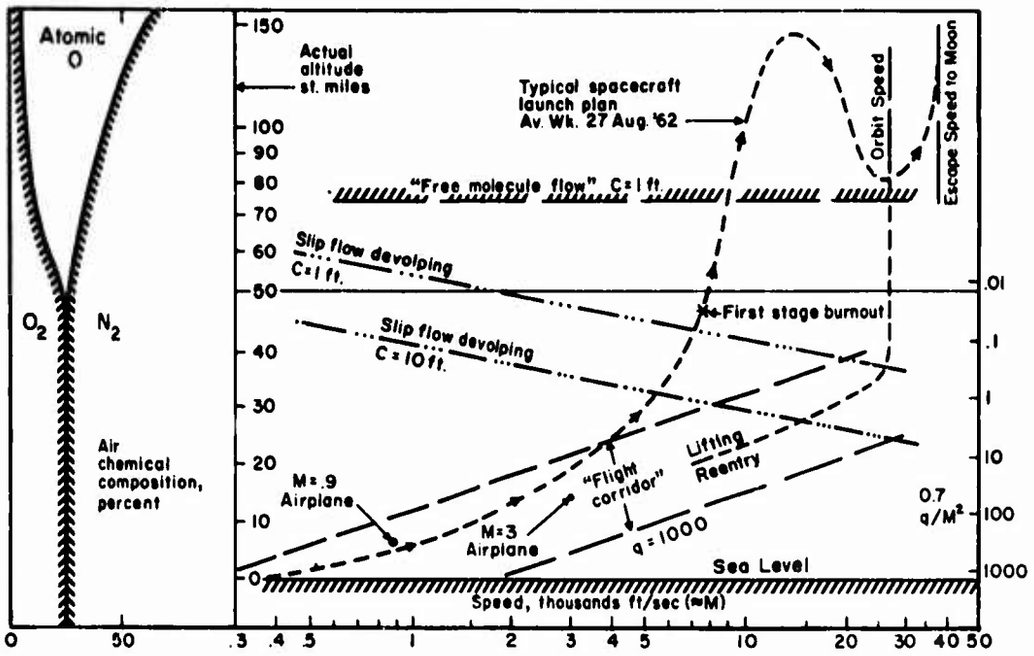

Fig. (2.2-29) Altitude versus speed and typical flight plans. (Ref. 58).

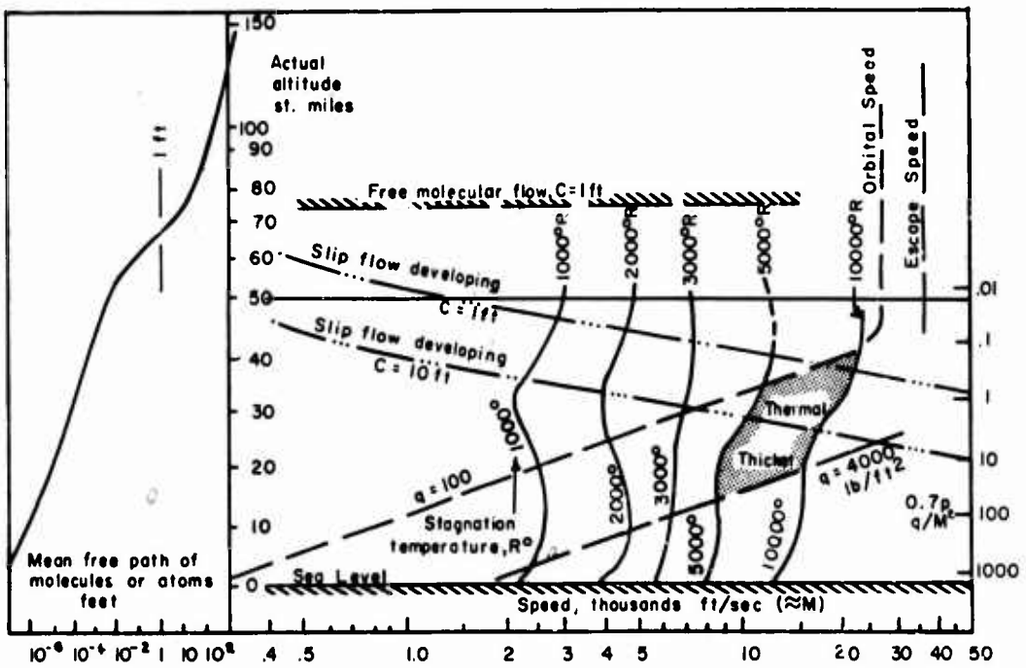

Fig (2.2-30) Altitude versus speed, vehicle wall temperatures, and mean free path of air particles. (Ref 58)

data. Some of the most important aerothermal characteristics of the inviscid flows can be easier formulated in an order-of-magnitude generalized form in terms of the involved temperature variations and the free stream (or flight) Mach Number.

At subsonic, transonic and supersonic speeds, the temperature effects on the air composition and the air properties are of secondary importance for aerodynamic force analysis purposes. The relevant data from classical kinetic theory of gases and classical thermodynamics concepts are sufficiently accurate for most of the theoretical investigations. At hypersonic speeds, the generally higher temperature levels in the regions behind the strong shocks and near the forward stagnation point can appreciably affect the aerothermal properties of air. An illustration of the conditions at the region of the stagnation point is given in Fig (2.2-31). Variations in air composition for four temperature levels are indicated in Fig (2.2-32). When related to the unit mass, the high temperatures affect the total number of contained particles (respectively increased unit volumes) and consequently the molecular weight of air also.

The specific heats represent calorically the amount of heat per unit mass of gas required to raise the temperature for one degree. Since at elevated temperatures the added heat is distributed among a greater number of intensified molecular degrees of freedom, i. e., since the generated amount of heat (by high compression, for instance) is not solely used up for an increase of the translational energy of molecules (which is measured by the concept of the kinetic absolute temperature), but has to be partially distributed for an intensification of the rotational, vibrational, dissociation and ionization internal energy levels also, the specific heats per unit mass of air (i.e., required for a unit rise of its temperature) are correspondingly increased, see Fig (2.2-33). It is evident that once air dissociation is set up, a manyfold increase in specific heats takes place.

The four temperature levels in Fig

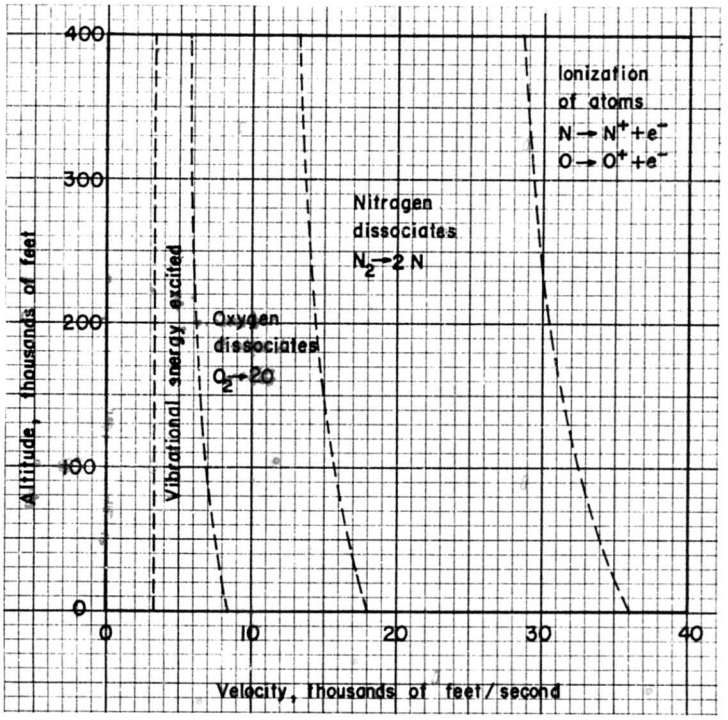

Fig. (2.2-31) State of the air at the stagnation point of a body. (Ref. 56).

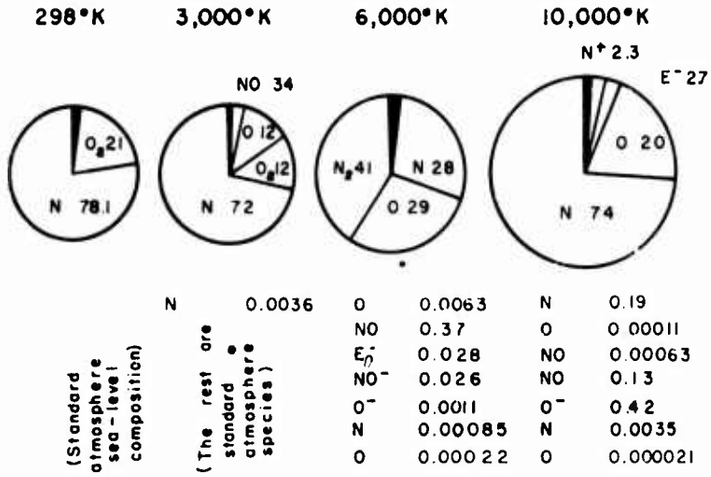

FIG (2.2-32) Fractional composition of air by volume as a function of temperature at standard density and pressure.

NUMBERS REPRESENT FRACTIONAL COMPOSITION OF AIR BY VOLUME. THE TOTAL NUMBER OF PARTICLES PER UNIT MASS IS ILLUSTRATED BY MAGNITUDE OF THE CORRESPONDING CIRCULAR SEGMENTS. (REF 59)

(2.2-32) have been chosen as representative indicators of the intensity and the extent of the structural changes in air with increasing temperatures, as encountered at hypersonic speeds. For instance, during the denser atmospheric flight phases of long range ballistic or winged vehicles, the temperatures in the flow regions behind the strong bow shock waves can reach an order of magnitude of 6000 °K. Respective to the air composition, the thermal sequence of events at different temperatures is represented by the following trend:

At ~1500 °K the excitation of the vibrational degrees of freedom of N_2 and O_2 sets up.

At ~3000 °K the molecules $O_2 \rightleftharpoons 2O$ dissociate. The free oxygen atoms react chemically with nitrogen, forming the nitric oxide (NO), which in its turn, decomposes into atoms of O and N as temperatures are further increased.

At ~6000 °K, the molecules O_2 are almost completely dissociated, while the dissociation of $N_2 \rightleftharpoons 2N$ starts and a partial ionization of O, N, NO atoms sets up.

At ~10,000 °K the molecular fractions of N_2 and O_2 become negligible, the air composition being predominantly atomistic, with a considerable fraction of nitrogen ions and an appreciable concentration of free electrons.

From the inviscid flow theory point, the resulting change in air properties do not significantly affect the analytical methods of calculation of the presumed equilibrium gas flows about slender bodies at relatively small angles of attack. The methods, developed for a perfect gas at subsonic and supersonic speeds, are formally extended to the hypersonic inviscid flow conditions, with corresponding modifications allowing for the hypersonic perfect gas flow pattern characteristics. The high temperature effects and the changed air properties affect mostly the entropy and the enthalpy (i.e., the energy equation) expressions, so that a specification of the free stream stagnation temperature (or the free stream specific heat ratio alternatively) appears as an additional governing natural variable, which, in conjunction with the Mach Number, enters into the idealized, equilibrium inviscid hypersonic flow computations.

Contrary to the inviscid flow case, the hypersonic boundary layer theories and the blunt body solutions are considerably influenced by the changed structural and physical properties of air. The high temperature effects are, in general, of significance whenever the heat, momentum and mass transfer phenomena become important, as, for instance, in case of skin-friction force analysis at large. The strong

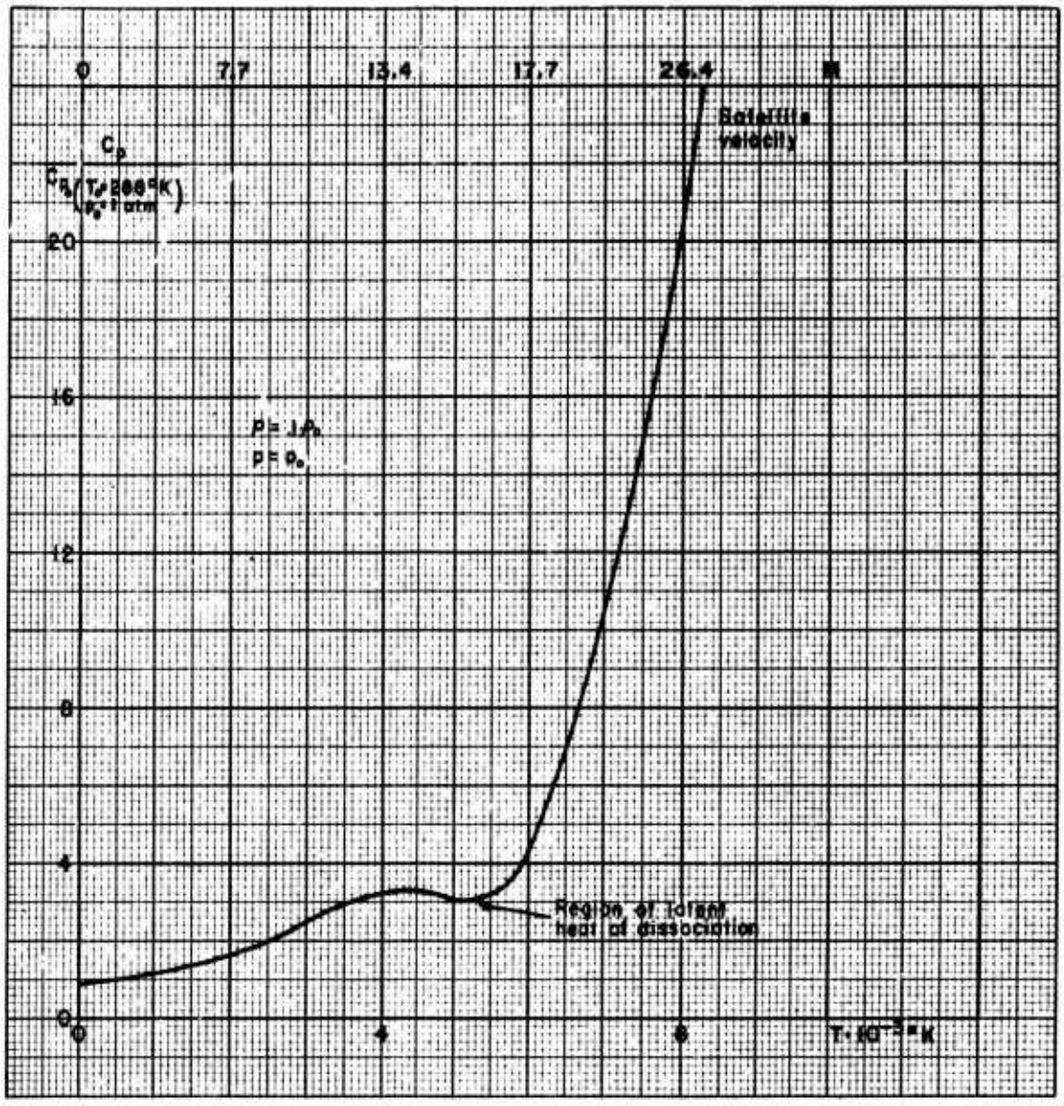

Fig. (2.2-33) Dependence of the specific heat of air upon temperature. (Ref. 59).

and concentrated temperature gradients in viscous and heat conducting flow regions not only change the viscosity, μ , and the heat conductivity, k , gas characteristics numerically, but also affect the local concentration rates of individual gas components and their equilibrium conditions, and subsequently the heat transfer rates, the heat currents orientation and the species diffusive fluxes.

Comparing the intensity of dissociative and recombination processes to the diffusivity rates, the viscous boundary layers fall into two types:

(a) "Frozen flow" boundary layers, if no dissociation or recombination takes place within the boundary layer, i.e., when these processes occur in the outside flow only, which is presumed to be in equilibrium (dissociation rates = recombination rates). The situation is realized when the characteristic time of the outside flow reactions is greater than the time necessary for a dissociated molecule or an atom to diffuse through the boundary layer. Upon reaching the body surface, the recombination process may additionally occur, if the surface has a lower temperature than the main outside flow.

These recombination rates at a relatively cooler surface depend upon the catalytic properties of the surface material.

(b) "Equilibrium flow" boundary layers, if the dissociative and recombination rates are high enough and the associated characteristic reaction times small enough, so that both the diffusive and the dissociative phenomena are taking place within the boundary layer itself, so that at each point the respective local concentration of atoms and molecules is a function of the local temperature only.

In general, the establishment of changing equilibrium conditions in a flowing gas is not an instantaneously accomplished process. As specified in Section 2.2.5, the equilibrium pressures and temperature changes, as well as the overall internal energy content build up are realized only after a finite time interval, which depends on both the instantaneous and on the preceding history of time rates at which the particle densities and the internal energy changes in a flowing gas are taking place (i.e., on the totality of fluid flow field variations in ρ, T° and ρ). In other words, the "relaxation times" and a successive realization of gaseous states in thermal equilibrium thus depend on the flight velocity and the flight altitude conditions.

As an illustration, in Fig (2.2-34) two equilibrium dissociation regions for two points (.3 m and 3 m respectively), measured along the surface from the forward stagnation point of a blunt body, are presented in terms of the flight speed and the flight altitude. The dissociation effects behind a strong, detached oblique shock are considered only, since they do play the most prominent percentage role in the establishment of the thermal equilibrium conditions. The dashed lines, indicating the degrees of dissociations of .01 and .04 respectively at the stagnation point, designate the tentative limits left of which the dissociation would be considered insignificant. The typified ballistic, glide and satellite trajectories are drawn for comparative flight dynamics illustrative purposes.

A relatively good electrical conductivity of a dissociated and ionized air flow behind the strong shocks at hypersonic speeds presents mostly a communication problem. The relative amount of free electrons is small (even at $T^{\circ} \sim 10{,}000^{\circ} K$) for significant airflow effects (see Fig 2.2-32), the dissociation remaining the primary factor. The elevated temperatures promote also an intensification of the radiation emissivity of hot gaseous species. The radiative flux is partially transmitted and absorbed by the body surface, affecting additionally the surface temperatures. But for the most part, the radiation is scattered and absorbed among the adjacent layers of the airstream itself.

(iv) Thermal Equilibrium Flow Analysis at High Mach Numbers

For the sake of correlating the general thermodynamic data from Sections 2.5 and 2.6, to the hypersonic flow conditions in particular, as may be needed for later aerodynamic force analysis purposes, a generalized examplary outline of the thermal equilibrium time history of a high speed flow across a strong shock is presented. The illustration is best representative for gas flow regions behind strong, oblique and detached shock waves associated with blunt bodies at hypersonic speeds. The respective temperature-time graph in Fig (2.2-35) sketches the relaxation time sequence along a streamline for various degrees of freedom.

The station 1 denotes the airflow in front of the shock wave, with pressures, densities, temperatures and the air composition assumed at near standard conditions; the (active) translational and the rotational degrees of molecular freedom are completely aroused and the internal energy content ($\epsilon_0 = \epsilon_t + \epsilon_r$) corresponds to its thermal equilibrium value at $T_1^{\circ} \sim 300^{\circ} K$, ($\gamma = 1.4$). The station 2 denotes conditions just behind a strong shock, the airflow being compressed to the corresponding higher values of pressure, density and temperature in terms of the free stream Mach Number, $M \gg 1$ and the shock wave angle, β , as specified by the respective across-the-shock conditions(59). It is supposed that $T_2^{\circ} \gg T_1^{\circ}$, so that the necessary thermal conditions for excitation of all inert degrees of molecular freedom are present. The relaxation time intervals required for a complete realization of the thermal equilibrium conditions for different degrees of freedom are different. The new translational and rotational thermal equilibriums behind the shock are realized

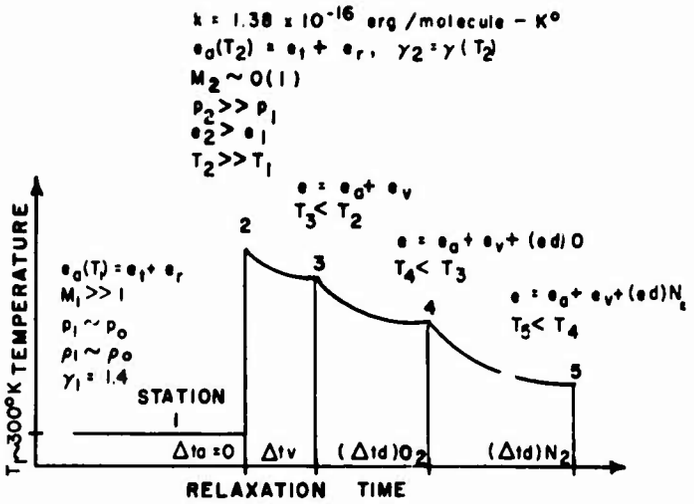

Fig (2.2-35) Variation of temperature with time from its free-stream value to its equilibrium values. (Ref 58)

almost instantaneously, while the vibrational mode is just set off.

The new internal energy equilibrium, $e_v(T_2^\circ)$, due to translational degrees is achieved in almost a single molecular collision within the highly compressed region of the shock itself(12); the total equilibrium transition between $e_t(T_1^\circ)$ and $e_t(T_2^\circ)$ is achieved in a spatial interval of the order of one or two mean free molecular paths, $\bar{\lambda}$. For ordinary monoatomic and diatomic gases at near standard conditions $\bar{\lambda}_o \sim 10^{-5}$ cm; it is a weak function of temperature and inversely proportional to density changes. Thus, since the temperature jump, $T_2^\circ \gg T_1^\circ$ is realized in the order of a mean free molecular path, the strong shock wave thickness itself is of the same order of magnitude.

The rotational degree approaches the equilibrium condition at an estimated number of collisions between 10 and 100. For all practical purposes, the corresponding relaxation time interval is still negligible, $\Delta t_r \sim 0$.(31)

The temperature of the air stream at the station 2 is then defined by (see Section 2.2.5):

$$e_a(T_2^\circ) = e_t(T_2^\circ) + e_r(T_2^\circ),$$

$$e_a(T_2^\circ) + \frac{p_2}{\rho_2} = \frac{\beta_a p_2}{\rho_2} = \beta_a R T_2^\circ,$$

$$\beta_a = \beta_t + \beta_r = \frac{7}{2} \text{ for air.}$$

(2.2-372)

At the station 3 the vibrational internal energy has achieved an equilibrium, while the dissociation process is practically only started. The relaxation time interval, Δt_v, reflects the considerably increased number of collisions required for a full realization of the internal vibrational energy, e_v. The corresponding temperature drop $T_3^\circ < T_2^\circ$, indicates the corresponding part of the translational energy Δe_t which has been used in the process. For diatomic molecules, the vibrational internal energy, e_v, is negligible at near standard conditions, constituting only about 1% of the active (translational and rotational) energy, e_a. From the equations (2.2-298) and (2.2-299) it is evident that $Z \to 0$ as $T^\circ \to \infty$, and $e_v \longrightarrow RT^\circ$. But, the gradient

$$\frac{de_v}{dT^\circ} = Cv_v \qquad (2.2\text{-}373)$$

is appreciable, even at lower temperatures at which (θ_v) itself may be not prominent; therefore, the specific heats ratio

$$\gamma = \frac{\left(\frac{7}{2}\right)R + Cv_v}{\left(\frac{5}{2}\right)R + Cv_v} \qquad (2.2\text{-}374)$$

is affected by excitation of the vibrational mode, causing a considerable departure from the perfect gas law. The respective numerical data can be found in Ref. 31.

The conditions at the station 3 can be computed in terms of the conditions at the station 2 by application of the mass, momentum and energy conservation principles. At the station 2 (see Section 2.2.5):

$$\gamma = \frac{n_a + 2}{n_a} = 1.4 \,, \qquad (2.2\text{-}375)$$

$$\beta_a = \frac{\gamma}{\gamma - 1} = \beta_t + \beta_r + 1 = \frac{3}{2} + 1 + 1 = \frac{7}{2} = 3.5. \qquad (2.2\text{-}376)$$

At the station 3, assuming $T_o^\circ \sim 300^\circ K$, according to Ref. 31:

$$\beta_a + \beta_v = 4.7 \,. \qquad (2.2\text{-}377)$$

The conservational principles:

$$\rho_3 V_3 = \rho_2 V_2 = \text{const} = C_1 \,,$$

$$\rho_3 + \rho_3 V_3^2 = p_2 + \rho_2 V_2^2 = \text{const} = C_2 \,,$$

$$4.7\left(\frac{p_3}{\rho_3}\right) + \left(\frac{V_3^2}{2}\right) = 3.5\left(\frac{p_2}{\rho_2}\right) + \left(\frac{V_2^2}{2}\right) = \text{const} = C_3 \qquad (2.2\text{-}378)$$

yield the solutions:

$$\rho_3 = \frac{4.7\,C_2 + \sqrt{(4.7\,C_2)^2 - 16.8\;C_3 C_1^2}}{2\,C_3} \,, \qquad (2.2\text{-}379)$$

$$p_3 = \frac{R_o}{M}\rho_3 T_3^\circ \,,$$

$$R_o = 8.31432 \times 10^7 \,(\text{erg}/\text{mole}\,^\circ K) \,,$$

$$M = 28.8 \,(\text{gr}/\text{mole}) \,. \qquad (2.2\text{-}380)$$

The stations 4 and 5 represent the equilibrium states for dissociation of O_2 and N_2 respectively. The equilibrium is characterized by the condition that the dissociation rates must be equal to the recombination rates for a given temperature. The final conditions at the stations 4 and 5 can be computed using the method from Ref. 60. The results of the computations at the station 4 are:

T_1°, °K	M_1	T_2°, °K	ρ_2/ρ_1	p_2/p_1	T_3°, °K	ρ_3/ρ_2	p_3/p_2	T_4°, °K	ρ_4/ρ_3	p_4/p_3
300	10	6116	5.7	116	4622	1.4	1.06	...	...	...
300	12	8683	5.8	168	6564	1.4	1.06	4100	1.37	1.03
300	14	11,716	5.8	228	8857	1.4	1.06	6440	1.18	1.03

Comparison of the results with the corresponding normal shock relationships (Rankine-Huyoniot) for perfect gases at $M_1 = 12$ are:

	Ref 60	Perfect gas
ρ_4 / ρ_1	11.1	5.8
T_4° / T_1°	13.65	21.8
p_4 / p_1	183.5	168

The streamwise distances and flow times corresponding to the equilibrium conditions at the station 4 are given in Ref. 60 in terms of flight Mach Number and flight altitude, H . The involved distances and times vary considerably with both M and H , so that no simple generalized conclusion can be stated.

The dissociation rates of N_2 are considerably slower than for O_2, and only at very small densities (relatively high flight altitudes) the dissociation of N_2 becomes significant.

But, even for the very low density conditions, the relaxation times, $(\Delta t d)_{N_2}$, are greater than the characteristic time intervals in which the airstream passes over a standard missile length. Thus, it can be concluded that for flight Mach Numbers of the order of 15 at any atmospheric sustained flight altitude, the dissociation effects due to N_2 are negligible for the aerodynamic pressure force analysis.

The above conclusion does not hold for relatively retarded viscous flow conditions in boundary layers. In Ref. 61, for laminar flows over flat plates at zero angle-of-attack, the

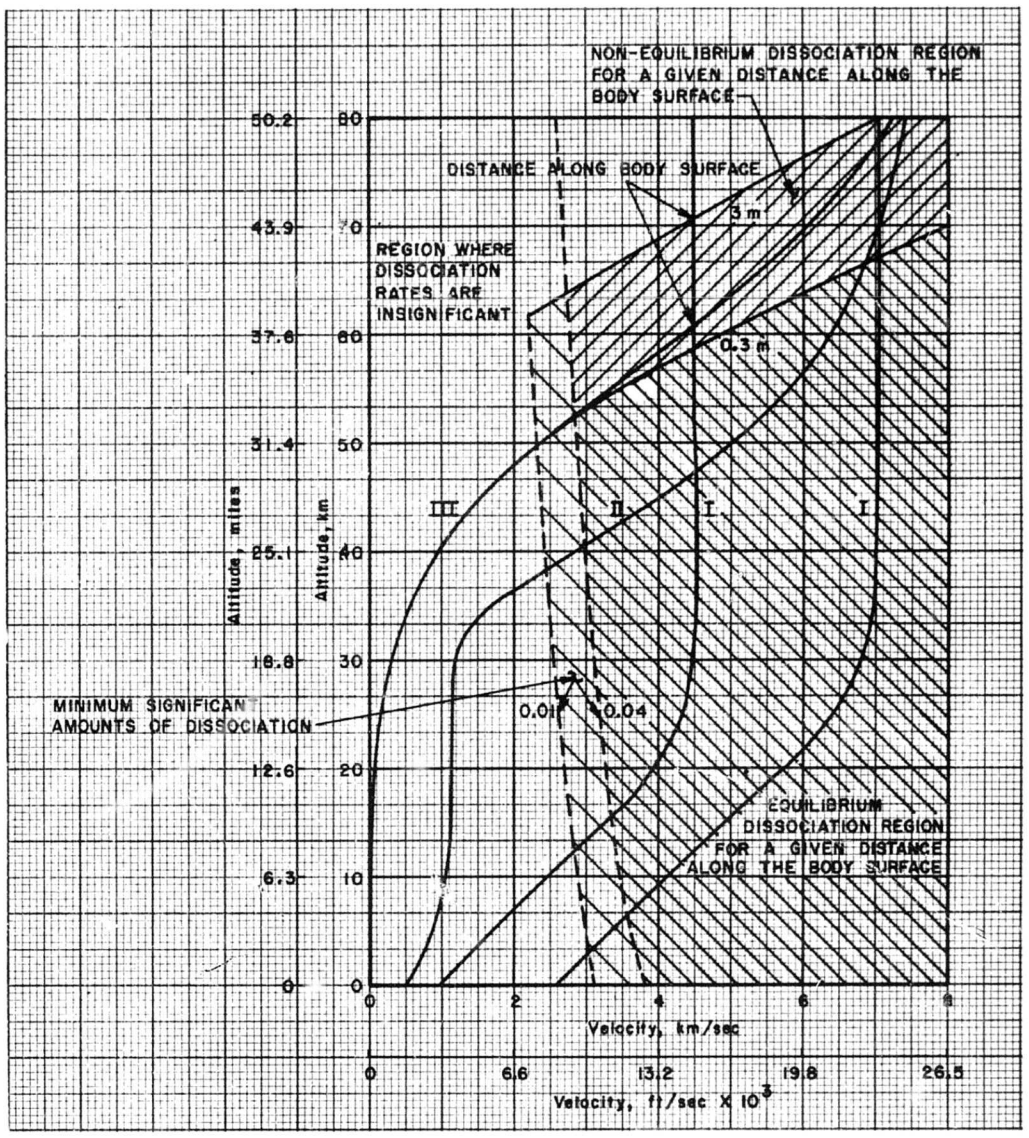

Fig. (2.2-34) Flight conditions for which relaxation phenomena connected with equilibrium dissociation can be important. Missile categories re-entering the dense layers of atmosphere: I- Ballistic; II- Glide; III- Satellite. (Ref. 59).

ratio of the local skin-friction coefficient for a viscous dissociated flow, C_{fd}, to that of a viscous perfect gas flow, C_f, while Re and M are kept constant, is given by:

$$\frac{C_{f_d}}{C_f} = \sqrt{\left[\frac{(\rho\mu)_d}{\rho\mu}\right]_w} \qquad (2.2\text{-}381)$$

where subscript w refers to the local conditions at the wall.

(v) References Related to the Thermal Effects in Flowing Gases

Useful numerical data respective to the variations of air properties and of its components with high temperatures can be especially found in the following references:

Ref. 58 - The section on air properties and air flow data.

Ref. 62 - Data sheets S 00.01.01 to 00.01.06
Data sheets S 00.02.03
Data sheets S 00.03.17 to 00.03.23

Ref. 63 - Chapters 1, 2, and 3.

2.2.7 REFERENCES

2.2-1. Goldstein, S. Modern Developments in Fluid Dynamics. New York: Oxford University Press, 1938.

2.2-2. Schlichting, H. Boundary Layer Theory. New York: McGraw-Hill Book Company, Inc., 1955.

2.2-3. Prandtl, L. Essentials of Fluid Dynamics. London: Blackie and Sons, Ltd., 1960.

2.2-4. Milne-Thompson, L. M. Theoretical Hydrodynamics. New York: The MacMillan Company, 1957.

2.2-5. Lamb, Sir Horace. Hydrodynamics. New York: Dover Publications, 1945.

2.2-6. Cope, W. F. "The Equations of Hydrodynamics in a Very General Form", London: R. and M., No. 1903, British A. R. C., 1942.

2.2-7. Patterson, G. N. Molecular Flow of Gases, New York: John Wiley and Sons, Inc., 1956.

2.2-8. Tsien, H. S. "Superaerodynamics, Mechanics of Rarefied Gases", Journal Aerospace Science, Vol. 13, No. 12, December, 1946.

2.2-9. Truitt, R. W. Fundamentals of Aerodynamic Heating. New York: The Ronald Press Company, 1960.

2.2-10. Truitt, R. W. Hypersonic Aerodynamics. New York: The Ronald Press Company, 1959.

2.2-11. Gaylord, E. W. and Hughes, W. F. Basic Equations of Engineering Science. New York: Schaum Publishing Company, 1964.

2.2-12. Liepmann, H. W. and Roshko, A. Elements of Gasdynamics. New York: John Wiley and Sons, Inc., 1957.

2.2-13. Chapman, S. and Cowling, T. G. Mathematical Theory of Non-Uniform Gases. Cambridge, England: Cambridge University Press, 1951.

2.2-14. Kuethe, A. M. and Schetzer, T. D. Foundations of Aerodynamics, Second Edition. New York: John Wiley and Sons, Inc., 1963.

2.2-15. Nelsen, N. C. and Loft, E. E. Space Mechanics, Englewood Cliffs, New Jersey: Prentice Hall, Inc., 1962.

2.2-16. Ipsen, D. C. Units, Dimensions and Dimensionless Numbers. New York: McGraw-Hill Book Company, Inc., 1960.

2.2-17. Hix, C. F. and Alley, R. P. Physical Laws and Effects, New York: John Wiley and Sons, Inc., 1958.

2.2-18. Eckert, E. R. G. "Mass, Momentum and Heat Transfer - a Survey of the Field "Recent Advances in Engineering Sciences, Proceedings of Conference on Science and Technology", September 9-12, 1957, Purdue University, Lafayette, Indiana.

2.2-19. Etkin, B. Dynamics of Flight. New York: John Wiley and Sons, Inc., 1959.

2.2-20. Chapman, S. and Cowling, T. G. Mathematical Theory of Non-Uniform Gases. Cambridge, England: Cambridge University Press, 1951.

2.2-21. Curtiss, C. F., Hirschfelder, J. O., and Bird, R. B. Molecular Theory of Gases and Liquids, Chapter 7, New York: John Wiley and Sons, Inc., 1954.

2.2-22. Uyehara, O. A. and Watson, K. M. "National Petroleum News," Technical Section, Vol. 36, P. 714, October 4, 1944.

2.2-23. Carr, N. L., Parent, J. D., and Peck, R. E. "Chemical Engineering Progress, Symposium Series, Vol. 51, No. 16, P. 91, 1955.

2.2-24. Comings, E. W., and Nathan, M. F., Ind. Eng. Chem., Vol. 39, P. 964, 1947.

2.2-25. Gamson, B. W. Chemical Engineering Progress, Vol. 45, P. 154, 1949.

2.2-26. Slattery, J. C. M. S. Thesis, Department of Chemical Engineering, University of Wisconsin, 1955.

2.2-27. NASA, USAF, USWB. "U. S. Standard Atmosphere, 1962".

2.2-28. Noolley, Harold W. "Effect of Dissociation on Thermodynamic Properties of Pure Diatomic Gases", NACA TN 3270, National Bureau of Standards, April, 1955.

2.2-29. Cambel, A. B., Duclos, D. P. and Anderson, T. P. Real Gases. New York: Academic Press Inc., 1963.

2.2-30. Present, R. D. Kinetic Theory of Gases, New York: McGraw-Hill Book Company, Inc., 1958.

2.2-31. Bethe, H. A., and Teller, E. "Deviations From Thermal Equilibrium in Short Waves", Rep. No. X-117, Ballistic Res. Lab., Aberdeen Proving Ground, 1945.

2.2-32. Enskog, D. "Kinetische Theorie der Vorgänge in mässig verdiinnten gasen", Inaugural Dissertation, University of Upsala, Sweden, 1917.

2.2-33. Chapman, S. "The Kinetic Theory of Simple and Composite Monoatomic Gases: Viscosity, Thermal Conduction and Diffusion", Proc. Royal Society, 93A, 1, 1917.

2.2-34. Chapman, S. "On the Kinetic Theory of A Gas, Part II -- A Composite Monoatomic Gas: Diffusion, Viscosity and Thermal Conduction", Phil. Trans. Royal Society, 217A, 115, 1917.

2.2-35. Chapman, S. "On the Law of Distribution of Molecular Velocities, and on the Theory of the Viscosity and Thermal Conduction in a Non-Uniform Simple Monoatomic Gas". Phil. Trans. Royal Society, 216A, 279, 1916.

2.2-36. Maxwell, T. C. Collected Works. Cambridge University Press, 1890.

2.2-37. Dryden, H. L., Murnaghan, F. D., and Bateman, H. "Report of the Committee on Hydrodynamics" National Research Council, Bulletin No. 84, Washington, 1932.

2.2-38. Sutherland, W. "The Viscosity of Gases and Molecular Force" Phil. Mag., 36, 507, (1893) and Phil. Mag. 17, 320, (1909).

2.2-39. Jeans, Sir James. An Introduction to the Kinetic Theory of Gases, Cambridge University Press, London, 1940.

2.2-40. Lewis, J. A. "Boundary Layer in Compressible Fluid". Air Material Command T.R. No. F-TR-1179-ND (Monograph V, Wright Field, 1948).

2.2-41. Lennard-Jones, T. E. "On the Determination of the Molecular Fields". Proc. Roy. Soc. A106, 441, 1924.

2.2-42. Chapman, D. R. and Rubesin, M. W. "Temperature and Velocity Profiles in the Compressible Laminar Boundary Layer with Arbitrary Distribution of Surface Temperature", J. Aero. Science, Vol. 16, p. 547, 1949.

2.2-43. Eucken, A. "Uber das Warmeleitvermogen, die spezifische Warme und die innere Riebung der Gase" Phys. Zeit., Vol. 14, P. 324, 1913.

2.2-44. Phillips, P. "The Viscosity of Carbon Dioxide". Proc. Royal Society, Vol. A87, P. 48, 1912.

2.2-45. Gibson, R. O., and Michels, A. "The Measurement of Viscosity in Gases at High Pressures--the Viscosity of Nitrogen to 1000 Atms". Proc. Royal Society, Vol. A134, P. 288, 1931.

2.2-46. Stokes, C. G. "Viscosity and Heat Conduction Losses", Trans. Cambridge Phil. Soc., Vol. 8, p. 297, 1845.

2.2-47. Liebermann, L. N. "Bulk Viscosity of Liquids" Physical Rev., Vol. 73, P. 537, 1948.

2.2-48. Liebermann, L. N. "The Second Viscosity of Liquids", Physical Rev., Vol. 75, P. 1415, 1949.

2.2-49. Born, M., and Green, H. S. "A General Kinetic Theory of Liquids"
Proc. Roy. Soc., Vol. A 188, P. 10, 1946.
Proc. Roy. Soc., Vol. 189, P. 103, 1947.
Proc. Roy. Soc., Vol. 190, P. 455, 1947.

2.2-50. Minzner, R. A., Ripley, W. S., and Condron, T. P. U.S. Extension to the ICAO Standard Atmosphere - Tables and Data to 300 Standard Geopotential Kilometers", Geophysical Res. Dir. and U. S. Weather Bureau, 1958.

2.2-51. Ailsenrath, Joseph and Beckett, Charles W., "Tables of Thermal Properties of Gases", NBS Cir. 564, U. S. Department of Commerce, 1955.

2.2-52. Kennard, Earle H. Kinetic Theory of Gases, New York: McGraw-Hill Book Company, Inc., 1938.

2.2-53. Dumond, Jesse W. M. and Cohen, E. Richard. "Fundamental Constants of Atomic Physics" Pt. 7 of Handbook of Physics, Chapter 10, E. U. Condon and Hugh Odishaw, eds., McGraw-Hill Book Co., Inc., 1958, PP. 7-143-7-173.

2.2-54. Jenson, Jorgen, Townsend, George, Kork, Jyri, and Kraft, Donald. Design to Orbital Flight, New York: McGraw-Hill Book Co., Inc., 1962.

2.2-55. Champion, Kenneth S. W., and Minzner, Raymond A. "Proposed Revision of U. S. Standard Atmosphere 90 to 700 Km", AFCRL-62-802, Air Force Cambridge Research Labs., July, 1962.

2.2-56. Hansen, C. F. and Heins, S. D. "A Review of the Thermodynamic Transport and Chemical Reaction Rate Properties of High Temperature Air", NACA TN 4359, 1958.

2.2-57. Johnson, Francis S. "Atmospheric Structure", Journal of Astronautics (ARS), August, 1962.

2.2-58. Wood, K. D. Aerospace Vehicle Design, Vol. I, Aircraft Design, Boulder, Colorado: Johnson Publishing Company, 1963.

2.2-59. Chernyi, G. G. Introduction to Hypersonic Flow, New York: Academic Press, 1961.

2.2-60. Wood, G. P. "Calculations of the Rate of Thermal Dissociation of Air Behind Normal Shock Waves at Mach Numbers of 10, 12, and 14", NACA TN 3634, 1956.

2.2-61. Kuo, Y. H. "Dissociation Effects in Hypersonic Viscous Flows", Journal Aero. Sciences, Vol. 24, No. 5 (May, 1957), PP. 345-350.

2.2-62. Royal Aeronautical Society Data Sheets, Aerodynamics, Vol. 1, Eleventh Issue, October, 1960.

2.2-63. Morrison, R. B. and Ingle, M. J. Design Data for Aeronautics and Astronautics, New York: John Wiley and Sons, Inc., 1962.

TABLE OF CONTENTS

Section 2.3 Skin-Friction Drag Coefficient Analysis

LIST OF FIGURES

Section 2.3 Skin-Friction Drag Coefficient Analysis

LIST OF TABLES

Section 2.3 Skin-Friction Drag Coefficient Analysis

LIST OF SYMBOLS

Section 2.3 Skin-Friction Drag Coefficient Analysis

I. GEOMETRY

AR - Aspect ratio,
$$AR = \frac{b^2}{S}$$

b - Span, ft.

b_F - Total fin span, ft.
$$b_F = b_{FEXP} + D = 2h_{FEXP} + D$$

b_{FEXP} - Exposed fin planform span, ft.
$$b_{FEXP} = 2h_{FEXP}$$

b_{FP} - Flat plate width, ft.

b_W - Total wing span, ft.

b_{WEXP} - Exposed fin planform span, ft.

c - Local chord, ft.

$\bar{c}$ - Mean geometric or aerodynamic chord, ft.

$\bar{c}_e$ - Mean "effective" geometric or aerodynamic chord, ft.

$\bar{c}_{FEXP}$ - Mean geometric chord of the fin's exposed planform, ft.
$$\bar{c}_{FEXP} = \frac{S_{FEXP}}{b_{FEXP}}$$

C_r - "Root" chord of the exposed wing or fin (i.e. at the wing-body juncture, or the fin-body juncture), ft.

C_t - Tip chord, ft.

$\bar{c}_{WEXP}$ - Mean geometric chord of the wing exposed planform, ft.
$$\bar{c}_{WEXP} = \frac{S_{WEXP}}{b_{WEXP}}$$

D - Reference body diameter; maximum diameter of missile body, ft.

D_{TR} - Local diameter at the nose cone section, where an assumed "instantaneous" transition from laminar to turbulent boundary layer occurs, see Fig. (2.3-42).

$D_{\Delta X}$ - Local diameter at the nose cone section, where an "equivalent" turbulent boundary layer is supposed to start, see Fig. (2.3-42).

d - Local diameter, ft.

h_{FEXP} - Exposed (one) fin height, ft.

L - Length, ft.; total missile length.
$L = L_N + L_{CYL} + L_{BT}$

L_{AFT} - Afterbody length, behind wing, ft.

L_{BT} - Length of the boattail body section, ft.

L_{CYL} - Length of the cylindrical body section, ft.

L_{FORE} - Forebody length, ahead of wing, ft.

L_{FP} - Flat plate length, ft.

L_N - Nose section length, ft.

N - Number of individual fins.

R - Local radius, ft.

S - Area of any missile part, sq. ft.

S_{EXP} - Exposed area of a missile part; planform exposed area of wings and fins; reference exposed area for the total pressure force coefficient definition on a missile part; sq. ft.

S_{FEXP} - One fin exposed planform area, ft.^{2}

$S_r \propto S_{REF}$ - Missile common reference area, sq. ft.,
$S = (\pi D^2)/4$

S_{WET} - Wetted area of missile part, sq. ft.

$S_{WETFEXP}$ - Total exposed fin wetted area, ft.^{2}
$S_{WETFEXP} = 2NS_{FEXP}$

$S_{WETWEXP}$ - Total exposed wing wetted area, ft.^{2}
$S_{WETWEXP} \approx 2S_{WEXP}$

S_{WEXP} - Total exposed wing planform area, ft.^{2}
$S_{WEXP} = b_{WEXP}\ \bar{c}_{WEXP}$

x - Longitudinal distance, ft.

x_{TR} - Distance from the leading edge of a flat plate (zero angle-of-attack) to an assumed point, where an instantaneous transition from laminar to turbulent boundary layer occurs, ft.

Δx - "Effective length of start of an "equivalent" turbulent boundary layer, ahead of a presumed "instantaneous" transition point of an "instantaneous" transition.

α - Angle of attack, degrees.

θ_N - Cone vertex angle; inscribed cone vertex angle for ogives; degrees.

λ - Taper ratio, nondimensional

II. PHYSICAL

a - Speed of sound, ft./sec.

C_D - Drag force coefficient, nondimensional, referred to the common reference area, S_r, and the flow conditions at "infinity", Standard Atmosphere at each flight altitude, H:

$$C_D = \frac{\text{Drag Force}}{q_H \; S_r}$$

C_{DO} - Zero-lift drag force coefficient, nondimensional, referred to the common reference area, S_r, and the flow conditions at "infinity", Standard Atmosphere at each flight altitude, H:

$$C_{DO} = \frac{\text{Zero - Lift Drag Force}}{q_H \; S_r}$$

C_{DOf} - Zero-lift skin-friction drag force coefficient, nondimensional, referred to the common reference area, S_r, and the flow conditions at "infinity", Standard Atmosphere at each flight altitude, H:

$$C_{DOf} = C_f \left(\frac{S_{WET}}{S_r} \right) \cos \left(V_H, t \right) \approx \frac{\iint_{S_{WET}} \tau \cos (V_H, t) \, dS}{q_H \; S_{WET}} \left(\frac{S_{WET}}{S_r} \right)$$

C_F - Total or average frictional force coefficient, referred to the wetted area, nondimensional.

$$C_F = \frac{F}{q_H \; S_{WET}}$$

C_{Fr} - Total or average frictional force coefficient, referred to the missile reference area (S_r), nondimensional

$$C_{Fr} = C_F \frac{S_{WET}}{S_r}$$

C_f - Average, or total compressible skin-friction coefficient, estimated on the respective wetted area (per unit area and referred to the free-stream dynamic pressure), nondimensional,

$$C_f = \frac{\text{Frictional Force}}{q_H}$$

$$C_f = \frac{1}{S_{WET}} \iint_{S_{WET}} C'_f \, dS$$

C'_f - Local value of the compressible skin-friction coefficient at some station x-ft. from the leading edge, nondimensional

$$C'_f = \frac{dC_f}{dS} \approx \frac{2 \tau'}{\rho_H V_H^2}$$

C_{fi} - Average or total incompressible ($M \approx 0$) skin friction coefficient, nondimensional.

C'_{fi} - Local value at some station x-ft. from the leading edge of the incompressible skin-friction coefficient ($M \approx 0$), nondimensional.

C_p - Specific heat coefficient at constant pressure, BTU per lb. ^oF, C_p .240 BTU/lb. ^oF for air at 59° F, Standard Sea-Level conditions.

C_R - Total resistance force coefficient, nondimensional,

$$C_R = \frac{R}{q_H S_r}$$

C_v - Specific heat coefficient at constant volume, BTU per lb. ^oF C_v .1715 BTU/lb. ^oF for air at 59° F, Standard Sea-Level conditions.

D_o - Zero-lift drag force, lb.

D_{ob} - Zero-lift base drag component, lb.

D_{of} - Aero-lift viscous, or skin-friction drag component, lb.

D_{op} - Zero-lift pressure drag, exclusive of base drag component, lb.

F - Total frictional force, lb.

g - Acceleration, 32.17 ft./sec.^{2} for Sea-Level conditions.

H - Altitude

h - Average dimensional heat transfer coefficient, BTU per sec. per sq. ft. ^oR.

h - Static enthalpy at any point, ft. lb.

h_t - Total enthalpy at any point, ft. lb.

J - Energy conversion factor,

$$J = 778.26 \text{ (ft / lb)/BTU}$$

k - Thermal conductivity (molecular), BTU per sec. per sq. ft., ^oF per ft.,

$$\frac{d(Q_o / S_{WET})}{dt} = q = k \frac{\partial T}{\partial y}$$

k - "Equivalent" surface roughness parameter; an average approximation of the actual surface roughness conditions through the concept of an "equivalent, uniformly distributed, sand-type" rough surface; in ft.

M - Mach Number, nondimensional; a similarity parameter,

$$M = \frac{V}{a}$$

Nu - Average Nusselt Number, nondimensional; a similarity parameter,

$$Nu = \frac{hL}{k} = \frac{L}{k}\left(\frac{q_W}{T_W - T_\delta}\right)$$

n_g - Acceleration, expressed in number g's.

P_r - Average Prandtl Number, nondimensional; a similarity parameter,

$$P_r = \frac{C_p \mu}{k}.$$

Q - Total rate of heat transfer, BTU per sec.,

$$Q = dQ_o / dt$$

Q_o - Total heat content, BTU.

q - Heat flux, BTU per sq. ft. sec.,

$$q = \frac{d(Q_o / S_{WET})}{dt} = \frac{Q}{S_{WET}}$$

q_H - Reference dynamic pressure, referred to conditions "at infinity" at a given altitude H ft., Standard Atmosphere,

$$q_H = \left(\frac{\rho V^2}{2}\right)_H = \frac{1}{2}(\gamma p M^2)_H \text{ lb./sq. ft.}$$

q_A - Same as q_H.

R - Total resistance force, lb.

R - Gas constant.

Re - Reynolds Number, nondimensional; a similarity parameter,

$$Re = \frac{VL}{\nu}$$

Re_{Cr} - Critical Reynolds Number, nondimensional, defining transition from laminar to turbulent boundary layer,

$$Re_{Cr} = \frac{X_{TR} V_H}{\nu_H}$$

Re_L - Same as Re.

Re_{TR} - Transitional Reynolds Number, nondimensional; alternative symbol for the "critical" value on a flat plate.

$Re_{\Delta X}$ - Reynolds Number value, nondimensional, corresponding to the "equivalent" turbulent boundary layer initiating distance ΔX, ahead of the presumed point of an "instantaneous" transition, see Fig. (2.3-42),

$$Re_{\Delta X} = \frac{\Delta X \, V_H}{\nu_H}$$

r - Local temperature recovery factor, nondimensional, expressing how close the recovery temperature, T_r, approaches the local free stream total (stagnation) temperature, $T_{t\delta}$,

$$r = \frac{T_r - T_\delta}{h_{t\delta} - h_\delta}$$

r_l - Local "enthalpy recovery factor", nondimensional

$$r_l = \frac{h_r - h_s}{h_{ts} - h_s}$$

St - Average Stanton Number, or the nondimensional heat transfer coefficient; a similarity parameter, whose average value may be defined from the known average skin-friction coefficient value, C_f , by introducing some kind of the Reynolds Analogy concept, for instance:

$$St = \frac{h}{\rho_\infty q_\infty V_\infty} = Pr^{-2/3}(C_f/2) = \frac{Nu}{Pr\ Re}$$

St' - Local value at some station x-ft. from the leading edge of the compressible flow of the heat-transfer coefficient, or local Stanton Number, nondimensional.

T - Local static temperature at any point, ^oR.

T' - A convenient "reference" static temperature, ^oR, serving to refer heat-transfer effects on skin-friction and heat-transfer coefficients in incompressible, laminar or turbulent boundary layers. The concept is used in the so-called "T" method of investigating boundary layer phenomena analytically (a semi-empirical approach).

T_{aw} - Local adiabatic wall temperature, ^oR , interchangeable with the recovery temperature concept, see definition of T_r .

T_e - Same as T_{we} .

T_H - Standard Atmosphere static temperature at an altitude H; under sea-level conditions.

$$T_{H=0} = 518.4^oR$$

T_r - Local recovery, or adiabatic, wall temperature, ^oR , i.e. the temperature of the fluid layer immediately next-to-surface (zero-velocity layer), provided the surface is insulated and an equilibrium steady thermal state is reached across the boundary layer section (a steady state temperature profile),

$$T_r = T_{aw}$$

Ts - Local total (stagnation) temperature at any point, ^oR ; total energy of fluid per unit mass

$$T_s = T + \frac{u^2}{2 C_p J}$$

T_w - Instantaneous actual local wall temperature of non-insulated surfaces; also referred to as "surface-face" temperature for insulated surfaces, i.e. the actual temperature, i.e. the actual instantaneous temperature of the next-to-wall fluid layer, prior to the achievement of a thermal steady equilibrium state of heat-transfer across the boundary layer section, when T_w becomes equal to T_r , meaning that the rate of frictional heat production equals the local heat transfer rate across the boundary layer on an insulated surface.

T_{we} - Local equilibrium skin-temperature of noninsulated surfaces, ^{o}R; it is eventually reached after a sufficiently long time interval under steady state flow conditions, when the actual temperature of the skin is equal to the temperature of the next-to-wall fluid layer, and the frictional heat created in the boundary layer is transported outward at a rate equal to the rate of its creation or, otherwise formulated when the rate of frictional heat generation in the boundary layer is equal to the combined rates of heat dissipation both into the free stream and through the non-insulated skin. Note that, due to radiation effects, which were not incorporated above, it is always

$(T_{we})_{RAD} < T_r = T_{tw}$

even if there is no inside "artificial cooling" of skin

T_{wer} - Same as $T_{we\,RAD}$.

$T_{we\,RAD}$ - Equilibrium wall temperature with radiation, ^{o}R

$T_{we\,RAD} < T_{we} < T_r = T_{tw}$

T_∞ - Local static temperature at the outer edge of the boundary layer; the same as T_δ.

T_δ - Same as T_∞.

t - Time, seconds.

$\vec{t}, \vec{n}$ - Local reference in the natural orthogonal Cartesian coordinate system in two dimensions: t is tangential to the local point on the surface, positive in downstream direction, while n is in the direction of the respective outward normal to the surface point.

U - See V_H or V_∞.

U_δ - Local free-stream velocity at the outer edge of a boundary layer, having a local thickness δ, ft./sec., tentatively equal to the free stream (inviscid) velocity "at infinity", ($U_\delta = U = V$), for flat plates at zero-angle-of-attack in a two dimensional flow. (Zero pressure gradient.)

$\frac{\partial u}{\partial y}$ - Local gradient of the velocity profile at any point.

u, v, w - Local velocity components in the x,y, & z directions at some point within the boundary layer, ft./sec.

V_H - Relative airspeed, or speed of flight, ft./sec. (see U)

V_A - Same as V_H.

x, y, z - Local coordinate axis at some point within the boundary layer: orthogonal Cartesian coordinate system, the x-axis being in the direction of the local tangent, while the z-axis is in the direction of the local normal.

Re_{crk} - Critical Reynolds Number for a rough plate, nondimensional.

Re_{crs} - Critical Reynolds Number for a smooth plate, nondimensional.

Re_δ^* - Reynolds Number, based on displacement thickness of the boundary layer.

U_c - Free stream velocity, ft./sec.

u' - Component of turbulent velocity fluctuation in x-direction ft./sec.

v' - Component of turbulent velocity fluctuation in y-direction ft./sec.

w' - Component of turbulent velocity fluctuation in z-direction ft./sec.

u - Mean average local velocity component in x-direction within the boundary layer, ft./sec.

v - Mean average local velocity component in y-direction within the boundary layer, ft./sec.

x - Station x ft. from the leading edge.

h - Local dimensional heat transfer coefficient, BTU/(sec.sq.ft.^{o}R),

$$h = \frac{q}{T_w - T_\delta} \left(\frac{BTU}{ft^2\ Sec.^{o}R} \right)$$

l - Mean free molecular path, ft.

Pr - Molecular Prandtl Number, nondimensional, defined in the laminar sublayer of a turbulent boundary layer,

$$Pr = \frac{Cp\mu}{k}$$

Pr_t - Prandtl Number, nondimensional, defined in the turbulent region of a turbulent boundary layer,

$$Pr = \frac{Cp\epsilon}{\kappa}$$

Re_θ^+ - Momentum thickness Reynolds Number, nondimensional,

$$Re_\theta^* = \frac{\theta^* U_\delta \rho_\delta}{\mu_\delta}$$

$$Re_x = 2\int_0^{Re_\theta} \frac{dRe_\theta}{C_f'}$$

S - Modified Reynolds analogy factor,

$$S_f' = \frac{1}{S}\left(\frac{C_f'}{2}\right),$$

$S = (P_r^*)^{2/3}$ for laminar boundary layers over smooth surfaces,

$S = f(P_r, C_f', M_\delta)$ for turbulent boundary layers over smooth surfaces, $0.80 \le S \le 0.835$ for $0 \le M_\delta \le 5$

$S = f(P_r^*, C_f', M_\delta, Re_L)$ alternatively for rough surfaces.

T - Time interval in which the mean individual velocity component fluctuations are evaluated, sec.

$$\bar{u}_1 = \frac{1}{T}\int_0^T u_1\, dt$$

etc.

u_τ - Frictional velocity, ft./sec.

$$u_\tau = (\tau_w / \rho)^{1/2}$$

V_* or V^* - Frictional velocity, ft./sec.

$$V_* = (\tau_w / \rho_w)^{1/2}$$

α - Frictional heating parameters,

$$\alpha = \frac{\tau_w}{2 C_p T_w \rho_w}$$

β - Heat-transfer parameter,

$$\beta = \frac{q_w (\tau_w / \rho_w)^{1/2}}{C_p T_w \tau_w}$$

σ - Root mean square value of fluctuating velocity components at any point, expressed in percents of resultant mean ordered velocity,

$$\sigma = \frac{100}{|V|} \left(\frac{\bar{u}_1^2 + \bar{v}_1^2 + \bar{w}_1^2}{3} \right)^{1/2}$$

ϵ - Eddy diffusivity of momentum, (virtual kinematic viscosity, resulting from the mechanism of turbulence), sq. ft. per sec., at the region "close to the wall" (laminar sublayer) it is only a function of the u and y as measured at the wall:

$$\epsilon = - \frac{\overline{u_1 v_1}}{(\partial u / \partial y)} ,$$

$$\epsilon = \epsilon(u, y) = n^2 u y$$

where n is an experimental constant at the region "away from the wall" (turbulent layer)

$$\epsilon = \epsilon \left(\frac{du}{dy} , \frac{d^2u}{dy^2} \right) = k^2 \frac{\left(\frac{du}{dy} \right)^3}{\left(\frac{d^2u}{dy^2} \right)^2}$$

where k is thermal conductivity.

ϵ_L - Eddy diffusivity of heat-transfer, (virtual thermal diffusivity resulting from the mechanism of turbulence), sq. ft. per sec.

$$\epsilon_L = \frac{\overline{T v}}{\left(\frac{\partial \bar{T}}{\partial y} \right)} ,$$

ω - Exponent in viscosity-temperature ratio:

$$\mu = T^\omega , \quad \omega \sim 0.76 \quad \text{for air}$$

γ - Specific heat ratio, nondimensional, $\gamma = \frac{C_p}{C_v} = 1.40$ for air, Standard Sea-Level conditions.

δ - Local boundary layer thickness, ft.

δ^* - Boundary layer displacement thickness, ft.

$$\delta^* = \int_0^\delta \left(1 - \frac{u}{u_\delta} \right) dy , \quad (2\text{-D, incompressible})$$

ϵ - Surface radiation emissivity.

θ^* - Local boundary layer momentum thickness, ft.; in two-dimensional cases,

$$\theta^* = \int_0^{\delta} \frac{\rho u}{\rho_\delta U_\delta} \left(1 - \frac{u}{U_\delta}\right) dy \text{ , (2-D, compressible)}$$

μ - Absolute coefficient of viscosity, slugs/ft. sec.

ν - Kinematic coefficient of viscosity, $ft^2/sec.$

$$\nu = \frac{\mu}{\rho}$$

ρ - Air density, $slug/ft.^3$

ρ_H - Air density at altitude H, ft. in $slug/ft.^3$; under Standard Sea-Level conditions.

ρ_∞ - Same as ρ_δ - local density of the outer edge of the boundary layer.

τ - Local shearing stress at any point of a wetted area, lb./sq. ft.

$$\tau = \mu \left(\frac{\partial u}{\partial y}\right)$$

τ_t - Local turbulent shearing stress at some point, or the Reynolds stress, lb./sq.ft.; turbulent shearing stress due to fluctuating eddying nature of turbulence,

$$\tau_t = -\rho \, \bar{u}_1 \bar{v}_1$$

τ_l - Local laminar shearing stress at some point, lb./sq.ft.; molecular shearing stress,

$$\tau_l = \mu \left(\frac{\partial u}{\partial y}\right)$$

θ^* - Boundary layer momentum thickness,

$$\theta^* = \int_0^{\delta} \frac{\rho u}{\rho_\delta U_\delta} \left(1 - \frac{u}{U_\delta}\right) dy \quad \text{for compressible flows}$$

κ - Eddy thermal conductivity, a property of turbulent transport mechanism,

$$\kappa = \frac{\bar{\rho} C_p V_1 T_1}{(\partial \bar{T}_1 / \partial y)}$$

δ^* - Displaced thickness boundary layer,

$$\delta^* = \int_0^{\infty} \left(1 - \frac{u}{U_o}\right) dy \quad \text{for incompressible flows,}$$

$$\delta^* = \int_0^{\infty} \left(1 - \frac{\rho u}{\rho_o U_o}\right) dy \quad \text{for compressible flows}$$

δ_k^* - Displacement thickness of the boundary layer at the station $x = x_k$

III. SUBSCRIPTS

i	- Referred to incompressible flow conditions.
l	- Referred to laminar flow conditions.
LAM	- Referred to laminar boundary layers.
t	- Referred to turbulent flow conditions.
TURB	- Referred to turbulent boundary layers.
w	- Reflects conditions at the wall.
H	- Referred to free stream conditions at infinity, same as (A).
δ	- Referred to local free stream conditions outside boundary layer, same as (∞).
B	- Refers to body in general.
BT	- Refers to the boattail section of body.
C	- Refers to cones.
CYL	- Refers to the cylindrical section of body.
CYL+BT	- Refers to cylindrical and boattail body sections, taken as an integral unit.
EXP	- Refers to the respective exposed area of a missile part.
F	- Refers to fins.
FORE	- Refers to the forebody, i.e. to the body section ahead of the wings.
FP	- Refers to the flat plate, zero angle-of-attack.
N	- Refers to nose section.
NC	- Refers to nose cones or ogives.
ROUGH	- Rough surfaces.
r	- Refers to the reference area, same as ref.
W	- Refers to wing.
WET	- Refers to the wetted area of a missile part.
ACC	- Means constant acceleration effects taken partially into account.
av	- Means an average value of the respective physical quantity

aw - Refers to the adiabatic wall conditions.

cr - Refers to the critical Reynolds Number value.

e - Refers to the equilibrium temperature condition.

f - Refers to the frictional force phenomena.

H - Refers to the conditions at any altitude H(ft) in a Standard Atmosphere (i.e. conditions "at infinity" at the given altitude).

INS - Means "insulated skin".

L - Refers alternatively to the laminar boundary layer; interchangeable with subscript "LAM ".

LAM - Refers to the laminar boundary layer.

M - Refers to the total missile configuration.

IM - Refers to Case IM for the total missile configuration, (fully turbulent boundary layer).

IIM - Refers to Case IIM for the total missile configuration (partially laminar, partially turbulent boundary layer, transition at the nose cone).

IIIM - Refers to Case IIIM for the total missile configuration) partially laminar, partially turbulent boundary layer, transition at point "B", see Fig. (2.3-43).

IVM - Refers to Case IVM for the total missile configuration (partially laminar, partially turbulent boundary layer, transition at forebody).

R - Means "rough surface" values.

RAD - Refers to the radiation effects.

r - Refers to the recovery temperature concept.

S - Alternatively refers to total, or stagnation, temperature concepts.

T - Refers to the turbulent boundary layer; interchangeable with subscript " TURB ".

T - Refers alternatively to skin temperature effects.

TR - Refers to the "transitional" Reynolds Number value; for flat plates, interchangeable with "C_r" subscript, assuming an "instantaneous" transition from laminar to turbulent boundary layer.

W - Refers to the conditions at the wall.

we - Refers to the wall equilibrium temperature.

Δx - Refers to the "equivalent" turbulent boundary layer start ahead of a presumed "instantaneous" transition point.

1 - Refers to nose cone.

2 - Refers to cylinder + boattail.

3 - Refers to wings.

4 - Refers to fins.

Δ - Means increment of a quantity.

θ - Refers to thermal equilibrium conditions for non-insulated surfaces.

∞ - Refers to local conditions outside the boundary layer.

IV. SUPERSCRIPTS

A - Refers to set of working graphs "A".

B - Refers to set of working graphs "B".

$*$ - Refers to physical and geometric quantities reduced to an "equivalent" flat plate, zero angle-of-attack.

$\overline{\ }$ - Defines the mean value of some quantity in a turbulent boundary layer; for a time-dependent fluctuating quantity, defines a time-average value.

$'$ - Denotes local value of some physical quantity; for instance, C_f' is the local skin-friction coefficient value at some section.

I - Refers to "CASE I" (fully turbulent b.l.).

II - Refers to "CASE II" (fully laminar b.l.).

III - Refers to "CASE III" (partially laminar, partially turbulent b.l.).

BLANK PAGE

2.3 SKIN FRICTION DRAG COEFFICIENT ANALYSIS

2.3.1 LAMINAR BOUNDARY LAYER FORMS OF CONTINUITY MOMENTUM AND ENERGY EQUATION -- CONTINUUM FLOW REGIME

The general governing equations of fluid motion (Section 2.2) have not been solved, except for a few simplified cases of viscous, non-conducting, incompressible fluid flows, around simple body geometries(1,2), i.e., assuming a constant viscosity, constant density and no heat-conduction. Other more elaborate flow cases are usually handled by semi-empirical and analytical approximate methods.

Using the Prandtl's boundary layer hypothesis(3), both the heat transfer and the viscous phenomena are restricted to a thin layer next to the body surface. Outside of the relatively thin boundary region the flow may be treated as inviscid. This hypothesis allows for a subsequent approximation of the general governing equations by introducing additional simplifying assumptions on the basis of an "order-of-magnitude" evaluation of the constituent physical variables. The resulting simplified expressions are called the boundary layer equations. Their most frequently encountered forms are listed below for two-dimensional boundary layer flow types.

(i) Steady, Compressible, Heat Conducting, Two-dimensional, Laminar Boundary Layer Equations.

CONTINUITY EQUATION:

$$\frac{\partial(\rho u)}{\partial x} + \frac{\partial(\rho v)}{\partial y} = 0 , \qquad (2.3-1)$$

MOMENTUM EQUATIONS:

In general, with ($F_i = 0$) and ($\partial/\partial t \equiv 0$) the two-dimensional Cartesian scalar form of the momentum equations is:

$$\rho u \frac{\partial u}{\partial x} + \rho v \frac{\partial u}{\partial y} = -\frac{\partial p}{\partial x} + \frac{\partial}{\partial x}\left(\mu \frac{\partial u}{\partial x}\right) + \frac{\partial}{\partial y}\left(\mu \frac{\partial u}{\partial y}\right) -$$

$$- \frac{2}{3}\frac{\partial}{\partial x}\left[\mu\left(\frac{\partial u}{\partial x} + \frac{\partial v}{\partial y}\right)\right] + \frac{\partial}{\partial x}\left(\mu \frac{\partial u}{\partial x}\right) + \frac{\partial}{\partial y}\left(\mu \frac{\partial v}{\partial x}\right) , \qquad (2.3-3)$$

$$\rho u \frac{\partial v}{\partial x} + \rho u \frac{\partial v}{\partial y} = -\frac{\partial p}{\partial y} + \frac{\partial}{\partial x}\left(\mu \frac{\partial v}{\partial y}\right) +$$

$$+ \frac{\partial}{\partial y}\left(\mu \frac{\partial v}{\partial y}\right) - \frac{2}{3}\frac{\partial}{\partial y}\left[\mu \frac{\partial u}{\partial x} + \frac{\partial v}{\partial y}\right] +$$

$$+ \frac{\partial}{\partial x}\left(\mu \frac{\partial v}{\partial y}\right) + \frac{\partial}{\partial y}\left(\mu \frac{\partial v}{\partial y}\right) , \qquad (2.3-4)$$

i.e., with,

$$\frac{v}{u} << 1 , \qquad \frac{\partial}{\partial x}\left(\mu \frac{\partial u}{\partial x}\right) \sim 0 ,$$

$$\therefore v \sim 0 , \quad \text{and} \quad \frac{\partial}{\partial x}\left[\mu\left(\frac{\partial u}{\partial x} + \frac{\partial v}{\partial y}\right)\right] \sim 0 ,$$

$$\frac{\partial v}{\partial x} \sim 0 , \qquad \frac{\partial}{\partial x}\left(\mu \frac{\partial u}{\partial x}\right) \sim 0 , \qquad (2.3-5)$$

the two-dimensional, steady, compressible, laminar boundary layer momentum equations become:

$$\rho u \frac{\partial u}{\partial x} + \rho v \frac{\partial u}{\partial y} = -\frac{\partial p}{\partial x} + \frac{\partial}{\partial y}\left(\mu \frac{\partial u}{\partial y}\right) , \qquad (2.3-6)$$

$$\frac{\partial \rho}{\partial y} = 0 . \qquad (2.3-7)$$

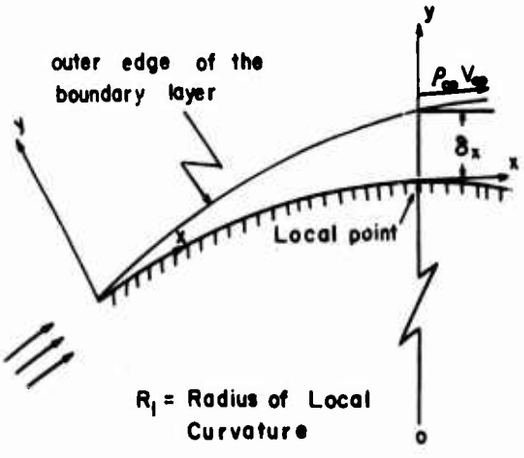

Fig. (2.3-1) Illustration of boundary layer terms.

ENERGY EQUATION:

The steady two-dimensional flow "enthalpy" form of the energy equation with ($F_i = 0$) and ($\partial/\partial t = 0$) and with the adopted assumptions that the viscous shear stress and the heat-conduction terms in the x_1-direction are negligible:

$$\rho u\left[C_p\frac{\partial T^*}{\partial x}+\frac{\partial}{\partial x}\left(\frac{u^2+v^2}{2}\right)\right]+\rho v\left[C_p\frac{\partial T^*}{\partial y}+\frac{\partial}{\partial y}\left(\frac{u^2+v^2}{2}\right)\right]=\frac{\partial}{\partial y}\left(k\frac{\partial T^*}{\partial y}\right)+\frac{\partial}{\partial y}\left(\mu u\frac{\partial u}{\partial y}\right). \tag{2.3-10}$$

In terms of the local stagnation temperature, T_0^*, concept and assuming:

$$C_p = \text{const}, \quad \frac{v}{u} << 1, \quad v^2 << u^2, \tag{2.3-11}$$

the alternative form of the energy equation (2.2-10) becomes:

$$\rho u\left(\frac{\partial T_0^*}{\partial x}\right)+\rho v\left(\frac{\partial T_0^*}{\partial y}\right)=$$

$$=\frac{\partial}{\partial y}\left(k\frac{\partial T_0^*}{\partial y}\right)+\frac{\partial}{\partial y}\left[\left(\frac{1}{Pr}-1\right)\mu\frac{\partial T^*}{\partial y}\right],$$

$$Pr=\frac{C_p\mu}{k}. \tag{2.3-12}$$

Combining the momentum equation (2.3-6) and the energy equation (2.3-10), another alternative form of the energy equation is obtained permitting for explicit variations in C_p, μ, and k:

$$\rho u C_p\frac{\partial T^*}{\partial x}+\rho v C_p\frac{\partial T^*}{\partial y}=u\frac{\partial p}{\partial x}+\frac{\partial}{\partial y}\left(k\frac{\partial T^*}{\partial y}\right)+\mu\left(\frac{\partial u}{\partial y}\right)^2,$$

$$C_p = C_p(T^*),$$
$$k = k(T^*),$$
$$\mu = \mu(T^*). \tag{2.3-13}$$

MAIN ASSUMPTIONS:

(1) A two-dimensional uniform steady ($\partial/\partial t = 0$) flow pattern is assumed ($u_3 = w_3 = 0$). The body surface may be two-dimensionally curved. Body forces are assumed zero ($F_i = 0$).

(2) The main reference coordinate system (Ox_i) has its origin at the forward stagnation point, (i.e., at the origin of the boundary layer) the ($x_1 = x$) axis being coincident with the body surface and oriented in the direction of the main flow, while the ($x_2 = y$) axis is perpendicular to it.

(3) The local coordinate system at any point on the body surface has the ($x_1 = x$) and ($x_2 = y$) axes locally tangential are normal to the body surface. Thus, for two-dimensionally curved surfaces a transformation (or an eventual approximation) of the local coordinate system to the main reference coordinate system is required.

(4) The boundary layer (momentum) thickness is very small compared with the distance from the stagnation point (or the characteristic body length),

$$\frac{\delta_x}{x} << 1 \quad \text{or} \quad \frac{\delta_L}{L} << 1, \tag{2.3-14}$$

and relatively very large compared with the mean free molecular path (for gaseous fluids),

$$\frac{\delta_x}{\lambda} >> 1 \quad \text{or} \quad \frac{\delta_L}{\lambda} >> 1. \tag{2.3-15}$$

The boundary layer thickness is thus of the order of y,

$$\frac{y}{x} << 1, \therefore \delta_x \sim O(y), \tag{2.3-16}$$

and grows parabolically,

$$\delta_x \sim \sqrt{x}. \tag{2.3-17}$$

(5) The slope (v/u) of a streamline inside the boundary layer is of the same order of magnitude as (δ_x/x), i.e.:

$$O\left(\frac{v}{u}\right) \sim O\left(\frac{\delta_x}{x}\right),$$
$$\therefore v << u. \tag{2.3-18}$$

(6) The viscous forces inside the boundary layer are of the same order of magnitude as the inertial forces, i.e.:

$$\frac{\frac{\partial}{\partial y}\left[\mu\frac{\partial u}{\partial y}\right]}{\rho u(\partial u/\partial x)} \sim O(1),$$
$$\therefore Re_x = \frac{V_\infty x}{\nu} >> 1. \tag{2.3-19}$$

or, with the assumption (4):

$$\frac{\delta_x}{x} \sim O\left(Re^{-\frac{1}{2}}\right).$$

(7) By an order of magnitude analysis(1,2) the y-momentum equation degenerates to

$$\frac{\partial p}{\partial y} = 0, \tag{2.3-20}$$

i.e., $p = p(x)$ only, estimated (in the first approximation) from the corresponding inviscid (perfect fluid) flow solutions for a given body geometry.

(8) The boundary layer equations are not valid near the stagnation point. Also, the surface curvature (if any) must be very small.

$$\frac{R}{\delta_x} >> 1 \quad , \tag{2.3-21}$$

i.e., the boundary layer equations are not valid near sharp corners.

The large radius of curvature assumption renders the velocity and the temperature gradient in the x-direction negligible,

$$\frac{\partial u}{\partial x} << \frac{\partial u}{\partial y} \quad , \qquad \frac{\partial T^\circ}{\partial x} << \frac{\partial T^\circ}{\partial y} \quad . \tag{2.3-22}$$

DISCUSSION OF BOUNDARY LAYER EQUATIONS

The two-dimensional form of the continuity equation (2.3-1) is not basically affected by the laminar boundary layer order-of-magnitude simplifying analysis.

The general two-dimensional forms of the momentum equations (2.3-3) and (2.3-4) for $F_i = 0$ reduce to the simplified laminar boundary layer forms (2.3-6) and (2.3-7) in view of the introduced assumptions that the velocity component, v, in the y-direction and the viscous forces variations in the x-direction are relatively negligibly small.

The general "enthalpy" form of the energy equation (2.3-8) for ($F_i = 0$) and ($\partial/\partial t = 0$) reduces to the simplified two-dimensional steady laminar boundary layer form (2.3-10) following the adopted assumptions that the velocity and the temperature gradients in the x-direction (i.e. that the viscous shear stresses and the heat conduction terms in the x-direction) are negligibly small.

Assuming that ($v/u << 1$) and ($C_p = \text{const}$) and introducing the concept of the local stagnation temperature, T_s°,

$$T_s^\circ = T^\circ + \frac{u^2+v^2}{2C_p} \sim T^\circ + \frac{u^2}{2C_p} \quad , \quad v << u, \tag{2.3-23}$$

it follows that:

$$\frac{1}{C_p}\frac{\partial}{\partial y}\left(\frac{u^2}{2}\right) = \frac{\partial T_s^\circ}{\partial y} - \frac{\partial T^\circ}{\partial y} \quad , \qquad \frac{1}{C_p}\frac{\partial}{\partial x}\left(\frac{u^2}{2}\right) = \frac{\partial T_s^\circ}{\partial x} - \frac{\partial T^\circ}{\partial x} \quad , \tag{2.3-24}$$

and the energy equation (2.3-10) takes the alternative form

$$\rho u\left(\frac{\partial T_s^\circ}{\partial x}\right) + \rho v\left(\frac{\partial T_s^\circ}{\partial y}\right) = \frac{\partial}{\partial y}\left(\mu \frac{\partial T_s^\circ}{\partial y}\right) + \frac{\partial}{\partial y}\left[\left(\frac{k}{C_p \mu} - 1\right)\mu \frac{\partial T^\circ}{\partial y}\right], \tag{2.3-25}$$

which, when the Prandtl Number concept is introduced,

$$Pr = \frac{C_p \mu}{k} \quad , \tag{2.3-26}$$

results in the energy equation (2.3-12), expressed in terms of the stagnation temperature.

Still another alternative form (2.3-13) of the energy equation is obtained by suitably combining the momentum (2.3-6) and the energy (2.3-10) equations(10).

In general, a simultaneous solution of the continuity equation (2.3-1), the momentum equation (2.3-6) and the energy equation (2.3-10), (2.3-12) or (2.3-13) (alternatively) is required for specified wall conditions, a known longitudinal pressure distribution, $p(x)$, and for a given flow variation of the gas properties(C_p, μ, k, ρ).

(ii) Integral Forms of the Momentum Boundary Layer Equations

The general two-dimensional unsteady compressible laminar boundary layer equations (momentum and mass) for an insulated flat plate with a pressure gradient:

$$\frac{\partial u}{\partial t} + u\frac{\partial u}{\partial x} + v\frac{\partial u}{\partial y} = -\frac{1}{\rho}\frac{\partial p}{\partial x} + \frac{1}{\rho}\frac{\partial}{\partial y}\left(\mu \frac{\partial u}{\partial y}\right)$$

$$\frac{\partial p}{\partial y} = 0$$

$$\frac{\partial \rho}{\partial t} + \frac{\partial}{\partial x}(\rho u) + \frac{\partial}{\partial y}(\rho v) = 0 \quad , \tag{2.3-2}$$

which are valid at any local point inside the boundary layer, can be integrated across the local cross-section of the boundary layer, yielding the general form of the von Karman momentum integral(7):

$$\int_{y=0}^{y=\delta} \frac{\partial}{\partial t}(\rho u)\,dy + \frac{\partial}{\partial x}\left[\int_{y=0}^{y=\delta} \rho u^2 dy\right] - V_\infty \frac{\partial}{\partial x}\left[\int_{y=0}^{y=\delta} \rho u\,dy\right] =$$

$$= -\tau_w - \delta_x \frac{\partial p}{\partial x}\,, \qquad (2.3\text{-}8)$$

where

V_∞ -is the local (x) free stream velocity value outside the boundary layer,

δ_x -is the local (x) boundary layer thickness,

τ_w -is the local shear stress at the wall.

For incompressible (ρ = const) viscous, unsteady flow conditions, the equation (2.3-2a) can be brought to a simpler form:

$$\frac{\tau_w}{\rho V_\infty^2} = \frac{\partial \theta_x}{\partial x} + \frac{1}{V_\infty}\frac{\partial V_\infty}{\partial x}(2\theta_x + \delta_x^*) + \frac{1}{V_\infty^2}\frac{\partial}{\partial t}(V_\infty \delta_x^*) \qquad (2.3\text{-}9)$$

where

$\delta_x^* = \int_{y=0}^{y=\delta} \left(1 - \frac{u}{V_\infty}\right) dy$ - is the so-called local (x) boundary layer "displacement thickness", representing the local velocity deficit in the boundary layer.

$\theta_x = \int_{y=0}^{y} \frac{u}{V_\infty}\left(1 - \frac{u}{V_\infty}\right) dy$ - is the so-called local (x) boundary layer "momentum thickness", representing the local momentum deficit in the boundary layer.

The boundary layer thickness, δ_x, is usually defined at a distance in the local y -direction where ($u \sim .99\, V_\infty$), measured from the wall.

Note that the expression (2.3-8) is derived by use of the momentum and the mass conservation principles only. The method is common in the boundary layer theories, the energy equation (2.3-10) being treated separately by a heat transfer investigation. The approach is restrictive and implicitly presupposes a known functional interdependence between the energy and the momentum equations, usually expressed conveniently through some form of the Reynolds analogy concept. But in more general cases, when such an approximate auxiliary interrelationship between viscous and thermal transport mechanisms is too complex, or when a more exact solution is sought, the set of three independent differential equations (2.3-1), (2.3-6) and (2.3-10) must be solved simultaneously.

The equations (2.3-8) and (2.3-9) provide, in a first approximation, a practical method for computation of the shear stress distribution, $\tau_w = f(x)$, over a given body geometry, provided the local velocity profiles, $u = u(y)$, are known(6).

(iii) The Thermal Boundary Layer Concept

Comparing the results from a few simple and approximate theoretical and semi-empirical laminar boundary layer analysis, a few general conclusions and concepts are condensed in this section for comparative purposes. The accompanying Figure (2.3-2) serves as an illustration for the thermal boundary layer conceptual interpretations in the text.

Viscous dissipation of the kinetic energy of the "ordered" flow within the boundary layer is realized through the shearing work performed on fluid particles. Assuming a "no slip" ($u_w = 0$) condition at the surface of an immersed solid body, the shearing work and the associated increase in the individual fluid particle (static) temperature, $T(y)$, in general falls off toward the outer edge of the boundary layer. The created temperature gradient ($\partial T / \partial y$) across the boundary layer results in heat conduction and a subsequent variation in the local value of all the fluid parameters which are intrinsically dependent on temperature, such as conductivity, k, viscosity, μ, specific heats, C_p and C_v, density, ρ, etc.

Thus the shear stress distribution in the y -direction across a boundary layer results in a velocity profile $u(y)$, and the associated momentum

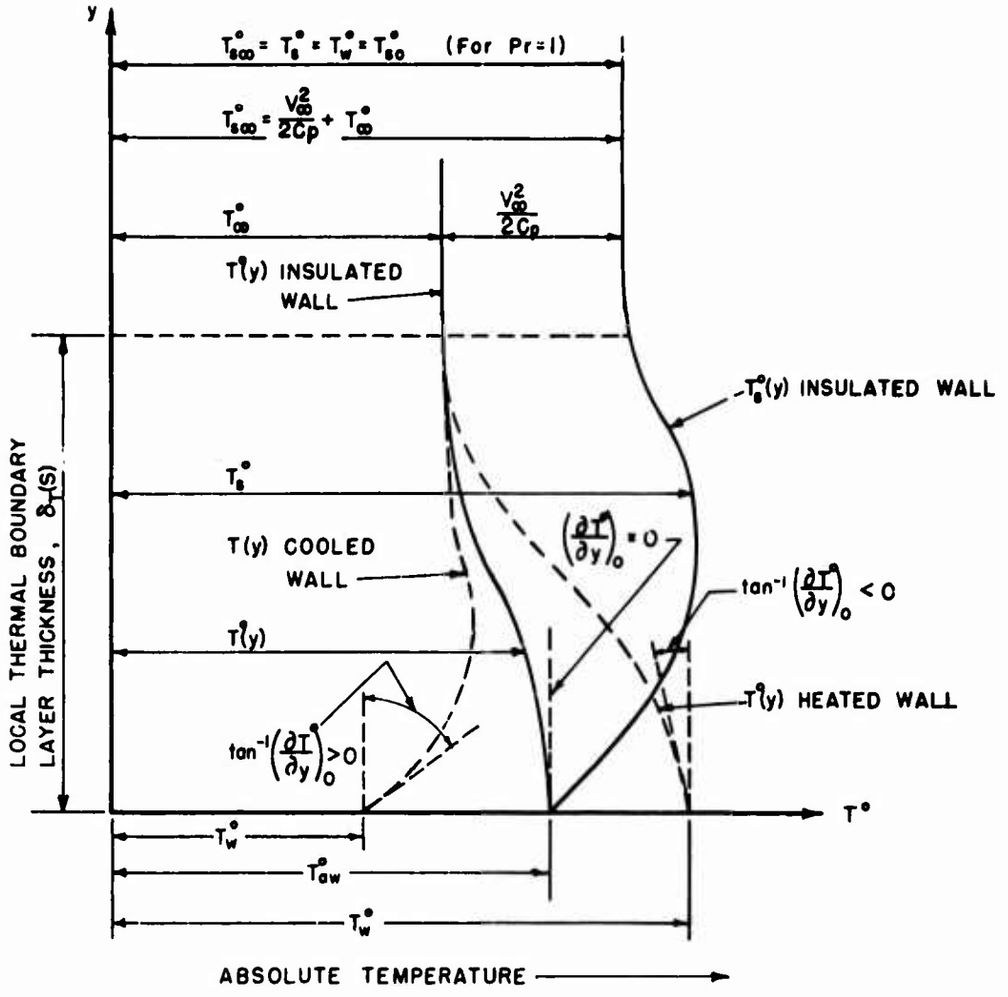

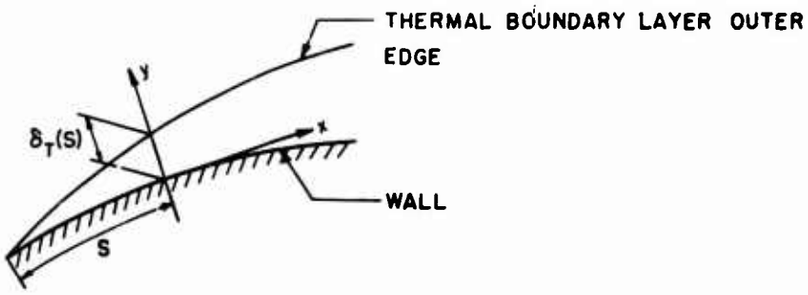

Fig. (2.3-2) TEMPERATURE PROFILES, STEADY STATE TWO-DIMENSIONAL THERMAL BOUNDARY LAYERS, CONTINUUM FLOW.

dissipation boundary layer thickness, δ_x, as well as in a temperature profile, $T(y)$, and a thermal boundary layer thickness, δ_T. The respective thicknesses of the two boundary layers, δ_x and δ_T, are not necessarily the same, but they are mutually interconnected, since their transport mechanisms can be physically traced to the same fundamental natural variable, the Peclet Number, $Pe = Re \cdot Pr$, see Section 2.2.

The thermal boundary layer concept for both insulated and non-insulated surfaces is illustrated in Fig (2.3-2). The said interdependence between the momentum loss and the heat conductivity within the boundary layers means that the skin-friction is partially dependent both on the mechanical energy losses and on the heat transfer rates, i.e., there is a definite implicit relationship between the skin-friction, the viscous shear stresses, and the heat transfer coefficients which can be summarized as follows:

The skin-friction coefficient is directly proportional to the velocity distribution profile shape (or the ordered flow momentum loss) within the boundary layer. The velocity profile in its turn depends on the shear stress, τ, viscosity, μ, and density, ρ, distributions for a given body geometry, surface condition, and the fluid flow regime (laminar, turbulent, continuum, slip, etc.). The viscosity and density distributions are again functions of the temperature profile, $\partial T / \partial y$, i.e., of the heat transfer rates.

In a continuum flow, the relative importance of heat transfer effects in practical applications varies with thermal conditions of the solid surface (insulated or non-insulated), the speed of flow (compressible or incompressible), and the type of boundary layer (laminar or turbulent):

For incompressible ($M < .4$) viscous flows along insulated surfaces, the heat transfer is relatively unimportant, both for laminar and for turbulent boundary layers.

For compressible ($M > .4$) flows over insulated surfaces, the importance of the heat transfer phenomena increases with the increase in the Mach Number, the turbulent boundary layers representing more severe case.

For noninsulated surfaces, the heat transfer phenomena are always important, the intensity of the temperature gradient value at the wall, $(\partial T / \partial y)_w$, being the measure of the relative importance.

(iv) The Adiabatic Wall Temperature and The Recovery Factor

The adiabatic wall temperature, T°_{aw}, is defined as the stagnation temperature value of the boundary layer stream particles in direct contact with an insulated (adiabatic) wall surface

$$y = 0 \ , \ \left(\frac{\partial T^\circ}{\partial y} \right)_0 = 0 \ , \qquad (2.3\text{-}26)$$

under the "no-slip" continuum flow wall conditions,

$$y = 0 \ , \quad u_0 = u_w = 0 \ ,$$
$$T^\circ_{aw} = T^\circ_{s0} \ , \qquad (2.3\text{-}27)$$

and assuming that the wall is treated as the "zero" streamline of the general flow, i.e.:

$$y = 0 \ , \quad v_0 = v = 0 \ . \qquad (2.3\text{-}28)$$

For perfect gas flows, the Prāndtl Number is less than or equal to one, ($Pr \leq 1$) and the local adiabatic (stagnation) wall temperature, T°_{aw}, is always less than the respective local free stream stagnation temperature, $T^\circ_{s\infty}$, outside the boundary layer. The difference is due to the very existence of the thermal boundary layer; i.e., due to the heat flux away from the wall across a finite thickness of the boundary layer. As a consequence, there is a temperature gradient, forming a local static temperature profile, $T^\circ(y)$, and a local stagnation temperature profile, $T^\circ_s(y)$, across the boundary layer, see Fig (2.3-2).

For an isentropic and compressible external flow, the general perfect gas relationship is given by(6).

$$\frac{T^\circ_1}{T^\circ_2} = \frac{1 + \frac{(\gamma-1)}{2} M_2^2}{1 + \frac{(\gamma-1)}{2} M_1^2} \qquad (2.3\text{-}29)$$

where subscripts (1) and (2) refer to any two points along a streamline.

The stagnation temperature at an insulated wall (i.e., in the absence of heat flux from the wall to the adjacent fluid layers), if the fluid were presumed to be brought to a rest isentropically, would be:

$$M_2 = 0 \ , \quad T_2^\circ = T_{s\infty}^\circ \ ,$$

$$M_1 = M_\infty \ , \quad T_1^\circ = T_\infty^\circ \ ,$$

$$\therefore \ T_{s\infty}^\circ = T_\infty^\circ \left(1 + \frac{\gamma-1}{2} M_\infty^2 \right) = T_\infty^\circ + \frac{V_\infty^2}{2C_p} \ ,$$

or (2.3-30)

$$C_p T_\infty^\circ + \frac{V_\infty^2}{2} = C_p T_{s\infty}^\circ \ ,$$

$$p_\infty \rho_\infty = R T_\infty^\circ \ ,$$

$$\frac{C_p}{R} = \frac{C_p - C_v}{R} = \frac{\gamma}{\gamma-1} \ ,$$

$$a_\infty^2 = \gamma R T_\infty^\circ \ ,$$

$$T_\infty^\circ \frac{\gamma-1}{2} M_\infty^2 = T_\infty^\circ \frac{\gamma-1}{2} \frac{V_\infty^2}{a_\infty^2} = \frac{(\gamma-1)V_\infty^2}{2\gamma R} = \frac{V_\infty^2}{2C_p} \ .$$

$$\therefore \ T_{s\infty}^\circ = T_\infty^\circ + \frac{V_\infty^2}{2C_p} \ .$$

(2.3-31)

Since, due to an outward heat flux in an adiabatic viscous flow within the boundary layer the recovery (stagnation) temperature is necessarily decreased, it follows that:

$$T_{s_0}^\circ = T_{aw}^\circ < T_{s\infty}^\circ \ ,$$

$$\therefore \ T_{aw}^\circ = T_\infty^\circ \left(1 + r \frac{\gamma-1}{2} M_\infty^2 \right), \quad r < 1 \ ,$$

(2.3-32)

where r is called the (adiabatic) recovery factor, and is less than unity for $Pr < 1$.

Note that the condition

$$y = 0 \ , \ \left(\frac{\partial T^\circ}{\partial y} \right)_0 = 0 \ ,$$

(2.3-33)

of the fluid layer directly next to the insulated wall is established only after a steady thermal equilibrium state is reached, i.e., after the static temperature profile $T^\circ(y)$ is realized.

The recovery factor, r , is thus a convenient measure of the stagnation temperature deficiency at the wall due to outward heat flux (or the total energy dissipation) across the thickness boundary layer. Using the above equations (2.3-30) and (2.3-32), the local recovery factor can be expressed as

$$r = \frac{T_{aw}^\circ - T_\infty^\circ}{V_\infty^2/2C_p} = \frac{T_{aw}^\circ - T_\infty^\circ}{T_{s\infty}^\circ - T_\infty^\circ} = \frac{.2}{(\gamma-1)M_\infty^2} \cdot \left(\frac{T_{aw}^\circ}{T_\infty^\circ} - 1 \right) \ .$$

(2.3-34)

(v) Main Aspects of Some Classical Treatments of The Laminar Boundary Layer Problem - The Karman-Tsien(4) and the Prandtl(3) Analyses - Steady, two-dimensional, Compressible, Laminar Boundary Layers for the Prandtl Number of Unity and an Insulated Wall Condition.

ASSUMPTIONS AND APPROXIMATIONS:

(a) $Pr = \frac{C_p \mu}{k} = 1$, μ = const., k = const.

(b) An insulated wall of a relatively small and continuously convex curvature.

(c) Due to the assumed value of ($P_r = 1$) and the wall insulation, the local stagnation temperature, T_s° , has the same value in all points within the boundary layer, equal to its local free stream (inviscid flow) value, $T_{s\infty}^\circ$.

(d) In addition to the solid boundary condition ($v_0 = v_w = 0$) the usual continuum flow "no slip" condition at the wall ($u_0 = u_w = 0$) is presumed valid.

Note: In case of insulated walls, the term "wall temperature", T_w° , is used conditionally, denoting actually the temperature of the fluid layer next to the wall, $T_{s_0}^\circ$, or T_{aw}° , where the subscript (o) refers to the fluid layer at $y = 0$.

CONSEQUENCES:

(1) Interpretations of the energy equation, valid both for insulated flat plates ($\partial p/\partial x = 0$) and for small curvature walls ($\partial p/\partial x \neq 0$):

The energy equation (2.3-12) takes the form:

$$\rho u \left(\frac{\partial T_s^\circ}{\partial x} \right) + \rho v \left(\frac{\partial T_s^\circ}{\partial y} \right) = \frac{\partial}{\partial y} \left(\mu \frac{\partial T_s^\circ}{\partial y} \right) ,$$

(2.3-35)

having as a particular solution:

$$T_s^\circ = T^\circ + \frac{u^2}{2C_p} = \text{const.} = T_{s\infty}^\circ , \qquad (2.3\text{-}36)$$

$$\therefore \frac{\partial}{\partial T}\left(C_p T^\circ + \frac{u^2}{2}\right) = 0 , \qquad (2.3\text{-}37)$$

$$C_p = -u \frac{\partial u}{\partial T^\circ} , \qquad (2.3\text{-}38)$$

i.e., the local stagnation temperature profile, $T_s^\circ(y)$, across the boundary layer (with $u_e = u_w = 0$) becomes (see Fig 2.3-2):

$$T_s^\circ = T_{s\infty}^\circ = T_{se}^\circ = T_{sw}^\circ = (T_w^\circ) = \text{const.} ,$$

$$T_{sw}^\circ = (T_w^\circ) > T^\circ(y) , \qquad (2.3\text{-}39)$$

i.e., the heat flows from the wall toward the outer edge of the boundary layer at all points (a positive heat flux, q), while the heat flux at the wall, q_w, is zero.

(2) The Prandtl Number Interpretation

The Prandtl Number can be interpreted as representing the ratio of viscous shear work to thermal heat conduction (see Section 2.2):

$$\frac{\mu u\left(\frac{\partial u}{\partial y}\right)}{k\left(\frac{\partial T^\circ}{\partial y}\right)} = \frac{\mu u\left(\frac{\partial u}{\partial T^\circ}\right)}{k} \sim Pr = \frac{\mu C_p}{k} , \qquad (2.3\text{-}40)$$

For viscous and heat conducting continuum gas flows, the Prandtl Number is always less than unity (no dissociation). Its approximate laminar boundary layer value for near standard sea-level temperatures is .75, and it is only a weak function of temperature.

In view of the equations (2.2-38) and (2.3-40) for ($Pr = 1$):

$$\frac{\mu u\left(\frac{\partial u}{\partial T^\circ}\right)}{k} = \frac{\mu C_p}{k} = Pr = 1 , \qquad (2.3\text{-}41)$$

i.e., the ratio of the viscous shear work is equivalent to the thermal heat conduction, which means that the viscous boundary layer, $\delta(x)$, and the thermal boundary layer, $\delta(T^\circ)$, have the same thicknesses locally. The recovery factor(r) for the case is unity, as follows from equations (2.3-34) and (2.3-39).

(3) Interpretations of the Momentum and the Energy Equations for Insulated Flat Plates (Zero Pressure Gradient).

The established steady viscous flow pattern and the wall temperature are uniform along an insulated flat plate: both the velocity and the temperature profiles are constant in the x-direction, the viscous and the thermal boundary layers having the same local and the same average thicknesses.

With $\left(\frac{\partial p}{\partial x} = 0\right)$, the momentum equation (2.3-6) in the x-direction becomes:

$$\rho u \frac{\partial u}{\partial x} + \rho v \frac{\partial u}{\partial y} = \frac{\partial}{\partial y}\left(\mu \frac{\partial u}{\partial y}\right) . \qquad (2.3\text{-}42)$$

For ($Pr = 1$) and an insulated plate, the momentum equation (2.3-42) and the energy equation (2.3-35) are simultaneously satisfied when the following parabolic temperature-velocity function is assumed[3]:

$$T_s^\circ = T^\circ + \frac{u^2}{2C_p} = Au + B \qquad (2.3\text{-}43)$$

where the constants (A) and (B) can be determined from the boundary conditions:

At the outer edge:

$$y = \delta_x , \quad u = V_\infty , \quad T_s^\circ = T_{s\infty}^\circ ,$$

At the plate:

$$y = 0 , \quad u = 0 , \quad T_s^\circ = T_{se}^\circ = T_{sw}^\circ = (T_w^\circ) ,$$

$$\therefore A = \frac{T_s^\circ - T_w^\circ}{V_\infty} , \quad B = T_w^\circ , \qquad (2.3\text{-}44)$$

and:

$$\frac{u}{V_\infty} = \frac{T_s^\circ - T_w^\circ}{T_{s\infty}^\circ - T_w^\circ} . \qquad (2.3\text{-}45)$$

Since:

$$\left.\begin{aligned} C_p &= \frac{\gamma}{\gamma-1} R \\ a_\infty^2 &= \gamma R T_\infty^\circ \end{aligned}\right\} \qquad C_p = \frac{a_\infty^2}{T_\infty^\circ(\gamma-1)} ,$$

$$\therefore \frac{1}{C_p} = M_\infty^2 \frac{\gamma-1}{V_\infty^2} T_\infty^\circ ,$$

(2.3-46)

the equations (2.3-43), (2.3-44) and (2.3-46) with ($T_{aw}^\circ = T_w^\circ$) yield:

$$\frac{T^\circ}{T_\infty^\circ} = \frac{T_w^\circ}{T_\infty^\circ} - \left(\frac{T_w^\circ}{T_\infty^\circ} - 1\right)\frac{u}{V_\infty} + \frac{\gamma-1}{2} M_\infty^2 \frac{u}{V_\infty}\left(1 - \frac{u}{V_\infty}\right) ,$$

(2.3-47)

or alternatively,

$$(T^\circ - T_w^\circ) = (T_{s\infty}^\circ - T_w^\circ)\frac{u}{V_\infty} - \frac{\gamma-1}{2} M_\infty^2 T_\infty^\circ \left(\frac{u}{V_\infty}\right)^2 .$$

(2.3-48)

(4) Heat Flux at any Local Point, q(y).

Fourier's law for the local heat flux per unit mass across the boundary layer in y -direction is by definition (see Section 2.2):

$$q = \frac{dQ}{dt} = -k\left(\frac{\partial T^\circ}{\partial y}\right) ,$$

(2.3-49)

or, by differentiating the equations (2.3-47) and (2.3-48) respectively, the local heat flux at any point within the boundary layer is:

$$q = \frac{k T_\infty^\circ}{V_\infty}\left[\left(\frac{T_w^\circ}{T_\infty^\circ} - 1\right) - \frac{\gamma-1}{2} M_\infty^2\right]\left(\frac{\partial u}{\partial y}\right) ,$$

(2.3-50)

$$q = \frac{k}{V_\infty}\left[(T_w^\circ - T_{s\infty}^\circ) + (\gamma-1) M_\infty^2 T_\infty^\circ \frac{u}{V_\infty}\right]\left(\frac{\partial u}{\partial y}\right) .$$

(2.3-51)

In terms of the local shear stress and the Prandtl Number definitions,

$$\tau = \mu\left(\frac{\partial u}{\partial y}\right) , \quad Pr = \frac{C_p \mu}{k} ,$$

(2.3-52)

the equation (2.3-51) takes the form:

$$q = \frac{C_p}{Pr}\frac{\tau}{V_\infty}\left[(T_w^\circ - T_{s\infty}^\circ) + (\gamma-1) M_\infty^2 T_\infty^\circ \frac{u}{V_\infty}\right] ,$$

(2.3-53)

(5) Heat Flux at the Wall, ($q_o = q_w$)

For the fluid layer at the wall (subscript "o") the velocity gradient in the y -direction is always positive:

$$y = 0, \left(\frac{\partial u}{\partial y}\right)_o > 0 \quad \text{for} \quad u_o = u_w = 0 .$$

(2.3-54)

(6) Insulated Wall (adiabatic Flow Conditions at the Wall)

At an insulated wall, there is no heat flux between the wall (subscript "w") and the fluid layer directly in contact with it (subscript "o"):

$$q_w = q_o = -k\left(\frac{\partial T^\circ}{\partial y}\right)_w = 0 ,$$

$$\therefore \left(\frac{\partial T^\circ}{\partial y}\right)_o = 0 \quad \text{since} \quad k \neq 0.$$

(2.3-55)

Then, in view of the equation (2.3-50):

$$\left(\frac{\gamma-1}{2}\right) M_\infty^2 = \left(\frac{T_w^\circ}{T_\infty^\circ} - 1\right) ,$$

$$q_w = 0 ,$$

(2.3-56)

is valid, in general, for any insulated wall.

When the additional assumptions ($Pr = 1$) and ($\gamma = 1$) are introduced, the equations (2.3-56) and (2.3-32) yield specifically:

$$T_{s\infty}^\circ = T_w^\circ = T_{aw}^\circ .$$

(2.3-57)

Under the adiabatic conditions (2.3-56) the energy equation

$$\frac{u^2}{2} + C_p T^\circ = \text{constant}$$

(2.3-58)

implies that the energy content per unit mass is constant throughout the boundary layer.

(7) Non-insulated Wall

Since $(\partial u/\partial y)_w$ is always positive, the heat flux equation (2.3-50) yields the following conditions at a non-insulated wall, see Fig (2.3-2):

For a cold wall:

$$\left(\frac{\gamma-1}{2}\right)M_\infty^2 > \left(\frac{T_w^\circ}{T_\infty^\circ}-1\right), \quad q_o = q_w < 0, \quad \left(\frac{\partial T^\circ}{\partial y}\right)_o > 0, \tag{2.3-59}$$

i.e., the heat flux is from the fluid to the wall, and for a hot wall:

$$\left(\frac{\gamma-1}{2}\right)M_\infty^2 < \left(\frac{T_w^\circ}{T_\infty^\circ}-1\right), \quad q_o = q_w > 0, \quad \left(\frac{\partial T^\circ}{\partial y}\right)_o < 0, \tag{2.3-60}$$

i.e., the heat flux is from the wall to the fluid.

Alternatively, analyzing the heat flux expression (2.3-53), and recalling that the heat flux is considered positive away from the wall, the following conclusion can be drawn, see Fig (2.3-2):

When ($T_w^\circ > T_{s\infty}^\circ$), the heat flux is positive at the wall ($q_w > 0$), and remains so throughout the boundary layer, ($q > 0$), i.e., it reflects the hot wall conditions.

When ($T_w^\circ < T_{s\infty}^\circ$), the heat flux is negative at the wall ($q_w < 0$), although at some points in the boundary layer it may be locally directed away from the wall ($q > 0$), i.e., the cold wall conditions are manifested.

The heat flux expression (2.3-53) can be further utilized for a later derivation of the Reynolds Analogy concept, provided the following clear discrimination of the temperature conditions at the wall are realized:

(a) The adiabatic flow conditions exist only if the wall is insulated. Then, for all Prandtl Number values ($Pr \leq 1$), the "adiabatic wall" temperature, T_{aw}°, is actually the stagnation temperature of the fluid layer next to the wall under the "no-slip" condition ($u_w = u_o = 0$), i.e.:

$$T_{aw}^\circ = T_{so}^\circ . \tag{2.3-61}$$

Under the adiabatic conditions, the "wall temperature" term, T_w°, is actually without a real meaning, since the wall is insulated and its temperature is not related to the fluid flow at all. Thus, the equality,

$$T_{aw}^\circ = T_{so}^\circ = (T_w^\circ), \tag{2.3-62}$$

for insulated walls can be used conditionally only, i.e., provided the adiabatic temperature of the fluid layer next to the wall, $T_{so}^\circ = T_{aw}^\circ$, is conditionally termed the "wall temperature," T_w.

When the real value of the Prandtl Number ($Pr < 1$) for nondissociated gases is used, the adiabatic wall temperature, T_{aw}°, is less than the corresponding free stream stagnation temperature, $T_{s\infty}^\circ$:

$$(T_w^\circ) = T_{so}^\circ = T_{aw}^\circ < T_{s\infty}^\circ \tag{2.3-63}$$

and also

$$T_{aw}^\circ < T_s^\circ(y), \quad T_s^\circ(y) \neq T_{s\infty}^\circ . \tag{2.3-64}$$

(b) When interpreting the non-insulated wall conditions the "adiabatic wall" temperature concept, T_{aw}°, is sometimes artificially introduced for the sake of comparison with the "insulated" (i.e., idealized) case. This artifice should be again interpreted as a conditional and useful convenience only, since for non-insulated walls the temperature relationship

$$T_{so}^\circ = T_w^\circ \gtrless T_{aw}^\circ < T_{s\infty}^\circ \tag{2.3-65}$$

is in force, where the wall temperature, (T_w°), is now a real quantity, and

$$T_w^\circ = T_{os}^\circ , \quad \therefore \; T_{aw}^\circ \neq T_{os}^\circ = T_w^\circ \neq T_s^\circ(y) \tag{2.3-66}$$

under the assumed "no-slip" condition ($u_w = u_o = 0$).

(c) The assumption (Pr=1) is sometimes used (rather inconsistently) both for the insulated and the non-insulated wall conditions. As specified earlier in the subparagraph (2), it represents an idealized approximation regarding the treatment of viscous and heat conduction effects within the boundary layers. When applied to the temperature distribution analysis, the approximation (Pr=1) renders the adiabatic wall temperature, T°_{aw} , equal to the free stream stagnation temperature, $T^\circ_{s\infty}$:

$$T^\circ_{aw} = T^\circ_{s\infty} \quad , \qquad (2.3\text{-}67)$$

which, for insulated walls leads to the very special overall temperature equality (see subparagraph 1):

$$T^\circ_{aw} = T^\circ_{os} = T^\circ_{s\infty} = T^\circ_s = (T^\circ_w) = \text{const.} \qquad (2.3\text{-}68)$$

(d) It should be noted that all the above temperature definitions are valid only under steady flow thermal equilibrium conditions. For unsteady flows or during the traditional thermal conditions, prior to the establishment of a steady equilibrium state, the discussed temperatures represent only an eventually limiting case.

(e) With the above idealized temperature definitions (2.3-68), assuming a Prandtl Number of unity (Pr = 1) and using the term "adiabatic wall temperature" conditionally ($T^\circ_{aw} = T^\circ_{so} = T^\circ_{s\infty}$), the heat flux at a non-insulated wall ($q_w \neq 0$) and the real wall temperature (T°_w) can be conveniently obtained from the equation (2.3-53) under the "no-slip" conditions ($u_o = u_w = 0$) in terms of the shear stress at the wall (τ_w) :

$$q_w = C_p \frac{\tau_w}{V_\infty}(T^\circ_w - T^\circ_{s\infty}) = C_p \frac{\tau_w}{V_\infty}(T^\circ_w - T^\circ_{aw}) \quad . \qquad (2.3\text{-}69)$$

(8) Reynolds Analogy Concept for Pr=1 .

The Reynolds analogy represents a functional relationship between the skin-friction and the heat transfer coefficients. The form of the functional relationships depends upon the assumptions and the approximations introduced in various semi-empirical or theoretical analyses of the boundary layer problem.

(a) Assuming (Pr = 1), and the insulated wall conditions, the local Reynolds analogy takes a very simple form for both incompressible and compressible laminar boundary layers (3) the incompressible flow approximation being more accurate:

$$\left(St_x\right)_\infty = \frac{(C_{fx})_\infty}{2} = \frac{(Nu_x)_\infty}{(Re_x)_\infty} \qquad (2.3\text{-}70)$$

which is obtained from Eq (2.3-69) and the following definitions:

$\left(C_{fx}\right)_\infty = \frac{\tau_w}{\frac{1}{2}\rho_\infty V_\infty^2}$ -is the local (x) skin friction coefficient by definition, based on local free stream value (∞) of the dynamic pressure.

$(St_x)_\infty = \frac{h}{C_p \rho_\infty V_\infty}$ -is the local (x) dimensionless heat transfer coefficient, based on local free stream (∞) values of (ρ_∞) and (V_∞). It is called the local Stanton Number. Alternatively:

$$\left(C_{hx}\right)_\infty = \frac{h}{C_p \rho_\infty V_\infty} = \frac{hx}{k_\infty} \cdot \frac{k_\infty}{C_p \mu_\infty} \cdot \frac{\mu_\infty}{x \rho_\infty V_\infty} = \frac{(N_{ux})_\infty}{Pr_\infty (Re\, x)_\infty} \quad ,$$

$Pr_\infty = 1$ by assumption.

$\left(N_{ux}\right)_\infty = \frac{hx}{k_\infty}$ -is another dimensionless local (x) heat transfer coefficient definition, called the local Nusselt Number.

$h = \frac{q_w}{T^\circ_w - T^\circ_{aw}} = C_\mu \frac{\tau_w}{V_\infty}$ -is the dimensional $\left[\frac{\text{ft. lb.}}{\text{sec.} - \text{ft}^2\ {}^\circ R}\right]$ local (x) coefficient of heat transfer, obtained directly from Eq (2.3-69). It manifests that the direction of heat flow at the flat plate surface depends upon the difference ($T^\circ_w - T^\circ_{aw}$) and that it is independent of the difference. ($T^\circ_w - T^\circ_\infty$).

$$q_w = \frac{C_{f\infty}}{2} \rho_\infty \; V_\infty (T_w^\circ - T_{aw}^\circ) \; C_p = \frac{dQ/dt}{dA}$$

- is the local (x) heat flux (dQ/dt) per unit area(dA)at the wall $\left[\frac{\text{ft.-lb.}}{\text{sec-ft}^2}\right]$. Alternatively, using the relationship,

$$T_{s\infty}^\circ = T_\infty^\circ + \frac{V_\infty^2}{2C_p} = T_{aw}^\circ \quad ,$$

the expression for the local heat flux per unit area at the wall(w) , becomes:

$$q_w = \frac{C_{f\infty}}{2} \; \frac{\rho_\infty}{2} \; V_\infty^3 \; \frac{T_w^\circ - T_{aw}^\circ}{T_{aw}^\circ - T_\infty^\circ} \quad .$$

Note: The above definitions are referred to the local free stream(∞)conditions. They can be (and are sometimes) defined with respect to the local wall(w) values of the fluid properties (k_w), (μ_w), (ρ_w), but retaining the reference local free stream velocity, (V_∞).

(b) When a more realistic compressible laminar boundary layer Prandtl Number value ($Pr < 1$) is introduced , the Reynolds analogy takes form(8):

$$\left[St_\infty\right]_x = \frac{\left[Cf_\infty\right]_x}{2} \; Pr^{-2/3} \quad , \; \text{[dimensionless]} \qquad (2.3\text{-}71)$$

$$\left[r_x\right] = \left[Pr_\infty\right]_x^{1/2} = \left[\frac{T_{aw}^\circ - T_\infty^\circ}{T_{s\infty}^\circ - T_\infty^\circ}\right]_x = \left[\frac{T_{aw}^\circ - T_\infty^\circ}{V_\infty^2 / 2C_{p\infty}}\right]_x \quad , \; \text{[dimensionless]} \qquad (2.3\text{-}72)$$

$$\left[T_{aw}^\circ\right]_x = \left[T_\infty^\circ\right]_x \left[1 + r \frac{\gamma - 1}{2} M_\infty^2\right]_x \quad , \; [^\circ R] \qquad (2.3\text{-}73)$$

$$\left[\frac{V_\infty^2}{2}\right]_x + \left[C_{p\infty} T_\infty^\circ\right]_x = C_{p\infty} T_{s\infty}^\circ \quad , \qquad (2.3\text{-}74)$$

$$\left[a_\infty^2\right]_x = \gamma R \left[T_\infty^\circ\right]_x = \left[\frac{V_\infty^2}{M_\infty^2}\right]_x \quad , \; \left[\frac{ft^2}{sec^2}\right] \qquad (2.3\text{-}75)$$

$$\left[\frac{2 V_\infty^2}{2 V_\infty^2} \; \frac{T_{aw}^\circ - T_\infty^\circ}{T_{aw}^\circ - T_\infty^\circ}\right]_x \equiv 1 \quad . \qquad (2.3\text{-}76)$$

The above expressions are valid for an insulated flat plate and Mach Numbers(8) low enough, so that, in a first approximation, the coefficients μ and k are treated as constants. For a range of Mach Numbers up to 5, the laminar boundary recovery layer factor value is (for air)(9):

$$r = .84 \sim .855$$

(c) The expression (2.3-71) is formulated in terms of local conditions. It can be shown(5,6)that it is equally valid for average or total values of Cf_A and St_A (referred to the ambient atmospheric conditions).

2.3.2 LAMINAR BOUNDARY LAYERS ON FLAT PLATES - CONTINUUM FLOW REGIME

A great number of laminar boundary layer solutions exists in technical literature for a wide range of Mach Numbers and temperature conditions, and for an array of simple body geometries and angles of attack. For the limited practical applications of the drag force analysis, the presumed small angle-of-attack variations are considered to have negligible effects on the average skin-friction coefficient values and the flow-separation phenomena are excluded. The flat plate results are in most cases considered adequate, since, in a first approximation, they can be easily corrected to three-dimensional body configurations, as later specified. Therefore, the few flat plate basic results from the commonly accepted simplified theoretical solutions are presented only. The results are generally found to be in a good agreement with the corresponding experimental evidence.

(i) Local Skin-friction and Heat Transfer Expressions for Two-Dimensional Compressible Laminar Boundary Layers on Flat Plates With Pr = 1 and $\partial p / \partial x = 0$.

For flat plates, the energy Eq (2.3-12) and the momentum Eq (2.3-6) take the simpler form when the energetic assumption $Pr = 1$ and the momentum assumption $(\partial p / \partial x) = 0$ are introduced respectively:

$$\left\{ \rho u \frac{\partial T_s^\circ}{\partial x} + \rho v \frac{\partial T_s^\circ}{\partial y} = \frac{\partial}{\partial y}\left(\mu \frac{\partial T_s^\circ}{\partial y}\right) \right. , \quad \left. Pr = \mu Cp/k = 1 \right. \qquad (2.3\text{-}77)$$

$$\left\{ \rho u \frac{\partial u}{\partial x} + \rho v \frac{\partial u}{\partial y} = \frac{\partial}{\partial y}\left(\mu \frac{\partial u}{\partial y}\right) \right. , \quad \left. \frac{\partial p}{\partial x} = 0 \right. \qquad (2.3\text{-}78)$$

where, in general:

$$\rho = \rho(x,y) \qquad T_s^\circ = T_s^\circ(x,y)$$
$$u = u(x,y) \qquad T_s^\circ = T_s^\circ(x,y)$$
$$v = v(x,y) \qquad \mu = \mu(T^\circ) = f(x,y)$$
$$k = Cp\mu \ . \qquad (2.3\text{-}79)$$

The energy Eq (2.3-77) for $Pr = 1$ is satisfied if the local stagnation temperature, T_s°, is constant everywhere:

$$T_s^\circ = T^\circ + \frac{u^2}{2Cp} = T_{s\infty}^\circ \ , \qquad (2.3\text{-}80)$$

which is a particular solution.

For $Pr = 1$, the very restrictive solution given by the Eq (2.2-80) reduces at the wall ($u = 0$) to:

$$T_{s\infty}^\circ = T_w^\circ = T_s^\circ = \text{const} \ , \qquad (2.3\text{-}81)$$

which represents the special case of a non-insulated wall in thermal equilibrium with the boundary layer flow having $k = Cp\,\mu = \text{const}$ characteristic. A less special case is to assume that the flat plate is insulated, i.e.:

$$T_{s\infty}^\circ = T_s^\circ = T_{aw}^\circ = \text{const} \ , \qquad (2.3\text{-}82)$$

where T_{aw}° is the adiabatic stagnation temperature of the fluid layer next-to-wall ($u = 0$). In both cases, the local heat flux at any point through the boundary layer

$$q = -k\frac{\partial T^\circ}{\partial y} = k\,\frac{u}{Cp}\,\frac{\partial u}{\partial y} = \mu u \frac{\partial u}{\partial y} \qquad (2.3\text{-}83)$$

is positive ($\partial u / \partial y > 0$), i.e., toward the outer edge of the boundary layer, while at the wall ($u = 0$):

$$q_w = 0 \ . \qquad (2.3\text{-}84)$$

The momentum Eq (2.3-78) for $\partial p/\partial x = 0$ and $Pr = 1$ is satisfied in general i.e., regardless of the special case (2.3-80), if(4):

$$T_s^\circ \equiv T^\circ + \frac{u^2}{2Cp} = Au + B \qquad (2.3\text{-}85)$$

where the constants A and B are found from the (non-insulated wall) boundary conditions:

when $u = V_\infty$ $\quad T_s^\circ = T_{s\infty}^\circ$ $\quad Pr = 1$

when $u = 0$ $\quad T_s^\circ = T_w^\circ$

$$\therefore A = \frac{T^\circ_{s\infty} - T^\circ_w}{V_\infty} \quad ,$$

$$B = T^\circ_w \quad , \quad T^\circ_s \neq T^\circ_{s\infty} \quad . \qquad (2.3\text{-}86)$$

Then, since:

$$\frac{u}{V_\infty} = \frac{T^\circ_s - T^\circ_w}{T^\circ_{s\infty} - T^\circ_w} \quad , \qquad (2.3\text{-}87)$$

$$\frac{1}{C_p} = M^2_\infty \frac{\gamma - 1}{V^2_\infty} \, T^\circ_\infty \quad . \qquad (2.3\text{-}88)$$

the explicit relation between the local temperature, T°, and the local velocity component, u, takes form(4):

$$\frac{T^\circ}{T^\circ_\infty} = \frac{T^\circ_w}{T^\circ_\infty} - \left(\frac{T^\circ_w}{T^\circ_\infty} - 1\right) \frac{u}{V_\infty} + \frac{\gamma - 1}{2} M^2_\infty \frac{u}{V_\infty} \left(1 - \frac{u}{V_\infty}\right) \qquad (2.3\text{-}89)$$

$$\therefore T^\circ - T^\circ_w = (T^\circ_{s\infty} - T^\circ_w) \frac{u}{V_\infty} - \frac{\gamma - 1}{2} M^2_\infty T^\circ_\infty \left(\frac{u}{V_\infty}\right)^2 \quad . \qquad (2.3\text{-}90)$$

Referring to the illustrative Fig (2.3-2), the temperature profiles for a non-insulated wall can be specifically reinterpreted in the terms of the von Karman-Tsien type(4) of solution given by the Eq (2.3-90), (i.e., for $Pr = 1$ and $\partial p / \partial x = 0$) as follows:

Defining the local heat flux as positive when directed toward the outer edge of the boundary layer $(+y)$ and differentiating the Eq (2.3-90):

$$q = -k \frac{\partial T^\circ}{\partial y} = \frac{k}{V_\infty} \left[T^\circ_w - T^\circ_{s\infty} + (\gamma - 1) M^2_\infty T^\circ_\infty \frac{u}{V_\infty} \right] \left(\frac{\partial u}{\partial y} \right) \qquad (2.3\text{-}91)$$

the following conclusions apply:

For a hot wall, $T^\circ_w > T^\circ_{s\infty}$, the local heat flux within the boundary layer is toward its outer edge, i.e., it is positive in all points.

For a cold wall, $T^\circ_w < T^\circ_{s\infty}$, near the plate the local heat flux is towards the wall (negative), but at some points away from the wall, the heat flux may reverse its trend towards the outer edge, depending on the T°_∞ value.

For an insulated wall, or for a special thermal equilibrium condition of a non-insulated wall, when

$$T^\circ_w = T^\circ_{s\infty} = T^\circ_s$$

or $$T^\circ_{aw} = T^\circ_{s\infty} = T^\circ_s$$

the local heat flux is always positive (away from the wall):

$$q = k(\gamma - 1) M^2_\infty T^\circ_\infty u \left(\frac{\partial u}{\partial y} \right) \quad . \qquad (2.3\text{-}92)$$

The heat flux at the wall ($u = 0$) is obtained from the Eq (2.3-91):

$$q_w = C_p \frac{\tau_w}{V_\infty} (T^\circ_w - T^\circ_{s\infty}) = C_p \frac{\tau_w}{V_\infty} (T^\circ_w - T^\circ_{aw}) \qquad (2.3\text{-}93)$$

or, alternatively, by differentiating Eq (2.3-89):

$$q_w = \frac{k T^\circ_\infty}{V_\infty} \left[\left(\frac{T^\circ_w}{T^\circ_\infty} - 1 \right) - \frac{\gamma - 1}{2} M^2_\infty \right] \left(\frac{\partial u}{\partial y} \right)_w \qquad (2.3\text{-}94)$$

where

$$\left(\frac{\partial u}{\partial y} \right)_w = \frac{\tau_w}{\mu} = \frac{C_p}{k} \tau_w \quad \text{for} \quad Pr = \frac{C_p \mu}{k} = 1 \, .$$

Since $(\partial u / \partial y)_w$ is always positive, the three conditions at the wall are:

For a hot wall:

$$\left(\frac{\gamma - 1}{2} \right) M^2_\infty < \left(\frac{T^\circ_w}{T^\circ_\infty} - 1 \right) \qquad (2.3\text{-}95)$$

the heat flux is $(q_w > 0)$, i.e., from the plate to the fluid.

For a cold wall:

$$\left(\frac{\gamma - 1}{2} \right) M^2_\infty > \left(\frac{T^\circ_w}{T^\circ_\infty} - 1 \right) \qquad (2.3\text{-}96a)$$

the heat flux is $(q_w < 0)$, i.e., from the fluid to the plate.

For an insulated wall (adiabatic conditions):

$$\frac{\gamma - 1}{2} M^2_\infty = \left(\frac{T^\circ_0}{T^\circ_\infty} - 1 \right) \qquad (2.3\text{-}96b)$$

$$q_w \equiv 0 \, , \quad \frac{T^\circ_w}{T^\circ_\infty} = 1 + \frac{\gamma - 1}{2} M^2_\infty \qquad (2.3\text{-}97)$$

$$T^\circ_0 = T^\circ_\infty \quad \text{and} \quad T^\circ_{aw} = T^\circ_s = T^\circ_{s\infty} \qquad (2.3\text{-}98)$$

where the subscript (0) denotes the layer next-to-wall ($u = 0$).

The combined conditions of $(\partial p / \partial x) = 0$ and $Pr = 1$, resulting in a more general (non-insulated wall) solution given by the Eq (2.3-81), imply that the viscous

and the thermal boundary layers have the same thicknesses:

$$\delta_x = \delta_T \ . \tag{2.3-99}$$

Furthermore, from Eq (2.3-93), the dimensional heat transfer coefficient

$$h = \frac{q_w}{T_w^\circ - T_{s\infty}^\circ} = \frac{q_w}{T_w^\circ - T_{aw}^\circ} \tag{2.3-100}$$

is obviously independent of $(T_w^\circ - T_\infty^\circ)$. Then, in view of Eq (2.3-99) and (2.3-93), a simple form of the Reynolds analogy concept is obtained with the subscript(∞) indicating the local reference free stream conditions outside the boundary layer:

$$Cf_\infty = \frac{\tau_w}{1/2\,\rho_\infty V_\infty^2} \ , \tag{2.3-101}$$

$$St_\infty = \frac{h}{Cp\,\rho_\infty V_\infty} \ , \tag{2.3-102}$$

$$\frac{q_w}{T_w^\circ - T_{aw}^\circ} = \frac{Cp\tau_w}{V_\infty} = h = \frac{1/2\,Cf_\infty \rho_\infty V_\infty^2 Cp}{V_\infty} \tag{2.3-103}$$

$$\therefore St_\infty = \frac{Cf_\infty}{2} \ , \quad Pr_\infty = 1 \ , \tag{2.3-104}$$

and since

$$St_\infty = \frac{h}{Cp\rho_\infty V_\infty} = \frac{hx}{k_\infty}\,\frac{k_\infty}{Cp\,\mu_\infty}\,\frac{\mu_\infty}{x\,\rho_\infty V_\infty} = \frac{Nu_\infty}{Pr_\infty\, Re_{x\infty}} \ ,$$

$$Pr_\infty = 1 \tag{2.3-105}$$

$$\therefore Nu_\infty = \frac{Cf_\infty}{2}\, Re_{x\infty} = St_\infty\, Re_{x\infty} \ . \tag{2.3-106}$$

The heat flux at a non-insulated wall can be expressed in terms of Cf_∞ and V_∞ using Eqs (2.3-103):

$$q_w = \frac{Cf_\infty}{2}\,\rho_\infty V_\infty\,(T_w^\circ - T_{aw}^\circ)\,Cp \ , \tag{2.3-103}$$

$$T_{t\infty}^\circ = T_\infty^\circ + \frac{V_\infty^2}{2Cp} = T_{aw}^\circ \ , \tag{2.3-107}$$

$$\therefore q_w = \frac{Cf_\infty}{2}\,\frac{\rho_\infty}{2}\,V_\infty^3\,\frac{T_w^\circ - T_{aw}^\circ}{T_{aw}^\circ - T_\infty^\circ}\left[(MLT^{-2})(T^{-1}L^{-2})\right]. \tag{2.3-108}$$

When the local skin-friction and the local heat transfer coefficients are defined respective to the wall (w) instead to the free stream (∞) reference conditions:

$$Cf_w = \frac{\tau_w}{(1/2)\rho_w V_\infty^2} \ , \quad St_w = \frac{h}{Cp\,\rho_w V_\infty} \ ,$$

$$Nu_w = \frac{hx}{k_w} \ , \quad Re_{xw} = \frac{\rho_w x V_\infty}{\mu_w} \ . \tag{2.3-109}$$

The local relationships are given by:

$$St_w = \frac{Cf_w}{2} \qquad Nu_w = \frac{Cf_w}{2Re_{xw}} = St_w\, Re_{xw} \ . \tag{2.3-110}$$

(ii) Some Special Solutions of Steady, Compressible Laminar Boundary Layers, $Pr = 1$, $\partial p/\partial x = 0$.

Two-Dimension Definition of the average skin-friction drag coefficient

For an arbitrary two-dimensional surface $s = s(x, z = b)$, see Fig (2.3-2), and an arbitrary S_{REF}:

$$D = C_D \frac{\rho_\infty V_\infty^2}{2} S_{REF} = b\int_0^S \left(\mu\,\frac{\partial u}{\partial y}\right)_w ds = b\int_0^S \tau_w\, ds \ , \tag{2.3-111}$$

$$\tau_w = Cf_\infty \frac{\rho_\infty V_\infty^2}{2} \tag{2.3-112}$$

$$\therefore C_D = \frac{b}{S_{REF}}\int_0^S Cf_\infty\, ds \tag{2.3-113}$$

For a flat plate (one side) $ds = dx$, $s = L_{FP}$.

For a given Mach Number, M_∞, the local skin friction coefficient on a flat plate takes the analytical form(5):

$$Cf_\infty = \text{const} \times Re_x^{(-1/2)} = \kappa\, Re_x^{(-1/2)} \ ; \tag{2.3-114}$$

and thus

$$C_D = \frac{b}{S_{REF}}\int_0^L Cf_\infty\, dx = \kappa\,\frac{b}{S_{REF}}\int_0^L Re_x^{(-1/2)} dx \ ,$$

$$C_D = \frac{\kappa b}{S_{REF}}\left(\frac{\mu_\infty}{\rho_\infty V_\infty}\right)^{1/2}\int_0^{L_{FP}} x^{(-1/2)} dx = 2\,\frac{\kappa b}{S_{REF}}\,L\left(\frac{\mu_\infty}{\rho_\infty V_\infty L}\right)^{1/2} ,$$

$$\therefore C_D = \frac{L\cdot b}{S_{REF}} \times 2\kappa\, Re_L^{(-1/2)} = \frac{S_{WET}}{S_{REF}}\, 2\kappa\, R_L^{(-1/2)} \ , \tag{2.3-115}$$

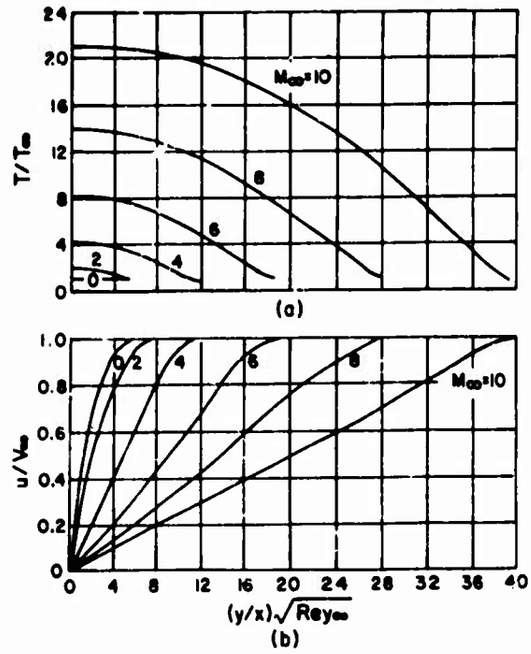

Fig. 2.3-3 Temperature and velocity profiles for insulated flat plate for Pr = 1 and ω = 0.76. (Ref. 4)

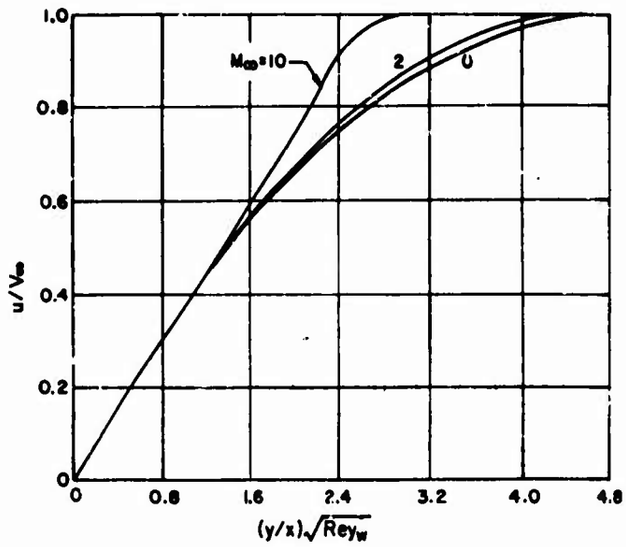

Fig. 2.3-5 Velocity profiles based on wall temperature, insulated flat plate, Pr = 1, ω = 0.76. (Ref. 4)

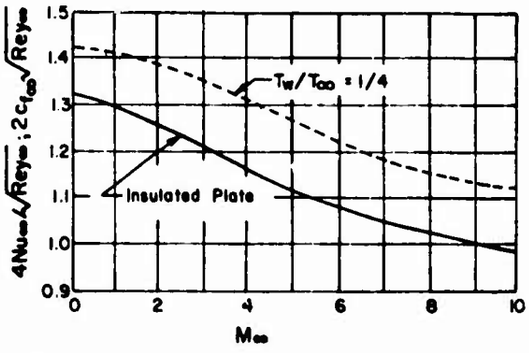

Fig. 2.3-4 Local skin-friction coefficient and local Nusselt number versus M∞ for Pr = 1 and ω = 0.76. (Ref. 4)

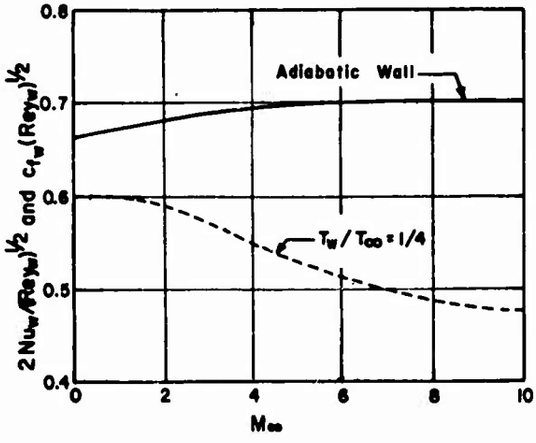

Fig. 2.3-6 Theoretical skin friction and heat transfer for flat plate based on wall temperature (Pr = 1, ω = 0.76). (Ref. 4)

and since at the distance L_{FP}, the local skin-friction coefficient is

$$(C_{f_\infty})_L = \kappa\, Re_L^{(-1/2)} \quad , \tag{2.3-116}$$

it follows that, in general, for compressible laminar boundary layers over non-insulated flat plates (one side):

$$C_D = \frac{S_{WET}}{S_{REF}}\, 2\,(C_{f_\infty})_L \quad , \tag{2.3-117}$$

or, in terms of the average skin-friction coefficient,

$$C_{f_{AV}} = \frac{b}{b \cdot L}\int_0^L C_{f_\infty}\, dx = 2\,\kappa\, Re_L^{(-1/2)}$$

$$\therefore C_{f_{AV}} = 2\,(C_{f_\infty})_L \quad . \tag{2.3-118}$$

(1) Von Karman - Tsien Solutions(4), Non-insulated, Smooth, Flat Plate at a Zero Angle-of-Attack (See Previous Subparagraph i):

Assumptions:

$$Pr = \frac{C_p \mu}{k} = 1, \quad \frac{\partial p}{\partial x} = 0$$

$$\mu(T^\circ) = \mu_\infty \left(\frac{T^\circ}{T^\circ_\infty}\right)^\omega, \qquad \omega = .76 \tag{2.3-119}$$

Local solutions for an insulated flat plate, Figs (2.3-3), (2.3-4), (2.3-5) and (2.3-6)

$$\frac{u}{V_\infty} = \frac{T^\circ - T^\circ_w}{T^\circ_\infty - T^\circ_w} = f\left[\left(\frac{y}{x}\right) Re_{x_\infty}^{1/2}\right] \quad , \tag{2.3-120}$$

$$\frac{T^\circ}{T^\circ_\infty} = \frac{T^\circ_w}{T^\circ_\infty} = 1 + \frac{\gamma - 1}{2} M_\infty^2 = f\left[\left(\frac{y}{x}\right) Re_{x_\infty}^{1/2}\right] \quad , \tag{2.3-121}$$

$$2C_{f_\infty} Re_{x_\infty}^{1/2} = 4\, Nu_\infty Re_{x_\infty}^{1/2} = f(M_\infty) \quad , \tag{2.3-122}$$

$$\frac{u}{V_\infty} = f\left[\left(\frac{y}{x}\right),\ Re_{x_w}^{1/2}\right] \quad ,$$

$$Re_{x_w}^{1/2} = Re_{x_\infty}\left(\frac{T^\circ_w}{T^\circ_\infty}\right)^{-\frac{(1+\omega)}{2}}, \quad \omega = .76 \quad , \tag{2.3-123}$$

$$2C_{f_w} Re_{x_w}^{1/2} = 4\, Nu_w Re_{x_w}^{1/2} = f(M_\infty) \quad . \tag{2.3-124}$$

Effects of a cool wall with $T^\circ_w / T^\circ_\infty = 1/4$ are illustrated in Figs (2.3-7), (2.3-4), (2.3-6).

Effects of a variable exponent ω, see Eq (2.3-119), are illustrated in Fig (2.3-8).

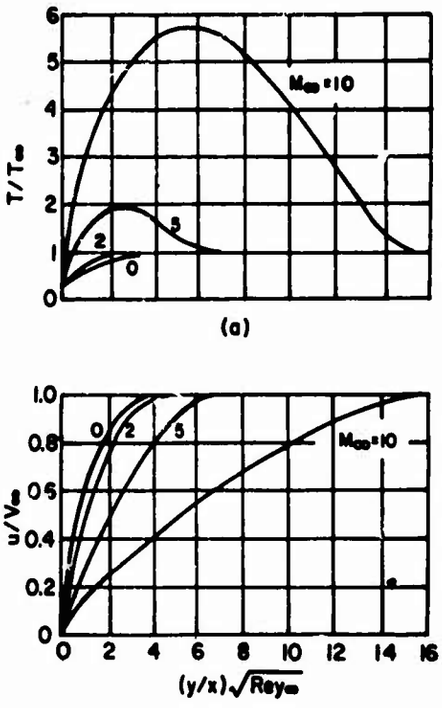

Fig.2.3-7 Temperature and velocity profiles, $T_w/T_\infty = 1/4$, $Pr = 1$, and $\omega = 0.76$. (Ref.4)

(2) Steady, Incompressible Laminar Boundary Layer Along a Smooth, Insulated Flat Plate at a Zero Angle-of-Attack Assuming a Linear Velocity Profile(5):

$$Pr = 1, \quad \frac{\partial p}{\partial x} = 0, \quad u = V_\infty\left(\frac{y}{\delta}\right) \quad ,$$

$$\delta_x = x\sqrt{12}\, Re_{x_\infty}^{-1/2}, \quad Re_{x_\delta} \equiv \frac{V_\infty\, x\, \rho_\infty}{\mu_\infty} \quad ,$$

$$\delta^*_x = \int_0^\delta \left[1 - \frac{u}{V_\infty}\right] dy = \frac{\delta_x}{2} \quad ,$$

$$C_{f_\infty} = \frac{1}{\sqrt{3}}\,(Re_{x_\infty})^{-1/2} \quad ,$$

$$\theta_x = \int_0^\delta \frac{u}{V_\infty}\left[1 - \frac{u}{V_\infty}\right] dy = \frac{\delta_x}{6} \quad , \tag{2.3-125}$$

$$\frac{\delta_x^*}{\theta_x} = 3 \,. \qquad (2.3\text{-}125)$$ cont'd

(3) The Blasius Solution[6], (Referred to as "Exact"):

Steady, two-dimensional, incompressible laminar boundary layer along a smooth, insulated flat plate at a zero angle-of-attack ($\partial p / \partial x = 0$, $Pr = 1$), see Fig (2.3-8):

$$\delta_x = 5.2\left(\frac{\nu x}{V_\infty}\right)^{1/2} = \frac{5.2\,x}{(Re_{x_\infty})^{1/2}} \,, \qquad (2.3\text{-}126)$$

$$\delta_x^* = \int_0^\infty \left(1 - \frac{u}{V_\infty}\right) dy = \frac{1.7208\,x}{(Re_{x_\infty})^{1/2}} \,, \qquad (2.3\text{-}127)$$

$$Cf_\infty = \frac{\tau_w}{\frac{1}{2}\rho_\infty V_\infty^2} = \frac{.664}{(Re_{x_\infty})^{1/2}} \,, \qquad (2.3\text{-}128)$$

$$Cf_{A\bar{V}} \frac{\int_0^L \tau_w dx}{\frac{1}{2}\rho V_\infty^2 L} = \frac{1}{L}\int_0^L Cf_\infty dx = \frac{1.328}{(Re_L)^{1/2}} = 2Cf_L \,. \qquad (2.3\text{-}129)$$

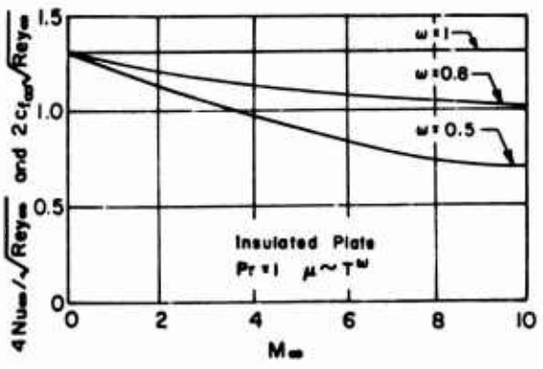

Fig. 2.3-8 Effect of variable viscosity on theoretical skin friction for flat plate. (Ref. 11)

(4) The Pohlhausen Solution[8] (Approximate):

Steady two-dimensional incompressible laminar boundary layer along insulated, body surfaces with a known inviscid flow pressure distribution ($\partial p / \partial x = f(x)$, $Pr = 1$) .

The solution is obtained by application of the Karman momentum integral, Eq (2.3-8), and by assuming a velocity profile shape given by a fourth degree polynomial. The analysis is sometimes called the Karman-Pohlhausen method. The results are in a good agreement with experimental evidence and with other theoretically more "exact" solutions, up to the point of boundary layer flow separation ($\partial p / \partial x > 0$). The inviscid pressure distribution $\partial p / \partial x = f(x)$ must be known.

For a flat plate at a zero angle-of-attack, ($\partial p / \partial x = 0$, $Pr = 1$) :

$$\theta_x = \int_0^\delta \frac{u}{V_\infty}\left(1 - \frac{u}{V_\infty}\right) dy = .686\,x\,Re_{x_\infty}^{-1/2} \,,$$

$$\frac{\theta_x}{\delta_x} = \frac{37}{315} \qquad \frac{\delta_x^*}{\theta_x} = 2.55 \,,$$

$$\frac{\delta_x^*}{\delta_x} = \frac{3}{10} \qquad Cf_\infty\, Re_{x_\infty}^{1/2} = .686 \,. \qquad (2.3\text{-}130)$$

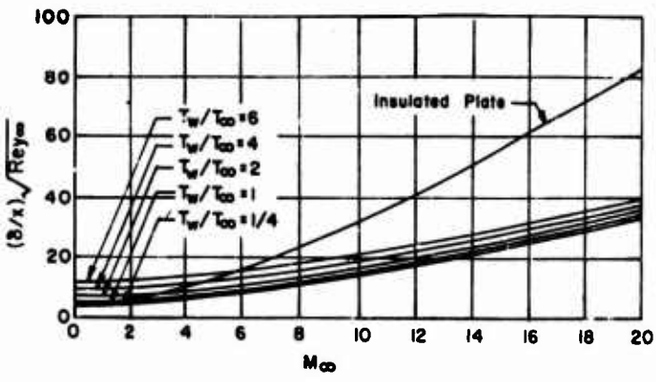

Fig. 2.3-9 Boundary-layer thickness on flat plate under Sutherland law, Pr = 0.75, (Ref. 4)

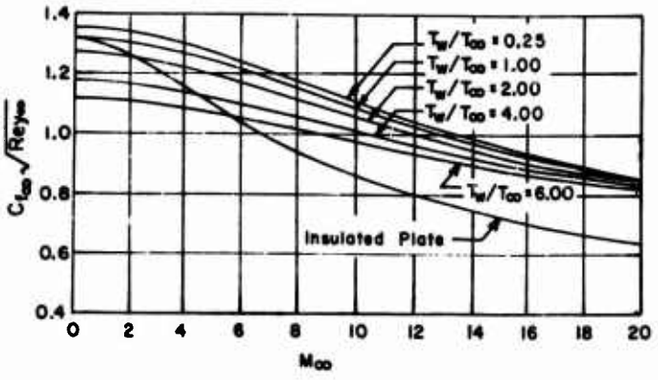

Fig. 2.3-10 Mean skin friction on flat plate under Sutherland law, Pr = 0.75, (Ref. 4)

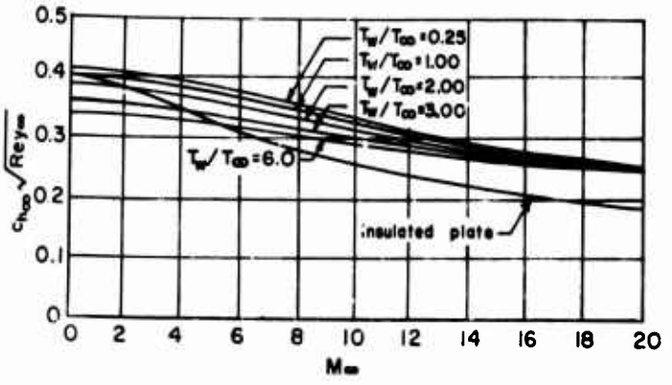

Fig.2.3–11 Heat transfer on flat plate under Sutherland law, Pr=0.75. (Ref. 4)

(5) Incompressible Laminar Boundary Layer, Insulated (one side) Flat Plate ($Pr = 1, \partial p/\partial x = 0$) - Comparative Table:

Linear	1.732	3.00	.578
Blasius	1.729	2.61	.664
Pohlhausen	1.752	2.55	.686
Karman-Tsien	--	--	.665
	$\left(\frac{\delta^*}{x}\right)Re_{x_\infty}^{1/2}$	$\frac{\delta^*}{\theta}$	$Cf_\infty Re_{x_\infty}^{1/2}$

(iii) Two Dimensional Compressible Laminar Boundary Layer on Flat Plates With Arbitrary Prandtl Number-van Driest Method(12)

When Prandtl Number is not unity, it becomes considerably more difficult to solve the governing laminar boundary layer equations, and usually the approximate analytical methods are used instead. The von Driest's solution(12), based on the Crocco's method and the Sutherland's law,

$$\frac{\mu}{\mu_\infty} = \left(\frac{T^\circ}{T_\infty^\circ}\right)^{3/2}\frac{T_\infty^\circ + S}{T^\circ + S} = \left(\frac{T^\circ}{T_\infty^\circ}\right)^{-1/2}\frac{1 + (S/T_\infty^\circ)}{1 + [(S/T_\infty^\circ)/(T^\circ/T_\infty^\circ)]},$$

$$\frac{S}{T_\infty^\circ} = .505 \ ,$$

$$Pr = .75 \ , \qquad (2.3\text{-}131)$$

is commonly accepted in practical applications for ($0 < M_A < 20$) and ($-250°F < T_A^\circ < 3250°F$).

The method is described in the section on turbulent boundary layers, the laminar boundary layer solutions are graphically illustrated below in Fig (2.3-9) to (2.3-11), (see preceding page).

(iv) Shock Wave Boundary Layer Interaction at Hypersonic Speeds, Laminar Boundary Layers

At hypersonic flow speeds, $M_A >> 1$, the boundary layer is thicker than at supersonic speeds for the same Reynolds Number value, primarily due to large temperature gradients near the body surface. The oblique strong bow shock wave is detached and tends to wrap up around the body contour, leaving a diminishing corridor for the inviscid flow region between the wave and the effective (real plus boundary layer) body thickness. The increased rate of growth of the boundary layer deflects the inviscid flow streamlines and thus effectively changes the pressure distribution, which in its turn, feeds back into the boundary layer and affects its growth, skin-friction and heat transfer rates.

In case of a steady, hypersonic laminar boundary layer over flat plates at zero angle-of-attack, the following practically important aspects and corrections can be noted(13,14):

The local, (x), deflection, θ_x, of the inviscid flow streamline by the boundary layer growth is computed on the basis of the Prandtl-Meyer relationship at hypersonic speeds(13):

$$\theta_x = K_i' \sqrt{C}\ \frac{M_\infty^2}{(Re_x)_\infty^{1/2}} \qquad (2.3\text{-}132)$$

where

$K_i' = .5985\,(\gamma - 1)$ for an insulated flat plate,

$K_i' = \frac{.865}{M_\infty^2}\left(\frac{T_w^\circ}{T_\infty^\circ}\right) + .166\,(\gamma - 1)$ for a non-insulated flat plate,

$\gamma = \frac{Cp}{Cv}$ - is the specific heats ratio,

T_w° - is the flat plate local wall temperature degrees absolute,

M_∞ - is the local undisturbed (i.e., not corrected for interference θ) Mach Number of the inviscid flow stream outside the

boundary layer (subscript ∞),

$C \approx .612$ - is the linear proportionality factor in the viscosity-temperature relation, $\mu = CT^{\circ}$,

$(Re_x)_\infty = \frac{\rho_\infty V_\infty x}{\mu_\infty}$ - is the local undisturbed (i.e., not corrected for θ) Reynolds Number referred to the local inviscid flow conditions outside the boundary layer (subscript ∞).

The local, (x), pressure disturbance of the inviscid stream, deflected by the θ_x angle due to boundary layer growth, is (in a first approximation):

$$\frac{p}{p_\infty} = \left(1 + \frac{\gamma-1}{2} M_\infty \theta_x\right)^{2\gamma/(\gamma-1)} \qquad (2.3\text{-}133)$$

$$\frac{p}{p_\infty} = \left[1 + \frac{\gamma-1}{2} K_i' \sqrt{C}\, \frac{M_\infty^3}{(Re_x)_\infty^{1/2}}\right]^{2\gamma/\gamma-1} \approx$$

$$\approx \left[1 + \gamma K_i' \sqrt{C}\, \bar{\chi}\right] \qquad (2.3\text{-}134)$$

and

$$\frac{T^{\circ}}{T_A^{\circ}} \approx 1 + (\gamma-1) K_i' \sqrt{C}\, \bar{\chi} \quad . \qquad (2.3\text{-}135)$$

$$\frac{\rho}{\rho_A} \approx 1 + K_i' \sqrt{C}\, \bar{\chi} \quad , \qquad (2.3\text{-}136)$$

$$\frac{V}{V_A} \approx 1 - K_i' \sqrt{C}\, \frac{M_\infty}{(Re_x)_\infty^{1/2}} \quad , \qquad (2.3\text{-}137)$$

where

$\bar{\chi} = \frac{M_\infty^3}{(Re_x)_\infty^{1/2}}$ -is the so-called interaction parameter, and the physical quantities without subscript (p, T°, ρ, V) denote the local corrected (for θ effects) values of the inviscid stream outside the boundary layer.

The parameter, $\bar{\chi}$, is a measure of the interaction intensity between the viscous and the inviscid flow patterns. A weak interaction is characterized by ($\bar{\chi} << 1$) , when ($p \sim p_\infty$) , and a strong interaction by $\bar{\chi} \sim O(1)$, when the corrective effects of the $p > p_\infty$ feed back into the boundary layer must be taken into account. Then, the corrected local boundary layer thickeness, δ_x , and the local skin friction coefficient, Cf , referred to the ambient flow conditions in front of the bow shock (subscript A) for a non-insulated flat plate and a weak interaction, $\bar{\chi} \sim O(1)$ are(13,14):

$$Cf \frac{(Re_x)_A^{1/2}}{C_A^{1/2}} = .783 \left(\frac{p}{p_A}\right)^{1/2} \quad , \qquad (2.3\text{-}138)$$

$$\frac{\delta (Re_x)_A^{1/2}}{x\, C_A^{1/2}} = 2.55\, \frac{\gamma-1}{2}\, M_A^2 \left(\frac{p}{p_A}\right)^{-1/2} \quad , \qquad (2.3\text{-}139)$$

where

$$\frac{p}{p_A} \approx 1 + .599\gamma(\gamma-1)\bar{\chi} + .090\gamma(\gamma-1)^2(\gamma+1)\bar{\chi}^2 \quad , \qquad (2.3\text{-}140)$$

$$C_A = \frac{\mu_w}{\mu_A} \frac{T_A^{\circ}}{T_w^{\circ}} \quad , \qquad (2.3\text{-}141)$$

$$(Re_x)_A = \frac{\rho_A V_A x}{\mu_A} \quad , \qquad (2.3\text{-}142)$$

$$M_A = \frac{V_A}{a_A} \quad , \quad a_A = (\gamma R T_A^{\circ})^{1/2} \quad , \qquad (2.3\text{-}143)$$

$$\bar{\chi} = \frac{M_\infty^3}{(Re_x)_\infty^{1/2}} \sim O(1) \quad .$$

Since for the case of the weak interaction, $\bar{\chi} \sim O(1)$, the ratio of the corrected local skin friction coefficient, Cf , (no subscript) and the non-interacting local skin friction coefficient, Cf_x, (as obtained from the classical compressible laminar boundary layer theories) is:

$$\frac{Cf \dfrac{(Re_x)_A^{1/2}}{C_A^{1/2}}}{Cf_x \dfrac{(Re_x)_A^{1/2}}{C_A^{1/2}}} = \frac{.783\left(\dfrac{p}{p_A}\right)^{1/2}}{.783} \quad , \qquad (2.3\text{-}144)$$

$$\therefore \frac{Cf}{Cf_x} = \left(\frac{p}{p_A}\right)^{1/2} , \quad \frac{p}{p_A} > 1 \quad , \qquad (2.3\text{-}145)$$

it follows that $Cf > Cf_x$. Similarly, from Eq (2.3-139), it can be shown that $\delta < \delta_x$. Thus, due to shock wave-boundary layer interaction, the skin friction increases, while the boundary layer thickness decreases. Allowing for a corresponding Reynolds Analogy concept, the heat transfer rates are then increased. The conclusions are for non-insulated flat plate and a weak interaction, $\bar{\chi} \sim O(1)$.

For the case of a strong interaction, $\chi >> 1$, and an insulated flat plate, the following results are obtained(15, 16):

$$Cf\,\frac{(Re_x)_A^{1/2}}{C_A^{1/2}} = .55\,\chi^{1/2} \quad , \qquad (2.3\text{-}146)$$

$$\frac{Cf}{Cf_x} = .83\,\chi^{1/2} \quad , \qquad (2.3\text{-}147)$$

where the redefined value of χ is:

$$\chi = \frac{M_A^3\, C_A^{1/2}}{(Re_x)_A^{1/2}} \qquad (2.3\text{-}148)$$

and

$$\frac{p}{p_A} = .52\chi + .92 \quad \text{for } \gamma = \frac{7}{5}\,,\ Pr = 1 \quad , \qquad (2.3\text{-}149)$$

i.e., for $\chi \gg 1$ the corrected local skin friction coefficient, Cf , can have a manifold value of its uncorrected (classical) estimates, Cf_x . The <u>average</u> skin friction values for an insulated flat plate of length, L , are:

$$Cf_{AV}\frac{(Re_L)_A^{1/2}}{C_A^{1/2}} = 2.20\,\chi^{1/2} \quad , \qquad (2.3\text{-}150)$$

$$\frac{Cf_{AV}}{(Cf_{AV})_{CLASSICAL}} = 1.66\,\chi^{1/2} \qquad (2.3\text{-}151)$$

2.3.3 TURBULENT BOUNDARY LAYERS ON FLAT PLATES - CONTINUUM FLOW REGIME

As already indicated in Section 2.2, the fundamental analytical formulations of the mass, momentum and energy conservation principles are obtained, in general, by two different approaches: (1) either by consideration of molecular systems, leading to the kinetic theory of transport processes, or (2) by application of the principles to microscopic systems, resulting in a more direct derivation of the usual differential forms of the equations of mass, momentum and energy conservations for fluids and fluid mixtures. Naturally, the two approaches are interrelated, leading to the same conclusions and consequences. The difference is that the kinetic theory analysis (1) allows both for a better substantially physical insight in the actual internal phenomena of any flow process and for a direct definition of the related transport coefficients, while the microscopic system approach(2) leads to a more straight forward derivation of the corresponding analytic differential expressions for direct computations, provided an adequate postulation of the intrinsic physical interrelationships between substantial variables is first achieved.

The above outline represents only possible methodical ways of investigations. When applied to the viscous flow phenomena, and the boundary layer problem in particular, neither approach has yielded an exact analytical (closed type) solution of the viscous flow problems over given body geometries, since the involved physical and the mathematical difficulties are beyond our present reach, except maybe in a few very simplified and idealized laminar boundary layer flow cases. The more important and the more complicated turbulent boundary layer internal mechanism is at present still inadequately functionally understood for a thorough physical interpretation. The very nature of turbulence, involving a fluctuating intermittent variation of many independent and mutually interrelated flow characteristics, suggests a statistical probability method of analysis. Such an approach seems to be practically too complex for direct engineering applications, and inevitably leads to considerable mathematical difficultics in finding adequate coherent solutions within a specific set of prescribed boundary conditions.

Since the equations of momentum, energy and mass conservation cannot be rigorously formulated and solved, all the existing turbulent boundary layer theories are semi-empirical and approximate only, judged both by physical and mathematical standards. The restricted accuracy of their solutions is directly related to the validity of approximations and limitations which have been adopted in the process of semi-empirical and mathematical simplifications. An illustration of a plausible scheme of such an approach to the problem may run as follows:

First, some analytically representative model of the turbulent boundary layer internal mechanism is adopted, presumably reflecting to an acceptable degree the existing empirical evidence for a given flow speed regime and specified boundary conditions. Some probable distributions of the influential flow parameters across and along the boundary layer are adopted, and the boundary conditions subsequently fixed. Then, since independent flow variables normally outnumber the physically available equations (continuity, mass and energy conservation), a necessary restriction to the eventually most influential among them is introduced by specifying known auxiliary functional interrelationships. As the flow variables are time-dependent at any point within the boundary layer, their time-averages are formulated. Since even then the instantaneous differential equations are not readily integrable, further restrictive assumptions and mathematical approximations are usually incorporated, based mainly on the related available experimental evidence.

The final theoretical results are then compared with the corresponding experimental or the other theoretical data, the degree of agreement between them being a measure of acceptability of the introduced theoretical assumptions and postulates. This "matching" of the related theoretical and experimental results requires special attention, since in many a case the inevitable human factor proved to be too much involved. A very good argumentation of this aspect is given by Nestler and Goetz(17).

A comparative investigation of the

technical literature related to the boundary layer problem usually results in a rather incoherent and frequently incompatible multitude of theoretical and experimental data. The variety of approaches and conclusions is so vast and conflicting, that a rational engineering selection and generalization seems a rather remote chance. Nevertheless, a few summary References can be useful in a critical selection of the necessary data for engineering purposes. Notably Nestler and Goetz[17], Smith and Walker[18], Eckert[19,20], Hoerner[21], Kurzweg[22], Ferrari[23], Coles[24], Rubesin and Johnson[25], Monaghan[26], Van Driest[27,28,29], Donaldson[30], Deissler and Loeffler[31], Tucker[32], etc. The quotations are only indicative, and by no means all inclusive.

(i) Two Dimensional Incompressible Turbulent Boundary Layers - Simplified Theoretical Considerations

A simplified form of governing equations for two-dimensional non-conducting, incompressible, turbulent boundary layers over flat plates can be derived on the following premises and notions:

(1) Turbulence

At any point in a general three-dimensional turbulent flow field the instantaneous velocity vector components are:

$$\begin{aligned} &\bar{u}(x,y,z) + u_1(x,y,z,t) && \text{in x-direction,}\\ &\bar{v}(x,y,z) + v_1(x,y,z,t) && \text{in y-direction,}\\ &\bar{w}(x,y,z) + w_1(x,y,z,t) && \text{in z-direction.} \end{aligned} \qquad (2.3\text{-}152)$$

where $\bar{u}$, $\bar{v}$, $\bar{w}$ are mean velocity components of the ordered flow, and u_1 , v_1 , w_1 , are instantaneous fluctuating velocity components due to turbulence.

The quantitative statistical measure of turbulence, in percents of the resultant mean ordered velocity, V , at any point in a three-dimensional turbulent field is expressed as a root mean square value of the fluctuations:

$$\sigma = \frac{100}{|V|}\left(\frac{\bar{u}_1^2+\bar{v}_1^2+\bar{w}_1^2}{3}\right)^{1/2} , \qquad (2.3\text{-}153)$$

where

$$\bar{u}_1 = \frac{1}{T}\int_0^T u_1\,dt ,$$

$$\bar{v}_1 = \frac{1}{T}\int_0^T v_1\,dt ,$$

$$\bar{w}_1 = \frac{1}{T}\int_0^T w_1\,dt . \qquad (2.3\text{-}154)$$

If time T is allowed to become sufficiently long in comparison with the duration of any of the individual velocity fluctuations, $\pm u_1$, $\pm v_1$, $\pm w_1$, then their time-average value becomes:

$$\bar{u}_1 = \bar{v}_1 = \bar{w}_1 = 0 \qquad (2.3\text{-}155)$$

Consequently, the mean resultant velocity of a turbulent flow. allowing for sufficient time, is $\bar{V}(x,y,z)$.

(2) Turbulent Shearing Stress at a Point

In a two-dimensional turbulent boundary layer on an arbitrary surface, the fluctuating instantaneous velocity components $(\pm u_1)$ and $(\pm v_1)$, induce a respective intermittent movement of fluid particles at any point in the turbulent flow field. A momentum transfer due to turbulence thus occurs. By fixing x and y axes tangentially and normally to the surface respectively, with x-axis pointed in the outside free-stream flow velocity direction, the instantaneous rate of turbulent momentum transfer per unit area in the y-direction is

$$\pm \rho u_1 v_1 . \qquad (2.3\text{-}156)$$

A positive momentum transfer in the positive y-direction will bear a negative sign, i.e., $-\rho u_1 v_1$.

To illustrate the point, assume that a fluid particle is moving instantaneously upward with its local fluctuating velocity $+v_1$. It will carry with it a distance $\delta y = v_1 dt$ a positive momentum transfer $(-\rho\, u_1 v_1)$, if at the same instant the fluctuating u_1 component for the distance δy is negative, i.e.,

$$u_1 = -\left(\frac{\partial u}{\partial y}\right)\delta y . \qquad (2.3\text{-}157)$$

The turbulent fluctuations are in general a random process. At any instant the turbulent momentum transfer carried by a fluid element in the y-direction can be positive or negative. But due to the very tendency of the

turbulent boundary layer growth, the momentum transfer shall be more often positive than negative, so that if its mean value is taken over sufficiently long time intervals:

$$\left| -\rho \overline{u_1 v_1} \right| > 0 \ , \qquad (2.3\text{-}158)$$

with ρ = const for incompressible flows.

Thus the mean rate of turbulent momentum transfer due to velocity fluctuations, taken for a sufficiently long time-interval, is the turbulent shearing stress component at the point, called sometimes the Reynolds stress:

$$\tau_t = -\rho \overline{u_1 v_1} \quad \text{for incompressible flows,} \qquad (2.3\text{-}159)$$

or $$\tau_t = -\beta \overline{u_1 v_1} \quad \text{for compressible flows.} \qquad (2.3\text{-}160)$$

(3) Laminar shearing stress

Apart from this pure turbulent shearing stress, caused by the time-averages of the fluctuating velocity components $(\pm u_1)$ and $(\pm v_1)$, at any point in a turbulent boundary layer exists a laminar shearing stress also, which is purely a consequence of the mean velocity gradient $(\partial \bar{u} / \partial y)_y$ at the point, i.e., a function of a mean turbulent velocity profile $\bar{u} = \bar{u}(y)$, interpreted in a similar manner as in the laminar flow case:

$$\tau_l = \mu \left(\frac{\partial \bar{u}}{\partial y} \right)_y \ . \qquad (2.3\text{-}161)$$

(4) Total Shearing Stress in Turbulent Boundary Layers

The total shearing stress at any arbitrary point in a two-dimensional incompressible turbulent boundary layer flow over a smooth, flat plate without pressure gradient, is:

$$\tau = \tau_l + \tau_t = \mu \left(\frac{\partial \bar{u}}{\partial y} \right)_y + \left(-\rho \overline{u_1 v_1} \right)_y \ . \qquad (2.3\text{-}162)$$

With no-slip condition at the wall, $u = u_1 = v_1 = 0$, the shearing stress at the wall is

$$\tau_w = \mu_w \left(\frac{\partial \bar{u}}{\partial y} \right)_{y=0} \ . \qquad (2.3\text{-}163)$$

For very small values of (y), a laminar sublayer is expected to exist, with $u_1 = v_1 = 0$, and $\tau = \tau_l = \mu (\partial u / \partial y)_{LAM}$. In the rest of real turbulent region, the turbulent mixing represents the predominant mechanism for vertical momentum transfer, and there, with a good approximation,

$$\tau = \tau_t = \left(-\rho \overline{u_1 v_1} \right)_{y_{TURB}} \ . \qquad (2.3\text{-}164)$$

(5) The Simplified Form of the Governing (Navier-Stokes) Equations

In view of the above definitions (1) to (4), the respectively simplified form of incompressible two-dimensional, turbulent boundary layer equations, can be formulated by an order-of-magnitude analysis in the same manner as for laminar boundary layers:

$$\frac{\partial u}{\partial x} + \frac{\partial v}{\partial y} = 0, \qquad \rho = \text{const.} \ , \qquad (2.3\text{-}164)$$

$$\rho \left(\frac{\partial u}{\partial t} + u \frac{\partial u}{\partial x} + v \frac{\partial u}{\partial y} \right) = -\frac{\partial p}{\partial x} + \frac{\partial}{\partial y} \left(\mu \frac{\partial u}{\partial y} \right),$$

$$\frac{\partial p}{\partial y} \equiv 0 \ . \qquad (2.3\text{-}165)$$

The implicit assumption is that the pressure is approximately constant through the boundary layer and that the momentum equation in y-direction is of higher order (negligible).

In the above form, the boundary layer equations are approximately applicable for arbitrary surfaces of small curvature also, (centrifugal force effects neglected).

For steady, incompressible, two-dimensional turbulent boundary layers, the fluctuating turbulent boundary layer quantities should be substituted:

$$u = \bar{u}(x,y) + u_1(x,y,t) \ ,$$

$$v = \bar{v}(x,y) + v_1(x,y,t) \ , \qquad \frac{\partial}{\partial t} \equiv 0 \ ,$$

$$p = \bar{p}(x,y) + p_1(x,y,t) \ , \qquad (2.3\text{-}166)$$

so that instantaneous turbulent boundary layer differential Navier-Stokes equations become:

$$\frac{\partial}{\partial x}(\bar{u} + u_1) + \frac{\partial}{\partial y}(\bar{v} + v_1) = 0, \qquad \rho = \text{const.} \ , \qquad (2.3\text{-}167)$$

$$\rho \left[(\bar{u} + u_1) \frac{\partial (\bar{u} + u_1)}{\partial x} + (\bar{v} + v_1) \frac{\partial (\bar{u} + u_1)}{\partial y} \right] =$$

$$= -\frac{\partial (\bar{p} + p_1)}{\partial x} + \frac{\partial}{\partial y} \left[\mu \frac{\partial}{\partial y} (\bar{u} + u_1) \right] \ . \qquad (2.3\text{-}168)$$

Introducing the concept of mean flow conditions, prevailing in sufficiently long time-intervals at any point of the boundary layer, and applying the time-averaging rule to the fluctuating components u_1, v_1, p_1, by which the mean time average of any individual fluctuating component or its derivative is zero, the above equations reduce to:

$$\frac{\partial \bar{u}}{\partial x} + \frac{\partial \bar{v}}{\partial y} = 0, \qquad \rho = \text{const.}, \tag{2.3-169}$$

$$\rho\left(\bar{u}\frac{\partial \bar{u}}{\partial x} + \bar{v}\frac{\partial \bar{u}}{\partial y}\right) = -\frac{\partial \bar{p}}{\partial x} + \frac{\partial}{\partial y}\left(\mu\frac{\partial \bar{u}}{\partial y} - \rho\overline{u_1 v_1}\right). \tag{2.3-170}$$

Applied to a flat-plate case, $\partial \bar{p}/\partial x = 0$, and omitting for convenience the bar symbols from mean values (except for mean time average $\bar{u}_1$, $\bar{v}_1$,), the equations read:

$$\frac{\partial u}{\partial x} + \frac{\partial v}{\partial y} = 0, \qquad \rho = \text{const.}, \tag{2.3-171}$$

$$\rho\left(u\frac{\partial u}{\partial x} + v\frac{\partial u}{\partial y}\right) = \frac{\partial}{\partial y}\left(\mu\frac{\partial u}{\partial y} - \rho\overline{u_1 v_1}\right). \tag{2.3-172}$$

(ii) Two-Dimensional Compressible Turbulent Boundary Layers - Simplified Theoretical Considerations

Since the compressibility introduces additional complexities in the analytical treatment of the turbulent boundary layers, i.e., since more independent variables and influential parameters appear, a subsequent reformulation and modification of the boundary layer structure and its mechanism, as reflected in various theories, is given below. It is stressed, however, that there is neither a unique approach to the problem, nor a common fixed specification of the inside flow parameters. As the knowledge in the field progresses, new concepts and formulations are introduced. Thus, the "definitions" as presented here are necessarily of a limited meaning, serving only as a general physical guidance in understanding the problem at large. In any specific theory, various modifications and alterations may occur.

(1) Compressible Turbulent Boundary Layer Structure

A direct consequence of the fluid compressibility is the respective pronounced variation in thermal flow conditions. At very low speeds, approximating the ideal incompressible case, the fluid motion can be regarded as non-conducting. With increase in flow-speeds, the flow processes may be considered either as adiabatic (insulated surfaces) or polytropic (due to surface cooling or heating effects). There is, in general, a pronounced coupling effect between surface-temperature conditions and the flow-induced temperature variations, as governed by the general conservation of energy law. It is usually assumed that the viscous and the thermal transport processes are compatible as expressed through the Reynolds analogy concept, allowing for separate analytical treatments of the momentum and the energy equations.

The turbulent boundary layer structure may be thought as made up of three regions:

(a) The "inner region", adjacent to the plate, called the laminar sublayer. In this region the conditions at the wall have a predominant effect, i.e., viscosity, μ_w, has a determining effect, the fluctuating velocities are absent, and the velocity profile is nearly linear:

$$\tau_l = \tau_w = \mu_w\left(\frac{\partial u}{\partial y}\right)_{y=0} \approx \mu_w\frac{u}{y},$$

$$\mu_w = \mu(T_w),$$

$$(\tau_w/\rho) = \nu\left(\frac{u}{y}\right), \qquad u_\tau = (\tau_w/\rho)^{1/2},$$

i.e., (2.3-173)

$$\frac{u}{u_\tau} = \frac{u_\tau y}{\nu} \quad \text{(Prandtl's "Law of the Wall")}, \tag{2.3-174}$$

where

$u_\tau = (\tau_w/\rho)^{1/2}$ - is called the friction velocity.

(b) The "outer region", comprising the major portion of the turbulent boundary layer next to the free stream, with a strong fluctuating turbulent mechanism, in which the velocity profile is regarded as independent of viscosity, μ, but strongly dependent on the friction velocity u_τ. This notion has been introduced by von Karman as the "velocity defect law":

$$\frac{V_\infty - u}{u_\tau} = f(y/\delta). \tag{2.3-175}$$

(c) The "overlapping" region between the laminar sublayer and the outer

turbulent region, with a mixed type of flow and a velocity profile(33):

$$\frac{u}{u_\tau} = 5.6 \log_{10} \frac{y u_\tau}{\nu} + 4.9 \qquad (2.3\text{-}176)$$

The turbulent velocity profiles in all the three regions agree well with many experimental data for incompressible turbulent boundary layers on smooth flat plates.

Alternatively, the outer portion of the boundary layer can be interpreted in two other ways:

Either the rest of the boundary layer structure between the laminar sublayer and the free stream is treated like one single region, characterized by presence of both molecular viscous and eddying fluctuating forces, or this region is further subdivided into two separate subregions:

- A fully turbulent "outer region", next to the free stream boundary, with a strong prevalence of turbulent fluctuating forces due to eddies, and

- A "buffer region" of "mixed" flow conditions, having both pure viscous and fluctuating turbulent stress components.

The boundary layer "structural concepts" as described above, have been used in many theories dealing with turbulent compressible boundary layer flows on smooth insulated plates at relatively low Mach Numbers ($M < 5$), see Ref. 34 to 37, for examples.

Generally, the supposed "laminar sublayer" is treated as void of any appreciable turbulence, the fluctuating effects being regarded as confined to the "outer regions". Consequently, the shearing stresses are also treated within the laminar sublayer in a laminar form:

$$\tau_l = \mu \left(\frac{\partial u}{\partial y}\right)_y . \qquad (2.3\text{-}177)$$

The results of such analytical approach in some cases agreed well within 5% with experimental evidence for the investigated relatively low supersonic speeds ($M < 5$), see Figs (2.3-12), (2.3-13), (2.3-14).

But more recent experimental evidence by Deissler and Loeffler(31) for velocity profile shapes at higher supersonic speeds ($M > 5$), indicates that a considerable portion of the turbulent shear is present in the so-called "laminar sublayer". Therefore, for the higher Mach-Number range, an improved model of the turbulent boundary layer has been attempted(31,51,58-63). There the boundary layer is divided into two regions:

- A region "near the wall", which is not void from the fluctuating turbulent mechanisms, but its turbulent flow parameters can be expressed (and and approximated) through conditions at the wall, which have a predominant influence,

- A region "away from the wall", similar to the "outer regions" as specified in earlier theories, in which the well known Karman's similarity law(64) is still retained and considered as the most reasonable way of expressing the turbulent flow parameters variations.

That region "away from the wall" displays a strong fluctuating pattern, created by interplay of both eddying and kinetic molecular effects. The intermittent nature of flow expresses itself as a particularly strong diffusivity of turbulence near the outer edge of the boundary layer. But since on the other hand in that "far-away" region, the temperature and velocity gradients are at the same time the smallest, i.e., since general intensity of turbulent and heat effects is the least, it follows that the quantities entering into the basic momentum, energy and continuity equations may be taken as unique fluctuating mean-time-averages across the whole span of the "away from the wall region".

Qualitatively, none of the "improved" theories brings up any radically new moments regarding final results, trends and conclusions as applicable to turbulent boundary layers in general. But an appreciable quantitative improvement of the final skin-friction and heat-transfer results seems evident, so that the existing gap between the theoretical predictions and the experimental results has been reduced to acceptable engineering tolerances for an increased range of Mach Numbers ($0 < M < 20$), see Fig (2.2-15).

TABLE (2.3-1)

Values of Re , ω , and r for Curves in Fig.(2.3-12)

Theory	Reference	r	ω	Re (Millions)
Clemmow II Van Driest II * Li-Nagamatsu (α =1)	39 84 41	1	0.76	10
Modified Frankl-Voishel	37	1	1	7
Rubesin	34	1	1	7
Clemmow III Li-Nagamatsu ($\alpha = \frac{1}{2}$) * Ferrari	39 41 45	1	0.768	11
Smith-Harrop	42	1	0.75	10
Eckert	85	1	0.8	Arbitrary
Li-Nagamatsu ($\alpha = \Lambda^{30}$)	41	1	0.768	11
Van Driest I Clemmow I * Li-Nagamatsu (α = 0)	27 39 41	1	0.76	10
Wilson	50	0.89	0.76	10
Monaghan	86	1	0.76	Arbitrary
Cope	44	1	1	10
Extended Frankl-Voishel	37	1	1	7
Tucker II	32	1	1	Arbitrary
Young-Janssen	46	...	...	7
von Karman	87	1	0.76	10
Tucker I	88	1	1	Arbitrary

*Same theory advanced by different investigators.

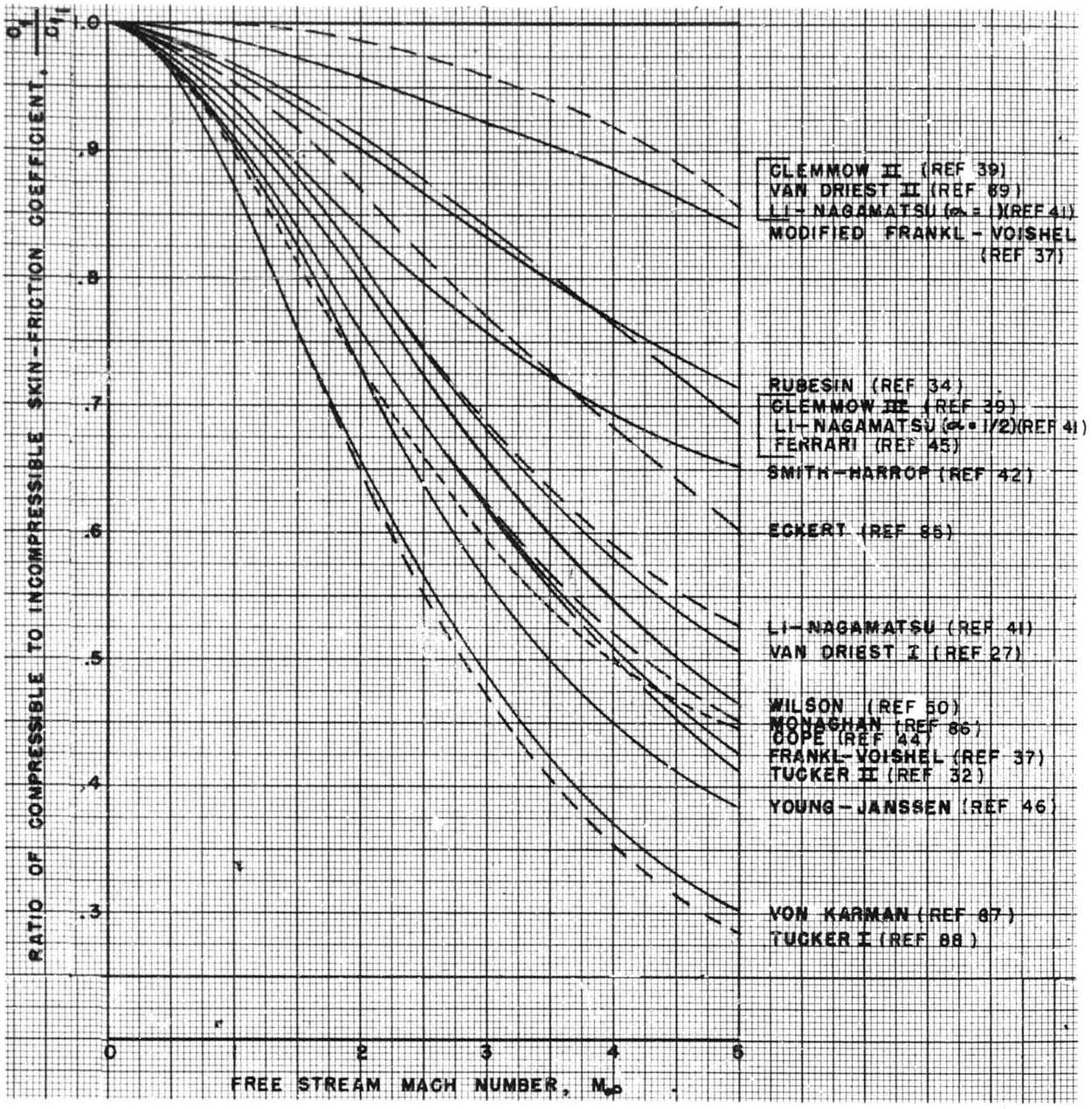

Fig (2.3-12) Theories of turbulent skin-friction for compressible flow over an insulated flat plate, assuming that $\frac{Cf}{Cf_i}$ is practically independ of Reynold's Number. (Ref 38).

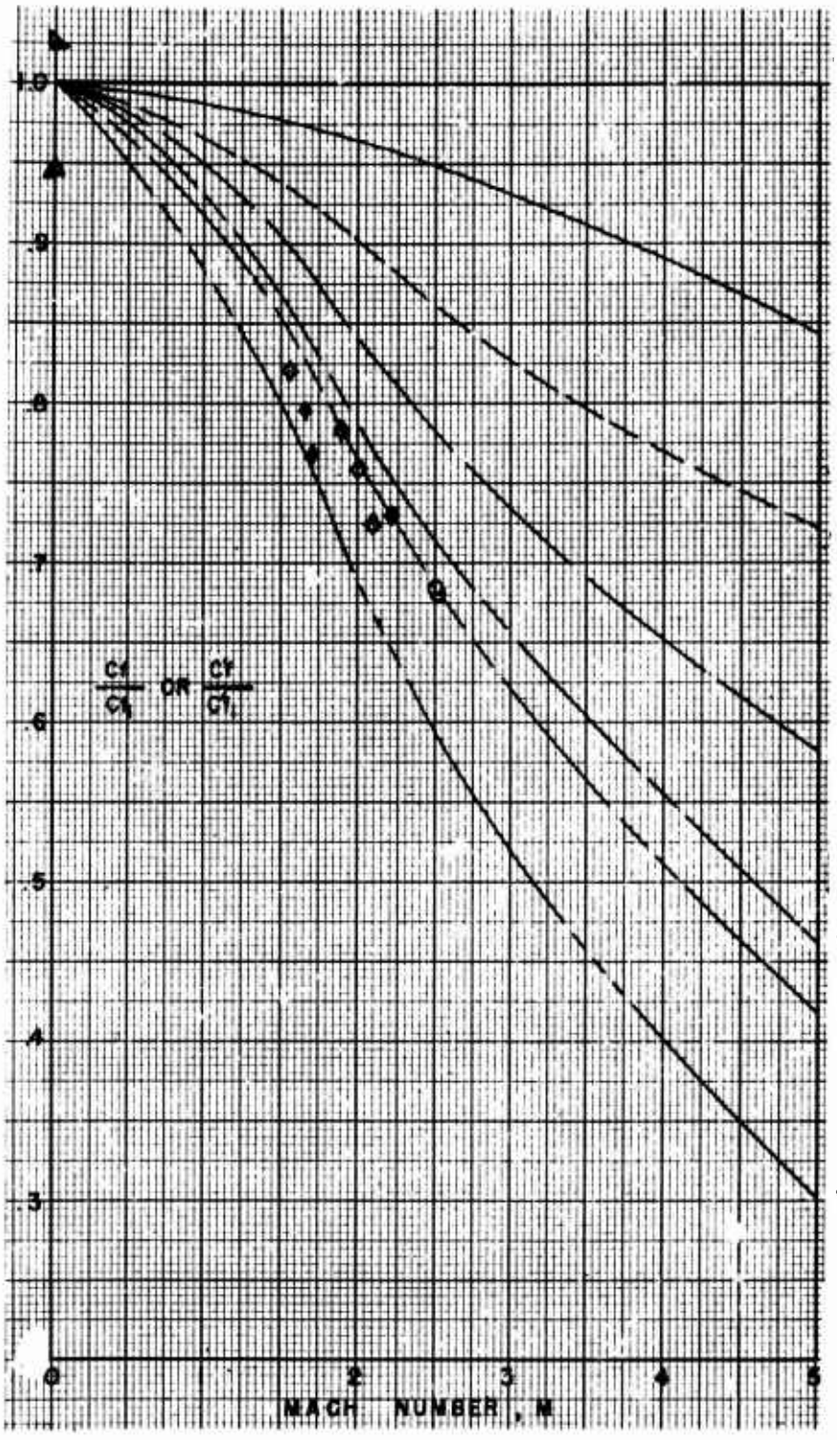

○ RESULTS FROM REF. 34
◊ WILSON, REF. 47
△ KEMPF, REF. 48
▷ WIESELBERGER, REF 49

FRANK & VOISHEL, REF 40

BUFFER-LAYER

VAN DRIEST, REF. 97

WILSON, REF. 50

EXTENDED FRANK & VOISHEL, REF 37

VON KÁRMÁN ESTIMATION, REF 87

Fig (2 3-13) Comparison of the variation with Mach Number of the average skin-friction coefficients determined from the various analyses for an insulated plate at $Re = 7 \times 10^6$, $r = 1, \omega = 1, a = 1, Pr = 1, \frac{C_f}{C_{f_i}} \neq f(Re_L)$: for comparison purposes the data is reduced to the same conditions. (Ref 33)

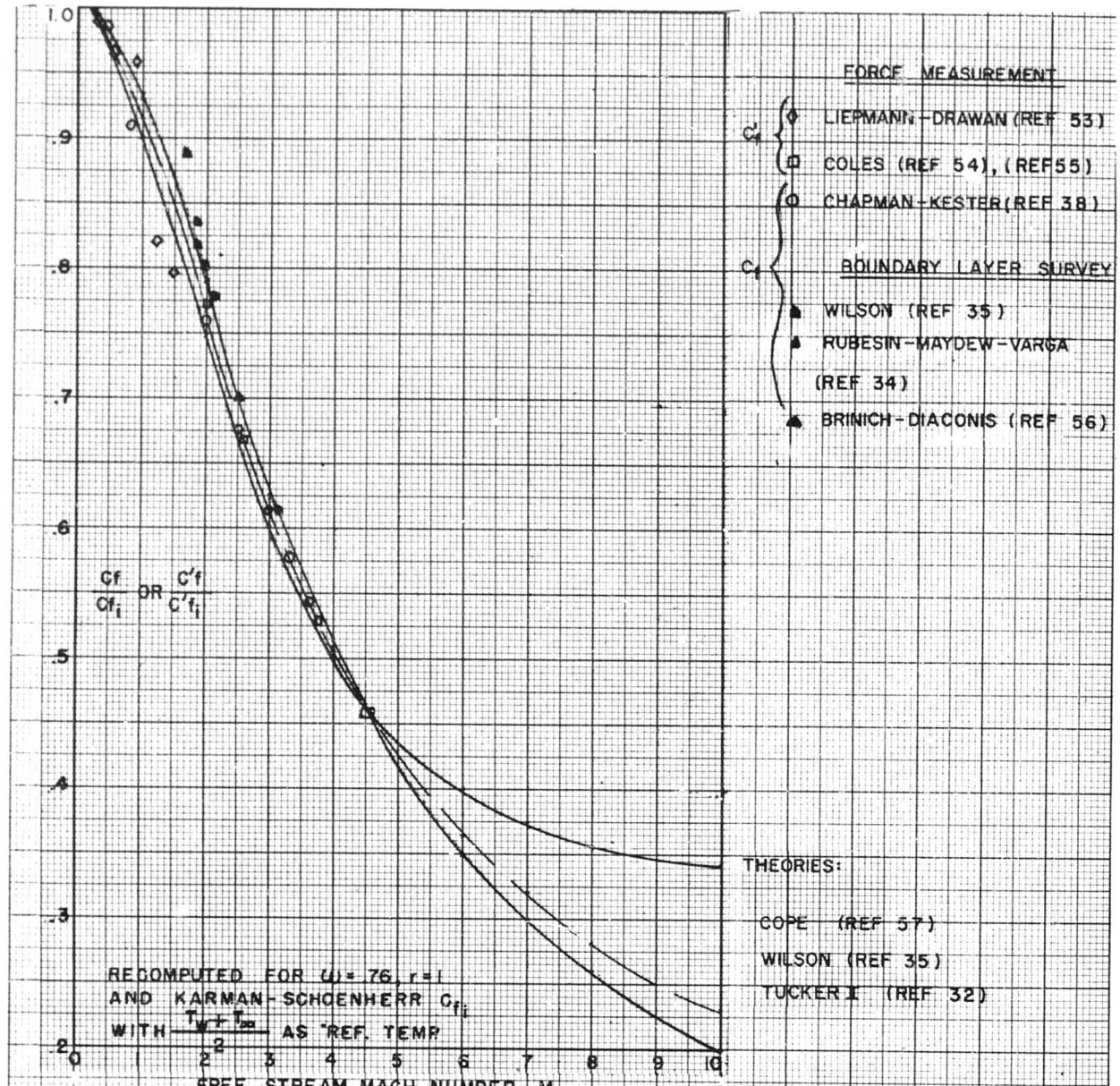

VALUES OF $(C_f/C_{f_i})_{exp}$

M_∞	$(C_f/C_{f_i})_{exp}$
0.51	0.985
0.81	0.929
1.98	0.764
2.49	0.671
2.95	0.623
3.36	0.578
3.60	0.551

VALUES OF Re FOR DATA OF THE ABOVE FIGURE

EXPERIMENT	$Re \cdot 10^6$
LIEPMANN-DRAWAN	1 (APPROX.)
COLES	8
CHAPMAN-KESTER	8 to 16
WILSON	10
RUBESIN-MAYDEW-VARGA	7
BRINICH-DIACONIS	3 to 18

Fig (2.3-14) Comparison of various experiments and theories; all data refered to the incompressible values given by Karman - Schoenherr equation. (Ref 38)

Note: The compressible turbulent boundary layer data are inevitably compared with the respective incompressible values, which are obtainable under considerably lesser restrictions and approximations. For the purpose, the commonly accepted basic reference incompressible turbulent boundary layer data are illustrated in Figs (2.3-16) and (2.3-17).

(2) Two-dimensional Turbulent Compressible Boundary Layer Equations

Following the same method as described in the section on incompressible two-dimensional boundary layers, the general instantaneous form of the differential two-dimensional compressible boundary layer equations on arbitrary surfaces can be derived in the form:

$$\frac{\partial}{\partial x}(\rho u) + \frac{\partial}{\partial y}(\rho v) = -\frac{\partial \rho}{\partial t} \quad , \qquad (2.3\text{-}178)$$

$$\rho\left(\frac{\partial u}{\partial t} + u\frac{\partial u}{\partial x} + v\frac{\partial u}{\partial y}\right) = -\frac{\partial p}{\partial x} +$$

$$+ \frac{\partial}{\partial y}\left(\mu\frac{\partial u}{\partial y}\right) \quad , \qquad (2.3\text{-}179)$$

$$\rho C_p\left(\frac{\partial T^\circ}{\partial t} + u\frac{\partial T^\circ}{\partial x} + v\frac{\partial T^\circ}{\partial y}\right) - \frac{\partial p}{\partial t} - u\frac{\partial p}{\partial x} =$$

$$= \frac{\partial}{\partial y}\left(k\frac{\partial T^\circ}{\partial y}\right) + \mu\left(\frac{\partial u}{\partial y}\right)^2 \quad . \qquad (2.3\text{-}180)$$

For steady, two-dimensional compressible turbulent boundary layers on smooth, flat plates, without pressure gradient and with time-derivatives omitted (since they are eliminated in a later time-averaging step), the instantaneous boundary layer equations reduce to:

$$\frac{\partial}{\partial x}(\rho u) + \frac{\partial}{\partial y}(\rho v) = 0 \quad , \qquad (2.3\text{-}181)$$

$$\rho\left(u\frac{\partial u}{\partial x} + v\frac{\partial u}{\partial y}\right) = \frac{\partial}{\partial y}\left(\mu\frac{\partial u}{\partial y}\right) \quad , \qquad (2.3\text{-}182)$$

$$\rho C_p\left(u\frac{\partial T^\circ}{\partial x} + v\frac{\partial T^\circ}{\partial y}\right) = \frac{\partial}{\partial y}\left(k\frac{\partial T^\circ}{\partial y}\right) + \mu\left(\frac{\partial u}{\partial y}\right)^2 . \qquad (2.3\text{-}183)$$

A direct solution of the above equations is beyond both mathematical and physical possibilities. The number of the instantaneous variables (ρ , u , v , μ , T°, C_p) exceeds the number of available physical equations. Additional sets of relationships are required.

- Each of the instantaneous variables, as formulated at any point within the flow field, reflects the two-fold nature of the turbulent flow, i.e., each of them comprises both the mean "ordered" motion component (superscript $\bar{}$) and the intermittent fluctuating component (subscript "1") due to turbulence. Thus, at any instant:

$$u(x,y,t) = \bar{u}(x,y) + u_1(x,y,t) \quad ,$$

$$v(x,y,t) = \bar{v}(x,y) + v_1(x,y,t) \quad , \qquad (2.3\text{-}184)$$

$$\rho(x,y,t) = \bar{\rho}(x,y) + \rho_1(x,y,t) \quad ,$$

$$T^\circ(x,y,t) = \bar{T}^\circ(x,y) + T_1^\circ(x,y,t) \quad ,$$

etc. $\qquad (2.3\text{-}185)$

An introduction of some kind of a time-averaging approach is necessary in order to bring the phenomena within the continuum theory realm. By considering sufficiently long time-intervals, the time-averages of the fluctuating components are determined as described in the incompressible case already. Furthermore, a variational law of the main mean independent variables ($\bar{\rho}$, $\bar{u}$, $\bar{T}^\circ$) across each of the complex boundary layer structural regions has to be established in accordance with experimental measurements. The boundary conditions, both outer and at interfaces between various boundary layer regions, must be specified, and the auxiliary expressions, interconnecting other variable fluid parameters ($\bar{\mu}$, $\bar{C_p}$, $\bar{k}$), established on the basis of experimental evidence.

(3) Compressible Boundary Layer Equations Expressed Through Mean Time Averages.

As described already in the incompressible case, the introduction of mean (superscript $\bar{}$) and fluctuating (subscript "1") time-averages into the instantaneous equations of motion allows for their subsequent reduction to the following expressions for the shear-stress and the heat-transfer, valid at

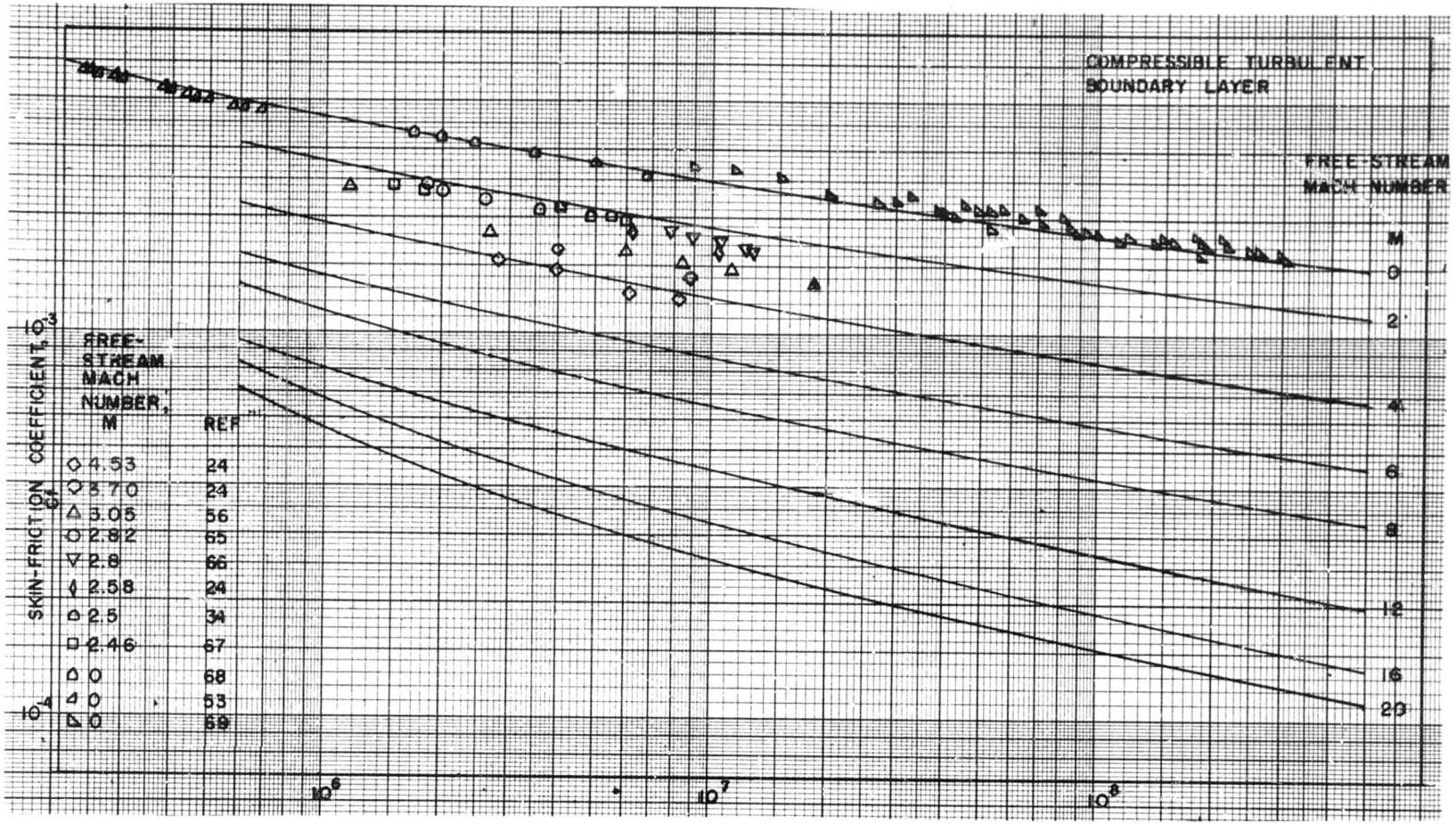

Fig (2.3-15) Predicted variation of skin-friction coefficient with longitudinal-distance Reynolds Number and Mach Number and comparison with experiment. (Ref. 31)

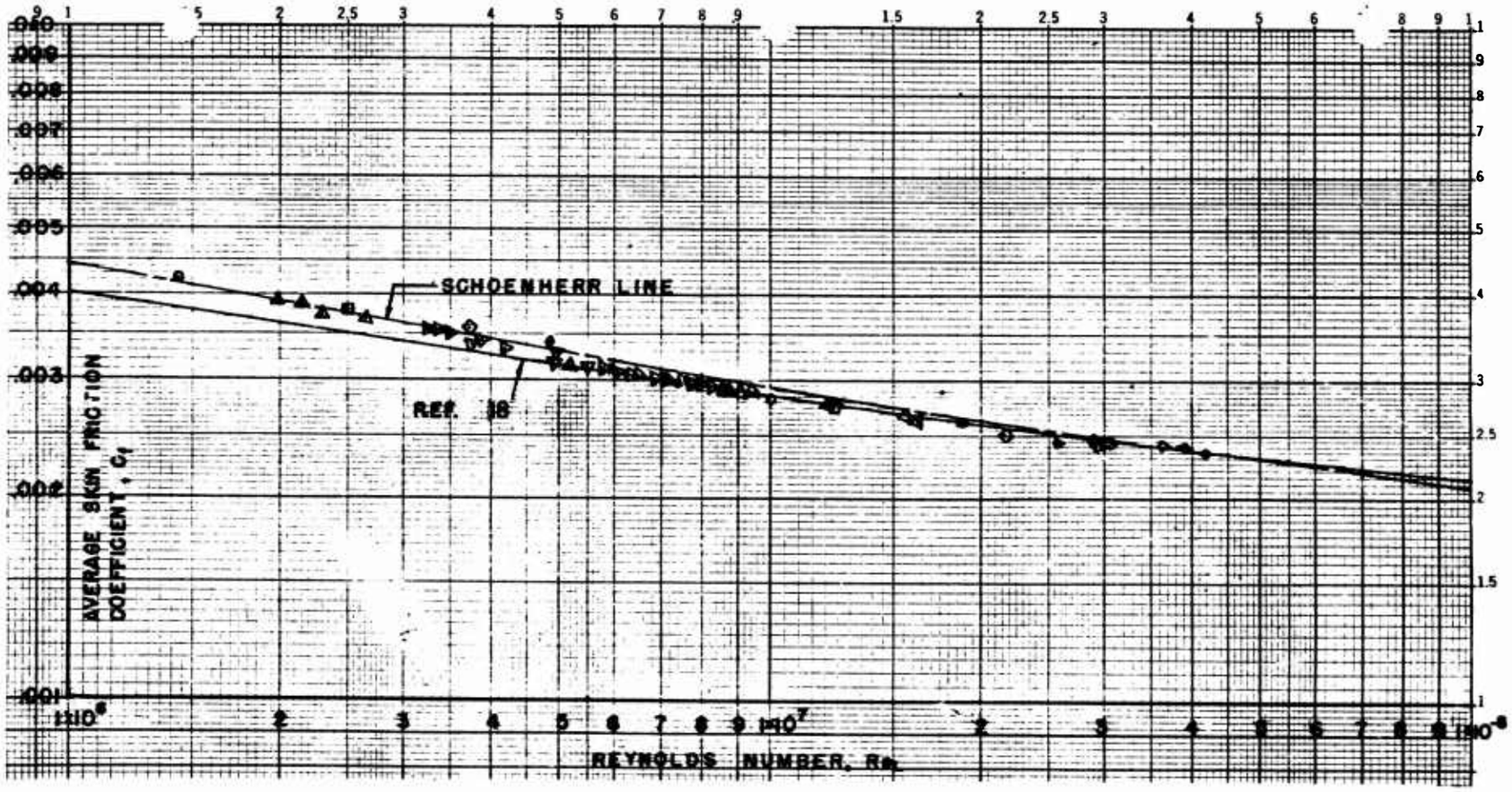

Fig (2.3-16) Variation of average skin friction coefficient with change in Reynolds Number, Re_L (Ref 18)

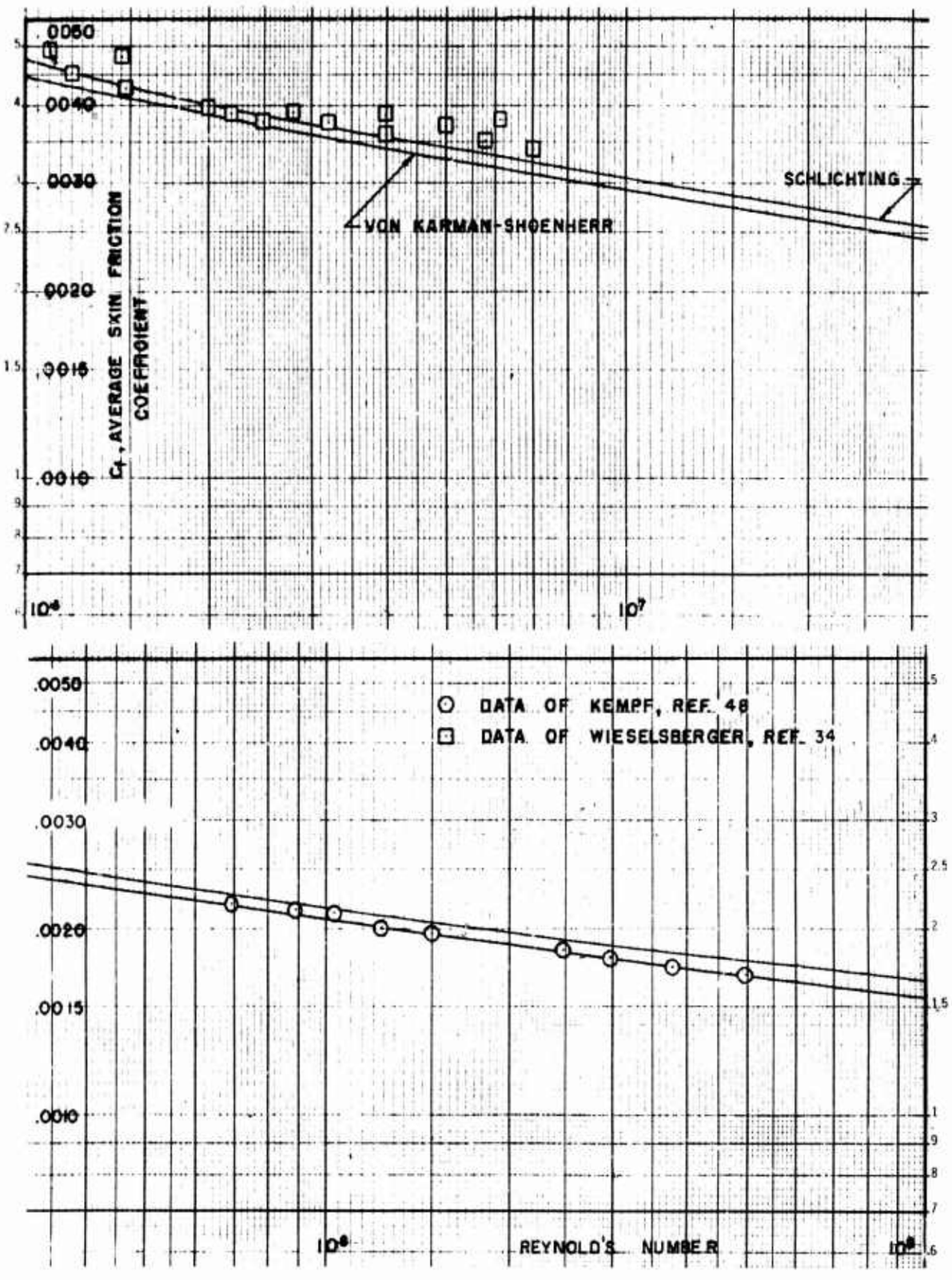

Fig (2.3-17) Average incompressible turbulent skin-friction coefficient variation with Mach Number, (Ref 34)

any general point inside the turbulent boundary layer:

$$\tau = \mu \frac{\partial \bar{u}}{\partial y} - \bar{\rho}\,\overline{u_1 v_1} \quad , \qquad (2.3\text{-}186)$$

$$q = -\bar{k}\frac{\partial \bar{T}}{\partial y} + \bar{\rho}\, C_p \overline{T_1 v_1} - \bar{u}\bar{\mu}\frac{\partial \bar{u}}{\partial y} + \bar{u}\bar{\rho}\,\overline{u_1 v_1} \quad , \qquad (2.3\text{-}187)$$

with $C_p = \text{const.}$

The assumption of $C_p \neq f(T)$ represents an allowable approximation for lower supersonic speeds ($M < 5$). It becomes less adequate as the temperature is increased, and breaks completely if dissociation and ionization processes take over at really high Mach Numbers.

Usually the "bars" over the time-averaged fluid variables, not involving the fluctuating effects, are dropped for the sake of convenience, i.e.:

$$\tau = \mu \frac{\partial u}{\partial y} - \rho\,\overline{u_1 v_1} \quad , \qquad (2.3\text{-}188)$$

$$q = -k\frac{\partial T}{\partial y} + \rho C_p \overline{T_1 v_1} - u\mu\frac{\partial u}{\partial y} + u\rho\,\overline{u_1 v_1} \quad . \qquad (2.3\text{-}189)$$

Definitions of the various terms in the above equations are:

$\mu \frac{\partial u}{\partial y} = \tau_l$, represents the molecular shearing stress.

$-\rho\,\overline{u_1 v_1} = \tau_t$, is the turbulent shear stress due to fluctuating eddying nature of turbulence.

$-k\frac{\partial T}{\partial y}$, represents the molecular heat transfer.

$\rho C_p \overline{T_1 v_1}$, represents the turbulent heat transfer due to fluctuating effects of turbulence.

$-u\mu\frac{\partial u}{\partial y}$, represents the molecular momentum dissipation term.

$u\rho\,\overline{u_1 v_1}$, represents the turbulent momentum dissipation term.

From the above definitions, two new terms, called the eddy-diffusivities of momentum and heat respectively, are defined as:

The eddy diffusivity of momentum,

$$\epsilon = -\frac{\overline{u_1 v_1}}{(\partial u/\partial y)} \quad . \qquad (2.3\text{-}190)$$

The eddy diffusivity of heat transfer,

$$\epsilon_h = -\frac{\overline{T_1 v_1}}{\partial T/\partial y} \quad . \qquad (2.3\text{-}191)$$

The physical meaning of these terms may be understood by noticing that the ratio

$$\frac{\epsilon}{(\mu/\rho)} \qquad (2.3\text{-}192)$$

is a measure of the turbulent (fluctuating) to molecular shear stresses, as may be seen from Eq (2.3-188) and that the ratio

$$\frac{\epsilon_h}{(k/\rho C_p)} \qquad (2.3\text{-}193)$$

is a measure of the turbulence (fluctuating) to molecular heat transfers.

With the above notation, Eqs. (2.3-188) and (2.3-189) can be written in the form,

$$\tau = (\mu + \rho\epsilon)\frac{\partial u}{\partial y} \quad , \qquad (2.3\text{-}194)$$

$$q = -(k + \rho C_p \epsilon_h)\frac{\partial T}{\partial y} - u(\mu + \rho\epsilon)\frac{\partial u}{\partial y} \quad , \qquad (2.3\text{-}195)$$

or, remembering that sufficiently far from leading edge variations in x-direction of any of these quantities is negligible as compared with variations in y-direction, i.e., assuming $u = u(y)$, $\mu = \mu(y)$, etc:

$$\tau = (\mu + \rho\epsilon)\frac{du}{dy} \quad , \qquad (2.3\text{-}196)$$

$$q = -(k + \rho C_p \epsilon_h)\frac{dT}{dy} - u(\mu + \rho\epsilon)\frac{du}{dy} \quad . \qquad (2.3\text{-}197)$$

This form of the boundary layer equations is suitable for functional evaluations of the various terms across the boundary layer cross-sectional regions and for interpretations of the various boundary conditions.

Particular solutions of the above equations can be found in Ref. (31) and (58), by Deissler and others.

(4) The Momentum Eddy Diffusivity, ϵ.

In the region "next-to-wall" for higher Mach Numbers it may be assumed that ϵ is a function of fluid properties measured relative to the surface:

$$\epsilon = \epsilon(u,y) = n^2 uy \quad , \qquad (2.3\text{-}198)$$

where (n) is an experimental constant(31)

In the region "away-from-wall" the application of the Karman's similarity hypothesis(64) is assumed valid as one of the best approximations available by now, yielding for the eddy diffusivity an expression of the form:

$$\epsilon = \epsilon\left(\frac{du}{dy}, \frac{d^2u}{dy^2}\right) = \varkappa^2 \frac{(du/dy)^3}{(d^2u/dy^2)^2} \quad , \qquad (2.3\text{-}199)$$

where $\varkappa$ is to be determined experimentally.

(5) Ratio of Eddy Diffusivities

When evaluating ratio of thermal and momentum transfer eddy diffusivities,

$$\alpha = \frac{\epsilon_h}{\epsilon} \qquad (2.3\text{-}200)$$

either Prandtl's or Karman's "mixing length" hypothesis can be used. If the Prandtl's(3) concept is used, the value of α equals unity, since according to this hypothesis a turbulent particle moves a given distance, and then suddenly mixes with the fluid, transferring both its heat and momentum contents instantaneously. The actual mechanism of turbulence is probably more complex, but even with such a simplification as this, the computed heat transfer coefficients happen to be in a reasonable agreement with experiments(61). The hypothesis is equivalent to the assumption that the momentum and the heat transfer boundary layer thicknesses are equal. The eddy diffusivity ratio is a form of a simple Reynolds analogy concept; more accurate interpretations of the phenomena lead to other "modified" Reynolds Analogy definitions.

(6) Recovery Factor and Related Thermal Definitions

Note: The following argumentation is of an empirical nature(33). A corresponding theoretical and idealized interpretation is given in Section 2.3.2 for $Pr = 1$.

The insulated wall case represents from engineering point of view an idealized limiting condition, which can be approximately realized in a slow ($q < .1$) accelerating flight from rest, or in steady flight regimes, see Fig (2.3-18). The "insulated" heat transfer conditions on smooth, flat plates serve also as a basic reference for formulation of heat transfer parameters, such as the recovery temperature, the recovery factor, the temperature profile as influenced by different skin-temperature conditions, etc.

The recovery factor, r, is defined under two simultaneous conditions: the surface is insulated, and a thermal equilibrium state across the boundary layer exists.

Fixing the reference coordinate system to a moving body, the fluid velocity relative to the body is supposedly reduced from its local free stream value to a zero value at the surface at any cross-section. This "no-slip" condition at the surface is a consequence of viscosity effects inside the boundary layer. Consequently, the static temperature of the fluid rises from its local free stream value, ($T_s^\circ = T_\infty^\circ$) to a higher skin-temperature at the body surface in general, T_w°.

If the surface is insulated, the temperature rise of the next-to-the-wall layer (subscript o) will reach at most (but not exactly) the free-stream stagnation (or total) temperature value ($T_{s\infty}^\circ = T_o^\circ$), see Fig. (2.3-19).

Assuming a steady flight regime, the highest insulated surface temperature (i.e. that of the fluid layer immediately next to the wall) is reached at any cross-section (for a given Mach Number and altitude), when

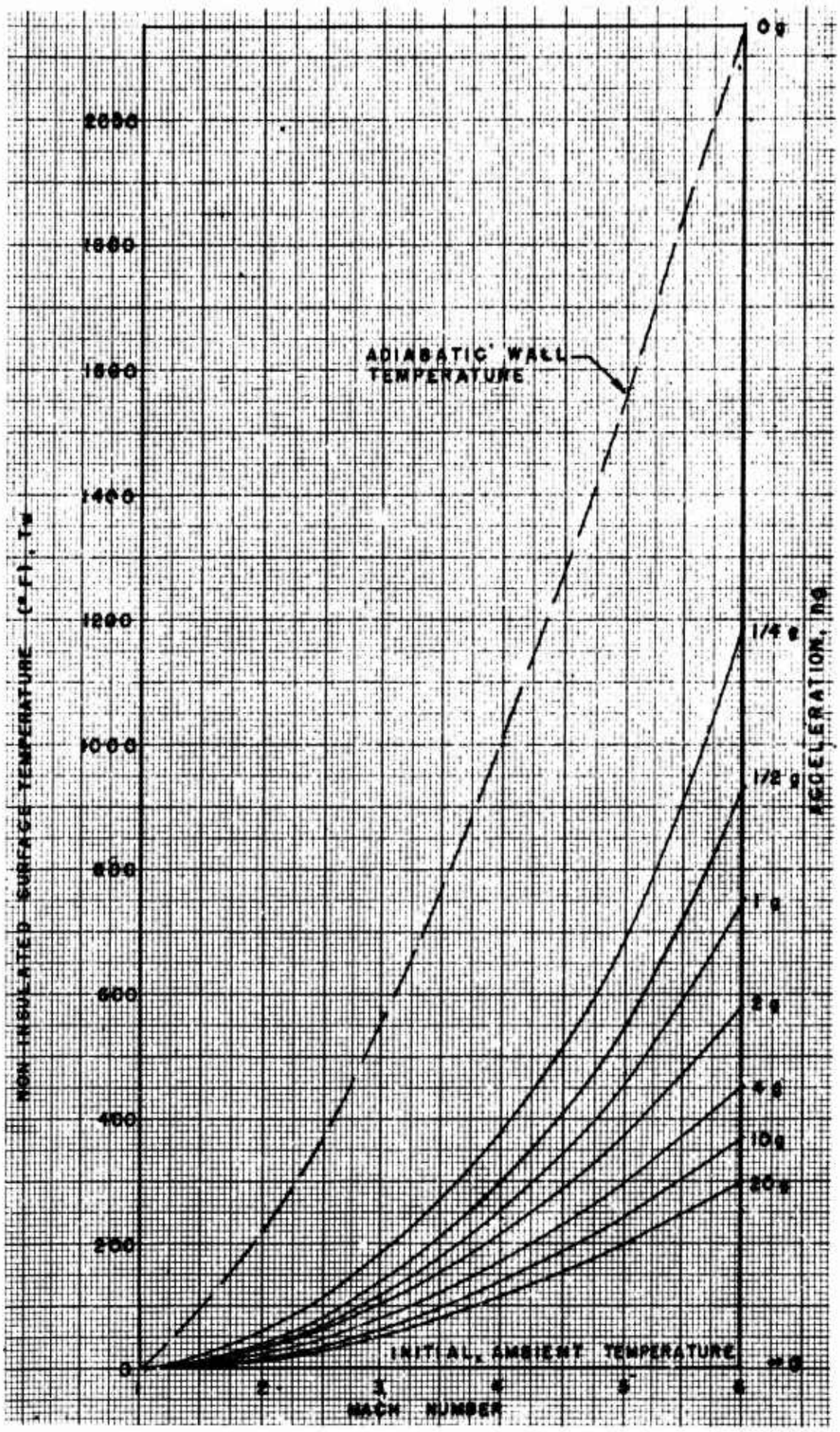

Fig (2.3-18) Comparison of surface temperatures for several accelerations calculated from heat flow in one dimension for flight at 50,000 feet. (Ref 70)

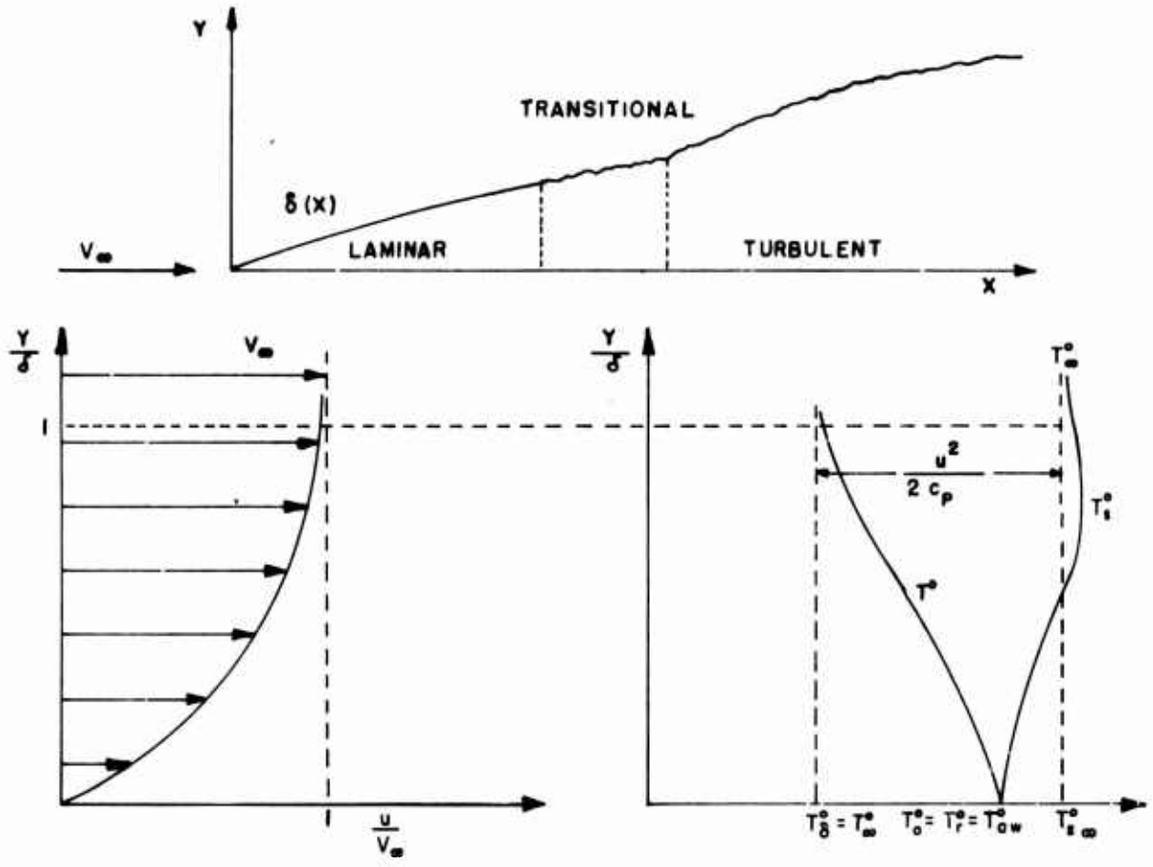

Fig(2.3-19) Velocity and temperature profiles in high speed boundary layer of insulated plate. (Ref. 33)

the rate of frictional heat output equals the rate of heat flux across the boundary layer outward. An equilibrium thermal condition is established. That particular maximum temperature of the insulated surface is called the recovery or adiabatic wall temperature:

$$T_r^\circ = T_{aw}^\circ \quad \text{, defined for } \left(\frac{\partial T^\circ}{\partial y}\right)_w = 0 \ . \tag{2.3-201}$$

All experimental evidence indicates that, both for laminar and turbulent boundary layers, the adiabatic wall temperature is less than the stagnation temperature of the free stream (for air):

$$T_{aw}^\circ < T_{s\infty}^\circ \ .$$

This is a consequence of the transport rates of the internal heat transfer mechanism within the viscous fluid flows: the amount of heat created by friction inside a boundary layer is less than heat transport rates (per unit time and unit area) across the boundary layer, i.e.:

$$c_p \mu < k \tag{2.3-202}$$

Expressed conveniently through the Prandtl Number concept,

$$P_r = \frac{c_p \mu}{k} \ , \tag{2.3-203}$$

it may be stated that the condition ($T_{aw}^\circ < T_{s\infty}^\circ$) is a consequence of the fact that the Prandtl Number value for air is less than unity ($Pr \sim .75$).

A suitable nondimensional parameter can be therefore introduced, serving as an indicator of the actual temperature conditions of an insulated surface when across the boundary layer a thermal equilibrium is established. This parameter is called the recovery factor. It defines the ratio of actual equilibrium temperature rise on an insulated surface and the free stream perfect fluid stagnation temperature rise, with the local free stream static temperature, T°_{∞} , taken as reference:

$$r = \frac{T^{\circ}_{aw} - T^{\circ}_{\infty}}{T^{\circ}_{s\infty} - T^{\circ}_{\infty}} = \frac{T^{\circ}_{aw} - T^{\circ}_{\infty}}{V^2_{\infty}/2C_p} < 1 \quad . \tag{2.3-204}$$

Obviously, since due to internal nature of viscous flows ($T^{\circ}_{aw} < T^{\circ}_{s\infty}$), i.e., ($Pr < 1$) , the recovery factor value for real gases must be less than unity also, ($r < 1$) .

Assumption of a Prandtl Number equal to unity leads to a value of the recovery factor equal to unity also, as sometimes is done in some approximate analyses, see Section 2.3.2.

In general, the adiabatic wall temperature, T°_{aw} , will be a function of the main viscous flow similarity parameters

$$T^{\circ}_{r} = T^{\circ}_{aw} = T^{\circ}(M \ , \ Re \ , P_r \ , \ St \ , \text{etc.}) \tag{2.3-205}$$

and the type of boundary layer flow (laminar or turbulent). Therefore, the numerical values of the recovery factor

$$r = \frac{T^{\circ}_{r} - T^{\circ}_{\infty}}{T^{\circ}_{s\infty} - T^{\circ}_{\infty}} = \frac{(T^{\circ}_{r}/T^{\circ}_{s\infty})(1 + \frac{\gamma - 1}{2} M^2_{\infty})}{\frac{\gamma - 1}{2} M^2_{\infty}} =$$

$$= f (M_{\infty} , Re_{\infty} , P_{r_{\infty}}) \tag{2.3-206}$$

will differ for laminar and turbulent boundary layers, since the ratio $(T^{\circ}_{r}/T^{\circ}_{s\infty})$ depends on the energy dissipation in the boundary layer. It has to be determined in all cases experimentally. Usually, its approximate value is used in many theoretical analyses. For instance, for flat plates:

$.85 \approx r = P_r^{1/2}$	for laminar flows up to $M = 5$, with the Prandtl Number evaluated at T_{aw} , i.e., $Pr \approx .72$.
$r = P_r^{1/3}$	for turbulent flows, with $Pr = .76$, (Squire[71]).
$.86 \leq r \leq .91$	for turbulent flows, from experimental evidence.
$r = r(M, P_r)$	for turbulent flows, (Eber[72])
$r = r(P_r, Re)$	for turbulent flows, (Seban[73])

etc.

Since at supersonic speeds there is no pressure gradient on flat plates and wedges, i.e., no Mach Number changes along the surfaces, it follows that in these cases the recovery factor shall have a constant value for all cross-sections (Re effects neglected).

A good summary of theoretical investigations regarding the recovery factor, r , and the adiabatic wall temperature, T°_{aw} , as well as temperature distributions within laminar boundary layers is presented by Johnson and Rubesin[74]. For supersonic flows over flat plates and bodies of revolution, a corresponding summary is given by van Driest[27], McAdams[75], and Kaye[76].

(7) The Actual Skin-Temperature of Noninsulated Surfaces, T°_{w} .

Apart from controlled experiments, the body skins are not insulated. The actual skin-temperature, T°_{w} , can obtain any value depending upon specific flight conditions (steady or accelerated) and the thermal and structural properties of the skin-material, even without artificial cooling or heating. Therefore, in general

$$T^{\circ}_{w} \neq T^{\circ}_{aw} \ , \tag{2.3-207}$$

in most cases. Theoretically, a non-insulated surface may reach a thermal equilibrium state only after an infinite time interval. Practically, if a steady flight condition is of a sufficient duration, a balance between the rates of frictional heat creation inside the boundary layer on one hand,

and the sum of heat-absorption rates by skin, the heat radiation rates and the heat transport rates inside the boundary layer on the other hand can be realized. Such an equilibrium skin-temperature, T°_{we} , is necessarily lower than T°_{aw} for no artificial skin-heating. So, in all actual thermal "equilibrium" states, with or without artificial cooling or heating of the skin:

$$T^{\circ}_{we} < T^{\circ}_{aw} . \qquad (2.3\text{-}208)$$

(8) Heat Transfer and Skin-friction Coefficients

For laminar compressible boundary layers, the relationship between heat transfer and the skin friction rests completely on the proportionality between the conductive heat transport, k , and viscosity, μ , coefficients in a continuous flow as expressed by Prandtl Number (see Section 2.3.2):

$$P_r = \frac{k}{C_p \mu} \approx 1 \qquad (2.3\text{-}209)$$

$$\text{i.e.} \quad S_t = P_r^{-2/3} (C_f/2) \qquad (2.3\text{-}210)$$

This simple relationship is used in the Pohlhausen's computations of the heat transfer to a non-insulated flat plate at a constant temperature, T°_{w} , with the restrictions that ρ , μ , k are constants, that $(\partial p / \partial x) = 0$, and that velocities are low enough, allowing for the dissipation term $\mu (\partial u / \partial y)^2$ in the energy equation to be neglected.

For turbulent compressible boundary layers it is also customary to relate the heat transfer and the skin-friction coefficients by some kind of simple or modified Reynolds analogy concept (see Ref. 36 by Rubesin for a summary of definitions through the general literature). The Reynolds analogy implies the order of compatibility between the turbulent thermal and momentum boundary layer thicknesses, as specified earlier already.

At moderate subsonic velocities, a dimensional form of the heat-transfer-coefficient between the turbulent boundary layer and the surface is defined as

$$\bar{h} = \frac{q}{T^{\circ}_{w} - T^{\circ}_{\infty}} , \qquad (2.3\text{-}211)$$

with $\bar{h}$ being the mean value of the heat-transfer coefficient, the heat flux, and (T°_{∞}) the average free stream or bulk temperature at a given cross section.

For high subsonic or supersonic speeds the above definition would yield (see Fig (2.3-19)):

$\bar{h} = 0$ for an insulated flat plate,

$\bar{h} > 0$ for a hot plate (heat flux from plate to the fluid),

$\bar{h} < 0$ for a cold plate (heat flux from fluid to plate),

which is evidently an inconvenience (see Section 2.2 for argumentations). Instead, a new arbitrary definition of the heat transfer coefficient is sometimes introduced:

$$h = \frac{q}{T_w - T_{aw}} \qquad (2.3\text{-}212)$$

where $\bar{h}$ is called the "effective heat transfer coefficient", and

$$T^{\circ}_{aw} = T^{\circ}_{\infty} + r \frac{V_{\infty}}{2 C_p} . \qquad (2.3\text{-}213)$$

Thus, the coefficient, $\bar{h}$, is always positive ($T^{\circ}_{w} < T^{\circ}_{aw}$), or in a limit equal to zero, ($T^{\circ}_{we} = T^{\circ}_{aw}$) , since both the actual wall temperature and the adiabatic wall temperature are evaluated for the same free stream static temperature, T°_{∞} .

A good review of experimental data for the local heat transfer coefficient at supersonic speeds is summarized in Ref. 74 by Johnson and others.

Alternatively, expressions for the local Nusselt and the local Stanton Numbers on flat, isothermal plates from Ref. 77 (Goldstein) supported by experiments from Ref. 76 (Kaye and others) are:

For incompressible laminar boundary layers:

$$N_u = \frac{hx}{k} = .33 \, Re_x^{1/2} \, P_r^{1/3} \qquad (2.3\text{-}214)$$

$$S_t = \frac{h}{C_p \rho_\delta U_\delta} = .33 \, Re_x^{-1/2} \, P_r^{-2/3} . \qquad (2.3\text{-}215)$$

For compressible turbulent boundary layers at either subsonic or supersonic speeds:

$$N_u = \frac{\bar{h}x}{k} = .030\, Re_x^{.8} P_r^{1/3} , \qquad (2.3\text{-}216)$$

$$S_t = \frac{\bar{h}}{C_p \rho_\delta U_\delta} = .030\, Re_x^{-.2} P_r^{-2/3} . \qquad (2.3\text{-}217)$$

In a more general case, the non-dimensional heat transfer coefficient is a function of the following variables:

$$S_t = f\left(M, Re, P_r, \frac{T_w^*}{T_\infty^*}, T_\infty^*, \frac{\partial p}{\partial x}, \frac{\partial T_w^*}{\partial x}, \frac{\bar{\lambda}}{\delta}, \gamma\right) \qquad (2.3\text{-}218)$$

where $\bar{\lambda}$ is the molecular mean free path.

For turbulent boundary layers, there are two possible definitions for the similarity parameter Pr :

- In the laminar sublayer

$$P_{r_l} = \frac{C_p \mu}{k} , \qquad (2.3\text{-}219)$$

- In the turbulent region

$$P_{r_t} = \frac{C_p \epsilon}{k} , \qquad (2.3\text{-}220)$$

where ϵ is the momentum diffusivity, defined earlier.

If the usual engineering approximation for moderate supersonic Mach Numbers ($Pr_l = Pr_t \approx 1$) is introduced, it follows as a consequence that across a turbulent boundary layer the total energy per unit mass is

$$C_p \bar{T} + \frac{\bar{u}^2}{2} \approx \text{const} . \qquad (2.3\text{-}221)$$

(9) "Reference" Temperature Ratios Which are Sometimes Used to Express the Skin Friction and the Heat Transfer Coefficients.

When investigating the cooling or heating effects on various flow parameters in the turbulent boundary layers over smooth, non-insulated surfaces, it is sometimes convenient to define a common "reference" temperature. Then, in a first approximation, the final skin-friction and heat-transfer coefficients can be presented as functions of Mach Number, Reynolds Number and the actual wall-to-the reference temperature ratio. Such "reference" temperatures, used in various theories, are:

(a) - The local adiabatic wall temperature, T_{aw}^* ,

(b) - The local free stream temperature, T_δ^* ,

(c) - The so-called T^{**} temperature, defined later.

Then:

(a) For an insulated flat plate the adiabatic local wall temperature in turbulent boundary layers is given by

$$T_{aw}^* = T_\delta^* + r \frac{V_\infty^2}{2 C_p} , \qquad r \approx .88 \text{ to } .91. \qquad (2.3\text{-}222)$$

The local skin friction and the local heat transfer coefficients on a non-insulated flat plate can be then tentatively expressed as functions of the actual wall-to-the adiabatic wall temperature ratio:

$$\frac{T_w^*}{T_{aw}^*} = \frac{1}{1 - \beta T_\delta^{*+} + r \alpha (U_\delta^+)^2} \qquad (2.3\text{-}223)$$

where: $\beta = \dfrac{q_w (\tau_w / \rho_w)^{1/2}}{C_p T_w^* \tau_w}$ (2.3-224)

is a heat transfer parameter,

T_δ^{*+} - a static temperature parameter, evaluated at the edge of the boundary layer cross-section, $y = \delta$.

$$T_\delta^{*+} = \frac{1 - (T_\delta^*/T_w^*)}{\beta} = \frac{(T_w^* - T_\delta^*) C_p \tau_w}{q_w (\tau_w/\rho_w)^{1/2}} \qquad (2.3\text{-}225)$$

$$a = \frac{\tau_w}{2 C_p T_w^* \rho_w}$$ - is a frictional heating parameter,

(2.3-226)

$$r = \frac{T_{aw}^* - T_\delta^*}{U_\delta^2 / 2C_p} = \frac{T_{aw}^* - T_\delta^*}{T_s^* - T_\delta^*}$$ - is the recovery factor.

(2.3-227)

U_δ^+ = a velocity parameter, evaluated at the edge of the boundary layer,

$$U_\delta^+ = \frac{U_\delta}{(\tau_w / \rho_w)^{1/2}} \quad , \; y = \delta \; , \; U_\delta = V_\infty \; .$$

(2.3-228)

(b) In some instances, mainly for direct engineering applications, the skin-friction coefficient is expressed in terms of the actual wall-to-the-free-stream temperature ratio directly, i.e., as function of (T_w^* / T_∞^*).

(c) The third alternative possibility, i.e., the use of the ratio $(T_w^* / T^{*\prime})$ as a reference parameter, actually evolves from a specific so-called "$T^{*\prime}$ method" of boundary layer solution, (for $M < 5$). It was first defined by Rubesin and Johnson[25] for laminar compressible boundary layers, and then later applied to turbulent boundary layers by Fischer and Norris[78], and others. They found out that the $T^{*\prime}$ method gives better results than the T_δ^* reference base, although there is no direct justification in applying a laminar boundary layer method to turbulent conditions.

The reference $T^{*\prime}$ temperature, as originally defined by Rubesin and Johnson, has been taken as that value of the static temperature inside a compressible laminar boundary layer at which the density, ρ, and the viscosity, μ, must be evaluated, if the incompressible flow relations are to apply. Thus, using the theoretical results of Crocco-Conforto for laminar incompressible flow on a flat plate, the following expression for $T^{*\prime}$ has been obtained for compressible turbulent boundary layers on smooth, flat, non-insulated plates[25]:

$$\frac{T^{*\prime}}{T_\infty^*} = 1 + .032\, M_\infty^2 + .58 \left(\frac{T_w^*}{T_\infty^*} - 1 \right) .$$

(2.3-229)

A further improvement of skin-friction results, see Fig (2.3-20), has been accomplished by Sommer and Shorts [80] and Tendeland[81] by changing the values of constants to:

$$\frac{T^{*\prime}}{T_\infty^*} = 1 + .035 M_\infty^2 + .45 \left(\frac{T_w^*}{T_\infty^*} - 1 \right)$$

(2.3-230)

where the subscript (∞) refers to the local free stream condition outside the boundary layer $(y = \delta)$.

(iii) Some Solutions for Turbulent Boundary Layers on Smooth Flat Plates

(1) Incompressible Turbulent Boundary Layers

First theoretical predictions of the turbulent skin-friction were forwarded by Karman and Prandtl for the case of a flat plate in a low-speed flow. They formulated the flow parameter variations due to turbulence by introducing the so-called "mixing" length hypotheses. Both theories are semi-empirical and were derived originally for an incompressible turbulent boundary layer only, not accounting for any additional effects, such as compressibility, heat transfer, pressure gradient, curvature, roughness, three-dimensional effects, etc. The results of the theories proved to be in general good agreement with respective experimental data, as long as the conditions and restrictions of the theories were preserved during the experiments. It is interesting to note that more recent measurements across the boundary layer, which were done using the relatively new hot-wire technique, indicate that the very "mixing length" hypothesis is questionable. The apparent agreement of the incompressible theory predictions with experimental data thus appears to be due to the fact that the arbitrary constants of integration, as formulated in the theory, can be subsequently adjusted so as to yield a desired agreement. As pointed out by Chapman[38], when compressibility effects are introduced, the arbitrary integration constants disappear, and the mixing length theory fails completely. Besides, in a compressible turbulent boundary layer several other influential flow parameters additionally appear, re-

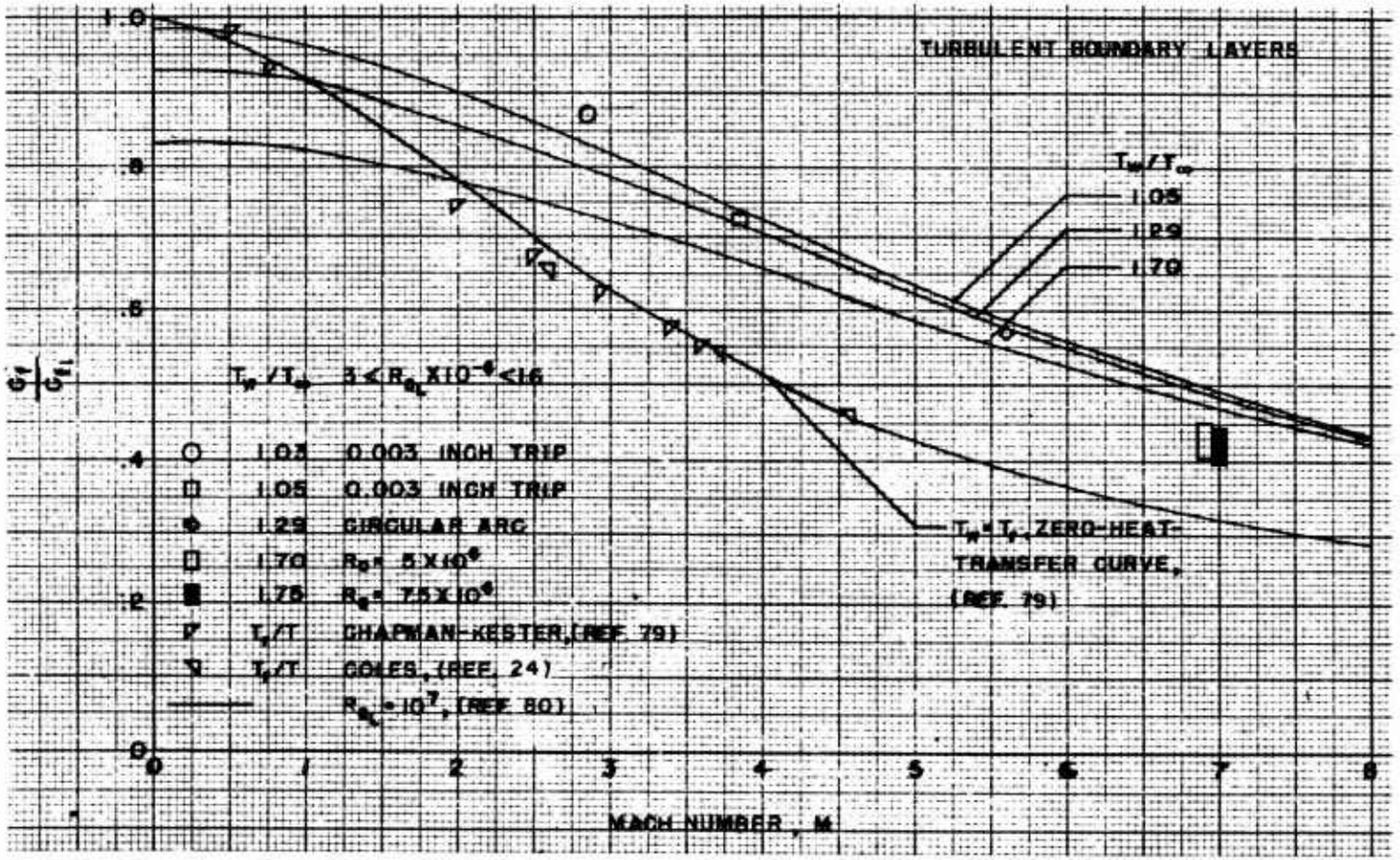

Fig(2.3-20) Comparison of skin-friction ratio as determined by use of compressible T' method with experimental values of skin-friction ratio. (Ref. 80)

flecting variation of fluid properties across the boundary layer, which are not considered in the classical mixing-length theory at all.

The mixing length hypothesis

Solution of the simplified boundary layer equations (2.3-181-183) is not possible in any form without resource to some physically plausible hypothesis regarding the local mean quantity $\overline{u_1 v_1}$ and its distribution across the boundary layer.

Therefore, based on experimental data of Nikuradse[82], Prandtl and Karman introduced their "Mixing-length" theories, expressing the time-averages of the fluctuating velocity components $\bar{u}_1$, $\bar{v}_1$ in terms of the mean velocity profile, $u(y)$, and a reference "mixing length" $l^2(x,y)$. Thus, it is assumed that:

$$\bar{u}_1 = -\, l \frac{\partial u}{\partial y} \quad ,$$

$$\bar{v}_1 = -\, l \frac{\partial u}{\partial y} \quad ,$$

$$\tau_1 = -\rho \overline{u_1 v_1} = \rho l^2 \frac{\partial u}{\partial y} \left| \frac{\partial u}{\partial y} \right| \quad , \tag{2.3-231}$$

at any point within a two-dimensional incompressible turbulent boundary layer on smooth, insulated flat plates. The absolute value sign is introduced in order that the turbulent shearing stress has the same sign as the mean turbulent velocity gradient.

The turbulent incompressible boundary layer equations of motion on flat plates then become:

$$\rho \left(u \frac{\partial u}{\partial x} + v \frac{\partial u}{\partial y} \right) = \frac{\partial}{\partial y} \left(\mu \frac{\partial u}{\partial y} + \right.$$

$$\left. + \rho l^2 \frac{\partial u}{\partial y} \left| \frac{\partial u}{\partial y} \right| \right) , \qquad \rho = \text{const.} \tag{2.3-232}$$

The "mixing length", $l^2(x,y)$, in the above equation can be expressed in two ways:

$$l = ky \quad , \quad \text{(Prandtl[3])} \tag{2.3-233}$$

$$l = k \frac{\partial u / \partial y}{\partial^2 u / \partial y^2} \quad \text{(Karman[64])} \tag{2.3-234}$$

where $k = .4$ is an empirical constant, assumed independent of the Mach Number, the Reynolds Number and the surface temperature.

Von Karman's, Schoenherr and Prandtl's solutions of the incompressible turbulent layers.

For an integration of the turbulent boundary layer equations (2.3-232) across any boundary layer cross-section, with the "mixing length" empirically defined by Eqs (2.3-233) and (2.3-234), the mean velocity variational law in the y direction should be first specified and the boundary conditions fixed.

Assuming, in a first approximation, that the maximum shearing conditions at the wall are dominant across the boundary layer, i.e., by approximating

$$\tau = \tau_w \tag{2.3-235}$$

Karman expressed the velocity profile in the form

$$\frac{u}{u_\tau} = \frac{1}{k} \left[\log_{10} \frac{y u_\tau}{\nu} + h(y/\delta) \right] \quad , \tag{2.3-236}$$

where the unknown function $h(y/\delta)$ has to be determined experimentally.

Defining the local values

$$C'_{fi} = \frac{\tau_w}{1/2 \rho U_\delta^2} = 2 \left(\frac{u_\tau}{u} \right)^2 \quad , \tag{2.3-237}$$

$$Re_x = \frac{U_\delta x}{\nu} \quad , \quad U_\delta = V_\infty \quad , \tag{2.3-238}$$

and integrating across the boundary layer, the von Karman local (superscript ′) incompressible (subscript i) turbulent skin-friction coefficient, C'_{fi}, expression on smooth, insulated flat plates without a pressure gradient is obtained:

$$\left(C'_{fi} \right)^{-1/2} = 1.7 + 4.15 \log_{10} \left(Re_x C'_{fi} \right) . \tag{2.3-239}$$

Schoenherr[52] developed the corresponding expression for the average skin-friction coefficient, C_{fi}, of turbulent incompressible boundary layers on smooth, insulated flat plates without pressure gradient:

$$\left(C_{fi} \right)^{-1/2} = 4.13 \log_{10} \left(Re_L C_{fi} \right) \quad , \tag{2.3-240}$$

where $C_{fi} = \dfrac{F}{1/2 \rho V_\infty^2 L}$, $U_\delta = V_\infty$, (2.3-241)

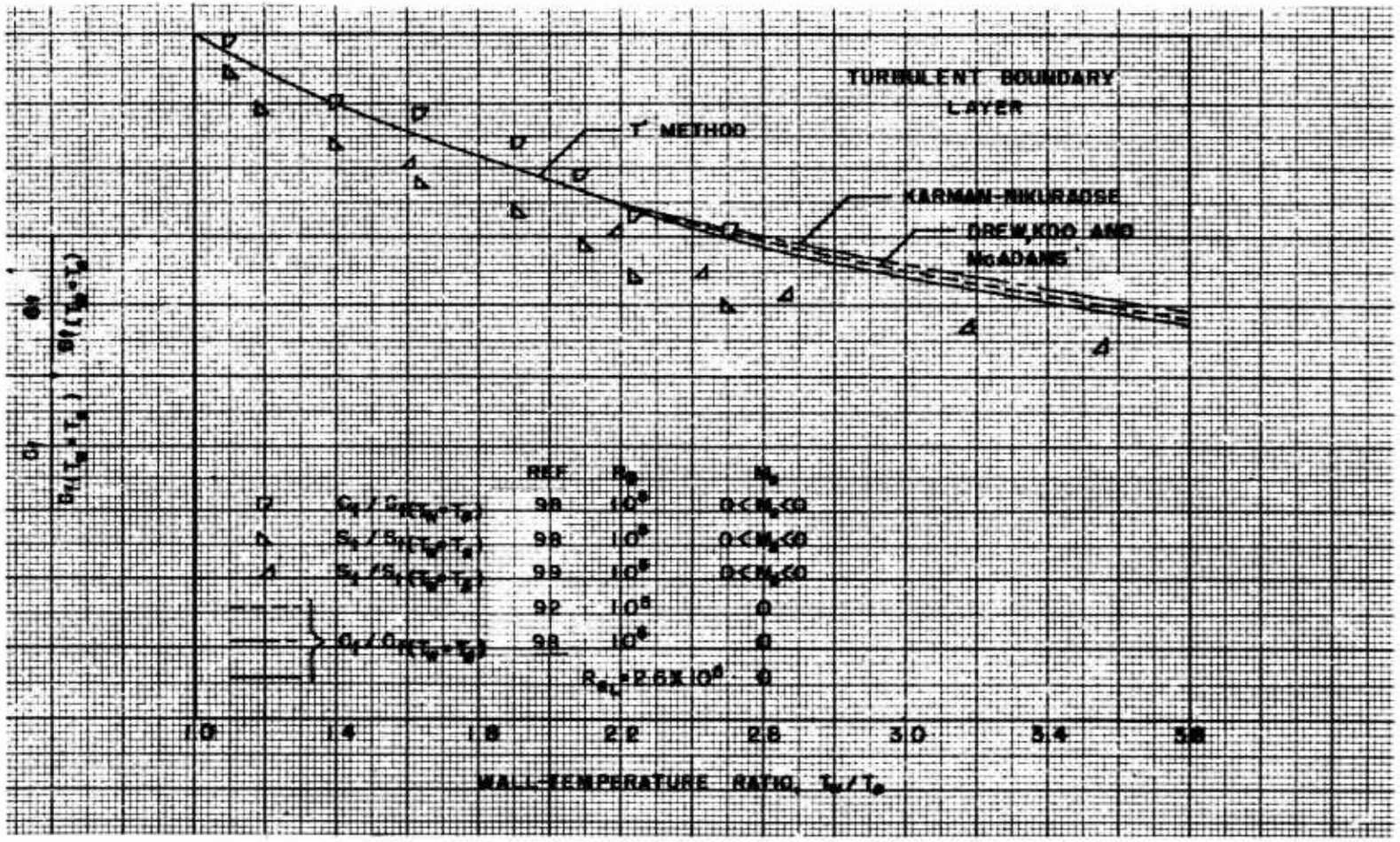

Fig (2.3-21) Comparison of skin-friction ratio as determined by use of T' method with experimental and theoretical results at subsonic speeds, (Ref 80)

F = friction force per unit width of plate of length L ,

$$Re_L = \frac{V_\infty L}{\nu_\infty} .$$

Prandtl[83] developed another expression for the average incompressible turbulent skin-friction coefficient on the basis of experimental results, giving

$$C_{f_I} = .455 \left(\log_{10} Re_L\right)^{-2.58} .$$

(2.3-242)

Both Schoenherr-von Karman's and Prandtl's expressions for the incompressible turbulent skin-friction coefficients are in very good agreement (within ± 5%) with the related experimental data, see Figs (2.3-16) and (2.3-17). Karman-Schoenherr curve has been adopted here as a working graph for the average, incompressible two-dimensional skin-friction coefficient estimates on insulated, smooth flat plates at a zero angle-of-attack.

(2) Some Approximate Analytical Solutions for Compressible Two-Dimensional Turbulent Boundary Layers or Smooth Flat Plates, With or Without Heating

There is a number of approximate analyses dealing with the skin-friction and the heat-transfer phenomena in compressible turbulent boundary layers, as affected by the internal variations of density, viscosity and thermal conductivity across and along the boundary layers with variations in Mach and Reynolds Numbers. Since a direct solution of the governing equations is not possible, a heavy reliance on experimental evidence is used when expressing cross-sectional internal relations between C_p, ρ, μ, k, and T° and when formulating changes of T_w, U_δ and T_δ long the surfaces. By introducing the concept of a "reference" (T^* or T') temperature, most of the flow variables and parameters (ρ, μ, C_p, k, r, Pr, Re) can be conveniently averaged across the boundary layer. Generally, the following line of argumentation is adopted:

The Prandtl Number, the recovery factor and the specific heat at constant pressure, are considered to be weak functions of temperature variations for moderate supersonic Mach Numbers. Therefore, they are usually taken as constants, evaluated at the reference temperature. For instance:

$$P_r^* = \frac{C_p^* \mu^*}{k^*} , \text{ or equivalent average value of } \sim .72,$$

$$r^* = \left(P_r^*\right)^{\frac{2}{3}} , \text{ or equivalent experimental value of } \sim .88, \text{ etc.}$$

The coefficient of viscosity, μ, is on the other hand a strong function of temperature. When the functional dependence is expressed by Sutherland's law,

$$\frac{\mu}{\mu^*} = \frac{T^* + 216}{T^\circ + 216} \left(\frac{T^\circ}{T^*}\right)^{\frac{3}{2}} ,$$

(2.3-243)

the solution of the boundary layer equations for a given $T^\circ(y)$ cross-sectional temperature profile requires machine computations. An approximate expression, easier for direct calculations, is therefore more frequently employed:

$$\frac{\mu}{\mu^*} = C\left(\frac{T^\circ}{T^*}\right)^{\omega} ,$$

(2.3-244)

where C is a coefficient which is a weak function of temperature, and ω is viscosity-temperature law exponent, usually taken as $\omega = .68$.

For a constant pressure, the density is inversely proportional to temperature

$$\rho^* = \frac{p}{RT^*} ,$$

(2.3-245)

and the local Reynolds Number becomes

$$Re_x^* = \frac{U_\delta \times \rho^*}{\mu^*} , \quad U_\delta = V_\infty .$$

(2.3-246)

Then, with the above expressions, and introducing other approximations, the local skin friction can be computed from the respectively simplified boundary layer equations, if the velocity profile $u = u(y)$ and the reference temperature, T^*, are defined. The computations are usually performed by step integrations across various boundary layer regions, with proper definitions of the intermediate boundaries. For instance, in the laminar sublayer it can be argued that the conditions at the wall are predominant,

so that the shear stress can be well approximated by:

$$\tau_w \approx \mu_w \left(\frac{\partial u}{\partial y}\right)_w \quad . \tag{2.3-247}$$

Similarly, in the boundary layer turbulent regions, with a specified τ^* and a specified $u=u(y)$ law, an iterative integrating procedure may be used to obtain the shear stress values. There, from the computed total shear stress, $\tau = \tau_l + \tau_t$, the local(superscript ′) skin-friction coefficient is then obtainable as

$$C_f' = \frac{\tau}{1/2 \rho^* U_\delta^2} \qquad U_\delta = V_\infty \tag{2.3-248}$$

Once the skin friction coefficient is determined, the local heat-transfer coefficient, S_t , can be computed from a corresponding form of the Reynolds analogy concept.

Sometimes, instead of the above iterative procedure, a semi-empirical average law of the skin-friction variation across the boundary layer may be introduced, such as the Shulz-Grunow formula for local turbulent skin-friction coefficient,

$$C_f' = \frac{.370}{(\log_{10} Re_x^*)^{2.584}} \quad , \tag{2.3-249}$$

or the Prandtl-Schlichting relationship for the average turbulent skin friction coefficient,

$$C_f = \frac{.455}{(\log_{10} Re_L^*)^{2.58}} \quad . \tag{2.3-250}$$

The actual detailed computational procedures are varied with each theory.

But, it should be noted that many of the present advanced theories, handling the compressibility and heat transfer effects in turbulent boundary layers, represent basically extensions, modifications or improvements of the Karman's incompressible "mixing length" theory, seeking to bring it in accordance with the far more complicated aspects of the compressibility influences. It should be also noted, that the usual broad scatter of the compressible skin-friction results from the present theories is additionally due to the inherent inadequacy of the "mixing length" hypothesis to represent the true mechanism of the compressible turbulence, see Fig (2.3-12).

The main premise used by Karman in his first formulation of the compressible turbulent boundary layer analytically[64], can be briefly expressed as follows:

The already known relationship between the skin-friction coefficient and the Reynolds Number from incompressible flows are modified for compressibility effects by simply expressing the fluid flow variables in these relationships in terms of the surface "reference" temperature instead of evaluating them at the free stream temperature. This represents a first approximation, and is equivalent to the assumption that the fluid properties next to the surface determine solely the skin-friction. This simple assumption represents a first approximation, yielding the largest decrease in the (C_f/C_{f_i}) ratio with the Mach Number variation. Since all other theories represent but modifications and improvements of this original analysis, it is no wonder that their results fall fan-like between the limiting Karman's incompressible and compressible cases, see Fig (2.3-12).

In the later theories, as a second approximation, the variations of fluid properties across the turbulent boundary layer are tentatively taken into account. The formulation of these variations and the boundary conditions differs in various theories, but the underlying assumptions are yet similar in as much as all of them incorporate the Karman's or Prandtl's "mixing length" hypothesis.

The leading edge effects of smooth flat plate are excluded by taking the boundary layer segments sufficiently far away, so that changes of all variables in x-direction are negligible with changes in y-direction at any given cross section.

Note: The symbolism used in the related technical literature shows a considerable nonuniformity. In the present text, the following equivalent conventions are found alternatively:

Subscripts $(_\delta)$ and $(_\infty)$ refer to the local inviscid stream conditions out side the boundary layer.

Subscripts $(_w)$, $(_{aw})$ and $(_r)$ refer to the local values at a non-insulated wall.

Subscript $(_o)$ refers to the local values at an insulated wall.

No subscript or ($_x$) refers to the local values inside the boundary layer (except for C_f and S_t).

Superscripts (*) and ($'$) refer to the reference T^* or T' temperature conditions (except for δ^*).

C_f, $C_{f_{aw}}$, $\bar{C}_f$, S_t, $S_{t_{aw}}$, $\bar{S}_t$ - refer to the compressible local skin friction and heat transfer coefficients, reduced to the ambient flight (A) or free stream conditions well ahead of the body.

C_{f_x}, C_{f_∞}, S_{t_x}, S_{t_∞} - refer to the compressible local skin friction and heat transfer coefficients, reduced to the local (x) inviscid stream conditions outside the boundary layer, (∞).

C_f' and S_t' - refer to the local compressible skin friction and heat transfer coefficients, reduced to the ambient (A) or free stream conditions well ahead of the body.

Subscript ($_i$) refers to the incompressible boundary layer conditions. Note that for a flat plate at a zero angle-of-attack:

$$\frac{C_f}{C_{f_i}} = \frac{C_f'}{C_{f_i}'} \quad \text{and} \quad \frac{S_t}{S_{t_i}} = \frac{S_t}{S_{t_i}'} .$$

(iii) A Summary of Main Theoretical Results for Turbulent Compressible Boundary Layers on Smooth, Flat Plates With Heat Transfer

Practical conclusions, which stem from the few best representative theories, are:

(1) Chapman and Kester Data

Results from sixteen theories, summarized by Chapman and Kester[38], for two-dimensional compressible turbulent skin-friction coefficients on aerodynamically smooth insulated surfaces without pressure gradients, predict in general widely different effects of Mach Number variation. Only a few of them (see Fig 2.3-12), agree with each other and with experimental data within 5% for moderate supersonic Mach Numbers ($M < 5$). It could be reasonably expected that the same order of discrepencies or agreements shall hold when the additional heat-transfer effects on non-insulated surfaces are considered, provided the thermal and the momentum boundary layer thicknesses can be still regarded comparable.

Note that in the comparative Fig (2.3-12) the reference C_{f_i} value is not unique, but rather as related to the representative particular theoretical expressions in each case. The respective references stated are listed in Table (2.3-1). It should be noted that both the total (C_f / C_{f_i}) and the local (C_f' / C_{f_i}') friction coefficient ratios follow the same law.

In recent years there have been numerous measurements of the compressible turbulent skin-friction coefficient of insulated flat plates. Some of the results are compiled in Fig. (2.3-14). Two basically different experimental measuring methods are presented with two types of symbols, respectively. Filled symbols denote data obtained by measurements performed within the boundary layer itself, with a subsequent calculation of the corresponding skin-friction coefficient by the momentum integral method. Unfilled symbols represent data obtained by direct force measurements. Comparison between these skin-friction measurements and the closest fitted respective theories is also presented. It should be noted that the flat plate measurement by Coles[54,55] are considered most reliable.

While replotting the data from the theories that yielded good agreements with experimental results within the limits of possible experimental uncertainties, the original values of C_f, which were in each case determined for different values of ω and Re_L (see Table (2.3-1), have been recalculated by Chapman[38], using a common reference basis of $Re_L = 10^7$, $\omega = .76$ and $r = 1$. Also, a common incompressible value of C_{f_i} in Fig (2.3-17) was adopted as given by the Karman-Schoenherr Equation:

$$\frac{.242}{(C_{f_i})^{1/2}} = \log_{10}(Re_L C_{f_i}) , \qquad (2.3\text{-}251)$$

$$C_{f_i}' = \frac{dC_{f_i}}{d(X/L)} = \frac{.557\, C_{f_i}}{.557 + 2(C_{f_i})^{1/2}} \qquad (2.3\text{-}252)$$

The "extended" Frankl-Voishe theory, by Rubesin and Varga[34] would agree also well with the experimental evidence, but the recalculations to a common C_{f_i}' value would prove too lengthy in this case.

For practical engineering purposes, it can be concluded from Fig (2.3-17) that the insulated smooth flat plate compressible turbulent C_f values with ± 5% of certainity may be predicted up to Mach Number of 5, as both theore-

tical and experimental evidence indicates. For higher Mach Numbers, the uncertainity increases rapidly.

Mach Number effects on the total skin-friction coefficient are generally large. For instance, an increase of Mach Number from 0 to 5 would reduce the total skin-friction coefficient in the order of 50% in case of aerodynamically nearly smooth insulated surfaces. This pronounced effect of Mach Number is found to be almost independent of Reynolds Number value for $10^6 \leq Re_L \leq 10^{10}$ (variation less than ± 5%, see Fig (2.3-14). The roughness and the heat-transfer effects, on the other hand, do change this tendency appreciably, tending in general to eliminate this reduction in the average skin-friction with Mach Number increase, as can be seen from Figs (2.3-34) and (2.3-35).

Regarding the heat transfer effects on the skin-friction coefficient values in turbulent boundary layers over non-insulated smooth surfaces, the existing theories incorporate a basic assumption of an assumed analogy between heat and momentum transport mechanism, linked through some type of Reynolds analogy parameter, Prandtl Number variations with temperature for higher Mach Numbers, etc. Due to this approach, the nondimensional heat transfer coefficient (Stanton Number, St) is usually not calculated directly, but rather as a function of the assumed analogy, i.e. as a ratio (St / C_f), see Ref. by Rubesin(36), Reichardt(89), Jakob(90), Shirokow(91), Colburn(92), etc. This handicaps the heat transfer theoretical predictions further, since the C_f theoretical value in itself varies widely with various theories.

(2) Deissler and Loeffler Data

An "improved" method of turbulent compressible boundary layers treatment at high Mach Numbers ($0<M<20$) is presented by Deissler and Loeffler(31). The concept of the "laminar sublayer" is discarded on the basis of some more recent measurements which showed a considerable turbulent shear-stress in the so-called "laminar" sublayer. Following similar attempts by Seiff(93) and Deissler(59,60), the boundary layer has been redivided into two regions: the "next-to-the-wall" region, with wall conditions decisive for all flow variables, and the predominantly turbulent "away-from-the wall" region, where the von Karman's(64) similarity expressions have been found in good agreement with the respective experimental evidence. Thus improved analysis has been extended by Deissler (31,94) to flow conditions at high Mach Numbers (up to 20), the non-insulated surface flows included. The compressible flow variables, i.e. the density, the viscosity and the thermal conductivity variations have been expressed in powers of the free stream reference temperature, while the Prandtl Number and the specific heats have been retained as constants.

Final results from these(31,94) and other references (especially from Rubesin(34) and Eckert(19), which contain good summaries of compressible boundary layer data) are presented in the respective figures, demonstrating the following:

- The ratio of C_f / C_{fi} decreases with the increase in Re_θ at a diminishing rate. For $Re_\theta \sim 6000$, data from various references are plotted in Fig (2.3-22), where:

$$Re_\theta = \frac{\theta^* U_\delta \rho_\delta}{\mu_\delta} \quad , \qquad \theta^* \equiv \int_0^\delta \frac{\rho u}{\rho_\delta U_\delta} \left(1 - \frac{u}{U_\delta}\right) dy \quad . \tag{2.3-253}$$

- Variations of (C_f / C_{fi}) with free stream Mach Number and momentum thickness Reynolds Number, Re_θ, for turbulent boundary layers on an insulated smooth flat plate are presented on Fig. (2.3-22). By using the relationship,

$$Re_x = 2 \int_0^{Re_\theta} \frac{dRe_\theta}{C_f'} \quad , \tag{2.3-254}$$

these data are replotted in Fig (2.3-15) with C_f as a function of M and Re_L.

- Variations of (St / St_i) with Mach Number and Re_θ following closely (due to Reynolds analogy) the pattern of the (C_f / C_{fi}) curves, are given in Fig (2.3-24). The Reynolds analogy factor variations with Mach and Reynolds Numbers are plotted in Fig (2.3-25). A replot of $St' = f(Re_x, M)$ is presented in Fig (2.3-26), using the integrated relationship, Eq (2.3-254) again.

Thus, from the presented theoretical results by Deissler(31), which have been found in good agreement with the respective experimental data, and from the other references stated above, the

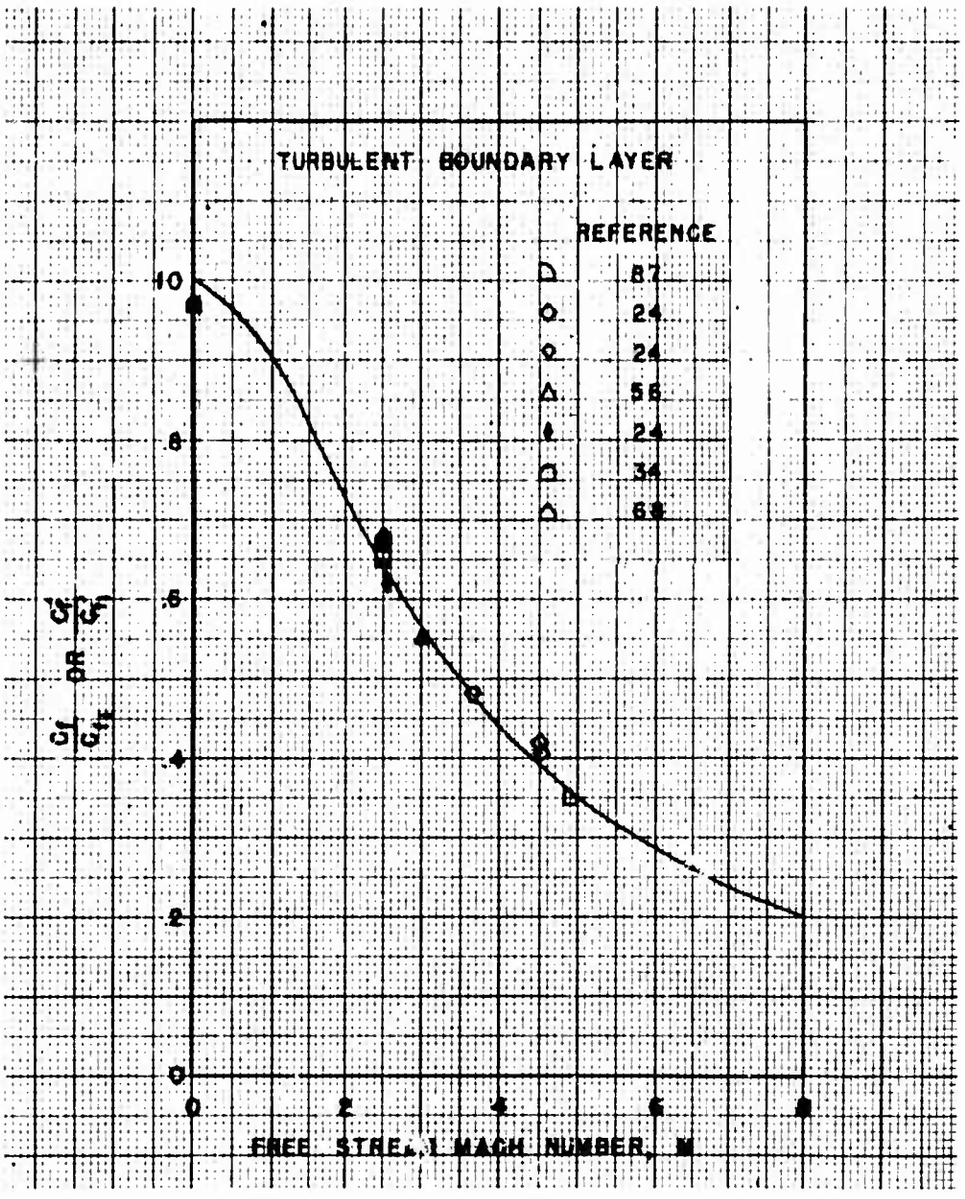

Fig (2.3-22) Momentum-thickness Reynolds Number, 6000 = Re_θ, insulated plate; heat flux parameter $\beta = 0$. (Ref. 31)

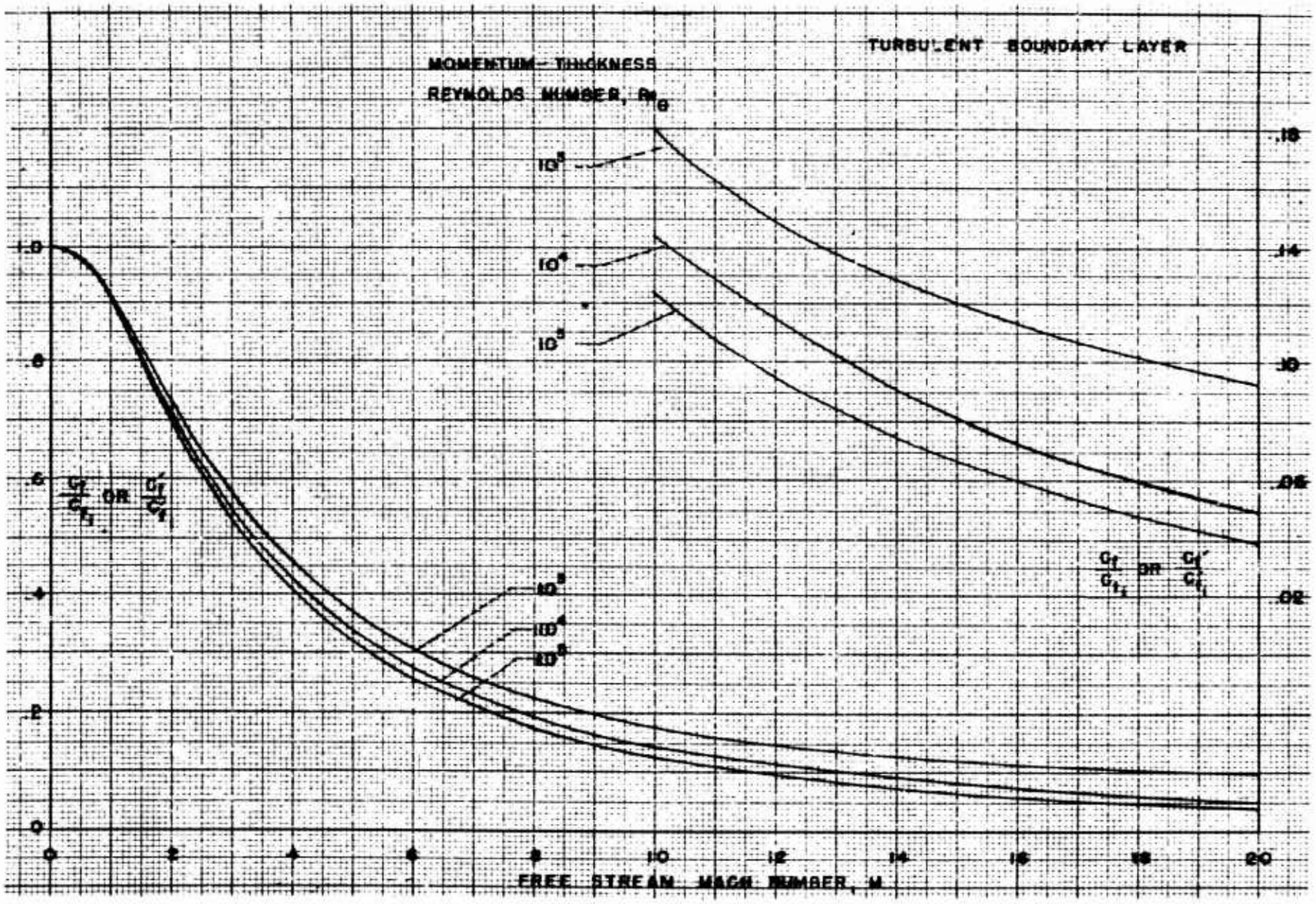

Fig (2.3-23) Variation of $\frac{Cf}{Cf_i}$ with Mach Number and comparison with experiment, Prandtl Number, 0.73. (Ref. 31)

Various values of momentum-thickness Reynolds Number; insulated plate; heat-flux parameter $\beta = 0$

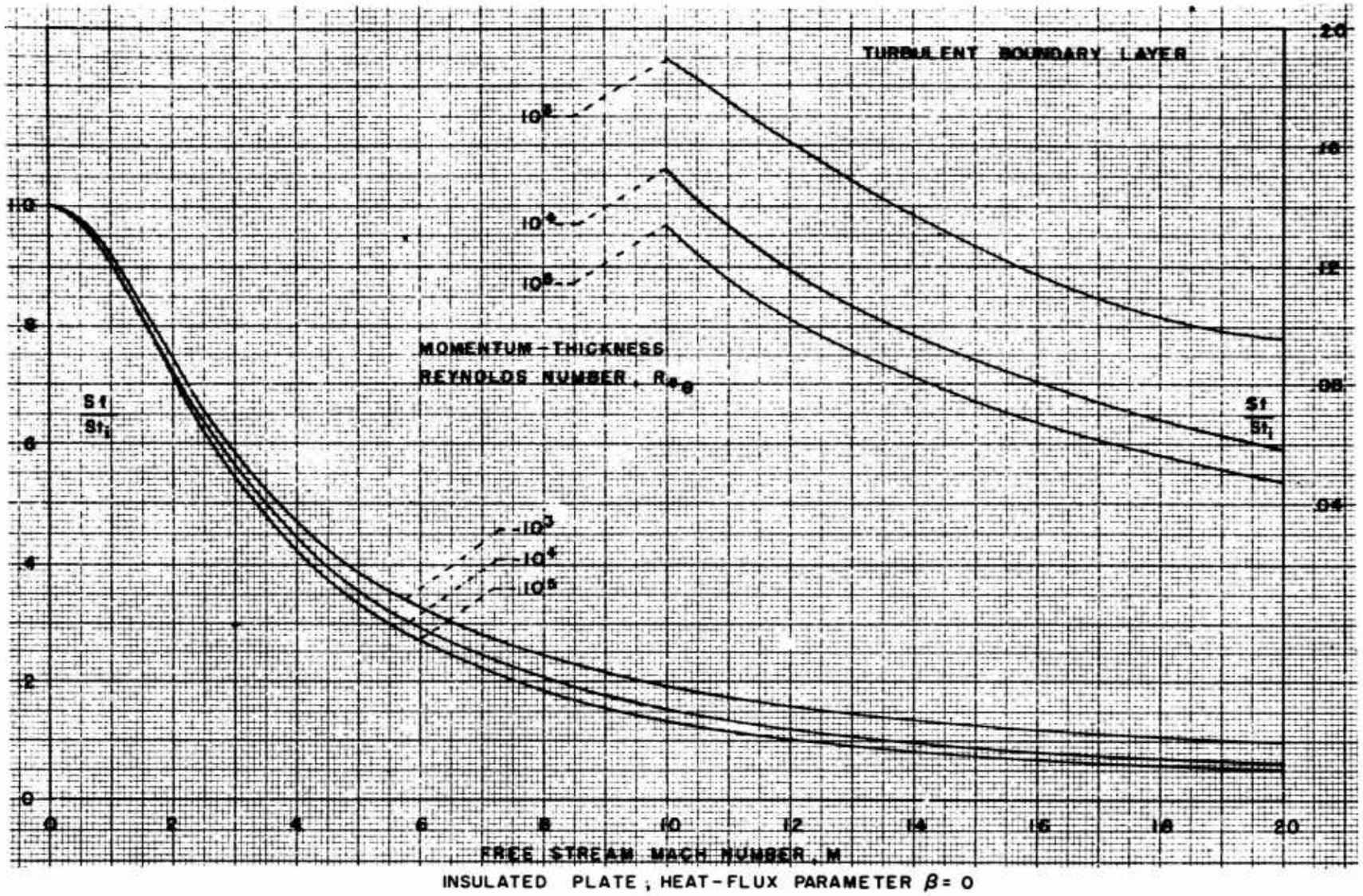

Fig (2.3-24) Variation of $\frac{St}{St_i}$ with Mach Number for various values of momentum-thickness Reynolds Number. Prandtl Number, 0.73. (Ref 31)

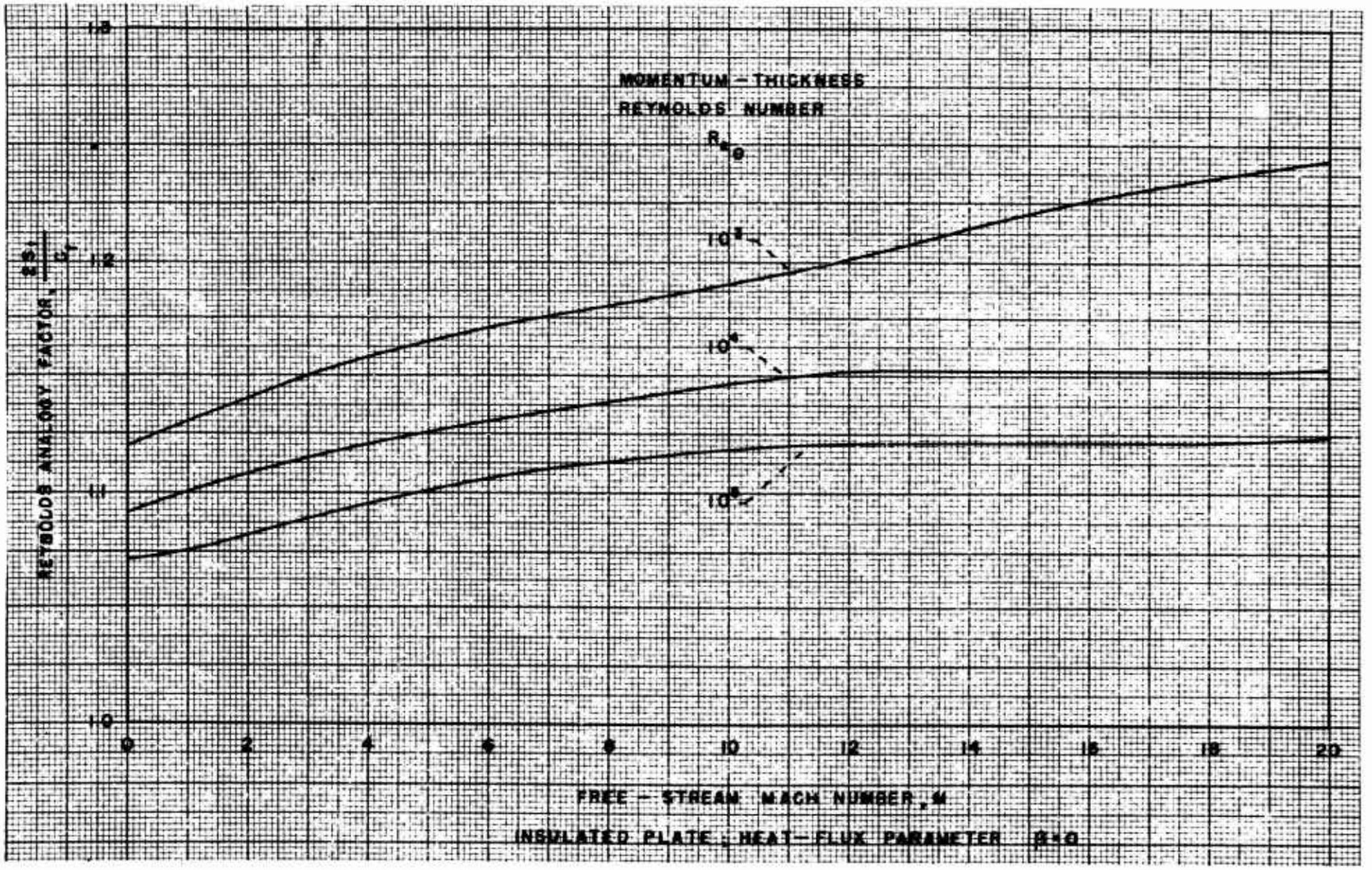

Fig(2.3-25) Predicted variation of Reynolds analogy factor with momentum-thickness Reynolds Number and Mach Number. Prandtl Number, 0.73. (Ref. 31)

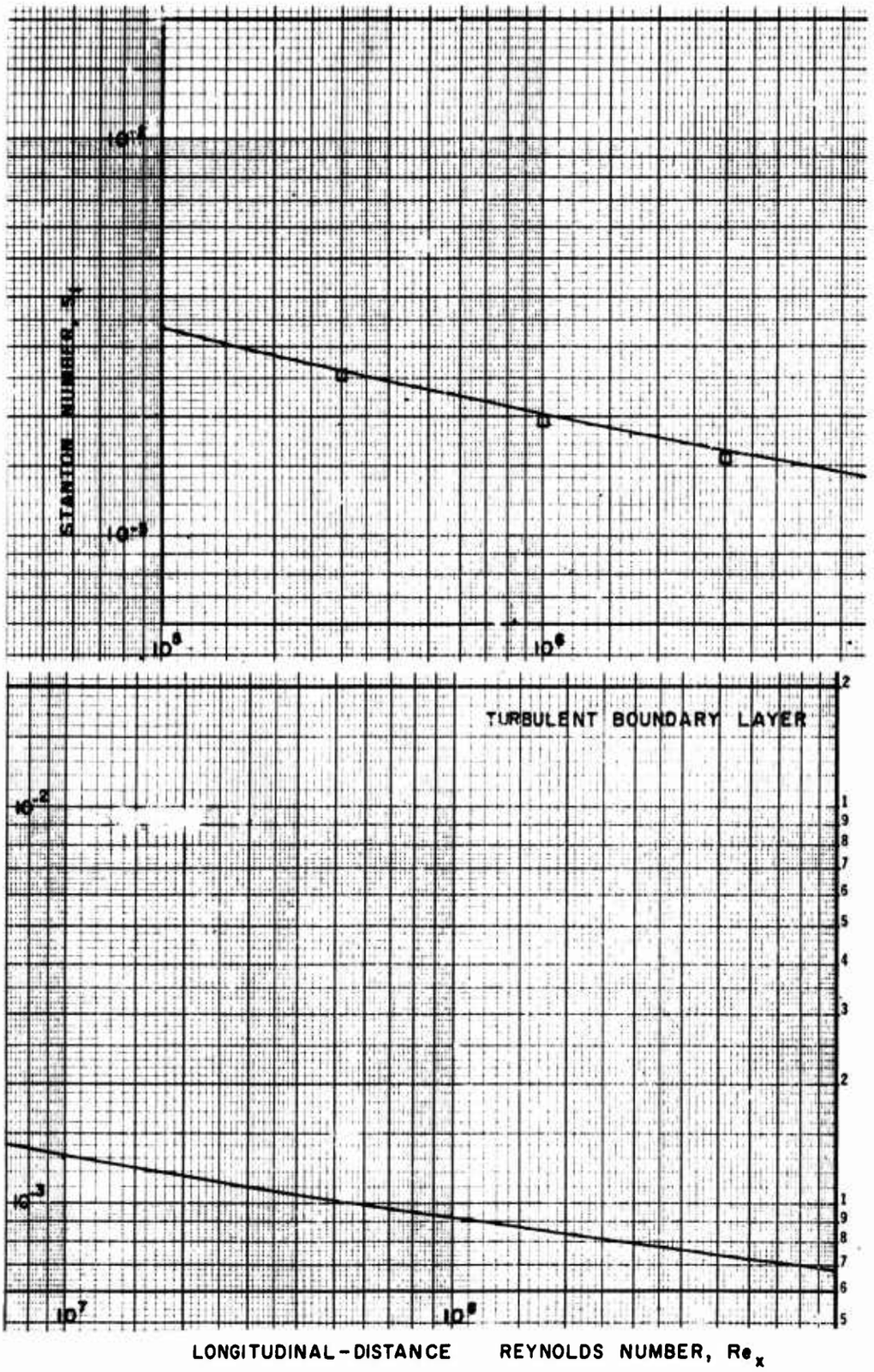

Fig (2.3-26) Predicted varation of Stanton Number with longitudinal-distance Reynolds Number for insulated plate and comparison with experiment for low-speed flow. Prandtl Number, 0.73; Mach Number, 0. (Ref 31)

following general conclusions may be drawn:

For insulated surfaces the skin-friction coefficient, C_f , and the heat-transfer coefficient, St , at a given Reynolds Number decrease as the Mach Number increases.

The incompressible values of the local skin-friction coefficients, plotted as functions of the local Reynolds Numbers, are in good agreement both with experiment and the Eckert's(19) results. Within 5% of accuracy, the law may be expressed analytically as:

$$C_{fi}' = .0292\, Re_x^{-.151} \quad . \qquad (2.3\text{-}255)$$

There is variation of both the skin-friction (C_f / C_{fi}) and the heat transfer (St / St_i) coefficient ratios with Reynolds Number, as indicated in Figs (2.3-23) and (2.3-24). The Reynolds Number effects on both (C_f / C_{fi}) and (St / St_i) increase appreciably with an increase in Mach Number.

Artificial surface cooling, used to offset the deteriorating structural effects of excessive frictional heating ($T_w < T_{aw}$), increases appreciably both C_f' and St' for smooth surfaces.

In a summary, all the existing results are pointing to the following common features of the two-dimensional compressible, turbulent boundary layers on smooth flat without pressure gradients:

The frictional heating tends to flatten the velocity profiles near the outer edge of boundary layer, especially so at high Mach Numbers ($M > 5$). This is not surprising, since heating of flat plates by other means produces essentially the same effect. Cooling of flat plate walls produce a corresponding counter-effect by increasing the respective velocity gradients.

At a given Reynolds Number value, both the skin friction (C_f) and the heat transfer coefficients (St) decrease as the Mach Number is increased; i.e., both are weak functions of the Reynolds Number for a given Mach Number for low supersonic speeds, ($M < 5$), but the Reynolds Number effects increase greatly with increase in Mach Number. The (C_f / C_{fi}) and (C_f' / C_{fi}') variational laws with the Mach and Reynolds Number changes are the same. So are the (St / St_i) and (St' / St_i') laws through the concept of a modified Reynolds analogy.

Cooling of flat plates (in order to offset the effects of excessive frictional skin-temperatures) increases both the skin-friction coefficient and the Stanton Number values for any given set of Mach and Reynolds Numbers.

The respective quantitative results from other analyses (Karman(87), Monaghan(26), Tucker(32), Van Dries(27), Clemmow(39), of the (C_f / C_{fi}) increase with the decreasing wall-to-free stream temperature ratio (T_w / T_δ) at a given value of Mach and Reynolds Numbers are summarized in Fig (2.3-27). The experimental data by Sommer and Short (80) are in good agreement with the Van Driest's and the Clemmow curves at $(T_w / T_\delta) \approx 1$, (highly cooled, plate, with no heat transport across the boundary layer), while Tucker and Managhan theories agree well for $T_w = T_r = T_{aw}$ (insulated plate).

With the free stream properties kept constant, the frictional heating at high Mach Numbers produces a thinning of the boundary layer at any given position on the plate (i.e., at a given value of x).

Experimental measurements by Tendeland(81) of the skin-friction and the heat-transfer coefficients for turbulent compressible boundary layers on smooth, flat plates with heat transfer, favorably agree with the corresponding theoretical predictions of the Sommer and Short's(80) method. The Van Driest's(27) respective theoretical results did not compare as well with the experimental evidence.

Sommer and Short(80) used the Karman-Schoenherr incompressible law for the average skin-friction coefficient,

$$\frac{.242}{(C_f)^{1/2}} = \log_{10}(C_f Re_L) \quad , \qquad (2.3\text{-}256)$$

with the density, the viscosity, and the Reynolds Number evaluated at the T' reference temperature rather than at T_δ :

$$\frac{T'}{T_\delta} = 1 + .035 M_\delta^2 + .45\left(\frac{T_w}{T_\delta} - 1\right) \quad , \quad T_\delta = T_\infty \quad , \qquad (2.3\text{-}257)$$

$$Re_L^* = \frac{U_\delta L}{\nu^*} = Re_L \frac{1}{\left(\frac{T'}{T_\delta}\right)\left(\frac{\mu^*}{\mu_\delta}\right)} \quad , \qquad (2.3\text{-}258)$$

$$\nu^* = \frac{\mu^*}{\rho^*} \quad , \qquad (2.3\text{-}259)$$

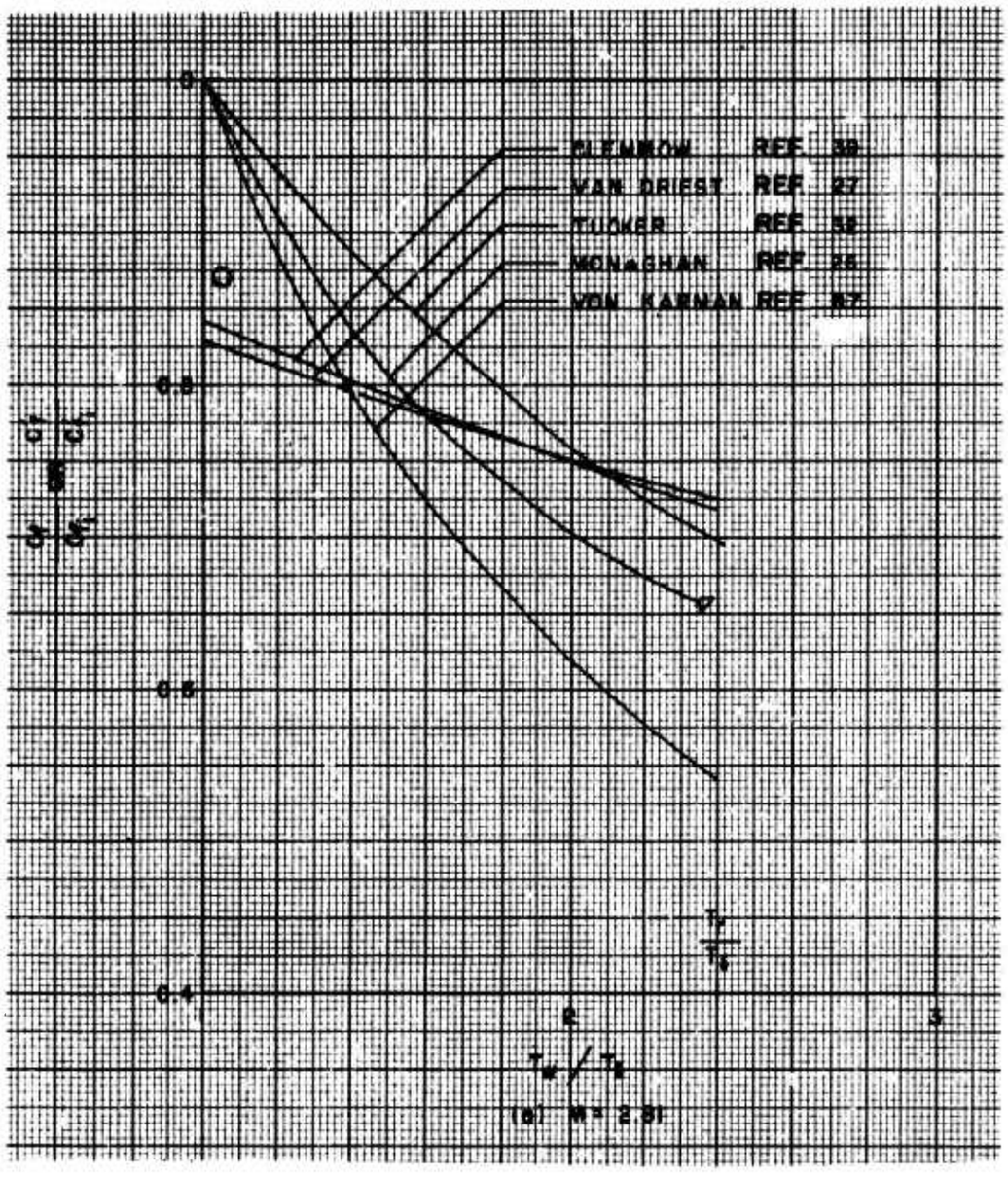

Fig (2.3-27) Comparison of experimental and theoretical results of the effect of wall-temperature ratio on skin-friction ratio at constant Mach Numbers. Turbulent boundary layers, flat plates, zero angle-of-attack. (Ref 80)

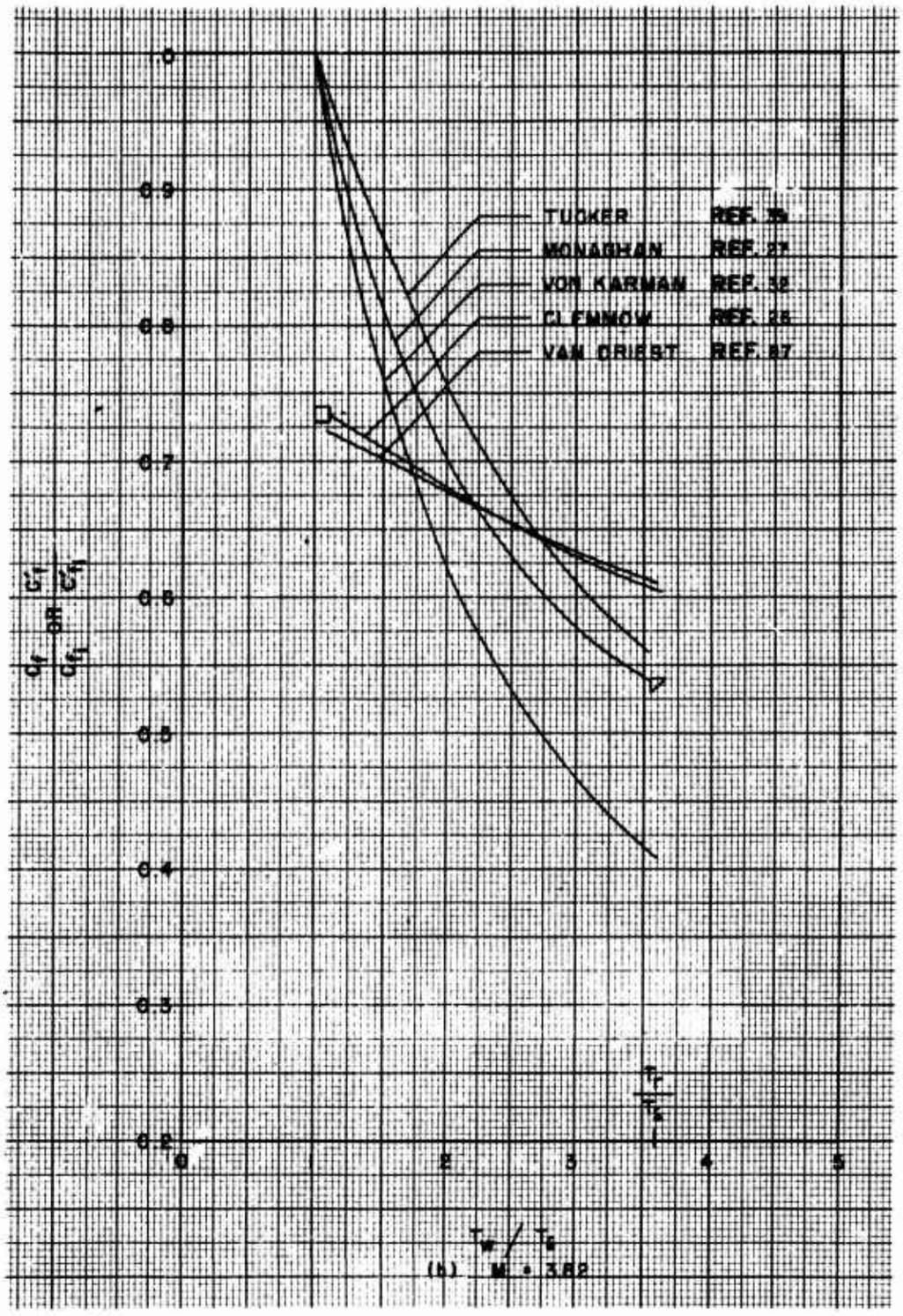

Fig (2.3 - 27) Continued.

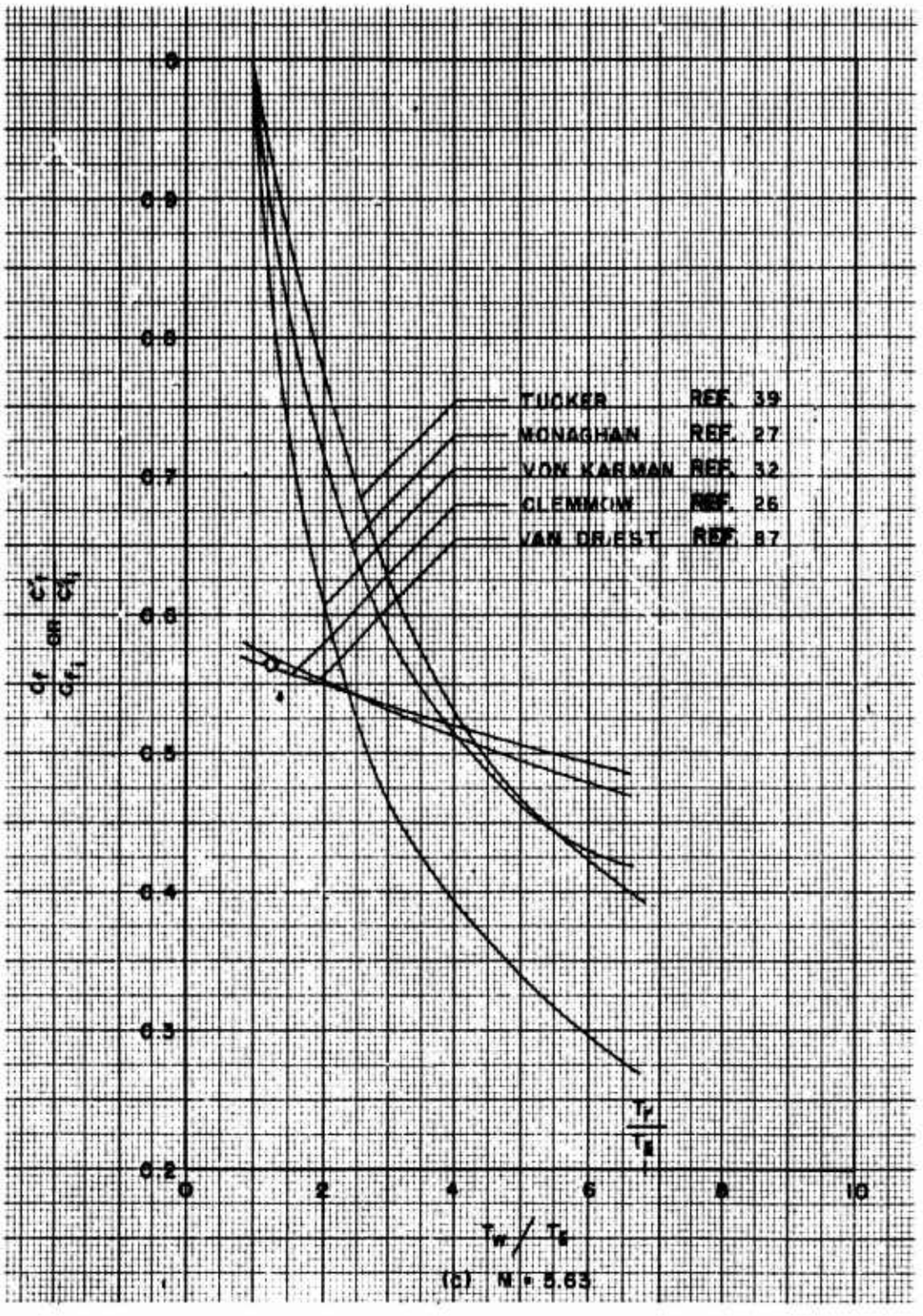

Fig (2.3-27) Continued.

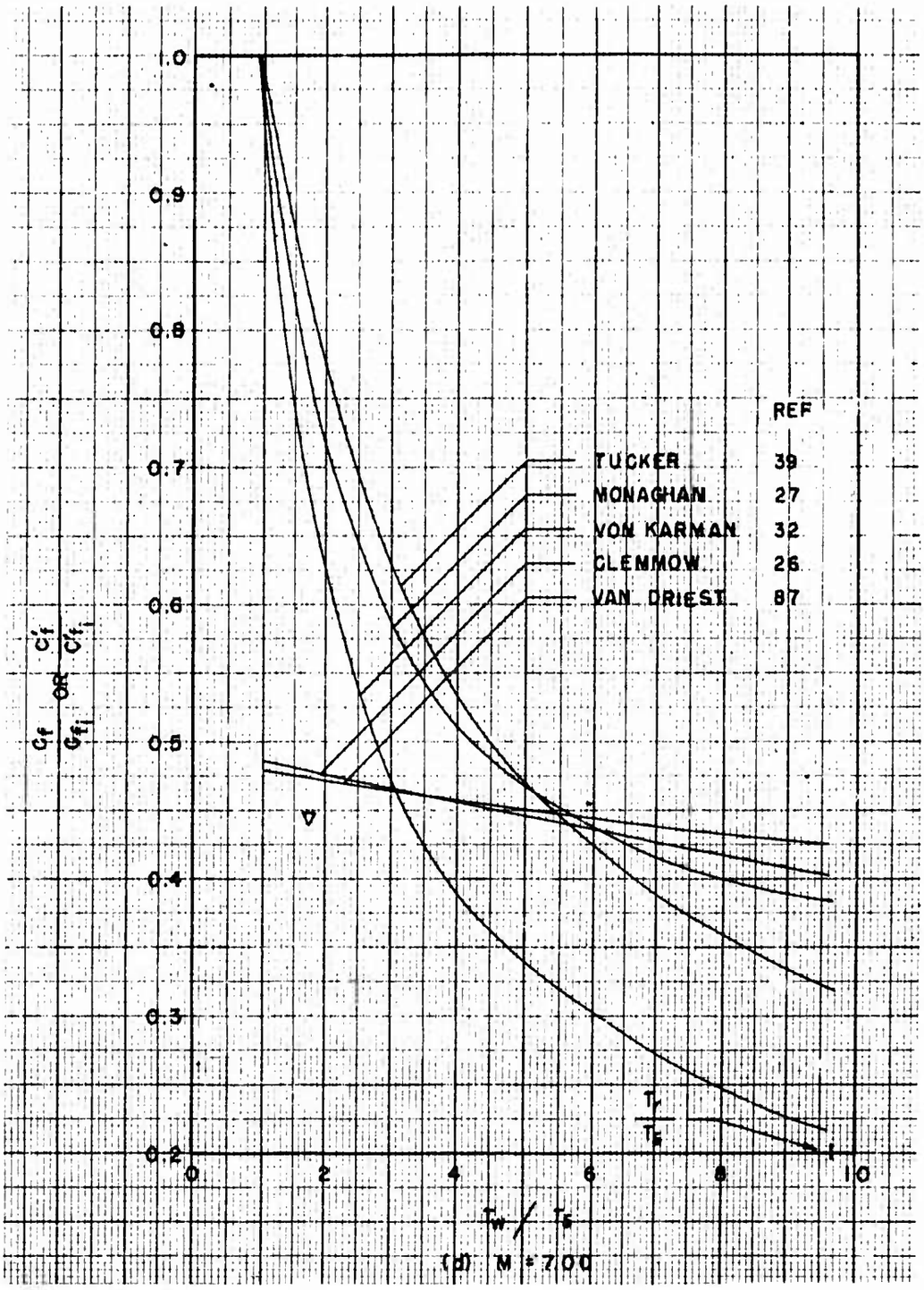

Fig (2.3-27) Continued.

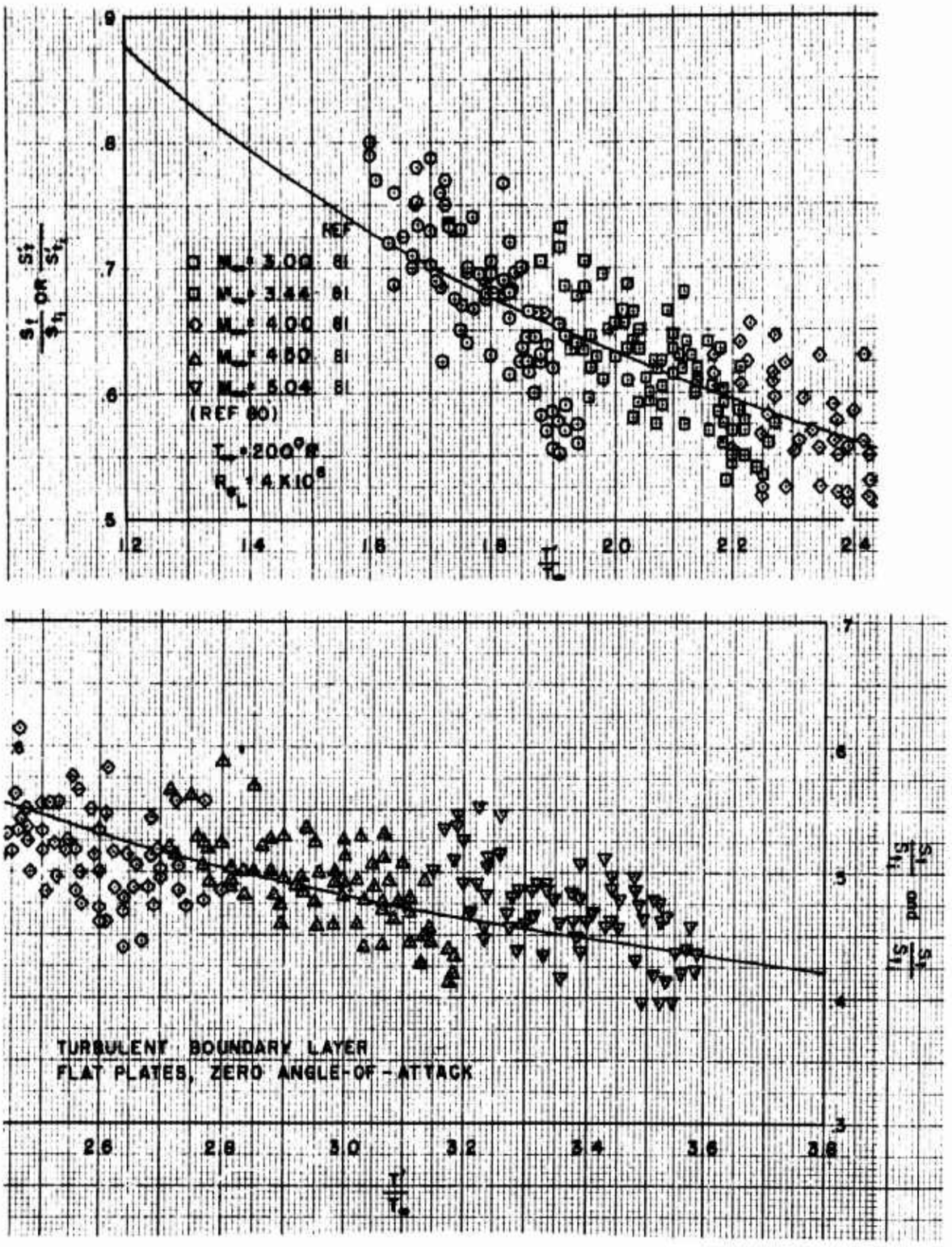

Fig (2.3-28) Comparison of Stanton Number ratio with temperature parameter ratio. (Ref 81)

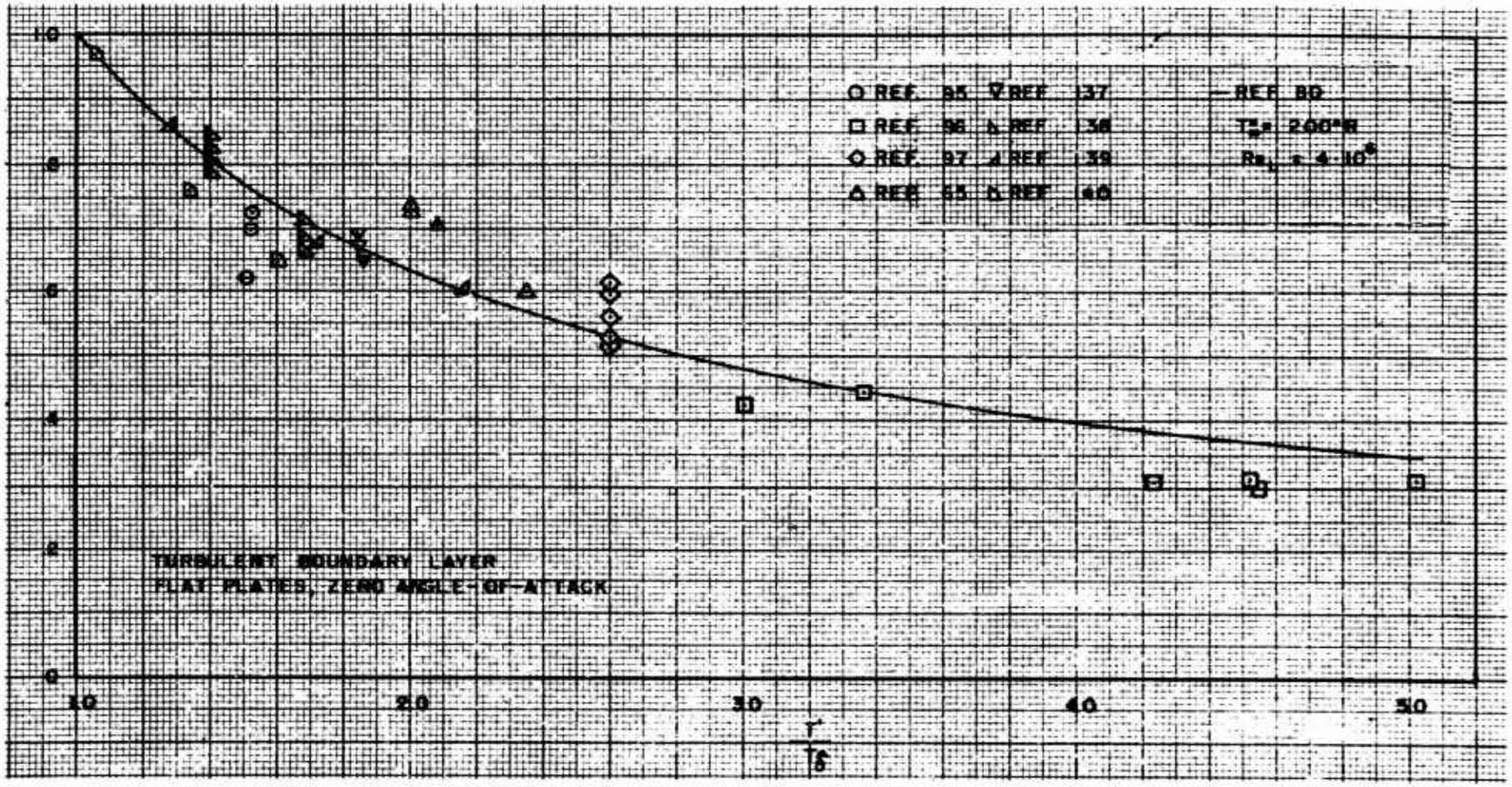

Fig (2.3-29) Comparison of Stanton Number ratio with temperature parameter ratio for various investigations. (Ref 81)

$$\frac{\mu^*}{\mu_\delta} = \left(\frac{T'}{T_\delta}\right)^{1.5}\left(\frac{T_\delta+S}{T'+S}\right) \quad , \quad \text{Sutherland law,}$$

and (2.3-260)

$$S_t^* = S_t\left(\frac{T'}{T_\delta}\right) \quad , \quad \text{Tendeland}^{(81)}. \qquad (2.3\text{-}261)$$

The computations of the heat transfer coefficient ratio, (St/St_i), as a function of (T'/T_δ) reference temperature ratio were preformed by using the modified Reynolds analogy method from Ref. 80. The Tendeland(81) results are presented on Figs. (2.3-28) and (2.3-29), and agree well with many experimental data.

Summary of T′ Expressions

The T′ method, or the mean-enthalpy method, is extensively used as a suitable reference temperature in boundary layer analyses. It was introduced by Rubesin and Johnson(25) for laminar compressible boundary layers, and then later applied by Fischer and Norris(78), and others to turbulent flows. They found that it gave better results than the T_δ reference temperature base. The same favorable results were obtained by Young and Janssen(46), and Sommer and Short(80).

The T′ reference temperature has been defined for laminar compressible boundary layers on insulated smooth flat plates as that specific temperature value at which the local density and the local viscosity must be evaluated, if incompressible skin-friction expressions are to apply to compressible cases. Using the theoretical results from Crocco-Conforto's analysis for laminar flows on flat plates, the following expression for the reference T′ temperature is obtained (subscript δ corresponding to subscript ∞ at a local station outside the boundary layer):

$$\frac{T'}{T_\delta} = 1 + .032M_\delta^2 + .58\left(\frac{T_w}{T_\delta} - 1\right). \qquad (2.3\text{-}262)$$

For turbulent boundary layers, the following expressions for the T′ reference temperature are used: (Sommer and Short(80)

$$\frac{T'}{T_\delta} = 1 + .035M_\delta^2 + .45\left(\frac{T_w}{T_\delta} - 1\right) \quad , \qquad (2.3\text{-}263)$$

Eckert(19):

$$T' = T_\delta + .5(T_w - T_\delta) + .22r\frac{\gamma-1}{2}M_\delta^2 T_\delta \quad , \qquad (2.3\text{-}264)$$

i.e., $$T' = T_\delta + .5(T_w - T_\delta) + .22r(T_{s\infty} - T_\delta), \qquad (2.3\text{-}265)$$

with

$r = (P_r^*)^{1/2}$ for turbulent boundary layers, and $r = (P_r^*)^{1/2}$ for laminar boundary layers.

Deissler and Loeffler(31):

$$\frac{T'}{T_\delta} = (1-C) + \left[(C-D)\frac{T_w}{T_{aw}} + D\right](1 + .176M_\delta^2) \quad , \qquad (2.3\text{-}266)$$

$$(C_f'/C_{f_i}') = \left(\frac{T'}{T_\delta}\right)^{-.875} \quad . \qquad (2.3\text{-}267)$$

$$T_{aw} = T_\delta + r\frac{U_\delta^2}{2C_f'} \quad , \quad U_\delta = V_\infty \quad , \qquad (2.3\text{-}268)$$

where $r = f(Re_\theta, M_\delta)$, and the experimental coefficients C and D are evaluated from the respective graphs in the Ref. 31. Thus, for instance, for Re_θ values near 10^5, the reference temperature is given by

$$\frac{T'}{T_\delta} = .44 + (.376\frac{T_w}{T_{aw}} + .184)(1 + .176M_\delta^2) \quad . \qquad (2.3\text{-}269)$$

After a substitution of the respective T′ -evaluated variables, the compressible turbulent boundary layer values of the skin friction coefficients, $C_f = f(M_\delta, Re_L)$, and the Stanton Number $St = f(M_\delta, Re_L)$ are obtained, see Figs (2.3-15), (2.3-24) and (2.3-25).

Instead of T′, the corresponding enthalpy expression can be used, if variations in C_p with temperature are strong:

$$h^* = h_\delta + .5(h_w - h_\delta) + .22\, r_h(h_{s\infty} - h_\delta), \qquad (2.3\text{-}270)$$

with the enthalpy recovery factor, r_h, given by the same type of expressions as r.

In all cases, the flow variables ρ, μ, C_p, k, are evaluated for the reference temperature $T^* = T'$, and used in some already known expression for the incompressible skin friction coefficient, such as:

(von Karman-Schoenherr, for turbulent incompressible flows),

$$\frac{.242}{(C_f)^{1/2}} = \log_{10}(C_f Re_L^*) ; \qquad (2.3\text{-}271)$$

(Schulz-Grunow formula for turbulent incompressible flows),

$$C_f' = \frac{.370}{(\log_{10} Re_x^*)^{2.584}} ; \qquad (2.3\text{-}272)$$

(Prandtl-Schlichting, for turbulent incompressible flows),

$$C_f = \frac{.455}{(\log_{10} Re_L^*)^{2.58}} . \qquad (2.3\text{-}273)$$

For Mach Numbers greater than 5, there are but few experimental data against which to check the T′ method. For subsonic Mach Numbers, the method is in reasonably good agreement with experiments, see Ref. (31,80,92,98,99) and Fig (2.3-26).

(3) Nestler and Goetz· A Comparative Analysis of Van Driest, Eckert, Donaldson, Bartz and Deissler-Loeffler Methods

The summary comparative data are taken from the well condensed and argumented presentation by Nestler and Goetz(17). It should be consulted for any additional information.

(a) Van Driest's Methods(27,28,29)

There are two Van Driest's semi-empirical methods of predicting the skin friction in turbulent, compressible boundary layers on smooth, flat plates with heat transfer. Both methods are based on the same assumptions:

-The Prandtl Number is assumed equal to unity both in the laminar sublayer and in the turbulent portion of the boundary layer.

- The shear stress distribution across the boundary layer is assumed constant:

$$\tau = \tau_w = \rho l^2 \left(\frac{du}{dy}\right)^2 . \qquad (2.3\text{-}274)$$

The difference between the two methods is in the assumed "mixing length" law. In the "1951" analysis(27), the Prandtl's law,

$$l = ky , \qquad (2.3\text{-}275)$$

is assumed to hold, while in the second "1954" analysis(28), the von Karman's expression,

$$l = k\left(\frac{du}{dy}\right)/\left(\frac{d^2u}{dy^2}\right) , \qquad (2.3\text{-}276)$$

is employed, which later proved to yield results in a better agreement with experimental evidence and is nowadays commonly preferred.

Apart from this difference in the "mixing length" assumptions, in both cases the method of solution remains the same, employing the Crocco's(100) relationship between the temperature distribution and the longitudinal velocity in the boundary layer and performing a subsequent integration of the assumed "mixing length" relationship to determine the velocity profile. The wall shearing stress expression is then obtained by application of the Karman momentum integral, with constants of the integrations fixed to match the incompressible insulated results of the Karman-Schoenherr relation, which is in a close agreement with the corresponding expression for the incompressible local skin-friction coefficient, C_{f_i}' , by Schultz-Grunow (Eq 2.3-272). The resulting Van Driest's local skin-friction coefficient expression for compressible boundary layers with heat transfer on smooth, flat plates at zero angle-of-attack, reads:

$$C_f'^{1/2}\left[.41 + \log_{10}(Re_x C_f') - f(\omega)\log_{10}\left(\frac{T_w}{T_\delta}\right)\right] = \frac{.242(\sin^{-1}\alpha + \sin^{-1}\beta)}{\left(\frac{\gamma-1}{2}M_\delta^2\right)^{1/2}} , \qquad (2.3\text{-}277)$$

where $\alpha = \frac{(2A^2-B)}{(B^2+4A^2)^{1/2}}$, $\beta = \frac{B}{(B^2+4A^2)^{1/2}}$,

$$A^2 = \frac{\left(\frac{\gamma-1}{2}\right)M_\delta^2}{(T_w/T_\delta)} , \quad B = \frac{\left(1+\frac{\gamma-1}{2}M_\delta^2\right)}{(T_w/T_\delta)} - 1 ;$$

and (2.3-278)

$f(\omega) = \omega + .5$ - is the Prandtl's mixing length law, Van Driest's first "1951" method.

$f(\omega) = \omega$ - is the von Karman's mixing length law, van Driest's second "1954" method.

$\omega = .76$, $\gamma = 1.4$

Van Driest uses the simple exponent viscosity law, $\mu \sim T^\omega$, instead of a more accurate (but less easy for computations) Sutherland's relationship; he states that this simplification does not introduce an appreciable error even at higher Mach Numbers. The

argument is based on one single examination for a free stream temperature T_δ of 400° R.

Regarding the assumed approximation of $Pr = 1$, van Driest shows that a more accurate value of $Pr = .75$ would introduce only a negligible correction, except for rare combinations of high Mach Numbers coupled with low $(T_w/T_{s\infty})$ ratios. Even then, for $M = 20$, $(T_w/T_\delta) = 1$ and for $Re_x = 10^6$, the $Pr = .75$ value would give an increase of 7% in the (Cf/Cf_i) value only.

(b) Eckert's Reference Temperature T' Method(20)

Using a modification of the T' method, which was introduced originally by Rubesin and Johnson(25) for laminar boundary layers, Eckert applied it to turbulent boundary layers obtaining results in good agreement with the related experimental data.

The Eckert's method may be considered as well representative of the T' reference temperature approach. It assumes an approximate expression for the wall shear stress,

$$\tau = \tau_w = C_{fi}'^{*} \rho^* \frac{U_\delta^2}{2\rho} \quad , \qquad (2.3\text{-}279)$$

where $C_{fi}'^{*}$ and ρ^* are evaluated for the reference temperature,

$$T' = T_\delta + .50(T_w - T_\delta) + .22(T_r - T_\delta) \quad , \qquad (2.3\text{-}280)$$

with the recovery temperature,

$$T_r = T_\delta \left[1 + r\frac{\gamma-1}{2} M_\delta^2\right] \qquad (2.3\text{-}281)$$

and the recovery factor for turbulent boundary layers,

$$r \cong Pr^{1/3} = .896 \quad \text{for} \quad Pr = .72 \quad , \qquad (2.3\text{-}282)$$

Further, introducing the Schultz-Grunow relationship for incompressible turbulent boundary layers, Eq (2.3-272):

$$C_{fi}'^{*} = \frac{.370}{(\log_{10} Re^*)^{2.58}}$$

with,

$$Re^* = \frac{\rho^* U_\delta x}{\mu} = Re_x \frac{\rho^*/\rho_\delta}{\mu^*/\mu_\delta} \quad , \qquad (2.3\text{-}283)$$

$$\frac{\rho^*}{\rho_\delta} = \frac{T_\delta}{T'} \quad , \qquad (2.3\text{-}284)$$

$$\frac{\mu^*}{\mu_\delta} = \left(\frac{T'}{T_\delta}\right)^{1.5} \left(\frac{1 + S/T_\delta}{T'/T_\delta + S/T_\delta}\right) \quad , \qquad (2.3\text{-}285)$$

where the Eq (2.3-285) is the Sutherland law(101), with $S = 198.6°$ R, the original Eq (2.3-279) is rewritten as

$$C_f' = \frac{\rho^*}{\rho_\delta} C_{fi}'^{*} = \frac{\tau_w}{\rho_\delta U_\delta^2/2\rho} \quad , \qquad (2.3\text{-}286)$$

$$\therefore \frac{C_f'}{C_{fi}'} = \frac{\rho^*}{\rho_\delta} \frac{C_{fi}'^{*}}{C_{fi}'} \quad . \qquad (2.3\text{-}287)$$

Thus Eqs (2.3-280) and (2.3-287) serve for computation of the local skin friction coefficient ratio (Cf'/Cf_i') by Eckert's method. The main feature of the results is that an increase in skin friction occurs with decreasing wall temperature for all Mach Numbers. This is in contrast to the van Driest's predictions, which result in a reverse trend at higher Mach Numbers, see comparative figures in Ref. 17.

The introduction of the Sutherland's law results in a definite dependency of the (Cf'/Cf_i') ratio on the inviscid stream temperature, (T_δ), which is not the case if the simpler law,

$$\frac{\mu^*}{\mu} = \left(\frac{T'}{T_\delta}\right)^{\omega} \quad , \qquad (2.3\text{-}288)$$

were used. In the Ref. 17 it is demonstrated that the difference for the range of $10^6 < Re_x < 10^9$ does not exceed 3%, the relatively higher value of the (Cf'/Cf_i') being associated with higher free stream temperatures, T_δ.

(c) Donaldson Method(30)

Donaldson presents a different method for the skin friction and the heat transfer estimates on smooth, flat, insulated plates. His method is based on the following assumptions:

- The shear stress in a laminar

sublayer is assumed constant,

$$\tau_l = \tau_w = \frac{\mu_l U_l}{\delta_l} \quad , \qquad (2.3\text{-}289)$$

where the subscript "$_l$" denotes conditions at the edge of the laminar sublayer.

The shear stress due to turbulence is defined by use of the Prandtl's mixing length hypothesis,

$$\tau_t = \rho l^2 \frac{\partial u}{\partial y} \left|\frac{\partial u}{\partial y}\right| , \qquad l = ky , \qquad (2.3\text{-}90)$$

with the velocity profile in turbulent region expressed by a power law ,

$$\frac{u}{U_\delta} = \left(\frac{y}{\delta}\right)^{1/n} . \qquad (2.3\text{-}291)$$

It is further assumed that the laminar and the turbulent shear stresses form a definite ratio,

$$R = \frac{\tau_l + \tau_t}{\tau_l} . \qquad (2.3\text{-}292)$$

The Crocco's(100) reference temperature concept is assumed to hold in the form,

$$T' = T_w - (T_w - T_r)\left(\frac{u}{U_\delta}\right) - (T_r - T_\delta)\left(\frac{u}{U_\delta}\right)^2 . \qquad (2.3\text{-}293)$$

With these assumptions, the final local skin-friction coefficient expression is obtained as:

$$C_f' = \frac{K}{F\, Re_\delta^{(2/n+1)}} , \qquad (2.3\text{-}294)$$

where,

$$Re_\delta = \frac{\rho_\delta U_\delta \delta}{\mu_\delta} ,$$

$$K = 2\left[n\left(\frac{R-1}{k^2}\right)\right]^{\frac{1-n}{1+n}} ,$$

$k = .4$ (mixing length constant) ,

$$F = \left\{1 + \frac{r(\gamma-1)}{2} M^2\left[1 - \left(\frac{u_l}{U_\delta}\right)^2\right] + \left(\frac{T_w - T_r}{T_\delta}\right)\left(1 - \frac{u_l}{U_\delta}\right)\right\}^{\frac{n-2\omega-1}{n+1}} ,$$

$$\frac{u_l}{U_\delta} = \left[\frac{n(R-1)}{k^2 Re_\delta}\right]^{\frac{1}{n+1}} \times F^{\frac{\omega+1}{n-2\omega-1}} . \qquad (2.3\text{-}295)$$

Obviously, a solution of the basic Eq (2.3-294) requires an iterative process, and an evaluation of constants from the incompressible data:

$$\frac{R-1}{k^2} = 22.5,$$

based on Prandtl's incompressible data,

$$n \approx 7 .$$

Results of the lengthy computations are obtained in terms of Re_δ . Their correlation to the usual Re_x values is then performed, using the expression (by Donaldson[30]):

$$C_f' = \left(\frac{K}{F_{aw}}\right)^{\frac{n+1}{n+3}} \left(\frac{n+1}{n+3}\,\frac{2\theta^*}{\delta}\right)^{\frac{2}{n+3}} \frac{1}{Re_x^{(2/n+3)}} , \qquad (2.3\text{-}296)$$

with F_{aw} being an average value along the plate, calculated for an average value of (u_l / U_δ), and

$$\frac{\theta^*}{\delta} = \int_0^\delta \frac{\rho}{\rho_\delta}\,\frac{u}{U_\delta}\left(1 - \frac{u}{U_\delta}\right) d\left(\frac{y}{\delta}\right) . \qquad (2.3\text{-}297)$$

Persh(102) tabulated values of θ^*/δ for $(0 < M_\delta < 20)$, $(5 < n < 11)$, $[-10 < (T_w - T_r)/T_\delta < +10]$.

(d) Deissler-Loeffler Method(31)

As already stated earlier, Deissler and Loeffler presented their analysis by dividing the turbulent compressible boundary layer into a region "next to the wall" and a region "away from the wall", characterized by the following assumptions:

In the region "away from the wall", the von Karman's mixing length hypothesis holds, yielding for the eddy diffusivity ,

$$\epsilon = K_1^2 \frac{(du/dy)^3}{(d^2u/dy^2)^2} , \qquad (2.3\text{-}298)$$

while in the region "next to the wall" (ϵ) is a function of (u) and (y) only

$$\epsilon = K_2^2 uy , \qquad (2.3\text{-}299)$$

where κ_1 and κ_2 are constants that should be determined from incompressible pipe flow data.

The viscosity-temperature relation is assumed to follow the simple power law,

$$\mu \sim T^{.68} , \qquad (2.3\text{-}300)$$

with the Prandtl Number value of .73.

It is argumented that the variable shear stress and heat transfer have a negligible effect on the velocity and the temperature profiles, i.e., the boundary layer momentum and energy equations may be solved assuming a constant shear stress and heat transfer.

It is assumed that the thermal and momentum eddy diffusivities are equal.

Thus calculated values of C_f' appear as functions of Re_Θ and M_δ. By a subsequent expression,

$$Re_x = 2\int_0^{Re_\Theta} \frac{dRe_\Theta}{C_f'} , \qquad (2.3\text{-}301)$$

and by introducing the reference T' temperature concept (for $Re_\Theta = 10^5$),

$$\frac{T'}{T_\delta} = .44 + (.376\,\frac{T_w}{T_r} + .184)(1 + .176\,M_\delta^2), \qquad (2.3\text{-}302)$$

the final form of the compressible-to-incompressible skin-friction coefficient ratio is obtained as:

$$\frac{C_f'}{C_{fi}'} = \left(\frac{T'}{T^\circ}\right)^{-.875} , \qquad (2.3\text{-}303)$$

with C_f' to be determined graphically from the plots of C_f' versus Re_Θ at $M_\delta = 0$.

(e) Bartz Method

Starting with the Blasius' incompressible equation,

$$C_{fi}' = .0456\left(\frac{\mu}{\rho U \delta}\right)^{.25} = \frac{\tau_w}{\frac{1}{2}\rho_\infty U_\infty^2} = \frac{\tau_w}{\frac{1}{2}\rho_A V_A^2} , \qquad (2.3\text{-}304)$$

and following the method of Tucker[32], Bartz assumed that ρ and μ could be evaluated at a reference temperature, T^*, representing an algebraic mean of the wall and the free stream temperatures,

$$T^* = \frac{1}{2}(T_w + T_\delta) \text{ with } \mu \sim T^{.6} . \qquad (2.3\text{-}305)$$

The resulting local compressible skin-friction coefficient is then obtained in terms of Re_δ,

$$C_f' = .0456\,Re_\delta^{-.25}\left[\frac{1}{2}\left(\frac{T_w}{T_\delta} + 1\right)\right]^{-.6} , \qquad (2.3\text{-}306)$$

which shows no explicit dependence on Mach Number, contrary to the Eckert's and van Driest's expressions and the experimental evidence.

(f) Comparisons With Experiments

Nestler and Goetz[17] performed a thorough and a very objective, detailed analysis of the relative agreements of the theories (a to e) with experimental evidence. Taking due care to eliminate the "human factor", i.e., avoiding temptations to match a chosen theoretical set of data with only such empirical evidence which might favorably support the theory, all the theories have been impartially related to two different sets of empirical data, obtained by two different experimental approaches:

By direct measurements of the skin-friction, with all the experimental evidence first correlated to the common Re_x and Re_Θ values,

By indirect determination of the skin-friction data, using a modified Reynolds Analogy concept and applying it to heat-transfer experimental data, with a critical pre-examination of the Reynolds Analogy expressions and the heat transfer measuring techniques themselves. Correlation of the experimental data has been again reduced to the common Re_x and Re_Θ bases.

By comparing the various theoretical predictions with such an average and common set of empirical data, the effects of Reynolds and Mach Numbers on the C_f' values in the cited theories can be summarized as follows:

When correlated with the experimental data of direct skin-friction measurements, based on common Re_x values, the Van Driest's "1954" method proves best, followed by Eckert's method as second. The Eckert's results prove

to be too low (10% utmost) for $M > 2$, particularly in case of slightly cooled wall conditions. The Deissler-Loeffler and Donaldson-Persh methods correlate reasonably well.

With this general sequence of the individual accuracies, it can be stated that, in an average for all the theories, the predictions of the compressible skin-friction coefficients for turbulent boundary layers over smooth, flat plates (in absence of pressure or temperature gradients, mass transfer or dissociation, and for near-insulated skin conditions), are in agreement with experimental evidence within $\pm 10\%$. for lower Reynolds Numbers, ($Re_x \sim 10^6$). For higher Reynolds Numbers, ($Re_x \sim 10^8$), or highly cooled walls, the tolerance should be increased up to $\pm$ 20% (due to lack of sufficient experimental evidence). Both recommended limits are for Mach Numbers up to 5. For higher Mach Numbers ($5 < M < 20$) a further deterioration in accuracy is to be expected.

The use of a modified Reynolds Analogy (supported by heat transfer measurements) for an indirect prediction of the skin friction coefficient values, yields a lesser agreement between theory and experiment, the limits of the average accuracy being additionally increased by $\pm 10\%$ in comparison with direct force measurement tolerances stated above. The best suited modified Reynolds Analogy concept is the simple Colburn form,

$$St = \frac{C_f}{2\, Pr^{2/3}} . \qquad (2.3\text{-}307)$$

It correlates the theoretical and the experimental data slightly better than other, more complex forms.

For engineering purposes, if the ready-made graphs are used, the van Driest's "1954" method, based on von Karman's similarity relation, is best and easiest to apply, due to sufficient graphical data. For numerical computations, the Eckert's method is simplest, without any appreciable sacrifice of accuracy, provided the Blasius' incompressible relation for local skin-friction coefficient,

$$C_f' = .0592\, Re_x^{-.2} , \qquad (2.3\text{-}308)$$

in the Eckert's reference temperature method is not used for values of Re_x above 10^7.

2.3.4 THREE DIMENSIONAL AND PRESSURE GRADIENT EFFECTS

The turbulent compressible boundary layers on slender bodies of revolution have been investigated by Seiff and Short(103), at Mach Numbers of 3.2 and 3.6 by a Mach-interferometer. The models were gun-launched. These measurements are particularly interesting from the engineering point of view, since the body skin temperatures were relatively cold compared to the recovery temperature, thus simulating the actual transient flight conditions encountered at early stages of missile trajectories.

The theoretical method of the reference T' temperature, as described by Sommer and Short(80), proved to be in good agreement with the experimental results of skin friction and heat transfer coefficient data when the modified Reynolds analogy is used.

In Fig. (2.3-30) a comparison of these test results(103) for relatively cool skin for ogive-cylinder and cones is compared with the "insulated" curves of a flat plate.

When pressure gradient-effects are introduced, an additional semi-empirical equation is required, expressing the pressure gradient $(\partial p/\partial x)$ effects on the velocity profile changes, and a corresponding modified skin-friction expression is needed, so that it reflects the pressure gradient existance along the surface. Depending upon definition of the additional semi-empirical pressure-gradient equation, several methods of solution exist in literature:

(1) By method of Lin and Tetervin, (104), a moment-of-momentum expression is used as the auxiliary equation, which has to be solved simultaneously with the von Karman momentum equation.

(2) By method of Maskell(105), the momentum equation is replaced by an empirical expression, allowing for a simplified solution. The Ludwieg-Tillman(106) skin friction formula, which accounts for the presence of pressure gradients, is then used to calculate the skin-friction distribution.

(3) In case of compressible turbulent boundary layers with heat transfer and pressure gradients on non-insulated surfaces, an approximate method for calculation of the skin friction and heat transfer coefficients is presented by Reshotko and Tucker(107). The method involves a simplification of the auxiliary Tetervin and Lin(104) moment-of-momentum expression by using a form of the Stewartson(108) transformation. Applying Eckert's(20) "reference" enthalpy concept, the semi-empirical Ludwieg-Tillman(106) skin friction expression is used in a form accounting for heat-transfer effects. Further simplification of the solution is then effected by using Maskell's(105) approximation for the shear-stress distribution through the boundary layer, together with a power-law velocity profile assumption. Then the heat transfer coefficients are estimated by a speculative extension of Reynolds analogy, as suggested by results from Ref. 109 (Reshotko). A final expression for skin-friction coefficient is then obtained in the form (see Fig 2.3-31):

$$\left(\frac{C_f'}{C_{fi}'}\right) = (1 + .144 M_8^2)^{-.578} \quad . \tag{2.3-309}$$

(4) A similar approach was previously used by Englert(110), and Mager,(111), in calculating compressible turbulent boundary layers over insulated surfaces with pressure gradients. In order to simplify the auxiliary moment of momentum equation of Tetervin and Lin(104), they used again the Stewartson transformation(108) and applied it to the Truckenbrodt(112) and Maskell(105) results respectively.

(5) The heat-transfer phenomena on smooth bodies of revolution and on cones for both laminar and turbulent compressible boundary layers have been analyzed by the following principal investigators:

The laminar heat-transfer analysis on a smooth flat plate with a uniform surface temperature is developed by Crocco(100). Effects of nonuniform surface temperatures were subsequently treated by Chapman and Rubesin(114), and the effects of body shape and longitudinal pressure gradients by Kalikhman(115) and by Scherrer(116). Mangler(117) has worked out a theoreti-

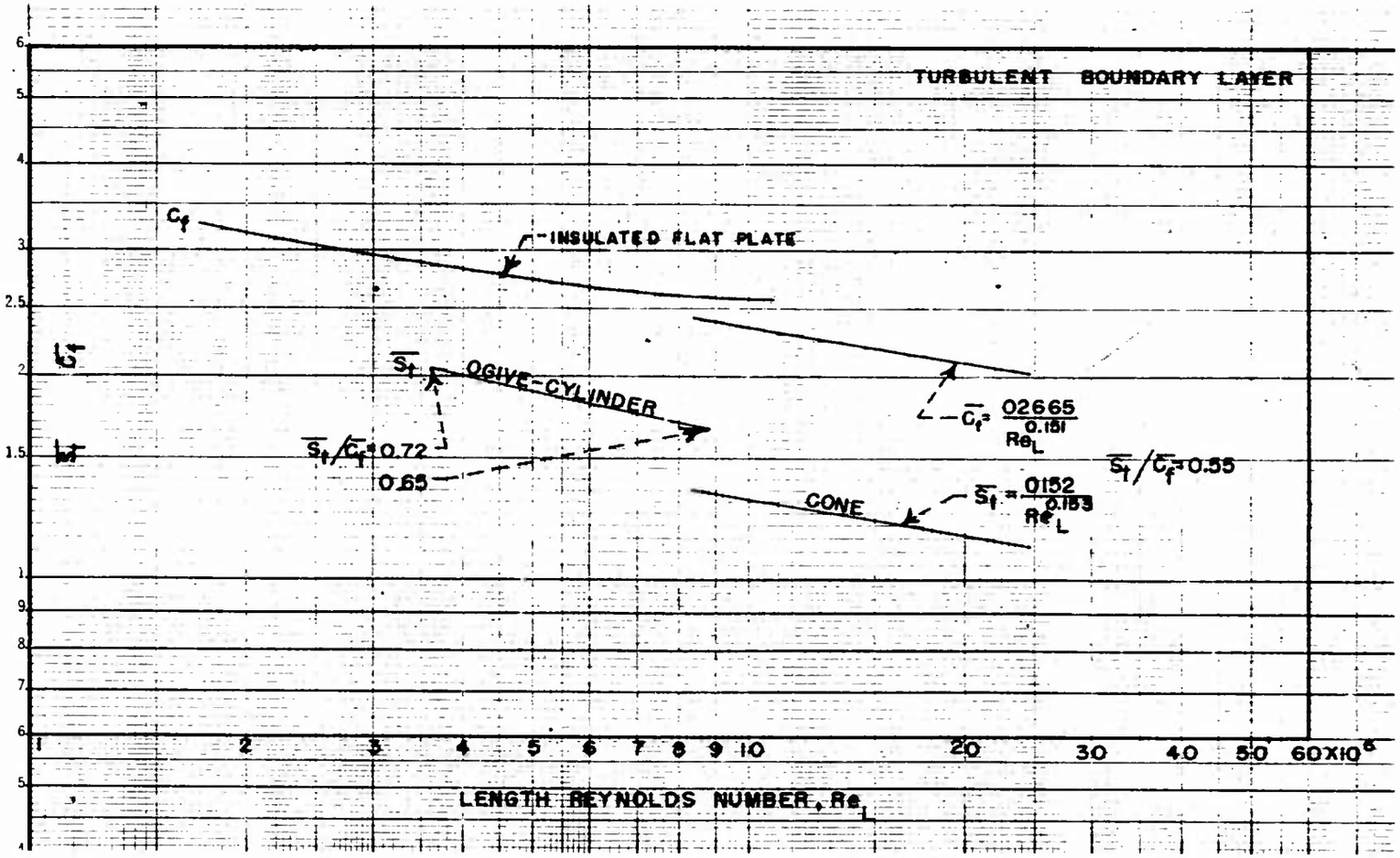

Fig (2.3-30) Average heat-transfer curves computed from experimental evidence and compared with $\overline{C_f}$ computed by T' method. (Ref. 103)

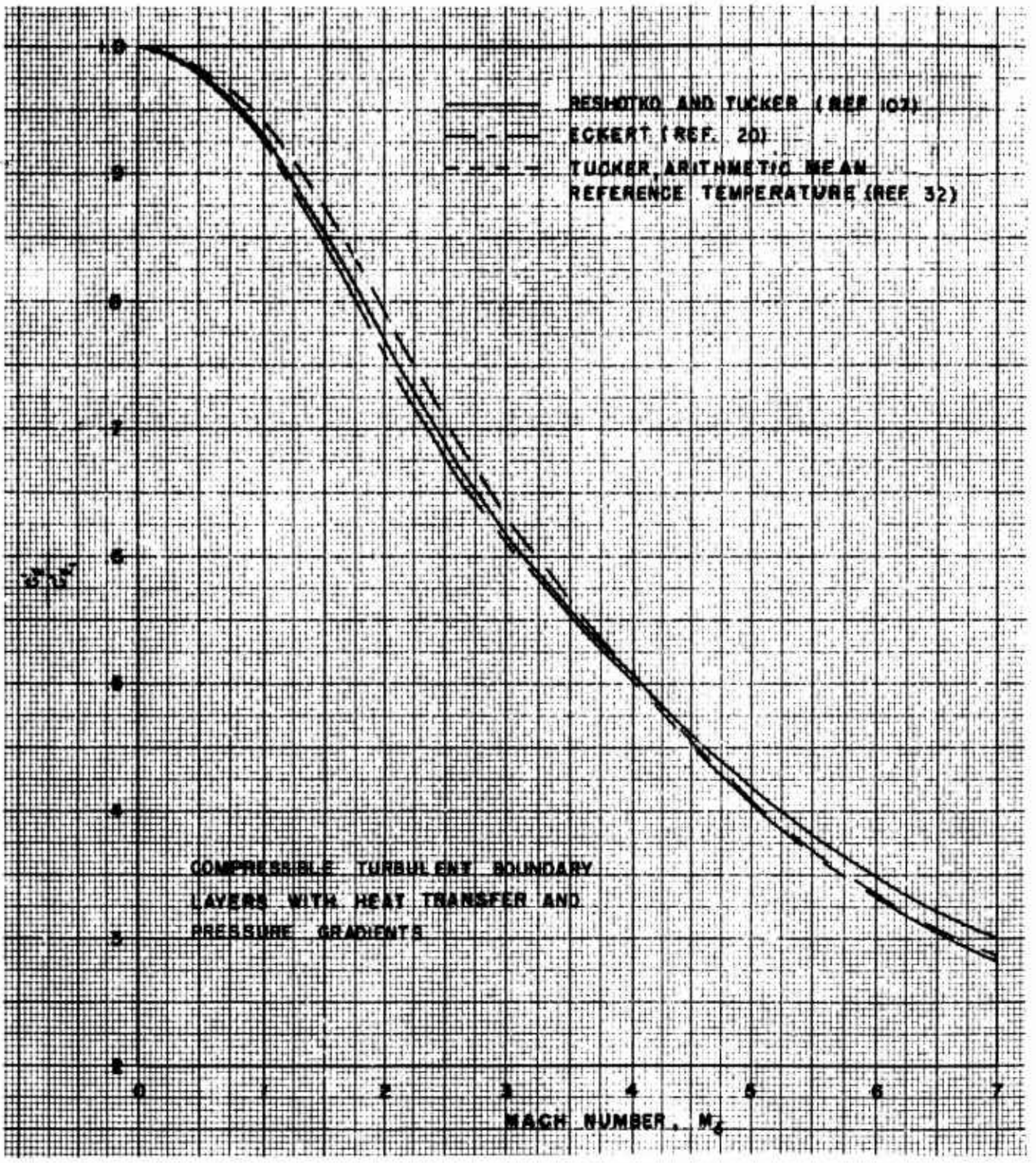

Fig (2.3-31) Skin-friction coefficient variation with Mach Number, comparative curves from Ref 20, 32, and 107.

cal relationship by which the heat transfer on a cone can be found, if the corresponding flat plate results are known for laminar boundary layers. In Ref. 113 (Scherrer), the applicability of available theoretical results of recovery factor and heat transfer parameters to smooth bodies of revolution and cones for both laminar and turbulent boundary layers is investigated. Respective experimental tests were conducted, with general conclusions indicating that:

- By adding heat to a laminar boundary layer, an earlier transition to turbulent boundary layer is promoted, and vice versa, by cooling laminar boundary layers the transition is delayed, although in a lesser degree than the theoretical results of Lees(118) would indicate.

- By using the theoretical recovery factors for laminar and turbulent boundary layers respectively, together with the local Mach Number values outside the boundary layers, the recovery temperature on cones in a negative pressure-gradient region on bodies of revolution can be computed with satisfactory accuracy.

- The theoretical heat-transfer parameters for laminar boundary layers on flat plates for uniform surface temperatures as computed by Rubesin(25), are found to be in good agreement for both heated and cooled bodies of revolution. For nonuniform surface temperatures, the laminar boundary layer values of heat transfer by Kalikhman(115) and Scherrer(113) are found in a good agreement with experiments, provided an exact analytical expression for the experimental surface temperature distribution is formulated.

(6) A comparative table of the compressible turbulent boundary layer cone-plate results from a few references is cited below:

$$\frac{C_f' \text{ cone}}{C_f' \text{ flat plate}} =$$

Reshotko & Tucker(107)	Gazley(119)	Van Driest(120)
= 1.192	= 1.176	= 1.150

$$\frac{St' \text{ cone}}{St' \text{ flat plate}} =$$

Reshotko & Tucker(107)	Gazley(119)	Van Driest(120)
= 1.192	= 1.176	= 1.150

(7) A correlation of the local and the total skin friction coefficients for cones (axisymmetric flow) and flat plates for laminar compressible boundary layers is given by Kurzweg(22) and Mangler(117):

$$C'_{f\,CONE} = \sqrt{3}\, C'_{f\,FLAT\ PLATE},$$
$$St'_{CONE} = \sqrt{3}\, St'_{FLAT\ PLATE}, \qquad (2.3\text{-}310)$$

$$C_{f\,CONE} = \frac{2}{3}\sqrt{3}\, C_{f\,FLAT\ PLATE}. \qquad (2.3\text{-}311)$$

Obviously the above relationships are independent of Mach Number, since for both flat plates and cones there is no pressure gradient variation and consequently no Mach Number changes along the surfaces, provided they are smooth and insulated (i.e., without extensive longitudinal skin-temperature variations).

(8) The three-dimensional turbulent compressible boundary layer effects for some specified body shapes can be expressed (for engineering purposes) through respective corrective factors applied to the corresponding two-dimensional flat plate values of the skin friction and the heat-transfer coefficients as follows (Eckert19):

For a two-dimensional wedge in a supersonic flow perpendicular to the leading edge, the conditions behind the shock correspond to the conditions outside the boundary layer on a flat plate with constant pressure in the flow direction and a corresponding after-shock Mach Number. Therefore, the laws of variation of the skin friction and the heat-transfer remain unchanged, i.e., as estimated for a flat plate, provided the equivalent Mach and Reynolds Numbers are correctly used.

For a cone, (axisymmetric flow): the two-dimensional flat-plate values of the average skin-friction coeffi-

cient in a turbuleny compressible boundary layer should be multiplied by a factor of 1.022, in order to obtain the average skin-friction coefficient value on the conical surface, expressed in terms of the same longitudinal distance (x) and under the same free stream flow conditions outside the boundary layer (∞ or δ) as existing on the equivalent surface flat plate.

For a slender cylindrical body, whose axis is aligned with free stream, and whose radius is large compared with the boundary layer thickness, the skin-friction and the heat-transfer coefficients are nearly equal to their flat-plate values for equivalent free stream Mach and Reynolds Numbers. No correction for three-dimensional effects is necessary. For extremely slender cylinders ($L/D > 30$), the boundary thickness becomes comparable with the cylinder radius, and appreciable departures from flat plate friction values occur, see Jakob and Dow[121] and Eckert[122].

For surfaces with small curvatures (not exceeding 5%), the pressure gradient effects on the final average skin friction coefficient values are negligible. The proper equivalent Mach and Reynolds Number values should be used in evaluating C_f and S_t from the flat-plate curves.

2.3.5 SURFACE ROUGHNESS EFFECTS

It is considered convenient to examine the surface roughness effects separately, since the available literature related to the problem, especially to high speed flows, is very scarce.

(i) The low-speed, incompressible case has been investigated at a length by Nikuradse(82), Clauser(123), Hama (124), Prandtl and Schlichting(125), etc.

The most extensive experimental investigation has been done by Nikuradse(82). Using these systematic data, the respective resistance charts were developed by Prandtl and Schlichting (125). A good summary of the present state of knowledge of the roughness effects on turbulent boundary layers at low speeds can be found in Ref. 123 (Clauser).

(ii) The most extensive and systematic set of data for compressible boundary layers flows over rough surfaces is presented by Goddard(126). The measurements of skin-friction coefficients were done by Goddard on sand-type roughened bodies of revolution within a Mach Number range from 1.98 to 4.54 and the Reynolds Numbers from 3×10^6 to 8×10^6. The results of the measurements and general analytical conclusions are in good agreement with the corresponding analytical data presented by Clutter(127).

The critical roughness, below which the surface is considered hydraulically smooth, is $k \approx 10\nu / v_*$. It is independent of Mach Number and it is of the same order of magnitude as the laminar sublayer on a smooth surface for both compressible and incompressible flows.

In general, there appears to be no appreciable wave drag component of individual roughness elements. If roughness is small compared with the laminar sublayer thickness, i.e., if it is below the above stated critical value, the turbulent skin-friction coefficient is approximately the same as for smooth walls, and the surface is considered as "hydraulically smooth". When the average height of roughness elements becomes of the same order of magnitude as the laminar sublayer, i.e., when above the critical size value, the skin friction coefficient increases considerably showing a marked departure from the smooth surface law. There is no firm information available regarding the heat transfer on rough surfaces and it may be only assumed that if a Reynolds analogy law, similar to that of the skin-friction coefficient. Since such a Reynolds analogy concept has not been verified, and since the experimental evidence by Granville(128) indicates that measured heat transfer rates are only slightly greater for the highest roughnesses tested (which were greater than critical), it could be approximately accepted that the heat-transfer is not materially affected by roughness of such surfaces.

Very rough surfaces are avoided in fabrication of high speed vehicles, and thus the range of practical interest is narrowed to the types of rough surfaces presented in Table (2.3-2), represented by their corresponding "equivalent" roughness k values.

Thus, for practical aerodynamic purposes, the heating rates on rough surfaces could be predicted about equally well by either the "1954" method of Van Driest(28), or by using the classical von Karman-Schoenherr incompressible relations and substituting in the gas properties as evaluated at the "reference" T′ temperature (Eckert19):

$$T' = T_\delta + .5(T_w - T_\delta) + .22(T_r - T_\delta), \quad T_r = T_{ow}. \tag{2.3-311}$$

Both methods seem to overestimate the turbulent heat rates to some degree.

(iii) Extensive working charts for direct engineering use have been developed by Clutter(127), including the roughness and the heat transfer effects on the skin friction coefficient for both laminar and turbulent compressible boundary layers over two-dimensional plates up to Mach Number of 5. Since the data from the Ref. 127 have been partially used in the proposed methods for the skin-friction estimates of this Report, it is considered necessary to present a brief discussion of the material.

The basic Nikuradze-Prandtl-Schlichting data of the incompressible skin-friction coefficient variations with Reynolds Number and surface roughness have been extended(127) to compressible laminar and turbulent flows

TABLE (2.3-2)

EQUIVALENT SURFACE ROUGHNESS ESTIMATES

Type of surface	Equivalent Sand Roughness k (inches)
Aerodynamically smooth	0
Polished metal or wood	$0.02 - 0.08 \times 10^{-3}$
Natural sheet metal	0.16×10^{-3}
Smooth matte paint, carefully applied	0.25×10^{-3}
Standard camouflage paint, average application	0.40×10^{-3}
Camouflage paint, mass-production spray	1.20×10^{-3}
Dip-galvanized metal surface	6×10^{-3}
Natural surface of cast iron	10×10^{-3}

(From Ref. 38)

with heat transfer.

The range of variation of the main flow parameters is:

(1) $0 \leq M \leq 5.0$,

(2) $10^5 \leq Re_L \leq 10^9$,

(3) $(T_w/T_\delta) = 1$ and $(T_w/T_{ow}) = 1$, denoting the thermal equilibrium and the insulated wall cases respectively, as two plausible actual flight extremes (see Figs (2.3-32), (2.3-33), (2.3-36) and (2.3-37).

(4) The location of the transition from laminar to turbulent boundary layer ranges from zero (fully turbulent boundary layer) to 50 per cent of body length.

The total skin-friction coefficient values as functions of Reynolds and Mach Numbers are graphically presented on Figures 1 to 10 in the Reference[127] for sand-roughened insulated and thermally in equilibrium ($T_w = T_\delta$) flat plates respectively, with various transition locations (from 0 to 50 percent of the flat plate length).

The local skin friction coefficient values for a sand-roughened flat plate with a wall temperature equal to the free stream temperature ($T_w = T_\delta$) are presented in the Fig. 11 of the Ref. 127 for the cited range of Reynolds and Mach Numbers.

The variations of the ratio of the compressible-to-incompressible values of skin friction coefficients (C_f / C_{fi}) for the "smooth" turbulent, the fully rough turbulent and the laminar types of flows on an insulated flat plate are presented in Fig. 12 of the Ref. 127 for the cited range of Mach and Reynolds Numbers.

The Mach Number variations of the ratio of compressible-to-incompressible values of skin-friction coefficients (C_f / C_{fi}) of an insulated flat plate are presented in Fig. 13 of the Ref. 127 for:

$$\frac{k v_*}{\nu_w} = 7.95 \text{ and } \frac{k v_*}{\nu_w} = 14.46 \ . \qquad (2.3\text{-}312)$$

The Mach Number variations of the ratio of compressible-to-incompressible values of skin-friction coefficients (C_f / C_{fi}) for laminar flows with and without heat transfer are presented in Fig. 14 of the Ref. 127.

Note: In all the presented cases (C_f / C_{fi}) = (C_f' / C_{fi}'), i.e., the total and the local compressible and incompressible skin friction coefficient ratios are equal, respectively.

Discussion of Applicability of the Graphs From the Reference 127 for Direct Design Purposes

For evenly distributed sand-roughness type surfaces the average individual height of the roughness elements promotes three basic types of boundary layer flows:

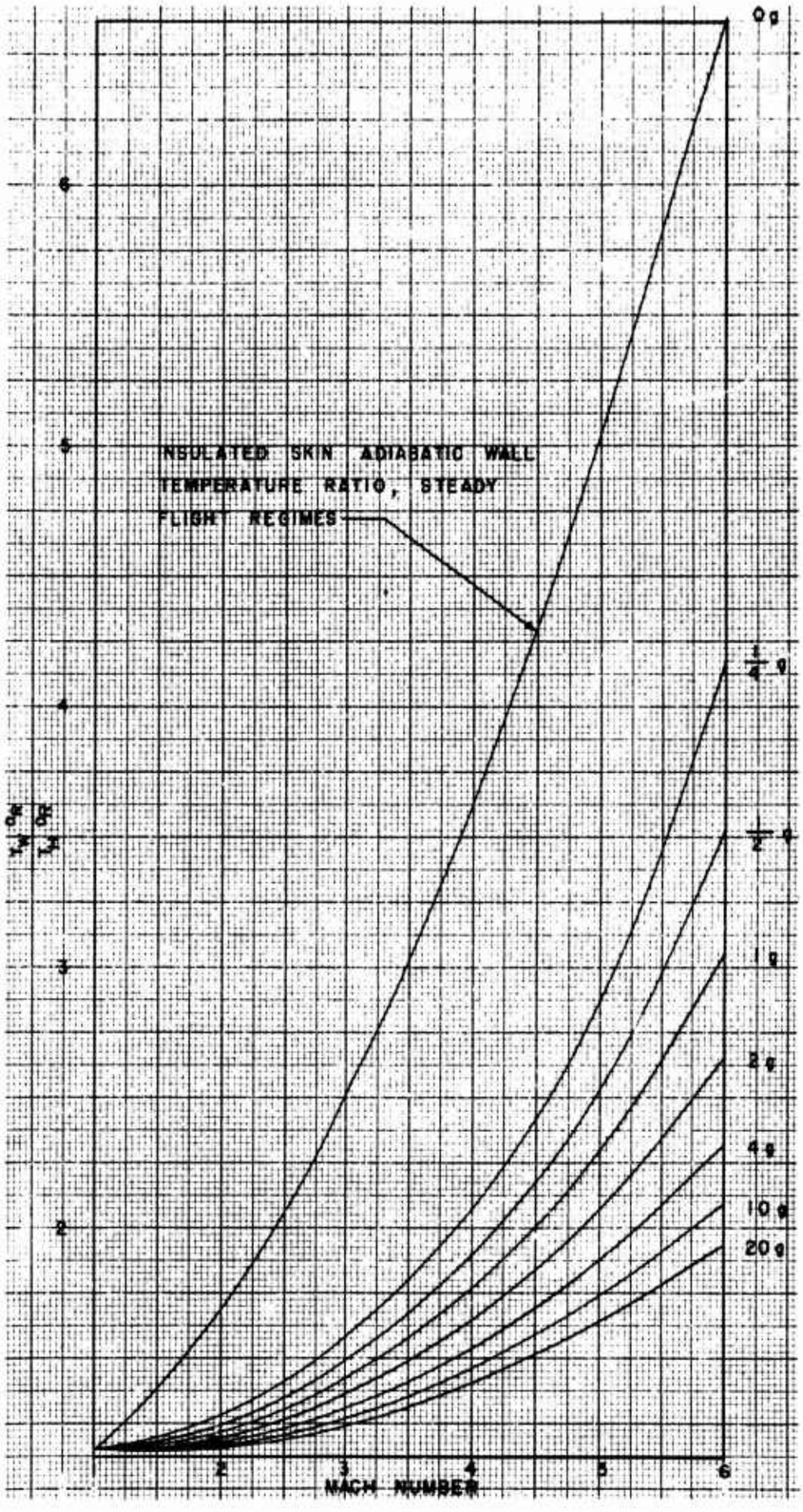

Fig (2.3-32) Skin-to-free stream temperature ratio in accelerated flight regime, sea level conditions. (Ref. 70)

Alternate Fig. (2.3-50)

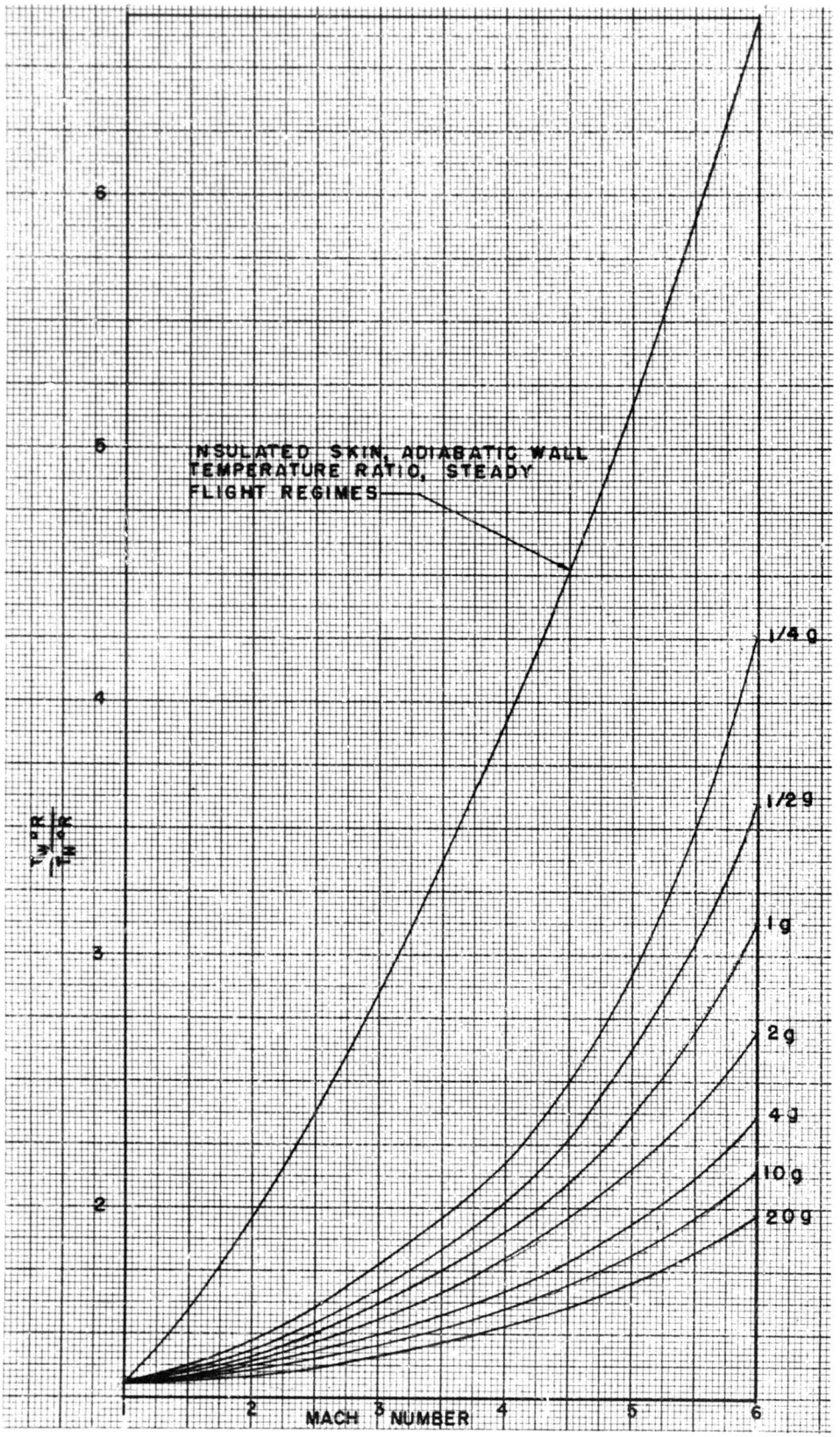

Fig (2.3-33) Skin-to-free stream temperature ratio in accelerated flight regime, isothermal altitudes. (Ref 70)

Alternate Fig. (2.3-51)

(1) Hydraulically Smooth Flow, existing when the roughness-element sizes are so small that the variation of the skin friction coefficient with Reynolds Number is the same as for an idealized smooth plate. This holds up to a certain critical Reynolds Number, which is a function of the roughness height. The hydraulically smooth flow is also called "sub-critical" (Prandtl).

(2) Transitional Region, the roughness element sizes are great enough to promote an increase of the skin function coefficient value above that of an ideal smooth plate, but the roughness element individual force drag is not yet an all-governing factor, i.e., there is still a classical functional relationship between the skin friction coefficient and Reynolds Number, only additionally affected by the roughness-elements sizes. This transitional region is in existence between the sub-critical (hydraulically smooth) and the fully rough types of boundary layer flows.

(3) Fully Rough Flow is established when the roughness element sizes are great enough to become a predominent factor. Both for the compressible (Goddard) and the incompressible (Prandtl-Schlichting-Nikuradse) fully rough flows of uniformly distributed sand-roughness type, the skin friction drag is a sum of the flow drags of the individual roughness elements, and there is no functional variation of C_f with Reynolds Number. The last feature is actually the basic criteria for the definition of a fully rough flow.

The experimental results for both hydraulically smooth and fully rough flows agree well with various semi-analytical investigations (Prandtl, Schiditing, Niknradse, Goddard). But in case of the transitional type of flow, the disagreement among various experimental and analytical results is of the order of 10% in C_f, mostly due to the fact that in any practical application the actual roughness size hardly could be estimated with a greater accuracy.

In preparing the graphs(127), the incompressible turbulent flow results for rough plates as theoretically formulated by Prandtl and Schlichting(83) supported by experimental investigations of flows in sand-roughened pipes by Niknradse(82), are used as a case. The subsequent corrections for variation of the skin-friction coefficients with the Reynolds Number, the Mach Number, the degree of roughness, the wall-to-free-stream temperature, and the location of the laminar-turbulent transition point are effected in accordance with the scheme presented in Table (2.3-3).

The procedure used in calculating the skin friction coefficient for turbulent boundary layers in accordance with the cited analytical expressions in Table (2.3-3) is as follows:

(a) Incompressible Turbulent Flows Over Rough, Insulated Flat Plates.

The Prandtl and Schlichiting(83) theories defining C_{fi} and C_{fi}' as functions of a turbulent velocity profile,

$$\frac{U}{V_*} = A \log_e \frac{y}{k} + B , \qquad (2.3\text{-}313)$$

are used, with a modified (Schlichitings value of the constant A = 5.85 (Prandtl originally specified A = 5.75), which sould be well representative for a flat plate, and with the constant B evaluated from the Niknradse's pipe tests as a function of kv_*/ν. The results of the calculations are presented in the examplary Fig. (2.3-34) as a cross-plot of the (L/k) and (Uk/ν) curves, respectively. They differ from the original Prandtl-Schlichiting's calculations from 1% to 7%, depending on Re_L and (L/k) values, and by 5% with the results of Ref. 128 (Granville). The full set of figures is given later.

The constant (L/k) curves show the variation of the total incompressible skin friction coefficient C_{fi} with the free stream Reynolds Number Re_L on a flat, sand-roughened insulated plate for given L and k, i.e., having a constant (L/k) ratio, for an entirely turbulent incompressible boundary layer. Such a curve of a constant (L/k) ratio is passing through all the three basic regions of "hydraulically smooth", "transitional" and "fully rough" flow types respectively.

For example, taking a hypothetical case of $(Uk/\nu) = 2 \times 10^2$, and $(L/k) = 1.10^5$, the three flow regimes could be defined from Fig. (2.3-34)

TABLE (2.3-3)

FORMULAE FOR COMPUTATIONS OF C_f AND C_f' IN REF. 127

FLOW CONDITION	FORMULA
$M = 0$ LAMINAR FLOW ZERO HEAT TRANSFER $M \neq 0$	$C_{fi} = 1.328 / \sqrt{Re_L}$ (SCHLICHTING, REF. 83 HOERNER, REF. 21) $\frac{C_f}{C_{fi}} = \frac{C_f'}{C_{fi}'} = \sqrt{\frac{\rho^*}{\rho_\delta}\frac{\mu^*}{\mu_\delta}}$ (ECKERT, REF. 19) The asterisk denotes the properties at Reference temperature. $T^* = 0.5 (T_\delta + T_w) + 0.22\, r \left(\frac{\gamma - 1}{2}\right) M_\delta^2\, T_\delta$
TURBULENT FLOW SMOOTH SURFACES $M = 0$ ZERO HEAT TRANSFER $M \neq 0$ WITH OR WITHOUT HEAT TRANSFER	$C_{fi} = \frac{0.455}{(\log Re_L)^{2.58}}$ (PRANDTL); $C_{fi} = (2 \log Re_L - 0.65)^{-2.3}$ (VAN DRIEST REF. 28): $\frac{0.242}{(C_f \frac{\gamma-1}{2} M^2)^{1/2}} (\sin^{-1}\alpha + \sin^{-1}\beta) = \log (Re_x \cdot C_f) - \omega \log \frac{T_w}{T_\delta}$ AND $\frac{0.242}{(C_f' \frac{\gamma-1}{2} M^2)^{1/2}} (\sin^{-1}\alpha + \sin^{-1}\beta) = 0.4 + \log (Re_x \cdot C_f') - \log \frac{T_w}{T_\delta}$ $\alpha = (2A^2 - B) / (B^2 + 4A^2)^{1/2}$ $\beta = B / (B^2 + 4A^2)^{1/2}$ $A^2 = \left(\frac{\gamma-1}{2} M^2\right) / \left(\frac{T_w}{T_\delta}\right)$ $B = \left[\left(1 + \frac{\gamma-1}{2} M^2\right) / \left(\frac{T_w}{T_\delta}\right)\right] - 1$
TURBULENT FLOW ROUGH SURFACE $M = 0$ ZERO HEAT TRANSFER $M \neq 0$ WITH OR WITHOUT HEAT TRANSFER	C_{fi} AND C_{fi}' ARE DETERMINED FROM RELATIONS FOR u/v_* BY METHOD OF PRANDTL AND SCHLICHTING (REF. 83) $u/v_* = A \log y/k + B$ WHERE A = 5.85 AND B IS A FUNCTION OF kv_*/ν GIVEN IN TABLE (2.3-2) $\frac{C_f}{C_{fi}} = \frac{\rho_w}{\rho_\delta} = \frac{T_\delta}{T_w}$ (GODDARD, REF. 127)

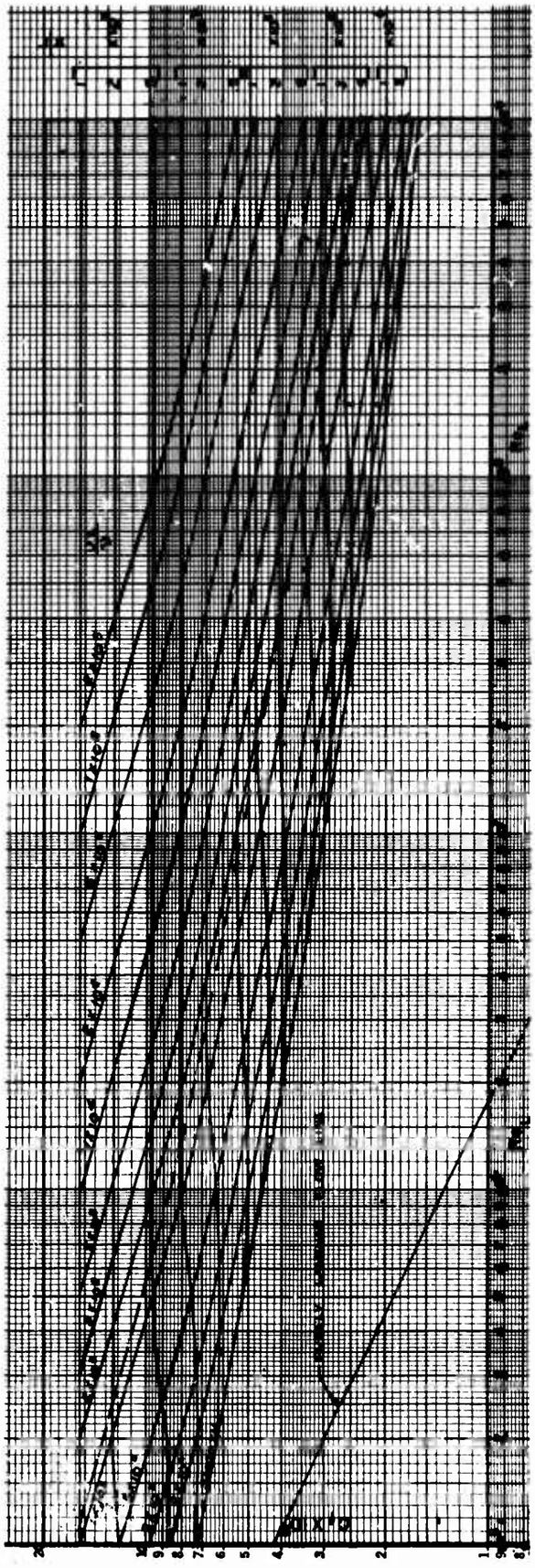

Fig (2.3-34) Total skin-friction for a sand-roughened insulated plate. M = 0. Transition at the leading edge. (Ref 127)

Alternate Fig.(2.3-44a)

"hydraulically smooth" pattern of flow for $10^5 < Re_L < 1.2 \times 10^7$,

"transitional" pattern of flow for $1.2 \times 10^7 < Re_L < 2 \times 10^8$,

"fully rough" pattern of flow for $2 \times 10^8 < Re_L$.

The region above the dashed line in Fig (2.3-34) represents a fully rough turbulent boundary layer flow.

The constant (Uk/ν) curves show the variation in C_{fi} with Reynolds Number Re_L under the same conditions for constant free stream velocity U and constant roughness height k, i.e., with the plate length L as a variable parameter.

Note: In case of a flat plate without pressure gradient at a zero-angle-of-attack, the free stream velocity at the outer edge of the boundary layer (U) is numerically equal to the free stream velocity at infinity, (V_H).

In order to use the Fig (2.3-34), an "equivalent sand roughness", approximating the actual surface conditions has to be defined for each particular design case by choosing the respective value for k from Table (2.3-2).

The "equivalent sand roughness" is specified as that value of k (from the Niknradse's original sand-rough experiments) that gives the same skin-friction coefficient as the actual surface-condition does in reality. These "equivalent sand-roughness" values of k, as related to various types of engineering rough surfaces, were calculated by Schlichiting and Hoerner.

When using the families of curves (Uk/ν) and (L/k) in the examplary Fig (2.3-34), the following procedure should be taken:

For a given free stream speed, U, altitude, H, flat plate length, L, and the equivalent sand roughness, k, (Table 2.3-2), find the values (Uk/ν) and (L/k). Draw interpolation curves $Uk/\nu = f_1(Re_L)$ and $L/k = f_2(Re_L)$, up to their mutual point of intersection, thus defining possible hydraulically smooth, transitional and fully rough turbulent flow regions for the investigated case. Calculate the corresponding value of the free stream Reynolds Number, Re_L, and read off from the combined interpolated curves of the (Uk/ν) and (L/k) the corresponding value of the total skin-friction coefficient, C_{fi}. Depending upon the actual case, the defined average flow condition will fall into one of the three possible flow regions ("hydraulically smooth", "transitional" or "fully rough") taken as prevailing.

(b) Compressible Turbulent Boundary Layers Over Rough, Insulated Flat Plates.

The compressibility effects on the total skin-friction coefficient are computed as indicated in Table (2.3-3) by using the following expressions:

$$\frac{.242}{C_f^{1/2}\left(\frac{\gamma-1}{2}M^2\right)^{1/2}}\left(\sin^{-1}\alpha + \sin^{-1}\beta\right) = .041 + \log(Re_L C_f) - \omega \log(T_W/T_\delta),$$

$$\alpha = (2A^2 - B)/(B^2 + 4A^2)^{1/2},$$

$$\beta = B/(B^2 + 4A^2)^{1/2},$$

$$A^2 = \left(\frac{\gamma-1}{2}M^2\right)/(T_W/T_\delta),$$

$$B = \left[\left(1 + \frac{\gamma-1}{2}M^2\right)/(T_W/T_\delta)\right] - 1,$$

$\omega = .76$ (von Karman's mixing law, method "1954").

(2.3-314)

By using the Van Driest's expression for fully turbulent boundary layers on smooth plates with or without heat transfer, and

$$\left(\frac{C_f}{C_{fi}}\right) = \frac{\rho_W}{\rho_\delta} = \frac{T_\delta}{T_W} = \frac{1}{\left(1 + r\frac{\gamma-1}{2}M^2\right)},$$

$r = .86$,

(2.3-315)

i.e., by using the Goddard's expression for fully rough plates, with or without heat transfer.

The laminar boundary layer case is not interpreted here, since for the engineering analysis purposes, it is assumed that the boundary layer flow over rough surfaces can be practically treated as fully turbulent, without introducing an appreciable error. Reasons and arguments supporting such an engineering approach are treated elsewhere; the conclusion which may be drawn for practical purposes is that the transition should be expected to occur at approximately 10% of body length (i.e., $X/L \sim .1$) under fairly low Reynolds Numbers, ($Re < 10^6$).

The results of calculations for com-

pletely turbulent boundary layers over insulated smooth plated and for fully rough insulated flows are presented in the examplary Fig. (2.3-35) as (C_f / C_{fi}) ratios plotted against M , and with Re_L as a parameter. The corresponding C_{fi} values should be obtained first from Fig (2.3-34).

For "transitional" rough flows an approximate expression, based on data by Goddard(126) and Nikuradze(82) is developed, yielding for an insulated rough plate:

$$\left(\frac{C_f}{C_{fi}}\right) = \left(\frac{C_f}{C_{fi}}\right)_s - \frac{\log_e\left(\frac{k v_*}{\nu_w}\right) - \log_e 4}{\log_e 75.9 - \log_e 4} \times$$

$$\times \left[\left(\frac{C_f}{C_{fi}}\right)_s - \left(\frac{C_f}{C_{fi}}\right)_{f.r.}\right] , \qquad (2.3\text{-}316)$$

where the subscripts ($_s$) and ($_{f.r.}$) denote the values at the limits of a smooth and a fully rough turbulent flow respectively. For the estimates of the ratio of the total skin friction coefficients (C_f / C_{fi}) , it was necessary to know the values of the parameter ($k v_* / \nu$) , which, in itself, is a function of the local skin friction coefficient:

$$C_f' = \frac{\tau_w}{\rho U_\delta^2/2} = \frac{v_*^2}{1/2\ U_\delta^2} . \qquad (2.3\text{-}317)$$

Combining the values of C_{fi} from Fig (2.3-34) with the corresponding data by Prandtl-Schlichting(83) and Fentor(129) for the C_f and C_{fi} variations with ($k v_* / \nu_w$) , and using the data from Fig 13a and 13b of the basic Ref. 127, which give variations of (C_f / C_{fi}) with Mach and Reynolds Numbers for the limiting values of ($k v_* / \nu_w$) = 7.95 (lower region of "transitional" flow), and ($k v_* / \nu_w$) = 14.46 (upper region of "transitional" flow), the variation of the total compressible skin-friction coefficient for "transitional" and "fully rough" turbulent boundary layers without heat transfer has been calculated in the basic Ref. 127 (Clutter) as a function of Mach Number, Reynolds Number, (L / k) and (Uk/ν) . The results are presented later in the respective working figures at the end of this section. The use of these graphs is the same as indicated earlier for the examplary figure (2.3-34).

(c) Compressible Turbulent Flows With Heat Transfer

In the basic Ref. 127 (Clutter), when calculating the heat transfer effects for "fully rough" flows, the local Stanton Number St' dependence on Reynolds analogy factor, S , and the local skin-friction coefficient C_f' are taken as being the same as for turbulent smooth flows, i.e.,

$$St' = \frac{1}{S}\left(\frac{C_f'}{2}\right) , \qquad (2.3\text{-}318)$$

$$S \approx .825 \quad \text{for} \quad 0 < M < 5 .$$

Although insufficient, the data from Refs. 130 (Nunner) and 131 (Bartz) indicate that this is not a good approximation, since it appears that the Reynolds analogy factor, S , changes significantly both with Pr^* and Re_x^* for fully rough flows.

The use of the charts (at the end of the section) is done in the same way as described for the examplary Fig (2.3-34).

Order of Accuracy of the C_f Estimates in Ref. 127 (Clutter)

The presented values of the average (C_f) and the local (C_f') skin-friction coefficients for the laminar and for the smooth turbulent flows with heat transfer agree with respective experimental data with ± 5%. For fully rough flows, the expected accuracy of the values in with ± 15% for no heat transfer. There is no reliable comparative experimental data for rough-plate flows with heat transfer.

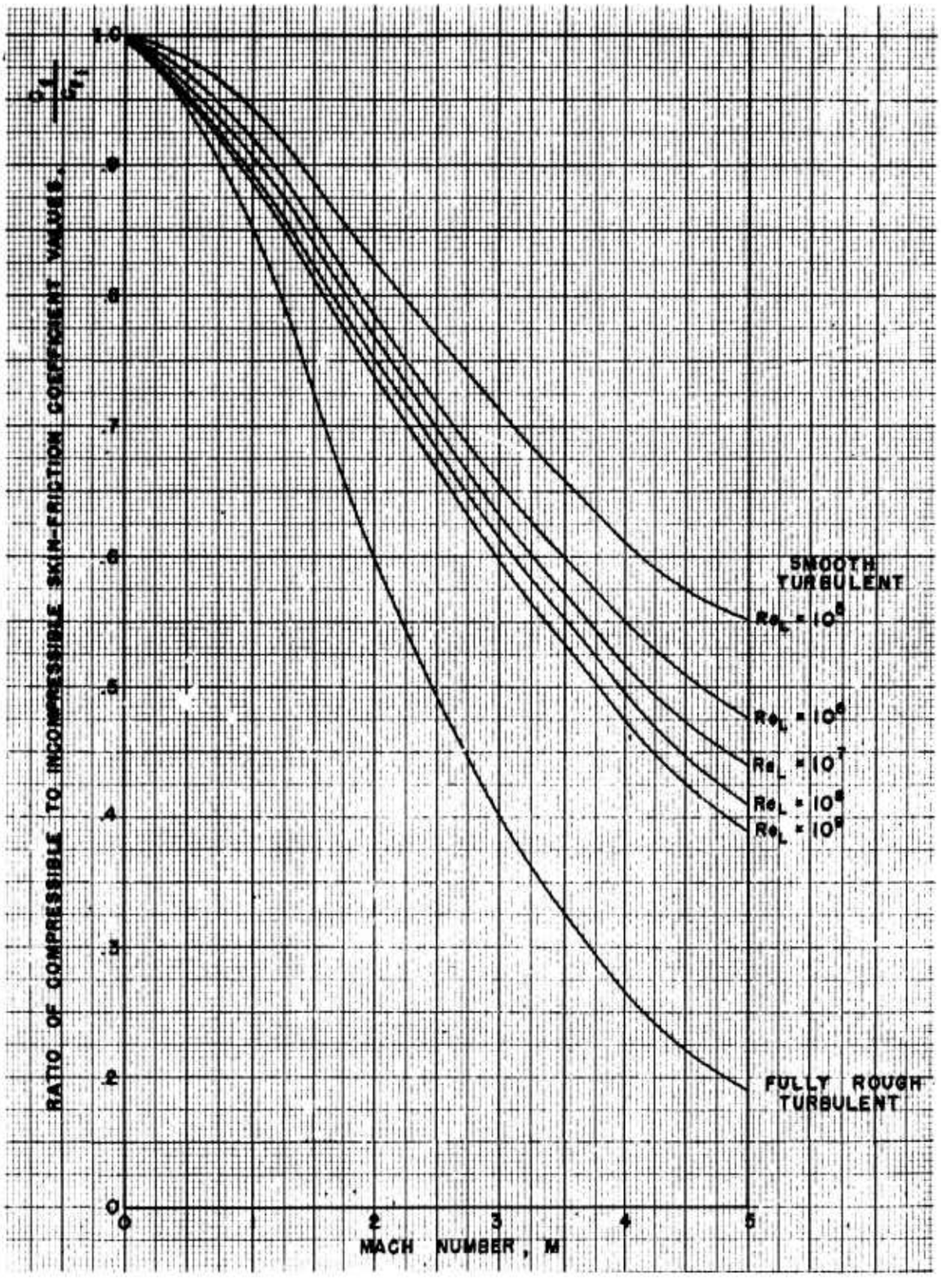

Fig(2.3-35) Mach Number variation of the ratio of the compressible to incompressible values of skin-friction coefficient for the various types of flow on an insulated plate. (Ref 127)

Alternate Fig. (2.3-47)

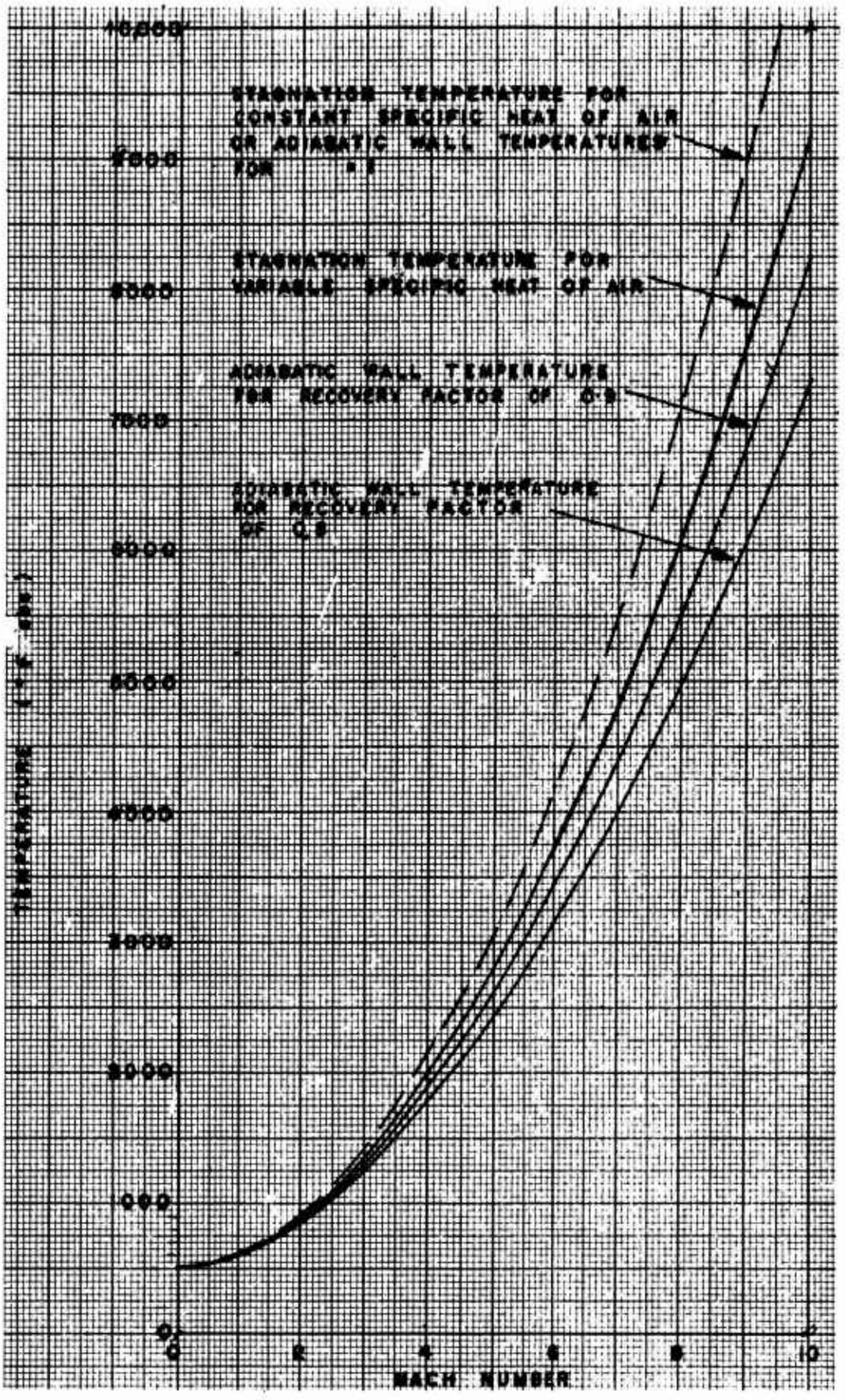

Fig(2.3-36) Stagnation and adiabatic wall temperatures for flight at constant speed in air at sea level. (Ref. 70)

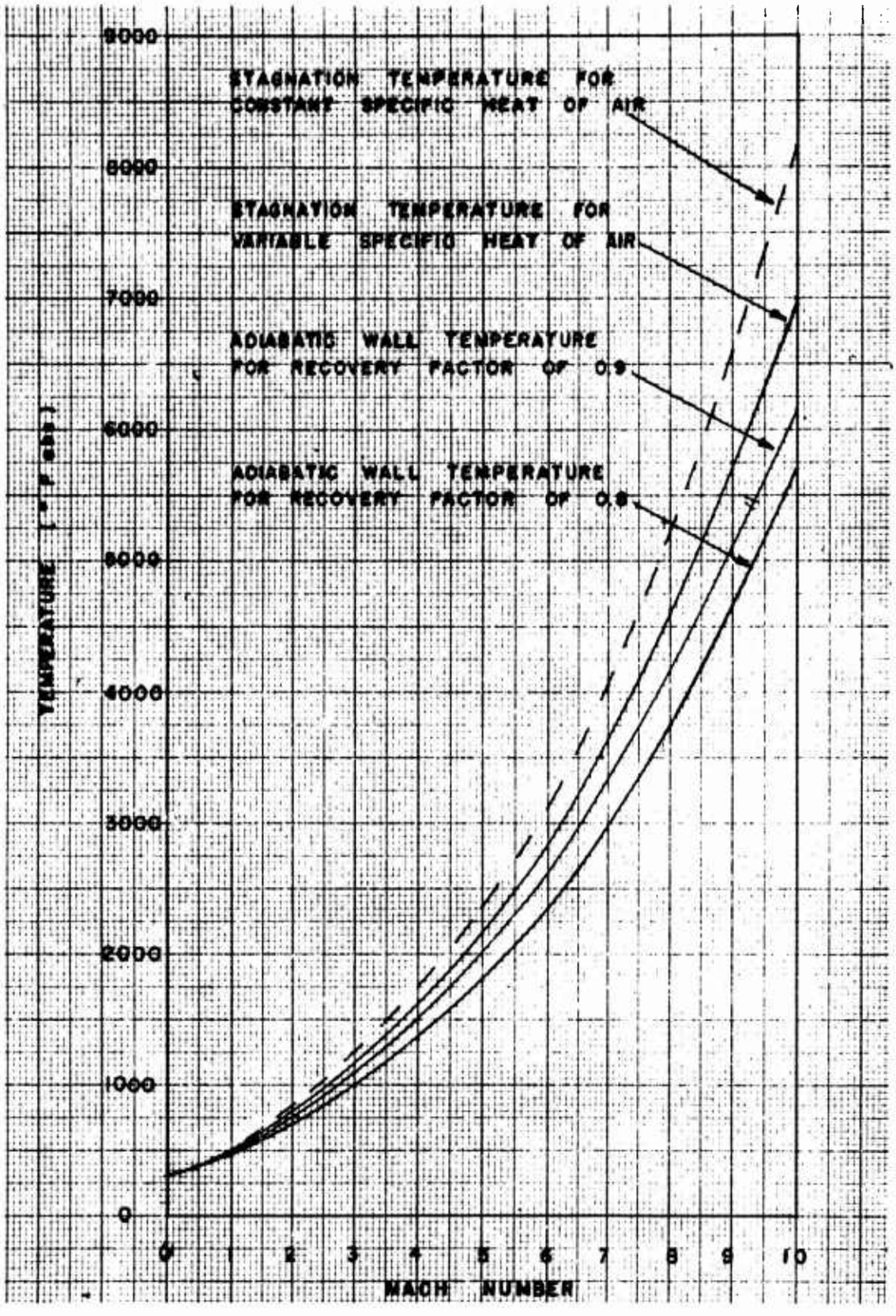

Fig (2.3-37) Stagnation and adiabatic wall temperatures for flight at constant speed in air from 35,000 to 105,000 feet. (Ref 70)

2.3.6 SKIN FRICTION DRAG COEFFICIENT - DEFINITIONS AND EXPRESSIONS USED IN THE PRESENTED METHODS OF ESTIMATES

In accordance with the conventions and limitations presented in Sections 1.6.4, 1.6.5, 1.7.3 and 1.7.4, the following summary skin-friction drag force coefficient expressions and definitions are adopted:

(i) Average Skin-friction Drag Coefficient - Basic Definition

$$C_{Dof} = \frac{Dof}{\frac{1}{2}\rho_A V_A^2 S_{REF}} = \frac{Dof}{q_A S_{REF}} = \frac{Dof}{\frac{1}{2}p_A \gamma_A M_A^2} , \tag{2.3-319}$$

$$Dof = \int_{S_{WET}} \tau_w (\vec{i} \cdot \vec{i}_a)\, dS = \int_{S_{WET}} \tau_w \cos(\vec{i}, \vec{i}_a)\, dS , \tag{2.3-320}$$

$$\therefore C_{Dof} = \frac{\int_{S_{WET}} \tau_w \cos(\vec{i}, \vec{i}_a)\, dS}{q_A S_{REF}} \tag{2.3-321}$$

(ii) Average Skin-friction Drag Coefficient in Terms of the Local (Superscript ′) and the Average Skin Friction Coefficient Definitions

$$C_f' = \left(\frac{\tau_w}{q}\right)\left(\frac{q}{q_A}\right) = \frac{\tau_w}{q_A} , \tag{2.3-322}$$

$$C_f = \frac{\int_{S_{WET}} \tau_w \cos(\vec{i} \cdot \vec{i}_a)\, dS}{q_A S_{WET}} = \frac{1}{S_{WET}} \int_{S_{WET}} C_f' \cos(\vec{i} \cdot \vec{i}_a)\, dS , \tag{2.3-323}$$

$$\therefore C_{Dof} = \frac{1}{S_{REF}} \int_{S_{WET}} C_f'\, dS = \frac{S_{WET}}{S_{REF}} C_f . \tag{2.3-324}$$

(iii) Average Skin-friction Drag Coefficient - Adopted Decomposition Scheme (Section 1.7.4):

$$C_{Dof} = C_{Dof_B} + C_{Dof_W} + C_{Dof_F} + C_{Dof_{PARTS}} , \tag{2.3-325}$$

$$C_{Dof_B} = C_{Dof_N} + C_{Dof_{CYL+BT}} = \frac{1}{S_{REF}} \left[\int_{S_{WET}} C_{f_N}' (\vec{i}_N \cdot \vec{i}_a)\, dS + \int_{S_{WET}} C_{f_{CYL+BT}}' (\vec{i}_{CYL+BT} \cdot \vec{i}_a)\, dS \right] ,$$

$$= \frac{1}{S_{REF}} \left[(S_{WET})_N C_{f_N} + (S_{WET})_{CYL+BT} C_{f_{CYL+BT}} \right] , \tag{2.3-326}$$

$$C_{Dof_W} = C_{Dof_{WEXP}} = \frac{1}{S_{REF}} \int_{S_{WET}} C_{f_W}' (\vec{i}_w \cdot \vec{i}_a)\, dS ,$$

$$= \frac{1}{S_{REF}} \left[(S_{WET})_{WEXP} C_{f_{WEXP}} \right] , \tag{2.3-327}$$

$$C_{Dof_F} = C_{Dof_{FEXP}} = \frac{1}{S_{REF}} \int_{S_{WET}} C_{f_F}' (\vec{i}_f \cdot \vec{i}_a)\, dS ,$$

$$= \frac{1}{S_{REF}} \left[(S_{WET})_{FEXP} C_{f_{FEXP}} \right] , \tag{2.3-328}$$

$$C_{Dof_{PARTS}} = \frac{1}{S_{REF}} \int_{S_{WET}} C_{f_{PARTS}}' (\vec{i}_F \cdot \vec{i}_a)\, dS ,$$

$$= \frac{1}{S_{REF}} (S_{WET})_{PARTS} C_{f_{PARTS}} , \tag{2.3-329}$$

$$\therefore C_{Dof} = C_{f_N} \frac{(S_{WET})_N}{S_{REF}} + C_{f_{CYL+BT}} \frac{(S_{WET})_{CYL+BT}}{S_{REF}} + \frac{(S_{WET})_{WEXP}}{S_{REF}} C_{f_{WEXP}} + \frac{(S_{WET})_{FEXP}}{S_{REF}} C_{f_{FEXP}} + \frac{(S_{WET})_{PARTS}}{S_{REF}} C_{f_{PARTS}} . \tag{2.3-330}$$

(iv) Average Skin-friction Coefficient - Functional Dependence

For any "i-th" part of a given vehicle configuration, the adopted convention for the skin friction drag coefficient and the skin-friction coefficient functional dependence on the flight speed and the flow type regimes:

$$(C_{Dof})_i = f_1\left[M_A, Re_A, Kn, H\right] , \qquad (2.3\text{-}331)$$

$$C_{f_i}' = f_2(q_A, M, Re, Kn, \gamma, Pr, St, \ldots\ldots) , \qquad (2.3\text{-}332)$$

i.e., the final average $(C_{Dof})_i$ results are interpreted in terms of the ambient flight reference variables (M_A, Re_A, Kn, H), while the actual computations of the local values of C_{f_i} are referred to all the influential viscous airflow variables evaluated locally (except for q_A).

(v) General Note

Symbols, subscripts and definitions relating to the expressions (2.3-1) through (2.3-14) are given in Sections (1.6.4), (1.6.5), (1.7.3) and (1.7.4), except for the superscript (′) which is here introduced to denote the local skin-friction coefficient (C_f') values.

The above expressions are applicable to the symmetric "vertical plane" flight conditions exclusively (see Section 1.6.5). Since the skin Friction drag variations with the aerodynamic angle-of-attack α_a are assumed negligible, the subscript (α) is deleted: the zero-lift skin-friction drag coefficient estimates ($\alpha_a = 0$) are assumed, in a first approximation, valid for the $\alpha_a \neq 0$ case also.

In the adopted definition for C_f', Eq (2.3-4), the local skin friction coefficient value is reduced to the reference ambient dynamic pressure, q_A . In some theoretical analysis, the local skin friction coefficient, C_f' , is instead directly referred to the local values of the shear stress at the wall, τ_w , and the local dynamic pressure, q , at the outer edge of the boundary layer. In such cases the necessary conversion is:

$$C_f' = C_{f_{local}}\left(\frac{q}{q_A}\right) = \frac{\tau_w}{q_A} , \qquad C_{f_{local}} = \frac{\tau_w}{q} . \qquad (2.3\text{-}333)$$

In the expression (2.2-15) the shear stress at the wall, τ_w , represents, in general, the average local value across the respective boundary layer section.

In the further text, the subscripts (A) and (H), referring to the ambient and flight altitude conditions shall be used interchangeably, while the subscript (∞) may refer either to the same (A) or (H) conditions "at infinity" well ahead of vehicle, or to the local free stream conditions at the outer edge of the boundary layer, when it becomes interchangeable with subscript $(_\delta)$. The inconvenience is due to differences existing in presentation of data in different theories; in each instance, the distinction shall be stressed.

2.3.7 ASSUMPTIONS AND LIMITATIONS ADOPTED IN EVALUATING SKIN-FRICTION

Note: All graphs are compiled at the end of the Section,2.3.

A quantative estimate of the skin-friction coefficient for missile design purposes proves to be a complex task. It involves a number of physical variables and conditions, which should be well representative of the actual flight conditions. In general, the skin-friction is dependent on the boundary layer properties and its time history, the body geometry and the flight regime.

The general limitations of the present analysis are specified in Section 1.2. In this section only the zero-lift drag values for rigid bodies are investigated, the angle-of-attack, aeroelastic, and eventual flow separation effects are not considered. The few most important criteria in the skin-friction estimates are:

(i) Type of the boundary layer flow: laminar, transitional, or turbulent.

(ii) Flow dimensionality: two-dimensional, axially symmetric, or a specific three dimensional.

(iii) Location of the transition point.

(iv) Body shape and surface curvature.

(v) Mach Number.

(vi) Reynolds Number.

(vii) Pressure gradients in the flow direction.

(viii) Surface roughness.

(ix) Heat transfer rates and the respective heat transfer parameters, i.e., heating or cooling of body.

(x) Surface-skin material properites.

(xi) Flight acceleration rates, influencing all time histories, and the surface temperature conditions in particular.

(xii) Changes in flight altitudes.

(xiii) Interference effects.

(xiv) Sound and noise levels.

(xv) Aeroelastic and Vibration phenomena.

Obviously, it is not possible to account for all of the multitude of factors; therefore, a reasonable selection of the relatively most significant among them has to be performed in such a way that an acceptable engineering estimate of C_f is obtained in terms of the desired order-of-accuracy.

(i) Choice of the Boundary Layer Type

The boundary layer status, i.e., the location of the transition point from laminar to turbulent boundary layer type, is a complex function of many external flow and body geometry parameters. The estimates of the extent and of the relative importance of laminar and turbulent boundary layer portions over given surfaces are mainly functions of three variables: flight altitude, Reynolds Number and Mach Number. A tentative boundary between laminar and turbulent boundary layers is presented in Fig. 1.20 in terms of flight altitude, Mach Number and Reynolds Number. For engineering purposes, two distinct steady flight cases may be readily distinguished: the low altitude ($H>35{,}000$ ft), supersonic regime ($M<5$, $Re>10^6$), with an overwhelmingly pronounced turbulent boundary layer, and the high altitude ($H>80{,}000$ ft), supersonic regime ($M<5$, $Re<10^6$) with an eventually predominant laminar boundary layer. Between the two extremes, a variety of "mixed flow conditions" (partially laminar, partially turbulent) may exist. This represents a considerable complication for a reasonable quick engineering drag estimate. Therefore, when an average drag force evaluation within a reasonable computational time limit is sought, the following procedure is proposed:

(1) For the continuum flow regime and the steady flight speeds where the laminar boundary layer does not comprise more than 10%-20% of the corresponding body length, (calculated for a plausible critical Reynolds Num-

ber of the order of 10^6) a turbulent boundary layer can be considered on all wetted surfaces as an acceptable engineering convenience. This does not imply, necessarily, that the laminar boundary layer is completely non-existent, but rather reflects an approximate evaluation procedure that should yield the conservative average C_f values which are acceptable within the usually uncertain limits of accuracy of the drag-force estimates in general. Taking into account all possible factors in free flight affecting the transition, such as atmospheric turbulence, adverse pressure gradients, surface curvature, surface roughness, surface temperature, local shock and Mach waves, etc., a probable critical Reynolds Number value of the order of 1×10^6 could be expected for normal operational flight conditions and for mass-production manufacturing tollerances. A few factors justifying the proposed relatively low value of Re_{cr} for engineering applications are:

(a) - The laminar flow length represents but a fraction (on the order of 10% in most cases) of the total body length. Also, even the so-called "laminar airfoils" in actual operational flight circumstances do not usually exhibit their "laminar" characteristics, which are obtainable only under very specific and idealized restrictions.

With the usually low aspects-ratio lifting or control surfaces for the semi-ballistic type of missiles, the three-dimensional tip-effects cover a relatively significant portion of the total exposed areas, inducing a flow pattern far from laminar. With the eventual delta or clipped delta planforms, as well as with conventional swept-back configurations, the inevitable spanwise flow-component thickens the boundary layer and through an additional pressure build-up creates conditions unfavorable for a laminar type of flow. The leading-edge local flow separation (bubble) phenomena with a subsequent re-attachment of flow (associated with very thin conventional airfoil shapes) works in the same sense.

(b) - A stronger influence of other factors on C_f, such as skin-temperature conditions at higher Mach Numbers and the relatively low accuracy with which it can be predicted under various flight conditions (especially involving accelerations) renders the "error" in assuming turbulent boundary layer prevailance rather insignificant.

(c) - In presence of atmospheric turbulence and gusts, or in accelerated regimes, which constitute the greater part of a missile flight history, the whole theory of the fundamental steady flow analysis is invalid, and even the mechanical reciprocity principle of relative motions does not hold(3). The "apparent mass" concept, reflecting the acceleration effects on the involved air masses, manifests itself as a corresponding drag increase. The "all turbulent" boundary layer assumption, with its slightly higher drag force value within the steady flow theory, may partially compensate for the actually unsteady flow "apparent mass" drag increaments.

Thus, it follows that the assumption of a turbulent boundary layer is a reasonable engineering proposition for actual atmospheric flight conditions. The evaluation procedure is simplified and the number of graphs reduced without adversely affecting the relatively low accuracy with which the drag force estimates can be performed in general, both theoretically and experimentally.

It should be pointed out, that the above arguments do not invalidate experimentally obtained laminar boundary layers under carefully planned but restricted test-conditions. The proposed method simply reflects, to the best belief and evidence, a practical and acceptable state of affairs under the prevailing atmospheric flight conditions.

(2) For higher altitudes and/or relatively low Re values, a wider extent of the laminar boundary layer may occur, provided the general surface smoothness is well accomplished. The criteria for the existence of the partially or totally established laminar flows may be accomplished through the proposed critical Reynolds Number value of 1×10^6. Evaluations of an average "mixed flow" skin-friction coefficient require then, correspondingly more elaborate expressions which are developed later.

(ii) Flow Dimensionality Effects

The laminar and the turbulent skin-friction coefficients on various missile surfaces (C_{f_N}, $C_{f_{CYL}}$, C_{f_W}, C_{f_F}) can be, in a first approximation, conveniently expressed through their equivalent two-dimensional flat plate values which are multiplied by respective corrective factors, in order

to account for the difference in flow-dimensionality and the pressure gradient variations. The flat, smooth plate data are most abundant for various flow speeds and boundary layer conditions. A more direct method of C_f estimates, pertinent to various geometries and the related flow patterns, can be used alternatively, if the respective data are available.

The equivalent flat plate is defined as having (1) the (one side) area equal to the total wetted area of the comparative body configuration, (2) the flat plate length equal to the wetted length of the comparative body configuration, and (3) the Reynolds Number of the flat plate and the Reynolds Number of the comparative body configuration are referred to the same ambient or free stream conditions far ahead of the body.

The equivalent flat plate corrective factors for principal body geometries are (see Section 2.3.4):

(1) Cones

The three dimensional average skin-friction coefficient on a cone is obtained by multiplying the two-dimensional equivalent flat plate average skin friction coefficient by 1.15 for laminar boundary layers, and by 1.022 for turbulent boundary layers[19]:

$$Cf_N = 1.15\ Cf_{FLAT\ PLATE}$$

OR

$$Cf_N = 1\ 022\ Cf_{FLAT\ PLATE}\ ,$$

(2.3-334)

Note that both flat plates and cones have a constant Mach Number and no pressure gradients along their respective surfaces.

(2) Ogives

Although there is a variation of the Mach Number and the pressure gradient on an ogive surface in an axisymmetric flow field, for engineering purposes, it can be assumed that the same corrective factors of 1.15 and 1.022, as specified for cones, may be used. It is experimentally proven that existance of small pressure gradients on slightly curved surfaces does not affect appreciably the skin-friction values[19,127].

(3) Cylindrical Bodies

For cylindrical bodies, with the longitudinal axis aligned streamwise and with radii large compared to the boundary layer thicknesses, the skin-friction and heat-transfer coefficients are nearly equal to their equivalent flat plate values for the same free stream Mach and Reynolds Numbers. No correction for three-dimensional effects is thus necessary. For very thin, slender cylinders ($L/D > 30$), the boundary layer thickness may become comparable with the cylinder radius, and appreciable departures from the equivalent flat plate friction values occur[19]. The latter case is of importance for wind-tunnel test models primarily, and far less so for full-flight configurations having the (L/D) ratio of the (optimum) order of 14 to 15. Thus, for full scale design purposes:

$$C_{f_{CYL}} = C_{f_{FLAT\ PLATE}} \qquad (2.3\text{-}335)$$

(4) Boattailed Afterbodies

As in the case of ogives, a mild boattailing of afterbodies, ($\theta_B < 15^o$), producing small pressure gradients, should have but little effect on the skin-friction values, provided no separation or flow-choaking effects (due to presence of fins) takes place. For zero-lift flight conditions, there is usually an afterbody expansion wave with a subsequent shock formation in the wake.

Therefore, it is accepted that the combination, cylinder plus boattail, could be treated as a unit with the $C_{f_{CYL+BT}}$ taken as a well representative average skin-friction value. The corresponding Reynolds Number value is computed and based on the total body length including the nose section:

$$Re_L = \frac{L V_H}{\nu_H}\ ,$$

where:

$$L = L_N + L_{CYL} + L_{BT}\ . \qquad (2.3\text{-}336)$$

In this way the preliminary existance of the boundary layer build-up on the nose surfaces is taken into account. In the final expression for the average skin-friction coefficient for the cylinder + boattail combination, the nose-cone fraction of the frictional effects should be then properly subtracted.

(5) Wings and Fins

Neglecting the three-dimensional tip-effects and the spanwise flow pressure build-up (for swept wings), and irrespective of the airfoil type (double wedge, modified double-wedged, biconvex), it is assumed (see Section 2.3.4) that the equivalent flat plate turbulent skin-friction coefficient should represent a good engineering approximation, i.e.,

$$C_{f_W} = C_{f_{FLAT\ PLATE}} \ , \quad C_{f_F} = C_{f_{FLAT\ PLATE}} \ , \tag{2.3-337}$$

with the respective Reynolds Number value based on the mean geometric (or aerodynamic) chord of the exposed wing or fin planform:

$$Re_{\bar{c}_{WEXP}} = \frac{\bar{c}_{WEXP} V_H}{\nu_H} \ , \quad Re_{\bar{c}_{FEXP}} = \frac{\bar{c}_{FEXP} V_H}{\nu_H} \ ,$$

$$\bar{c}_{WEXP} = \frac{S_{WEXP}}{b_{WEXP}} \ , \quad \bar{c}_{FEXP} = \frac{S_{FEXP}}{b_{FEXP}} \ . \tag{2.3-338}$$

(6) Alternatively, the actual individual values of the average skin friction coefficient for a given body configuration, Mach Number, Reynolds Number and ambient flight altitude can be used, when available. Partial compiled data for usual configurational shapes and auxilliary vehicle parts are obtainable from Ref. 21 (Hoerner)[132] (R.A.S. Data Sheets), Ref. 133 (Design Data for Aeronautics and Astronautics), Ref. 134 (Wood), Ref. 135 (Nielsen), Ref. 136 (Corning), etc.

(7) The quantitative value of the equivalent, two-dimensional, flat plate average skin-friction coefficient, C_f, is a function of many independent variable usually acting simultaneously under operational flight conditions. In evaluating procedures, only the most influential among the factors are taken into account:

Mach Number, M_H.
Reynolds Number, $(Re_L)_H$.
Surface roughness, k.
Skin-temperature condition, (T_W / T_H).
Flight altitude, H.
Flight regime: steady or transient.

Each of the main factors has to be explicitly specified for any particular skin-friction computation.

(iii) Reynolds and Mach Number Effects

The Reynolds and Mach Number effects have a pronounced effect on the skin-friction drag values. In the subsequent proposed methods of frictional drag estimates, this influence is taken into account by a proper choice of the respective semi-analytical laws as pertinent to two-dimensional, smooth, rough, insulated or cooled flat plates respectively, see Figs. (2.3-44) to (2.3-49).

The average two-dimensional skin-friction coefficient on a smooth insulated flat plate is a strong function of both Reynolds and Mach Numbers. There is a marked decrease in the compressible C_f values with increase in Mach and Reynolds Numbers. The same holds for rough insulated surfaces, although somewhat modified by the intensity of the so-called equivalent surface roughness conditions, expressed by parameters $(V_H k/\nu_H)$ and (L/K), see Figs. (2.3-44) and (2.3-45).

This trend persists also for the average compressible-to-incompressible skin-friction ratios (C_f / C_{f_i}) on insulated flat plates with both smooth and rough surfaces, see Figs. (2.3-47) and (2.3-49), the Reynolds Number effects getting more pronounced for higher supersonic speeds $(M > 3)$. The correct value of the Reynolds and Mach Numbers therefore should be used in all computations.

Generally, the Reynolds Number is a function of the true flight speed, V_H, the characteristic body length, L or $\bar{c}$, and the kinematic coefficient of viscosity, ν_H. Since

$$Re_L = \frac{V_H L}{\nu_H} \quad \text{or} \quad Re_{\bar{c}} = \frac{V_H \bar{c}}{\nu_H}$$

and $\mu_H = \mu(T_H), \ \nu_H = (\mu_H / \rho_H)$,

$T_H = T(H)$,

$\rho_H = \rho(H)$, (2.3-339)

it follows that the Reynolds Number is an implicit function of flight altitude, H, for any given set of

flight speeds, V_H, and body geometry, L, or $\bar{C}$.

The flight Mach Number, $M_H = V_H / a_H$, in view of the relationships $a_H = a(T_H)$ and $T_H = T(H)$, is again an implicit function of flight altitude, H, for a given relative flight speed, V_H.

Therefore, it follows that the skin-friction coefficient must be evaluated separately for every flight altitude. But, from the respective quantitative values of the variational laws (see Standard Atmosphere, Section 2.2.6):

$$\mu_H = \mu(T_H), \quad T_H = T(H), \quad \rho_H = \rho(H), \qquad (2.3\text{-}340)$$

it can be shown that for flights in the lower atmospheric layers (below 35,000 ft.), the calculated variations with altitude in absolute values of the average skin-friction coefficients will not be pronounced. With increase in height (H>35,000 ft.), these effects get more appreciable. As a "rule of thumb" for engineering purposes, it is recommended that the drag calculations be performed for the following altitude steps (in ft.):

H=0; 35,000; 60,000; 80,000 and for each additional 20,000 feet of altitude.

For any other intermediate altitude, the drag coefficient value can then be interpolated within the general limited accuracy of the drag coefficient estimates at large.

In order to facilitate numerical evaluations of the $Re_H = Re(H)$ and $M_H = M(H)$ functions for computational uses, i.e., for a given relative flight speed, V_H, and a specified characteristic length, L or $\bar{C}$, special auxilliary graphs are presented in the Figs. (1.31) and (1.32) and the Table (1.7-2) for direct reading of these relationships for a Standard Atmosphere (see Section 2.2-6):

$$(Re/L)_H = f(M_H, H).$$

These working graphs have been computed from the expressions:

$$(Re/L)_H = \frac{V_H \rho_H}{\mu_H} \quad \text{and} \quad V_H = M_H a_H, \qquad (2.3\text{-}341)$$

$$\text{i.e.,} \quad (Re/L)_H = M_H \frac{a_H \rho_H}{\mu_H} = M \times K(H), \qquad (2.3\text{-}342)$$

$$\text{where} \quad K(H) = \frac{a_H \rho_H}{\mu_H} = \frac{a_H}{\nu_H}. \qquad (2.3\text{-}343)$$

Other important altitude dependent variations of flight dynamics parameters are compiled in Ref. 132 (R.A.S. Data Sheets).

(iv) Surface Roughness Effects

The surface roughness effects, encountered with different types of manufactured surface conditions, have been expressed through an "equivalent roughness parameter", k, as determined by experimentally investigated sand-roughened flat plates with different grain sizes. The related Figs (2.3-44) and (2.3-45) of the average skin-friction coefficient variations are reproduced directly from Ref. 127 (Clutter). The possible "rough" types of flows are thus sub-divided into three categories: "hydraulically smooth", "transitional" and "fully rough", each of them exhibiting a distinct functional dependence of the skin-friction and heat-transfer coefficients on Mach and Reynolds Numbers. The respective average skin-friction values of compressible turbulent boundary layers apply to insulated flat plates without pressure gradient. Corrections for transient or steady equilibrium heat-transfer conditions, reflecting actual surface temperatures as function of various possible flight regimes can be correctively taken into account as examplified later. A detailed account respective to the data is given in Section 2.3.5. Here, only a summary is given:

Based on the Nikuradse-Prandtl-Schlichting charts of the incompressible turbulent skin-friction coefficient variations with the Reynolds Number and surface roughness, an extension to the compressible flows with heat transfer has been worked out in Ref. 127 (Clutter), using Van Driest's turbulent compressible boundary layer equations, see Table (2.3-3).

The range of the main flow parameters:

$0 \leq M \leq 5.0$,

$10^5 \leq Re \leq 10^9$,

$(T_w/T_\delta) = (T_w/T_H) = 1$ and $(T_w = T_{aw})$, (insulated case).

The "equivalent sand roughness" parameter, k, is introduced in order to correlate actual experimentally investigated sand-roughened surfaces to those used in missile design and operation. The correlating values of k are given in Table (2.2-2). According to the physical nature of turbulent boundary layer flows over "sand-roughened" insulated surfaces, and according to subsequent variational laws of the "insulated" skin-friction coefficient with Reynolds and Mach Number changes, the following three distinct types of rough surface flows have been found:

(1) Hydraulically Smooth Flow - existing when the roughness-element sizes are so small that the variation of the skin-friction coefficient with Reynolds Number is of the same trend as for an idealized smooth flat plate. This type of flow persists up to a certain critical Reynolds Number based on roughness height. Physically, hydraulically smooth flows are realized when the individual roughness-element heights are less than the laminar sublayer thickness in compressible turbulent boundary layers.

(2) Transitional Type of Flow - in existance when the roughness element sizes are great enough to promote an increase of the skin-friction coefficient value above that of an ideal smooth flat plate, but the individual drag force of the roughness elements is not yet an all-important factor, i.e., there is still some modified functional relationship between the skin-friction coefficient and the Reynolds Number. This transitional region lies between the hydraulically smooth (or subcritical) and the fully rough types of boundary layer flows.

(3) Fully Rough Flow - established when the individual element sizes are great enough to become the governing factor. Both for compressible (Goddard[126]) and incompressible (Prandtl-Schlichting-Nikuradse) fully rough flows of uniformly distributed sand-roughness, the skin-friction drag is a sum of the flow drags of the individual roughness elements, and there is no variation in the $C_{f_{INS}}$ with Reynolds Number. The last feature is actually a basic criteria for definition of fully rough flows.

All three types of flows are presented in Figs. (2.3-44a) to (2.3-44h) for insulated rough surfaces (i.e., $T_w = T_{aw}$), the dotted line representing the border of the fully rough flows (from the line up). The insulated average skin-friction values are cross-plotted against Reynolds Numbers for various Mach Numbers from 0 to 5. The roughness effects are conveniently represented by two parameters: (L/K) and $(VK/\nu)_H$.

The constant (L/K) curves show the variation of the average skin-friction coefficient, $C_{f_{INS}}$, with the free-stream Reynolds Number, $(Re_L)_H$, on a flat, sand-roughened, insulated plate for given (L) and (H) in an entirely turbulent incompressible boundary layer. Such a curve of a constant (L/K) ratio passes through all the three basic flow regions: "hydraulically smooth", "transitional" and "fully rough".

The constant $(VK/\nu)_H$ curves represent variations in $C_{f_{INS}}$ with Reynolds Number, $(Re_L)_H$, under the same conditions for a constant stream velocity, $(U = V_H)$ and constant roughness height, k, i.e., with the plate length, L, as a variable parameter.

As an order-of-magnitude rule, for the possible equivalent missile-surface conditions, as represented by (k) values in the Table (2.2-2), the roughness-influence shall be felt as a 5% to 10% increase in the $C_{f_{INS}}$ values, i.e., very close to "hydraulically smooth" case.

Heat-transfer effects are conveniently represented by the wall-to-free stream temperature ratio $(T_w/T_\delta$ or $T_w/T_H)$ on non-insulated rough plates. These effects have been computed by Clutter(127) for the extreme condition of $(T_w/T_\delta) = 1$, which could represent either a highly cooled skin or initial (take-off) conditions. Due to the general lack of reliable experimental data, it was tacitly assumed that for "hydraulically smooth" non-insulated plates, the variations in the average skin-friction coefficient, C_f, with heat-transfer rates follow the same pattern as defined for ideally smooth plates as expressed by Van Driest's formula, see Table (2.2-3). The re-

spective calculated values of C_f, versus Reynolds Number, Re_L, for various Mach Numbers are presented as the curves $(T_W / T_\delta) = (T_W / T_H) = 1$ on Fig (2.3-45).

The graphs in Figs (2.3-44) and (2.3-45) are for the fully turbulent boundary layers, i.e., for the transition at the leading edge. Additional graphs, similar in form, but with the transition from laminar to turbulent boundary layer occurring at various distances from the leading edge can be found in the basic Reference 127. Another set of data regarding skin-roughness effects on the skin-friction coefficient values on insulated flat plates is presented in Ref. 132 (R.A.S. Aerodynamics Data Sheets).

(v) Skin-temperatures and Flight Regimes

The non-insulated missile skins generally undergo intricate temperature changes that are strongly affected by the variations in actual flight conditions and flight regimes, as well as by respective body geometry, actual mass distribution and the surface conditions. A summary of the heat-transfer phenomena, including definitions, is presented in Section 2.2.

The heat transfer rates may have a very pronounced effect on the skin-friction coefficient, especially at higher supersonic speeds. Since the skin-temperature conditions depend on the boundary layer, the thermal properties of the skin-material and the flight conditions (acceleration, altitude and time), exact time-histories of skin temperatures should be known in each particular case. In a design phase of a missile this is almost impossible, as it requires a most complex and lengthly trial-and-error iteration of the interrelationships between the drag, the vehicle flight performances and a definite structural design. Therefore, relying on the available scarce unclassified experimental data, an approximate evaluating procedure is basically proposed. It is believed to be acceptable within the general accuracy with which the skin-friction can be predicted for steady flight conditions in particular.

Alternatively, an iterative computational procedure for determination of the local skin friction coefficient data in terms of the local heat transfer rates during the generally accelerated (transient) aerothermal conditions on a prescribed trajectory is exampli-fied for all regimes (continuum, slip, transitional and free molecule) in Section 2.4. Since the method yields only a local skin-friction coefficient value, a subsequent integration of a sufficient number of the local values is required in order to obtain the average skin friction coefficient value. The procedure is obviously lenthy and of importance more for the heat transfer than for skin friction drag analysis. The more so in view of the fact that the heat transfer effects become pronounced at higher Mach Numbers, when the skin friction contribution to the total drag force coefficient is but a minor part, the wave or pressure drag playing a predominant role (see Section 1.7.4), even for zero-lift conditions.

As stated, the missile flight histories usually involve appreciable accelerations and altitude changes that, even without artificail cooling devices, decisively affect the skin-temperature adjustment rates and the overall heat transfer conditions, see Figs (1.21) to (1.25) and (1.27). During the accelerated flight phases neither the equilibrium (non-insulated) skin temperatures, T_{we}, nor the adiabatic (insulated) skin temperatures are achieved in general, see Sections 2.2.5 and 2.2.6 . For instance, for short duration boost periods, with acceleration rates of 10 to 20 g's, the early stage skin temperature conditions are more likely to follow close to the "ambient temperature" curve on Fig (2.3-50) and (2.3-51) and the skin-friction coefficient should be estimated for the condition closer to $T_W = T_\delta$ from Figs. (2.3-39) and (2.3-40). This may yield values far greater than for the respective adiabatic "insulated" case, see Figs (2.3-56) and (2.3-57).

The determination of the actual time-histories of the skin temperature variations with flight speed, altitude changes and accelerations, requires a complex iteration of the flight performance and the drag force estimates for a strictly specified structural and aerodynamic missile configuration on a prescribed trajectory. Obviously, this is beyond the framework and possibilities of the general aerodynamic force design phase. An order of magnitude approach, based on experimental evidence, should be used instead. With this in mind, the possible flight regimes are tentatively grouped into

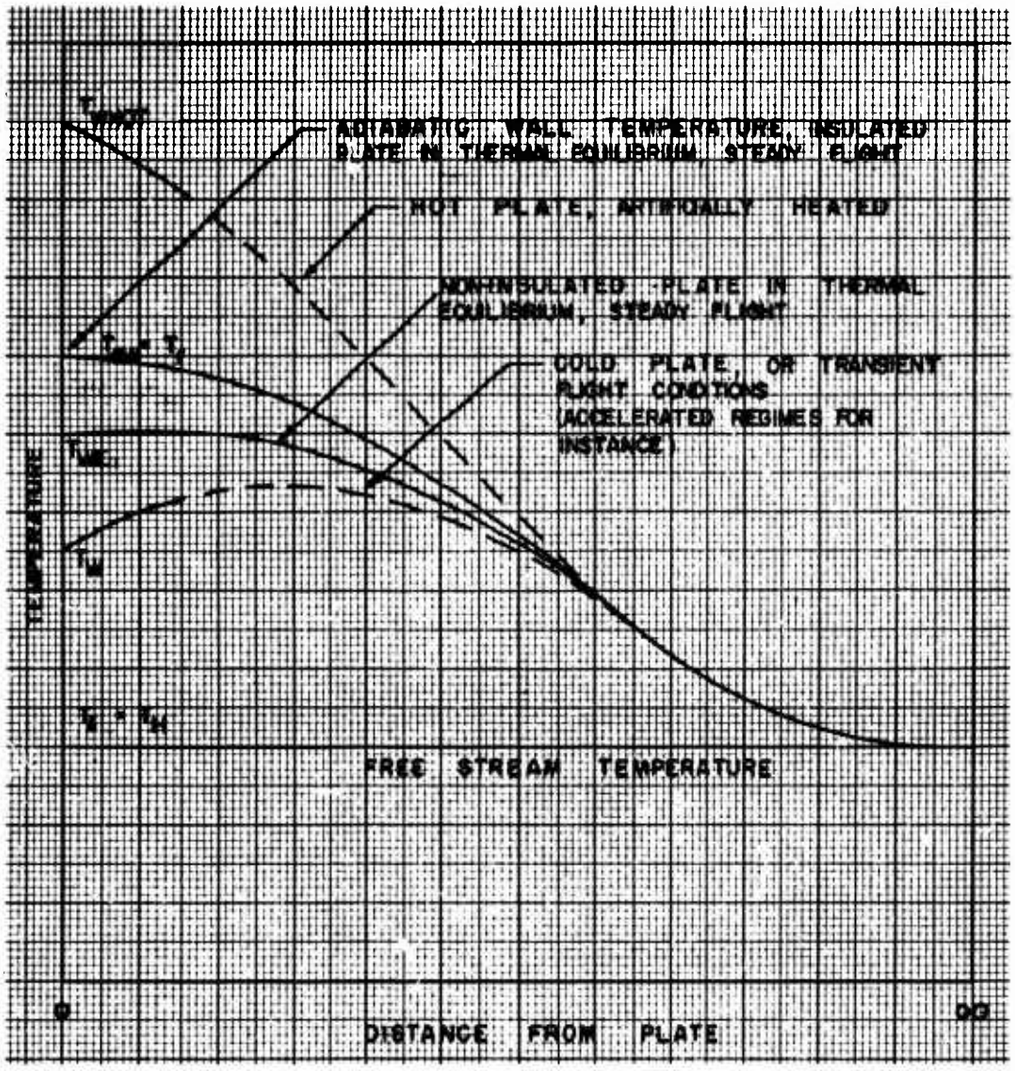

Fig (2.3-39) Distribution of temperature in the boundary layer with fixed stream for hot, insulated, and cold plates.

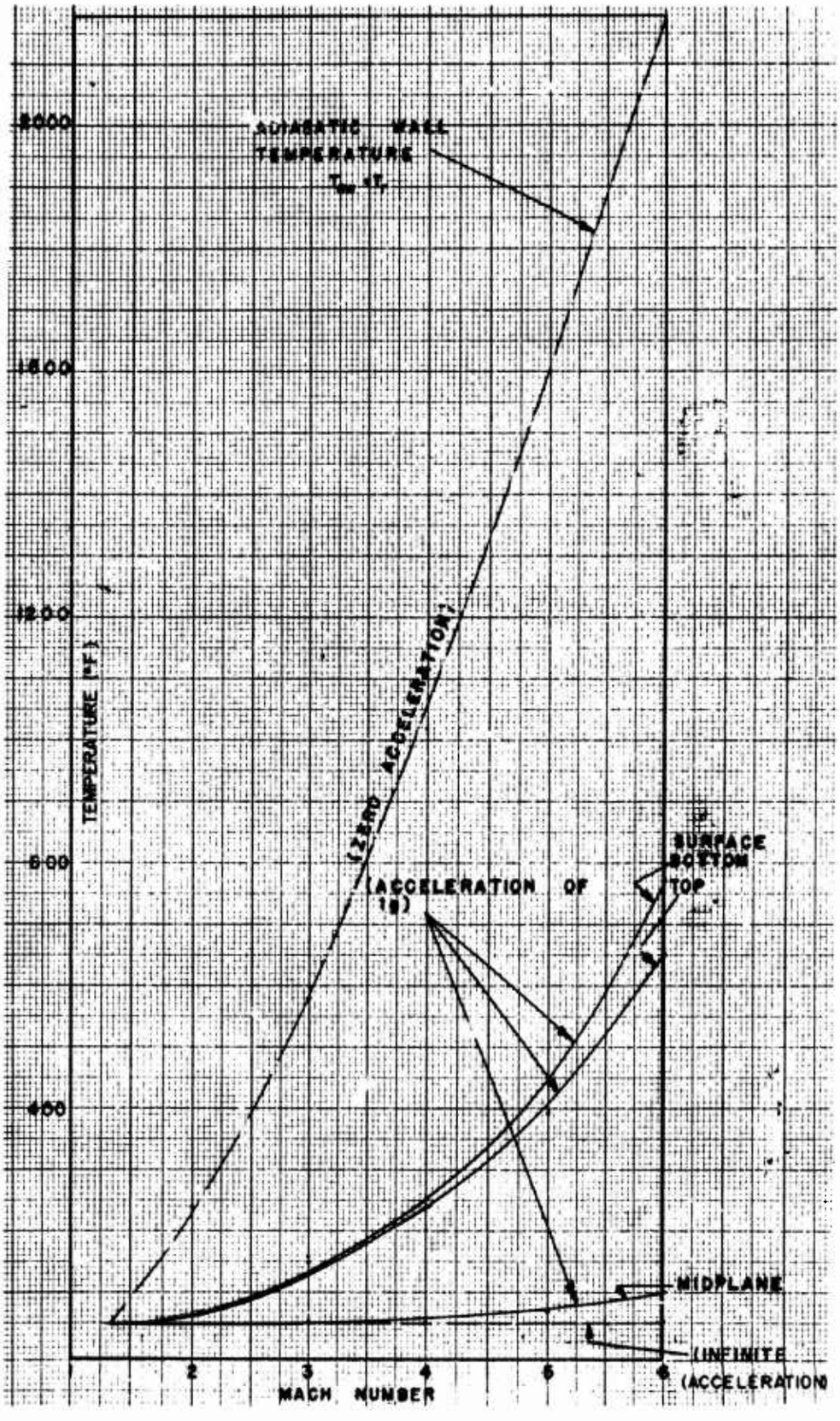

Fig (2.3-40) Temperature distribution at midchord from calculations of two dimensional heat flow for constant acceleration of 1g from a Mach Number of 1.4 at 50,000 feet. (Ref. 70)

two categories:

(1) Transient flight conditions, characterized in general by the actual skin-temperatures being variable and less than in the respective thermal equilibrium, steady flight cases, i.e.,

$$T_w < T_{we} < T_{aw} = T_r \leq T_{s\infty}, \quad (2.3\text{-}344)$$

for non-insulated and insulated surfaces alike, see Figs (2.3-34), (2.3-39) and (2.3-40).

The transient skin-temperature conditions are in existance whenever accelerations or appreciable altitude changes are involved. Also, the transient skin-temperature conditions prevail in steady rectilinear flight prior to the achievement of a thermal equilibrium.

(2) Steady-state thermal equilibrium flight conditions, $(T_w = T_{aw})$ or $(T_w = T_{we})$, which are realized only after sufficient time intervals in a steady flight without appreciable altitude changes.

The respective preliminary engineering design estimates of the skin-temperature effects on the average skin-friction coefficient, are specified in Methods I, II and III, and based on the following assumptions:

(1) It is assumed that an average isothermal condition, characterized by an average skin-temperature, T_w, exists on all missile surfaces. The leading edges of the lifting surfaces and the nose cone tips are excluded from this consideration. The approximation may be accepted on the rest of the missile configuration: cylindrical bodies, wing and fin surfaces away from the leading edge.

(2) It is assumed that the missile skin is made of steel with a thickness of the usual order of magnitude (.10" to .50"). This restriction is forced by lack of other experimental data in preparing the corresponding working charts. When other skin thicknesses and temperature data are available, they should be substituted instead.

(3) Flights are restricted to the lower atmospheric layers, not exceeding 400,000 feet. Flight speeds are in the supersonic bracket of Mach Numbers($M < 5$). Real rarefied gas effects, or high Mach Number ionization and dissociation effects, are non-existant.

(4) There is no artificial cooling of the missile skin involving auxiliary coolant injection in the boundary layer.

(5) For steady, prolonged flight regimes, or quasi-steady regimes, and relatively small altitude variations ($\Delta H \sim 0$ to 20,000ft.), it can be assumed that

$$T_w = T_{we} \approx T_{aw} \approx T_{s\infty} \quad (2.3\text{-}345)$$

The quasi-steady regimes are in this sense conceived to have acceleration rates small enough ($n_g < 0.1g$) so that the skin temperature rise is proportional to the heat transfer, i.e., that a thermal equilibrium exists between the boundary layer laminae next to the surface and the non-insulated skin; the skin is allowed to heat-up to the equilibrium temperature, ($T_{we} \approx T_{aw}$). This condition has been experimentally verified by Kaye[20] for a steel, 0.20" thick skin of a supersonic biconvex airfoil wing.

Since the non-insulated, (without artificial cooling) skin-equilibrium temperature,

$$T_{we} = T(M_H, H), \quad (2.3\text{-}346)$$

is very close to the adiabatic or recovery wall temperature, $(T_{aw} = T_r)$ of an insulated skin (except for skin-radiation effects), i.e.:

$$T_{we} \approx T_{aw} = T_r, \quad (2.3\text{-}347)$$

the average skin-friction values for steady or quasi-steady flight regimes should follow closely the curves for insulated skin on the working charts in Figs. (2.3-50) and (2.3-51).

The expected accuracy of estimates should be within the tolerances of the skin-friction estimates in general, i.e., of the order of ± 15%.

(6) For pronounced unsteady flight regimes, involving appreciable accelerations and/or altitude variations, the skin-temperature adjustment lags appreciably behind the velocity and altitude changes. The nigher the acceleration rates, the less time is left for the skin-temperature to adjust

to the changing thermal conditions within the boundary layer, i.e., to an increased frictional-heat production. The higher the accelerations, the greater the initial (i.e., prior to acceleration) temperature lag behind its respective maximum possible thermal equilibrium value, (T_{we}). Subsequently, if the high-acceleration (ng>20g) phase started from rest (boost phase), the initial skin-temperature (T_{WIN}) should be close to the ambient static temperature (T_H) and would change insignificantly for the usually short duration of the boost-launch phase. For such short time durations, no radiation effects are of importance.

The chart in Fig (2.3-52) can then be used as an order-of-magnitude guide in predicting skin-temperature conditions for short-duration transient flight regimes. It should be stated that the experimental data in the Fig (2.3-52) are a convenient replot of the respective experimental data from Figs (2.3-50) and (2.3-51), which have been originally obtained for a biconvex airfoil wing with a skin of steel sheet material .20" thick(70). The curves are for constant accelerations with the initial skin-temperature, T_{WN}, equal to the ambient temperature, T_H, at altitudes above 35,000 feet (isothermal layers of the Standard Atmosphere) and at sea-level conditions respectively. Due to the lack of other data, it can be approximated that the relative ratio of the instantaneous actual skin-temperature, $T_W = T(H, M_H, ng)$, to the ambient temperature, $T_H = T(H)$, i.e.,

$$T_W / T_H = f(M_H, ng, H), \qquad (2.3\text{-}348)$$

may be taken as a first order engineering estimate for all flight altitudes up to 100,000 ft. Obviously, more accurate data should be substituted instead, when available. The applicability of the curves from Fig. (2.3-52) is restricted to accelerated flight phases, starting from Mach Number 1 on. In the subsonic, short-duration, high-acceleration boost phase, it can be assumed that the initial skin-temperature is very close to the static ambient temperature, i.e., $T_{WIN} \approx T_H$.

Note: If it is desired to represent the skin-friction (and the drag-force in general) variations in boost phase as a function of time, then an approximate knowledge of time-histories of Mach Number and acceleration changes during the boost phase is required in advance. This can be roughly estimated by the usual approximate simple boost-phase performance calculations in which the drag force is taken as "constant" by an average, very rough, guess. Then, from the known $M = M(t, H)$ and $ng = f(t, H)$ laws, for a set of intermediate Mach Numbers, $0, M_1, M_2, M_3 \cdots M_n$, and the corresponding set of acceleration values, $(ng)_{max}, (ng)_1, (ng)_2, (ng)_3, \ldots (ng)_n$, the respective (T_W / T_H) temperature ratios from Fig (2.3-52) can be read, and from $(C_f / C_{f_i}) = f[M_H, H, Re_L, (T_W / T_H), K]$, graphs in Figs (2.3-44) to (2.3-57), the skin friction drag estimated as a function of time are then obtained. With the proper knowledge of the drag-force variation with time and altitude, the boost-phase performance can be then more accurately recalculated in a second approximation, etc. This iterative approach, although technically feasible and eventually attractive, is still inadequate, since it does not incorporate the additional drag rise due to the "apparent mass" effects as created by the accelerated motion of a body through a real fluid. The problem belongs to the general type of the unsteady fluid flow theory, which is as yet not amenable to an easy engineering approach.

Alternatively, in case of a prefixed accelerated flight trajectory from launch, including the later atmospheric re-entry conditions, the transient local temperature time history and the respective local skin friction coefficient time-dependent values, can be computed by the iterative method of Section 2.4.

(7) An equilibrium surface temperature, allowing for radiation when necessary, can be estimated from Figs (2.3-53) and (2.3-54). The equilibrium is achieved when convective heat input from the boundary layer to the surfaces equals the heat loss from the surface through radiation. The solar radiation is neglected. The governing equation for equilibrium temperature, $T_{wer} = (T_{we})_{radiation} < T_{aw}$, is taken directly from Ref. 132 (R.A.S. Aerodynamics Data Sheets):

$$1.829 \times 10^{14} \frac{\rho_H h M_H}{\epsilon T_\delta^{2.5}} \left[1 + .2 r M_\delta^2 - \left(\frac{T_{wer}}{T_\delta}\right)\right] = \left(\frac{T_{wer}}{T_\delta}\right)^4 - \left(\frac{T_\infty}{T_\delta}\right)^4, \qquad (2.3\text{-}349)$$

where

$r = .90$ - is the temperature recovery factor for turbulent boundary layers,

T_∞ - exceptionally here refers to the static ambient temperature far ahead of the body, i.e., $T_\infty \cong T_A = T_H$,

T_δ - refers to the local inviscid stream temperature outside the boundary layer,

$(T_\infty / T_\delta) \approx 1.0$ - for slender bodies and wings, zero angle-of-attack,

ϵ - surface emissivity, see Table (2.3-4),

$h = Q_\delta / [\rho_\delta U_\delta (i_{o_w} - i_w)]$ - a form of heat transfer coefficient. The values of h can be determined from Fig (2.3-53).

(8) In a general summary note, it can be said that the temperature ratio, T_W / T_H, has a marked influence on the average skin-friction values for supersonic Mach Numbers; the absolute value of (C_f / C_{f_i}) rapidly increases as the ratio (T_W / T_H) decreases toward unity, while the influences of both the Reynolds and the Mach Numbers are diminishing. Since the difference in skin-friction values for high Mach Numbers may reach almost 50% for the two possible thermal extremes, $(T_W = T_H)$ and $(T_W = T_H)$ respectively, it is evident that an accurate evaluation of the frictional drag at supersonic speeds should start from the estimates of the thermal skin-conditions as influenced by various flight regimes. Here, proposed "order-of-magnitude" methods may thus proved inadequate for some special transient unsteady flight regime analyses, intended for more elaborate heat transfer and structural design purposes. A resource to more accurate temperature time-histories from other sources should be then used, and the drag increments due to the acceleration effects from the unsteady flow theory computed.

Generally speaking, when the aerodynamic data are used on a prescribed flight trajectory, the skin-friction drag coefficient estimates, and consequently the total drag values, should be presented as flight dynamic variables:

$$C_{Dof} = f\left[M_H, H, t, (Re_L)_H, \quad (T_W / T_H), ng\right] \qquad (2.3\text{-}350)$$

TABLE (2.3-4)
EMISSIVITIES, ϵ

Material	50°C	250°C	550°C
Aluminum			
Polished	0.04	0.05	0.08
Oxidised	0.11	0 12	0.18
Chromium	0.08	0.17	0.26
Glass	0·9	—	—
Graphite	0.41	0.49	0.54
Iron			
Pure, polished	0.06	0.08	0.13
Wrought, polished	0.28	0.27	—
smooth	0.35	—	—
Cast	0.21	—	—
Cast, oxidised	0.63	0.66	0.76
Nickel			
Electrolytic	0.04	0.06	0.10
Oxidised	0.39	0.49	0.67
Steel			
Polished	0.07	0.10	0.14
Carbonised	0.52	0.53	0.56
Oxidised	0.79	0.79	0.79
Zinc			
Pure, polished	0.02	0.03	0.04
On Sheet Iron	0.23	—	—

$$\frac{°C}{5} = \frac{°F-32}{9}$$

Pigments	50°C	400°C
Lampblack paint	0.96	0.97
Blue (Co_2O_3)	0.87	0.86
Red (Fe_2O_3)	0.96	0.70
Green (Cu_2O_3)	0.95	0.67
Yellow (PbO)	0.74	0.49
Yellow ($PbCrO_4$)	0.95	0.59
White (ZnO)	0.97	0.91
White (ThO_2)	0.93	0.53

SEE FIG. (2.3-54)

REF. 132 ROYAL AERONAUTICAL SOCIETY DATA SHEETS, AERODYNAMICS, VOL I, S.00.03.20

2.3.8 LAMINAR, TURBULENT AND MIXED FLOW EXPRESSIONS FOR THE ZERO-LIFT SKIN-FRICTION DRAG COEFFICIENT, COMMON TO ALL METHODS OF EVALUATION

Note: Except for illustrative figures, all graphs are compiled at the end of the Section 2.3.

Following the guidelines stated in the previous Sections (2.3.5, 2.3.6, 2.3.7 and in Section 1.7, the estimates of the zero-lift skin-friction drag coefficients are performed separately for each principal missile part. Possible variations in the boundary layer flow are represented by the following three distinct cases:

Case I. A fully turbulent boundary layer is assumed on all missile parts for the whole range of Reynolds and Mach Numbers under investigation, i.e., transition phenomena occur in the regions of the leading edge or the nose tip. It represents an engineering convenience allowing for a relatively simple and quick drag force analysis. Justifications and limitations for such an approach to the drag force problem have been analyzed earlier; the results may be regarded as conservative when compared to more elaborate and more idealistic treatments stated below, but there is no conclusive evidence that this simplified analysis falls short of engineering expectancies when compared to actual flight conditions and measurements, provided the general representative flight conditions are within the possible turbulent boundary layer limits, see Fig (1.20).

Case II. Eventual existence of a fully laminar boundary layer on some missile parts is taken into account. This corresponds to some Mach Number and flight altitude combinations, and an assumed critical (transitional) Reynolds Number value, see Fig (1.20).

Case III. A partially laminar, partially turbulent boundary layer combination on each missile part is considered separately. For shortness, the combination is arbitrarily labeled as the "mixed flow" case. It represents the most general approach to the drag force problem and involves a rather elaborate and time-consuming estimate of the related critical Reynolds Numbers, which are a strong function of Mach Number, flight altitude, skin-temperature, the individual body geometry and the boundary layer prehistory on the other (preceding) missile parts, if so the case.

In all three cases, the two-dimensional equivalent flat plate skin-friction estimates are taken as a common basis, since they constitute the best investigated domain, both theoretically and experimentally, for a wide range of Mach Number, Reynolds Number and skin-temperature conditions. But, as the flat plate results usually reflect the conditions of no pressure gradient, a uniform skin-temperature and the existance of either a completely laminar or a completely turbulent boundary layer, their application to wings and bodies required additional corrections. Among these corrections are nonuniform pressure and temperature distributions, variations in the associated shock-wave patterns, three dimensional flow effects, etc., affecting the relative co-existance of laminar and turbulent boundary layers. In view of all this, a simplified approximate treatment of the necessary corrections for the mixed flow conditions on different body shapes is suggested instead:

(1) For slender, aerodynamically clean body shapes, having relatively small longitudinal surface curvatures, the associated pressure field variations are assumed to have little influence on the average skin-friction results. Therefore, the effects of small pressure gradients are neglected, since their small contribution in general is well beyond the possible accuracy of the drag estimates, see Section 2.3.4 .

(2) Skin-temperature effects, including the flow acceleration and the skin radiation influence are treated in a progressive way. First, the basic drag coefficient expressions are derived assuming an "insulated" skin. These results may be directly used for some flight conditions as specified later. The effects of the "non-insulated", but still presumably uniform, skin-temperature conditions are then added to the basic "insulated" case as corrections , comprising effects of the accelerated flight and the skin radiation, when necessary. The general, non-uniform skin-temperature distribution is not treated.

(3) Differences in body geometries are represented by proper estimates of the associated wetted areas of the equivalent flat plate in each case. The associated variations in flow dimensionality and the flow conditions behind various shock wave patterns are reduced to a comparable basis by a relatively simple change in reference flow quantities: the final skin-friction and the Reynolds Number expressions are related to a common set of the free stream parameters far ahead of the body. This allows for a direct conversion between the general body (three dimensional) and the equivalent flat plate (two-dimensional) skin-friction results, see Section 2.3.7.

An estimating procedure for flat, insulated plates is outlined first, followed by a corrective treatment of the fundamental results for different body geometries and skin-temperature conditions.

(i) Flat Plate

(1) The critical Reynolds Number, Re_{cr}, determining the type of boundary layer, is assumed to be of the order of 1×10^6. Nevertheless, all the proposed explicit expressions are derived in a form suitable for use with any other transitional Reynolds Number value.

(2) For computational convenience, it is assumed that the transition from laminar to turbulent boundary layer takes place instantaneously when the mixed flow case is considered, see Fig (2.3-41). Although physically incorrect, the approximation is well within the possible accuracy of skin-friction estimates.

With any acceptable critical Reynolds Number value, location of the instantaneous transition point, T , is formally fixed by

$$X_{TR} = \frac{Re_{cr}\nu_H}{V_H} = L_{FP}\frac{Re_{cr}}{Re_L} = f(M,H) \qquad (2.3\text{-}351)$$

where the ratio

$$\frac{\nu_H}{V_H} = \frac{L_{FP}}{Re_L} \qquad (2.3\text{-}352)$$

can be obtained directly from Figs (1.31) and (1.32) or from Table (1.7-2) as a function of the flight Mach Number and the flight altitude.

(3) To compute the correct Reynolds Number value, Re_{TURB} , which shall be needed later for determination of the average skin-friction coefficient for the turbulent portion of the boundary layer, a fictious "effective" beginning of the turbulent boundary layer is tentatively specified. On smooth flat plates this "effective" length can be defined approximately by assuming that the turbulent portion of the boundary layer started some distance, ΔX, ahead of the transition point, T , see Fig (2.3-41a). Then, by matching the respective laminar and turbulent momentum thicknesses at the point, T , i.e.:

$$(\theta^*_{LAM})_{AT\ T} = (\theta^*_{TURB})_{AT\ T} = \theta^*_{TRANS} \qquad (2.3\text{-}353)$$

the required distance, ΔX , and the associated average turbulent skin-friction coefficient, $\Delta C_{f_{TURB}}$, can be determined within acceptable limits of accuracy as follows:

Using the Eq (2.3-353) and the fundamental relationship,

$$C_f = \frac{2\theta^*}{X} \ , \qquad (2.3\text{-}354)$$

which is valid for both laminar and turbulent boundary layers, either compressible or incompressible, it is obtained that

$$2\theta^*_{TR} = C_{f_{LAMFP}} X_{TR} = \Delta C_{f_{TURBFP}} \Delta X \qquad (2.3\text{-}355)$$

$$\Delta C_{f_{TURBFP}} = C_{f_{LAMFP}} \frac{X_{TR}}{\Delta X} \qquad (2.3\text{-}356)$$

where $C_{f_{LAMFP}}$ and $\Delta C_{f_{TURBFP}}$ are the flat plate average skin-friction coefficients related to the laminar, X_{TR} , and the turbulent, ΔX , portions respectively.

For any pre-chosen value of Re_{CR} , determining both X_{TR} and $C_{f_{LAMFP}}$, the expression (2.3-356) contains two unknown variables, ΔX , and $\Delta C_{f_{TURBFP}}$, which are functions of Mach Number and flight altitude. The unknown quantities could be found by any trial-and-error method in each specific case. Here, ready graphs are presented for this purpose, see Fig (2.3-58), whereby, $Re_{\Delta X}$, ΔX and the associated value of $\Delta C_{f_{TURBFP}}$ are directly obtainable

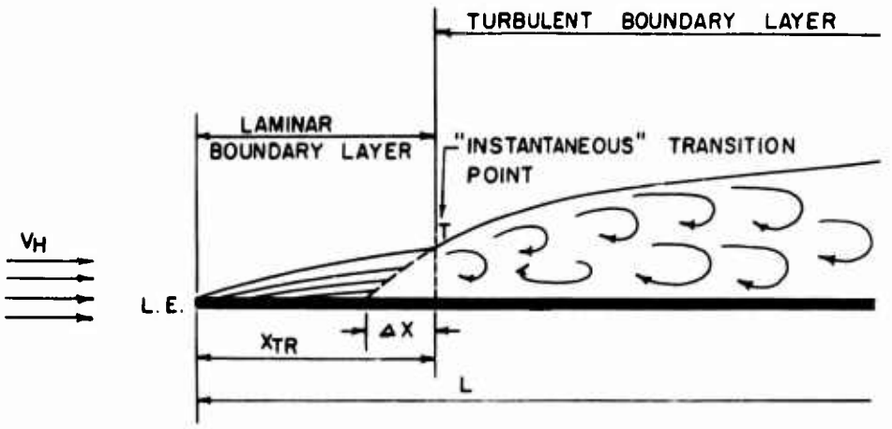

FIG. (2.3-41) SKETCH OF THE "MIXED FLOW" GEOMETRY ON A SMOOTH, FLAT PLATE (AN ENGINEERING APPROXIMATION)

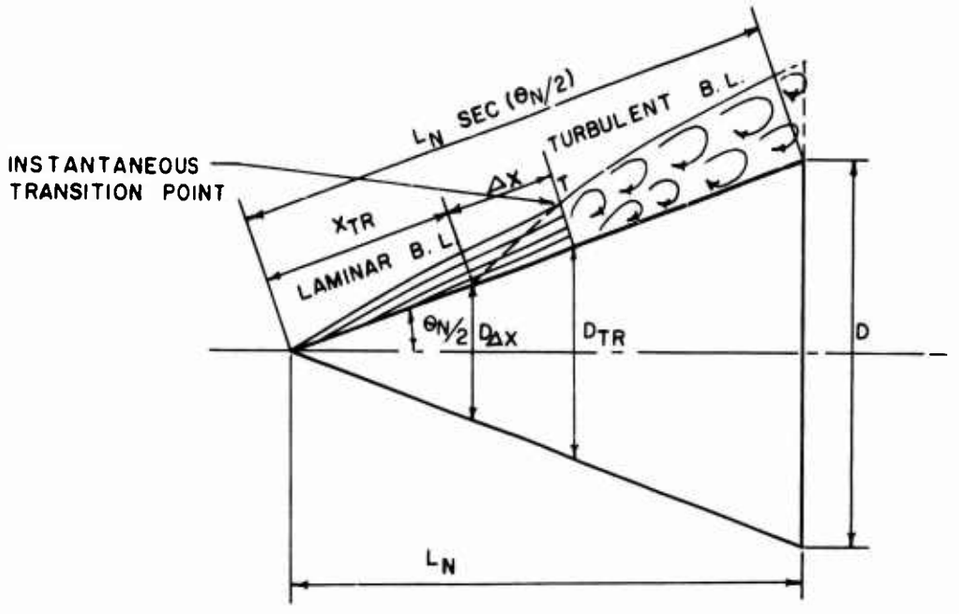

FIG. (2.3-42) EVALUATION OF THE AVERAGE SKIN-FRICTION AND THE WETTED AREAS ON NOSE CONES FOR PARTIALLY LAMINAR, PARTIALLY TURBULENT BOUNDARY LAYERS.

as functions of Re_{CR} and M. The computations have been performed using the respective data from Fig. (2.3-44) "smooth" curve (van Driest).

Alternatively, if an average value of Re_{CR} is assumed to be 1×10^6, independent of Mach Number and flight altitude, the following simpler, but less accurate, analysis can be used:

At the point of a supposedly "instantaneous" transition, T, not only the expression (2.3-353) holds, but likewise the actual boundary layer thicknesses are the same:

$$(\delta_{LAM})_{AT\ T} = (\delta_{TURB})_{AT\ T} = \delta_{TRANS} \qquad (2.3\text{-}357)$$

The above relationship is valid for both compressible and incompressible boundary layers. It is further assumed that for relatively low Mach Numbers ($M < 5$), the respective ratios of compressible-to-incompressible laminar and turbulent boundary layer thicknesses are approximately equal numerically, i.e.,

$$\frac{(\delta_{LAM})_M}{(\delta_{LAM})_{M=0}} = \frac{(\delta_{TURB})_M}{(\delta_{TURB})_{M=0}} = K . \qquad (2.3\text{-}358)$$

The ratio is plotted in Fig (2.3-59).

The approximate relationship (2.3-359) can be reduced to a still simpler form through the rather accurate Blasius's incompressible, flat plate, formulae

$$\frac{5.2\,X_{TR}}{Re_{Cr}^{1/2}} = \frac{.37\,\Delta X}{Re_{Cr}^{.2}} \qquad (2.3\text{-}359)$$

for laminar and turbulent incompressible boundary layers respectively, i.e., with $Re_{Cr} = 1 \times 10^6$.

$$\Delta X = \frac{5.2}{.37}\, 10^{-1.8} X_{TR} = .222\, X_{TR} = .222\, L_{FP} \frac{10^6}{Re_L} . \qquad (2.3\text{-}360)$$

With this, the Eq (2.3-356) reduces to

$$\Delta C_{f_{TURBFP}} = 4.5\, C_{f_{LAMFP}} . \qquad (2.3\text{-}361)$$

In both cases, either by using Fig (2.3-58) or the approximate expression (2.3-361), the correct Reynolds Number value for evaluation of the turbulent portion of the boundary layer is

$$Re_{TURBFP} = \frac{(\Delta X + L_{FP} - X_{TR})\, V_H}{\upsilon_H} , \qquad (2.3\text{-}362)$$

or, in terms of Re_L,

$$Re_{TURBFP} = \left(\frac{\Delta X}{L_{FP}} + \frac{L_{FP} - X_{TR}}{L_{FP}}\right) Re_L , \qquad (2.3\text{-}363)$$

and alternatively, from Eq (2.3-360),

$$Re_{TURBFP} = \left[1 - .778\, \frac{X_{TR}}{L_{FP}}\right] Re_L , \qquad (2.3\text{-}364)$$

$$Re_{TURBFP} = Re_L - .778 \times 10^6 , \qquad (2.3\text{-}365)$$

to the Re_{TURBFP} value in Eqs (2.3-363) or (2.3-365) corresponds an average turbulent skin-friction coefficient,

$$C_{f_{TURBFB}} = f(Re_{TURBFP}, M) ,$$

obtainable readily from the respective graphs in Figs. (2.3-44) and (2.3-47). Note that the $C_{f_{TURBFP}}$ average value refers to the "effective" total length of the turbulent boundary layer, $(L - X_{TR} + \Delta X)$. It reflects the fact that the turbulent boundary layer at the transition point, T, continues the existance of the preceding laminar boundary layer portion, i.e., the turbulence is not started from a zero boundary layer condition. A correct combination of the $C_{f_{LAMFP}}$, $C_{f_{TURBFP}}$ and $\Delta C_{f_{TURBFP}}$ values and the respective associated wetted areas is then required for evaluation of the total average zero-lift skin-friction drag coefficient.

Note: Instead of introducing the approximation (2.3-58), the Blasius' incompressible laminar-to-turbulent relationship (2.3-359) might be combined with the respective van Driest's expression for compressible-to-incompressible relationship (see Fig 2.3-59). But the relative increase in the accuracy of Re_{TURBFP} estimates, which might be obtainable in this way, is hardly necessary for practical aims, since both the concept of an

"instantaneous" transition and the estimates of the true Re_{Cr} values are largely provisional.

(4) Evaluation of the zero-lift skin-friction drag coefficient, $C_{Dof_{FP}}$, for smooth flat plates has to be performed by fractions in the general case of a "mixed" boundary layer condition as follows:

Case III:

By definition, the average two-dimensional skin-friction coefficient is,

$$C_{f_{FP}} = \frac{\int_0^X C_{f_X}' dx}{X} = f(Re_X, M) \ , \quad b_{FP} = \text{constant} \ , \tag{2.3-367}$$

where C_{f_X}' is its local value at any station x. Then, for one side of a flat plate,

$$(L \times b)_{FP} C_{Dof_{FP}} = (X_{TR} b)_{FP} \frac{\int_0^{X_{TR}} C_{f_{LAM}}' dx}{X_{TR}} + \\ + (L_{FP} - X_{TR}) b_{FP} \frac{\int_{X_{TR}}^{L_{FP}} C_{f_{TURB}}' dx}{L_{FP} - X_{TR}} \ . \tag{2.3-368}$$

The first term in Eq (2.3-368) is readily obtainable from

$$C_{f_{LAMFP}} = \frac{\int_0^{X_{TR}} C_{f_{LAM}}' dx}{X_{TR}} = f(Re, \ M \ , Re < Re_{Cr} \ . \tag{2.3-369}$$

Using a formally and physically correct transformation of the type,

$$\int_{X_{TR}}^{L_{FP}} = \int_0^{L_{FP}-X_{TR}} \int_{X_{TR}-\Delta x - X_{TR}+\Delta x}^{L_{FP}-X_{TR}} = \\ = \int_{X_{TR}-\Delta x}^{L_{FP}} - \int_{X_{TR}-\Delta x}^{X_{TR}} \ , \tag{2.3-370}$$

the second term in Eq (2.3-368) can be brought to the convenient form,

$$(L_{FP} - X_{TR}) b_{FP} \frac{\int_{X_{TR}}^{L_{FP}} C_{f_{TURBFP}}' dx}{(L_{FP} - X_{TR})} = \\ = b_{FP} \left[\int_{X_{TR}-\Delta x}^{L_{FP}} C_{f_{TURBFP}}' dx - \int_{X_{TR}-\Delta x}^{X_{TR}} C_{f_{TURBFP}}' dx \right] ,$$

$$(L_{FP} - X_{TR}) b_{FP} \frac{\int_{X_{TR}}^{L_{FP}} C_{f_{TURBFP}}' dx}{(L_{FP} - X_{TR})} = \\ = b_{FP}(L_{FP} - X_{TR} + \Delta x) \frac{\int_{X_{TR}-\Delta x}^{L_{FP}} C_{f_{TURBFP}}' dx}{(L_{FP} - X_{TR} + \Delta x)} - \\ - b_{FP} \Delta x \int_{X_{TR}-\Delta x}^{X_{TR}} \frac{C_{f_{TURBFP}}' dx}{\Delta x} \ ,$$

$$\therefore \ (L_{FP} - X_{TR}) b_{FP} \frac{\int_{X_{TR}}^{L_{FP}} C_{f_{TURBFP}}' dx}{(L_{FP} - X_{TR})} = \\ = b_{FP}(L_{FP} - X_{TR} + \Delta x) C_{f_{TURBFP}} - b_{FP} \Delta x \Delta C_{f_{TURBFP}} \ , \tag{2.3-371}$$

where $C_{f_{TURBFP}}$ and $\Delta C_{f_{TURBFP}}$ are specified by Eqs (2.3-366) and (2.3-356) respectively.

Thus, for the "mixed" boundary layer on one side of a smooth flat plate, using the average skin-friction coefficient notation associated with the respective wetted areas, Eq (2.3-368) takes the form:

$$(L \times b)_{FP} C_{Dof_{FP}} = (X_{TR} b_{FP}) C_{f_{LAMFP}} + \\ + b_{FP}(L_{FP} - X_{TR} + \Delta x) C_{f_{TURBFP}} - (b_{FP} \Delta x) \Delta C_{f_{TURBFP}} , \tag{2.3-372}$$

and with

$$\Delta x \Delta C_{f_{TURBFP}} = X_{TR} C_{f_{LAMFP}} \ ,$$

$$X_{TR} = L_{FP} \frac{Re_{Cr}}{Re_L} \ ,$$

$$\Delta x = L_{FP} \frac{Re_{\Delta x}}{Re_L} = f(M, Re_{Cr}) \quad \text{from Fig (2.3-58)} \ , \tag{2.3-373}$$

it becomes, for two-dimensional flow over one side of a flat plate,

$$L_{FP} C_{Dof_{FP}} = \left[L_{FP} \left(1 - \frac{Re_{Cr} - Re_{\Delta x}}{Re_L}\right) \right] C_{f_{TURBFP}} \ , \tag{2.3-374}$$

$$\therefore C_{Dof_{FP}} = \left(1 - \frac{Re_{Cr} - Re_{\Delta x}}{Re_L}\right) C_{f_{TURBFP}} = \\ = \frac{Re_{TURBFP}}{Re_L} C_{f_{TURBFP}} \ , \tag{2.3-375}$$

where

$$C_{f_{TURBFP}} = f(Re_{TURBFP}, M) \quad ,$$

$$Re_{TURBFP} = \frac{(\Delta X + L_{FP} - X_{TR})V_H}{\nu_H} = Re_L\left(1 - \frac{Re_{Cr} - Re_{\Delta X}}{Re_L}\right) . \tag{2.3-376}$$

Alternatively, in case of the approximate assumption that

$$\Delta X = .222 X_{TR} = .222 L_{FP} \frac{10^6}{Re_L} \quad , \tag{2.3-377}$$

Eq (2.3-375) reduces to a very simple form,

$$C_{Dof_{FP}} = \left(1 - .778 \frac{10^6}{Re_L}\right) C_{f_{TURBFP}} \quad . \tag{2.3-378}$$

where

$$C_{f_{TURBFP}} = f(Re_{TURBFP}, M) \quad ,$$

$$Re_{TURBFP} = \left(1 - .778 \frac{10^6}{Re_L}\right) \quad . \tag{2.3-379}$$

Then, in the case of a fully turbulent or a fully laminar boundary layer on a flat plate, Eqs (2.3-375) and (2.3-378) reduce to:

Case I: fully turbulent boundary layer, transition assumed at the leading edge:

$$X_{TR} = \Delta X = 0 \quad ,$$

$$Re_{Cr} = Re_{\Delta X} = 0 \quad ,$$

$$C_{Dof_{FP}} = C_{f_{TURBFP}} = f_1(Re_{TURBFP}, M) \quad ,$$

$$Re_{TURBFP} = Re_L \quad , \tag{2.3-380}$$

Case II: fully laminar boundary layer:

$$X_{TR} > L_{FP} \quad , \quad \Delta X = 0 \quad ,$$

$$Re_{Cr} \geq Re_L \quad , \quad Re_{\Delta X} = 0$$

$$C_{Dof_{FP}} = C_{f_{LAMFP}} = f_2(Re_L, M) \quad . \tag{2.3-381}$$

(5) For rough flat plates, the above outlined analysis is less accurate; nevertheless, in order to avoid any additional complications, it is proposed that the very simple expressions (2.3-375) and (2.3-378) be used for mixed flow conditions. This involves an error still practically insignificant, since even in the simpler cases of a fully laminar or a fully turbulent boundary layer the values of the "rough" C_f's can be determined only within ± 15%.

By applying the foregoing equivalent flat plate method to individual missile parts, the corresponding three-dimensional expressions for C_{Dof} are determined next.

(ii) Nose Section (Conical or Ogive)

The three-dimensional zero-lift skin-friction drag coefficient for nose cones is (see Fig 2.3-42):

$$C_{Dof_N} = C_{f_N} \frac{S_{NWET}}{S_r} \cos(\theta_N/2) \quad . \tag{2.3-382}$$

According to Eckert[19], Mangler[141], and Hantsche and Wendt[11], the average three-dimensional skin-friction coefficient, C_{f_N} , is expressed through its corresponding two-dimensional, flat plate value by multiplying the equivalent flat plate average skin-friction coefficient, $C_{f_{LAMFP}}$ with a factor $\kappa = 1.15$ for laminar boundary layers, or by multiplying the equivalent flat plate average skin-friction coefficient, $C_{f_{TURFP}}$, with a factor $\kappa = 1.022$ for turbulent boundary layers. These corrective factors comprise all the three-dimensional effects existing on a cone, provided the following "equivalent" flat plate and cone reference parameters are taken as common (see Fig 2.3-42):

(1) The "equivalent" flat plate (one side) and the cone are of equal wetted areas, ($b_{FP} L_{FP} = S_{NWET}$).

(2) The "equivalent" flat plate has a length equal to the slant height of the cone, $L_{FP} = L_N \sec(\theta_N/2)$.

(3) Differences in dynamic pressures outside the boundary layer are taken into account by referring the cone and the equivalent (superscript*) flat plate Reynolds Numbers to the common free ambient stream parameters at infinity (i.e., well ahead of body):

$$Re^*_{FP} = Re_L = \frac{L_{FP} V_H}{\nu_H} = Re_{LN} \sec(\theta_N/2) =$$

$$= \frac{L_N V_H}{\nu_H} \sec(\theta_N/2) = Re^*_N \quad . \tag{2.3-383}$$

Thus, Eq (2.3-382), expressed through the "equivalent" flat plate concept takes alternatively the forms:

Case I:

$$C_{Dof_N} = 1.022\ C_{f_{TURFP}} \frac{S_{WETCONE}}{S_r} \cos(\Theta_N/2)\ , \tag{2.3-384}$$

Case II:

$$C_{Dof_N} = 1.15\ C_{f_{LAMFP}} \frac{S_{WETCONE}}{S_r} \cos(\Theta_N/2)\ , \tag{2.3-385}$$

Case III:

$$C_{Dof_N} = \left[1.15\ C_{f_{LAMFP}} \frac{S_{WETLAMCONE}}{S_r} + \right.$$
$$+ 1.022\ C_{f_{TURFP}} \frac{S_{WETTURCONE}}{S_r} -$$
$$\left. - 1.022\ \Delta C_{f_{TURFP}} \frac{S_{\Delta XCONE}}{S_r}\right] \cos(\Theta_N/2)\ . \tag{2.3-386}$$

Explicit expressions for the three cases are derived below, using the flat plate analysis data from the previous paragraph (i).

Case I: a fully turbulent boundary layer, i.e., the transition at the leading edge is assumed in a first approximation. The imposed condition is:

$$X_{TR}=0,\quad Re_{Cr}=0,\quad \Delta X=0\ .$$

Then, from Fig (2.3-43),

$$\frac{S_{NWET}}{S_r} = \frac{\pi D}{2} L_N \sec(\Theta_N/2) = \frac{\pi D^2}{4} \operatorname{cosec}(\Theta_N/2)\ ,$$

$$S_r = \frac{\pi D^2}{4}\ ,$$

$$\left(\frac{S_{NWET}}{S_r}\right)_T^I = 2(L_N/D)\sec(\Theta_N/2) = \operatorname{cosec}(\Theta_N/2)\ ,$$

$$\left(C_{Dof_N}\right)_T^I = 1.022\ C_{f_{TURFP}} \left(\frac{S_{NWET}}{S_r}\right)_T^I \cos(\Theta_N/2)\ ,$$

$$\left(C_{Dof_N}\right)_T^I = 1.022\ C_{f_{TURFP}} \cot(\Theta_N/2) = G_1 C_{f_{IT}}^I\ , \tag{2.3-387}$$

where, for convenience of later tabulations,

$G_1 = 1.022 \cot(\Theta_N/2)$ is a geometric factor,

$$C_{f_{IT}}^I = C_{f_{TURFP}} = f(Re_{FP}^*, M) = f(Re_N^*, M)\ ,$$

$$Re_{FP}^* = \frac{V_H L_N}{\nu_N} \sec(\Theta_N/2) = Re_{LN}\sec(\Theta_N/2) = Re_N^*\ . \tag{2.3-388}$$

Case II: a fully laminar boundary layer exists. The necessary conditions is:

$$Re_N^* = Re_{FP}^* = \frac{L_N V_H}{\nu_H} \sec(\Theta_N/2) \le Re_{Cr} = (1\times 10^6 \text{ eventually}),$$

$$\left(\frac{S_{NWET}}{S_r}\right)_L^{II} = 2(L_N/D)\sec(\Theta_N/2) = \operatorname{cosec}(\Theta_N/2)\ ,$$

$$\left(C_{Dof_N}\right)_L^{II} = 1.15\ C_{f_{LAMFP}} \left(\frac{S_{NWET}}{S_r}\right)_L^{II} \cos(\Theta_N/2)\ ,$$

$$\left(C_{Dof_N}\right)_L^{II} = 1.15 \frac{1.022}{1.022} C_{f_{LAMFP}} \cot(\Theta_N/2) = 1.125\, G_1 C_{f_{IL}}^{II}\ , \tag{2.3-389}$$

where,

$$G_1 = 1.022 \cot(\Theta_N/2)\ ,$$

$$C_{f_{IL}}^{II} = C_{f_{LAMFP}} = f(Re_{FP}^*, M) = f(Re_N^*, M)\ ,$$

$$Re_{FP}^* = \frac{V_H L_N}{\nu_H} \sec(\Theta_N/2) = Re_N^*\ . \tag{2.3-390}$$

Case III: a partially laminar, partially turbulent boundary layer. The necessary condition for the "mixed" boundary layer existence is:

$$Re_N^* = Re_{FP}^* = \frac{L_N V_H}{\nu_H} \sec(\Theta_N/2) > Re_{Cr} = (1\times 10^6 \text{ eventually}).$$

Combining Eq (2.3-386) in connection with Fig (2.3-43), and the corresponding Eq (2.3-375) from the flat plate analysis, it follows that in a first approximation:

$$\left(C_{Dof_N}\right)_{L+T}^{III} = \left[1.15\ C_{f_{LAMFP}} \frac{S_{WETLAMCONE}}{S_r} + \right.$$
$$+ 1.022\ C_{f_{TURFP}} \frac{S_{WETTURCONE}}{S_r} - \tag{2.3-391}$$
$$\left. - 1.022\ \Delta C_{f_{TURFP}} \frac{S_{\Delta XWETCONE}}{S_r}\right] \cos(\Theta_N/2)\ ,$$

$$\Delta C_{f_{TURFP}} = \frac{X_{TR}}{\Delta X_N} C_{f_{LAMFP}} = \frac{Re_{Cr}}{Re_{\Delta XN}} C_{f_{LAMFP}}\ , \tag{2.3-392}$$

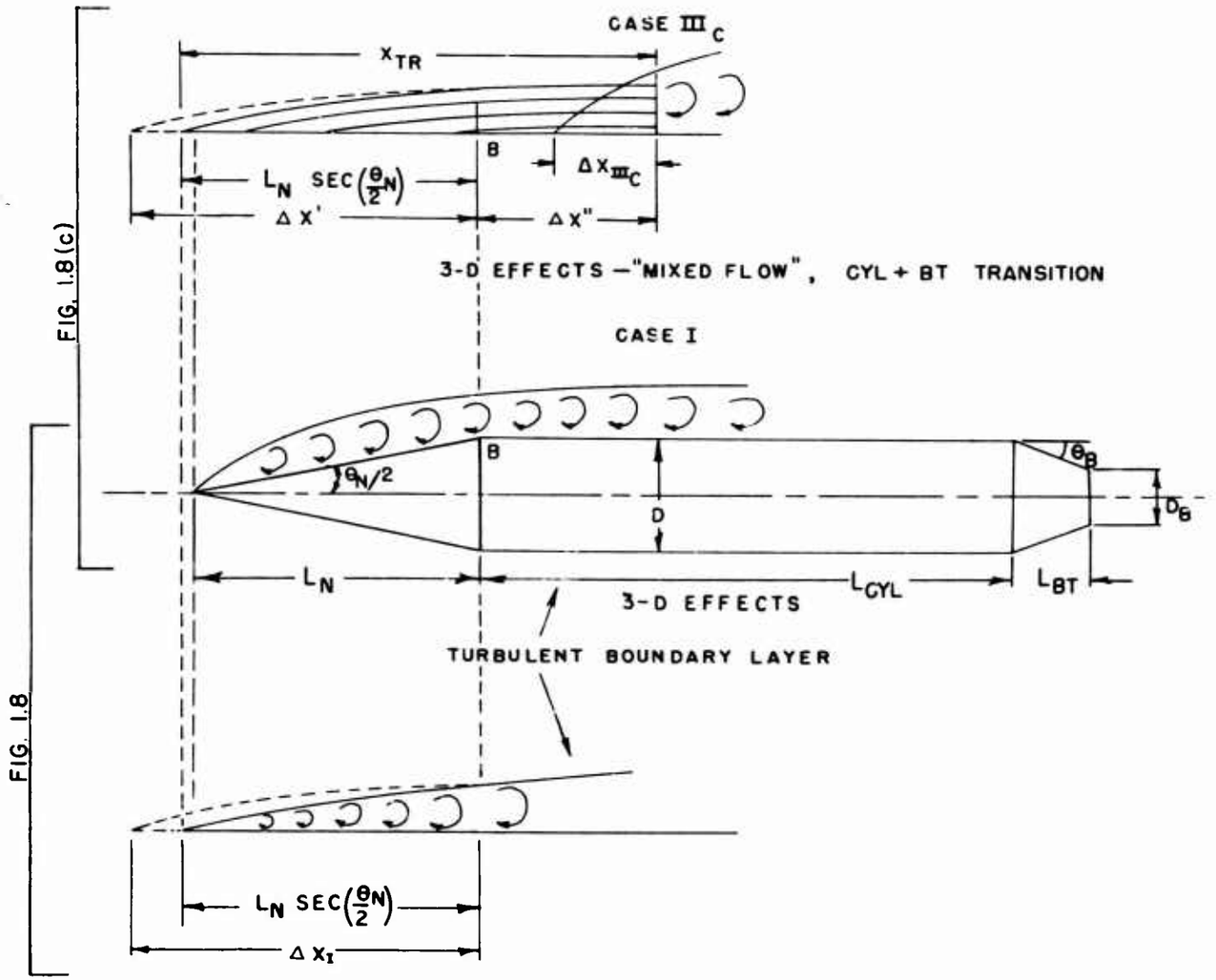

FIG (2.3-43) USE OF "EQUIVALENT" FLAT PLATE CONCEPT

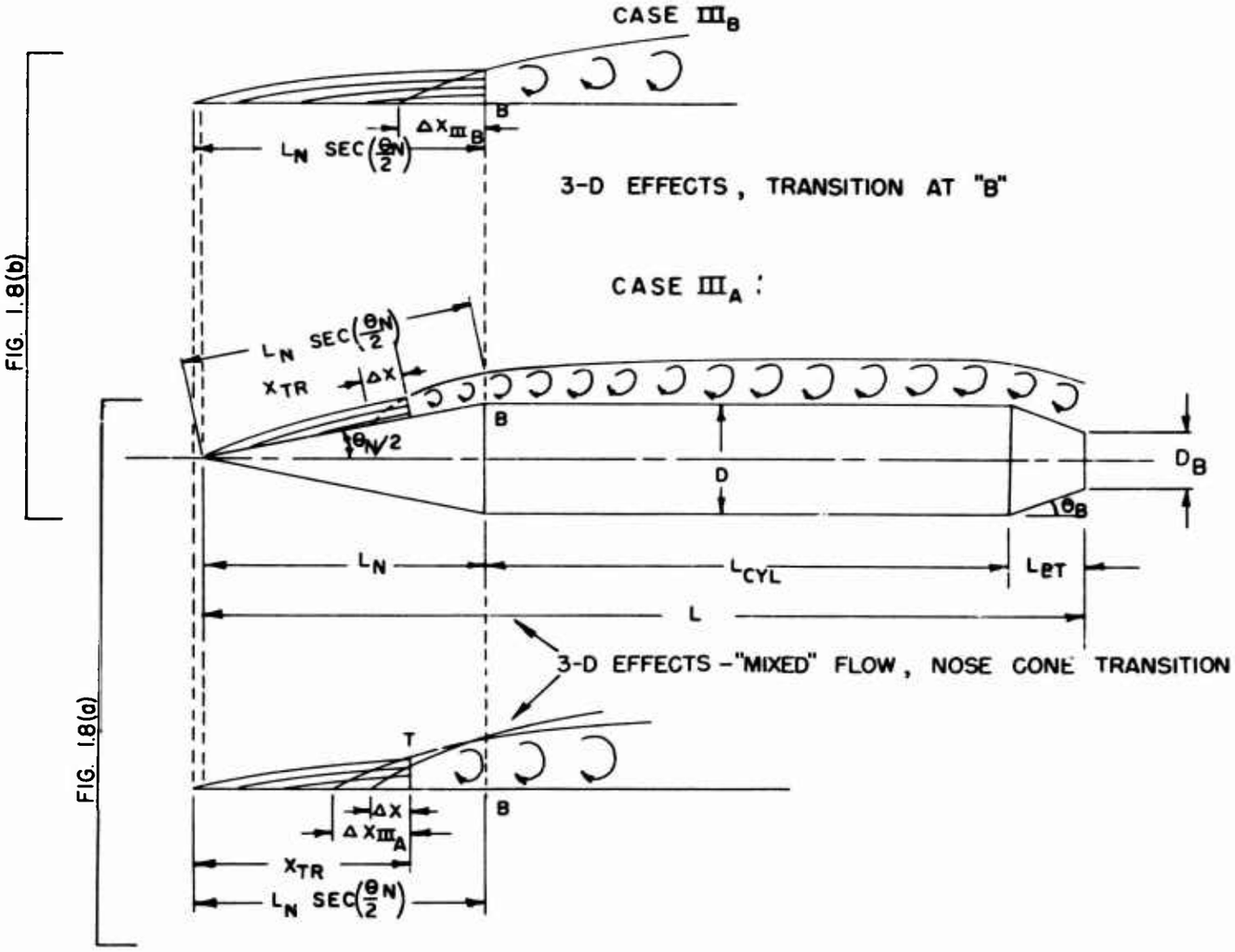

FIG. (2.3-43) Continued

$$X_{TR} = L_N\left[\sec(\Theta_N/2)\right]\frac{Re_{cr}}{Re^*_{FP}} \quad ,$$

$$Cf_{LAMFP} = f_1(Re_{cr}, M) \quad ,$$

$$Cf_{TURFP} = f_2(Re^*_{TURFP}, M) \quad ,$$

$$Re^*_{TURFP} = Re^*_{FP}\left[1-\left(\frac{Re_{cr}}{Re^*_{FP}} - \frac{Re_{\Delta XN}}{Re^*_{FP}}\right)\right] = (Re^*_{TURFP})^{III}_{NOSE} =$$

$$= Re^*_{TURN} \quad ,$$

$$Re^*_{FP} = Re_{LN}\sec(\Theta_N/2) = Re^*_N \quad .$$

$$Re_{\Delta XN} = \frac{\Delta X_N V_H}{\nu_H} \quad , \text{ from Fig. (2.3-58)}$$

$$Re_{LN} = \frac{L_N V_H}{\nu_H} \quad ,$$

$$Re_{CR} = \frac{X_{TR} V_H}{\nu_H} = (1\times10^6 \text{ eventually}) \quad .$$

(2.3-393)

The respective wetted areas in Eq (2.3-391) are (see Fig 2.3-42):

$$S_{WETCONELAM} = \frac{\pi D_{TR}}{2} X_{TR} =$$

$$= \frac{\pi D^2}{4}\left[\operatorname{cosec}(\Theta_N/2)\right]\left(\frac{Re_{cr}}{Re^*_{FP}}\right)^2 \quad ,$$

(2.3-394)

$$S_{WETCONETUR} = \frac{\pi D}{2} L_N \sec(\Theta_N/2) - \frac{\pi D_{\Delta X}}{2}(X_{TR} - \Delta X_N) =$$

$$= \frac{\pi D^2}{4}\left[\operatorname{cosec}(\Theta_N/2)\right]\left[1-\left(\frac{Re_{cr}}{Re^*_{FP}} - \frac{Re_{\Delta XN}}{Re^*_{FP}}\right)^2\right] \quad ,$$

(2.3-395)

$$S_{\Delta XWETCONE} = S_{WETLAMCONE} - \frac{\pi D_{\Delta X}}{2}(X_{TR} - \Delta X_N) =$$

$$= \frac{\pi D^2}{4}\left[\operatorname{cosec}(\Theta_N/2)\right]\left[\left(\frac{Re_{cr}}{Re^*_{FP}}\right)^2 - \left(\frac{Re_{cr}}{Re^*_{FP}} - \frac{Re_{\Delta XN}}{Re^*_{FP}}\right)^2\right] \quad ,$$

(2.3-396)

$$S_f = \frac{\pi D^2}{4} \quad .$$

Thus, Eq (2.3-386) takes the form:

$$(C_{DofN})^{III}_{L+T} = \left\{1.15\,\frac{1.022}{1.022}\,Cf_{LAMFP}\left(\frac{Re_{cr}}{Re^*_{FP}}\right)^2 + \right.$$

$$+ 1.022\, Cf_{TURFP} \times$$

$$\times\left[1-\left(\frac{Re_{cr}}{Re^*_{FP}} - \frac{Re_{\Delta XN}}{Re^*_{FP}}\right)^2\right] - 1.022\, Cf_{LAMFP}\left(\frac{Re_{cr}}{Re_{\Delta XN}}\right) \times$$

$$\left.\times\left[\left(\frac{Re_{cr}}{Re^*_{FP}}\right)^2 - \left(\frac{Re_{cr}}{Re^*_{FP}} - \frac{Re_{\Delta XN}}{Re^*_{FP}}\right)^2\right]\right\}\cot(\Theta_N/2) \quad ,$$

(2.3-397)

or, after rearrangements:

$$(C_{DofN})^{III}_{L+T} = \left\{1.022\, Cf_{LAMFP}\left(\frac{Re_{cr}}{Re^*_{FP}}\right)\left(\frac{Re_{\Delta XN}}{Re^*_{FP}} - \right.\right.$$

$$\left. - .875\frac{Re_{cr}}{Re^*_{FP}}\right) + 1.022\, Cf_{TURFP}\left(\frac{Re^*_{TURFP}}{Re^*_{FP}}\right)$$

$$\left.\left[1+\left(\frac{Re_{cr}}{Re^*_{FP}} - \frac{Re_{\Delta XN}}{Re^*_{FP}}\right)\right]\right\}\cot(\Theta_N/2) \quad ,$$

(2.3-398)

$$(C_{DofN})^{III}_{L+T} = G_1 \times\left\{Cf^{III}_{IL}\left(\frac{Re_{cr}}{Re^*_{FP}}\right)\left[\frac{Re_{\Delta XN}}{Re^*_{FP}} - \right.\right.$$

$$\left. - .875\frac{Re_{cr}}{Re^*_{FP}}\right] + Cf^{III}_{IT}\left(\frac{Re^*_{TURFP}}{Re^*_{FP}}\right)$$

$$\left.\left[1+\left(\frac{Re_{cr}}{Re^*_{FP}} - \frac{Re_{\Delta XN}}{Re^*_{FP}}\right)\right]\right\} \quad ,$$

(2.3-399)

$$\therefore (C_{DofN})^{III}_{L+T} = G_1 \times\left\{Cf^{III}_{IL} R_o\left[R'_o - .875 R_o\right] + \right.$$

$$\left. + Cf^{III}_{IT}\left[1-(R_o - R'_o)^2\right]\right\} \quad , \quad (2.3\text{-}400)$$

where,

$$G_1 = 1.022\cot(\Theta_N/2) \quad ,$$

$$Cf^{III}_{IL} = Cf_{LAMFP} = f_1(Re_{cr}, M) \quad ,$$

$$Cf^{III}_{IT} = Cf_{TURFP} = f_2(Re^*_{TURFP}, M) = f_2(Re^*_{TURN}, M) \quad ,$$

$$Re_{cr} = \frac{X_{TR} V_H}{\nu_H} ,$$

$$Re^*_{FP} = Re_{L_N} \sec(\Theta_N/2) = \frac{L_N V_H}{\nu_H} \sec(\Theta_N/2) = Re^*_N ,$$

$$Re_{\Delta XN} = \frac{\Delta X_N V_H}{\nu_H} , \text{ from Fig.(2.3-58),}$$

$$Re^*_{TURFP} = Re^*_{FP}\left[1-\left(\frac{Re_{cr}}{Re^*_{FP}} - \frac{Re_{\Delta XN}}{Re^*_{FP}}\right)\right] = Re^*_{TURN} = \left(Re^*_{TURFP}\right)^{III}_{NOSE} ,$$

$$R_o = \frac{Re_{cr}}{Re^*_{FP}} ,$$

$$R'_o = \frac{Re_{\Delta XN}}{Re^*_{FP}} . \qquad (2.3\text{-}401)$$

Assuming that $Re_{cr} = 1 \times 10^6$, Eq (2.3-400) takes the simpler form by virtue of the relationships (2.3-360):

$$\Delta X_N = .222 X_{TR} = .222 L_N\left[\sec(\Theta_N/2)\right]10^6/Re^*_{FP} = .222 L_N 10^6/Re_{L_N} .$$

$$Re_{\Delta XN} = .222 \times 10^6 ,$$

$$Re^*_{FP} = Re_{L_N}\sec(\Theta_N/2) = Re^*_N ,$$

$$Re_{L_N} = L_N V_H/\nu_H , \qquad (2.3\text{-}402)$$

$$Re^*_{TURFP} = Re^*_{FP} - .778 \times 10^6 = Re^*_N\left[1-.778\frac{10^6}{Re^*_N}\right] = Re^*_{TURN} ,$$

$$(C_{DOfN})^{III}_{L+T} = G_1\left\{C^{III}_{fIT}\left[1-(.778\frac{10^6}{Re^*_N})^2\right] - .653\, C^{III}_{fIL}(\frac{10^6}{Re^*_N})^2\right\} ,$$

$$\therefore (C_{DOfN})^{III}_{L+T} = G_1\left\{C^{III}_{fIT}\left[1-.606R_o^2\right] - .653\, C^{III}_{fIL} R_o^2\right\} ,$$

where, (2.3-403)

$$G_1 = 1.022\cot(\Theta_N/2) ,$$

$$C^{III}_{fIL} = C_{fLAMFP} = f_1(10^6, M) ,$$

$$C^{III}_{fIT} = C_{fTURFP} = f_2\left[Re^*_N(1-.778\frac{10^6}{Re^*_N}), M\right],$$

$$R_O = (\frac{10^6}{Re^*_N}) . \qquad (2.3\text{-}404)$$

Obviously, Eq (2.3-403) reduces to Eqs (2.3-387) or (2.3-389) for fully turbulent and fully laminar flows respectively:

For fully turbulent flow:

$$X_{TR} = 0 , \; Re_{cr} = 0 ,$$

$$(C_{DOfN})^I_T = G_1 C^I_{fIT} = G_1 \times f_1(Re^*_{TURN} = Re^*_{FP} = Re^*_N, M) . \qquad (2.3\text{-}405)$$

For fully laminar flow:

$$X_{TR} = L_N \sec(\Theta_N/2) , Re_{cr} = Re^*_{FP} = Re_{L_N}\sec(\Theta_N/2) = Re^*_N ,$$

$$C^{II}_{fIL} L_N \sec(\Theta_N/2) = C^{II}_{fIT}\Delta X , C^{II}_{fIT} = \Delta C_{fT} ,$$

$$\Delta X = .222 L_N \sec(\Theta_N/2) ,$$

$$C^{II}_{fIT} = (C^{II}_{fIL}/.222) ,$$

$$\therefore (C_{DOfN})^{II}_L = G_1\left\{\frac{C^{II}_{fIL}}{.222}\left[1-(.778)^2\right] - .653\, C^{II}_{fIL}\right\} ,$$

$$(C_{DOfN})^{II}_L = G_1\left\{1.778\, C^{II}_{fIL} - .653\, C^{II}_{fIL}\right\} = 1.125\, C^{II}_{fIL} G_1 ,$$

(2.3-406)

(iii) Cylinder + Boattail (Conical Frustrum)

There is no significant difference between the flat plate two-dimensional and the cylindrical body three-dimensional skin-friction coefficient values, (Eckert[19]), provided the ratio of boundary layer displacement thickness to cylinder diameter is less than 4%.

$$\frac{\delta^*}{D} < .04 \qquad (2.3\text{-}407)$$

Based on experimental data, the above condition may be extended for practical purposes up to

$$\left(\frac{L_{CYL}+L_{BT}}{D}\right) \sim O(10) \qquad (2.3\text{-}408$$

without introducing any appreciable error.

Evaluation of the transitional Reynolds Number values remains open to circumstantial criteria. For supersonic speeds, the wind-tunnel experimental evidence (Pitts[142]) suggests a definite transition at the wing-body juncture, especially so far zero-angle-of-attack conditions: the three-dimensional pattern of shock-

waves arising from the wings leading edge usually intersects the body in such a manner that a sharp pressure rise at, or in the vicinity of, the wing-body juncture promotes a boundary layer transition. It would be safe to assume that the possible extent of the laminar boundary layer should be limited to the "forebody" region at utmost.

The explicit expressions, taking into account the influence of the nose-cone boundary layer pre-existence, are derived in the following text for all the three cases of the boundary layer types. The method of derivations is the same as for the flat plate, see paragraph (i).

Case I: fully turbulent boundary layer on both the cylindrical part and the nose cone is assumed, i.e., transition is at the nose tip:

$$Re_N^* > Re_{cr} \ , \ X_{TR} = 0 \ .$$

The actual turbulent boundary layer build up on the nose cone incorporates three-dimensional flow effects, $C_{f_N} = 1.022\, C_{f_{TURFP}}$. Therefore, although for cylinders the three-dimensional effects are negligible, $C_{f_{CYL}} \approx C_{f_{TURFP}}$, the boundary layer growth along the effective (slant) missile length, interpreted in terms of an equivalent two-dimensional flat plat average skin-friction coefficient, takes the form (see Fig 2.3-43):

$$(2\theta^*)_{AT\ POINT\ B} = 1.022\,(C_{f_{TURFP}})^I_{NOSE}\, L_N \sec(\theta_N/2) =$$

$$= (C_{f_{TURFP}})^I_{NOSE} \times \Delta X_I \ , \qquad (2.3\text{-}409)$$

$$\Delta X_I = 1.022\, L_N \sec(\theta_N/2) \ , \qquad (2.3\text{-}410)$$

and

$$(C_{f_{TURFP}})^I_{CYL+BT} = (C_{f_{TURFP}})^I_{TOTAL} \ ,$$

$$\frac{\Delta X_I + L_{CYL} + L_{BT}\sec(\theta_B)}{L_{CYL} + L_{BT}\sec(\theta_B)} -$$

$$-(C_{f_{TURFP}})^I_{NOSE}\,\frac{\Delta X_I}{L_{CYL} + L_{BT}\sec(\theta_B)} \ , \qquad (2.3\text{-}411)$$

$$(C_{f_{TURFP}})^I_{CYL+BT} = (C_{f_{TURFP}})^I_{TOTAL}\left[1 + \frac{Re^I_{\Delta X}}{Re_{CYL} + Re^*_{BT}}\right] -$$

$$- (C_{f_{TURFP}})^I_{NOSE}\left[\frac{Re^I_{\Delta X}}{Re_{CYL+BT}}\right] \ , \qquad (2.3\text{-}412)$$

where,

$$(C_{f_{TURFP}})^I_{TOTAL} = f\left[Re^{*I}_{TOTAL},\ M\right] = C^I_{f2T} \ ,$$

$$Re^{*I}_{TOTAL} = Re^I_{\Delta X} + Re_{CYL} + Re^*_{BT} \ ,$$

$$Re^*_{BT} = Re_{BT}\sec(\theta_B) = \frac{\left[L_{BT}\sec(\theta_B)\right] V_H}{\nu_H} \ ,$$

$$Re^I_{\Delta X} = \frac{\Delta X_I V_H}{\nu_H} = 1.022\, Re^*_N = 1.022\, Re_{L_N}\sec(\theta_N/2) \ ,$$

$$Re_{CYL} = \frac{L_{CYL} V_H}{\nu_H} \ ,$$

$$Re^*_N = (Re^*_{TURFP})^I_{NOSE} = Re^*_N \sec(\theta_N/2) =$$

$$= \frac{\left[L_N \sec(\theta_N/2)\right] V_H}{\nu_H} \ ,$$

$$(C_{f_{TURFP}})^I_{NOSE} = C^I_{f_{IT}} = f(Re^*_N,\ M) \ . \qquad (2.3\text{-}413)$$

The corresponding zero-lift skin-friction drag force coefficient is:

$$(C_{DOf_{CYL+BT}})^I_T = (C_{f_{TURFP}})^I_{CYL+BT}\,\frac{S_{WET(CYL+BT)}}{S_r} \ , \qquad (2.3\text{-}414)$$

$$S_{WET(CYL+BT)} = \pi D L_{CYL} + \frac{\pi D^2}{4}\left[(\text{cosec}\ \theta_B)\left(1 - \frac{D_B}{D}\right) + 2\left(\frac{D_B}{D}\right)\left(\frac{L_{BT}}{D}\right)\sec(\theta_B)\right] \ , \qquad (2.3\text{-}415)$$

$$S_{WET(CYL+BT)} = \frac{\pi D^2}{4}\left\{4\left(\frac{L_{CYL}}{D}\right) + (\text{cosec}\ \theta_B)\left(1 - \frac{D_B}{D}\right) + 2\left(\frac{D_B}{D}\right)\left(\frac{L_{BT}}{D}\right)\sec(\theta_B)\right\} \ , \qquad (2.3\text{-}416)$$

$$\therefore (C_{DOf_{CYL+BT}})^I_T = \left\{C^I_{f2T}\left[1 + \frac{1.022 Re^*_N}{Re_{CYL} + Re^*_{BT}}\right] - C_{f_{IT}}\left[\frac{1.022 Re^*_N}{Re_{CYL} + Re^*_{BT}}\right]\right\}\frac{S_{WET(CYL+BT)}}{S_r} \ , \qquad (2.3\text{-}417)$$

and finally,

$$(C_{DOf_{CYL+BT}})^I_T = \left\{C^I_{f2T}\left[1 + R_I\right] - C^I_{f_{IT}} R_I\right\} G_2 \ , \qquad (2.3\text{-}418)$$

where,

$$C^I_{f2T} = (C_{f_{TURFP}})^I_{TOTAL} = f\left(Re^{*I}_{TOTAL},\ M\right) \ ,$$

$$Re^{*I}_{TOTAL} = Re^I_{\Delta X} + Re_{CYL} + Re^*_{BT} =$$

$$= 1.022\, Re^*_N + Re_{CYL} + Re^*_{BT} \ ,$$

$$Re^{*}_{BT} = Re_{BT}\sec(\Theta_B) = \frac{L_{BT}V_H}{\nu_H}\sec(\Theta_B) \ ,$$

$$Re_{CYL} = \frac{L_{CYL}V_H}{\nu_H} \ ,$$

$$Re^{I}_{\Delta X} = 1.022\,Re^{*}_{N} \ ,$$

$$Re^{*}_{N} = Re_{L_N}\sec\left(\frac{\Theta_N}{2}\right) = \frac{L_N V_H}{\nu_H}\sec\left(\frac{\Theta_N}{2}\right) \ ,$$

$$R_1 = \frac{1.022\,Re^{*}_{N}}{Re_{CYL} + Re^{*}_{BT}} \ ,$$

$$C^{I}_{fIT} = \left(C_{fTURFP}\right)^{I}_{NOSE} = f\left(Re^{*}_{N}, M\right) \ ,$$

$$G_2 = \left[4\left(\frac{L_{CYL}}{D}\right) + (\text{cosec}\ \Theta_B)\left(1 - \frac{D_B}{D}\right) + 2\left(\frac{D_B}{D}\right)\left(\frac{L_{BT}}{D}\right)\sec(\Theta_B)\right] .$$

(2.3-4

Case III A: A partially laminar, partially turbulent boundary layer on the nose cone; turbulent boundary layer on the cylinder, (see Fig 2.3-43). The necessary condition is:

$$Re^{*}_{N} = Re_{L_N}\sec\left(\frac{\Theta_N}{2}\right) > Re_{Cr} = (1 \times 10^6 \text{ eventually})$$

(2.3-420)

Following the same pattern of derivations as in Case I for cylindrical bodies and using Eqs (2.3-392) and (2.3-387) from Case III for nose cones:

$$(2\Theta^{*})_{AT\ POINT\ B} = 1.022\left(C_{fTURFP}\right)^{III}_{NOSE} \times$$

$$\times \left[\Delta X + L_N\sec(\Theta_N/2) - X_{TR}\right]^{III}_{NOSE} =$$

$$= \left(C_{fTURFP}\right)^{III}_{NOSE}\Delta X_{III\,A} \ ,$$

(2.3-421)

$$\therefore \Delta X_{III\,A} = 1.022\left[\Delta X + L_N\sec(\Theta_N/2) - X_{TR}\right]^{III}_{NOSE} \ ,$$

and (2.3-422)

$$\left(C_{fTURFP}\right)^{III\,A}_{CYL+BT} = \left(C_{fTURFP}\right)^{III\,A}_{TOTAL} \times$$

$$\times \frac{\Delta X_{III\,A} + L_{CYL} + L_{BT}\sec(\Theta_B)}{L_{CYL} + L_{BT}\sec(\Theta_B)} -$$

(2.3-423)

$$- \left(C_{fTURFP}\right)^{III}_{NOSE}\frac{\Delta X_{III\,A}}{L_{CYL} + L_{BT}\sec(\Theta_B)}$$

(2.3-423)

$$\therefore \left(C_{fTURFP}\right)^{III\,A}_{CYL+BT} = \left(C_{fTURFP}\right)^{III\,A}_{TOTAL} \times$$

$$\times \left[1 + \frac{1.022\left(Re^{*}_{TURFP}\right)^{III}_{NOSE}}{Re_{CYL} + Re^{*}_{BT}}\right] -$$

$$- \left(C_{fTURFP}\right)^{III}_{NOSE}\left[\frac{1.022\left(Re^{*}_{TURFP}\right)^{III}_{NOSE}}{Re_{CYL} + Re^{*}_{BT}}\right]$$

(2.3-424)

The respective zero-lift skin-friction drag coefficient is:

$$\left(C_{DOf\,CYL+BT}\right)^{III\,A}_{T} = \left(C_{fTURFP}\right)^{III\,A}_{CYL+BT}\frac{S_{WET(CYL+BT)}}{S_r} \ ,$$

$$\therefore \left(C_{DOf\,CYL+BT}\right)^{III\,A}_{T} = \left\{C^{III\,A}_{f2T}\left[1 + R_2\right] - C^{III}_{fIT}R_2\right\}G_2$$

where, (2.3-425)

$$C^{III\,A}_{f2T} = \left(C_{fTURFP}\right)^{III\,A}_{TOTAL} = f\left(Re^{*III\,A}_{TOTAL}, M\right) \ ,$$

$$Re^{*III\,A}_{TOTAL} = 1.022\left(Re^{*}_{TURFP}\right)^{III}_{NOSE} + Re_{CYL} + Re^{*}_{BT} \ ,$$

$$\left(Re^{*}_{TURFP}\right)^{III}_{NOSE} = Re^{*}_{TURN} = Re_{\Delta XN} + Re^{*}_{FP} - Re_{cr} =$$

$$= Re_{\Delta XN} + Re^{*}_{N} - Re_{cr} \ ,$$

$$Re_{\Delta XN} = \frac{\Delta X\, V_H}{\nu_H} \ , \text{ for nose cones, see Fig(2.3-58),}$$

$$Re^{*}_{N} = Re^{*}_{FP} = Re_{L_N}\sec(\Theta_N/2) = \frac{L_N V_H}{\nu_H}\sec(\Theta_N/2) \ ,$$

$$Re_{CYL} = \frac{L_{CYL}V_H}{\nu_H} \ ,$$

$$Re^{*}_{BT} = Re_{BT}\sec(\Theta_B) = \frac{L_{BT}V_H}{\nu_H}\sec(\Theta_B) \ ,$$

$$C^{III}_{fIT} = \left(C_{fTURFP}\right)^{III}_{NOSE} = f\left[\left(Re^{*}_{TURF}\right)^{III}_{NOSE}, M\right] =$$

$$= f\left[Re^{*}_{TURN}, M\right] \ ,$$

$$R_2 = \frac{1.022\left(Re^{*}_{TURFP}\right)^{III}_{NOSE}}{Re_{CYL} + Re_{BT}} = \frac{Re^{*}_{TURN} \times 1.022}{Re_{CYL} + Re_{BT}} \ ,$$

$$G_2 = \left[4\left(\frac{L_{CYL}}{D}\right) + (\text{cosec}\ \Theta_B)\left(1 - \frac{D_B}{D}\right) + 2\left(\frac{D_B}{D}\right)\left(\frac{L_{BT}}{D}\right) \times \sec(\Theta_B)\right] .$$

(2.3-426)

Case III B: A fully laminar boundary layer on the nose cone; a fully turbulent boundary layer on the cylinder. The necessary condition is:

$$Re^{*}_{FP} = Re^{*}_{N} = Re_{L_N}\sec(\Theta_N/2) = Re_{Cr} =$$

$$= (1 \times 10^6 \text{ eventually}) \ .$$

(2.3-427)

From Fig (2.3-43) in this case:

$$(2\theta^*)_{\text{AT POINT B}} = 1.15(Cf_{LAMFP})^{II}_{NOSE} L_N \sec(\theta_N/2) =$$

$$= (\Delta Cf_{TURFP})^{IIIB}_{CYL} \Delta X_{IIIB} ,$$

$$(\Delta Cf_{TURFP})^{IIIB}_{CYL} = Cf^{II}_{IL} \frac{1.15 Re^*_N}{Re^{IIIB}_{\Delta X}} \rightarrow \text{from Fig. (2.3-58)}$$

$$Re^{IIIB}_{\Delta X} = f(1.15\, Re^*_N , M) \rightarrow \text{from Fig. (2.3-58)} \qquad (2.3\text{-}428)$$

and

$$(Cf_{TURFP})^{IIIB}_{CYL+BT} = (Cf_{TURFP})^{IIIB}_{TOTAL} \times$$

$$\times \frac{\Delta X_{IIIB} + L_{CYL} + L_{BT}\sec(\theta_B)}{L_{CYL} + L_{BT}\sec(\theta_B)} -$$

$$-(\Delta Cf_{TURFP})^{IIIB}_{CYL} \frac{\Delta X_{IIIB}}{L_{CYL} + L_{BT}\sec(\theta_B)} ,$$

(2.3-429)

$$(Cf_{TURFP})^{IIIB}_{CYL+BT} = (Cf_{TURFP})^{IIIB}_{TOTAL} \left[1 + \frac{Re^{IIIB}_{\Delta X}}{Re_{CYL} + Re^*_{BT}}\right] -$$

$$-(\Delta Cf_{TURFP})^{IIIB}_{CYL} \left[\frac{Re^{IIIB}_{\Delta X}}{Re_{CYL} + Re^*_{BT}}\right] . \qquad (2.3\text{-}430)$$

The zero-lift skin-friction drag coefficient is:

$$(C_{DOf_{CYL+BT}})^{IIIB}_T = (Cf_{TURFP})^{IIIB}_{CYL+BT} \frac{S_{WET\,(CYL+BT)}}{S_r} ,$$

$$(C_{DOf_{CYL+BT}})^{IIIB}_T = \left\{Cf^{IIIB}_{2T}\left[1+R_3\right] - (\Delta Cf_{TURFP})^{IIIB}_{CYL} R_3\right\} G_2 .$$

(2.3-431)

where,

$$Cf^{IIIB}_{2T} = (Cf_{TURFP})^{IIIB}_{TOTAL} = f_1(Re^{*IIIB}_{TOTAL} , M) ,$$

$$Re^{*IIIB}_{TOTAL} = Re^{IIIB}_{\Delta X} + Re_{CYL} + Re^*_{BT} ,$$

$$Re^*_{BT} = Re_{BT}\sec(\theta_B) = \frac{L_{BT} V_H}{\nu_H}\sec(\theta_B) ,$$

$$Re_{CYL} = \frac{L_{CYL} V_H}{\nu_H} ,$$

$$Re^{IIIB}_{\Delta X} = f(1.15\, Re^*_N , M) \rightarrow \text{from Fig. 2.3-58} ,$$

$$(\Delta Cf_{TURFP})^{III}_{CYL} = Cf^{II}_{IL} \frac{1.15 Re^*_N}{Re^{IIIB}_{\Delta X}} , \text{ or directly from Fig. 2.3-58,}$$

$$Re^*_N = Re^*_{FP} = Re_{L_N}\sec(\theta_N/2) = \frac{L_N V_H}{\nu_H}\sec(\theta_N/2) ,$$

$$R_3 = \frac{Re^{IIIB}_{\Delta X}}{Re_{CYL} + Re^*_{BT}} ,$$

$$Cf^{II}_{IL} = f_2(Re^*_N , M) ,$$

$$G_2 = \left[4\left(\frac{L_{CYL}}{D}\right) + (\text{cosec}\ \theta_B)\left(1 - \frac{D_B}{D}\right) + 2\left(\frac{D_B}{D}\right)\left(\frac{L_{BT}}{D}\right)\sec(\theta_B)\right].$$

(2.3-432)

Case III C: A fully laminar boundary layer on the nose cone; a partially laminar, partially turbulent boundary layer on the cylinder. The maximum extent of the laminar boundary layer on the cylinder is restricted to forebody. The necessary condition is:

$$Re^*_N = Re^*_{FP} < Re_{cr} \lesssim Re^*_{FOREBODY} . \qquad (2.3\text{-}433)$$

The average skin-friction coefficient of the "mixed" boundary layer in terms of an equivalent flat plate is (see Fig 2.3-43):

$$1.022\,(Cf_{LAMFP})^{II}_{NOSE} \times L_N \sec(\theta_N/2) = (Cf_{LAMFP})^{II}_{NOSE} \Delta X' ,$$

$$\Delta X' = 1.022\, L_N \sec(\theta_N/2) ,$$

and (2.3-434)

$$(Cf_{LAMFP})^{IIIC}_{TOTAL} (\Delta X' + \Delta X'') = (\Delta Cf_{TURFP})^{IIIC}_{CYL} \Delta X_{IIIC} ,$$

$$\Delta X' + \Delta X'' = X_{TR} + .022 L_N \sec(\theta_N/2) =$$

$$= \left[L_N \sec(\theta_N/2)\right]\left[.022 + \frac{Re_{cr}}{Re^*_N}\right] ,$$

$$X_{TR} = Re_{cr}\frac{\nu_H}{V_H} = \left[L_N \sec(\theta_N/2)\right]\frac{Re_{cr}}{Re^*_N} ,$$

$$\Delta X_{IIIC} = Re^{IIIC}_{\Delta X}\frac{\nu_H}{V_H} , \text{ from Fig. 2.3-58 ,}$$

$$Re^{IIIC}_{\Delta X} = f(Re_{cr} , M), \text{ from Fig. 2.3-58 ,}$$

$$(\Delta Cf_{TURFP})^{IIIC}_{CYL} = f(Re^{IIIC}_{\Delta X} , M) , \text{ from Fig. 2.3-58 ,}$$

$$\Delta X'' = X_{TR} - L_N \sec(\theta_N/2) ,$$

so that, (2.3-435)

$$(Cf_{LAM+TUR})^{IIIC}_{CYL+BT}\left[L_{CYL} + L_{BT}\sec(\theta_B)\right] =$$

$$= (C_{f_{TURFP}})^{III C}_{TOTAL} \left[L_{CYL} - \Delta X' + \Delta X_{III C} + L_{BT} \sec(\Theta_B) \right] -$$

$$- (C_{f_{LAMFP}})^{I}_{NOSE} \left[\Delta X' \right] , \qquad (2.3\text{-}36)$$

$$\therefore (C_{f_{LAM+TUR}})^{III C}_{CYL+BT} = (C_{f_{TURFP}})^{III C}_{TOTAL} \times$$

$$\times \left[1 + \frac{\Delta X_{III C} - X_{TR} + L_N \sec(\Theta_N/2)}{L_{CYL} + L_{BT} \sec(\Theta_B)} \right] -$$

$$- \left[(C_{f_{LAMFP}})^{II}_{NOSE} \frac{1.022\, L_N \sec(\Theta_N/2)}{L_{CYL} + L_{BT} \sec(\Theta_B)} \right] . \qquad (2.3\text{-}437)$$

The average skin-friction drag coefficient is then:

$$(C_{DOf_{CYL+BT}})^{III C}_{L+T} = (C_{f_{L+T}})^{III C}_{CYL+BT} \frac{S_{WET\,(CYL+BT)}}{S_r} , \qquad (2.3\text{-}238)$$

$$(C_{DOf_{CYL+BT}})^{III C}_{L+T} = \left\{ C^{III C}_{f2T} \left[1 + R_4 + \frac{R_1}{1.022} \right] - C^{II}_{fIL} R_1 \right\} G_2 , \qquad (2.3\text{-}239)$$

where,

$$C^{III C}_{f2T} = (C_{f_{TURFP}})^{III C}_{TOTAL} = f_2 \left[Re^{*III C}_{TOTAL} , M \right] ,$$

$$Re^{*III C}_{TOTAL} = Re^{*III C}_{TURFP} + Re_{CYL} + Re^{*}_{BT} ,$$

$$Re^{*III C}_{TURFP} = Re^{*}_{N} + Re^{III C}_{\Delta X} - Re_{cr} ,$$

$$Re^{*}_{N} = Re^{*}_{FP} = Re_{L_N} \sec(\Theta_N/2) = \frac{L_N V_H}{\nu_H} \sec(\Theta_N/2) ,$$

$$Re_{CYL} = \frac{L_{CYL} V_H}{\nu_H} ,$$

$$Re^{*}_{BT} = Re_{BT} \sec(\Theta_B) = \frac{L_{BT} V_H}{\nu_H} \sec(\Theta_B) ,$$

$$Re_{cr} = \frac{X_{TR} V_H}{\nu_H} = (1 \times 10^6 \text{ eventually}) ,$$

$$Re^{III C}_{\Delta X} = f(Re_{cr} , M) \quad \text{from Fig. (2.3-58)} ,$$

$$C^{I}_{fIL} = f_2(Re^{*}_{N} , M) ,$$

$$R_1 = \frac{1.022\, Re^{*}_{N}}{Re_{CYL} + Re^{*}_{BT}} ,$$

$$R_4 = \frac{Re^{III C}_{\Delta X} - Re_{cr}}{Re_{CYL} + Re^{*}_{BT}} ,$$

$$G_2 = \left[4 \left(\frac{L_{CYL}}{D} \right) + (\text{cosec } \Theta_B) \left(1 - \frac{D_B}{D} \right) + \right.$$

$$\left. + 2 \left(\frac{D_B}{D} \right) \left(\frac{L_{BT}}{D} \right) \sec(\Theta_B) \right] . \qquad (2.3\text{-}440)$$

Alternatively, if $Re_{cr} = 1 \times 10^6$ is chosen, together with the approximation expressed by Eq (2.3-377), the final Eqs (2.3-418), (2.3-425), (2.3-431) and (2.3-439) reduce to the following simpler forms for $C_{DOf_{CYL+BT}}$:

Case I: Eq (2.3-418) unchanged.

Case III A:

$$(C_{DOf_{CYL+BT}})^{III A}_{T} = \left\{ C^{III A}_{f2T} \left[1 + R_2 \right] - C^{III}_{fIT} R_2 \right\} G_2 , \qquad (2.3\text{-}441)$$

where,

$$C^{III A}_{f2T} = (C_{f_{TURFP}})^{III A}_{TOTAL} = f\,(Re^{III A}_{TOTAL} , M) ,$$

$$Re^{III A}_{TOTAL} = 1.022\, Re^{*}_{N} - .795 \times 10^6 + Re_{CYL} + Re^{*}_{BT} ,$$

$$Re^{*}_{N} = Re^{*}_{FP} = Re_{L_N} \sec(\Theta_N/2) = \frac{L_N V_H}{\nu_H} \sec(\Theta_N/2) ,$$

$$Re^{*}_{BT} = Re_{BT} \sec(\Theta_B) = \frac{L_{BT} V_H}{\nu_H} \sec(\Theta_B) ,$$

$$Re_{CYL} = \frac{L_{CYL} V_H}{\nu_H} ,$$

$$R_2 = \frac{1.022\, Re^{*}_{N} - .795 \times 10^6}{Re_{CYL} + Re^{*}_{BT}} ,$$

$$C^{III}_{fIT} = (C_{f_{TURFP}})^{III}_{NOSE} = f\left[(Re^{*}_{N} - .778 \times 10^6) , M \right] ,$$

$$G_2 = \left[4 \left(\frac{L_{CYL}}{D} \right) + (\text{cosec } \Theta_B) \left(1 - \frac{D_B}{D} \right) + \right.$$

$$\left. + 2 \left(\frac{D_B}{D} \right) \left(\frac{L_{BT}}{D} \right) (\sec \Theta_B) \right] . \qquad (2.3\text{-}442)$$

Case III B:

$$(C_{DOf\,CYL+BT})^{III B}_{T} = \left\{ C^{III B}_{f2T} \left[1 + R_3 \right] - 4.5\, C^{II}_{fIL} R_3 \right\} G_2 , \qquad (2.3\text{-}443)$$

where,

$$C^{III B}_{f2T} = (C_{f_{TURFP}})^{III B}_{CYL+BT} = f_1 \left[Re^{*III B}_{TOTAL} , M \right] ,$$

$$Re^{*III B}_{TOTAL} = .255 \times 10^6 + Re_{CYL} + Re^{*}_{BT} ,$$

$$Re^{*}_{BT} = Re_{BT} \sec(\Theta_B) = \frac{L_{BT} V_H}{\nu_H} \sec(\Theta_B) ,$$

$$Re_{CYL} = \frac{L_{CYL} V_H}{\nu_H} ,$$

$$R_3 = \frac{.255 \times 10^6}{Re_{CYL} + Re^*_{BT}} ,$$

$$C^{II}_{fIL} = f_2(10^6, M) = (C_{f_{LAMFP}})^{II}_{NOSE} ,$$

$$G_2 = \left[4\left(\frac{L_{CYL}}{D}\right) + (\operatorname{cosec} \Theta_B)\left(1 - \frac{D_B}{D}\right) + \right.$$
$$\left. + 2\left(\frac{D_B}{D}\right)\left(\frac{L_{BT}}{D}\right) \sec \Theta_B \right] . \qquad (2.3\text{-}444)$$

Case III C:

$$(C_{D_{0f\,CYL+BT}})^{III\,C}_{L+T} =$$
$$= \left\{ C^{III\,C}_{f2T}\left[1 + R_4 + \frac{R_1}{1.022}\right] - C^{II}_{fIL} R_1 \right\} G_2 , \qquad (2.3\text{-}445)$$

where,

$$C^{III\,C}_{f2T} = (C_{f_{TURFP}})^{III\,C}_{TOTAL} =$$
$$= f_1\left[\left(Re^*_N - .788 \times 10^6 + Re_{CYL} + Re^*_{BT}\right), M\right] ,$$

$$C^{II}_{fIL} = (C_{f_{LAMFP}})^{II}_{NOSE} = f_2\left(Re^*_N, M\right) ,$$

$$Re^*_N = Re^*_{FP} = Re_{LN} \sec\left(\Theta_N/2\right) = \frac{L_N V_H}{\nu_H} \sec\left(\Theta_N/2\right) ,$$

$$Re_{CYL} = \frac{L_{CYL} V_H}{\nu_H} ,$$

$$Re^*_{BT} = Re_{BT} \sec\left(\Theta_B\right) = \frac{L_{BT} V_H}{\nu_H} \sec\left(\Theta_B\right) ,$$

$$R_1 = \frac{1.022\, Re^*_N}{Re_{CYL} + Re^*_{BT}} ,$$

$$R_4 = -\frac{.778 \times 10^6}{Re_{CYL} + Re^*_{BT}} ,$$

$$G_2 = \left[4\left(\frac{L_{CYL}}{D}\right) + (\operatorname{cosec} \Theta_B)\left(1 - \frac{D_B}{D}\right) + \right.$$
$$\left. + 2\left(\frac{D_B}{D}\right)\left(\frac{L_{BT}}{D}\right) \sec\left(\Theta_B\right)\right] . \qquad (2.3\text{-}446)$$

(iv) Cylinder + Boattail (Parabolic)

In a first approximation, the Eqs (2.3-418), (2.3-425), (2.3-431) and (2.3-439) can be used.

(v) Wings and Fins

It is assumed that the wings (or fings) are of relatively small thickness ratio (~ 6%). Then, within a first approximation, the total wetted surface may be taken equal to twice the exposed planform area. No corrections for the three-dimensional flow effects are performed, see Section 2.3.4.

Experiments by Vincenti[143] indicate that for triangular double-wedge wings at zero-angle-of-attack, under controlled wind-tunnel flow conditions, the transition from laminar to turbulent boundary layer is induced at the ridge line if the flow at the ridge is subsonic. The transition is caused by a corresponding rapid increase in pressure directly behind the "subsonic" ridge line. For "supersonic" ridge lines the pressure rise is delayed to the point where the Mach lines associate with the ridge line. A greater laminar flow area may be expected with the transition shifted somewhat backward. Considering the types of wings and profiles specified in Table (2.5-6), Section 2.5, it seems recommendable that under actual flight conditions the laminar boundary layer on lifting surfaces should be restricted to the ridge line at utmost. With a critical Reynolds Number fixed at 1×10^6, the practical limit for laminar boundary layer existance is thus restricted to,

$$X_{TR} \geq X_{LAM} \leq X_{RIDGE} \approx 1/2\, c , \qquad (2.3\text{-}447)$$

where c is the local wing chord.

For practical quick estimates, it is proposed that in a first approximation the skin-friction drag due to wings (or fins) be computed assuming either a fully turbulent boundary layer or a partially laminar, partially turbulent boundary layer. The procedure is thus simplified, and the eventual "error" in comparison with more idealistic fully laminar flow conditions is on the safe side of the total drag predictions under actual atmospheric flight conditions and the manufactured surface conditions, which may render a theoretically idealized laminar boundary layer existence very dubious. Nevertheless, if the idealized laminar boundary layer alternative is accepted for any justifiable reason, the computational procedure of Case I (fully turbulent boundary layer) can be always easily substituted by the corresponding Case II method (fully laminar boundary layer), see the flat plate paragraph (i).

Case I: A fully turbulent boundary

layer is supposed, i.e., a transition at the leading edge is assumed: $X_{TR} = 0$.

Taking the equivalent flat plate skin-friction results for a basic reference, the zero-lift skin-friction drag coefficient for exposed wing surfaces is

$$(C_{D0f_{WEXP}})^{I}_{T} = (C_{f_{TURFP}})^{I}_{W} \frac{S_{WETWEXP}}{S_r} \quad , \qquad (2.3\text{-}448)$$

$$(C_{D0f_{WEXP}})^{I}_{T} = C_{f_{3T}}^{I} G_3 \quad , \qquad (2.3\text{-}449)$$

where,

$$C_{f_{3T}}^{I} = (C_{f_{TURFP}})^{I}_{W} = f(Re_{\bar{c}_W}, M) \quad ,$$

$$Re_{\bar{c}_W} = \frac{\bar{C}_{WEXP} V_H}{\nu_H} \quad ,$$

$$\bar{C}_{WEXP} = \frac{S_{WEXP}}{b_{WEXP}} \quad ,$$

$$G_3 = 2.55\left(\frac{\bar{C}_{WEXP}}{D}\right)\left(\frac{b_{WEXP}}{D}\right) = \frac{S_{WEXPWET}}{S_r} \quad . \qquad (2.3\text{-}450)$$

In the same way, for fins:

$$(C_{D0f_{FEXP}})^{I}_{T} = N\, C_{f_{4T}}^{I} G_4 \quad , \qquad (2.3\text{-}451)$$

where,

$$C_{f_{4T}}^{I} = (C_{f_{TURFP}})^{I}_{F} = f(Re_{\bar{c}_F}, M),$$

$$Re_{\bar{c}_F} = \frac{\bar{C}_{FEXP} V_H}{\nu_H} \quad ,$$

$$\bar{C}_{FEXP} = \frac{S_{FEXP}}{b_{FEXP}} \quad ,$$

$$h_{FEXP} = \frac{b_{FEXP}}{2} = \frac{b_F - D}{2} \quad ,$$

N = number of individual fins ,

S_{FEXP} = planform area of one fin ,

$$G_4 = 2.55\left(\frac{\bar{C}_{FEXP}}{D}\right)\left(\frac{h_{FEXP}}{D}\right) = \frac{S_{WETFEXP}}{S_r} \quad . \qquad (2.3\text{-}452)$$

Case III: partially laminar, partially turbulent boundary layer. Extent of the laminar boundary restricted to ($\bar{c}/2$). The necessary conditions are:

$$X_{LAM} \leq \bar{c}/2 \lesseqgtr X_{TR} \quad ,$$

$$Re_{cr} = \frac{X_{TR} V_H}{\nu_H} = (1 \times 10^6 \text{ eventually}) \qquad (2.3\text{-}453)$$

Using the corresponding equivalent flat plate results, paragraph (i), the zero-lift skin-friction drag coefficient is for wings,

$$(C_{D0f_{WEXP}})^{III}_{L+T} = (C_{f_{FP}})^{III}_{MIXED} \frac{S_{WETWEXP}}{S_r} \quad , \qquad (2.3\text{-}455)$$

i.e., with

$$(C_{f_{FP}})^{III}_{MIXED} = (C_{f_{TURFP}}^{III})_{TOTAL}\left[1 - \frac{Re_{cr} - Re_{\Delta X}}{Re_{\bar{c}_W}}\right] =$$

$$= (C_{f_{TURFP}}^{III})_{TOTAL} \frac{Re_{TURFP}}{Re_{\bar{c}_W}} \quad , \qquad (2.3\text{-}456)$$

it follow that

$$(C_{D0f_{WEXP}})^{III}_{L+T} = C_{f_{3T}}^{III} G_3 R_5, \qquad (2.3\text{-}457)$$

where,

$$C_{f_{3T}}^{III} = (C_{f_{TURFP}}^{III})_{TOTAL} = f\left[(Re_{TURFP})^{III}_{W}, M\right] \quad ,$$

$$(Re_{TURFP}^{III})_W = Re_{\bar{c}_W}\left(1 - \frac{Re_{TRW} - Re_{\Delta XW}}{Re_{\bar{c}_W}}\right) = Re_{\bar{c}_W} R_5 \quad ,$$

$$Re_{\bar{c}_W} = \frac{\bar{C}_{WEXP} V_H}{\nu_H} \quad ,$$

$$\bar{C}_{WEXP} = \frac{S_{WEXP}}{b_{WEXP}} \quad ,$$

$$Re_{TRW} = \frac{X_{TRW} V_H}{\nu_H} \leq \frac{Re_{\bar{c}_W}}{2} \geq Re_{cr} = (1 \times 10^6 \text{ eventually}) \quad ,$$

$$Re_{\Delta XW} = f\left[(Re_{TRW} \leq \tfrac{1}{2} Re_{\bar{c}_W}), M\right] \quad , \text{ from Fig. (2.3-58)}$$

$$R_5 = \frac{(Re_{TURFP}^{III})_W}{Re_{\bar{c}_W}} = \left(1 - \frac{Re_{TRW} - Re_{\Delta XW}}{Re_{\bar{c}_W}}\right) \quad ,$$

$$G_3 = 2.55\left(\frac{\bar{C}_{WEXP}}{D}\right)\left(\frac{b_{WEXP}}{D}\right) \quad . \qquad (2.3\text{-}458)$$

Alternatively, with $Re_{cr} = 1 \times 10^6$ and $\Delta X = .222\, X_{TR}$, Eq (2.3-457) takes the simpler approximate form:

$$(C_{D0f_{WEXP}})^{III}_{L+T} = C_{f_{3T}}^{III} G_3 R_5 \quad ,$$

(2.3-459)

where,

$$C_{f_{3T}}^{III} = (C_{f_{TURFP}}^{III})_{TOTAL} = f\left[(Re_{TURFP})_W^{III}, M\right] ,$$

$$(Re_{TURFP})_W^{III} = Re_{\bar{c}_W}\left[1 - \frac{.778 Re_{TRW}}{Re_{\bar{c}_W}}\right] = Re_{\bar{c}_W} R_5 ,$$

$$Re_{\Delta XW} = .222 \times 10^6 ,$$

$$Re_{TRW} = \frac{X_{TR} V_H}{\nu_H} \leq \frac{1}{2} Re_{\bar{c}_W} \geq Re_{cr} = 1 \times 10^6 ,$$

$$R_5 = \frac{(Re_{TURFP})_W^{III}}{Re_{\bar{c}_W}} = \left(1 - \frac{.778 \times 10^6}{Re_{\bar{c}_W}}\right) ,$$

$$G_3 = 2.55\left(\frac{\bar{C}_{WEXP}}{D}\right)\left(\frac{b_{WEXP}}{D}\right) . \qquad (2.3\text{-}460)$$

In the same way, the zero-lift skin-friction drag coefficient for N fins is

$$(C_{DOfFEXP})_{L+T}^{III} = N C_{f_{4T}}^{III} R_6 G_4 , \qquad (2.3\text{-}461)$$

where N is the number of individual fins, and:

$$C_{f_{4T}}^{III} = (C_{fTURFP})_{TOTAL}^{III} = f\left[(Re_{TURFP})_F^{III}, M\right] ,$$

$$(Re_{TURFP})_F^{III} = Re_{\bar{c}_F}\left[1 - \frac{Re_{TRF} - Re_{\Delta XF}}{Re_{\bar{c}_F}}\right] ,$$

$$Re_{TRF} = \frac{X_{TRF} V_H}{\nu_H} \leq \frac{1}{2} Re_{\bar{c}_F} \geq Re_{cr} = (1 \times 10^6 \text{ eventually}) ,$$

$$Re_{\Delta XF} = f(Re_{TRF} \leq \tfrac{1}{2} Re_{\bar{c}_F}, M) \rightarrow \text{from Fig. (2.3-58)}$$

$$Re_{\bar{c}_F} = \frac{\bar{C}_{FEXP} V_H}{\nu_H} ,$$

$$C_{FEXP} = \frac{S_{FEXP}}{b_{FEXP}} ,$$

$$Re_{TRF} = \frac{X_{TRF} V_H}{\nu_H} \leq \frac{1}{2} Re_{\bar{c}_F} ,$$

$$R_6 = \frac{(Re_{TURFP})_F^{III}}{Re_{\bar{c}_F}} = \left[1 - \frac{Re_{TRF} - Re_{\Delta XF}}{Re_{\bar{c}_F}}\right] ,$$

$$G_4 = 2.55\left(\frac{\bar{C}_{FEXP}}{D}\right)\left(\frac{h_{FEXP}}{D}\right) = \frac{S_{WETFEXP}}{Sr} ,$$

$$h_{FEXP} = \frac{b_{FEXP}}{2} = \frac{b_F - D}{2} .$$

(2.3-462)

Alternatively, with $Re_{cr} = 1 \times 10^6 \geq Re_{TR}$ and $\Delta X = .222 X_{TR}$, Eq (2.3-461) reduces to the approximate form,

$$(C_{DOfFEXP})_{L+T}^{III} = N C_{f_{4T}}^{III} R_6 G_4 ,$$

(2.3-463)

where N is the number of individual fins, and:

$$C_{f_{4T}}^{III} = (C_{fTURFP})_{TOTAL}^{III} = f\left[(Re_{TURFP})_F^{III}, M\right] ,$$

$$(Re_{TURFP})_F^{III} = Re_{\bar{c}_F}\left[1 - \frac{.778 \times 10^6}{Re_{\bar{c}_F}}\right] = Re_{\bar{c}_F} R_6 ,$$

$$Re_{\Delta XF} = .222 \times 10^6 ,$$

$$Re_{\bar{c}_F} = \frac{\bar{C}_{FEXP} V_H}{\nu_H} ,$$

$$R_6 = \frac{(Re_{TURFP})_F^{III}}{Re_{\bar{c}_F}} = \left[1 - \frac{.778 \times 10^6}{Re_{\bar{c}_F}}\right] ,$$

$$G_4 = 2.55\left(\frac{\bar{C}_{FEXP}}{D}\right)\left(\frac{h_{FEXP}}{D}\right) . \qquad (2.3\text{-}464)$$

(vi) Within the state limitations, the explicit step-by-step instructions for the total zero-lift skin-friction drag coefficient computations are presented in the following Section, 2.3.9. A corresponding tabular form for the computations is also given in Tables (2.3-5) to (2.3-16).

2.3.9 INSTRUCTIONS FOR USE OF THE PROPOSED METHODS FOR SKIN-FRICTION DRAG COEFFICIENT ESTIMATES

Note: All tables related to this section, 2.3.9, are compiled at the end of the section. All graphs are compiled at the end of the overall Section 2.3.

(i) The Total Zero-lift Skin-friction Drag Coefficient Expressions

The results of the analytical procedures presented in the preceding Section 2.3.8 are summarized in Table (2.3-5a) to (2.3-5f), meant to serve as basic reference data. They should be used in connection with other instructive Tables (2.3-6) to (2.3-16) for direct computations of the total zero-lift skin-friction drag coefficient by the various methods.

In view of the developments presented in the preceding Section 2.3.8, the basic expression for the total skin-friction drag coefficient for all the three boundary layer types (Case I, II and III respectively) can be re-written in a common form as:

$$C_{Dof_M} = C_{f_1} G_1 + C_{f_2} G_2 + C_{f_3} G_3 + C_{f_4} G_4 N + \Delta C_{Dof_{PARTS}} , \qquad (2.3\text{-}465)$$

where C_{Dof_M} is the total missile zero-lift skin-friction drag coefficient and C_{f_1}, C_{f_2}, C_{f_3} and C_{f_4} are the average skin-friction coefficients related to the nose, cylinder + boattail, wings and fins, respectively, while G_1, G_2, G_3, G_4 are the corresponding geometric factors.

The last term, $\Delta C_{Dof_{PARTS}}$, refers to all other external configurational shapes, and should be evaluated separately by using the corresponding data from the related technical literature, such as Refs. 21, 132, 133, 134, 135, 136, etc. It will not be treated here, since a generalized analytical approach is cumbersome for the particular geometrical forms, such as canopies, nacelles, turrets, landing gears, cabin-domes, etc.

The numerical values of the average skin friction coefficients depend upon many variables, pertinent to any selected flight condition and the associated boundary layer status. Selecting the few most important parameters as independent variables, the average skin-friction coefficient can be conveniently expressed as an explicit function of:

$$C_f = f\left[Re, Re_{cr}, M, H, (T_W/T_H), k, ng, t, \text{body shape} \right]_H , \qquad (2.3\text{-}466)$$

where

M_H - is the flight Mach Number at a given altitude,

$(Re_{cr})_H$ - is the critical Reynolds Number, serving as a criteria of the boundary layer status on the respective missile part,

$(Re)_H$ - is the Reynolds Number of the particular missile part, based on its characteristic length, L, and the ambient flight condition ρ_H, V_H, and μ_H,

H - is the flight altitude,

(T_W/T_H) - is the skin to ambient temperature (average) ratio,

k - is the "equivalent" surface-roughness parameter, (see Table (2.3-2),

ng - is the total acceleration, in multiples of g,

t - is the time.

Regarding the boundary layer status as referred to the total missile configuration, the different individual cases (analyzed in the preceding section) can be combined to form the following resultant possibilities:

Case I M: a fully turbulent boundary layer is assumed on all missile parts. It represents the simplest approach to the problem; results may be judged on the conservative side when compared to a more accurate approach, with the actual "degree of accuracy" remaining debatable under the actual atmospheric flight conditions. The corresponding expression is (omitting the term $\Delta C_{Dof_{PARTS}}$):

$$C_{DofIM} = C_{f_1}^I G_1 + C_{f_2}^I G_2 + C_{f_3}^I G_3 + C_{f_4}^I G_4 N , \qquad (2.3\text{-}467)$$

$$\therefore C_{DOfIM} = C_{f_{1T}}^{I} G_1 + \left\{ C_{f_{2T}}^{I} \left[1 + R_1 \right] - C_{f_{1T}}^{I} R_1 \right\} G_2 +$$

$$+ C_{f_{3T}}^{I} G_3 + C_{f_{4T}}^{I} N G_4 \qquad (2.3\text{-}468)$$

or

$$C_{DOfIM} = (C_{DOfN})_T^I + (C_{DOfCYL+BT})_T^I +$$

$$+ (C_{DOfWEXP})_T^I + (C_{DOfFEXP})_T^I \qquad (2.3\text{-}469)$$

where $(C_{DOfN})_T^I$, $(C_{DOfCYL+BT})_T^I$, $(C_{DOfWEXP})_T^I$, $(C_{DOfFEXP})_T^I$ are given by Eqs (2.3-387), (2.3-418), (2.3-449) and (2.3-451), respectively.

Case II M: a partially laminar, partially turbulent boundary layer exists on the nose cone; a fully turbulent boundary layer on the cylindrical part of missile body; a partially laminar. partially turbulent boundary layer on wings and fins, up to $(\bar{C}/2)$ at the most. The Reynolds Number criteria are:

(1) for nose cones: $Re_N^* > Re_{cr}$ (Case III),

(2) for cylinder + boattail (Case III A),

(3) for wings: $Re_{cr} \geq Re_{TRW} \leq (Re_{\bar{C}_W}/2)$

$X_{TRW} \leq (\bar{C}_{WEXP}/2)$ (Case III),

(4) for fins: $Re_{cr} \geq Re_{TRF} \leq (Re_{\bar{C}_F}/2)$

$X_{TRF} \leq (\bar{C}_{FEXP}/2)$ (Case III),

and

$$C_{DOfIIM} = C_{f_1}^{III} G_1 + C_{f_2}^{IIIA} G_2 + C_{f_3}^{III} G_3 + C_{f_4}^{III} G_4 N ,$$

(2.3-470)

$$C_{DOfIIM} = \left\{ C_{f_{1T}}^{III} \left[1 - (R_0 - R_0')^2 \right] + \right.$$

$$\left. + C_{f_{1L}}^{III} R_0 \left[R_0' - .875 R_0 \right] \right\} G_1 + \left\{ C_{f_{2T}}^{IIIA} \left[1 + R_2 \right] - \right.$$

$$\left. - C_{f_{1T}}^{III} R_2 \right\} G_2 + C_{f_{3T}}^{III} R_5 G_3 + C_{f_{4T}}^{III} R_6 N G_4$$

or (2.3-471)

$$C_{DOfIIM} = (C_{DOfN})_{L+T}^{III} + (C_{DOfCYL+BT})_T^{IIIA} +$$

$$+ (C_{DOfWEXP})_{L+T}^{III} + (C_{DOfFEXP})_{L+T}^{III} ,$$

(2.3-472)

where

$(C_{DOfN})_{L+T}^{III}$, $(C_{DOfCYL+BT})_T^{IIIA}$,

$(C_{DOfWEXP})_{L+T}^{III}$ and $(C_{DOfFEXP})_{L+T}^{III}$

are given by Eqs (2.3-400), (2.3-425), (2.3-457) and (2.3-461), respectively.

Case III M: a fully laminar boundary layer on the nose cone, with transition occurring at the point B, see Fig (2.3-42); a fully turbulent boundary layer on the cylindrical part of the body; a partially laminar, partially turbulent boundary layer on wings and fins, with the laminar portion up to $(\bar{C}/2)$ at the most. The Reynolds Number criteria are:

(1) for nose-cones: $Re_N^* \leq Re_{cr}$ (Case II),

(2) for cylinder + boattail (Case III B),

(3) for wings $Re_{cr} \geq Re_{TRW} \leq (Re_{\bar{C}_W}/2)$

$X_{TRW} \leq (\bar{C}_{WEXP}/2)$

(Case III),

(4) for fins: $Re_{cr} \geq Re_{TRF} \leq (Re_{\bar{C}_F}/2)$

$X_{TRF} \leq (\bar{C}_{FEXP}/2)$

(Case III),

and

$$C_{DOf_{III M}} = C_{f_1}^{I} G_1 + C_{f_2}^{IIIB} G_2 + C_{f_3}^{III} G_3 + C_{f_4}^{III} G_4 N ,$$

(2.3-473)

$$\therefore C_{DOf_{III M}} = 1.125\, C_{f_{1L}}^{II} G_1 + \left\{ C_{f_{2T}}^{IIIB} \left[1 + R_3 \right] - \right.$$

$$\left. - (\Delta C_{f_{TURFP}}^{IIIB})_{CYL} R_3 \right\} G_2 + C_{f_{3T}}^{III} G_3 R_5 + C_{f_{4T}}^{III} R_6 G_4 N$$

(2.3-474)

or

$$C_{DOf_{III M}} = (C_{DOf_N})_L^{II} + (C_{DOf_{CYL+BT}})_T^{IIIB} +$$

$$+ (C_{DOf_{WEXP}})_{L+T}^{III} + (C_{DOf_{FEXP}})_{L+T}^{III} ,$$

(2.3-475)

where $(C_{Dof_N})_L^{II}$, $(C_{Dof_{CLY+BT}})_T^{IIIB}$, $(C_{Dof_{WEXP}})_{L+T}^{III}$, and $(C_{Dof_{FEXP}})_{L+T}^{III}$ are given by Eqs (2.3-389), (2.3-431), (2.3-457) and (2.3-461).

Case IV M: a fully laminar boundary layer on the nose cone; a partially laminar, partially turbulent boundary layer on the cylindrical part of body, the extent of laminar portion restricted to the wing-body juncture at the most; a partially laminar, partially turbulent boundary layer at wings and fins, with the laminar portion up to $(\bar{C}/2)$ at the most. The Reynolds Number criteria are:

(1) for nose cones: $Re_N^* < Re_{cr}$ (Case II),

(2) for cylinder + boattail: (Case III C),

(3) for wings: $Re_{cr} \geq Re_{TRW} \leq (Re_{\bar{C}W}/2)$

$$x_{TRW} \leq (\bar{C}_{WEXP}/2)$$

(Case III),

(4) for fins: $Re_{cr} \geq Re_{TRF} \leq (Re_{\bar{C}F}/2)$

$$x_{TRF} \leq (\bar{C}_{FEXP}/2)$$

(Case III),

and

$$C_{Dof_{IV\,M}} = C_{f_1}^{II} G_1 + C_{f_2}^{III C} G_2 + C_{f_3}^{III} G_3 + C_{f_4}^{III} G_4 N \ ,$$

(2.3-476)

$$\therefore C_{Dof_{IV\,M}} = 1.125 C_{f_{IL}}^{II} G_1 + \left\{ C_{f_{2T}}^{III C} \left[1 + R_4 + \frac{R_1}{1.022} \right] - C_{f_{IL}}^{II} R_1 \right\} G_2 + C_{f_{3T}}^{III} R_5 G_3 + C_{f_{4T}}^{III} R_6 G_4 N$$

(2.3-477)

or

$$C_{Dof_{IV\,M}} = (C_{Dof_N})_L^{II} + (C_{Dof_{CYL+BT}})_T^{III C} + (C_{Dof_{WEXP}})_{L+T}^{III} + (C_{Dof_{FEXP}})_{L+T}^{III}$$

(2.3-478)

where $(C_{Dof_N})_L^{II}$, $(C_{Dof_{CLY+BT}})_T^{III C}$, $(C_{Dof_{WEXP}})_{L+T}^{III}$ and $(C_{Dof_{FEXP}})_{L+T}^{III}$ are given by Eqs (2.3-389), (2.3-445), (2.3-457) and (2.3-461), respectively.

The preceding basic expressions, (2.3-468), (2.3-471), (2.3-474) and (2.3-477) are used with all methods. The respective average skin-friction coefficients, C_f's, in general follow the functional law expressed by (2.3-465). Since the defined four "cases" reflect the possible boundary layer status only, the above basic two-dimensional, insulated, smooth flat plate values of C_f's need to be additionally corrected for skin-temperature, skin-roughness and acceleration effects, which are estimated in form of ΔC_f increments, and algebraically added to the basic C_f's values. These incremental estimates are linked with corresponding flight regimes as specified by the proposed methods in the coming text and in the Section 2.3.7 . The underlying assumptions, limitations and eventual accuracy levels of the different methods are stated in each case.

(ii) The Basic Data Preparation, Common to All Methods

To avoid a possible mishandling of the basic geometry and the flow parameters in various C_{Dof} expressions, as they are changed in different methods, a tabulation of the data, common to all methods is suggested, see Tables (2.3-5a) to (2.3-5f) and Figs (1.36) and (1.37).

(1) For the given missile geometry define and tabulated all the characteristic lengths, angles and geometric ratios from a convenient three-view drawing:

Missile:

total length, $L = L_N + L_{CYL} + L_{BT}$, ft,

maximum diameter, D, ft,

fineness ratio, (L/D),

reference area, $Sr = (\pi D^2/4)$, sq. ft.

Nose Section: cone or ogive:

nose length, L_N, ft,

(inscribed) cone vertex angle, Θ_N, degrees,

fineness ratio, (L_N/D).

Cylindrical Section:

cylinder length, L_{CYL}, ft,

diameter, D, ft,

fineness ratio, (L_{CYL}/D).

Boattail Section:

boattail length, L_{BT}, ft,

base diameter, D_B, ft,

boattail angle, θ_B, degrees,

fineness ratio, (L_{BT}/D),

diameter ratio, (D_B/D).

Exposed Wing:

exposed planform area, S_{WEXP}, sq ft,

exposed planform span, b_{WEXP}, ft,

mean geometric or aerodynamic chord, $\bar{C}_{WEXP} = (S_{WEXP}/b_{WEXP})$, ft,

chord-diameter ratio, $(\bar{C}_{WEXP}/D)$,

span-diameter ratio, (b_{WEXP}/D).

Exposed Fins:

number of fins, N,

exposed planform area of one fin, S_{FEXP}, sq.ft,

fin height, h_{FEXP}, ft,

mean geometric or aerodynamic chord, $\bar{C}_{FEXP} = (S_{FEXP}/h_{FEXP})$, ft,

chord-diameter ratio, $(\bar{C}_{FEXP}/D)$,

height-diameter ratio, (h_{FEXP}/D).

(2) Compute the geometry factors, G's, in the general expression (2.3-465) for C_{D0f_M}:

Nose section, cone or ogive:

$$G_1 = 1.022 \cot(\theta_N/2), \quad (2.3\text{-}479)$$

$$1.125\, G_1 = 1.15 \cot(\theta_N/2). \quad (2.3\text{-}480)$$

Cylinder + boattail (conical or ogive frustrum):

$$G_2 = \left[4\left(\frac{L_{CYL}}{D}\right) + (\operatorname{cosec}\theta_B)\left(1 - \frac{D_B}{D}\right) + 2\left(\frac{D_B}{D}\right)\left(\frac{L_{BT}}{D}\right)(\sec\theta_B)\right], \quad (2.3\text{-}481)$$

Exposed wings:

$$G_3 = 2.55\left(\frac{\bar{C}_{WEXP}}{D}\right)\left(\frac{b_{WEXP}}{D}\right). \quad (2.3\text{-}482)$$

Exposed fins:

$$G_4 = 2.55\left(\frac{\bar{C}_{FEXP}}{D}\right)\left(\frac{h_{FEXP}}{D}\right), \text{ one fin.} \quad (2.3\text{-}483)$$

$$NG_4 = 2.55\left(\frac{\bar{C}_{FEXP}}{D}\right)\left(\frac{h_{FEXP}}{D}\right)N, \text{ for N fins} \quad (2.3\text{-}484)$$

(3) Compute the Reynolds Number values for the basic Eqs (2.3-468), (2.3-471), (2.3-474), and (2.3-477), using Fig (1.31) or Table (1.7-2) for the functional relationship, $(V_H/\nu_H) = (Re/L) = f(M,H)$:

Nose section, cones or ogives:

$$Re_{L_N} = \frac{L_N V_H}{\nu_H} = f(L_N, M, H), \quad (2.3\text{-}485)$$

$$Re_N^* = Re_{L_N}(\sec\theta_N/2), \quad (2.3\text{-}486)$$

for Cases I and II. Separately, for Case III:

$$Re_{cr} = \frac{X_{TR} V_H}{\nu_H} = f(M, H, X_{TR}), \quad (2.3\text{-}487)$$

$$Re_{\Delta XN} = f(Re_{cr}, M), \text{ from Fig. 2.15}, \quad (2.3\text{-}488)$$

$$Re_{TURN}^{*\,III} = \left[1 - \left(\frac{Re_{cr}}{Re_N^*} - \frac{Re_{\Delta XN}}{Re_N^*}\right)\right] Re_N^* =$$

$$= Re_N^*\left[1 - (R_0 - R_0')\right], \quad (2.3\text{-}489)$$

$$R_0 = \frac{Re_{cr}}{Re_N^*}, \quad (2.3\text{-}490)$$

$$R_0' = \frac{Re_{\Delta XN}}{Re_N^*}, \quad (2.3\text{-}491)$$

$$R_0\left[R_0' - .875\, R_0\right], \quad (2.3\text{-}492)$$

$$\left[1 - (R_0 - R_0')^2\right], \quad (2.3\text{-}493)$$

with any arbitrary critical Reynolds Number value; or, alternatively with the proposed approximation:

$$Re_{cr} = 1 \times 10^6 = \text{constant}, \quad (2.3\text{-}494)$$

$$Re_{\Delta XN} = .222 \times 10^6 = \text{constant}, \quad (2.3\text{-}495)$$

$$Re_{TURN}^{*\,III} = Re_N^*\left(1 - .778\frac{10^6}{Re_N^*}\right) = Re_N^*(1 - .778 R_0), \quad (2.3\text{-}496)$$

$$R_0' = \frac{Re_{\Delta X N}}{Re_N^*} = \frac{.222 \times 10^6}{Re_N^*}, \quad (2.3\text{-}497)$$

$$R_0 = \frac{Re_{Cr}}{Re_N^*} = \frac{10^6}{Re_N^*}, \quad (2.3\text{-}498)$$

$$R_0 \left[R_0' - .875 R_0\right] = -.653 R_0^2, \quad (2.3\text{-}499)$$

$$\left[1 - (R_0 - R_0')^2\right] = \left[1 - .606 R_0^2\right]. \quad (2.3\text{-}500)$$

Cylinder + boattail (conical or parabolic frustrum), with an arbitrary critical Reynolds Number value.

Case I:

$$Re_{TOTAL}^{*I} = 1.022\, Re_N^* + Re_{CYL} + Re_{BT}^*, \quad (2.3\text{-}501)$$

$$Re_{CYL} = \frac{L_{CYL} V_H}{\nu_H} = f\left(L_{CYL}, M, H\right), \quad (2.3\text{-}502)$$

$$Re_{BT}^* = Re_{BT} \sec(\theta_B) = \frac{L_{BT} V_H}{\nu_H} \sec(\theta_B), \quad (2.3\text{-}503)$$

$$R_1 = \frac{1.022\, Re_N^*}{Re_{CYL} + Re_{BT}^*}. \quad (2.3\text{-}504)$$

Case III A:

$$Re_{TOTAL}^{*IIIA} = \left(Re_{TURFP}^{*III}\right)_{NOSE} + Re_{CYL} + Re_{BT}^*, \quad (2.3\text{-}505)$$

$$\left(Re_{TURFP}^{*III}\right)_{NOSE} = 1.022\, Re_{TURN}^*, \quad (2.3\text{-}506)$$

$$Re_{Cr} = \frac{X_{TR} V_H}{\nu_H}, \quad (2.3\text{-}507)$$

$$R_2 = \frac{1.022\, Re_{TURN}^*}{Re_{CYL} + Re_{BT}^*}. \quad (2.3\text{-}508)$$

Case III B:

$$Re_{TOTAL}^{*IIIB} = Re_{\Delta X}^{IIIB} + Re_{CYL} + Re_{BT}^*, \quad (2.3\text{-}509)$$

$$Re_{\Delta X}^{IIIB} = f\left(M, Re_{Cr}\right), \text{ from Fig. (2.3-58)}, \quad (2.3\text{-}510)$$

$$Re_{Cr} = Re_N^*, \quad (2.3\text{-}511)$$

$$R_3 = \frac{Re_{\Delta X}^{IIIB}}{Re_{CYL} + Re_{BT}^*}. \quad (2.3\text{-}512)$$

Case III C:

$$Re_{TOTAL}^{*IIIC} = Re_{TUR}^{*IIIC} + Re_{CYL} + Re_{BT}^*, \quad (2.3\text{-}513)$$

$$Re_{TUR}^{*IIIC} = Re_N^* + Re_{\Delta X}^{IIIC} - Re_{Cr}^{IIIC}, \quad (2.3\text{-}514)$$

$$Re_{Cr}^{IIIC} = f(X_{TR}, M, H), \quad (2.3\text{-}515)$$

$$Re_{\Delta X}^{IIIC} = f(Re_{Cr}^{IIIC}, M, H), \text{ from (2.3-58)}, \quad (2.3\text{-}516)$$

$$R_1 = \frac{1.022\, Re_N^*}{Re_{CYL} + Re_{BT}^*}, \quad (2.3\text{-}517)$$

$$R_4 = \frac{Re_{\Delta X}^{IIIC} - Re_{Cr}^{IIIC}}{Re_{CYL} - Re_{BT}^*}. \quad (2.3\text{-}518)$$

Alternatively, with $Re_{Cr}^{IIIC} = 1 \times 10^6$ and $\Delta X = .222 X_{TR}$:

Case III A:

$$Re_{TOTAL}^{*IIIA} = \left(Re_{TURFP}^{III}\right)_{NOSE} + Re_{CYL} + Re_{BT}^*, \quad (2.3\text{-}519)$$

$$\left(Re_{TURFP}^{III}\right)_{NOSE} = 1.022\, Re_{TURN}^* = 1.022\left[1 - .778 \frac{10^6}{Re_N^*}\right] Re_N^*, \quad (2.3\text{-}520)$$

$$R_2 = \frac{1.022\, Re_{TURN}^*}{Re_{CYL} + Re_{BT}^*}, \quad (2.3\text{-}521)$$

Case III B:

$$Re_{TOTAL}^{*IIIB} = Re_{\Delta X}^{IIIB} + Re_{CYL} + Re_{BT}^*, \quad (2.3\text{-}522)$$

$$Re_{\Delta X}^{IIIB} = .255 \times 10^6, \quad (2.3\text{-}523)$$

$$R_3 = \frac{.255 \times 10^6}{Re_{CYL} + Re_{BT}^*}. \quad (2.3\text{-}524)$$

Case III C:

$$Re_{TOTAL}^{*IIIC} = Re_{TUR}^{*IIIC} + Re_{CYL} + Re_{BT}^*, \quad (2.3\text{-}525)$$

$$Re_{TUR}^{*IIIC} = Re_{\Delta X}^{IIIC} + Re_N^* - Re_{Cr}^{IIIC} = \left[Re_N^* - .778 \times 10^6\right], \quad (2.3\text{-}526)$$

$$Re_{\Delta X}^{IIIC} = .222 \times 10^6, \quad (2.3\text{-}527)$$

$$Re_{Cr}^{IIIC} = 1 \times 10^6, \text{ but less than } Re_{FOREBODY}^*, \quad (2.3\text{-}528)$$

$$Re_{FOREBODY}^* = \frac{L_{FORE} V_H}{\nu_H}, \quad (2.3\text{-}529)$$

$$R_1 = \frac{1.022\, Re_N^*}{Re_{CYL} + Re_{BT}^*}, \quad (2.3\text{-}530)$$

$$R_4 = \frac{.778 \times 10^6}{Re_{CYL} + Re_{BT}}. \quad (2.3\text{-}531)$$

Exposed Wings and Fins, with an arbitrary critical Reynolds Number value.

Case I:

$$Re_{\bar{c}_W} = \frac{\bar{C}_{WEXP} V_H}{\nu_H} = f(\bar{C}_{WEXP}, M, H) \ , \quad (2.3\text{-}532)$$

$$Re_{\bar{c}_F} = \frac{\bar{C}_{FEXP} V_H}{\nu_H} = f(\bar{C}_{FEXP}, M, H) \ . \quad (2.3\text{-}533)$$

Case III:

$$(Re^{III}_{TUR})_W = Re_{\bar{c}_W} R_5 \ , \quad (2.3\text{-}534)$$

$$Re_{TRW} = \frac{X_{TRW} V_H}{\nu_H} \leq \frac{1}{2} Re_{\bar{c}_W} \ , \quad (2.3\text{-}535)$$

$(Re_{\Delta X})_W = f(Re_{TRW}, M)$, from Fig. (2.3-58), (2.3-536)

$$R_5 = \left[1 - \frac{Re_{TRW} - Re_{\Delta XW}}{Re_{\bar{c}_W}}\right] \ , \quad (2.3\text{-}537)$$

$$(Re^{III}_{TUR})_F = Re_{\bar{c}_F} R_6 \ , \quad (2.3\text{-}538)$$

$$Re_{TRF} = \frac{X_{TRF} V_H}{\nu_H} \leq \frac{1}{2} Re_{\bar{c}_F} \ , \quad (2.3\text{-}539)$$

$(Re_{\Delta X})_F = f(Re_{TRF}, M)$, from Fig. (2.3-58), (2.3-540)

$$R_6 = \left[1 - \frac{Re_{TRF} - Re_{\Delta XF}}{Re_{\bar{c}_F}}\right] \ . \quad (2.3\text{-}541)$$

Alternatively, with $Re_{TR} = 1 \times 10^6 \leq (Re_{\bar{c}}/2)$ and $\Delta X = .222 X_{TR}$:

$$Re_{TRW} = 1 \times 10^6 \leq \frac{1}{2} Re_{\bar{c}_W} \ , \quad (2.3\text{-}542)$$

$$Re_{\Delta XW} = .222 \times 10^6 , \quad (2.3\text{-}543)$$

$$R_5 = \left[1 - \frac{.778 \times 10^6}{Re_{\bar{c}_W}}\right] \ , \quad (2.3\text{-}544)$$

$$Re_{TRF} = 1 \times 10 \leq \frac{1}{2} Re_{\bar{c}_F} \ , \quad (2.3\text{-}545)$$

$$Re_{\Delta XF} = .222 \times 10^6 , \quad (2.3\text{-}546)$$

$$R_6 = \left[1 - \frac{.778 \times 10^6}{Re_{\bar{c}_F}}\right] \ . \quad (2.3\text{-}547)$$

(iii) Limitations in Applicability of the Proposed Methods I, II, and III for Computations of the Skin Friction Drag Coefficient Values.

The general limitations and approximations respective to the validity of the presented aerodynamic drag force analyses are enumerated in Section 1.2 and further analytically elaborated in Sections 1.6 to 1.8. The more important practical aspects regarding the skin friction in particular are then discussed in Sections 2.3.2 to 2.3.9. In a brief summary, the main assumptions and limitations, common to all the presently proposed methods of the skin friction drag force evaluations are:

(1) The effects of atmospheric turbulence as well as gust effects, are not taken into account. A Standard Atmosphere in a steady equilibrium state, rotating as a unit with Earth, is assumed.

(2) The apparent mass and the time lag effects in accelerated flight regimes are not included, i.e., a true non-uniform and unsteady motion is not analyzed. All flight regimes are interpreted as steady, or quasi-steady.

(3) The missile configurations are treated as aerodynamically slender so that the equivalent flat plate results can be correctively applied. The entropic loss of the energy of ordered motion through the oblique shock patterns are neglected. Also, shock wave-boundary layer interference effects are assumed negligible.

(4) There are no appreciable flow separation phenomena.

(5) The effects of pressure gradients in the flow direction are neglected; the flow dimensionality effects are only partially taken into account (nose cones).

(6) The representative average and uniform surface roughness and temperature distributions are assumed, and estimated as functions of different flight regimes.

(7) The noise, aeroelastic and vibrational effects are neglected.

(8) Symmetric flight cases are investigated only.

(9) The skin-friction drag coefficient estimates are performed for given sets of Mach, Reynolds and Knudsen Numbers, i.e., for given sets of ambient flight speed, V, ambient flight altitude, H, and a continuum flow regime restrictively. Therefore, prior to actual computations, the respective general boundaries of validity for the here proposed methods of the skin-friction drag coefficient estimates must be established:

(a) Either for the vehicle as a whole, or for each individual vehicle part (which is more accurate), the domains of the continuum, the slip, the transitional and the free molecular flow regimes are determined using the respective Knudsen Number criteria. For the purpose, the graphs and the boundary expressions from Section 1.7 should be used, as specified in terms of M_H, Re_H and H.

(b) For the restrictive continuum flow domain, the prevailance of the laminar and the turbulent boundary layer types for various configurational parts of a given vehicle should be ascertained on the basis of a chosen critical Reynolds Number value. Then, referring to Fig 1.20, the conditions for predominantly laminar, predominantly turbulent or for mixed boundary layer flow types can be obtained in terms of M_H, Re_H and H.

(10) The slip, the transitional and the free molecular flow regimes are nominally excluded from the present analysis. They are considered separately in the next Section, 2.4. Nevertheless, the slip and the transitional flow regimes can be, in a first approximation and for practical purposes, tentatively included in the present analysis of this Section, 2.3, either by using the same graphs as for the continuum laminar flow regime, or by resorting to somewhat more accurate graphs from Section 2.4. The relative acceptability of such an approximative treatment is argued on the basis that (for a given Mach and Reynolds Number values), (1) the skin friction drag coefficient data in the laminar continuum and the laminar slip flow regimes are numerically of the same order of value, and (2) the fractional skin friction drag contribution to the total drag force becomes pronouncedly less with the increase in Mach Number values, when the wave (or pressure) drag effects constitute a major portion of the overall air resistance.

TABLE (2.3-5a)

AVERAGE SKIN-FRICTION DRAG COEFFICIENT, C_{Daf} — BASIC DATA

1. INITIAL GEOMETRY DATA, SEE FIGS. 1.36 and 1.37												
NO.	DESCRIPTION	MISSILE		NOSE SECTION		CYLINDRICAL SECTION		BOATTAIL SECTION		WINGS (EXPOSED)		FINS (EXPOSED)
	GENERAL	——		OGIVE		——		——		——		N =
(1)	CHARACTERISTIC LENGTH L or $\bar{C}$, ft	L		L_N		L_{cyl}		L_{BT}		$\bar{C}_w$		$\bar{C}_F$
(2)	MAXIMUM DIAMETER D, ft	D		D		D		D_B		b_w		h_F
(3)	FINENESS RATIO (L/D)	$\frac{L}{D}$		$\frac{L_N}{D}$		$\frac{L_{cyl}}{D}$		$\frac{L_{BT}}{D}$		—		—
(4)	OTHER RATIOS:	—		—		—		$\frac{D_B}{D}$		$\frac{\bar{C}_w}{D}$		$\frac{\bar{C}_F}{D}$
(5)		—		—		—		—		$\frac{b_w}{D}$		$\frac{h_F}{D}$
(6)	CHARACTERISTIC ANGLE, $\theta°$	—		$\frac{\theta_N}{2}$		—		θ_B		—		—
(7)		—	COT $\frac{\theta_N}{2}$			—	COSEC	θ_B		—		—
(8)		—	SEC $\frac{\theta_N}{2}$			—	SEC	θ_B		—		—

2. COMPUTATION OF GEOMETRY FACTOR, G_n
(9) NOSE SECTION EQUATION (2.3-479) G_1 = 1.022 × (7)$_N$ =
(10) CYLINDER + BOATTAIL EQUATION (2.3-481) G_2 = [1 × (3)$_{CYL}$ + (7)$_{BT}$ × [1 − (4)$_{BT}$] + 2[(4)$_{BT}$ × (3)$_{BT}$ × (8)$_{BT}$]] =
(11) WINGS, EQUATION (2.3-482) G_3 = 2.55 × [(4)$_w$ × (5)$_w$] =
(12) N FINS, EQUATION (2.3-484) N G_4 = 2.55 × [(4)$_F$ × (5)$_F$]N =

NOTES:

SUBSONIC $\frac{T_w}{T_H} \approx 1$

STEADY SUPERSONIC $\frac{T_w}{T_H} = \frac{T_{aw}}{T_H}$, FIGS (2.3-50) and (2.3-51)

TRANSIENT ACCELERATED $\frac{T_w}{T_H}$ = f(M,ng,h), FIGS (2.3-50) and (2.3-51) or as prescribed by cooling system

C_{Daf} — BASIC DATA

3. FLIGHT REGIME DATA					
(13)	(14)	(15)	(16)	(18) T − (2.3-2)	(21) T − (1.7-2) or FIG. 1.31
MACH NO. M	ALTITUDE H, ft	TIME t, sec	ACCELERATION ng	ROUGHNESS k, ft	$Re = \frac{V}{L\sqrt{\nu}}$
0 or .2					
.5					
M_{cr}					
1.0					
1.2					
1.5					
2.0					
2.5					
3.0					
3.5					
4.0					
4.5					
5.0					

$\frac{Re}{L}$ = f(M,H), FIGS 1.31 and 1.32

k (feet) — (2.3-2)

$Sr = \frac{\pi D^2}{4}$

$\bar{C}_{FEXP} = \frac{S_{FEXP}}{S_{REXP}}$

$\bar{C}_{WEXP} = \frac{S_{WEXP}}{S_{WEXP}}$

TABLE (2.3-5b)

AVERAGE SKIN-FRICTION DRAG COEFFICIENT, C_{Daf} — BASIC DATA

4. REYNOLDS NUMBERS AND ROUGHNESS PARAMETERS											
	NOSE SECTION k = $\frac{L_N \sec(\theta_N/2)}{k}$ =			CYLINDER + BOATTAIL k = $\frac{L_{cyl}+L_{BT}+L \sec(\theta_N/2)}{k}$ =			WINGS k = $\frac{\bar{C}_{WEXP}}{k}$ =			FINS k = $\frac{\bar{C}_{FEXP}}{k}$ =		
(13)	(17)	(22)	(23)	(17)	(26)	(27)	(17)	(30)	(31)	(17)	(34)	(35)
MACH NO. M	$\frac{T_w}{T_H}$	Re_{L_N}	$\left(\frac{kV}{\sqrt{\nu}}\right)_H$	$\frac{T_w}{T_H}$	$Re_{L_{CYL+BT}}$	$\left(\frac{kV}{\sqrt{\nu}}\right)_H$	$\frac{T_w}{T_H}$	$Re_{\bar{C}_w}$	$\left(\frac{kV}{\sqrt{\nu}}\right)_H$	$\frac{T_w}{T_H}$	$Re_{\bar{C}_F}$	$\left(\frac{kV}{\sqrt{\nu}}\right)_H$
0 or .2												
.5												
M_{cr}												
1.0												
1.2												
1.5												
2.0												
2.5												
3.0												
3.5												
4.0												
4.5												
5.0	etc.											

NOTE: FOR ITEMIZED REYNOLDS NUMBER DATA, CORRESPONDING TO VARIOUS BOUNDARY LAYER CASES, SEE THE FOLLOWING TABLE (2.3-5c)

TABLE (2.3-5c)

AVERAGE SKIN-FRICTION DRAG COEFFICIENT,

5 REYNOLDS NUMBER VALUES, BASIC EQS (2.3-487), (2.3-488), (2.3-400),

MACH NO	CASE I AND II (22) Re_{LN}	(36) $\bar{R}^{*}_{RN}$	(37) Re_{cr}	(38) Re_{ABN}	(39) R_B	(40) R_B'	(41) $(R_B - R_B')$
GENERAL or $Re_{cr} = 1 \times 10^6$	FIG. 1.31	(22) x (8)$_N$	or 1×10^6	FIG (2.3-58) or $.222 \times 10^6$	(37) / (38)	(39) / (38)	(39) − (40) $.778 \times$ (39)
M	EQ (2.3-485)	EQ (2.3-486)	EQ (2.3-487)	EQ (2.3-488)	EQ (2.3-490)	EQ (2.3-491)	
0 or .2							
.5							
M_{cr}							
1.0							
1.2							
1.5							
2.0							
3.0							
4.0							
5.0							

NOTE

CASE I – FULLY TURBULENT B.L., TRANSITION AT THE NOSE TIP, SEE FIG (2.3-42)

CASE II – FULLY LAMINAR B.L., TRANSITION AT THE CYLINDRICAL PART OF FOREBODY, SEE FIG (2.3-42)

CASE III – PARTIALLY LAMINAR, PARTIALLY TURBULENT B.L. ON THE NOSE SECTION, SEE FIG (2.3-42)

$\bar{R}^{*}_{RN} = Re_{LN} \sec\left(\frac{\Theta_N}{2}\right)$, EQ (2.3-486)

$Re_{cr} = \frac{x_{cr} V_N}{\nu} = f(M,H)$ or $(1 \times 10^6) = \text{const}$, EQ (2.3-487)

$Re_{ABN} = f(M, Re_{cr})$ or $(.222 \times 10^6) = \text{const}$, EQ (2.3-488)

$R_B = \frac{Re_{cr}}{\bar{R}^{*}_{RN}}$ or $\frac{10^6}{\bar{R}^{*}_{RN}}$, EQ (2.3-490)

C_{Daf} – BASIC DATA

NOSE SECTION (CONES OR OGIVES)

CASE III (42)	(43) $\bar{R}^{*III}_{RETURN}$	(44)	(45)	(46)	(47)	(48)
$1 - (41)$	(42) x (36)	.875 x (39) or (39)^2	(40) − (44) or NON-EXISTANT	(45) x (39) or $-.653 \times$ (44)	(41)^2 or $.608 \times$ (44)	$1 - (47)$
	EQ (2.3-489)			EQ (2.3-442)		EQ (2.3-493)

(2.3-42)

$R_B' = \frac{Re_{ABN}}{\bar{R}^{*}_{RN}}$ or $\frac{.222 \times 10^6}{\bar{R}^{*}_{RN}}$, EQ (2.3-491)

$\bar{R}^{*}_{RETURN} = \left[1 - (R_B - R_B')\right] \bar{R}^{*}_{RN}$ or $\left[1 - .778 R_B\right]$, EQ (2.3-489)

(46) $= R_B\left[R_B' - .875 R_B\right]$ or $\left[-.653 R_B^2\right]$, EQ (2.3-492)

(48) $= \left[1 - (R_B - R_B')^2\right]$ or $\left[1 - .606 R_B^2\right]$, EQ (2.3-403)

TABLE (2.3-5d)

AVERAGE SKIN-FRICTION DRAG COEFFICIENT,

6 REYNOLDS NUMBER VALUES, BASIC EQS (2.3-418), (2.3-425),

MACH NO	CASE I (49) Re_{CYL}	(50) Re_{BT}	(51) $\bar{R}^{*}_{BT}$	(52) $1.022 \bar{R}^{*}_{RN}$	(53)
GENERAL or $Re_{cr} = 1 \times 10^6$	FIG 1.31	FIG 1.31	(50) x (8)$_{BT}$	1.022 x (36)	(49) + (51)
M	EQ (2.3-502)		EQ (2.3-503)		
0 or .2					
.5					
M_{cr}					
1.0					
1.2					
1.5					
2.0					
3.0					
4.0					
5.0					

NOTE

CASE I: FULLY TURBULENT B.L. ON BOTH NOSE CONE AND CYLINDER AND

CASE III A PARTIALLY LAMINAR, PARTIALLY TURBULENT B.L. ON NOSE CONE, FULLY

$Re_{CYL} = \frac{L_{CYL} V_N}{\nu_N} = f(M,H)$, see FIG 1.31, EQ (2.3-502)

$\bar{R}^{*}_{BT} = Re_{BT} \sec(\Theta_B) \left(\frac{L_{BT} V_N}{\nu_N}\right) \sec(\Theta_B)$, see FIG 1.31, EQ (2.3-503)

$\bar{R}^{*I}_{TOTAL} = 1.022 \bar{R}^{*}_{RN} + Re_{CYL} + \bar{R}^{*}_{BT}$, EQ (2.3-504)

$R_I = \frac{1.022 \bar{R}^{*}_{RN}}{Re_{CYL} + \bar{R}^{*}_{BT}}$, EQ (2.3-504)

C_{Daf} — BASIC DATA

CYLINDER + BOATTAIL (FRUSTRUMS, CONICAL OR PARABOLIC)

CASE III A (54) $\bar{R}^{*I}_{TOTAL}$	(55) R_I	(56) $(\bar{R}^{*III}_{RETURN})_{NOSE}$	(57) $\bar{R}^{*IIIA}_{TOTAL}$	(58) R_B
(53) + (52)	(52)/(53)	1.022 x (43)	(56) + (53)	(56) / (53)
EQ (2.3-501)	EQ (2.3-504)	EQ (2.3-506)	EQ (2.3-505)	EQ (2.3-508)

BOATTAIL

TURBULENT B.L. ON CYLINDER AND BOATTAIL

$\sec(\Theta_B) = (8)_{BT}$, TABLE (2.3-5a)

$\bar{R}^{*IIIA}_{TOTAL} = 1.022 \bar{R}^{*}_{RETURN} + Re_{CYL} + \bar{R}^{*}_{BT}$, EQ (2.3-505)

$R_B = \frac{1.022 \bar{R}^{*}_{RETURN}}{Re_{CYL} + R_{BT}}$, EQ (2.3-508)

$(\bar{R}^{*III}_{RETURN})_{NOSE} = 1.022 \bar{R}^{*III}_{RETURN}$, EQ (2.3-506)

TABLE (2.3-5e)

AVERAGE SKIN-FRICTION DRAG COEFFICIENT, C_{Daf} — BASIC DATA

8 REYNOLDS NUMBER VALUES, BASIC EQ (2.3-431), (2.3-439), CYLINDER + BOATTAIL (FRUSTRUMS - CONICAL OR PARABOLIC)

CASE III B, $Re_{Cr}^{IIIB} < Re_{B}^{B}$ (54)

MACH NO	(59) $Re_{\Delta x}^{IIIB}$	(60) Re_{TOTAL}^{IIIB}	(61) R_B	(62) Re_{Cr}^{IIIC}	(63) $Re_{\Delta x}^{IIIC}$
GENERAL or $Re_{Cr} = 1 \times 10^6$	FIG (2.3-58) or 255×10^6	(53) + (59)	(59)/(53)	1×10^6	FIG (2.3-58) or 222×10^6
M	EQ (2.3-510)	EQ (2.3-509)	EQ (2.3-512)	EQ (2.3-515)	EQ (2.3-516)
0 OR .2					
5					
M_{Cr}					
1.0					
1.2					
1.5					
2.0					
3.0					
4.0					
5.0					

NOTE

CASE III B FULLY LAMINAR B.L. ON NOSE CONE, FULLY TURBULENT B.L. ON CYLINDER AND BOATTAIL

CASE III C FULLY LAMINAR B.L. ON NOSE CONE, PARTIALLY LAMINAR, PARTIALLY TURBULENT B.L. ON CYLINDER AND BOATTAIL

$Re_{TOTAL}^{IIIB} = Re_{\Delta x}^{B} + Re_{CYL} + Re_{BT}^{B}$, EQ (2.3-509)

$Re_{\Delta x}^{IIIB}$ FROM FIG 1.31 OR $255 \times 10^6 \pm$ const., EQ (2.3-510)

$Re_{Cr} = Re_{N}^{B}$ OR 1×10^6, EQ (2.3-486)

$R_B = \dfrac{Re_{\Delta x}^{IIIB}}{Re_{CYL} + Re_{BT}^{B}}$, EQ (2.3-512)

$Re_{TOTAL}^{IIIC} = Re_{TURB} + Re_{CYL} + Re_{BT}^{B}$, EQ (2.3-525)

— BASIC DATA

BOATTAIL (FRUSTRUMS - CONICAL OR PARABOLIC)

CASE III C, $Re_{Cr}^{IIIC} < Re_{FOREBODY}^{B}$ (64)

(64) Re_{FORE}^{B}	(65) (63) − (62) or $.778 \times 10^6$	(66) Re_{TURB}^{IIIC}	(67) Re_{TOTAL}^{IIIC}	(68) R_B
FIG 1.31		(56) + (65)	(66) + (61)	(65)/(63)
EQ (2.3-529)		EQ (2.3-526)	EQ (2.3-525)	EQ (2.3-518)

BOATTAIL B.L. ON CYLINDER AND BOATTAIL

$Re_{TUR}^{IIIC} = Re_{N}^{B} + Re_{\Delta x}^{IIIC} - Re_{Cr}^{IIIC}$, EQ (2.3-526)

$Re_{Cr}^{IIIC} = \left(\dfrac{X_{TR} V_N}{\sqrt{\gamma}_N}\right) = f(M,H)$, EQ (2.3-515)

$Re_{\Delta x}^{IIIC}$ FROM FIG. 1.31 OR 222×10^6, EQ (2.3-516)

$R_B = \dfrac{Re_{\Delta x}^{IIIC} - Re_{Cr}^{IIIC}}{Re_{CYL} + Re_{BT}^{IIIC}}$, EQ (2.3-518)

$Re_{FOREBODY}^{B} = \dfrac{L_{FOREBODY} V_N}{\sqrt{\gamma}_N}$, SEE FIGS. (1.31) AND (1.32), EQ (2.3-529)

TABLE (2.3-5f)

AVERAGE SKIN-FRICTION DRAG COEFFICIENT, C_{Daf} — BASIC DATA

7 REYNOLDS NUMBER VALUES, BASIC EQS. (2.3-449), (2.3-451), (2.3-457), (2.3-481), WINGS AND FINS

MACH NO	CASE I WINGS (50) $Re_{\Sigma_W}^{I}$	CASE I FINS (54) $Re_{\Sigma_F}^{I}$	CASE III WINGS (69) $Re_{\Sigma_W}^{III}/2$	(70) Re_{TRW}	(71) $Re_{\Delta XW}$	(72)	(73)	(74) R_S
GENERAL or $Re_{Cr} = 1 \times 10^6$	FIG. 1.31	FIG 1.31	(50)/2	or 1×10^6 up to $Re_{\Sigma_W}/2$	FIG (2.3-58) or $.222 \times 10^6$	(70) − (71) or $.778 \times 10^6$	(72)/(50)	1 − (73)
M	EQ. (2.3-532)	EQ. (2.3-533)		EQ. (2.3-535)	EQ. (2.3-536)			EQ. (2.3-537)
0 or 2								
5								
M_{Cr}								
1.0								
1.2								
1.5								
2.0								
3.0								
4.0								
5.0 etc.								

NOTE:

CASE I FULLY TURBULENT B.L. ON WINGS AND FINS, i.e. TRANSITION AT THE LEADING EDGE

CASE III PARTIALLY LAMINAR, PARTIALLY TURBULENT B.L., EXTENT OF L.B.L. RESTRICTED UP TO $(\bar{c}/2)$.

$Re_{TRW} = \dfrac{X - V_N}{\sqrt{\gamma}_N} \leq (1/2)\, Re_{\Sigma W}$, EQ (2.3-535)

$Re_{TRF} = \dfrac{X_{TR} V_N}{\sqrt{\gamma}_N} \leq (1/2)\, Re_{\Sigma F}$, EQ (2.3-539)

$Re_{\Delta XW}$ = FROM FIG (2.3-58) or $.222 \times 10^6$, EQ (2.3-536)

$Re_{\Sigma W} = \dfrac{\bar{C}_{EXP} V_N}{\sqrt{\gamma}_N}$, EQ (2.3-532)

$Re_{\Sigma F} = \dfrac{\bar{C}_{EXP} V_N}{\sqrt{\gamma}_N}$, EQ (2.3-533)

$R_S = \left[1 - \dfrac{Re_{TRW} - Re_{\Delta XW}}{Re_{\Sigma W}}\right]$, EQ (2.3-537)

$Re_{TURW}^{III} = Re_{\Sigma W} \times R_S$, EQ (2.3-534)

$Re_{TURF}^{III} = Re_{\Sigma F} \times R_S$, EQ (2.3-538)

$R_S = \left[1 - \dfrac{Re_{TRF} - Re_{\Delta XF}}{Re_{\Sigma F}}\right]$, EQ (2.3-541)

C_{Daf} — BASIC DATA

(2.3-451), (2.3-457), (2.3-481), WINGS AND FINS

CASE III $Re_{TR} \leq (Re_{C}/2)$

(75) Re_{TURW}^{III}	(76) $Re_{\Sigma F}/2$	(77) Re_{TRF}	(78) $Re_{\Delta XF}$	(79)	(80)	(81) R_S	(82) Re_{TURF}^{III}
(30) × (74)	(34)/2	or 1×10^6	FIG (2.3-58) or 222×10^6	(77) − (78) or 778×10^6	(79)/(34)	1 − (80)	(34) × (81)
EQ. (2.3-534)		EQ. (2.3-539)	EQ. (2.3-540)			EQ. (2.3-541)	EQ. (2.3-538)

2.3.10 METHOD I, TABLES (2.3-6) to (2.3-10)

Assumptions: the actual surface finish is treated as aerodynamically smooth, ($k = 0$) ; the skin is assumed as nearly "insulated", i.e., the average skin surface temperature is approximated by the uniform adiabatic wall temperature ($T_w = T_{aw}$) ; radiation effects are not taken into account.

Applicability: high quality surface-finish prototypes; prolonged, steady flight regimes, ($M = const$) , or slow-acceleration take-offs ($n_g < 1.0g$) and not involving appreciable or rapid altitude changes, ($\Delta H < 20{,}000$ ft).

Working graphs and tables: two different sets of working charts can be used alternatively.

(i) Set A: Direct Estimates for Laminar and Turbulent B. L.

Figs (2.3-44) - Average, two-dimensional, compressible skin-friction coefficient $(C_{fINS})^A$ for laminar and turbulent boundary layers on insulated flat plates. Use "smooth" curves (Van Driest).

(ii) Set B: Indirect Estimates for Laminar and Turbulent B. L.

Fig (2.3-46) - Average, two-dimensional, incompressible skin-friction coefficient $(C_{fiINS})^B$, for turbulent boundary layers on insulated, smooth flat plates. (Karman - Schoenherr).

Fig (2.3-48) - Average, two-dimensional incompressible skin-friction coefficient for laminar b.l. (Blasius) on smooth, insulated flat plates, zero-angle-of-attack.

Fig (2.3-47) and Fig (2.3-49) - Variations of $(C_f/C_{fi})^B_{INS}$ ratio with the Mach (and Reynolds) Number changes for turbulent and laminar boundary layers on insulated, smooth, flat plates (Van Driest).

The expected accuracy of the working graphs: the individual values of $(C_{fi})_{INS}$, (C_{fINS}) and $(C_f/C_{fi})_{INS}$ agree with the majority of the acceptable experimental and theoretical evidence within ±10% for turbulent boundary layers on smooth, insulated flat plates and for Mach Numbers up to 5. Accuracy of the corresponding laminar boundary layer values is within ±5%, under the same general conditions.

Computational procedure - see Tables (2.3-6) to (2.3-10).

(i) Using the set of graphs "A":

(1) From Figs (2.3-44) read-off through the lowest ("smooth") curves the corresponding average, two-dimensional, compressible, insulated flat plate skin-friction coefficient values,

$$C^A_{fINS} = f(M, Re) ,$$

for the specified flight speed regime (M_H) and the flight altitude, (H)

For every missile componental part (nose cone, cylinder + boattail, wings, fins) a corresponding set of readings should be taken:

$$(C^A_{fINS})_{NOSE} = C^A_{f1} , \qquad (C^A_{fINS})_{CYL+BT} = C^A_{f2} ,$$

$$(C^A_{fINS})_{WINGS} = C^A_{f3} , \qquad (C^A_{fINS})_{FINS} = C^A_{f4} ,$$

(2.3-548)

following the explicit stepwise instructions in tables (2.3-6) to (2.3-10).

For quick estimates, a fully turbulent boundary layer can be assumed on all missile parts, i.e., the Case I M, Section 2.3.9, and the related Eqs (2.3-468), (2.3-387), (2.3-418), (2.3-449) and (2.3-451), should be used. The C_{DofM} estimates shall be then on the conservative side.

When allowing for eventual co-existance of both laminar and turbulent boundary layers by choosing a definite value for the transitional Reynolds Number (Re_{cr}) , all three remaining Cases II M, III M and IV M may be encountered on any missile part, depending upon the particular set of Mach Number and flight altitude values. In a first approximation, it has been recommended that the critical Reynolds Number value be fixed,

$$Re_{cr} = 1 \times 10^6 = const ,$$

for all missile parts, Mach Numbers and flight altitudes. This, together with the approximation (see Section 2.3.8 and Fig 2.3-58),

$$\Delta X = .222 X_{TR} = \text{const}, \qquad (2.3\text{-}549)$$

renders the computational procedure simpler, without affecting seriously the accuracy of the $C_{D_{OfM}}$ estimates under actual atmospheric flight conditions and the usual manufacturing skin-finish tolerances. The respective Eqs (2.3-403), (2.3-441), (2.3-459), (2.3-461), (2.3-471), or Eqs (2.3-389), (2.3-443), (2.3-459), (2.3-461), (2.3-474) or Eqs (2.3-389), (2.3-445), (2.3-459), (2.3-461), (2.3-477) should be used, corresponding to the Case II M, Case III M and Case IV M of the Section 2.3.9, respectively.

(2) The total zero-lift skin-friction coefficient is then obtained by summing up the partial estimates according to the Eq (2.3-468) for Case I M, or Eqs (2.3-471), (2.3-474) and (2.3-477) for Cases II M, III M and IV M respectively.

The steps are clearly indicated in Tables (2.3-6) to (2.3-10). The initial basic data for three-dimensional flow effects and body geometries, common to all methods, should be taken from the preliminary Tables, (2.3-5a) to (2.3-5f).

Using the set of graphs "B":

(1) From Fig (2.3-46) read-off the average, two-dimensional, incompressible, insulated, smooth flat plate turbulent skin-friction coefficient values, or from Fig (2.3-48) read off the respective laminar skin-friction coefficient values,

$$(C_{f_l})^B_{INS} = f(Re), \quad M=0,$$

for a specified flight altitude, H. Thus, a set of $(C_{f_l INS})^B$ values for each component missile part is obtained. Follow all instructions stated under Step 1 for the set of graphs "A".

(2) From Figs (2.3-47) to (2.3-49), evaluate the ratios of the compressible-to-incompressible values of,

$$(C_f/C_{f_l})^B_{INS} = f(M, Re), \qquad (2.3\text{-}550)$$

which, with the corresponding $(C_{f_l INS})^B$ values already determined in step 1, shall give the explicit compressible, insulated, two-dimensional, smooth flat plate average skin-friction coefficient values:

$$(C_f{}^B{}_{INS})_{NOSE} = C_{f_1}{}^B, \quad (C_f{}^B{}_{INS})_{CYL+BT} = C_{f_2}{}^B,$$

$$(C_f{}^B{}_{INS})_{WINGS} = C_{f_3}{}^B, \quad (C_f{}^B{}_{INS})_{FINS} = C_{f_4}{}^B, \qquad (2.3\text{-}551)$$

respectively. All other instructions are the same as Step 1 for the "A" set of working graphs.

(3) The same as in step (2) for the "A" set of charts.

TABLE (2.3-6)

AVERAGE SKIN-FRICTION DRAG COEFFICIENT, $C_{D_{OF}}$ - METHOD I

PROLONGED, STEADY FLIGHT REGIMES ($0 \leq n_g \leq 1.0$), SMOOTH SURFACES ($k \approx 0$), INSULATED SKIN ($T_W / T_H \approx T_{aw} / T_H$), NO RADIATION ($\varepsilon = 0$)

BASIC CASE I_M: FULLY TURBULENT B.L. ON ALL MISSILE PARTS

WORKING CHARTS: SET "A"

		NOSE SECTION				
(13)	(14)	(82)	(83)	(84)	(85)	(85)
MACH NO. M	ALTITUDE H, ft	Re^{*}_{N}	$C^{A}_{f_{INS}} = \left(C^{I}_{f_{IT}}\right)^{A}$	$\left(C^{I}_{f_{IT}}\right)^{A} G_1$	R_i	$1 + R_i$
T (2.3-5)	T (2.3-5)	T (2.3-5)	FIG. (2.3-44)	(83) x (9)	T (2.3-5)	1 + (85)
0 OR .2						
.5						
M_{cr}						
1.0						
1.2						
1.5						
2.0						
3.0						
4.0						
5.0, ETC.						

NOTE: SUBSCRIPT "INS" MEANS "INSULATED SKIN"
SUBSCRIPT "T" MEANS "TURBULENT B.L."
SUPERSCRIPT "A" MEANS SET OF CHARTS "A"
SUPERSCRIPT "I" MEANS INDIVIDUAL "CASE I", RELATED TO CORRESPONDING MISSILE
SUBSCRIPT "IM" MEANS "CASE IM" FOR THE WHOLE MISSILE CONFIGURATION

BASIC EQ. (2.3-46B) $\left(C_{D_{OF}}\right)^{A}_{IM} = \left(C^{I}_{f_{IT}}\right)^{A} G_1 + \left\{\left(C^{I}_{f_{2T}}\right)^{A} \left[1 + R_i\right] - \left(C^{I}_{f_{IT}}\right)^{A} R_i\right\} G_2 + \left(C^{I}_{f_{3T}}\right)^{A} G_3 + \left(C^{I}_{f_{4T}}\right)^{A} G_4 \times N$

$C^{I}_{f_{IT}} = f\left(Re^{*}_{N}, M\right)$, T.B.L. $\qquad C^{I}_{f_{3T}} = f\left(Re_{aw}, M\right)$, T.B.L.

$C^{I}_{f_{2T}} = f\left(Re^{*I}_{TOTAL}, M\right)$, T.B.L. $\qquad C^{I}_{f_{4T}} = f\left(Re_{cr}, M\right)$, T.B.L.

		CYLINDER + BOATTAIL				
(54)	(86)	(87)	(88)	(89)	(90)	
Re^{*I}_{TOTAL}	$C^{A}_{f_{INS}} = \left(C^{I}_{f_{2T}}\right)^{A}$				$(89)^{A} G_2$	
T (2.3-5)	FIG. (2.3-44)	(86) x (85)	(83) x (55)	(87) − (88)	(89) x (10)	

G_1 = (9) =

PART. G_2 = (10) =

G_3 = (11) =

NG_4 = (12) =

TABLE (2.3-6) (CONTINUED)

		WINGS			
(13)	(14)	(90)	(91)	(92)	(94)
MACH NO. M	ALTITUDE H, ft	Re_{aw}	$C^{A}_{f_{INS}} = \left(C^{I}_{f_{3T}}\right)^{A}$	$\left(C^{I}_{f_{3T}}\right)^{A} G_3$	Re_{cr}
T (2.3-5)	T (2.3-5)	T (2.3-5)	FIG (2.3-44)	(91) x (9)	T (2.3-5)
0 OR .2					
.5					
M_{cr}					
1.0					
1.2					
1.5					
2.0					
3.0					
4.0					
5.0, ETC.					

FINS, N =		MISSILE		
(93)	(94)	(95)	(96)	(97)
$C^{A}_{f_{INS}} = \left(C^{I}_{f_{4T}}\right)^{A}$	$\left(C^{I}_{f_{4T}}\right)^{A} NG_4$			$\left(C_{D_{OF\,IM}}\right)^{A}$
FIG (2.3-44)	(93) x (12)	(84) + (90)	(94) + (92)	(95) + (96)

TABLE

AVERAGE SKIN FRICTION DRAG

PROLONGED, STEADY FLIGHT REGIMES ($0.5 \le n_g \le 1.0$), SMOOTH SURFACES ($\epsilon = 0$),

BASIC CASE IM FULLY TURBULENT B.L. ON WORKING CHARTS: SET "B"

		NOSE SECTION					CYLINDER + BOATTAIL	
(13)	(14)	(36)	(98)	(99)	(100)	(101)	(35)	(85)
MACH NO. M	ALTITUDE H, ft	Re°_{BN}	$(C_{f_i})^{B}_{INS}$	$(C_f/C_{f_i})^{B}_{INS}$	$C_{f_{INS}} = (C_{f_i})^{I}_{T} (C_f/C_{f_i})^{B}_{INS}$	$(C_{f_T})^{I}_{B_1} \times G_1$	R_1	$1 + R_1$
		T(2.3-5)	T(2.3-5)	FIG(2.3-46)	FIG(2.3-47)	(99) × (98)	(100) × (9)	T(2.3-5)	T(2.3-6)
0 or 2									
.5									
Mcr									
1.0									
1.2									
1.5									
2.0									
3.0									
4.0									
5.0, ETC.									

NOTE:

SUBSCRIPT "i" MEANS "INCOMPRESSIBLE"

SUBSCRIPT "INS" MEANS "INSULATED SKIN"

SUBSCRIPT "T" MEANS "TURBULENT B.L."

SUBSCRIPT "IM" MEANS "CASE IM" FOR THE WHOLE MISSILE CONFIGURATION

SUPERSCRIPT "I" MEANS INDIVIDUAL "CASE I", RELATED TO CORRESPONDING MISSILE PARTS

SUPERSCRIPT "B" MEANS SET OF CHARTS "B"

BASIC EQ (2.3-46R) $(C_{DOF})^{B}_{IM} = (C_{f_{iT}})^{I}_{B} G_1 + \left[(C_{f_{ST}})^{I}_{B} [1 + R_1] - (C_{f_{iT}})^{I}_{B} R_1\right] G_2 + (C_{f_{BT}})^{I}_{B} G_3 + (C_{f_{AT}})^{I}_{B} G_4$

(2.3-71)

COEFFICIENT, C_{DOF} — METHOD I

INSULATED SKIN ($T_w / T_R = T_{aw} / T_R = 1$, NO RADIATION ($\epsilon = 0$))

ALL MISSILE PARTS

(34)	(106)	(43)	(104)	(105)	(108)	(107)	(109)
$Re^{\circ}_{I\,TOTAL}$	$(C_{f_i})^{B}_{INS}$	$(C_f/C_{f_i})^{B}_{INS}$	$C_{f_{INS}} = C_{f_{BT}}^{I}$				$(107)^{B} \times G_2$
T(2.3-5)	FIG(2.3-46)	FIG(2.3-47)	(43) × (103)	(104) × (85)	(100) × (35)	(105) − (106)	(107) × (10)

$C_{f_{iT}} = f(Re^{\circ}_{BN}, M), T\,B\,L$

$C_{f_{ST}} = f(Re^{\circ}_{I\,TOTAL}, M), T\,B\,L$

$C_{f_{BT}} = f(Re_{BW}, M), T\,B\,L$

$C_{f_{AT}} = f(Re_{BF}, M), T\,B\,L$

TABLE (2.3-7)

		WINGS				
(13)	(14)	(30)	(108)	(110)	(111)	(112)
MACH NO. M	ALTITUDE H, ft	Re_{B_W}	$(C_{f_i})^{B}_{INS}$	$(C_f/C_{f_i})^{B}_{INS}$	$C_{f_{INS}} = (C_{f_T})^{I}_{BT}$	$(C_{f_T})^{I}_{BT} \times G_3$
T(2.3-5)	T(2.3-5)	T(2.3-5)	FIG(2.3-46)	FIG(2.3-47)	(108) × (110)	(111) × (11)
0 or .2						
.5						
Mcr						
1.0						
1.2						
1.5						
2.0						
3.0						
4.0						
5.0, ETC						

(CONTINUED)

	FINS N =				MISSILE		
(34)	(113)	(114)	(115)	(116)	(117)	(118)	(119)
Re_{B_F}	$(C_{f_i})^{B}_{INS}$	$(C_f/C_{f_i})^{B}_{INS}$	$C_{f_{INS}} = (C_{f_{AT}})^{I}_{B}$	$(C_{f_{AT}})^{I}_{B} \times G_4$			$(C_{DOF_{IM}})^{B}$
T(2.3-5)	FIG(2.3-46)	FIG(2.3-47)	(113) × (114)	(115) × (12)	(101) + (108)	(112) + (116)	(117) + (118)

COMMON NOTES ON TABLES (2.3-8), (2.3-9) and (2.3-10)

SUBSCRIPT "INS" MEANS "INSULATED SKIN"
SUBSCRIPT "T" MEANS "TURBULENT B.L." VALUE
SUBSCRIPT "L" MEANS "LAMINAR B.L. ' VALUE
SUBSCRIPTS "IIM,IIIM,IVM" MEAN "CASE IIM, CASE IIIM, CASE IVM RESPECTIVELY, FOR THE TOTAL MISSILE CONFIGURATION
SUPERSCRIPTS "I,II,III,IIIA,IIIC" MEAN INDIVIDUAL "CASE I,II,III,IIIA,IIIB,IIIC" RESPECTIVELY, RELATED TO VARIOUS MISSILE PARTS
SUPERSCRIPT "A" MEANS USE OF CHARTS "A"

CASE II M: NOSE CONE: PARTIALLY LAMINAR, PARTIALLY TURBULENT B.L.: $Re_{cr} < Re^{*}_{N}$ (INDIVIDUAL CASE III)
CYLINDER + BOATTAIL: FULLY TURBULENT B.L. (INDIVIDUAL CASE IIIA)
WINGS AND FINS: PARTIALLY LAMINAR, PARTIALLY TURBULENT B.L: $Re_{cr} \geq Re_{TR} \leq \frac{Re\,\bar{c}}{2}$.
(INDIVIDUAL CASE III)
TABLE (2.3-8)
GOVERNING EQ. (2.3-471):

$$(C_{D_{0f_{IIM}}})^{A} = \left\{(C^{III}_{f_{1L}})^{A}\, Ro\left[R\acute{o}-.875Ro\right] + (C^{III}_{f_{1T}})^{A}\left[1-(Ro-R\acute{o})^{2}\right]\right\} G_1 +$$

$$+ \left\{(C^{IIIA}_{f_{2T}})^{A}\left[1+R_2\right] - (C^{III}_{f_{1T}})^{A} R_2\right\} G_2 + (C^{III}_{f_{3T}})^{A} G_{3T} R_5 + (C^{III}_{f_{4T}})^{A} N G_4 R_6$$

CASE III M: NOSE CONE: FULLY LAMINAR B.L.: $Re_{cr} = Re^{*}_{N}$ (INDIVIDUAL CASE II)
CYLINDER + BOATTAIL: FULLY TURBULENT B.L. (INDIVIDUAL CASE IIIB)
WINGS AND FINS: PARTIALLY LAMINAR, PARTIALLY TURBULENT B.L.: $Re_{cr} \geq Re_{TR} \leq \frac{Re\,\bar{c}}{2}$ (INDIVIDUAL CASE III)
TABLE (2.3-9)
GOVERNING EQ. (2.3-474):

$$(C_{D_{0f_{IIIM}}})^{A} = 1.125\,(C^{II}_{f_{1L}})^{A}\, G_1 + \left\{(C^{IIIB}_{f_{2T}})^{A}\left[1+R_3\right] - (\Delta C^{IIIB}_{f_{TURFP}})^{A} R_3\right\} G_2 +$$

$$+ (C^{III}_{f_{3T}})^{A}\, G_3 R_5 + (C^{III}_{f_{4T}})^{A}\, N G_4 R_6$$

COMMON NOTES ON TABLES (2.3-8), (2.3-9) and (2.3-10)(cont'd)

CASE IV M: NOSE CONE: FULLY LAMINAR B.L.: $Re_{cr} > Re_N^*$ (INDIVIDUAL CASE II)
CYLINDER + BOATTAIL: PARTIALLY LAMINAR, PARTIALLY TURBULENT B.L.: $Re_N > Re_{TR} \geq Re_{FORE}$, $Re_{cr} \geq Re_{TR}$ (INDIVIDUAL CASE IIIC)
WINGS AND FINS: PARTIALLY LAMINAR, PARTIALLY TURBULENT B.L.: $Re_{cr} > Re_{TR} \leq \frac{Re\,\bar{c}}{2}$ (INDIVIDUAL CASE III)
TABLE (2.3-10)
GOVERNING EQ. (2.3-477): $(C_{D\,of\,IV\,M})^A = 1.125\,(C_{fIL}^{II})^A\,G_1 + \left\{ (C_{f2T}^{IIc})^A \left[1 + R_4 + \frac{R_1}{1.022} \right] - (C_{f3T}^{II})^A\,R_1 \right\} G_2 +$

$$+ (C_{f3T}^{III})^A\,G_3\,R_5 + (C_{f4T}^{III})^A\,R_6\,NG_4$$

ALL THE THREE CASES IIM, IIIM AND IVM MAY BE SUCCESSIVELY PRESENTED FOR A GIVEN FLIGHT REGIME AS MACH AND REYNOLDS NUMBER VARY WITH ALTITUDE. EACH OF THEM SHOULD BE COMPUTED UP TO THE MACH NUMBER AND FLIGHT ALTITUDE COMBINATIONS FOR WHICH THE "CRITICAL" OR "TRANSITIONAL" REYNOLDS NUMBER AND THE FLIGHT REYNOLDS NUMBER VALUES SATISY THE REQUIRED LIMITING CRITERIA FOR THE PARTICULAR CASE.

NOTE: IF SET B OF WORKING CHARTS WERE USED, THE COMPUTATIONAL PROCEDURE AND THE GOVERNING EQUATIONS SHOULD REMAIN THE SAME, BUT BEFORE OBTAINING C_{fINS}^B VALUES, TWO PRIOR STEPS WOULD BE REQUIRED: ESTIMATES OF C_{fiINS}^B AND OF $(C_f / C_{fiINS})^B$ SIMILAR TO THE PROCEDURE IN TABLE (2.3-7) FOR CASE IM.

TABLE (2.3-8)

AVERAGE SKIN FRICTION DRAG COEFFICIENT

NOTE:

$(C_{FIL})^{\overline{III}}_{B} = f_1(Re_{cr}, M)$, L & L

$(C_{FIT})^{\overline{III}}_{B} = f_2(Re^{*}_{TURN}, M)$, T & L

$(C_{FT})^{\overline{III}}_{B} = f[\beta Re_{T-APP}(\overline{III}_{B}), M]$, T & L

PROLONGED, STEADY FLIGHT REGIMES ($0 \leq \alpha \leq 10$), SMOOTH SURFACES ($\epsilon = 0$),

CASE IIM: NOSE CONE PARTIALLY LAMINAR, PARTIALLY TURBULENT B.L.,
CYLINDER + BOATTAIL: FULLY TURBULENT B.L.
WINGS AND FINS: PARTIALLY LAMINAR, PARTIALLY TURBULENT
WORKING GRAPHS: SET "A" ONLY

		NOSE SECTION $Re_{cr} < Re^{*}_{TR}$				
(13)	(14)	(37)	(38)	(44)	(46)	(45)
MACH NO M	ALTITUDE H, ft	Re_{cr}	Re^{A}_{TR}			$Re^{*\overline{III}}_{RETURN}$
		EQ (2.3-487)	EQ (2.3-488)	EQ (2.3-492)	EQ (2.3-493)	EQ (2.3-489)
T (2.3-5)	T (2.3-5)	T (2.3-5)	T (2.3-5)	T (2.3-5)	T (2.3-5)	T (2.3-5)
0 or .2						
.5						
M_{cr}						
1.0						
1.2						
1.5						
2.0						
3.0						
4.0						
5.0, ETC.						

NOTE:

SUBSCRIPT "INS" MEANS "INSULATED SKIN"

SUBSCRIPT "T" MEANS "TURBULENT B.L." VALUE

SUBSCRIPT "L" MEANS "LAMINAR B.L." VALUE

SUBSCRIPTS "IIM, IIIM, IVM" MEAN "CASE IIM, CASE IIIM, CASE IVM" RESPECTIVELY, FOR

SUPERSCRIPTS "I, II, III, IIIA, IIIB, IIIC" MEAN INDIVIDUAL "CASE I, II, III, IIIA, IIIB, IIIC"

SUPERSCRIPT "A" MEANS USE OF SET OF CHARTS "A"

GOVERNING EQ (2.3-471): $(C_{DOF\,IIM})^{A} = \left\{(C_{FIL})^{\overline{III}A}_{B}\left[R_{B'} - .873R_{N}\right] + (C_{FIT})^{\overline{III}A}_{B}\left[1 - (R_{B} - R_{B'})^{.2}\right]\right\}\frac{S_1}{S_B} + \left\{(C_{FBT})^{\overline{III}A}_{B}\left[1 + R_{B}\right] - (C_{FIT})^{\overline{III}A}_{B}\right\}$

NOTE FOR SET "B" THE COMPUTATIONAL SEQUENCE IS THE SAME, BUT BEFORE OBTAINING OF $C^{A}_{f_{INS}}$ AND OF $(C_f/C_{f_1})^{A}_{INS}$ — SIMILAR TO THE PROCEDURE IN TABLE (2.3-7)

C_{DOF} — METHOD I

INSULATED SKIN ($T_W/T_H \approx T_{AW}/T_H$), NO RADIATION ($\epsilon = 0$)

$Re_{cr} < Re_{TR}$

B.L., $Re_{cr} > Re_{TR} \leq Re_{RE}/2$.

(120)	(121)	(122)	(123)	(124)	(125)
$C^{A}_{f_{INS}} \cdot (C_{FIL})^{\overline{III}A}_{B}$	$C^{A}_{f_{INS}} \cdot (C_{FIT})^{\overline{III}A}_{B}$				$(C_{DOF_{IN}})^{\overline{III}A}_{L+T}$
					EQ (2.3-400)
FIG (2.3-44)	FIG (2.3-44)	(46) x (120)	(46) x (121)	(122) + (123)	(124) x (9)

THE TOTAL MISSILE CONFIGURATION

RESPECTIVELY, RELATED TO VARIOUS MISSILE PARTS

$R_{S_2}) G_2 + (C_{FBT})^{\overline{III}A}_{B} G_3 \; R_3 + (C_{FAT})^{\overline{III}A}_{N} G_4 R_4$

$C^{A}_{f_{INS}}$ VALUES, TWO PRIOR STEPS ARE REQUIRED ESTIMATES FOR CASE IM.

TABLE (2.3-8) CONTINUED (1)

AVERAGE SKIN-FRICTION DRAG COEFFICIENT, C_{DOF} — METHOD I

(CASE IIM)

		CYLINDER + BOATTAIL		
(13)	(14)	(57)	(124)	(58)
MACH NO M	ALTITUDE H, ft	$Re^{\overline{III}A}_{TOTAL}$	$C^{A}_{f_{INS}} \cdot (C_{FBT})^{\overline{III}A}_{B}$	R_B
		EQ (2.3-505)		EQ (2.3-506)
T (2.3-5)	T (2.3-5)	T (2.3-5)	FIG (2.3-44)	T (2.3-5)
0 OR .2				
.5				
M_{cr}				
1.0				
1.2				
1.5				
2.0				
3.0				
4.0				
5.0, ETC				

NOTE:

$(C_{FBT})^{\overline{III}A}_{B} = f(Re^{\overline{III}A}_{TOTAL}, M)$, T & L

(27)	(28)	(29)	(30)	(31)
				$(C_{DOF_{CYL+BT}})^{A}_{T}$
				EQ (2.3-425)
1 + (58)	(29) x (27)	(21) + (58)	(28) - (29)	(30) x (10)

TABLE (2.3-8), CONTINUED (2)

AVERAGE SKIN-FRICTION DRAG COEFFICIENT $C_{D_{OF}}$ — METHOD I

(CASE II M)

		WINGS $Re_{cr} \geq Re_{TURB} \leq (Re_{\Sigma_W}/2)$		
(13)	(14)	(30)	(69)	(70)
MACH NO M	ALTITUDE H, ft	Re_{Σ_W}	$Re_{\Sigma_W}/2$	$Re_{cr} \geq Re_{TURB}$
		EQ (2.3-532)	(30)/2	EQ (2.3-535)
T (2.3-5)	T (2.3-5)	T (2.3-5)	T (2.3-5)	T (2.3-5)
0 or .2				
.5				
M_{cr}				
1.0				
1.2				
1.5				
2.0				
3.0				
4.0				
5.0, ETC				

(74)	(75)	(32)	(33)	(134)
R_δ	Re^{Σ}_{TURB}	$C_{f_{TURB}} = (C_{f_{ST}})^{A}$	$(C_{f_{ST}})^{\Sigma}_{A} R_\delta$	$(C_{D_{OF}})^{A}_{L+T}$
EQ (2.3-537)	EQ (2.3-534)			EQ (2.3-487)
T (2.3-5)	T (2.3-5)	FIG (2.3-44)	(32) x (74)	(33) x (11)

NOTE

$(C_{f_{ST}})^{A} = f(Re^{\Sigma}_{TURB}, M)$, TBL

TABLE (2.3-8) CONTINUED (3)

AVERAGE SKIN-FRICTION DRAG COEFFICIENT, $C_{D_{OF}}$ — METHOD I

(CASE II M)

		N FINS, $Re_{cr} \geq Re_{TRF} \leq (Re_{\Sigma_W}/2)$				
(13)	(14)	(34)	(76)	(77)	(81)	(82)
MACH NO M	ALTITUDE H, ft	Re_{Σ_F}	$\frac{Re_{\Sigma_F}}{2}$	$Re_{cr} \geq Re_{TRF}$	R_δ	(Re^{Σ}_{TURF})
		EQ (2.3-533)	(34)/2	EQ (2.3-539)	EQ (2.3-541)	EQ (2.3-538)
T (2.3-5)	T (2.3-5)	T (2.3-5)	T (2.3-5)	T (2.3-5)	T (2.3-5)	T (2.3-5)
0 OR .2						
.5						
M_{cr}						
1.0						
1.2						
1.8						
2.0						
3.0						
4.0						
5.0, ETC						

			MISSILE		
(35)	(36)	(37)	(38)	(39)	(40)
$C_{f_{TURB}} = (C_{f_{ST}})^{A}$	$(C_{f_{ST}})^{\Sigma}_{A} \times N \times S_B$	$(C_{D_{OF}})^{A}_{L+T}$			$(C_{D_{OF_{MI}}})^{A}$
		EQ (2.3-461)			EQ (2.3-471)
FIG (2.3-44)	(12) x (36)	(36) x (81)	(25) + (31)	(34) + (37)	(38) + (39)

NOTE

$(C_{f_{ST}})^{A} = f(Re^{\Sigma}_{TURF}, M)$, TBL

TABLE (2.3-9)

AVERAGE SKIN-FRICTION DRAG
PROLONGED, STEADY FLIGHT REGIMES
INSULATED SKIN ($T_w/T_o \approx T_{aw}/T_o$)
CASE III M NOSE CONE FULLY
CYLINDER + BOATTAIL
WINGS AND FINS
$Re_{cr} \triangleq Re_{TR} \triangleq Re_E/2$

WORKING GRAPHS SET "A" ONLY

		NOSE SECTION, $Re_{cr} = Re_n^o$			
(13)	(14)	(38)	(41)	(42)	(43)
MACH NO. M	ALTITUDE H, ft	$Re_{cr} = Re_n^o$	$C_{f_{TURB}}^o = \left(C_{f_{TR}}^{III}\right)^A$	$1.328\left(C_{f_{TR}}^{III}\right)^A$	$\left(C_{DOF_{III}}^{III}\right)^A$
		EQ (2.3-406)		EQ (2.3-408)	EQ (2.3-369)
T (2.3-5)	T (2.3-5)	T (2.3-5)	FIG (2.3-44)	1.328 × (41)	(42) × (9)
0 OR 2					
.9					
M_{cr}					
1.0					
1.2					
1.5					
2.0					
3.0					
4.0					
5.0, ETC.					

NOTE $\left(C_{f_{TR}}^{III}\right)^A = f_1\left(Re_n^o = Re_{cr}, M\right)$, TBL

$\left(C_{DOF}^{III\,0}\right)^A = f\left(Re_{TOTAL}^{o\;III\,0}, M\right)$, TBL

$\left(\Delta C_{f_{TURBP}}^{III\,0}\right)^A = \left(C_{f_{TR}}^{III}\right)^A \left(Re_n^o / Re_{TR}^{III\,0}\right) \times 1.15$, TBL

CASE III M NOSE CONE: FULLY
CYLINDER + BOATTAIL:
WINGS AND FINS:
GOVERNING EQ (2.3-474)

COEFFICIENT, C_{DOF} - METHOD I
$(0 < Re_E < 10)$, SMOOTH SURFACES $(\varepsilon = 0)$
, NO RADIATION $(\mathcal{E} = 0)$
LAMINAR B.L., $Re_{cr} = Re_n^o$,
FULLY TURBULENT B.L.
PARTIALLY LAMINAR, PARTIALLY TURBULENT B.L.

		CYLINDER + BOATTAIL					
(39)	(41)	(39)	(44)	(45)	(46)	(47)	
$Re_{TOTAL}^{o\;III\,0}$	R_b	$Re_{AE}^{III\,0}$	Re_n^o / Re_{AE}^{III}	$1.15\left(C_{f_{TR}}^{III}\right)^A$	$\left(\Delta C_{f_{TURBP}}^{III\,0}\right)^A$	$C_{f_{TURB}}^A = \left(C_{f_{TR}}^{III\,0}\right)^A$	
EQ (2.3-509)	EQ (2.3-512)	EQ (2.3-510)					
T (2.3-5)	T (2.3-5)	T (2.3-5)	(39) / (39)	1.15 × (41)	(45) × (46)	FIG (2.3-44)	

LAMINAR B.L. $Re_{cr} = Re_n^o$ (INDIVIDUAL CASE III)
FULLY TURBULENT B.L. (INDIVIDUAL CASE III 8)
PARTIALLY LAMINAR, PARTIALLY TURBULENT B.L.: $Re_{cr}\ Re_{TR}\ \frac{Re_E}{2}$, (INDIVIDUAL CASE III)

$(C_{DOF_{III\,M}})^A = 1.328\left(C_{f_{TR}}^{III} Y^B_{TR} + \left[\left(C_{f_{TR}}^{III\,0}\right)^A (1 + R_b) - \left(\Delta C_{f_{TURBP}}^{III\,0}\right)^A R_b\right] C_{B_2} + \left(C_{f_{TR}}^{III}\right)^A / D_2\, R_2 + \left(C_{f_{TR}}^{III}\right)^A N C_{B_1} R_B\right)$

TABLE (2.3-9) (CONTINUED)

AVERAGE SKIN-FRICTION DRAG
(CASE III M)
COEFFICIENT, C_{DOF} - METHOD I

		CYLINDER + BOATTAIL (CONTINUED)			
(13)	(14)	(48)	(49)	(50)	(51)
MACH NO. M	ALTITUDE H, ft	$1 + R_b$			
T (2.3-5)	T (2.3-5)	1 + (41)	(48) × (47)	(48) × (41)	(49) − (50)
0 OR 2					
.9					
M_{cr}					
1.0					
1.2					
1.5					
2.0					
3.0					
4.0					
5.0, ETC.					

(2.3-9) (CONTINUED)
(CASE III M)
DRAG COEFFICIENT, C_{DOF} - METHOD I

	WINGS AND FINS		MISSILE		
(18)	(134)	(137)	(133)	(135)	(136)
$\left(C_{DOF_{CYL+BT}}^{III\,0}\right)^A_{F_B}$	$\left(C_{DOF_W}^{III}\right)^A$	$\left(C_{DOF_F}^{III}\right)^A$			$\left(C_{DOF_{III\,M}}\right)^A$
EQ (2.3-431)	EQ (2.3-457)	EQ (2.3-461)		T (2.3-8)	EQ (2.3-474)
(51) × (18)	T (2.3-8)	T (2.3-8)	(143) + (132)	(134) + (137)	(133) + (135)

TABLE

AVERAGE SKIN-FRICTION DRAG COEFFICIENT
PROLONGED, STEADY FLIGHT REGIMES (0 ≤ n_z
INSULATED SKIN ($T_w/T_\infty \approx T_{aw}/T_\infty$), NO
CASE IX M NOSE CONE FULLY LAMINAR B L ,
CYLINDER + BOATTAIL PARTIALLY

WORKING GRAPHS: SET "A" ONLY

WINGS AND FINS PARTIALLY LAMINAR

		NOSE SECTION, $Re_{cr} > Re^{a}_{n}$				
(13)	(14)	(37)	(36)	(101)	(106)	(103)
MACH NO M	ALTITUDE H ft	Re_{cr}	Re^{M}_{n}	$C^{A}_{f\,NS} \cdot \left(C^{M}_{f\,IL}\right)^{A}$	$1.125\left(C^{M}_{f\,IL}\right)^{A}$	$\left(C_{DofN}\right)^{A}$
		EQ (2.3-487)	EQ (2.3-486)	T (2.3-9)	T (2.3-9)	T (2.3-9)
T (2.3-5)	T (2.3-5)	T (2.3-5)	T (2.3-5)	FIG. (2.3-44)	1.125 × (101)	(102) × (8)
0 OR .2						
.5						
M_{cr}						
1.0						
1.2						
1.5						
2.0						
3.0						
4.0						
5.0, ETC						

NOTE: SUBSCRIPT "INC" MEANS "INSULATED SKIN".
SUBSCRIPT "T" MEANS "TURBULENT B L" VALUE
SUBSCRIPT "L" MEANS "LAMINAR B L" VALUE
SUBSCRIPTS "IIM, IIIM, IIXM" MEANS "CASE IIM, CASE IIIM, CASE IIXM" RESPECTIVELY FOR THE TOTAL MISSILE CONFIGURATION
SUPERSCRIPTS "I, II, IIA, IIB, IIC" MEAN INDIVIDUAL "CASE I, II, IIA, IIB, IIC" RESPECTIVELY RELATED TO VARIOUS MISSILE PARTS.
SUPERSCRIPT "A" MEANS USE OF SET OF CHARTS "A"

(2.3-10)

C_{DOf} METHOD I

$\bar{s}$ (0), SMOOTH SURFACE ($k = 0$)

RADIATION ($\epsilon = 0$)

$Re_{cr} > Re^{a}_{n}$

LAMINAR, PARTIALLY TURBULENT B L $Re^{a}_{n} > Re_{TR} \geq Re^{a}_{FORE}$

$Re_{cr} = Re_{TR} = Re^{IIC}_{cr}$

PARTIALLY TURBULENT B L $Re_{cr} \geq Re_{TR} = (Re_{cr}/2)$

CYLINDER + BOATTAIL, $Re^{a}_{n} > Re_{TR} \geq Re^{a}_{FORE}$, $Re_{cr} \geq Re_{TR}$					
(62)	(64)	(67)	(66)	(68)	(69)
Re^{IIC}_{cr}	Re^{a}_{FORE}	$Re^{a\,IIC}_{TOTAL}$	$C^{A}_{f\,NS} \cdot \left(C^{IIC}_{f\,ST}\right)^{A}$	R_c	R_l
EQ (2.3-515)	EQ (2.3-514)	EQ (2.3-513)		EQ (2.3-518)	EQ (2.3-517)
T (2.3-5)	T (2.3-5)	T (2.3-5)	FIG (2.3-44)	T (2.3-5)	T (2.3-5)

GOVERNING EQ (2.3-477)

$$\left(C_{DofIIM}\right)^{A} = 1.128\left(C^{M}_{f\,IL}\right)^{A} G_1 + \left\{\left(C^{IIC}_{f\,ST}\right)^{A}\left[1 + R_c - \frac{R_l}{1.022}\right] - \left(C^{M}_{f\,IL}\right)^{A} R_l\right\} G_2 + \left(C^{IIC}_{f\,ST}\right)^{A} G_3 R_b + \left(C^{IIC}_{f\,ST}\right)^{A} R_l$$

$$\left(C^{M}_{f\,IL}\right)^{A} = f_1\left(Re^{M}_{n}, M\right), \text{ L B L} \qquad \left(C^{IIC}_{f\,ST}\right)^{A} = f\left(Re^{a\,IIC}_{TOTAL}, M\right), \text{ T B L}$$

TABLE (2.3-10) (CONTINUED)
AVERAGE SKIN-FRICTION DRAG COEFFICIENT, C_{Dof} - METHOD I
(CASE IXM)

		CYLINDER + BOATTAIL, (CONTINUED)					
(13)	(14)	(104)	(107)	(108)	(109)	(104)	(110)
MACH NO M	ALTITUDE H, ft	$1 + R_c$	$\frac{R_l}{1.022}$			$\left(C^{M}_{f\,IL}\right)^{A}$	
						T (2.3-9)	
T (2.3-5)	T (2.3-5)	1 + (69)	(69)/1.022	(110) + (107)	(108) × (109)	FIG. (2.3-44)	(69) × (104)
0 OR .2							
.5							
M_{cr}							
1.0							
1.2							
1.5							
2.0							
3.0							
4.0							
5.0, ETC.							

NOTE: $\left(C^{M}_{f\,IL}\right)^{A} = f_1\left(Re^{M}_{n}, M\right)$, L B L

		WINGS AND FINS		MISSIL.		
(101)	(104)	(124)	(127)	(133)	(135)	(134)
	$\left(C_{Dof\,IIC\,CYL+BT}\right)^{A}$	$\left(C_{Dof\,IIM}\right)^{A}_{L+T}$	$\left(C_{Dof\,IIM}\right)^{A}_{L+T}$			$\left(C_{Dof\,IIM}\right)^{A}$
	EQ (2.3-439)	EQ (2.3-467)	EQ (2.3-461)		T (2.3-8)	EQ (2.3-477)
(101) - (104)	(82) × (10)	T (2.3-8)	T (2.3-8)	(133) + (104)	(134) + (127)	(133) + (108)

2.3.11 METHOD II, TABLES (2.3-11) AND (2.3-12)

Assumptions: The actual surface finish is considered aerodynamically smooth, ($k=0$); the non insulated skin thermal conditions are approximated by the respective average (T_w/T_H) ratios corresponding to different flight regimes stated below; the skin-temperature distribution is assumed to be uniform; the radiation effects can be taken into account, if needed.

Applicability: High quality surface-finish prototypes; prolonged, steady flight regimes, ($M = const$), or quasi-steady accelerated phases ($n_g > 0$) treated within the steady flow theory (apparent mass effects not included).

Working graphs and tables: Two sets of working charts can be used alternatively:

Set A: DIRECT ESTIMATES FOR LAMINAR AND TURBULENT B. L.

Fig. (2.3-44) - Average, two-dimensional, compressible skin-friction coefficient $(C_{f\,INS})^A$ for laminar and turbulent boundary layers on insulated flat plates. Use "smooth" curves. (Van Driest)

Fig. (2.3-45) - Average, two-dimensional, compressible skin-friction coefficient $(C_f)_T^A$ for laminar and turbulent boundary layers on non-insulated flat plates, for the specific case of $(T_W/T_H=1)$. Use "smooth" curves. (Van Driest).

Set B: INDIRECT ESTIMATES FOR LAMINAR AND TURBULENT B. L.

Fig. (2.3-46) - Average, two-dimensional incompressible skin-friction coefficient $(C_{fi\,INS})^B$ for turbulent boundary layers on insulated, smooth flat plates. (Karman-Schoenherr).

Fig. (2.3-48) - Laminar boundary layer (Blasius): Average two-dimensional, incompressible skin-friction coefficient; smooth, insulated flat plates; zero angle-of-attack.

Fig. (2.3-47) and Fig. (2.3-49) - Variations of $(C_f/C_{fi})^B_{INS}$ ratio with the Mach (and Reynolds) Number changes for turbulent and laminar boundary layers on insulated, smooth, flat plates. (Van Driest).

GRAPHS COMMON TO BOTH SETS:

Fig. 1.31 - Plot of Reynolds Number versus Mach Number for altitudes from 0 to 35,000 feet.

Fig. 1.32 - Plot of Reynolds Number versus Mach Number for altitudes from 40,000 feet to 80,000 feet.

Fig. (2.3-50) - Skin-free stream temperature ratios (T_{we}/T_H) in accelerated flight regimes, isothermal altitudes.

Fig. (2.3-51) - Skin-free stream temperature ratios (T_{we}/T_H) in accelerated flight regimes, sea-level conditions.

Fig. (2.3-52) - Skin-to-adiabatic temperature ratios (T_{we}/T_{aw}) versus Mach Number for non-insulated skin, accelerations from 0 to 20g.

Fig. (2.3-55) - Adiabatic temperatures of perfectly insulated surfaces, neglecting radiation, $T_{aw} = f(M_H, T_H)$.

Fig. (2.3-54) - Determination of equilibrium temperatures with radiation, $(T_{wer}/T_H) = f(\epsilon, M, T_H, h)$.

Fig. (2.3-53) - Heat-transfer coefficients for laminar and turbulent boundary layers,

$$h_i = f(Re) \text{ and}$$

$$(h/h_i) = f\left[(T_W - T_H)/(T_{aw} - T_H), M_H\right]$$

Fig. (2.3-58) - Estimates of the equivalent turbulent boundary layer Reynolds Number $Re_{\Delta x}$, and of the respective product, $\Delta C_{f_{TURBFP}} Re_{\Delta x}$ in terms of Re_{cr}.

Fig. (2.3-56) and Fig. (2.3-57) - Average compressible turbulent boundary layer skin-friction coefficient incremental ratio $(\Delta C_{f_T} / C_{fi\,INS})$ due to actual skin-temperature ratio (T_W/T_H), both for accelerated and steady flight regimes (with radiation effects included).

The expected accuracy of the working graphs: The individual values of $(C_{fi\,INS})$, $(C_{f\,INS})$ and $(C_f/C_{fi})_{INS}$ agree with most of the acceptable experimental and theoretical evidence within ± 10% for turbulent boundary layers on smooth, insulated flat plates, and for Mach Numbers up to 5. Accuracy of the corresponding laminar boundary layer values is within ± 5% under the same general conditions.

The ΔC_{f_T} estimates in Figs (2.3-56) and (2.3-57) are recalculated from the Van Driest's(27) and Sommer and

Short's[80] data. Due to lack of a unified general experimental evidence, the accuracy level is somewhat uncertain, even assuming a uniform skin-temperature distribution; the most that can be hoped is that the estimates may be expected to conform with the overall accuracy of within the usual ± 10%, provided the skin-temperature is guessed correctly.

The estimates of $(T_{we}/T_H) = f(ng, M, H)$ ratios in Figs (2.3-50) and (2.3-51) are based and recalculated from the unique experimental evidence presented by Kaye[70] for a steel, 20" thick skin of a supersonic, bi-convex airfoil wing, assuming a mean-average, uniform temperature distribution. The reliability of a broader application of the specific results remains questionable.

Figs. 1.31 and 1.32 are within the general validity of the Standard Atmosphere concept; the relationship can be computed to any desired degree of accuracy.

The adiabatic wall temperatures, T_{aw}, in Fig (2.3-55) are computed by classical thermodynamic concepts with variable specific heats.

Figs (2.3-53), (2.3-54) and (2.3-55) reflect a first-order approximation, including the empirical estimate of an "emissivity factor", ϵ, see Table (2.3-4). Within the mean-average uniform temperature concept, a reasonable accuracy of the (T_{wer}/T_H) predictions should be of the order of ±5%, see Ref. 132 (R.A.S. Data Sheets).

Computational procedure:

The computational procedure with the proposed method II is tentatively subdivided into three best representative flight cases. Each of the three procedures is clearly indicated in the respective computational tables (2.3-11) to (2.3-14), in a self-explanatory manner. The skin-friction coefficient estimates are two-dimensional, average flat plate values; corrections for flow three-dimensionality and specific body geometries are included additionally in the usual "factoring" form.

(i) Steady, Prolonged Flight Regimes, No Radiation Effects, Tables (2.3-6) to (2.3-10)

The computational procedure is identical with that of the Method I, since in this case, in a first approximation:

$$(T_W/T_H) = (T_{we}/T_H) \approx (T_{aw}/T_H) \qquad (2.3\text{-}552)$$

which is the same condition specified earlier for an "insulated" skin. Therefore, the Tables (2.3-6) to (2.3-10) from Method I can be used directly, representing Cases I M, II M, III M and IV M, alternatively.

(ii) Steady, Prolonged Flight Regimes, Radiation Effects on Skin-temperature Taken into Account, Table (2.3-11)

First, estimates of a mean uniform skin-temperature distribution due to radiation effects should be performed for all missile parts. These estimates should cover the prescribed Mach Numbers and flight altitude changes. Since the skin-temperature is, among other factors, strongly influenced by the boundary layer flow-type and the associated Reynolds Number values, the same four Cases (IM, IIM, IIIM, IVM), specified in Method I, might be here present also. This would appreciably complicate the already lengthy computational procedure; instead, a turbulent boundary layer is assumed on all missile parts (Case IM, Method I). Such an approximation seems well acceptable for engineering purposes since the proposed method of finding a mean, presumably, uniform skin-temperature distribution due to radiation is in itself grossly approximate. Once the incremental drag term due to radiation effects is determined for each missile part, a total zero-lift drag force coefficient increment for the whole missile configuration can be found by using the slightly modified "governing" Eq. (2.3-468) of the Case IM:

$$(\Delta C_{D0f_{IMT}})^A_{RAD} = (\Delta C_{fiT})^A_{RAD} G_1 + \left\{(\Delta C^I_{f2T})^A_{RAD}[1+R_1] - (\Delta C^I_{fiT})^A_{RAD} R_1\right\} G_2 + (\Delta C^I_{f3T})^A_{RAD} G_3 + (\Delta C^I_{f4T})^A_{RAD} G_4 N,$$

or

(2.3-468a)

$$(\Delta C_{Dof_{IMT}})^{B}_{RAD} = (\Delta C_{f_{1T}})^{B}_{RAD} G_1 +$$

$$+ \left\{ (\Delta C^{I}_{f_{2T}})^{B}_{RAD} [1 + R_1] - (\Delta C^{I}_{f_{1T}})^{B}_{RAD} R_1 \right\} G_2 +$$

$$+ (\Delta C^{I}_{f_{3T}})^{B}_{RAD} G_3 + (\Delta C^{I}_{f_{4T}})^{B}_{RAD} G_4 N ,$$

(2.3-468b)

depending upon the alternative choice of sets "A" or "B" as working graphs. In the above equations (2.3-468a) or (2.3-468b), the subscripts "1T", "2T", "3T" and "4T" refer to the thermal (T) effects within the turbulent boundary layer, for nose section (1), cylinder + boattail (2), wings (3) and fins (4), respectively.

The total incremental drag coefficient value due to radiation $(\Delta C_{Dof_{IMT}})_{RAD}$ is then added to any of the already computed missile drag coefficient values without radiation ($C_{Dof_{IM}}$), ($C_{Dof_{IIM}}$), ($C_{Dof_{IIIM}}$), or ($C_{Dof_{IVM}}$) as performed by Method I for various actually selected boundary layer flow types. The whole procedure is self-instructively indicated in the Table (2.3-11). The computational steps are as follows:

(1) For a given flight altitude and Mach Number range, enter in Table (2.3-11) the Reynolds Number values,

$$Re^{*}_{N} , \; Re^{*}_{TOTAL} , \; R_1 , \; 1 + R_1 , \; Re_{\bar{c}_W} , \; Re_{\bar{c}_F} ,$$

(2.3-553)

from Table (2.3-5), for nose section, cylinder + boattail, wings and fins, respectively. They serve as the assumed approximate Reynolds Numbers for skin-temperature estimates in presence of radiation. The approximation involves a supposedly fully turbulent boundary layer on all missile parts, as already stated.

(2) From Figs (2.3-53) and (2.3-54) determine the temperature ratio (T_{wer}/T_H) with skin-to-ambient atmosphere radiation taken into account as follows:

Corresponding to given values of Re , M_H , and H , determine first the incompressible turbulent boundary layer heat transfer coefficient $h_i = f(Re)$ from Fig (2.3-53a), and then the compressible-to-incompressible ratio, $(h/h_i) = f(M_H, T_{wer}/T_H)$ from Fig (2.3-53b). Since the value of actual skin-temperature $(T_w = T_{wer})$ is not known in advance, the determination of the necessary ratio (h/h_i) should be done in two approximations:

In a first approximation, assume $[(T_w - T_H)/(T_{aw} - T_H)] = 1$ and read off $(h/h_i) = f(M_H)$ for turbulent flows. From Table (2.3-4) determine the emissivity factor, ϵ , as a function of the skin material and its surface condition. With the respective values of ϵ , T_H , ρ_H and h , compute the parameter,

$$\left[\left(\frac{\epsilon T_H^{2.5}}{\rho_H h} \right) \frac{1}{10^{14}} \right]_{FIRST \; APPROX}$$

(2.3-554)

and from Fig (2.3-54) determine the respective value of the (T_{wer}/T_H) ratio, i.e., in the first approximation the required skin temperature,

$$(T_w = T_{wer})_{FIRST \; APPROX} .$$

(2.3-555)

In a second approximation, read off the corresponding value of $(T_{aw}/T_H) = f(M_H)$ from Fig (2.3-54), assuming $(\epsilon = 0)$. With the (T_{aw}) and $(T_w = T_{wer})$ first approximation, compute the necessary ratio,

$$\left(\frac{T_w - T_H}{T_{aw} - T_H} \right) ,$$

(2.3-556)

and then repeat the procedure of finding (h/h_i) and (T_{wer}/T_H) ratios as outlinded in the first step above. This second approximate value of (T_{wer}/T_H) may be regarded as sufficiently accurate for the practical engineering analysis.

Important note: On Figs (2.3-53) and (2.3-54) all temperatures must be taken in °Kelvin and °Centigrade respectively. General conversion formulae are:

$$°R = (9/5) \, °K ,$$

$$\frac{°C}{5} = \frac{°F - 32}{9} = \frac{°K - 273.16}{5} = \frac{°R - 491.69}{9} ,$$

i.e., $\left(\frac{T_{wer}}{T_H} \right)_{KELVIN} =$

(2.3-557)

$$= \left(\frac{T_{wer}}{T_H} \right)_{FAHRENHEIT \; OR \; RANKINE \; ABSOLUTE} ,$$

(2.3-558)

and

$$\left(\frac{T_w - T_H}{T_{aw} - T_H}\right)_{KELVIN} = \left(\frac{T_w - T_H}{T_{aw} - T_H}\right)_{FAHRENHEIT\ ABSOLUTE\ OR\ RANKINE} \quad (2.3\text{-}559)$$

(3) Insert in the Table (2.3-11) the skin-friction coefficient values, already computed in the Tables (2.3-6) or (2.3-7) (Case IM, Method I), for various missile parts (without radiation) as follows:

If the set "B" of the working charts has been used, insert in Table (2.3-11) the values of

$$(C_{fi_{INS}}^{B})_{NOSE}\ ,\quad (C_{fi_{INS}}^{B})_{CYL+BT}\ ,$$

$$(C_{fi_{INS}}^{B})_{WING}\ ,\quad (C_{fi_{INS}}^{B})_{FINS}\ , \quad (2.3\text{-}560)$$

as already computed in Table (2.3-7). The subscript "i" means "incompressible" and the subscript "INS" means "insulated". The average skin friction coefficient values are for a smooth flat plate.

If the set "A" of the working charts has been used, first insert in the Table (2.3-11) the compressible two-dimensional values of the average skin friction coefficients as computed in Table (2.3-6):

$$(C_{fi_{INS}}^{A})_{NOSE}\ ,\quad (C_{fi_{INS}}^{A})_{CYL+BT}\ ,$$

$$(C_{fi_{INS}}^{A})_{WING}\ ,\quad (C_{fi_{INS}}^{A})_{FINS} \quad (2.3\text{-}561)$$

and then compute the corresponding incompressible two-dimensional values:

$$(C_{fi_{INS}}^{A})_{NOSE}\ ,\quad (C_{fi_{INS}}^{A})_{CYL+BT}\ ,$$

$$(C_{fi_{INS}}^{A})_{WING}\ ,\quad (C_{fi_{INS}}^{A})_{FINS} \quad (2.3\text{-}562)$$

by using related data from Fig (2.3-47), in which the compressible-to-incompressible average skin-friction coefficient ratios,

$$(C_f / C_{fi})\ , \quad (2.3\text{-}563)$$

are plotted versus Mach and Reynolds Numbers.

In the case of the set "B" of working graphs, it has been necessary to find the respective incompressible skin-friction coefficient values because the basic working graphs for skin-temperature effects or the frictional phenomena represent a replot from Ref. 27 (Van Driest) in the form of

$$(\Delta C_{fT} / C_{fi_{INS}}) = f(M, Re, T_W)\ , \quad (2.3\text{-}564)$$

for smooth, flat plates (two dimensional values, see Figs (2.3-56) and (2.3-57)).

(4) For the earlier determined values of $(T_W / T_H) = (T_{wer} / T_H)$ from step (2), determine from Figs (2.3-56) or (2.3-57) the incremental ratio,

$$\left(\frac{\Delta C_{fT}}{C_{fi_{INS}}}\right)_{RAD} = f\left(Re, M_H, \frac{T_{wer}}{T_H} = \frac{T_w}{T_H}\right)\ , \quad (2.3\text{-}565)$$

and compute the explicit value of (ΔC_{fT}) using the value of $(C_{fi}^{A}{}_{INS})$ or $(C_{fi}^{B}{}_{INS})$ from step (3).

(5) Using the Eq (2.3-468a) or (2.3-468b), find the total drag force coefficient increment due to the radiation effects, $(\Delta C_{Dof}{}^{IMT})_{RAD}$, by performing in Table (2.3-11), the indicated algebraic operations for nose cone, cylinder + boattail, wings and fins, and by summing up the resultant components.

(6) This incremental value, $(\Delta C_{Dof}{}^{IMT})_{RAD}$ is then added to the drag coefficient estimates without radiation, evaluated previously by Method I for the chosen boundary layer status on various missile parts (Cases IM, IIM, IIIM or IVM respectively):

$$(C_{Dof\,IMT})_{RAD}^{A} = (C_{Dof\,IM})^{A} + (\Delta C_{Dof\,IMT})_{RAD}^{A}\ ,$$

$$(C_{Dof\,IIMT})_{RAD}^{A} = (C_{Dof\,IIM})^{A} + (\Delta C_{Dof\,IMT})_{RAD}^{A}\ ,$$

$$(C_{Dof\,IIIMT})_{RAD}^{A} = (C_{Dof\,IIIM})^{A} + (\Delta C_{Dof\,IMT})_{RAD}^{A}\ ,$$

$$(C_{Dof\,IVMT})_{RAD}^{A} = (C_{Dof\,IVM})^{A} + (\Delta C_{Dof\,IMT})_{RAD}^{A}\ , \quad (2.3\text{-}566)$$

or

$$(C_{Dof\,IMT})_{RAD}^{B} = (C_{Dof\,IM})^{B} + (\Delta C_{Dof\,IMT})_{RAD}^{B}\ ,$$

$$(C_{Dof\,IIMT})_{RAD}^{B} = (C_{Dof\,IIM})^{B} + (\Delta C_{Dof\,IMT})_{RAD}^{B}\ ,$$

$$(C_{Dof\,IIIMT})_{RAD}^{B} = (C_{Dof\,IIIM})^{B} + (\Delta C_{Dof\,IMT})_{RAD}^{B}\ ,$$

$$(C_{Dof\,IVMT})_{RAD}^{B} = (C_{Dof\,IVM})^{B} + (\Delta C_{Dof\,IMT})_{RAD}^{B}\ , \quad (2.3\text{-}567)$$

for the working sets of charts "A" or "B", respectively, see Table (2.3-11).

(iii) Constant Acceleration Flight Regimes, $n_q>0$; Radiation Effects on Skin-temperature Neglected, Table (2.3-12)

The only constant acceleration effects accounted for are the corresponding change in the average skin-temperature conditions.

The contribution of the radiation phenomena on the average skin-temperature conditions in accelerated flight regimes is neglected, since the predominant effects of the acceleration itself are estimated only roughly by the proposed method (see earlier text), i.e., by neglecting the apparent mass effects and all other unsteady flow phenomena (except for the skin-temperature changes).

For the same reasons, it is assumed that a fully turbulent boundary layer exists on all missile surfaces, so that the simplest evaluation formulae, similar to the fundamental Case IM, may be used. This yields the total increment of the zero-lift drag coefficient due to the changed thermal conditions in acceleration in the form:

$$(\Delta C_{D0fIMT})^{A}_{ACC} = (\Delta C_{fIT})^{A}_{ACC} G_1 + \left\{ (\Delta C_{f2T})^{A}_{ACC} [1+R_1] - (\Delta C_{fIT})^{A}_{ACC} R_1 \right\} G_2 + (\Delta C_{f3T})^{A}_{ACC} G_3 + (\Delta C_{f4T})^{A}_{ACC} G_4 N , \quad (2.3\text{-}468c)$$

or

$$(\Delta C_{D0fIMT})^{B}_{ACC} = (\Delta C_{fIT})^{B}_{ACC} G_1 + \left\{ (\Delta C_{f2T})^{B}_{ACC} [1+R_1] - (\Delta C_{fIT})^{B}_{ACC} R_1 \right\} G_2 + (\Delta C_{f3T})^{B}_{ACC} G_3 + (\Delta C_{f4T})^{B}_{ACC} G_4 N , \quad (2.3\text{-}468d)$$

depending upon the set of working charts that has been used. It should be noticed that the "B" set permits a shorter evaluation procedure.

In the above Eqs (2.3-468c) or (2.3-468d), the subscript "acc" means "due to acceleration", and the subscript "T" means the skin-temperature effects of a fully turbulent boundary layer. All other subscripts and superscripts have the same meanings as in Method I, Case IM.

The partial skin-friction coefficient increments, due to the acceleration effects on the presumed average skin-temperature change:

$$(\Delta C_{fIT})^{I}_{ACC} , \ (\Delta C_{f2T})^{I}_{ACC} , \ (\Delta C_{f3T})^{I}_{ACC} , \ (\Delta C_{f4T})^{I}_{ACC} , \quad (2.3\text{-}568)$$

refer to the nose section, cylinder and boattail, wings and fins respectively. They are expressed in Figs (2.3-56) and (2.3-57) as a functional incremental relationship,

$$\left(\frac{\Delta C_{fT}}{C_{fiINS}}\right) = f(M, Re) , \quad (2.3\text{-}569)$$

based on Van Driest's[27] semi-empirical theory, where the reference two-dimensional skin-friction coefficient,

$$C_{fiINS} = f(R_e) , \quad (2.3\text{-}570)$$

refers to smooth, insulated (ins), flat plates at a zero angle-of-attack in an incompressible (i), viscous turbulent flow, as determined from charts in Fig (2.3-46) (set B) directly, or from Figs (2.3-44) and (2.3-47) indirectly (set A) for each missile part.

The total three-dimensional zero-lift drag coefficient corrective increment due to the acceleration effects on the skin thermal conditions:

$$(\Delta C_{D0fIMT})_{ACC} \quad (2.3\text{-}571)$$

as specified by Eqs (2.3-468c) or (2.3-468d) (for the assumed fully turbulent boundary layers), are then added to the basic zero-lift skin-friction drag coefficient values,

$$(C_{D0fIM}) , \ (C_{D0fIIM}) , \ (C_{D0fIIIM}) , \ (C_{D0fIVM}) , \quad (2.3\text{-}572)$$

which have been computed by Method I for an insulated skin-condition and the assumed (laminar, turbulent or mixed) boundary layer status.

To summarize, the stepwise, self-explanatory computational procedure for the incremental drag coefficient value due to acceleration effects on the skin-friction is performed in

Table (2.3-12), as follows:

(1) From Figs. 1.31 and 1.32, estimate the Reynolds Number value for the given flight altitude, H , and the flight Mach Number, M_H.

(2) From Figs (2.3-50) and (2.3-51), read off the respective (T_W/T_H) ratio as function of the given ng value.

(3) Using charts "B" or "A":

From Fig (2.3-46), read off the average incompressible skin-friction coefficient on an insulated flat plate, or use the already computed values from Table (2.3-7):

$$(C_{fi})^{B}_{INS} = f(R_e) , \qquad (2.3\text{-}573)$$

if the set of charts "B" has been adopted; or, if the alternative set of working charts "A" is used, from Fig (2.3-44) read the value (smooth curves) of the average compressible skin-friction coefficient on an insulated flat plate, or use the already computed values from Table (2.3-6),

$$C^{A}_{f_{INS}} = f(R_e, M) , \qquad (2.3\text{-}574)$$

and then determine the corresponding compressible-to-incompressible skin-friction ratios from Fig (2.3-47), i.e., finally compute the explicit incompressible values of

$$(C_{fi})^{A}_{INS} .$$

(4) From Fig (2.3-56) or (2.3-57), read off the incremental ratio

$$\left(\frac{\Delta C_{fT}}{C_{fi_{INS}}}\right)^{A\ OR\ B}_{ACC} = f(R_e, M, H, T_W/T_H) , \qquad (2.3\text{-}575)$$

using the value of T_W/T_H from step 2. The explicit value of $(\Delta C_{fT})^{A\,or\,B}_{ACC}$, should then be multiplied by the corresponding geometry, (G) , and Reynolds Number, (R) , parameters as indicated for each missile part in the governing Eqs (2.3-486c) or (2.3-486d).

(5) For subsonic speeds (short-duration acceleration from launch or during take off), the skin-temperature conditions may be approximated with the ambient temperature, i.e., $(T_W = T_H)$ and Fig. (2.3-45) for M = .5 can be used directly by reading off the smooth curve, yielding:

$$(C_{fT})^{A}_{\substack{ACC \\ SUB}} = f(R_e) . \qquad (2.3\text{-}576)$$

(6) Repeat the procedure for each chosen set of accelerations, (ng), Mach Numbers, (M_H), Reynolds Numbers (Re) and altitudes, (H), as the need may be.

The final zero-lift friction drag coefficient increments due to acceleration effects on the skin-friction,

$$(\Delta C_{D_{of_{IMT}}})^{A\ or\ B}_{ACC} , \qquad (2.3\text{-}577)$$

are then added to the corresponding fundamental zero-lift skin-friction drag coefficient values that were estimated earlier by Method I for insulated skins:

$$(C_{D_{of_{IMT}}})^{A\ or\ B}_{ACC} =$$

$$\text{or} \quad = (C_{D_{of_{IM}}})^{A\ or\ B} + (\Delta C_{D_{of_{IMT}}})^{A\ or\ B}_{ACC} ,$$

$$(C_{D_{of_{IIMT}}})^{A\ or\ B}_{ACC} =$$

$$\text{or} \quad = (C_{D_{of_{IIM}}})^{A\ or\ B} + (\Delta C_{D_{of_{IMT}}})^{A\ or\ B}_{ACC} ,$$

$$(C_{D_{of_{IIIMT}}})^{A\ or\ B}_{ACC} =$$

$$= (C_{D_{of_{IIIM}}})^{A\ or\ B} + (\Delta C_{D_{of_{IMT}}})^{A\ or\ B}_{ACC} ,$$

or

$$(C_{D_{of_{IVMT}}})^{A\ or\ B}_{ACC} =$$

$$= (C_{D_{of_{IVM}}})^{A\ or\ B} + (\Delta C_{D_{of_{IMT}}})^{A\ or\ B}_{ACC} , \qquad (2.3\text{-}578)$$

where subscripts IM, IIM, IIIM, and IVM denote the corresponding cases of the actual boundary layer status, as defined in the Method I.

Working charts — A: Figs – (2.3-44), (2.3-45)

B: Figs – (2.3-46), (2.3-47), (2.3-48), (2.3-49)

MACH NO M	ALTITUDE H ft	$\dot{q}_{RAD}$	h_i	T_H °K	ρ_H slug/ft³	ε	h/h_i	h	$T_H^{2.5}$ °K$^{2.5}$
(13)	(14)	(36)	(165)	(166)	(167)	(168)	(169)	(170)	(171)
? (2.3-5)	? (2.3-5)	T (2.3-5)	FIG (2.3-53)	5/9 °R		T (2.3-41)	FIG (2.3-53)	(165)×(169)	(166)$^{2.5}$
Qor.2									
.5									
M_{cr}									
1.0									
1.2									
1.5									
2.0									
2.5									
3.0									
3.5									
4.0									
4.5									
5.0	etc.								

NOTES:

h = thermal conductivity of air = $\dfrac{Q_H}{\sqrt{R}\sqrt{T_H}\,C_p(T_{aw}-T_w)}$ $\left[\dfrac{C.H.U.}{°K\cdot ft\,sec}\right]$

Q_H = convective heat transfer $\left[\dfrac{C.H.U.}{slug\ °K}\right]$

TABLE (2.3-11)

AVERAGE SKIN-FRICTION DRAG COEFFICIENT, $(\Delta C_{DO\,FIT})_{RAD}$ – METHOD II, STEADY, PROLONGED FLIGHT REGIMES, RADIATIONS EFFECTS, $\dot{q}=0$, T_{wall}/T_H

$(\Delta C_{DO\,FIT})_{RAD} = (\Delta C_{f\,FIT})_{RAD}\,G_i$

FIRST APPROXIMATION $\left[(T_w - T_H)/(T_{aw} - T_H)\right] = 1$

$\varepsilon \times T_H^{2.5}$	$h\,\rho_H$	$\dfrac{\varepsilon\,T_H^{2.5}}{h\,\rho_H}$	$\dfrac{1}{10^4} \times$ (174)	$\left(\dfrac{T_{wall}}{T_H}\right)_{Prod}$ °K	$T_{wall} - T_{H_{Prod}}$ °K	$\left(\dfrac{T_{aw}}{T_H}\right)_{\varepsilon=0}$ °K	T_{aw} °K	$\left(\dfrac{T_w}{T_H}\right)_{Prod}$ °K	$T_{aw} - T_H$ °K
(172)	(173)	(174)	(175)	(176)	(177)	(178)	(179)	(180)	(181)
(171)×(168)	(170)×(167)	(172)/(173)		FIG (2.3-54)	(176)×(166)	FIG (2.3-54)	(178)×(166)	(177)-(166)	(179)-(166)

SUBSCRIPT "RAD" MEANS "RADIATION"

SUBSCRIPT "i" MEANS "INCOMPRESSIBLE"

SUBSCRIPT "INS" MEANS "INSULATED"

SUBSCRIPT "T" MEANS "THERMAL"

PREFIX "Δ" MEANS "INCREMENT"

SUPERSCRIPT "G" MEANS CHARTS "A"

SUPERSCRIPT "B" MEANS CHARTS "B"

CONVERTION FORMULAE

$\dfrac{°C}{5} = \dfrac{°F-32}{9} = \dfrac{°K-273.16}{5} = \dfrac{°R-491.69}{9}$

$\left(\dfrac{T_{wall}}{T_H}\right)_{KELVIN} = \left(\dfrac{T_{wall}}{T_H}\right)_{FAHRENHEIT\ ABSOLUTE\ OR\ RANKIN}$

TABLE (2.3-11) CONTINUED

NOSE SECTION

SECOND APPROXIMATION

$\left(\dfrac{T_w - T_H}{T_{aw} - T_H}\right)_{Prod}$	(h/h_i)	h	$h\,\rho_H$	$\dfrac{\varepsilon\,T_H^{2.5}}{h\,\rho_H}$	$\dfrac{1}{10^4} \times$ (186)	$\left(\dfrac{T_{wall}}{T_H}\right)_{Sec}$ °K
(182)	(183)	(184)	(185)	(186)	(187)	(188)
(180)/(181)	FIG (2.3-53)	(183)×(165)	(184)×(167)	(172)/(185)		FIG (2.3-54)

$\left(\dfrac{T_w - T_H}{T_{aw} - T_H}\right)_{KELVIN} = \left(\dfrac{T_w - T_H}{T_{aw} - T_H}\right)_{FAHRENHEIT\ ABSOLUTE\ OR\ RANKIN}$

$°R = 9/5\,°K = °F + 459.69$

Figures common to both sets, "A" and "B": FIGS. (1.31), (1.32), (2.3-50), (2.3-57), (2.3-52), (2.3-53), (2.3-54), (2.3-55), (2.3-56), (2.3-57), (2.3-58)

FINAL ESTIMATES

$(C_f)^B_{INS}$	$(C_{f\,FIT})^A$	$\left(\dfrac{C_{f\,FIT}}{C_{f\,INS}}\right)^A$	$(C_f)^A_{INS}$	$\dfrac{\Delta C_{FT}}{C_{f\,INS\,RAD}}$	$(\Delta C_{f\,FIT})^B_{RAD}$	$(\Delta C_{f\,FIT})^A_{RAD}$	G_i	$(\Delta C_{DO\,FIT})^B_{RAD}$	$(\Delta C_{DO\,FIT})^A_{RAD}$
(100)	(84)	(189)	(190)	(191)	(192)	(193)	(9)	(194)	(195)
FIG (2.3-46) or T-(2.3-7)	FIG (2.3-44) or T-(2.3-6)	(2.3-47) FIG or (2.3-49)	(84)/(189)	(2.3-56) FIG or (2.3-57)	(191)×(100)	(190)×(191)	T (2.3-5)	(9)×(192)	(9)×(193)
	ALTERNATIVELY					OR			OR

$(\Delta C_{DO\,FIT})^B_{RAD} = (\Delta C_{f\,FIT})^B_{RAD}\,G_i$

$(\Delta C_{DO\,FIT})^A_{RAD} = (\Delta C_{f\,FIT})^A_{RAD}\,G_i$

SUBSCRIPT "i" REFERS TO NOSE CONE

TABLE (2.3-11) CONTINUED (1)

AVERAGE SKIN-FRICTION DRAG COEFFICIENT, $(\Delta C_{D0f2T})_{RAD}$ — METHOD II

STEADY, PROLONGED FLIGHT REGIMES, RADIATION EFFECTS, k=0, T_{wr}/T_H

$$(\Delta C_{D0f2T})_{RAD} = \left\{(\Delta C_{f2T})_{RAD}[1+R_i] - (\Delta C_{f1T})_{RAD} R_i\right\} G_2$$

Working charts: A Figs – (SEE NOSE SECTION); B Figs – (SEE NOSE SECTION)

Figures common to both sets, "A" and "B" (SEE NOSE SECTION)

MACH NO. M	ALTITUDE H ft	Re_{TURN}	h_i	ϵ	T_H °K	ρ_H slug/ft³	FIRST APPROXIMATION h/h_i	h	$T_H^{2.5}$ °K	$\epsilon \cdot T_H^{[illegible]}$
(13)	(14)	(42)	[illegible]	[illegible]	[illegible]	[illegible]	[illegible]	[illegible]	(171)	(172)
T (2.3-5)	T (2.3-5)	T (2.3-5)	FIG (2.3-55)	(2.3-11)	S/D °R	T (2.3-11)	FIG (2.3-53) or T-(2.3-11)	[illegible] · [illegible]	(2.3-11)	(2.3-11)
0 or 2										
5										
M_{cr}										
10										
12										
15										
20										
25										
30										
35										
40										
45										
50	air									

$[(T_w - T_H)/(T_{aw} - T_H)] = 1$: $h\,\rho_H$	$\frac{\epsilon T_H^{2.5}}{h\,\rho_H}$	$\frac{1}{10^{14}} \times$ [illegible]	$(T_{aw}/T_H)_{First}$ °K	$T_{aw} = T_{w\,First}$ °K	CYLINDER + BOATTAIL, SECOND APPROXIMATION: (T_{aw}/T_H) $\epsilon = 0$	T_{aw} °K	$(T_w - T_H)_{First}$ °K	$(T_{aw} - T_H)$ °K	$\left(\frac{T_w - T_H}{T_{aw} - T_H}\right)_{First}$
[illegible]	[illegible]	[illegible]	[illegible]	[illegible]	(178)	(179)	[illegible]	(181)	[illegible]
[illegible] × (167)	(172)/[illegible]		FIG (2.3-54)	[illegible] × [illegible]	FIG (2.3-55) T-(2.3-11)	T (2.3-11)	[illegible] − [illegible]	T (2.3-11)	[illegible]/(181)

NOTES:

SUBSCRIPT "RAD" MEANS "RADIATION"
SUBSCRIPT "i" MEANS "INCOMPRESSIBLE"
SUBSCRIPT "INS" MEANS "INSULATED"
SUBSCRIPT "T" MEANS "THERMAL"
PREFIX "Δ" MEANS "INCREMENT"
SUPERSCRIPT "A" MEANS CHARTS "A"
SUPERSCRIPT "B" MEANS CHARTS "B"

h = thermal conductivity of air = $\frac{Q_H}{\rho_H V_H C_p (T_{aw} - T_w)}$ $\left[\frac{C.H.U.}{°K, ft\ sec}\right]$

Q_H = convective heat transfer $\left[\frac{C.H.U.}{slug\ °K}\right]$

CONVERSION FORMULAE:

$$\frac{°C}{5} = \frac{°F - 32}{9} = \frac{°K - 273.16}{5} = \frac{°R - 491.69}{9}, \quad \left(\frac{T_w - T_H}{T_{aw} - T_H}\right)_{KELVIN} = \left(\frac{T_w - T_H}{T_{aw} - T_H}\right)_{FAHRENHEIT\ ABSOLUTE\ OR\ RANKIN}$$

$$\left(\frac{T_{aw}}{T_H}\right)_{KELVIN} = \left(\frac{T_{aw}}{T_H}\right)_{FAHRENHEIT\ ABSOLUTE\ OR\ RANKIN}, \quad °R = 9/5\,°K = °F + 459.69$$

TABLE (2.3-11) CONTINUED (1a)

CYLINDER + BOATTAIL, SECOND APPROXIMATION: h/h_i	h	$(h\,\rho_H)$	$\frac{\epsilon T_H^{2.5}}{h\,\rho_H}$	$\frac{1}{10^{14}} \times$ [illegible]	$\left(\frac{T_{wr}}{T_H}\right)_{Sec}$ °K	$(C_{f1})^B_{INS}$	$(C_{f2T})^B$	$\left(\frac{C_{f2T}}{C_{f1\,INS}}\right)^A$	$(C_{f1})^A_{INS}$	$\left(\frac{\Delta C_{fT}}{C_{f1\,INS}}\right)_{RAD}$	$(\Delta C_{f2T})^B_{RAD}$
[illegible]	(207)	[illegible]	[illegible]	(210)	(211)	[illegible]	[illegible]	[illegible]	[illegible]	(214)	[illegible]
FIG (2.3-53)	[illegible] × [illegible]	(207) × (167)	(172)/[illegible]		FIG (2.3-55)	FIG (2.3-44) or T-(2.3-7)	FIG (2.3-44) or T-(2.3-6)	(2.3-41) FIG or (2.3-40)	[illegible]/[illegible]	(2.3-56) FIG or (2.3-56)	[illegible] × [illegible]
						ALTERNATIVELY					

FINAL ESTIMATES: $(\Delta C_{f2T})^A_{RAD}$	$1+R_i$	R_i	$(\Delta C_{f2T})^B_{RAD} \times (1+R_i)$	$(\Delta C_{f1T})^B_{RAD} \times R_i$	$(\Delta C_{f2T})^A_{RAD} \times (1+R_i)$	$(\Delta C_{f1T})^A_{RAD} \times R_i$			$(\Delta C_{D0f2T})^B_{RAD}$	$(\Delta C_{D0f2T})^A_{RAD}$
[illegible]	(85)	(86)	(217)	(218)	[illegible]	[illegible]	[illegible]	[illegible]	[illegible]	[illegible]
[illegible] + [illegible]	T (2.3-6)	T (2.3-6)	[illegible] × (85)	[illegible] × (86)	[illegible] × (85)	[illegible] × (86)	(217) − [illegible]	[illegible] − [illegible]	[illegible] × (10)	[illegible] × (10)
OR					OR		OR		OR	

$$(\Delta C_{D0f2T})^B_{RAD} = \left\{(\Delta C_{f2T})^B_{RAD}[1+R_i] - (\Delta C_{f1T})^B_{RAD} R_i\right\} G_2$$

$$(\Delta C_{D0f2T})^A_{RAD} = \left\{(\Delta C_{f2T})^A_{RAD}[1+R_i] - (\Delta C_{f1T})^A_{RAD} R_i\right\} G_2$$

SUBSCRIPT "2" REFERS TO CYLINDER + BOATTAIL

SUBSCRIPT "1" REFERS TO NOSE CONE

TABLE (2.3-11) CONTINUED (2)

METHOD E,

$(\Delta C_{DOF3T})_{RAD} = (\Delta C_{F3T})_{RAD}\, G_3$

Working charts: A Figs — (SEE NOSE SECTION)

B Figs — (SEE NOSE SECTION)

MACH NO M (15) T	ALTITUDE H ft (16) T	Re^{C}_{CW} (30) T	h_1 (220) FIG (2.3-53)	T_H °K (66) $T_H/9$	ρ_H slugs/ft³ (67) T	$\mathcal{E}$ (66) T	FIRST APPROXIMATION h/h_1 (100) T	h (228) (65)×(228)	$T_H^{2.5}$ °K (71) T	$\mathcal{E} = T_H^{2.8}$ (172) T
		(2.3-5)	(2.3-53)		(2.3-11)	(2.3-11)	(2.3-11)		(2.3-11)	(2.3-11)
0 or 2										
5										
Mar										
10										
12										
15										
20										
25										
30										
35										
40										
45										
50	etc									

NOTES

SUBSCRIPT "RAD" MEANS "RADIATION"

SUBSCRIPT "I" MEANS "INCOMPRESSIBLE"

SUBSCRIPT "INS" MEANS "INSULATED"

SUBSCRIPT "T" MEANS "THERMAL"

PREFIX "Δ" MEANS "INCREMENT"

SUPERSCRIPT "A" MEANS CHARTS "A"

SUPERSCRIPT "B" MEANS CHARTS "B"

h = thermal conductivity of air = $\frac{Q_m}{{}_mV_m C_p (T_{aw} - T_w)}$

Q = convective heat transfer $\frac{C\,H\,U}{slug\ ^\circ K}$

AVERAGE SKIN FRICTION DRAG COEFFICIENT, $(\Delta C_{DOF3T})_{RAD}$

STEADY, PROLONGED FLIGHT REGIMES, RADIATION EFFECTS, $\kappa = 0$, T_{wgr}/T_H

Figures common to both sets, "A" and "B" (SEE NOSE SECTION)

$(T_w - T_H)/(T_{aw} - T_H) = t$					WINGS SECOND APPROXIMATION				
$h = \rho_H$ (67)	$\mathcal{E}\, T_H^{2.8} / h\, \rho_H$ (220) (172)/(227)	$\frac{1}{10^8} = (228)$	$\left(\frac{T_{wgr}}{T_H}\right)_{Prref}$ (230) FIG (2.3-54)	$T_{wgr} = T_{wPrref}$ °K (231) (93)×(166)	$\left(\frac{T_{aw}}{T_H}\right)_{\mathcal{E}=0}$ (70) T (2.3-11)	T_{aw} °K (70) T (2.3-11)	$\left(\frac{T_w - T_H}{T_{aw} - T_H}\right)_{Prref}$ (230) (93)÷(166)	$T_{aw} - T_H$ °K (81) T (2.3-11)	$\left(\frac{T_w - T_H}{T_{aw} - T_H}\right)_{ref}$ (232) (94)/ etc

$\frac{C\,H\,U}{ft\ sec\ ^\circ K}$

TABLE (2.3-11) CONTINUED (2a)

WINGS SECOND APPROXIMATION $\left(\frac{h}{h_1}\right)$ (234) FIG (2.3-53)	h (233) (234)×(225)	$h\,\rho_H$ (236) (235)×(100)	$\frac{\mathcal{E}\, T_H^{2.8}}{h\,\rho_H}$ (237) (172)/(236)	$\frac{1}{10^8} = (238)$	$\left(\frac{T_{wgr}}{T_H}\right)_{Prref}$ (239) FIG (2.3-54)	$(C_{f_1})^B_{INS}$ (109) T (2.3-7)	$(C_{f3T})^A$ (91) T (2.3-7)	$\left(\frac{C_{f3T}}{C_{f1TINS}}\right)^A$ (240) FIG (2.3-47) (2.3-49)	$(C_{f1})^A_{INS}$ (241) (91)/(240)

ALTERNATIVELY

CONVERSION FORMULAE

$\frac{^\circ C}{5} = \frac{^\circ F - 32}{9}$, $\frac{^\circ K - 273.16}{5} = \frac{^\circ R - 491.69}{9}$, $\frac{T_w - T_H}{T_{aw} - T_H}$ KELVIN = $\frac{T_w - T_H}{T_{aw} - T_H}$ FAHRENHEIT ABSOLUTE OR RANKIN

$\frac{T_{wgr}}{T_H}$ KELVIN = $\frac{T_{wgr}}{T_H}$ FAHRENHEIT ABSOLUTE OR RANKIN, $^\circ R = 9/5\ ^\circ K = ^\circ F + 459.69$

FINAL ESTIMATES $\left(\frac{\Delta C_{f3T}}{C_{f1INS}}\right)_{RAD}$ (242) FIG (2.3-58)	$(\Delta C_{f3T})^B_{RAD}$ (243) (242)×(109)	$(\Delta C_{f3T})^A_{RAD}$ (244) (242)×(241)	G_3 (11) T (2.3-5)	$(\Delta C_{DOF3T})^B_{RAD}$ (245) = (11)	$(\Delta C_{DOF3T})^A_{RAD}$ (246) (245)×(11)
		OR			OR

$(\Delta C_{DOF3T})^A_{RAD} = (\Delta C_{F3T})^A_{RAD}\, G_3$

$(\Delta C_{DOF3T})^B_{RAD} = (\Delta C_{F3T})^B_{RAD}\, G_3$

SUBSCRIPT "3" REFERS TO WINGS

Working charts — A Figs — B Figs — (SEE NOSE SECTION) AVERAGE SKIN-FRICTION DRAG FLIGHT REGIMES, RADIATION

MACH NO M	ALTITUDE h f_t	Re_{CF}	h_1	T_H °K	ρ_H slugs/ft³	$\mathcal{E}$	FIRST h/h_1	FIRST h
(13)	(14)	(34)	(247)	(88)	(187)	(186)	(185)	(248)
T (2.3-5)	T (2.3-5)	T (2.3-5)	FIG (2.3-53)	β/g °R	T (2.3-11)	T (2.3-11)	T (2.3-11)	(88) × (247)
Or .2								
.5								
M								
1.0								
1.2								
1.5								
2.0								
2.5								
3.0								
3.0								
4.0								
4.5								
5.0	etc.							

NOTES

h = thermal conductivity of air = $\frac{q_H}{\rho_H V_H c_p (T_{aw} - T_W)}$ $\left[\frac{C.H.U.}{°K,\ ft\ sec}\right]$

q_H = convective heat transfer $\left[\frac{C.H.U.}{slug \cdot °K}\right]$

TABLE (2.3-11) CONTINUED (3)

COEFFICIENT, $(\Delta C_{DOf4T})_{RAD}$ — METHOD II, STEADY, PROLONGED EFFECTS, $k \approx 0$, T_{WER} / T_H, $(\Delta C_{DOf4T})_{RAD} = (\Delta C_{f4T})_{RAD}^{NG_4}$

APPROXIMATION: $\{(T_W - T_H)/(T_{aw} - T_H)\} = 1$

$T_H^{2.5}$ °K	$\mathcal{E} \times T_H^{2.5}$	$h\rho_H$	$\frac{\mathcal{E} T_H^{2.5}}{h\rho_H}$	$\frac{1}{10^{12}} \times$ (250)	$\left(\frac{T_{WER}}{T_H}\right)_{First}$ °K	$T_{WER} - T_{W\ First}$ °K
(171)	(172)	(249)	(250)	(251)	(252)	(253)
T (2.3-11)	T (2.3-11)	(248) × (187)	(172) / (249)		FIG (2.3-54)	(236) (180)

SUBSCRIPT "RAD" MEANS "RADIATION"
SUBSCRIPT "I" MEANS "INCOMPRESSIBLE"
SUBSCRIPT "INS" MEANS "INSULATED"
SUBSCRIPT "T" MEANS "THERMAL"
PREFIX "Δ" MEANS "INCREMENT"
SUPERSCRIPT "A" MEANS CHARTS "A"
SUPERSCRIPT "B" MEANS CHARTS "B"

TABLE (2.3-11) CONTINUED (3)a

FINS — SECOND APPROXIMATION

$\left(\frac{T_{aw}}{T_H}\right)_{F=1}$ °K	T_{aw} °K	$\left(\frac{T_W - T_H}{T_{aw} - T_H}\right)_{First}$ °K	$T_{aw} - T_H$ °K	$\left(\frac{T_W - T_H}{T_{aw} - T_H}\right)_{First}$	$\left(\frac{h}{h_1}\right)$	h	$h\rho_H$	$\frac{\mathcal{E} T_H^{2.5}}{h\rho_H}$	$\frac{1}{10^{12}} \times$ (257)	$\left(\frac{T_{WE}}{T_H}\right)_{sec}$ °K
(178)	(179)	(254)	(181)	(253)	(254)	(255)	(256)	(257)	(258)	(259)
T (2.3-11)	T (2.3-11)	(253) − (66)	T (2.3-11)	(254) / (181)	FIG (2.3-53)	(254) × (247)	(256) × (187)	(172) / (256)		FIG (2.3-54)

CONVERSION FORMULA

$\frac{°C}{5} = \frac{°F - 32}{9} = \frac{°K - 273.16}{5} = \frac{°R - 491.69}{9}$, $\left(\frac{T_W - T_H}{T_{aw} - T_H}\right)_{KELVIN} = \left(\frac{T_W - T_H}{T_{aw} - T_H}\right)_{FAHRENHEIT\ ABSOLUTE\ OR\ RANKIN}$

$\left(\frac{T_{WER}}{T_H}\right)_{KELVIN} = \left(\frac{T_{WER}}{T_H}\right)_{FAHRENHEIT\ ABSOLUTE\ OR\ RANKIN}$, °R = 9/5 °K = °F + 459.69

Figures common to both sets, "A" and "B". (SEE NOSE SECTION)

FINAL ESTIMATES

$(C_{f1})^2_{INS}$	$(C^2_{f4T})^A$	$\left(\frac{I}{C_{f1T}/C_{f1INS}}\right)^A$	$(C_{f1})^A_{INS}$	$\left(\frac{\Delta C_{fT}}{C_{f1}}\right)_{RAD}$	$(\Delta C_{f4T})^B_{RAD}$	$(\Delta C_{f4T})^A_{RAD}$	NG_4	$(\Delta C_{DOf4T})^B_{RAD}$	$(\Delta C_{DOf4T})^A_{RAD}$
(113)	(93)	(260)	(261)	(262)	(263)	(264)	(12)	(265)	(266)
T (2.3-7)	T (2.3-7)	FIG (2.3-47)	(93) / (260)	FIG (2.3-56)	(262) × (113)	(262) (261)	T (2.3-5)	(18) × (263)	(12) × (264)
						OR			OR

ALTERNATIVELY

$(\Delta C_{DOf4T})^A_{RAD} = (\Delta C_{f4T})^A_{RAD}\ NG_4$

$(\Delta C_{DOf4T})^B_{RAD} = (\Delta C_{f4T})^B_{RAD}\ NG_4$

SUBSCRIPT "4" REFERS TO FINS

TABLE (2.3-11) SUMMARY

AVERAGE SKIN FRICTION DRAG COEFFICIENT, $(\Delta C_{D_{OF}T})^{A}_{RAD}$

STEADY, PROLONGED FLIGHT REGIMES, RADIATIONS

$(\Delta C_{D_{OF}T})^{A}_{RAD} = (\Delta C_{D_{OF}NT})^{A}_{RAD} + (\Delta C_{D_{OF}CT})^{A}_{RAD} + (\Delta C_{D_{OF}ST})^{A}_{RAD} + (\Delta C_{D_{OF}WT})^{A}_{RAD} + (\Delta C_{D_{OF}HT})^{A}_{RAD}$ —OR— $(\Delta C_{D_{OF}T})^{A}_{RAD} + (\Delta C_{FHT})^{A}_{RAD} G_1$

(MISSILE) (NOSE SECTION) (CYL + BOATTAIL) (WINGS) (FINS)

WORKING SET OF CHARTS "A"

MACH NO M	ALTITUDE H ft	$(\Delta C_{D_{OF}T})^{A}_{RAD}$ INCREMENT						
		NOSE SECTION $(\Delta C_{D_{OF}NT})^{A}_{RAD}$	CYL + BOATTAIL $(\Delta C_{D_{OF}CT})^{A}_{RAD}$	WINGS $(\Delta C_{D_{OF}ST})^{A}_{RAD}$	FINS $(\Delta C_{D_{OF}WT})^{A}_{RAD}$			MISSILE $(\Delta C_{D_{OF}T})^{A}_{RAD}$
(13)	(14)	(195)	(224)	(246)	(266)	(274)	(275)	(276)
T (2.3-5)	T (2.3-5)	T (2.3-11)	T (2.3-11)	T (2.3-11)	T (2.3-11)	(195) + (274)	(246) + (266)	(274) + (275)
0 OR 2								
.5								
M_{cr}								
1.0								
1.2								
1.5								
2.0								
3.0								
4.0								
5.0	etc							

NOTES SEE EARLIER

THE COMPUTED VALUES OF $(\Delta C_{D_{OF}T})^{A}_{RAD}$ ARE ADDED TO THE CORRESPONDING NO-RADIATION $C_{D_{OF}}$ ESTIMATES FROM METHOD I

$(C_{D_{OF_{SMT}}})^{A}_{RAD} = C_{D_{OF_{SM}}} + (\Delta C_{D_{OF}T})^{A}_{RAD}$,

OR $(C_{D_{OF_{CMT}}})^{A}_{RAD} = C_{D_{OF_{CM}}} + (\Delta C_{D_{OF}T})^{A}_{RAD}$,

OR $(C_{D_{OF_{WMT}}})^{A}_{RAD} = C_{D_{OF_{WM}}} + (\Delta C_{D_{OF}T})^{A}_{RAD}$,

OR $(C_{D_{OF_{HMT}}})^{A}_{RAD} = C_{D_{OF_{HM}}} + (\Delta C_{D_{OF}T})^{A}_{RAD}$

— METHOD II

EFFECTS, $k \approx 0$, T_{Wor} / T_H

$+ \left\{(\Delta C_{FBT})^{A}_{RAD}[1+R] - (\Delta C_{FHT})^{A}_{RAD} R_i\right\} G_2 + (\Delta C_{FST})^{A}_{RAD} G_3 + (\Delta C_{FWT})^{A}_{RAD} N G_4$

MISSILE TOTAL $(C_{D_{OF_{MT}}})_{RAD}$							
CASE I M		CASE II M		CASE III M		CASE IV M	
$C_{D_{OF_{IM}}}$	$(C_{D_{OF_{IMT}}})^{A}_{RAD}$	$C_{D_{OF_{IIM}}}$	$(C_{D_{OF_{IIMT}}})^{A}_{RAD}$	$C_{D_{OF_{IIIM}}}$	$(C_{D_{OF_{IIIMT}}})^{A}_{RAD}$	$C_{D_{OF_{IVM}}}$	$(C_{D_{OF_{IVMT}}})^{A}_{RAD}$
(97)	(277)	(140)	(278)	(154)	(278)	(164)	(280)
T (2.3-6)	(97) + (276)	T (2.3-8)	(140) + (278)	T (2.3-9)	(154) + (278)	T (2.3-10)	(164) + (278)

SEE EARLIER

TABLE (2.3-11)

AVERAGE SKIN FRICTION DRAG COEFFIENT, $(\Delta C_{D_{OF}T})^{B}_{RAD}$ —

STEADY, PROLONGED FLIGHT REGIMES, RADIATIONS EFFECTS,

$(\Delta C_{D_{OF}T})^{B}_{RAD} = (\Delta C_{D_{OF}NT})^{B}_{RAD} + (\Delta C_{D_{OF}CT})^{B}_{RAD} + (\Delta C_{D_{OF}ST})^{B}_{RAD} + (\Delta C_{D_{OF}WT})^{B}_{RAD}$ —OR—

(MISSILE) (NOSE SECTION) (CYL + BOATTAIL) (WINGS) (FINS)

WORKING SET OF CHARTS "B"

MACH NO M	ALTITUDE H ft	$(\Delta C_{D_{OF}T})^{B}_{RAD}$ INCREMENT						
		NOSE SECTION $(\Delta C_{D_{OF}NT})^{B}_{RAD}$	CYL + BOATTAIL $(\Delta C_{D_{OF}CT})^{B}_{RAD}$	WINGS $(\Delta C_{D_{OF}ST})^{B}_{RAD}$	FINS $(\Delta C_{D_{OF}WT})^{B}_{RAD}$			MISSILE $(\Delta C_{D_{OF}T})^{B}_{RAD}$
(13)	(14)	(194)	(223)	(245)	(265)	(267)	(268)	(268)
T (2.3-5)	T (2.3-5)	T (2.3-11)	T (2.3-11)	T (2.3-11)	T (2.3-11)	(194) + (223)	(245) + (265)	(267) + (268)
0 or 2								
.5								
M_{cr}								
1.0								
1.2								
1.5								
2.0								
3.0								
4.0								
5.0	etc							

NOTES SEE EARLIER

THE COMPUTED VALUES OF $(\Delta C_{D_{OF}T})^{B}_{RAD}$ ARE ADDED TO THE CORRESPONDING NO-RADIATION $C_{D_{OF}}$ ESTIMATES FROM METHOD I

$(C_{D_{OF_{SMT}}})^{B}_{RAD} = C_{D_{OF_{SM}}} + (\Delta C_{D_{OF}T})^{B}_{RAD}$,

OR $(C_{D_{OF_{CMT}}})^{B}_{RAD} = C_{D_{OF_{CM}}} + (\Delta C_{D_{OF}T})^{B}_{RAD}$,

OR $(C_{D_{OF_{WMT}}})^{B}_{RAD} = C_{D_{OF_{WM}}} + (\Delta C_{D_{OF}T})^{B}_{RAD}$,

OR $(C_{D_{OF_{HMT}}})^{B}_{RAD} = C_{D_{OF_{HM}}} + (\Delta C_{D_{OF}T})^{B}_{RAD}$

SUMMARY CONTINUED

METHOD II

$k \approx 0$, T_{Wor} / T_H

$(\Delta C_{D_{OF}T})^{B}_{RAD} = (\Delta C_{FHT})^{B}_{RAD} G_1 + \left\{(\Delta C_{FBT})^{B}_{RAD}[1+R_i] - (\Delta C_{FHT})^{B}_{RAD} R_i\right\} G_2 + (\Delta C_{FST})^{B}_{RAD} G_3 + (\Delta C_{FWT})^{B}_{RAD} N G_4$

MISSILE TOTAL $(C_{D_{OF_{MT}}})_{RAD}$							
CASE I M		CASE II M		CASE III M		CASE IV M	
$C_{D_{OF_{IM}}}$	$(C_{D_{OF_{IMT}}})^{B}_{RAD}$	$C_{D_{OF_{IIM}}}$	$(C_{D_{OF_{IIMT}}})^{B}_{RAD}$	$C_{D_{OF_{IIIM}}}$	$(C_{D_{OF_{IIIMT}}})^{B}_{RAD}$	$C_{D_{OF_{IVM}}}$	$(C_{D_{OF_{IVMT}}})^{B}_{RAD}$
(119)	(270)	(140)	(271)	(154)	(272)	(164)	(273)
T (2.3-7)	(119) + (269)	T (2.3-8)	(140) + (269)	T (2.3-9)	(154) + (268)	T (2.3-10)	(164) + (269)

TABLE (2 3-12)

AVERAGE SKIN-FRICTION DRAG COEFFICIENT, $\Delta C_{D_{OFT}}$ - METHOD II. $h = 0$, $(T_w/T_\infty) = f(M,H,ng)$

CONSTANT ACCELERATION FLIGHT REGIMES FROM START (V=0)

$$\left(\Delta C_{D_{OFT}}\right)_{ACC} = \left(\Delta C_{f_{IT}}\right)_{ACC} G_1 + \left\{\left(\Delta C_{f_{RT}}\right)_{ACC}\left[1 + R_1\right] - \left(\Delta C_{f_{IT}}\right)_{ACC} R_1\right\} G_2 + \left(\Delta C_{f_{RT}}\right)_{ACC} G_3 + \left(\Delta C_{f_{BT}}\right)_{ACC} G_4 N$$

MACH NO M	ALTITUDE H, ft	TIME t, sec	ACCELERATION ng	T_w/T_∞ °R	NOSE SECTION, $\left(\Delta C_{f_{IT}}\right)_{ACC} G_1$				
					Re^{I}_{NS}	$\left(C_{f_I}\right)^{B}_{NS}$	$\left(\Delta C_{f_{IT}}/C_{f_{I\,NS}}\right)^{M}_{ACC}$	$\left(\Delta C_{f_{IT}}\right)^{N}_{ACC}$	$\left(\Delta C_{D_{OFT}}\right)^{N}_{ACC}$
(1)	(14)	(18)	(16)	(17)	(96)	(98)	(99)	(100)	(101)
T (2 3-5)	T (2 3-5)	T (2 3-5)	T (2 3-8)	FIG (2 5-80)	T (2 3-6)	T (2 3-7)	FIG (2 3-56)	(96) × (99)	(100) × (1)
					SET "B"				
0 or 2									
5									
M_{CR}									
10									
12									
15									
20									
25									
30									
35									
40									
45									
50	etc								

NOTE. (Same as from Method I) $\left(\Delta C_{D_{OFT}}\right)_{ACC} = \left(\Delta C_{f_{IT}}\right)_{ACC} G_1$

$C^{A}_{f_{RNS}} = \left(C^{I}_{f_{IT}}\right)_{q}$	$\left(C_{f_{RNS}}/C_{f_{I\,NS}}\right)^{M}$	$\left(C_R\right)^{B}_{NS}$	$\left(\Delta C_{f_{IT}}/C_{f_{RNS\,ACC}}\right)^{M}$	$\left(\Delta C_{f_{IT}}\right)^{N}_{ACC}$	$\left(C_{D_{OFT}}\right)^{N}_{ACC}$
(95)	(97)	(98)	(99)	(100)	(101)
T (2 3-6)	FIG (2 3-47)	(97) / (98)	FIG (2 3-56)	(98) × (99)	(100) × (1)
on	SET "A"				

TABLE (2 3-12)

AVERAGE SKIN-FRICTION DRAG COEFFICIENT,

$\left\{\left(\Delta C_{f_{RT}}\right)_{ACC}\left[1 + R_1\right] - \left(\Delta C_{f_{IT}}\right)_{ACC} R_1\right\} G_2$, CYLINDER + BOATTAIL

Re^{FT}_{TOTAL}	$\left(C_{f_L}\right)^{B}_{NS}$	$\left(\Delta C_{f_{RT}}/C_{f_{L\,NS}}\right)^{M}_{ACC}$	$\left(\Delta C_{f_{IT}}\right)^{N}_{ACC}$	$\left[1 + R_1\right]$						$\left(\Delta C_{D_{OFT}}\right)^{N}_{ACC}$
(94)	(102)	(103)	(99)	(88)	(99C)	(88)	(99E)	(99F)	(99G)	(99T)
T (2 3-6)	T (2 3-7)	FIG (2 3-56)	(102) × (103)	T (2 3-6)	(99B) × (88)	T (2 3-6)	(99D) × (88)	(99C) - (99E)	(99F) × (10)	
	SET "B"									

NOTE $\left(\Delta C_{D_{OFT}}\right)_{ACC} = \left\{\left(\Delta C_{f_{RT}}\right)_{ACC}\left[1 + R_1\right] - \left(\Delta C_{f_{IT}}\right)_{ACC} R_1\right\} G_2$

CONTINUED (1)

$\left(\Delta C_{D_{OFT}}\right)_{ACC}$ - METHOD II: $h = 0$, $(T_w/T_\infty) = f(M,H,ng)$

$C^{A}_{f_{RNS}} = \left(C^{I}_{f_{IT}}\right)_{q}$	$\left(C_{f_{RNS}}/C_{f_{I\,NS}}\right)^{M}$	$\left(C_R\right)^{B}_{NS}$	$\left(\Delta C_{f_{IT}}/C_{f_{RNS\,ACC}}\right)^{M}$	$\left(\Delta C_{f_{RT}}\right)^{N}_{ACC}$					$\left(\Delta C_{D_{OFT}}\right)^{N}_{ACC}$
(95)	(97)	(98)	(99)	(99T)	(99B)	(99D)	(99F)	(99C)	(99)
T (2 3-6)	FIG (2 3-47)	(97) / (98)	FIG (2 3-56)	(98) × (99)	(99T) × (88)	(99T) × (88)	(99T) × (88)	(99C) - (99E)	(99G) × (10)
	SET "A"								

TABLE (2.3-12)

AVERAGE SKIN-FRICTION DRAG COEFFICIENT, WINGS, $(\Delta C_{fST})_{ACC}^{B}$ G_s

R_{eEff} (30)	$(C_f)^B_{WB}$ (109)	$(\Delta C_{fST}/C_{f_{WB}})^B_{ACC}$ (308)	$(\Delta C_{fST})^B_{ACC}$ (309)	$(\Delta C_{DOfST})_{ACC}$ (309) × (11)
T (2.3-6)	T (2.3-7)	FIG (2.3-56)	(309) × (109)	
SET "B"				

NOTE $(\Delta C_{DOfST})^B_{ACC} = (\Delta C_{fST})^B_{ACC}\, G_s$

CONTINUED (2)

$(C_{DOfST})_{ACC}$ - METHOD II $h = 0$, $(T_w/T_H) = f(M,H,ng)$

$(\frac{1}{C_{fST}})^A = C_{f_{WB}}{}^A$ (91)	$(C_f/C_N)^A_{WB}$ (308)	$(C_n)^A_{WB}$ (308) / (308)	$(\Delta C_{fST}/C_{L_{WB}})^A_{ACC}$ (307)	$(\Delta C_{fST})^A_{ACC}$ (308)	$(\Delta C_{DOfST})^A_{ACC}$ (309) × (11)
T (2.3-6)	FIG (2.3-47)	(91) / (308)	FIG (2.3-56)	(307) × (308)	
SET "A"					

TABLE (2.3-12)

AVERAGE SKIN-FRICTION DRAG COEFFICIENT, N FINS, $(\Delta C_{fST})_{ACC}\, G_s{}^N$

R_{eEff} (30)	$(C_f)^B_{WB}$ (115)	$(\Delta C_{fST}/C_{f_{LIMB_{ACC}}})$ (310)	$(\Delta C_{fST})^B_{ACC}$ (311)	$(\Delta C_{DOfST})_{ACC}$ (312)
T (2.3-6)	T (2.3-7)	FIG (2.3-56)	(310) × (115)	(311) × (12)
SET "B"				

NOTES $(\Delta C_{DOfST})_{ACC} = (\Delta C_{fST})_{ACC}\, G_s{}^N$

CONTINUED (3)

$(\Delta C_{DOfT})_{ACC}$ - METHOD II $h = 0$, $(T_w/T_H) = f(M,H,ng)$

$(\Delta C_{fST})_{ACC}\, G_s{}^N$

$(\frac{1}{C_{fST}})^A = (C_{f_{WB}})^A$ (93)	$(C_f/C_{fl})^A_{WB}$ (315)	$(C_{fl})^A_{WB}$ (314)	$(\Delta C_{fST}/C_{f_{WB_{ACC}}})^A$ (313)	$(\Delta C_{fST})^A_{ACC}$ (310)	$(\Delta C_{DOfST})^A_{ACC}$ (317)
T (2.3-6)	FIG (2.3-47)	(93) / (315)	FIG (2.3-56)	(310) × (314)	(310) × (12)
SET "A"					

TABLE (2.3-12) SUMMARY

TOTAL AVERAGE SKIN-FRICTION DRAG COEFFICIENT INCREMENT, $(\Delta C_{DOF(T)})_{ACC}$

CONSTANT ACCELERATION FLIGHT REGIMES FROM

$(\Delta C_{DOF(SM)})_{ACC} = (\Delta C_{DOF(T)})_{ACC} + (\Delta C_{DOF(ET)})_{ACC} + (\Delta C_{DOF(ST)})_{ACC} + (\Delta C_{DOF(F)})_{ACC}$

MISSILE = NOSE SECTION + (CYLINDER + BOATTAIL) + WINGS + FINS

MACH NO	ALTITUDE	TIME	ACCELERATION	T_w/T_H	SET OF CHARTS "A", $(\Delta C_{DOF(TM)})^A_{ACC}$ INCREMENT						
					NOSE SECTION	CYL. + BOATTAIL	WINGS	FINS			MISSILE
M	H, ft	t, SEC	ng	°R	$(\Delta C_{DOF(T)})^A_{ACC}$	$(\Delta C_{DOF(ET)})^A_{ACC}$	$(\Delta C_{DOF(ST)})^A_{ACC}$	$(\Delta C_{DOF(F)})^A_{ACC}$	(307) + (310)	(308) + (311)	$(\Delta C_{DOF(TM)})^A_{ACC}$
(3)	(14)	(18)	(6)	(17)	(307)	(308)	(309)	(311)	(310)	(311)	(312)
T	T	T	T	FIG	T	T	T	T			(310) + (312)
(2.3-5)	(2.3-5)	(2.3-5)	(2.3-5)	(2.3-5)	(2.3-12)	(2.3-12)	(2.3-12)	(2.3-12)			
0 OR 2											
5											
M_{CR}											
10											
12											
15											
20											
25											
30											
35											
40											
45											
50	etc										

NOTE SEE (2.3-11) AND (2.3-6), (2.3-7), (2.3-8), (2.3-9), (2.3-10)

METHOD II $\alpha \approx 0$, $(T_w/T_H) = F(M, H, ng)$

START (V = 0)

MISSILE TOTAL DRAG COEFFICIEN

CASE IM		CASE IIM		CASE IIIM		CASE IV M	
$(C_{DOF(TM)})^A$	$(C_{DOF(SM)})^A_{ACC}$	$(C_{DOF(TM)})^A$	$(C_{DOF(SM)})^A_{ACC}$	$(C_{DOF(TM)})^A$	$(C_{DOF(SM)})^A_{ACC}$	$(C_{DOF(TM)})^A$	$(C_{DOF(SM)})^A_{ACC}$
(39)	(323)	(40)	(324)	(164)	(325)	(164)	(326)
T		T		T		T	
(2.3-7)	(39) + (321)	(2.3-8)	(40) + (322)	(2.3-9)	(164) + (321)	(2.3-10)	(164) + (322)

$(C_{DOF(SM)})^A_{ACC} = (C_{DOF(TM)})^A + (\Delta C_{DOF(SM)})^A_{ACC}$, $(C_{DOF(IIM)})^A_{ACC} = (C_{DOF(IIM)})^A + (\Delta C_{DOF(SM)})^A_{ACC}$, $(C_{DOF(IIIM)})^A_{ACC} = (C_{DOF(IIIM)})^A + (\Delta C_{DOF(SM)})^A_{ACC}$

$(C_{DOF(IVM)})^A_{ACC} = (C_{DOF(IVM)})^A + (\Delta C_{DOF(SM)})^A_{ACC}$, $(C_{DOF(VM)})^A_{ACC} = (C_{DOF(VM)})^A + (\Delta C_{DOF(SM)})^A_{ACC}$, $(C_{DOF(VIM)})^A_{ACC} = (C_{DOF(VIM)})^A + (\Delta C_{DOF(SM)})^A_{ACC}$

TABLE (2.3-12) SUMMARY (2)

TOTAL AVERAGE SKIN-FRICTION DRAG COEFFICIENT INCREMENT,

CONSTANT ACCELERATION FLIGHT REGIMES FROM START (V = 0)

$(\Delta C_{DOF(SM)})_{ACC} = (\Delta C_{DOF(T)})_{ACC} + (\Delta C_{DOF(ET)})_{ACC} + (\Delta C_{DOF(ST)})_{ACC} + (\Delta C_{DOF(F)})_{ACC}$

MISSILE = NOSE SECTION + (CYLINDER + BOATTAIL) + WINGS + FINS

MACH NO	ALTITUDE	TIME	ACCELERATION	T_w/T_H	SET OF CHARTS "B", $(\Delta C_{DOF(TM)})^B_{ACC}$ INCREMENT						
					NOSE SECTION	CYL. + BOATTAIL	WINGS	FINS			MISSILE
M	H, ft	t, SEC	ng	°R	$(\Delta C_{DOF(T)})^B_{ACC}$	$(\Delta C_{DOF(ET)})^B_{ACC}$	$(\Delta C_{DOF(ST)})^B_{ACC}$	$(\Delta C_{DOF(F)})^B_{ACC}$	(313) + (316)	(314) + (317)	$(\Delta C_{DOF(TM)})^B_{ACC}$
(13)	(14)	(18)	(16)	(17)	(313)	(314)	(315)	(317)	(316)	(317)	(318)
T	T	T	T	FIG	T	T	T	T			(315) + (316)
(2.3-5)	(2.3-5)	(2.3-5)	(2.3-5)	(2.3-5)	(2.3-12)	(2.3-12)	(2.3-12)	(2.3-12)			
0 OR 2											
5											
M_{CR}											
10											
12											
15											
20											
25											
30											
35											
40											
45											
50											

NOTE SEE (2.3-11) AND (2.3-6), (2.3-7), (2.3-8), (2.3-9), (2.3-10)

$(\Delta C_{DOF(T)})_{ACC}$ - METHOD II $\alpha \approx 0$, $(T_w/T_H) = f(M, H, ng)$

MISSILE TOTAL DRAG COEFFICIENT

CASE IM		CASE IIM		CASE IIIM		CASE IV M	
$(C_{DOF(TM)})^B$	$(C_{DOF(SM)})^B_{ACC}$	$(C_{DOF(TM)})^B$	$(C_{DOF(SM)})^B_{ACC}$	$(C_{DOF(TM)})^B$	$(C_{DOF(SM)})^B_{ACC}$	$(C_{DOF(TM)})^B$	$(C_{DOF(SM)})^B_{ACC}$
(39)	(318)	(40)	(319)	(164)	(320)	(164)	(321)
T		T		T		T	
(2.3-7)	(39) + (318)	(2.3-8)	(40) + (319)	(2.3-9)	(164) + (320)	(2.3-10)	(164) + (321)

$(C_{DOF(SM)})^B_{ACC} = (C_{DOF(TM)})^B + (\Delta C_{DOF(SM)})^B_{ACC}$, $(C_{DOF(IIM)})^B_{ACC} = (C_{DOF(IIM)})^B + (\Delta C_{DOF(SM)})^B_{ACC}$, $(C_{DOF(IIIM)})^B_{ACC} = (C_{DOF(IIIM)})^B + (\Delta C_{DOF(SM)})^B_{ACC}$

2.3-12 METHOD III, TABLES (2.3-13), (2.3-14), (2.3-15)

Assumptions: The actual surface finish is approximated by an "equivalent surface roughness" parameter (k) (see Table (2.3-2)) matched and derived from experimental data of the frictional behavior of uniformly "sand-type" roughened flat plates. The corresponding skin-thermal conditions are approximated by the (T_w/T_H) ratio for various flight regimes, estimated in the same way as in the case of "aerodynamically" smooth surfaces, i.e., the eventual roughness effects upon skin-temperature distribution are not taken into account due to lack of any generalized data.

Applicability: The same as for Method II, with the skin-roughness aditionally taken into account.

Working graphs and tables:

Set A Only: Direct Estimates for Laminar and Turbulent Boundary Layers.

Note that roughness effects on skin-friction for laminar boundary layers are negligible, i.e., even here the "smooth" laminar curves are valid. But, the turbulent boundary layer is treated using the corresponding "rough" curves, presented in the following figures:

Fig.(2.3-44) - Average, two-dimensional, compressible skin-friction coefficient $(C_{f_{INS}})^A$ for laminar (smooth curves) and turbulent (rough curves) boundary layers on insulated flat plates. (Clutter(127)).

Fig.(2.3-45) - Average, two-dimensional, compressible skin-friction coefficient $(C_{f_T})^A$ for laminar (smooth curves) and turbulent (rough curves) boundary layers on non-insulated flap plates for the specific case of $(T_{W/T_H}) = 1$.

Graphs Common to Both Sets--see Method II.

Accuracy of the working graphs:

The C_f values for "rough curves" in Fig (2.3-44) are expected to be accurate within ±15%, (Clutter(127). The corresponding "rough curves" in Fig (2.3-45) involve additionally uncertainty of temperature effects upon the C_f values, due to an approximate application of the "smooth" flat plate laws, (Van Driest(127)).

For accuracy of the figures "common to both sets"--see Method II.

Computational procedure:

As in Method II, the computation procedure is tentatively subdivided into three representative flight cases. Each of the procedures is represented for Method III in the respective Tables (2.3-13) to (2.3-15) in a self-instructive way.

(i) Steady, Prolonged Flight Regimes, No Radiation Effects, Table (2.3-13)

(1) and (2)--repeat the steps (1) and (2) described in Method I.

(3) Determine the "equivalent surface roughness" parameter, k, from Table (2.3-2). Calculate the respective sets of $(V_H k/\nu_H)$ and (L/k) values, corresponding to the investigated flight regime.

(4) For the given values of $(V_H k/\nu_H)$ and (L/k), interpolate the $(V_H k/\nu_H)$ = const and (L/k) = const curves, if necessary, on Fig (2.3-44), and read off the average compressible adiabatic-wall flat plate skin-friction values.

$$(C_{f_T}^A)_{ROUGH} = (C_{f_{INS}}^A)_{ROUGH} = \quad (2.3\text{-}579)$$

$$= f\left[Re, M_H, (L/k), (V_H k/\nu_H), (T_{aw}/T_H)\right]$$

for a given flight altitude, H, and Reynolds Number, Re, Mach Number, M_H and the specific values of the roughness parameters.

(5) The rest of the procedure is the same as specified in Method I. The respective step-by-step self-indicative computation scheme is presented in Table (2.3-13).

(ii) Steady, Prolonged Flight Regimes, Radiation Effects on Skin Temperature Taken Into Account, Table (2.3-14)

Assuming that the radiation effects of a rough surface follow the same law as specified for the smooth surfaces, the computational procedure stays the same as indicated in Method II and the corresponding Table (2.3-11).

When fulfilling the clearly indicated stepwise computations in the Table (2.3-11), the only quantities that can differ in the rough case from their smooth values are:

ϵ - the emissivity coefficient, Table (2.3-2)

$C_{fi_{INS}}$ - the incompressible, two-dimensional value of the average skin-friction coefficient on insulated rough flat plates, estimated directly from Fig (2.3-44),(M=0)for the nose-cone, the cylinder and boattail, the wings and the fins respectively.

The computed rough-surface values of the average, three-dimensional, zero-lift skin-friction drag coefficient increment for the total missile configuration,

$$(\Delta C_{Dof_{IMTR}})^{A}_{RAD} \quad , \qquad (2.3\text{-}580)$$

should be then added to the fundamental, insulated values, obtained earlier by Method III (i), see Table (2.3-12):

$$(C_{Dof_{IMTR}})^{A}_{RAD} = (C_{Dof_{IMR}})^{A} + (\Delta C_{Dof_{IMTR}})^{A}_{RAD} \quad . \qquad (2.3\text{-}581)$$

However, in a first approximation, instead of the above estimates of $(\Delta C^{A}_{Dof_{IMT}})_{RAD}$ for rough-surfaces, the smooth-surface results from Method II(i) may be alternatively used in view of the rather inadequate margin of accuracy inherent to the temperature and roughness estimates in general, i.e.,

$$(\Delta C_{Dof_{IMTR}})^{A}_{RAD} \approx (\Delta C_{Dof_{IMT}})^{A}_{RAD} \quad . \qquad (2.3\text{-}582)$$

Note that here only the set of charts A is used, since the rough surface data are found only there.

(iii) Constant Acceleration Flight Regimes, $n_g > 0$, No Radiation Effects, Table (2.3-15)

Following the same line of arguments presented above for radiation effects Method III (ii), the Table (2.3-12) may be used for the computations of the average skin-friction drag coefficient increment due to constant acceleration effects,

$$(\Delta C_{Dof_{IMTR}})^{A}_{ACC} \quad , \qquad (2.3\text{-}583)$$

or the already computed smooth-surface results, from Method II (iii), may be used alternatively, i.e., with the approximation,

$$(\Delta C_{Dof_{IMTR}})^{A}_{ACC} \approx (\Delta C_{Dof_{IMT}})^{A}_{ACC} \quad . \qquad (2.3\text{-}584)$$

The total missile zero-lift average skin-friction drag coefficient is then likewise obtained from (see Table 2.3-12):

$$(C_{Dof_{IMTR}})^{A}_{ACC} = (C_{Dof_{IMR}})^{A} + (\Delta C_{Dof_{IMTR}})^{A}_{ACC}$$

or

$$(C_{Dof_{IMTR}})^{A}_{ACC} \approx (C_{Dof_{IMR}})^{A} + (\Delta C_{Dof_{IMT}})^{A}_{ACC} \quad . \qquad (2.3\text{-}585)$$

Working charts A
Figs — (2 3 44) and (2 3 45)

TABLE (2 3 13)
AVERAGE SKIN-FRICTION DRAG COEFFICIENT,

STEADY, PROLONGED FLIGHT REGIMES, NO

FULLY TURBULENT B L ASSUMED ON ALL MISSILE PARTS $(C_{DOF(TURB)})^A = (C_{f_{TR}})^A G_1 + \left\{(C_{f_{STR}})^A [\ + R_i] - \right.$

		NOSE SECTION					
		$\bar{x}$(ft) = , $L_N \sec(\theta_N/2)$ = , $[L_N \sec\theta_N/2)]/R$ =				$\bar{x}$(ft) = ,	
MACH NO M	ALTITUDE H ft	$Re^{\bar{x}}_{Re_N}$	$\left(\frac{V\bar{x}}{\nu}\right)_H$	$(C_f)^A_{RNS\ ROUGH} + (C_{f_{STR}})^A$	$(C_{DOF(TURB)})^A$	$Re^{\bar{x}}_{TOTAL}$	$\left(\frac{V\bar{x}}{\nu}\right)_H$
(13)	(14)	(30)	(23)	(32C)	(32I)	(24)	(27)
T = (2 3 5)	T = (2 3 5)	T-(2 3 5)	T-(2 3 5)	T-(2 3 44)	(32C) x (9)	T-(2 3 5)	T-(2 3 5)
0 or 2							
5							
M_{cr}							
10							
12							
15							
20							
30							
40							
50	etc						

NOTES

Subscript "T" means turbulent boundary layer

Subscript "R" means rough surface

Subscripts "1", "2", "3", and "4" mean NOSE CONE, CYL + BOATTAIL, WINGS and FINS,

Subscript "IM" means Case IM for the missile

Superscript "A" means set of working charts "A"

C_{DOF} — METHOD III

Figures common to both sets, — see Method II

RADIATION, R F O, $(T_w/T_N) + (T_{aw}/T_N)$

$\left(C_{f_{STR}}\right)^A R_i\Big\}\ G_2 + (C_{f_{STR}})^A G_3 + (C_{f_{STR}})^A N\, G_4$

	CYLINDER + BOATTAIL					
	$L_N \sec(\theta_N/2) + L_{CYL} + L_{BT}$ = ,			$[L_{CYL} + L_{BT} + L_N \sec(\theta_N/2)]/R$ = ,		
$(C_f)^A_{RNS\ ROUGH} + (C_{f_{STR}})^A$	$1 + R_i$	R_i				$(C_{DOF(CYL + BT)R})^A$
(32I)	(35)	(35)	(32F)	(32S)	(32H)	(32B)
FIG (2 3 44)	T-(2 3 61)	T-(2 3 5)	(32I) x (35)	(32C) x (35)	(32B) - (32S)	(32H) x (10)

$(C_{DOF(TURB)})^A = (C_{f_{TR}})^A G_1$

$(C_{DOF(CYL + BT)R})^A = \left\{(C_{f_{STR}})^A [\ + R_i] - (C_{f_{STR}})^A R_i\right\} G_2$

$(C_{DOF(TURB)})^A = (C_{f_{STR}})^A G_3$

$(C_{DOF_{FR}})^A = (C_{f_{STR}})^A G_4\ N$

respectively

TABLE (2 3 - 13)
AVERAGE SKIN-FRICTION DRAG COEFFICIENT,

STEADY PROLONGED FLIGHT REGIMES, NO RADIATION,

FULLY TURBULENT B.L. ASSUMED ON ALL MISSILE PARTS $(C_{DOF(TURB)})^A = (C_{f_{TR}})^A G_1 +$

		WINGS				FINS			MISSILE		
		$\bar{x}$(ft) = , $\bar{c}_{EXP}$ = , $(\bar{c}_{EXP}/b)$ =				$\bar{c}_{EXP}$ = , $(\bar{c}_{EXP}/b)$ =					
MACH NO M	ALTITUDE H ft	$Re^{\bar{x}}_{Re_W}$	$\left(\frac{V\bar{x}}{\nu}\right)_H$	$(C_{f_{STR}})^A - (C_f)^A_{RNS\ ROUGH}$	$(C_{DOF(TURB)})^A$	$\left(\frac{V\bar{x}}{\nu}\right)_H$	$(C_{f_{STR}})^A - (C_f)^A_{RNS\ ROUGH}$	$(C_{DOF(TURB)})^A$			$(C_{DOF(TURB)})^A$
(13)	(14)	(30)	(31)	(32S)	(32F)	(35)	(32B)	(32G)	(33O)	(33I)	(33Z)
T = (2 3 5)	T = (2 3 5)	T-(2 3 5)	T-(2 3 5)	T-(2 3 44)	(32B) x (11)	T-(2 3 5)	T-(2 3 44)	(35) x (12)	(32I) + (32S)	(32I) + (32G)	(33O) + (33I)
0 or 2											
5											
M_{cr}											
10											
12											
15											
20											
30											
40											
50	etc										

NOTES

$(C_{DOF(TURB)})^A = (C_{f_{STR}})^A G_3$

$(C_{DOF_{FR}})^A = (C_{f_{STR}})^A G_4$

CONTINUED
C_{DOF} — METHOD III

R F O, $T_w/T_N = T_{aw}/T_N$

$\left\{(C_{f_{STR}})^A [\ + R_i] - (C_{f_{STR}})^A R_i\right\} G_2 + (C_{f_{STR}})^A G_3 + (C_{f_{STR}})^A N\, G_4$

T (2 3-4) METHOD III (iii)

AVERAGE SKIN FRICTION DRAG COEFFICIENT INCREMEN $(\Delta C_{D_{OF_{MISTR}}})^{A}_{RAD}$,
STEADY, PROLONGED FLIGHT REGIMES, FULLY
SET OF WORKING CHARTS

$(C_{D_{OF_{MISTR}}})^{A}_{RAD} = (C_{D_{OF_{MISS}}})^{A} + (\Delta C_{D_{OF_{MISTR}}})^{A}_{RAD}$, WHERE $(\Delta C_{D_{OF_{MISTR}}})^{A}_{RAD}$ =

MACH NO M (13)	ALTITUDE H, ft (14)	NOSE CONE $(\Delta C_{D_{OF_{TRN}}})^{A}_{RAD}$ (195)	CYLINDER + BOATTAIL $(\Delta C_{D_{OF_{TRCYL+BT}}})^{A}_{RAD}$ (224)	WINGS $(\Delta C_{D_{OF_{TRW}}})^{A}_{RAD}$ (246)	FINS $(\Delta C_{D_{OF_{TRF}}})^{A}_{RAD}$ (268)
T-(2 3-5)	T-(2 3-5)	T-(2 3-11)	T-(2 3-11)	T-(2 3-11)	T-(2 3-11)
0 or .2					
.5					
M_{cr}					
1.0					
1.2					
1.5					
2.0					
3.0					
4.0					
5.0 etc					

NOTE

SEE TABLES (2 3-11) AND (2 3-5)

SUBSCRIPT "R" MEANS "ROUGH SURFACE"

(SUMMARY)

DUE TO RADIATION EFFECTS ON ROUGH SURFACES
TURBULENT BOUNDARY LAYER
"A" ONLY
$(\Delta C_{D_{OF_{MIST}}})^{A}_{RAD}$ FROM T-112 EVENTUALLY

MISSILE $(\Delta C_{D_{OF_{MIST}}})^{A}_{RAD}$			TOTAL MISSILE $(C_{D_{OF_{MIS}}})^{A}$	$(C_{D_{OF_{MISTR}}})^{A}_{RAD}$
(274)	(275)	(276)	(333)	(334)
(195) + (224)	(246) + (268)	(274) + (275)		(270) + (330)
T-(2 3-11)	T-(2 3-11)	T-(2 3-11)	T-(2 3-13)	

T-(2 3-5) METHOD III

AVERAGE SKIN FRICTION DRAG COEFFICIENT INCREMENT, $(\Delta C_{D_{OF_{MISTR}}})^{A}_{ACC}$,
SURFACES, STEADY, ACCELERATED FLIGHT REGIMES,
SET OF WORKING CHARTS

$(C_{D_{OF_{MISTR}}})^{A}_{ACC} = (C_{D_{OF_{MISS}}})^{A} + (\Delta C_{D_{OF_{MISTR}}})^{A}_{ACC}$, WHERE $(\Delta C_{D_{OF_{MISTR}}})^{A}_{ACC}$ =

MACH NO M (13)	ALTITUDE H, ft (14)	NOSE CONE $(\Delta C_{D_{OF_{TRN}}})^{A}_{ACC}$ (307 A)	CYLINDER + BOATTAIL $(\Delta C_{D_{OF_{TRCYL+BT}}})^{A}_{ACC}$ (301)	WINGS $(\Delta C_{D_{OF_{TRW}}})^{A}_{ACC}$ (309)	FINS $(\Delta C_{D_{OF_{TRF}}})^{A}_{ACC}$ (317)
T-(2 3-5)	T-(2 3-5)	T-(2 3-12)	T-(2 3-12)	T-(2 3-12)	T-(2 3-12)
0 or .2					
.5					
M_{cr}					
1.0					
1.2					
1.5					
2.0					
3.0					
4.0					
5.0					

NOTE

SEE TABLES (2 3-12) AND (2 3-5)

SUBSCRIPT "R" MEANS "ROUGH SURFACE"

(iii) (SUMMARY)

DUE TO CONSTANT ACCELERATION EFFECTS ON ROUGH
FULLY TURBULENT BOUNDARY LAYER
"A" ONLY
$\approx (\Delta C_{D_{OF_{MIST}}})^{A}_{ACC}$ FROM T-113 , EVENTUALLY

MISSILE $(\Delta C_{D_{OF_{MIST}}})^{A}_{ACC}$			TOTAL MISSILE $(C_{D_{OF_{MIS}}})^{A}$	$(C_{D_{OF_{MISTR}}})^{A}_{ACC}$
(320)	(321)	(322)	(332)	(335)
(307) + (301)	(309) + (317)	(320) + (321)		(332) + (330)
T-(2 3-12)	T-(2 3-12)	T-(2 3-12)	T-(2 3-13)	

2.3.13 FINAL SUMMARY RESULTS, C_{Dof_M}, TABLE (2.3-16)

The results of the C_{Dof_M} estimates for different skin roughness, skin-temperature and boundary layer conditions, both in steady flight and with constant acceleration, are summarized in Table (2.3-16). A schematic instructive outline of the proposed methods and procedures of estimates is attached to the Table (2.3-16) as a guide.

Since individual specifications of a variety of skin-friction coefficients and of their increments necessitates a rather elaborate symbolic notation, a partial reference list of nomenclature is provided below for convenience.

Subscripts

"i" - refers to "incompressible" flow values

"INS" - refers to "insulated" skin conditions

"L" - refers to "laminar" boundary layers

"T" - refers to "turbulent" boundary layers

"TUR" "T" - alternatively refers to skin-temperature effects (caused by radiation or acceleration)

"L+T" - refers to partially laminar, partially turbulent boundary layers

"R" - refers to "rough" surfaces

"ACC" - refers to "acceleration" effects

"RAD" - refers to "radiation" effects

"IM" - refers to total missile, turbulent boundary layer (Case IM)

"IIM" - refers to total missile, partially turbulent boundary layer, transition at the nose section (Case IIM)

"IIIM" - refers to total missile, partially laminar, partially turbulent boundary layer, transition at the nose-cylinder junction (Case IIIM)

"IVM" - refers to total missile, partially laminar, partially turbulent boundary layer, transition at the cylindrical part of body (Case IVM)

"M" - refers to total missile configuration

"1" - refers to nose section individual value

"2" - refers to cylinder + boattail value

"3" - refers to wing's individual value

"4" - refers to fin's individual value

Superscripts

"I" - refers to the individual "Case I" (fully turbulent boundary layer) of the respective missile part

"II" - refers to the individual "Case II" (fully laminar boundary layer) of the respective missile part

"III" - refers to partially laminar, partially turbulent boundary layer on the respective missile part (Case III)

"IIIA" "IIIB" "IIIC" - refer to the boundary layer condition on cylinder + boattail, as affected by the boundary layer condition on the nose-section (Cases IIIA, IIIB, IIIC)

"A" - refers to set of working graphs "A"

"B" - refers to set of working graphs "B".

Symbol "Δ" denotes an incremental value.

Example:

$(\Delta C_{Dof_{IMT}})^{A}_{RAD}$ - the increment (Δ) of the zero-lift (0) average skin-friction (f) drag coefficient (C_{Df}) due to thermal conditions (T) of a smooth skin (no R), caused by radiation effects (RAD), if a turbulent boundary layer on all missile surfaces is assumed (IM). Numerical evaluation is performed using set of working graphs "A".

TABLE (2.3-16)
AVERAGE SKIN-FRICTION DRAG COEFFICIENT OF THE TOTAL MISSILE, C_{Dof_M}
A COMPARATIVE SUMMARY TABLE FOR ALL METHODS AND CASES (FROM 2.3-6 TO 2.3-15)

STEADY FLIGHT REGIME, $n_g = 0$

MACH NO	ALTITUDE (ft)	(1) NO RADIATION, $\varepsilon = 0$, SMOOTH SKIN, $h = 0$ METHOD I = METHOD II (1) — SET OF WORKING GRAPHS "A"				(1) NO RADIATION, $\varepsilon = 0$, SMOOTH SKIN, $h = 0$ METHOD I = METHOD II (1) — SET OF WORKING GRAPHS "B"				(2) NO RADIATION, $\varepsilon = 0$, ROUGH SKIN, $h \neq 0$ METHOD III (1) — SET OF WORKING GRAPHS "A" ONLY
		CASE I M	CASE II M	CASE III M	CASE IV M	CASE I M	CASE II M	CASE III M	CASE IV M	CASE I M ONLY
M	H	$(C_{Dof_{IM}})^A$	$(C_{Dof_{IIM}})^A$	$(C_{Dof_{IIIM}})^A$	$(C_{Dof_{IVM}})^A$	$(C_{Dof_{IM}})^B$	$(C_{Dof_{IIM}})^B$	$(C_{Dof_{IIIM}})^B$	$(C_{Dof_{IVM}})^B$	$(C_{Dof_{IMR}})^A$
(13)	(14)	(97)	(140)	(154)	(164)	(19)	(140) ALTERNATE	(154) ALTERNATE	(164) ALTERNATE	(332)
T(2.3-5)	T(2.3-5)	T(2.3-6)	T(2.3-8)	T(2.3-9)	T(2.3-10)	T(2.3-7)	T(2.3-8)	T(2.3-9)	T(2.3-10)	T(2.3-13)
0 or .2										
.5										
M_{cr}										
1.0										
1.2										
1.5										
2.0										
3.0										
4.0										
5.0, ETC										

NOTES

$$(C_{Dof_{IM}})^{A\,or\,B} = (C_{f_{IT}}^{I})^{A\,or\,B} G_1 + \left\{(C_{f_{ST}}^{I})^{A\,or\,B}[1+R_1] - (C_{f_{IT}}^{I})^{A\,or\,B} R_1\right\} G_2 + (C_{f_{ST}}^{I})^{A\,or\,B} G_3 +$$

$$(C_{Dof_{IIM}})^{A\,or\,B} = \left\{(C_{f_{IL}}^{II})^{A\,or\,B} R_0 [R_0' - .875 R_B] + (C_{f_{IT}}^{II})^{A\,or\,B}[1-(R_0 - R_0')]\right\} G_1 + \left\{(C_{f_{ST}}^{II})^{A\,or\,B} + (\Delta C_{f_{TURB}}^{II A})^{A\,or\,B}\right\}$$

$$(C_{Dof_{IIIM}})^{A\,or\,B} = 1.25 (C_{f_{IL}}^{III})^{A\,or\,B} G_1 + \left\{(C_{f_{ST}}^{III})^{A\,or\,B}[1+R_B] - (\Delta C_{f_{TURB}}^{III})^{A\,or\,B} R_B\right\} G_2 +$$

$$(C_{Dof_{IVM}})^{A\,or\,B} = 1.25 (C_{f_{IL}}^{IV})^{A\,or\,B} G_1 + \left\{(C_{f_{ST}}^{IV})^{A\,or\,B}[1+R_B + R_1/1.022] - (C_{f_{IL}}^{IV})^{A\,or\,B} R_1\right\} G_2$$

$$(C_{f_{ST}}^{I})^{A\,or\,B} G_3 N$$

$$[1+R_B] - (C_{f_{IT}}^{III})^{A\,or\,B} R_B\Big\} G_2 + (C_{f_{ST}}^{III})^{A\,or\,B} G_3 R_3 + (C_{f_{ST}}^{III})^{A\,or\,B} N G_4 R_B$$

$$(C_{f_{ST}}^{III})^{A\,or\,B} G_3 R_3 + (C_{f_{ST}}^{III})^{A\,or\,B} N G_4 R_B$$

$$+ (C_{f_{ST}}^{IV})^{A\,or\,B} G_3 R_3 + (C_{f_{ST}}^{IV})^{A\,or\,B} G_4 N R_B$$

$$(C_{Dof_{IMR}})^A = (C_{f_{ITR}})^A G_1 + \left\{(C_{f_{STR}})^A[1+R_1] - (C_{f_{ITR}})^A R_1\right\} G_2 + (C_{f_{STR}})^A G_3 + (C_{f_{ATR}})^A G_4 N$$

TABLE (2.3-16) CONTINUED (1)

STEADY FLIGHT REGIME, $n_g = 0$

	(3) RADIATION, $\varepsilon \neq 0$, SMOOTH SKIN, $h = 0$ METHOD II (1) — SET OF WORKING GRAPHS "A"				(3) RADIATION, $\varepsilon \neq 0$, SMOOTH SKIN, $h = 0$ METHOD II (1) — SET OF WORKING GRAPHS "B"				(4) RADIATION, $\varepsilon \neq 0$, ROUGH SKIN, $h \neq 0$ METHOD III (1) — SET OF WORKING GRAPHS "A" ONLY
	CASE I M	CASE II M	CASE III M	CASE IV M	CASE I M	CASE II M	CASE III M	CASE IV M	CASE I M ONLY
	$(C_{Dof_{IMT}})^A_{RAD}$	$(C_{Dof_{IIMT}})^A_{RAD}$	$(C_{Dof_{IIIMT}})^A_{RAD}$	$(C_{Dof_{IVMT}})^A_{RAD}$	$(C_{Dof_{IMT}})^B_{RAD}$	$(C_{Dof_{IIMT}})^B_{RAD}$	$(C_{Dof_{IIIMT}})^B_{RAD}$	$(C_{Dof_{IVMT}})^B_{RAD}$	$(C_{Dof_{IMTR}})^A_{RAD}$
	(277)	(278)	(279)	(280)	(270)	(271)	(272)	(273)	(334)
	T(2.3-11)	T(2.3-11)	T(2.3-11)	T(2.3-11)	T(2.3-11)	T(2.3-11)	T(2.3-11)	T(2.3-11)	T(2.3-11)

$$(C_{Dof_{IMT}})^A_{RAD} = (C_{Dof_{IM}})^A + (\Delta C_{Dof_{IMT}})^A_{RAD}$$

$$(C_{Dof_{IIMT}})^A_{RAD} = (C_{Dof_{IIM}})^A + (\Delta C_{Dof_{IIMT}})^A_{RAD}$$

$$(C_{Dof_{IIIMT}})^A_{RAD} = (C_{Dof_{IIIM}})^A + (\Delta C_{Dof_{IIMT}})^A_{RAD}$$

$$(C_{Dof_{IVMT}})^A_{RAD} = (C_{Dof_{IVM}})^A + (\Delta C_{Dof_{IMT}})^A_{RAD}$$

$$(C_{Dof_{IMT}})^B_{RAD} = (C_{Dof_{IM}})^B + (\Delta C_{Dof_{IT}})^B_{RAD}$$

$$(C_{Dof_{IIMT}})^B_{RAD} = (C_{Dof_{IIM}})^B + (\Delta C_{Dof_{IT}})^B_{RAD}$$

$$(C_{Dof_{IIIMT}})^B_{RAD} = (C_{Dof_{IIIM}})^B + (\Delta C_{Dof_{IT}})^B_{RAD}$$

$$(C_{Dof_{IVMT}})^B_{RAD} = (C_{Dof_{IVM}})^B + (\Delta C_{Dof_{IT}})^B_{RAD}$$

$$(C_{Dof_{IMTR}})^A_{RAD} = (C_{Dof_{IMR}})^A + (\Delta C_{Dof_{IMTR}})^A_{RAD}$$

TABLE (2.3-16) CONTINUED (2)

ACCELERATED FLIGHT REGIME

CONSTANT ACCELERATION (gs)	TIME (sec)	(i) NO RADIATION, $\delta = 0$, SMOOTH SKIN, $\alpha = 0$ METHOD II (iii) SET OF WORKING GRAPHS "A" CASE I M	CASE II M	CASE III M	CASE IV M	(ii) NO RADIATION, $\delta = 0$, SMOOTH SKIN, $\alpha = 0$ METHOD III (iii) SET OF WORKING GRAPHS "A" ONLY CASE I M ONLY
+8	t	$(C_{DOF\,I\,WT})^{A}_{+8}$	$(C_{DOF\,II\,WT})^{A}_{ACC}$	$(C_{DOF\,III\,WT})^{A}_{ACC}$	$(C_{DOF\,IV\,WT})^{A}_{ACC}$	$(C_{DOF\,WING})^{A}_{ACC}$
(14)	(15)	(323)	(324)	(325)	(326)	(335)
T (2.3-5)	T (2.3-5)	T (2.3-12)	T (2.3-12)	T (2.3-12)	T (2.3-12)	T (2.3-13)

$$(C_{DOF\,I\,WT})^{A}_{ACC} = (C_{DOF\,I\,W})^{A} + (\Delta C_{DOF\,I\,WT})^{A}_{ACC}$$

$$(C_{DOF\,II\,WT})^{A}_{ACC} = (C_{DOF\,II\,W})^{A} + (\Delta C_{DOF\,II\,WT})^{A}_{ACC}$$

$$(C_{DOF\,III\,WT})^{A}_{ACC} = (C_{DOF\,III\,W})^{A} + (\Delta C_{DOF\,III\,WT})^{A}_{ACC}$$

$$(C_{DOF\,IV\,WT})^{A}_{ACC} = (C_{DOF\,IV\,W})^{A} + (\Delta C_{DOF\,IV\,WT})^{A}_{ACC}$$

SET OF WORKING GRAPHS "B"

CASE I M	CASE II M	CASE III M	CASE IV M
$(C_{DOF\,I\,WT})^{B}_{ACC}$	$(C_{DOF\,II\,WT})^{B}_{ACC}$	$(C_{DOF\,III\,WT})^{B}_{ACC}$	$(C_{DOF\,IV\,WT})^{B}_{ACC}$
(316)	(317)	(318)	(319)
T (2.3-12)	T (2.3-12)	T (2.3-12)	T (2.3-12)

$$(C_{DOF\,I\,WT})^{B}_{ACC} = (C_{DOF\,I\,W})^{B} + (\Delta C_{DOF\,I\,WT})^{B}_{ACC}$$

$$(C_{DOF\,II\,WT})^{B}_{ACC} = (C_{DOF\,II\,W})^{B} + (\Delta C_{DOF\,II\,WT})^{B}_{ACC}$$

$$(C_{DOF\,III\,WT})^{B}_{ACC} = (C_{DOF\,III\,W})^{B} + (\Delta C_{DOF\,III\,WT})^{B}_{ACC}$$

$$(C_{DOF\,IV\,WT})^{B}_{ACC} = (C_{DOF\,IV\,W})^{B} + (\Delta C_{DOF\,IV\,WT})^{B}_{ACC}$$

$$(C_{DOF\,WING})^{A}_{ACC} = (C_{DOF\,WING})^{A} + (\Delta C_{DOF\,WING})^{A}_{ACC}$$

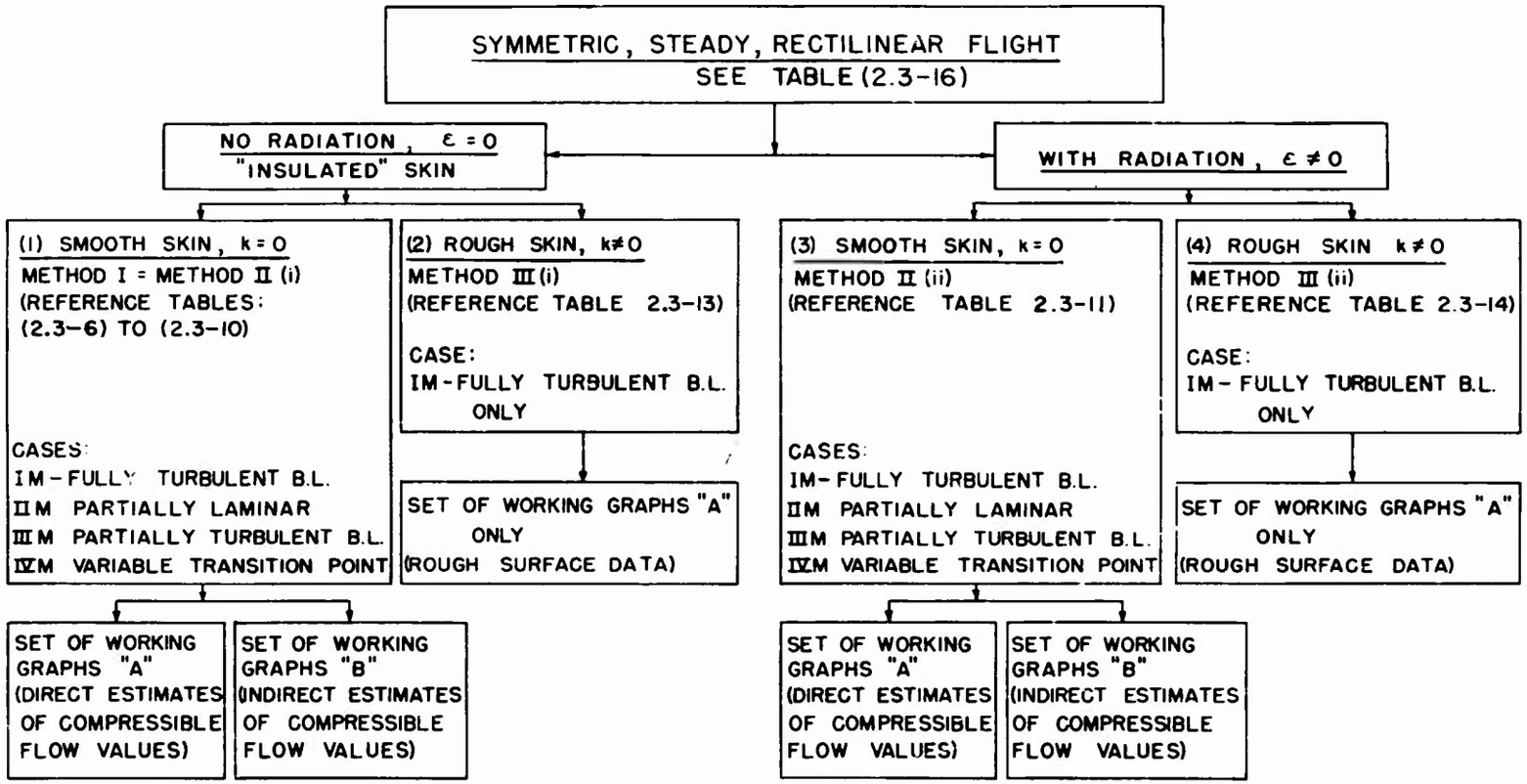

TABLE 2.3-16 SUPPLEMENT

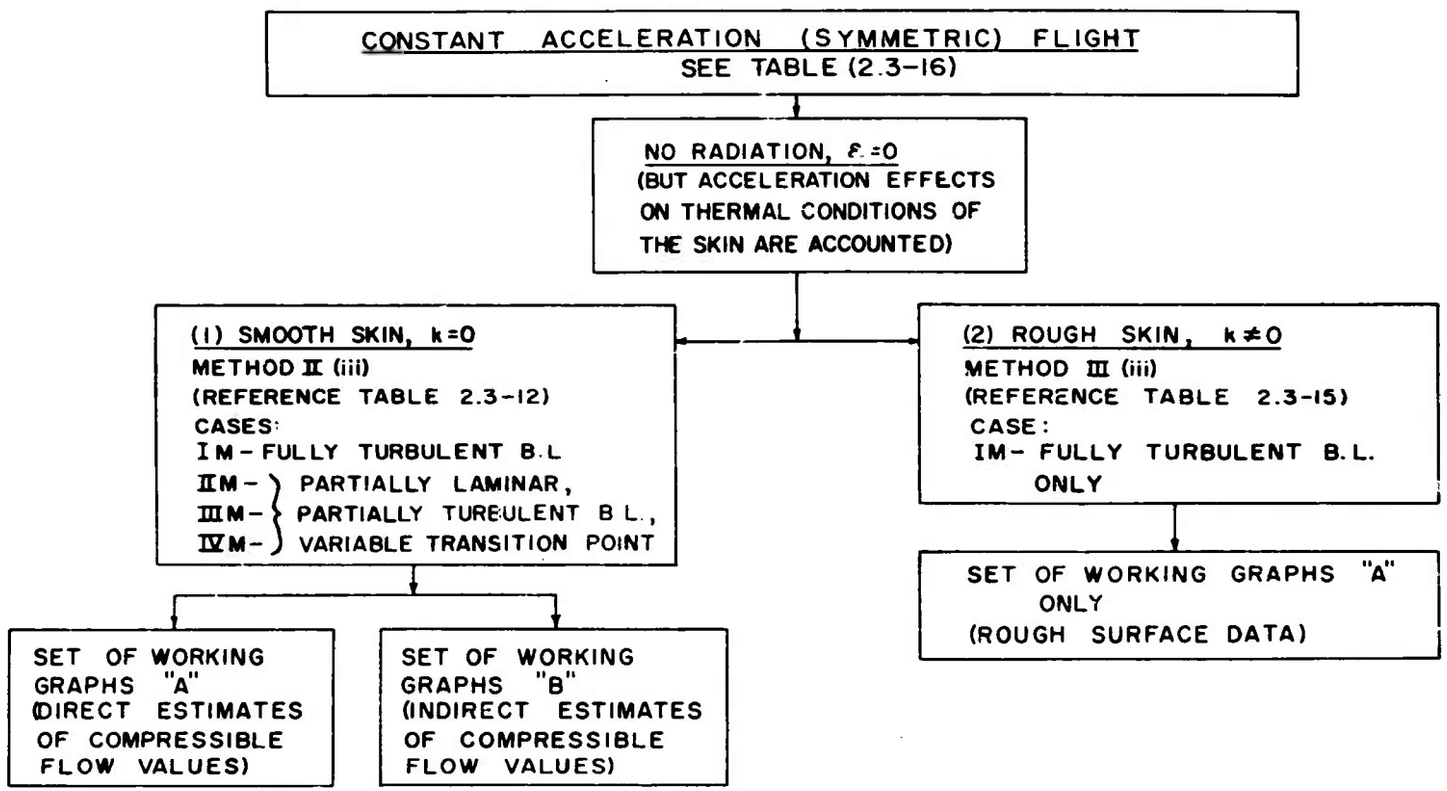

TABLE 2.3-16 SUPPLEMENT

Fig. (2.3-44a) see Fig. (2.3-34)

Note: For all Figs. (2 3-44a) to (2.3-44b) the "smooth" curve values can be obtained directly from Fig. (2.3-63) also.

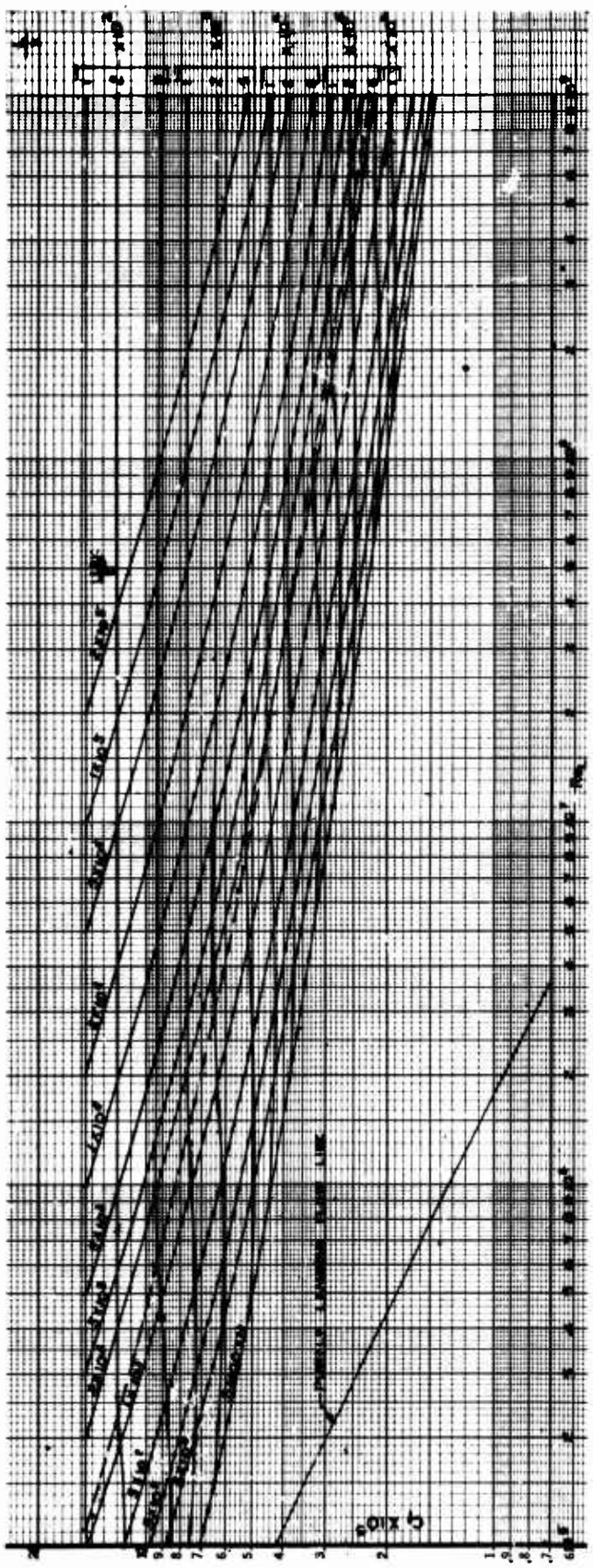

Fig. (2.3-44b) Total skin friction for a sand-roughned insulated plate M=0.5. Transition at the leading edge. (Ref. 127).

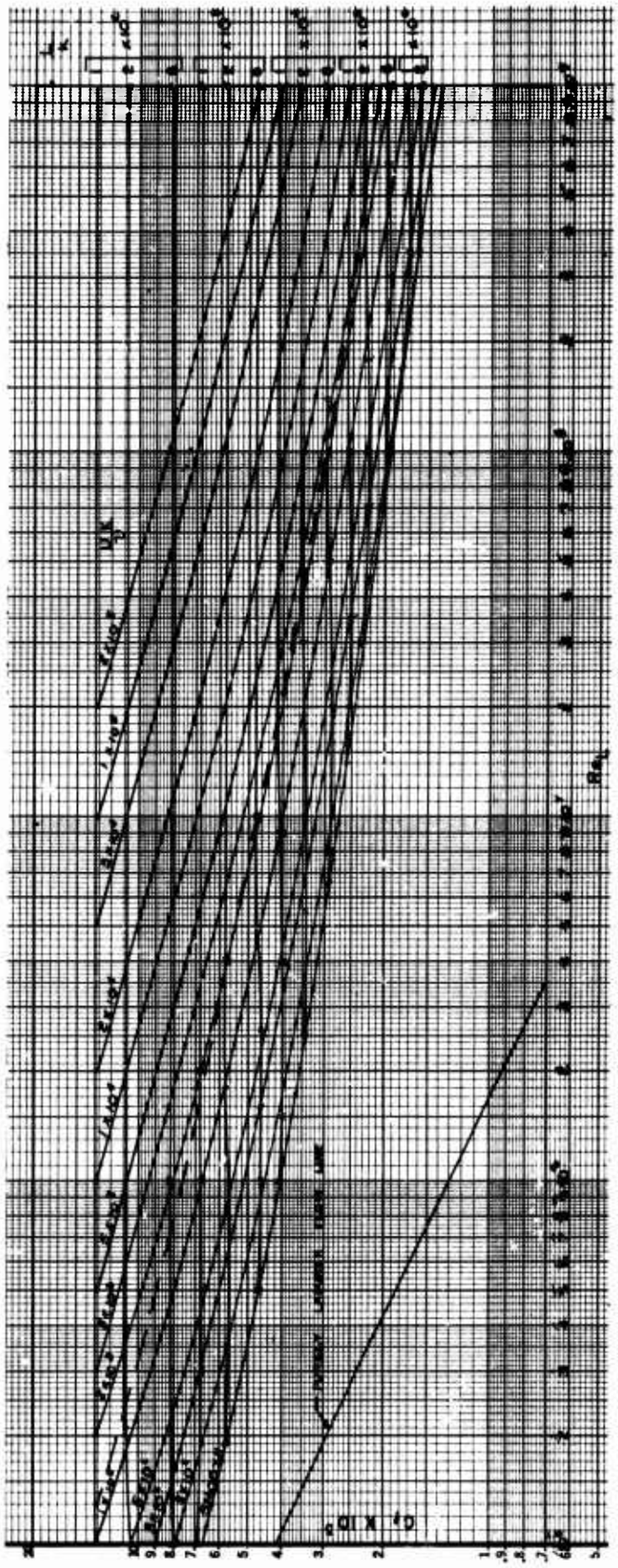

Fig. (2.3-44c) Total skin friction for a sand-roughened insulated plate. M = 1.0. Transition at the leading edge. (Ref. 127).

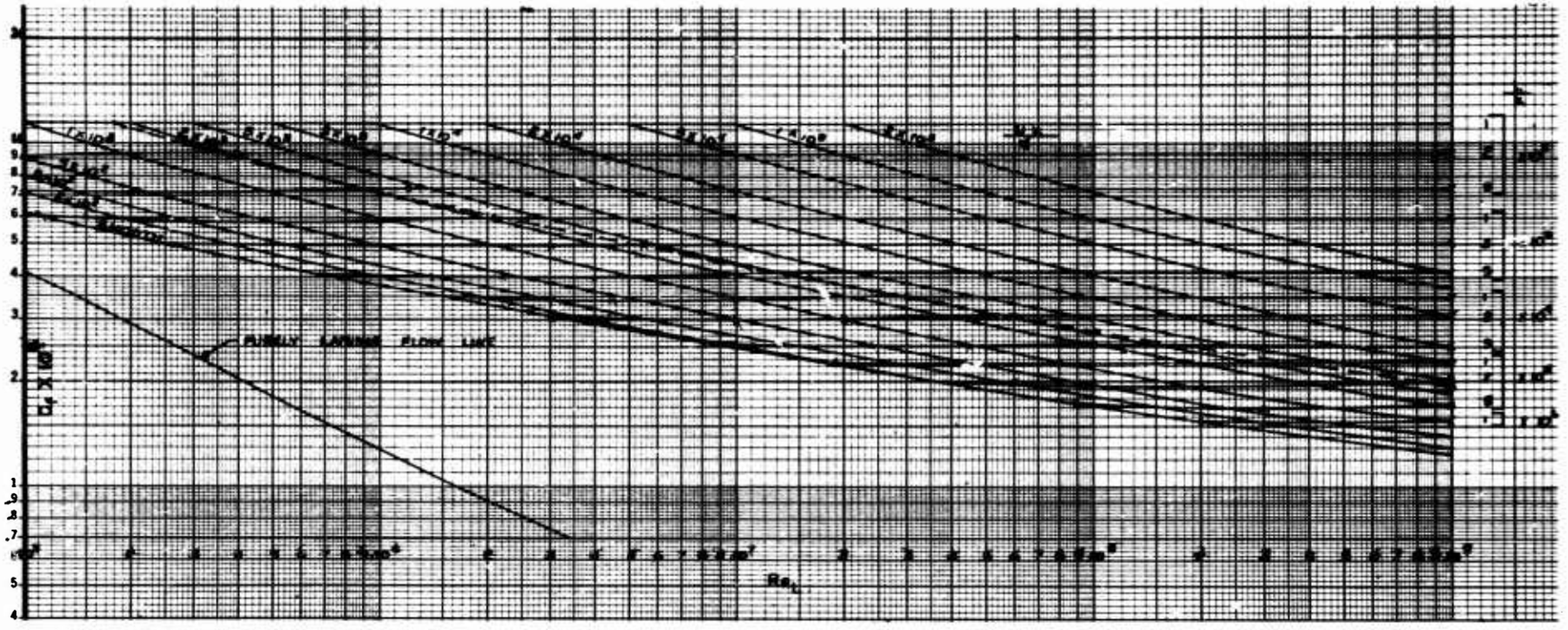

Fig. (2.3-44d) Total skin friction for a sand-roughened insulated plate. M = 1.5. Transition at the leading edge. (Ref. 127).

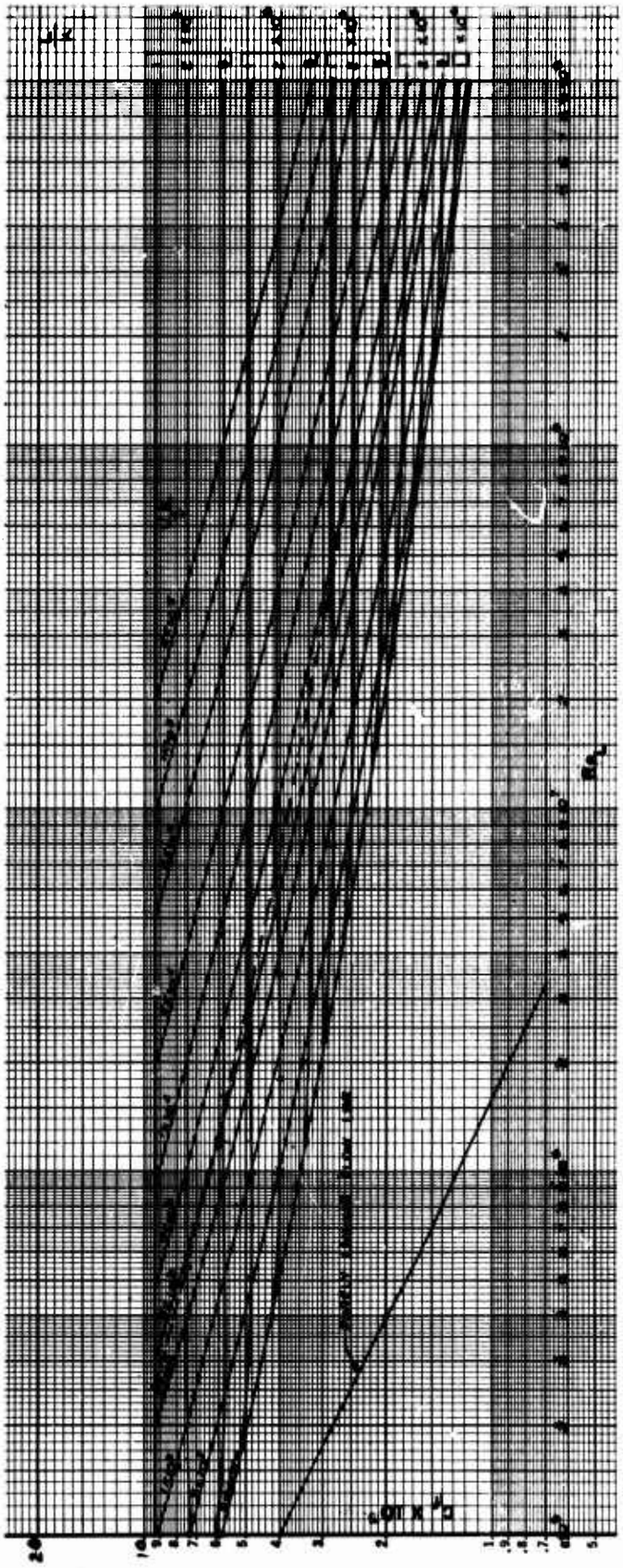

Fig. (2.3-44e) Total skin friction for a sand-roughened insulated plate. M = 2.0. Transition at the leading edge. (Ref. 127).

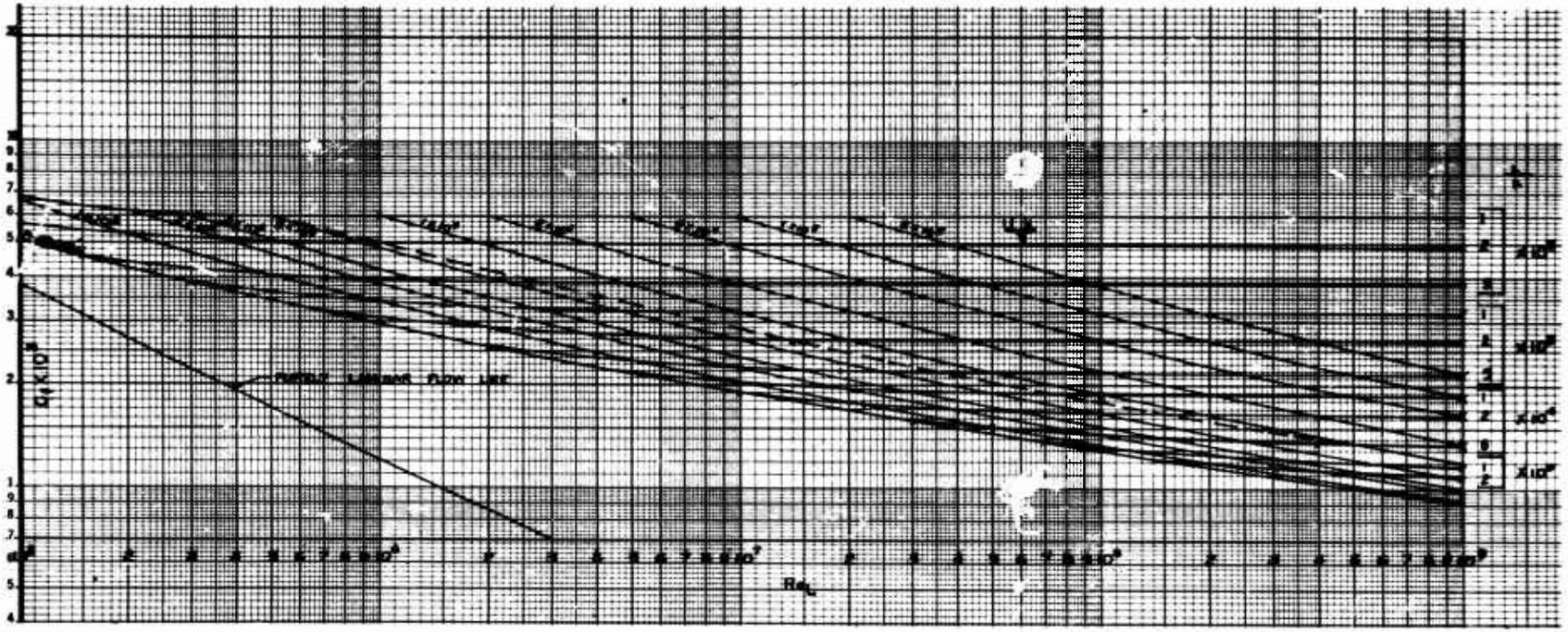

Fig. (2.3-44f) Total skin friction for a sand-roughened insulated plate. M = 3.0. Transition at the leading edge. (Ref. 127).

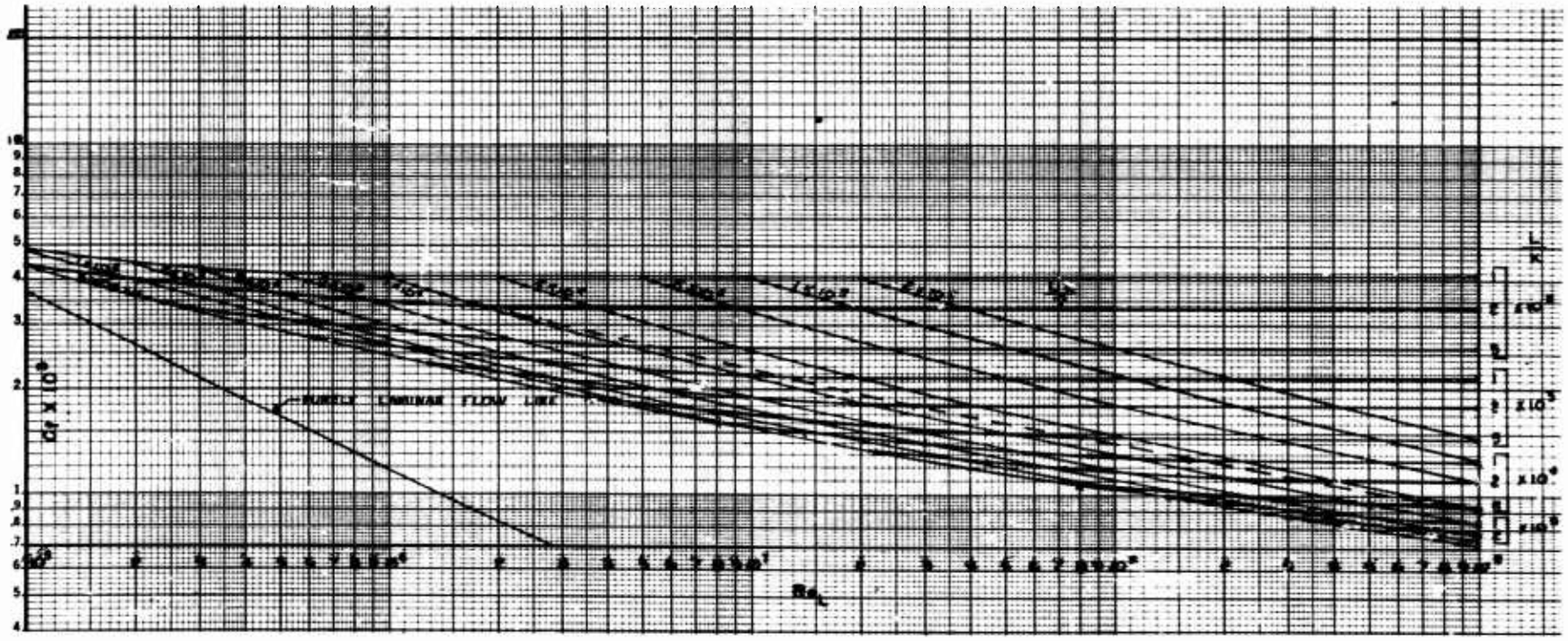

Fig. (2.3-44g) Total skin friction for a sand-roughened insulated plate. M= 4.0. Transition at the leading edge. (Ref 127).

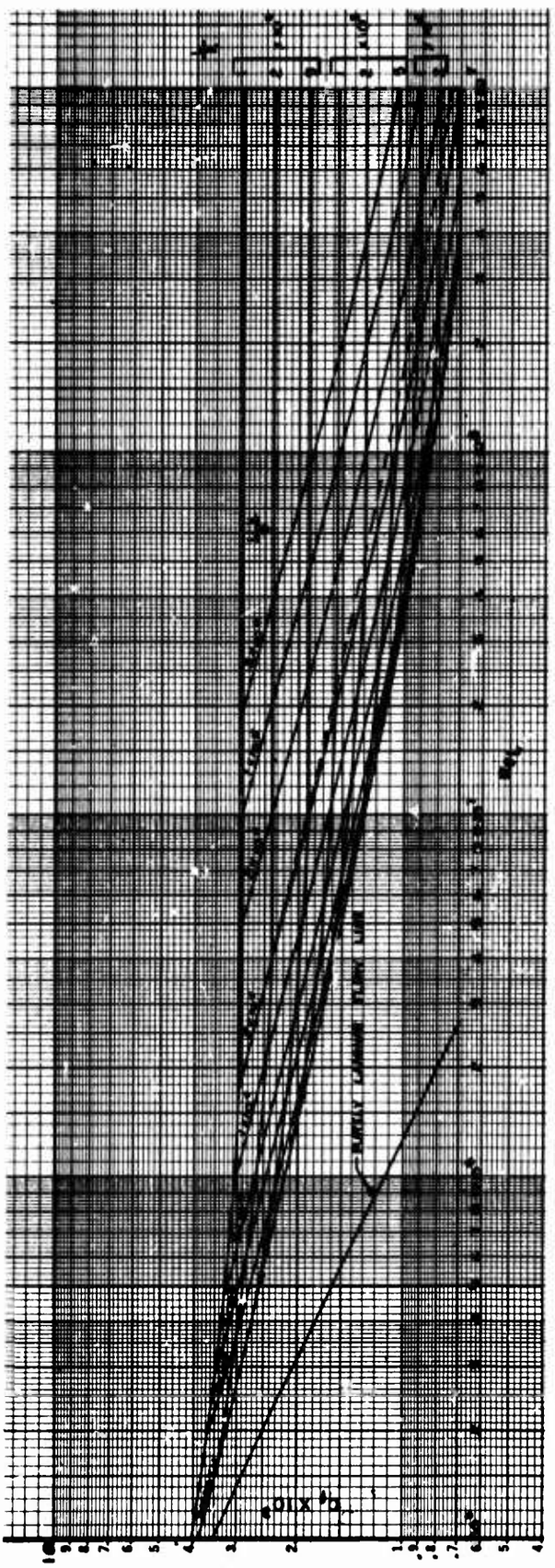

Fig. (2.3-44h) Total skin friction for a sand-roughened insulated plate. M = 5.0
Transition at the leading edge. (Ref. 127).

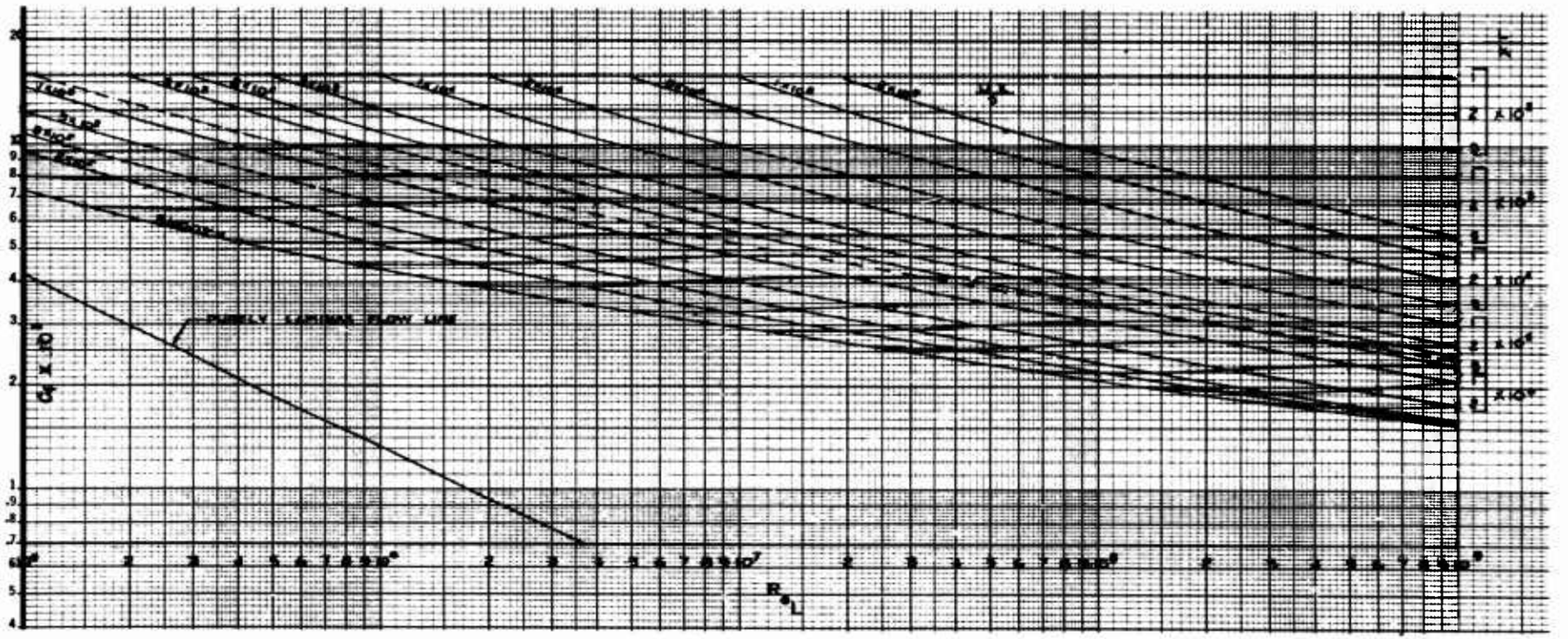

Fig. (2.3-45) Total skin friction for a sand-roughened plate with a wall temperature equal to free stream temperature. M = 0.5. Transition at leading edge. (Ref. 127).

Note: For all Fig. (2.3-45) the "smooth" curve value can be obtained directly from Fig. (2.3-60) to (2.3-63) for different T_w / T_s temperature ratios.

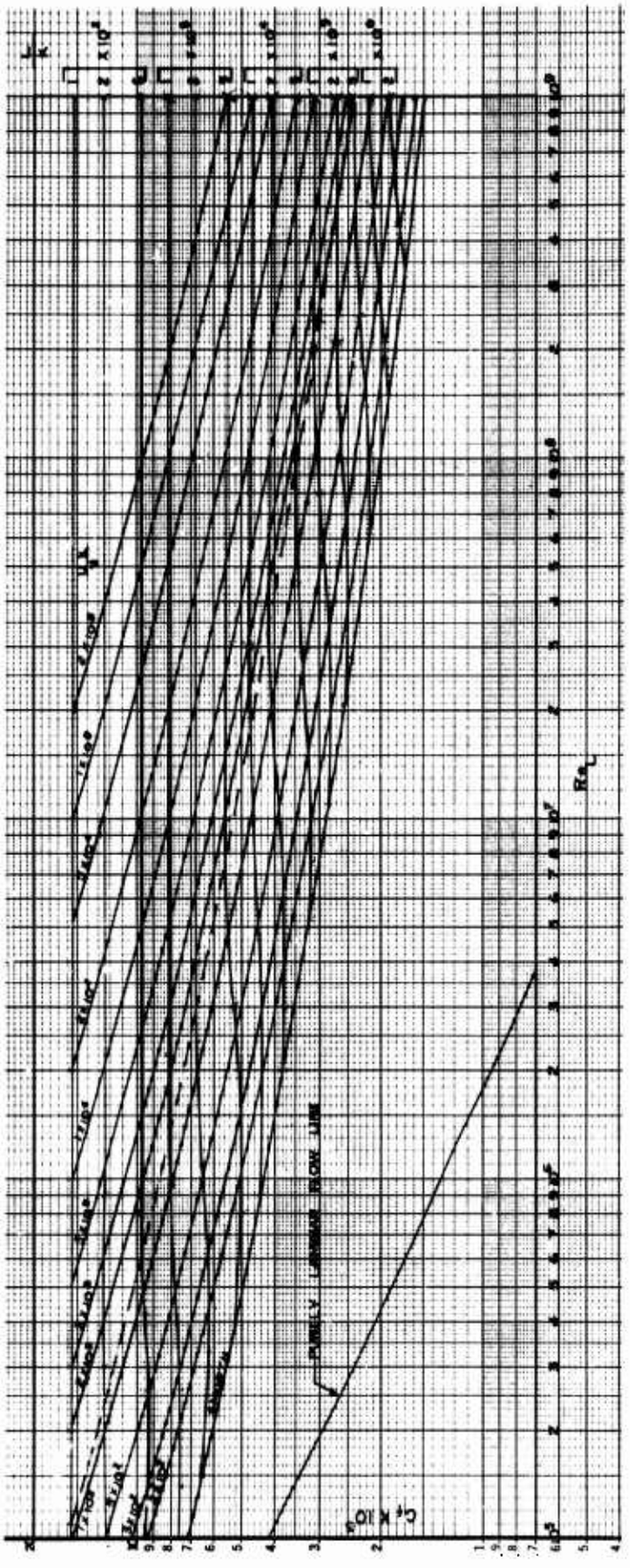

Fig. (2.3-45) Continued (1) M=1.0

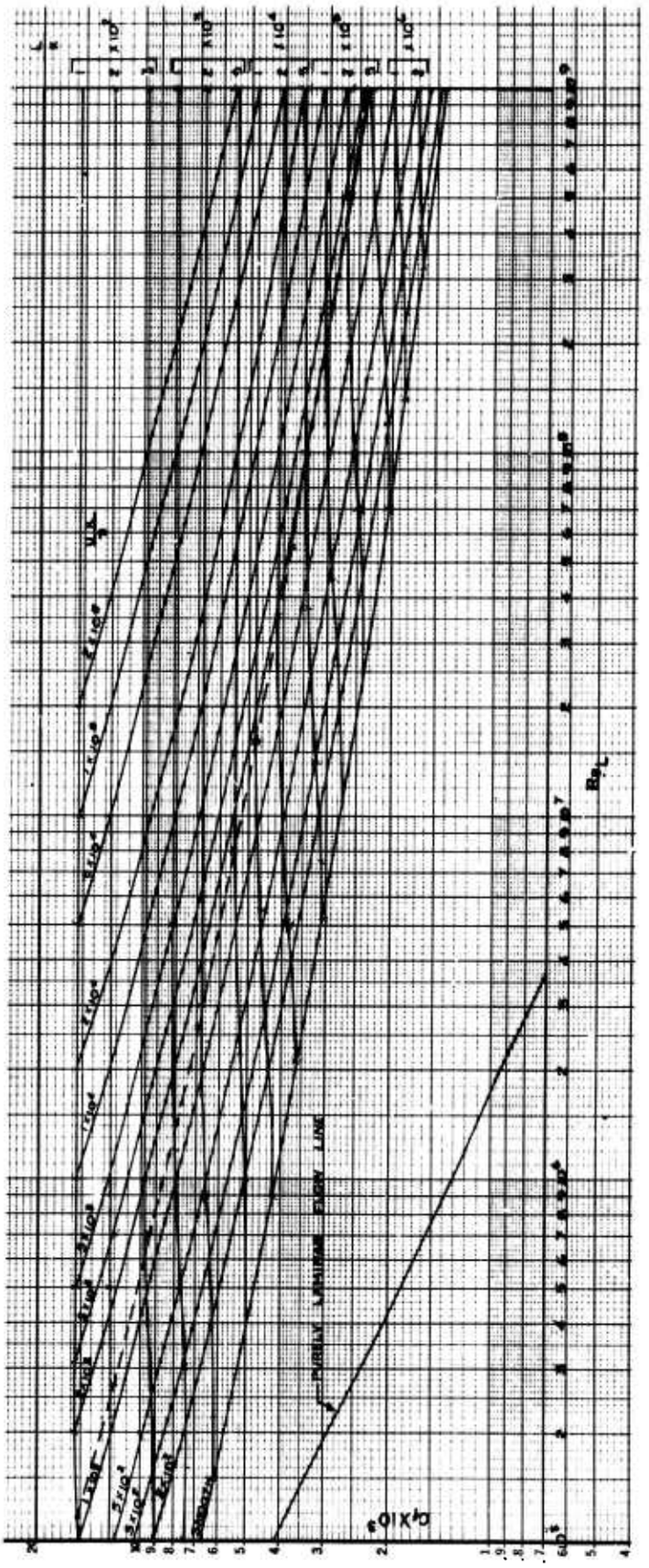

Fig. (2.3-45) Continued (2) M = 1.5

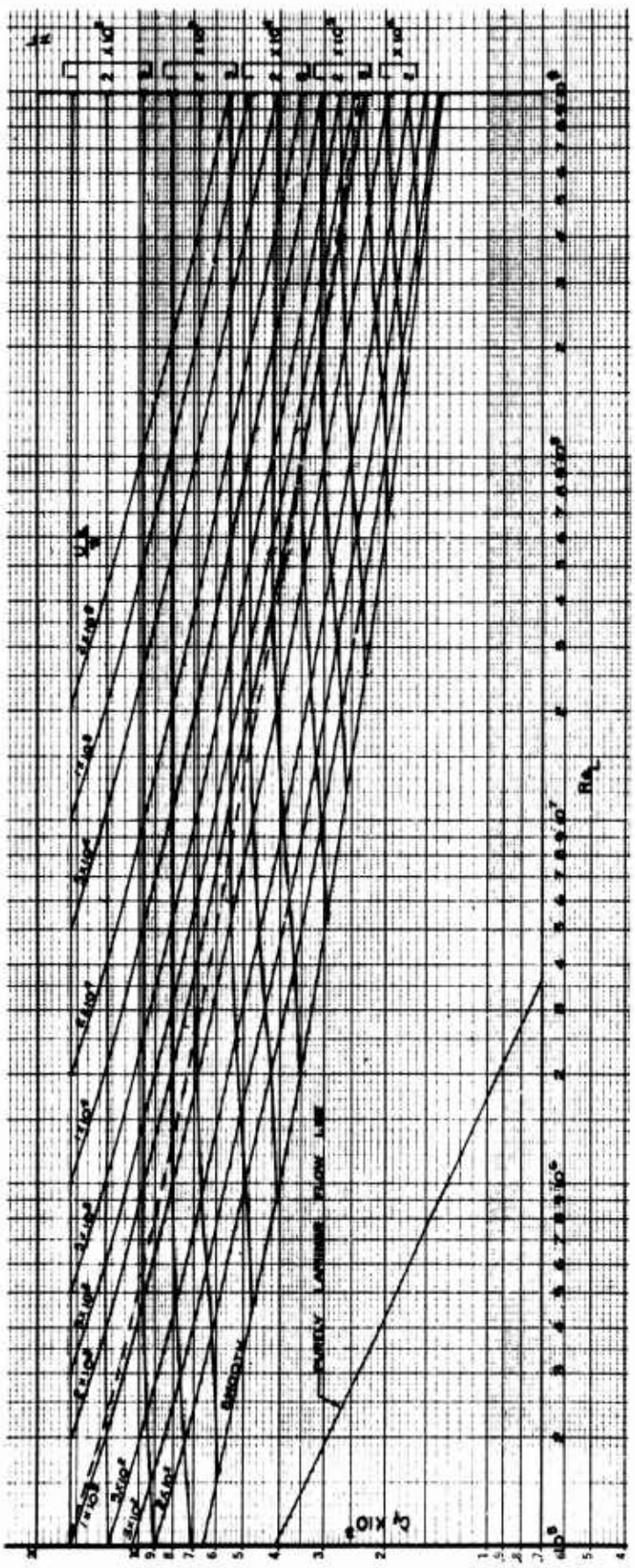

Fig. (2.3-45) Continued (3) M = 2.0

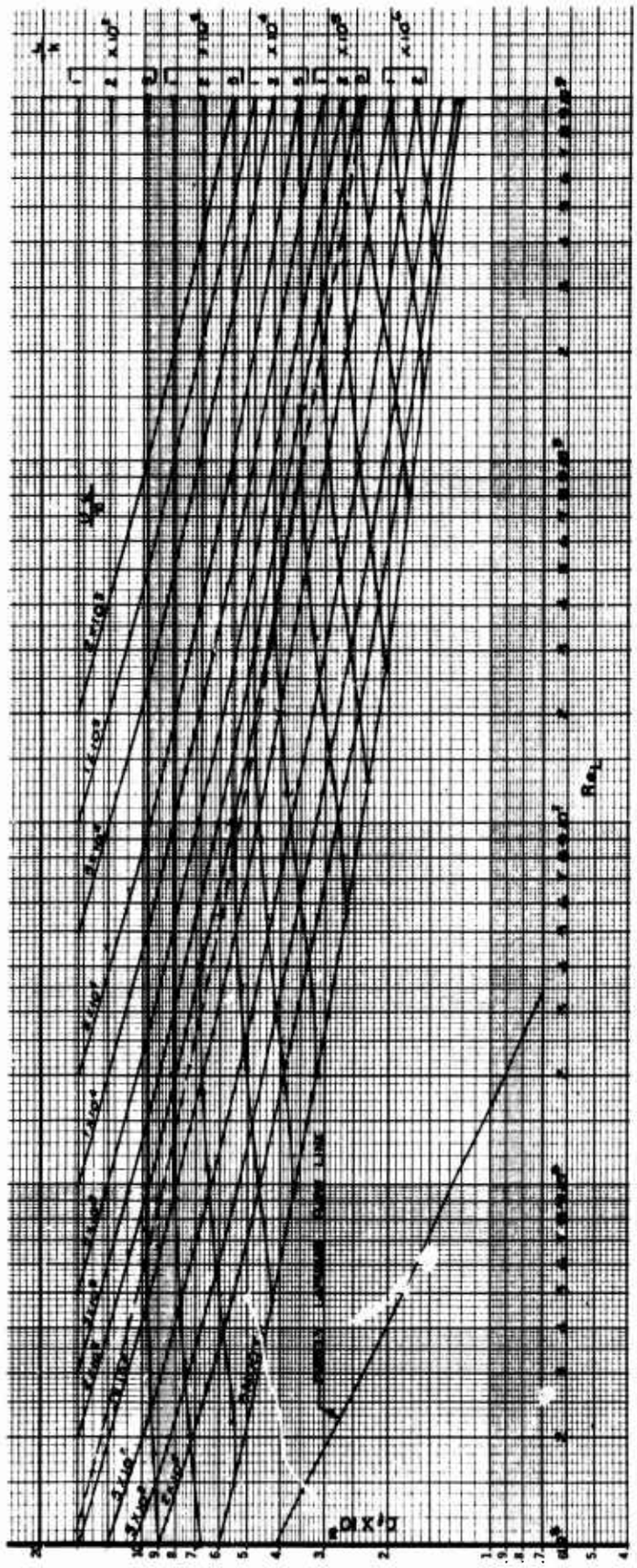

Fig. (2.3-45) Continued (4) M=3.0

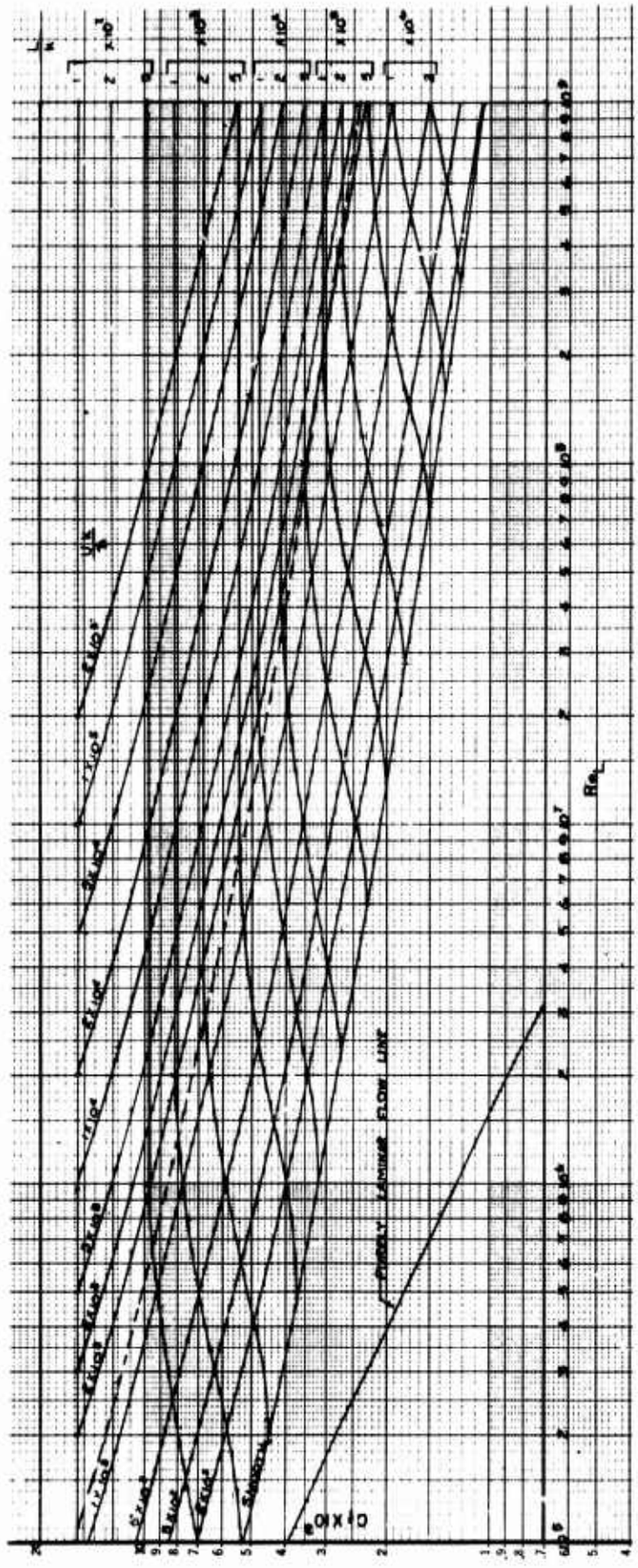

Fig. (2.3-45) Continued (5) M = 4.0

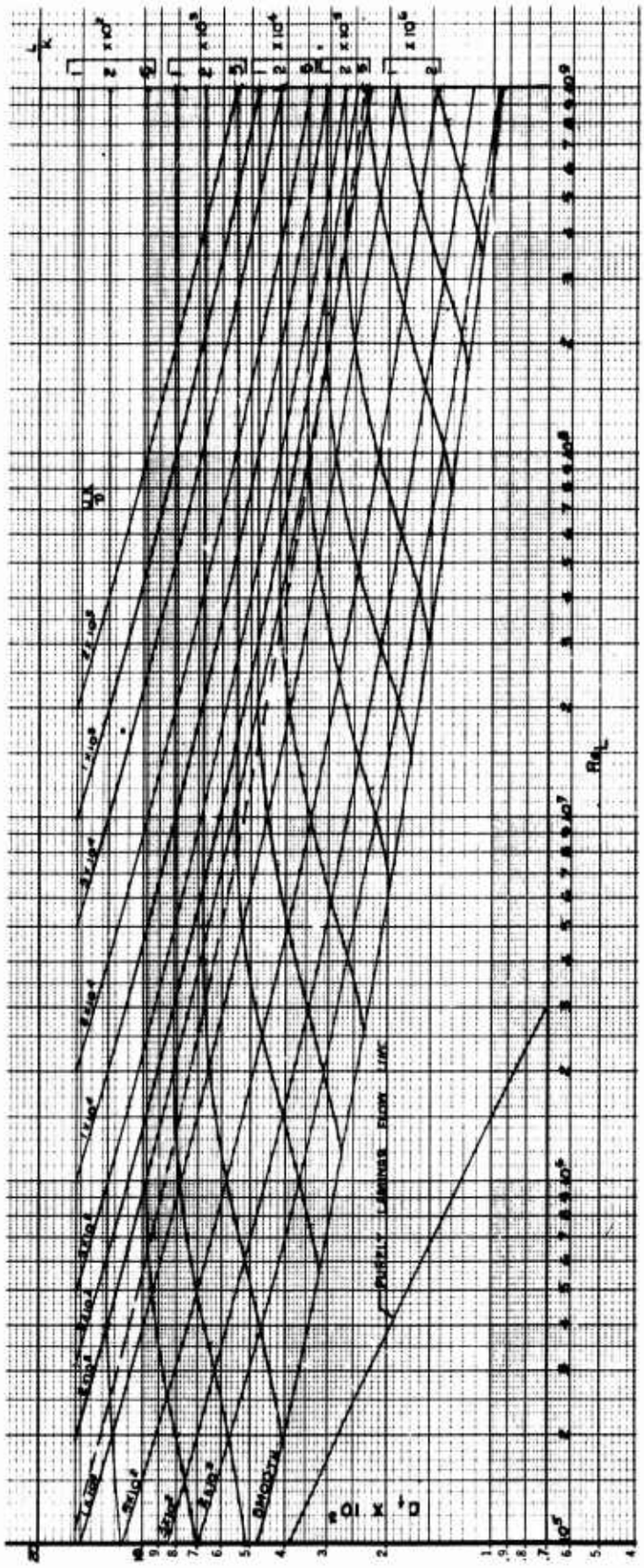

Fig. (2 3-45) Continued (6) M=50

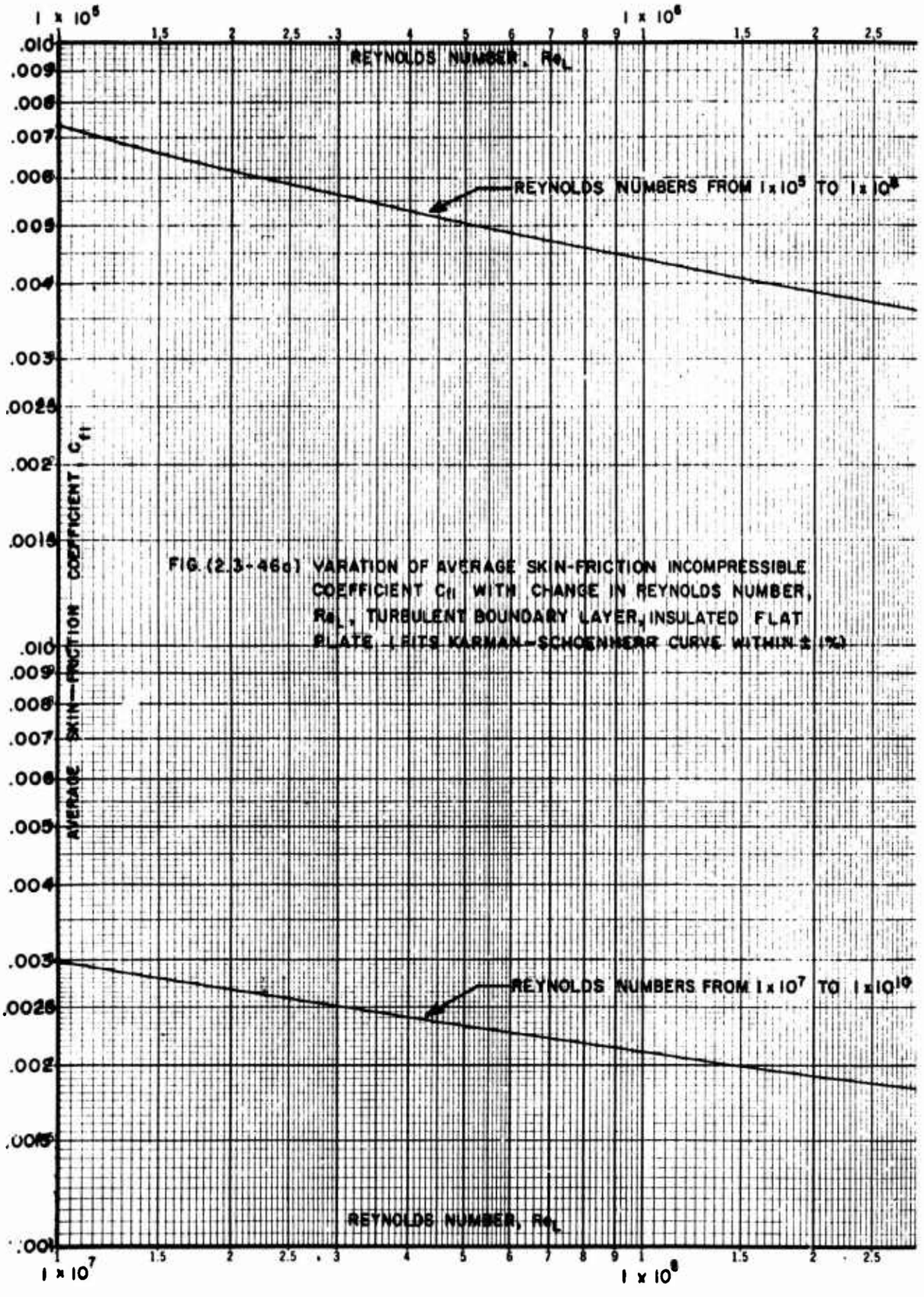

FIG. (2.3-46c) VARIATION OF AVERAGE SKIN-FRICTION INCOMPRESSIBLE COEFFICIENT C_{ff} WITH CHANGE IN REYNOLDS NUMBER, Re_L, TURBULENT BOUNDARY LAYER, INSULATED FLAT PLATE, (FITS KARMAN-SCHOENHERR CURVE WITHIN ± 1%)

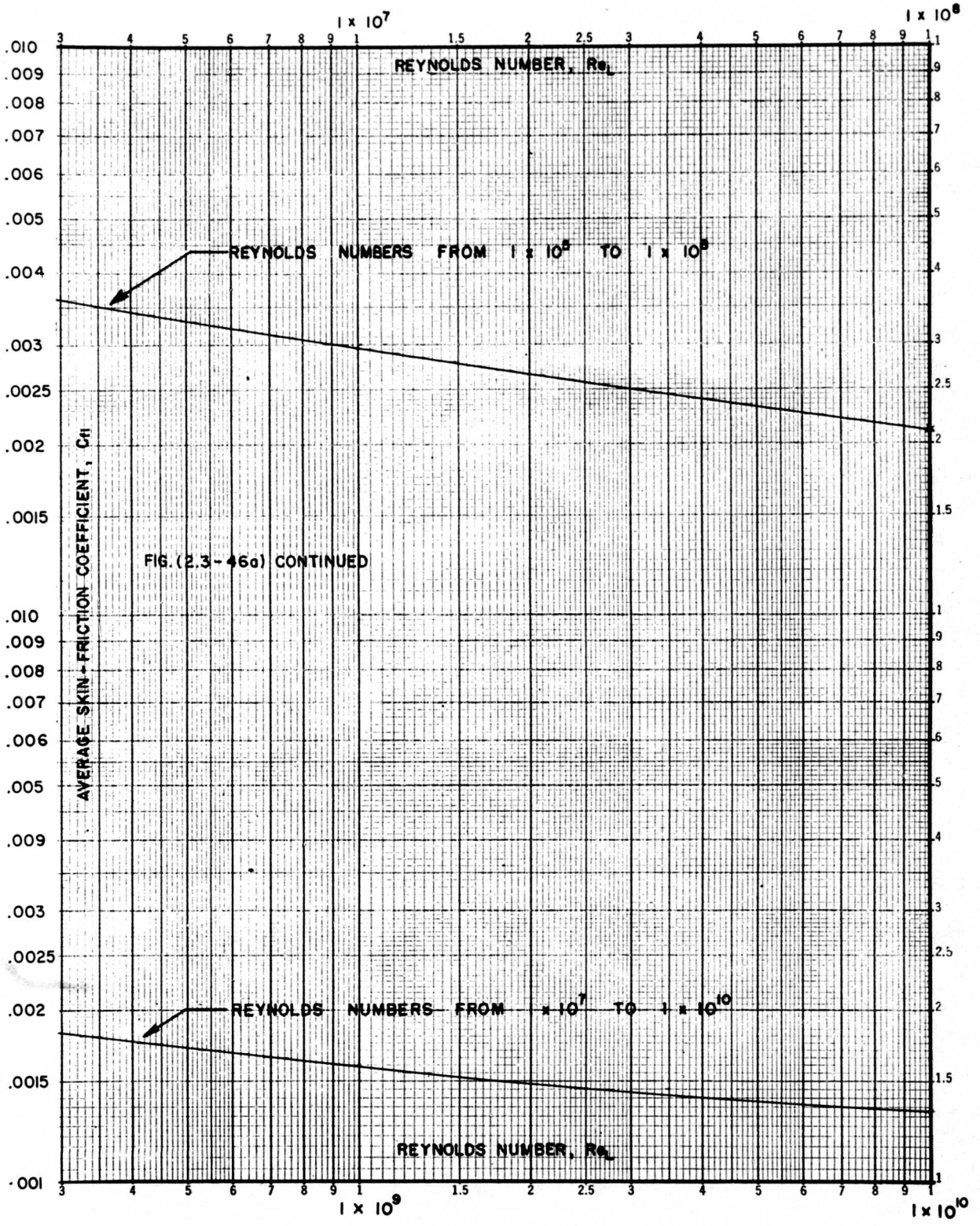

FIG. (2.3-46a) CONTINUED

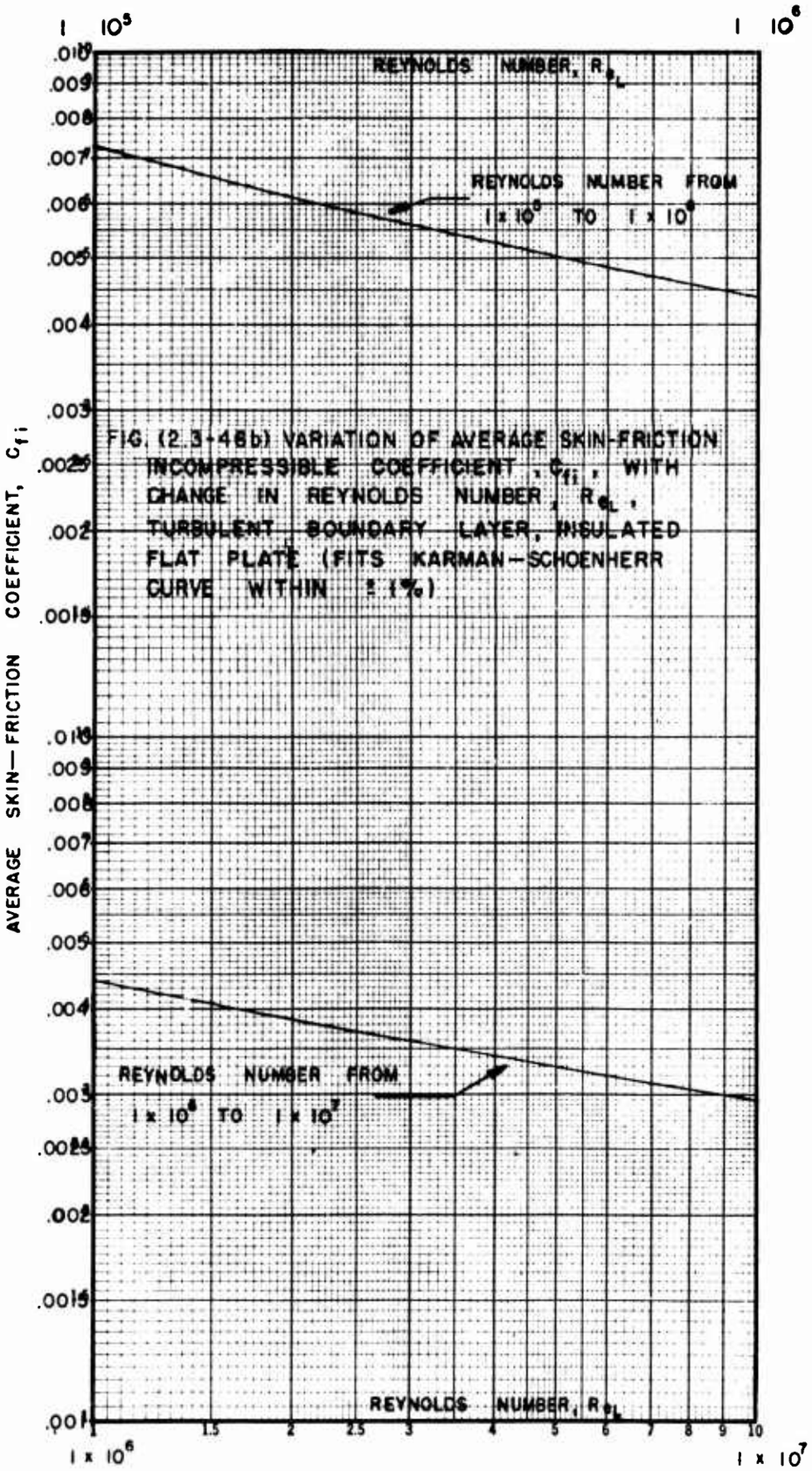

FIG. (2.3-46b) VARIATION OF AVERAGE SKIN-FRICTION INCOMPRESSIBLE COEFFICIENT, C_{fi}, WITH CHANGE IN REYNOLDS NUMBER, $R_{\theta L}$, TURBULENT BOUNDARY LAYER, INSULATED FLAT PLATE (FITS KARMAN-SCHOENHERR CURVE WITHIN ± 1%)

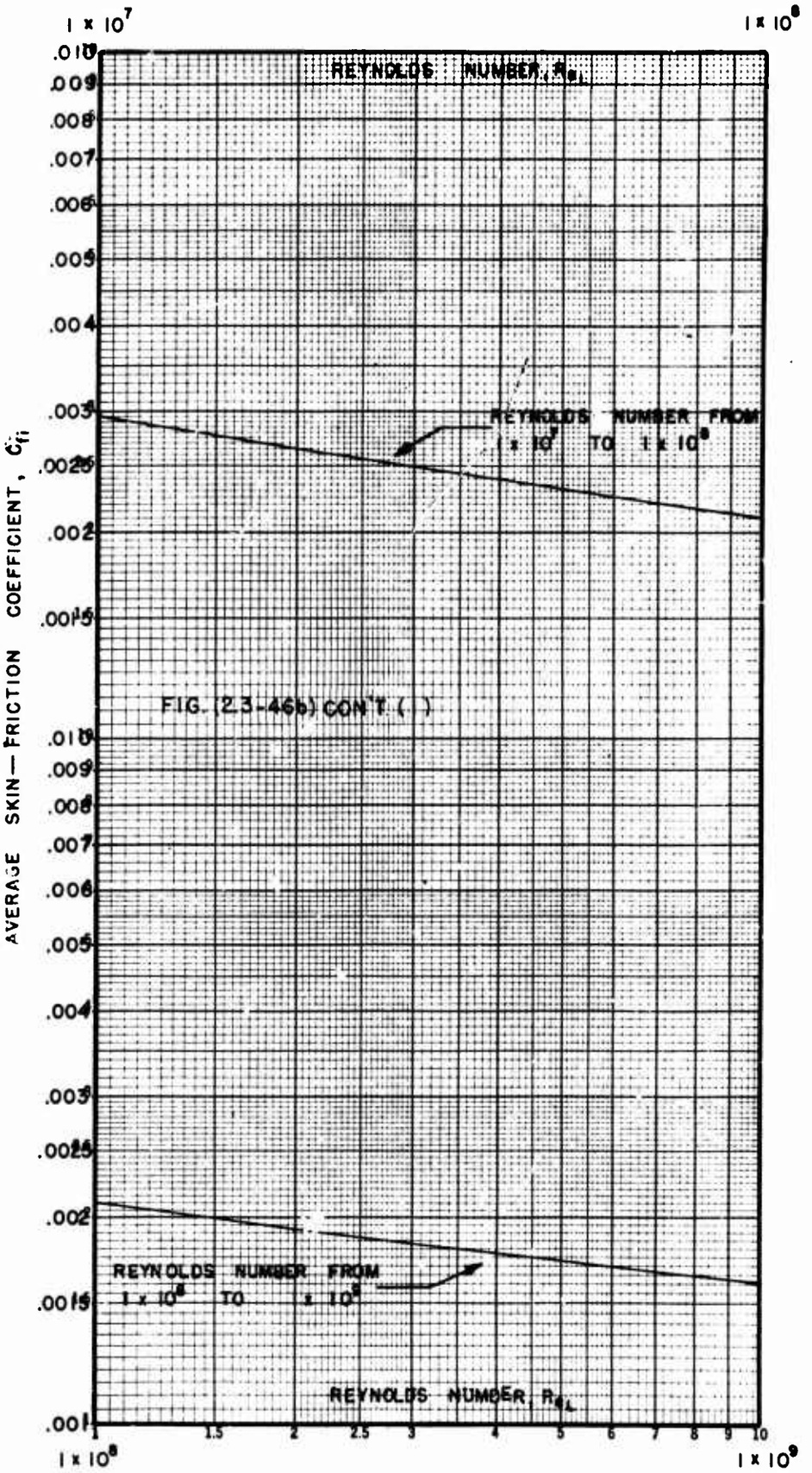
1 x 10^7
1 x 10^8
REYNOLDS NUMBER, R_{θ_L}
AVERAGE SKIN — FRICTION COEFFICIENT, C_{fi}
.010
.009
.008
.007
.006
.005
.004
.003
.0025
.002
.0015
.001
REYNOLDS NUMBER FROM 1 x 10^7 TO 1 x 10^8
FIG. (2.3-46b) CON'T. ( )
REYNOLDS NUMBER FROM 1 x 10^8 TO x 10^8
1
1.5
2
2.5
3
4
5
6
7
8
9
10
1 x 10^8
1 x 10^9

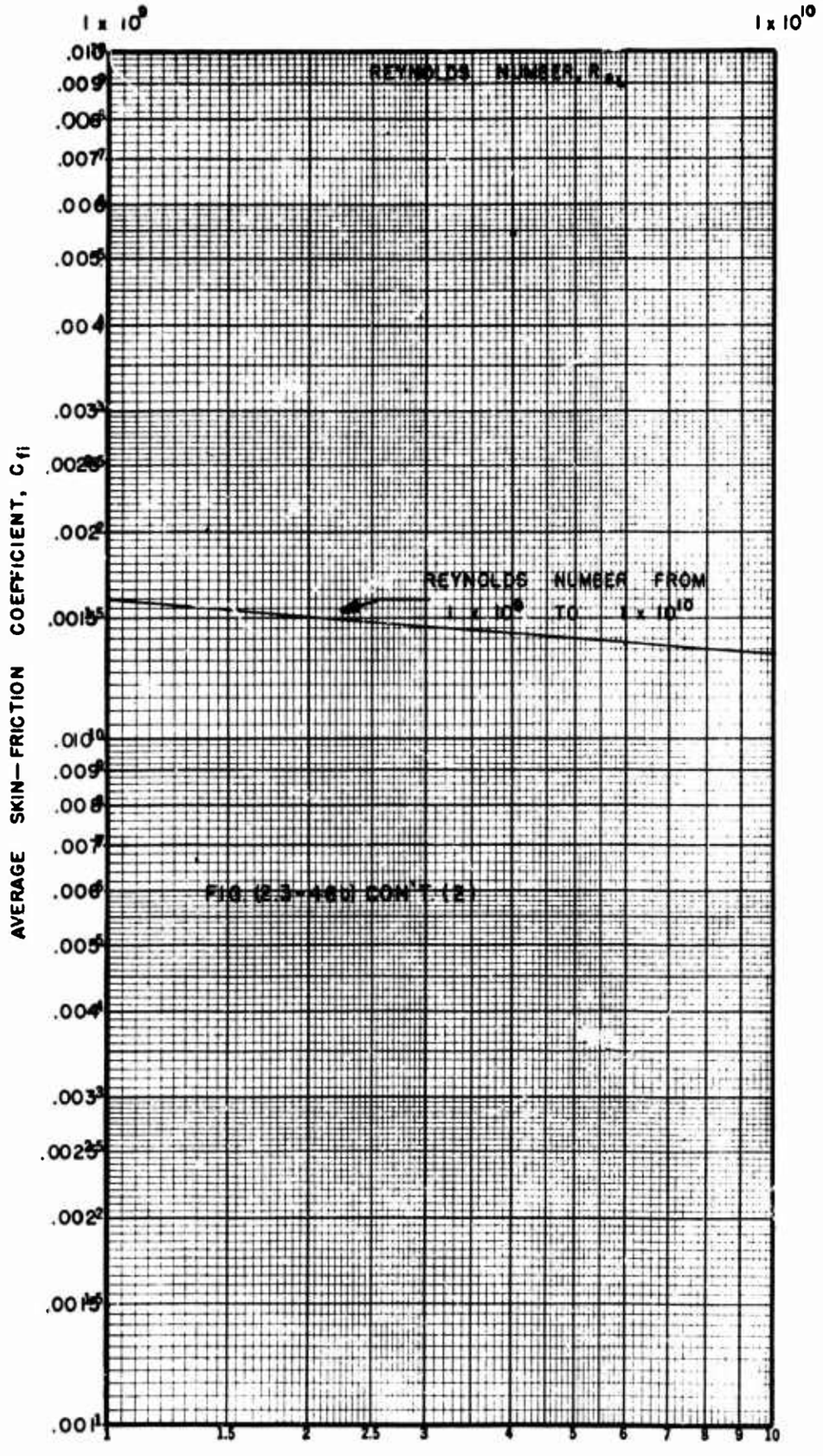
1 x 10^9
1 x 10^10
REYNOLDS NUMBER, R_ex
AVERAGE SKIN—FRICTION COEFFICIENT, C_fi
REYNOLDS NUMBER FROM 1 x 10^9 TO 1 x 10^10
FIG (2.3-46d) CON'T-(2)
.010
.009
.008
.007
.006
.005
.004
.003
.002
.001
1
1.5
2
2.5
3
4
5
6
7
8
9
10

Fig.(2.3-47) see Fig.(2.3-35)

Important note: Alternatively use Fig.(2.3-60) for Mach Numbers up to 20.

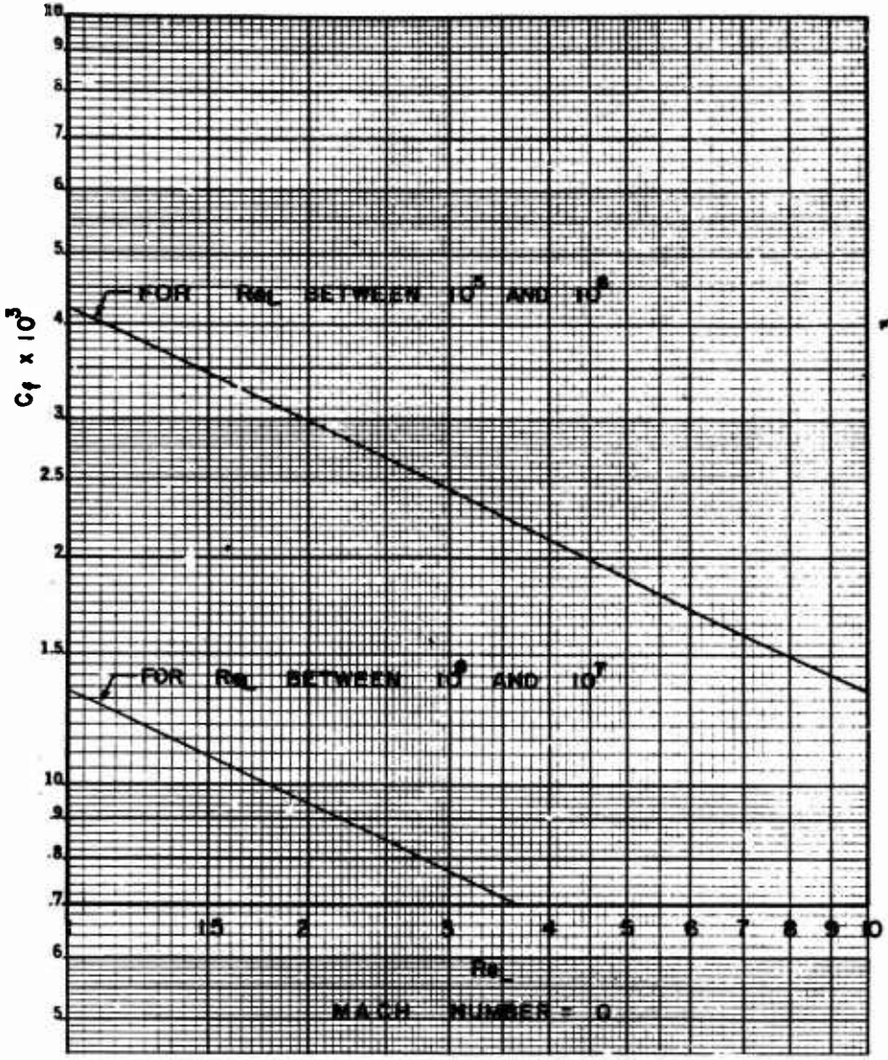

Fig. (2.3-48) Laminar boundrary layer (blasius), average skin friction coefficient, smooth, insulated flat plate, zero angle of attack.

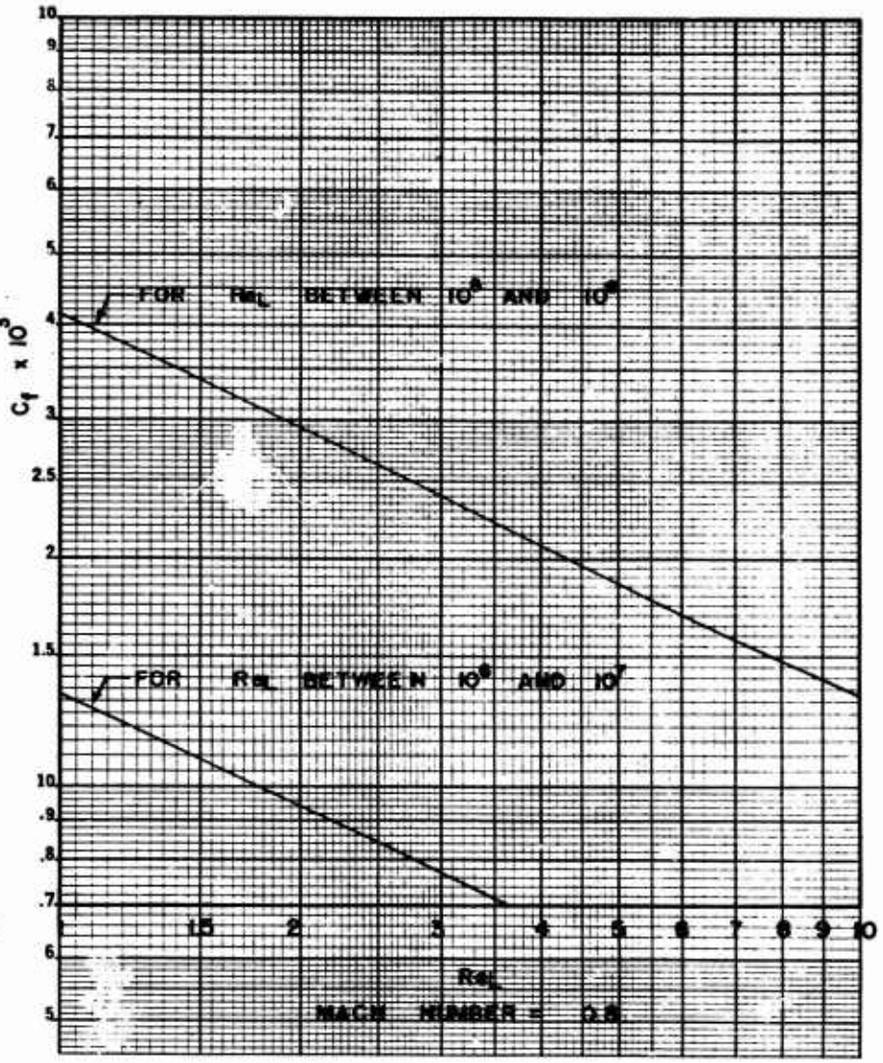

Fig. (2.3-48) continued (1)

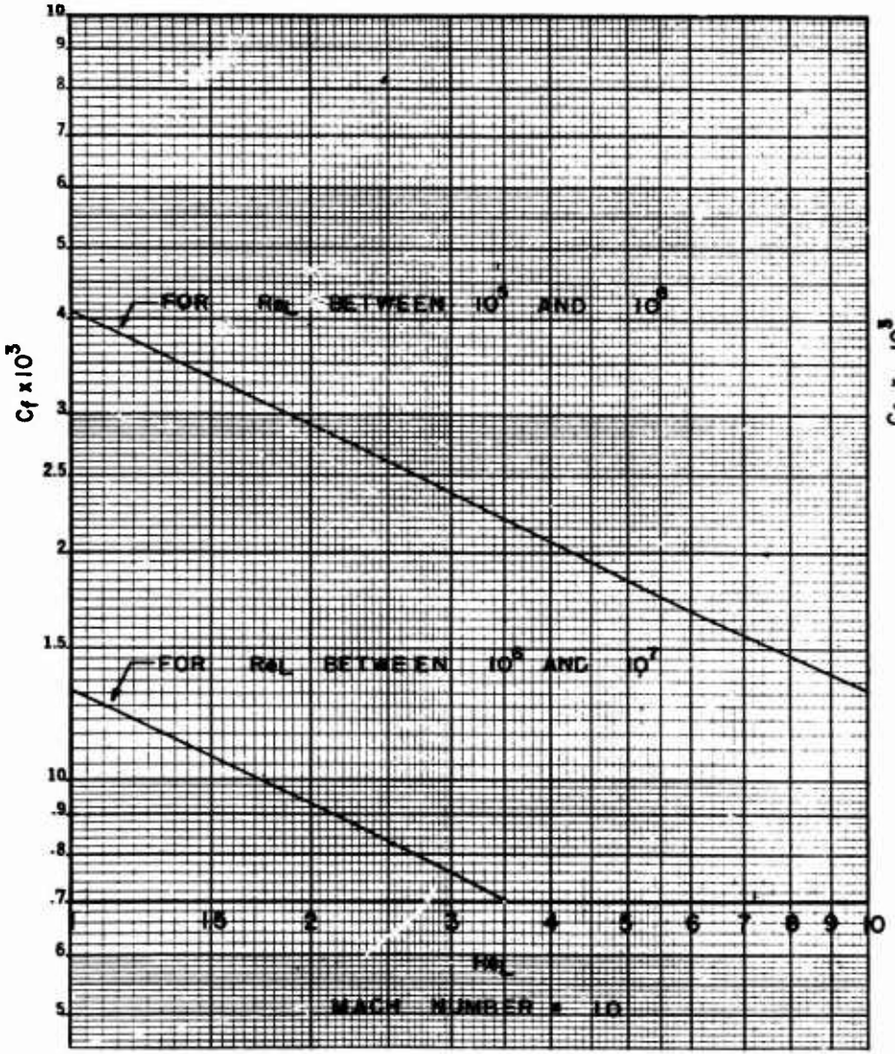

Fig. (2.3-48) continued (2)

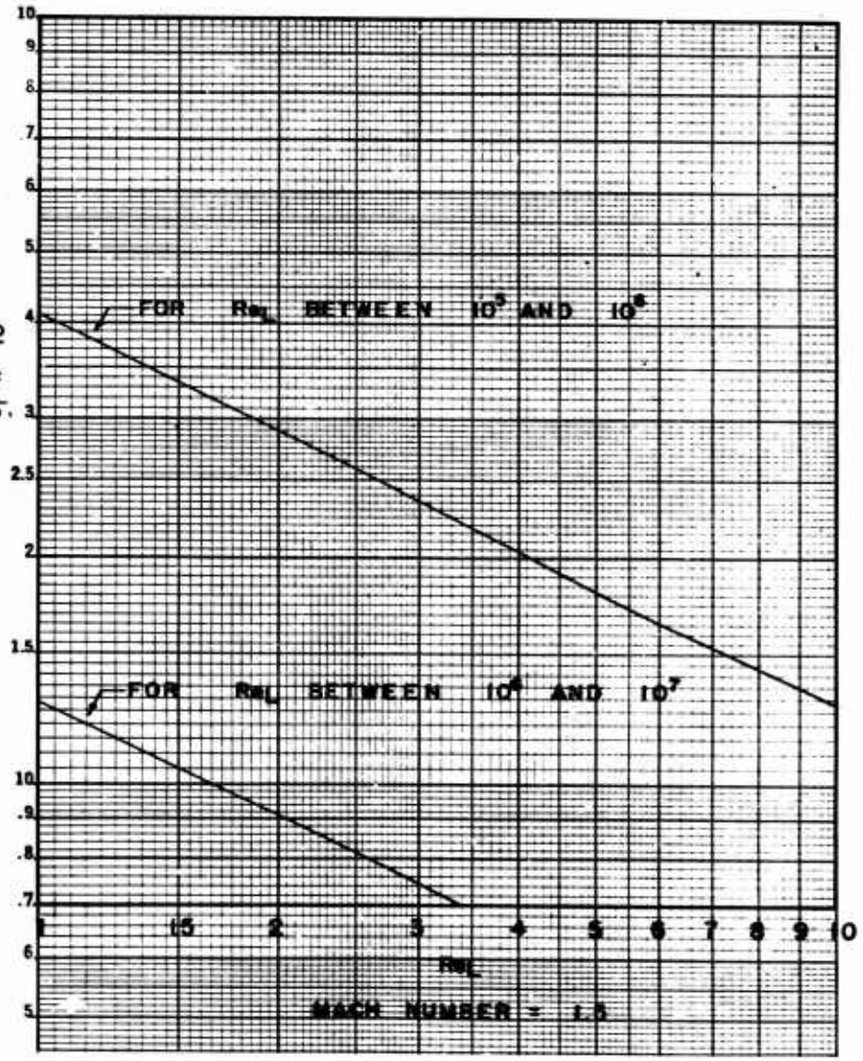

Fig. (2.3-48) continued (3)

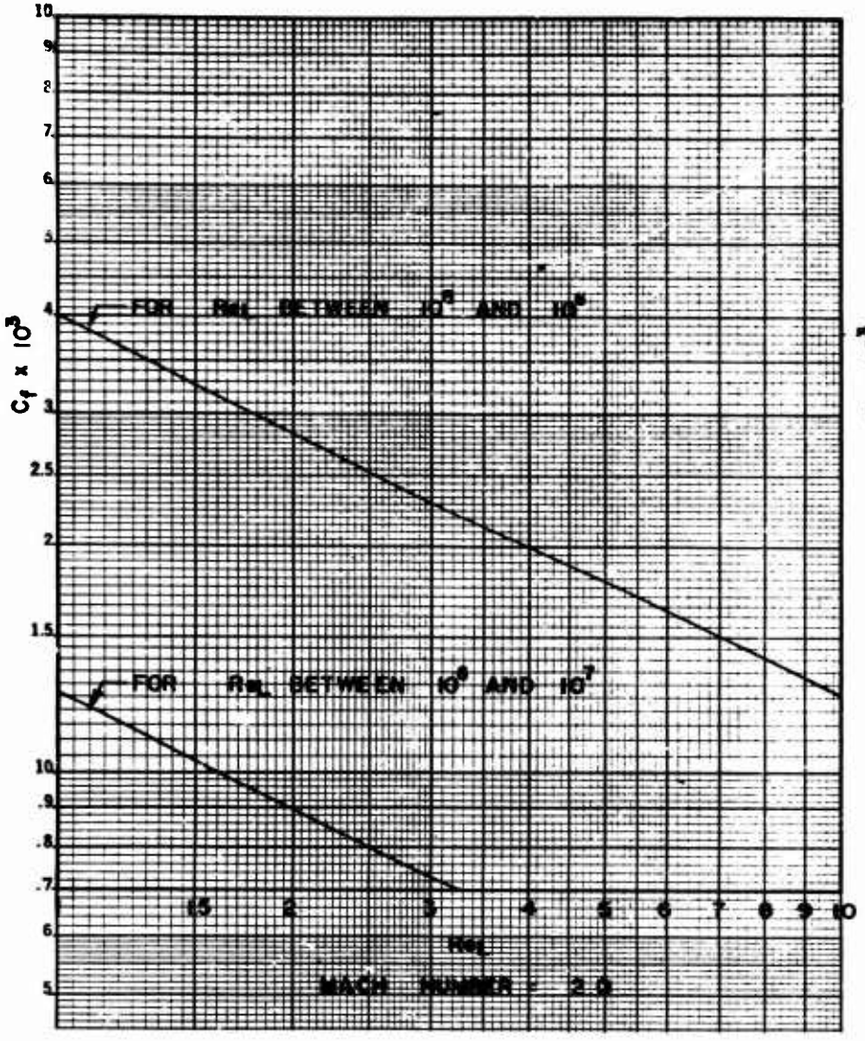

Fig. (2.3-48) continued (4)

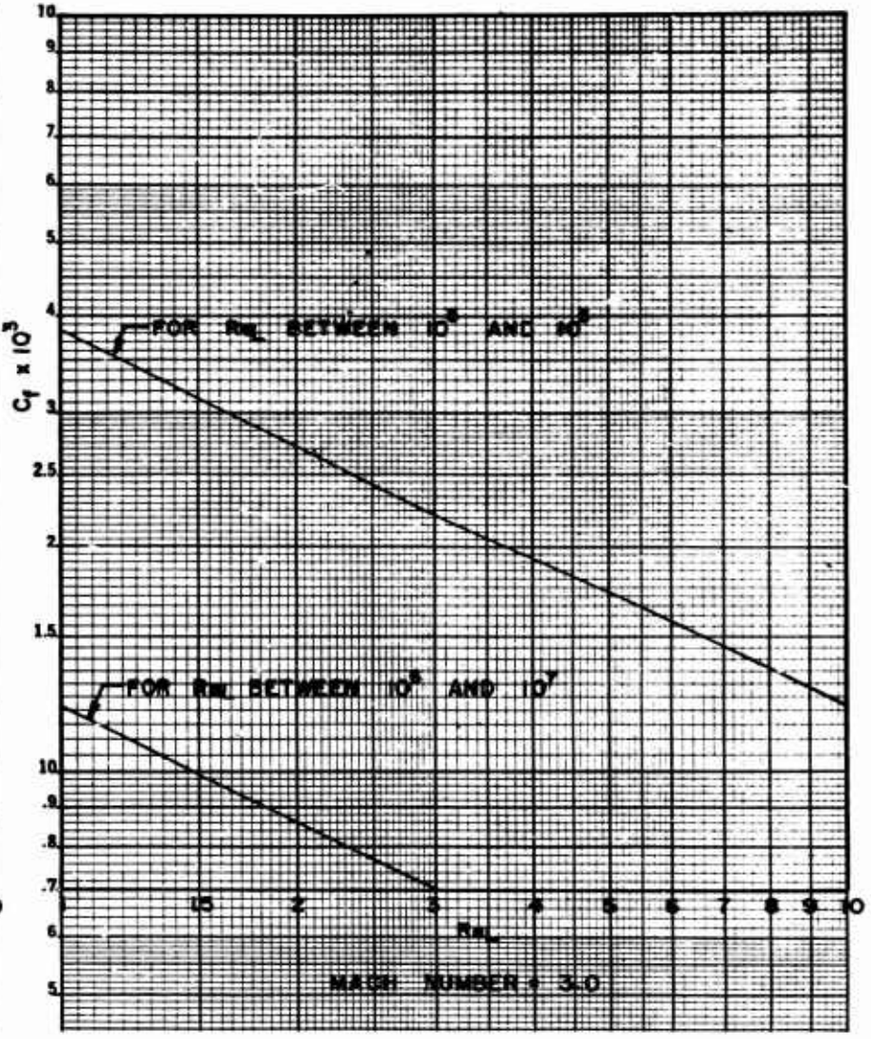

Fig. (2.3-48) continued (5)

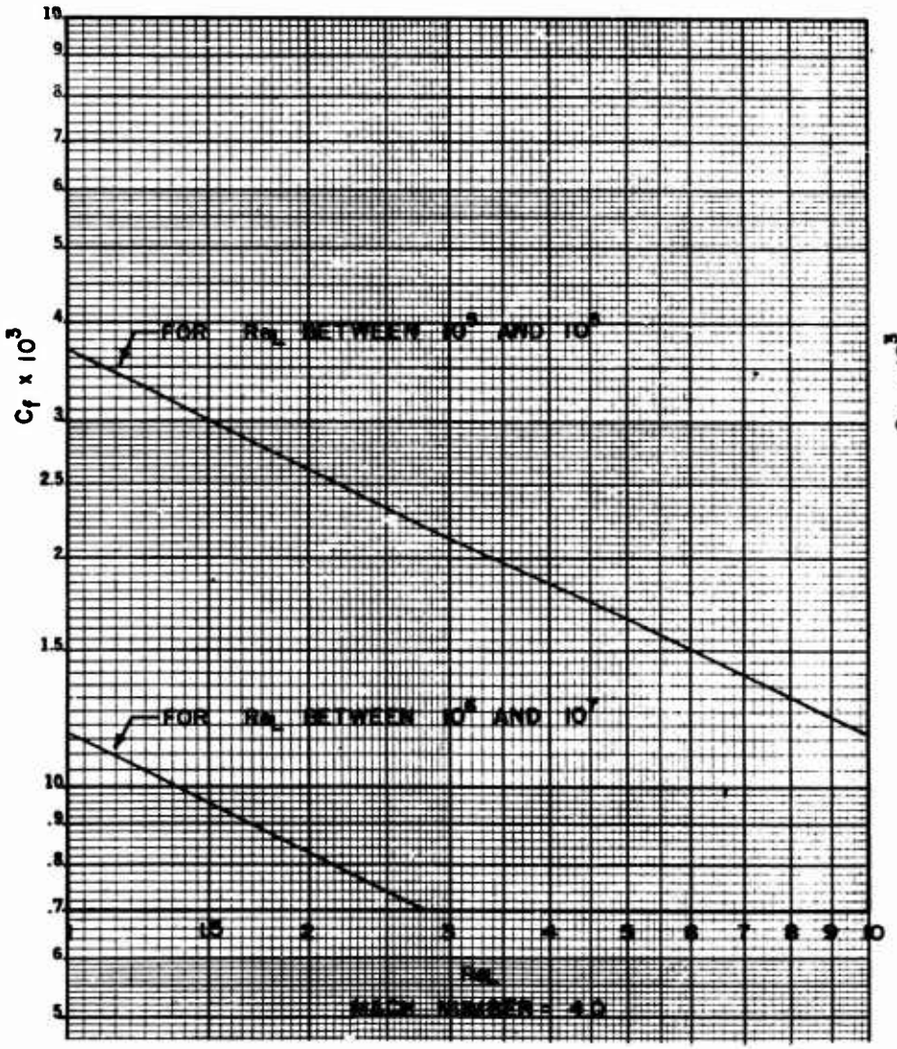

Fig. (2.3-48) continued (6)

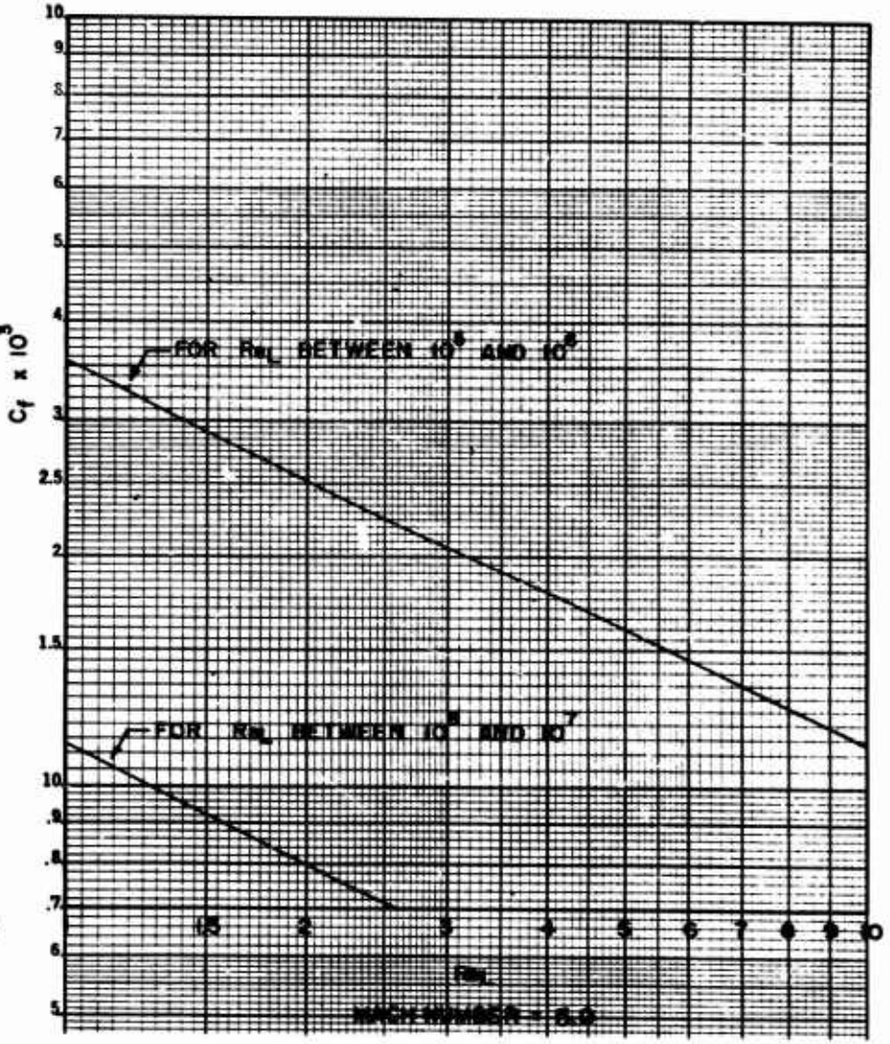

Fig. (2.3-48) continued (7)

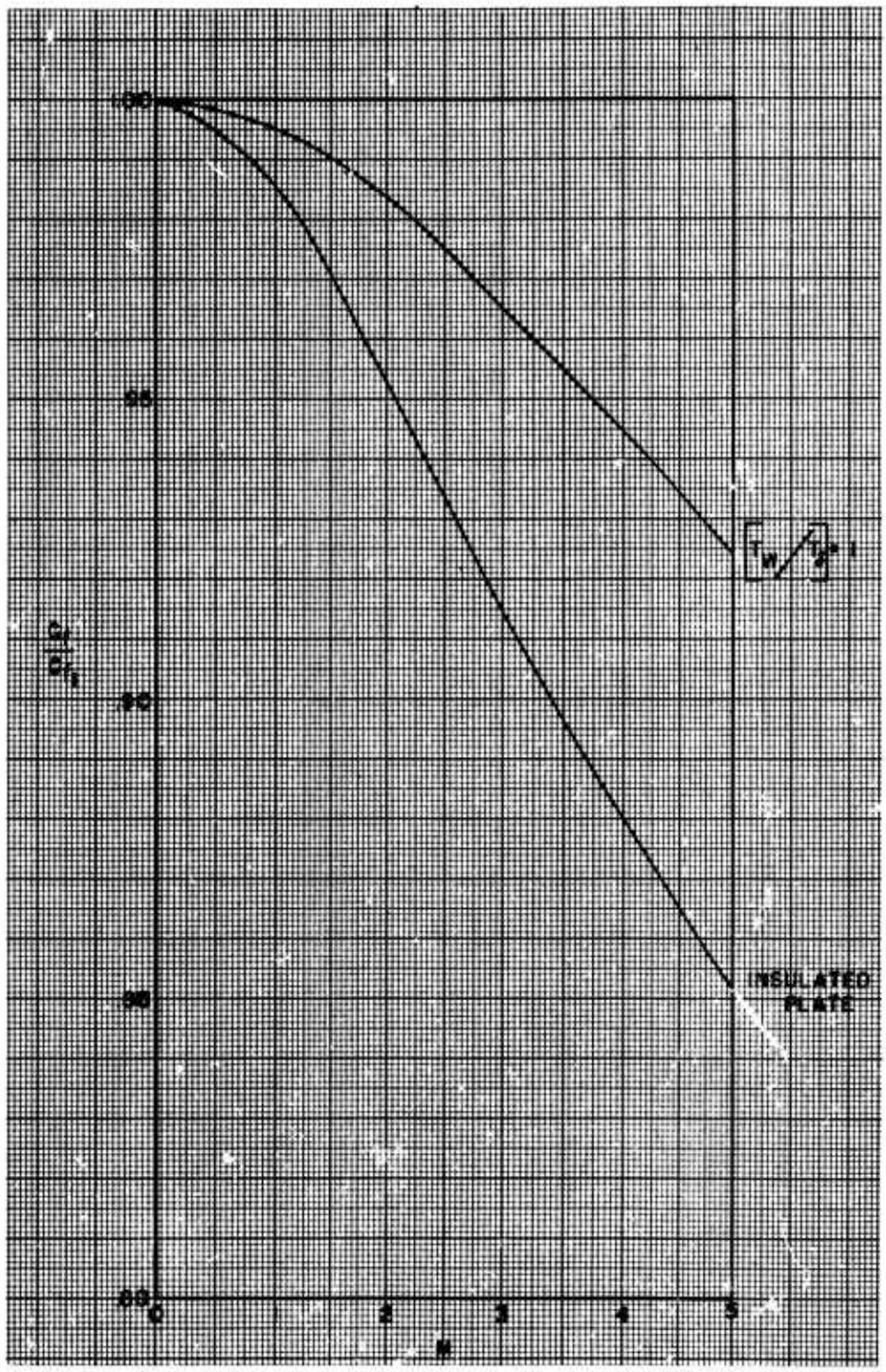

Fig. (2.3-49) Mach number variation of the ratio of the incompressible values of skin-friction coefficient for laminar flow with and without heat transfer. (Ref. 127).

Fig. (2.3-50) see Fig. (2.3-32)

Fig. (2 3-51) see Fig. (2.3-33)

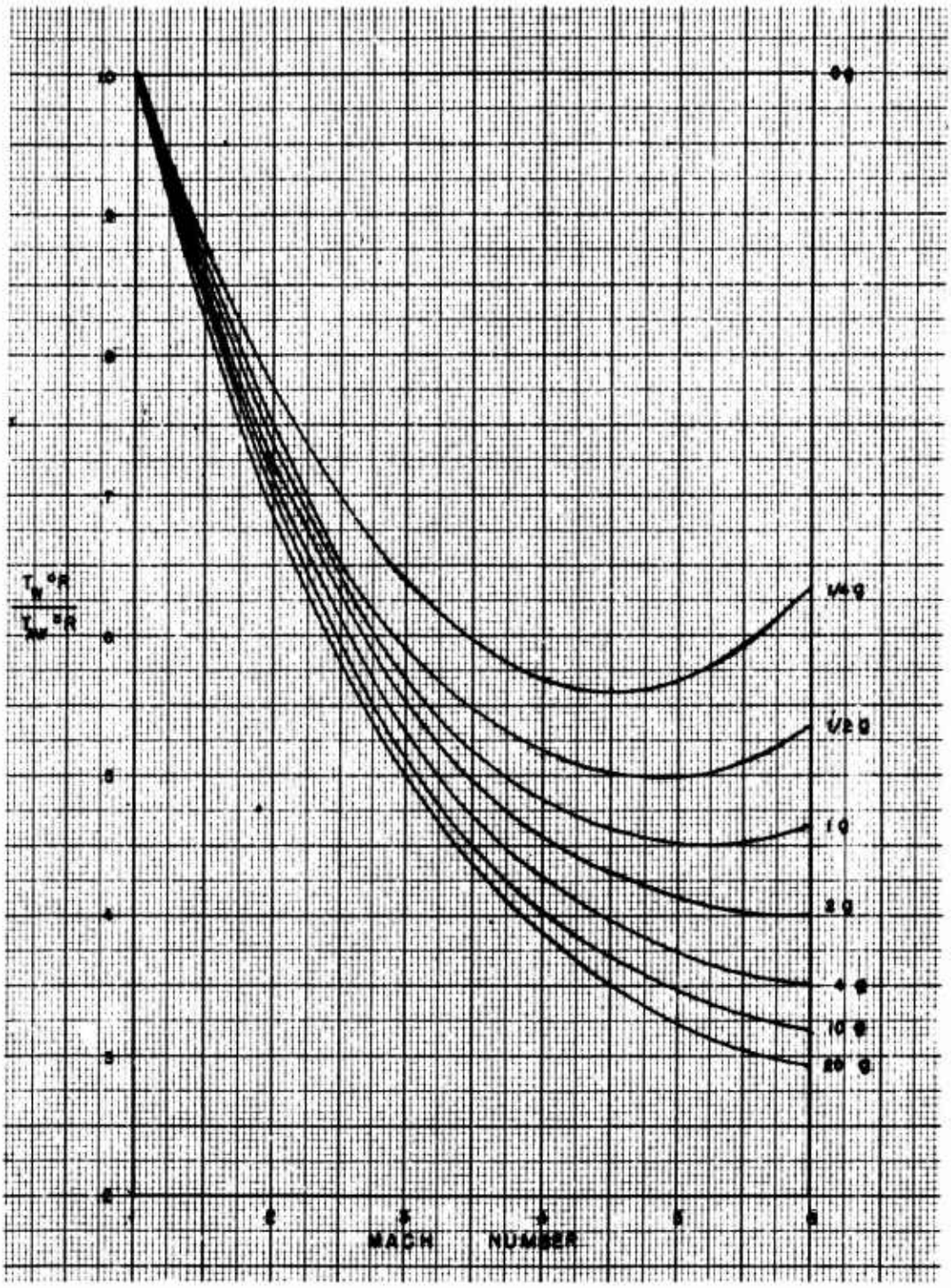

Fig. (2.3-52) Temperature ratio vs. Mach Number for non insulated skins, accelerations from 0g to 20g. (Ref. 70).

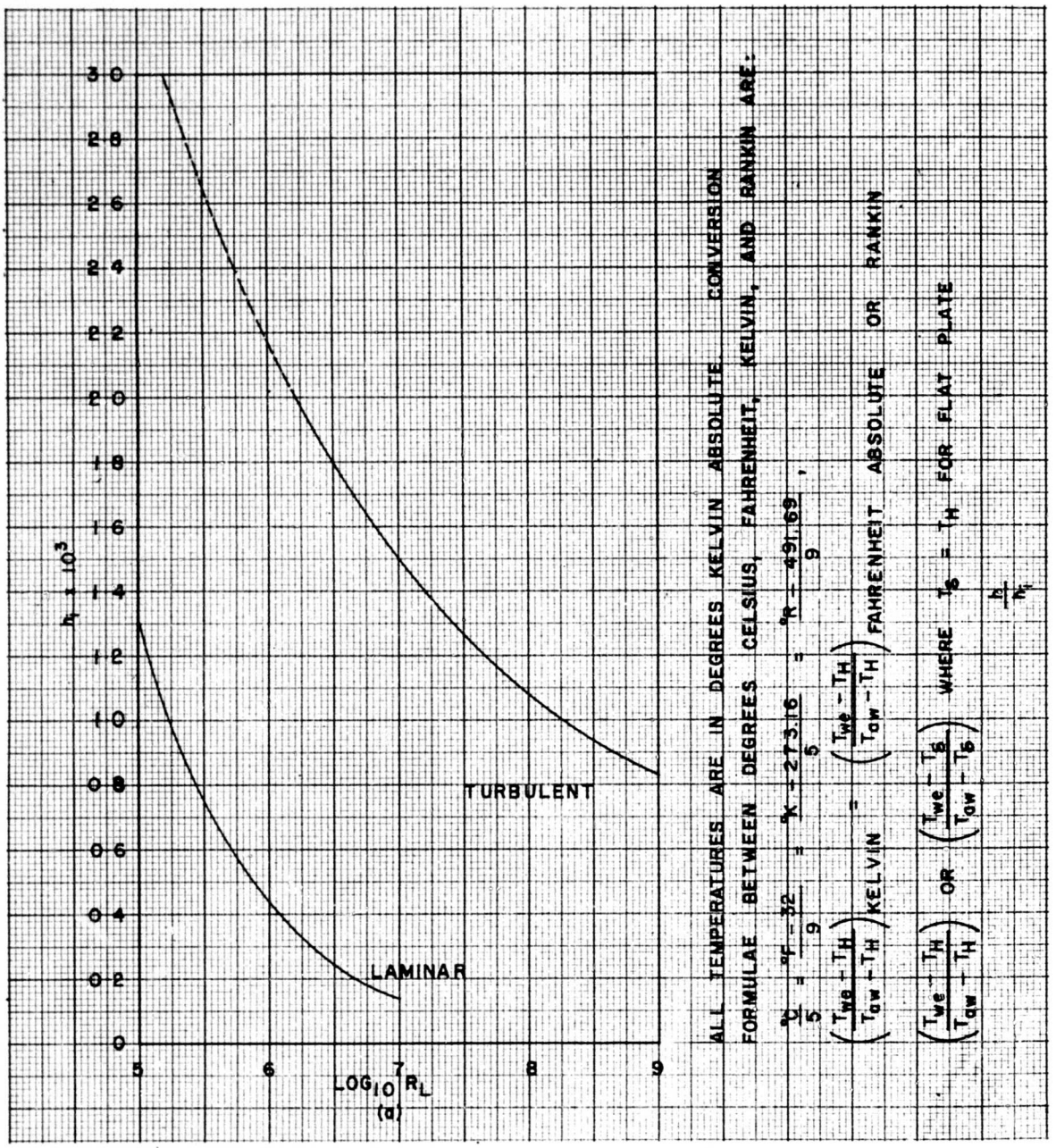

Fig. (2.3-53) Heat transfer coefficients for laminar and turbulent boundry layers. (Ref. 132 R.A.S. Data Sheets, Areodynamics, Vol. I, S.00.03.19)

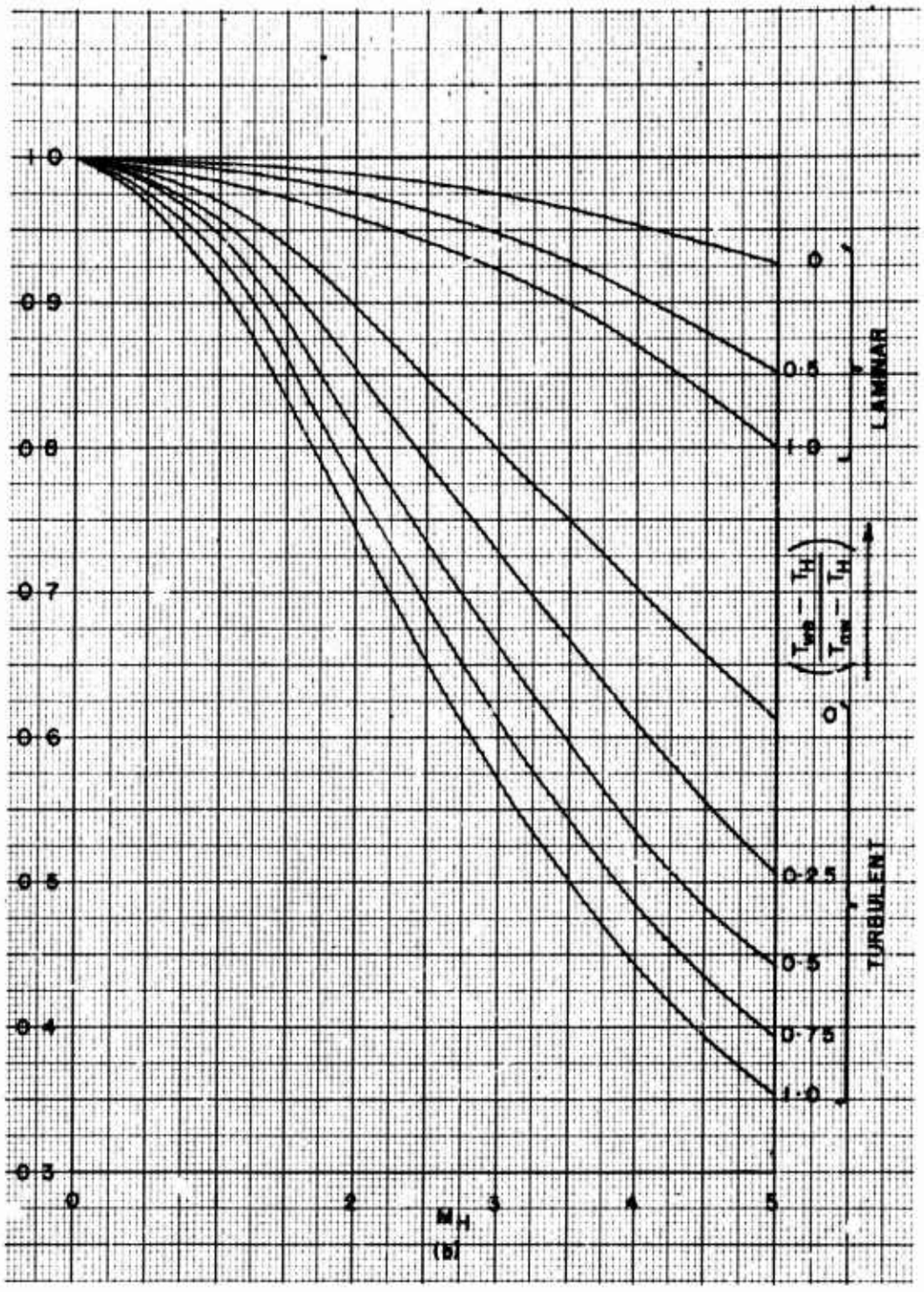

Fig. (2.3-53) Continued.

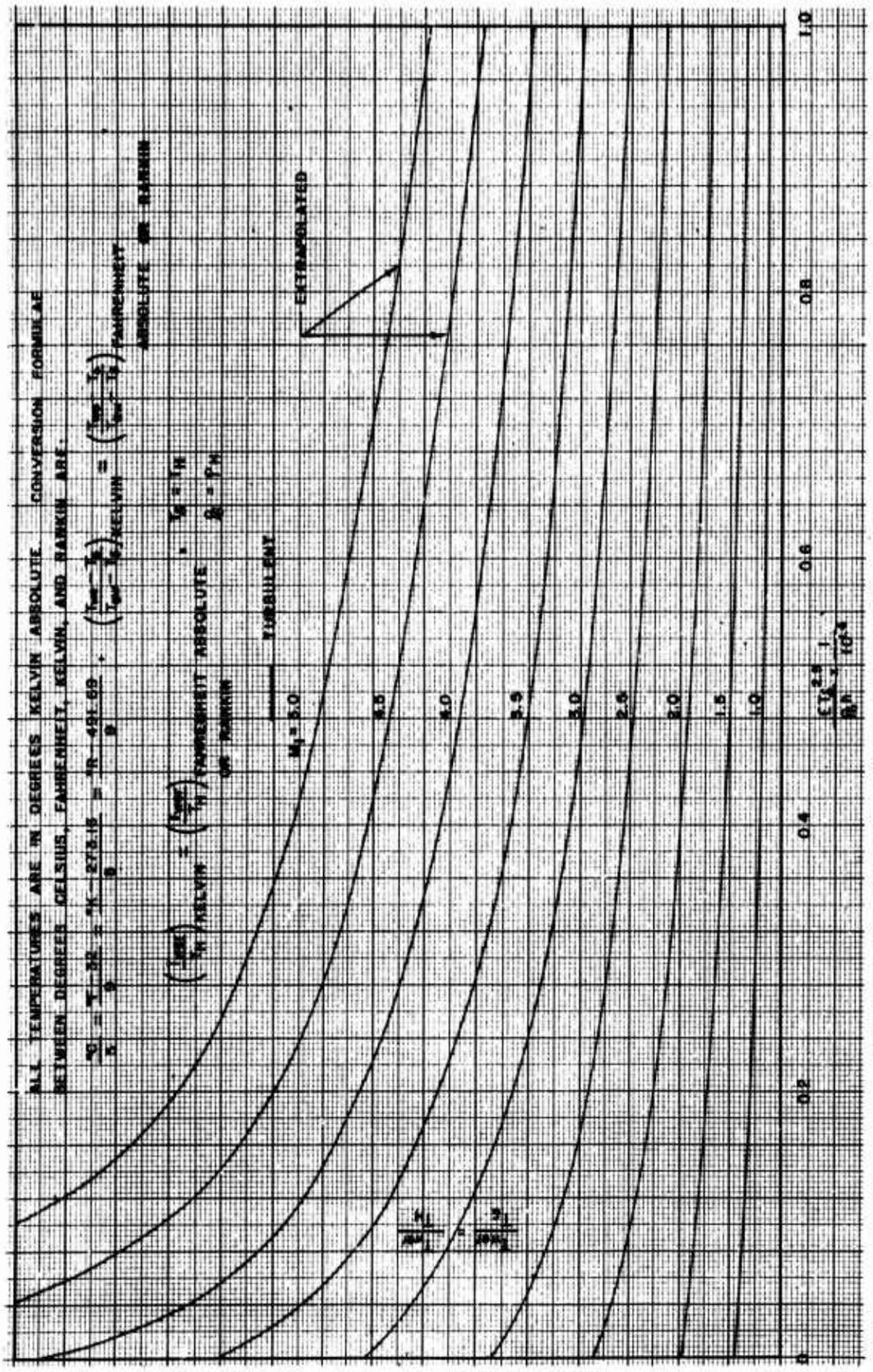

Fig. (2.3-54a) Determination of equilibrium temperatures with radiation.
(Ref. 132, R.A.S. Data Sheets, Aerodynamics, Vol I, S.00.03.20) – Turbulent B.L.
(See Table 2.3-2)

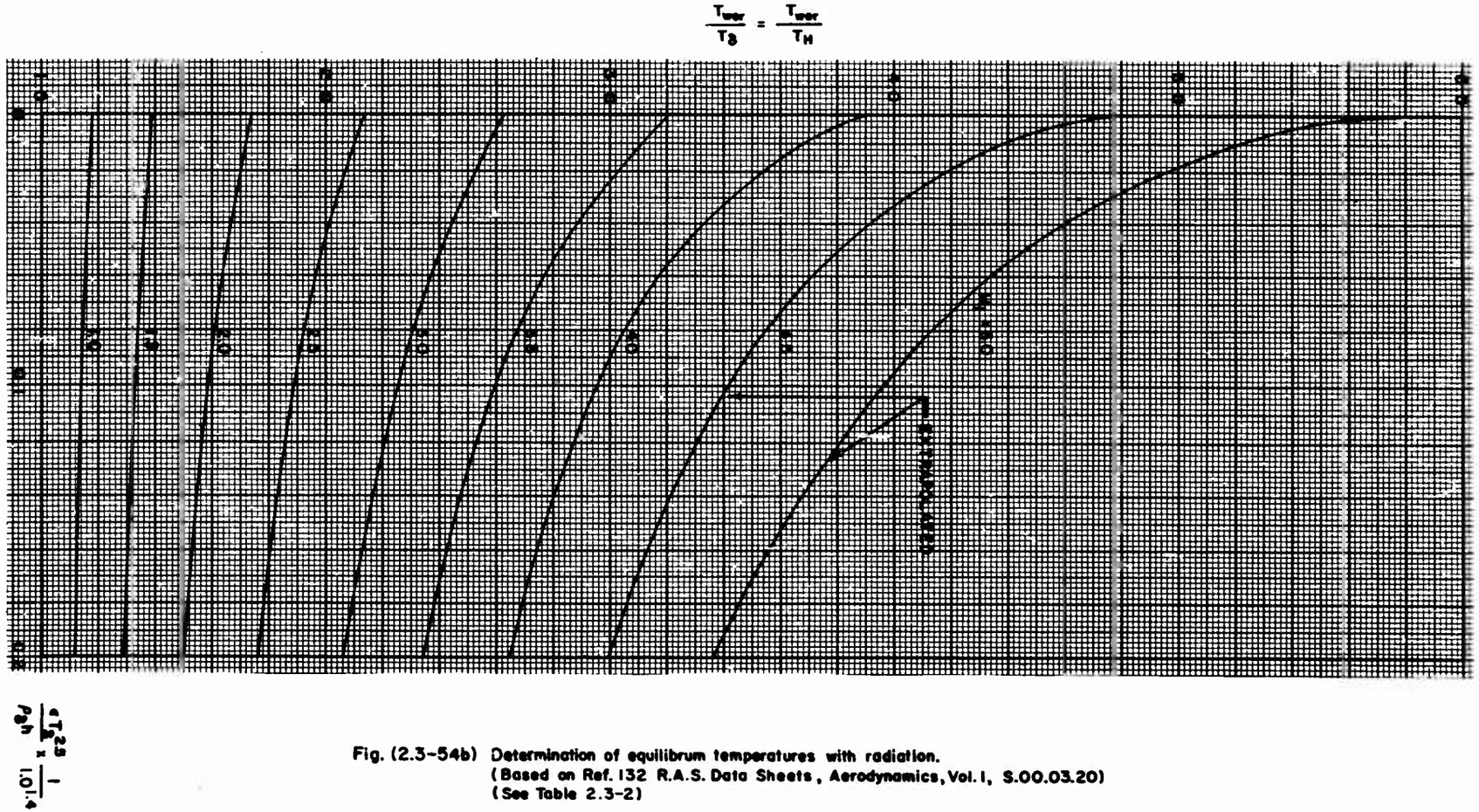

Fig. (2.3-54b) Determination of equilibrum temperatures with radiation.
(Based on Ref. 132 R.A.S. Data Sheets, Aerodynamics, Vol. I, S.00.03.20)
(See Table 2.3-2)

$$°R = \frac{9}{5}\,°K = F + 459.69$$

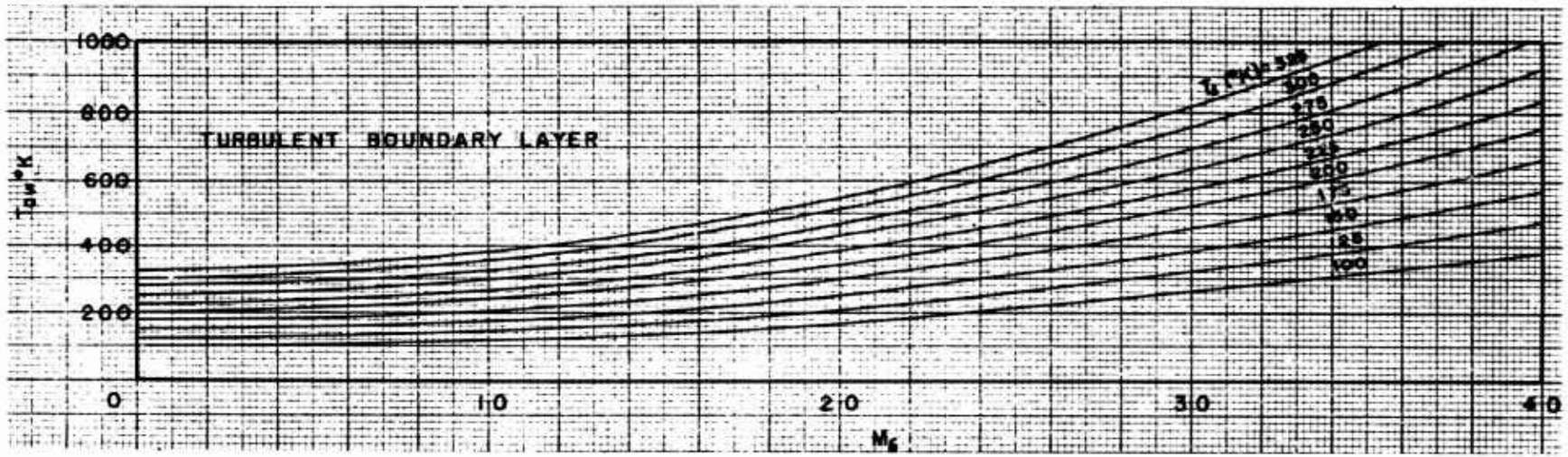

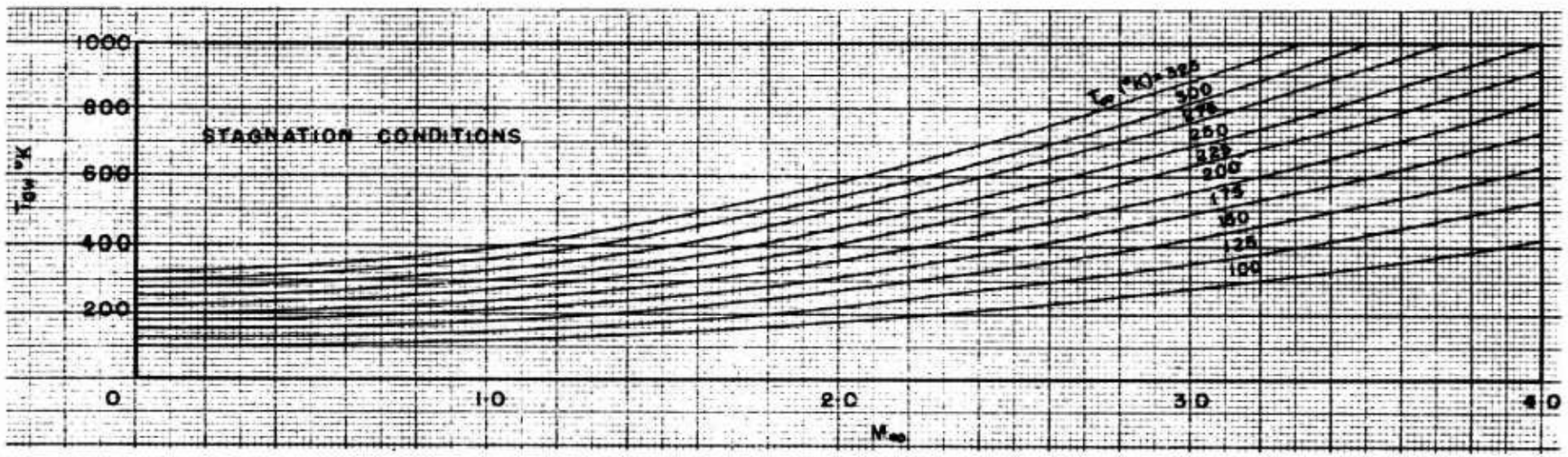

Fig. (2.3-55) Temperatures at a perfectly insulated surface, neglecting radiation.
(Ref. R.A.S. Data Sheets, Aerodynamics, Vol. I, S.00.03.18)

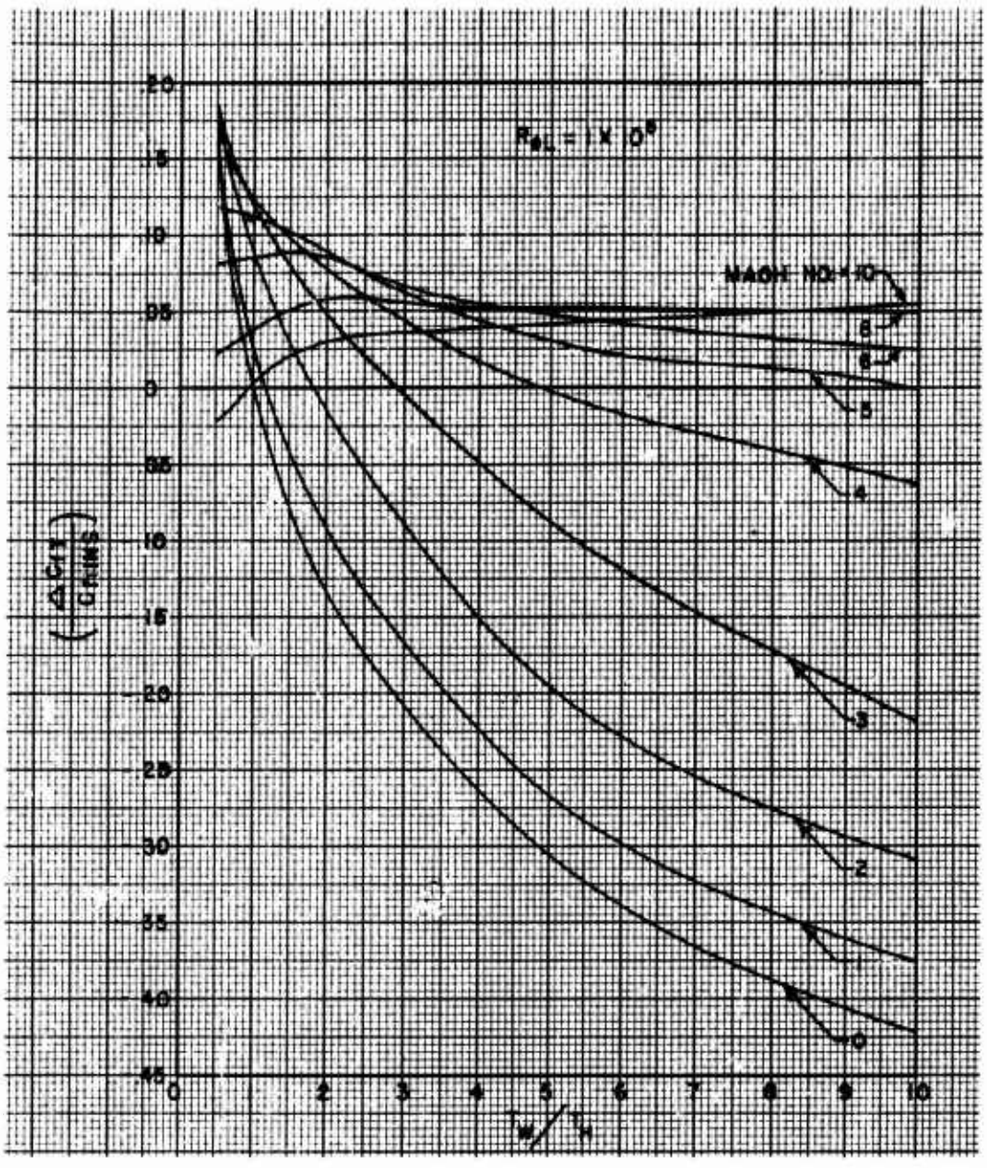

Fig (2.3-56) Skin-friction coefficient increment over its incompressible insulated value, due to actual skin temperature condition. Repilot from Fig (2.3-57)

Average values, T.B.L.

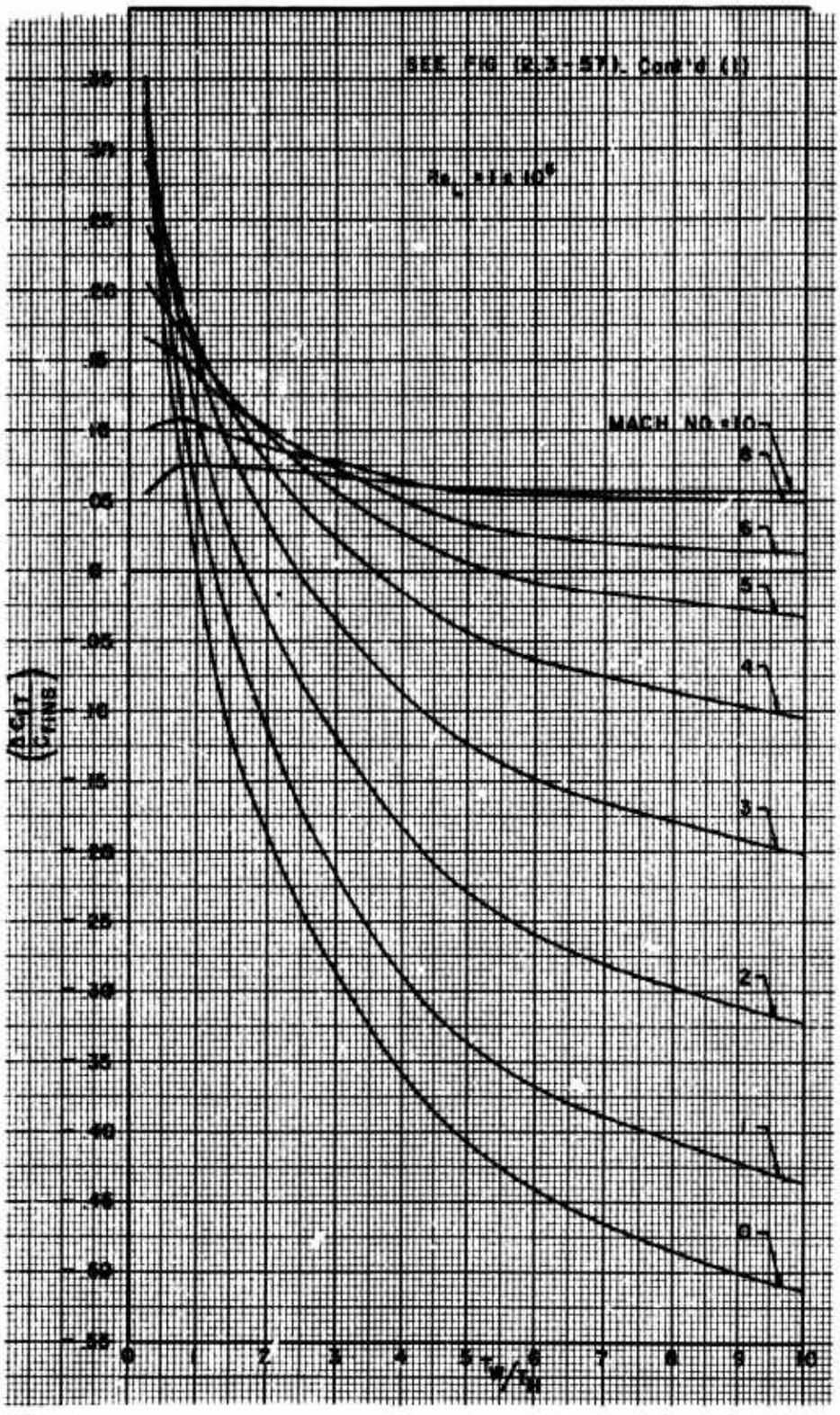

Fig (2.3-56) Continued (1)

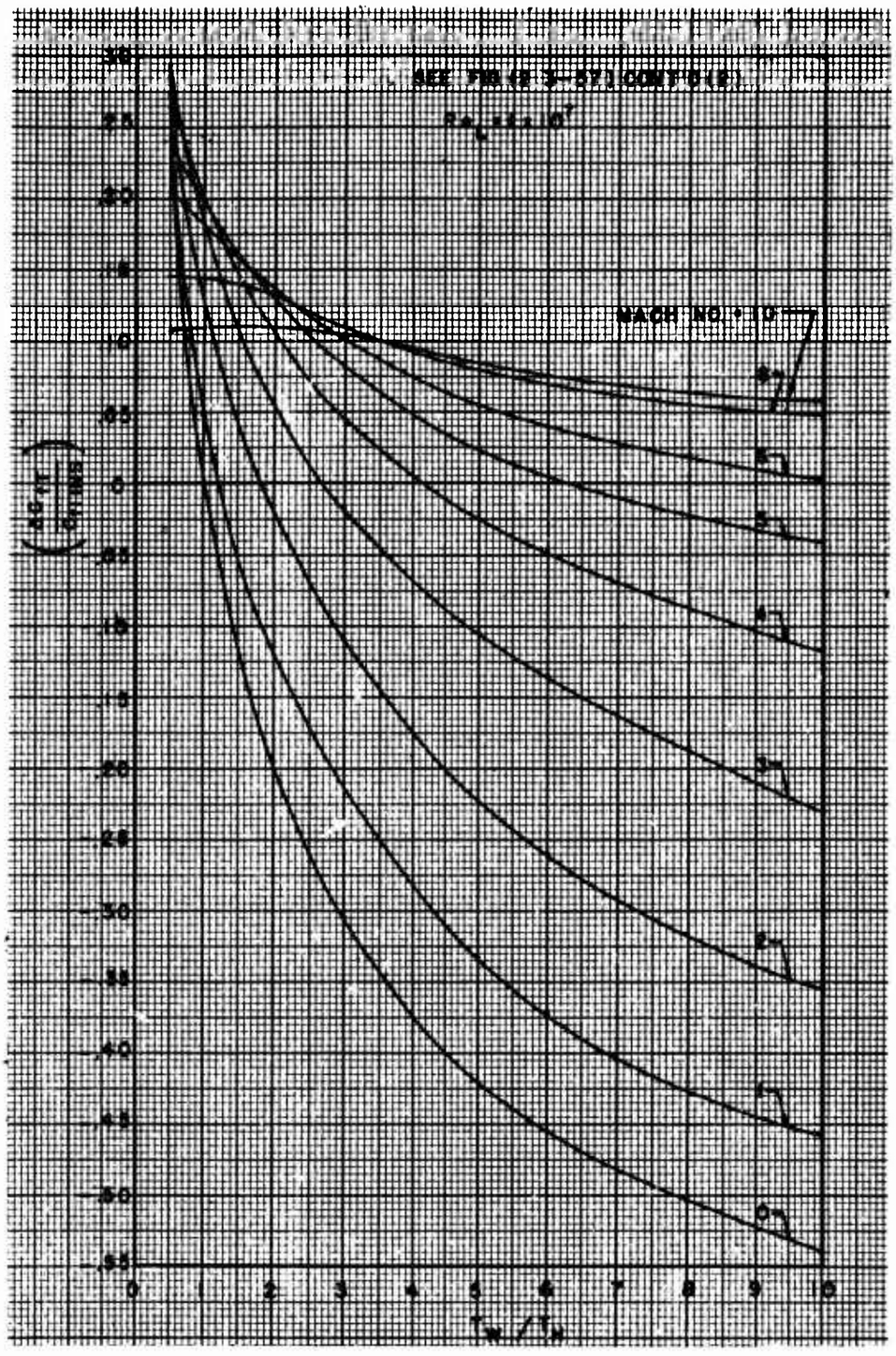

Fig (2.3-56) Continued (2)

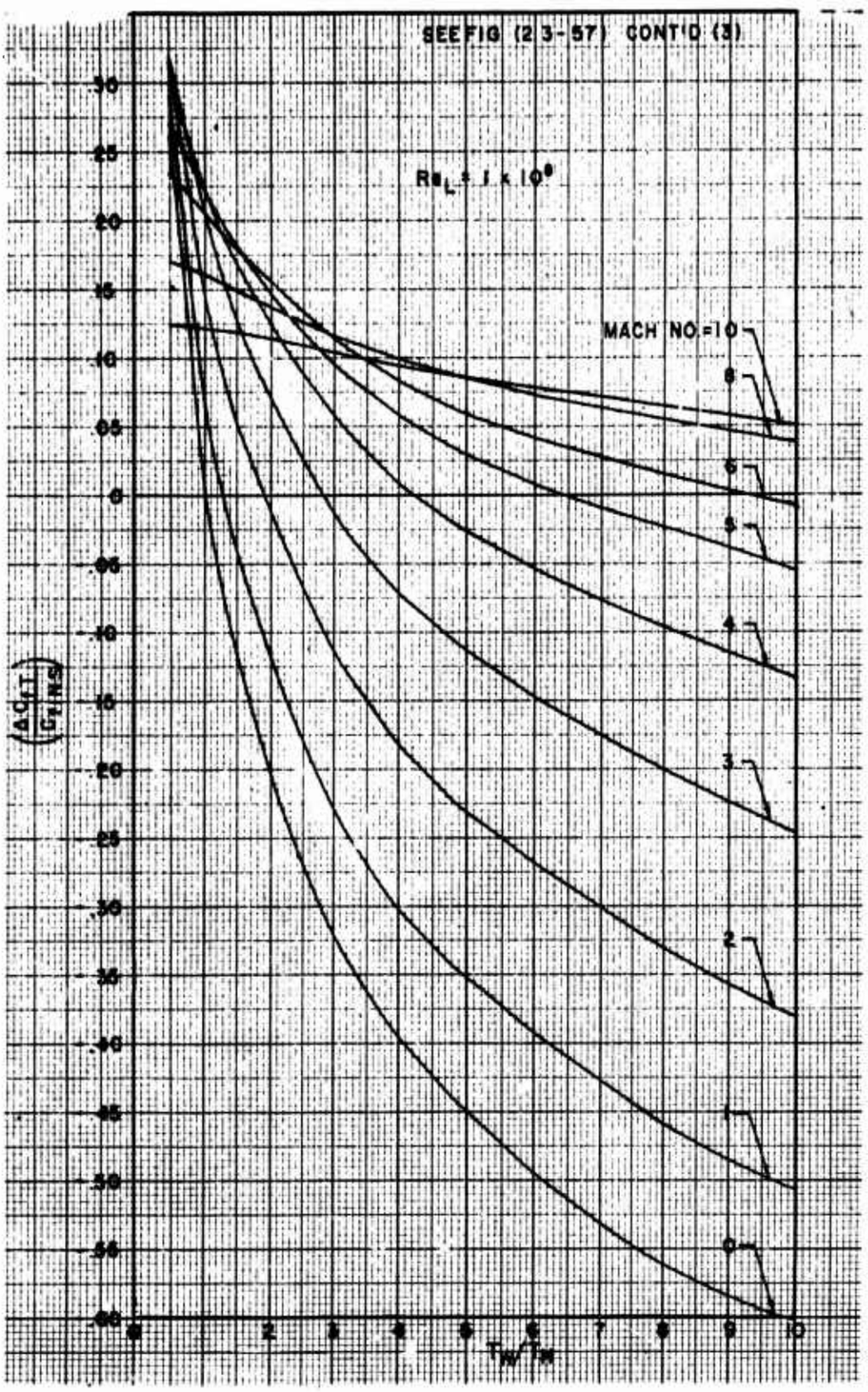

Fig (2.3-56) Continued (3)

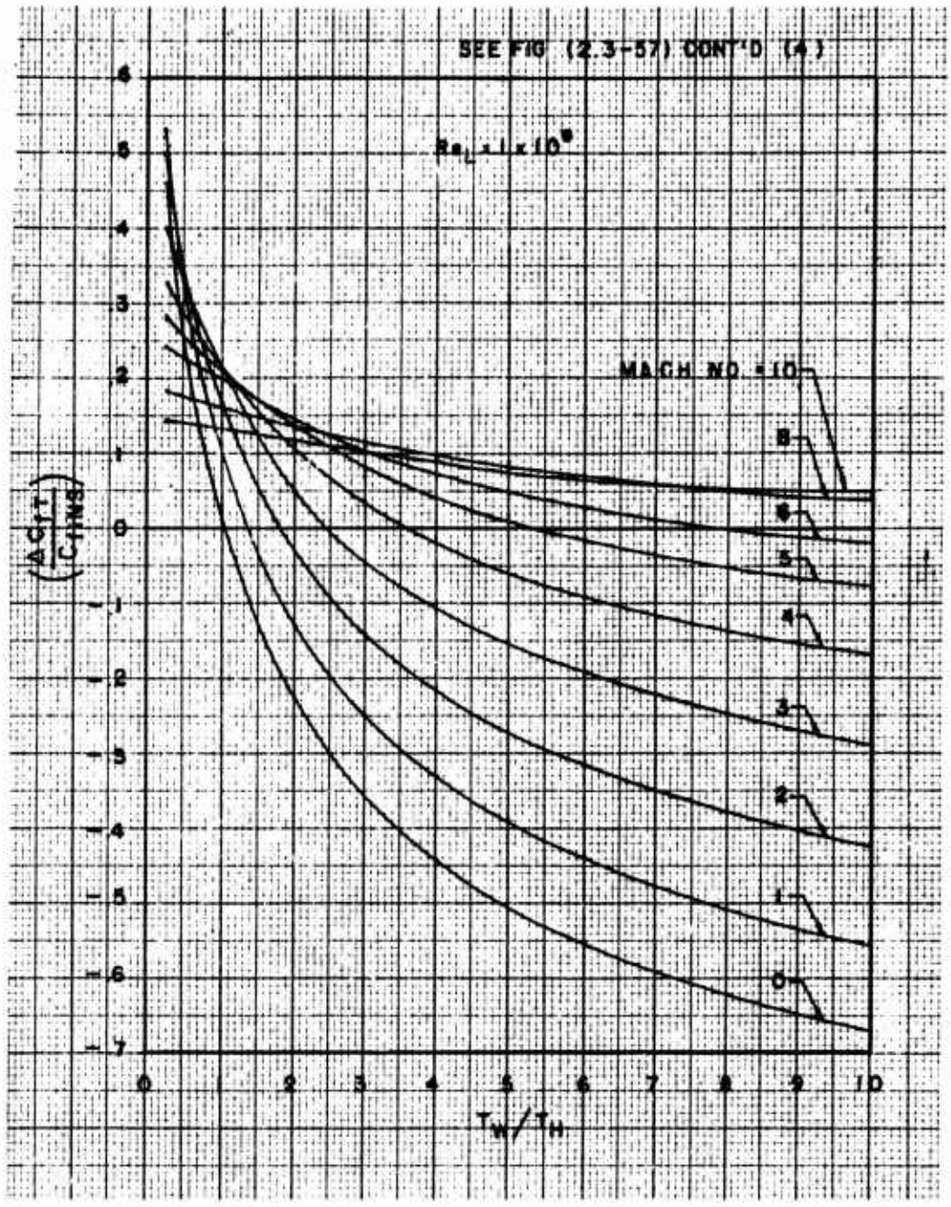

Fig (2.3-56) Continued (4)

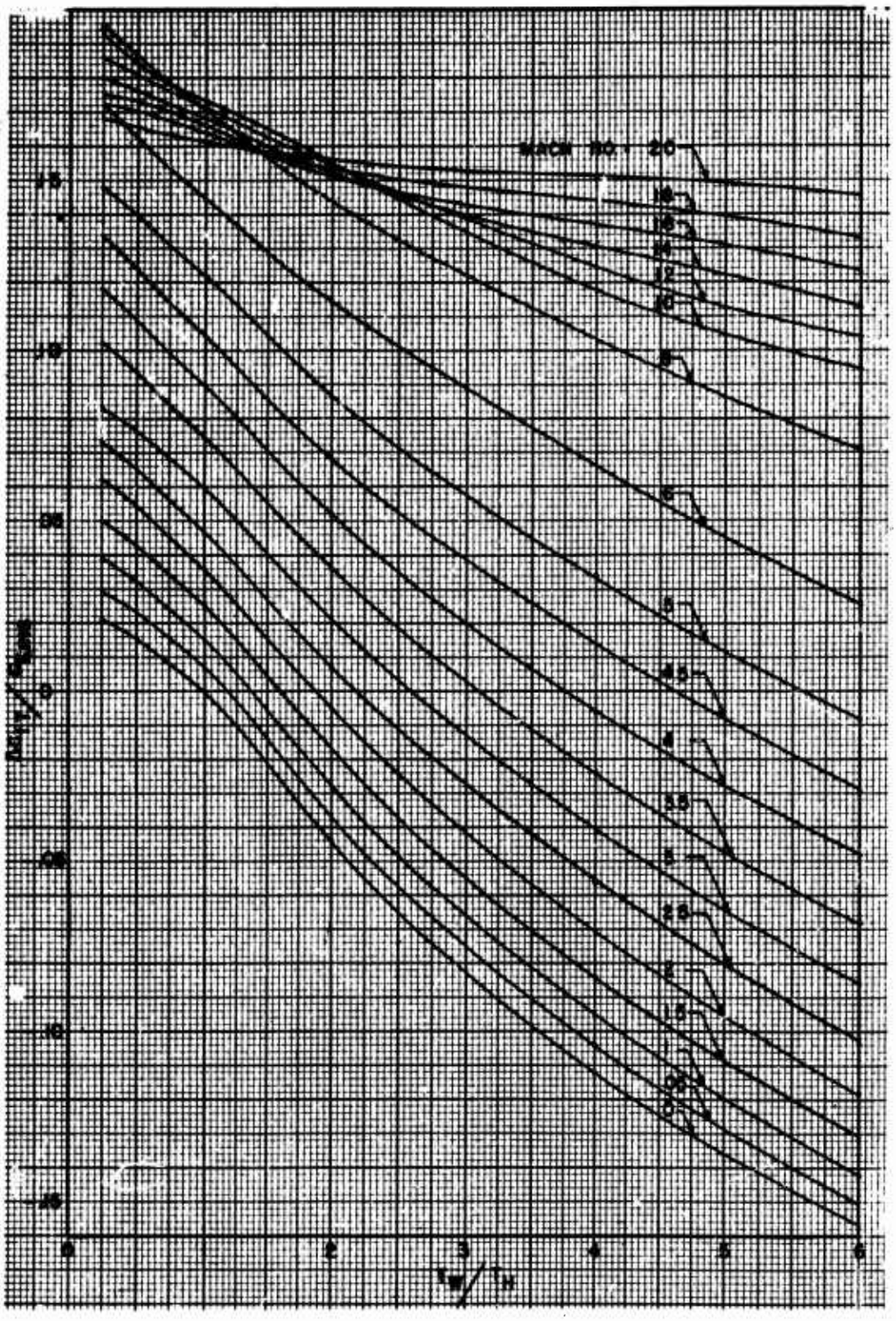

Fig (2.3-56) Continued (5)

Average compressible skin-friction increment due to skin temperature, turbulent B.L.

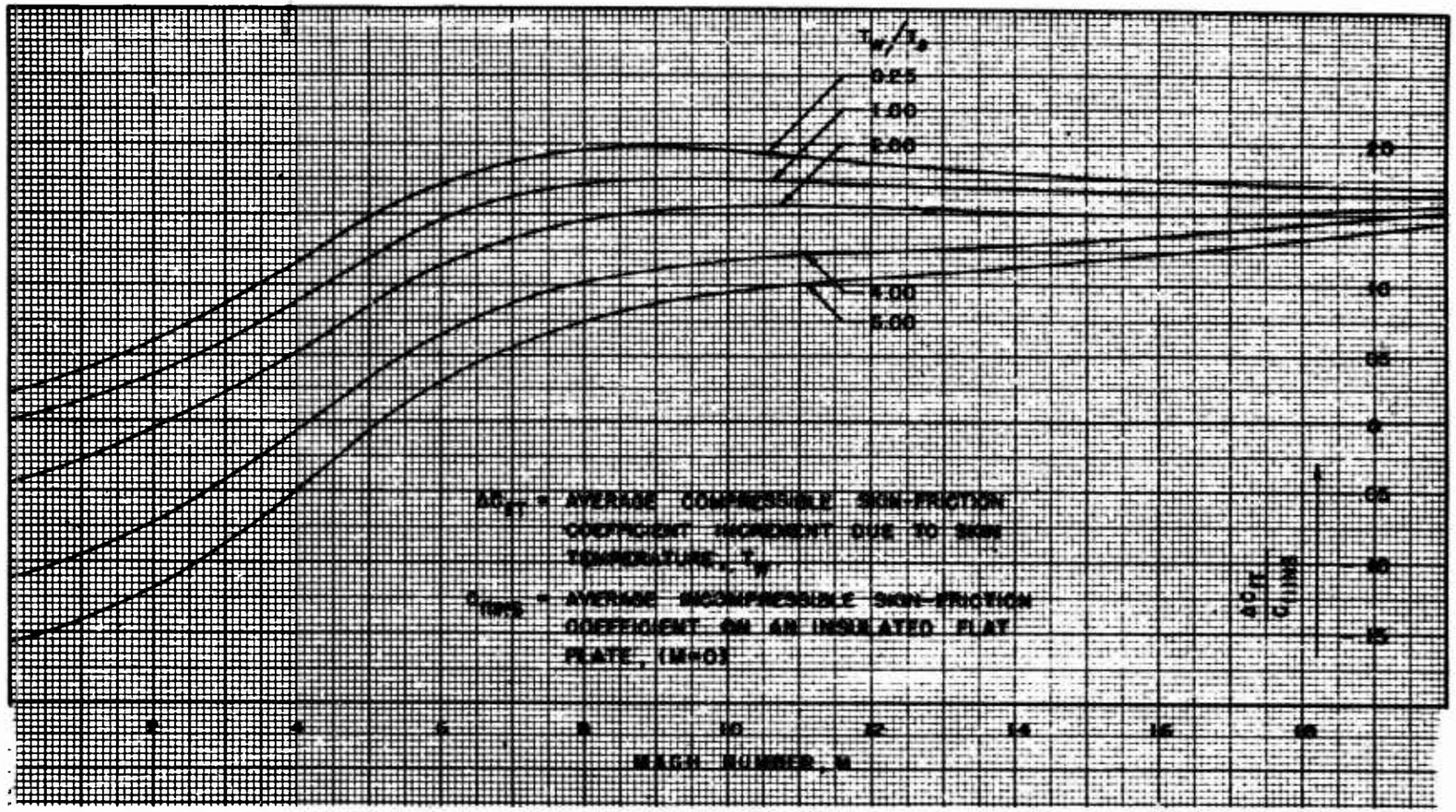

Fig (2.3-56) Continued (6)

Mean skin-friction coefficient for flat plate as a function of Mach Number and temperature ratio; turbulent B.L. (Von Driest, Ref (2.3-27))

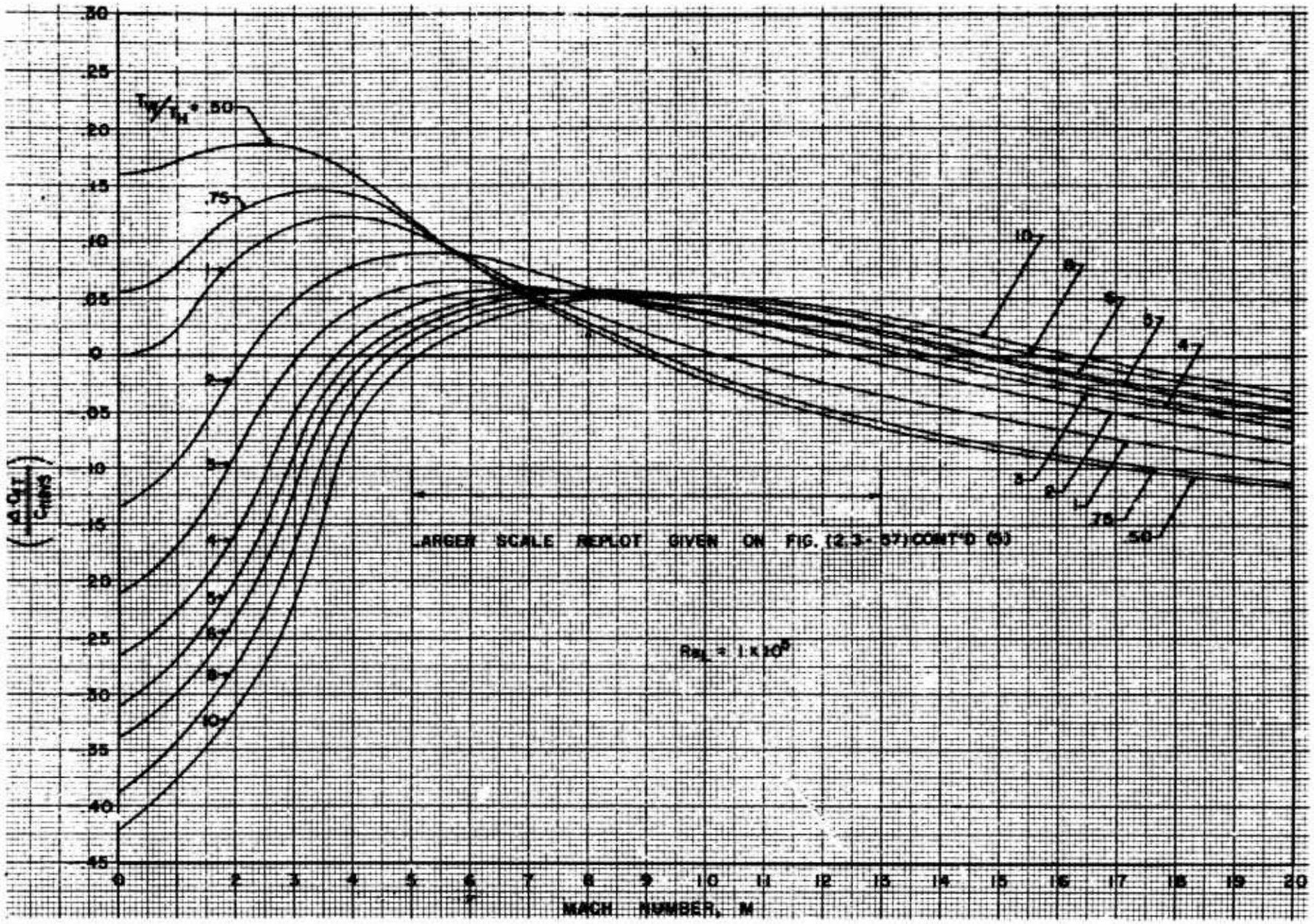

Fig (2.3-57) Skin-friction coeffient increment over its incompressible insulated value, due to actual skin temperature condition average values, T.B.L.. (Replot from Ref 27)

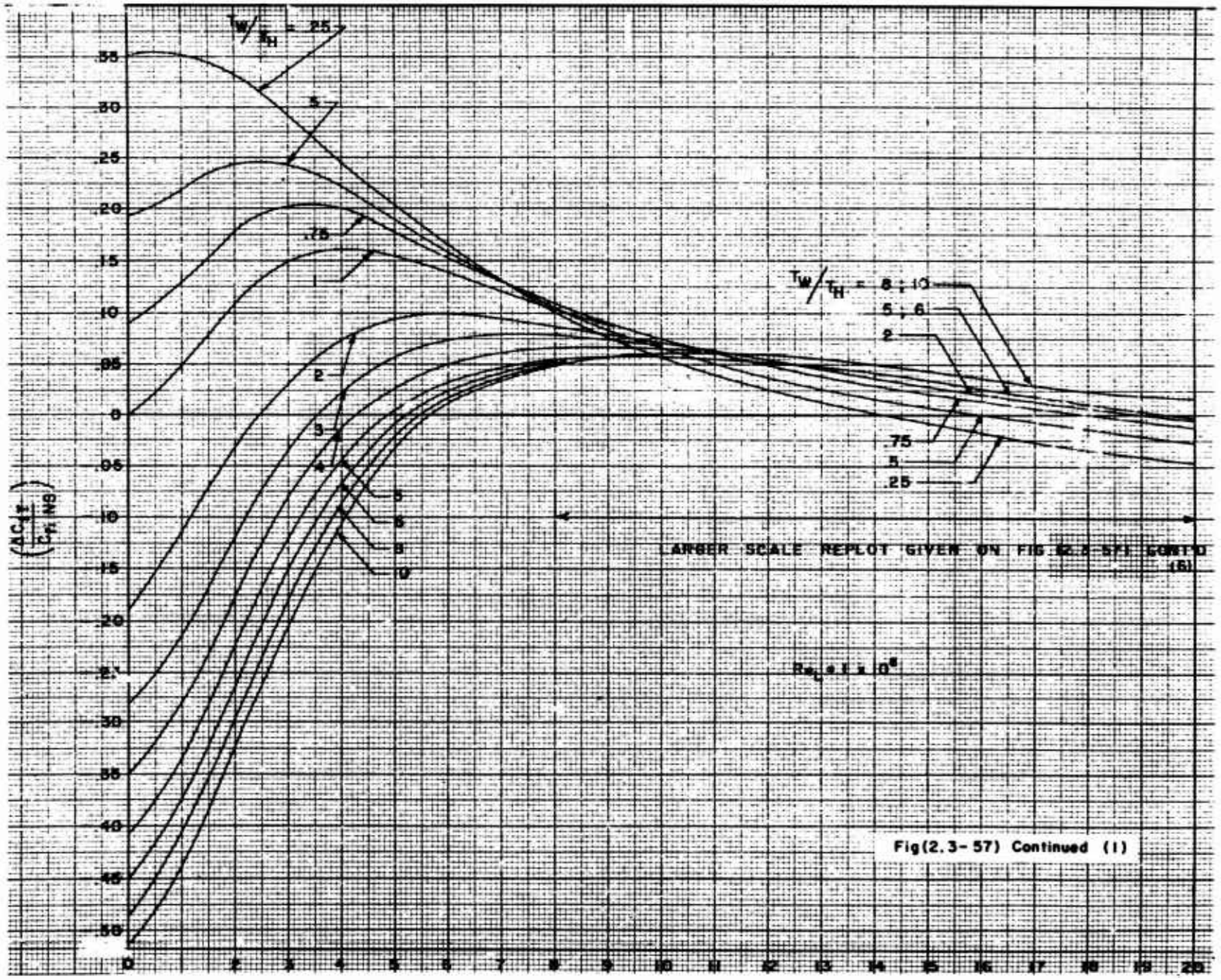

LARGER SCALE REPLOT GIVEN ON FIG. 2.3-57(1) CONT'D (1)

Fig(2.3-57) Continued (1)

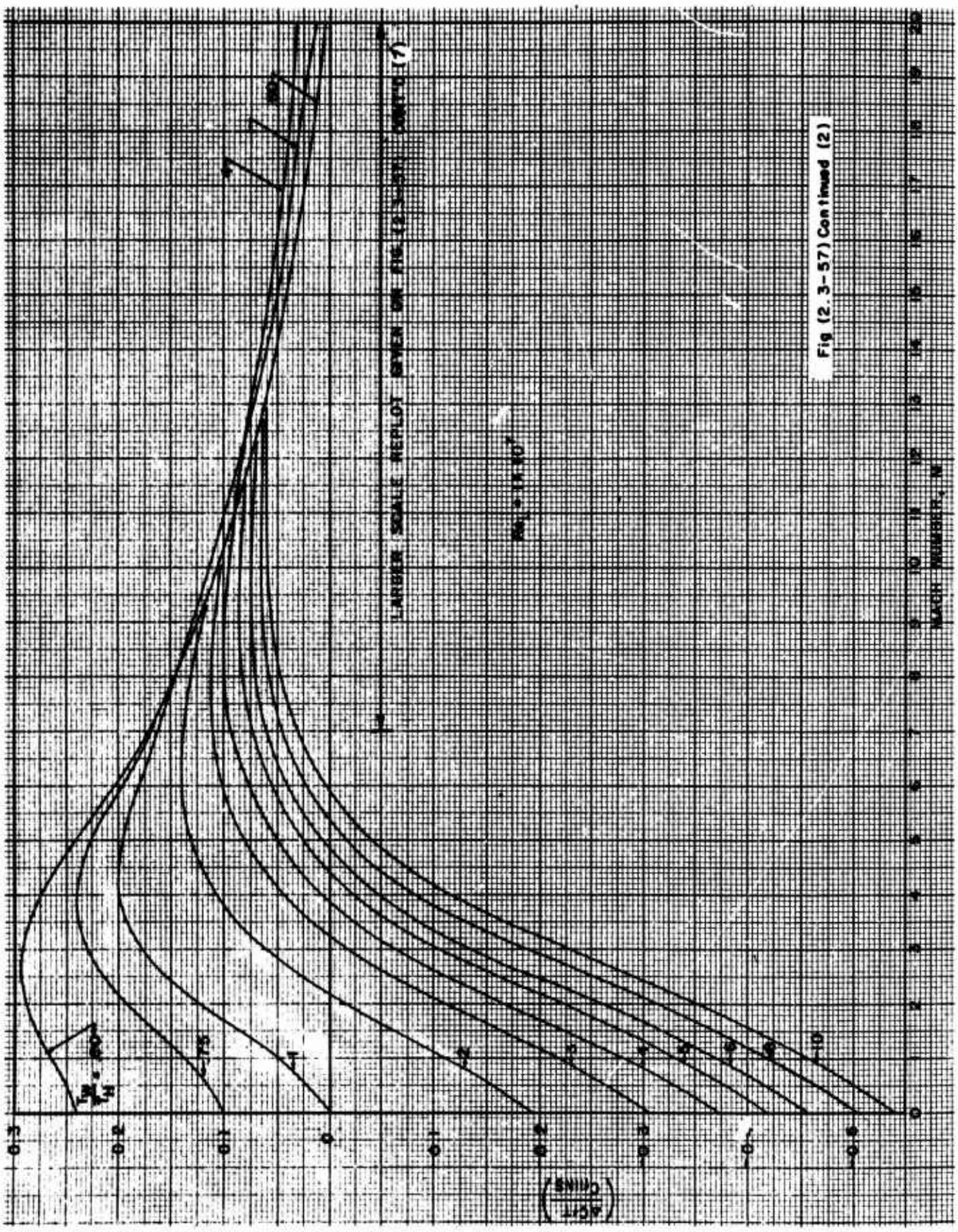
LARGER SCALE REPLOT GIVEN ON FIG. 2.3-57(1)
MACH NUMBER, M
Fig (2.3-57) Continued (2)

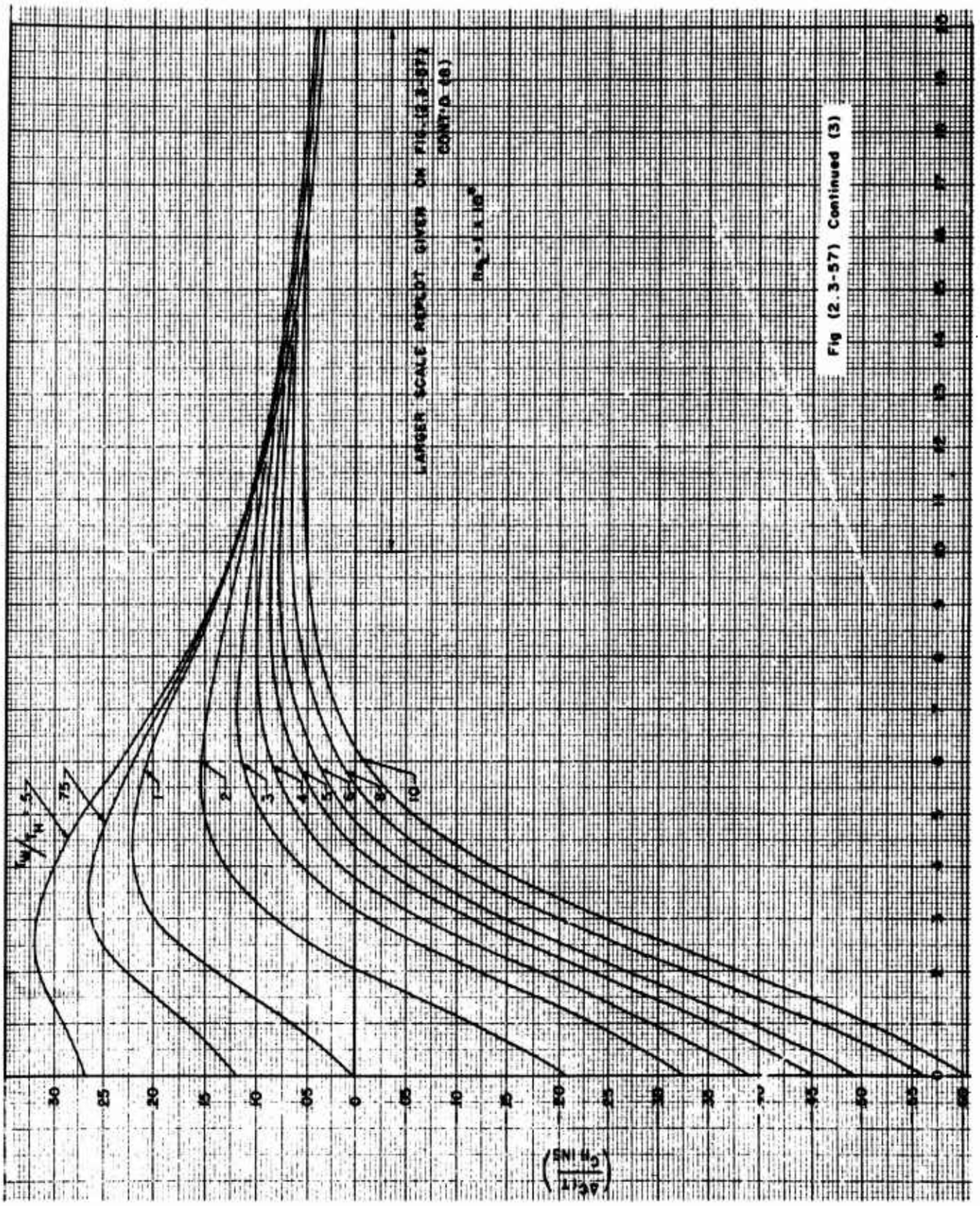

Fig (2.3-57) Continued (3)

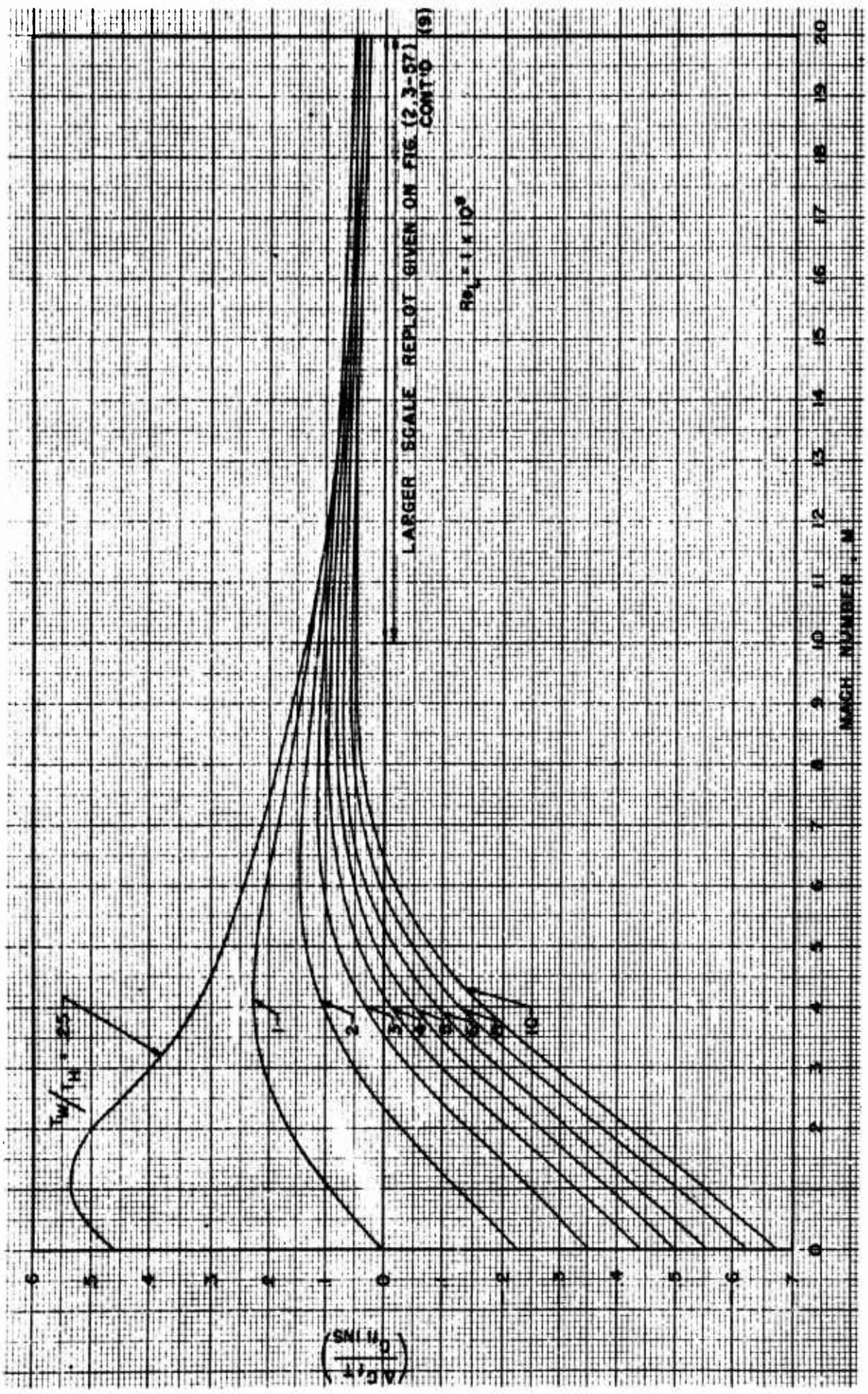

Fig (2.3-57) Continued (4)

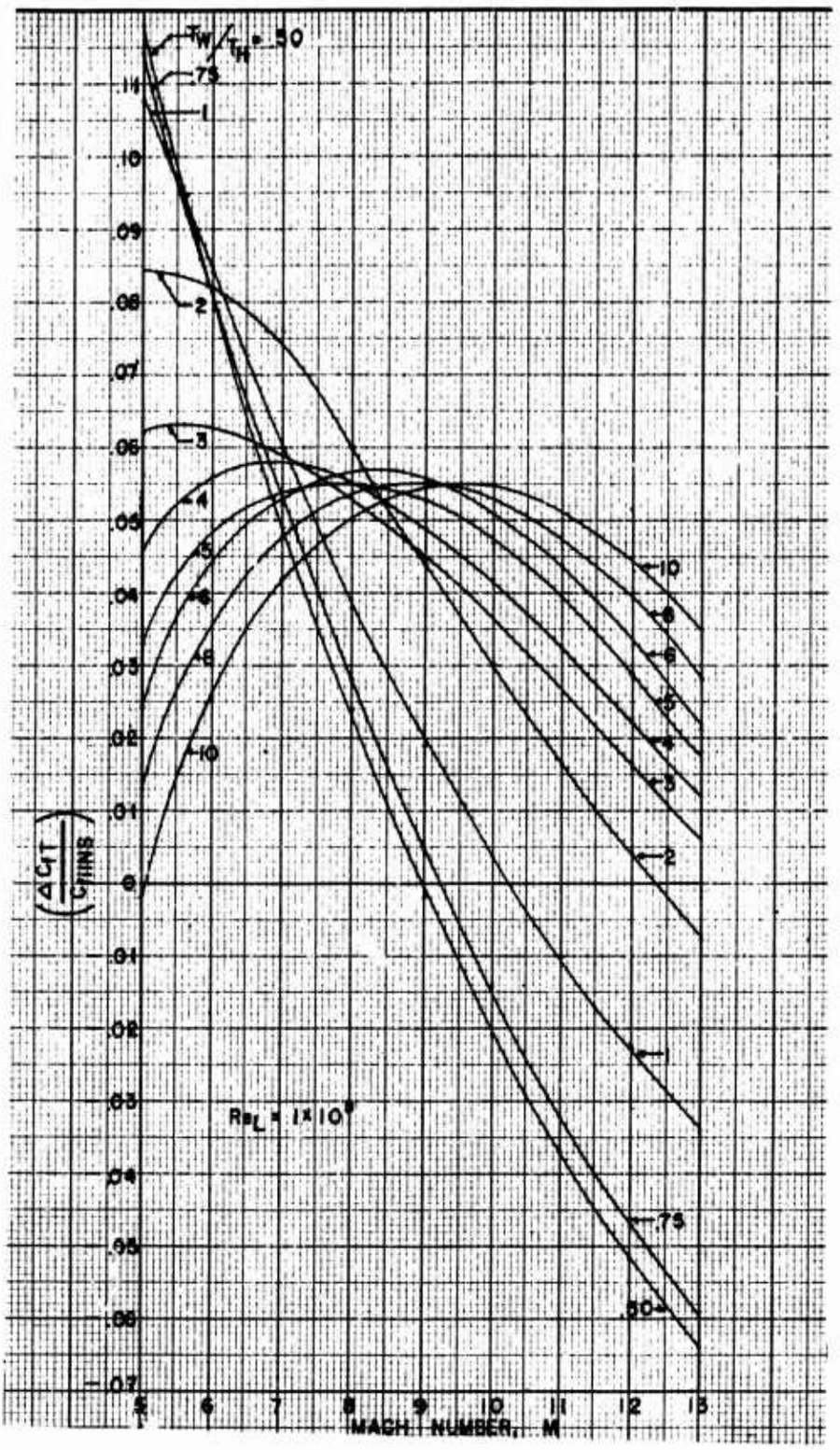

Fig (2.3-57) Continued (5)

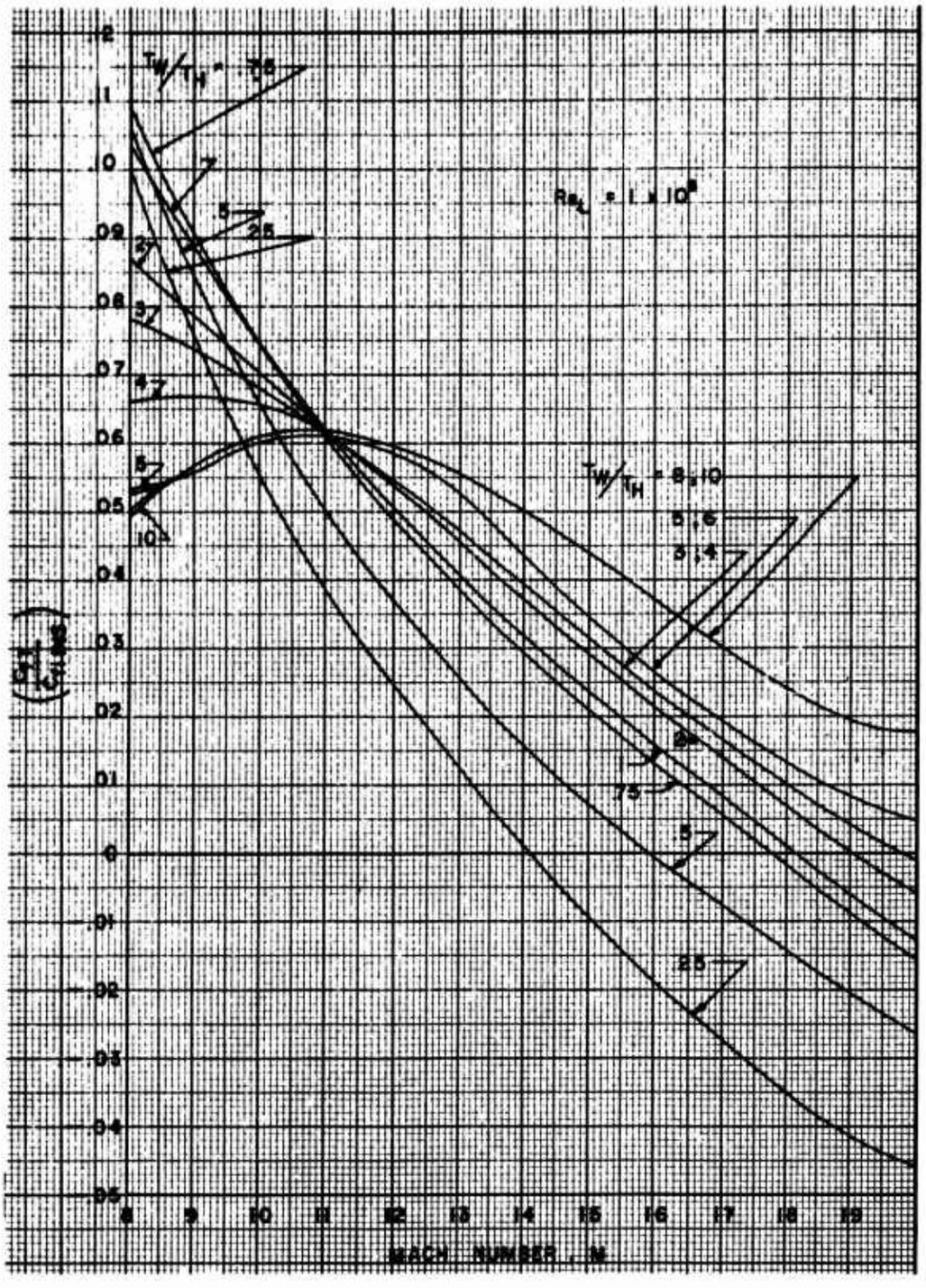

Fig (2.3-57) Continued (6)

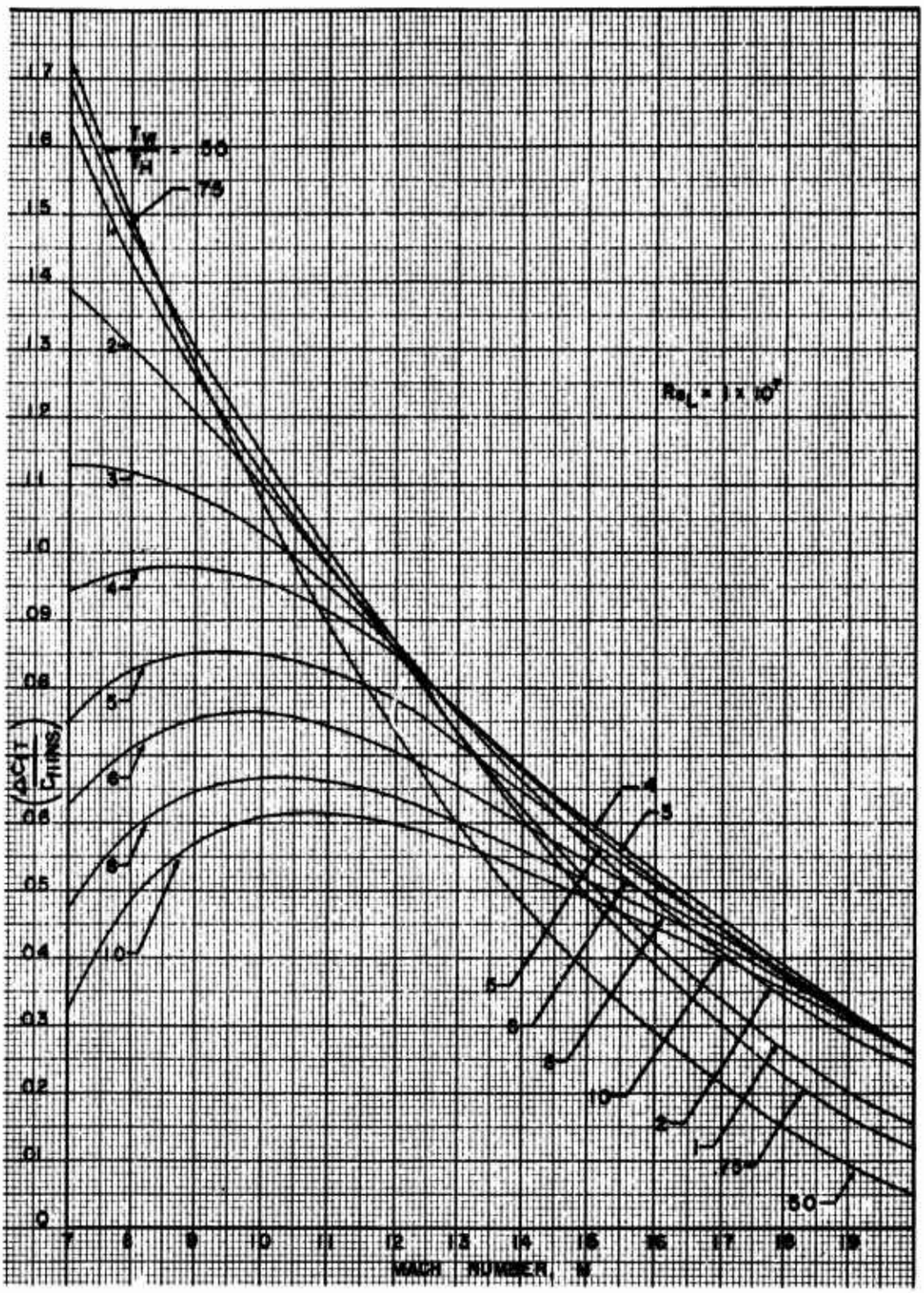

Fig (2.3-37) Continued (7)

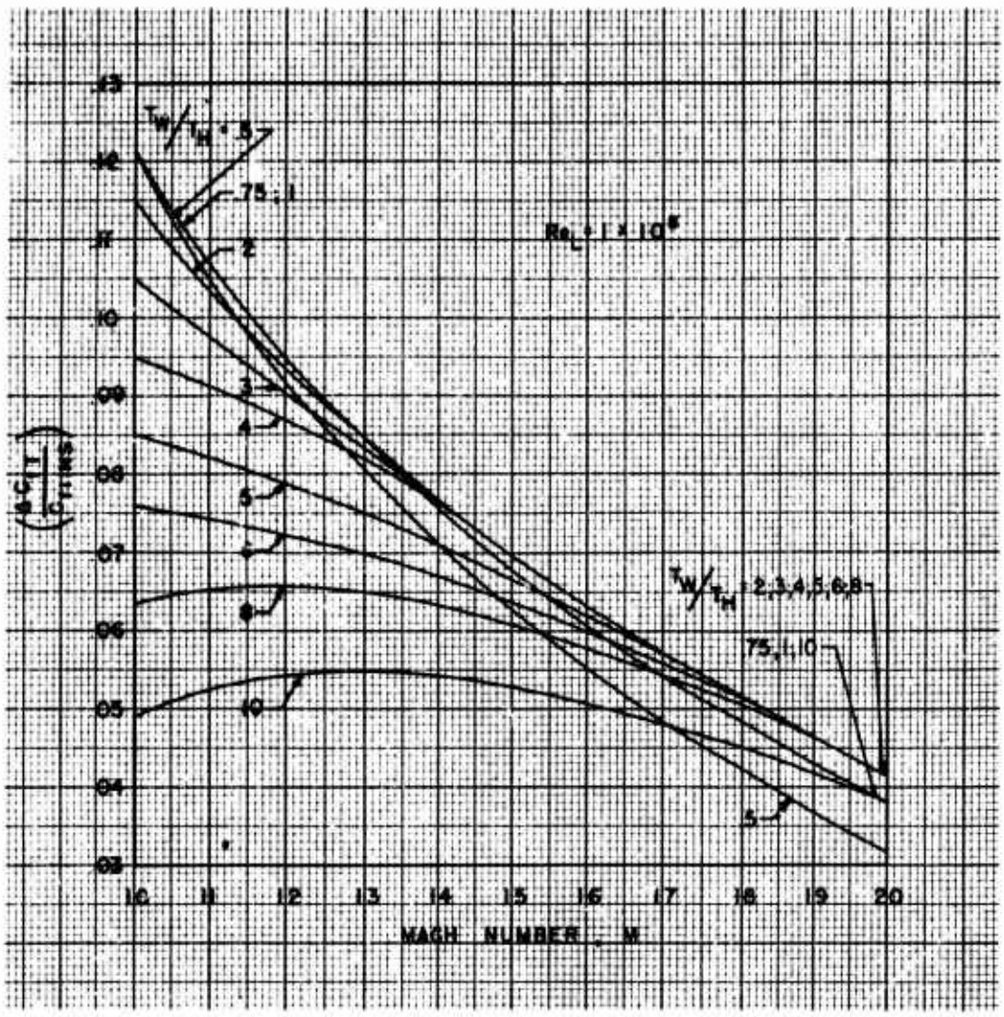

Fig (2.3-57) Continued (8)

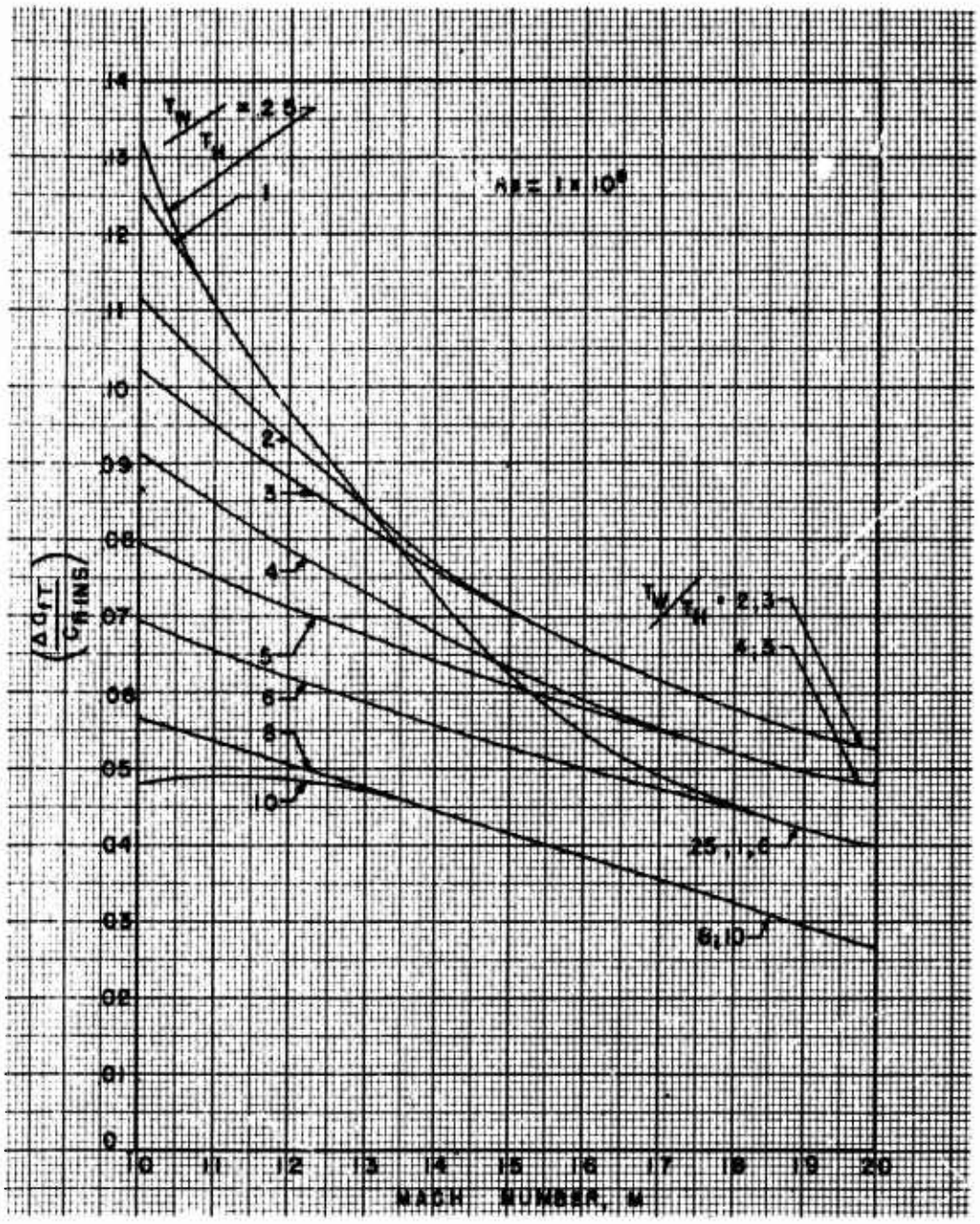

Fig (2.3-57) Continued (9)

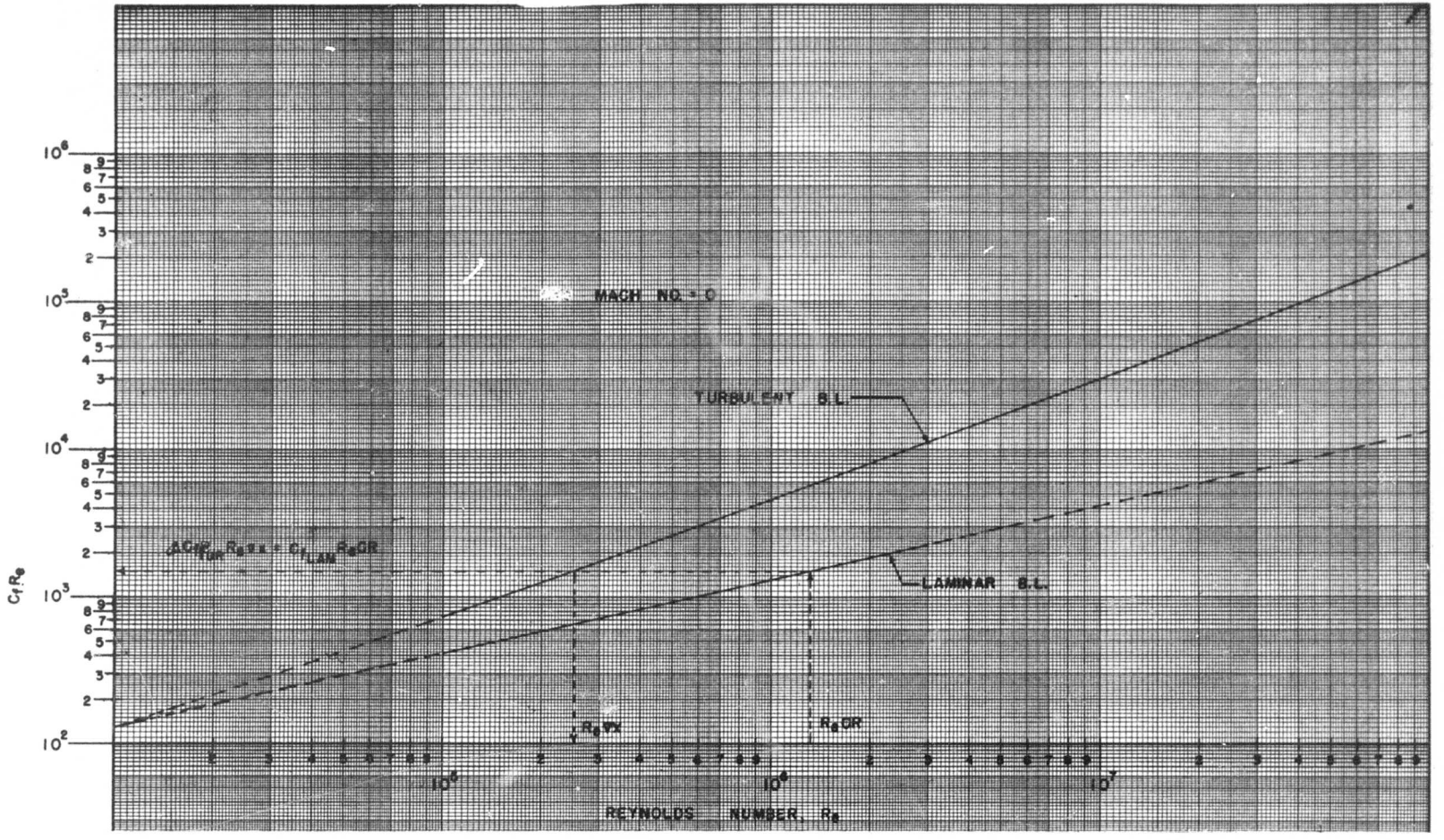

Fig (2.3-58) Estimates of the equivalent turbulent boundary layer Reynolds Number, $Re_{\Delta x}$, and the respective product, $\Delta Cf_{TUR} Re_{\Delta x}$, in terms of Re_{cr}.

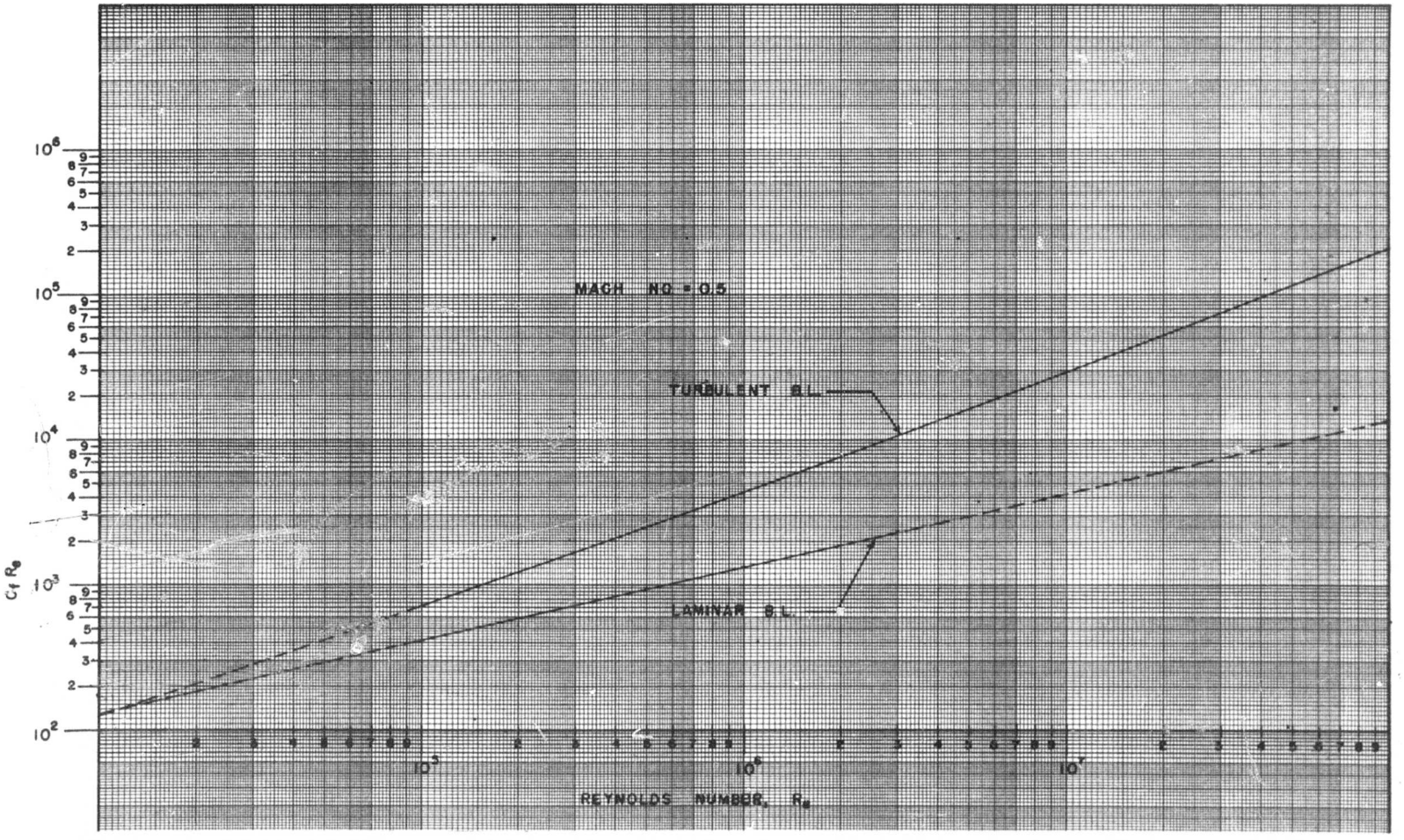

Fig (2.3-58) Continued (1)

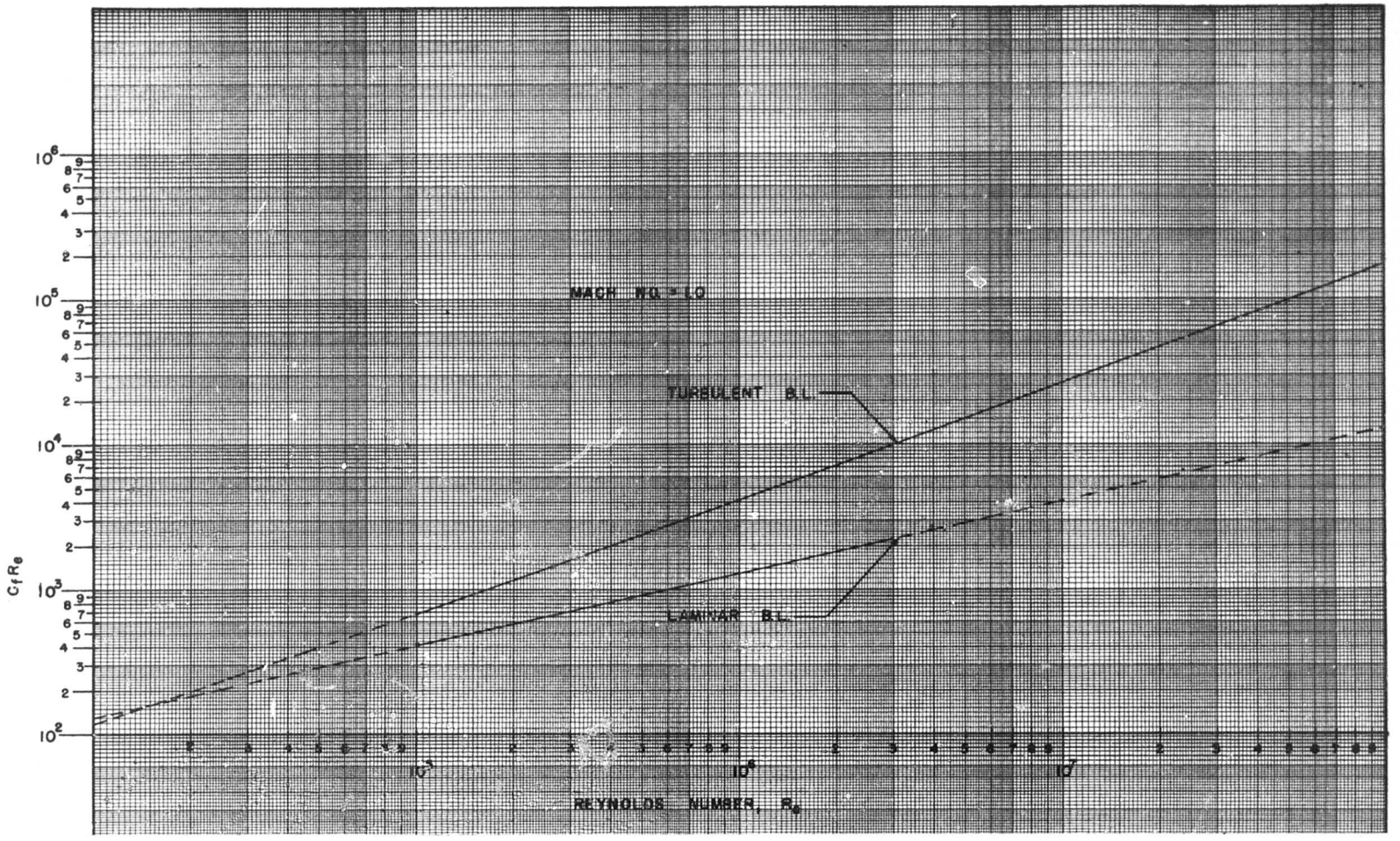

Fig (2.3-58) Continued (2)

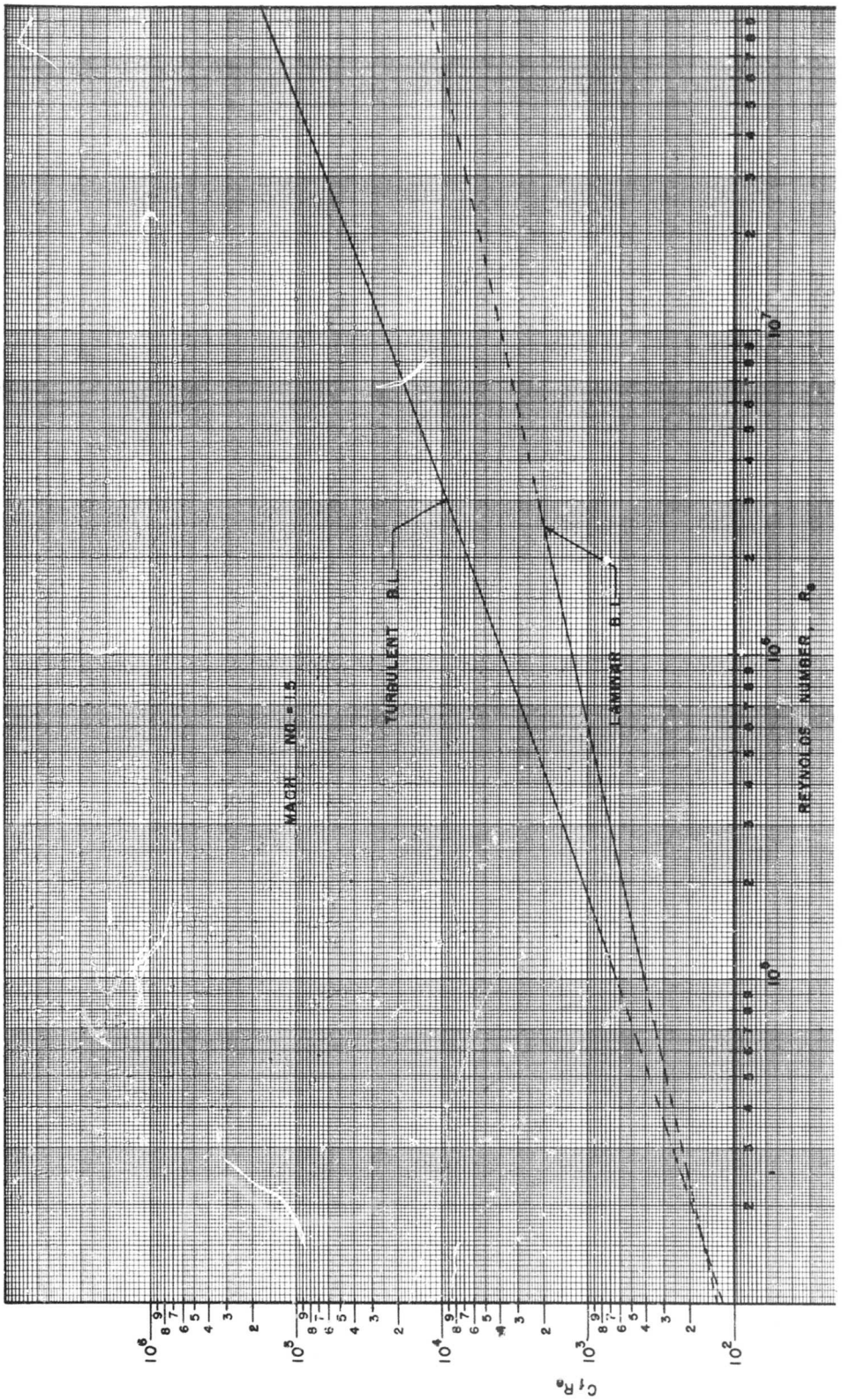

Fig (2.3-58) Continued (3)

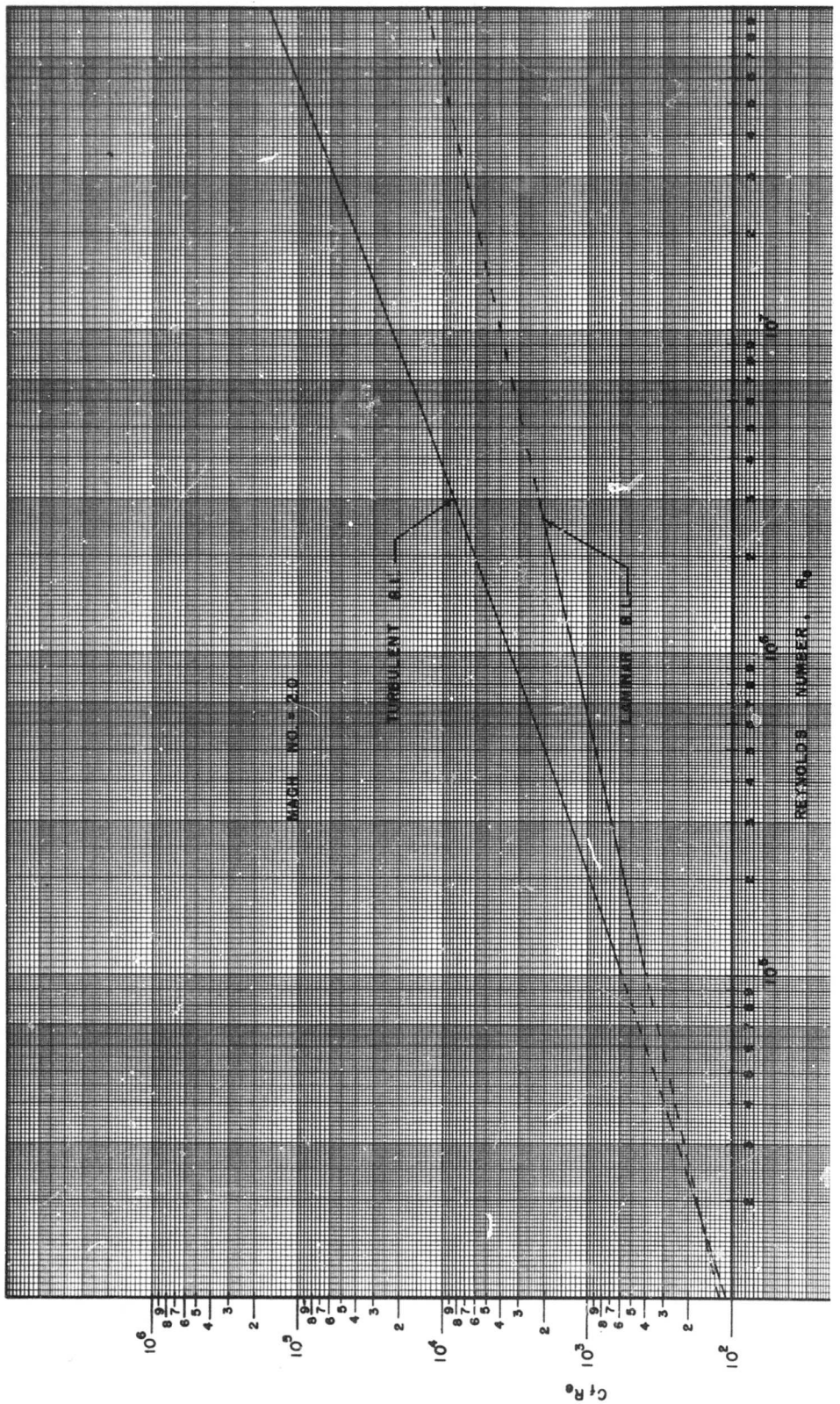

Fig(2.3-58) Continued (4)

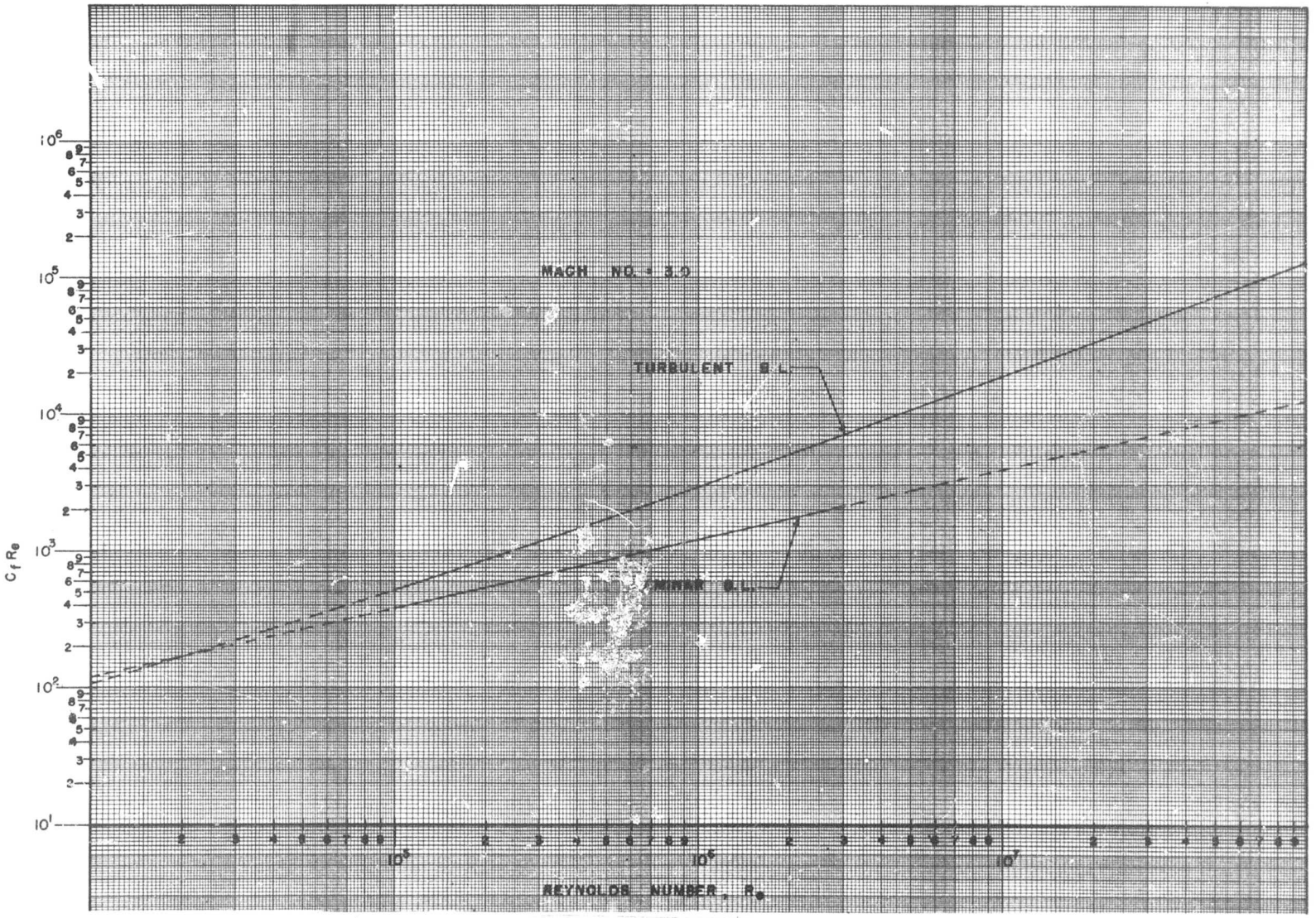

Fig (2.3-58) Continued (5)

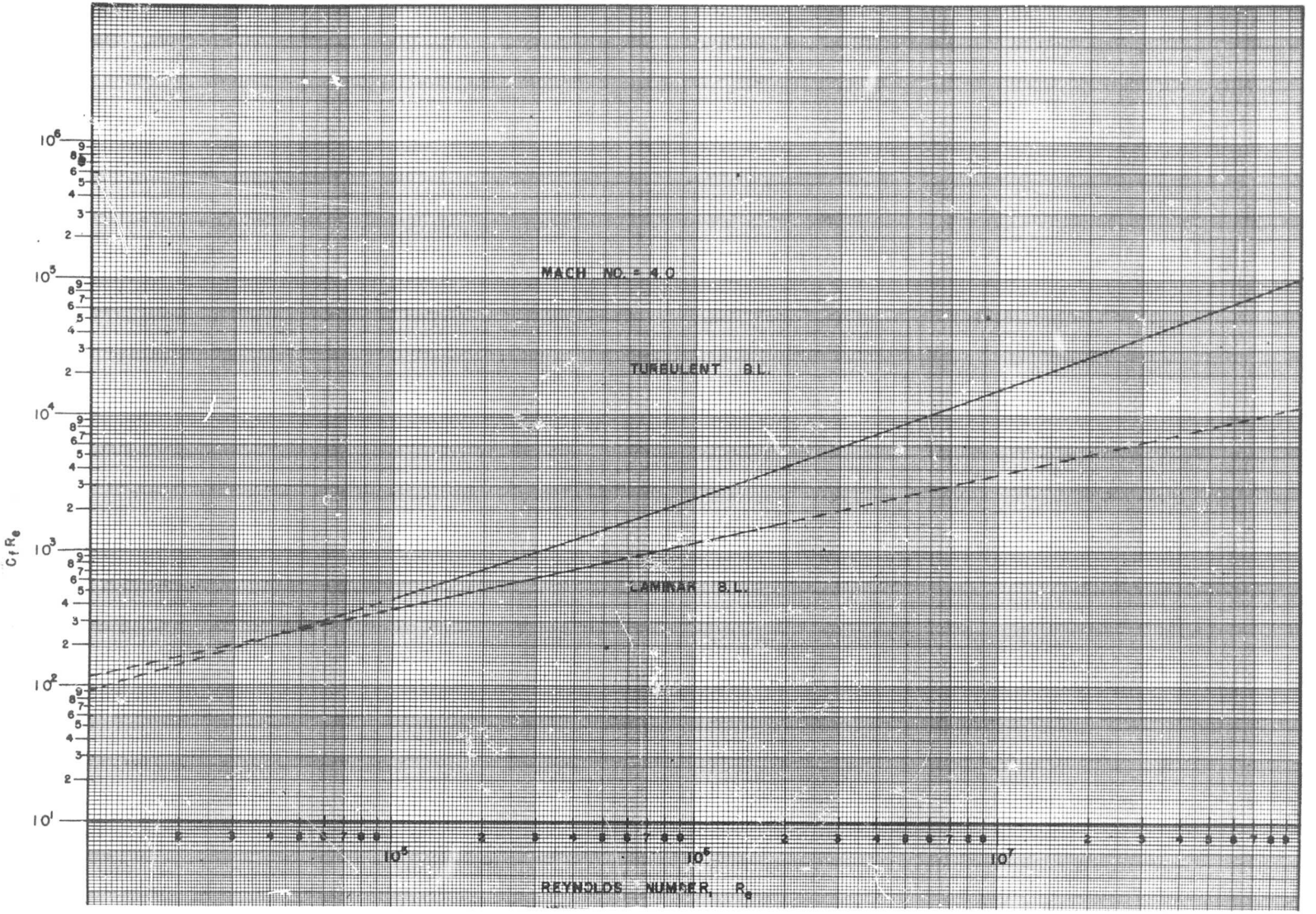

Fig (2.3-58) Continued (6)

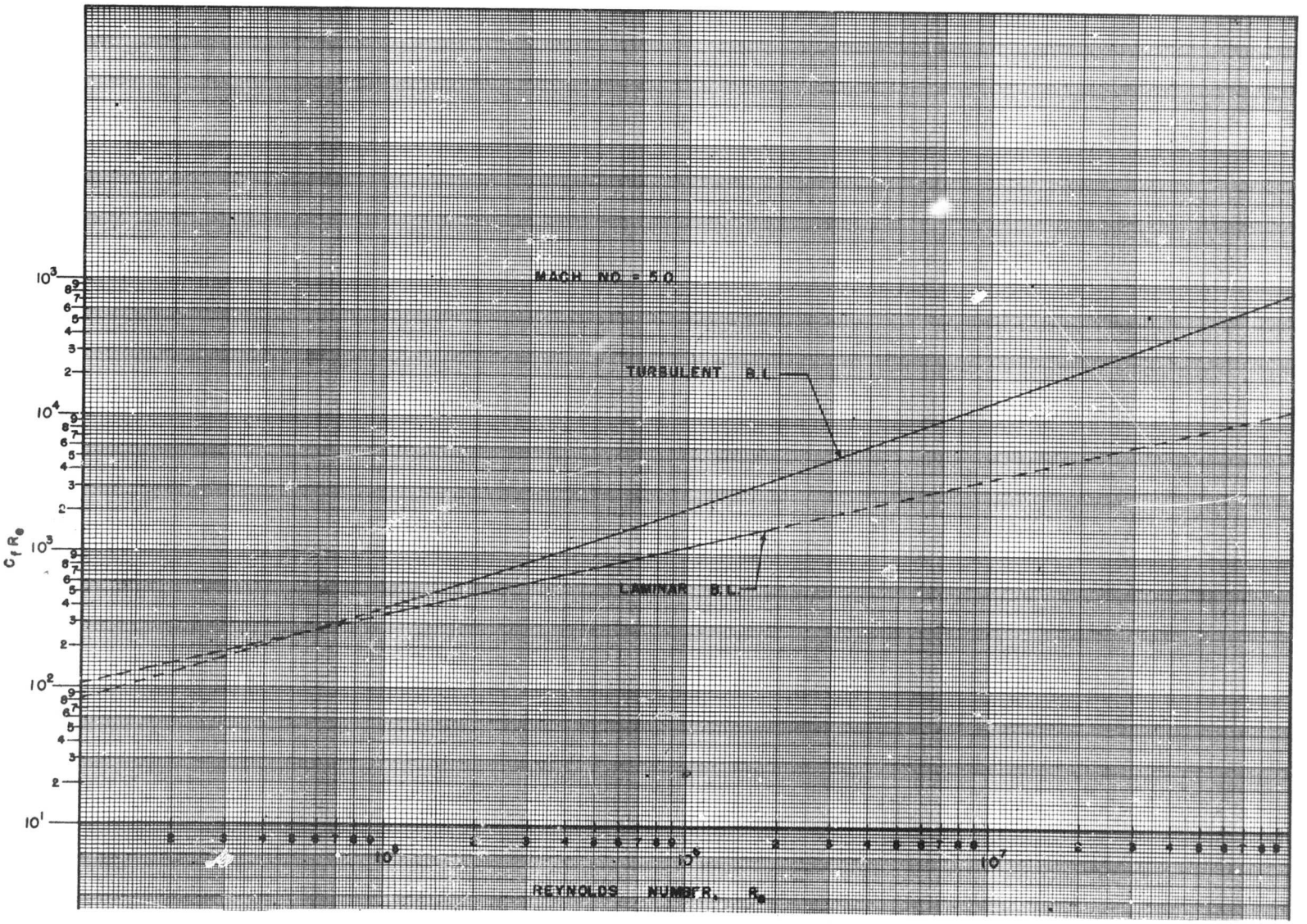

Fig(2.3-58) Continued (7)

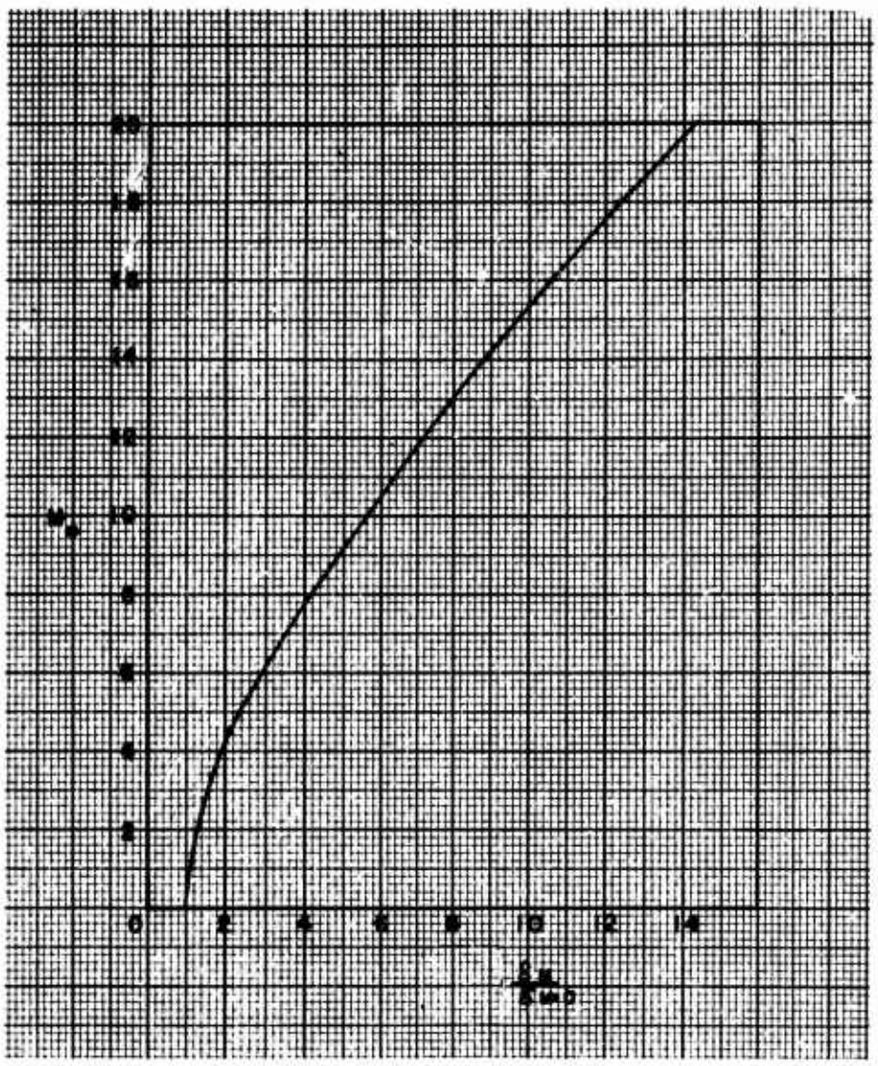

Fig (2.3-59) Compressible-to-incompressible laminar boundary layer thickness ratio ($\delta_M/\delta_{M=0}$) versus Mach Number; smooth, insulated flat plate. (Von Driest)

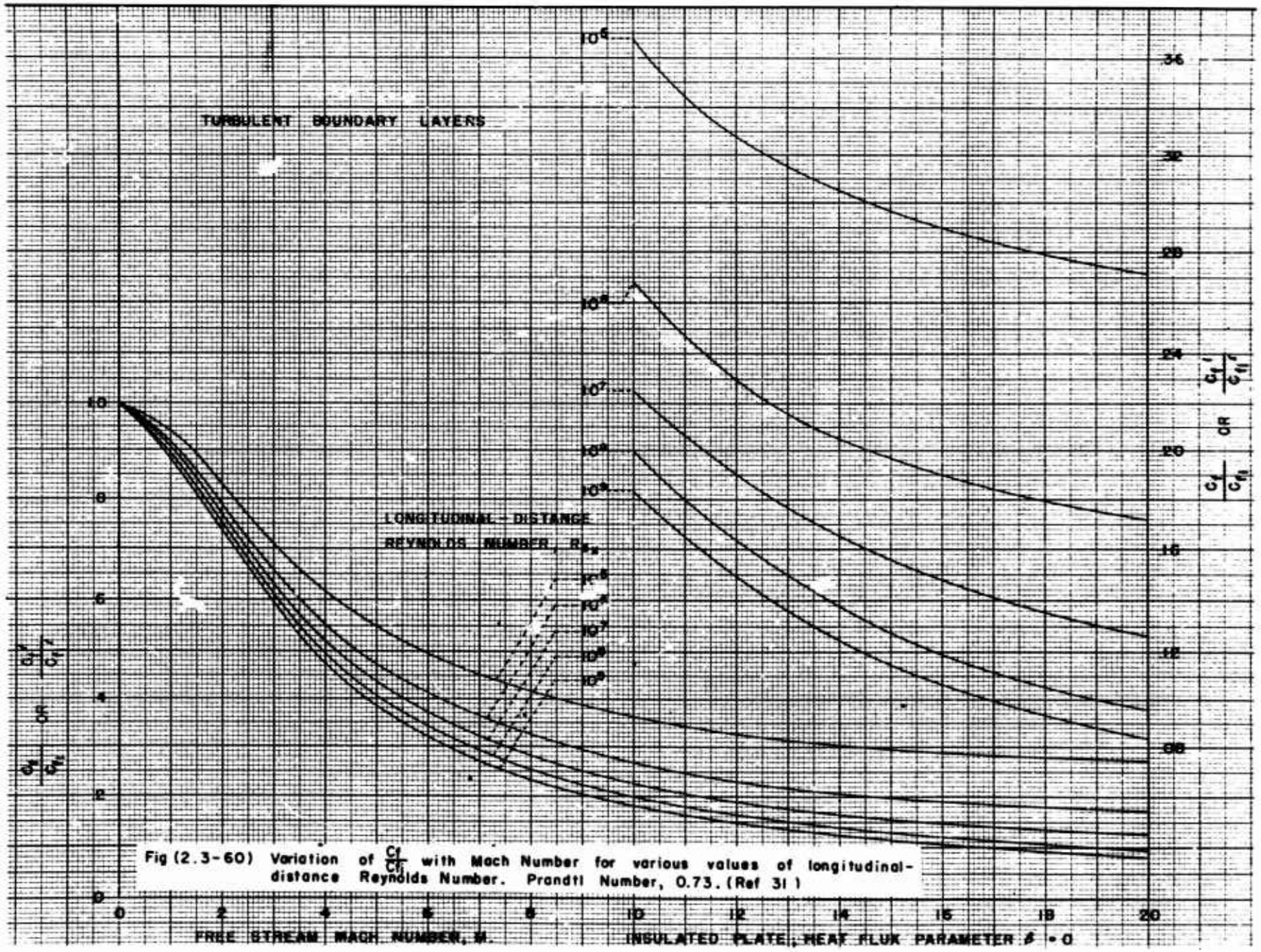

Fig (2.3-60) Variation of $\frac{C_f}{C_{f_0}}$ with Mach Number for various values of longitudinal-distance Reynolds Number. Prandtl Number, 0.73. (Ref 31)

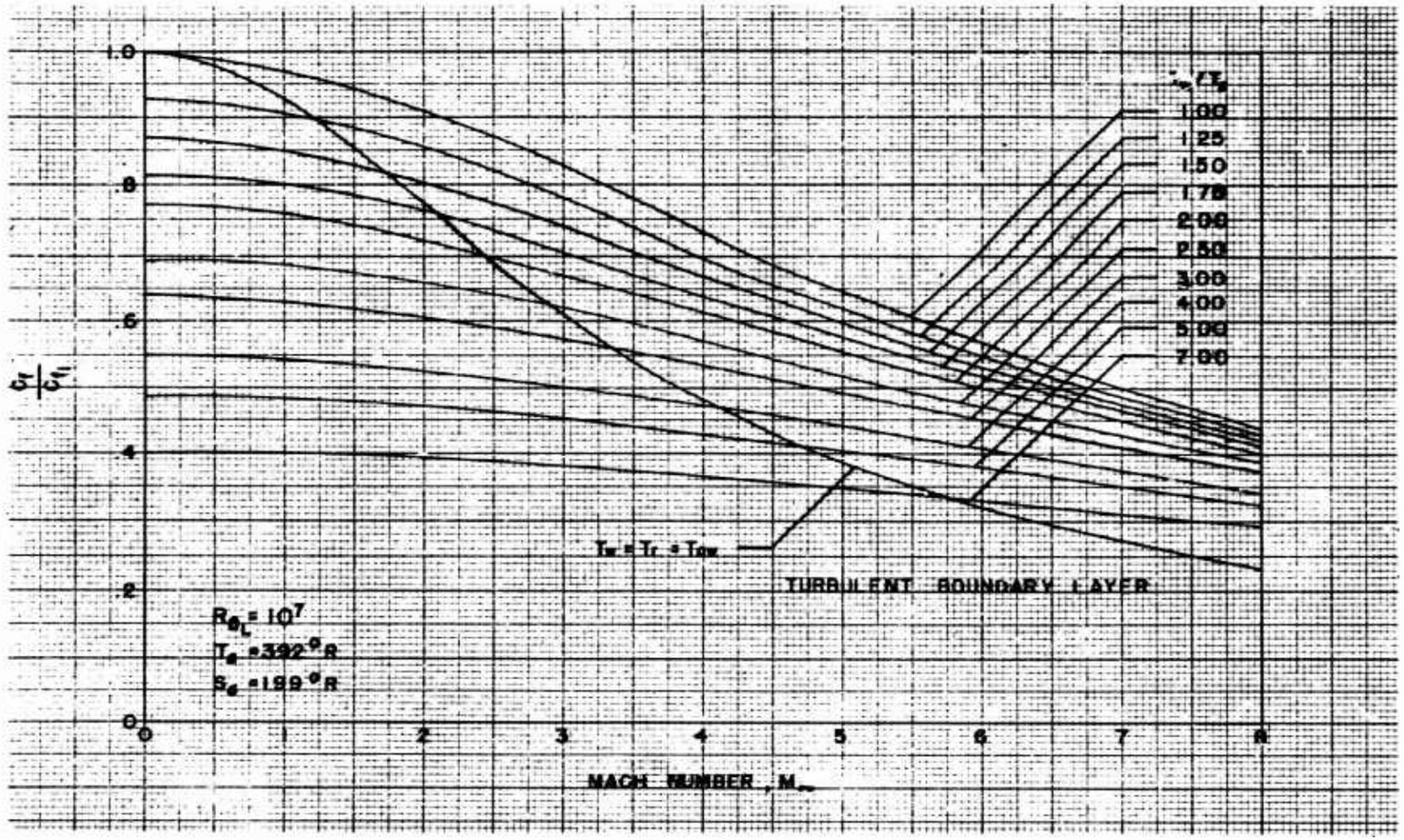

Fig (2.3-61) Effect of Mach Number on skin-friction ratio at standard isothermal attiltude, as determined by use of T' method at constant values of wall-temperature ratio, (Ref 80)

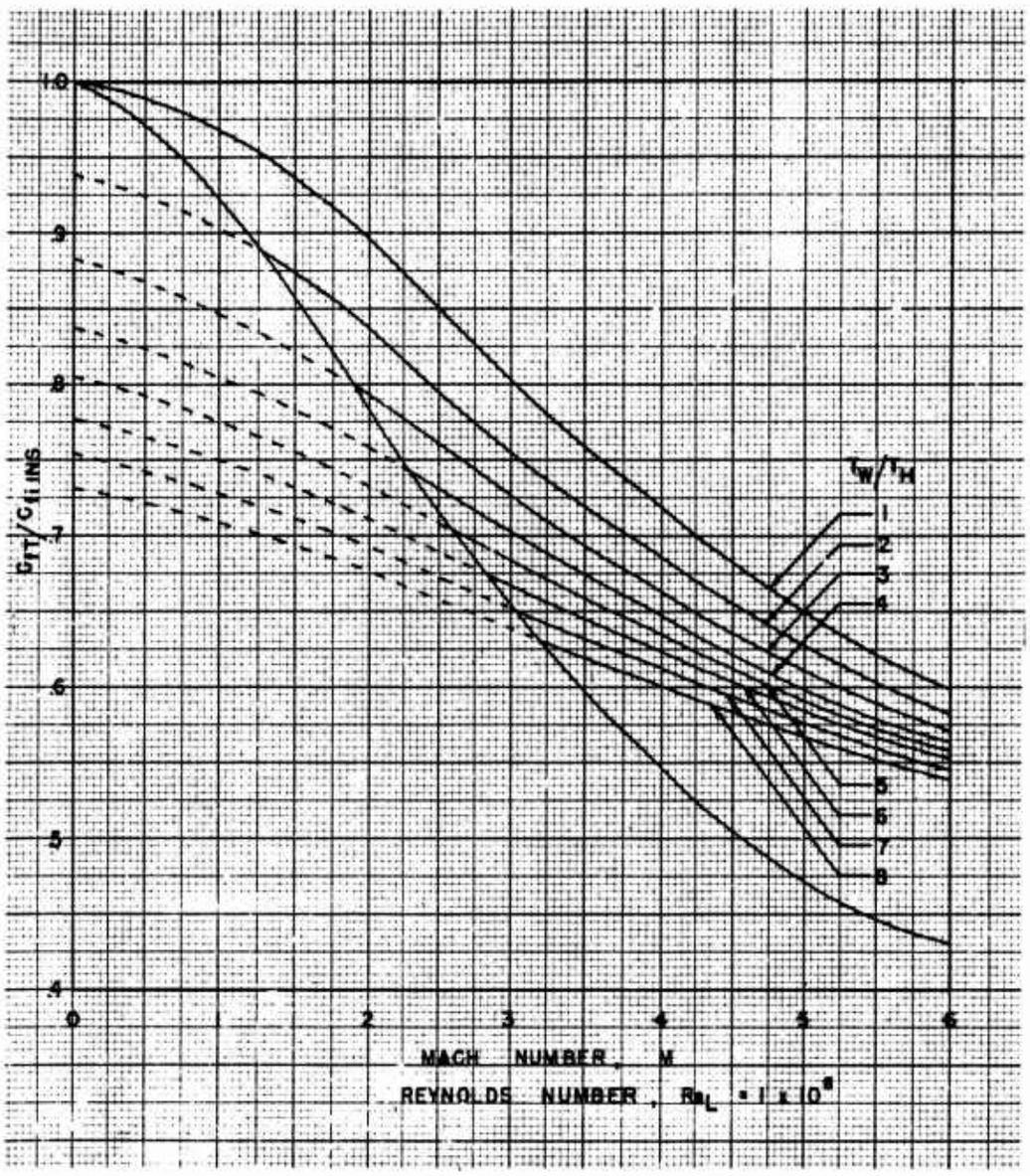

Fig(2.3-62) Skin-friction coefficient ratio $C_{f_T}/C_{fi\,INS}$ due to actual skin temperature conditions (T_W/T_H) for flat plates, compressible boundary layer. (Replot from Ref 80 and Ref 27)

Turbulent boundary layers

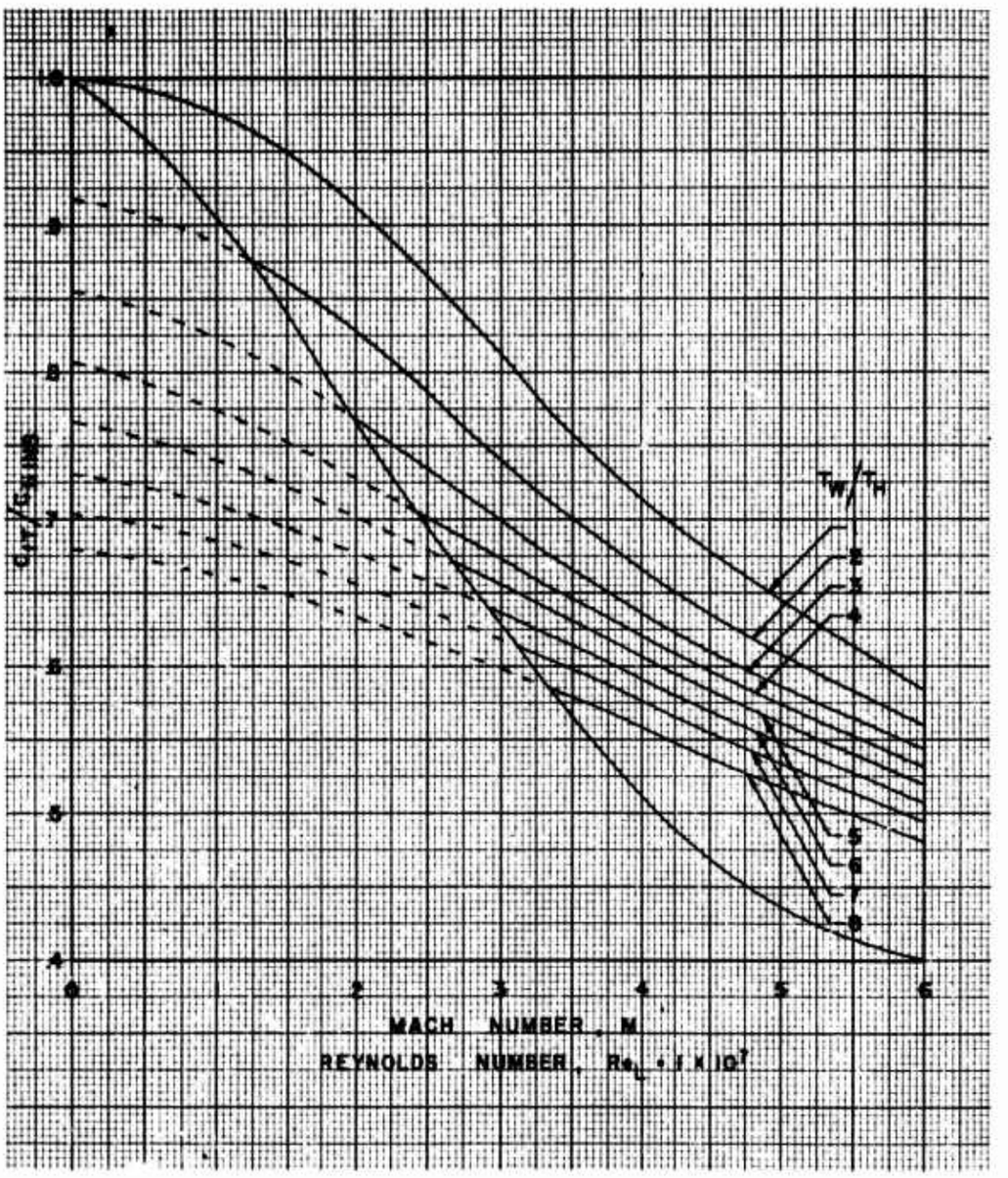

Fig (2.3-62) Continued (1)

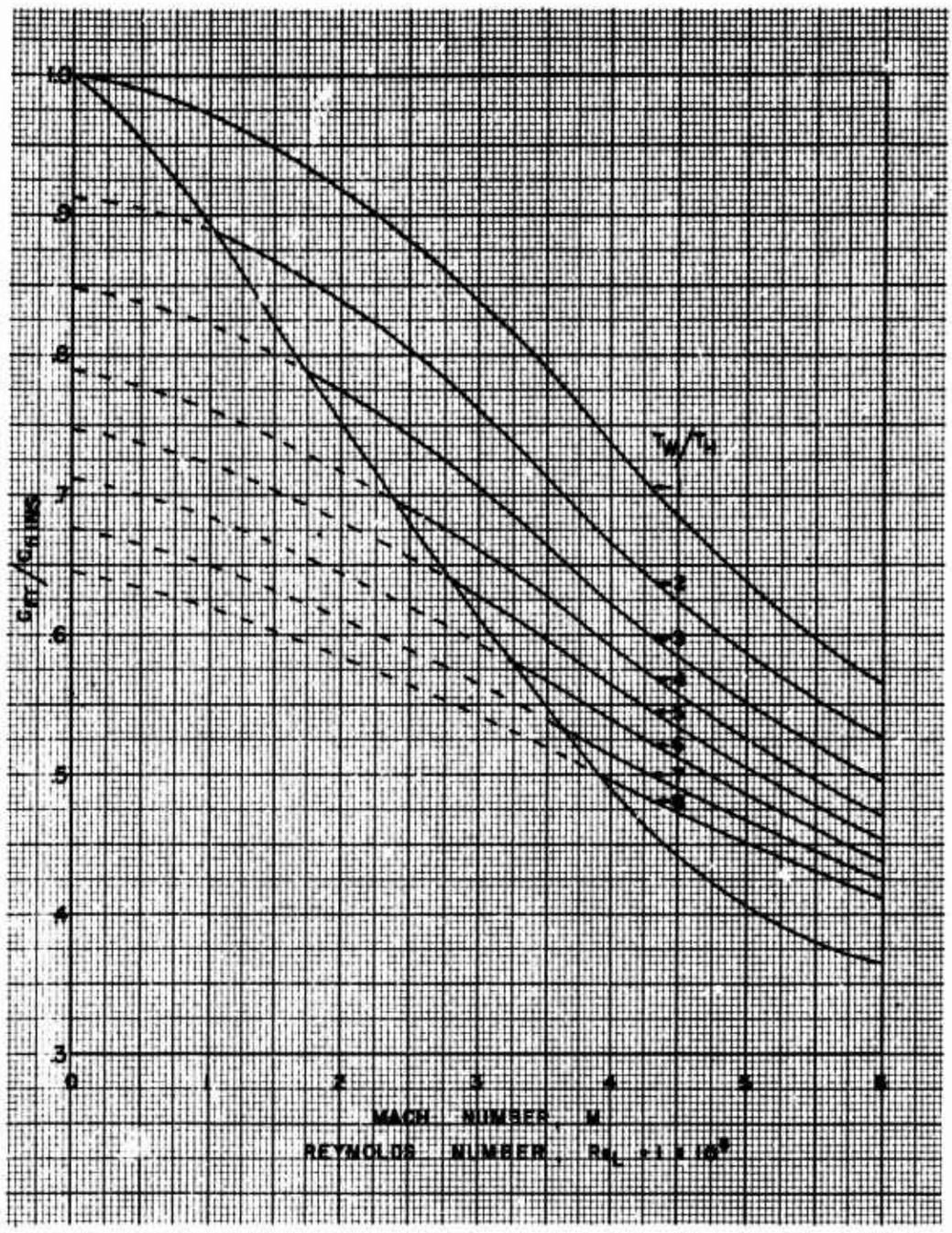

Fig (2.3-62) Continued (2)

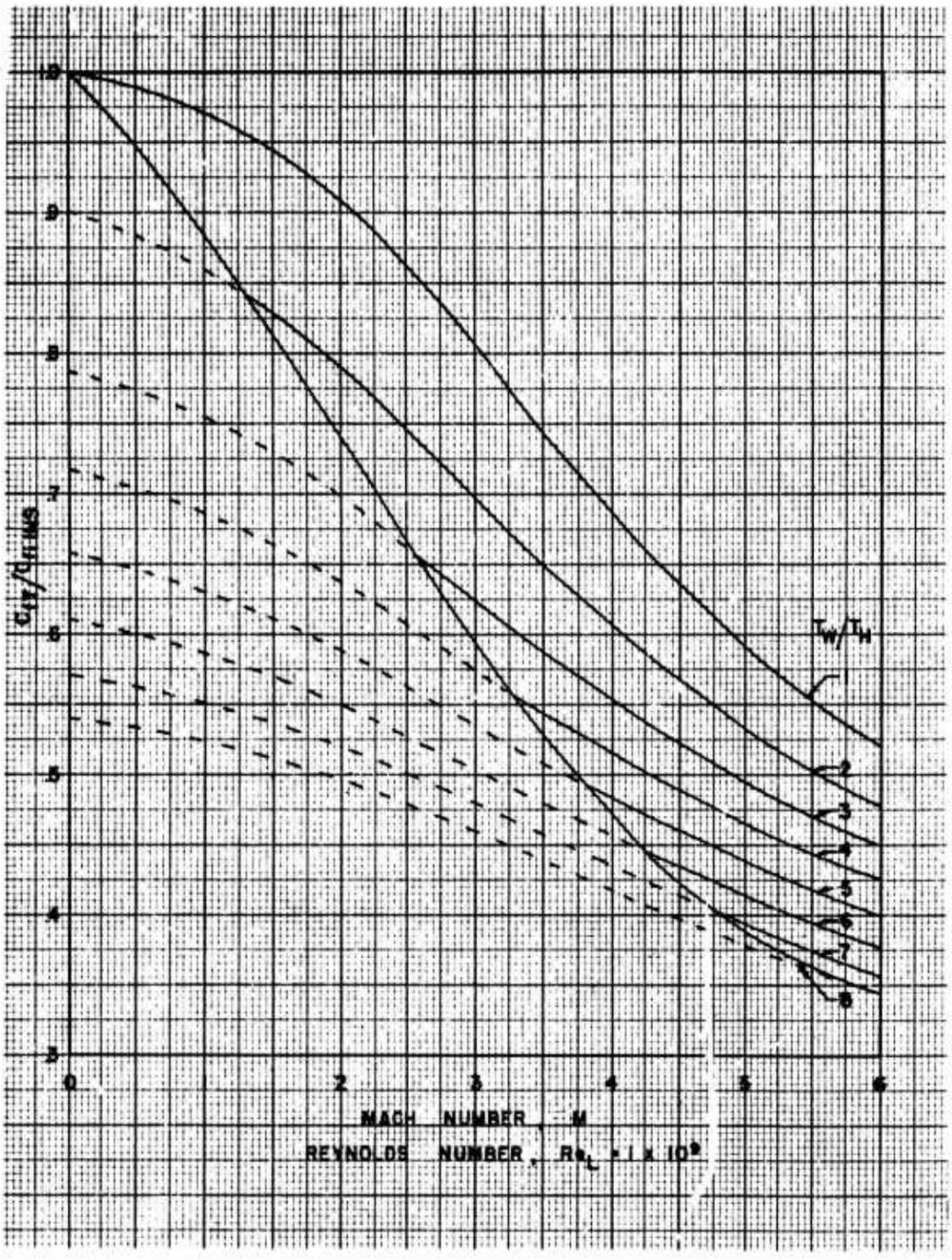

Fig (2.3-62) Continued (3)

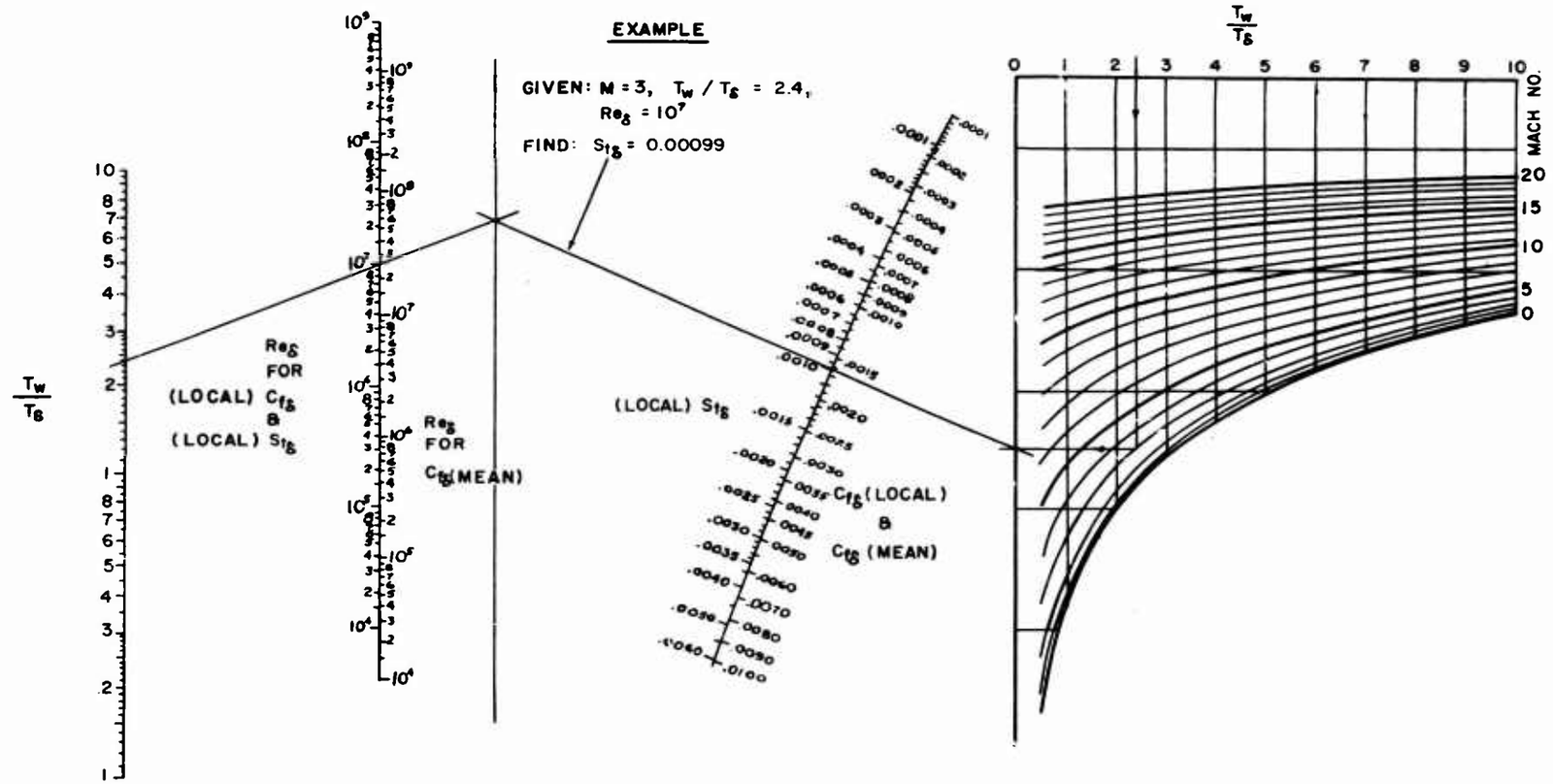

Fig (2.3-63) Nomograh for coefficient of friction and heat transfer of a turbulent boundary layer on a flat plate for air. (For computational purposes, the original Ref 23-27 should be used.)

2.3.14 REFERENCES

2.3-1 Goldstein, S. Modern Developments in Fluid Dynamics. New York: Oxford University Press, 1938.

2.3-2 Schlichting, H. Boundary Layer Theory. New York: McGraw-Hill Book Company, Inc., 1955.

2.3-3 Prandtl, L. Essentials of Fluid Dynamics. London: Blackie and Sons, Ltd., 1960.

2.3-4 Milne-Thompson, L. M. Theoretical Hydrodynamics. New York: The Mac Millan Company, 1957.

2.3-5 Truitt, R. W. Fundamentals of Aerodynamic Heating. New York: New York: The Ronald Press Company, 1960.

2.3-6 Kuethe, A. M. and Schetzer, T. D. Foundations of Aerodynamics, Second Edition. New York: John Wiley and Sons, Inc., 1963.

2.3-7 Von Karman, T. "Uber laminare und turbulente Reibung", Z. Angew. Math. U. Mech., Vol. 1, pp. 233-251, 1921, translated as NACA TM 1092, 1946.

2.3-8 Pohlhausen, E. Der Warmeaustausch Zwischen festen korpern und flussigkeiten mit kleiner Reibung und Kleiner Warmeleitung, Zeit. f. Angew, Math. U. Mech., Vol. 1, p. 115, 1921.

2.3-9 Mack, L. M. Report 20-80, Jet Propulsion Laboratory, Calif. Institute of Technology, 1954.

2.3-10 Liepmann, H. W. and Dhawan, S. Proc. 1st U. S. Nat. Congress Applied Mech., p. 869, 1951.

2.3-11 Hantzsche, W., and Wendt, H. Die laminare Grenzschicht bei einemmit Uberschallgeschwindig-keit angestromten nichtangestallten Kreiskegel, Jahrbuch, 1941, der deutschen Luftfahrt forschung, Sec. I, 1941, p. 76.

2.3-12 Van Driest, E. R. Investigation of the Laminar Boundary Layer in Compressible Fluids Using the Grocco Method, NACA TN 2595, 1952.

2.3-13 Lees, L. and Probstein, R. F. Hypersonic Viscous Flow Over a Flat Plate. Rep. No. 195, Princeton University, Aero. Engr. Lab., 1952.

2.3-14 Bertram, M. H. Boundary-Layer Displacement Effects in Air at Mach Numbers of 6.8 and 9.6. NACA TN 4133, 1958.

2.3-15 Lees, L. Hypersonic Flow. Fifth International Aeronautical Conference, Los Angeles, California, June 20-23, 1955. New York.

2.3-16 Lees, L. "Influence of the Leading-edge Shock Wave on the Laminar Boundary Layer at Hypersonic Speeds", Journal Aero. Sciences, Vol. 23, No. 6, 1956.

2.3-17 Nestler, D. E. and Goetz, R. "Survey of Theoretical and Experimental Determinations of Skin-friction in Compressible Boundary Layers"- II The Turbulent Boundary Layer on a Flat Plate. General Electric Company, Thermodynamics Technical Memorandum #109, July 1958.

2.3-18 Smith, Donald W. and Walker, John H. "Skin-Friction Measurements in Incompressible Flow", NASA TR R-26, 1959.

2.3-19 Eckert, E. R. G. "Survey of Heat Transfer at High Speeds", WADC Technical Report 54-70, April, 1954.

2.3-20 Eckert, E. R. G. "Engineering Relations for Friction and Heat Transfer to Surfaces in High Velocity Flow", J. Aero. Sci., Vol. 22, No. 8, August, 1955.

2.3-21 Hoerner, S. F. "Fluid Dynamics Drag" Author's Publication.

2.3-22 Kurzweg, H. H. "The Status of Heat Transfer and Friction Investigations at Supersonic Speeds", AGARD AG 19/P9, June, 1955.

2.3-23 Ferrari, Carlo. "Comparison of Theoretical and Experimental Results for the Turbulent Boundary Layer in Supersonic Flow Along a Flat Plate", Vol. 18, No. 8, August, 1951.

2.3-24 Coles, Donald. "Measurements in the Boundary Layer on a Smooth Flat Plate in Supersonic Flow. I. The Problem of the Turbulent Boundary Layer", REP. 20 - 69, C.I.T. Jet Propulsion Lab., Pasadena, June 1, 1953.

2.3-25 Rubesin, Morris W., and Johnson, H. A. "A Critical Review of Skin-Friction and Heat Transfer Solutions of the Laminar Boundary Layer of a Flat Plate", ASME Trans., Vol. 71, No. 5, July, 1949.

2.3-26 Monagham, R. J. "A Review of Assessment of Various Formulae for Turbulent Skin-Friction in Compressible Flow", British RAE TN Aero. 2182, 1952.

2.3-27 Van Driest, E. R. "Turbulent Boundary Layer in Compressible Fluids", Journal Aero. Science, Vol. 18, No. 3, March 1951, p. 145.

2.3-28 Van Driest, E. R. "The Problem of Aerodynamic Heating", Aeronautical Engineering Review, October, 1956, pp. 26-41.

2.3-29 Van Driest, E. R. "The Turbulent Boundary Layer with Variable Prandtl Number", North American Aviation Report AL-1914, April 2, 1954.

2.3-30 Donaldson, C. DuP. "On the Form of the Turbulent skin-friction Law and Its Extension to Compressible Flows", NACA TN 2692, May 1952.

2.3-31 Deissler, R. G. and Loeffler, A. L., Jr. "Analysis of Turbulent Flow and Heat-Transfer on a Flat Plate at High Mach Numbers with Variable Fluid Properties", NASA TR R-17, 1959.

2.3-32 Tucker, Maurice. "Approximate Calculation of Turbulent Boundary-Layer Development in Compressible Flow", NACA TN 2337, 1951.

2.3-33 Nielsen, Y. N. Missile Aerodynamics McGraw-Hill Series in Missile and Space Technology, McGraw-Hill Book Company, Inc., New York, 1960.

2.3-34 Rubesin, Maydew and Varga: "An Analytical and Experimental Investigation of the Skin-Friction of the Turbulent Boundary Layer on a Flat Plate at Supersonic Speeds," NACA TN 2305, 1951.

2.3-35 Wilson, Robert E. "Turbulent Boundary Layer Characteristics of Supersonic Speeds-Theory and Experiment", Journal Aero. Sci.

Vol. 17, No. 9, September, 1950.

2.3-36 Rubesin, Morris W. "A Modified Reynolds Analogy for the Compressible Turbulent Boundary Layer on a Flat Plate", NACA TN 2917, March, 1953.

2.3-37 Frankl, F. and Voishel, V. "Turbulent Friction in the Boundary Layer of a Flat Plate in a Two-Dimensional Compressible Flow at High Speeds", NACA TM 1083, December, 1943.

2.3-38 Chapman, D. R. and Kester, R. H. "Measurements of Turbulent Skin-Friction on Cylinders in Axial Flow at Subsonic and Supersonic Velocities", J. Aero. Sci., Vol. 20, No. 7, July, 1953, p. 441.

2.3-39 Clemmow, D. M. "The Turbulent Boundary Layer Flow of a Compressible Fluid Along a Flat Plate", British, Director of Guided Weapons Research and Development, REP. 50/6, August, 1950.

2.3-40 Frankl, F., and Voishel, V. "Friction in the Turbulent Boundary Layer of a Compressible Gas at High Speeds", NACA TM 1032, 1942.

2.3-41 Li, Ting-Yi, and Nagamatsu, Henry T. "Effects of Density Fluctuations on the Turbulent Skin-Friction of an Insulated Flat Plate at High Supersonic Speeds", GALCIT Memo No. 5, May 24, 1951.

2.3-42 Smith, F. and Harrop, R. "The Turbulent Boundary Layer With Heat Transfer and Compressible Flow". TN No. Aero. 1759, British R.A.E., February, 1946.

2.3-43 Van Driest, E. R. "The Turbulent Boundary Layer for Compressible Fluids on a Flat Plate with Heat-Transfer", North American Aviation, Aerophysics Lab., AL-1006, February 20, 1950.

2.3-44 Cope, W. F. "The Turbulent Boundary Layer in Compressible Flow", NPL Engr. Dept., British ARC 7634, November, 1943.

2.3-45 Ferrari, Carlo. "Study of the Boundary Layer at Supersonic Speeds in Turbulent Flow: Case of Flow Along a Flat Plate", Quart. Appl. Math, Vol. 8, No. 1, April, 1950.

2.3-46 Young, George B. W., and Janssen, Earl. "The Compressible Boundary Layer", J. Aero. Sci., Vol. 19, No. 4, April, 1952.

2.3-47 Wilson, R. E., Young, E. C., and Thompson, M. J. "2nd Interim Report on Experimentally Determined Turbulent Boundary Layer Characteristics at Supersonic Speeds", Univ. of Texas, Defense Research Lab., UT/DRL 196, January 25, 1949.

2.3-48 Kempf, von Gunther. "Wietere Reibungsergebnisse an Ebenen Glatten Und Rauhen Flachen", Hydrodynamische Probleme Des Schiffsantriebs, Vol. 1, 1932.

2.3-49 Schlichting, H. "Lecture Series, Boundary Layer Theory, Part II - Turbulent Flows", NACA TM 1218, 1949.

2.3-50 Wilson, R. E. "Turbulent Boundary Layer Characteristics at Supersonic Speeds-Theory and Experiment", Univ. of Texas, Defense Research Lab., CM569, November 21, 1949.

2.3-51 Von Karman, Th. "The Analogy Between Fluid Friction and Heat-Transfer", Trans. A.S.M.E., Vol. 61, No. 8, November, 1939.

2.3-52 Schoenherr, Karl E. "Resistance of Flat Surfaces Moving Through a Fluid", Soc. Nav. Arch, and Marine Engrs. Trans., Vol. 40, 1932.

2.3-53 Dhawan, Satish. "Direct Measurements of Skin-Friction", NACA REP 1121, 1953.

2.3-54 Coles, Donald. "Direct Measurement of Supersonic Skin-Friction", Reader's Forum, J. Aero. Sci., Vol. 19, No. 10, October, 1952.

2.3-55 Coles, Donald and Goddard, Frank E. "Direct Measurement of Skin-Friction on a Smooth Flat Plate at Supersonic Speeds", Paper presented at VIIIth Internation Congress on Theoretical and Applied Mechanics at Istanbul, Turkey, August 22, 1952.

2.3-56 Brinich, Paul F. and Diaconis, Nick S. "Boundary Layer Development and Skin-Friction at Mach Number 3.05", NACA TN 2742, 1952.

2.3-57 Cope, W. F. "Measurement of Skin-Friction in a Turbulent Boundary Layer at a Mach Number of 2.5, Including the Effect of a Shock Wave", Proc. Roy. Soc., Ser. A, Vol. 215, No. 1120, November, 1952.

2.3-58 Deissler, Robert G. "Analytical and Experimental Investigation of Adiabatic Turbulent Flow in Smooth Tubes", NACA TN 2138, 1950.

2.3-59 Deissler, R. G. "Investigation of Turbulent Flow and Heat-Transfer in Smooth Tubes, Including the Effects of Variable Fluid Properties", Trans, ASME, Vol. 73, No. 2, February, 1951.

2.3-60 Deissler, R. G. "Heat-Transfer and Fluid Friction for Fully Developed Turbulent Flow of Air and Supercritical Water with Variable Fluid Properties", Trans. ASME, Vol. 76, No. 1, Jan., 1954.

2.3-61 Deissler, R. G. and Eian, C. S. "Analytical and Experimental Investigation of Fully Developed Turbulent Flow of Air in a Smooth Tube with Heat-Transfer with Variable Fluid Properties", NACA TN 2629, 1952.

2.3-62 Deissler, Robert G. "Turbulent Heat-Transfer and Friction in the Entrance Regions of Smooth Passages", Trans. ASME, Vol. 77, No. 8, November, 1955.

2.3-63 Deissler, Robert G. "Analysis of Turbulent Heat-Transfer, Mass Transfer, and Friction in Smooth Tubes at High Prandtl and Schmidt Numbers", NACA Rep. 1210, 1955. (Supercedes NACA TN 3145).

2.3-64 Von Karman, Th. "Mechanical Similitude and Turbulence", NACA TN 611, 1931.

2.3-65 Monaghan, R. J. and Cooke, J. R. "The Measurement of Heat-Transfer and Skin-Friction at Supersonic Speeds. Pt.IV. Tests on a Flat Plate at M = 2.82, Tech. Note AERO. 2171, British RAE, June, 1952.

2.3-66 Spivack, H. M. "Experiments in the Turbulent Boundary Layer of a Supersonic Flow", REP. CM-615 (AL-1052), Aerophys. Lab., North American Aviation, Inc., January 16, 1950.

2.3-67 Monaghan, R. J. and Johnson, J. E. "The Measurement of Heat-Transfer and Skin-Friction at Supersonic Speeds. Pt. II. Boundary-Layer Measurements on a Flat Plate at M = 2.5 and Zero Heat-Transfer", C. P. 64, British ARC, 1952.

2.3-68 Schultz - Grunow, F. "New Frictional Resistance Law for Smooth Plates". NACA TM 986, 1941. (Also Luftfahrtforschung, Vol. 17, No. 8, August 20, 1940).

2.3-69 Kempf, Gunther. "Neue Ergebnisse Der Widerstands-Forschung", Werft Reederei Hafen, Bd. 10, June 1929.

2.3-70 Kaye, Joseph. "The Transient Temperature Distribution in a Wing Flying at Supersonic Speeds", Journal Aero. Sci., Vol. 17, No. 12, December, 1950.

2.3-71 Squire, H. B. "Heat-Transfer Calculations for Airfoils", British Air Ministry R. and M. No. 1986, 1942.

2.3-72 Eber, G. R. "Recent Investigation of Temperature Recovery and Heat Transmission on Cones and Cylinders in Axial Flow in the N.O.L. Aeroballistic Wind Tunnel", Journal Aero. Science, Vol. 19, No. 1, January, 1952.

2.3-73 Seban, R. A. "Analysis for the Heat-Transfer to Turbulent Boundary Layers in High Velocity Flow", Ph.D. Thesis, University of California, Berkeley, California, 1948.

2.3-74 Johnson, H. A., Rubesin, M. W., Sauer, F. M., Slack, E. G., and Possner, L. "A Design Manual for Determining the Thermal Characteristics of High Speed Aircraft", A.A.F. Technical Report 5632, 1947.

2.3-75 McAdams, W. H., Nicolai, L. A., and Keenan, J. H. "Measurements of Recovery Factors and Coefficients of Heat-Transfer in a Tube for Subsonic Flow of Air", Trans. A.I.C.E., Vol. 42, 1946.

2.3-76 Kaye, J., Keenan, J. H., and McAdams, W. H. "Report of Progress on Measurements of Friction Coefficients, Recovery Factors, and Heat Transfer Coefficients for Supersonic Flow of Air in a Pipe", presented at the Fluids Mechanics and Heat-Transfer Institute, Berkeley, Calif., June, 1949.

2.3-77 Goldstein, S. Modern Developments in Fluid Mechanics, Oxford University Press, 1938.

2.3-78 Fischer, W. W. and Norris, R. H. "Supersonic Convective Heat-Transfer Correlation from Skin-Temperature Measurements on a V-2 Rocket in Flight", ASME Trans., Vol. 71, No. 5, July, 1949.

2.3-79 Chapman, Dean R., and Kester, Robert H. "Turbulent Boundary-Layer and Skin-Friction Measurements in Axial Flow Along Cylinders at Mach Numbers Between 0.5 and 3.6", NACA TN 3097, 1954.

2.3-80 Sommer, S: C. and Short, Barbara J. "Free Flight Measurements of Turbulent-Boundary-Layer Skin-Friction in the Presence of Severe Aerodynamic Heating at Mach Numbers from 2.8 to 7.0" NACA Technical Note 3391, Ames Aeronautical Laboratory, Moffett Field, Calif., 1955.

2.3-81 Tendeland, Thorval. "Effects of Mach Number and Wall Temperature Ratio on Turbulent Heat-Transfer at Mach Numbers from 3 to 5", NASA TR R-16, 1959.

2.3-82 Nikuradze, J. "Laws of Flow in Rough Pipes", NACA TM 1292, November, 1950.

2.3-83 Prandtl, L. and Schlichting, H. "Das Widerstandsgesetz Rauher Platten", Werft-Reederei Hafen, Jan. 1, 1934, No. 1, pp. 1-4.

2.3-84 "Proceedings of the Bureau of Ordnance Symposium on Aeroballistics", Nov. 16-17, 1950, Comments by E. R. Van Driest and paper by R. E. Wilson, NAVORD REP. 1651.

2.3-85 Eckert, Hans Ulrich. "Characteristics of the Turbulent Boundary Layer on a Flat Plate in Compressible Flow from Measurements of Friction in Pipes", J. Aero. Sci., Vol. 17, No. 9, September, 1950.

2.3-86 Monagham, R. J. "Comparison Between Experimental Measurements and a Suggested Formula for the Variation of Turbulent Skin-Friction in a Compressible Flow", British ARC C.P. No. 45 (13260), 1951.

2.3-87 Von Karman, Th. "The Problem of Resistance in Compressible Fluids", Reale Accademia D'Italia, Roma. (Paper read at the 5th Volta Congress at Rome, Sept. 30 - Oct. 6, 1935).

2.3-88 Tucker, Maurice. "Approximate Turbulent Boundary Layer Development in Plane Compressible Flow Along Thermally Insulated Surfaces with Application to Supersonic-Tunnel Contour Correction", NACA TN 2045, 1950.

2.3-89 Reichardt, H. "Heat-Transfer Through Turbulent Friction Layers", NACA TM 1047, 1943.

2.3-90 Jokob, Max. Heat-Transfer , Vol. 1, John Wiley and Sons, Inc., New York, 1949.

2.3-91 Schirokow, M. "The Influence of the Laminar Boundary Layer on Heat-Transfer at High Speeds", Tech. Phys. of the USSR, Vol. 3, No. 12, 1936.

2.3-92 Colburn, Allan P. "A Method of Correlating Forced Convection Heat-Transfer Data and a Comparison with Fluid Friction", American Inst. of Chem. Engrs. Trans., Vol. XXIX, 1933.

2.3-93 Seiff, Alvin, James Carlton S., Canning, Thomas N., and Boissevain, Alfred G. "The Ames Supersonic Free-Flight Wind Tunnel", NACA RM AS2A24, 1952.

2.3-94 Deissler, R. G. and Loeffler, A. L., Jr. "Turbulent Flow and Heat-Transfer on a Flat Plate at High Mach Number with Variable Fluid Properties", Paper No. 55 - A - 133, ASME, 1955.

2.3-95 Brevoort, Maurice J., and Rashis, Bernard. "Turbulent-Heat Transfer Measurements at a Mach Number of 2.06", NACA TN 3374, 1955.

2.3-96 Lobb, R. Kenneth, Winkler, Eva M., and Persh, Jerome. "Experimental Investigation of Turbulent Boundary Layers in Hypersonic Flow", I.A.S. Preprint No. 452, 1954.

2.3-97 DeCoursin, D. G., Bradfield, W. S., and Sheppard, J. J. "Aerodynamic Heating and Heat Transfer Phenomena at Mach Numbers 2.7 through 5.7", Res. Rep. 101, Univ. of Minnesota, 1954. (Also available as WADC TR 53-379, February, 1954).

2.3-98 Loudermilk, Warren H., and Grele, Milton D. "Heat-Transfer from High-Temperature Surfaces to Fluids. II-Correlation of Heat-Transfer and Friction Data for Air Flowing in Inconel Tube with Rounded Entrance", NACA RM E8L03, 1949.

2.3-99 Desmon, L. G. and Sams, E. W. "Correlation of Forced-Convection Heat-Transfer Data for Air Flowing in Smooth Platinum Tube with Long-Approach Entrance at High Surface and Inlet-Air Temperatures", NACA RM E50H23, 1950.

2.3-100 Crocco, L. "Su di un valore massimo del coefficiente di transmissione del calose da una limina piana a un fluido seconente", Rendiconti R. Accademia del Lincei, Vol. 14, Dec., 1931.

2.3-101 Ames Research Staff. "Equations, Tables and Charts for Compressible Flow" NACA Rep. 1135, 1953.

2.3-102 Persh. "A Theoretical Investigation of Turbulent Boundary Layer Flow with Heat Transfer at Supersonic and Hypersonic Speeds", NAVORD Rep. 3854, May 1955.

2.3-103 Seiff, Alvin and Short, Barbara J. "An Investigation of Supersonic Turbulent Boundary Layers on Slender Bodies of Revolution in Free-Flight by Use of a Mach-Zehnder Interferometer and Shadowgraphs", NACA TN 4364, September, 1958.

2.3-104 Tetervin, Neal and Lin, Chia Chiao. "A General Intergral From of the Boundary-Layer Equation for Incompressible Flow with an Application to the Calculation of the Separation Point of Turbulent Boundary Layers", NACA REP. 1046, 1951. (Supersedes NACA TN 2158)

2.3-105 Maskell, E. C. "Approximate Calculation of the Turbulent Boundary Layer in Two-Dimensional Incompressible Flow", REP. No. AERO 2443, British RAE, November, 1951.

2.3-106 Ludwieg, H. and Tillman, W. "Investigations of the Wall-shearing Stress in Turbulent Boundary Layers", NACA TM 1285, May, 1960.

2.3-107 Reshotko, Eli and Tucker, Maurice. "Approximate Calculation of the Compressible Turbulent Boundary Layer with Heat-Transfer and Arbitrary Pressure Gradient", NACT TN 4154, December, 1957. (P. III -III - 58)

2.3-108 Cohen, Clarence B., and Reshotko, Eli. "The Compressible Laminar Boundary Layer with Heat Transfer and Arbitrary Pressure Gradients", NACA REP. 1294, 1956. (Supersedes NACA TN 3326).

2.3-109 Reshotko, Eli. "Simplified Method for Estimating Compressible Laminar Heat-Transfer with Pressure Gradient", NACA TN 3888, 1956.

2.3-110 Englert, Gerald W. "Estimation of Compressible Boundary-Layer Growth Over Insulated Surfaces with Pressure Gradient", NACA TN 4022, 1957.

2.3-111 Prandtl, L. and Schlichting, H. "Das Widerstandsgestz Rauher Platten". Werft-Reederei Hafen, Jan. 1, 1934, No. 1, pp. 1-4.

2.3-112 Truckenbrodt, E. "A Method of Quadrature for Calculation of the Laminar and Turbulent Boundary Layer in Case of Plane and Rotationally Symmetrical Flow", NACA TM 1379, 1955.

2.3-113 Scherrer, Richard. "Comparison of Theoretical and Experimental Heat-Transfer Characteristics of Bodies of Revolution at Supersonic Speeds", NACA REP 1055, 1951.

2.3-114 Chapman, Dean R., and Rubesin, Morris W. "Temperature and Velocity Profiles in the Compressible Laminar Boundary Layer with Arbitrary Distribution on Surface Temperature", Journal Aero. Sci., Vol. 16, No. 9, Sept., 1949.

2.3-115 Kalikhman, L. E. "Heat Transmission in the Boundary Layer", NACA TM 1229, 1949.

2.3-116 Scherrer, Richard. "The Effects of Aerodynamic Heating and Heat-Transfer on the Surface Temperature of a Body of Revolution in Steady Supersonic Flight", NACA REP. 917, 1948. (Formerly TN 1300, 1947).

2.3-117 Mangler, W. "Compressible Boundary Layers on Bodies of Revolution", M.A.P. Rolkenrode, VG83 (Rep. and Trans. 47T), March 15, 1946).

2.3-118 Lees, Lester. "The Stability of the Laminar Boundary Layer in a Compressible Fluid", NACA REP. 876, 1947, (Formerly NACA TN 1360).

2.3-119 Gazley, C., Jr. "Theoretical Evaluation of the Turbulent Skin Friction and Heat Transfer on a Cone in Supersonic Flight", Rep. R49A0524, General Electric Co., Nov., 1949. (Proj. Hermes (TU1-2000A) U. S. Army Ord.).

2.3-120 Van Driest, E. R. "Turbulent Boundary Layer on a Cone in a Supersonic Flow at Zero-Angle-of-Attack", Journal Aero. Science, Vol. 19, No. 1, Jan., 1952.

2.3-121 Jakob, Max and Dow, W. M. "Heat Transfer from a Cylindrical Surface to Air in Parallel Flow With and Without Unheated Starting Sections", Trans. ASME, Vol. 68, No. 2, Feb., 1946.

2.3-122 Eckert, Hans Ulrich. "Simplified Treatment of the Turbulent Boundary Layer Along a Cylinder in Compressible Flow" J. Aero. Sci., Vol. 19, No. 1, January, 1952.

2.3-123 Clauser, F. H. The Turbulent Boundary Layer, Advances in Applied Mechanics, Vol. IV, Academic Press, Inc., New York, 1956.

2.3-124 Hama, F. R. "Boundary Layer Characteristics for Smooth and Rough Surfaces", Transactions of the Society of Naval Architects and Marine Engineers, Vol. 62, 1954.

2.3-125 Prandtl, L., and Schlichting, H. "Das Widerstandsgesetz rauher Plattern", Werft, Reederei und Hafen, Vol. 15, No. 1, Jan. 1, 1934 (an account in English is given in Durand, Aerodynamic Theory, Vol. 3, 1936).

2.3-126 Goddard, F. E., Jr. "Effect of Uniformly Distributed Roughness on Turbulent Skin-Friction Drag at Supersonic Speeds" Journal of the Aero-Space Sciences, Vol. 26, No. 1, Jan., 1959, pp. 1-15 and 24.

2.3-127 Clutter, Darwin W. "Charts for Determining Skin-Friction Coefficients on Smooth and on Rough Flat Plates at Mach Numbers up to 5.0 with and without Heat Transfer" Report No. ES 29074, Douglas Aircraft Co., El Segundo, Calif., April 15, 1959.

2.3-128 Granville, P. S. "The Frictional Resistance and Turbulent Boundary Layer of Rough Surfaces" David Taylor Model Basin Report 1024, June, 1958.

2.3-129 Fenter, F. W. "The Effect of Heat-Transfer on the Turbulent Skin-Friction of Uniformly Rough Surfaces in Compressible Flow", The University of Texas, Defense Research Laboratory, Report DRL-368, CM-839, April, 1956.

2.3-130 Nunner, W. "Warmeubergang und Druckabfall in rauhen Rohren", VDI-Forschungshft, Ausgabe B, Vol. 22, 1956.

2.3-131 Hastrup, R. C., Sabersky, R. H. Bartz, D. R. and Noel, M. B. "Friction and Heat-Transfer in a Rough Tube at Varying Prandtl Numbers", Jet Propulsion, Vol. 28, No. 4, April, 1958.

2.3-132 Royal Aeronautical Society Data Sheets, Aerodynamics, Vol. I, Eleventh Issue, October, 1960.

2.3-133 Morrison, R. B. and Ingle, M. J. Design Data for Aeronautics and Astronautics, New York: John Wiley and Sons, Inc., 1962.

2.3-134 Wood, K. D. Aerospace Vehicle Design, Volume I, Aircraft Design, Boulder Colorado: Johnson Publishing Co., 1963.

2.3-135 Nielson, Y. N. Missile Aerodynamics. New York: McGraw-Hill, Inc., 1962.

2.3-136 Corning, G. Aerospace Vehicle Design. Ann Arbor, Michigan: Braun-Bromfield, Inc., 1964.

2.3-137 Fallis, W. B. "Heat-Transfer in the Transitional and Turbulent Boundary Layers of a Flat Plate at Supersonic Speeds", UTIA REP. No. 19, Univ. of Toronto, Inst. of Aerophysics, May, 1952.

2.3-138 Pappas, C. C. "Measurement of Heat Transfer in the Turbulent Boundary Layer on a Flat Plate in Supersonic Flow and Comparison with Skin-Friction Results", NACA TN 3222, 1954.

2.3-139 Desmon, Leland G., and Sams, Eldon W. "Correlation of Forced-Convection Heat-Transfer Data for Air Flowing in Smooth Platinum Tube with Long-Approach Entrance at High Surface and Inlet-Air Temperatures", NACA RM E50H23, 1950.

2.3-140 Humble, Leroy V., Lowdermild, Warren H. and Desmon, Leland G. "Measurements of Average Heat-Transfer and Friction Coefficients for Subsonic Flow of Air in Smooth Tubes at High Surface and Fluid Temperatures", NACA REP. 1020, 1951.

2.3-141 Mangler, W. "Boundary Layers on Bodies of Revolution in Symmetrical Flow" Aerodynamische Versuchsanstalt Gottingen, E.V., Rept. 45-A-17. Translated by M. S. Medvedeff, Goodyear Aircraft Corp., Akron, Ohio, March 6, 1946.

2.3-142 Pitts, William C., Nielsen, Jack N., and Gionfriddo, Maurice P. "Comparison Between Theory and Experiment for Interference Pressure Field Between Wing and Body at Supersonic Speeds" NACA TN 3128, 1954.

2.3-143 Vincenti, Walter G. "Comparison Between Theory and Experiment for Wings at Supersonic Speeds" NACA TR 1033, 1951.